

THE JOURNAL OF  
PHYSICAL CHEMISTRY

---

Volume 69, Number 4 April 1965

Nuclear Magnetic Resonance, Dielectric, Near-Infrared, and Cryoscopic Studies of Solubilized and Emulsified Water. The System Cyclohexane-Carbon Tetrachloride-Duomeen T Dioleate . . . . .	<b>P. D. Cratin and B. K. Robertson</b>	1087
Substituent Effects on Intramolecular Energy Transfer. I. Absorption and Phosphorescence Spectra of Rare Earth $\beta$ -Diketone Chelates . . . . .	<b>W. F. Sager, N. Filipescu, and F. A. Serafin</b>	1092
Intrinsic Viscosity Studies of Stereoregular Poly(methyl methacrylate) in 2,2,3,3-Tetrafluoropropanol . . . . .	<b>Eugene Hamori, Longine R. Prusinowski, Peter G. Sparks, and R. E. Hughes</b>	1101
The Extraction of Acids by Basic Organic Solvents. V. Trioctyl Phosphine Oxide-HClO <sub>4</sub> and Trioctyl Phosphine Oxide-HReO <sub>4</sub> . . . . .	<b>T. J. Conocchioli, M. I. Tocher, and R. M. Diamond</b>	1106
The Differential Thermal Analysis of Perchlorates. VII. Catalytic Decompositions of the Alkali Metal Perchlorates by Manganese Dioxide . . . . .	<b>Meyer M. Markowitz and Daniel A. Boryta</b>	1114
Remarks on Refractive Index Mixture Rules . . . . .	<b>Wilfried Heller</b>	1123
The Virial Theory of Adsorption and the Surface Areas of Solids . . . . .	<b>Robert Wolfe and John R. Sams</b>	1129
Multicomponent Diffusion Involving High Polymers. I. Diffusion of Monodisperse Polystyrene in Mixed Solvents . . . . .	<b>E. L. Cussler, Jr., and E. N. Lightfoot</b>	1135
Multicomponent Diffusion Involving High Polymers. II. Characterization of Polydispersity from Diffusion Data . . . . .	<b>E. L. Cussler, Jr.</b>	1144
Photooxidation of Tertiary Nitrogen Compounds by Methylene Blue . . . . .	<b>F. C. Goodspeed, B. L. Scott, and J. G. Burr</b>	1149
Disulfur Monoxide. III. Its Infrared Spectrum and Thermodynamic Functions . . . . .	<b>Uldis Blukis and Rollie J. Myers</b>	1154
Linear Energy Transfer Effects in the Radiolysis of Liquid Aromatic Hydrocarbons . . . . .	<b>J. Y. Yang, J. D. Strong, and J. G. Burr</b>	1157
Dielectric Dispersion of Protein Solutions Containing Small Zwitterions . . . . .	<b>Rufus Lumry and Robert Hon-Sang Yue</b>	1162
Variation of Chain Dimensions of Polystyrene with Concentration . . . . .	<b>J. Leonard and H. Daoust</b>	1174
Ion-Exchange Kinetics. V. Ion Exchange Accompanied by Reactions . . . . .	<b>F. Helfferich</b>	1178
An Infrared Study of High-Area Metal Films Evaporated in Carbon Monoxide . . . . .	<b>C. W. Garland, R. C. Lord, and P. F. Troiano</b>	1138
Infrared Spectrum of Carbon Monoxide Chemisorbed on Evaporated Nickel Films . . . . .	<b>C. W. Garland, R. C. Lord, and P. F. Troiano</b>	1195
Thermoelectric Properties of the Molten Silver Nitrate-Sodium Nitrate System . . . . .	<b>Benson Ross Sundheim and Jordan D. Kellner</b>	1204
Heat Capacities and Thermodynamic Properties of Globular Molecules. XIII. Transition and Fusion of Pentaerythrityl Chloride and Bromide, Transition of Pentaerythrityl Iodide . . . . .	<b>H. Lawrence Clever, Wen-Kuei Wong, and Edgar F. Westrum, Jr.</b>	1209
Heat Capacities and Thermodynamic Properties of Globular Molecules. XIV. Tetraphosphorus Trisulfide, Tetraphosphorus Triselenide, and Tetraphosphorus Decasulfide between 5 and 350°K. . . . .	<b>H. Lawrence Clever, Edgar F. Westrum, Jr., and A. W. Cordes</b>	1214
Calorimetric Determination of the Mean $\beta$ -Energy and Half-Life of Promethium-147 . . . . .	<b>E. J. Wheelwright, D. M. Fleming, and F. P. Roberts</b>	1220
The Decomposition Pressure and Melting Point of Thorium Mononitride . . . . .	<b>W. M. Olson and R. N. R. Mulford</b>	1223

6462 Sodium trichloroacetate \$22.50/kg  
 2333 Boron tribromide, 99.5% \$5.00/10g  
 \$24.00/100g



**RARE  
 CHEMICALS**

**FINE**

CATALOG  
 NUMBER **5**

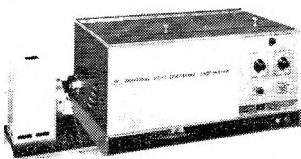
SEND FOR CATALOG #5

TELEPHONE  
 AREA CODE 516  
 GENERAL 3-6262



TWX 516-433-8184  
 TELEX: 01-26464  
 CABLE: KALABOR PLAINVIEWNEWYORK  
**LABORATORIES, INC.**  
 121 EXPRESS STREET, ENGINEERS HILL, PLAINVIEW, NEW YORK

**NOW YOU CAN MEASURE  
 MOLECULAR WEIGHTS  
 from 300 TO 1 BILLION\*  
 with ONE INSTRUMENT . . .**



**the BRICE-PHOENIX UNIVERSAL  
 LIGHT SCATTERING PHOTOMETER**

Sounds improbable, doesn't it? But it is true. And not only does it measure molecular and micellar weights from 300 to 1 Billion, but it also measures size, shape, mass, interactions in solutions, turbidity, dissymmetry, and depolarization. With features such as absolute calibration, wavelength selection, and temperature control one would expect to pay much more than the actual price of the BRICE-PHOENIX LIGHT-SCATTERING PHOTOMETER. As a matter of fact it is far below the cost of other instruments with more limited ranges.

Certainly you will want more information. Send for Bulletin BP-2000.

\*See DISSYMMETRIES, Anal. Chem. 36, 42A (1964); 36, 66A (1964); Science 143, 617 (1964) and 144, 449 (1964)



**PHOENIX PRECISION INSTRUMENT COMPANY**  
 A Subsidiary of CENCO INSTRUMENTS CORP.  
 3803-05 N. 5th Street, Phila., Penna. 19140, U.S.A.

**3<sup>RD</sup>**

**CUMULATIVE  
 ANALYTICAL  
 CHEMISTRY  
 INDEX**

1959-1963

The third ANALYTICAL CHEMISTRY INDEX, which covers the last five years is now available. It contains a complete author and subject index of every article and feature printed in ANALYTICAL CHEMISTRY during the period 1959-1963, volumes 31 through 35 inclusive. This useful reference volume costs only \$7.

Use the space below to order your copy of this important index today.

**Reprint Department  
 ACS APPLIED PUBLICATIONS**

1155 16th St., N.W. / Washington, D.C. 20036

Gentlemen:

Please accept this as my order for \_\_\_\_\_ copies of the third CUMULATIVE ANALYTICAL CHEMISTRY INDEX (1959-1963) at \$7 each.

- My payment is enclosed.
- Bill me.
- Bill Company.

NAME \_\_\_\_\_

MAILING ADDRESS \_\_\_\_\_

CITY \_\_\_\_\_

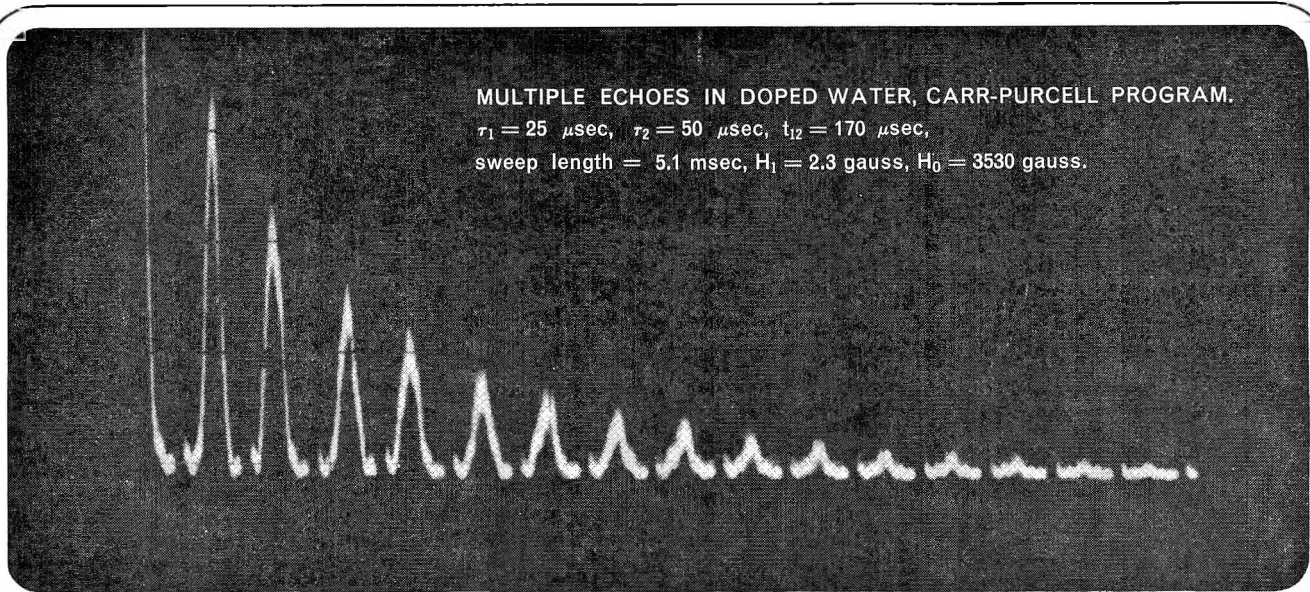
STATE \_\_\_\_\_

ZIP CODE \_\_\_\_\_

COMPANY NAME \_\_\_\_\_

Signature \_\_\_\_\_

The Estimation of Diffusion Coefficients for Ternary Systems of Strong and Weak Electrolytes	Richard P. Wendt	1227
The Occurrence of Metastable Tetragonal Zirconia as a Crystallite Size Effect	Ronald C. Garvie	1238
The Effect of Solvent and of Solutes on the Absorption Spectrum of Solvated Electrons	M. Anbar and Edwin J. Hart	1244
Influence of Electrolytes on the Solution Properties of Neutralized Poly-N-vinylimidazole	Kang-Jen Liu and Harry P. Gregor	1248
Metal-Polyelectrolyte Complexes. X. Poly-N-vinylimidazole Complexes with Zinc(II) and with Copper(II) and Nitrilotriacetic Acid	Kang-Jen Liu and Harry P. Gregor	1252
Kinetic Theory of Inhibition and Passivation in Electrochemical Reactions	D. Gilroy and B. E. Conway	1259
The Heat of Hydration of Cobalt Sulfate Hexahydrate to Heptahydrate. Their Solubilities and Heats of Solution	G. E. Brodale and W. F. Giauque	1268
The Heat Capacities and Entropies of Cobalt Sulfate Heptahydrate and Hexahydrate from 15 to 330°K.	R. V. G. Rao and W. F. Giauque	1272
Kinetics of the Thermal Rearrangement between 3-Methyl-1,5-hexadiene and 1,5-Heptadiene	Akira Amano and Masao Uchiyama	1278
Toward a Generalized Theory of Gas Chromatography at High Solute Concentrations	D. L. Peterson and F. Helfferich	1283
Microwave Absorption and Molecular Structure in Liquids. LXII. The Three Dielectric Dispersion Regions of the Normal Primary Alcohols	S. K. Garg and C. P. Smyth	1294
Microwave Absorption and Molecular Structure in Liquids. LXIV. The Dielectric Behavior of Mixtures of Polar Nonassociative Liquids	Edward Forest and Charles P. Smyth	1302
Wettability of Metals under Continuous Condensing Conditions	Robert A. Erb	1306
Thermodynamic Parameters of Hydrophobic Bond Formation in a Model System	Henry Schneider, Gordon C. Kresheck, and Harold A. Scheraga	1310
Pulse Radiolysis of Aqueous Hydrogen Solutions. I. Rate Constants for Reaction of $e_{aq}^-$ with Itself and Other Transients. II. The Interconvertibility of $e_{aq}^-$ and $H^1$	Max S. Matheson and Joseph Rabani	1324
Solvents Having High Dielectric Constants. XV. Thermodynamic Properties of Solutions of Hydrochloric Acid in N-Methylacetamide by Electromotive Force Measurements	Lyle R. Dawson, William H. Zuber, Jr., and Hartley C. Eckstrom	1335
The Dispersion of the Conductance of a Salt in Low Dielectric Solvents	T. R. Nanney and W. R. Gilkerson	1338
The Fluorescence of Benzene and Benzene- $d_6$	John A. Poole	1343
Carbon-13 Magnetic Resonance Spectra of 1-Substituted 1-Hexynes	Daniel D. Traficante and Gary E. Maciel	1348
The Thermal Unimolecular Decomposition of Norbornylene	B. C. Roquette	1351
Galvanostatic Studies of Carbon Monoxide Adsorption on Platinum Electrodes	S. B. Brummer and J. I. Ford	1355
Comparison of Adsorbed Formic Acid and Carbon Monoxide on Platinum Electrodes	S. B. Brummer	1363
The Radiolysis of Acetone in Air-Free Aqueous Solutions	Peter Riesz	1366
Mass Spectrometric Knudsen Cell Measurements of the Vapor Pressure of Palladium and the Partial Pressure of Palladium Oxide	J. H. Norman, H. Gene Staley, and Wayne E. Bell	1373
Properties of Organic-Water Mixtures. II. Solubilities and Activity Coefficients of Sodium Chloride and Potassium Chloride in N,N-Dialkylamides Containing Water	C. F. Coleman	1377
Rate Constants of Some Reactions of H Atoms in Aqueous Solution	Gil Navon and Gabriel Stein	1384
Electron Transfer between Atomic Hydrogen and Cobalt(III) Complexes in Aqueous Solution	Gil Navon and Gabriel Stein	1390
Pore Area and Adsorption Hysteresis for Packed Spheres	Raymond Venable and William H. Wade	1395
Electrical Properties of Ferromagnetic $CrO_x$ ( $1.89 < x < 2.02$ )	D. S. Chapin, J. A. Kafalas, and J. M. Honig	1402
Thermodynamics of Vaporization of Liquid Thallous Iodide	Daniel Cubicciotti	1410



Now available from Magnion . . .

# SPIN ECHO\* SPECTROMETERS

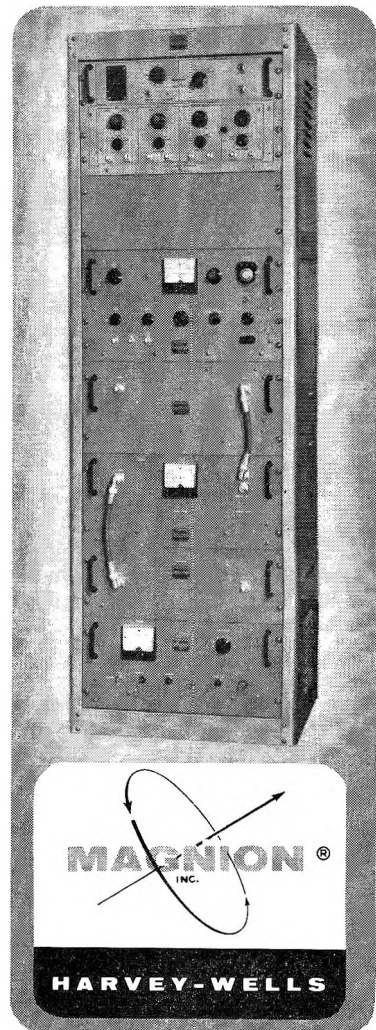
Versatile, pulsed-NMR systems designed for a broad range of experimental applications, including the study of:

- Kinetics of exchange reactions
- Diffusion of liquids and gases
- Atomic and molecular motion
- Internal rotation
- Polymer dynamics
- Spin-spin and spin-lattice interaction
- Nuclear resonance in the rotating frame
- Paramagnetic impurities

Magnion Series ELH Spin Echo Systems, now in use in a number of laboratories, are providing researchers with a powerful and flexible experimental tool. They are available with low or high power (100 or 1000 Watts) output, for liquid or solid samples, and can be used over a wide range of sample temperatures (4.2°K to 500°K). They provide automatic pulse programming, with a broad variety of available sequences from single pulses to complex Carr-Purcell burst patterns. And they are compatible with samples having extremely long relaxation times.

Magnion offers the broadest line of advanced electromagnet equipment available and furnishes complete Superconducting or Iron Core Electromagnet systems for Spin Echo use.

For detailed data on Magnion's Spin Echo Spectrometer Systems, write today to: **MAGNION, INC.**, 144 Middlesex Turnpike, Burlington, Massachusetts.



\*MANUFACTURED UNDER EXCLUSIVE LICENSE TO U. S. PATENT NO. 2,887,673. ISSUED TO E. L. HAHN

Production, Identity, and Annealing of the Radiolytic Products Formed in Crystalline  
Cesium Bromate by Cobalt-60  $\gamma$ -Rays . . . . . **G. E. Boyd and Q. V. Larson** 1413

Relation between Specific Heat and Total Emittance in Tantalum, Niobium, Tungsten, and Molybdenum  
. . . . . **H. V. L. Narasimhamurty, A. S. Iyer, and M. Hoch** 1420

#### NOTES

On the Calculation of the Vibrational De-excitation Probabilities. . . . . **H. Shin** 1424

Carbon-13 Chemical Shift Viewed as a Constitutive Property. II. Substituted Hydrocarbons  
. . . . . **George B. Savitsky, Robert M. Pearson, and Keishi Namikawa** 1425

Carbon-13 Isotope Effects in the Oxidation of Acetic Acid. . . . . **Mieczyslaw Zielinski** 1428

Magnetic Resonance of the Triplet State of Oriented Pyrene Molecules . . . . . **O. Hayes Griffith** 1429

Computation of Statistical Complexions. III. An Exact High Speed Method  
. . . . . **E. W. Schlag, R. A. Sandsmark, and W. G. Valance** 1431

Comparison of Water Sorption and Deuterium-Hydrogen  
Exchange Sites in Poly-L-valine . . . . . **W. W. Brandt and R. S. Budrys** 1432

#### COMMUNICATIONS TO THE EDITOR

The Importance of Xenon Fluorides in the Xenon-Photosensitized Reactions of the Perfluoroalkanes  
. . . . . **Glenn H. Miller and J. R. Dacey** 1434

The Spectroscopy and Photosensitization of Various Photochromic Spiropyrans  
. . . . . **Ralph S. Becker and J. K. Roy** 1435

## AUTHOR INDEX

- Amano, A., 1278  
 Anbar, M., 1244  
 Becker, R. S., 1435  
 Bell, W. E., 1373  
 Blukis, U., 1154  
 Boryta, D. A., 1114  
 Boyd, G. E., 1413  
 Brandt, W. W., 1432  
 Brodale, G. E., 1268  
 Brummer, S. B., 1355, 1363  
 Budrys, R. S., 1432  
 Burr, J. G., 1149, 1157  
 Chapin, D. S., 1402  
 Clever, H. L., 1209, 1214  
 Coleman, C. F., 1377  
 Conocchioli, T. J., 1106  
 Conway, B. E., 1259  
 Cordes, A. W., 1214  
 Cratin, P. D., 1087  
 Cubicciotti, D., 1410  
 Cussler, E. L., Jr., 1135, 1144  
 Dacey, J. R., 1434  
 Daoust, H., 1174  
 Dawson, L. R., 1335  
 Diamond, R. M., 1106  
 Eckstrom, H. C., 1335  
 Erb, R. A., 1306  
 Filipescu, N., 1092  
 Fleming, D. M., 1220  
 Ford, J. I., 1355  
 Forest, E., 1302  
 Garg, S. K., 1294  
 Garland, C. W., 1188, 1195  
 Garvie, R. C., 1238  
 Giauque, W. F., 1268, 1272  
 Gilkerson, W. R., 1338  
 Gilroy, D., 1259  
 Goodspeed, F. C., 1149  
 Gregor, H. P., 1248, 1252  
 Griffith, O. H., 1429  
 Hamori, E., 1101  
 Hart, E. J., 1244  
 Helfferich, F., 1178, 1283  
 Heller, W., 1123  
 Hoch, M., 1420  
 Honig, J. M., 1402  
 Hughes, R. E., 1101  
 Iyer, A. S., 1420  
 Kafalas, J. A., 1402  
 Kellner, J. D., 1204  
 Kresheck, G. C., 1310  
 Larson, Q. V., 1413  
 Leonard, J., 1174  
 Lightfoot, E. N., 1135  
 Liu, K.-J., 1248, 1252  
 Lord, R. C., 1188, 1195  
 Lumry, R., 1162  
 Maciel, G. E., 1348  
 Markowitz, M. M., 1114  
 Matheson, M. S., 1324  
 Miller, G. H., 1434  
 Mulford, R. N. R., 1223  
 Myers, R. J., 1154  
 Namikawa, K., 1425  
 Nanney, T. R., 1338  
 Narasimhamurty, H. V. L., 1420  
 Navon, G., 1384, 1390  
 Norman, J. H., 1373  
 Olson, W. M., 1223  
 Pearson, R. M., 1425  
 Peterson, D. L., 1283  
 Poole, J. A., 1343  
 Prusinowski, L. R., 1101  
 Rabani, J., 1324  
 Rao, R. V. G., 1272  
 Riesz, P., 1366  
 Roberts, F. P., 1220  
 Robertson, B. K., 1087  
 Roquette, B. C., 1351  
 Roy, J. K., 1435  
 Sager, W. F., 1092  
 Sams, J. R., 1129  
 Sandsmark, R. A., 1431  
 Savitsky, G. B., 1425  
 Scheraga, H. A., 1310  
 Schlag, E. W., 1431  
 Schneider, H., 1310  
 Scott, B. L., 1149  
 Serafin, F. A., 1092  
 Shin, H., 1424  
 Smyth, C. P., 1294, 1302  
 Sparks, P. G., 1101  
 Staley, H. G., 1373  
 Stein, G., 1384, 1390  
 Strong, J. D., 1157  
 Sundheim, B. R., 1204  
 Tocher, M. I., 1106  
 Traficante, D. D., 1348  
 Troiano, P. F., 1188, 1195  
 Uchiyama, M., 1278  
 Valance, W. G., 1431  
 Venable, R., 1395  
 Wade, W. H., 1395  
 Wendt, R. P., 1227  
 Westrum, E. F., Jr., 1209, 1214  
 Wheelwright, E. J., 1220  
 Wolfe, R., 1129  
 Wong, W.-K., 1209  
 Yang, J. Y., 1157  
 Yue, R. H.-S., 1162  
 Zielinski, M., 1428  
 Zuber, W. H., Jr., 1335

THE JOURNAL OF  
PHYSICAL CHEMISTRY

Registered in U. S. Patent Office © Copyright, 1965, by the American Chemical Society

VOLUME 69, NUMBER 4 APRIL 15, 1965

**Nuclear Magnetic Resonance, Dielectric, Near-Infrared, and  
Cryoscopic Studies of Solubilized and Emulsified Water. The  
System Cyclohexane–Carbon Tetrachloride–Duomeen T Dioleate**

by P. D. Cratin and B. K. Robertson<sup>1</sup>

*Department of Chemistry, Spring Hill College, Mobile, Alabama (Received February 19, 1964)*

Nuclear magnetic resonance, dielectric, near-infrared, and cryoscopic methods have been used to demonstrate the existence of two distinct water species in water-in-oil emulsions formed from cyclohexane, carbon tetrachloride, and Duomeen T Dioleate (TDO). The solubilized species appears to be very strongly associated with the carboxyl groups of the surfactant; emulsified water appears only after the surfactant has been "saturated" with the solubilized moiety. The authors postulate that the surfactant–water complexes are a series of hydrates having the general formula  $TDO \cdot nH_2O$ . The marked increase in dielectric constant with decreasing frequency has been attributed to interfacial polarization. Dielectric studies suggest that micelles build up in cyclohexane (but are absent in carbon tetrachloride) before solubilization occurs; cryoscopic measurements indicate no such buildup.

**Introduction**

It is not unreasonable to believe that water *solubilized* in an organic medium through the action of a surfactant should manifest properties which are substantially different from those exhibited by water *emulsified* in the same medium. Especially interesting, then, is the transition region where the solubilization point is slightly exceeded, and emulsion droplets first appear. Do two distinct water species exist in this region—each having its own set of properties due to environmental differences—or are all the water molecules equivalent and therefore indistinguishable? This problem—and related ones—have been subject to much theoretical

interest during the past few years<sup>2–4</sup>; lacking, however, has been the experimental evidence needed to answer this question unequivocally, even for a single system.

In an attempt to solve this problem, the authors have employed nuclear magnetic resonance, dielectric, spectral, and cryoscopic methods to study the properties of

(1) Department of Chemistry, Texas A and M University, College Station, Texas.

(2) M. E. L. McBain and E. Hutchinson, "Solubilization and Related Phenomena," Academic Press, Inc., New York, N. Y., 1955, pp. 188–190.

(3) J. H. Schulman and T. S. McRoberts, *Trans. Faraday Soc.*, **42B**, 165 (1946).

(4) A. V. Tobolsky and B. J. Ludwig, *Am. Scientist*, **51**, 400 (1963).

solubilized and emulsified water in the system cyclohexane-carbon tetrachloride-Duomeen T Dioleate.

### Experimental

**Reagents.** Duomeen T Dioleate (tallow 1,3-propylenediamine dioleate) was obtained in the commercial grade, "100% active," from Armour Industrial Chemical Co. and used without further purification. The molecular weight determined from cryoscopic measurements agreed with that given by the manufacturer, about 1000, but was higher than the theoretical formula weight, 750. (The discrepancy is probably due to the presence of high molecular weight tertiary amines in the sample.)

Cyclohexane and carbon tetrachloride were reagent grade chemicals purchased from Fisher Scientific Co. and Baker Chemical Co., respectively. Inasmuch as there were no detectable differences in the dielectric constants of the reagent grade chemicals and those of spectroscopic grade materials, further purification was deemed unnecessary.

Distilled water was used in all experimental runs.

**Apparatus.** Many of the practical difficulties associated with employing conventional permittivity cells (*i.e.*, those having immersed electrodes) were overcome by using the Wayne Kerr (D121) cell, which has non-contacting electrodes. Since the electrodes contact neither the solution nor the sample container, surface adsorption and catalysis, poisoning, boundary effects, etc., are not encountered. Such a cell is limited, however, to use with solutions whose dielectric constants do not exceed 5.

In this study, the dielectric constants were calculated using capacitance values obtained with a Wayne Kerr universal bridge (B221) and the D121 permittivity cell at 159, 1592, and 15,000 c.p.s. Because the frequency of the bridge oscillator was fixed at 1592 c.p.s., a General Radio oscillator (1210 C) and power supply (1203 B) were used to achieve the remaining frequencies. A Ballantine vacuum tube voltmeter (300-H) served as the null detector.

N.m.r. spectra were obtained with a Varian 60-Mc. proton resonance spectrometer.

Near-infrared spectra were obtained with a Beckman DK-1 recording spectrophotometer using 1-cm. Corex cells.

A Beckmann freezing point apparatus was used for all cryoscopic measurements. The temperature sensor was a Sargent thermistor bridge equipped with a low-range thermometric element. The bridge unbalance was fed into a Hewlett-Packard (425A) d.c. microvolt-ammeter and amplified, and the output was displayed on a Varian (G-11A) recorder.

**Technique and Reproducibility of Emulsions.** One of the difficulties in any emulsion study is that of reproducibly formulating the systems with which one is to work. In this investigation we feel that we have overcome this problem—within limits—by using sonic energy to generate our emulsions. (The criterion of reproducibility is the dielectric constant.)

A Sonifier 75-H sonic generator proved most effective in bringing about rapid solution and emulsification of water in the organic phase, which contained weighed amounts of surfactant. The resulting mixture was subjected to sonic energy until solution (or emulsification, as the case may be) was complete, usually in about 10 sec. The liquid was rapidly transferred to the previously calibrated dielectric cell, and the capacitance was determined as quickly as possible, in most cases within 30 sec. Table I illustrates the typical precision with which emulsions were reproduced in this study.

Table I: Precision of Emulsion Formulation<sup>a</sup>

% H <sub>2</sub> O	Dielectric constant, $\epsilon$		Ratio $\epsilon_A/\epsilon_B$
	Run A	Run B	
0.00	2.08	2.08	1.000
0.90	2.15	2.155	1.002
1.88	2.22	2.23	1.005
2.97	2.31	2.33	1.009
4.14	2.43	2.44	1.004
5.45	2.565	2.58	1.006
6.88	2.74	2.74	1.000
8.53	2.93	2.93	1.000
10.3	3.15	3.15	1.000
12.4	3.48	3.48	1.000

<sup>a</sup> Organic phase consisted of 72 ml. of cyclohexane, 28 ml. of carbon tetrachloride, and 0.30 g. of TDO.  $T = 25^\circ$ .

### Results and Discussion

1. **Nuclear Magnetic Resonance Studies.** Conclusive evidence for the existence of two distinct water species in an emulsion was gathered from studies of the n.m.r. spectra, whose tracings are shown in Figure 1. The first (partial) spectrum gives the chemical shifts assigned<sup>5a</sup> to the carboxyl protons at 7.22 p.p.m.<sup>5b</sup> and to the olefinic hydrogens at 3.88 p.p.m. When 0.15% H<sub>2</sub>O is added to the solution, the chemical shift of the carboxyl protons moves to higher magnetic field strengths, and the peak area ascribed to these protons increases. Once the solubilization point is reached—

(5) J. D. Roberts, "Nuclear Magnetic Resonance," McGraw-Hill Book Co., Inc., New York, N. Y., 1959, p. 23. (b) All measurements were made relative to the methylene protons of cyclohexane set at zero p.p.m.



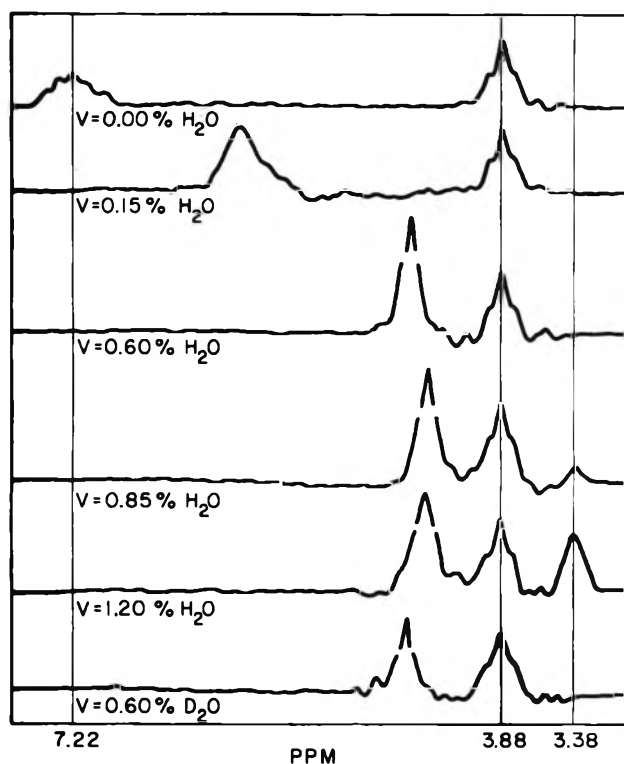


Figure 1. Nuclear magnetic resonance spectra of mixtures containing 4.0 g. of TDO in 100 ml. of cyclohexane and varying quantities of water.

that is, when the solution becomes saturated with solubilized water—the upfield movement of the chemical shift and the increase in peak area cease. (In this example, the solubilization point occurs at 0.62%  $H_2O$ .)

Water added after the solubilization point is reached causes the sample to become turbid; the protons of this “excess” water—actually, emulsified water—are seen in the n.m.r. spectrum as a distinct signal occurring at 3.38 p.p.m. (0.85% spectrum). Increasing the water concentration to 1.20% increases the peak area of the emulsified species but does not affect that of the solubilized moiety.

The last spectrum of Figure 1 shows how heavy water,  $D_2O$ , affects the magnitude and change of the carboxyl proton chemical shift. Inasmuch as deuterium does not respond to n.m.r., the use of  $D_2O$  removes the contribution of the water protons.

The existence of a single n.m.r. signal up to the solubilization point indicates a very rapid exchange of protons between the solubilized water and the carboxyl groups. Once the solubilization point is exceeded, a new n.m.r. signal characteristic of the protons of free (*i.e.*, emulsified) water appears. That two distinct signals are noted in the n.m.r. spectrum shows that (1) two distinct water species coexist in these emulsions and

(2) the rate of proton exchange between the solubilized water and the emulsified species is indeed a very slow one.

2. *Dielectric Constants. A. Frequency Dependence of Dielectric Constants.* The dependence of the dielectric constant on the frequency at which measurement is made is depicted in Figure 2. In the range 1592–15,000 c.p.s., the values of the dielectric constants are identical (within experimental error) and appear to be independent of the frequency. Somewhere below 1592 c.p.s., the dielectric constant begins to increase as the frequency decreases. The cause of this phenomenon is interfacial polarization.<sup>6</sup> As pointed out by Smyth,<sup>7</sup> interfacial polarization arises only when the bulk phases differ appreciably in dielectric constant ( $\epsilon$ ) and electrical conductivity ( $k$ ) so that  $\epsilon_1 k_2 \neq \epsilon_2 k_1$ . Under these conditions, a charge accumulates at the oil-water interface. This accumulation of charge requires current to flow through the dielectric phase; the current flows so slowly that it is observed only in the low frequency range of measurement.

*B. Dielectric Constants and Water Concentration.* According to Callinan and co-workers,<sup>8</sup> there is a linear relationship between the logarithm of the dielectric constant and the volume % of water in an oil-continuous phase emulsion. Our findings agreed with theirs, provided that the water content was high and the surfactant concentration was low. When the reverse was true, the addition of water effected little or no change in the dielectric constant.

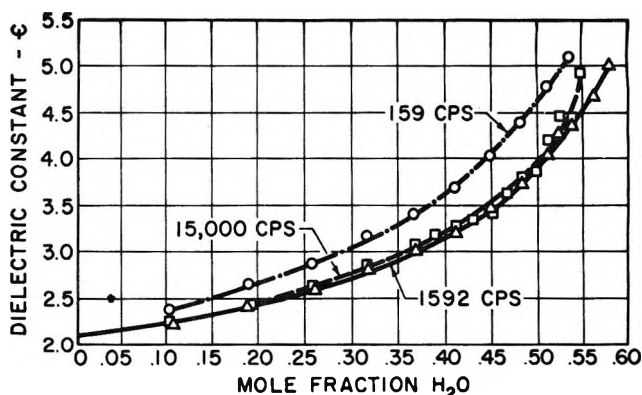


Figure 2. Dependence of the dielectric constant upon frequency of a mixture containing 72 ml. of cyclohexane, 28 ml. of carbon tetrachloride, and 0.30 g. of TDO as a function of the water concentration.

(6) T. Hanai, *Kolloid Z.*, 177, 57 (1961).

(7) C. P. Smyth, "Dielectric Behavior and Structure," McGraw-Hill Book Co., Inc., New York, N. Y., 1955, pp. 52–54.

(8) T. D. Callinan, R. M. Roe, and J. B. Romans, *Anal. Chem.*, 28, 1911 (1956).

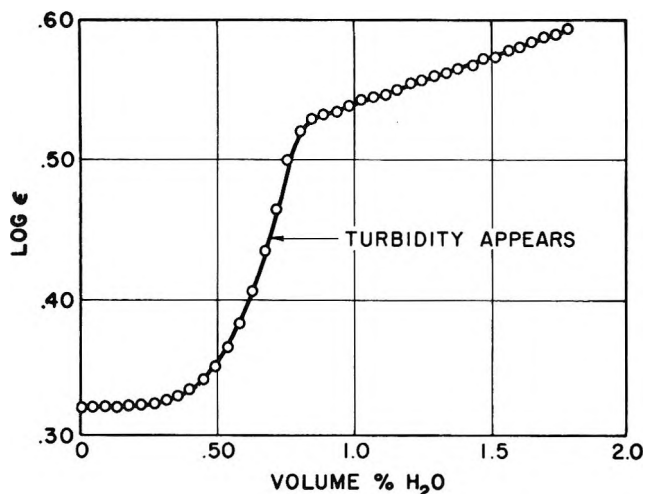


Figure 3. Dependence of the logarithm of the dielectric constant upon the water concentration of a mixture containing 4.0 g. of TDO in 100 ml. of cyclohexane.

A typical example of how low water and high surfactant concentrations affect the dielectric constant is given in Figure 3. With the addition of small quantities of water, up to 0.25%  $H_2O$  in this case, there is no perceptible change in  $\log \epsilon$ . Between 0.25 and 0.75%  $H_2O$ , the change in  $\log \epsilon$  is much more pronounced. At approximately 0.75%  $H_2O$ , the relationship between  $\log \epsilon$  and %  $H_2O$  becomes linear and remains so until demulsification begins. The solubilization point, as determined by the first appearance of turbidity, occurred at 0.62%  $H_2O$ . A graph of  $\Delta \log \epsilon / \Delta V$  vs.  $V$  showed that the maximum in the first-derivative plot corresponded to the solubilization point. Once again, it is quite evident that solubilized water exhibits polar properties that are substantially different from those manifested by the emulsified species.

It was not surprising to find that the quantity of water solubilized was directly proportional to the amount of surfactant present; it was unusual, we thought, that the composition of the organic phase should play such a dominant role in determining the solubilizing power of the surfactant. These phenomena are discussed in detail in section 5 of this paper.

3. *Near-Infrared Spectral Studies.* Near-infrared spectra were obtained on the cyclohexane-surfactant system containing varying quantities of water, using the former components as a blank. In all cases, an absorption band occurred at  $1.935 \mu$ . As shown in Figure 4, when the peak height (which is directly proportional to the absorbance) is plotted vs. the water concentration, two intersecting straight lines result. The first line, passing through the origin, gives only the response due to solubilized water. The second line

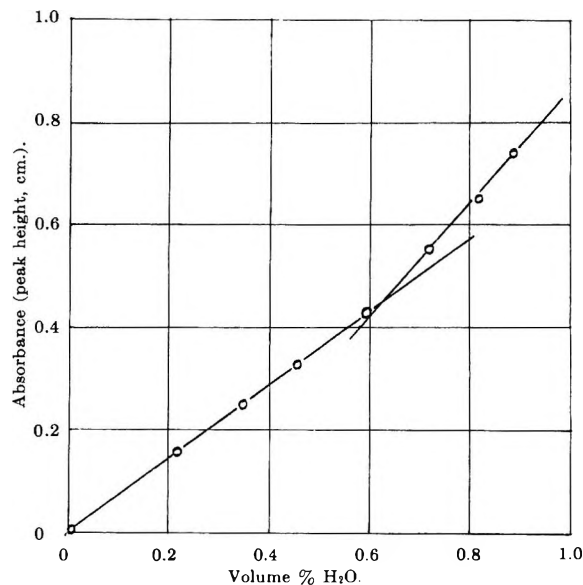


Figure 4. Near-infrared absorbance ( $1.935 \mu$ ) of a mixture containing 4.0 g. of TDO in 100 ml. of cyclohexane as a function of the water concentration.

probably results from a combination of several factors: (1) the absorption of light by the solubilized species, (2) the absorption of light by the emulsified moiety, and (3) the scattering of light by the emulsion droplets themselves. We believe that the effect of scattering contributes very little to the over-all effect, for, although the particle size and wave length of light used in the measurement are of the same order of magnitude, there is only one point where absorption occurs, *i.e.*,  $1.935 \mu$ . Were the scattering significant, a more or less broad absorption would be noted over a relatively large range of wave lengths. The intersection of these lines corresponds to the solubilization point found by other methods, 0.62%  $H_2O$ .

4. *Cryoscopic Measurements.* The large freezing-point depression constant of cyclohexane ( $K_f = 20$ ) made this solvent attractive for use in determining the molecular weight of TDO by the cryoscopic method.<sup>9</sup>

The molecular weight<sup>10</sup> was found to be about 1000 by this method; thus, the number of micelles in cyclohexane at  $6.5^\circ$  (the freezing point) is indeed negligible. It should be emphasized, however, that micellization and solubilization are temperature-dependent properties of this system<sup>11</sup> so that the conclusions drawn from measurements made at freezing temperatures may not be valid for the system at room temperature.

(9) F. Daniels, *et al.*, "Experimental Physical Chemistry," McGraw-Hill Book Co., Inc., New York, N. Y., 1956, p. 65 ff.

(10) Theoretical formula weight = 750.

(11) See ref. 2, pp. 113-122, 149 ff.

To determine the degree of dissociation of the TDO-H<sub>2</sub>O complex, additional cryoscopic studies were made using water as the solute in cyclohexane-surfactant mixtures. Water concentrations as high as 1 *m* caused no depression of the freezing points of these mixtures. We interpret this to mean that, in the solubilization range, each water molecule is bound to the carboxyl groups of the surfactant so tightly that no detectable dissociation takes place. Once emulsification occurs, the water droplets are too large (1  $\mu$  in diameter) to manifest colligative properties.

Thus, it appears that at this temperature water is tied up with the surfactant, not in micelles, but as hydrated species. This disagrees with Pink's findings<sup>12</sup> but lends support to some early work carried out by Weichherz.<sup>13,14</sup>

5. *Solubilization Point and Surfactant Concentration.* The dependence of the solubilization point on the composition of the organic phase was determined as a function of the surfactant concentration in mixtures containing varying percentages of cyclohexane and carbon tetrachloride. As one would predict, the quantity of water solubilized is directly proportional to the amount of surfactant present for a fixed composition of the organic phase. There is, however, wide variance in the solubilizing power of a fixed quantity of surfactant from one composition to another. Figure 5 graphically depicts the total amount of water solubilized as a function of the amount of surfactant present in cyclohexane, carbon tetrachloride, and two of their mixtures. The slopes of the lines are interpreted to be average, albeit approximate, formulas of the water-surfactant complexes in each system. These are in cyclohexane, TDO·10-11H<sub>2</sub>O; in 72-28, TDO·8-9H<sub>2</sub>O; in 50-50, TDO·7-8H<sub>2</sub>O; and in carbon tetrachloride, TDO·5-6H<sub>2</sub>O.

We can envision two interpretations of these data: (1) if we assume that the complexes are built up from a surfactant molecule and *n* molecules of water, *i.e.*, a series of hydrates having the general formula TDO·*n*-H<sub>2</sub>O, then the solubilization point merely represents the place where one (or more) of the hydrates precipitates from solution, and all higher hydrates are similarly insoluble; (2) if we extrapolate the curves in Figure 5 to zero water concentration, we find that those representing 100 and 50% CCl<sub>4</sub> pass through the origin, whereas those of the 100 and 72% cyclohexane do not. According to Ross,<sup>15,16</sup> the intercept gives a measure of the c.m.c. of the surfactant since this is the concentration of material needed before any water can be solubilized. If this is true, then micelles *are* present in the 100 and 72% cyclohexane samples and are absent in the 100 and 50% CCl<sub>4</sub> solutions.

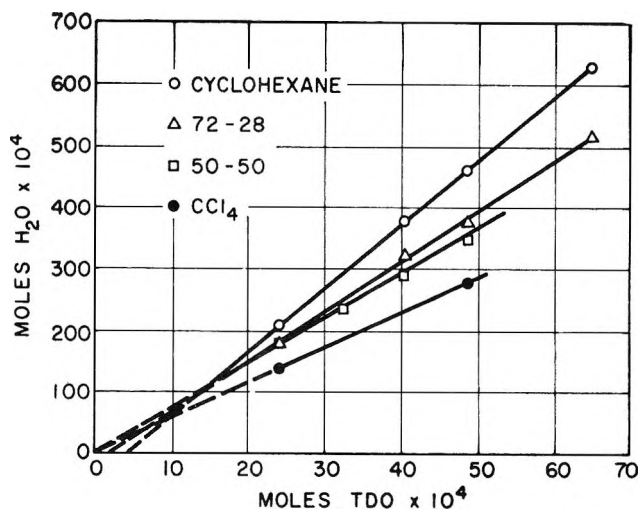


Figure 5. Quantitative solubilization of water as functions of amount of surfactant and composition of organic phase.

The problem is quite perplexing. From cryoscopic studies, there appear to be few, if any, micelles in cyclohexane, and results can be interpreted on the basis of hydrate formation; as noted before, however, the fact that micelles are absent at 6.5° does not necessarily mean they are absent at 25°. On the other hand, the solubilization plots mentioned in this section lead one to believe that a c.m.c. does exist in 100 and 72% cyclohexane mixtures. Unfortunately, the n.m.r. spectra give no additional information as to the aggregation of the "complex."

The extreme solubility of the surfactant in cyclohexane prohibited our using surface tension measurements to determine a c.m.c. by that method. (It may be well to mention that TDO is practically insoluble in water; it does, however, show some surface activity here.)

6. *Temperature and Salt Effects.* Although no quantitative data were obtained on our systems, it was noted qualitatively that the solubilization point was dependent upon the temperature and salt content.

An increase in temperature lowered the amount of water that could be solubilized. This indicates that the formation of the surfactant-water complex is an exothermic process.

Sodium chloride decreased the quantity of water solubilized by the surfactant. This is probably due to

(12) R. C. Pink, *J. Chem. Soc.*, 53 (1939).

(13) J. Weichherz, *Kolloid-Z.*, 47, 133 (1929).

(14) J. Weichherz, *ibid.*, 49, 158 (1929).

(15) S. Ross and J. B. Hudson, *J. Colloid Sci.*, 12, 523 (1957).

(16) S. Ross, private communication.

the competition of the salt and the TDO for the water molecules.

*Acknowledgment.* We wish to express our appreciation to the Jersey Production Research Co. for permis-

sion to publish this work and to Dr. Walt Naegele of Esso Research and Engineering for his help in obtaining and interpreting the n.m.r. spectra. We also extend thanks to Mr. J. W. Coryell, who aided us in the cryoscopic and surface tension measurements.

## Substituent Effects on Intramolecular Energy Transfer. I. Absorption and Phosphorescence Spectra of Rare Earth $\beta$ -Diketone Chelates

by W. F. Sager, N. Filipescu, and F. A. Serafin

*Department of Chemistry, The George Washington University, Washington 6, D. C. (Received June 1, 1964)*

The absorption and phosphorescence spectra of differently substituted rare earth  $\beta$ -diketonates have been investigated. The influence of the substituents on the electronic states of the organic ligand is discussed in relation to the over-all intramolecular energy migration.

### Introduction

Rare earth ions incorporated in organic chelates by coordination through a donor atom such as oxygen or nitrogen when excited in the region of light absorption associated primarily with the organic ligand exhibit characteristic intra-4f parity-forbidden fluorescence similar to the inorganic single crystal system. Direct excitation of the metal ion is not responsible for the line emission which, instead, is the result of an intramolecular energy transfer from the excited electronic states of the organic complex to the localized 4f energy levels of the chelated ion. The efficiency of excitation varies greatly with the nature of the ligand, temperature, and solvent.<sup>1</sup> The over-all absorption-line emission under near-ultraviolet excitation involves (1) ground singlet  $\rightarrow$  excited singlet absorption, (2) radiationless intersystem crossing from the excited singlet to the lowest lying triplet state, (3) transfer of energy to the chelated ion, and (4) characteristic ionic fluorescent emission. Recent studies of the emission spectra of rare earth  $\beta$ -diketonates have been concerned with the path of energy migration within these complex molecules.<sup>2</sup> In these investigations only a

restricted number of chelating agents have been studied (dibenzoylmethane, benzoylacetone, and acetylacetone). The present work is concerned with the influence of substituents attached to a  $\beta$ -diketone rare earth chelate structure on the emission spectra under excitation with near-ultraviolet radiation, the intramolecular energy transfer, and the quantum states involved. The first part covers the investigation of the absorption spectra and phosphorescence spectra of a number of substituted gadolinium  $\beta$ -diketone chelates, indicative of the excited electronic states of the organic ligand.

### Experimental

*Preparation of  $\beta$ -Diketones.* The following diketones, reagent grade, were purchased: dibenzoylmethane, benzoylacetone, theonyltrifluoroacetone, acetylacetone

(1) S. I. Weissman, *J. Chem. Phys.*, **10**, 214 (1942).

(2) (a) G. A. Crosby, R. E. Whan, and R. M. Alire, *ibid.*, **34**, 743 (1961); (b) R. E. Whan and G. A. Crosby, *J. Mol. Spectry.*, **8**, 315 (1962); (c) G. A. Crosby, R. E. Whan, and J. J. Freeman, *J. Phys. Chem.*, **66**, 2493 (1962); (d) J. J. Freeman and G. A. Crosby, *ibid.*, **67**, 2717 (1963); (e) G. A. Crosby and R. E. Whan, *ibid.*, **36**, 863 (1962).

(Eastman), trifluoroacetylacetone (K & K), hexafluoroacetylacetone (Columbia). All the other  $\beta$ -diketones were synthesized. The symmetrically substituted dibenzoylmethanes (di-*p*-methoxy, di-*m*-methoxy, di-*p*-nitro, di-*m*-nitro, and di-*p*-fluoro), as well as difuroylmethane, ditheonylmethane, di-1-naphthoylemethane, and di-2-naphthoylemethane, were prepared from the acid chloride with vinyl acetate, by the procedure described by Sieglitz and Horn.<sup>3</sup> Diisonicotylmethide was synthesized from 4-acetylpyridine and ethyl isonicotinate in condensation reaction with sodamide.<sup>4</sup> The monosubstituted *p*-methoxy-, *m*-methoxy-, and *p*-phenyldibenzoylmethanes were prepared from the substituted ethyl benzoate in condensation reaction with acetophenone or the substituted acetophenone with ethyl benzoate by the sodium amide procedure. The *m*-nitro- and *p*-nitrodibenzoylmethanes were synthesized from the nitro-substituted benzoyl chloride in condensation with the sodium salt of acetophenone.<sup>4,5</sup> Benzoyltrifluoroacetone was obtained from acetophenone and ethyl trifluoroacetate as described by Reid and Calvin.<sup>6</sup> The prepared  $\beta$ -diketones, as well as those purchased, were distilled, sublimed, or recrystallized from appropriate solvents.

**Preparation of  $\beta$ -Diketone Chelates.** Rare earth chlorides were purchased from the American Potash and Chemical Corp. (99.999% purity). The procedure involving the rare earth chloride, the  $\beta$ -diketone, and piperidine, as precipitating agent, in absolute ethanol was employed for the preparation of most of the chelates.<sup>7</sup> The acetylacetonates, trifluoroacetylacetonates, and hexafluoroacetylacetonates were prepared by titration with aqueous ammonia of a mixture of the diketone and the rare earth chloride in water with a pH meter in the reaction beaker, as described by Moeller and Ulrich.<sup>8</sup> The benzoylacetonates were synthesized from the sodium salt of the  $\beta$ -diketone and the rare earth halide.<sup>2b</sup> The chelates were purified by washing, recrystallization, and vacuum drying for prolonged periods of time at temperatures below decomposition.

**Spectroscopic Measurements.** All absorption spectra were measured in the near-ultraviolet and visible range with a Cary Model 14 recording spectrophotometer, in Spectrograde methanol at 20°. All measurements were performed on fresh solutions at concentrations of  $10^{-5}$  M in chelate. The phosphorescence spectra of the gadolinium chelates were recorded on the same spectrophotometer using the fluorescence attachment. The compounds were dissolved at a concentration of  $\sim 10^{-5}$  M in EPA (5 parts diethyl ether, 5 parts 3-methylpentane, and 2 parts absolute ethanol by volume). The diethyl ether and the methylpentane were distilled from magnesium ethoxide. The

fresh solutions of gadolinium chelates were introduced into 10-mm. quartz tubes and immersed in liquid nitrogen in a transparent quartz dewar. The frozen samples were irradiated with two sources—a beam from the internal mercury vapor lamp in the Cary Model 14 illuminating the sample from the photocell side and one from an external mercury vapor lamp 9 W, Model SL 3660 (Ultraviolet Products, Inc.) normal to the sample-slit beam. For all the aromatic  $\beta$ -diketone chelates, the exciting light was filtered through an aqueous  $\text{CuSO}_4$  solution and a Corning 5840 filter (3000–4000 Å. transmission range) whereas, for the aliphatic  $\beta$ -diketonates (acetylacetonates, trifluoroacetylacetonate, and hexafluoroacetylacetonate), the internal Cary 14 ultraviolet source was filtered through a  $\text{NiSO}_4$  water solution and a Corning 9863 filter and coupled with an external short-wave ultraviolet lamp 9 W, Model SL 2537, perpendicular to the sample-slit direction. The log scale was used on the recorder, and all the phosphorescence spectra were extrapolated to an equivalent 0.5-mm. slit for comparison. A semiquantitative evaluation of the relative intensities is possible by comparing the area under the curve of a given band on a linear relative intensity =  $f(\nu)$  scale.

## Discussion

Two series of  $\beta$ -diketone chelates have been prepared. Substituents with different configurations and electro-negativities have been attached (through synthesis) in various positions, either on a dibenzoylmethide structure (series A) or directly to the  $\beta$ -diketone chelate ring (series B).

Both symmetrically and asymmetrically substituted  $\beta$ -diketonates were synthesized with aromatic and/or aliphatic substituents appended to the chelating ring.

**Absorption Spectra in Near-Ultraviolet-Visible.** The ultraviolet-visible absorption spectra of the different chelates are illustrated in Figures 2, 3, 4, and 5. The absorption spectrum of a given tris chelate did not show any significant modification on changing the metallic ion, and actually the spectrum is very similar to that of the hydrogen chelate (the free  $\beta$ -diketone). This indicates that the absorption spectrum is characteristic of any one of the three chelate groups surrounding the ion. The molar concentration ( $\sim 10^{-5}$  M) was only approximative because analysis of chelates indicated

(3) A. Sieglitz and O. Horn, *Ber.*, **84**, 607 (1951).

(4) R. Adams, "Organic Reactions," Vol. III, John Wiley and Sons, Inc., New York, N. Y., 1954.

(5) B. O. Linn and C. R. Hauser, *J. Am. Chem. Soc.*, **78**, 6066 (1956).

(6) J. C. Reid and M. Calvin, *ibid.*, **72**, 2948 (1950).

(7) G. A. Crosby and M. Kasha, *Spectrochim. Acta*, **10**, 377 (1958).

(8) T. Moeller and W. F. Ulrich, *J. Inorg. Nucl. Chem.*, **2**, 164 (1956).

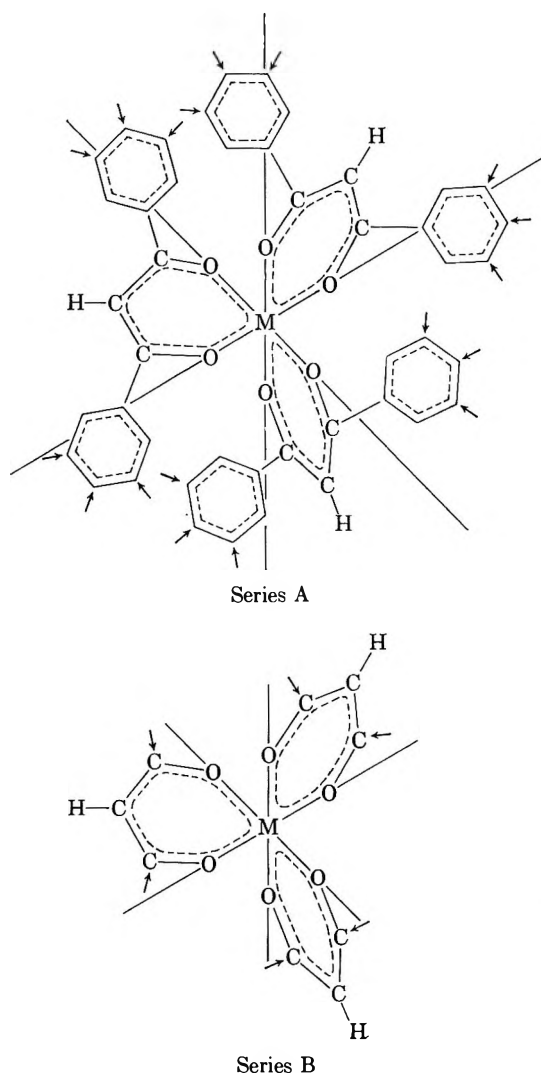
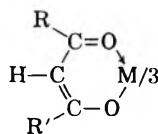


Figure 1. Substituted  $\beta$ -diketone tris chelates.

departure from the exact empirical formula. Therefore, no accurate extinction coefficient measurement was possible.

The predominant feature of the ultraviolet absorption spectra of the tris diketonates studied is the strong band occurring usually from 280 to 380  $m\mu$ . This band is due to the same kind of electronic transition in each case, probably a  $\pi-\pi^*$  type or "K" transition associated with the conjugated system.



This system in which R and R' represent the different substituents attached to the  $\beta$ -diketone ring is common to all of the investigated chelates. The six-

Table I

	Abbreviation
Series A	
Dibenzoylmethide	DBM
<i>p</i> -Methoxydibenzoylmethide	<i>p</i> M
Di- <i>p</i> -methoxydibenzoylmethide	<i>Dp</i> M
<i>p</i> -Nitrodibenzoylmethide	<i>p</i> N
Di- <i>p</i> -nitrodibenzoylmethide	<i>Dp</i> N
<i>m</i> -Methoxydibenzoylmethide	<i>m</i> M
Di- <i>m</i> -methoxydibenzoylmethide	<i>Dm</i> M
<i>m</i> -Nitrodibenzoylmethide	<i>m</i> N
Di- <i>m</i> -nitrodibenzoylmethide	<i>Dm</i> N
<i>p</i> -Phenyldibenzoylmethide	<i>p</i> Ph
Di- <i>p</i> -fluorodibenzoylmethide	<i>Dp</i> F
Series B	
Dibenzoylmethide	DBM
Difuroylmethide	DFuM
Ditheonylmethide	DTM
Diisonicotylmethide	DPyM
Di-1-naphthoylmethide	D1NM
Di-2-naphthoylmethide	D2NM
Theonyltrifluoroacetate	TTA
Benzoylacetate	BA
Acetylacetate	AcA
Trifluoroacetylacetate	TFAcA
Hexafluoroacetylacetate	HFAcA

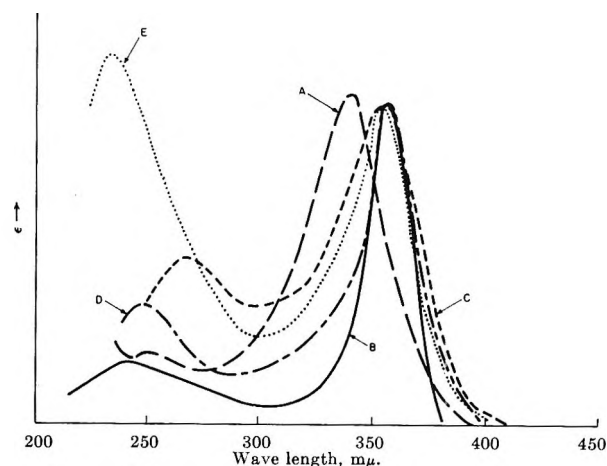


Figure 2. Absorption spectra: A, dibenzoylmethides; B, *p*-methoxydibenzoylmethides; C, *p*-nitrodibenzoylmethides; D, *m*-methoxydibenzoylmethides; E, *m*-nitrodibenzoylmethides.

member enolate ring is planar and has a  $C_{2v}$  symmetry if  $R = R'$ ; the pairs of M-O, O-C, and C-C distances are of equal length with C-C and C-O distances of 1.39 and 1.28 Å, intermediate between single and double bonds.<sup>9</sup> There is some evidence<sup>10</sup> that an enolate type

(9) R. B. Roof, *Acta Cryst.*, 9, 781 (1956).

(10) R. H. Holm and F. A. Cotton, *J. Am. Chem. Soc.*, 80, 5658 (1958).

Table II

M <sup>3+</sup> chelate	DBM	pM	DpM	pN	DpN	nM	DmM	mN	DmN	pPh	DpF
$\lambda_{\max}$ , m $\mu$	363	358	364	352	362	355	352	353	363	355	350

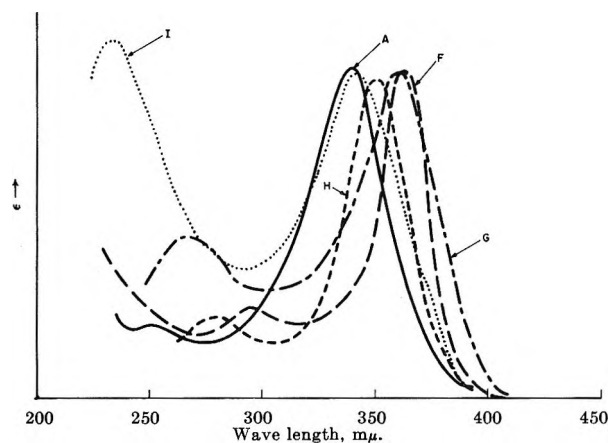


Figure 3. Absorption spectra: A, dibenzoylmethides; F, dianisoylmethides; G, di-*p*-nitrodibenzoylmethides; H, di-*m*-methoxydibenzoylmethides; I, di-*m*-nitrodibenzoylmethides.

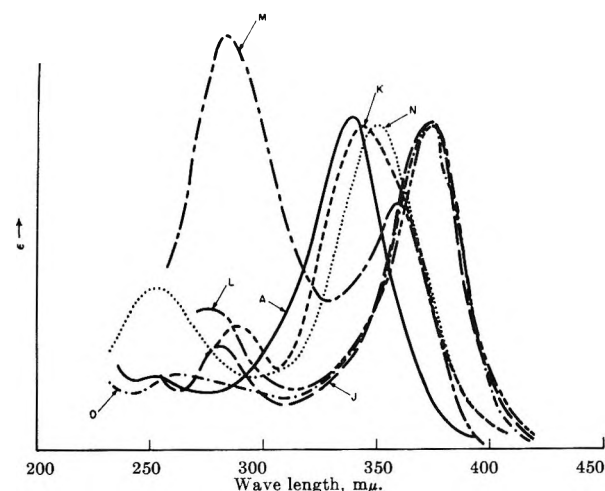


Figure 4. Absorption spectra: A, dibenzoylmethides; J, difuroylmethides; K, di-1-naphthoylmethides; L, di-2-naphthoylmethides; M, *p*-phenyldibenzoylmethides; N, di-*p*-fluorodibenzoylmethides; O, ditheonylmethides.

resonance tends to equalize the pairs of C-C, M-O, and C-O distances although a benzoid resonance has also been suggested for the  $\beta$ -diketonate ring. Six oxygen atoms of the ligand octahedrally surround the trivalent rare earth ion, and the ion uses  $d^2sp^3$  type hybrid orbitals to form six bonds with the nearest neighbors, formed by hybridization of  $5d_{x^2-y^2}$ ,  $5d_{z^2}$ ,  $6s$ ,  $6p$ ,  $6p_y$ , and  $6p_z$  orbitals. The metal orbitals available for  $\pi$ -bonding

with the  $\pi$ -electrons of the ligand (oxygen atoms) are the empty  $5d_{zz}$ ,  $5d_{yz}$ , and  $5d_{zy}$  orbitals.

In series A (*meta*- and *para*-substituted dibenzoylmethides), the main absorption peak ( $\lambda_{\max}$ ) is found at longer wave lengths than in acetylacetonates or other aliphatic substituted  $\beta$ -diketonates, as expected on increasing the length of the conjugated system as a whole, compared to enol resonance alone in the acetylacetonates. *para* substitution shifts the main molecular absorption peak toward red for both  $\text{CH}_3\text{O}$  and  $\text{NO}_2$  groups, in monosubstituted and (more) in disubstituted dibenzoylmethides. Di-*p*-fluoro and *p*-phenyl substitution results also in a bathochromic shift compared to the monosubstituted chelates.

Methoxy or nitro groups substituted in *para* position accept the positive charge more easily on the ether oxygen or on the nitrogen atom, respectively. These polar configurations represent cross conjugation and compete with the enolate ring resonance, thereby decreasing the stabilization of the ground state and resulting in a net bathochromic shift for  $\lambda_{\max}$  in absorption.

Table III

M <sup>3+</sup> chelate	DBM	pM	DpM	DBM	pN	DpN
$\lambda_{\max}$ , m $\mu$	343	358	364	343	352	362

The effect of *para* substituents on the location of the main molecular absorption peak is smaller than the effect of substituents on the absorption spectra of most benzene derivatives.<sup>11</sup> This indicates a limited resonance interaction between substituents attached to the dibenzoylmethide system and the chelated enolate ring. The fact that the di-*para*-substituted dibenzoylmethides have the absorption maxima at longer wave lengths than the mono-*para*-substituted chelates, which in turn show a bathochromic shift with regard to the unsubstituted dibenzoylmethide, implies that introduction of the first group induces only a small asymmetry in the enolate ring. This asymmetry has a restricted effect on the energetic location of the excited singlet but plays an important role in the fluores-

(11) (a) L. Doub and J. M. Vandenberg, *J. Am. Chem. Soc.*, **69**, 2714 (1947); **71**, 2414 (1949); (b) G. S. Hammond, W. G. Borduin, and G. A. Guter, *ibid.*, **81**, 4682 (1959).

cent emission of the chelated ion when transfer of energy to the ion is possible. The fact that some of the resonance structures mentioned increase the availability of electrons at the carbonyl oxygen does not imply an increased stabilization of the ground state, just as substitution of a methoxy group for a methyl in cross conjugation with C=O in acetylacetonate decreases the stability of the chelate. Fluorine and phenyl *para* substitution on dibenzoylmethide results also in a bathochromic shift for the same reason. The

Table IV

M <sup>3+</sup> chelate	DBM	DpF	pPh
$\lambda_{\max}$ , m $\mu$	343	350	355

*meta* substitution of CH<sub>3</sub>O and NO<sub>2</sub> shifts  $\lambda_{\max}$  toward the red less significantly than does *para* substitution, and the shift is more pronounced for mono- than for di-*meta*-substituted dibenzoylmethides. Only inductive effects can be attributed to *meta* substituents.

For series B,  $\lambda_{\max}$  values of the main absorption band are given in Table V.

Table V

M <sup>3+</sup> chelate	DTM	DFuM	D2NM	DPyM	D1NM	DBM	TTA	BTA	BA	HFACa	TFACa	AcA
$\lambda_{\max}$ , m $\mu$	375	372	372	363	346	343	340	325	323	304	294	293

The aromatic substituents on  $\beta$ -diketone chelates (DFuM, DTM, D1NM, D2NM, and DPyM) determine a red shift for  $\lambda_{\max}$  compared to DBM owing to an increased resonance with the substituents: for D1NM and D2NM analogous to *p*Ph, and for DFuM, DTM, and DPyM, the polarity of the heteroatom enhances the contribution of polar structures resulting in a destabilization of the ground state through interference with resonance in the enolate ring. Less competition with the chelate ring resonance expected for aliphatic substituents results in a hypsochromic shift

Table VI

M <sup>3+</sup> chelate	DBM	TTA	BTA	BA	HFACa	TFACa	AcA
$\lambda_{\max}$ , m $\mu$	343	340	325	323	304	294	293

for  $\lambda_{\max}$ . There are a few published data on the effect of fluorine substitution in aliphatic  $\beta$ -diketones on the absorption spectra.<sup>6,10,12</sup> A continuous red shift was ob-

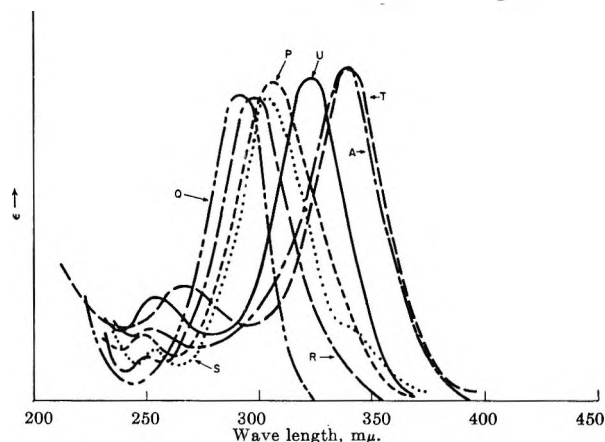


Figure 5. Absorption spectra: A, dibenzoylmethides; P, benzoylacetates; Q, acetylacetates; R, trifluoroacetylacetates; S, hexafluoroacetylacetates; T, theonyltrifluoroacetates; U, benzoyltrifluoroacetates.

served for  $\lambda_{\max}$  from acetylacetonate to trifluoroacetylacetonate and hexafluoroacetylacetonate. This shift can be accounted for by assuming that the introduction of the electronegative fluorine causes an increase in the contribution of the ionic resonance forms in the excited

states which stabilize this state reducing the energy difference between the excited and ground states.

*Phosphorescence Spectra of Gadolinium Chelates.* Gadolinium chelates were selected for the determination of phosphorescence spectra owing to enhanced phosphorescence-fluorescence ratios ( $\phi_p/\phi_f > 100$ ) compared to those of other lanthanide chelates. The strong phosphorescence from Gd chelates is justified by the absence of any ionic resonance level below the triplet state of the chelates, coupled with the strong paramagnetic effect of the Gd ion. Electric dipole and magnetic dipole transitions between pure singlet and pure triplet states are rigorously forbidden on account of the orthogonality of the spin-wave functions. The intervention of spin-orbit coupling (introduced by atoms with high atomic number and by paramagnetic atoms) brings about a mixing of singlet and triplet states, destroying their purity and permitting inter-

(12) R. L. Belford, A. E. Martell, and M. Calvin, *J. Inorg. Nucl. Chem.*, **2**, 11 (1956); E. M. Larsen, G. Terry, and J. Leddy, *J. Am. Chem. Soc.*, **75**, 5107 (1953).



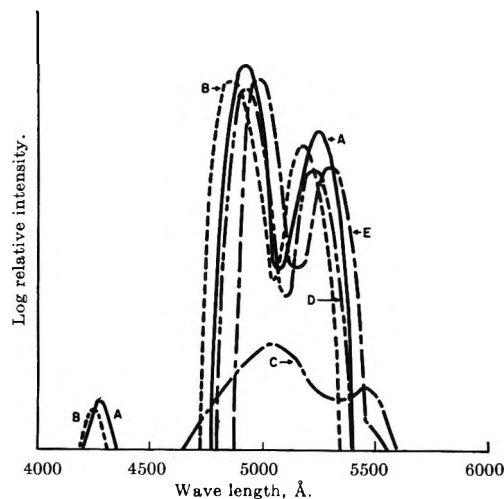


Figure 6. Phosphorescence spectra (Gd chelates): A, dibenzoylmethide; B, *p*-methoxydibenzoylmethide; C, *p*-nitrodibenzoylmethide; D, *m*-methoxydibenzoylmethide; E, *m*-nitrodibenzoylmethide.

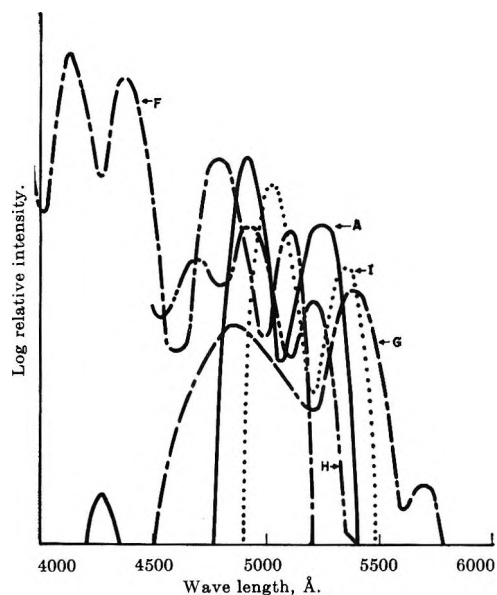


Figure 7. Phosphorescence spectra (Gd chelates): A, dibenzoylmethide; F, di-*p*-methoxydibenzoylmethide; G, di-*p*-nitrodibenzoylmethide; H, di-*m*-methoxydibenzoylmethide; I, di-*m*-nitrodibenzoylmethide.

combinations between nominal singlet and triplet states.<sup>13</sup> Most of the triplet excitation occurs by intersystem crossing from the excited singlet. This radiationless transition is significantly increased under the perturbation effects introduced by the electric and magnetic fields of the heavy paramagnetic gadolinium ion. The emission from gadolinium  $\beta$ -diketonates consists essentially of phosphorescence, with the exception of DpM, DmM, *p*Ph, DpN, and DPyM,

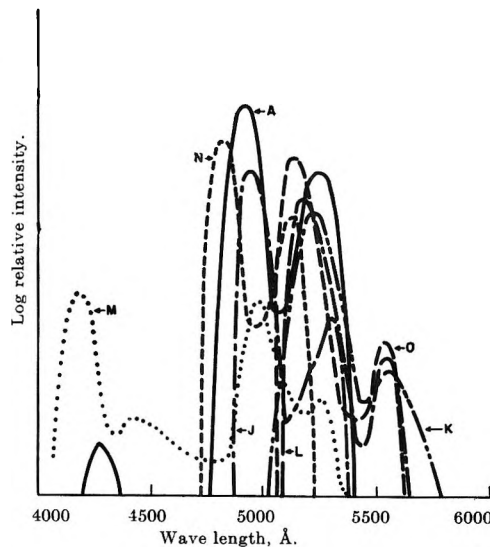


Figure 8. Phosphorescence spectra (Gd chelates): A, dibenzoylmethide; J, difuroylmethide; K, di-1-naphthoylmethide; L, di-2-naphthoylmethide; M, *p*-phenyldibenzoylmethide; N, di-*p*-fluorodibenzoylmethide; O, ditheonylmethide.

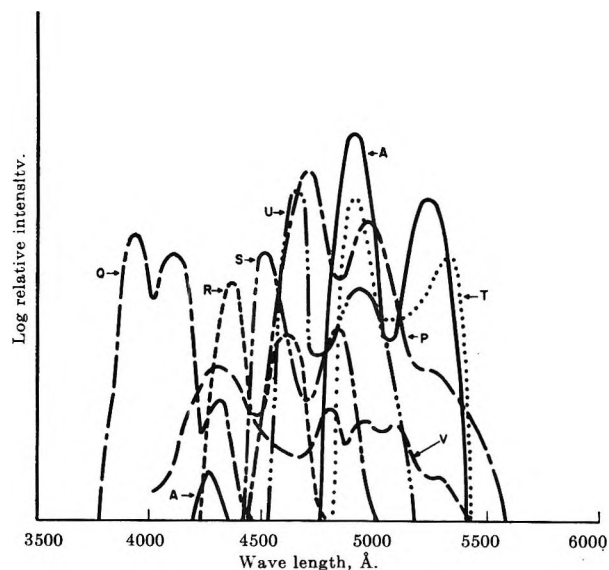


Figure 9. Phosphorescence spectra (Gd chelates): A, dibenzoylmethide; P, benzoylacetate; Q, acetylacetate; R, trifluoroacetylacetate; S, hexafluoroacetylacetate; T, theonyltrifluoroacetate; U, benzoyltrifluoroacetate; V, dipyridoylmethide.

which exhibited some fluorescence at shorter wave length. The phosphorescence band emission was well defined, and the bands represent the fall from the phosphorescent state to a number of vibrational states of the ground state. Two clearly defined bands

(13) (a) M. Kasha and S. P. McGlynn, *Ann. Rev. Phys. Chem.*, **1**, 403 (1956); (b) M. Kasha, *Discussions Faraday Soc.*, **9**, 14 (1950).

Table VII: Phosphorescence Spectra of Gd Chelates

Gd chelate	0 → 0 transition				0 → 1 transition		$\Delta\bar{\nu} = \bar{\nu}_p - \bar{\nu}_p'$ , cm. <sup>-1</sup>
	$\lambda_{\max}$ , m $\mu$	$\bar{\nu}_p$ , cm. <sup>-1</sup>	$\Delta\bar{\nu}_p$ , cm. <sup>-1</sup>	$\Delta E_R$ , kcal.	$\lambda_{\max}$ , m $\mu$	$\bar{\nu}_p'$ , cm. <sup>-1</sup>	
DBM	492	20,300	420	-22.8	523	19,100	1200
pM	485	20,700	440	-21.7	517	19,300	1400
DpM	477	21,000	560	-20.5	509	19,600	1400
pN	506	19,700	1800	-20.5	542	18,500	1200
DpN	536	18,600	1400	-24.8	570	17,500	1100
mM	493	20,300	440	-22.8	523	19,100	1200
DmM	493	20,300	800	-21.7	520	19,200	1100
mN	498	20,100	460	-23.4	529	18,900	1200
DmN	502	19,900	420	-23.8	534	18,700	1200
pPh	498	20,100	800	-22.4	525	19,000	1100
DpF	482	20,800	400	-21.5	513	19,500	1300
DFuM	493	20,300	320	-23.0	530	18,800	1500
DTM	513	19,500	260	-25.6	554	18,000	1500
D1NM	522	19,100	800	-25.2	555	18,000	1100
D2NM	518	19,300	420	-25.7	554	18,000	1300
DPyM	480	20,800	640	-20.8	508	20,800	1100
BA	470	21,200	440	-20.3	498	20,000	1200
BTA	465	21,500	440	-19.4	493	20,300	1200
TTA	492	20,400	440	-22.5	532	18,800	1600
AcA	394	25,300	800	-7.5	412	24,300	1000
TFAcA	437	22,800	720	-14.8	462	21,700	1100
HFAcA	452	22,200	440	-17.4	482	20,800	1400

are observed for all chelates investigated (a third band of lower intensity was recorded for several chelates). The band at shorter wave length is assumed to be the 0 → 0 transition<sup>2a,b,14</sup> while the second band takes the 0 → 1 designation, representing the transition from the lowest triplet state to a vibrationally excited ground state. The fact that the 0 → 0 band is the strongest and relatively sharp indicates that, according to the Franck-Condon principle, the phosphorescent state does not differ greatly from the ground state in size or in shape, reflected in high probability of direct transition from T to S<sub>0</sub> without vibration. This assumption can be made considering that the phosphorescent state is practically vibrationless at liquid nitrogen temperature. The frequency differences between the 0 → 0 and 0 → 1 bands vary from 1100 to 1600 cm.<sup>-1</sup> in the investigated chelates. This separation coincides with the infrared absorption frequency range found by some investigators for the C-O or C-C bond in  $\beta$ -diketone chelates.<sup>15</sup> The vibration frequency may be indicative of the intermediate single-double bond character of the C-O or C-C bonds in these compounds.

The triplet state is associated with a biradical structure formed by the separation (with parallel spin) of two electrons of a double bond. These two odd electrons repel each other, and in a conjugated system they tend to arrange as far apart as allowed by

resonance to a configuration giving the most important contribution to the description of the lowest triplet.

The evaluation of  $\Delta E_R$  (the resonance energy in the ground singlet less the resonance energy in the triplet state) has been made using the relation  $\Delta E_R = (\bar{\nu}_p + \Delta\bar{\nu}_p)hc - B$  where  $\bar{\nu}_p$  is the frequency of the 0 → 0 band at the peak,  $\Delta\bar{\nu}_p$  is the "half-width" of the same band, and  $B$  is the value for breaking the C=O bond, taken as 82 kcal.<sup>14</sup> The values for  $\Delta E_R$  vary from -7.5 kcal. for AcA to -25.7 kcal. for D2NM. These negative values of  $\Delta E_R$  could be interpreted as resulting from a significant odd-electron resonance in the triplet state.

Resonance in the triplet state of a dibenzoylmethide involving *para* substituents (both CH<sub>3</sub>O and NO<sub>2</sub>) can be considered as localizing one of the odd electrons on the substituent, while the other is primarily found on one of the two  $\beta$ -diketone oxygen atoms. The strong acid auxochrome nitro group in *para* position lowers the energy of the triplet state considerably whereas, in *meta*, the same trend is smaller owing only to an inductive effect. An opposite shift in  $\lambda_{\max}$  is observed for the basic auxochrome methoxy-substituted dibenzoylmethides. Di-*p*-fluoro substitution on di-

(14) G. N. Lewis and M. Kasha, *J. Am. Chem. Soc.*, **66**, 2100 (1944).

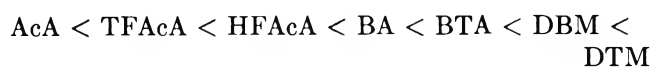
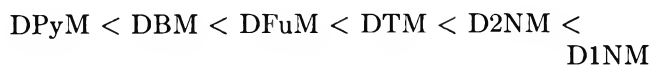
(15) (a) L. J. Bellamy and R. F. Branch, *J. Chem. Soc.*, 4491 (1954);  
(b) J. Lecompte, *Discussions Faraday Soc.*, **9**, 125 (1950).

Table VIII: Relative Intensities of Phosphorescence Spectra

Gd chelate	$\Delta\nu_{0\rightarrow 0}$ , cm. <sup>-1</sup>	$\Delta\nu'_{0\rightarrow 0}$ , cm. <sup>-1</sup>	$h_{\max, 0\rightarrow 0}$ , R.U. <sup>a</sup>	Rel. int. 0 $\rightarrow$ 0, A.U. <sup>b</sup>	$\Delta\nu_{0\rightarrow 1}$ , cm. <sup>-1</sup>	$\Delta\nu'_{0\rightarrow 1}$ , cm. <sup>-1</sup>	$h_{\max, 0\rightarrow 1}$ , R.U.	Rel. int. 0 $\rightarrow$ 1, A.U.	Total rel. int., A.U.
DBM	1400	420	10 <sup>3.6</sup>	2,229,920	1400	640	10 <sup>3.2</sup>	1,061,950	3,291,870
pM	1400	440	10 <sup>3.5</sup>	1,802,340	1200	680	10 <sup>3.1</sup>	806,400	2,608,740
DpM	1400	560	10 <sup>2.6</sup>	251,200	1200	680	10 <sup>2.2</sup>	101,300	352,500
pN	2200	1800	10 <sup>0.26</sup>	2,900	1400	1000	10 <sup>0.05</sup>	850	3,750
DpN	2400	1400	10 <sup>1.6</sup>	52,000	2000	1000	10 <sup>0.9</sup>	7,950	59,950
mM	1400	440	10 <sup>2.1</sup>	71,820	1400	720	10 <sup>1.5</sup>	22,720	94,540
DmM	1400	800	10 <sup>0.6</sup>	3,000	1400	600	10 <sup>0.3</sup>	1,300	4,300
mN	1400	460	10 <sup>2.7</sup>	290,580	1400	640	10 <sup>2.3</sup>	134,000	424,580
DmN	1400	420	10 <sup>2.3</sup>	112,000	1400	640	10 <sup>1.7</sup>	33,500	145,500
pPh	1400	800	10 <sup>1.1</sup>	9,800	1400	800	10 <sup>0.6</sup>	2,950	12,750
DpF	1200	400	10 <sup>3.3</sup>	997,500	1400	640	10 <sup>3</sup>	670,000	1,667,500
DFuM	1000	320	10 <sup>2.1</sup>	51,700	1400	800	10 <sup>1.3</sup>	14,960	66,660
DTM	1200	260	10 <sup>3.2</sup>	682,000	1000	460	10 <sup>2.3</sup>	95,550	777,550
D1NM	1400	800	10	8,000	1600	720	10 <sup>0.6</sup>	3,040	11,040
D2NM	1400	420	10 <sup>2.1</sup>	70,560	1200	640	10 <sup>1.2</sup>	9,920	80,480
DPyM	1400	620	10 <sup>1.1</sup>	8,550	1600	800	10 <sup>0.5</sup>	2,560	11,110
TTA	1400	440	10 <sup>3</sup>	570,000	1400	720	10 <sup>2.5</sup>	224,360	794,360
BTA	1400	440	10 <sup>3</sup>	226,860	1200	800	10 <sup>2.5</sup>	70,000	296,860
BA	1400	440	10 <sup>2.6</sup>	570,000	1200	720	10 <sup>2</sup>	208,560	778,560
AcA	1400	800	10 <sup>2.5</sup>	237,000	1400	800	10 <sup>2</sup>	75,000	312,000
TFAcA	1400	720	10 <sup>2.3</sup>	141,800	1600	800	10 <sup>2.1</sup>	101,000	242,800
HFAcA	1400	440	10 <sup>3</sup>	570,000	1400	720	10 <sup>2.6</sup>	282,580	852,580

<sup>a</sup> Recorder units. <sup>b</sup> Arbitrary units.

benzoylmethane results in a hypsochromic shift similar to *p*-methoxy, suggesting a predominant resonance effect over the inductive effect. A red shift of different magnitude in  $\lambda_{\max}$  (0  $\rightarrow$  0 band) of dibenzoylmethide is observed for the aromatic  $\beta$ -diketonates in series B (DFuM, DTM, D1NM, D2NM), whereas a large hypsochromic shift occurs on replacing the phenyl groups with aliphatic substituents (AcA, TFAcA, HFAcA). A trifluoromethyl group confers a weaker blue shift compared to a methyl radical. The results can be summarized as



The phosphorescence spectra were recorded on a log scale (log relative intensity *vs.* wave length), and the relative intensity is taken as the area under the two main peaks (0  $\rightarrow$  0 and 0  $\rightarrow$  1) on a linear scale of relative intensity *vs.* frequency. The approximate area has been evaluated as equal to  $(0.25\Delta\nu + 0.5\Delta\nu')h_{\max}$ ,

where  $\Delta\nu$  is the spectral range where the band is observed,  $\Delta\nu'$  is the width of the band at  $1/2h_{\max}$ , and  $h_{\max}$  is the height of the band at the peak. The results are tabulated in Table VIII.

The phosphorescence emission is the result of inter-system crossing from the excited singlet and competitive deactivation of the lowest triplet by a radiative process (phosphorescence) and nonradiative vibrational coupling to the surroundings. Inefficient inter-system crossing and nonradiative deactivation of the triplet decrease the phosphorescence intensity. Both processes are substituent dependent. If one considers the radiationless deactivation of the triplet as insignificant in a solid matrix at 77°K.,<sup>2</sup> the relative phosphorescence intensity can be taken as an approximate measure of the S' $\rightarrow$ T intersystem crossing efficiency (or the amount of energy available at the triplet state level for chelates of Eu, Tb, Sm, etc., ions having resonance levels below the triplet). The atomic number and paramagnetic characteristics of the gadolinium ion are not very different from those of its neighbors (europium and terbium), and, therefore, a similar efficiency of the S' $\rightarrow$ T intersystem crossing is expected when Gd is replaced by either Eu or Tb.

There is no apparent correlation between the S'-T energy gap ( $\Delta E$ ) and intersystem crossing efficiency in the gadolinium chelates investigated. The energy dif-

ference between the lowest excited singlet and the lowest triplet changes in an orderly manner in series A as a function of substituents attached to the dibenzoylmethide if one considers resonance, inductive, and asymmetry effects. Methoxy, fluoro, and phenyl groups attached in the *para* position have a strong resonance effect (tendency to decrease  $\Delta E$  stabilizing the polar S' singlet more than the triplet) and a comparatively small inductive effect, of different directions for CH<sub>3</sub>O, F, and C<sub>6</sub>H<sub>5</sub>. Monosubstituted dibenzoylmethides tend to have a smaller  $\Delta E$  because of asymmetry which again tends to stabilize the polar, excited singlet state more. But this effect is overcome by resonance in DpM compared to that in pM.

Table IX

M <sup>3+</sup> chelate $\Delta E$ , cm. <sup>-1</sup>	DpM	pM	DpF	pPh	DBM
	6500	7200	7800	8000	8800

A methoxy group substituted in the *meta* position has only inductive and asymmetry effects. The inductive effect tends to decrease  $\Delta E$ , but the asym-

Table X

M <sup>3+</sup> chelate $\Delta E$ , cm. <sup>-1</sup>	mM	DmM	DBM
	7800	8100	8800

metry effect is stronger, resulting in a smaller  $\Delta E$  for the monosubstituted chelate.

The acid auxochrome nitro group has a less pronounced effect on  $\Delta E$ , with smaller values for the monosubstituted dibenzoylmethides than for the disubstituted chelates.

Table XI

M <sup>3+</sup> chelate $\Delta E$ , cm. <sup>-1</sup>	mN	pN	DBM	DpN	DmN
	8200	8700	8800	9000	9200

In the aliphatic  $\beta$ -diketonates the stabilization of the triplet is more substantial for the asymmetrical TFAcA than for the two symmetrical AcA and HFAcA which may indicate that, although the excited singlet is normally associated with a polar state, the triplet is probably more polarizable for this system. This would explain the close energetic values of the excited states of AcA and TFAcA whereas the triplet of the asymmetrical TFAcA is at significantly lower energy.

The assumption that the radiationless deactivation of the lowest triplet is negligible<sup>2</sup> is questionable, and probably decay time measurements on the phosphorescence emission of the Gd chelates will contribute to the elucidation of the process. If the assumption is correct then the relative phosphorescence intensity is a valuable indication of the amount of energy at the triplet level of the ligand available for transfer to ions such as europium and terbium.

# Intrinsic Viscosity Studies of Stereoregular Poly(methyl methacrylate) in 2,2,3,3-Tetrafluoropropanol<sup>1a</sup>

by Eugene Hamori, Longine R. Prusinowski, Peter G. Sparks, and R. E. Hughes<sup>1b</sup>

*John Harrison Laboratory of Chemistry, University of Pennsylvania, Philadelphia, Pennsylvania  
(Received July 18, 1964)*

Intrinsic viscosity-molecular weight relationships were established for atactic and isotactic poly(methyl methacrylate) in 2,2,3,3-tetrafluoropropanol at 25°. Contrary to usual observations in thermodynamically good solvents, a significant difference between the Mark-Houwink  $K'$  values was observed for the two polymers. Moreover, in contrast to the usual results in poor solvents, significantly larger values for  $K'$  and for the unperturbed chain dimensions, calculated by the Kurata-Stockmayer-Roig extrapolation method, were found for the atactic polymer.

## Introduction

A number of studies of stereoregular polymers have been concerned with the effects of tacticity on the dilute solution properties of the polymer chains. Thus, for example, intrinsic viscosity studies of isotactic polypropylene,<sup>2-5</sup> isotactic, atactic, and syndiotactic poly(methyl methacrylate),<sup>6-8</sup> isotactic polystyrene,<sup>9-13</sup> and, recently, isotactic, atactic, and syndiotactic poly(isopropyl acrylate)<sup>14-16</sup> showed no significant differences in the intrinsic viscosity-molecular weight relationships among the different stereochemical forms in thermodynamically good solvents<sup>2,3,6,9,11-13</sup>; in solvents near the Flory temperature, however, and in poor solvents, significant differences were reported.<sup>4,7,8</sup>

Preliminary studies carried out in this laboratory indicated that 2,2,3,3-tetrafluoropropanol (TFP) is an excellent solvent for acrylate and methacrylate polymers.<sup>14-16</sup> In fact, it appears that it is thermodynamically the best solvent for poly(methyl methacrylate) (PMMA) among those for which systematic intrinsic viscosity-molecular weight studies have been reported. Work on the poly(isopropyl acrylate)-TFP system<sup>14</sup> showed differences between the Mark-Houwink constants for the isotactic and atactic forms which could be best accounted for by assuming strong ordered associations between the solvent molecules and the polymer segments.

It is the purpose of the present study to establish the intrinsic viscosity-molecular weight relationships for

isotactic and atactic PMMA in TFP and to compare the relationships between the two stereoregular forms in this and other solvents.

## Experimental

*Polymer Preparation.* The atactic PMMA sample

- (1) (a) Supported in part by the Advanced Research Projects Agency under Contract SD-63; (b) author to whom correspondence is to be addressed at the Department of Chemistry, Cornell University, Ithaca, N. Y.
- (2) F. Danusso and G. Moraglio, *Makromol. Chem.*, **28**, 250 (1958).
- (3) J. B. Kinsinger and R. E. Hughes, *J. Phys. Chem.*, **63**, 2002 (1959).
- (4) J. B. Kinsinger and R. E. Hughes, *ibid.*, **67**, 1922 (1963).
- (5) P. Parrini, F. Sebastiano, and G. Messina, *Makromol. Chem.*, **38**, 27 (1960).
- (6) V. M. Tsvetkov, V. S. Skazka, and N. M. Krinoruchko, *Vysokomolekul. Soedin.*, **2**, 1045 (1960).
- (7) S. Krause and E. Cohn-Ginsberg, *Polymer*, **3**, 565 (1962).
- (8) S. Krause and E. Cohn-Ginsberg, *J. Phys. Chem.*, **67**, 1479 (1963).
- (9) G. Natta, F. Danusso, and G. Moraglio, *Makromol. Chem.*, **20**, 37 (1956).
- (10) F. W. Peaker, *J. Polymer Sci.*, **22**, 25 (1956).
- (11) F. Danusso and G. Moraglio, *ibid.*, **24**, 161 (1957).
- (12) L. Trossarelli, E. Campi, and G. Saini, *ibid.*, **35**, 205 (1959).
- (13) W. R. Krigbaum, D. K. Carpenter, and S. J. Newman, *J. Phys. Chem.*, **62**, 1586 (1958).
- (14) E. Hamori, Ph.D. Dissertation, University of Pennsylvania, 1964.
- (15) R. A. Wessling, Ph.D. Dissertation, University of Pennsylvania, 1962.
- (16) J. E. Mark, Ph.D. Dissertation, University of Pennsylvania, 1962.

was prepared<sup>17a</sup> by a low conversion (12%), bulk polymerization at 60°, using a 2,2'-azobisisobutyronitrile initiator.<sup>17b</sup> The intrinsic viscosity of the unfractionated polymer in benzene at 25° was 1.15 dl./g., indicating<sup>19</sup> a viscosity average molecular weight of  $4.62 \times 10^5$ .

The two samples of isotactic PMMA used in the studies were made by different processes. Sample I(F) was prepared from freshly distilled, uninhibited monomer in toluene at -70° using 9-fluorenyllithium as initiator. The polymer was isolated by precipitation in petroleum ether and dried under vacuum; subsequently, it was washed in a 90-10 water-methanol mixture containing 5% HCl and in distilled water. The number-average molecular weight of this sample, determined<sup>7</sup> by ultraviolet end-group analysis,<sup>20</sup> was  $2.92 \times 10^4$ . Its intrinsic viscosity in acetone at 30° was 0.505 dl./g.<sup>7</sup>; this corresponds<sup>19</sup> to a viscosity-average molecular weight of  $3.09 \times 10^5$ .

Sample I(P) was prepared from degassed, uninhibited monomer in toluene at 12° using phenylmagnesium bromide as initiator and was isolated and washed as described above. The intrinsic viscosity of the unfractionated sample in chloroform at 25° was 4.65 dl./g., indicating<sup>19</sup> a viscosity-average molecular weight of  $1.65 \times 10^6$ . The number-average molecular weight, obtained by osmometry, was  $1.15 \times 10^4$ . The stereoregularity of the isotactic samples was characterized by analysis of the relative intensities of certain infrared absorption peaks, in terms of a parameter called the *J* value which has been shown<sup>18b,21</sup> to be a useful index for the number of stereochemical inversions in the chain. Isotactic PMMA samples have *J* values between 25 and 35, the more isotactic samples having lower *J* values. *J* values found for samples I(F) and I(P) were 33 and 28, respectively.

**Fractionation.** The atactic polymer was carefully fractionated into the 13 fractions from a 1% reagent grade benzene solution at 33.5° using cyclohexane as the nonsolvent. The fractions were redissolved in benzene, filtered, and freeze-dried. To obtain a more monodisperse high molecular weight sample, fraction 1 was refractionated to yield 1a.

The isotactic polymer, I(P), was fractionated from a 0.5% reagent grade benzene solution at 40° using *n*-hexane as the nonsolvent, following the technique used by Krause and Cohn-Ginsberg.<sup>7</sup> Eleven fractions were obtained and number 11 was refractionated into seven subfractions to obtain additional lower molecular weight fractions. The four fractions of sample I(F) which were utilized were fractionated by a similar technique.<sup>7</sup> All fractions were dissolved in benzene, filtered, and freeze-dried.

**Intrinsic Viscosity Measurements.** In an associated study it was found that intrinsic viscosity measurements in TFP were particularly sensitive to the presence of traces of water so considerable care was taken in purification and storage of the solvent. Technical grade TFP (2500 ml.), which was generously provided by E. I. du Pont de Nemours and Co., Wilmington, Del., was refluxed for 4 hr. over 50 g. of KOH; the brown mixture was distilled through a 50-cm. column packed with glass helices and a 2000-ml. cut was taken between 104 and 109°. This fraction was redistilled over 40 g. of sodium trifluoroacetate through a vacuum-jacketed Stedman column equipped with a Shell head and rated at 125 theoretical plates at total reflux. A main fraction of 1300 ml. was collected over 5 days at 108°. The purified solvent showed no water content when analyzed in a gas chromatograph.

The intrinsic viscosities of the polymer fractions in TFP were determined by the usual double extrapolation of data obtained from a calibrated Cannon-Ubbelohde viscometer at  $25 \pm 0.005^\circ$ . The viscosity-average molecular weight of each fraction was determined from its intrinsic viscosity in benzene at  $25 \pm 0.005^\circ$ , assuming the relationship obtained for fractions of atactic PMMA in this solvent at this temperature<sup>22</sup>

$$[\eta] = 5.7 \times 10^{-5} M^{0.76} \quad (1)$$

where  $[\eta]$  is the intrinsic viscosity in deciliters per gram. The use of this relation for the isotactic polymer is supported by the equivalence<sup>7</sup> of the two polymers in the same solvent at 30°.

**Osmometry.** Osmotic pressure measurements were made in toluene at 37° for several atactic and isotactic fractions. A Mechrolab automatic osmometer was used and the data were analyzed by usual techniques.

## Results and Discussion

In Table I the intrinsic viscosities in TFP and in benzene are given for all of the fractions studied along

(17) (a) The authors are indebted to Mr. Robert P. Fellman and Mr. James Rorapaugh of the Rohm and Haas Co., Bristol, Pa., for the preparation of the polymers used in this study. (b) PMMA as prepared by this technique has a stereosequence distribution closer to syndiotacticity than complete randomness.<sup>18a,b</sup> Some workers prefer to call it conventional PMMA.<sup>7</sup>

(18) (a) F. A. Bovey and G. V. D. Tiers, *J. Polymer Sci.*, **44**, 173 (1960); (b) T. G. Fox, Jr., W. E. Goode, S. Gratch, C. M. Huggett, J. F. Kincaid, A. Spell, and J. D. Stroupe, *ibid.*, **31**, 173 (1958).

(19) E. Cohn-Ginsberg, T. G. Fox, Jr., and H. F. Mason, *Polymer*, **3**, 97 (1962).

(20) D. L. Glusker, E. Stiles, and B. Yoncoskie, *J. Polymer Sci.*, **49**, 297 (1961).

(21) W. E. Goode, F. H. Owens, R. P. Fellman, W. H. Snyder, and J. E. Moore, *ibid.*, **46**, 317 (1960).

(22) P. J. Flory, "Principles of Polymer Chemistry," Cornell University Press, Ithaca, N. Y., 1953, p. 312.

**Table I:** Intrinsic Viscosity-Molecular Weight Data for Poly(methyl methacrylate) Fractions

Atactic fractions	$[\eta]$ in	$[\eta]$ in	$\bar{M}_v$ $\times 10^{-5}$	$\bar{M}_n$ $\times 10^{-5}$	$\bar{M}_v/\bar{M}_n$
	benzene at 25°, dl./g.	TFP at 25°, dl./g.			
A1a	1.94	3.72	9.15	..	...
A2	1.47	2.72	6.38	..	...
A4	1.22	2.13	4.96	..	...
A8	0.680	1.28	2.31	..	...
A9	0.623	1.08	2.06	..	...
A10	0.401	0.775	1.15	1.13	1.0
A11	0.295	0.485	0.77	0.70	1.1
Isotactic fractions					
I(P)-8	2.01	3.50	9.95	..	...
I(P)-9	1.86	2.90	8.71	..	...
I(P)-10	1.40	2.26	5.98	..	...
I(P)-11c	0.937	1.50	3.53	..	...
I(P)-11e	0.610	1.02	2.00	1.32	1.5
I(P)-11f	0.434	0.701	1.28	0.86	1.5
I(F)-10	0.358	0.521	0.99	0.69	1.4
I(P)-11g	0.324	0.483	0.87	..	...
I(F)-11	0.196	0.268	0.45	0.26	1.7
I(F)-12	0.165	0.234	0.36	0.20	1.8
I(F)-13	0.138	0.196	0.28	0.15	1.9

with corresponding viscosity- and number-average molecular weights. Careful fractionation procedures were followed to obtain reasonably narrow molecular weight distributions for the fractions and the  $\bar{M}_v/\bar{M}_n$  ratios given in Table I indicate that satisfactory fractionation was achieved for these highly polydispersed systems. Due to a shortage of polymer, the ratios could not be obtained for the high molecular weight fractions.

The relationships between the intrinsic viscosity and the viscosity-average molecular weight are shown in Figure 1 for the atactic and isotactic polymers in TFP at 25°. A least-squares analysis of the data yielded the constants for the Mark-Houwink relationship,<sup>23</sup>  $[\eta] = K'M^a$ , which are presented in Table II along with their standard deviations. Comparison of the Mark-Houwink constants in Table II with the values reported for other solvents<sup>19,24</sup> shows that TFP must be considered an exceptionally good solvent for poly(methyl methacrylate) in a thermodynamic sense.

The magnitude of this strong interaction between TFP and the polymer chain is shown in a striking way by comparison of intrinsic viscosities calculated for a hypothetical atactic PMMA fraction, of molecular weight  $1 \times 10^5$ , in a number of common solvents. The results in dl./g. are as follows: acetone,<sup>25</sup> 0.24; benzene,<sup>22</sup> 0.36; ethylene dichloride,<sup>26</sup> 0.42; chloro-

**Table II:** Mark-Houwink Constants for Poly(methyl methacrylate) in 2,2,3,3-Tetrafluoropropanol at 25°

Tacticity	$K' \times 10^6$	$a$
Atactic	$7.20 \pm 0.06$	$0.79 \pm 0.01$
Isotactic	$7.05 \pm 0.05$	$0.78 \pm 0.02$

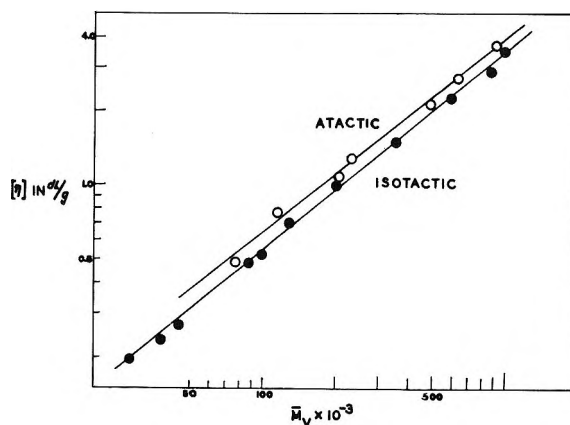


Figure 1. Intrinsic viscosity-molecular weight plot of PMMA fractions in TFP at 25°.

form,<sup>27</sup> 0.48; and in TFP, the value of 0.64 is calculated from the present data.

The intrinsic viscosity-molecular weight relationship can be expressed<sup>24</sup> in terms of a hydrodynamic expansion factor  $\alpha_n$  and a quantity  $K$  which is a measure of the unperturbed mean-square displacement ( $\bar{r}_0^2$ ) of the chain; in the expression

$$[\eta] = KM^{1/2}\alpha_n^3 = \Phi_0(\bar{r}_0^2/M)^{3/2}M^{1/2}\alpha_n^3 \quad (2)$$

the hydrodynamic constant,  $\Phi_0 = 2.87 \times 10^{21}$ , is related to the Flory parameter  $\Phi$  and the statistical expansion factor,  $\alpha$ , by the equation,  $\Phi = \Phi_0(\alpha_n/\alpha)^3$ . At the Flory  $\Theta$ -temperature,  $\alpha_n \rightarrow \alpha \rightarrow 1$  and the unperturbed chain dimensions can be calculated directly from measurements using eq. 2; for measurements at higher temperatures, the dependence of  $\alpha_n$  on  $M$  must be ascertained.

In the original Flory-Fox-Schaeffgen extrapolation method,<sup>28</sup> it is assumed that  $\alpha = \alpha_n$  and that Flory's<sup>29</sup> equation

(23) H. Mark, "Der Feste Körper," Leipzig, 1938; R. Houwink, *J. Prakt. Chem.*, **157**, 15 (1940).

(24) M. Kurata and W. H. Stockmayer, *Fortschr. Hochpolymer. Forsch.*, **3**, 196 (1963).

(25) J. Bischoff and V. Desreux, *Bull. soc. chim. Belges*, **61**, 10 (1952).

(26) F. W. Billmeyer, Jr., and C. B. DeTham, *J. Am. Chem. Soc.*, **77**, 4763 (1955).

(27) S. M. Chinai, J. D. Matlack, A. L. Resnick, and R. J. Samuels, *J. Polymer Sci.*, **17**, 391 (1955).

$$\alpha^5 - \alpha^3 = C_M(1 - 2\chi_1)M^{1/2} \quad (3)$$

defines  $\alpha$  in terms of the molecular weight and thermodynamic parameters. A linear extrapolation of  $[\eta]^{2/3}M^{-1/3}$  vs.  $M/[\eta]$  to the ordinate intercept then yields  $K^{2/3}$ , from which the unperturbed dimensions can be calculated. The validity of the assumptions and the applicability of the method have often<sup>24,30</sup> been questioned, especially for polar polymers and for good solvents. Moreover, the accuracy of the extrapolation is a sensitive function of the molecular weight range investigated and of experimental error. Some of these difficulties emerged in the treatment of the careful measurements of Krause and Cohn-Ginsberg<sup>7</sup> and in the analysis of the present data which yielded standard deviations in  $K^{2/3}$  almost as large as the quantity itself.

A more successful analysis of the data involved the application of the Kurata-Stockmayer-Roig<sup>31</sup> expression

$$[\eta]^{2/3}M^{-1/3} = K^{2/3} + 0.363\Phi_0B\{g(\alpha_\eta)M^{2/3}[\eta]^{-1/3}\} \quad (4)$$

in which  $B$  is a parameter characteristic of the polymer-solvent interaction and

$$g(\alpha_\eta) = 8\alpha_\eta^3(3\alpha_\eta^2 + 1)^{-3/2}$$

This equation, which is based upon a semiempirical relation between  $\alpha_\eta$  and  $M$ , yields a value for  $K$  upon linear extrapolation of a plot of the left-hand side vs. the quantity in braces on the right. Since  $\alpha_\eta$  is initially unknown, it is necessary to set  $g(\alpha_\eta)$  equal to unity for the first extrapolation and to use the resulting value of  $K$  in eq. 2 to calculate a first approximation to  $\alpha_\eta$  which, in turn, can be used to provide a better value of  $K$ . This iterative procedure was performed in a computer by a least-squares analysis which converged for all of the pertinent quantities in three cycles. The final Kurata-Stockmayer-Roig plot is shown in Figure 2 along with similar results obtained in other good solvents. The parameter  $(\bar{r}_0^2/M)^{1/2}$  which characterizes the unperturbed dimensions of the polymer is listed for a variety of solvents in Table III.

It is of interest to compare these results with those obtained from the application of a more recent approach to the calculation of unperturbed dimensions, that of Stockmayer and Fixman,<sup>30</sup> in which the hydrodynamic expansion factor assumes the particularly simple form

$$\alpha_\eta^3 = 1 + 0.51B(\bar{r}_0^2/M)^{-3/2}M^{1/2} \quad (5)$$

Inserting this expression into eq. 2 yields a linear equation in  $[\eta]M^{-1/2}$  and  $M^{1/2}$ , the ordinate intercept of which is  $K$ . Such an analysis of the TFP data for isotactic and atactic PMMA produced values of 659 and

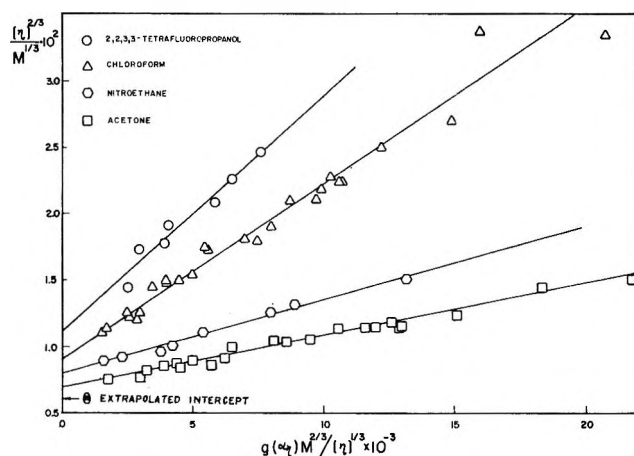


Figure 2. Kurata-Stockmayer-Roig analysis of atactic PMMA data in various solvents at 25°. Data for chloroform, nitroethane, and acetone are from ref. 24; extrapolated intercept for Flory  $\Theta$ -solvents is from Fox, *et al.*, ref. a in Table III.

Table III: Calculated Unperturbed Dimensions of Poly(methyl methacrylate) in Various Solvents

Solvent	Temp., °C.	Tacticity	$(\bar{r}_0^2/M)^{1/2} \times 10^{11}$	Ref.
$\Theta$ -Solvents <sup>a</sup>	30-70	Atactic	$551 \pm 10^b$	<sup>a</sup>
Acetone	25	Atactic	$600 \pm 15$	24
Benzene	25	Atactic	$635 \pm 20$	24
Nitroethane	25	Atactic	$638 \pm 20$	24
Chloroform	25	Atactic	$685 \pm 20$	24
TFP	25	Atactic	$740 \pm 60^c$	This work
TFP	25	Isotactic	$673 \pm 50^c$	This work

<sup>a</sup> T. G. Fox, Jr., J. B. Kinsinger, Jr., H. F. Mason, and E. M. Schuele, *Polymer*, **3**, 111 (1962). <sup>b</sup> Fox's original value (612) was corrected for the different  $\Phi_0$  used in the remainder of the data. <sup>c</sup> The higher standard deviations obtained here appear to be due to the more limited molecular weight range investigated.

739, respectively, for  $(\bar{r}_0^2/M)^{1/2} \times 10^{11}$ , in excellent agreement with the values 673 and 740 obtained from the Kurata-Stockmayer-Roig method.

From eq. 4 it can be seen that the slopes of the lines in Figure 2 are proportional to the polymer-solvent interaction parameter  $B$ ; moreover, an increase in the intercept indicates an increase in the unperturbed dimensions of the polymer chain. The quantity  $\bar{r}_0^2/M$  has long been regarded as a constant characterizing the unperturbed configuration of a polymer chain and,

(28) P. J. Flory and T. G. Fox, Jr., *J. Am. Chem. Soc.*, **73**, 1904 (1951).

(29) See ref. 22, Chapter XIV.

(30) W. H. Stockmayer and M. Fixman, *J. Polymer Sci.*, **1**, 137 (1963).

(31) M. Kurata, W. H. Stockmayer, and A. Rieg, *J. Chem. Phys.*, **33**, 151 (1960).



in the case of nonpolar polymers at least, this constancy has been supported<sup>24</sup> by the extrapolation of Kurata–Stockmayer–Roig plots from a spectrum of solvents to a common intercept. The systematic increase in intercept with increasing slope (polymer–solvent interaction parameter) shown in Figure 2 for the polar polymer PMMA in a number of solvents indicates either the inconstancy of the unperturbed dimensions or the inapplicability of the viscosity theory. In view of the consistency of the results, it is easier to believe the former than the latter and to suspect that specific solvent–polymer segment interactions sufficiently alter the configurational properties of the chain so that the extrapolations in different solvents are essentially for different polymer chains.

A number of investigations have demonstrated that the Mark–Houwink constants are experimentally indistinguishable in good solvents<sup>2,3,6,9,11–13</sup> for isotactic and atactic forms of the same polymer; significant differences have been observed, however, in thermodynamically poor solvents.<sup>4,7</sup> It appears that the stronger polymer–solvent interaction in good solvents

minimizes the effects of the structure-dependent segment–segment interactions in the polymer. Thus, it is particularly interesting to note that these differences reappear for the highly extended PMMA chain in the strongly interacting solvent TFP; the  $K'$  value is significantly higher for the atactic form of the polymer. Moreover, as shown in Table III, the parameter characterizing the unperturbed dimensions is also larger for the atactic polymer.

This structure sensitivity is noteworthy in that it is the reverse of that found for the same polymers in poorer solvents such as acetone<sup>7</sup> and under  $\Theta$ -conditions<sup>8</sup> where both parameters were found to be higher for the isotactic polymer. The complexity of the situation is further compounded by the results of extensive studies of the stereoregular forms of another polar polymer, poly(isopropyl acrylate), which were recently completed in this laboratory<sup>14–16</sup>; once again, the polymers were highly extended by the strongly interacting solvent TFP, but this time both  $K'$  and  $\bar{r}_0^2/M$  were higher for the isotactic polymer. These results will be reported shortly in a more extended discussion.

## The Extraction of Acids by Basic Organic Solvents. V. Trioctyl

### Phosphine Oxide-HClO<sub>4</sub> and Trioctyl Phosphine Oxide-HReO<sub>4</sub><sup>1</sup>

by T. J. Conocchioli, M. I. Tocher, and R. M. Diamond

Lawrence Radiation Laboratory, University of California, Berkeley, California (Received July 15, 1964)

The extraction of HClO<sub>4</sub> and HReO<sub>4</sub> into dilute solutions of trioctyl phosphine oxide (TOPO) in CCl<sub>4</sub> has been studied, and the nature of the extracting complex has been determined. It has been found that for TOPO concentrations <0.1 M in CCl<sub>4</sub> and for aqueous acid concentrations low enough so that the stoichiometric ratio of TOPO/H<sup>+</sup> in the organic phase is >6, the only extracting species are the water complex, TOPO·H<sub>2</sub>O, and the trisolvated hydronium ion, H<sub>3</sub>O<sup>+</sup>·3TOPO, which is ion-paired with the ClO<sub>4</sub><sup>-</sup>. For higher concentrations of acid in the organic phase, the predominant species appears to become the 1:1 complex, TOPOH<sup>+</sup>...ClO<sub>4</sub><sup>-</sup>. These results are compared with those for tributyl phosphate extraction and the model proposed earlier.

Solvent extraction systems composed of inorganic acid, water, and an organic base, either pure or diluted with an "inert" organic liquid, can be interpreted on the basis of a model which views the extraction as a competition among water, the extractant, and the anion for solvating the proton. The nature of this process is further dependent upon the dielectric constant and the possibly acidic or basic character of the diluent, if one is present. Two previous papers have described the extraction of aqueous HClO<sub>4</sub>, HReO<sub>4</sub>, and HBr by solutions of tributyl phosphate in CCl<sub>4</sub>.<sup>2,3</sup> In these systems the extracted acid species was H<sub>3</sub>O<sup>+</sup>·3TBP·y·H<sub>2</sub>O...X<sup>-</sup>, where 0 ≤ y ≤ 3. That is, the TBP is not basic enough to take the proton alone out of the water phase, but extracts a partially hydrated hydronium ion; water is a stronger base than TBP.

The extractant used in the present study was tri-*n*-octyl phosphine oxide (TOPO), a stronger base than TBP. Thus it might be expected to compete better with water for the proton, and so permit less water in the extracted complex. The choice of TOPO was also influenced by the fact that it has only one basic site—the phosphoryl oxygen—as opposed to TBP which has three additional ester oxygens.

A number of studies have been conducted on the extraction of mineral and complex acids by TOPO.<sup>4-9</sup> A few have suggested the nature of the extracting adduct but most have neglected the presence of water in

any such complex. This study will show that an investigation of the TOPO-H<sub>2</sub>O system and of the water content in the presence of acid extraction must be included to explain the extraction mechanism of strong acids satisfactorily.

The acid chosen was HClO<sub>4</sub> because ClO<sub>4</sub><sup>-</sup> is a very weak base, and so does not enter the competition. Perchloric acid is also a good model for the strong complex metal acids such as HFeCl<sub>4</sub>, HAuCl<sub>4</sub>, HReO<sub>4</sub>, etc. In addition, ReO<sub>4</sub><sup>-</sup> was used in tracer form because it also is a very weak base like ClO<sub>4</sub><sup>-</sup> and has a convenient isotope, Re<sup>186</sup> (*t*<sub>1/2</sub> = 90 hr.), which made possible the extension of the studies to more dilute solutions. The

(1) This work was supported by the U. S. Atomic Energy Commission, A.E.C. No. W7405-eng-48.

(2) D. C. Whitney and R. M. Diamond, *J. Phys. Chem.*, **67**, 209 (1963).

(3) D. C. Whitney and R. M. Diamond, *ibid.*, **67**, 2583 (1963).

(4) J. C. White and W. J. Ross, "Separations by Solvent Extraction with TOPO," National Academy of Sciences Report NAS-NS-3102, 1961.

(5) R. A. Zingaro and J. C. White, *J. Inorg. Nucl. Chem.*, **12**, 315 (1960).

(6) B. Martin, D. W. Ockenden, and J. K. Foreman, *ibid.*, **21**, 96 (1961).

(7) W. J. Ross and J. C. White, "The Solvent Extraction of Iron with TOPO," Oak Ridge National Laboratory Report ORNL-2382, 1957.

(8) G. E. Boyd and Q. V. Larson, *J. Phys. Chem.*, **64**, 988 (1960).

(9) M. I. Tocher, D. C. Whitney, and R. M. Diamond, *ibid.*, **68**, 368 (1964).

solvent used was  $\text{CCl}_4$ , which has a low dielectric constant ( $\epsilon = 2.2$ ) and so cannot easily support a charge separation of even moderately sized ions. Thus the attraction between the proton and the anion in such a medium is increased over the value in water, and the extracting complex might be expected to be an ion pair.

The method of studying the complex was that suggested by Hesford, *et al.*,<sup>10-12</sup> in which the activity of one component of the system is varied while all others are kept constant, thereby showing the dependence of the extracting complex on that particular component. Because concentrations (as opposed to activities) are what are usually measured, one must use caution in drawing conclusions about the nature of the complex from such studies. This problem may be minimized by limiting the concentration of extractant to only a few tenths molar and choosing experimental conditions such that only a few per cent of the extractant are involved in the complex. Thus, the organic phase retains the properties of the diluent, and changes in concentration of the extractant, acid, and water in that phase will have only a slight effect on their activity coefficients. After the nature of the complex in dilute solution is established, studies may be extended to more concentrated solutions to see if, in fact, more complex interactions are occurring in the organic phase.

### Experimental

The TOPO used was Eastman White Label product. Purification by equilibration with mild base, washing with distilled water, and recrystallization gave a product with a behavior identical with that of the original product; therefore, the material was used as obtained. A stock solution of 0.1 *M* TOPO in  $\text{CCl}_4$  (Baker and Adamson reagent grade) was prepared by weighing the desired amount of TOPO and making up to volume in a volumetric flask. All dilutions of TOPO were made in volumetric glassware from the stock solution. Solutions which had to be dried were stored over molecular sieves (Linde Co., 0.16-cm. diameter pellets), but could not be left for long periods due to the uptake of TOPO itself. At time of use, these solutions were filtered under mild vacuum in order to remove suspended particles of molecular sieves.

The  $\text{HClO}_4$  solutions were prepared by diluting G. F. Smith reagent grade  $\text{HClO}_4$  (70-72%) with distilled water. Determinations of aqueous acid concentrations were made by standard analytical methods, *i.e.*, titration with standard base to the red end point of phenol red (pH 7). Matheson Coleman and Bell stabilized and premixed single-solution Karl Fischer reagent was used in the water determinations. Methanol used in the Karl Fischer analysis blank was Baker and Adam-

son Electronic grade ( $\leq 0.1\%$   $\text{H}_2\text{O}$ ). The pyridine used was Baker and Adamson reagent grade (0.1%  $\text{H}_2\text{O}$ ).

The radioactive  $\text{Re}^{186}\text{O}_4^-$  tracer was prepared by irradiating  $\text{KReO}_4$  with neutrons in the Livermore pool-type reactor. The product was dissolved in distilled water to give an approximately  $10^{-3}$  *M*  $\text{KReO}_4$  solution which was further diluted before use.

*Procedure.* Equal volumes of aqueous acid and of TOPO solutions in  $\text{CCl}_4$  were equilibrated in glass-stoppered bottles. Samples were normally shaken from 1 to 3 hr. with a wrist-action shaker. Some samples were shaken as much as 6 hr. with no detectable difference in extraction; previous work in this laboratory had indicated that equilibrium is attained in similar systems in less than 30 min. After equilibration, samples were transferred to centrifuge cones and centrifuged for 1 to 3 min.; the organic phase was withdrawn with a pipet. The acid content of the organic phase was determined by a direct two-phase titration using 0.0100 or 0.1000 *M*  $\text{NaOH}$ , with stirring of the phases continued throughout the titration. Phenol red (pH 7) was used as the indicator, and determinations were made to its red end point. An indicator blank was run using water-saturated TOPO solutions; the amount of  $\text{NaOH}$  used for the blank was one-half the total titration for the smallest amount of organic-phase acid measured ( $1 \times 10^{-4}$  *M*) and vanishingly small for higher concentrations.

The water content of the organic phase was determined by the Karl Fischer method, using a direct visual end point and a pyridine-methanol blank.<sup>13</sup> The Karl Fischer reagent was standardized by titration of samples of methanol with known water content. A Beckman IR-5 double-beam recording spectrophotometer was also used to determine the water bound to the TOPO molecules by means of the peak heights of the symmetric and antisymmetric stretching modes of water. Dry  $\text{CCl}_4$  or a dry TOPO solution in  $\text{CCl}_4$  of the same concentration as the sample was used as a reference. Sample solutions and reference were contained in matched 2.0- or 0.2-mm. cells with  $\text{CaF}_2$  windows or 0.5-mm. cells with  $\text{AgCl}$  windows.

In the tracer studies, between 10 and 40  $\mu\text{l.}$  of  $\text{KReO}_4$  tracer was added to the mixture of aqueous acid and

(10) E. Hesford, H. A. C. McKay, and D. Scargill, *J. Inorg. Nucl. Chem.*, **4**, 321 (1957).

(11) E. Hesford and H. A. C. McKay, *Trans. Faraday Soc.*, **54**, 573 (1958).

(12) E. Hesford, H. A. C. McKay, and E. E. Jackson, *J. Inorg. Nucl. Chem.*, **9**, 229 (1959).

(13) J. Mitchell, Jr., and D. M. Smith, "Aquametry," Interscience Publishers, Inc., New York, N. Y., 1948, p. 235.

organic extractant before shaking. After shaking, centrifugation, and separation,  $\gamma$  counting was done on 2-ml. aliquots of each phase with a well-type Na(Tl)I scintillation crystal and a single-channel analyzer. The total number of counts/minute in both phases (corrected for background) was equated to the quantity of macro  $\text{HClO}_4$  originally taken. The fraction of the total counts found in each phase times the original quantity of  $\text{HClO}_4$  taken gave the amount of acid in that phase, under the assumption that  $\text{HClO}_4$  and  $\text{HReO}_4$  behave similarly (but see later). All experimental work was done at room temperature,  $23 \pm 2^\circ$ , with no detectable changes in extraction over this range.

### Results

Investigation was first made of the TOPO- $\text{H}_2\text{O}$  system. Solutions of 0.002 to 0.5  $M$  TOPO in  $\text{CCl}_4$  were equilibrated with water, and the water content in the organic phase was determined by the Karl Fischer method. These values must then be corrected for the amount of water dissolved in  $\text{CCl}_4$  alone, namely, the solubility of  $\text{H}_2\text{O}$  in  $\text{CCl}_4$  (0.010  $M$ ) times the volume fraction of  $\text{CCl}_4$  in the solution. However, the lowest concentration of TOPO-bound water was best determined from infrared analyses which can distinguish the two kinds of water. The fundamental vibrational stretching modes of unbound water molecules, the anti-symmetric and symmetric stretches, are at 2.70 and 2.76  $\mu$ , respectively, with the shorter wave length peak showing the greater absorbance. The positions and relative magnitudes of these peaks are nearly the same for gaseous  $\text{H}_2\text{O}$  and for  $\text{H}_2\text{O}$  dissolved in  $\text{CCl}_4$ , indicating that there is little hydrogen bonding present in the latter case.<sup>14</sup> But, when water is hydrogen bonded through its OH groups, the ratio of peak heights changes, and the absorption moves to longer wavelengths. For the water extracted into dilute TOPO solutions ( $\leq 0.1 M$ ) the two stretching modes appear at 2.71 and 2.97  $\mu$ , respectively, and the 2.97  $\mu$  peak shows the greater absorbance. These changes indicate the hydrogen bonding of water to the TOPO and a corresponding weakening of the O-H bond involved.

Spectra were taken of water-saturated TOPO solutions ranging in concentration from 0.001 to 0.5  $M$  TOPO. Calibration curves relating the absorption peak height of the 2.71 and 2.97  $\mu$  peaks to the water content were normalized to the Karl Fischer titration values in the region around 0.06  $M$  TOPO; here, the water concentrations were sufficiently high so that the titrations were subject to relatively small experimental error. A plot of log organic-phase water vs. log total TOPO, determined by either peak, gave results in

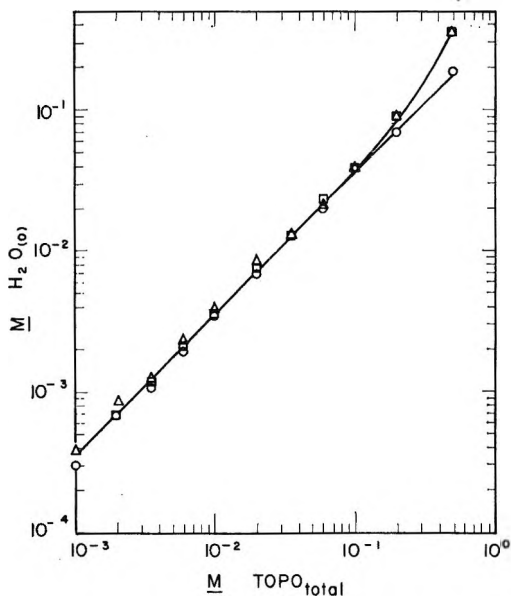


Figure 1. Variation of water content of organic phase ( $\text{CCl}_4$  diluent) with TOPO concentration, corrected for solubility of  $\text{H}_2\text{O}$  in  $\text{CCl}_4$ :  $\square$  Karl Fischer;  $\circ$  2.75  $\mu$  peak; and  $\triangle$  3.0  $\mu$  peak.

good agreement with the corrected Karl Fischer values for solutions as high in concentration as 0.1  $M$  TOPO, as shown in Figure 1. At this point the curves of the two peaks diverged; that of the 2.97  $\mu$  peak rose faster than that of the 2.71  $\mu$  peak and approximated the Karl Fischer values.

The next series of experiments had to do with the  $\text{HClO}_4$  extraction itself. Concentrations of acid from 0.01 to 11  $M$   $\text{HClO}_4$  were equilibrated with dilute solutions of TOPO in  $\text{CCl}_4$  ranging from 0.01 to 0.1  $M$ , and the organic-phase acid content was determined at each external (aqueous) acid concentration. Figure 2 shows a plot of log organic-phase acid concentrations vs. log equilibrium aqueous acid activities. It should be noted that the experimental organic-phase acid concentrations must be corrected for the amount of acid extracted by  $\text{CCl}_4$  without TOPO present; however, the extraction of  $\text{HClO}_4$  into  $\text{CCl}_4$  was found to be negligible over the range of  $\text{HClO}_4$  concentrations used.

The  $\text{ReO}_4^-$  tracer extractions from macroconcentrations of  $\text{HClO}_4$  were used to extend the range of aqueous acid concentrations investigated toward more dilute solutions, namely down to 0.001  $M$   $\text{HClO}_4$ . A log-log plot of the organic phase acid concentration (as calculated from the  $\text{ReO}_4^-$  tracer distribution) vs. the equilibrium aqueous  $\text{HClO}_4$  activity is given in Figure 3.

(14) G. C. Pimentel and A. L. McClennan, "The Hydrogen Bond," W. H. Freeman and Co., San Francisco, Calif., 1960.

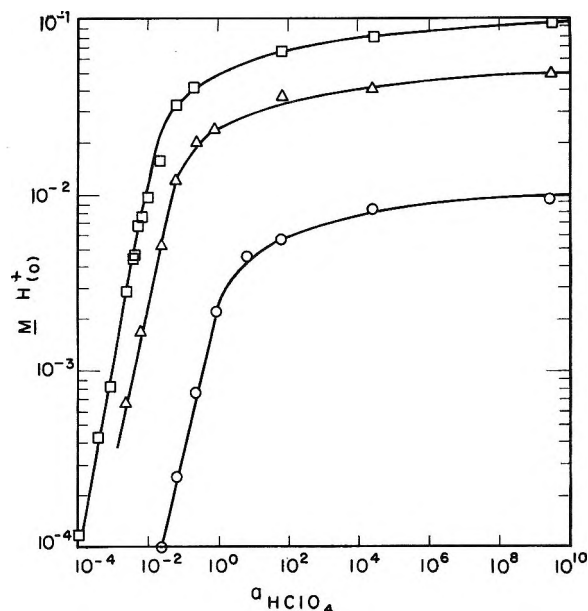


Figure 2. Variation of organic-phase acid content ( $\text{CCl}_4$  diluent) with aqueous  $\text{HClO}_4$  activity for total TOPO concentrations of  $\square$  0.1  $M$ ;  $\triangle$  0.05  $M$ ; and  $\circ$  0.01  $M$ .

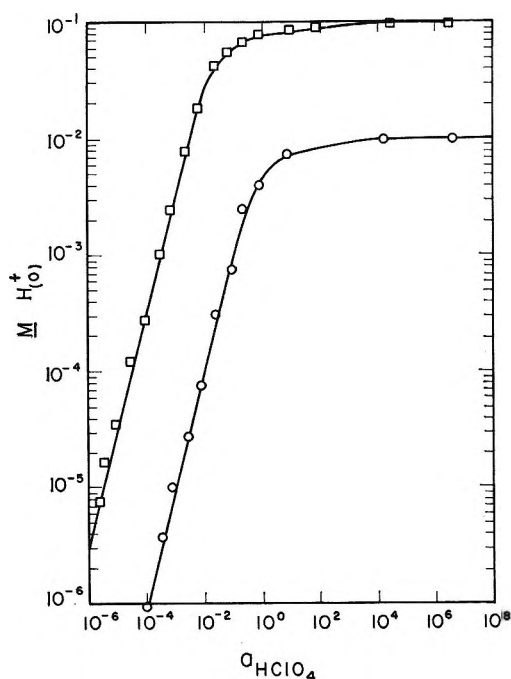


Figure 3. Variation of organic-phase acid content (measured by  $\text{HReO}_4$  tracer,  $\text{CCl}_4$  diluent) with aqueous  $\text{HClO}_4$  activity for total TOPO concentrations of  $\square$  0.1  $M$  and  $\circ$  0.01  $M$ .

Determinations were also made of the amount of  $\text{H}_2\text{O}$  extracting with  $\text{HClO}_4$ . Solutions of 0.05 and 0.1  $M$  TOPO were equilibrated with aqueous solutions of acid ranging from 0.01 to 11  $M$  in  $\text{HClO}_4$  and the

amounts of  $\text{H}^+$  and  $\text{H}_2\text{O}$  in the organic phase were measured, the latter by the Karl Fischer method. The water values, however, include the water dissolved in  $\text{CCl}_4$  alone, which quantity may be calculated as the product of the solubility of pure water in  $\text{CCl}_4$ , the aqueous water activity, and the volume fraction of  $\text{CCl}_4$ . The amount of water extracted minus this  $\text{CCl}_4$  water is shown in Figure 4 plotted vs. the organic phase acid concentration. Infrared spectra were also recorded for 0.1  $M$  TOPO solutions equilibrated with various concentrations of aqueous acid. Because a dry TOPO solution was used as a reference, the water absorption peaks (after correction for  $\text{H}_2\text{O}$  in  $\text{CCl}_4$  alone) gave an experimental determination of the amount of water bonded to TOPO, but not in the acid complex.

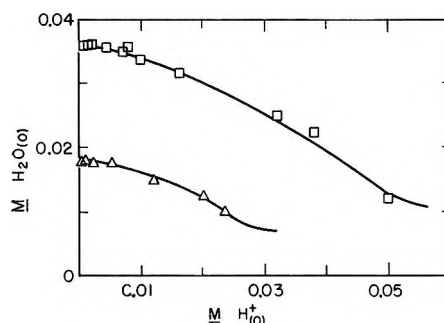
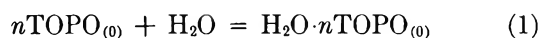


Figure 4. Variation of organic-phase water content ( $\text{CCl}_4$  diluent corrected for solubility of  $\text{H}_2\text{O}$  in  $\text{CCl}_4$ ) with organic-phase  $\text{HClO}_4$  acid content:  $\square$  0.1  $M$  TOPO and  $\triangle$  0.05  $M$  TOPO.

## Discussion

**TOPO- $\text{H}_2\text{O}$ .** It is assumed that the TOPO-water system is maintained independently of any TOPO-acid system so that TOPO molecules bonded to water are not readily available for acid extraction. Therefore, the initial investigation was of the extraction of pure water by TOPO (eq. 1, where (o) indicates the organic



phase). The corresponding equilibrium constant is given in eq. 2 where parentheses signify activities;

$$K_{\text{H}_2\text{O}} = \frac{(\text{H}_2\text{O} \cdot n\text{TOPO})}{(\text{TOPO})^n (\text{H}_2\text{O})} = \frac{[\text{H}_2\text{O} \cdot n\text{TOPO}] \gamma_{\text{H}_2\text{O} \cdot n\text{TOPO}}}{[\text{TOPO}]^n \gamma_{\text{TOPO}}^n (\text{H}_2\text{O})} \quad (2)$$

brackets, concentrations;  $\gamma$ , activity coefficients; and where  $[\text{TOPO}]$  always means the equilibrium TOPO concentration. Initial or total concentration will be specifically indicated.

Although very little is known about activity coefficients in organic solutions, the assumption was made

that the ratio of activity coefficients  $\gamma_{\text{H}_2\text{O}\cdot n\text{TOPO}}/\gamma_{\text{TOPO}}^n$  was constant; thus, organic-phase concentrations were used instead of thermodynamic activities. This does not seem unreasonable as the solutions of TOPO were kept dilute so that the properties of the  $\text{CCl}_4$  diluent were essentially retained. As will be seen later, the results of the extraction studies substantiate this assumption. Thus, eq. 2 may be rewritten

$$K'_{\text{H}_2\text{O}} = \frac{[\text{H}_2\text{O}\cdot n\text{TOPO}]}{[\text{TOPO}]^n(\text{H}_2\text{O})} \quad (3)$$

Taking logarithms and rearranging yields

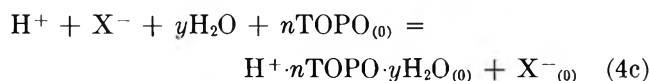
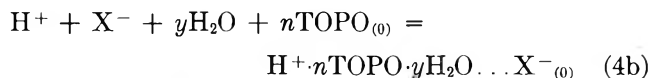
$$\log [\text{H}_2\text{O}\cdot n\text{TOPO}] = n \log [\text{TOPO}] + \log K'_{\text{H}_2\text{O}} + \log (\text{H}_2\text{O}) \quad (3a)$$

Assuming that the water activity is approximately equal to 1, since the solubility of TOPO in water is negligibly small, a plot of  $\log [\text{H}_2\text{O}\cdot n\text{TOPO}]$  vs.  $\log [\text{TOPO}]$  will determine  $n$ , the number of TOPO molecules per water molecule. The equilibrium TOPO concentration may be calculated as  $[\text{TOPO}] = [\text{TOPO}]_{\text{total}} - n[\text{H}_2\text{O}\cdot n\text{TOPO}]$  in which  $[\text{TOPO}]_{\text{total}}$  is the initial TOPO concentration and  $n[\text{H}_2\text{O}\cdot n\text{TOPO}]$  is  $n$  times the water content in the organic phase (exclusive of water just dissolved in the  $\text{CCl}_4$ ).

It can be seen that the log-log plot of organic-phase water vs. log initial TOPO concentration is linear from 0.001 to 0.1  $M$  TOPO with a slope of 1.0. Correction to equilibrium TOPO yields a value of  $n = 1.0$  and  $K'_{\text{H}_2\text{O}} = 0.56$ , which means that at TOPO concentrations below 0.1  $M$  in  $\text{CCl}_4$ , 36% of the total TOPO is bonded to  $\text{H}_2\text{O}$ , and the water-TOPO complex contains only one TOPO. This is analogous to the earlier studied TBP- $\text{CCl}_4$  system,<sup>2</sup> and the larger value of  $K'_{\text{H}_2\text{O}}$  is an indication of the greater basicity of TOPO over TBP.

Above 0.1  $M$  TOPO, the curve rises more steeply than a slope of unity. This rise indicates either the introduction of a new TOPO- $\text{H}_2\text{O}$  complex or the breakdown of the assumptions made for dilute solutions. The linear portion of the curve, however, supports the assumption of a constant activity coefficient ratio for TOPO species in the organic phase in the region of concentrations in  $\text{CCl}_4$  below 0.1  $M$ .

*TOPO-H<sub>2</sub>O-HClO<sub>4</sub> (HReO<sub>4</sub>)*. The reaction for the extraction of dilute acids by dilute solutions of TOPO may be written as eq. 4a, b, or c, depending upon whether



the extracting species is (a) molecular, (b) ionic but associated, or (c) ionic and dissociated. The assumption is made that the anion in eq. 4b and 4c is not hydrated or complexed by the extractant in the organic phase, and  $\text{ClO}_4^-$  and  $\text{ReO}_4^-$  appear to satisfy this requirement.

The equilibrium constants for eq. 4a, 4b, and 4c, respectively, are given by eq. 5a, 5b, and 5c.

$$K_{\text{HX}} = \frac{(\text{HX}\cdot n\text{TOPO}\cdot y\text{H}_2\text{O})}{(\text{TOPO})^n(\text{H}_2\text{O})^y(\text{H}^+\text{X}^-)} = \frac{[\text{HX}\cdot n\text{TOPO}\cdot y\text{H}_2\text{O}]\gamma}{[\text{TOPO}]^n\gamma_{\text{TOPO}}^n(\text{H}_2\text{O})^y(\text{H}^+\text{X}^-)} \quad (5a)$$

$$K_{\text{HX}} = \frac{(\text{H}^+\cdot n\text{TOPO}\cdot y\text{H}_2\text{O}\dots\text{X}^-)}{(\text{TOPO})^n(\text{H}_2\text{O})^y(\text{H}^+\text{X}^-)} = \frac{[\text{H}^+\cdot n\text{TOPO}\cdot y\text{H}_2\text{O}\dots\text{X}^-]\gamma}{[\text{TOPO}]^n\gamma_{\text{TOPO}}^n(\text{H}_2\text{O})^y(\text{H}^+\text{X}^-)} \quad (5b)$$

$$K_{\text{HX}} = \frac{(\text{H}^+\cdot n\text{TOPO}\cdot y\text{H}_2\text{O})(\text{X}^-)}{(\text{TOPO})^n(\text{H}_2\text{O})^y(\text{H}^+\text{X}^-)} = \frac{[\text{H}^+\cdot n\text{TOPO}\cdot y\text{H}_2\text{O}]\gamma_+[\text{X}^-]\gamma_-}{[\text{TOPO}]^n\gamma_{\text{TOPO}}^n(\text{H}_2\text{O})^y(\text{H}^+\text{X}^-)} \quad (5c)$$

It is again assumed that the ratio  $\gamma/\gamma_{\text{TOPO}}^n$  or  $\gamma_+\gamma_-/\gamma_{\text{TOPO}}^n$  is a constant, as the TOPO solutions are in a dilute, near-ideal region. Substituting  $[\text{H}^+]_{(o)}^m$  to represent the extracted acid in the organic phase, with  $m = 1$  for cases (a) and (b) and  $m = 2$  for case (c), leads to the simpler general expression of eq. 6. Thus, if the

$$K'_{\text{HX}} = \frac{[\text{H}^+]_{(o)}^m}{[\text{TOPO}]^n(\text{H}_2\text{O})^y(\text{H}^+\text{X}^-)} \quad (6)$$

equilibrium TOPO concentration and water activity are kept constant, the slope of the plot of  $\log [\text{H}^+]_{(o)}$  vs.  $\log (\text{H}^+\text{X}^-)$  will yield  $1/m$ . Figures 2 and 3 show that below an aqueous acid activity of unity for 0.01  $M$  TOPO and of about  $10^{-2}$  for 0.1  $M$  TOPO a log-log plot of  $[\text{H}^+]_{(o)}$  vs.  $[\text{TOPO}]_{\text{total}}$  does give a slope of about unity. Experimentally, however, as the amount of extracted acid increases, the amount of TOPO tied up in the complex also increases and so  $[\text{TOPO}]$  decreases. Therefore, the raw data must be corrected to a fixed equilibrium TOPO concentration, to satisfy the requirement of eq. 6. Equation 7 may be used (as will be

$$[H^+]_{(o)}' = [H^+]_{(o)} \frac{[TOPO]'^3}{[TOPO]^3} \quad (7)$$

justified below) where  $[H^+]_{(o)}'$  is the corrected organic-phase concentration corresponding to a fixed equilibrium TOPO concentration,  $[TOPO]'$ , taken to be the initial concentration; and the unprimed values are the experimental equilibrium concentrations, *i.e.*,  $[TOPO]$  is the actual concentration of unbonded TOPO. The latter does not include TOPO·H<sub>2</sub>O or TOPO bound to the proton; thus, these corrections must be evaluated. The concentration of TOPO used in the acid complex will be  $n[H^+]_{(o)}$  with  $n = 3$  as shown below, so that

$$[TOPO] = [TOPO]_{total} - [TOPO \cdot H_2O] - 3[H^+]_{(o)} \quad (8)$$

Substitution of the value of TOPO·H<sub>2</sub>O from eq. 3 yields eq. 9. The use of eq. 7 and 9 permits the data

$$[TOPO] = \frac{[TOPO]_{total} - 3[H^+]_{(o)}}{1 + K'_{H_2O}(H_2O)} \quad (9)$$

plotted in Figure 2 to be corrected to a constant equilibrium TOPO concentration, and these corrected data are shown in Figure 5. Slopes of  $1/m = 1$  are obtained, so  $m = 1$  and the species is either molecular or ion-paired. This conclusion agrees with conductivity measurements made by Hesford and McKay for extracts of HClO<sub>4</sub> in TBP-benzene solutions in which the conductivity was negligibly small at concentrations similar to those used in this study<sup>15</sup> and is certainly what one would expect for a solvent system with a dielectric constant as low as that of CCl<sub>4</sub> ( $\epsilon = 2.2$ ).

Figure 3 shows a plot of  $\log [H^+]_{(o)}$  vs.  $\log$  aqueous acid for tracer HReO<sub>4</sub> in macro HClO<sub>4</sub> at two values of initial TOPO concentration. Again the linear portion

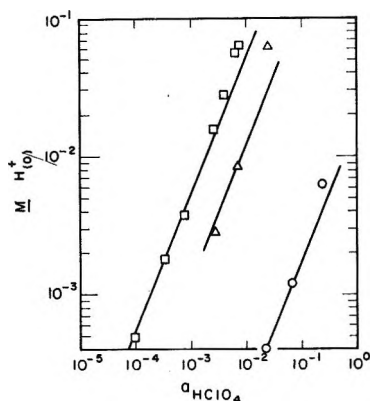


Figure 5. Variation of organic-phase acid content (CCl<sub>4</sub> diluent) with aqueous HClO<sub>4</sub> activity for fixed TOPO concentrations of  $\square$  0.1 M;  $\triangle$  0.05 M; and  $\circ$  0.01 M. All lines drawn with slopes of 1.0.

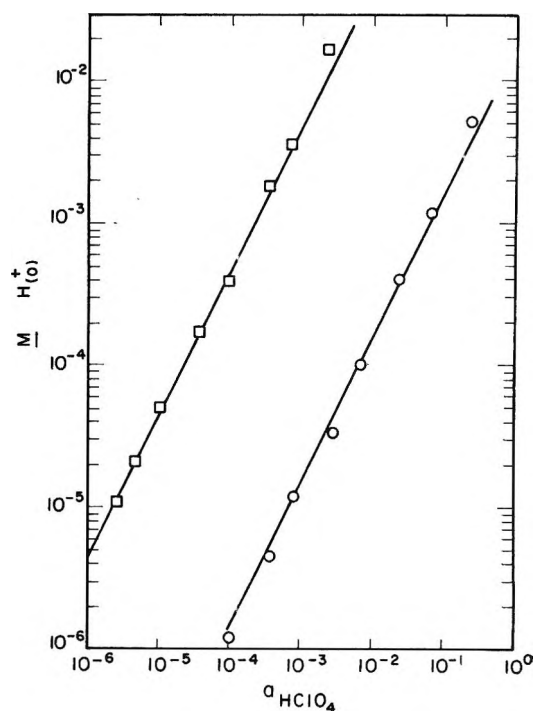


Figure 6. Variation of organic-phase acid content (measured by HReO<sub>4</sub> tracer, CCl<sub>4</sub> diluent) with aqueous HClO<sub>4</sub> activity for fixed TOPO concentrations of  $\square$  0.1 M and  $\circ$  0.01 M. Both lines drawn with slopes of 1.0.

of the curve has a slope of approximately 1, and after correction to a constant equilibrium TOPO value, Figure 6 shows that the corrected values again yield  $m = 1$  over an extended range of acid concentration. It must be noted that the extraction of HReO<sub>4</sub> tracer in HClO<sub>4</sub> differs somewhat from the extraction of HClO<sub>4</sub> itself and is, in fact, slightly higher; the conclusions that can be drawn from an analysis of the slopes, however, are not affected.

From eq. 6, it can be seen that if the aqueous HClO<sub>4</sub> activity is kept constant, a plot of  $\log [H^+]_{(o)}$  vs.  $\log [TOPO]$  will yield a curve, the slope of which is  $n/m$ . For a molecular or ion-paired complex,  $m = 1$ , and the slope equals  $n$ , the number of TOPO molecules bound in the complex. The experimental plot of  $\log [H^+]_{(o)}$  vs.  $\log [TOPO]_{total}$ , is given in Figure 7 for HReO<sub>4</sub> tracer in HClO<sub>4</sub>. A slope of about 2.5 is obtained, but the use of eq. 6 to determine  $n$  requires that  $\log [H^+]_{(o)}$  be plotted against  $\log [TOPO]$ , not  $\log [TOPO]_{total}$ , so that the amount of TOPO bound to water and to the acid must be subtracted, as in eq. 9. Since such a correction will steepen the slope and so increase the value of  $n$ , a trial value of  $n = 3$  was used

(15) E. Hesford and H. A. C. McKay, *J. Inorg. Nucl. Chem.*, **13**, 156 (1960).

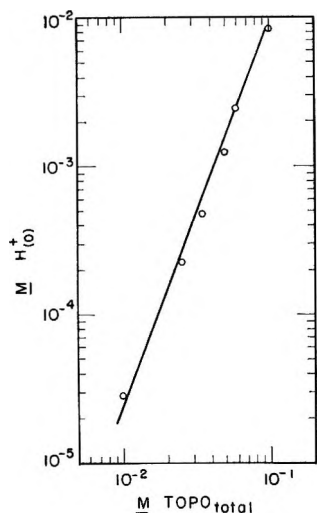


Figure 7. Variation of organic-phase acid content (measured by  $\text{HReO}_4$  tracer,  $\text{CCl}_4$  diluent) with initial TOPO concentration for aqueous  $\text{HClO}_4$  activity of  $2.8 \times 10^{-3}$ .

in eq. 9. The resulting curve for  $\log [\text{H}^+]_{(o)}$  vs.  $\log [\text{TOPO}]$  yielded a slope of 3 until about 40% of the total TOPO was complexed by acid (Figure 8). Corrections using  $n = 2$  and  $n = 4$  did not yield the corresponding slopes. Therefore,  $n$  is, in fact, equal to 3, just as in the corresponding TBP system.<sup>2</sup>

The number of water molecules per proton,  $y$ , remains to be determined. The Karl Fischer titrations gave values for the total amount of water present. These values then had to be corrected for the solubility of water in the  $\text{CCl}_4$  and for the amount of water involved in the  $\text{TOPO-H}_2\text{O}$  complex in order to yield values for  $y$ . The former term is calculated in the way previously described, while the water bound as  $\text{TOPO-H}_2\text{O}$  can be calculated from eq. 3 assuming that the  $\text{TOPO-H}_2\text{O}$  system is maintained independently of the  $\text{TOPO-acid-H}_2\text{O}$  system and that no other  $\text{TOPO-acid}$  complex exists. In Figure 9 is shown a plot of the water bound in the acid complex,  $[\text{H}_2\text{O}]_{\text{acid}}$ , vs.  $[\text{H}^+]_{(o)}$ . It can be seen that the curve passes through the origin and that its slope is initially 1.

If, then, the stoichiometric ratio of  $\text{TOPO}/\text{H}^+$  is greater than about 6, the ratios of  $\text{TOPO}/\text{H}^+$  and of  $\text{H}_2\text{O}/\text{H}^+$  in the organic phase complex are 3 and 1, respectively. These ratios strongly suggest that the hydronium ion is the species about which the three TOPO molecules are coordinated, because each of the three hydrogens is a possible acidic bonding site for the basic phosphoryl oxygens. This is similar to the species described for the extraction of  $\text{HClO}_4$  by dilute TBP solutions in  $\text{CCl}_4$ .<sup>2</sup> But with the less basic extractants such as TBP or ethers, water competes better with the extractant for the protonic sites on the hy-

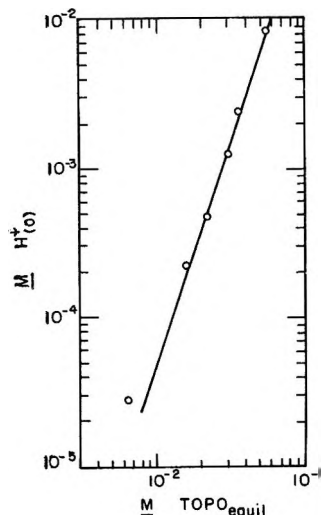


Figure 8. Variation of organic-phase acid content (measured by  $\text{HReO}_4$  tracer,  $\text{CCl}_4$  diluent) with equilibrium TOPO concentration for aqueous  $\text{HClO}_4$  activity of  $2.8 \times 10^{-3}$ . Line drawn with slope of 3.0.

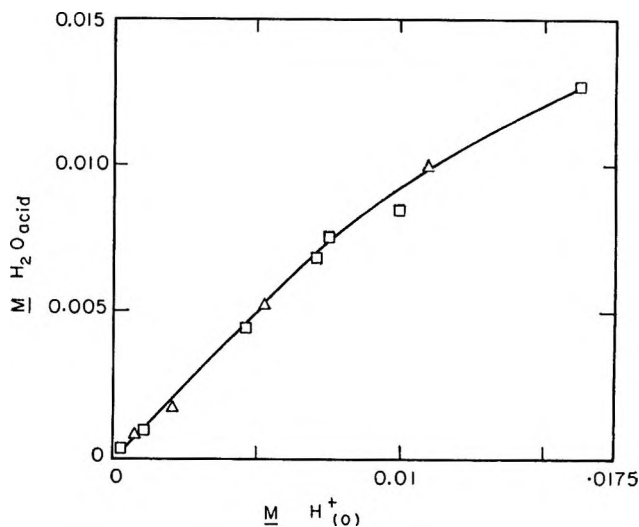


Figure 9. Variation of organic-phase water content ( $\text{CCl}_4$  diluent;  $M \text{H}_2\text{O}_{\text{acid}}$  does not include  $\text{H}_2\text{O}$  dissolved in  $\text{CCl}_4$  nor complexed in  $\text{TOPO-H}_2\text{O}$ ) with organic-phase  $\text{HClO}_4$  acid content:  $\square$  0.1  $M$  TOPO and  $\triangle$  0.05  $N$  TOPO.

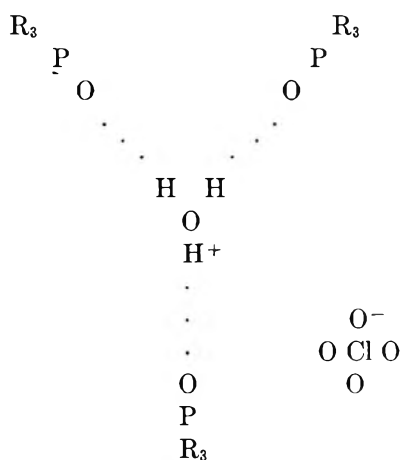
dronium ion, and so additional water molecules may be bound in the complex as bridges between the  $\text{H}_3\text{O}^+$  and the TBP molecules. Water to proton ratios varying from 1 to 4 may be found depending upon the concentrations of the components. The more basic TOPO molecules do not permit any additional water to bind directly to the  $\text{H}_3\text{O}^+$  ion and so the ratio of water to acid does not exceed unity. With the still more basic amine systems, the amine takes the proton away from



even the hydronium ion, forming an ammonium ion and an almost anhydrous organic phase.<sup>16</sup>

Additionally, the species in the TOPO-CCl<sub>4</sub> solutions is expected to be an ion pair rather than a molecular complex because (a) it seems unlikely that a molecular acid could coordinate three TOPO molecules plus a water molecule about itself; and (b) the ClO<sub>4</sub><sup>-</sup> ion is a very weak base and extraction of molecular HClO<sub>4</sub> in dilute solution would not be expected.

On the basis of the foregoing considerations, it may be stated that in CCl<sub>4</sub> solutions of TOPO up to 0.1 *M* and with aqueous HClO<sub>4</sub> acid concentrations up to about 0.2 *M* the species may be written H<sub>3</sub>O<sup>+</sup>·3TOPO·ClO<sub>4</sub><sup>-</sup>, and the most likely structure for the extracting complex is



*TOPO-Concentrated HClO<sub>4</sub>.* The curves shown in Figures 2 and 3 deviate from the initial slope of 1 when the amount of TOPO bound in the extracted complex exceeds about 50% of the total TOPO concentration. For the TOPO concentrations used in this study, 10<sup>-2</sup> to 10<sup>-1</sup> *M*, this corresponds to aqueous HClO<sub>4</sub> concentrations greater than about 1 and 10<sup>-2</sup> *M*, respectively. The assumptions used for the interpretation of extraction into dilute solutions are probably no longer valid, but some inferences and conclusions can be drawn from stoichiometric considerations.

In the concentrated acid region the log [H<sup>+</sup>]<sub>(o)</sub> vs. log (HClO<sub>4</sub>) curve (see Figure 2) approaches as a limit a value of the organic-phase H<sup>+</sup> equal to the total TOPO concentration, although even at the highest initial HClO<sub>4</sub> concentration, the stoichiometric TOPO/

H<sup>+</sup> ratio is not quite 1. When the stoichiometric TOPO/H<sup>+</sup> ratio falls below 3, a new species must be involved besides the previously described H<sub>3</sub>O<sup>+</sup>·3TOPO·ClO<sub>4</sub><sup>-</sup>. The asymptotic limit suggests that at high organic-phase acid concentrations, only one TOPO molecule is associated with the proton. The water activity in concentrated HClO<sub>4</sub> has been reduced considerably, and TOPO certainly competes more favorably as a base for the proton. It appears to become, in fact, the primary solvating molecule leading to a complex of the form TOPOH<sup>+</sup>·ClO<sub>4</sub><sup>-</sup>. This would be similar to the formation of an ammonium salt by the still more basic trialkylamine. However, the water content in the organic phase does not go to zero, suggesting that a hydrated species may also be involved, very possibly TOPOH<sup>+</sup>·OH<sub>2</sub>·ClO<sub>4</sub><sup>-</sup>.

### Conclusions

For the system of dilute HClO<sub>4</sub>-H<sub>2</sub>O-TOPO, water best solvates the proton, and the H<sub>3</sub>O<sup>+</sup> ion is extracted over a considerable range of TOPO and acid concentrations. The species present is H<sub>3</sub>O<sup>+</sup>·3TOPO·ClO<sub>4</sub><sup>-</sup>, an ion pair in the CCl<sub>4</sub> diluent. This trisolvated species is similar to the one proposed for the extraction of HClO<sub>4</sub> by dilute TBP (a weaker base) in CCl<sub>4</sub>, except that TBP cannot entirely displace the water molecules from about the hydronium ion.<sup>2,3</sup> But as the acid concentration is increased, the water activity falls and the amount of free TOPO decreases, so that a transition occurs to a monosolvated species, TOPOH<sup>+</sup>·ClO<sub>4</sub><sup>-</sup>, and probably the hydrate, TOPOH<sup>+</sup>·OH<sub>2</sub>·ClO<sub>4</sub><sup>-</sup>.

In general, it is suggested for systems involving dilute acid, water, and dilute extractant where the anion of the acid is a very weak base and the extractant is a base weaker or comparable to water that the hydronium ion is the basis for extraction. In addition, in low dielectric constant media, the complex can be expected to be ion-paired. Subsequent reports will discuss the cases where the anion is the strongest relative base in the system and where the extractant is the strongest base. Also, the effect of high dielectric constant solvents will be presented.

(16) J. J. Bucher and R. M. Diamond, "Extraction of HClO<sub>4</sub> by Trilaurylamine," Lawrence Radiation Laboratory Report, UCRL 11616-Rev. Sept. 1964.

## The Differential Thermal Analysis of Perchlorates. VII. Catalytic

### Decompositions of the Alkali Metal Perchlorates by Manganese Dioxide

by Meyer M. Markowitz and Daniel A. Boryta

Footo Mineral Company, Research and Engineering Center, Exton, Pennsylvania (Received August 3, 1964)

The thermal stabilities of the pure alkali metal perchlorates ( $MClO_4$ ) and of admixtures with 10 mole %  $MnO_2$  catalyst follow the order  $Li < Na < K, Rb, Cs$ . For both pure and catalyst-containing materials, rapid decomposition is preceded by liquid phase formation. Analyses of molten perchlorates near their fusion temperatures show that fusion is coincident with decomposition except for  $LiClO_4$  which has a congruent melting point; the simultaneous occurrence of fusion and decomposition is in contrast to the behavior manifested by  $MClO_3$  salts, each of which possesses a congruent melting point and a significant range of liquid phase stability. Catalysis of  $MClO_4$  pyrolysis by basic substances yielding  $O^{2-}$  ion, in conjunction with other evidence, suggests the presence of O atoms in decomposing perchlorates. A proposed mechanism for  $Cl_2$  evolution from  $MClO_4$  melts (order of extent of  $Cl_2$  release:  $Li \gg Na > K > Rb, Cs = O$ ) stipulates an autoionization equilibrium of the type  $ClO_4^- \rightarrow ClO_3^+ + O^{2-}$ , so that  $Cl_2$  release occurs through the reaction  $ClO_4^- + ClO_3^+ \rightarrow [Cl_2O_7] \rightarrow Cl_2 + 7/2O_2$ . Such a scheme removes acidic oxides (*e.g.*,  $P_2O_5$ ,  $B_2O_3$ ,  $WO_3$ ,  $MoO_3$ , etc.) from consideration as true catalysts inasmuch as they function by removal of oxide ions and hence undergo specific, irreversible reactions with  $MClO_4$  salts. In this regard,  $MnO_2$  is primarily a true catalytic agent for  $MClO_4$  decomposition, but it also does appear to undergo a small amount of chemical reaction with  $LiClO_4$ , in particular, to foster  $Cl_2$  evolution, *viz.*,  $LiClO_4 + MnO_2 \rightarrow LiMnO_2 + 1/2Cl_2 + 2O_2$ .

#### Introduction

Though the catalytic decomposition of  $KClO_3$  by  $MnO_2$  has been extensively studied in the past,<sup>1</sup> relatively little care had been taken to ensure the purity and structural properties of the materials used and to secure comparable data for the other  $MClO_3$  salts.<sup>2</sup> The  $MClO_4$  compounds in these regards have suffered even greater neglect. Accordingly, in the present study, previously well-characterized reactants were employed to ascertain the course of changes during the pyrolyses of the pure  $MClO_4$  salts and of  $MClO_4$  samples containing 10 mole %  $MnO_2$ .

#### Experimental

Differential thermal analysis (d.t.a.), thermogravimetric analysis (t.g.a.), and  $Cl_2$  evolution experiments were performed as previously described.<sup>2</sup> Vycor (96%  $SiO_2$ ) or quartz was used as the sample container because of the high temperatures encountered in this

study and because these materials tend to undergo less interaction with molten  $MClO_3$  and  $MClO_4$  salts to produce  $Cl_2$  than does soft or borosilicate glass.<sup>3,4</sup>

*Materials.* The preparation and handling of the five  $MClO_4$  salts have been detailed elsewhere.<sup>5</sup> All samples were ground to pass a 325 mesh sieve. Each of these materials and subsequently produced reaction residues was analyzed for  $Cl^-$  content titrimetrically by the Mohr method and for  $ClO_3^-$  content as additional  $Cl^-$  after reduction with aqueous  $SO_2$ .  $ClO_4^-$  was determined gravimetrically as nitron perchlorate after

(1) "Gmelins Handbuch der anorganischen Chemie," 8 Auflage, System No. 6, "Chlor," Verlag Chemie, G.m.b.h., Berlin, 1926, pp. 340-346.

(2) M. M. Markowitz, D. A. Boryta, and H. Stewart, Jr., *J. Phys. Chem.*, **68**, 2282 (1964).

(3) W. Farmer and J. B. Firth, *J. Chem. Soc.*, **125**, 82 (1924).

(4) W. H. Sodeau, *ibid.*, **77**, 137 (1900).

(5) M. M. Markowitz, D. A. Boryta, and R. F. Harris, *J. Phys. Chem.*, **65**, 261 (1961).

removal of  $\text{ClO}_3^-$ . No  $\text{Cl}^-$  or  $\text{ClO}_3^-$  was found in any of the  $\text{MClO}_4$  compounds. Analyses of products:  $\text{LiClO}_4$ :  $\text{ClO}_4^-$ , 93.8 (calcd. 93.5);  $\text{NaClO}_4$ :  $\text{ClO}_4^-$ , 81.4 (calcd. 81.2);  $\text{KClO}_4$ :  $\text{ClO}_4^-$ , 71.7 (calcd. 71.9);  $\text{RbClO}_4$ :  $\text{ClO}_4^-$ , 19.14 (calcd. 19.18);  $\text{CsClO}_4$ :  $\text{ClO}_4^-$ , 15.20 (calcd. 15.27). Because of the possible susceptibility of these salts to catalysis of thermal decomposition by trace impurities,<sup>6,7</sup> the compounds were also analyzed spectrographically; B, Co, Cr, Mo, Pb, Sn, Ti, V, and Zn were uniformly found to be absent, whereas Al, Ca, Cu, Fe, Mg, Mn, Ni, and Si were generally present to the extent of 1–10 p.p.m.

Chemically analyzed  $\text{MnO}_2$  as tetragonal pyrolusite was available from an earlier study.<sup>2</sup> The screen analysis was 100% through 200 mesh, 43.7% through 325 mesh, and 56.3% on 325 mesh. In order to avoid promotion of catalysis and other effects due to trace impurities,<sup>8,9</sup> the material was analyzed spectrographically and was found free of Pb, Ti, and V with less than 50–100 p.p.m. of Al, Ca, Cu, Ni, and Si, and 300 p.p.m. of Fe. It should be noted that despite the many studies performed concerning the catalytic effects of  $\text{MnO}_2$  on the pyrolysis of  $\text{KClO}_3$ , systematic characterization of the catalyst appears to have been consistently omitted.<sup>10,11</sup>

*Thermal Profiles of Pure Perchlorate Salts.* The pertinent data obtained from the d.t.a. (Figure 1) and t.g.a. (Figure 2) curves for the pure  $\text{MClO}_4$  compounds are summarized in Tables I and II, respectively.

**Table I:** Thermal Behavior of  $\text{MClO}_4$  Salts and of 90 Mole %  $\text{MClO}_4$ -10 mole %  $\text{MnO}_2$  Mixtures from D.t.a. Experiments

Sample	Crystallographic transition, °C.	$\text{MClO}_4$ fusion, °C.	Onset of rapid dec., °C.	MCl fusion, °C.
$\text{LiClO}_4$	...	247	438	611
$\text{LiClO}_4\text{-MnO}_2$	...	247	402	612
$\text{NaClO}_4$	309	468	525	800
$\text{NaClO}_4\text{-MnO}_2$	311	450	485	801
$\text{KClO}_4$	303	580	580	773
$\text{KClO}_4\text{-MnO}_2$	300	529	529	769
$\text{RbClO}_4$	284	597	597	726
$\text{RbClO}_4\text{-MnO}_2$	285	545	545	722
$\text{CsClO}_4$	225	577	577	650
$\text{CsClO}_4\text{-MnO}_2$	228	522	522	642

The initial endotherm for each  $\text{MClO}_4$  salt but  $\text{LiClO}_4$  denotes a reversible crystallographic transition from the rhombic to the cubic form. The initial endotherm for  $\text{LiClO}_4$  corresponds to its congruent melting point (247°). By using accurately weighed

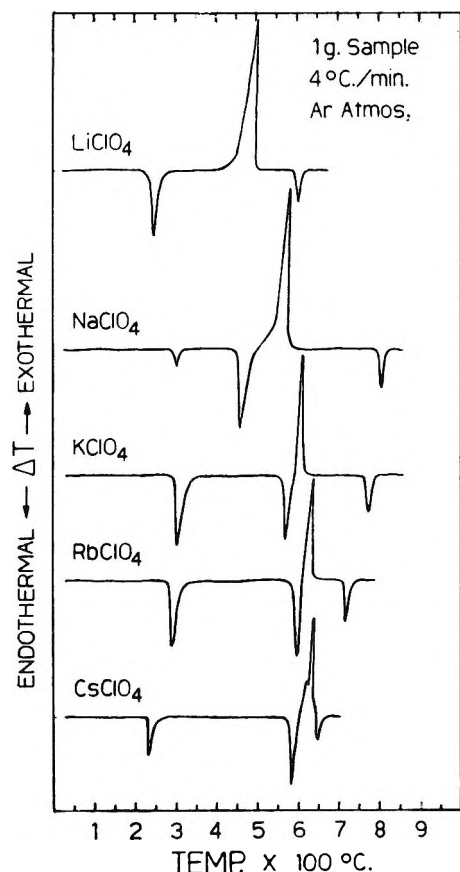


Figure 1. D.t.a. curves for pure alkali metal perchlorates.

**Table II:** Thermal Behavior of  $\text{MClO}_4$  Salts and of 90 Mole %  $\text{MClO}_4$ -10 Mole %  $\text{MnO}_2$  Mixtures from T.g.a. Experiments

Sample	2% dec. temp., °C.	% wt. loss of $\text{MClO}_4$ based on conversion to MCl	$\text{Cl}_2$ evolution, % of total available Cl
$\text{LiClO}_4$	470	103.0	1.22
$\text{LiClO}_4\text{-MnO}_2$	402	102.2	3.81
$\text{NaClO}_4$	522	102.4	0.20
$\text{NaClO}_4\text{-MnO}_2$	440	101.5	Trace
$\text{KClO}_4$	583	101.5	Variable: none or a faint trace
$\text{KClO}_4\text{-MnO}_2$	477	100.6	Trace
$\text{RbClO}_4$	611	101.9	None
$\text{RbClO}_4\text{-MnO}_2$	485	100.6	Trace
$\text{CsClO}_4$	601	101.6	None
$\text{CsClO}_4\text{-MnO}_2$	466	100.7	None

(6) A. Glasner and A. E. Simchen, *Bull. soc. chim. France*, 233 (1951).

(7) A. E. Simchen, *J. Phys. Chem.*, **65**, 1093 (1961).

(8) J. A. Burrows and F. E. Brown, *J. Am. Chem. Soc.*, **48**, 1790 (1926).

(9) H. A. Neville, *ibid.*, **45**, 2330 (1923).

(10) F. E. Brown, J. A. Burrows, and H. M. McLaughlin, *ibid.*, **45**, 1343 (1923).

(11) H. M. McLaughlin and F. E. Brown, *ibid.*, **50**, 782 (1928).

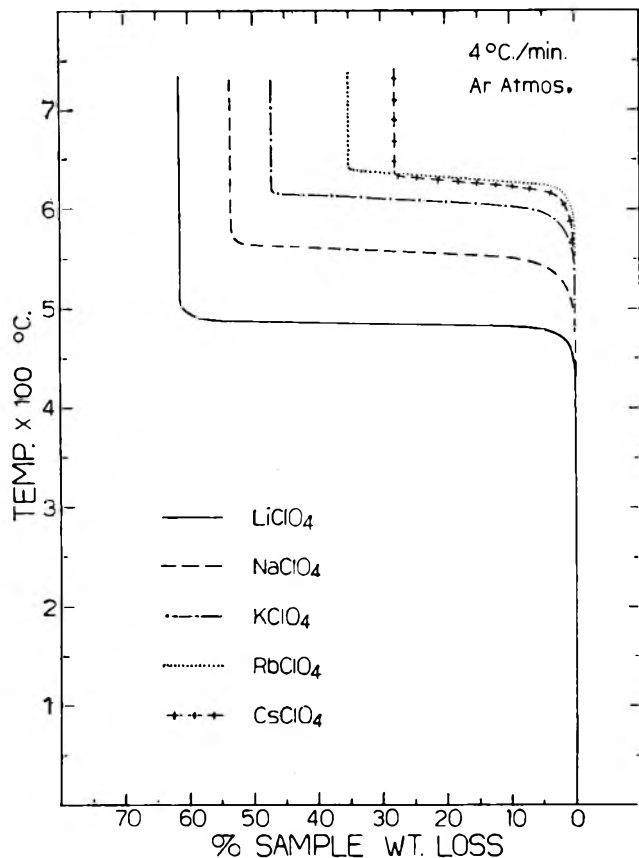


Figure 2. T.g.a. curves for pure alkali metal perchlorates.

$MClO_4$  samples during each d.t.a. run in combination with the known value of the heat of transition of  $KClO_4$  (3.29 kcal./mole),<sup>12</sup> it was possible to estimate the heats of transition of  $NaClO_4$  ( $0.6 \pm 0.1$  kcal./mole),  $RbClO_4$  ( $3.0 \pm 0.1$  kcal./mole), and  $CsClO_4$  ( $2.0 \pm 0.2$  kcal./mole). For  $NaClO_4$ ,  $KClO_4$ ,  $RbClO_4$ , and  $CsClO_4$  the succeeding endotherm refers to fusion of the  $MClO_4$  salt together with any of the decomposition products which have accumulated up to that temperature. The t.g.a. data indicate some small weight losses for these materials within the range of the fusion temperatures. To confirm the concordance of fusion and decomposition phenomena for these substances, they were heated as in a d.t.a. experiment close to their fusion temperatures, and the clear melts were then removed from the furnace, quenched, and analyzed; the results obtained are presented in Table III. As seen,  $KClO_4$ ,  $RbClO_4$ , and  $CsClO_4$  have undergone appreciable decomposition coincident with fusion;  $NaClO_4$  is but slightly decomposed. That  $NaClO_4$  decomposes at a slow but significant rate upon fusion was further demonstrated in the present study by maintaining a sample for 48 hr. at  $470^\circ$ , after which period the compound had decomposed to  $NaCl$  to the extent of 98.8%. The

Table III: Compositions of Fused, Quenched  $MClO_4$  and of 90 Mole %  $MClO_4$ -10 Mole %  $MnO_2$  Residues near Fusion Temperatures

$MClO_4$	Temp., °C.	Mole fraction		
		$MClO_4$	$MClO_3$	$MCl$
$NaClO_4$	469	0.9929	0.0000	0.0071
90% $NaClO_4$ -10% $MnO_2$	458	0.9698	0.0001	0.0301
$KClO_4$	584	0.8623	0.0558	0.0819
90% $KClO_4$ -10% $MnO_2$	539	0.8082	0.0187	0.1731
$RbClO_4$	595	0.8877	0.0335	0.0788
90% $RbClO_4$ -10% $MnO_2$	564	0.7837	0.0542	0.1621
$CsClO_4$	573	0.9550	0.0232	0.0218
90% $CsClO_4$ -10% $MnO_2$	535	0.8394	0.0056	0.1550

considerable thermal stability of molten  $LiClO_4$  near its melting point has been abundantly proven.<sup>13</sup> The presence of chlorate in the residues of Table III is consistent with the known thermal decomposition behavior of  $MClO_4$  compounds. Indeed, it can be considered virtually axiomatic in the chemistry of pure  $MClO_3$  and  $MClO_4$  compounds that at decomposition temperatures the presence of one also betokens the presence of the other.<sup>2,12,14,15</sup>

It is significant to note that the observed fusion temperatures of  $NaClO_4$ ,  $KClO_4$ ,  $RbClO_4$ , and  $CsClO_4$  are functions of the heating rate used. This dependency would, in part, account for the diversity of values given in the literature for the liquefaction of many thermally unstable materials. Thus, in the present investigation, 1-g. samples of  $KClO_4$  heated over the range of  $10^\circ/\text{min.}$  to  $1^\circ/\text{min.}$  gave a spread of  $20^\circ$  for the fusion temperature, this temperature decreasing with decreasing heating rate. Clearly then, the heating rate determines the average residence time at any temperature and thereby the extent of decomposition occurring up to the liquidus temperature of the reaction residue formed. Accordingly, for thermally unstable materials of this type, neglecting heat-transfer effects, a rapid heating rate would approach the fusion temperature more closely than a slow heating rate.

Each of the d.t.a. curves of Figure 1 manifests an exotherm in the higher temperature regions which is associated with the major portions of the thermal decomposition processes of the perchlorate salt to produce ultimately the corresponding metal chloride ( $MCl$ ).

(12) K. A. Hofmann and P. H. Marian, *Sitzber. preuss. Akad. Wiss. Physik. Math. Kl.*, 448 (1932).

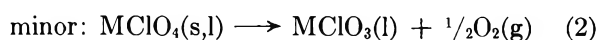
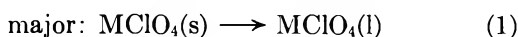
(13) M. M. Markowitz, *J. Phys. Chem.*, **62**, 827 (1958).

(14) A. E. Harvey, C. J. Wassink, T. A. Rodgers, and K. H. Stern, *Ann. N. Y. Acad. Sci.*, **78**, 971 (1960).

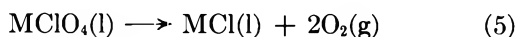
(15) M. M. Markowitz, D. A. Boryta, and H. Stewart, Jr., *J. Chem. Eng. Data*, **9**, 573 (1964).

The temperature intervals ( $T_r - T_f$ ) between fusion ( $T_f$ ) and the onset of rapid decomposition ( $T_r$ ) follow the order Li ( $191^\circ$ ) > Na ( $57^\circ$ ) > K, Rb, Cs =  $0^\circ$  and the sequence of thermal stabilities from Table I is found to be Li < Na < Cs < K < Rb. This order follows the order of fusion temperatures under the prevailing thermal treatment rather than the anticipated order of stabilities based solely on considerations of polarizing power<sup>5</sup> as occasioned by the steadily decreasing ionic potential in passing from Li<sup>+</sup> to Cs<sup>+</sup>.

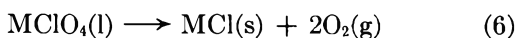
The reactions observed for each of the MClO<sub>4</sub> salts but LiClO<sub>4</sub> during fusion can be represented by the over-all equations



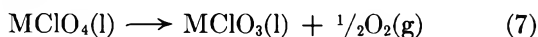
These equations are followed with rising temperature by the processes giving rise to the succeeding exotherm which encompasses the reactions



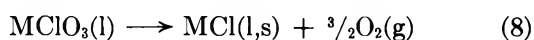
followed by



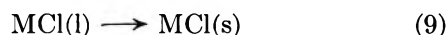
each concomitant with



and



and simultaneously with reaction 6



At decomposition temperatures, molten LiClO<sub>4</sub> would exhibit substantially the same series of events, *i.e.*, reactions 5-9; LiClO<sub>3</sub> is known to be an intermediate in the thermal decomposition of LiClO<sub>4</sub>. Reaction 1 is, of course, endothermic as is reaction 2 for all the MClO<sub>4</sub> compounds, a conclusion reached from estimates of their heats of reaction.<sup>15</sup> Thus, the fusion endotherms for NaClO<sub>4</sub>, KClO<sub>4</sub>, RbClO<sub>4</sub>, and CsClO<sub>4</sub> represent the resultant of two endothermic processes (reactions 1 and 2) and two exothermic processes (reactions 3 and 4). The composite decomposition exotherms encompassing eq. 5-9 are consistent with the exothermic natures of reactions 5, 6, 8, and 9 as moderated by the occurrence of endothermic reaction 7 to but a slight degree. Calculations based on available high-temperature heat of formation data for

LiClO<sub>4</sub>, NaClO<sub>4</sub>, and KClO<sub>4</sub> permit verification of this latter statement.<sup>15,16</sup> It would be anticipated that reaction 6 is more exothermic than reaction 5 by approximately the magnitude of the heat of fusion of the respective chloride (*viz.*, LiCl (4.74 kcal./mole), NaCl (6.85 kcal./mole), KCl (6.28 kcal./mole), RbCl (4.40 kcal./mole), and CsCl (3.60 kcal./mole)). However, the d.t.a. exotherms would appear to indicate no discontinuities at any point which could be attributed to augmented heat release due to reaction product crystallization (eq. 6, 8, and 9). Generalizing from the phase diagram for the system KClO<sub>4</sub>-KCl (KClO<sub>3</sub>) constructed from the compositions of decomposed KClO<sub>4</sub> samples at different temperatures,<sup>17</sup> it would seem that the onset of KCl precipitation occurs quite close to the virtual completion of KClO<sub>4</sub> decomposition by reaction 5. This is due to the increasing solubility with rising temperature of the KCl in the decomposing liquid KClO<sub>4</sub>-KCl (KClO<sub>3</sub>) solution. Furthermore, thermodynamic considerations show that the exothermicity of reaction 5 is, at reaction temperatures, about the same magnitude as for process 9. Reaction 6 is expected to occur to only a small extent and therefore its high level of heat release would make but a small contribution to the over-all enthalpy change. Accordingly, the heat evolution during the latter part of perchlorate decomposition attributable to reactions 6, 8, and 9 stems primarily from reaction 9, *i.e.*, reaction product crystallization. Thus, the observed exotherm is smooth and indicates no significantly different levels of heat release.

A resolution of the decomposition exotherm for KClO<sub>4</sub> has been claimed through the use of small sample sizes (0.086 g.) and bare thermocouples.<sup>18</sup> However, the possible catalytic effects of oxide-coated surfaces of the chromel-alumel sensors on the course of KClO<sub>4</sub> decomposition were not determined.<sup>15</sup> In addition, during the present investigation sample sizes from 3 to 0.1 g. of KClO<sub>4</sub> in d.t.a. experiments with shielded thermocouples yielded substantially identical thermograms without further resolution of the decomposition exotherm.

Both the final endotherms from the d.t.a. data (Table I) and the aggregate weight losses from the t.g.a. results (Table II) show that the final decomposition products of the MClO<sub>4</sub> salts are preponderantly the corresponding MCl compounds. The somewhat higher

(16) Dow Chemical Co., "Joint Army-Navy-Air Force Thermochemical Tables," Supplements of Dec. 31, 1960, Dec. 31, 1961, June 30, 1962, and June 30, 1963, Midland, Mich.

(17) A. E. Harvey, Jr., M. T. Edmison, E. D. Jones, R. A. Seybert, and K. A. Catto, *J. Am. Chem. Soc.*, **76**, 3270 (1954).

(18) D. A. Anderson and E. S. Freeman, *Nature*, **195**, 1297 (1962).

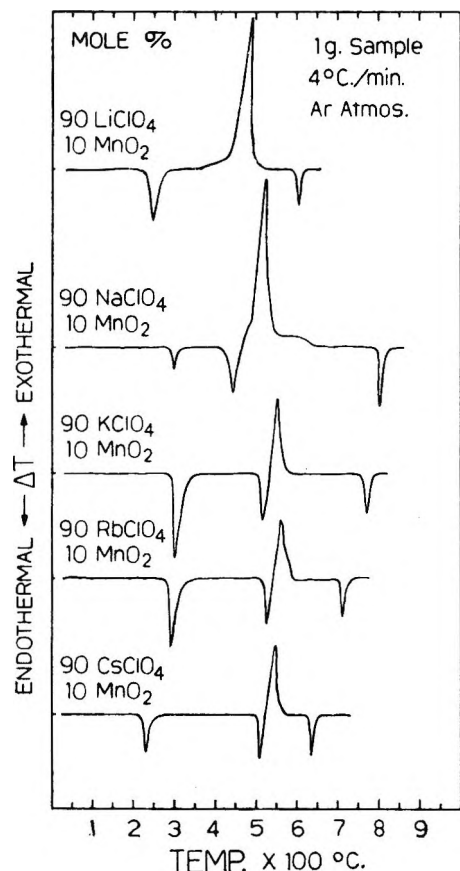


Figure 3. D.t.a. curves for 90 mole %  $MClO_4$ -10 mole %  $MnO_2$  mixtures.

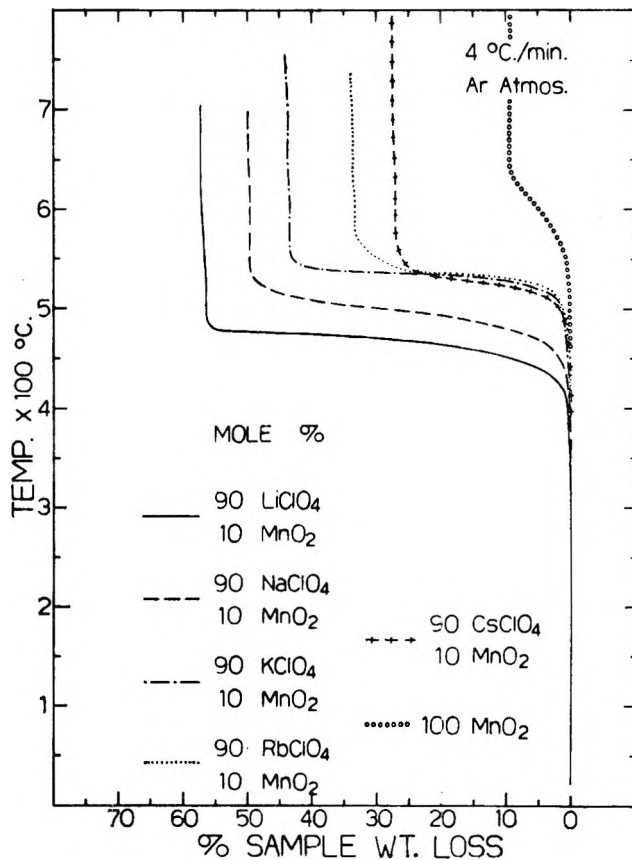


Figure 4. T.g.a. curves for 90 mole %  $MClO_4$ -10 mole %  $MnO_2$  mixtures.

than theoretical weight losses for the  $MClO_4$  compounds are due in part to loss of sample by carryover during the turbulent decomposition reactions.

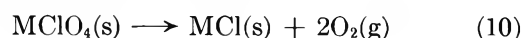
*Thermal Profiles of 90 Mole %  $MClO_4$ -10 Mole %  $MnO_2$  Mixtures.* The pertinent data obtained from the d.t.a. (Figure 3) and t.g.a. (Figure 4) curves for these mixtures are summarized in Tables I and II, respectively.

The d.t.a. curves for the mixtures with catalyst (Figure 3) show a number of pronounced differences upon comparison with the corresponding curves for the pure  $MClO_4$  compounds. The liquidus temperatures for  $NaClO_4$ - $MnO_2$ ,  $KClO_4$ - $MnO_2$ ,  $RbClO_4$ - $MnO_2$ , and  $CsClO_4$ - $MnO_2$  are considerably lower than for the pure perchlorate salts, thereby indicating that up to fusion, considerably greater perchlorate decomposition has occurred in the mixtures. Furthermore, the fusion endotherms are smaller than would be expected merely on the basis of sample dilution by an inert, infusible substance. Thus, it appears that the fusion endotherms are composites of the endothermic phase transition from the solid to the liquid state

(reaction 1) but decreased in magnitude by an augmented extent to occurrence of the exothermic reaction 3. In the same vein the successive decomposition exotherms are smaller in both peak temperature achieved and in over-all heat release, thereby also substantiating the greater degree of decomposition during fusion. These interpretations are reflected in the data of Table III where at appreciably lower temperatures the  $MClO_4$ - $MnO_2$  samples have decomposed to a greater extent than have the pure  $MClO_4$  salts.

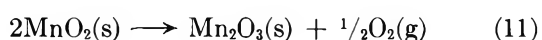
The data from the t.g.a. experiments (Table II) indicate the occurrence of considerable solid-state decomposition of  $NaClO_4$ ,  $KClO_4$ ,  $RbClO_4$ , and  $CsClO_4$  in admixtures with  $MnO_2$  prior to fusion inasmuch as the 2% decomposition temperatures are appreciably below the observed d.t.a.-determined fusion temperatures. Despite the low melting points<sup>2</sup> for  $NaClO_3$  (263°),  $KClO_3$  (357°),  $RbClO_3$  (342°), and  $CsClO_3$  (388°), it is unlikely that any liquid  $MClO_3$  will accumulate in the pre-bulk fusion decomposition stage because of the relative ease of catalysis of chlorate decomposition by the  $MnO_2$  present<sup>2</sup>; rather, in this

region it is felt that the decomposition of the  $\text{MClO}_4$  salts follows essentially the reaction



It should be noted that the  $[\text{MClO}_3/\text{MCl}]$  ratios at fusion for the  $\text{MnO}_2$ -containing mixtures of Table III are lower than for the pure salts.

As the final reaction product endotherms (Figure 3, Table I) and t.g.a. weight loss data (Figure 4, Table II) indicate, the corresponding chlorides constitute the final decomposition products of the  $\text{MClO}_4$  compounds. The total weight losses were corrected to account for the reaction



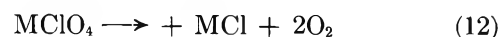
which is known to go to completion at about  $650^\circ$  under the conditions employed in the present study (Figure 4). The reaction product ( $\text{Mn}_2\text{O}_3$ ) was identified by chemical and X-ray analyses.

The clear, colorless aqueous extracts from the residues of the catalyzed mixtures of Table III were qualitatively tested for water-soluble Mn by treatment with  $\text{KIO}_4$  and dilute  $\text{H}_2\text{SO}_4$ , followed by boiling. No water-extractable Mn was found, thereby indicating that manganates and permanganates were not formed in the course of catalysis up to this point and that the catalytic action of the  $\text{MnO}_2$  probably proceeded heterogeneously on the catalyst surface with little or no contribution from homogeneous solution catalysis, unlike the effects found for  $\text{KClO}_3$ - $\text{MnO}_2$  mixtures.<sup>19</sup> X-Ray powder patterns from the mixtures of Table III showed that the  $\text{MnO}_2$  was unaltered. Similar behavior was found for the aqueous extract and residual catalyst from a  $\text{LiClO}_4$ - $\text{MnO}_2$  sample heated up to  $402^\circ$  and then quenched.

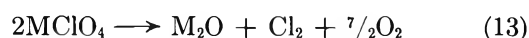
In another series of experiments, each of the five  $\text{MClO}_4$ - $\text{MnO}_2$  mixtures was decomposed at about  $600^\circ$  under flowing Ar, cooled, and then extracted with water. Only the  $\text{LiClO}_4$ - $\text{MnO}_2$  mixture showed the presence of water-soluble Mn. X-Ray powder patterns of the catalyst from this decomposed sample showed the presence of some  $\text{Mn}(\text{OH})_2$ , probably stemming from the hydrolysis of  $\text{LiMnO}_2$ , the formation of which will be discussed in a later section; the X-ray patterns from the other catalyst residues corresponded to unchanged pyrolusite. Thus, for  $\text{NaClO}_4$ ,  $\text{KClO}_4$ ,  $\text{RbClO}_4$ , and  $\text{CsClO}_4$ , catalytic decomposition by  $\text{MnO}_2$  appears to involve primarily heterogeneous effects, while in the case of  $\text{LiClO}_4$  some catalyst solution effects in the melt also seem probable. It should be noted that some type of specific interaction between  $\text{LiClO}_4$  and  $\text{MnO}_2$  is indicated by the enhanced  $\text{Cl}_2$  release during decomposition in the presence of the

catalyst (Table II). This aspect will be covered in greater detail subsequently.

*Chlorine Evolution from Decomposing Perchlorate Melts.* As evidenced from the d.t.a. and t.g.a. studies, the preponderant decomposition reactions of the  $\text{MClO}_4$  compounds are such as to follow the general equation



Indeed this would be anticipated on the basis of the greater thermodynamic stabilities of the product chlorides over the equivalent oxides which would be produced by the alternate mode of decomposition as represented by



Nevertheless, as shown in the last column of Table II, reaction 13 does occur to some small extent for all but pure  $\text{RbClO}_4$  and  $\text{CsClO}_4$  and for all the  $\text{MClO}_4$ - $\text{MnO}_2$  mixtures except  $\text{CsClO}_4$ - $\text{MnO}_2$ .

The instances of  $\text{LiClO}_4$  and of the  $\text{LiClO}_4$ - $\text{MnO}_2$  sample were studied most intensively and extensively because the  $\text{Cl}_2$  evolution phenomenon appeared greatest here. The entry of 1.22% in Table II for  $\text{LiClO}_4$  represents the average of 18 determinations with an average deviation of  $\pm 0.16\%$ . The extent of  $\text{Cl}_2$  release appears to be relatively independent of the average rate of  $\text{LiClO}_4$  decomposition. This was shown by decomposing samples of  $\text{LiClO}_4$  in isothermal experiments at  $50^\circ$  intervals over the temperature range from  $400$  to  $700^\circ$ . In these experiments the average degree of  $\text{Cl}_2$  evolution was  $1.22 \pm 0.22\%$  (average of 11 runs). Interestingly, attempts to secure an alkali balance concordant with the  $\text{Cl}_2$  release were unsuccessful. Thus in 12 experiments only  $42.8 \pm 6.2\%$  of the  $\text{Li}_2\text{O}$  could be titrated with standard  $0.1 N$   $\text{HCl}$ , thereby suggesting attack of the silica structure of the container surfaces by the base liberated at the high temperatures.

Previous workers had found that  $\text{BaO}_2$  was effective in eliminating  $\text{Cl}_2$  release from burning halate and perchlorate-metal fuel composites.<sup>20,21</sup> Accordingly, it was shown subsequently that  $\text{Cl}_2$  release from decomposing  $\text{LiClO}_4$  could be completely suppressed by the incorporation of 5 wt. %  $\text{Li}_2\text{O}_2$  or its equivalent of  $\text{Li}_2\text{O}$ ,  $\text{LiOH}$ ,  $\text{Na}_2\text{O}_2$ , or  $\text{Li}_2\text{CO}_3$ . However, in silica containers such suppression was usually obtained only after the container had first been pretreated with a

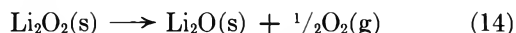
(19) J. M. Gaidis and E. G. Rochow, *J. Chem. Educ.*, **40**, 78 (1963).

(20) W. H. Schechter, R. R. Miller, R. M. Bovard, C. B. Jackson, and J. R. Pappenheimer, *Ind. Eng. Chem.*, **42**, 2348 (1950).

(21) J. F. O'Brien, *Proc. Iowa Acad. Sci.*, **66**, 194 (1959).

reaction mixture at decomposition temperatures when but about 0.2% Cl<sub>2</sub> was released; succeeding experiments with base-containing LiClO<sub>4</sub> in the same container always gave Cl<sub>2</sub>-free O<sub>2</sub>. Clearly then some interaction between the glass surface and the LiClO<sub>4</sub> is indicated. No Cl<sub>2</sub> was obtained from reaction of 80 mole % LiClO<sub>4</sub> (5 wt. % Li<sub>2</sub>O<sub>2</sub>)-20 mole % Mn mixtures when held in stainless steel vessels.<sup>22</sup>

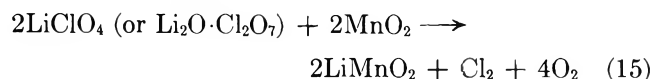
D.t.a. and t.g.a. experiments showed that the presence of oxide-producing substances in LiClO<sub>4</sub> drastically reduced the thermal stability of the perchlorate. Thus, the 2% decomposition temperature of LiClO<sub>4</sub> dropped from 470 to 281° (5.0 wt. % Li<sub>2</sub>O<sub>2</sub>), 306° (4.35 wt. % Li<sub>2</sub>O), 311° (8.11 wt. % Na<sub>2</sub>O<sub>2</sub>), 410° (5.21 wt. % LiOH), and 431° (7.89 wt. % Li<sub>2</sub>CO<sub>3</sub>). Except for the inversion of Li<sub>2</sub>O<sub>2</sub> and Li<sub>2</sub>O, this is the order of ease of formation of O<sup>2-</sup> ions from the various anions. The decomposition accelerating effects due to the presence of base in MClO<sub>3</sub> and MClO<sub>4</sub> melts had been previously noted for KClO<sub>4</sub>,<sup>17,19</sup> NaClO<sub>4</sub> and NaClO<sub>3</sub>,<sup>23</sup> and KClO<sub>3</sub>.<sup>24</sup> The promotion of LiClO<sub>4</sub> pyrolysis by Li<sub>2</sub>O was further demonstrated in some isothermal experiments. Thus, samples containing 90 wt. % LiClO<sub>4</sub>-10 wt. % Li<sub>2</sub>O heated for 20-, 30-, and 60-min. periods at 336° under flowing Ar showed, respectively, 13.0, 56.9, and 89.2% losses of LiClO<sub>4</sub> content, whereas pure LiClO<sub>4</sub> similarly heated for 1 hr. showed no change in LiClO<sub>4</sub> assay. In addition, each of the samples containing Li<sub>2</sub>O showed the presence of trace amounts of O<sub>2</sub><sup>2-</sup> ion after heating as determined by the Ti(SO<sub>4</sub>)<sub>2</sub>-H<sub>2</sub>SO<sub>4</sub> and KMnO<sub>4</sub> tests for H<sub>2</sub>O<sub>2</sub>. Similarly, a sample of 95 wt. % LiClO<sub>4</sub>-5 wt. % Li<sub>2</sub>O maintained at 275° for 16 hr. under flowing Ar was 13.2% decomposed with respect to LiClO<sub>4</sub> content; pure LiClO<sub>4</sub> under the same heating conditions is unchanged.<sup>13</sup> The heated LiClO<sub>4</sub>-Li<sub>2</sub>O sample was found to contain O<sub>2</sub><sup>2-</sup> ion. Li<sub>2</sub>O<sub>2</sub> itself starts to decompose rapidly at about 300° as per<sup>25</sup>



It should be noted that the formation of O<sub>2</sub><sup>2-</sup> ions has been conjectured to account for the catalysis of the thermal decomposition of KClO<sub>4</sub> by MgO<sup>17</sup> and of NaClO<sub>3</sub> and NaClO<sub>4</sub> by NaOH.<sup>23</sup> However, these experiments with LiClO<sub>4</sub> appear to be the first to demonstrate the formation of O<sub>2</sub><sup>2-</sup> ions in a decomposing perchlorate melt.

Of considerable interest is the ability of Li<sub>2</sub>O<sub>2</sub> additions to LiClO<sub>4</sub>-MnO<sub>2</sub> mixtures to counterbalance the tendency for enhanced Cl<sub>2</sub> evolution due to the presence of the MnO<sub>2</sub> (Table II). Thus, but 0.20% Cl<sub>2</sub> was obtained from the LiClO<sub>4</sub> in a 90 mole % (5 wt. % Li<sub>2</sub>O<sub>2</sub>)-10 mole % MnO<sub>2</sub> mixture, whereas the 90 mole

% LiClO<sub>4</sub>-10 mole % MnO<sub>2</sub> mixture alone yielded 3.81% Cl<sub>2</sub> upon decomposition. It is known from the combustion of 80 mole % LiClO<sub>4</sub>-20 mole % Mn and 80 mole % LiClO<sub>4</sub> (5 wt. % Li<sub>2</sub>O<sub>2</sub>)-20 mole % Mn mixtures that the final combustion product residue contains, in part, lithium manganite, LiMnO<sub>2</sub>,<sup>22</sup> in addition to MnO and Mn<sub>3</sub>O<sub>4</sub>. This observation would lead to the conclusion that the promotion of Cl<sub>2</sub> production from LiClO<sub>4</sub> by MnO<sub>2</sub> is due to a specific interaction stemming from the amphoteric nature of the Mn compound so that an acid-base reaction of the type below may proceed to some extent at these elevated temperatures.



Clearly, in the presence of added Li<sub>2</sub>O equivalents, the Cl<sub>2</sub> may be removed by virtue of the combination



or the MnO<sub>2</sub> may react directly with the Li<sub>2</sub>O present,<sup>26</sup> viz.



In any case, it is probably the LiMnO<sub>2</sub> that leads to the presence of water-soluble Mn in the extracts from LiClO<sub>4</sub>-MnO<sub>2</sub> residues formed at high temperatures.

### Discussion of Results

The d.t.a. curves (Figures 1 and 3) demonstrate that the thermal decompositions of MClO<sub>4</sub> compounds are exothermic, as are the decompositions of heavy metal azides and fulminates, rather than endothermic, as characterizes many other pyrolysis reactions which yield both a condensed phase residue and a gas as reaction products (*e.g.*, the decompositions of salt hydrates, hydroxides, peroxides, carbonates, sulfates, etc.). The common characteristics for such exothermic decompositions appear to be both a highly favorable negative free energy change for the reaction path manifested in contrast to the equilibrium type dissociation reactions of the endothermic decompositions (*i.e.*,  $\Delta F^\circ \cong 0$ ) and a change in the oxidation states

(22) M. M. Markowitz and E. W. Dezmelyk, "A Study of the Application of Lithium Chemicals to Air Regeneration Techniques in Manned, Sealed Environments," Technical Documentary Report No. AMRL-TDR-64-1, Wright-Patterson Air Force Base, Ohio, Feb. 1964.

(23) R. P. Seward and H. W. Otto, *J. Phys. Chem.*, **65**, 2078 (1961).

(24) G. J. Fowler and J. Grant, *J. Chem. Soc.*, **57**, 272 (1890).

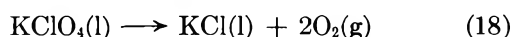
(25) T. V. Rode, T. A. Dobrynina, and G. A. Gol'der, *Izv. Akad. Nauk SSSR, Otd. Khim.*, 611 (1955).

(26) W. D. Johnston and R. R. Heikes, *J. Am. Chem. Soc.*, **78**, 3255 (1956).

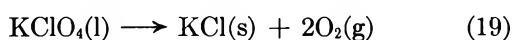


of the constituent atoms of the disrupted anion (*viz.*, for  $\text{ClO}_4^-$ ,  $\text{Cl}^+ \rightarrow \text{Cl}^-$ , and  $\text{O}^{2-} \rightarrow \frac{1}{2}\text{O}_2$ ).

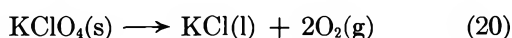
The signs of the enthalpy changes accompanying the thermal breakdown of  $\text{KClO}_4$  have been a matter of some dispute.<sup>18,27</sup> However, recently available high-temperature enthalpy data<sup>16</sup> have permitted more exact calculations which are in substantial agreement with the d.t.a. behavior observed in the present study. At rapid decomposition the bulk of the pyrolysis occurs through the reactions



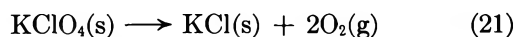
and



The heat of formation of liquid  $\text{KClO}_4$  is not known but estimated heat of formation data are available for solid  $\text{KClO}_4$  up to 1500°K. Thus, the heats of reaction ( $\Delta H_r^\circ$ ) for the changes



and



may be computed. Taking an average reaction temperature of 900°K.,  $\Delta H_r^\circ(20) = -4.50$  kcal./mole and  $\Delta H_r^\circ(21) = -10.51$  kcal./mole. Inasmuch as the change

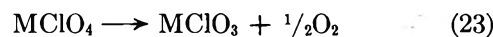


is endothermic,  $\Delta H_r^\circ(18)$  and  $\Delta H_r^\circ(19)$  will be more exothermic than  $\Delta H_r^\circ(20)$  and  $\Delta H_r^\circ(21)$  by the heat of fusion of  $\text{KClO}_4$  at 900°K. Assuming a reasonably low entropy of fusion for  $\text{KClO}_4$  (2.5 e.u.)<sup>28</sup> because of the crystallographic transition,  $\Delta H_r^\circ(22) = 2.3$  kcal./mole; thus,  $\Delta H_r^\circ(18) = -6.8$  kcal./mole and  $\Delta H_r^\circ(19) = -12.8$  kcal./mole. As noted earlier,  $\Delta H_r^\circ(18) \cong -\Delta H^\circ_{\text{fusion}}(\text{KCl}) \cong -6$  kcal./mole.

It is of interest to contrast the thermal behavior of  $\text{MClO}_4$  compounds with that of the corresponding  $\text{MClO}_3$  salts.<sup>2,15</sup> Thus, the latter possess congruent melting points whereas the former, except for  $\text{LiClO}_4$ , concomitantly fuse and decompose. Both  $\text{LiClO}_4$  and  $\text{LiClO}_3$ , however, manifest the longest intervals between congruent melting and the onset of rapid decomposition when compared with the other alkali metal derivatives. It seems clear then that the melting points observed for  $\text{NaClO}_4$ ,  $\text{KClO}_4$ ,  $\text{RbClO}_4$ , and  $\text{CsClO}_4$  are functions of the extents of decomposition up to the liquidus temperatures observed and as such are dependent on the experimental techniques employed and the thermal history of the samples used.<sup>7</sup>

Rapid decomposition of the heavier  $\text{MClO}_4$  salts sets in after fusion of the solid perchlorates for both the pure materials (Figure 1, Table I) and for the  $\text{MClO}_4$ - $\text{MnO}_2$  mixtures (Figure 3, Table I). This type of behavior would indicate that increased anion mobility facilitates the pyrolytic processes, as pointed out in an earlier study.<sup>5</sup> The d.t.a. data give the order of thermal stability of the perchlorates as  $\text{Li} < \text{Na} < \text{Cs} < \text{K} < \text{Rb}$ , which conforms to the order of their fusion temperatures rather than to the inverse order of polarizing power or ionic potential of the cation. However, it may be seen that the degree of differentiation of thermal stability among  $\text{KClO}_4$ ,  $\text{RbClO}_4$ , and  $\text{CsClO}_4$  is small, despite the appreciable variation in cation size in proceeding from  $\text{K}^+$  (1.33 Å.) to  $\text{Cs}^+$  (1.65 Å.), so that the order  $\text{Li} < \text{Na} < \text{K}, \text{Rb}, \text{Cs}$  seems most generally appropriate. This is the conclusion reached from a similar study of the five  $\text{MClO}_3$  compounds<sup>2,15</sup> and suggests that for both chlorate and perchlorates a leveling effect in polarizing power occurs among the  $\text{M}^+$  ions for values of the ionic potential at and below that of  $\text{K}^+$ .

As would be anticipated, the  $\text{MClO}_4$  salts are thermally more stable than the corresponding chlorates.<sup>2,15</sup> Consequently, but small quantities of chlorate are formed in the course of  $\text{MClO}_4$  pyrolysis,<sup>7,12,14,17,29</sup> whereas the converse is true during the thermal decompositions of  $\text{MClO}_3$  compounds. Indeed, such behavior would tend to substantiate that the equilibrium



tends to lie to the left as indicated by thermodynamic considerations.<sup>15</sup> Furthermore, the smooth continuous nature of the perchlorate decomposition exotherms tends to rule out any substantial accumulation of  $\text{MClO}_3$  intermediate.

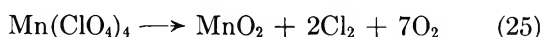
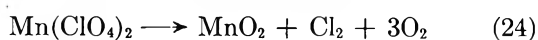
As with the pure  $\text{MClO}_4$  compounds, the order of thermal stability of the  $\text{MnO}_2$ -containing samples is best expressed as  $\text{Li} < \text{Na} < \text{K}, \text{Rb}, \text{Cs}$ . Qualitatively, the catalytic effects of  $\text{MnO}_2$  appear to be less pronounced with the  $\text{MClO}_4$  salts than with the  $\text{MClO}_3$  compounds. Thus, for example, for  $\text{NaClO}_4$ ,  $\text{KClO}_4$ ,  $\text{RbClO}_4$ , and  $\text{CsClO}_4$  the 2% decomposition temperatures are reduced about 100° whereas for the chlorates<sup>2</sup> the reduction is about 150° in the presence of  $\text{MnO}_2$ . In either instance, however, the mechanisms of the

(27) M. M. Markowitz, *J. Phys. Chem.*, **61**, 505 (1957).

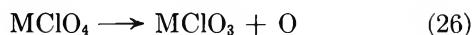
(28) R. R. Wenner, "Thermochemical Calculations," McGraw-Hill Book Co., New York, N. Y., 1941, pp. 23-26.

(29) A. Glasner and L. Weidenfeld, *J. Am. Chem. Soc.*, **74**, 2462, 2467 (1952).

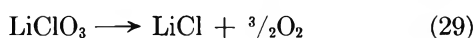
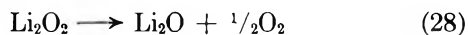
catalysis appear obscure at present. Thus, it has been suggested that a manganese chlorate or perchlorate is alternately formed and decomposed in the catalytic process.<sup>7</sup> However, the decomposition of a manganese perchlorate ( $\text{Mn}(\text{ClO}_4)_2$  or  $\text{Mn}(\text{ClO}_4)_4$ ) would be expected to yield  $\text{MnO}_2$  as a reaction product and thereby promote abundant evolution of  $\text{Cl}_2$  as per reactions 24 and 25,<sup>30</sup> a circumstance which has been shown not to prevail. Currently proposed mechanisms



for perchlorate decompositions appear to favor the production of O atoms as the primary pyrolytic step, *viz.*,<sup>5,14,17,29,31</sup>



Accordingly, it seems possible that the role of  $\text{MnO}_2$  as a catalyst is to favor the abstraction of atomic O, perhaps by formation of some transient peroxide derivative as is formed with the more basic oxides such as  $\text{Li}_2\text{O}$  and  $\text{MgO}$ . These more basic materials seem to function as more efficient catalysts for perchlorate decomposition than does  $\text{MnO}_2$  as clearly demonstrated in the present study with  $\text{LiClO}_4$  through the postulated reaction sequence

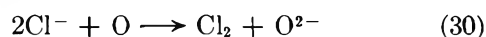


Virtually no information appears to be available concerning the catalytic activity of  $\text{MnO}_2$  as a function of its structural properties (*e.g.*, surface area and crystal form). Furthermore, a clear resolution between heterogeneous and homogeneous catalytic effects remains to be performed, although this investigation indicates homogeneous solution effects to be important only in the  $\text{LiClO}_4$ - $\text{MnO}_2$  system.

In addition to  $\text{O}^{2-}$  ion catalysis of the pyrolyses of  $\text{LiClO}_4$ ,  $\text{KClO}_4$ ,<sup>17</sup> and  $\text{NaClO}_4$ ,<sup>23</sup> there are a number of other pieces of evidence pointing to the existence of O atoms during the decompositions of  $\text{MClO}_4$  salts. The direct transfer of O atoms to Mn metal is suggested by the formation of  $\text{Mn}_3\text{O}_4$  in an 80 mole %  $\text{LiClO}_4$ -20 mole % Mn mixture maintained for several hours at 225°. The oxidation of the metal occurs apparently without liquid phase formation and without any loss in system weight.<sup>32</sup> The formation of reactive O atoms would also help to explain the low temperature pre-ignition reactions observed between  $\text{KClO}_4$  and various carbonaceous fuels where rapid

oxidation is found to occur considerably below the normal range of decomposition temperatures of the oxidant.<sup>33</sup> Furthermore, the oxidation of bromides and iodides to the respective halates by  $\text{KClO}_4$ ,<sup>29,34</sup> without appreciable  $\text{O}_2$  evolution points to direct O-transfer reactions. The inability to oxygenate chlorates to perchlorates by high-pressure treatment with molecular  $\text{O}_2$ ,<sup>15,35</sup> despite the favorable thermodynamic potential for such reactions would indicate the need for the participation of a kinetically more reactive form of oxygen to achieve the conversion.<sup>31</sup> In this same regard, it should be pointed out that despite the thermodynamic potential for oxygenation of  $\text{Li}_2\text{O}$  by molecular  $\text{O}_2$  at moderate pressures, it has not been possible to bring about this reaction by application of even very high pressures of  $\text{O}_2$ , whereas the peroxygenation of  $\text{Li}_2\text{O}$  can be performed in decomposing  $\text{LiClO}_4$  melts as demonstrated here. Thus, an appreciable body of chemical evidence exists to support the kinetic view for the presence of O atoms in decomposing perchlorates.<sup>14,17,29,31</sup>

For the pure  $\text{MClO}_4$  salts the degree of  $\text{Cl}_2$  release during decomposition follows the order  $\text{Li} \gg \text{Na} > \text{K} > \text{Rb}$ ,  $\text{Cs} = \text{O}$  (Table II). Of all the  $\text{MClO}_4$  compounds,  $\text{LiClO}_4$  is the only one for which conversion to oxide (reaction 13) is thermodynamically possible as well as the more familiar decomposition to chloride by reaction 12.<sup>36</sup> The preponderant occurrence of reaction 12 over reaction 13 is due to the greater thermodynamic stabilities of the  $\text{MCl}$  compounds relative to the equivalent oxides.<sup>36</sup> However, the mechanism by which the small amount of  $\text{Cl}_2$  is formed from the decomposing  $\text{MClO}_4$  compounds merits some further consideration. The presence of O atoms may cause a reaction such as



A more general explanation might be based on the autoionization of perchlorate melts, much as occurs with molten nitrates<sup>37,38</sup>

(30) J. G. F. Druce, *J. Chem. Soc.*, 966 (1938).

(31) K. H. Stern and M. Bufalini, *J. Phys. Chem.*, **64**, 1781 (1960).

(32) M. M. Markowitz, D. A. Boryta, and H. Stewart, Jr., "Generation of Oxygen Gas by the Combustion of Heterogeneous, Dilute Metal-Alkali Metal Perchlorate Mixtures," Preprint No. 63-504, American Institute of Aeronautics and Astronautics, Heterogeneous Combustion Conference, Palm Beach, Fla., Dec. 11-13, 1963.

(33) E. Hoffmann and S. Patai, *J. Chem. Soc.*, 1797 (1955).

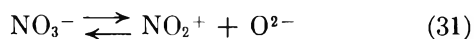
(34) A. Glasner and L. Weidenfeld, *Nature*, **166**, 109 (1950).

(35) M. Dode and J. Basset, *Bull. soc. chim. France*, [5] **2**, 344 (1935).

(36) M. M. Markowitz, *J. Inorg. Nucl. Chem.*, **25**, 407 (1963).

(37) J. M. Crewe, Fisons Fertilizer, Ltd., private communication.

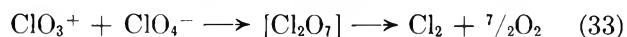
(38) R. W. Kust and F. R. Duke, *J. Am. Chem. Soc.*, **85**, 3338 (1963).



Thus, for the perchlorates the self-ionization equilibrium might be represented as



and  $\text{Cl}_2$  evolution would then ensue by the reaction



Such a mechanism would also be consistent with the oxide-donating or basic properties of perchlorates, so that an  $\text{O}^{2-}$  ion acceptor or acid would move reaction 32 to the right and thus increase the rate and extent of reaction 33. A number of investigators have

noted that catalysts for  $\text{MClO}_3$  and  $\text{MClO}_4$  decompositions can generally be divided into two categories: oxide catalysts (*e.g.*,  $\text{Fe}_2\text{O}_3$ ,  $\text{MnO}_2$ ,  $\text{Bi}_2\text{O}_3$ ,  $\text{CuO}$ ,  $\text{SnO}_2$ , etc.) which yield substantially  $\text{Cl}_2$ -free  $\text{O}_2$  and oxide catalysts (*e.g.*,  $\text{P}_2\text{O}_5$ ,  $\text{B}_2\text{O}_3$ ,  $\text{WO}_3$ ,  $\text{MoO}_3$ ,  $\text{V}_2\text{O}_5$ , etc.) which cause much  $\text{Cl}_2$  production. It now seems clear that the first group of materials represents true catalytic agents while the second group of substances are polymeric acids, capable of  $\text{O}^{2-}$  ion capture and thus enter into specific, irreversible chemical reactions with the Cl-containing oxy anions.

*Acknowledgment.* The aid and encouragement given by B. Schrier during the performance of this work are greatly appreciated.

## Remarks on Refractive Index Mixture Rules

by Wilfried Heller

*Department of Chemistry, Wayne State University, Detroit 2, Michigan (Received August 20, 1964)*

The most important refractive index mixture rules used for determining the refractive index of a solute are scrutinized regarding their relative merits and interrelations. The Dale-Gladstone and the Biot-Arago equations are found to follow from either the Lorentz-Lorenz equation or the Wiener equation if the solution is dilute and if, in addition, the refractive indices of solute and solvent are nearly the same. A mixture rule proposed by the writer represents the limiting form of the Wiener equation in case of dilute solutions without restriction as to the value of the refractive indices. The performance of all equations is tested on literature data. The results are in line with expectation on the basis of theoretical analysis. The special case of solutes of colloidal dimensions, where none of the equations applies satisfactorily, is briefly discussed.

It is often desirable to know the refractive index of a solute. This index can be derived from the refractive indices of solution and solvent on using a suitable "mixture rule." There are several available. Little is known about the conditions under which each may usefully be applied nor about their interrelation. The present paper deals with both problems.

*I. The Principal Mixture Rules.* Omitting mixture rules of minor significance one has the choice among eq. 1-5. Here,  $n_{12}$ ,  $n_1$ , and  $n_2$  are the refrac-

$$\frac{n_{12}^2 - 1}{n_{12}^2 + 2} = \phi \frac{n_1^2 - 1}{n_1^2 + 2} + \phi_2 \frac{n_2^2 - 1}{n_2^2 + 2} \quad (1)$$

$$\frac{n_{12}^2 - n_1^2}{n_{12}^2 + 2n_1^2} = \phi_2 \frac{n_2^2 - n_1^2}{n_2^2 + 2n_1^2} \quad (2)$$

$$\frac{n_{12} - n_1}{n_1} = \frac{3}{2} \phi_2 \left( \frac{m^2 - 1}{m^2 + 2} \right) \quad (3)$$

$$(n_{12} - 1) = \phi_1(n_1 - 1) + \phi_2(n_2 - 1) \quad (4)$$

$$n_{12} = \phi_1 n_1 + \phi_2 n_2 \quad (5)$$

tive indices of solution, solvent, and solute, respectively,  $\phi_1$  and  $\phi_2$  are the volume fractions of the respective components in the solution, and  $n = n_2/n_1$ . The volume fraction  $\phi_i$  may be obtained from either  $\phi_i = c_i/\rho_i$ , where  $c_i$  is the concentration in g./cm.<sup>3</sup> and  $\rho_i$  is the density of the  $i$ th component, or from  $\phi_i = p_i \rho_{ij}/\rho_i$ , where  $p_i$  is the weight fraction of the  $i$ th component and  $\rho_{ij}$ , the density of the mixture of the two components. Equations 1 and 4 are always found to be formulated in an alternate form, which is referred to as "specific refraction" (dimension cm.<sup>3</sup> g.<sup>-1</sup>)

$$\frac{(n_{12}^2 - 1)}{(n_{12}^2 + 2)} \frac{1}{\rho_{12}} = \frac{(n_1^2 - 1)}{(n_1^2 + 2)} \frac{p_1}{\rho_1} + \frac{(n_2^2 - 1)}{(n_2^2 + 2)} \frac{p_2}{\rho_2} \quad (1')$$

$$\frac{(n_{12} - 1)}{\rho_{12}} = \frac{(n_1 - 1)}{\rho_1} p_1 + \frac{(n_2 - 1)}{\rho_2} p_2 \quad (4')$$

The formulation given first which contains only dimensionless quantities is customary for the other three equations.

Equations 2 and 3 differ from the others by the absence of  $\phi_1$  in the formulation. They can therefore be strictly valid only in the case of volume additivity; *i.e.*, if  $\phi_1 = V_1^0/(V_1^0 + V_2^0)$ ,  $\phi_2 = V_2^0/(V_1^0 + V_2^0)$  where the superscript 0 defines the volumina of the components prior to mixing.

Equation 1', which is by far the best known, is due to Lorentz.<sup>1</sup> It is generally referred to as the Lorentz-Lorenz equation, although only the equation for a one-component system was derived independently by both authors.<sup>2</sup> Equation 2 is due to Wiener<sup>3</sup> and it is written here in the form which applies to isotropic bodies of spherically symmetrical shape and, in addition, in the best known simplified form which presupposes volume additivity. Equation 3 has been derived by the writer<sup>4</sup> on assuming equivalence of the light scattering equations of Debye<sup>5</sup> and Rayleigh.<sup>6</sup> Equations 4' and 5 are empirical equations, in contradistinction to those just mentioned. Of these, eq. 4' is widely known as the Dale-Gladstone<sup>7</sup> equation, although it follows directly from an equation given by Newton (prior to 1728)<sup>8</sup> and is identical with equations given by Beer<sup>9a</sup> and Landolt.<sup>9b</sup> Equation 5 finally has been proposed independently and repeatedly by at least five different authors, the earliest ones having been Arago and Biot.<sup>10</sup>

The theoretical mixture rules all have in common that they are based upon the electromagnetic theory

of light with the implicit restriction that the molecules (or particles) may be considered as dipoles or assemblies of dipoles induced by an external field. A series of failures of specific ones of these mixture rules reported in the literature is due to this restriction having been overlooked, others are due to the fact that other restrictions (homogeneous, undistorted electromagnetic field) had not been recognized (see section VIII).

II. *The Relation between Equations 1 and 2.* The major difference between eq. 1 and 2 is that the reference dielectric constant in the latter equation is that of the solvent,  $n_1^2$ , while in the former the reference is that of the vacuum,  $n_0^2 = 1.0$ . It is of interest to ascertain whether or when these two equations are equivalent. For this purpose, one has to transform the former for the case of volume additivity. On substituting in eq. 1  $(1 - \phi_2)$  for  $\phi_1$ , and on slight rearrangement, eq. 6

$$\frac{n_{12}^2 - 1}{n_{12}^2 + 2} - \frac{n_1^2 - 1}{n_1^2 + 2} = \phi_2 \left[ \frac{(n_2^2 - 1)}{(n_2^2 + 2)} - \frac{(n_1^2 - 1)}{(n_1^2 + 2)} \right] \quad (6)$$

results. Subsequent consolidation yields eq. 6a which,

$$\frac{3n_{12}^2 - 3n_1^2}{(n_{12}^2 + 2)(n_1^2 + 2)} = \phi_2 \left[ \frac{3n_2^2 - 3n_1^2}{(n_2^2 + 2)(n_1^2 + 2)} \right] \quad (6a)$$

after obvious cancellations, yields eq. 6b.

$$\frac{n_{12}^2 - n_1^2}{n_{12}^2 + 2} = \phi_2 \left( \frac{n_2^2 - n_1^2}{n_2^2 + 2} \right) \quad (6b)$$

Equations 2 and 6b are identical if and only if  $n_1$  approaches 1.0.

Equation 6b represents a relatively simple formulation of the Lorentz-Lorenz equation not given previously. It is of interest because its use involves fewer calculations than that of the original equation. On the other hand, it can give results identical with those of eq. 1 only if the solution process is accompanied by neither a contraction nor an expansion, *i.e.*, if the

- (1) H. A. Lorentz, "Theory of Electrons," Leipzig, 1906.
- (2) H. A. Lorentz, *Wied. Ann.*, **9**, 641 (1880); L. Lorenz, *ibid.*, **11**, 70 (1880).
- (3) O. Wiener, *Leipzig. Ber.*, **62**, 256 (1910).
- (4) W. Heller, *Phys. Rev.*, **68**, 5 (1945).
- (5) P. Debye, *J. Appl. Phys.*, **15**, 338 (1944).
- (6) Lord Rayleigh, see, *e.g.*, *Phil. Mag.*, **47**, 375 (1899).
- (7) D. Dale and F. Gladstone, *Phil. Trans.*, **148**, 887 (1858); **153**, 317 (1864).
- (8) See, *e.g.*, E. Mach, "Die Prinzipien der physikalischen Optik," Leipzig, 1921, Chapter IV.
- (9) (a) D. Beer, "Einleitung in die höhere Optik," 1853, p. 35; (b) H. H. Landolt, *Liebigs Ann. Chem. Suppl.*, **4**, 1 (1865).
- (10) D. F. J. Arago and J. B. Biot, *e.g.*, *Mém. acad. France*, **7** (1806).

volume of the solution is the sum of the volumes of the components prior to solution. The same restriction applies to the Wiener equation in the form given (eq. 2) and also to eq. 3.

Solving the Wiener equation for the refractive index of the solute, one obtains eq. 7 where  $\bar{V}$  is the partial

$$n_2^2 = \left[ \frac{(2/\bar{V})(dn/dc)(n_1 + n_{12}) + (n_{12}^2 + 2n_1^2)}{(n_{12}^2 + 2n_1^2) - (1/\bar{V})(dn/dc)(n_1 + n_2)} \right] n_1^2 \quad (7)$$

specific volume of the solute,  $c$  is the concentration of the solute in g./cm.<sup>3</sup> and  $(dn/dc)$  is the slope of  $(n_{12} - n_1)$  vs.  $c$  plots. This slope is constant at low  $c$  values. It is defined by eq. 8.

$$\frac{dn}{dc} = f(c) = \frac{(n_2^2 - n_1^2)(n_{12}^2 + 2n_1^2)\bar{V}}{(n_2^2 + 2n_1^2)(n_1 + n_{12})} \quad (8)$$

It is clear from these equations that  $n_2$  cannot be obtained from differential refractometric (interferometric) measurements of  $(n_{12} - n_1)$  alone if either the Lorentz-Lorenz or the Wiener equation is used. The explicit value of  $n_{12}$  must also be known.

III. *The Relation between Equations 4 and 5.* The very widely used Dale-Gladstone equation is found to be identical with Biot's eq. 5 if, in both cases, volume additivity is assumed. This follows quickly on replacing, in the former,  $(n_2 - 1)\phi_2$  by  $n_2\phi_2 + \phi_1 - 1$  and, in the latter,  $n_1\phi_1$  by  $n_1 - n_1\phi_2$ .

On solving either eq. 4 or 5 for  $n_2$ , on assuming such volume additivity, one obtains eq. 9. The slope of

$$n_2 = (1/\bar{V})(dn/dc) + n_1 \quad (9)$$

$(n_{12} - n_1)$  vs.  $c$  curves represents here, therefore, eq. 10.

$$(dn/dc) = \bar{V}(n_2 - n_1) = \bar{V}n_1(m - 1) \quad (10)$$

The Dale-Gladstone equation does not reduce to the Biot equation if volume additivity is not assumed. In that case

$$n_2 = \frac{\rho_2}{c_2} \left[ (n_{12} - 1) - \frac{\rho_{12}}{\rho_1} (n_1 - 1) \right] + \frac{\rho_2}{\rho_1} (n_1 - 1) \quad (11)$$

Equation 5, on the other hand, yields eq. 12. The

$$n_2 = \frac{\rho_2}{c_2} (n_{12} - \frac{\rho_{12}}{\rho_1} n_1) + \frac{\rho_2}{\rho_1} n_1 \quad (12)$$

expressions for  $dn/dc$  follow from eq. 11 and 12 as eq. 13 and 14, respectively.

$$\frac{dn}{dc} = \left( \frac{n_2 - 1}{\rho_2} \right) - \left( \frac{n_1 - 1}{\rho_1} \right) \quad (13)$$

$$\frac{dn}{dc} = \frac{n_2}{\rho_2} - \frac{n_1}{\rho_1} \quad (14)$$

In the general case of nonadditivity of volumes, the Dale-Gladstone equation differs therefore from the Biot equation. It will be noted, however, that both equations for  $dn/dc$  are identical, again, if  $\rho_2 \rightarrow \rho_1$ .

IV. *Equation 3 and Its Relation to Equations 4 and 5.* In order to determine  $n_2$  from eq. 3, it has to be rearranged to eq. 15 where  $A = 2/3\bar{V}$ . This is the form

$$n_2^2 = \frac{n_1^3 + 2An_1^2(dn/dc)}{n_1 - A(dn/dc)} \quad (15)$$

in which this equation was given originally<sup>4</sup> except for the use of the volume fraction,  $\phi_2$ , instead of  $c$  and  $\bar{V}$ . According to this equation the slope (eq. 16) is a con-

$$(dn/dc) = \frac{3}{2}\bar{V}n_1 \left( \frac{m^2 - 1}{m^2 + 2} \right) \quad (16)$$

stant like that of eq. 10, but differs from it in value. In contradistinction, the slope derived from eq. 8 varies with concentration, although the variation is only slight at low  $c$ .

The validity of eq. 15 was tested extensively<sup>4</sup> on systems where volume additivity should apply. The  $n_2$ -values obtained agreed with those calculated from the DG (Dale-Gladstone) equation if  $(n_2 - n_1)$  was small, but disagreed with the latter more the larger this difference. In view of the firm entrenchment of the DG equation, it was assumed without further scrutiny of the situation that this indicated a more restricted validity of eq. 3. This assumption overrated the performance of the DG equation and underrated that of eq. 3.

On assuming that  $n_2 \rightarrow n_1$ ,  $(m^2 - 1) \rightarrow 2(n_2 - n_1)/n_1$  and  $(m^2 + 2) = [(n_2^2 + 2n_1^2)/n_1^2] \rightarrow 3$  so that  $(m^2 - 1)/(m^2 + 2) \rightarrow 2(n_2 - n_1)/3n_1$ . Equation 16 therefore reduces to eq. 10 if  $n_2 \rightarrow n_1$ . Consequently, the DG equation formulated for volume additivity is a limiting case of eq. 3. The correction factors developed<sup>4</sup> for eq. 15 should therefore be used instead in order to correct data calculated from eq. 4 or 5.

V. *Relation between Equations 3 and 2.* If one operates in dilute solutions,  $n_{12} \rightarrow n_1$ . In that case, eq. 8 reduces to eq. 17. This becomes identical with

$$\frac{dn}{dc} = \frac{3}{2}\bar{V} \left( \frac{n_2^2 - n_1^2}{n_2^2 + 2n_1^2} \right) n_1 \quad (17)$$

eq. 16 on introducing  $m$  in place of the individual  $n$  values. Consequently, eq. 3 is simply a limiting form of the Wiener equation inasmuch as it applies only to dilute solutions. Since one will want to derive  $n_2$

from dilute solution only in order to avoid solute-solute interaction effects, this limitation of eq. 3 cannot be considered as a shortcoming. On the other hand, it has the important advantage over the Wiener equation that differential measurements of  $(n_{12} - n_1)$  are sufficient in order to derive either  $dn/dc$  or  $n_2$  values. Such differential measurements can be made with far higher precision than individual  $n$  measurements.

VI. *Relation between Equations 1' and 4'*. Of particular interest is the relation existing between the two best known mixture rules, that of Lorentz-Lorenz and Dale-Gladstone, on formulating them in the conventional manner as given by eq. 1' and 4', respectively. On assuming the solution to be very dilute ( $n_{12} \rightarrow n_1$ ), the former simplifies to eq. 18. On as-

$$\frac{n_{12} - 1}{\rho_{12}} = \left( \frac{n_1^2 - 1}{n_1 + 1} \right) \frac{p_1}{\rho_1} + \left[ \frac{(n_2^2 - 1)(n_1^2 + 2)}{(n_2^2 + 2)(n_1 + 1)} \right] \frac{p_2}{\rho_2} \quad (18)$$

suming, in addition, that  $n_2 \rightarrow n_1$  one obtains eq. 4',

$$\frac{n_{12} - 1}{\rho_{12}} = (n_1 - 1) \frac{p_1}{\rho_1} + (n_2 - 1) \frac{p_2}{\rho_2} \quad (4')$$

*i.e.*, the Dale-Gladstone equation. It is surprising that this very simple relationship between these two equations apparently has thus far escaped attention. It relieves the latter from the classical attribute of being an "empirical" equation. Although established as an empirical equation,<sup>7</sup> it may now clearly be considered as a theoretical equation valid in the doubly limiting case that  $n_{12} \rightarrow n_1$  and  $n_2 \rightarrow n_1$ . This interrelation explains also the well known fact that in certain instances both equations perform equally well while in others only the Lorentz-Lorenz equation gives acceptable results.

It is of interest to recall (see sections IV and V) that the Dale-Gladstone equation, if written in the form requiring volume additivity is, similarly, a doubly limited version of the Wiener equation (2).

VII. *Conclusions*. It follows from the preceding discussion that the mixture rules of widest applicability should be the Lorentz-Lorenz and the Wiener equations.

All other equations are more limited in applicability than the two equations just named. The Dale-Gladstone equation, in particular, is doubly limited in scope. It can be expected to give results identical with those obtained from the former only if the solutions are very dilute and if, in addition, the refractive indices of solute and solvent are very similar.

Equation 3 assumes an intermediate role. It only requires that the solutions are dilute, in which case its

performance is equal to that of the Wiener equation. Equation 3 shares with the Dale-Gladstone equation the advantage over the two first named equations that the refractive index of the solute can be obtained from differential measurements alone, thus guaranteeing a high degree of precision of the data obtained for the refractive index of the solute.

The Biot equation, finally, shares the advantages and disadvantages of the Dale-Gladstone equation. In case of volume additivity, the performance of both equations should be identical.

VIII. *Conditions under which None of the Preceding Equations Applies*. It remains to recall briefly the restrictions existing for the application of all mixture rules discussed here. The derivation of eq. 1 and 2 is based upon the assumption that (a) dipoles are induced in a homogeneous isotropic system so that the electromagnetic field (originally: the electrostatic field) is throughout undistorted. This applies as long as the solute molecules (or dispersed particles) are small compared to the wave length. An additional restriction is that (b) the solute (particle) is spherically symmetrical except in the special case that the polarizabilities of solvent and solute molecules are nearly the same. (The case of small nonspherical solutes differing in polarizability from the solvent has also been treated by Wiener,<sup>3</sup> but shall not be considered here.) Equations 1 and 2 and, consequently, all the others, will therefore break down if compact molecules (particles) have colloidal size. On passing from the colloidal range into the upper microscopic range, the difficulties are bound to disappear again since one then has effectively a mixture of two homogeneous media. In fact, eq. 5 has been found to hold very well in the latter instance.

The complications arising within the colloidal range have been treated by Zimm and Dandliker.<sup>11</sup> The refractive index,  $n_2$ , derived from any mixture rule should then, generally, be too small and may even assume values  $<1.0$ . (In other words, particles may then behave as if they were completely nonrefracting.) The actual experimental variation of  $n_2$  with particle size is in accord with expectation.<sup>12</sup> Fortunately, one may, even in such cases, obtain significant  $n_2$  values from application of the mixture rules discussed by using correction factors calculated from the Zimm-Dandliker equation.<sup>13</sup> Whether such corrections are necessary in a given case can and must be ascertained

(11) B. H. Zimm and W. B. Dandliker, *J. Phys. Chem.*, **58**, 644 (1954).

(12) W. Heller and T. L. Pugh, *J. Colloid Sci.*, **12**, 294 (1957).

(13) M. Nakagaki and W. Heller, *J. Appl. Phys.*, **27**, 975 (1956).

by combining a light scattering experiment with the refractometric experiment. If there is dissymmetry, *i.e.*, if the intensity of light scattered at an angle of observation of  $45^\circ$ , with respect to the direction of the incident beam, is appreciably larger than at  $135^\circ$ , then application of these corrections is possibly, but not necessarily, indicated. Absence of dissymmetry, on the other hand, is conclusive proof that the mixture rules discussed here can be applied without risk of the complications just defined.

*IX. Test of the Principal Mixture Rules Discussed.* In order to check the conclusions arrived at with respect to the interrelation and relative merits of the various mixture rules, a test on model systems appeared desirable. The simplest and most conclusive test consists of comparing the refractive index of solutions determined experimentally with that calculated from the refractive index and density of the pure components and the densities of the solutions. For this purpose, the mixture rules discussed take the following forms

$$n_{12} = \left( \frac{2A' + 1}{1 - A'} \right)^{1/2} \quad (1a)$$

where

$$A' = \left[ \left( \frac{n_1^2 - 1}{n_1^2 + 2} \right) \frac{1}{\rho_1} - \left( \frac{n_1^2 - 1}{n_1^2 + 2} \right) \frac{p_2 (n_2^2 - 1) p_2}{\rho_1 (n_2^2 + 2) \rho_2} \right] \rho_{12}$$

$$n_{12} = \left[ \frac{2B(p_2 \rho_{12} / \rho_2) + n_1^2}{1 - B(p_2 \rho_{12} / \rho_2)} \right]^{1/2} \quad (1a)^*$$

where  $B = (n_2^2 - n_1^2) / (n_2^2 + 2)$

$$n_{12} = n_1 \left( \frac{1 + 2C}{1 - C} \right)^{1/2} \quad (2a)^*$$

where

$$C = (p_2 \rho_{12} / \rho_2) \left( \frac{m^2 - 1}{m^2 + 2} \right)$$

$$n_{12} = (3/2)(p_2 \rho_{12} / \rho_2) \left( \frac{m^2 - 1}{m^2 + 2} \right) n_1 + n_1 \quad (3a)^*$$

$$n_{12} = \rho_{12} \left[ \left( \frac{n_1 - 1}{\rho_1} \right) - (n_1 - 1) \frac{p_2}{\rho_1} + (n_2 - 1) \frac{p_2}{\rho_2} \right] + 1 \quad (4a)$$

$$n_{12} = \rho_{12} \left[ \frac{n_1}{\rho_1} + p_2 \left( \frac{n_2}{\rho_2} - \frac{n_1}{\rho_1} \right) \right] \quad (5a)$$

$$n_{12} = (n_2 - n_1)(p_2 \rho_{12} / \rho_2) + n_1 \quad (4a)^* \text{ and } (5a)^*$$

Asterisks indicate that the respective equation is formulated for the case of volume additivity (no volume

expansion or contraction during mixing of the pure components).

In view of the availability of numerous literature data, experimentation appeared unnecessary. Among the data scrutinized, two sets were selected. One pertains to a system which comes close to volume additivity. The second deviates appreciably from volume additivity. In addition  $n_2$  and  $n_1$  differ more than in the first system.

The first system represents mixtures of ethylene bromide and ethanol. The respective data are very old,<sup>14</sup> but are outstanding by their precision. They have, incidentally, been used previously, by Nernst<sup>15</sup> for a test of eq. 1' and 4'. Table I gives the results.<sup>16</sup>  $\Delta V$  is the per cent change in volume on mixing the pure components. It is defined by  $\Delta V = (\rho_{12 \text{ calcd}} / \rho_{12 \text{ exptl}}) \times 100 - 100$  where

$$\frac{1}{\rho_{12 \text{ calcd}}} = \frac{1}{\rho_1} + p_2 \left( \frac{1}{\rho_2} - \frac{1}{\rho_1} \right) \quad (19)$$

It is seen that even at a weight concentration of ethylene bromide as large as 30%, the volume expansion is still slightly less than 0.05%.

Considering first the Lorentz-Lorenz equation,<sup>17</sup> it is seen to perform very well and far better than all others at small and moderate concentrations. The small negative deviations are accounted for by the volume dilation without one having to assume a change in molecular polarizabilities on mixing of the components. The system may therefore be considered as a nearly ideal one for the test of the various other mixture rules. It is very interesting that the simplified form of the Lorentz-Lorenz equation in which volume changes on mixing are neglected (eq. 1a') performs nearly as well at low and better at very high concentrations. The latter result is due to the fact that the deviation from volume additivity leads to a positive deviation<sup>18</sup> of the results and therefore to a reduction in the over-all deviation.

The performance of the Wiener equation (2a) should be compared to that of the Lorentz-Lorenz equation (1a'). The error committed on using the former is about five times larger. One can therefore anticipate that the Wiener equation in the full form which does

(14) F. Schuett, *Z. physik. Chem.* (Leipzig), **9**, 349 (1892).

(15) W. Nernst, "Theoretische Chemie," F. Enke, Stuttgart, 1913, p. 104. See also the discussion by D. A. G. Bruggeman, *Physik.-Z.*, **37**, 906 (1936).

(16) The numerical calculations were carried out by Sanford Perlman, a graduate student at Wayne State University.

(17) The respective  $\Delta n$  values given in Table I agree throughout with those calculated by Nernst from the same primary data except for differences, in a few instances, by one unit in the fifth decimal.

(18) This deviation represents an error in the value of  $\phi_2$ .

**Table I:** Mixtures of Propyl Alcohol (1) and Ethylene Bromide (2)<sup>a</sup>

$p_2 \times 10^2$	$\rho_{12}$	$\Delta V^b$	$n_{12}^c$	$(n_{12}^{\text{calcd}} - n_{12}^{\text{obsd}}) \times 10^6$							
				Eq. 1a	Eq. 1a'	Eq. 2a	Eq. 3a	Eq. 4a	Eq. 4a'	Eq. 5a	Eq. 5a'
0	0.80659	0.0	1.386161	0.0	0.0	0.0	0.0	0.0	0.0	0.0	0.0
10.0084	0.86081	0.012	1.391892	-1.2	4.3	23.2	22.8	30.8	35.6	18.3	35.6
20.9516	0.92908	0.030	1.399136	-2.8	10.4	51.1	48.9	66.2	77.8	35.9	77.8
29.8351	0.99300	0.048	1.405958	-5.5	15.7	74.7	69.5	95.0	113.5	46.9	113.5
40.7320	1.08453	0.073	1.415815	-12.3	20.2	101.8	90.1	127.5	155.7	54.4	155.7
49.9484	1.17623	0.098	1.425748	-17.9	25.9	125.8	105.0	154.4	192.3	56.2	192.3
60.0940	1.29695	0.131	1.439013	-33.4	25.6	142.9	105.7	171.0	221.5	40.2	221.5
70.0123	1.44175	0.159	1.455063	-45.4	27.1	155.2	91.7	180.3	241.6	21.4	241.6
80.0893	1.62640	0.183	1.475796	-55.9	29.0	154.4	46.2	168.9	239.7	-14.4	239.7
90.1912	1.86652	0.186	1.503227	-57.6	30.2	123.4	-62.5	115.8	187.6	-70.0	187.6
100	2.18300	0.0	1.540399	0.0	0.0	0.0	-324.3	0.0	0.0	0.0	0.0

<sup>a</sup> Data apply to the sodium D-line and temperature of 18.0°. <sup>b</sup>  $\Delta V$  = per cent volume change on mixing. <sup>c</sup> Observed refractive index.

**Table II:** Mixtures of Bromoform (1) and Acetone (2)<sup>a</sup>

$p_2 \times 10^2$	$\rho_{12}$	$\Delta V^b$	$n_{12}^c$	$(n_{12}^{\text{calcd}} - n_{12}^{\text{obsd}}) \times 10^6$							
				Eq. 1a	Eq. 1a'	Eq. 2a	Eq. 3a	Eq. 4a	Eq. 4a'	Eq. 5a	Eq. 5a'
0	2.8794	0.0	1.59445	0.0	0.0	0.0	0.0	0.0	0.0	0.0	0.0
2.0469	2.720	0.375	1.57705	-36.4	-94.3	22.8	19.8	-170.3	52.2	-544.6	52.2
5.4395	2.507	0.292	1.55251	-45.9	-253.6	-1.6	-19.3	-112.9	60.0	-403.8	60.0
9.8916	2.283	-0.223	1.52637	-32.2	-477.2	-122.2	-169.3	94.8	-37.8	317.9	-37.8
13.403	2.127	-0.298	1.50838	-32.1	-524.9	-127.6	-201.3	142.5	-35.2	441.5	-35.2

<sup>a</sup>  $n_2 = 1.35657$ ,  $\rho_2 = 0.7847$ , at 25° using sodium D-line. <sup>b</sup> Per cent volume change on mixing. <sup>c</sup> Observed refractive index.

not assume volume additivity (not discussed here) will give for the system under discussion an error about four times larger at the lowest concentration considered. Equation 3a performs, as expected, as well as the Wiener equation at the lowest concentrations. It performs better at higher concentrations. The latter is due, again, to partial compensation of deviations of opposite sign. The remaining equations perform less well than the others at the lowest concentration with the exception of the Biot equation in its general form. The latter performs surprisingly well. Summarizing, it can be stated that all those equations which are interrelated in a simple quantitative manner perform at low concentrations as anticipated in the preceding sections of this paper. It will be noted, in particular, that the Lorentz-Lorenz equation performs by far the best. It is followed by the Wiener equation. In contradistinction, the Dale-Gladstone equation is relatively unsatisfactory. At higher concentrations, a statement about the relative merits of all equations is very difficult; it is clear, however, that the Lorentz-

Lorentz equation (1a) is preferable to all others since the variation of the deviation with concentration is monotonic without a maximum or a change in sign.

The second system tested represents mixtures of bromoform and acetone.<sup>19</sup> Here, the volume change during mixing is considerably larger (by about one order of magnitude) at low and moderate concentrations ( $0.02 < p_2 < 0.13$ ). The results are given in Table II. At the lowest concentrations ( $p \leq 0.05$ ) the situation is the same as for the preceding system: the Lorentz-Lorenz equation (1a), the Wiener equation (2a), and eq. 3a perform best. The Dale-Gladstone equation (4a) and the Biot equation (5a) are very unsatisfactory. It is important to note that use of those variants of the latter two equations which presuppose volume additivity (which does not apply here) considerably improves the results (eq. 4a' and 5a', respectively). This is due to partial compensation of deviations of opposite sign.

(19) V. C. G. Trew, *Trans. Faraday Soc.*, 28, 509 (1932).



Such a compensation of deviations of opposite sign is apparent also by the change of sign, in the net deviations observed, as a function of the concentration  $p$  of the solute. The latter compensatory effect manifests itself for all equations except the Lorentz-Lorenz equation. This applies to both systems discussed. An interesting result of this superposition of deviations of opposite sign is that at certain concentrations some of the equations given may actually *appear* to be superior in performance to the Lorentz-Lorenz equation. Thus, Bauer and Lewin,<sup>20</sup> on considering experimental  $n_{12}$  values obtained on a solution of acetone in water ( $p = 0.6561$ ), find that the Dale-Gladstone equation gives a value which is in better agreement with experiment than that derived from the Lorentz-Lorenz equation. Similarly, eq. 4a' and 5a' will give for the acetone-

bromoform system (Table II) better results than eq. 1a if  $p > 0.13$ . On the basis of the analysis given here, it is now clear that such cases of apparently better performance of equations other than 1, 2, and 3 are purely fortuitous and are due to a compensation of major deviations of opposite sign effective over a limited range of concentrations. Equations 1, 2, and 3 are the safest to use *at low solute concentrations* irrespective of whether volume additivity applies or volume expansion occurs on mixing. Over an *extensive concentration range*, the Lorentz-Lorenz equation alone appears to be the most reliable equation.

---

(20) N. Bauer and S. Z. Lewin, "Technique of Organic Chemistry," Vol. I, Part II, A. Weissberger, Ed., Interscience Publishers, Inc., New York, N. Y., 1960, p. 1157.

## The Virial Theory of Adsorption and the Surface Areas of Solids

by Robert Wolfe and John R. Sams

Department of Chemistry, University of British Columbia, Vancouver 8, Canada (Received August 29, 1964)

---

The high-temperature adsorption theory provides several methods for estimating surface areas of solids. These have the advantage over such methods as B.E.T. and point B of providing unambiguous values which are independent of any estimate of adsorbate cross section. The method proposed by Barker and Everett is used to calculate the area of a highly graphitized carbon black from both argon and xenon adsorption data at low surface coverages. Essentially perfect agreement between the values is obtained by this method, whereas those found from monolayer coverage data differ by more than 20%.

---

### Introduction

For a number of years, the Brunauer-Emmett-Teller equation<sup>1</sup> has been the basis for the most widely used method of determining the surface areas of solids. It has the advantages of being a simple and rapid method and does not require elaborate experimental apparatus or laborious measurements. For fairly rough, semiquantitative determinations it is a very useful and handy method. On the other hand, it has certain inherent disadvantages which not only limit its

usefulness in very precise work, but render it quite unsatisfactory in trying to determine an "absolute" or even an "unambiguous" surface area.

The first of these is that the monolayer volume,  $v_m$ , as calculated from the B.E.T. equation, is a fairly strong function of the temperature. This is illustrated by Figure 1, for the adsorption of argon on the highly

---

(1) S. Brunauer, P. H. Emmett, and E. Teller, *J. Am. Chem. Soc.*, **60**, 309 (1938).

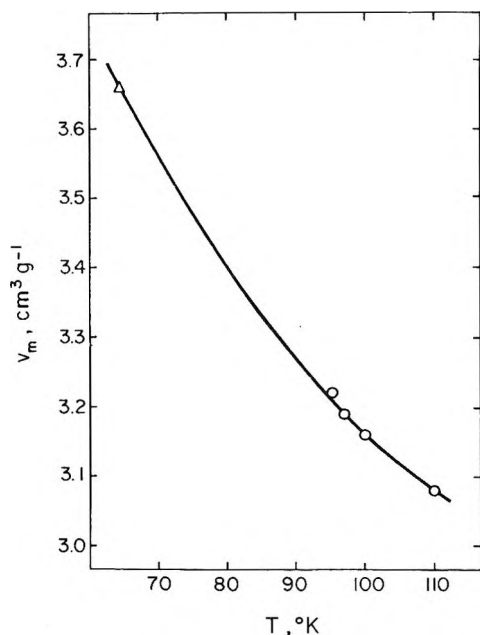


Figure 1. Dependence of monolayer volume capacity on temperature for argon on graphitic carbon:  $\Delta$ , data of Prenzlów and Halsey;  $\circ$ , data of Sams, Constabaris, and Halsey.

graphitized carbon black P33 (2700).<sup>2,3</sup> A much more serious criticism of B.E.T. areas is that the values are often strongly dependent on the adsorbate used. Thus, Pace and Siebert<sup>4</sup> found that for the same graphitized carbon black helium adsorption gave an area of 267 m<sup>2</sup> g<sup>-1</sup>, whereas argon adsorption gave 86 m<sup>2</sup> g<sup>-1</sup>. Moreover, as long as one must make more or less arbitrary assumptions in assigning an effective cross-sectional area to the admolecule, an unambiguous area determination is clearly impossible. As we have pointed out,<sup>3</sup> the uncertainty involved in assuming a particular type of packing for the admolecules can easily lead to a variation of 30–40% in the calculated areas.

The high-temperature adsorption theory developed by Halsey and co-workers<sup>5</sup> obviates much of the uncertainty involved in choosing a "size" for the admolecule. In the second-order (or Henry's law) region of the isotherm this two-parameter theory allows the evaluation of the gas–solid interaction energy,  $\epsilon_{gs}$ , and a capacity factor  $As_0$ , where  $A$  is the surface area of the adsorbent and  $s_0$  the apparent value of the gas–solid separation for which the potential energy vanishes. If  $\epsilon_{gs}$  is identified with the attractive part of the dispersion energy expression,<sup>6</sup> then from any one of the familiar equations (*e.g.*, Kirkwood–Müller, London, etc.) for the dispersion constant one can calculate  $s_0$  and hence obtain a value for the area which is independent of any estimate of adsorbate cross section.

Three points should be made in connection with such areas. (1) The results depend slightly on the exact form of the function chosen to represent the interaction potential. For three different assumed potential models,<sup>6</sup> the values for a given adsorbate–adsorbent pair agree to within  $\pm 4\%$ . (2) There is also a dependency on the nature of the measuring gas. For the rare gases Ne, Ar, Kr, and Xe on a highly graphitized carbon black<sup>6</sup> this amounts to only  $\pm 5\%$ , but much larger variations have been observed<sup>5</sup> with heterogeneous surfaces. (3) The area values depend markedly on the equation used to evaluate the dispersion energy constant. The London formula gives areas which are greater by nearly a factor of two than those found from the Kirkwood–Müller formula.<sup>6</sup> One might hope to estimate  $s_0$  independently by noting that this quantity is the sum of an effective radius of the solid atoms and an effective radius of the gas molecules. One does not really know, of course, what radii to assign, but if data for several gases on a given adsorbate are available, a plot of  $As_0$  against, say, the van der Waals radii of the adsorbates should give a straight line whose slope is the area.<sup>6</sup>

Third-order interaction data provide another means of separating the capacity factor  $As_0$ .<sup>7</sup> The third-order region corresponds to small deviations from Henry's law behavior, and in this region the adsorbate can be treated as an imperfect two-dimensional gas.<sup>8</sup> As in the second-order treatment, one obtains a two-parameter model and can evaluate  $\epsilon_2$ , the virtual two-dimensional gas–gas interaction energy, and  $A/\sigma_2^2$ , where  $\sigma_2$  is the two-dimensional collision diameter. The assumption of a value for  $\sigma_2$  then gives another independent estimate of the area.<sup>9</sup> Barker and Everett have shown that by combining two-dimensional gas data with Henry's law data one can, by a series of successive approximations, arrive at an unambiguous value for the area. We present below a brief outline of their procedure and apply the method to the data of Constabaris, *et al.*,<sup>10</sup> for the adsorption of argon and

(2) C. F. Prenzlów and G. D. Halsey, *J. Phys. Chem.*, **61**, 1158 (1957).

(3) J. R. Sams, G. Constabaris, and G. D. Halsey, *ibid.*, **66**, 2154 (1962).

(4) E. L. Pace and A. R. Siebert, *ibid.*, **64**, 961 (1960).

(5) W. A. Steele and G. D. Halsey, *J. Chem. Phys.*, **22**, 971 (1954); M. P. Freeman and G. D. Halsey, *J. Phys. Chem.*, **59**, 181 (1955).

(6) J. R. Sams, G. Constabaris, and G. D. Halsey, *ibid.*, **64**, 1689 (1960).

(7) J. A. Barker and D. H. Everett, *Trans. Faraday Soc.*, **58**, 1608 (1962).

(8) J. R. Sams, G. Constabaris, and G. D. Halsey, *J. Chem. Phys.*, **36**, 1334 (1962).

(9) D. H. Everett, *Soc. Chem. Ind. Monograph*, **14**, 98 (1960).

xenon on the highly graphitized carbon black P33 (2700).

### Analysis of Data

*Experimental Results.* High-temperature adsorption data can be discussed most conveniently with reference to two volume terms, both of which are defined by the perfect gas law. The first of these is the apparent volume, which relates the total number of moles of gas in the system,  $n_b$ , to the experimentally determined pressure  $p$  and Kelvin temperature  $T$

$$V_a = n_b RT/p \quad (1)$$

The second is the excess volume, which gives the number of moles of gas adsorbed,  $n_a$ , at pressure  $p$  and temperature  $T$

$$V_x = n_a RT/p \quad (2)$$

These two are related very simply by

$$V_x = V_a - V_{DS} \quad (3)$$

where  $V_{DS}$  is the total dead-space volume of the apparatus. Since  $n_b$ ,  $p$ , and  $T$  are directly measured in any adsorption experiment, the apparent volume is known, and hence the excess volume, which is directly related to quantities of theoretical interest, is readily obtained. It is, in fact, the simplest and most straightforward way of representing the data.

In general,  $V_x$  is a function of pressure as well as of temperature, although if the temperature is sufficiently high this pressure dependence vanishes. In this case, Henry's law is obeyed, and we can express the adsorption isotherm as

$$n_a = k_H A p \quad (4)$$

From eq. 2 and 4 we see that the excess volume (extrapolated to zero pressure if the temperature is not sufficiently high to yield a pressure-independent quantity) is effectively the Henry's law constant for the isotherm, *i.e.*

$$V_x^0 = k_H A RT \quad (5)$$

and it may perhaps be more easily visualized as such. We might also point out in passing the relationship between  $V_x$  and the more commonly used  $V_{STP}$ , the volume of gas adsorbed at STP, *viz.*

$$V_{STP} = (273.15p/76.000T)V_x \quad (6)$$

Thus  $V_x$  data can be converted readily to  $V_{STP}$  data, although there is no advantage in doing so.

In the absence of lateral adsorbate interactions, the Henry's law constant, or  $V_x^0$ , is the only theoretically significant quantity. However, with the on-

set of lateral interactions (that is to say, in the third-order interaction region) the excess volume becomes a linear function of the pressure,<sup>11</sup> and one needs also to determine the quantity  $dV_x/dp$ , as we shall see below. The point we wish to stress is that the only data one requires in applying the present method are measurements of the apparent volume as a function of pressure at each temperature of interest. Moreover, if the temperature range is carefully selected so that the  $V_x$  vs.  $p$  plots are linear, then only two points are needed at each temperature to completely determine the slope and intercept. Note that if one uses  $V_{STP}$  data rather than  $V_x$  data, it is necessary to determine the slope and curvature of the isotherm, which is both more difficult and less accurate.

$V_x^0$  and  $dV_x/dp$  can be related directly to theoretically significant quantities, namely, the second and third gas-surface virial coefficients,  $B_{AS}$  and  $C_{AAS}$ .<sup>5</sup> Thus

$$V_x^0 = B_{AS} \quad (7)$$

$$dV_x/dp = C_{AAS}/RT \quad (8)$$

These in turn allow the experimental determination of the two-dimensional gas second virial coefficient  $B_2$  through the equation<sup>8</sup>

$$-B_2/A = C_{AAS}/2B_{AS}^2 = RT(dV_x/dp)/2(V_x^0)^2 \quad (9)$$

We can thus obtain experimental measurements of the virial coefficients  $B_{AS}$  and  $B_2/A$ .

*Method of Calculation.* Theoretical expressions for  $B_{AS}$  and  $B_2$  have been derived elsewhere<sup>6-8</sup> and we quote only the results. The exact functional forms are not

$$B_{AS} = A s_0 f(\epsilon_{gs}/kT) \quad (10)$$

$$B_2 = \pi \sigma^2 f(\epsilon_2/kT) \quad (11)$$

essential to our line of reasoning, and we omit the details to avoid complication. Values of  $f_{gs}$  and  $f_2$  as functions of reduced temperature  $T^* = kT/\epsilon$  are given in Tables I and II, respectively.<sup>12</sup> We have assumed a Lennard-

(10) G. Constabaris, J. R. Sams, and G. D. Halsey, *J. Chem. Phys.*, **37**, 915 (1962).

(11) At lower temperatures and/or higher pressures, where higher-order interactions are also present, this functional relationship is rather more complex, but this does not concern us here.

(12) We are indebted to Prof. D. H. Everett for calling our attention to the fact that our earlier tabulation<sup>8</sup> of  $f_2$  values for the Lennard-Jones (12-6) potential is in error. This was owing to the use of an incorrect  $\Gamma$ -function in the computer program used to evaluate the integral. None of our conclusions<sup>8,13</sup> is affected by this error, although the numerical values for interaction energies and areas are slightly altered. The present results may be considered to revise the previous ones. Barker and Everett<sup>7</sup> have also published a table of  $f_2$  values for the (12-6) potential, but the range of their table is not sufficient for our purposes.

(13) J. R. Sams, *J. Chem. Phys.*, **37**, 1881 (1962).

Jones (12-6) potential for the gas-gas interaction and a (12-3) potential for the gas-surface interaction.

Expression 11 is derived on the assumption that the adsorbate forms a strictly two-dimensional layer.

**Table I:** Reduced Gas-Surface Second Virial Coefficient as a Function of Reduced Temperature; Lennard-Jones (12-3) Potential

$T_{gs}^*$	$B_{AS} = A s_0 B_{AS}^*$ $B_{AS}^*$	$T_{gs}^* = kT/\epsilon_{gs}$ $T_{gs}^*$	$B_{AS}^*$
0.1111	1486.270	0.1449	217.9940
0.1124	1354.720	0.1471	199.2723
0.1136	1234.945	0.1493	182.1870
0.1149	1125.892	0.1515	166.5962
0.1163	1026.586	0.1538	152.3641
0.1176	936.1513	0.1563	139.3717
0.1190	853.7797	0.1587	127.5081
0.1205	778.7531	0.1613	116.6750
0.1220	710.4072	0.1639	106.7796
0.1235	648.1442	0.1667	97.7404
0.1250	591.4142	0.1695	89.4806
0.1266	539.7232	0.1724	81.9323
0.1282	492.6172	0.1754	75.0326
0.1299	449.6863	0.1786	68.7244
0.1316	410.5551	0.1818	62.9560
0.1333	374.8834	0.1852	57.6798
0.1351	342.3623	0.1887	52.8529
0.1370	312.7090	0.1923	48.4358
0.1389	285.6702	0.1961	44.3929
0.1408	261.0092	0.2000	40.6914
0.1429	238.5151	0.2041	37.3017

**Table II:** Reduced Two-Dimensional Second Virial Coefficient as a Function of Reduced Temperature; Lennard-Jones (12-6) Potential

$T^*$	$B_2 = \frac{1}{2}\pi\bar{N}\sigma_2^2 B_2^*$ $B_2^*$	$T^* = kT/\epsilon_2$ $T^*$	$B_2^*$
1.042	-0.59854	1.724	0.09955
1.064	-0.55698	1.786	0.13121
1.087	-0.51596	1.852	0.16238
1.111	-0.47552	1.923	0.19306
1.136	-0.43564	2.000	0.22324
1.163	-0.39630	2.083	0.25294
1.191	-0.35752	2.174	0.28212
1.220	-0.31928	2.273	0.31078
1.250	-0.28156	2.381	0.33894
1.282	-0.24436	2.500	0.36656
1.316	-0.20770	2.632	0.39364
1.351	-0.17155	2.778	0.42016
1.389	-0.13591	2.941	0.44610
1.429	-0.10078	3.125	0.47142
1.471	-0.06615	3.333	0.49612
1.515	-0.03202	3.571	0.52012
1.563	0.00161	3.846	0.54338
1.613	0.03475	4.546	0.58744
1.667	0.06740	5.000	0.60802

When account is taken of the nonplanarity of the adsorbed layer, it is found that  $B_2$  must be replaced by  $(B_2 - \alpha)$ . The correction term  $\alpha$  depends on  $\epsilon_{gs}/kT$ ,  $\epsilon_2/kT$ , and the ratio  $s_0/\sigma_2$ . Tables of  $\alpha$  values, calculated from the equations of Barker and Everett,<sup>7</sup> are given in Table III.

The procedure now is to determine the best fit of experimental values of  $B_2/A$ , as a function of temperature, to the theoretical curve of  $B_2$  vs.  $\epsilon_2/kT$  by

**Table III:** Reduced Nonplanarity Correction  $\alpha^*$ ; Lennard-Jones (12-6) Potential;  $\alpha \equiv \frac{1}{2}\pi\bar{N}\sigma_2^2\alpha^*$ ;  $T^* \equiv kT/\epsilon$

$T_2^{*-1}$	$s_0/\sigma$						
	0.70	0.75	0.80	0.85	0.90	0.95	1.00
A. $T_{gs}^{*-1} = 8.000$							
0.250	0.0115	0.0128	0.0140	0.0153	0.0165	0.0178	0.0190
0.300	0.0113	0.0126	0.0138	0.0151	0.0163	0.0176	0.0188
0.350	0.0111	0.0124	0.0136	0.0149	0.0161	0.0174	0.0186
0.400	0.0109	0.0122	0.0134	0.0147	0.0159	0.0172	0.0184
0.450	0.0107	0.0120	0.0132	0.0145	0.0157	0.0170	0.0182
0.500	0.0105	0.0118	0.0130	0.0143	0.0155	0.0168	0.0180
0.550	0.0103	0.0116	0.0128	0.0141	0.0153	0.0166	0.0178
0.600	0.0101	0.0114	0.0126	0.0139	0.0151	0.0164	0.0176
0.650	0.0099	0.0112	0.0124	0.0137	0.0149	0.0162	0.0174
B. $T_{gs}^{*-1} = 7.500$							
0.250	0.0136	0.0150	0.0164	0.0178	0.0192	0.0206	0.0221
0.300	0.0133	0.0147	0.0161	0.0175	0.0189	0.0203	0.0218
0.350	0.0131	0.0145	0.0159	0.0173	0.0187	0.0201	0.0214
0.400	0.0128	0.0142	0.0156	0.0170	0.0184	0.0198	0.0211
0.450	0.0126	0.0139	0.0153	0.0167	0.0181	0.0195	0.0208
0.500	0.0123	0.0137	0.0151	0.0164	0.0178	0.0192	0.0205
0.550	0.0121	0.0134	0.0148	0.0161	0.0175	0.0189	0.0202
0.600	0.0118	0.0132	0.0145	0.0159	0.0172	0.0186	0.0199
0.650	0.0115	0.0129	0.0142	0.0156	0.0169	0.0183	0.0196
C. $T_{gs}^{*-1} = 7.000$							
0.250	0.0162	0.0178	0.0194	0.0210	0.0226	0.0242	0.0258
0.300	0.0158	0.0174	0.0190	0.0206	0.0222	0.0238	0.0254
0.350	0.0155	0.0171	0.0187	0.0202	0.0218	0.0234	0.0249
0.400	0.0152	0.0168	0.0183	0.0198	0.0214	0.0229	0.0245
0.450	0.0149	0.0164	0.0179	0.0195	0.0210	0.0225	0.0240
0.500	0.0145	0.0161	0.0176	0.0191	0.0206	0.0221	0.0236
0.550	0.0142	0.0157	0.0172	0.0187	0.0202	0.0217	0.0232
0.600	0.0139	0.0154	0.0168	0.0183	0.0198	0.0213	0.0227
0.650	0.0136	0.0150	0.0165	0.0179	0.0194	0.0208	0.0223
D. $T_{gs}^{*-1} = 6.500$							
0.250	0.0194	0.0213	0.0231	0.0250	0.0268	0.0287	0.0305
0.300	0.0190	0.0208	0.0227	0.0245	0.0263	0.0281	0.0299
0.350	0.0186	0.0204	0.0222	0.0239	0.0257	0.0275	0.0293
0.400	0.0182	0.0199	0.0217	0.0234	0.0252	0.0269	0.0287
0.450	0.0178	0.0195	0.0212	0.0229	0.0246	0.0263	0.0280
0.500	0.0174	0.0190	0.0207	0.0224	0.0241	0.0258	0.0274
0.550	0.0169	0.0186	0.0202	0.0219	0.0235	0.0252	0.0268
0.600	0.0165	0.0181	0.0197	0.0214	0.0230	0.0246	0.0262
0.650	0.0161	0.0177	0.0193	0.0208	0.0224	0.0240	0.0256
E. $T_{gs}^{*-1} = 6.000$							
0.250	0.0236	0.0258	0.0279	0.0301	0.0323	0.0344	0.0365
0.300	0.0231	0.0252	0.0273	0.0294	0.0315	0.0336	0.0357
0.350	0.0225	0.0246	0.0266	0.0287	0.0307	0.0328	0.0348
0.400	0.0220	0.0240	0.0260	0.0280	0.0300	0.0320	0.0340
0.450	0.0215	0.0234	0.0253	0.0273	0.0292	0.0312	0.0331
0.500	0.0209	0.0228	0.0247	0.0266	0.0285	0.0304	0.0323
0.550	0.0204	0.0222	0.0241	0.0259	0.0277	0.0296	0.0314
0.600	0.0199	0.0216	0.0234	0.0252	0.0270	0.0288	0.0306
0.650	0.0193	0.0211	0.0228	0.0245	0.0262	0.0280	0.0297

adjusting the two parameters  $\epsilon_2$  and  $A/\sigma_2^2$ . It is found that  $\epsilon_2$  is somewhat less than the gas phase energy  $\epsilon_3$ , owing to the nonadditivity of the gas-gas and gas-surface interactions. If it is assumed that the surface affects only the attractive part of the potential and not the repulsive part, then the three-dimensional potential parameters  $\epsilon_3$  and  $\sigma_3$  together with  $\epsilon_2$  permit the estimation of  $\sigma_2$  through the equation<sup>7</sup>

$$\sigma_2 = \sigma_3(\epsilon_3/\epsilon_2)^{1/2} \quad (12)$$

Once  $\sigma_2$  is known, the area is determined. One now calculates values of  $V_x^0/A$  for each temperature and fits these to the theoretical curve of  $B_{AS}/As_0$  vs.  $\epsilon_{gs}/kT$  by adjusting  $\epsilon_{gs}$  and  $s_0$ . One is then in a position to calculate a first estimate of the correction term  $\alpha$ , and thence a theoretical curve of  $(B_2 - \alpha)$  vs.  $\epsilon_2/kT$ . One returns now to the experimental values of  $B_2/A$  and repeats the entire series of calculations, fitting now to  $(B_2 - \alpha)$  vs.  $\epsilon_2/kT$ . This yields new values for all the fitting parameters and the area, and one merely iterates the calculation until no further changes in the values are observed.

## Results and Discussion

The method outlined in the preceding section has been used to analyze second-order and third-order data for argon and xenon on graphitic carbon,<sup>10</sup> and the results are presented in Table IV. In both cases four iterations of the calculations were required for convergence, and although this renders the present method rather more laborious than the determination of B.E.T. areas, the results are gratifying. The final areas for the two adsorbates differ by only 1.6% which can be considered essentially perfect agreement. Note that the values after the final iteration appear to be very slightly higher than the preceding ones, but this is principally due to round-off errors and is not significant.

Similar results have also been obtained for krypton<sup>14</sup> and for methane and tetradeuteriomethane<sup>15</sup> interacting with this same solid, and the areas obtained are included in Table IV. The krypton value is slightly lower than those for argon and xenon, although the difference is not large. We might mention that the krypton results were obtained at somewhat higher reduced temperatures than those for argon and xenon, and the data are consequently subject to larger relative errors. The methane area is in good agreement with the rare gas results, but the deuteriomethane area is considerably smaller. We feel that this rather low value for deuteriomethane may possibly result from some systematic error in the  $C_{AAS}$  data, because the areas determined for  $CH_4$  and  $CD_4$  from Henry's law

**Table IV:** Parameters of Best Fit and Surface Areas Determined by the Method of Barker and Everett for Argon and Xenon on the Graphitized Carbon Black P33 (2700)

Iteration	$\epsilon_2/k$ , °K.	$\sigma_2$ , Å.	$A$ , m. <sup>2</sup> g. <sup>-1</sup>	$\epsilon_{gs}/k$ , °K.	$s_0$ , Å.
Argon					
1	99	3.46	9.80	1110	2.82
2	96	3.47	8.70	1110	3.18
3	95	3.47	8.53	1110	3.24
4	95	3.47	8.54		
Xenon					
1	192	4.13	10.22	1916	3.05
2	185	4.14	8.92	1916	3.49
3	184	4.14	8.65	1916	3.53
4	184	4.14	8.68		
Areas obtained for other gases					
			Krypton	8.2 m. <sup>2</sup> g. <sup>-1</sup>	
			Methane	8.8 m. <sup>2</sup> g. <sup>-1</sup>	
			Tetradeuteriomethane	7.3 m. <sup>2</sup> g. <sup>-1</sup>	

measurements alone are the same within 10%, that for  $CD_4$  apparently being the *higher*.<sup>16</sup> Assuming the  $CD_4$  value in Table IV to be spurious, the remaining four gases are seen to agree closely. The average value is 8.55 m.<sup>2</sup> g.<sup>-1</sup> and the standard deviation is 0.23 m.<sup>2</sup> g.<sup>-1</sup>. Nevertheless, it is disconcerting that the  $CD_4$  value should be so low.

There are several features of the calculations which deserve comment. Firstly, the two-dimensional interaction energies are seen to be somewhat smaller than the corresponding gas phase values, and a comparison of these quantities shows that  $\epsilon_2/\epsilon_3$  is 0.80 for argon and 0.82 for xenon. These differences arise because the gas-gas and gas-surface interaction potentials are not pairwise additive and a significant three-body term exists. Yaris<sup>17</sup> has estimated the magnitudes of the three-body dispersion energies in these systems using the variational theory and finds values of  $\epsilon_2/\epsilon_3$  of 0.88 for argon and 0.84 for xenon, in quite good agreement with the experimental results.

Note that the two-dimensional interaction energy falls slightly with the introduction of the term  $\alpha$  to account for the nonplanarity of the adsorbed film. This is as one would expect if, on the average, a given admolecule is spending a considerable fraction of the time interacting with other molecules which are not coplanar to it. At the same time, the values of the

(14) J. R. Sams, *Mol. Phys.*, in press.

(15) J. R. Sams, *J. Chem. Phys.*, to be published.

(16) R. Yaris and J. R. Sams, *ibid.*, **37**, 571 (1962).

(17) R. Yaris, Thesis, University of Washington, 1962.

parameter  $A/\sigma_2^2$  required to fit the data are also lowered. As  $\sigma_2$  depends only on the twelfth root of  $\epsilon_2$ , it remains essentially constant, so that all the decrease in  $A/\sigma_2^2$  is absorbed by  $A$ .

The nature of the two-dimensional gas fit is also of interest. In the case of the xenon data, the fit becomes progressively better with each iteration, the standard deviation in  $A/\sigma_2^2$  decreasing from 0.99 to 0.84, although the fit is never particularly sharp. The situation with the argon data is somewhat different, as the initial fit is the best, having a standard deviation of 0.32. On introducing the  $\alpha$  correction term, the standard deviation increases to 0.48, then declines again to a value of 0.38 on the final iteration. The argon data appear to fit the model considerably better than do the xenon data, probably because the former are more extensive.

The fifth and sixth columns of Table IV give the results for the fit of the Henry's law data. In all cases the gas-surface interaction energy remains unchanged and all the effect of altering the estimate of the area is absorbed by  $s_0$ , which increased by about 13% for both argon and xenon. This was to have been expected, since one is dividing the  $V_x^0$  by a constant, which leaves the slope of the (logarithmic) plot unaltered.

A large number of B.E.T. and "point B" estimates of the monolayer volume capacity of this graphitized black have been published,<sup>2,3,18-20</sup> the adsorbates studied being nitrogen, oxygen, argon, krypton, and xenon. Areas estimated from these  $v_m$  data range from 10 to 15 m.<sup>2</sup> g.<sup>-1</sup>. In particular, the values for argon and xenon adsorption at 78°K. are 11.4 and 14.8 m.<sup>2</sup> g.<sup>-1</sup>, respectively.<sup>19</sup> These figures are based on effective cross-sectional areas of 13.8 Å.<sup>2</sup> for argon and 20.2 Å.<sup>2</sup> for xenon. There is considerable uncertainty concerning the effective area of the xenon atom,<sup>21</sup> the most frequently used value being about 24 Å.<sup>2</sup>. This, of course, would increase the area for xenon adsorption to something over 17 m.<sup>2</sup> g.<sup>-1</sup>. Differences in B.E.T. areas observed with different adsorbates have often been attributed to the existence in the adsorbent of pores having a cross section smaller than the apparent cross section of one of the adsorbates, but such an explanation obviously cannot be invoked here.

Instead of using adsorbate cross sections based on solid or liquid densities, one might assume two-dimensional hexagonal packing of the adsorbate and employ second virial coefficient molecular diameters at the potential minimum to compute the area. This has previously been done for argon adsorption on P33, in which case the area is lowered by about 7% (from 11.4 to 10.6 m.<sup>2</sup> g.<sup>-1</sup>).<sup>3</sup> The area for xenon adsorption

computed on this basis is 13.2 m.<sup>2</sup> g.<sup>-1</sup>. If second virial zero-interaction diameters<sup>22</sup> are used, the values are 8.4 and 10.5 m.<sup>2</sup> g.<sup>-1</sup>, respectively, which at least are in more substantial agreement with the results found here.

The B.E.T. and point B areas for this black are not so consistent as the values obtained from the present method, and the *absolute* uncertainty involved in assigning effective adsorbate cross sections is very large. For example, at 78°K. the rare gases are solids while nitrogen and oxygen are liquids, and moreover, as Prenzlow and Halsey<sup>2</sup> have pointed out, the adsorbed layer may have little reference to either solid or liquid since the strongest interaction is with the surface of dissimilar substance rather than with neighboring admolecules. In view of the fact that high temperature adsorption methods appear capable of providing consistent and unambiguous surface areas, whereas the B.E.T. method is not, it is unfortunate that they have not been more widely used.

Finally, it is interesting to compare the results of Table IV with those obtained from Henry's law data alone. As we pointed out above, such values are

Table V: Comparison of Areas Obtained from Henry's Law Data for Argon and Xenon on Graphitic Carbon by Five Different Dispersion Energy Equations

Adsorbate	Formula used				Mar- genau- Pollard
	Kirkwood- Müller	Slater- Kirkwood	London	Bardeen	
Ar	9.33	13.81	16.15	18.81	12.73
Xe	9.48	14.63	16.71	14.42	13.40

strongly dependent on the equation used to calculate the dispersion energy constant, and the present results (which are obtained using no assumptions external to the model) provide a means for evaluating the various formulas which have been used. In Table V are quoted areas for P33 obtained from argon and xenon adsorption in the Henry's law region, using five different formulas for the dispersion constant.<sup>9</sup> It is clear that the only equation which yields results in

(18) M. H. Polley, W. D. Schaeffer, and W. R. Smith, *J. Phys. Chem.*, **57**, 469 (1953).

(19) J. H. Singleton and G. D. Halsey, *ibid.*, **58**, 330, 1011 (1954).

(20) S. Ross and W. Winkler, *J. Colloid Sci.*, **10**, 319, 330 (1955).

(21) See D. Brennan, M. J. Graham, and F. H. Hayes, *Nature*, **199**, 1152 (1963), for a discussion of this point and numerous references.

(22) J. O. Hirschfelder, C. F. Curtiss, and R. B. Bird, "Molecular Theory of Gases and Liquids," John Wiley and Sons, Inc., New York, N. Y., 1954, p. 1110.

good agreement with the present calculations is that of Kirkwood and Müller. Salem<sup>23</sup> has noted that this formula gives an upper bound to the dispersion energy, and hence it gives a lower bound to the area which can be calculated from a dispersion energy constant. A good case can be made<sup>24</sup> for reducing both the Slater-Kirkwood and London estimates by a multiplicative factor of  $2^{-1/3}$ , which would bring them into more reasonable agreement with the Kirkwood-Müller values, but would still leave them 20-30% above the area obtained in the present paper. At least it appears

that Henry's law data in conjunction with the Kirkwood-Müller formula will yield areas in which one can have considerable confidence.

*Acknowledgment.* Financial support from the National Research Council and the Research Fund of the University of British Columbia is gratefully acknowledged.

---

(23) L. Salem, *Mol. Phys.*, **3**, 441 (1960).

(24) J. R. Sams and E. Yaris, *J. Phys. Chem.*, **67**, 1931 (1963).

## Multicomponent Diffusion Involving High Polymers. I. Diffusion of Monodisperse Polystyrene in Mixed Solvents

by E. L. Cussler, Jr.,\* and E. N. Lightfoot

*Department of Chemical Engineering, University of Wisconsin, Madison, Wisconsin  
(Received September 15, 1964)*

---

Multicomponent diffusion coefficients at three compositions of the ternary system polystyrene-toluene-cyclohexane were measured at 28.00° with a Gouy interferometer. The strong concentration dependence of the diffusion coefficients was removed by repeating all experiments at the same average concentration but different concentration differences and extrapolating the results to zero concentration difference. That the polymer behaves as a single species is shown by binary data. The multicomponent diffusion coefficients measured show the largest deviations from Fick's law yet observed. Because of these large deviations, the data offer the opportunity of evaluating multicomponent flux equations. The two most promising forms are briefly discussed, stressing the restraints on the various coefficients. Experimentally, they are compared as to accuracy of measurement, variation with composition, and molecular significance.

---

Diffusion in some multicomponent systems deviates sharply from the predictions of Fick's law, and more general flux equations are required to describe the concentration profiles within experimental error. The purpose of this paper is to seek a liquid system where these deviations are large and to choose the best set of flux equations to describe these effects. Large deviations have previously been reported for gases of very different molecular weight<sup>1,2</sup> and for aqueous systems

of electrolytes whose solutes have radically different mobility.<sup>3</sup> Since large deviations in physical size and mobility appear to cause large deviations from Fick's

---

\* Department of Physical Chemistry, University of Adelaide, Adelaide, South Australia.

(1) J. B. Duncan and H. L. Toor, *A.I.Ch.E. J.*, **8**, 38 (1962).

(2) W. E. Stewart and R. Prober, *Ind. Eng. Chem. Fundamentals*, **3**, 224 (1964).

(3) R. P. Wendt, *J. Phys. Chem.*, **66**, 1279 (1962).

law, the system polystyrene-cyclohexane-toluene was chosen for experimental investigation. The results were used to determine the set of multicomponent diffusion coefficients which are most nearly independent of concentration, which can be best estimated from binary data, and which represent known physical occurrences.

A wide variety of multicomponent flux equations have been proposed either on the basis of a physical model or from irreversible thermodynamic arguments. Although each set of flux equations defines a set of multicomponent diffusion coefficients, these different sets are interrelated.<sup>4-6</sup> The differences in the sets originate in the choice of the driving force, in the specification of a reference velocity, and in the treatment of the restraints on the system. The two most promising forms are the generalized Stefan-Maxwell equations and the generalized Fick's law equations.

The generalized Stefan-Maxwell equations have the form

$$\nabla \phi_i = \sum_{j=1}^n \phi_i \phi_j R_{ij} (\mathbf{v}_j - \mathbf{v}_i) \quad (1)$$

where  $\phi_i$  is the volume fraction of species  $i$  and  $\mathbf{v}_i$  is the velocity of species  $i$ . The coefficients  $R_{ij}$  of this type equation are independent of reference velocity and are similar to the "generalized Stefan-Maxwell coefficients" and to the frictional coefficients defined by other investigators.<sup>7-12</sup> In the special case of an

$$R_{ij} = R_{ji} \quad (2)$$

ideal gas, the  $R_{ij}$  are symmetric<sup>8,13,14</sup> and are identically equal to the binary diffusion coefficients.<sup>15</sup> In all cases, they reduce to the binary limit at infinite dilution

$$\lim_{(\phi_i + \phi_j) \rightarrow 1} R_{ij} = \frac{1}{\mathcal{D}_{ij}} \quad (3)$$

where  $\mathcal{D}_{ij}$  is the binary diffusion coefficient. In general, however, the  $R_{ij}$  need not be positive, although the eigenvalues of the coefficient matrix must be positive.<sup>2,4</sup> Because of their simple limits, the  $R_{ij}$  are often easily estimated from binary data.

For the solution of practical problems, the generalized Fick's law equations relative to constant volume are the best set

$$-\mathbf{j}_i = -\rho_i (\mathbf{v}_i - \mathbf{v}^0) = \sum_{j=1}^{n-1} D_{ij} \nabla \rho_j \quad (4)$$

where  $\rho_i$  is the mass density of species  $i$ . In many experimental cases, the volume average velocity is zero. The  $D_{ij}$  are in general not reciprocal, so that in the absence of activity data, four coefficients are re-

quired in a ternary experiment. The  $D_{ij}$  have the following binary limits<sup>16,17</sup>

$$\lim_{(\rho_i + \rho_n) \rightarrow \rho} D_{ii} = \mathcal{D}_{in} \quad (5)$$

$$\lim_{\rho_j \rightarrow \rho} D_{ii} = \mathcal{D}_{ij} \quad (6)$$

$$\lim_{\rho_i \rightarrow 0} D_{ij(j \neq i)} = 0 \quad (7)$$

$$\lim_{\rho_i \rightarrow \hat{\rho}} D_{ij(i \neq j)} = \frac{\bar{V}_j}{\bar{V}_i} [\mathcal{D}_{ni} - \mathcal{D}_{ji}] \quad (8)$$

Again, the eigenvalues of the diffusion coefficient matrix must be positive. For a ternary system, this is equivalent to

$$D_{11} + D_{22} > 0 \quad (9)$$

$$(D_{11} - D_{22})^2 + 4D_{12}D_{21} > 0 \quad (10)$$

Thus, there is no theoretical reason for *any single* coefficient to be positive. However, for a wide class of dilute electrolytes, the terms  $D_{ij(i \neq j)}$  are small relative to the  $D_{ii}$  and may be neglected.<sup>18</sup>

## Experimental

*Materials.* The polystyrene used in the experiments, designated S-109, was supplied by Dr. H. W. McCormick of the Dow Chemical Co. It had a number-average molecular weight of 182,000 and a weight-average weight of 193,000. It contained as an impurity 300 p.p.m. of acrowax, a lubricant which had been added in earlier experiments by other investigators. Acrowax is a complex nitrogen derivative of the higher fatty acids manufactured by the Glyco Products Co. New York, N. Y.<sup>19</sup> Whether this con-

(4) S. R. de Groot and P. Mazur, "Non-Equilibrium Thermodynamics," North-Holland Publishing Co., Amsterdam, 1962.

(5) C. Truesdell, *J. Chem. Phys.*, **37**, 2336 (1962).

(6) E. N. Lightfoot, E. L. Cussler, Jr., and R. L. Rettig, *Chem. Eng. (Tokyo)*, **28**, 480 (1964).

(7) E. N. Lightfoot, E. L. Cussler, Jr., and R. L. Rettig, *A.I.Ch.E. J.*, **8**, 708 (1962).

(8) L. Onsager, *Ann. N. Y. Acad. Sci.*, **46**, 241 (1945).

(9) O. Lamm, *Acta Chem. Scand.*, **11**, 362 (1957).

(10) R. W. Laity, *J. Phys. Chem.*, **63**, 80 (1959).

(11) R. J. Bearman, *ibid.*, **65**, 1961 (1961).

(12) P. J. Dunlop, *ibid.*, **68**, 26 (1964).

(13) L. Onsager, *Phys. Rev.*, **37**, 405 (1931).

(14) L. Onsager, *ibid.*, **38**, 2265 (1931).

(15) C. F. Curtiss and J. O. Hirschfelder, *J. Chem. Phys.*, **17**, 550 (1949).

(16) I. J. O'Donnell and L. J. Gosting in "Structure of Electrolytic Solutions," W. J. Hamer, Ed., John Wiley and Sons, New York, N. Y., 1959.

(17) F. O. Shuck and H. L. Toor, *J. Phys. Chem.*, **67**, 540 (1963).

(18) R. L. Baldwin, P. J. Dunlop, and L. J. Gosting, *J. Am. Chem. Soc.*, **77**, 5235 (1955).



centration of impurity is significant must be determined experimentally. Reagent grade cyclohexane and toluene were used in all experiments.

*Solutions.* The desired solution concentrations for each experiment were calculated by assuming the densities were additive. Densities were taken to be 1.040, 0.77148, and 0.85821 for polystyrene, cyclohexane, and toluene, respectively. After two experiments were made, approximate values of the partial specific volumes were calculated. These were used to estimate the remaining compositions.

All solutions were prepared by weight on a B-5 Mettler balance, always against a sealed tare. All weights in air were corrected to those under vacuum. A definite order for making the ternary solutions was followed. After the polymer was weighed, the approximate amount of cyclohexane was added. The sample was placed in an oven at 40° and stirred slowly with a magnetic stirrer for at least 24 hr. Then the sample was brought up to the desired weight with cyclohexane which had been warmed to 35°. After the desired weight of toluene was added, the experiment was immediately begun. In this way, volatility losses were minimized and polymer precipitation avoided.

Solution densities were measured in 25-ml. short neck Pyrex pycnometers, which had been calibrated at least three times with air-saturated water. The density of the water at 28° was taken to be 0.99626 g./cm.<sup>3</sup>. Because of the limited amount of polymer available only one sample of each solution was measured. The samples were weighed against a sealed tare with the balance described above. Partial specific volumes were found by the usual method.<sup>20</sup>

*Apparatus.* In these experiments, free diffusion was studied using the Gouy interferometer belonging to Professor L. J. Gosting. A general description of the apparatus is available elsewhere.<sup>21</sup> The wave optical theory has been highly developed, and tables of the theoretical constants used are readily obtained.<sup>22-24</sup> The particular apparatus used in these experiments has been described in previous publications.<sup>3,25-27</sup>

The diffusion cell, manufactured of fused silica by the Pyrocell Manufacturing Co., is similar to the Tiselius cells described previously<sup>25,28-30</sup> but has a reference channel parallel to the diffusion channel.<sup>31</sup> In order that ordinary Rayleigh photographs may be taken during the experiment, the channel is filled with the less dense of the two diffusing solutions. The internal diameter  $a$  of the cell along the optical path is 2.4960 cm.; the optical lever arm  $b$  measured from the center of the cell to the photographic plate is 304.99 cm.

The flanges of the cell were greased with an outer band of Lubriscal grease and an inner band of Fisher

Non-Aq grease. The Non-Aq grease was washed six times in toluene and six times in cyclohexane to remove any impurities which would dissolve in the solvents during the experiment. Before being filled the cell and cell holder were heated to the experimental temperature of 28°.

The temperature was measured by a mercury-in-glass thermometer calibrated against a standard thermometer belonging to Professor L. J. Gosting.<sup>25</sup> It was found to read 28.044° at a true 28.000°.

*General Experimental Procedure.* In each experiment with the Gouy interferometer, diffusion occurs across a sharp initial boundary between the less dense upper solution and the more dense lower solution. This boundary was formed by sharpening with a single prong 23-gage stainless steel capillary.<sup>32</sup> Because of the high viscosity of the polymer solutions, an aspirator operating through a 5-l. surge tank was required to obtain the desired flow of 1-2 ml./min. through the capillary. All tubing in this apparatus was of polyethylene. This technique came at least as close to infinite sharpening as that previously used.

Three groups of reference photographs are required in the Gouy procedure.<sup>25,33</sup> These establish the position of the cell relative to the reference channel and allow determination of the fractional number of fringes. The integral number of fringes is found from one or two Rayleigh photographs taken during the experiment.<sup>33,34</sup> Reference photographs were taken with Kodak Tri-X Panchromatic, Kodak Super-Ortho Press, or Kodak Spectroscopic plates.

During the diffusion between the two solutions, 7-20 photographs of the Gouy interference fringes were taken on Kodak Super-Ortho Press or Kodak Spectro-

(19) A. B. Warth, "The Chemistry and Technology of Waxes," Reinhold Publishing Corp., New York, N. Y., 1956.

(20) P. J. Dunlop and L. J. Gosting, *J. Phys. Chem.*, **63**, 86 (1959).

(21) L. J. Gosting, *Advan. Protein Chem.*, **11**, 476 (1956).

(22) G. Kegeles and L. J. Gosting, *J. Am. Chem. Soc.*, **69**, 2516 (1947).

(23) L. J. Gosting and M. S. Morris, *ibid.*, **71**, 1998 (1949).

(24) L. J. Gosting and L. Onsager, *ibid.*, **74**, 6066 (1952).

(25) L. J. Gosting, E. M. Hanson, G. Kegeles, and M. S. Morris, *Rev. Sci. Instr.*, **20**, 209 (1949).

(26) P. J. Dunlop and L. J. Gosting, *J. Am. Chem. Soc.*, **75**, 5073 (1953).

(27) P. J. Dunlop and L. J. Gosting, *ibid.*, **77**, 5238 (1955).

(28) A. Tiselius, *Trans. Faraday Soc.*, **33**, 524 (1937).

(29) L. G. Longworth, *Chem. Rev.*, **30**, 323 (1942).

(30) J. St. L. Philpot and G. H. Cook, *Research*, **1**, 234 (1948).

(31) R. L. Rettig, Ph.D. Thesis, University of Wisconsin, 1964.

(32) D. S. Kahn and A. Polson, *J. Phys. Colloid Chem.*, **51**, 816 (1947).

(33) L. J. Gosting, *J. Am. Chem. Soc.*, **72**, 4418 (1950).

(34) R. P. Wendt and L. J. Gosting, *J. Phys. Chem.*, **63**, 1287 (1959).

scopic plates. The Tri-X Panchromatic plates gave less distinct images and so were not used for the diffraction photographs. The intensity minima of the fringe pattern were measured with a Gaertner M 2001 RS toolmakers microscope fitted with a projection screen.<sup>3,25</sup> Between 16 and 20 intensity minima were measured on each photograph, including the minima numbered 0 to 6.

The quantity  $C_t$ , which is the maximum value of refractive index gradient predicted by ray optics, is found by extrapolating  $Y/e^{-\xi^2}$  vs.  $Z_j^{2/3}$  to  $Z_j^{2/3} = 0$  where  $Y$  is the fringe displacement on the plate, equal to the derivatives of refractive index  $\partial n/\partial x$ ,<sup>26,35</sup>  $Z_j$  is the reduced fringe number,<sup>22,23</sup> and  $e^{-\xi^2}$  is found from the fringe number.<sup>23</sup> In a binary experiment, the values of  $Y/e^{-\xi^2}$  for fringes 0 to 6 were fit to a straight line in  $Z_j^{2/3}$  by least squares. This technique generally did not work for ternary experiments or for experiments where  $D_{ij}$  is a strong function of composition. After an unsuccessful attempt at a parabolic fit in  $Z_j^{2/3}$ ,  $C_t$  was found by a manual extrapolation. Using this value of  $C_t$ , an initial value of the reduced height-area ratio  $\mathcal{D}_A'$  for each plate was found

$$\mathcal{D}_A' = \frac{(J\lambda b)^2}{4\pi C_t^2 t} \quad (11)$$

The true value of  $\mathcal{D}_A$ , corrected for the fact that the initial boundary was not infinitely sharp, is found from

$$\mathcal{D}_A' = \mathcal{D}_A \left( 1 + \frac{\Delta t}{t} \right) \quad (12)$$

where  $\Delta t$  is the starting time correction.<sup>36,37</sup>

In the special case of zero polymer gradient at the composition 5% polystyrene, 5% toluene, and 90% cyclohexane, the first four fringes were too faint to be photographed by the usual exposures. If the exposures were increased so the first four were visible, the lower minima (fringe no. 6 or greater) were completely obscured. In this case, two sets of photographs are required, one set giving the first four fringes and a second set measuring the lower portion of the pattern. Both maxima and minima of the first five fringes of the first set of pictures were measured.  $C_t$  was found by the usual extrapolation, and  $\mathcal{D}_A$  and  $\Delta t$  were calculated from the relations given above. Then, reversing this procedure, values of  $C_t$  for each of the times of the second set of photographs were calculated. In this way, both  $\mathcal{D}_A$  and  $Q$  (described below) could be experimentally determined.

For each experiment, the average deviation of the refractive index profile from Gaussian shape was found as the area under the fringe deviation graph  $Q$ .<sup>35,38</sup>

$Q$  is found by plotting the dimensionless difference of the ideal refractive index gradient and the actual refractive index gradient vs. the reduced fringe number and then integrating over the reduced fringe member

$$Q = \int_0^1 \left( e^{-\xi^2} - \frac{Y}{C_t} \right) df(j) \quad (13)$$

For values of  $Q$  less than  $40 \times 10^{-4}$ , the data were fit to a fifth-order polynomial and integrated by machine. For higher values of  $Q$ , integrations were by Simpson's one-third rule using intervals of 0.05 in  $f(j)$ .

*Procedure for Binary Experiments.* In the binary theory of the Gouy interferometer, three basic assumptions are made. These are that the diffusion coefficient is not a function of concentration, that the refractive index is a linear function of the concentration, and that the partial specific volumes of both species are constant. If these assumptions are obeyed, then the reduced height-area ratio equals the binary diffusion coefficient and the area under the fringe deviation graph  $Q$  is zero.

However, in a wide variety of systems such as those studied here, the assumptions above are not valid. For example, the assumption that the diffusion coefficient is not a function of composition is valid only at the  $\theta$  temperature.<sup>39-41</sup> A limited theory for these cases has been developed by Gosting and Fujita<sup>42</sup> and by Fujita.<sup>43</sup> They solved the concentration profile and the refractive index profile for the assumptions

$$\mathcal{D}_{ij} = \mathcal{D}_{ij}(\bar{\rho})(1 + k_1(\rho - \bar{\rho}) + k_2(\rho - \bar{\rho})^2 + \dots) \quad (14)$$

$$n = n(\bar{\rho})(1 + R_1(\rho - \bar{\rho}) + R_2(\rho - \bar{\rho})^2 + \dots) \quad (15)$$

$$\bar{V}_i = \bar{V}_i(\bar{\rho})(1 + m_1(\rho - \bar{\rho}) + m_2(\rho - \bar{\rho})^2 + \dots) \quad (16)$$

where  $\bar{\rho}$  is the average mass concentration of the solute between the upper and lower solutions. The principal result of their work is that

$$\mathcal{D}_A = \mathcal{D}_{ij}(\bar{\rho})(1 + P(\Delta\rho)^2 + \dots) \quad (17)$$

(35) D. F. Akeley and L. J. Gosting, *J. Am. Chem. Soc.*, **75**, 4685 (1953).

(36) L. G. Longworth, *ibid.*, **69**, 2510 (1947).

(37) H. Fujita, *J. Phys. Soc. Japan*, **11**, 1018 (1956).

(38) H. Fujita and L. J. Gosting, *J. Phys. Chem.*, **64**, 1256 (1960).

(39) V. N. Tsvetkov and S. I. Kleinin, *J. Polymer Sci.*, **30**, 187 (1958).

(40) S. I. Kleinin, H. Benoit, and M. Daune, *Compt. rend.*, **250**, 3174 (1960).

(41) R. Varoqui, M. Jacob, L. Freund, and M. Daune, *J. chim. phys.*, **59**, 161 (1962).

(42) L. J. Gosting and H. Fujita, *J. Am. Chem. Soc.*, **79**, 1359 (1957).

(43) H. Fujita, *ibid.*, **83**, 2862 (1961).

In addition, although no exact theory is available, we postulate that

$$Q = S(\Delta\rho)^2 + \dots \quad (18)$$

In other words, to find the true value of the diffusion coefficient  $\mathfrak{D}_{ij}$  at the average composition, the reduced height-area ratio  $\mathfrak{D}_A$  is measured at least two times at the same average composition  $\bar{p}$  but at different  $\Delta\rho$ . The various values of  $\mathfrak{D}_A$  are graphed *vs.*  $(\Delta\rho)^2$  and extrapolated to  $(\Delta\rho)^2 = 0$  to obtain the true value of the diffusion coefficient. A similar extrapolation for  $Q$  will give a zero intercept.

If one of the species contains an impurity or a precipitate, the limiting intercept of  $Q$  may be nonzero.<sup>35</sup> For a polymer, a nonzero intercept may result from the polydispersity of the sample.<sup>44</sup> Before starting ternary experiments, binary runs of each pair of components must be made to ensure that impurities and polydispersity are not significant.

In summary, for a binary experiment, the critical parameter is  $Q$ . If, at finite  $\Delta\rho$ ,  $Q$  is zero, then the reduced height-area ratio  $\mathfrak{D}_A$  equals the diffusion coefficient at average composition  $\mathfrak{D}_{ij}(\bar{p})$ . If  $Q$  is nonzero, the experiment is repeated three times at the same  $\bar{p}$  but different  $(\Delta\rho)$ . Then  $Q$  and  $\mathfrak{D}_A$  are extrapolated *vs.*  $(\Delta\rho)^2$ . If  $Q$  is zero at  $(\Delta\rho)^2 = 0$ , then  $\mathfrak{D}_A$  equals  $\mathfrak{D}_{ij}(\bar{p})$ . If  $Q$  is nonzero at  $(\Delta\rho)^2 = 0$  for a system of two solvents, then the system must contain an impurity or a precipitate. If  $Q$  is nonzero at  $(\Delta\rho)^2 = 0$  for a system of solvent and a polymer, the system may contain an impurity or a precipitate, or the polymer may be too polydisperse to be treated as a single species.

*Procedure for Ternary Experiments.* The basic method for ternary experiments was described in earlier work.<sup>21, 38, 45, 46</sup> As in the binary case, three basic assumptions are made: that all four diffusion coefficients are not functions of composition, that the refractive index is a linear function of the composition of each species, and that the partial specific volumes of all species are constant. Since only two independent parameters,  $\mathfrak{D}_A$  and  $Q$ , are measured in each experiment, it is necessary to repeat each experiment at least twice at the same average composition but at different values of  $\Delta\rho_1$  and  $\Delta\rho_2$ .

The choice of  $\Delta\rho_1$  and  $\Delta\rho_2$  is governed by two restrictions. First, the absolute magnitudes of  $\Delta\rho_1$  and  $\Delta\rho_2$  are chosen so that the total number of fringes  $J$  is about 50–100.<sup>18</sup> The relative values of  $\Delta\rho_1$  and  $\Delta\rho_2$  are fixed by defining a new parameter  $\alpha$ , the fraction of the refractive index gradient due to component 1.<sup>35, 46</sup> In most previous work, the values of  $\alpha$  used for each experiment were 0.0, 0.2, 0.8, and 1.0. By solving

the multicomponent flux equations for the refractive index profile,  $\mathfrak{D}_A$  and  $Q$  may be found in terms of the four diffusion coefficients and  $\alpha$ .<sup>38, 45</sup>

$$1/\sqrt{\mathfrak{D}_A} = I_A + S_A\alpha \quad (19)$$

$$\frac{Q}{\sqrt{\mathfrak{D}_A}} = E_0 + E_1\alpha - E_2\alpha^2 \quad (20)$$

The five constants  $I_A$ ,  $S_A$ ,  $E_0$ ,  $E_1$ , and  $E_2$  are functions of  $\alpha$  and of the four diffusion coefficients. The values of these constants best fitting the data are found by trial and error.

However, for the systems studied in this work, the diffusion coefficients are strong functions of concentration; the refractive index varies nonlinearly with concentration; the partial specific volumes are not constant. To adapt the above theory to systems of this type, we must re-examine the parameter  $\alpha$ . Because of the nonlinear refractive index, the value for  $\alpha$  is not known except at the values of 0 and 1, *i.e.*, at the points where  $\Delta\rho_1 = 0$  and  $\Delta\rho_2 = 0$ . Thus if we consider these two points only, we can define an  $\alpha$  for the system.

We next assume that at small values of  $\Delta\rho_1$ ,  $\mathfrak{D}_A$  and  $Q$  vary with  $(\Delta\rho_i)^2$ . This is analogous to the binary case but, because it has no theoretical basis, must be verified experimentally. If it is verified, then parallel to the above equations, we have

$$\lim_{\substack{(\Delta\rho_1)^2 \rightarrow 0 \\ \Delta\rho_2 = 0}} \left( \frac{1}{\sqrt{\mathfrak{D}_A}} \right) = I_A \quad (21)$$

$$\lim_{\substack{\Delta\rho_1 = 0 \\ (\Delta\rho_2)^2 \rightarrow 0}} \frac{1}{\sqrt{\mathfrak{D}_A}} = I_A + S_A \quad (22)$$

$$\lim_{\substack{(\Delta\rho_1)^2 \rightarrow 0 \\ \Delta\rho_2 = 0}} \frac{Q}{\sqrt{\mathfrak{D}_A}} = E_0 \quad (23)$$

$$\lim_{\substack{\Delta\rho_1 = 0 \\ (\Delta\rho_2)^2 \rightarrow 0}} \frac{Q}{\sqrt{\mathfrak{D}_A}} = E_0 + E_1 - E_2 \quad (24)$$

We must repeat each experiment a minimum of four times, twice with  $\Delta\rho_1 = 0$  and with  $\Delta\rho_2$  equal to two different values, and twice with  $\Delta\rho_2 = 0$  and  $\Delta\rho_1$  equal to two different values. In this work, however, each experiment was repeated six times in order to check the linearity in  $(\Delta\rho_i)^2$  of the extrapolation of  $\mathfrak{D}_A$  and  $Q$ .

In practice, because the densities of the solutions

(44) E. L. Cussler, Jr., *J. Phys. Chem.*, **69**, 1144 (1965).

(45) H. Fujita and L. J. Gosting, *J. Am. Chem. Soc.*, **78**, 1099 (1956).

(46) L. A. Woolf, D. G. Miller, and L. J. Gosting, *ibid.*, **84**, 317 (1962).

**Table I:** Binary Runs for Sucrose-Water and Cyclohexane-Toluene

Expt. no. <sup>a</sup>	System	<i>T</i>	$\omega_1$	<i>J</i>	$\mathcal{D}_A \times 10^6$	<i>Q</i> × 10 <sup>4</sup>
2	1 = sucrose 2 = water	24.950 ± 0.006	0.00739	99.560	0.5164	0.5
13	1 = cyclohexane 2 = toluene	28.001 ± 0.003	0.0815	73.393	2.256	0.9
14	1 = cyclohexane 2 = toluene	28.003 ± 0.002	0.4597	66.847	1.944	-1.7
15	1 = cyclohexane 2 = toluene	28.003 ± 0.002	0.9000	64.330	1.776	0.7

<sup>a</sup> Experiments numbered chronologically.

**Table II:** Binary Diffusion Coefficients of Polystyrene<sup>a</sup>

Experiment no.	Solvent	Average mass fraction polymer	Mass fraction difference	<i>T</i>	<i>J</i>	$\mathcal{D}_A$ (exptl.) × 10 <sup>7</sup>	$\mathcal{D}_A$ (calcd.) × 10 <sup>7</sup>	<i>Q</i> (exptl.) × 10 <sup>4</sup>	<i>Q</i> (calcd.) × 10 <sup>4</sup>
8	Toluene	0.0500	0.01571	28.006 ± 0.002	66.543	9.082	9.078	21.1	21.1
23	Toluene	0.0500	0.01172	28.006 ± 0.003	52.040	8.930	8.935	11.7	11.8
24	Toluene	0.0500	0.00954	28.000 ± 0.002	41.246	8.874	8.871	7.3	7.3
(Limit A)	Toluene	0.0500	0.00000	...	0.000	...	8.752	...	-0.6
10	Cyclohexane	0.0500	0.01154	27.990 ± 0.002	69.396	0.7932	0.794	99.5	97.4
1	Cyclohexane	0.0500	0.00825	27.995 ± 0.004	49.632	0.871	0.878	55.6	60.6
52	Cyclohexane	0.0500	0.00338	28.000 ± 0.003	20.197	0.9820	0.987	11.9	9.2
(Limit B)	Cyclohexane	0.0500	0.00000	...	0.000	...	1.010	...	1.8

<sup>a</sup> Experiments numbered chronologically.

could not be exactly predicted, the values of  $\alpha$  for experiments were not exactly 0 or 1, but several thousandths off these values. The values of  $\mathcal{D}_A$  and *Q* must be corrected to  $\alpha = 0$  or 1 before the extrapolation can be made. These corrections were made as follows: Using the two experiments with the smallest values of  $\Delta\rho_1$  and  $\Delta\rho_2$ , initial values of  $I_A$ ,  $S_A$ ,  $E_0$ ,  $E_1$ , and  $E_2$  were calculated. These values were used to correct the values of  $\mathcal{D}_A$  and *Q* for the six experiments to  $\alpha = 0$  or  $\alpha = 1$ . The corrected values were extrapolated *vs.* the appropriate  $(\Delta\rho_i)^2$  to give the actual intercepts in terms of the five constants. Using these new constants, new correction factors were calculated, and the cycle was repeated until no significant change occurred.

One further point about the ternary theory requires emphasis. The labeling of the components as 1, 2, and 3 is of course arbitrary. However, in some cases, free convection may be caused by coupling between fluxes.<sup>47,48</sup> The restraint that free convection does not occur may restrict the species whose gradient is zero. Unfortunately, this may be determined only by trial and error.

## Results

Binary runs for the system sucrose-water and for three compositions of the system toluene-cyclohexane are shown in Table I. The sucrose run was made to check cell alignment and experimental procedure. Its value of  $\mathcal{D}_A$  differs from that of Gosting and Morris<sup>23</sup> by 0.1%, well within the expected error of 0.3%. The area under the fringe deviation graph *Q* is equal to zero within the expected error of  $\pm 2 \times 10^{-4}$ . The three binary experiments on cyclohexane-toluene also show *Q* = 0 within this error, indicating that the solvents contain no significant impurities.

The data required for the binary diffusion coefficients of 5 wt. % polystyrene in cyclohexane and in toluene are given in Table II. The experimental values  $\mathcal{D}_A$  (exptl.) and *Q* (exptl.) are plotted *vs.* the square of the mass fraction difference  $(\Delta\omega)^2$  for each trio of experiments. A straight line is drawn through the experimental points to the intercept at  $(\Delta\omega)^2 = 0$ . This intercept is reported in Table II as "limit." The ex-

(47) R. Wendt, *J. Phys. Chem.*, **66**, 1740 (1962).

(48) G. Reinfelds and L. J. Gosting, *ibid.*, **68**, 2464 (1964).

Table III: Initial Data for the System Polystyrene-Cyclohexane-Toluene at 28<sup>aa</sup>

Expt. no. <sup>b</sup> Type plates <sup>c</sup> Temp., °C.	Ternary point 1: toluene regarded as solvent			Ternary point 2: cyclohexane regarded as solvent			Ternary point 3: cyclohexane regarded as solvent					
	25 S	27 S	46 S	21 TO	22 TO	26 S	45 S	44 O	43 S	34 S	38 S	39 S
$\omega_1$	28.002 ± 0.002	28.001 ± 0.002	28.005 ± 0.002	28.001 ± 0.002	28.006 ± 0.003	28.000 ± 0.003	28.005 ± 0.002	28.001 ± 0.002	28.008 ± 0.003	27.997 ± 0.002	27.998 ± 0.002	28.002 ± 0.002
$\omega_2$	0.0500	0.0500	0.0500	0.0500	0.0500	0.0500	0.0500	0.0500	0.0498	0.0500	0.0500	0.0500
$\Delta\rho_1$	0.0500	0.0501	0.0501	0.0500	0.0501	0.0500	0.0500	0.0500	0.4748	0.4750	0.4749	0.4748
$\Delta\rho_2$	0.00012	0.00002	0.00004	0.00000	0.01557	0.00892	0.00000	0.00003	-0.00004	0.00000	0.00905	0.00624
$J$	-0.03243	-0.02072	-0.01323	-0.00000 > 0 <sup>d</sup>	0.00001	-0.00003	0.00000	0.02547	0.01739	0.00004	0.00006	-0.00241
$\mathcal{D}_A$ (exptl.) × 10 <sup>7</sup>	160.870	100.974	63.998	0.00	77.755	39.211	80.405	101.478	66.585	86.478	70.638	40.693
$\mathcal{D}_A$ (calcd.) × 10 <sup>7</sup>	183.0	189.2	185.0	7.938	8.298	8.149	128.5	128.5	123.3	7.300	7.340	5.903
$Q$ (exptl.) × 10 <sup>4</sup>	183.4	188.2	186.0	7.945	8.286	8.154	128.3	127.9	123.1	7.300	7.340	7.338
$Q$ (calcd.) × 10 <sup>4</sup>	150.9	106.5	121.9	-104.7	-67.8	-81.6	376.7	371.3	379.1	193	-77.9	192
	151	107	122	-104.7	-67.7	-81.8	377	371	379	193		
				85.6								

Expt. no. <sup>b</sup> Type plates <sup>c</sup> Temp., °C.	Ternary point 2: cyclohexane regarded as solvent			Ternary point 3: cyclohexane regarded as solvent		
	28 S	41 S	42 S	29 S	35 S	36 S
$\omega_1$	28.000 ± 0.002	27.999 ± 0.002	28.005 ± 0.003	28.002 ± 0.003	27.997 ± 0.002	27.998 ± 0.002
$\omega_2$	0.0500	0.0500	0.0500	0.0500	0.0503	0.0500
$\Delta\rho_1$	0.8997	0.8999	0.8999	0.8999	0.8993	0.8996
$\Delta\rho_2$	-0.00000	-0.00001	0.00001	0.00000	0.00932	0.00655
$J$	0.02379	0.02001	0.01546	0.00009	0.00006	0.002548
$\mathcal{D}_A$ (exptl.) × 10 <sup>7</sup>	77.103	64.836	49.990	100.974	70.519	60.268
$\mathcal{D}_A$ (calcd.) × 10 <sup>7</sup>	60.00	68.54	77.04	1.705	1.742	2.346
$Q$ (exptl.) × 10 <sup>4</sup>	60.00	68.60	77.03	1.705	1.742	2.350
$Q$ (calcd.) × 10 <sup>4</sup>	1134	1057	928	48.3	13.8	419
	1143	1039	937	48.8	14.6	407

<sup>a</sup> Units  $\Delta\rho_i$  in g./cm<sup>3</sup>;  $\mathcal{D}_A$  in cm<sup>2</sup>/sec. <sup>b</sup> Experiments numbered chronologically. <sup>c</sup> S, Spectroscopic plates; O, Super-Ortho Press plates; TO, Tri-X Panchromatic plates for reference photographs and Super-Ortho Press for diffusion photographs. <sup>d</sup> The notation 0.00000 > 0 indicates this quantity is finite. <sup>e</sup> Experiment 39 is not included in extrapolation.

**Table IV:** Multicomponent Diffusion Coefficients and Partial Specific Volumes

Column	1	2	3 <sup>a</sup>	4	5	6
Solvent	1 = polystyrene 2 = cyclohexane 3 = toluene			1 = polystyrene 2 = toluene 3 = cyclohexane		
Ternary pt.	1	Binary limit	1	3	2	Binary limit
$\omega_1$	0.0500	0.0500	0.0500	0.0500	0.0500	0.0500
$\omega_2$	0.0500	0.9500	0.9000	0.4751	0.0503	0.0000
$\bar{V}_1$	0.9133	...	0.9133	0.9030	0.9464	...
$\bar{V}_2$	1.340	...	1.164	1.171	1.162	...
$\bar{V}_3$	1.164	...	1.340	1.305	1.299	...
$D_{11} \times 10^7$	8.9	(8.7) <sup>c</sup>	10.0	5.8	1.8	1.010 <sup>b</sup>
$D_{12} \times 10^7$	-1.6	(0.0) <sup>c</sup>	1.3	-6.7	-6.7	(0) <sup>c</sup>
$D_{21} \times 10^7$	-8.9	(175) <sup>c</sup>	169.6	14.5	-0.9	0.0 <sup>b</sup>
$D_{22} \times 10^7$	203.1	(226) <sup>c</sup>	202.0	171.8	178.9	(178) <sup>c</sup>
$R_{12} \times 10^{-6}$	9.6 ± 0.10	11.3 ± 0.1 <sup>b</sup>	11.4 ± 2	8.7 ± 1	12 ± 6	...
$R_{13} \times 10^{-6}$	11.4 ± 2	...	9.86 ± 2	21.5 ± 6	57.8 ± 1	99.0 ± 0.5
$R_{21} \times 10^{-5}$	11.5 ± 2	11.3 ± 0.1 <sup>b</sup>	12.7 ± 0.5	4.14 ± 0.40	-7 ± 8	...
$R_{23} \times 10^{-6}$	1.0 ± 0.1	(0.445) <sup>c</sup>	0.056 ± 0.010	0.39 ± 0.20	0.9 ± 1	(0.564) <sup>c</sup>

<sup>a</sup> Values calculated from multicomponent coefficients in column 1. <sup>b</sup> Limiting values found from eq. 11, 21, and 23 and data in Table II. <sup>c</sup> Values estimated with eq. 21-24 from binary data in Tables I and II assuming  $\rho_1 = 0$  are in parentheses.

trapolation is tested by reading the smoothed values  $\mathcal{D}_A$  (calcd.) and  $Q$  (calcd.) at the known values of  $(\Delta\omega)^2$ . These values are also reported in Table II.

Initial data for eighteen ternary experiments at three different average compositions are given in Table III. Parallel to the binary experiment,  $\mathcal{D}_A$  (exptl.) and  $Q$  (exptl.) are the actual experimental parameters, while  $\mathcal{D}_A$  (calcd.) and  $Q$  (calcd.) again test the extrapolation in  $(\Delta\rho_i)^2$ . The limiting values of  $\mathcal{D}_A$  and  $Q$  at  $(\Delta\rho_i)^2 = 0$  are included in the table as "limit."

The values of the partial specific volumes for the three ternary compositions are given in Table IV. Since the partial specific volumes are not constant, these are averages across the concentration increment and are known only to  $\pm 5\%$ . The generalized Fick's law coefficients and the generalized Stefan-Maxwell coefficients are also reported in Table IV. The diffusion coefficients of ternary point 1 considering toluene as the solvent are given in column 1; the coefficients for points 1, 3, and 2 considering cyclohexane as the solvent are given in columns 3, 4, and 5, respectively. The binary limits of the multicomponent coefficients considering cyclohexane as the solvent are given in columns 2 and 6. Those limits which are exact are written without parentheses; those found by assuming the polymer concentration equals zero are written in parentheses.

## Discussion

The binary data in Table II show that the binary diffusion coefficient of polystyrene is a strong function

of composition. In the system polystyrene-toluene, this results in a strong variation of  $\mathcal{D}_A$  with  $(\Delta\omega)^2$ . These conclusions are partially supported by literature data.<sup>49</sup> As predicted by the theory, the effects of concentration may be eliminated by the straight line extrapolation *vs.*  $(\Delta\omega)^2$  at small values of  $(\Delta\omega)^2$ . The agreement with this extrapolation is very good, providing further verification of the theory. The values of  $\mathcal{D}_A$  read from the straight line differ from the observed values by less than 0.1%, well within the expected error of 0.3%. In addition, the postulate that the concentration effects in the parameter  $Q$  may be eliminated by extrapolation in  $(\Delta\omega)^2$  is experimentally verified. The extremely good agreement is fortuitous, since  $Q$  is known to only  $\pm 2 \times 10^{-4}$ . The value of zero for  $Q$  at  $(\Delta\omega)^2 = 0$  indicated that in toluene the polymer behaves as a single species.<sup>44</sup> Thus the limiting value of  $\mathcal{D}_A$  at  $(\Delta\omega)^2 = 0$  equals the binary diffusion coefficient at the average polymer concentration.

The system polystyrene-cyclohexane also shows sharp variation of  $\mathcal{D}_A$  with  $(\Delta\omega)^2$ . However, the refractive index varies linearly with concentration in this system since  $J/\Delta\omega$  is a constant. The variations of  $\mathcal{D}_A$  and  $Q$ , which are much larger for this system, are again removed by extrapolating *vs.*  $(\Delta\omega)^2$ . However, the agreement is less good. The values of  $\mathcal{D}_A$  read from the straight line differ by 0.6% from the

(49) G. C. Park, *J. chim. phys.*, **55**, 134 (1958).

experimental ones, twice the expected error. The parameter  $Q$  shows similar deviations. The concentration effects in this system are probably large enough to require that the  $(\Delta\omega)^4$  term be included in the extrapolation. The intercept of  $Q \times 10^4$  is  $2 \pm 2$ . The nonzero intercept may be due to the precipitation of a small amount of polystyrene of molecular weight greater than 250,000.<sup>50</sup> Such an impurity, which would result in a positive intercept, would be consistent with the slight cloudiness observed in these solutions. However, since the value of the intercept is equal to the expected error, this system is safely treated as a binary. Once again,  $\mathfrak{D}_A$  at  $(\Delta\omega)^2 = 0$  equals the binary diffusion coefficient at the average composition.

The ternary data summarized in Table III show that both  $\mathfrak{D}_A$  and  $Q$  are strong functions of  $(\Delta\rho_i)^2$ . As one would suspect from the binary results, the effects are largest where the cyclohexane concentration is large (ternary point 2). The assumption that  $\mathfrak{D}_A$  and  $Q$  vary linearly with  $(\Delta\rho_i)^2$  at small values of  $(\Delta\rho_i)^2$  is verified by the results at all three compositions. The variation of  $\mathfrak{D}_A$  from the straight line is in all cases less than 0.5%, which is less than the expected error for a ternary experiment of 0.6%. The departures of  $Q \times 10^4$  from a straight line are less than the expected error of  $\pm 2$  except for expt. 28, 41, and 42. In these three experiments, which show the largest deviations from Gaussian behavior yet reported,  $Q \times 10^4$  is known to only  $\pm 20$ . The cause of this large error is not known. The most probable explanation is that the variation of  $Q$  with  $(\Delta\rho_i)^4$  is significant in the extrapolation *vs.*  $(\Delta\rho_i)^2$ .

The values of  $\mathfrak{D}_A$  and  $Q$  at  $(\Delta\rho_i)^2 = 0$  provide the input data from which the  $D_{ij}$  and the  $R_{ij}$  are calculated. The  $D_{ij}$ , found by the usual procedure,<sup>38</sup> are known to  $\pm 0.8 \times 10^{-7}$ . The  $R_{ij}$  are known less accurately. Because the defining equations of the  $R_{ij}$  are nonlinear, the equations must be forced into the generalized Fick's law form (or its inverse) and then solved.<sup>2</sup> Thus it is the  $D_{ij}$  which are always measured, and the  $R_{ij}$  calculated from them, with a resultant loss of accuracy. As an example

$$R_{12} = \frac{1}{\rho_1 \bar{V}_2} \left( \frac{D_{12}}{D_{11}D_{22} - D_{21}D_{12}} \right) \quad (25)$$

$D_{12}$  may be known to only one significant figure. Thus if  $\rho_1$  is very small,  $R_{12}$  will be poorly known.

*Deviations from Fick's Law.* This system shows some of the largest deviations from Fick's law which have been observed. The cross term coefficients ( $D_{12}$  and  $D_{21}$ ) are large relative to the main term coefficients ( $D_{11}$  and  $D_{22}$ ). In particular, the coefficient

$D_{12}$  was greater than  $D_{11}$  for two of the three ternary points measured. Some of this deviation is due to designating one species (cyclohexane) as the solvent; but a significant part of the deviations are caused by sharp gradients in thermodynamic forces. At 28°, binary solutions of polystyrene-toluene and polystyrene-cyclohexane behave very differently. Quantitatively this difference is described by the chemical potential of the solvent<sup>51</sup>

$$\frac{\mu_S - \mu_S^0}{RT} = -\psi_1 \left( 1 - \frac{\theta}{T} \right) \phi_P^2 \quad (26)$$

where  $\mu_S$  is the chemical potential of the solvent,  $\phi_P$  is the volume fraction of polymer, and  $\psi_1$  and  $\theta$  are experimental constants. For toluene,  $\theta = 160^\circ\text{K}$ ., while for cyclohexane,  $\theta = 307.2^\circ\text{K}$ . Thus, at 28° polystyrene has a chemical potential of opposite sign in each of the two solvents. The result of this behavior is that these ternary solutions are nonhomogeneous: a molecule of polystyrene is surrounded by a cloud of high toluene concentration. This nonhomogeneity is responsible for a significant portion of the deviations from Fick's law.

However, the main cause of the concentration dependence of  $D_{ij}$  is the choice of one species as the solvent. If the component designated as the "solvent" is present only in small concentrations, the cross terms can become very large. This is shown theoretically by eq. 8 and experimentally by columns 1 and 3 of Table IV. In spite of the lack of accuracy in their measurement, the  $R_{ij}$  show smaller concentration dependence than the  $D_{ij}$ , since they do not depend on labeling one species as "solvent." They are preferable for problems where no single species is always present in excess.

Neither the  $D_{ij}$  or the  $R_{ij}$  have any known molecular significance. Since the  $D_{ij}$  are macroscopic phenomenological coefficients, their physical significance would be expected to be complex. However, because the  $R_{ij}$  are defined in a parallel form to the Stefan-Maxwell equations used for ideal gases, it was hoped that they would represent particular molecular interactions. Thus they would have a simple relation with binary coefficients, as is the case for ideal gases. No simple relation is found experimentally.

In general, then, no fully satisfactory set of flux equations is yet known. The two most promising sets are the generalized Fick's law coefficients  $D_{ij}$  defined relative to volume average velocity and the generalized

(50) A. R. Schultz and P. J. Flory, *J. Am. Chem. Soc.*, **74**, 4760 (1952).

(51) P. J. Flory, "Principles of Polymer Chemistry," Cornell University Press, Ithaca, N. Y., 1954, pp. 522, 523, 625.

Stefan–Maxwell coefficients  $R_{ij}$  based on volume fraction driving force. The  $D_{ij}$  may be measured more accurately experimentally, but show greater concentration dependence than the  $R_{ij}$ . Neither set may generally be predicted from binary data. The molecular significance of neither set is known.

*Acknowledgments.* The authors wish to thank Professors P. J. Dunlop and L. J. Gosting for many helpful discussions of this research, and Professor Gosting for the loan of the Gouy interferometer used in the experimental work. This work was supported by National Science Foundation Grant No. 86-4403.

## Multicomponent Diffusion Involving High Polymers. II.

### Characterization of Polydispersity from Diffusion Data

by E. L. Cussler, Jr.\*

*Department of Chemical Engineering, University of Wisconsin, Madison, Wisconsin  
(Received September 15, 1964)*

Polydispersity may be described by average diffusion coefficients. This work develops the theory for the determination of these coefficients with the Gouy interferometer. If a particular form of the distribution function of diffusion coefficients is assumed, number-average and weight-average molecular weights may be calculated. Two polystyrenes of broad molecular weight distribution are studied in cyclohexane at 35°.

If a polymer sample is sufficiently dilute, the various species diffuse independently. In this case, diffusion data can be used to measure the polydispersity; that is, the distribution of the sizes of the polymer molecules. Usually, instead of actually measuring this distribution, average molecular weights are determined by osmotic pressure, light scattering, or ultracentrifuge measurements. In a similar fashion, Daune and Benoit<sup>1</sup> suggested measurement of the average diffusion coefficients  $D_1$  and  $D_2$

$$D_1 = \left[ \int_0^\infty D^{-1/2} g(D) dD \right]^2 \quad (1)$$

$$D_2 = \frac{\int_0^\infty D^{-1/2} g(D) dD}{\int_0^\infty D^{-3/2} g(D) dD} \quad (2)$$

where  $D$  is the diffusion coefficient and  $g(D)$  is the distribution of diffusion coefficients. Using a Jamin

interferometer, Daune, Benoit, and co-workers<sup>2–5</sup> evaluated  $D_1$  and  $D_2$  for several systems. This paper develops the theory of measurement of average diffusion coefficients with the Gouy interferometer and presents results for two polystyrenes.

*Theory.* The Gouy interferometer measures the refractive index gradient for one-dimensional, isothermal diffusion.<sup>6</sup> If the solution is sufficiently dilute, each polymer species diffuses independently. For a con-

\* Department of Physical Chemistry, University of Adelaide, Adelaide, South Australia.

- (1) M. Daune and H. Benoit, *J. chim. phys.*, **51**, 233 (1955).
- (2) M. Daune, H. Benoit, and Ch. Sadron, *J. Polymer Sci.*, **16**, 483 (1955).
- (3) M. Daune, H. Benoit, and G. Scheibling, *J. chim. phys.*, **54**, 924 (1957).
- (4) R. N. Mukherjea and P. Remmp, *ibid.*, **56**, 94 (1959).
- (5) R. Varoqui, M. Jacob, L. Freund, and M. Daune, *ibid.*, **59**, 161 (1962).
- (6) L. J. Gosting, *Advan. Protein Chem.*, **11**, 476 (1956).



stant diffusion coefficient  $D$  and constant partial specific volumes, the concentration profile for free diffusion is

$$\frac{\rho - \rho_0}{\frac{\Delta\rho_0}{2}} = \operatorname{erf} \frac{x}{\sqrt{4Dt}} \quad (3)$$

where  $\rho$  is the mass concentration,  $\rho_0$  the average mass concentration,  $\Delta\rho$  the mass concentration difference,  $x$  the cell coordinate, and  $t$  the time. Except at the  $\Theta$ -temperature, the assumption of constant  $D$  is poor.<sup>5,7,8</sup> Experiments at temperatures other than the  $\Theta$ -temperature must be repeated at different  $\Delta\rho$  to ensure that the concentration dependence of the diffusion coefficient is not significant. The concentration dependence of the measured parameters may be removed by extrapolating *vs.* the concentration difference squared.<sup>9,10</sup>

If each species varies linearly with refractive index, the refractive index profile is

$$\frac{n - n_0}{\left(\frac{\Delta n}{2}\right)} = \int_0^{\infty} \operatorname{erf} \frac{x}{\sqrt{4Dt}} g(D) dD \quad (4)$$

The refractive index gradient  $\partial n/\partial x$  is

$$\frac{\partial n}{\partial x} = \frac{\Delta n}{2} \int_0^{\infty} \frac{e^{-x^2/4Dt}}{\sqrt{\pi Dt}} g(D) dD \quad (5)$$

with a maximum at  $x = 0$

$$\left(\frac{\partial n}{\partial x}\right)_{\max} = \frac{\Delta n}{\sqrt{4\pi t}} \int_0^{\infty} g(D) D^{-1/2} dD \quad (6)$$

Combining eq. 6 with eq. 1

$$D_1 = \frac{(\Delta n)^2}{4\pi t (\partial n/\partial x)_{\max}^2} \quad (7)$$

$D_1$  is identical with the "reduced height-area ratio"  $\mathfrak{D}_A$ ,<sup>11</sup> which is measured by the Gouy method.

The second average diffusion coefficient  $D_2$  is found from the deviation of the refractive index gradient given in eq. 5 from Gaussian shape. We define an "idealized cell coordinate"  $\zeta$  as the value of  $x/\sqrt{4Dt}$  for a particular fringe if the polymer were monodisperse. This parameter  $\zeta$  is a function only of the Gouy fringe number  $j$ . Next, we define the "fringe deviation"  $\Omega$  as<sup>12</sup>

$$\Omega = e^{-\zeta^2} - \frac{(\partial n/\partial x)}{(\partial n/\partial x)_{\max}} \quad (8)$$

Combining eq. 5, 7, and 8 gives

$$\Omega = e^{-\zeta^2} - \int_0^{\infty} g(D) \sqrt{\frac{D_1}{D}} e^{-x^2/4Dt} dD \quad (9)$$

If we find  $x$  as a function of  $\zeta$ , we may expand eq. 9 as a power series in  $\zeta$  to obtain an expression for  $D_2$ . This derivation is given in the Appendix. The result is

$$\Omega = \frac{1}{3} \left[ \left(\frac{D_1}{D_2}\right) - 1 \right] \zeta^2 + 0(\zeta^4) \quad (10)$$

This equation allows determination of the second average diffusion coefficient.<sup>13,14</sup>

Unfortunately, the two average diffusion coefficients defined above do not have the same physical significance as the number-average and weight-average molecular weights. The ratio of these average molecular weights is often the desired result. To obtain them, Daune and Benoit postulated a two-parameter form of the distribution function

$$g(D) = \frac{1}{D_0} \frac{\beta^\beta}{\Gamma(\beta)} \left(\frac{D_0}{D}\right)^{\beta+2} e^{-\beta(D_0/D)} \quad (11)$$

The parameters  $D_0$  and  $\beta$  may be found from  $D_1$  and  $D_2$ . The average molecular weights are found using the relation

$$f(M) dM = g(D) dD \quad (12)$$

where  $f(M)$  is the distribution of molecular weights.

To determine how well the assumed distribution function fits the data, we require another experimental parameter, the area under the fringe deviation graph  $Q$

$$Q = \int_0^1 \Omega df(j) \quad (13)$$

where  $f(j)$  is the interference condition discussed in detail in the Appendix. The parameter  $Q$  is used in the analysis of coupled ternary diffusion problems<sup>15</sup> and has proved the most successful method of analyzing the deviations of the refractive index profile from Gaussian shape.

(7) S. I. Klenine, H. Benoit, and M. Daune, *Compt. rend.*, **250**, 3174 (1960).

(8) V. N. Tsvetkov and S. I. Klenine, *J. Polymer Sci.*, **30**, 187 (1958).

(9) L. J. Gosting and H. Fujita, *J. Am. Chem. Soc.*, **79**, 1359 (1957).

(10) E. L. Cussler, Jr., and E. N. Lightfoot, *J. Phys. Chem.*, **69**, 1135 (1965).

(11) P. J. Dunlop and L. J. Gosting, *J. Am. Chem. Soc.*, **77**, 5238 (1955).

(12) D. A. Akeley and L. J. Gosting, *ibid.*, **75**, 5685 (1953).

(13) The reduced second moment and the reduced fourth moment defined for the Gouy theory do not give useful average diffusion coefficients.

(14) R. L. Baldwin, P. J. Dunlop, and L. J. Gosting, *J. Am. Chem. Soc.*, **77**, 5235 (1955).

(15) H. Fujita and L. J. Gosting, *J. Phys. Chem.*, **64**, 1256 (1960).

To evaluate  $Q$  in terms of the distribution functions, we combine eq. 8 and 13 to obtain

$$Q = \int_0^\infty e^{-\zeta^2} \frac{\partial f(j)}{\partial \zeta} d\zeta - \int_0^\infty \frac{\partial n / \partial x}{(\partial n / \partial x)_{\max}} \frac{\partial f(j)}{\partial y} dy \quad (14)$$

where  $y = x\sqrt{4D_A t}$ . These derivatives may be found by differentiating eq. 23 and 25 in the Appendix. The results are

$$\frac{\partial f(j)}{\partial \zeta} = \frac{4}{\sqrt{\pi}} \zeta^2 e^{-\zeta^2} \quad (15)$$

$$\frac{\partial f(j)}{\partial y} = \frac{4}{\sqrt{\pi}} \int_0^\infty g(D) y^2 \delta^3 e^{-y^2 \delta^2} dD \quad (16)$$

where  $\delta = (D_A/D)^{1/2}$ . By inserting these derivatives into eq. 14, subscripting the two different integration variables previously called  $D$ , and integrating over  $\zeta$  and  $y$ , we obtain

$$Q = 2^{-3/2} - \int_0^\infty \int_0^\infty g(D_i) g(D_j) \frac{(D_i/D_i)^{1/2}}{(D_j/D_i + 1)^{3/2}} dD_i dD_j \quad (17)$$

If the species is monodisperse,  $g(D)$  becomes the Dirac  $\delta$  function and  $Q$  is zero.

For the form of  $g(D)$  given in eq. 11, we have

$$Q = 2^{-3/2} - \left(\frac{D_A}{D_0}\right)^{1/2} \int_0^\infty \int_0^\infty \frac{\left(\frac{D_0}{D_i}\right)^{\beta+1/2} \left(\frac{D_0}{D_j}\right)^{\beta+1/2}}{\left(\frac{D_0}{D_i} + \frac{D_0}{D_j}\right)^{\beta+3/2}} \times \exp\left[-\beta\left(\frac{D_0}{D_i} + \frac{D_0}{D_j}\right)\right] d\left(\frac{D_0}{D_i}\right) d\left(\frac{D_0}{D_j}\right) \quad (18)$$

Using the variable substitutions

$$\frac{D_0}{D_i} = r \cos \theta; \quad \frac{D_0}{D_j} = r \sin \theta \quad (19)$$

the above equation may be directly integrated

$$Q = 2^{-3/2} - \frac{\Gamma(2\beta + 5/2)\Gamma(\beta + 5/2)}{\Gamma(2\beta + 4)\Gamma(\beta + 1)} \quad (20)$$

Thus, a measurement of  $Q$  provides a check on the parameter  $\beta$ .

From an experiment with the Gouy interferometer, we find the two average diffusion coefficients  $D_1$  and  $D_2$ . From these two true averages, we may determine values for  $D_0$  and  $\beta$  of the assumed distribution. At the same time, we can obtain a value of  $\beta$  from  $Q$  which is based on the assumption that the polymer

does fit this type of distribution. Comparison of the values of  $\beta$  obtained in these two ways shows how well the sample fits the assumed distribution. If we decide that, for our purposes, this assumption is satisfied, we may use our knowledge of  $g(D)$  to calculate  $M_n$  and  $M_w$ .

## Experimental

*Materials and Solutions.* Two polystyrene samples were studied. The first was National Bureau of Standards standard sample No. 706, a polystyrene of broad molecular weight distribution. The number-average molecular weight by osmotic pressure measurements with No. 600 cellophane membranes was 136,500. This value should be the upper limit of the true value. The National Bureau of Standards reported weight-average molecular weights of 257,800 (measured by light scattering) and 288,100 (measured by sedimentation equilibrium). A value for the weight-average molecular weight of 278,000 was obtained from sedimentation equilibrium by Osterhault.<sup>16</sup> The sample used in these experiments was provided by Dr. Osterhault.

The second polymer sample, designated 19F, was provided by Professor J. D. Ferry of the Department of Chemistry at the University of Wisconsin. It was originally supplied by Dr. R. F. Boyer of the Dow Chemical Co. as a preparation having substantially the most probable molecular weight distribution. It had a number-average molecular weight of 197,000 by osmotic measurements,<sup>17</sup> and a weight-average molecular weight of 370,000 by light scattering measurements<sup>18</sup> and of 375,000 by sedimentation velocity experiments.<sup>19</sup> However, a value of 456,000 has been reported for sedimentation equilibrium experiments.<sup>16</sup> Both polymers were studied in reagent grade cyclohexane at 35°.

*Apparatus.* The Gouy interferometer<sup>6,11,12,20-22</sup> used in these experiments has been fully described elsewhere. The temperature was measured to  $\pm 0.002^\circ$  with a mercury-in-glass thermometer calibrated against a standard thermometer belonging to Professor J. W. Williams. It was found to read  $34.966^\circ$  at a true

(16) H. W. Osterhault, Ph.D. Thesis, University of Wisconsin, 1964.

(17) L. E. Grandine, Jr., Ph.D. Thesis, University of Wisconsin, 1952.

(18) D. J. Streeter and R. F. Boyer, *Ind. Eng. Chem.*, **43**, 1790 (1951).

(19) J. F. Blair and J. W. Williams, *J. Phys. Chem.*, **68**, 161 (1964).

(20) L. J. Gosting, E. M. Hanson, G. Kegeles, and M. S. Morris, *Rev. Sci. Instr.*, **20**, 209 (1949).

(21) L. A. Woolf, D. G. Miller, and L. J. Gosting, *J. Am. Chem. Soc.*, **84**, 317 (1962).

(22) R. L. Rettig, Ph.D. Thesis, University of Wisconsin, 1964.

Table I: Polystyrene in Cyclohexane at 35°

Expt. no.	Polymer	Average mass fraction	Mass fraction difference	$T, ^\circ\text{C.}$	$J$	$D_1 \times 10^7$	$D_2 \times 10^7$	$Q \times 10^4$	$\beta$ from $D_1/D_2$	$\beta$ from $Q$	$\beta$ from $M_w/M_n$
47	NBS 706	0.00721	0.01442	$35.003 \pm 0.004$	86.483	2.578	2.124	169.6	2.70	2.80	2.38
48	19F	0.00629	0.01259	$35.014 \pm 0.002$	76.019	2.070	1.676	191.3	2.38	2.36	2.38

35.000°. A 110-volt constant input heater equipped with a Variac was used to supplement the usual temperature control. All calculations were made on an IBM 1620 computer belonging to the Wisconsin College of Engineering.

### Results

The experimental results for polymers NBS 706 and 19F are given in Table I. In this table,  $D_1$  and  $D_2$  are reported separately, although it is  $D_1$  and  $D_1/D_2$  which are found experimentally. These values are used to determine a value of  $\beta$  from eq. 1, 2, and 10. The value of  $\beta$  for  $Q$  is found from eq. 20. For comparison with these values, a value of  $\beta$  has been calculated from  $M_w/M_n$  by assuming  $D = kM^{-0.5}$ . The value of 0.5 is given by the theory of a flexible chain polymer in a poor solvent. Experimental values of the exponent range from 0.48 to 0.51.<sup>23,24</sup> The ratio of  $M_w/M_n$  was based on light scattering data and osmotic pressure data for the calculations. Thus, values of  $\beta$  obtained from  $D_1/D_2$ , from  $Q$ , and from  $M_w/M_n$  can be compared.

### Discussion

The average diffusion coefficients  $D_1$  and  $D_2$  reported above are reproducible within 0.5%. As such, they are an accurate, reproducible method of analyzing polydispersity. Their chief disadvantage is that they are not in common use. The assumption of a particular form of distribution function  $g(D)$  which is necessary to convert the diffusion data into molecular weight data prevents the calculation of the accurate molecular weights which are commonly reported. This is shown by both polydisperse polymers which were studied.

For polymer NBS 706, the values obtained for  $\beta$  from  $D_1/D_2$  and  $Q$  differ by about 4%, indicating that the Shultz distribution is not a good assumption for this polymer. This is in agreement with results obtained on this polymer from sedimentation equilibrium.<sup>14</sup> Sedimentation equilibrium measures  $M_w$ ,  $M_z$ , and  $M_{z+1}$  and fits these parameters to a Shultz-type distribution. Thus, the procedure weights the larger molecules more heavily. It gives  $M_w/M_n = 1.67$ . The Gouy technique reported in this paper

weights the smaller molecules more heavily. Using the value of  $\beta = 2.70$ ,  $M_w/M_n = 2.18$ . These values bracket the directly measured value of 1.887.

For polymer 19F, the values obtained for  $\beta$  by the two methods differ by less than 1%, indicating that the actual distribution function is nearly the assumed form. Thus, the value of  $\beta$  found from  $M_w/M_n$  should be nearly the same. It is. However, since there is disagreement about the actual value of  $M_w/M_n$  for this polymer,<sup>16</sup> this close agreement must be viewed with some skepticism.

The success of this technique depends on the goal of the experimentalist. If he is interested in the molecular weight distribution of the polymer as a goal in itself, then he should use the established methods of fractionation or of the ultracentrifuge. If his goal is the measurement of some other physical property, such as viscosity or chemical potential, then he can use the technique of average diffusion coefficients. If a  $\theta$ -solvent is known, one experiment is sufficient; if not, at least two are required. The result is an accurately known ratio  $D_1/D_2$  characterizing polydispersity. From this ratio,  $M_w/M_n$  may be calculated. The diffusion data provide an internal check on the probable success of this calculation in the comparison of the distribution found from the average diffusion coefficient ratio  $D_1/D_2$  and that found from the area under the fringe deviation graph  $Q$ . This check and the accuracy with which  $D_1/D_2$  is known are the strengths of this technique.

*Acknowledgment.* The author is indebted to Professors L. J. Gosting and E. N. Lightfoot and to Dr. Hans W. Osterhaut for discussions during the course of this work. He is also anxious to thank Professor Gosting for the loan of the Gouy interferometer used in the experiments. The work was supported by National Science Foundation Grant No. 86-4403.

### Appendix

The interference condition derived from wave optics for the Gouy interferometer is<sup>25</sup>

(23) H. W. McCormick, *J. Polymer Sci.*, **36**, 341 (1959).

(24) H. J. Cantow, *Macromol. Chem.*, **30**, 169 (1959).

$$f(j) = \frac{j + 3/4 + C}{J} \quad (21)$$

where  $J$  is the total number of fringes;  $j$  is the fringe number, measured from the bottom of the pattern; and  $C$  is a small wave optical correction factor. In terms of the refractive index, this is

$$f(j) = \frac{2}{\Delta n} \left[ (n - n_0) - x \frac{\partial n}{\partial x} \right] \quad (22)$$

which for our system is combined with eq. 4 and 5 to give

$$f(j) = \int_0^\infty g(D) \left[ \operatorname{erf} \left( \frac{x}{\sqrt{4Dt}} \right) - \frac{x^2}{\sqrt{\pi Dt}} e^{-x^2/4Dt} \right] dD \quad (23)$$

We next define an "idealized cell coordinate"  $\zeta$  by

$$\frac{n - n_0}{\Delta n/2} = \operatorname{erf} \zeta \quad (24)$$

If the system were monodisperse, then  $\zeta = x/\sqrt{4Dt}$ . In terms of  $\zeta$ , the interference condition is

$$f(j) = \operatorname{erf} \zeta - \frac{2}{\sqrt{\pi}} \zeta e^{-\zeta^2} \quad (25)$$

We want to find  $\Omega$  (cf. eq. 10) as a power series in  $\zeta$ . In principle, this is simple. We want to combine eq. 23 and 25 and solve for  $x$  in terms of  $\zeta$ . Then we want to insert this result into eq. 5 to find  $dn/dx$  in terms of  $\zeta$  and then combine with eq. 8 to give the desired equation. In practice, this is difficult.

First we define the new variables  $y$  and  $\delta$

$$y = \frac{x}{\sqrt{4D_A t}} \quad \delta = \sqrt{\frac{D_A}{D}} \quad (26)$$

Then we define a generalized interference condition of the arbitrary variable,  $\xi$

$$f(\xi) = \operatorname{erf} \xi - \frac{2}{\sqrt{\pi}} \xi e^{-\xi^2} \quad (27)$$

For example

$$f(\zeta) = \int_0^\infty g(D) f(y\delta) dD \quad (28)$$

If we define a deviation variable  $\sigma$  by the relation

$$\sigma = f(y) - f(\zeta) \quad (29)$$

then

$$\sigma = \int_0^\infty g(D) [f(y) - f(y\delta)] dD \quad (30)$$

Expanding this as a Taylor series, we may write

$$\sigma = \sum_{l=0}^{\infty} \frac{\sigma^l}{l!} \frac{\partial^l}{\partial f(\zeta)^l} \left[ \int_0^\infty g(D) (f(\zeta) - f(\delta\zeta)) dD \right] \quad (31)$$

Neglecting all but the first two terms and solving for  $\sigma$  gives

$$\sigma = \frac{\int_0^\infty g(D) (f(\zeta) - f(\delta\zeta)) dD}{\int_0^\infty g(D) \delta^3 e^{-\zeta^2(\delta^2 - 1)} dD} \quad (32)$$

Now, from eq. 5 and 6, we expand  $(\partial n/\partial x)/(\partial n/\partial x)_{\max}$  as a Taylor series in  $\sigma$

$$\frac{(\partial n/\partial x)}{(\partial n/\partial x)_{\max}} = \sum_{m=0}^{\infty} \frac{\sigma^m}{m!} \frac{\partial^m}{\partial f(\zeta)^m} \left[ \int_0^\infty g(D) \delta e^{-\zeta^2 \delta^2} dD \right] \quad (33)$$

Neglecting all but the first two terms and substituting eq. 32 for  $\sigma$  gives

$$\frac{(\partial n/\partial x)}{(\partial n/\partial x)_{\max}} = \int_0^\infty g(D) \delta e^{-\zeta^2 \delta^2} dD - \frac{\sqrt{\pi}}{2\zeta} \left[ \int_0^\infty g(D) (f(\zeta) - f(\delta\zeta)) dD \right] \quad (34)$$

Substituting this into the definition of  $\Omega$  (eq. 8) and expanding for small values of  $\Omega$  gives

$$\Omega = 1/3 \left[ \int_0^\infty g(D) \delta^3 dD - 1 \right] \zeta^2 + 0(\zeta^4) \quad (35)$$

which is identical with eq. 10. This equation gives a method of determining  $D_1/D_2$  for the Gouy interferometer.

(25) L. J. Gosting and L. Onsager, *J. Am. Chem. Soc.*, **74**, 6066 (1952).

## Photooxidation of Tertiary Nitrogen Compounds by Methylene Blue

by F. C. Goodspeed, B. L. Scott, and J. G. Burr

*North American Aviation Science Center, Thousand Oaks, California (Received September 17, 1964)*

The photooxidation of diethylglycine by methylene blue in buffered aqueous solutions consumes 1 mole of diethylglycine and gives 1 mole of carbon dioxide, 1 mole of formaldehyde, and 1 mole of diethylamine for each mole of dye which is decolorized. Similarly, the photooxidation of EDTA gives a mole of carbon dioxide for each mole of reduced dye plus formaldehyde and a nonvolatile aldehyde. A mechanism is described and supported for the photoreaction consisting of electron transfer from  $\text{OH}^-$  to the dye, abstraction of hydrogen from the diethylglycine or EDTA by the dye semiquinone, and oxidation of the resulting amine radical by  $\text{OH}$  or  $\text{H}_2\text{O}_2$ . It is concluded that any reducing agent which functions by donating a hydrogen atom to the dye and which thus forms a radical oxidizable by  $\text{OH}$  or  $\text{H}_2\text{O}_2$  will be irreversibly consumed in the dye photoreduction.

Oster<sup>1</sup> has studied the photooxidation of ethylenediaminetetraacetic acid (EDTA) by methylene blue, and more recently Silverman<sup>2</sup> has evaluated solar cell systems composed of proflavine, ascorbic acid, and EDTA, as well as proflavine-iron systems stabilized by EDTA.

Explanations which have been proposed for the irreversibility of the EDTA oxidation by methylene blue are amine oxide formation at the nitrogen<sup>1</sup> atom and oxidation at the  $\alpha$ -carbon.<sup>3</sup> The stoichiometry of the reaction has not been determined to date, although  $\text{CO}_2$  and formaldehyde have been detected as reaction products from photooxidation of EDTA by other dyes.<sup>4</sup>

The present work was undertaken in order to learn more about the nature of the photoreduction and the identity of the products as a possible guide to reducing agents which are not irreversibly oxidized in the reaction. To this end, the EDTA concentration dependence and light intensity dependence of the methylene blue photoreduction rate were determined. Volatile oxidation products ( $\text{CO}_2$  and  $\text{CH}_2\text{O}$ ) were determined quantitatively. A complete material balance was obtained for the photooxidation of methylene blue-diethylglycine solutions, including the relative amounts of carbon dioxide, formaldehyde, and diethylamine formed and diethylglycine consumed for each mole of methylene blue reduced. Diethylglycine represents a model of the reactive center of EDTA. Relative rates of photoreduction of methylene blue with several molecules containing tertiary nitrogen groups

and labile C-H bonds were determined to study the relationships between the structure of these molecules and their effectiveness as photoreducing agents.

### Experimental

*Equipment.* The light source was a 1000-w. G.E. projector bulb, run at 100 v. from a Stabiline EMT 4102 voltage stabilizer. The light source was mounted in an aluminum box equipped with a blower. This unit was attached to an Ealing optical bench. A Baird Atomics interference filter with maximum transmission at 6640 Å. and a half-width of 100 Å. was used to obtain the desired band of irradiation. A Cary Model 14 spectrophotometer equipped with a modified cell compartment was used for absorption measurements.

The irradiation cell was a Pyrex cylinder (with Pyrex windows), 55-mm. i.d., 60-mm. path, equipped with 14/35  $\frac{3}{8}$  joints for gas exhaust and addition of reagents when required. The cell was also equipped with a side-arm mounted cell, 20-mm. i.d. and 5-mm. path length, which was used for absorption measurements with the spectrophotometer.

(1) G. Oster and N. Wotherspoon, *J. Am. Chem. Soc.*, **79**, 4836 (1957).

(2) H. Silverman, W. Momyer, and M. Eisenberg, Proceedings of the 14th Annual Power Sources Conference, 1960, p. 72.

(3) D. Mauzerall, *J. Am. Chem. Soc.*, **82**, 1832 (1960).

(4) W. R. Frissel, W. Choong, and C. G. MacKenzie, *J. Biol. Chem.* **234**, 1297 (1959).

Argon, used as a purge gas, was purified by passage over calcium metal at 600° to remove oxygen. Residual oxygen was just at detectable limits polarographically after this treatment (50–75 p.p.b.) whereas the untreated argon showed oxygen at 5–10 p.p.m.

**Materials.** Methylene blue was National Aniline, histological grade. Proflavine, acridine orange, acridine yellow, and fluorescein were from Allied Chemical; riboflavine phosphate was from Merck. EDTA was Fisher Certified Reagent. Trimethyl- and triethylamine, nitrilotriacetic acid, triethanolamine, dimethylacetamide, diethylglycine sodium salt, and formaldehyde were from Eastman. Methylene blue was not photoreduced in buffered solutions unless one of the amines was present; this shows that small amounts of possible hydrogen donors were not present in these reagents. The excellent yield of oxidation products from the diethylglycine and from the EDTA show that the reactions observed were those of the reagents and not of impurities.

**Procedures.** Photoreduction rates were determined using the cell described above. One hundred milliliters of the solution was placed in the main cell and degassed for 15 min. with the purified argon; an initial absorbance was read using the side-arm cell. Concentrations were determined from a calibration curve constructed using the side-arm cell with known concentrations of methylene blue.

Carbon dioxide was determined using the same cell equipped with a barium hydroxide trap in the argon exit line. The exit gas was passed through the trap during the photoreaction. At the end of the reaction the bleached solution was acidified and the bulk of the carbon dioxide was evolved. The barium carbonate precipitate was transferred to a crucible, vacuum dried at 110°, and weighed. Blank determinations on unirradiated solutions gave negligible correction.

Formaldehyde was determined by the chromotropic acid colorimetric technique. Aliquots (1 ml.) of the dye solutions, identical with the solutions in which CO<sub>2</sub> formation was measured, were placed in one arm of an inverted U-trap with detachable arms, a stopcock, and a  $\text{F}$  joint for attachment to a vacuum system. The solution was then degassed to a residual pressure of  $1 \times 10^{-5}$  mm. and irradiated. The liquid was vacuum distilled into the other arm of the U-trap, leaving non-volatile, ionic reaction components behind. This was to ensure that free formaldehyde was being determined, since the chromotropic acid technique does not distinguish between free and bound formyl groups. Bound formyl groups were similarly determined in the residue from the distillation after dissolving this in 1 ml. of water. One milliliter of an unirradiated solu-

tion, similarly treated, was used as a blank in the spectrophotometer.

Diethylamine was determined spectrophotometrically as its nitrosamine, using the method of Morgan.<sup>5</sup> In this procedure, the aqueous amine solution is treated with nitrous acid, the nitrosamine is extracted by cyclohexane, and its concentration in the cyclohexane is measured by the optical density at 2350 Å. The absorptivity obeyed Beer's law over the concentration region used,  $2 \times 10^{-4}$  to  $1 \times 10^{-5}$  M in diethylamine. The results were somewhat low for the higher concentration, because of incomplete extraction of the nitrosamine by the cyclohexane.<sup>5</sup>

Diethylglycine consumption was measured in the following manner. Duplicate 100-ml. samples of a solution  $1.6 \times 10^{-3}$  M in DEG and  $2.67 \times 10^{-4}$  M in methylene blue in a 0.01 F pH 7 phosphate buffer were degassed by evacuation on a vacuum line and the ampoules were sealed off. One ampoule contained a 1-cm. quartz Cary cell on a side arm; this solution was photolyzed until the methylene blue concentration, as determined by absorption at about 6400 Å., had decreased to 1% of the initial value (the other ampoule was kept in the dark). Both ampoules were then opened and the DEG was separated from the methylene blue and phosphate by running the samples through a short column of Dowex 50W-X8 cationic exchange resin. The DEG was then eluted with 1 F HCl, and the DEG solution was evaporated to dryness in a current of nitrogen. The residue was taken up in a mixture of benzene and methanol, and the DEG was determined by potentiometric titration with NaOMe solution.<sup>6</sup>

## Results

The photooxidation of EDTA by methylene blue was shown to be first order in EDTA (Table III), zero order in dye (Table II), and approximately proportional to the  $2/3$  power of the intensity (Table I) over a range of concentration of  $5 \times 10^{-4}$  to  $5 \times 10^{-6}$  M in dye and  $5 \times 10^{-3}$  to  $1 \times 10^{-4}$  M in EDTA. The rate was the same, within experimental error, in D<sub>2</sub>O and in H<sub>2</sub>O. Carbon dioxide was formed in a mole for mole ratio to the dye consumed (Table IV). Approximately 0.1 mole of free formaldehyde and 0.4 mole of bound formyl groups were formed per mole of dye consumed.

Carbon dioxide, formaldehyde, and diethylamine were produced from methylene blue–diethylglycine photolyses (Table V) in a mole for mole ratio to bleached dye, within experimental error. The high

(5) D. J. Morgan, *Mikrochim. Acta*, 104 (1958).

(6) E. G. Parry and C. L. Atkin, this laboratory, to be published. We gratefully acknowledge the help of Parry and Atkin.

**Table I:** Rate of Reduction as a Function of Intensity

$I_a^a$	$\Delta C/\Delta t$	$[\Delta C/\Delta t]/I^2/11$
1.00	69	69
0.473	39	65
0.263	28	68
0.113	17	72

<sup>a</sup> Arbitrary units.**Table II:** Rate of Reduction as a Function of Dye Concentration

Dye concn., $M \times 10^5$	$\Delta C/\Delta t, M/\text{min.} \times 10^7$
4.52	
4.12	10
3.77	9
3.32	11
2.94	9.5
2.51	10.75
2.06	11
1.65	10.25
1.21	11
0.79	10.25

**Table III:** Data for Calculating Reaction Order in EDTA<sup>a</sup>

EDTA concn., $M \times 10^4$	$R, \mu\text{moles}/\text{min.}^b$	$R/R_0^c$	
		Obsd.	Calcd. for 1st order
1	7.3	1	1
5	36.4	5	5
10	75.1	10.3	10
20	150	20.4	20
30	224	30.5	30

<sup>a</sup> Methylene blue concentration  $5 \times 10^{-5} M$  for all runs.  
<sup>b</sup> Of dye reduced. <sup>c</sup>  $R_0$  = rate for  $1 \times 10^{-4} M$  EDTA.

values for  $\text{CO}_2$  may be real, but probably arise from incomplete removal of dissolved  $\text{CO}_2$  in the slightly basic solution before photolysis. Diethylglycine was consumed also in a mole for mole ratio with the bleached dye, since the results of the experiment described above (Experimental) were that 9.35  $\mu\text{moles}$  of diethylglycine was consumed when 9.39  $\mu\text{moles}$  of dye was bleached.

The relative reaction rates shown in Table VI were normalized to an arbitrary rate of 1000 for EDTA. The various compounds were run at the same dye concentration and pH. Some were in higher concentration than the EDTA in the reference runs, to obtain measurable rates with our apparatus.

The precision of the rate measurements (Tables I-III) is judged to be about 10% reproducibility from

**Table IV:** Methylene Blue-EDTA Reaction Products<sup>a</sup>

Ratio, EDTA/dye	Dye reduced <sup>b</sup>	EDTA in soln. <sup>b</sup>	$\text{CO}_2$ formed <sup>b</sup>	Ratio, moles $\text{CO}_2/\text{moles dye}$	$\text{CH}_2\text{O}^b$	Bound formyl <sup>b</sup>
5:1	50.0	250	47.7	0.95		
5:1	50.0	250	44.2	0.89		
5:1	50.0	250	52.2	1.04		
2.5:1	100	250	95.0	0.95		
2.5:1	100	250	79.0	0.79		
2.5:1	50	125	48.0	1.14		
1.25:1	50	62.5	56.8	1.14		
1.25:1	50	62.5	48.7	0.97		
	1.0	100			0.12	0.37
	1.0	100			0.11	0.36

<sup>a</sup> With 0.1  $M \text{HPO}_4^{2-} + \text{H}_2\text{PO}_4^-$  buffer, pH 6.5. <sup>b</sup> In micro-moles.**Table V:** Methylene Blue-Diethylglycine Reaction Products<sup>a</sup>

MB <sup>b</sup>	DEG <sup>b</sup>	$\text{CH}_2\text{O}^b$	$\text{CO}_2^b$	Diethyl-amine <sup>b</sup>	Ratio of product to dye
1.0	50	0.91			0.91
1.00	50	1.08			1.08
1.0	50	0.94			0.94
50	2500		65		1.3
50	2500		64		1.3
50	2500		65		1.3
2.0	200			1.93	0.965
2.0	200			2.04	1.02
2.0	200			1.70	0.85
2.0	200			1.93	0.965

<sup>a</sup> With 0.1  $M \text{HPO}_4^{2-} + \text{H}_2\text{PO}_4^-$  buffer, pH 7.4. <sup>b</sup> In micro-moles.**Table VI:** Relative Photoreduction Rates of Methylene<sup>a</sup>

Compd.	Relative rate of dye reduction
EDTA	1000
Nitrioltriacetic acid	69
2'2'2''-Nitrioltriethanol	55
N,N-Diethylglycine	7
2,4-Pentanedione	6
2-Dimethylaminoethyl acetate	1
N,N-Diethylacetamide	1

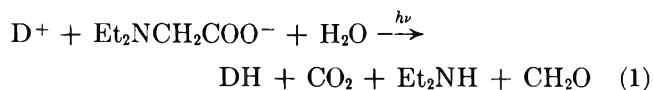
<sup>a</sup> All run at pH 7.5, in 0.1  $M \text{HPO}_4^{2-}$  and  $\text{HPO}_4^-$  buffer.

the scatter of the rate constants during a run. The amount of error in measurements of product yields can

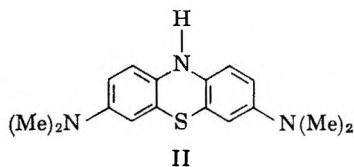
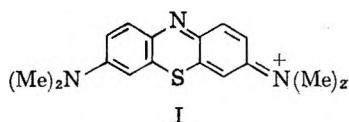
be judged from the comparison of the results of multiplicate experiments reported in Tables IV and V; determinations of formaldehyde, bound aldehyde, and diethylamine appear to show less than 10% error. The determinations of carbon dioxide appear to be less reproducible with deviations of more than 10% in many cases; we think that this larger error is owing to the difficulty of freeing these slightly basic solutions from dissolved carbon dioxide prior to a run.

### Discussion

The analytical results obtained in this investigation show that the stoichiometric equation for the photooxidation of diethylglycine (DEG) by methylene blue ( $D^+$ ) can be written as eq. 1, where  $D^+$  is I and DH is



II. The net effect is transfer of an electron and a hydrogen atom to the dye, and decomposition of both a molecule of water and a molecule of diethylglycine.

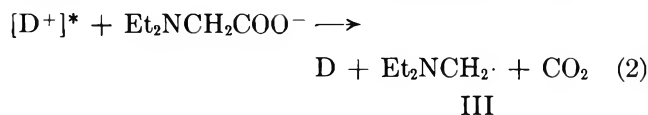


The photooxidation of the EDTA probably follows an analogous stoichiometry, but we shall center our discussion about diethylglycine.

We have measured every quantity in eq. 1 except the consumption of water, and this must follow by difference. The equality between the consumption of diethylglycine and the formation of formaldehyde, diethylamine and formaldehyde, and leucomethylene blue shows that no other products are formed in this photooxidation, and furthermore that only 1 mole of diethylglycine is concerned in the reaction. This is in agreement with the first-order dependence of the photoreduction rate on diethylglycine concentration. These results also exclude the possibility that traces of organic or other impurities are actually responsible for the photoreduction of the dye.

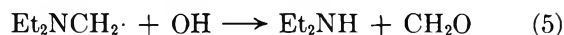
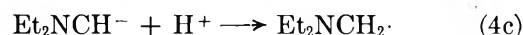
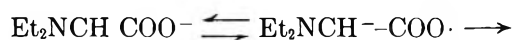
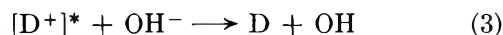
A proper explanation of the reaction must account for both electron transfer and hydrogen transfer to the dye, and for the intervention of a strong oxidizing agent

which contains oxygen. Either a water molecule (or an  $OH^-$ ) or the amino acid can be considered as the source of the electron, but only the amine can be considered as the source of hydrogen. The water cannot be a source of hydrogen because the dye is not photoreduced in the buffered water solution. On the other hand, the amino acid cannot be the source of both the electron and the hydrogen since this set of processes cannot account for the oxidation of the amine. Electron transfer from the amine to the photoexcited dye would produce an unstable radical (eq. 2) which would decompose to give



an amine radical and carbon dioxide. The only reasonable fate for the amine radical III would be recombination or hydrogen abstraction; an oxidized product would not be expected. (An unstable methylol amine might result if the amine radical III transferred an electron to a second photoexcited dye molecule, forming a cation  $Et_2NCH_2^+$  which could combine with an  $OH^-$ . However, double electron transfer from the same amine molecule is statistically improbable when the amine concentration is so large.)

A simple sequence of events which explains our observed stoichiometry consists of electron transfer from  $OH^-$  to the photoactivated dye molecule, followed by hydrogen abstraction from the amine and oxidation of the amine radical by  $OH$  (eq. 3-5). Other mechanisms



can be written which account for our observed stoichiometry but at some point in each of them an electron must be transferred from  $OH^-$  or  $H_2O$  to an acceptor, and of all the possible acceptors for this electron, we think that transfer to the photoactivated dye cation,  $D^+$ , is the most energetically feasible. It should be noted that only the photoactivation-electron transfer step is endothermic; all of the subsequent reactions are spontaneous.

We agree with Holmstrom and Oster<sup>7</sup> that water

(7) B. Holmstrom and G. Oster, *J. Am. Chem. Soc.*, **83**, 1867 (1961)

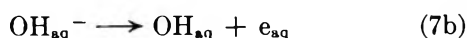
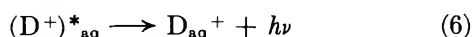


alone cannot supply both electrons or an electron plus a hydrogen. However, the proven stoichiometry (eq. 1) demonstrated in our experiments compels us to consider a water molecule as one of the reactants, and thus as a source of one of the electrons when a source of hydrogen such as trimethylamine, diethylglycine, or EDTA is present. The strongest evidence for our mechanism is the complete material balance obtained, but some supporting evidence can be cited. For example, this mechanism explains the equality of the photooxidation rates in  $H_2O$  and  $D_2O$ , since the oxidation potentials of  $OH^-$  and  $OD^-$  should be the same.

Electron transfer from  $OH^-$  to dye has been cited to explain the photoreduction of riboflavin.<sup>8</sup> The presence of  $H_2O_2$  in light faded air-free dye solutions has been reported,<sup>9</sup> and  $H_2O_2$  is postulated as a reactive intermediate in the photooxidation of nicotine by methylene blue.<sup>10</sup> Trimethylamine oxide has been reported as a product of the air-free photooxidation of trimethylamine by methylene blue,<sup>11</sup> and methionine sulfide results from the photooxidation of methionine by riboflavin<sup>8b</sup>; each of these products strongly suggests the intervention of hydrogen peroxide or an OH radical during the photo process.

Our evidence does not provide any detailed understanding of the way in which the water molecule can supply the electron. The photoreactive state of the dye is probably the triplet<sup>1,12</sup> since EDTA in low concentrations does not quench the dye fluorescence yet is oxidized by the activated dye,<sup>12</sup> and the lifetime of the activated dye appears to be in excess of  $10^{-5}$  sec.

The electron transfer from  $OH^-$  to the photoactivated dye, ( $D^+$ ), must be exothermic, spontaneous, and with a fairly high rate constant if this process is to compete with other reactions of the photoactivated dye. The exothermicity of this process is very difficult to estimate from thermodynamic data. The decrease in energy content of the dye (eq. 3) is the sum of the excitation energy of the triplet dye in solution (eq. 6) and the electron affinity of solvated dye cation for solvated electrons (eq. 7), *i.e.*, (3) = (6) + (7). This is



probably greater than the excitation energy of the triplet dye, which in turn can only be estimated to be

somewhat less than the singlet excitation energy, 1.9 e.v.

Similarly, the electron affinity of  $OH_{aq}$  differs from the electron affinity of  $OH_g$ , variously estimated from 1.95 to 3.61 e.v. with a most probable value of 2.82 e.v.,<sup>13</sup> by the solvation energy of OH and the solvation energy of the electron. The solvation energy of the OH is probably quite small, but that of the electron may be quite large. It does not seem entirely unreasonable that these solvation energies and electron affinities are such that process 3 is indeed exothermic.

This mechanism should be valid for the photooxidation of EDTA and for the other substances listed in Table IV. The low yield of formyl product from EDTA, and the division of formyl between bound formyl and formaldehyde suggests that the  $-N-CH_2-$  formed is less easily oxidized by HO, and that the oxidized EDTA is more stable than the corresponding product from diethylglycine. The relative photoreduction rates shown in Table IV must then represent the relative abstractability of hydrogen from the various compounds. Unfortunately, there does not appear to be independent information about the hydrogen atom donor ability of such unusual and diverse compounds.

The ability of these hydrogen donors to promote the photoreduction of these dyes is owing to the ability of the dye semiquinone to function both as a hydrogen extractor and also as an electron acceptor. Photoreductions of dyes by substrates which are only electron donors, such as ferrous ion, simply proceeds by successive electron transfers followed by proton additions to the negative ions. In the absence of a substrate capable of transferring an electron to the semiquinone, certain hydrogen donors can promote the reaction by transferring a hydrogen atom to the semiquinone.

The practical consequence of this is that any reducing agent which functions by donating a hydrogen atom and which forms a radical oxidized by OH or  $H_2O_2$  will therefore be irreversibly consumed in the photoreduction of the dye.

(8) (a) G. Strauss and W. J. Nickerson, *J. Am. Chem. Soc.*, **83**, 3187 (1961); (b) W. J. Nickerson and G. Strauss, *ibid.*, **82**, 5007 (1960).

(9) L. P. Vernon, *Biochim. Biophys. Acta*, **36**, 177 (1959).

(10) L. Weil and J. Maher, *Arch. Biochem.*, **29**, 241 (1950).

(11) H. Obata and M. Koisumi, *Bull. Chem. Soc. Japan*, **30**, 136 (1957).

(12) G. Oster, J. S. Bellin, R. K. Kimball, and M. E. Schrader, *J. Am. Chem. Soc.*, **81**, 5095 (1959).

(13) F. M. Page, *Discussions Faraday Soc.*, **19**, 87 (1955).

## Disulfur Monoxide. III. Its Infrared Spectrum and Thermodynamic Functions

by Uldis Blukis and Rollie J. Myers

*Inorganic Materials Research Division, Lawrence Radiation Laboratory, and Department of Chemistry, College of Chemistry, University of California, Berkeley, California (Received September 21, 1964)*

A study of the infrared spectrum of frozen films of  $S_2O$  has led to a complete infrared assignment including the bending frequency at  $388 \pm 2 \text{ cm.}^{-1}$ . The thermodynamic functions  $(F^\circ - H^\circ_0)/T$  and  $(H^\circ - H^\circ_0)/T$  for gaseous  $S_2O$  are tabulated for 273.15–3000°K. Estimates of the standard enthalpy of formation for gaseous  $S_2O$  are given, and its thermodynamic stability is discussed.

### Introduction

Now that disulfur monoxide,  $S_2O$ , is a well-established molecular species,<sup>1</sup> its chemical and physical properties can be studied. Current work is being done on its chemical reactions.<sup>2</sup> This paper is concerned with its thermodynamic properties and an assignment of its vibration spectrum. A previous determination of the standard enthalpy of formation of  $S_2O$  has been obtained from ionization potentials,<sup>3</sup> but, since this is only an approximate minimum value, other possible values will be discussed.

### Experimental

The samples of  $S_2O$ , containing about 50%  $SO_2$ , were prepared by the usual discharge method.<sup>1</sup> For our infrared studies the samples were sprayed on a salt window cooled to 77°K. in a low temperature cell.<sup>4</sup> To study the decomposition of  $S_2O$ , several spectra were taken after the window had been allowed to warm to 100 and to 280°K., but the spectra were always taken after the window was cooled back to 77°K. These spectra were taken several years ago on a modified Perkin-Elmer Model 12C single-beam instrument utilizing either KBr or CsI optics. The wave length scale in the CsI region was determined from the water bands that appeared in the background of the single-beam instrument.

### Infrared Results

In the region 600–1400  $\text{cm.}^{-1}$  two bands were observed in the frozen films which could be ascribed to  $S_2O$ . The frequencies of these bands were identical, within our resolution, to the 679 and 1165  $\text{cm.}^{-1}$  found by Jones<sup>5</sup> in the gas phase. The 1165- $\text{cm.}^{-1}$  band is

close to an  $SO_2$  absorption,<sup>6</sup> and the two could never be entirely resolved. The 679- $\text{cm.}^{-1}$  absorption is completely free of  $SO_2$  absorption. When the salt window was warmed to 100°K., the  $S_2O$  bands at 1165 and 679  $\text{cm.}^{-1}$  decreased greatly. After warming to 280°K. the 679- $\text{cm.}^{-1}$  band could not be observed, but an absorption of about one-third the original intensity remained at 1130  $\text{cm.}^{-1}$ . These observations are consistent with diffusion of  $S_2O$  in an  $SO_2$  matrix at 100°K. followed by decomposition into  $SO_2$  and sulfur. Since the band near 1100  $\text{cm.}^{-1}$  can be ascribed to an S–O stretch, it is clear, as observed by Schenk,<sup>7</sup> that some oxygen remains bonded to the produced sulfur at temperatures as high as 280°K.

Since  $S_2O$  is a bent triatomic molecule, it should have one bending and two stretching frequencies. The 1165 and 679  $\text{cm.}^{-1}$  can be readily assigned to the two stretches, and the bend would normally be found at a lower frequency. A measurement of microwave satellite intensities<sup>1b</sup> gave a value of  $370 \pm 30 \text{ cm.}^{-1}$  for the lowest frequency vibration for  $S_2O$ , and the spectroscopic temperature coefficient measurements<sup>8</sup> indicate that there is a frequency of about 450  $\text{cm.}^{-1}$ . In the

(1) (a) D. J. Meschi and R. J. Myers, *J. Am. Chem. Soc.*, **78**, 6220 (1956); (b) *J. Mol. Spectry.*, **3**, 405 (1959).

(2) P. W. Schenk and R. Steudel, *Angew. Chem.*, **75**, 793 (1963); P. W. Schenk and W. Holst, *Z. anorg. allgem. Chem.*, **319**, 337 (1963).

(3) R. Hagemann, *Compt. rend.*, **255**, 1102 (1962).

(4) E. D. Becker and G. C. Pimentel, *J. Chem. Phys.*, **25**, 224 (1956).

(5) A. V. Jones, *ibid.*, **18**, 1263 (1950).

(6) R. N. Wiener and E. R. Nixon, *ibid.*, **25**, 175 (1956); P. A. Giguère and M. Falk, *Can. J. Chem.*, **34**, 1833 (1956).

(7) P. W. Schenk, *Z. anorg. allgem. chem.*, **248**, 297 (1941).

(8) E. Kondrat'eva and V. Kondrat'ev, *Zh. Fiz. Khim.*, **14**, 1528 (1940).

range 300–450  $\text{cm}^{-1}$  a single  $\text{S}_2\text{O}$  band was found at  $388 \pm 2 \text{ cm}^{-1}$  in a frozen film at  $77^\circ\text{K}$ . This band had the same warm-up characteristics as did the  $679\text{-cm}^{-1}$  absorption. The bending frequency in the gas phase would be expected to differ from  $388 \text{ cm}^{-1}$  by less than  $10 \text{ cm}^{-1}$ .

### Thermodynamic Functions

On the basis of the infrared measurements in this paper and the previous work,<sup>5</sup> we know, without doubt, all three fundamental vibrational frequencies for  $\text{S}_2\text{O}$ . The microwave work<sup>1b</sup> has also supplied the rotational constants and the symmetry ( $C_6$ ). The thermodynamic functions for gaseous  $\text{S}_2\text{O}$  on the basis of a rigid-rotor, harmonic-oscillator model were calculated from these data, and they are listed in Table I.

Table I: Thermodynamic Functions for  $\text{S}_2\text{O}^a$

$T$	$-(F^\circ - H^\circ_0)/T$	$(H^\circ - H^\circ_0)/T$
273.15	53.78	8.78
298.15	54.56	8.92
400	57.25	9.45
500	59.41	9.91
600	61.26	10.30
700	62.87	10.64
800	64.31	10.92
900	65.61	11.16
1000	66.80	11.37
1100	67.88	11.55
1200	68.91	11.70
1300	69.85	11.84
1400	70.72	11.97
1500	71.56	12.08
2000	75.09	12.48
2500	77.90	12.74
3000	80.24	12.92

<sup>a</sup> In  $\text{cal.}/(\text{mole } ^\circ\text{K.})$  calculated using  $I_a I_b I_c = 618.14 \times 10^{-117} \text{ g.}^3 \text{ cm.}^6$ ,  $M(\text{S}_2\text{O}) = 80.12 \text{ g./mole}$ ,  $P = 1 \text{ atm.}$ ,  $\nu_1 679 \text{ cm.}^{-1}$ ,  $\nu_2 388 \text{ cm.}^{-1}$ , and  $\nu_3 1165 \text{ cm.}^{-1}$ .

### Thermodynamic Stability

$\text{S}_2\text{O}$ , called "sulfur monoxide" or " $\text{S}_2\text{O}_2$ " in the older literature, has been produced in a variety of non-equilibrium systems.<sup>1a,9</sup> Possibly, it is present in significant amounts in those high temperature oxygen-sulfur equilibria which are rich in sulfur. For a study of the thermodynamic stability of  $\text{S}_2\text{O}$  in these and similar systems the standard enthalpy of formation  $\Delta H^\circ_0 [2\text{S}(\text{rh}) + \frac{1}{2}\text{O}_2(\text{g}) \rightarrow \text{S}_2\text{O}(\text{g}), \text{ at } 0^\circ\text{K.}]$  is needed. In the absence of a direct measurement an estimated  $\Delta H^\circ_0$  would be useful.

An approximate value for  $\Delta H^\circ_0$  can be based on bond energies. The corresponding bond distances and

angles in  $\text{S}_2$ ,  $\text{SO}$ ,  $\text{S}_2\text{O}$ , and  $\text{SO}_2$  are similar.<sup>1b,10</sup> Furthermore, the bond dissociation energies  $D_0(\text{S-O})$  and  $D_0(\text{OS-O})$  are nearly equal.<sup>11</sup> These observations imply that  $D_0(\text{S-S})$  and  $D_0(\text{S-O})$  may be used to calculate  $\Delta H^\circ_0$  for  $\text{S}_2\text{O}$ . With these assumptions  $\Delta H^\circ_0 = -34 \text{ kcal./mole}$  is obtained. From measurements of ionization potentials, ultraviolet spectrum, and equilibria in the sulfur-oxygen system experimental lower limits for  $\Delta H^\circ_0$  can be established. These limits indicate that  $\text{S}_2\text{O}$  is less stable than is indicated by the bond energy calculation.

Hagemann<sup>3</sup> has measured the appearance potentials of  $\text{SO}^+$  from both  $\text{SO}_2$  and  $\text{S}_2\text{O}$ . His measurements give a value of  $2.0 \pm 0.4 \text{ e.v.}$  for the energy required to produce  $\text{S}_2\text{O} + \text{O}$  from  $\text{SO}_2 + \text{S}$ . This value gives  $\Delta H^\circ_0 = -17 \pm 9 \text{ kcal./mole}$ . Hagemann implies in his paper that this value is a lower limit for  $\Delta H^\circ_0$ .

In his work on the ultraviolet absorption spectrum of  $\text{S}_2\text{O}$  Jones<sup>5</sup> noted a well-defined predissociation limit at  $3153.8 \text{ \AA.}$  in a progression which starts from the ground vibrational state. This value corresponds to an energy for photodissociation of  $90.5 \text{ kcal./mole}$ . If  $\text{S}_2 + \text{O}$  were the products of this dissociation, then a minimum  $\Delta H^\circ_0$  for  $\text{S}_2\text{O}$  would be  $-1 \text{ kcal./mole}$ . This value seems to be somewhat too high. If  $\text{SO} + \text{S}$  were the products, then a minimum  $\Delta H^\circ_0$  would be  $-23 \text{ kcal./mole}$ . These are minimum values because of the unknown amount of excess energy carried off by the products. Excess energy in the form of electronic excitation is unlikely because the first excited states of both the S atom and SO are sufficiently high<sup>12</sup> to give a value for  $\Delta H^\circ_0$  of about  $0 \text{ kcal./mole}$ . Photodissociation studies of  $\text{SO}_2$ <sup>13</sup> and  $\text{NO}_2$ <sup>14</sup> have shown that the excess rotational and vibrational energy of the products can be small.

The most complete study of sulfur-oxygen vapor in equilibrium has been done by Dewing and Richardson.<sup>15</sup> They used silver beads in equilibrium with the

(9) R. G. W. Norrish and G. A. Oldershaw, *Proc. Roy. Soc. (London)*, **A249**, 498 (1959); R. G. W. Norrish and A. P. Zeelenberg, *ibid.*, **A240**, 293 (1957); A. L. Myerson, F. R. Taylor, and P. L. Hanst, *J. Chem. Phys.*, **26**, 1309 (1957).

(10) P. A. Giguère, *J. Phys. Chem.*, **64**, 190 (1960).

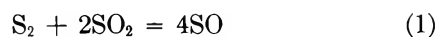
(11) All the thermodynamic data are taken from Table I of this paper and Appendix 7 of G. N. Lewis, M. Randall, K. S. Pitzer, and L. Brewer, "Thermodynamics," McGraw-Hill Book Co., Inc., New York, N. Y., 1961. There is some uncertainty about the values of 101 and 123.5 kcal./mole used for the dissociation energies of  $\text{S}_2$  and SO, respectively. See R. Colin, P. Goldfinger, and M. Jeunehomme, *Nature*, **187**, 408 (1960); also see W. D. McGrath and J. F. McGarrey, *J. Chem. Phys.*, **37**, 1574 (1962).

(12) The  $^1\Delta$  state of SO is not known, but its energy should be similar to that found in  $\text{O}_2$ .

(13) P. Warnek, F. F. Marmo, and J. O. Sullivan, *J. Chem. Phys.*, **40**, 1132 (1964).

(14) J. N. Pitts, J. H. Sharp, and S. I. Chan, *ibid.*, **40**, 3655 (1964).

vapor at 1000–1500°K. They interpreted their results in terms of the gas phase equilibrium



but the equilibrium



may also have been significant. If, so, then the relationship between the apparent equilibrium constant calculated by Dewing and Richardson ( $K_a$ ) and those for equilibria 1 and 2 would be

$$K_a^{1/4} = K^{1/4} + 3K_2^{1/4}P(\text{S}_2)^{1/2} \quad (3)$$

In their experiments the equilibrium pressure of  $\text{S}_2$ ,  $P(\text{S}_2)$ , ranged from only 2.9 to  $3.9 \times 10^{-3}$  atm. Therefore, a variation of  $K_a$  would not have been detected even if relatively large amounts of  $\text{S}_2\text{O}$  were present. If we assume that under their experimental conditions, equilibrium 2 is dominant, then with the help of eq. 3 we calculate a value of  $\Delta H^\circ_0 = -15$  kcal./mole for  $\text{S}_2\text{O}$  from Dewing and Richardson's data. This value represents a rather well-established lower limit for  $\Delta H^\circ_0$ .

In their silver bead experiments Dewing and Richardson arrived at a value for the  $\Delta H^\circ_0$  of SO, neglecting equilibrium 2, which can be taken to be in error by  $-3$  kcal./mole (this is the largest error consistent with the accepted values of  $D_0(\text{S-S})$  and  $D_0(\text{S-O})$  and their errors<sup>11</sup>). If this  $-3$  kcal./mole error is ascribed to equilibrium 2, then eq. 3 allows one to calculate  $\Delta H^\circ_0 = -13$  kcal./mole for  $\text{S}_2\text{O}$ . This value is only slightly larger than the  $-15$  kcal./mole value which was based upon the complete neglect of equilibrium 1. Since it seems improbable<sup>11</sup> that equilibrium 1 can be neglected, the silver bead data of Dewing and Richardson make  $\Delta H^\circ_0 = -13$  kcal./mole a realistic lower limit for the heat of formation of  $\text{S}_2\text{O}$ . While the bond energy and predissociation values all indicate a more negative  $\Delta H^\circ_0$  value for  $\text{S}_2\text{O}$ , the only well-established equilib-

rium data in sulfur-rich systems show that  $\text{S}_2\text{O}$  cannot be more stable than is allowed by a  $\Delta H^\circ_0 = -13$  kcal./mole.

Since  $\text{S}_2\text{O}$  can be produced in relatively high yield in a number of high temperature systems, it seems possible that the actual value of  $\Delta H^\circ_0$  is fairly close to the lower limit of  $-13$  kcal./mole. We are aware of only one experiment reported in the literature on which a useful upper limit for  $\Delta H^\circ_0$  of  $\text{S}_2\text{O}$  can be based. Schenk<sup>16</sup> reported that  $\text{S}_2\text{O}$  can be prepared in 5% yield (based upon  $\text{SO}_2$ ) by heating  $\text{SO}_2$  and sulfur vapor with a Nernst glower. If we assume that Gibbs free energy is an applicable criterion of equilibrium in this case and that the net reaction is given by eq. 2, then one can write

$$\Delta F = \Delta F^\circ - RT \ln [P(\text{SO}_2)^{-2}P(\text{S}_2)^{-3}P(\text{S}_2\text{O})^4] \quad (4)$$

A useful upper limit for  $\Delta H^\circ_0$  can be calculated if  $\Delta F$  is set equal to zero under Schenk's conditions.<sup>16</sup> Schenk does not describe his experimental conditions in great detail, but reasonable assumptions ( $T \sim 2000^\circ\text{K}$ . and  $P(\text{SO}_2)^{-2}P(\text{S}_2)^{-3}P(\text{S}_2\text{O})^4 \geq 10^{-12}$ ) give a maximum  $\Delta H^\circ_0$  of 2 kcal./mole. This value is also a reasonable upper limit on the basis of bond energies.

The range that our limits place on the relative importance of SO and  $\text{S}_2\text{O}$  in sulfur-rich systems is still rather large. If one assumes that at  $1000^\circ\text{K}$ .  $P(\text{SO}_2) = P(\text{S}_2) = 0.5$  atm., then  $P(\text{SO}) \sim 10^{-4}$  atm. If  $\Delta H^\circ_0$  for  $\text{S}_2\text{O}$  is  $-13$  kcal./mole, then in this system  $P(\text{S}_2\text{O}) \sim 10^{-2}$  atm., but, if  $\Delta H^\circ_0 = 2$  kcal./mole, then  $P(\text{S}_2\text{O}) \sim 10^{-6}$  atm. Only further experimental data will be able to remove this uncertainty.

*Acknowledgment.* This work was performed under the auspices of the United States Atomic Energy Commission.

(15) E. W. Dewing and F. D. Richardson, *Trans. Faraday Soc.*, **54**, 679 (1958).

(16) P. W. Schenk, *Z. anorg. allgem. Chem.*, **229**, 305 (1936).

## Linear Energy Transfer Effects in the Radiolysis of

### Liquid Aromatic Hydrocarbons<sup>1</sup>

by J. Y. Yang, J. D. Strong, and J. G. Burr

North American Aviation Science Center, Thousand Oaks, California (Received September 26, 1964)

Liquid benzene and *o*-terphenyl have been exposed to radiations of LET values ranging from 0.02 to 25 e.v./Å.;  $G(\text{H}_2)$  and  $G(\text{reactant} \rightarrow \text{polymer})$  values have been determined under these conditions. There is little change in product yields for radiations with LET from 0.02 to 2 e.v./Å., but the yields increase sharply with LET above 2 e.v./Å. A number of observations cannot be explained by a reaction model based on competition between a unimolecular reaction and a bimolecular reaction involving activated species. It is suggested that the above observations may be explained by thermal spike effects.

Although linear energy transfer (LET) effects in the radiolysis of water and aqueous solutions are reasonably well documented,<sup>2</sup> comparatively little attention has been given to such effects in the radiolysis of organic liquids. Early investigations by Schuler and co-workers<sup>3-5</sup> indicated that product yields from irradiations of aliphatic hydrocarbons are independent of LET values, and it was concluded that bimolecular radical reactions in the ionizing track are unimportant in such aliphatic systems. Recently, however, evidences for a track effect in the radiolysis of liquid cyclohexane<sup>6a</sup> and cyclohexene<sup>6b</sup> have been reported.

In the radiolysis of aromatic hydrocarbons, definite, although small, effects attributed to changes in LET have been reported by a number of investigators.<sup>7-12</sup> The observed effects cannot be explained by a model similar to that proposed for the aqueous system.<sup>13</sup> Intuitive feelings thus far have led to a general belief in a bimolecular reaction of activated intermediates to account for the increased product yield found for very densely ionizing radiation. Recently, Hochanadel<sup>14,15</sup> has proposed that differences in the decomposition of inorganic salt crystals induced by radiations of varying LET can be attributed principally to a temperature effect in the ionizing track. It is logical, therefore, to consider also such a thermal spike effect as the cause for the LET dependence of radiolysis yields in aromatic hydrocarbons.

### Experimental

**Materials.** Phillips 66 Research Grade benzene and Eastman Kodak White Label *o*-, *m*-, and *p*-terphenyls were used without further purification. All reagents were analyzed by gas chromatography and found not to contain any significant impurity. Polonium-210

(1) Work supported in part by the U. S. Atomic Energy Commission under Contract AT-(11-1)-GEN-8, at the Atomic International Division of North American Aviation, Inc., and presented at the 140th and 148th National Meetings of the American Chemical Society, Chicago, Ill., Sept. 1961 and Sept. 1964, respectively.

(2) A. O. Allen, "The Radiation Chemistry of Water and Aqueous Solutions," D. Van Nostrand Company, Inc., New York, N. Y., 1961.

(3) R. H. Schuler and A. O. Allen, *J. Am. Chem. Soc.*, **77**, 507 (1955).

(4) H. A. Dewhurst and R. H. Schuler, *ibid.*, **81**, 3210 (1959).

(5) R. H. Schuler, *J. Phys. Chem.*, **63**, 925 (1959).

(6) (a) J. W. Falconer and M. Burton, *ibid.*, **67**, 1743 (1963); (b) W. G. Burns and J. A. Winter, *Discussions Faraday Soc.*, **36**, 124 (1963).

(7) W. G. Burns, W. Wild, and T. F. Williams, *Proc. 2nd Intern. Conf. Peaceful Uses At. Energy*, **29**, 266 (1959).

(8) W. G. Burns, *Trans. Faraday Soc.*, **58**, 961 (1962).

(9) W. G. Burns and C. R. V. Reed, *ibid.*, **59**, 101 (1963).

(10) T. Gauman and R. H. Schuler, *J. Phys. Chem.*, **65**, 703 (1961).

(11) T. Gauman, *Helv. Chim. Acta*, **44**, 1337 (1961).

(12) J. Y. Yang, F. C. Goodspeed, and J. G. Burr, *Chem. Ind. (London)*, 1018 (1962).

(13) A. H. Samuel and J. L. Magee, *J. Chem. Phys.*, **21**, 1080 (1953).

(14) C. J. Hochanadel, *Radiation Res.*, **16**, 286 (1962).

(15) C. J. Hochanadel, *J. Phys. Chem.*, **67**, 2229 (1963).

sources were purchased from the Mound Laboratory of the Monsanto Chemical Co.

**Irradiations.** The experimental procedure for  $^{210}\text{Po}$   $\alpha$ -radiolysis has been described in our earlier report.<sup>12</sup> The irradiation apparatus was almost identical with that described subsequently by Falconer and Burton,<sup>6</sup> except that our  $^{210}\text{Po}$  source housing was constructed of glass, and the source was positioned by simply raising and lowering the attached rod with the guiding shaft serving also as the helium gas exit. Efficient stirring was essential to avoid polymer deposition on the housing window, and this was accomplished by a glass-enclosed magnetic stirrer pivoting on a sharp point in a small well. The stirring bar enclosure was made disk shaped to minimize the necessary sample size and thus in effect increase the  $\alpha$ -dose rate.

Helium ion and deuteron irradiations were carried out with the 60-in. cyclotron at the Crocker Laboratory, University of California (Berkeley). The samples were irradiated in glass cells with 1-mil stainless steel foil windows as shown in Figure 1. The windows and the keeper rings were cemented in place with a one-component epoxy bonding agent. The tungsten lead was used as a ground to prevent any charge build-up in the organic liquid. Samples were loaded into the reservoir side of the cells and degassed by a conventional freeze-thaw technique. During irradiation, the samples were stirred by the use of a shaker assembly designed by Garrison and co-workers.<sup>16</sup> Benzene samples were irradiated at about  $35^\circ$  by cooling with circulating water. *o*-Terphenyl samples were preheated to  $100^\circ$  in a steam bath and were found to reach an equilibrium temperature of about  $150^\circ$  due to heat generated upon irradiation by the cyclotron beam.

$\gamma$ -Radiolyses of terphenyl samples were carried out in a cobalt-60 source of the general Hochanadel-Ghormley type. The dose rate, as measured by ceric dosimetry and also by  $G(\text{H}_2)$  from benzene, was  $1.84 \times 10^{17}$  e.v./g.-min.

**Dosimetry.** Dose rate measurements for  $^{210}\text{Po}$   $\alpha$ -radiolysis were made by ceric sulfate dosimetry, using the value of 2.88 as  $G(\text{Ce}^{3+})$ .<sup>17</sup> For cyclotron irradiations, beam currents were measured by a monitoring circuit described by Garrison and co-workers<sup>18,19</sup> and the total radiation energy absorbed in each sample was calculated from range-energy data. The energies of the particles accelerated in the cyclotron were 48 Mev. for helium ions and 24 Mev. for deuterons, and energies for the attenuated beams reaching the samples were calculated to be 44 and 22 Mev., respectively. The reliability of the above dose absorption calculation was confirmed by measurements of LET independent

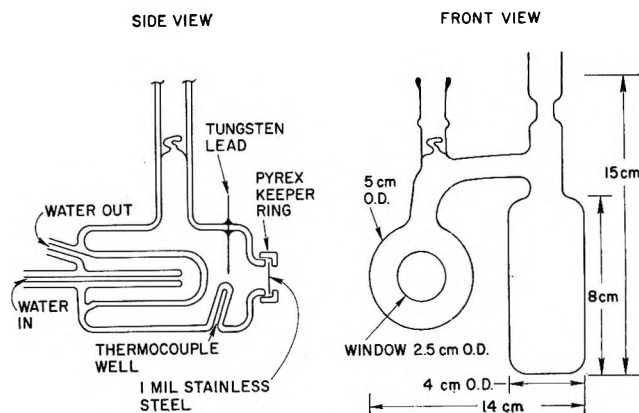


Figure 1.  $\text{He}^{2+}$  and  $\text{D}^+$  irradiation cell.

yields of hydrogen and cyclohexene from the radiolysis of cyclohexane under identical conditions.

**Analysis.** The gas yields were obtained by conventional volume and pressure measurements. Polymer yields ( $\text{C}_{12}$  and higher products) were determined by a vacuum sublimation technique. Product analysis for irradiated *o*-terphenyl has been described earlier.<sup>12</sup> Benzene sublimation was carried out by initially cooling the irradiated sample to liquid nitrogen temperature and then allowing the sample to warm up to  $0^\circ$  while being evacuated. The residue was weighed and redissolved in cyclohexane to allow correction for any benzene content detectable by gas chromatography ( $\beta, \beta'$ -oxydipropionitrile column at  $80^\circ$ ). The residue weight was also corrected for dimeric products carried over in the original distillation by analysis of the distillate by gas chromatography using a polyester succinate column at  $180^\circ$ .

## Results

The predominant decomposition products from radiolysis of aromatic hydrocarbons are always mixtures of high molecular weight substances. Since the composition and the molecular weight of these polymeric mixtures are not well defined, the product yields are often expressed as  $G(-\text{reactant})$ , the number of reactant molecules converted per 100 e.v. energy absorbed.  $G(-\textit{o}$ -terphenyl) values from  $^{210}\text{Po}$   $\alpha$ -radiolysis have been reported in our earlier note<sup>12</sup> as a function of temperature. The value at  $150^\circ$  was found to be 0.63. Polymer yields from benzene irradiated

(16) W. M. Garrison, H. R. Haymond, and B. M. Weeks, *Radiation Res.*, **1**, 97 (1954).

(17) J. Weiss and N. Miller, *J. Phys. Chem.*, **63**, 888 (1959).

(18) W. M. Garrison, et al., *Rev. Sci. Instr.*, **24**, 462 (1953).

(19) W. M. Garrison, B. M. Weeks, J. O. Ward, and W. Bennett, *J. Chem. Phys.*, **27**, 1214 (1957).

with  $^{210}\text{Po}$   $\alpha$ -particles have now been determined with benzene damage up to 1%, and  $G(-\text{benzene})$  was found to be 1.37 at 25° and 1.43 at 35°. Our data on  $G(-\text{reactant})$  as well as  $G(\text{H}_2)$  values for cyclotron irradiations of benzene and *o*-terphenyl are summarized in Table I. The results for  $^{60}\text{Co}$   $\gamma$ -radiolysis of *o*-, *m*-, and *p*-terphenyls are reported in Table II.

**Table I:** Cyclotron Irradiation of *o*-Terphenyl and Benzene

Sample	Particle	Energy, Mev.	Beam current, $\mu\text{a.}$	Total dose, e.v. $\times 10^{-22}$	$G(\text{H}_2)$	$G(-\text{reactant})$
<i>o</i> -Terphenyl	He $^{2+}$	44	2	4.95	0.0139	0.29
	He $^{2+}$	44	2	4.95	0.0143	0.29
	He $^{2+}$	44	2	4.95	0.0141	0.29
	D $^+$	22	1.5	4.95		0.22
	D $^+$	22	2	4.95	0.0116	0.25
	D $^+$	22	2	4.95		0.26
	D $^+$	22	2	4.95		0.25
Benzene	He $^{2+}$	44	1.5	2.50	0.061	1.0
	He $^{2+}$	44	1.5	2.50	0.071	1.1
	D $^+$	22	1.5	2.50	0.048	
	D $^+$	22	1.5	2.50	0.044	

**Table II:** Initial Yields<sup>a</sup> of High Boilers from  $\gamma$ -Irradiated Terphenyls

Temp., °C.	$G(-\text{terphenyl})$		
	<i>o</i> -Terphenyl	<i>m</i> -Terphenyl	<i>p</i> -Terphenyl
100	0.19	0.12	0.034 <sup>b</sup>
200	0.19	0.17	0.074 <sup>b</sup>
300	0.24	0.17	0.17

<sup>a</sup> Final HB content about 2-3%. Total doses were  $3.7 \times 10^{22}$  e.v./g. <sup>b</sup> Solid phase.

The ionizing track density for a charged particle in liquid hydrocarbons is not far different from that in the aqueous medium. The linear energy transfer value for the  $^{60}\text{Co}$   $\gamma$ -radiation is thus about 0.04 e.v./ $\text{\AA}$ ., and that for a  $^{210}\text{Po}$   $\alpha$ -particle, attenuated through 0.0003-in. stainless steel foil, is near the Bragg ionization peak value of about 25 e.v./ $\text{\AA}$ ..<sup>20</sup> The LET values for high energy helium ions and deuterons can be calculated by equations given by Schuler and Allen<sup>21</sup>; the value for 22-Mev. deuterons is 0.44 e.v./ $\text{\AA}$ ., and that for 44-Mev. helium ions is 1.75 e.v./ $\text{\AA}$ .

Our observed hydrogen yields for benzene radiolysis with high energy helium ions and deuterons agree well with those reported by Gauman and Schuler,<sup>10</sup> and the  $G(-\text{benzene})$  value is essentially the same as that

obtained by Burns<sup>8</sup> for ionizing particles of intermediate linear energy transfer. There is some discrepancy between our  $G(-\text{reactant})$  values for  $^{210}\text{Po}$   $\alpha$ -radiolyses of benzene and *o*-terphenyl and those of  $G(-\text{benzene}) = 2.1$  at 25° and  $G(-\text{o-terphenyl}) = 0.93$  at 100° as reported by Burns and Reed<sup>9</sup> for irradiations with particles from the  $^{10}\text{B}(n,\alpha)^7\text{Li}$  reaction. The ionizing track densities for both the  $^{210}\text{Po}$   $\alpha$ -particles and the particles from the  $^{10}\text{B}(n,\alpha)^7\text{Li}$  reaction are expected to be nearly the same, but the condition for pile irradiations is complicated by the necessary presence of organoboron compounds. It may not be entirely valid to compare results from these two sets of experiments. In any case, we are in qualitative agreement that there is little change in product yields for radiations in LET values from 0.02 to 2 e.v./ $\text{\AA}$ ., and that the yields increase sharply with increasing LET above 2 e.v./ $\text{\AA}$ .. Such correlations are presented graphically in Figure 2.

Another significant observation is a dependence of the rate of radiation-induced decomposition on the

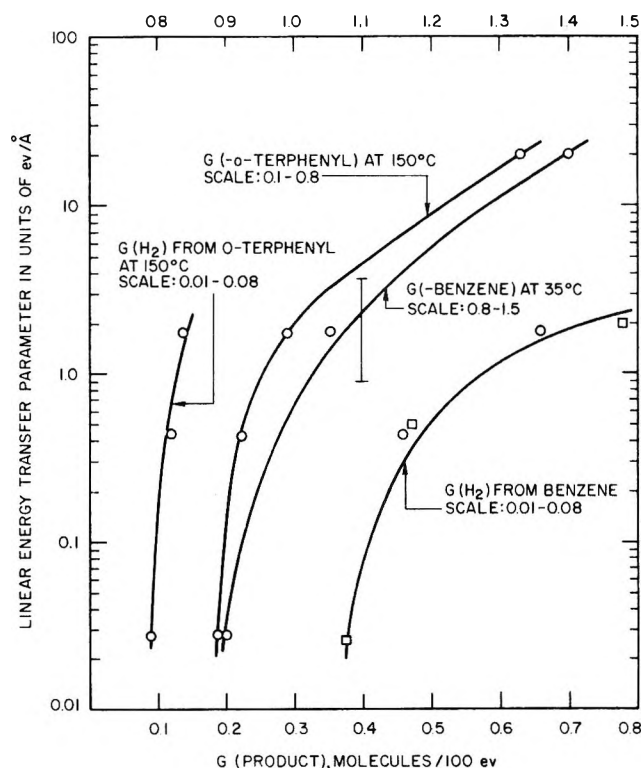


**Figure 2.** Radiation damages to liquid benzene and *o*-terphenyl:  $\square$ , Gauman and Schuler;  $\circ$ , Burns' data.

(20) E. Collinson, F. S. Dainton, and J. Kroh, *Nature*, **187**, 475 (1960).

(21) R. H. Schuler and A. O. Allen, *J. Am. Chem. Soc.*, **79**, 1565 (1957).

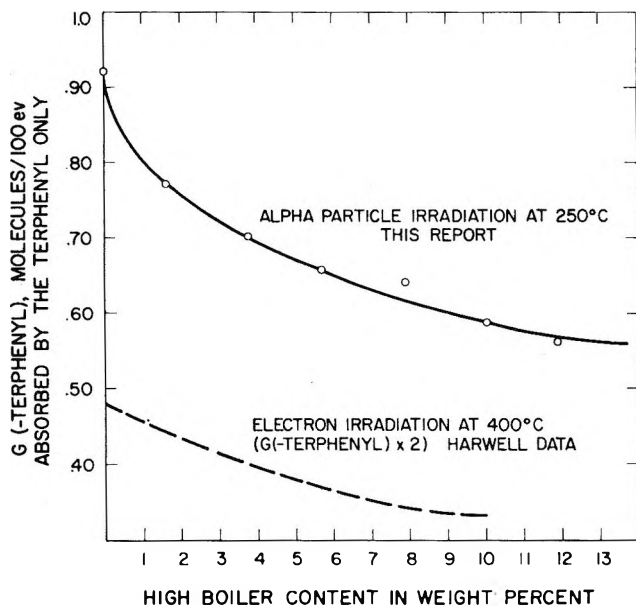


Figure 3.  $G(-o\text{-terphenyl})$  as functions of the polymer content.

polymer content of the substrate. Figure 3 is a plot of the  $G(-o\text{-terphenyl})$  values (corrected for energy absorption in  $o\text{-terphenyl}$  alone) vs. the polymer content. Such a marked inhibitory effect of the polymer on the radiation damage to  $o\text{-terphenyl}$  indicates an important competition between the product and the substrate in reactions with active intermediates. Parallel results are observed in irradiations by  $^{210}\text{Po}$   $\alpha$ -particles and by fast electrons. Apparently such scavenging processes are LET independent.

## Discussion

Comprehensive analyses of possible mechanisms for radiation-induced decomposition of aromatic hydrocarbons are given by Burns and Reed<sup>8,9</sup> and by Burr and co-workers.<sup>22</sup> We shall therefore center our attention only to implications of LET effects on the product yields.

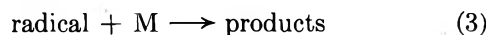
The observed effect is distinctly different from that in the aqueous system and cannot arise from competition between track recombination and diffusion out of the track by radicals and hydrogen atoms. As we have pointed out in our earlier note,<sup>12</sup> in organic systems the radicals can react readily with the solvent molecules and the particle track must be more diffuse than in irradiated aqueous systems. Consequently bimolecular reactions involving long-lived excited species have been proposed often<sup>8-12,22,23</sup> as most compatible with the increase in radiation damage with increasing LET. A competition between product formation *via* a bimolecular reaction of excited molecules,

eq. 1, and a unimolecular deactivation of the intermediate, eq. 2, is suggested specifically by Burns and



Reed.<sup>8,9</sup>

It is not apparent that the above model can account satisfactorily for the observed LET effects. A qualitative analysis based on such a model has to take into consideration not only diffusion of activated species but also complications due to radical diffusion as a result of reaction 3, which is necessary to account



for the observed high molecular weight products as well as the protective effects of certain additives. Simplified calculations based on reactions 1 and 2 will account only for a linear increase in yield with LET. Our intuitive estimate on the effect of diffusion of radicals and activated species is one of depressed yield at high LET rather than the observed sharp increase. A similar conclusion was made recently by Schuler.<sup>24</sup>

Schuler<sup>24</sup> has proposed, further, two very interesting models, the knock-on model and the charge-displacement model. Both these models can reasonably account for observed LET effects in liquid aromatic hydrocarbons. However, they are highly speculative and require large departure from normal considerations of radiation-induced processes.

All the above models are based on a consideration that the only significant change in experimental conditions due to variations in LET is a change in the track concentration of reactive intermediates. Recent evidences indicate, however, that a temperature effect cannot be neglected for high LET radiations.<sup>14,15,25</sup> It may be considered that for relatively low LET radiations the track temperature increase will be small and the reaction rate increase negligible. For high LET radiations, however, a sharp product yield increase may be expected from a large temperature effect.

Thermal spike calculations<sup>26</sup> based on reactions between activated intermediates and surrounding molecules gave results in qualitative agreement with our observations. Such calculations were made, however,

(22) J. G. Burr, *et al.*, *Nucl. Sci. Eng.*, **11**, 218 (1961).

(23) J. M. Scarborough and J. G. Burr, *J. Chem. Phys.*, **37**, 1890 (1962).

(24) R. H. Schuler, *Trans. Faraday Soc.*, **61**, 100 (1965).

(25) J. L. Magee, *Discussions Faraday Soc.*, **36**, 232 (1963).

(26) T. Wolfram and J. A. Brinkman, private communications. We will provide details of these calculations on request.



with oversimplified and sometimes unrealistic assumptions. We think, however, the thermal spike model<sup>27</sup> should be considered as an alternative explanation for the observed LET effects and further efforts made to bring it to a computational level equivalent to that of the diffusion model.

*Acknowledgment.* We wish to thank Dr. Warren M. Garrison, Mr. Boyd M. Weeks, and the 60-in. cyclotron staff at the Crocker Radiation Laboratory, University of California (Berkeley), for their assistance in carrying out helium ion and deuteron irradiations.

We are indebted to Mr. John A. Brinkman and Dr. Thomas Wolfram of our laboratory for calculating the radiation damage yield due to a thermal spike, and to Dr. Mark Cher of our laboratory for valuable suggestions. We wish to acknowledge further the generosity of Dr. W. G. Burns of A.E.R.E., Harwell, England, for furnishing us some of his unpublished preliminary reports.

---

(27) F. Seitz and J. S. Koehler, "Solid State Physics," Vol. II, Academic Press, Inc., New York, N. Y., 1956, p. 351.

## Dielectric Dispersion of Protein Solutions Containing Small Zwitterions<sup>1</sup>

by Rufus Lumry and Robert Hon-Sang Yue

Laboratory for Biophysical Chemistry, School of Chemistry, University of Minnesota, Minneapolis, Minnesota  
(Received September 28, 1964)

The molecular mechanism responsible for the dielectric-dispersion behavior of small globular proteins has been examined using measurements in the presence and absence of small dissolved zwitterions. The zwitterions eliminate complications due to electroviscous effects and dielectric effects of the ion atmosphere. They have relatively little influence on the Kirkwood-Shumaker effect. The kinetics of the latter are analyzed on the basis of known rates for proton processes to show that in the range of pH from 6.5 to 9, little complication due to these effects is to be expected. The agreement between results obtained with and without zwitterions over a range of solvent conditions demonstrates that for sufficiently small proteins the solution dielectric properties are controlled by and measure the mean-square permanent dipole moment of the protein and the rotational relaxation behavior of the protein. The dielectric parameters for metmyoglobin, carboxymyoglobin, oxidized and reduced cytochrome-c, and chymotrypsinogen A are given for a variety of solution conditions. Distinct anomalies were found only in the cytochrome-c forms where relaxation time and dielectric increment increase with decreasing concentration of protein and in mixtures of bovine serum albumin with oxidized cytochrome-c. No differences were detected between oxidized and reduced cytochrome-c or between oxidized and reduced myoglobin. The results provide confidence in the use of the dielectric dispersion method for some protein solutions and suggest several uses of the method for the study of the kinetics and equilibria of protein aggregation reactions.

### Introduction

As a source of information about the physical parameters of protein molecules, the method of dielectric dispersion has much to recommend it. It is simple, capable of considerable precision, and under certain conditions can provide, in addition to dielectric relaxation times, the distribution of such times and information about the first moment of the charge distribution.<sup>2</sup> These quantities cannot for the most part be interpreted in terms of specific protein models in any useful way at the present any more than can data from any other hydrodynamic measurement. However, providing that the specific processes measured by the method are known, the quantities can be of considerable help to protein chemists especially in studying changes in conformation and charge distribution. They may also ultimately have some utility as a means of determining the rate constants for aggregation processes or some conformation changes. Some years ago, Oncley and Wyman and their respective co-workers<sup>3</sup>

developed the method as applied to proteins and collected considerable information about well-known proteins. In recent years Takashima<sup>4-10</sup> has been the principal worker in this area. The method has not grown in popularity because the possibility of several kinds of complication has led to uncertainty regarding the actual molecular processes which determine the measured dielectric parameters. In particular, the

(1) This work was supported by the Office of Naval Research, Department of Defense, Contract No. NONR 710 (55).

(2) C. P. Smyth, "Dielectric Behavior and Structure," McGraw-Hill Book Co., Inc., New York, N. Y., 1955.

(3) E. J. Cohn and J. T. Edsall, "Proteins, Amino Acids and Peptides," Reinhold Publishing Corp., New York, N. Y., 1943.

(4) S. Takashima, *J. Am. Chem. Soc.*, **78**, 541 (1956).

(5) S. Takashima and R. Lumry, *ibid.*, **80**, 4238 (1958).

(6) S. Takashima and R. Lumry, *ibid.*, **80**, 4244 (1958).

(7) S. Takashima, *ibid.*, **80**, 4478 (1958).

(8) S. Takashima, *J. Polymer Sci.*, **56**, 257 (1962).

(9) S. Takashima, *Arch. Biochem. Biophys.*, **77**, 454 (1958).

(10) S. Takashima, *Biochim. Biophys. Acta*, **79**, 531 (1964).

dielectric relaxation and measured dielectric moment may have more to do with the behavior of the ion atmosphere of the protein than with the rotational diffusion and permanent moment of the rigid protein dipole. There are three types of complication which may be important.

1. Because of high ionic conductance of singly charged ions it is not possible to work at sufficiently high salt concentrations to damp out the electroviscous effects resulting essentially from the dragging of ion atmosphere ions and solvent by the moving protein groups. This effect is a minimum at the prevailing isoelectric point but is still nonzero because the condition of zero net charge for the protein system is partially achieved by balancing molecules with instantaneous net positive charge against those with net negative charge. Effects can become quite large at pH values some distance from the isoelectric point.

2. If a protein molecule is charged, its ion atmosphere has the opposite average charge and on the average a complementary electrical distribution. The ion atmosphere can thus respond to the applied electrical field to undergo periodic polarization. The problem has been discussed particularly by O'Konski.<sup>11</sup> The characteristic relaxation time for this process has been estimated at  $M^{-1} \times 10^{-10}$  sec.,<sup>12</sup> in which  $M$  is the molar concentration of salt. Thus the ion-atmosphere relaxation time for  $10^{-4}$  M KCl is  $5 \times 10^{-7}$  sec. and close to the expected rotational relaxation time of a protein of medium size or medium asymmetry. Increasing salt concentration reduces electroviscous effects and decreases the time for ion-atmosphere relaxation but also reduces the precision of the method. The method becomes inapplicable at salt concentrations much above  $10^{-3}$  M. Decreasing salt concentration decreases the magnitude of the ion-atmosphere dispersion but increases the electroviscous effect and shifts the ion-atmosphere relaxation time right into the range of rotational relaxation times. It is clear that no suitable compromise of salt concentration exists which will eliminate the possibility of complications. The ion-atmosphere effect is an example of the Maxwell-Wagner effect<sup>13</sup> and can be quite large if the ionic strength is appreciable. Because of technical limitations, most protein dielectric work is done at such low ionic strength that there is usually only one small ion per protein molecule. Hence it can be anticipated that the magnitude of the effect usually will be very small.

3. In 1952, Kirkwood and Shumaker<sup>14</sup> suggested that the probable process measured in dielectric dispersion measurements in protein solutions was the field-induced migration of protons from acid groups on

the surface of the proteins to unprotonated basic groups of the protein. Kinetically, the rate of such migration will depend on the particular acidic and basic groups involved and their orientation and also weakly on the salt concentration which, as it increases, will increasingly stabilize an existing charge distribution on the protein relative to rapid changes in this distribution. Kirkwood and Shumaker did not estimate the relaxation times for the migratory process, but suggested that the apparent dielectric increment produced in this way might be of the order found in protein studies. Since that time there has been little further development of this idea and until recently little clarification of the kinetic problems involved. Takashima<sup>8</sup> has attempted with some success to show that protein dielectric dispersion studies are to be interpreted in terms of classical Debye behavior of a rigid dipole. Very recently, Scheider<sup>15</sup> has considered theoretically the kinetic problems and has concluded from theory and experiment that the Debye behavior is the principal cause of the dielectric relaxation in bovine serum albumin.

The first two general classes of effects include Maxwell-Wagner effects dependent on the difference in dielectric constant and conductance across a phase boundary and are thus associated with the protein as a suspended particle and Debye-Falkenhagen effects which are direct consequences of the structure of the ion atmosphere about a charge particle. O'Konski<sup>11</sup> has developed a more general approach to the problem in which he shows that both types of effects can be treated as manifestations of a common set of electrostatic conditions dependent on dielectric constant, surface conductivity, and particle volume conductivity. Schwarz<sup>16</sup> and Eigen and Schwarz<sup>17</sup> have arrived at somewhat similar conclusions. These studies plus numerous investigations of large colloidal particles and particularly of large colloidal particles and polymer molecules with large axial ratios clearly demonstrate that the static and dynamic properties of such particles in their interaction with an electric field are dominated by ion-atmosphere effects which completely

(11) C. T. O'Konski, *J. Phys. Chem.*, **64**, 605 (1960).

(12) H. Falkenhagen, "Electrolytes," The Clarendon Press, Oxford, 1934.

(13) K. W. Wagner, *Arch. Elektrotech.*, **2**, 371 (1914).

(14) J. G. Kirkwood and J. B. Shumaker, *Proc. Natl. Acad. Sci. U. S.*, **38**, 855 (1952).

(15) W. Scheider, "Relaxation Spectra of Permanent and Fluctuating Dipole Moments," Thesis, Harvard University, 1962.

(16) G. Schwarz, *Z. Physik*, **145**, 563 (1956).

(17) M. Eigen and G. Schwarz, *Z. physik. Chem. (Frankfurt)*, **4**, 380 (1955); *J. Colloid Sci.*, **12**, 181 (1957).

overshadow any influence of the permanent dipole moment. The discussion of Eigen and Schwarz<sup>18</sup> on these matters is particularly illuminating. The ion-atmosphere effects drop off very rapidly with decreasing particle length and axial ratio, so that at some upper limit of size and shape of the charged particle the permanent-moment effects can be expected to assume a dominant role in the interaction with an applied field. The basic problem in the use of the dielectric dispersion method for globular proteins has been to decide whether the ion atmosphere or the permanent moment dominates or indeed what is the range of size, shape, charge density, and ionic strength in which effects attributable separately to ion atmosphere and to permanent moment appear.

In view of the potential utility of the dielectric dispersion method and our own interest in interpreting at the molecular level a series of experiments on hemoglobin made some years ago by Takashima and Lumry,<sup>5,6</sup> we have devoted some attention to method modifications which might allow unequivocal interpretation of the data. Of these, the most successful appears to be the use of relatively high concentrations of small zwitterions instead of singly charged ions. Zwitterions have been used effectively in dielectric experiments by Shack and co-workers<sup>19</sup> and by Shaw, *et al.*,<sup>20</sup> studying  $\beta$ -lactoglobulin. Their particular use was justified in the latter experiments by a need to salt-in the globulin. Since in the cases reported zwitterions act effectively to salt-in proteins,<sup>3</sup> it appears probable that to at least a first approximation insofar as the protein is concerned, an ion atmosphere of such ions is equivalent to an ion atmosphere of single-charged ions. The zwitterion atmosphere can be made concentrated without serious loss in method precision. As a result, electroviscous effects can be eliminated and the ion-atmosphere relaxation time made very small since aside from small effects due to the asymmetry of the protein field there is no net ion displacement and the relaxation process becomes rapid. In fact, the latter will not be very much longer than the characteristic rotational time of the small zwitterion. Hence, with such an atmosphere the only probable sources of dielectric relaxation in the radiofrequency range are Debye rotator behavior and perhaps the Kirkwood-Shumaker effect. Although the change in type of ion atmosphere should alter the time constants of the latter effect, it is not obvious that this effect can be eliminated. However, a realistic look at the Kirkwood-Shumaker effect in terms of rate constants for protonic processes suggests that in most instances the effect cannot practically alter relaxation times for protein solutions except under very limited conditions.

It may, however, make a small contribution to the observed moment.

In this paper are described results obtained with and without zwitterions on several small proteins of current interest. The Kirkwood-Shumaker effect will be considered at the end.

### Experimental

*Material.* Sigma Chemical Co. Type III horse-heart cytochrome-c (Lot No. 31B-647) was used. The material was 95% pure by carbon monoxide binding and autoxidation tests. About 10 mg. of reagent grade potassium ferricyanide was added to 5 ml. of cytochrome-c solution to ensure that all the cytochrome-c was in the ferric state. In making reduced cytochrome-c solution, oxidized cytochrome-c solution was reduced using platinum black with hydrogen gas until there was no further change in the absorbancy.

Worthington Biochemical Corp. chymotrypsinogen A Lot No. CG685-90 was used.

Sperm whale metmyoglobin was kindly furnished by Dr. H. Mizukami. It was chromatographed on a carboxymethyl cellulose column using the pH and ionic gradient technique (0.01 *M* phosphate buffer pH 6.05 to 0.1 *M* phosphate buffer pH 7.60). Only the main component was used for the experiment. Carboxymyoglobin was made by reducing the metmyoglobin with a very small amount of sodium borohydride in the presence of carbon monoxide.

Sigma Chemical Co. bovine plasma albumin Lot No. A42B-98 was used.

Carboxypeptidase A was obtained from Worthington Biochemical Corp.

Reagent grade glycine and  $\beta$ -alanine were recrystallized from ethyl alcohol-water at the isoionic pH.

All protein concentrations were measured spectrophotometrically with a Beckman DU spectrophotometer. Optical densities for a 1% solution in a 1-cm. spectrophotometric cell at the respective wave length are: oxidized cytochrome-c at 530  $m\mu$ , 7.66; reduced cytochrome-c at 530  $m\mu$ , 22.4; metmyoglobin at 408  $m\mu$ , 87.0; carboxymyoglobin at 580  $m\mu$ , 7.55; chymotrypsinogen A at 280  $m\mu$ , 19.7. These values were determined by the dry-weight method. Viscosity was measured with Oswald viscometers at 15.00  $\pm$  0.02°.

*Instrumental.* A standard replacement bridge

(18) M. Eigen and G. Schwarz, "Symposium on Electrolytes-trieste 1959," Pergamon Press, London, 1961.

(19) J. Shack, "Dielectric Absorption of Protein Solutions," Ph.D. Dissertation, Harvard University, 1939.

(20) T. N. Shaw, E. F. Jensen, and H. Lineweaver, *J. Chem. Phys.*, 12, 439 (1944).

method employing a Boonton Radio Model 250A RX meter, essentially an admittance bridge, was used for all experiments.<sup>21</sup> The bridge conductance scale was shifted to a maximum value of 120 pf. by fixed parallel inductance coils at each of the 14 frequencies in the range 0.5 to 20 Mc. The measuring cell has been described<sup>5</sup> but was modified for this work by covering the brass electrode support for the upper electrode with a Teflon cylinder compressed against the top of this electrode. The Teflon was effective in eliminating contact between brass and the solution and thus removed previous drift problems even when using conductivity water. The cell was rigidly joined to the instrument input terminals by the shortest possible brass rods hollowed to receive banana plugs mounted on the cell. The equivalent circuit was determined from readings on known KCl concentrations. The resistance and capacitance of the solution in the cell were computed from eq. 1a and 1b.<sup>22</sup>  $L_x$ , the residual series inductance, was  $0.75 \times 10^{-7}$  henrys and  $R_x$ , the residual series resistance was 0.40 ohms. Both quantities were constant independent of plate separation and cell contents.

$$R = \left( \frac{R_p}{1 + R_p^2 C_p^2 \omega^2} - R_x \right) + \frac{\left( \frac{R_p^2 C_p \omega}{1 + R_p^2 C_p^2 \omega^2} + L_x \omega \right)^2}{\left( \frac{R_p}{1 + R_p^2 C_p^2 \omega^2} - R_x \right)} \quad (1a)$$

$$C = \left[ \frac{\left( \frac{R_p^2}{1 + R_p^2 C_p^2 \omega^2} + L_x \omega \right)}{\left( \frac{R_p}{1 + R_p^2 C_p^2 \omega^2} - R_x \right)^2 \omega + \left( \frac{R_p^2 C_p \omega}{1 + R_p^2 C_p^2 \omega^2} + L_x \omega \right)^2 \omega} \right] - C_x \quad (1b)$$

$R$  was the resistance of the solution in the cell in ohms;  $C$  was the capacitance of the solution in the cell;  $C_x$  was the residual capacitance of the cell;  $R_p$  was the equivalent parallel resistance; and  $C_p$  was the equivalent parallel capacitance. Using different plate separations and plotting  $C - C_x$  vs. the reciprocal of the distance between electrodes, the intercept gave  $C_x$  and it was found to be 20.0 pf. The real and imaginary parts of the complex dielectric constant of the cell were calculated<sup>23</sup> from  $\epsilon' = C/C_0$  in which  $C_0 = C_{KCl}/D_{water}$ ;  $C_{KCl}$  = capacitance of a dilute KCl solution at the same fixed plate separation; and  $D_{water}$  = low frequency dielectric constant of water taken as 82.0 at 15.0°.  $\epsilon'' = G_p/C_0 \omega$  in which  $G_p = (1/R - 1/R_0)$ .  $R_0$  is the low frequency resistance outside the dispersion frequency range. The dielectric constant of the solution at high frequency well outside the dispersion range was taken as  $(82.0 - 0.060c)$  in which  $c$  is the concentration of protein in grams/liter of solvent.<sup>3</sup> The

dipole moment,  $\mu$ , of the protein was estimated from eq. 2 using Wyman's value of 8.5<sup>3</sup> for the constant  $h$

$$\mu^2 = \left( \frac{9000kT}{4Nh} \right) \left( M \frac{\epsilon'_0 - \epsilon'_\infty}{c} \right) \quad (2)$$

where  $k$  is the Boltzmann constant,  $N$  is Avogadro's number, and  $M$  is the molecular weight of the protein.

An interesting and useful by-product of the investigation was the finding that electrode polarization effects at our lower frequencies are a consequence of the simultaneous presence of zwitterions and single-charged ions. In the range  $0-5 \times 10^{-4}$  M KCl and as high as 2%  $\beta$ -alanine neither kind of ion by itself produced polarization at our lowest frequency, 0.5 Mc. The polarization observed when both kinds of ion were present was roughly proportional to the product of their concentrations. Since the polarization contribution from the protein was negligible when 1 or 2% glycine or  $\beta$ -alanine was present, it was possible to correct for polarization contributions by subtracting the values of  $\epsilon'$  observed with a zwitterion solution containing no protein from the value of  $\epsilon'$

observed when both zwitterion and protein were present and the zwitterion concentration was the same in both experiments. Some experimental results of the polarization effects in solutions containing singly-charged and zwitterions are given in Figure 1. Results from a typical experiment on a protein solution showing the effect of the correction are given in Figure 2. In view of the confusion attending any understanding of electrode-polarization processes, this result is of some interest since in zwitterion-free solutions the protein as dipole may be contributing to electrode polarization.

*Procedure.* Just before use, the protein solutions

(21) We are indebted to Dr. O. Schmitt for making this instrument available.

(22) Dr. D. Britton provided valuable aid in programming and computing.

(23) "International Critical Tables of Numerical Data, Physics, Chemistry and Technology," McGraw-Hill Book Co., Inc., New York, N. Y., 1929.

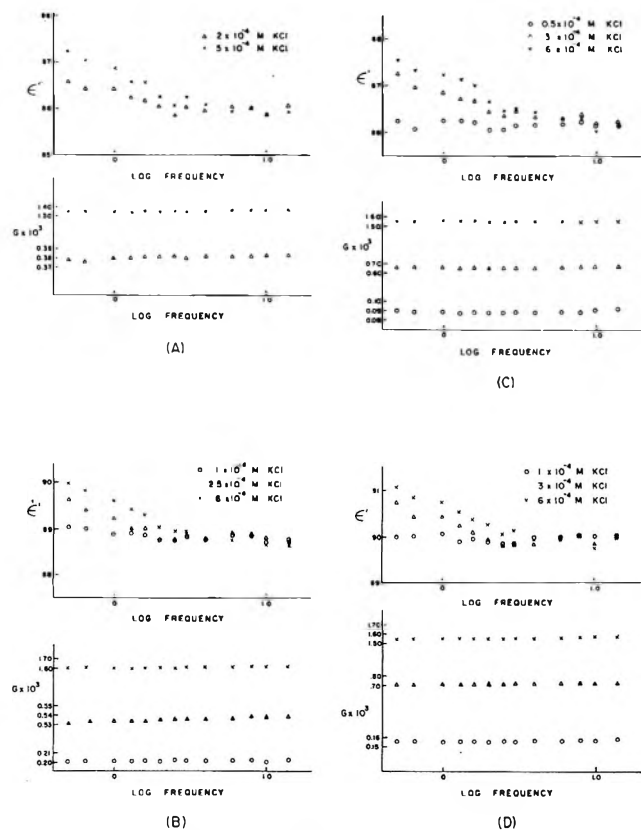


Figure 1. Electrode polarization produced by simultaneous presence of zwitterions and singly charged ions: (A) 1% glycine, (B) 2% glycine, (C) 1%  $\beta$ -alanine, and (D) 20%  $\beta$ -alanine. The frequency scale is log Mc.

were desalted on a Dintzis column.<sup>24</sup> The pH was then adjusted slowly with dilute HCl or KOH plus the desired amount of KCl solution necessary to allow balance of the bridge. The zwitterion solution was then added. Nitrogen in equilibrium with water at the cell temperature was passed through the closed cell until the bridge readings became constant. At a plate separation of 1.02 cm. the equivalent parallel solution capacitance was about 100 pf. and could be read with a precision of 0.15%. The equivalent parallel solution resistance could be read to about 0.4% at all but the highest frequencies. Solution conductance was in the range of  $1 \times 10^{-5}$  to  $4 \times 10^{-3}$  mho.

## Results

*Solubility of Carboxypeptidase A in  $\beta$ -Alanine.* In order to test for the effectiveness of zwitterions as salting-in agents for proteins and thus presumably for their adequacy in providing an ion atmosphere similar to that provided by singly charged ions, the saturated solubility of carboxypeptidase A, which is extremely low in pure water, was determined in 0.268 M KCl and 0.225 M  $\beta$ -alanine solutions. The ratio of

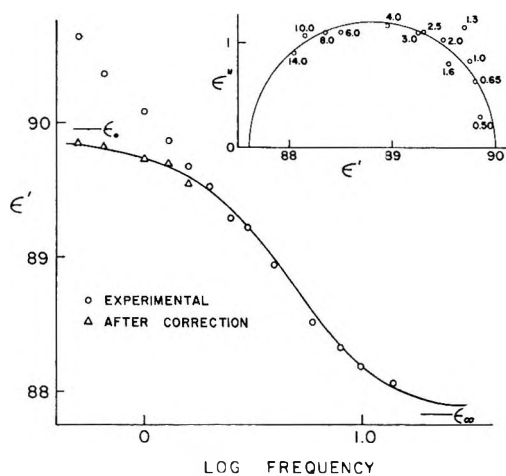


Figure 2. Dielectric dispersion curve for 1.41% metmyoglobin in 2% glycine and  $3 \times 10^{-4}$  M salt at pH 7.20. The insert is the Cole-Cole plot for the same experiment. The frequency scale is log Mc.

dissolved protein to total charge concentrations in the two solutions was identical. The efficiency of zwitterions as salting-in agents has previously been demonstrated by Richards on hemoglobin<sup>25</sup> and by Joseph on  $\beta$ -lactoglobulin.<sup>26</sup>

There is no understanding of the variation in solubility of different globular proteins. Nevertheless, the salting-in effect can be attributed to a favorable interaction between ionized groups of the protein and the local ion atmosphere about these groups as well as to a smaller influence of salt ions on ionic activity coefficients. An ion atmosphere constructed from zwitterions has a long-range character totally different from one composed of singly charged ions. On the other hand, the short-range effects as those which exist between a given charged group and its nearest neighbors are much less different. That this is so appears to be verified by the effectiveness of zwitterions as salting-in agents. Since it is the long-range behavior of the ion atmosphere which is responsible for Maxwell-Wagner and Debye-Falkenhagen effects and since the zwitterion atmosphere will have little long-range character, we may hope to eliminate or usefully alter the characteristics of the ion atmosphere which complicate the analysis of dielectric dispersion data if we replace single-charged ions by zwitterions.

*Myoglobin.* Myoglobin, Mb, has a small dielectric increment and it was not possible to work at protein concentrations lower than 1%. The results for met-Mb are shown in Table I. In these experiments as in most

(24) H. M. Dintzis, Ph.D. Dissertation, Harvard University, 1952.

(25) M. M. Richards, *J. Biol. Chem.*, **122**, 727 (1938).

(26) N. R. Joseph, *ibid.*, **116**, 353 (1936).

**Table I:** Metmyoglobin<sup>a</sup>

% protein	Amino acid	Salt concn., <sup>b</sup> <i>M</i>	pH	$\tau \times 10^8$ , sec.	$\Delta D$	$\alpha$
3.05 <sup>c</sup>	...	$1 \times 10^{-5}$	8.10	3.54	0.18	0
2.20	...	$1.2 \times 10^{-4}$	7.88	3.3	0.21	0.11
2.20	...	$2.7 \times 10^{-4}$	7.88	3.9	0.23	0.09
2.20	...	$6 \times 10^{-4}$	6.70	3.3	0.19	$\sim 0^d$
1.90	...	$2 \times 10^{-5}$	8.35	3.5	0.20	0.02
1.49	...	$5 \times 10^{-5}$	8.00	3.2	0.17	0.01
1.19	...	$1 \times 10^{-5}$	8.00	3.2	0.18	0
1.41	2% glycine	$3 \times 10^{-4}$	7.20	3.1 <sup>e</sup>	0.17	0
1.41	2% glycine	$4.5 \times 10^{-4}$	7.20	3.2 <sup>e</sup>	0.16	$\sim 0^d$
1.41	2% glycine	$5 \times 10^{-4}$	7.20	3.2 <sup>e</sup>	0.17	$\sim 0^d$
1.19	2% $\beta$ -alanine	$3.5 \times 10^{-4}$	7.00	3.0	0.18	0
1.19	2% $\beta$ -alanine	$4.5 \times 10^{-4}$	7.00	3.3 <sup>e</sup>	0.17	$\sim 0^d$
1.19	2% $\beta$ -alanine	$5.5 \times 10^{-4}$	7.00	3.2 <sup>e</sup>	0.16	$\sim 0^d$

<sup>a</sup> Dielectric parameters from Cole-Cole plots unless noted.

<sup>b</sup> Calculated as KCl concentration from conductance measurements. <sup>c</sup> Not chromatographed. <sup>d</sup> From capacitance dispersion. <sup>e</sup> Not corrected for solvent viscosity. Correction factors to water reference for 1% glycine, 2% glycine, 1%  $\beta$ -alanine, and 2%  $\beta$ -alanine are 1.0147, 1.0353, 1.0221, and 1.0461, respectively.

others, a wide range of salt and protein concentrations and pH was employed in order to look for changing dielectric behavior which might result from the dependence of the several possible mechanisms of dielectric relaxation on these variables. It was the purpose of these experiments to validate the method and not to provide exhaustive information on any protein. In fact, the Boonton RX meter is not an instrument of sufficient precision for detailed work on proteins. Where possible, the values of  $\tau$ , the reciprocal of the critical frequency times  $2\pi$ ;  $\Delta D$ , the dielectric increment; and  $\alpha$ , the dispersion parameter for the relaxation times were determined from Cole-Cole plots<sup>2</sup> of the real and imaginary parts of the dielectric constants determined at the several frequencies. Above  $10^{-3}$  *M* concentrations of singly ionized salts it was not possible to measure the dispersion of conductance and a set of capacitance *vs.* log frequency curves calculated from the Cole-Cole equation was used to determine  $\alpha$  from the capacitance dispersion. In the myoglobin experiments,  $\alpha$  was zero within the accuracy of curve fitting so that dispersion corresponds to the classic Debye equation for a single critical frequency.<sup>27</sup> There is no evidence in this work for more than one relaxation time as is consistent with X-ray diffraction results which show that the molecule has no large asymmetry. Without zwitterions the results were somewhat erratic but there was no significant effect of pH, protein concentration,

or salt concentration on the dielectric parameters. With added zwitterions, the average value of  $\tau$  was  $3.2 \times 10^{-3}$  sec. and the average value of  $\Delta D$  was 0.17 l./g., leading to an estimate of the dipole moment of 126 D. The presence of the zwitterion in concentrations up to 0.224 *M* altered the dielectric behavior neither quantitatively nor qualitatively. There is some indication of an increased dielectric increment at pH values above the isoelectric point as would be expected, but the change is small and at the limit of errors. Results for the carbon monoxide derivative of reduced myoglobin are given in Table II. Once

**Table II:** Carbon Monoxide Myoglobin<sup>a</sup>

% protein	Amino acid	Salt concn., <sup>b</sup> <i>M</i>	pH	$\tau \times 10^8$ , sec.	$\Delta D$	$\alpha$
1.39	...	$5 \times 10^{-5}$	7.75	2.8	0.17	0
1.39	...	$2.5 \times 10^{-4}$	7.75	4.1	0.21	0.09
1.39	1% glycine	$5 \times 10^{-4}$	7.00	3.1 <sup>d</sup>	0.17	$\sim 0^e$
1.39	2% glycine	$5 \times 10^{-4}$	7.00	2.8	0.19	0
1.39	2% glycine	$5.5 \times 10^{-4}$	7.00	3.0 <sup>d</sup>	0.19	$\sim 0^e$
1.39	2% glycine	$6 \times 10^{-4}$	7.00	3.1 <sup>d</sup>	0.19	$\sim 0^e$

<sup>a</sup> Dielectric parameters from Cole-Cole plots unless noted.

<sup>b</sup> Calculated as KCl concentration from conductance. <sup>c</sup> Capacitance dispersion only. <sup>d</sup> Not corrected for solvent viscosity. See Table I, footnote *e*.

again there was no evidence within experimental errors for more than one relaxation process. The results were erratic without the zwitterion but within error the addition of zwitterion had no effect on the dielectric behavior. The average value of  $\tau$  in the zwitterion solution was  $3.0 \times 10^{-8}$  sec. and that of  $\Delta D$  was 0.19 l./g., leading to a dipole moment estimate of 133 D. These  $\tau$ -results are to be compared with a value reported by Marcey and Wyman,<sup>28</sup>  $2.9 \times 10^{-8}$  sec. for horse-heart met-Mb, and with those of Takashima,<sup>8</sup> who found  $\tau = 2.9 \times 10^{-8}$  sec. and  $\Delta D = 0.19$  l./g. at 10° working with bovine met-Mb. Neither these authors nor the present authors detected deviations from a single relaxation process. All of these results are identical within error. The ratios of the viscosity of 1% glycine, 2% glycine, 1%  $\beta$ -alanine, and 2%  $\beta$ -alanine to that of water at 15.0° were found in this work to be 1.0147, 1.0353, 1.0221, and 1.0461, respectively. Hence the viscosity corrections for zwitterion solutions are negligible within error of the method.

(27) P. Debye, "Polar Molecules," Reinhold Publishing Co., New York, N. Y., 1929.

(28) H. O. Marcey and J. Wyman, Jr., *J. Am. Chem. Soc.*, **64**, 638 (1942).

According to Kendrew and co-workers,<sup>29</sup> met-Mb is a flattened disk of approximate dimensions of  $43 \times 35 \times 23 \text{ \AA}$ . Assuming a spherical shape for the protein and the conventional Stokes law from the relationship between radius,  $R$ , viscosity,  $\eta$ , and relaxation time,  $\tau = 4\pi\eta R^3/kT$ ,  $R$  is estimated from our data as  $21.3 \text{ \AA}$  for met-Mb and  $20.9 \text{ \AA}$  for COMb. Considering the assumptions, the absence of an estimate of hydration, and the fact that the orientation of the dipolar axis is unknown, the agreement with X-ray diffraction dimensions is as good as can be expected.

**Cytochrome-c.** In contrast to Mb, cytochrome-c has an unusually large moment especially at low protein concentration and could be studied at concentrations as low as 0.1%. Neither glycine nor  $\beta$ -alanine could be used at the high isoionic point of oxidized cytochrome-c, reported as 10.65 at  $0^\circ$ ,<sup>30</sup> since a considerable concentration of the  $\text{NH}_2$  form is present. A guanidinium zwitterion would have been successful. The results were somewhat erratic, particularly  $\alpha$  which, however, was small or zero within error. The experimental results shown in Table III are in the

Table III: Oxidized Cytochrome-c<sup>a</sup>

% protein	Amino acid	Salt concn., <sup>b</sup> M	pH	$\tau \times 10^8$ , sec.	$\Delta D$	$\alpha$
0.79	...	$5 \times 10^{-4}$	8.48	1.9	0.67	$\sim 0^c$
0.70	...	$3.5 \times 10^{-4}$	9.70	2.8	0.64	$\sim 0^c$
0.80	...	$3.5 \times 10^{-4}$	9.65	3.6	0.64	0.07
1.73	...	$2.5 \times 10^{-4}$	10.00	2.65	0.42	0.01
0.534	...	$1.6 \times 10^{-4}$	9.70	2.5	0.49	0.05
0.855	...	$3 \times 10^{-4}$	9.80	3.2	0.59	0.05
0.795	2% glycine	$6.5 \times 10^{-4}$	7.00	2.4 <sup>d</sup>	0.67	$\sim 0^e$
0.795	2% glycine	$6.5 \times 10^{-4}$	7.00	2.1 <sup>d</sup>	0.69	$\sim 0^e$
0.1087	2% glycine	$5.5 \times 10^{-4}$	7.00	4.0 <sup>d</sup>	1.1	?
0.1087	2% glycine	$4 \times 10^{-4}$	7.00	3.5 <sup>d</sup>	1.1	?
0.534	2% $\beta$ -alanine	$5.5 \times 10^{-4}$	7.00	2.1 <sup>d</sup>	0.82	$\sim 0^e$
1.73	2% $\beta$ -alanine	$1 \times 10^{-4}$	7.00	1.9 <sup>d</sup>	0.58	$\sim 0^e$
0.855	2% $\beta$ -alanine	$5 \times 10^{-4}$	7.00	2.0 <sup>d</sup>	0.70	$\sim 0^e$
0.855	2% $\beta$ -alanine	$5 \times 10^{-4}$	7.00	2.0 <sup>d</sup>	0.70	$\sim 0^e$
0.855	2% $\beta$ -alanine	$5 \times 10^{-4}$	7.00	2.0 <sup>d</sup>	0.72	$\sim 0^e$

<sup>a</sup> Dielectric parameters from Cole-Cole plots unless noted. <sup>b</sup> Calculated as KCl concentration from conductance. <sup>c</sup> Capacitance dispersion based on frequencies larger than one megacycle. The low frequency results were anomalous. <sup>d</sup> Not corrected for solvent viscosity. See Table I footnote e. <sup>e</sup> Capacitance dispersion only.

nature of survey since it became obvious that the dielectric parameters are quite sensitive to protein concentration. This is apparent in the experiments at high zwitterion concentration. The results in glycine and  $\beta$ -alanine solutions are shown in Figure 3. The dielectric parameters become very large at low concentration. In general, at concentrations much

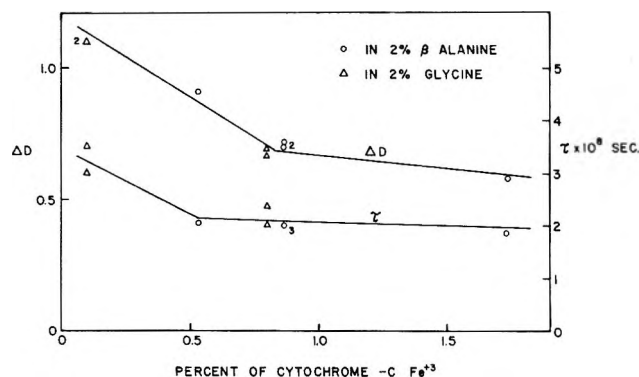


Figure 3. Dielectric increment and relaxation time of oxidized cytochrome-c at pH 7.00.

above 0.1%, the capacitance dispersion curves for the experiments of this figure follow the simple dispersion equation very closely. At 0.1% protein the data were not sufficiently precise to establish the form of the capacitance dispersion curves, yet the large increases in estimated  $\tau$  and  $\Delta D$  there and the more precise value at high protein concentrations suggest an unfolding process or an aggregation. The occurrence of such processes on lowering the protein concentration would be remarkable but at both high and low salt concentrations there are large increases in reduced viscosity of the protein solutions which follow the same dependence on protein concentration. These were first observed by Takashima<sup>31</sup> and have since been found in our laboratory<sup>32</sup> and in that of Kowalsky.<sup>33</sup> This behavior is currently under investigation and we have deferred further dielectric studies until a clearer interpretation of the viscosity behavior becomes available. The matter is of some concern since oxidation-reduction potentials and spectra are usually determined in low protein concentration whereas physical properties are studied at high protein concentrations. It is worth noting that both Dintzis<sup>24</sup> and Scheider<sup>15</sup> observed a large increase in dielectric increment with decreasing protein concentration for both bovine plasma albumin BPA and human plasma albumin. There may be a common cause for such behavior in these proteins and in cytochrome-c.

There is also a significant indication that the relaxation time is longer at the isoionic point than at pH 7.0. Also the dielectric increment is smaller as would be expected. The relaxation time is  $2 \times 10^{-8}$  sec. at

(29) J. C. Kendrew, G. Bodo, H. M. Dintzis, R. D. Parrish, and H. Wyckoff, *Nature*, **181**, 662 (1958).

(30) D. Keilin and E. F. Hartree, *Biochem. J.*, **39**, 289 (1945).

(31) S. Takashima, unpublished results.

(32) J. F. Sullivan and R. Lumry, unpublished results.

(33) A. Kowalsky, unpublished results.



higher protein concentrations which, assuming a spherical protein, corresponds to a diameter of 36.5 Å. The ratio of relaxation times for met-Mb and oxidized cytochrome-c at pH 7 in the presence of zwitterions is 1.5. The ratio of molecular weights without attempting to correct for hydration is 1.4.

A few results obtained with reduced cytochrome-c are given in Table IV. Although the range of con-

Table IV: Reduced Cytochrome-c

% pro- tein	Amino acid	Salt concn., <sup>a</sup> M	pH	$\tau \times 10^8$ , sec.	$\Delta D$	$\alpha$
0.79	...	$5 \times 10^{-4}$	6.40	2.4	0.95	0.05 <sup>b</sup>
0.62	...	$2 \times 10^{-4}$	9.80	2.3	0.61	$\sim 0^c$
0.50	2% $\beta$ -alanine	$4 \times 10^{-4}$	8.30	2.4 <sup>d</sup>	0.76	$\sim 0^c$

<sup>a</sup> Calculated as KCl concentration from conductance. <sup>b</sup> Dielectric parameters from Cole-Cole plot. <sup>c</sup> Capacitance dispersion only. <sup>d</sup> Not corrected for solvent viscosity. See Table I, footnote e.

centrations examined was not adequate for an unequivocal interpretation, the relaxation time appears to be independent of pH and the dielectric increment strongly dependent on pH. The dielectric parameters also increase with decreasing protein concentration.

*Chymotrypsinogen A.* The results of studies of chymotrypsinogen A, CGN, are given in Table V.

Table V: Chymotrypsinogen A<sup>a</sup>

% pro- tein	Amino acid	Salt concn., <sup>b</sup> M	pH	$\tau \times 10^8$ , sec.	$\Delta D$	$\alpha$
0.80	...	$1 \times 10^{-4}$	9.00	6.1	1.07	0.10
0.75	...	$1 \times 10^{-4}$	8.50	6.6	1.24	0.10
0.97	...	$1 \times 10^{-4}$	8.70	7.1	0.95	0.09
0.97	...	$2.3 \times 10^{-4}$	8.00	6.0	1.04	0.09
0.97	...	$4 \times 10^{-4}$	6.90	5.3	1.20	0.08
0.97	...	$5 \times 10^{-4}$	6.00	5.3	1.20	0.09
0.97	...	$5.5 \times 10^{-4}$	5.00	4.8	1.00	0.07
0.88	...	$1 \times 10^{-4}$	7.50	6.4	1.00	0.09
0.70 <sup>c</sup>	2% $\beta$ -alanine	$3.5 \times 10^{-4}$	7.00	4.7 <sup>d</sup>	1.20	0
0.70 <sup>c</sup>	2% $\beta$ -alanine	$5 \times 10^{-4}$	6.00	4.7 <sup>d</sup>	1.20	0

<sup>a</sup> Dielectric parameters from Cole-Cole plots. <sup>b</sup> Calculated as KCl concentration from conductance. <sup>c</sup> Abnormal protein—see text. <sup>d</sup> Not corrected for solvent viscosity. See Table I, footnote e.

Those obtained in 2%  $\beta$ -alanine solutions are particularly noteworthy since the protein was found to have a very low sedimentation constant ( $S_{20,w}$ ) of 1.8S in

these solutions compared with that of the essentially monomeric protein in solutions of singly-charged ions which is about 2.7S. Dreyer and co-workers<sup>34</sup> observed low sedimentation constants in glycine buffer at pH 3.0 and 0.1 M ionic strength but in our work at neutral pH values no such effects of glycine were observed. Difference-spectrum studies in  $\beta$ -alanine did not indicate denaturation and the Cole-Cole plot was a perfect half-circle with dielectric parameters in the range expected for native proteins of this size. Further work on this interesting effect of small zwitterions on the chymotrypsin family of proteins is in progress. For the present, the effect is important insofar as it shows that zwitterions must be used with caution in dielectric studies of some proteins.

With no added zwitterions,  $\alpha$  was significantly different from zero, suggesting more than one dispersion process. The dielectric increment did not change with pH, which is not surprising since there are only two histidine residues, but there is an indication that the relaxation time increases with increasing pH. Some aspects of this behavior are associated with dimerization and higher aggregation reactions and will be discussed in another place.

*Bovine Plasma Albumin Plus Oxidized Cytochrome-c.* Figure 4 shows the typical results of an experiment in which two proteins different in dielectric properties are combined in the same zwitterion solution. By itself, a 1.5% solution of BPA in parallel experiments was found to have  $\tau = 1.2 \times 10^{-7}$  sec. and  $\Delta D = 0.20$ . The behavior of bovine serum albumin in dielectric dispersion experiments is variable and complicated,<sup>15,21</sup> so no attempt was made to obtain other than relative information. The results of Figure 4 were obtained from a solution containing 1.50% BPA plus 0.50% oxidized cytochrome-c in 2%  $\beta$ -alanine solution. The

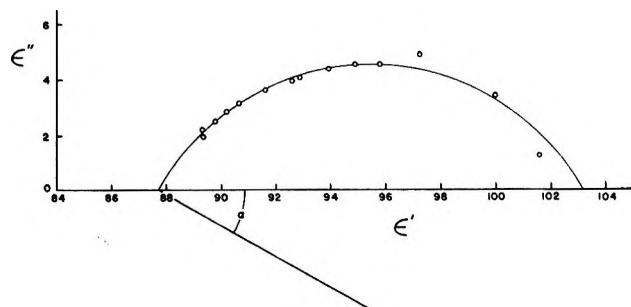


Figure 4. Cole-Cole plot for 1.50% bovine serum albumin and 0.50% oxidized cytochrome-c in 2%  $\beta$ -alanine and  $2 \times 10^{-4}$  M salt at pH 6.70.

(34) W. J. Dreyer, R. D. Wade, and H. Neurath, *Arch. Biochem. Biophys.*, 59, 145 (1955).

pH was 6.70 and thus between the isoelectric points of the two proteins in this solution. If no heterogeneous association of the two proteins occurs, the Cole-Cole plot should be resolvable into two circular arcs since the critical frequencies are well separated. Somewhat similar results would be expected in the case that an association occurs but has an association-dissociation relaxation time small with respect to the period of the experimental frequencies. However, it is to be expected that the relaxation time for the protein association-dissociation process would be long relative to 1 Mc. Then, if aggregation occurs with long time constants, a wide variety of different Cole-Cole plots is possible. As shown in Figure 4, a deceptively simple Cole-Cole plot consisting of a single arc is observed over most of the frequency range and only at lowest frequencies is complex behavior suggested. Only a large  $\alpha$  value of 0.22 reveals the complexity of the situation although the average dielectric increment of 0.78 is considerably higher than might have been expected even on the basis of extensive aggregation. The mean relaxation time from Figure 4 was  $7.1 \times 10^{-8}$  sec. The sedimentation pattern for the solution consisted of a major component with  $S_{20,w} = 5.0S$  and a red component of a very low concentration with the sedimentation constant of monomeric cytochrome-c. The molar ratio of cytochrome-c to BPA was 2:1 and it was apparent from the color of the heavy peak that most of the cytochrome-c moves with bovine serum albumin. It might be assumed on the basis of the sedimentation experiments that there were only two components: pure cytochrome-c and a 1:2 compound of bovine serum albumin and cytochrome-c. If it then be assumed that the relaxation time for the formation equilibrium of the compound is long with respect to  $10^{-7}$  sec., the characteristic time of the experiment, the Cole-Cole plot would be expected to consist of two displaced semicircles. This behavior was not observed. The value of  $\alpha$  observed is not remarkable but the very large apparent dielectric increment is.

There would appear to be three possible explanations for this peculiar behavior. In the first, we can suppose that the relaxation time for compound association-dissociation is the same order as  $10^{-7}$  sec. Then at low frequencies the dielectric experiment "sees" only a weighted average of all forms. At high frequencies it "sees" the separate compounds so that high and low frequency results cannot be expected to be compatible. In this case neither dielectric increment nor critical frequency has much immediate significance.

In the second case, it may be assumed that compound equilibrium is either slow or fast relative to  $10^{-7}$  sec., but that there is a wide variety of compounds con-

sisting of different proportions of cytochrome-c to BPA and including some forms making very high contributions to the measured dielectric increment. An appropriate distribution of these compounds could explain the Cole-Cole plot. If this case is correct, it would seem possible to use dielectric dispersion studies to detect heterogeneity not indicated in sedimentation experiments as is the case here.

The third possibility is more serious. It is possible that the dielectric properties of a heterogeneous protein solution are not additive functions of the contributions from the several species. This situation would make useful analysis very difficult. Much more extensive dielectric dispersion studies of mixed protein systems are necessary and this form of study should provide not only a test of the last alternative but also much unique information about the kinetics and thermodynamics of aggregation reactions.

## Discussion

*Value of the Method.* Although the results of this work are generally favorable to the method of dielectric dispersion for protein study, they also indicate possible complexities which must be understood before the full power of the method becomes available for general protein study. The effect of  $\beta$ -alanine on CGN demonstrates the need for caution in choosing "inert" small zwitterions for this work. At the same time it shows that the method can be used to study reactions of this type and particularly to characterize altered forms. In fact, the method is potentially the best way to detect the presence of unfolding in such reactions and has real advantages over viscosity.

The experiments with the heterogeneous mixture of BPA and cytochrome-c indicate that the method is not yet applicable to at least some heterogeneous systems. Similarly, the peculiar behavior of cytochrome-c as protein concentration is lowered must be further investigated. Studies with hemoglobin by Takashima and Lumry<sup>7</sup> showed no such effect down to about 0.2% protein to suggest that the phenomenon is not general, and Scheider<sup>15</sup> has concluded that similar behavior of BPA on lowering concentration is probably an artifact.

Aside from these reservations, our experiments provide considerable confidence in the method when used with caution. Of equal importance, they lead to two significant conclusions. The first of these is that small zwitterions can be used effectively in some protein solutions to correct for electrode polarizations, to eliminate electroviscous effects, and finally to eliminate complications due to polarization processes of the counterion atmosphere. The second conclusion is that dielectric parameters obtained in the absence of

zwitterions and at low salt are generally free of ion atmosphere and electroviscous effects. This is apparent from the similarity of results obtained with and without zwitterions. Electroviscous effects are expected to be a minimum at the isoelectric point but even in experiments carried out at pH values some distance from the isoelectric point, there is little evidence in this work for the occurrence of new dispersion processes in zwitterion-free solutions. This simple situation may not always exist, however, since Shutt<sup>35</sup> observed a strong pH dependence of dispersion behavior in ovalbumin solutions which suggests the appearance of some relaxation mechanism other than dipole rotation at conditions of large net charge. On the other hand, Takashima<sup>36</sup> could not confirm these findings.

It may also be noted that even though heterogeneity as measured by  $\alpha$  was not large for most of our protein solutions, the presence of zwitterions reduced  $\alpha$  to zero and considerably improved precision. No reason for this behavior can be given. If a protein molecule has high asymmetry, multiple relaxation processes should in general be detectable. Our proteins with the exception of BPA may be too symmetrical to make multiple relaxation detectable. On the other hand, some of the multiple dispersion previously reported may be incorrect or due in part to small ion-atmosphere effects eliminated by the use of zwitterions.

Although new studies using zwitterions of proteins previously investigated are necessary to support any general conclusion, our results indicate that the dielectric relaxation processes of proteins thus far studied are primarily those of protein orientation.

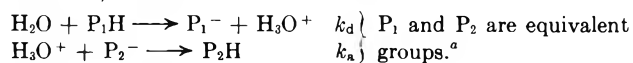
It is interesting to note that insofar as dielectric dispersion is concerned, within our experimental errors met-Mb and COMb are identical. Similarly, insofar as the dependence on protein concentrations allows comparisons, oxidized and reduced cytochrome-c are very similar. Hence any conformational differences between iron(II) and iron(III) forms of these proteins have only a small effect on the charge distribution or shape.

*The Kirkwood-Shumaker Effect.* This effect can only be due to proton migration by two mechanisms.

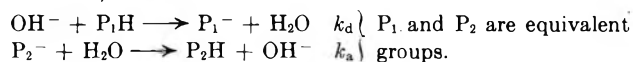
(1) *The Indirect-Transfer Process.* The indirect process shown in Table VI occurs when a proton leaves an acid group and migrates to a basic group on the same or a different protein molecule. At low hydrogen ion concentrations and low protein concentrations the protein has a better chance of being picked up by the molecule from which it was released. The effective time constant is as usual the reciprocal of the sum of the true first-order rate constant for dissociation plus

Table VI

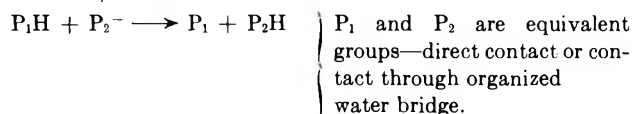
Two-center, indirect acid



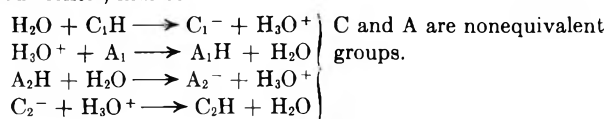
Two-center, indirect base



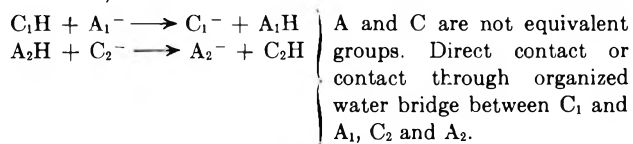
Two-center, direct



Four-center, indirect acid



Four-center, direct



<sup>a</sup> P<sub>1</sub> and P<sub>2</sub>, for example, do not need to be on the same molecule. At low ionic strength or low zwitterion concentration there is a correlation among charges on a given protein molecule. These fluctuations are an important aspect of the Kirkwood-Shumaker theory but their times in low electric field are very similar to the values for the group-pair processes. The fluctuations can occur no faster than the appropriate transfer processes and the charge-charge correlation has only the effect of slightly modifying the rates of these processes.

the pseudo-first-order constant for association and is thus usually the reciprocal of the larger of these two. The magnitude of the effect depends on the product of the number of the proton-donating and proton-accepting sites on a single protein molecule, and thus this magnitude is significant only near the pH equal to the effective pK<sub>a</sub> or pK<sub>b</sub> of the group involved depending on whether the mechanism is protolysis or hydrolysis. Thus if there is a large number, say 100, of a particular kind of group with essentially the same effective pK, at one pH unit from pK each protein molecule has about 10 sites of one kind and 90 of the other. A 10% perturbation of the charge distribution away from the purely random distribution and due to the applied electric field could thus produce a mean-

(35) W. J. Shutt, *Trans. Faraday Soc.*, **30**, 893 (1934).

(36) S. Takashima, Abstracts, 148th National Meeting of the American Chemical Society, Chicago, Ill., Aug. 31, 1964, p. 31C.

square dipole moment of from  $10^2 d^2$  to  $5 \times 10^3 d^2$  depending on the dimension of the protein. This is generally considerably less than is observed experimentally. The smaller the protein the smaller the contribution from this source. Since a 10% perturbation is much larger than can occur in this kind of experiment, these contributions are certainly an upper limit of the effect. At 2 pH units from the  $pK$  of the group the effect would be negligible. However, if the characteristic time of the proton migration is of the same order as the rotational relaxation time and the experiments are carried out very near the  $pK$  of the responsible group, multiple or complex dispersion with a contribution from the Kirkwood-Shumaker effect may be detected. This matter has also been discussed by Scheider.<sup>15</sup>

If the Kirkwood-Shumaker relaxation time is very short relative to the rotational relaxation time, the proton migration will always be in phase with the applied field in the frequency range of rotational relaxation and the dielectric increment will contain the contributions from both processes. The relaxation time in this frequency range will, however, be that for rotational relaxation. If  $\epsilon_\infty$  can be chosen experimentally in a frequency range below that of the dispersion of the Kirkwood-Shumaker process,  $\epsilon_0 - \epsilon_\infty$  will be independent of the latter process and the correct dielectric increment due to the dipole moment of the protein can be determined.

It is important to note that the perturbing field used in most dielectric dispersion experiments is much smaller than  $kT$  and cannot produce a net change in the number of different kinds of protein charged groups. The field can only influence normal charge fluctuations to occur in such a way as to lower the electrostatic potential energy. Thus in the presence of the applied field a proton will tend to migrate from one carboxyl group to a carboxylate group lying close to the negative electrode. Migration from ammonium to a carboxylate group can occur only if the reverse process also occurs at some other place in the protein system. Both migrations can be influenced by the field in this "four-center" process. Two-center and four-center indirect-transfer processes are shown in Table VI. It is to be noted, however, that insofar as relaxation times are concerned, all four-center indirect processes can be considered as a sum of two-center indirect processes. Four-center processes between groups with well-separated  $pK_a$  values can make only minor contributions to the induced moment since the magnitude of the contribution depends on the product of concentrations of acidic and basic forms of both kinds of groups. This product can be large only if the

$pK_a$  values are close together and close to the pH of the experiment.

(2) *The Direct-Transfer Process.* Proton migration can occur through direct contact of donating and accepting groups or through complete hydrogen-bonded water bridges between such groups. Once again the contribution to dielectric increment will be significant only at pH values such that appreciable concentrations of both donor and acceptor groups exist. Although there is no precise description of protein hydration, hydration water will be organized to favor charge hydration and in so doing may effect a slight increase in the average length of water bridges for proton migration. It is unlikely that the effect will be large and thus unlikely that two-center direct processes can occur at a sufficient distance to make an important contribution to the induced moment unless there are many of them. It is also unlikely that side chains of glutamic, aspartic, histidine, or lysine residues have the freedom of motion which would allow direct contact for proton transfer to occur over appreciable distances. This is a consequence of the hydrophobic character of their tethering chains which generally requires the hydrocarbon sections to be well surrounded by other hydrocarbon parts of the protein. In fact, these tethers probably make at least as large a contribution to hydrophobic binding as any other side chains. This situation also explains why it is unlikely that we need consider dielectric effects due to the perturbation of charge group positions by rotation along the tethering chains.

The direct-transfer processes are diagrammed in Table VI. The times of these processes can be variously estimated from the protolysis, hydrolysis, and direct-transfer processes of small molecules when the rates for the appropriate models are known. The calculated times for the protein groups may be slightly different from true values since the local proton concentration about a protein which has just released a proton will be slightly higher than the bulk average. This effect has been discussed by Scheider.<sup>15</sup> Furthermore, the times may be a bit smaller because of the solid-angle limitations on proton and water approach to protein charged groups in diffusion-controlled processes.

The times estimated in Table VII are reasonable approximations and will have to be improved with direct studies of proteins. Table VII is incomplete since a few additional model reactions remain to be studied.

A consideration of Table VII shows that for rotational relaxation times in the range of  $10^{-7}$  to  $5 \times 10^{-9}$  sec. in the pH range from 6.5 to 9, proton migration processes

Table VII

Type of mechanism	Group	Model	$\tau$ is the larger of	Ref.
Two-center proton migration times				
Indirect acid	-COO <sup>-</sup>	Acetic acid	$10^{-6}$ or $3 \times 10^{-11}[\text{H}^+]^{-1}$ sec.	<i>a</i>
Indirect acid	-NH <sub>2</sub>	Ammonia	$5 \times 10^{-2}$ or $3 \times 10^{-11}[\text{H}^+]^{-1}$ sec.	<i>a</i>
Indirect acid	Imidazole	Imidazole	$5 \times 10^{-4}$ or $5 \times 10^{-11}[\text{H}^+]^{-1}$ sec.	<i>a</i>
Indirect base	-COO <sup>-</sup>	Acetic acid	$1$ or $10^{-11}[\text{OH}^-]^{-1}$ sec.	<i>b</i>
Indirect base	-NH <sub>2</sub>	Methylamine	$5 \times 10^{-3}$ or $3 \times 10^{-11}[\text{OH}^-]^{-1}$ sec.	<i>c</i>
Indirect base	Imidazole	Imidazole	$5 \times 10^{-4}$ or $3 \times 10^{-11}[\text{OH}^-]^{-1}$ sec.	<i>a</i>
Direct	-COO <sup>-</sup> , -COOH	Acetic acid formate	$2 \times 10^{-8}$ sec.	<i>a</i>
Direct	-NH <sub>2</sub> , -NH <sub>3</sub> <sup>+</sup>	Methylamine	$10^{-9}$ sec. (direct) $10^{-8}$ sec. (through single water molecule bridge)	<i>d</i>
Four-center proton migration times				
Direct	$\left\{ \begin{array}{l} -\text{COOH} + -\text{NH}_2 \\ -\text{NH}_3^+ + -\text{COO}^- \end{array} \right.$	Acetic acid-hydrazine	$10^{-6}$ sec.	<i>a</i>
Direct	$\left\{ \begin{array}{l} -\text{COOH} + -\text{Im} \\ -\text{ImH}^+ + -\text{COO}^- \end{array} \right.$	Acetic acid-imidazole	$2 \times 10^{-7}$ sec.	<i>a</i>

<sup>a</sup> M. Eigen and L. De Maeyer in "Technique of Organic Chemistry," A. Weissberger, Ed., Vol. VIII, Part II, Interscience Publishers, Inc., New York, N. Y., 1963, p. 1031. <sup>b</sup> Z. Luz and S. Meiboom, *J. Am. Chem. Soc.*, **85**, 3923 (1963). <sup>c</sup> Calculated from data in footnote *a*. <sup>d</sup> S. Meiboom, A. Loewenstein, and S. Alexander, *J. Chem. Phys.*, **29**, 969 (1958).

are almost invariably too slow or too improbable because of the concentrations of donor and acceptor to make contributions to dielectric behavior. Only the direct reactions are sufficiently rapid to provide complications. With the information currently available, the only such process which might provide a detectable contribution would be the four-center direct exchange between imidazolium and carboxylate groups. Concentration factors make its importance unlikely even at pH 7, the  $pK_a$  of the imidazole, and it is certainly unimportant at much higher pH values.

In general, the groups with proton relaxation times in the range of small globular protein rotational relaxation times have  $pK$  values outside the central pH range and thus are of little interest unless the protein average moment is very small. Experiments with large proteins and at pH values near carboxyl and ammonium  $pK$  values may be complicated by Kirkwood-Shumaker effects. However, Takashima<sup>36</sup> has reported dielectric dispersion experiments with ovalbumin and BPA over a wide range of hydrogen ion concentrations including pH values near the  $pK_a$  values of these two important ionizing groups, and he has not found either new dispersion processes or changes in dielectric behavior which indicate any contribution for the Kirkwood-Shumaker effect.

Except under the unusual circumstances in which the Kirkwood-Shumaker effect may still present complications, it would now appear possible to carry out meaningful dielectric dispersion experiments on globular proteins at least as large as BPA. Each new pro-

tein should first be examined using a zwitterion atmosphere and probably any drastic change in solution composition such as a large change of pH should also be examined in this way. If the zwitterion-protein solution demonstrates normal dispersion, and especially if this dispersion is essentially identical with that obtained in the absence of zwitterions, the dispersion can be assumed to be due to rotational relaxation and the electrostatic interaction to be due to the root-mean-square moment of the protein itself. It is to be noted that although the apparent value of this moment must depend on the ion atmosphere, the presence of large concentrations of zwitterions has little if any effect on it. This behavior is another manifestation of the absence of long-range order in the zwitterion atmosphere.

It may also be useful in some cases to apply a viscosity test for rigid rotator behavior in dielectric dispersion. Takashima<sup>8</sup> studied the effect of solvent viscosity on the dielectric dispersion of met-Mb, ovalbumin, hemoglobin, and catalase. The first three proteins manifested behavior expected for a rigid rotator and not that expected if the viscosity dependence were due to changes in the motional times of small ions. The viscosity test is not infallible but can be useful either to supplement the zwitterion test or to replace it when the latter is inapplicable. Takashima's results with the first three proteins cannot be generalized to all globular proteins, since he found that the dispersion behavior of catalase was independent of solvent viscosity. This is a most interesting

result and suggests that further dielectric studies of catalase may lead to a more profound understanding of the method.

It is to be hoped that the combination of studies by Takashima, Scheider, and those reported here will help to restore confidence and interest in the dielectric dispersion method for protein study since the method is potentially a powerful tool for such investigations.

Much work is obviously required to make the method suitable for routine use. There is a variety of applications of the method which when developed will provide useful and often unique information about globular proteins. In addition, it may be noted that the by-product investigations in the present work present new and interesting phenomena for investigation.

## Variation of Chain Dimensions of Polystyrene with Concentration<sup>1</sup>

by J. Leonard and H. Daoust

Department of Chemistry, Université de Montréal, Montréal, Canada (Received September 28, 1964)

Osmotic pressures of polystyrene solutions have been measured at 25° for concentrations up to 17%, using dioxane and chlorobenzene as solvents. The data have been analyzed according to three different theories which deal with the concentration dependence of polymer dimensions. The variational theory developed by Fixman seems to give a more complete picture of the behavior of polymer chains in solution. The theories of Eizner and Grimley are theoretically applicable only in the dilute concentration range.

### Introduction

According to Fixman,<sup>2</sup> the apparent second virial coefficient,  $S$ , varies with concentration for polymers in good solvents; it has been shown that the same phenomenon exists also for intermediate solvents.<sup>3</sup> In the model used by Fixman, it is assumed that the intermolecular potential of average force of the system of polymer molecules in solution is a sum of pair potentials. The radial distribution function is calculated on the basis of the model of Flory and Krigbaum, through a variational solution of the Born-Green-Kirkwood equation. The concentration dependence of the excluded volume factor  $\alpha$  has been obtained by the minimization of the free energy with respect to  $\alpha$ . We here recall the most important relations needed in the application of Fixman's treatment. The empirical definition of  $S$  is given by

$$S = (\Pi/c - RT/M)(RTc)^{-1} \quad (1)$$

where  $\Pi$  is the osmotic pressure;  $c$ , the polymer con-

centration; and  $M$ , the molecular weight of the polymer. In Fixman's variational theory,<sup>2</sup>  $S$  is defined by

$$RTS = 2\pi A_0 \alpha_0^3 B'^{-1/2} M^{-2} N_0 (1 - \eta) \quad (2)$$

where  $A_0$  is the intermolecular potential parameter defined by

$$A_0 = 5.63(\alpha_0^2 - 1) \quad (3)$$

and where  $\alpha_0$  is the excluded volume expansion factor at zero concentration.  $B'$  is given by

$$B' = 9.61/R_0^2 \quad (4)$$

$R_0^2$  being the mean square end-to-end distance.  $N_0$

(1) This paper has been presented in part at the 145th National Meeting of the American Chemical Society, New York, N. Y., Sept. 8-13, 1963.

(2) M. Fixman, *J. Chem. Phys.*, **33**, 370 (1960); *Ann. N. Y. Acad. Sci.*, **89**, 657 (1961); *J. Polymer Sci.*, **47**, 91 (1960).

(3) J. Leonard and H. Daoust, *ibid.*, **57**, 53 (1962).

is the Avogadro number, and  $(1 - \eta)$ , where  $\eta = \alpha(1 + \delta)^{-3/2}$ , is concentration dependent. For  $A_0 > 1.064$ ,  $a = 1$  and  $\delta$  is the only variable which needs to be calculated at each concentration. The variation of the chain dimension with concentration is implicitly given by eq. 2.

Another interesting theory on the relationship between concentration and dimensions of macromolecules in solution has been derived by Eizner.<sup>4</sup> According to this theory, the variation of the excluded volume expansion factor is given by

$$\alpha = \alpha_0(1 - \kappa_1 c - \kappa_2 c^2 - \dots) \quad (5)$$

When the smoothed density model proposed by Flory and co-workers to describe the intra- and intermolecular interactions in polymer solutions is used to calculate the coefficients  $\kappa_1$  and  $\kappa_2$  in eq. 5, the following relations

$$\kappa_1 = A_2 M L_1(\alpha_0) \quad (6)$$

and

$$\kappa_2 = A_3 M L_2(\alpha_0) \quad (7)$$

are obtained by the minimization of the free energy of the solution with respect to  $\alpha$ .  $A_2$  is the second virial coefficient, and  $A_3$  is the third virial coefficient as calculated according to Stockmeyer and Casassa.<sup>5</sup> The quantities  $L_1(\alpha_0)$  and  $L_2(\alpha_0)$  are easily calculated when  $\alpha_0$  is known.

Finally, Grimley<sup>6</sup> has derived the relation

$$\langle s^2 \rangle = \langle s^2 \rangle_0 (1 + Kc) \quad (8)$$

for the variation of the mean square radius of gyration of flexible polymer molecules with concentration in the dilute range.  $\langle s^2 \rangle_0$  is the mean square radius of gyration at infinite dilution, and  $K$  is defined by

$$K = (2/3\pi)^{1/2} M^2 (\partial A / \partial M) \quad (9)$$

In the light of the previously mentioned theories, we have studied the variation of the chain dimensions of polystyrene using chlorobenzene and dioxane as solvents.

## Experimental

**Materials.** The polystyrene fraction used in this investigation was obtained by fractionating a commercial sample of Lustrex HF-77, supplied by Monsanto of Canada. The fractionation was carried out at 25° using the butanone-methanol pair, the initial polymer concentration being 3.3% *P/V*. Linearity of the polystyrene fraction was checked by the viscometric method developed by Manson and Cragg.<sup>7</sup> Reagent grade solvents were distilled before use.

**Osmotic Pressures.** A specially designed osmometer<sup>8,8</sup> was used for measurements of osmotic pressures of solutions having a concentration above 3% *P/V*. For lower concentrations, block osmometers<sup>9</sup> were used. All measurements were done at 25°.

**Viscosity Measurements.** They have been carried out with a modified Ubbelohde capillary viscometer<sup>10</sup> at 25°.

## Results and Discussion

Table I gives the experimental data on polystyrene-chlorobenzene and on polystyrene-dioxane systems at

**Table I:** Osmotic Pressures of the Polystyrene Solutions at 25°

In chlorobenzene			In dioxane		
$c \times 10^2$ , g./cc.	$\Pi/c$ , cm.	$RTS$ $\times 10^{-4}$	$c \times 10^2$ , g./cc.	$\Pi/c$ , cm.	$RTS$ $\times 10^{-4}$
0.00	2.57		0.00	2.60	
0.282	2.90	1.15	0.502	3.08	0.96
0.468	3.20	1.34	0.691	3.13	0.77
0.498	3.44	1.74	0.983	3.42	0.83
0.616	3.49	1.48	1.007	3.33	0.72
0.953	4.05	1.55	1.416	3.89	0.91
1.638	5.28	1.65	1.976	4.24	0.83
2.770	7.75	1.87	3.094	7.29	1.52
2.883	7.64	1.76	3.853	8.68	1.58
4.059	10.00	1.83	5.301	11.64	1.71
5.185	12.04	1.83	7.603	16.93	1.88
5.759	13.11	1.83	8.126	18.20	1.92
7.472	18.05	2.07	8.590	19.37	1.95
8.659	22.55	2.31	9.916	22.80	2.04
9.761	26.31	2.43	13.356	30.86	2.12
10.866	29.72	2.50	14.273	32.96	2.13
12.821	36.39	2.64	15.351	36.04	2.18
14.340	41.76	2.73	15.920	38.10	2.23
			17.066	43.39	2.39

25°. The number-average molecular weight of the fraction used was 98,400 as determined by the value of  $(\Pi/c)_0$  extrapolated from data in chlorobenzene and 97,300 in dioxane. The value of the mean square end-to-end distance at  $\theta$ -temperature was determined using the structural parameter  $(R_0^2/M)^{1/2} = 0.70 \times 10^{-8}$  (in c.g.s. units) as evaluated by Krigbaum and Car-

(4) Yu. E. Eizner, *Visokomol. Soedin.*, **3**, 748 (1961).

(5) W. H. Stockmeyer and C. E. Casassa, *J. Chem. Phys.*, **20**, 1560 (1952).

(6) T. B. Grimley, *Trans. Faraday Soc.*, **57**, 1974 (1961).

(7) J. A. Manson and L. H. Cragg, *Can. J. Chem.*, **30**, 482 (1952).

(8) P. J. Flory and H. Daoust, *J. Polymer Sci.*, **25**, 429 (1957).

(9) W. R. Krigbaum and P. J. Flory, *J. Am. Chem. Soc.*, **75**, 1775 (1953).

(10) D. A. Henderson and N. R. Legge, *J. Polymer Sci.*, **19**, 215 (1956).

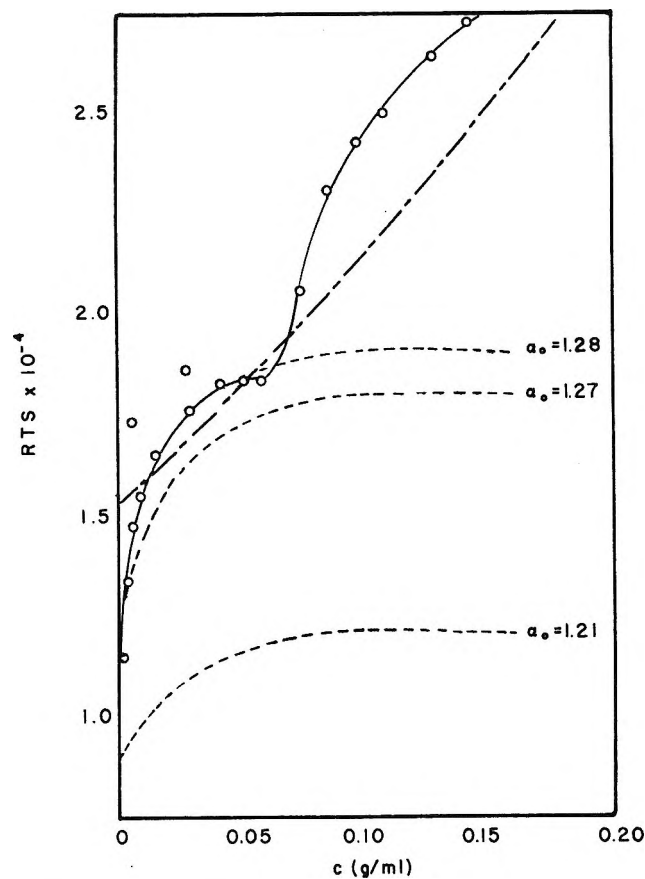


Figure 1. Apparent second virial coefficient against concentration (in g./ml.): —, for polystyrene in chlorobenzene. - - -, F-H curve; - · - ·, Fixman's curves for different values of  $\alpha_0$ .

penter.<sup>11</sup> The variation of the second virial coefficient with concentration for polystyrene in chlorobenzene is shown in Figure 1. The theoretical curve was calculated using eq. 2 with  $\alpha_0 = 1.28$ ,  $A_0 = 3.6$ , and  $R_0 = 220 \times 10^{-8}$  cm. The value of  $\alpha_0$  has been selected to give the best correlation between theory and experimental values. Good agreement is so obtained up to 6% in polymer. If the exponent 2.43 is used in the estimation of  $\alpha_0$  from viscosity measurements ( $\alpha_0^{2.43} = [\eta]/[\eta_0]$ ) as suggested by the Kurata and Yamakawa treatment of viscometric data,<sup>12</sup> a value of 1.27 is obtained for  $\alpha_0$ , in very good agreement with that selected. The value of  $[\eta_0]$  for the fraction of polystyrene used in this investigation has been estimated from the relation  $[\eta_0] = K_{25}M^{1/2}$  with  $K_{25} = 8.2 \times 10^{-4}$  as reported.<sup>13</sup> Now, it is interesting to compare the average curve obtained from the Flory-Huggins (F-H) theory on concentrated polymer solutions, assuming a constant value for the free energy interaction parameter,  $\chi$ . From the definition of  $S$  and by putting<sup>8</sup>  $y = \chi_1\varphi^2 + \chi_2\varphi^3$ , where  $y = -H_1V_1/RT - \ln(1 - \varphi) - \varphi + \varphi/x$ ,

$\varphi$  being the volume fraction of the polymer,  $V_1$ , the molar volume of solvent, and  $x$ , the ratio of molar volumes of polymer and solvent, it can be shown that the average F-H curve can be represented by

$$RTS = RT[(\bar{v}_2^2/V_1)^{1/2} - \chi] + (\bar{v}_2^3/3V_1)c + (\bar{v}_2^4/4V_1)c^2 \quad (10)$$

With  $y/\varphi^2 = 0.42$  (average value =  $\chi$ ),  $V_1 = 102.2$  ml., and the partial specific volume of polystyrene<sup>14</sup>  $\bar{V}_2 = 0.891$  ml. g.<sup>-1</sup>, eq. 10 becomes  $RTS \times 10^{-4} = 1.53 + 5.83c + 3.90c^2$ . It is obvious from Figure 1 that Fixman's treatment gives a better correlation with experimental results in the low concentration range than the F-H treatment.

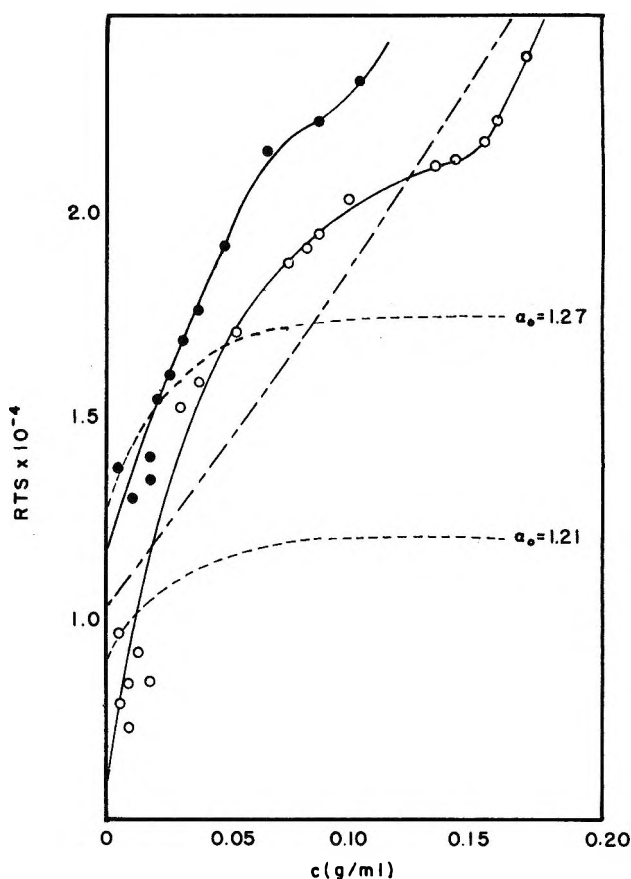


Figure 2. Apparent second virial coefficient against concentration (in g./ml.): ●, for polystyrene in toluene<sup>15</sup>; ○, for polystyrene in dioxane; —, F-H curve for dioxane solutions; - - -, Fixman's curves for dioxane solutions.

(11) W. R. Krigbaum and D. K. Carpenter, *J. Phys. Chem.*, **59**, 1166 (1955).

(12) M. Kurata and H. Yamakawa, *J. Chem. Phys.*, **32**, 1852 (1960).

(13) P. J. Flory, "Principles of Polymer Chemistry," Cornell University Press, New York, N. Y., Chapter XIV.

(14) G. Goyer, Ph.D. Thesis, Université de Montréal, 1951.



The correlation is not so good in dioxane (see Figure 2). The viscometric value of  $\alpha_0$  is 1.21 (with the exponent 2.43), and the average Fixman's theoretical curve has been traced using  $\alpha_0 = 1.27$ ,  $A_0 = 3.4$ , and  $R_0 = 218 \times 10^{-8}$  cm. This discrepancy is not due to experimental errors since the same type of results are obtained when the data of Shick, Doty, and Zimm<sup>15</sup> are plotted according to eq. 1 as shown in Figure 1. Using the values  $\chi = 0.46$ ,  $V_1 = 85.7$  ml., and  $\bar{v}_2 = 0.933$  ml. g.<sup>-1</sup> in eq. 10, the F-H curve for this system can be represented by  $RTS \times 10^{-4} = 1.02 + 7.98c + 5.58c^2$ .

Figure 3 shows the variation of  $\alpha$  with concentration as predicted by the different theories mentioned previously. In Fixman's treatment,  $\alpha_0$  is the only empirical parameter needed;  $A_0$  is then calculated by eq. 3, and the value of  $\alpha$  at any concentration, for that value of  $A_0$ , is interpolated using Fixman's tables.<sup>2</sup> The calculation of the curves from eq. 5 has been done with determined values of  $A_2$  from the osmotic pressures in the dilute range and  $A_3$  estimated from the relation<sup>5</sup>  $A_3 = A_2^2 M g (J \alpha_0^{-3})$  where  $(J \alpha_0^{-3})$  is a function of  $\alpha_0$  only.

It has been impossible to estimate the parameter  $K$  from eq. 8 for the polystyrene-chlorobenzene system since no data on the variation of  $A_2$  with  $M$  are available in the literature. However, in the case of the polystyrene-dioxane system, the value of  $K$  has been calculated using the results of Cragg, *et al.*,<sup>17</sup> and our value for  $A_2$  at 25°. Table II gives the different parameters needed in the calculation of the variation of  $\alpha$  with concentration according to the different

Table II: Thermodynamic Parameters at 25°

Solvent	$\alpha_0$	$A_2 \times 10^4$	$A_3 \times 10^4$	$\kappa_1$	$\kappa_2$	$K$
Chlorobenzene	1.28	5.41	62.2	1.97	-12.2	...
Dioxane	1.21	3.08	16.2	1.05	-7.9	-0.56

theories. It is recalled that, in the first derivation of his variational theory, Fixman kept  $\alpha$  independent of concentration. Then, by making  $\alpha$  concentration dependent, Fixman has shown that correlations between theory and experiments were slightly improved.

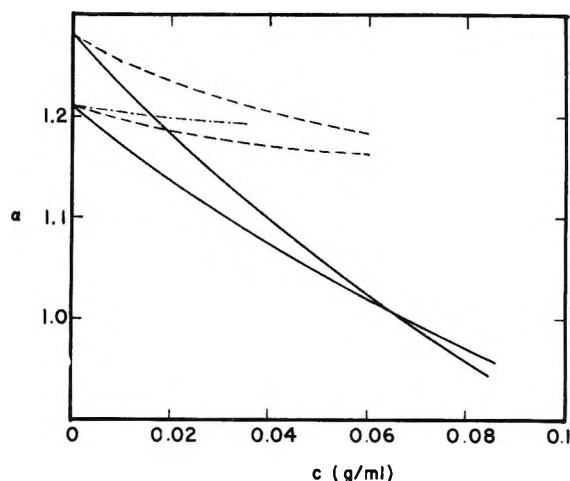


Figure 3. Variation of  $\alpha$  with concentration: upper curves, chlorobenzene; lower curves, dioxane. —, Fixman's theory; - - -, Eizner's theory; - · -, Grimley's theory.

Both Eizner's and Grimley's theories give a slow decrease in  $\alpha$  with increasing concentration whereas Fixman's treatment gives a rather fast decrease. However, according to this treatment, the polymer dimensions in a given solvent might decrease below those measured in a  $\theta$ -solvent. In a recent review of the theoretical studies of concentrated polymer solutions, Fixman<sup>18</sup> has shown that  $\alpha$  decreases first rapidly and then gradually as concentration increases, but  $\alpha$  never becomes smaller than unity. This last prediction has been experimentally proven by Picot and Benoit,<sup>19</sup> who studied the scattering of light by moderately concentrated solutions of high molecular weight fractions of polymers.

*Acknowledgments.* The authors are pleased to acknowledge the financial assistance of the National Research Council of Canada. J. L. wishes to thank the Department of Education of the Province of Quebec for the award of a bursary while doing this research.

(15) M. Shick, P. Doty, and B. Zimm, *J. Am. Chem. Soc.*, **72**, 530 (1950).

(16) D. J. Streeter and R. F. Boyer, *Ind. Eng. Chem.*, **43**, 1790 (1951).

(17) L. H. Cragg, E. T. Dumitru, and J. E. Simkins, *J. Am. Chem. Soc.*, **74**, 1977 (1952).

(18) M. Fixman, *ibid.*, **86**, 3524 (1964).

(19) C. Picot and H. Benoit, private communication.

## Ion-Exchange Kinetics. V. Ion Exchange Accompanied by Reactions

by F. Helfferich

Shell Development Company, Emeryville, California (Received September 29, 1964)

A theoretical analysis of various ion-exchange processes involving ionic reactions such as neutralization and complex formation is presented. The derived rate laws differ appreciably from those for ordinary ion exchange in the absence of reactions. Co-ion diffusion can affect the rate or even be the sole rate-controlling step. Although still much in need of verification by systematic experimental studies, the proposed rate laws are in agreement with earlier experimental observations by other authors.

### Introduction

It has long been known that ion-exchange rates are controlled by diffusion.<sup>1,2</sup> Quantitative theories based on diffusion equations<sup>1-4</sup> are now well confirmed for simple systems.<sup>1,2,5-13</sup> All previous theories, however, are based on the premise that the exchanging ions retain their identity, that is, are not consumed by accompanying chemical reactions. Obviously, this underlying assumption is not admissible if the ions, in the course of ion exchange, undergo neutralization, association, or complex-formation reactions. The purpose of this communication is to investigate, from a theoretical viewpoint, the effects of accompanying reactions on the kinetics of ion exchange.

### Types of Reactions

Eleven characteristic examples of ion-exchange processes involving reactions of the ions are compiled in Table I. Chemically, the reactions would best be classified as neutralizations, hydrolyses, and complex formations. For a quantitative treatment, however, it is more convenient to classify the processes by types as follows. In processes of type I, the counterions released by the ion exchanger are consumed by reactions with the co-ions from the solution (reactions 1 to 4 in Table I). In those of type II, the counterions originating from the solution are consumed by reactions with the fixed ionic groups of the ion exchanger (reactions 5 to 7). In those of type III, undissociated fixed ionogenic groups of the ion exchanger are ionized by reactions with the co-ions from the solution (reactions 8 to 10). In those of type IV, fixed ionogenic groups are converted from one undis-

sociated form to another by reactions with the counterions from the solution (reaction 11).

### Theory

The theoretical treatment will be based on the following simplifying assumptions commonly used in theories of ion-exchange kinetics. It is assumed that the systems are isothermal, that the ion-exchanger particles are spherical, uniform, and of equal size, and that the individual diffusion coefficients of the ions are constant. Furthermore, swelling changes of the ion exchanger, activity-coefficient gradients, and coupling effects other than by electric fields are neglected. Also, the treatment remains restricted to systems in which the rates of the chemical reactions are fast enough not to limit the exchange rates. Of course, equations based on these assumptions can only represent ideal limiting rate laws.

(1) G. E. Boyd, A. W. Adamson, and L. S. Myers, Jr., *J. Am. Chem. Soc.*, **69**, 2836 (1947).

(2) F. Helfferich, "Ion Exchange," McGraw-Hill Book Co., Inc., New York, N. Y., 1962, Chapter 6 (also gives references to earlier work).

(3) R. Schlögl and F. Helfferich, *J. Chem. Phys.*, **26**, 5 (1957).

(4) F. Helfferich and M. S. Plesset, *ibid.*, **28**, 418 (1958).

(5) F. Helfferich, *J. Phys. Chem.*, **66**, 39 (1962); **67**, 1157 (1963).

(6) J. C. W. Kuo and M. M. David, *A.I.Ch.E. J.*, **9**, 365 (1963).

(7) B. Hering and H. Bliss, *ibid.*, **9**, 495 (1963).

(8) C. Heitner-Wirguin and G. Markovits, *J. Phys. Chem.*, **67**, 2263 (1963).

(9) M. Gopala Rao and M. M. David, *A.I.Ch.E. J.*, **10**, 213 (1964).

(10) A. Schwarz, J. A. Marinsky, and K. S. Spiegler, *J. Phys. Chem.*, **68**, 918 (1964).

(11) R. H. Doremus, *ibid.*, **68**, 2212 (1964).

(12) A. Varon and W. Rieman, III, *ibid.*, **68**, 2716 (1964).

(13) T. G. Smith and J. S. Dranoff, *Ind. Eng. Chem. Fundamentals*, **3**, 195 (1964).

**Table I:** Typical Ion-Exchange Processes Involving Reactions<sup>a</sup>

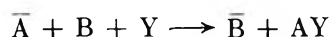
Type of process	Reaction	Reactants		Products	
		Resin	Solution	Resin	Solution
I	1	$-\text{SO}_3^- + \text{H}^+$	$+ \text{Na}^+ + \text{OH}^-$	$\rightarrow -\text{SO}_3^- + \text{Na}^+$	$+ \text{H}_2\text{O}$
	2	$-\text{N}(\text{CH}_3)_3^+ + \text{OH}^-$	$+ \text{H}^+ + \text{Cl}^-$	$\rightarrow -\text{N}(\text{CH}_3)_3^+ + \text{Cl}^-$	$+ \text{H}_2\text{O}$
	3	$-\text{SO}_3^- + \text{H}^+$	$+ \text{Na}^+ + \text{AcO}^-$	$\rightarrow -\text{SO}_3^- + \text{Na}^+$	$+ \text{AcOH}$
	4	$4(-\text{SO}_3^-) + 2\text{Ni}^{2+}$	$+ 4\text{Na}^+ + \text{EDTA}^{4-}$	$\rightarrow 4(-\text{SO}_3^-) + 4\text{Na}^+$	$+ \text{Ni}_2\text{EDTA}$
II	5	$-\text{COO}^- + \text{Na}^+$	$+ \text{H}^+ + \text{Cl}^-$	$\rightarrow -\text{COOH}$	$+ \text{Na}^+ + \text{Cl}^-$
	6	$-\text{NH}_3^+ + \text{Cl}^-$	$+ \text{Na}^+ + \text{OH}^-$	$\rightarrow -\text{NH}_2$	$+ \text{Na}^+ + \text{Cl}^- + \text{H}_2\text{O}$
	7	$-\text{N}(\text{CH}_2\text{COO})_2^{2-} + 2\text{Na}^+$	$+ \text{Ni}^{2+} + 2\text{Cl}^-$	$\rightarrow -\text{N}(\text{CH}_2\text{COO})_2\text{Ni}$	$+ 2\text{Na}^+ + 2\text{Cl}^-$
III	8	$-\text{COOH}$	$+ \text{Na}^+ + \text{OH}^-$	$\rightarrow -\text{COO}^- + \text{Na}^+$	$+ \text{H}_2\text{O}$
	9	$-\text{NH}_2$	$+ \text{H}^+ + \text{Cl}^-$	$\rightarrow -\text{NH}_3^+ + \text{Cl}^-$	
	10	$2[-\text{N}(\text{CH}_2\text{COO})_2\text{N}]$	$+ 4\text{Na}^+ + \text{EDTA}^{4-}$	$\rightarrow 2[-\text{N}(\text{CH}_2\text{COO})_2^{2-}] + 4\text{Na}^+$	$+ \text{Ni}_2\text{EDTA}$
IV	11	$-\text{N}(\text{CH}_2\text{COO})_2\text{Ni}$	$+ 2\text{H}^+ + 2\text{Cl}^-$	$\rightarrow -\text{N}(\text{CH}_2\text{COOH})_2$	$+ \text{Ni}^{2+} + 2\text{Cl}^-$

<sup>a</sup> From F. Helfferich in "Advances in Ion Exchange," Vol. I, J. A. Marinsky, Ed., Marcel Dekker, Inc., New York, N. Y., to be published. Reproduced with permission of Marcel Dekker, Inc.

In particular, the assumptions of isothermal behavior and absence of swelling changes are less justified here than in ordinary ion exchange, since the ionic reactions may release considerable heat and may make the ion exchanger swell or shrink appreciably. Moreover, although most reactions of ions and particularly neutralization and hydrolysis are fast, reactions of certain complexes are slow and may become rate-controlling. To systems involving such slow reactions the theoretical treatment is not applicable.

For simplicity, all rate laws will be derived for systems with the ion exchanger initially containing counterions of species A only and solutions initially containing counterions of species B only. Extensions to other initial conditions—provided the initial distribution within the ion exchanger is uniform—can in most cases be achieved without difficulties.

*Type I: Consumption of the Counterion Released by the Ion Exchanger.* Processes of type I can be written in general form



As in ordinary ion exchange, the rate can be controlled by diffusion within the particle or in an adherent Nernst "film."<sup>1,2</sup>

With *particle-diffusion control*, the reaction consuming A does not interfere with interdiffusion in the ion exchanger because the co-ion Y is efficiently excluded from the interior. The reaction does affect, however, the boundary condition at the particle surface. Here, A is eliminated as soon as it is released by the ion exchanger, at least as long as the solution still contains Y. The boundary condition thus is

$$t \geq 0, r = r_0, \bar{C}_A(r_0, t) = 0 \quad (1)$$

even for exchanges with solutions of limited volume, in which the concentration of A at the interface would otherwise build up. The numerical solutions tabulated for ordinary ion exchange with the simple constant boundary condition (1)<sup>2,7,14a,b</sup> thus apply even if the solution volume is not large compared to the amount of ion exchanger. Provided that  $CV > \bar{CV}$ , i.e., that the amount of B in the solution is sufficient to convert the ion exchanger completely to the B form, fractional attainment  $F$  of equilibrium for *any* solution volume is therefore given by

$$F(t) = G(t) \quad (CV > \bar{CV}) \quad (2)$$

where  $G(t)$  is the tabulated fractional attainment of equilibrium for the corresponding ordinary ion exchange with *infinite* solution volume.

If, in a solution of limited volume, the amount of B (and Y) is smaller than the amount of A in the ion exchanger ( $CV < \bar{CV}$ ), then, of course, the ion exchanger cannot be completely converted to the B form. Conversion then proceeds with a finite rate until all B and Y is used up, and equilibrium is attained in a finite time  $t_c$ . Since the boundary condition (1) remains valid to the end, the function  $G(t)$  still describes fractional conversion of the ion exchanger, but equilibrium is attained when

$$t = t_c, G(t) = \frac{CV}{\bar{CV}} \quad (CV < \bar{CV}) \quad (3)$$

Accordingly, one has for fractional attainment of equilibrium

(14) (a) M. S. Plesset, F. Helfferich, and J. N. Franklin, *J. Chem. Phys.*, **29**, 1064 (1958); (b) F. Helfferich, *ibid.*, **38**, 1688 (1963).

$$0 \leq t \leq t_c, F(t) = \frac{\overline{CV}}{CV} G(t) \\ (CV < \overline{CV}) \quad (4) \\ t \geq t_c, F(t) = 1$$

The time  $t_c$  for complete exhaustion of the solution is readily found as the value of  $t$  for which the tabulated function  $G(t)$  reaches the value stated in eq. 3.

With *film-diffusion control*, the reaction consuming A interferes deeply with the mechanism of ion exchange, as may be illustrated with the neutralization reaction 1 in Table I. Electroneutrality in the film requires that

$$C_H + C_{Na} = C_{OH} \quad (5)$$

so that

$$C_H \leq C_{OH} \quad (6)$$

However,  $C_H$  and  $C_{OH}$  are also linked by the dissociation equilibrium

$$C_H C_{OH} = K_{H_2O} \cong 10^{-14} \text{ mole}^2/\text{l.}^2 \quad (7)$$

It follows from the conditions (6) and (7) that, in the film

$$C_H \leq 10^{-7} M \quad (8)$$

Accordingly, as long as the bulk-solution concentration of NaOH is well above  $10^{-7} M$ ,  $H^+$  cannot make headway into the film but is consumed right at the particle surface. The physical process occurring thus is diffusion of  $Na^+$  and  $OH^-$  across the film to the particle surface, where  $Na^+$  continues into the ion exchanger while  $OH^-$  reacts with  $H^+$  from the ion exchanger to form  $H_2O$ . In general terms, the rate-controlling step is film diffusion of the *counterion and co-ion from the solution*, rather than interdiffusion of the two counterions as in ordinary ion exchange.<sup>3</sup>

Since, throughout the film,  $C_H$  is negligible compared to  $C_{Na}$  and  $C_{OH}$ , film diffusion obeys the well-known equation for diffusion of a binary electrolyte

$$J_{Na} = J_{OH} = -D \text{ grad } C_{Na} \quad (9)$$

where  $D$  is the "Nernst" diffusion coefficient

$$D = \frac{2D_{Na}D_{OH}}{D_{Na} + D_{OH}} = \text{constant}^{15} \quad (10)$$

The boundary condition at the particle surface is also particularly simple. Since the ratio  $C_{Na}/C_H$  at the particle surface will not greatly exceed the ratio  $\overline{C}_{Na}/\overline{C}_H$  in the ion exchanger (unless the latter has an unusually high preference for  $H^+$ ), eq. 5 and 7 limit  $C_{Na}$  and  $C_{OH}$  at the particle surface to below about  $10^{-6} M$  until conversion is almost complete. For all practical

purposes, the latter concentrations thus are negligible compared to the bulk-solution concentrations. With the usual assumptions of quasi-stationary film diffusion and negligible film curvature<sup>1,2</sup> one then obtains the following rate laws by integration of eq. 9: for constant solution concentration ( $CV \gg \overline{CV}$ )

$$0 \leq t < t_c, F(t) = \frac{3DCt}{r_0\delta\overline{C}} \quad (11)$$

$$t \geq t_c, F(t) = 1$$

$$t_c = \frac{r_0\delta\overline{C}}{3DC}$$

for  $CV > \overline{CV}$

$$0 \leq t < t_c, F(t) = \frac{CV}{\overline{CV}} \left[ 1 - \exp\left(-\frac{3D\overline{V}t}{r_0\delta V}\right) \right] \\ t \geq t_c, F(t) = 1 \quad (12)$$

$$t_c = \frac{r_0\delta V}{3D\overline{V}} \ln \frac{CV}{CV - \overline{CV}}$$

and for  $CV < \overline{CV}$

$$F(t) = 1 - \exp\left(-\frac{3D\overline{V}t}{r_0\delta V}\right) \quad (13)$$

(Derivations are given in the Appendix.) Again, equilibrium can be attained in a finite time,  $t_c$ . With film-diffusion control, however, this happens if  $CV > \overline{CV}$ , whereas with particle-diffusion control it happens if  $CV < \overline{CV}$  (see eq. 4). The limiting law (11) is furthermore remarkable in that fractional attainment of equilibrium is a *linear* function of time.

The rate laws (11), (12), and (13) also hold for other processes of type I; one merely has to use for  $D$ , instead of eq. 10, the general expression

$$D = \frac{D_B D_Y (z_B - z_Y)}{z_B D_B - z_Y D_Y} \quad (14)$$

For processes such as reactions 3 and 4 (Table I), in which the association product AY is *not* the solvent itself, the validity range of eq. 11 to 13 calls for a comment. The derivation is based on the premise that the concentrations of A, B, and Y at the particle surface are negligible compared to the bulk-solution concentrations of B and Y and remain so up to almost complete attainment of equilibrium. The concentra-

(15) This coefficient is constant with the stated premise that the individual  $D_i$  of the ions are constant. Actually, of course,  $D$  shows a slight concentration dependence which, however, is minor compared to the large variations of  $D$  in ordinary ion exchange (even with constant  $D_i$ ) as well as compared to the large effects resulting from the theory.

tions at the particle surface depend, of course, on the concentration of AY, which has to diffuse away from the surface. Since a material balance for Y requires that  $J_Y = -J_{AY}$  and since  $D$  and  $D_{AY}$  will not differ by orders of magnitude, the concentration of AY at the surface should be of the same order as the bulk-solution concentrations of B and Y. With this in mind and with the dissociation constant of AY one can readily estimate the minimum solution concentration required for validity of eq. 11 to 13. For reaction 3, the limit is somewhat above 0.1  $M$ , and for reaction 4 of the order of  $10^{-6} M$ . At lower concentration, the process will, of course, still be controlled by film diffusion, but deviations from the rate laws (11) to (13) should become noticeable.

A criterion whether a process of type I is controlled by film or particle diffusion is readily derived. As the half-times for film-diffusion and particle-diffusion control (with  $CV \gg \bar{C}\bar{V}$ ) are<sup>2</sup>

$$t_{1/2} = \frac{r_0 \delta \bar{C}}{6DC}; \quad t_{1/2} \cong 0.03 \frac{r_0^2}{\bar{D}} \quad (15)$$

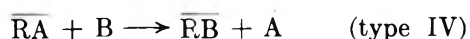
respectively, it follows that

$$\frac{6\bar{D}\bar{C}\delta}{DCr_0} \gg 1 \text{ (film-diffusion control)} \quad (16)$$

$$\frac{6\bar{D}\bar{C}\delta}{DCr_0} \ll 1 \text{ (particle-diffusion control)}$$

Here,  $\bar{D}$  is the average interdiffusion coefficient in the particle and  $D$  is given by eq. 14. This criterion is not very different from that for ordinary ion exchange and is derived in the same manner.<sup>2</sup>

*Types II and IV: Consumption of the Counterion Originating from the Solution.* Processes of the types II and IV can be written in general form



Reaction 5 from Table I may serve to illustrate the kinetic behavior to be expected in such systems.

When the weak-acid ion exchanger in the  $\text{Na}^+$  form comes in contact with the acid,  $-\text{COO}^-$  groups at the particle surface will rapidly trap  $\text{H}^+$  ions and be converted to undissociated  $-\text{COOH}$  groups. Further conversion of the resin requires diffusion of  $\text{H}^+$  across the outer, already converted shell to the  $\text{Na}^+$ -form core, and of  $\text{Na}^+$  from the core across the shell into the solution. As all  $\text{H}^+$  ions arriving at the inner boundary of the shell are at once trapped by  $-\text{COO}^-$  groups, the boundary between core and shell will remain sharp while retreating, with progressing con-

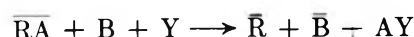
version, to the particle center. In the absence of  $\text{Cl}^-$  co-ions, interdiffusion of  $\text{Na}^+$  and  $\text{H}^+$  across the shell would be extremely slow because electroneutrality would permit the presence of only as few mobile cations as there are anionic  $-\text{COO}^-$  groups. However, the scarcity of such groups in the shell results in almost complete elimination of Donnan exclusion of mobile co-ions. Accordingly,  $\text{H}^+$  and  $\text{Cl}^-$  from the solution can invade the shell and thereby greatly boost the interdiffusion rate. Nevertheless, the concentration of  $\text{Cl}^-$  in the shell will hardly be higher than in the external solution, and one readily sees that shell diffusion then is much slower than film diffusion for all but extremely small particles. Film-diffusion control can therefore be ruled out for all practical purposes.

One remarkable feature is that the exchange rate, although controlled by particle diffusion of counterions, depends on the solution concentration. As the latter is increased, invasion increases and so does the exchange rate. The rate of particle-diffusion controlled ordinary ion exchange, in contrast, is independent of the solution concentration.<sup>1,2,4</sup>

Other reactions of type II should follow the same pattern. This is also true for reactions of type IV, because the arguments advanced for reactions of type II remain valid even if the fixed groups in the particle core are largely undissociated, provided that the groups have higher affinity for B than for A. (In the opposite case, with higher affinity of the groups for A, a sharp boundary between shell and core should not exist, but this case is of little practical interest because a very large excess of B would be required to achieve significant conversion of the ion exchanger to the B form.)

Quantitative rate laws for processes of types II and IV have not as yet been obtained. The chief obstacle is that the rate-controlling shell diffusion is a three-ion problem; as in film-diffusion controlled ordinary ion exchange,<sup>3</sup> the presence of the co-ion in concentrations comparable to those of the counterions makes reduction of the problem to one single explicit flux equation impossible.

*Type III: Ionization of Undissociated Fixed Ionogenic Groups by Reaction with the Co-ion.* The process, written in general terms, is



Neutralization of the free-acid form of a weak-acid resin by  $\text{NaOH}$  (reaction 8, Table I) will be used as an example.

In principle, conversion of the resin can occur by two different particle-diffusion mechanisms. The first is interdiffusion of  $\text{H}^+$  and  $\text{Na}^+$  in the absence of mobile co-ions and differs from ordinary particle-diffusion

controlled exchange merely in that the fixed carboxylic groups trap and thus localize most of the  $H^+$ , thus slowing the process greatly. The second mechanism is invasion of a  $Na^+$ -form outer shell by  $Na^+$  and  $OH^-$  from the solution; when having crossed the shell,  $OH^-$  abstracts a proton from a  $-COOH$  group and forms water while  $Na^+$  takes over the task of balancing the negative charge of the newly formed  $-COO^-$  group. Again, the boundary between shell and core remains sharp while retreating toward the particle center.

With the first mechanism, the conversion rate is independent of the solution concentration. With the second mechanism, the rate depends on the extent of electrolyte invasion of the  $Na^+$ -form shell and thus increases greatly with increasing solution concentration. Since the mechanisms constitute alternative paths, the system will follow the faster one, namely, the first at low solution concentrations and the second at high solution concentrations. As can be verified with the equations derived below, both particle-diffusion mechanisms are so slow that rate control by film diffusion can be ruled out for all practical purposes.

A quantitative treatment of the first mechanism with the assumptions stated at the outset and particularly with a constant diffusion coefficient  $\bar{D}_H$  of the "free"  $H^+$  ions and a mass-action law for the dissociation of the carboxylic acid groups

$$\frac{\bar{C}_R - \bar{C}_{H^+}}{\bar{C}_{RH}} = K_{RH} = \text{constant} \quad (17)$$

leads to the flux equation

$$\bar{J}_{Na} = -\bar{D} \text{grad } \bar{C}_{Na} \quad (18)$$

where

$$\bar{D} = \frac{\bar{D}_{Na}[A(A - K_{RH}) - \bar{C}_{Na}(\bar{C}_{Na} - K_{RH})]}{A(A - K_{RH}) - \bar{C}_{Na}A(1 - 2\bar{D}_{Na}/\bar{D}_H)} \quad (19)$$

$$A \equiv [(\bar{C}_{Na} - K_{RH})^2 + 4K_{RH}\bar{C}]^{1/2}$$

(Derivation is given in the Appendix.) The interdiffusion coefficient  $\bar{D}$  depends strongly on composition and varies between the limits

$$\bar{C}_{Na} \rightarrow 0, \bar{D} = \bar{D}_{Na}; \quad \bar{C}_{Na} \rightarrow \bar{C}, \bar{D} = \frac{K_{RH}}{\bar{C} + K_{RH}} \bar{D}_H \quad (20)$$

being within one order of magnitude above the lower limit over most of the composition range. An analytical solution of eq. 18 and 19 has not been found. Although numerical integrations could easily be accomplished by an available computer program,<sup>16</sup>

the results would be of little value because swelling of the resin upon conversion must be expected to cause appreciable deviations from the calculated behavior. Nevertheless, eq. 19 permits the order of magnitude of the conversion rate to be estimated; for example, for conventional resins with carboxylic acid groups (Amberlite IRC-50, Duolite C-101) one has  $K_{RH} \approx 1.5 \times 10^{-5}$  mole/l.,<sup>17</sup>  $\bar{C} \approx 5$  moles/l., and  $\bar{D}_H \approx 10^{-5}$  cm.<sup>2</sup>/sec.,<sup>18</sup> and the integral average of the apparent interdiffusion coefficient  $\bar{D}$  in eq. 19 then is of the order of  $10^{-9}$  to  $10^{-10}$  cm.<sup>2</sup>/sec. Another conclusion from eq. 19 is that  $\bar{D}$  is higher near the particle center than in the outer shells and is at its lowest when the resin is almost completely converted to the  $Na^+$  form; accordingly, there should be no sharp boundary between core and shell,<sup>2,4</sup> and conversion should become extremely slow when approaching completion. In both these features the first mechanism differs drastically from the second.

The second mechanism involves diffusion of  $Na^+$  and  $OH^-$  from the solution across the outer  $Na^+$ -form shell to the inner core. In the shell, the concentration of  $Na^+$  always greatly exceeds that of  $OH^-$ . In coupled diffusion of two ions (in the absence of other mobile ions) the rate is controlled by the minority species,<sup>2,4</sup> in the present case by  $OH^-$

$$\bar{J}_{Na} = -\bar{D}_{OH} \text{grad } \bar{C}_{Na} \quad (21)$$

(Derivation is given in the Appendix.) In general terms, conversion by the second mechanism is controlled by *particle diffusion of the co-ion*, a quite unique situation in ion exchange. For a constant solution concentration and the respective constant boundary condition

$$t \geq 0, r = r_0, \bar{C}_{OH}(r_0, t) = \bar{C}^0_{OH} = \text{constant} \quad (22)$$

an analytical solution has been obtained

$$0 \leq \tau < 1/2, \\ F(\tau) = 1 - \{1/2 + \sin [1/3 \sin^{-1}(1 - 4\tau)]\}^3 \\ (|\sin^{-1}| \leq \pi/2) \\ \tau \geq 1/2, F(\tau) = 1 \quad (23)$$

where

$$\tau \equiv \frac{3\bar{D}_{OH}\bar{C}^0_{OHT}}{r_0^2\bar{C}} \quad (24)$$

(Derivation is given in the Appendix.) Complete conversion is attained in a finite time corresponding to

(16) F. Helfferich, "Diffusion with Variable Diffusion Coefficient," IBM SHARE program 3187 (1964).

(17) I. Michaeli and A. Katchalsky, *J. Polymer Sci.*, **23**, 683 (1957).

(18) Estimated by use of an equation given by J. S. Mackie and P. Meares, *Proc. Roy. Soc. (London)*, **A232**, 498 (1955).

$\tau = 1/2$ . The function  $F(\tau)$  in eq. 23 is tabulated in Table II. Incidentally, the respective rate law for a finite slab of thickness  $x_0$  is

$$0 \leq \tau' < 1/2, F(\tau') = (2\tau')^{1/2} \quad (25)$$

$$\tau' \geq 1/2, F(\tau') = 1$$

where

$$\tau' \equiv \frac{\bar{D}_{OH}\bar{C}_{OH}^0}{x_0^2\bar{C}} \quad (26)$$

(Derivation is given in the Appendix.) Since the rate-controlling diffusion step occurs in the  $Na^+$ -form outer shell of the particle or slab, the values of  $\bar{D}_{OH}$ ,  $\tau_0$ , and  $x_0$  in eq. 24 and 26 should be those for the resin in the  $Na^+$  form.

**Table II:** Rate Law for Processes of Type III, High-Concentration Mechanism (eq. 23)

$F(\tau)$	$\tau$	$F(\tau)$	$\tau$
0.05	0.000426	0.55	0.06916
0.1	0.001745	0.6	0.08568
0.15	0.004025	0.65	0.1050
0.2	0.007339	0.7	0.1278
0.25	0.01178	0.75	0.1547
0.3	0.01744	0.8	0.1860
0.35	0.02444	0.85	0.2265
0.4	0.03293	0.9	0.2768
0.45	0.04307	0.95	0.3464
0.5	0.05506	1.0	0.5000

A criterion whether reaction 8 proceeds by the first or the second mechanism is readily derived by comparing the respective half-times of conversion (see eq. 15, 19, and Table II). With simplifications one obtains

$$\frac{K_{RH}\bar{D}_H}{\bar{C}_{OH}^0\bar{D}_{OH}} \gg 1 \quad (\text{first mechanism}) \quad (27)$$

$$\frac{K_{RH}\bar{D}_H}{\bar{C}_{OH}^0\bar{C}_{OH}} \ll 1 \quad (\text{second mechanism})$$

With  $K_{RH} \approx 1.5 \times 10^{-5}$  mole/l.,  $\bar{D}_H/\bar{D}_{OH} \approx 5$ , and electrolyte invasion data one finds that the limit between the two mechanisms is in the range of solution concentrations of  $10^{-3}$  to  $10^{-2}$  M.

Extension of the quantitative treatment to other processes of type III is straightforward if the ions A, B, and Y are univalent (as, for example, in reaction 9). If A has a higher valence, however, the applicability of mass action equations such as eq. 17 for the associa-

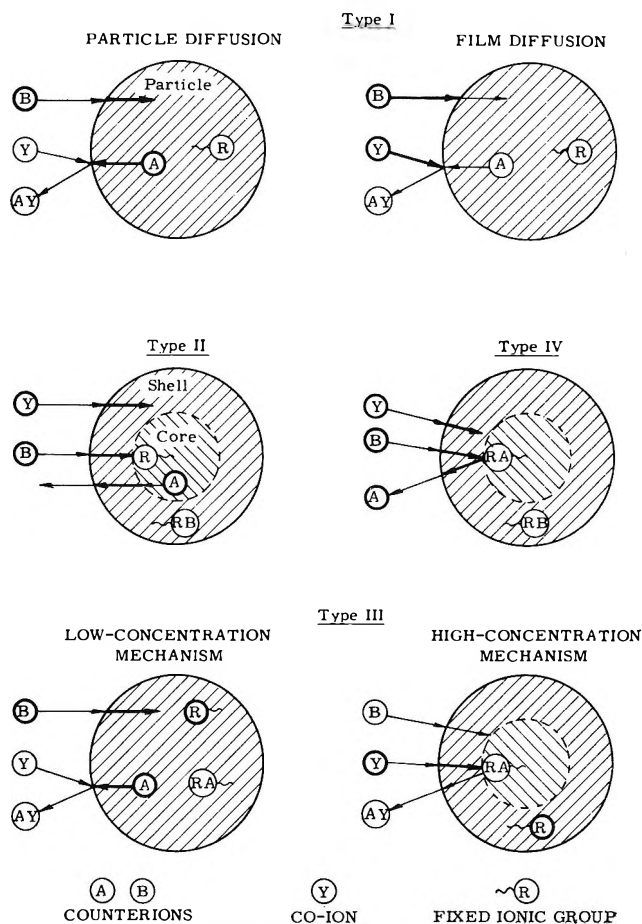


Figure 1. Schematic picture of mechanisms. Heavy circles indicate ions controlling or affecting the rate, heavy arrows indicate rate-controlling diffusion steps.

(From F. Helfferich, ref. a in Table I.

Reproduced with permission of Marcel Dekker, Inc.)

tion becomes doubtful, so that results obtained for the first mechanism will be even more questionable. On the other hand, the rate laws (23) and (25) for the second mechanism should remain valid for ions of any valences, with merely the substitutions of  $|z_Y|\bar{C}_Y^0$  for  $\bar{C}_{OH}^0$  and  $\bar{D}_Y$  for  $\bar{D}_{OH}$ .

**Discussion**

The rate laws derived in the previous section differ appreciably from those for ordinary ion exchange. Several aspects warrant comment.

A noteworthy feature of film-diffusion controlled processes of type I is the constancy of the effective diffusion coefficient. With constant  $D$ , the Nernst film concept can be applied without hesitation. In ordinary ion exchange, in contrast,  $D$  is not constant and the adequacy of the Nernst film model therefore is somewhat in doubt. The theory for film-diffusion controlled processes of type I thus is not only simpler,

but also inspires more confidence than that for ordinary ion exchange. With particle-diffusion control, the theories for processes of type I and ordinary ion exchange should be about equally reliable since they differ only in the boundary condition.

Film-diffusion controlled reaction 1 has received earlier theoretical treatment. Calderbank<sup>19</sup> has argued that the rate should be controlled by diffusion of  $H^+$  (i.e.,  $D = D_H$ ) because, throughout the film,  $C_H$  is much smaller than  $C_{Na}$ . This argument, however, is untenable because it is based on an equation valid only for interdiffusion of two counterions in the absence of other mobile ions and thus is not applicable to the film, where  $OH^-$  is present. Indeed, the present treatment shows that  $H^+$  does not even diffuse across the film but is eliminated at the particle surface. On the other hand, Harriott,<sup>20</sup> without giving a theoretical derivation, has used the proper diffusion coefficient in accordance with eq. 10.

Experimental evidence is scanty, but so far supports the rate laws derived here. The results of recent cursory studies comparing film-diffusion controlled reaction 1 with ordinary  $Na^+-H^+$ ,  $H^+-Na^+$ , and  $K^+-NH_4^+$  exchanges (with chloride solutions) are in much better agreement with eq. 10 than with Calderbank's assumption and therefore they have confirmed the validity of the rate law eq. 13 up to almost complete exhaustion of the solution.<sup>21</sup> Further studies of reactions 1 and 2 are under way.<sup>22</sup> That reaction 3 and analogous processes are faster than ordinary  $H^+$ -metal ion exchange, at least with solutions of only modest volume, has been observed long ago<sup>23</sup> and is in qualitative agreement with the theory presented here.

The theories for processes of types II, III, and IV are still much in need of verification by systematic experimental studies. Nevertheless, at least a semi-quantitative agreement with earlier experimental observations can be reported. It has been found that the rates of processes analogous to reactions 5 and 7 are much lower than those of ordinary ion exchange, are controlled by particle diffusion, and increase with increasing solution concentration,<sup>12,24-26</sup> as the present theory demands. Rates of processes analogous to reactions 8 and 10 are in order-of-magnitude agreement with the present theory.<sup>8,27-30</sup> Unfortunately, the most detailed and accurate measurements of reaction 8<sup>27,28</sup> were carried out with mixed  $NaOH-NaCl$  solutions, a fact which greatly complicates their comparison with the theory.

A striking and unusual feature, and one amenable to experimental verification, is the sharp boundary between converted shell and unconverted core in processes of types II and IV and of type III at high solu-

tion concentrations. Measurements of intraparticle concentration profiles thus suggest themselves as a more powerful tool for testing the theories than measurements merely of conversion as a function of time. In particular, concentration profile measurements could provide evidence for or against the dual mechanism of processes of type III, where the theory predicts a sharp boundary at high solution concentrations and no such boundary at low solution concentrations.

The author hopes that this theoretical analysis will help to stimulate systematic experimental work to confirm or refute the hypotheses.

### Appendix

A list of the symbols used in this work, with their respective definitions and units, is given in Table III.

*Derivation of Eq. 11, 12, and 13.* Since  $D$  is constant (see eq. 14) and  $A$  is virtually absent from the film, the quasi-stationary concentration profiles of  $B$  and  $Y$  are linear. Since, furthermore, the concentrations of  $B$  and  $Y$  at the particle surface are negligible compared with those in the bulk solution, the quasi-stationary flux is

$$-J_B(t) = D \frac{C_B'(t)}{\delta} \quad (28)$$

For  $CV \gg \bar{CV}$ , the boundary concentration  $C_B'$  remains constant and so does the flux. The intra-

$$t \geq 0, |z_B| C_B'(t) = C = \text{constant} \quad (29)$$

particle concentration  $\bar{C}_B(t)$  is calculated from the material balance

$$\bar{V} \frac{d\bar{C}_B}{dt} = -J_B S = -J_P \frac{3\bar{V}}{r_0} \quad (30)$$

After substitution with eq. 28 and 29, integration of eq. 30 over  $t$  with the initial condition shown in (31)

(19) P. H. Calderbank and S. J. R. Jones, *Trans. Inst. Chem. Engrs.* (London), **39**, 363 (1961).

(20) P. Harriott, *A.I.Ch.E. J.*, **8**, 93 (1962).

(21) C. P. Strand, G. D. Towell, and G. H. Ackerman, unpublished results, 1963.

(22) J. S. Dranoff, in preparation.

(23) F. C. Nachod and W. Wood, *J. Am. Chem. Soc.*, **67**, 629 (1945).

(24) K. Haagen, *Z. Elektrochem.*, **57**, 178 (1953).

(25) D. Reichenberg, personal communication, 1957.

(26) G. Dickel and E. Hübner, *Kolloid-Z.*, **179**, 60 (1961); however, see also F. Helfferich, *ibid.*, **185**, 157 (1962).

(27) D. K. Hale and D. Reichenberg, *Discussions Faraday Soc.*, **7**, 79 (1949).

(28) D. E. Conway, J. H. S. Green, and D. Reichenberg, *Trans. Faraday Soc.*, **50**, 511 (1954).

(29) I. Saunders and R. S. Srivastava in "Ion Exchange and its Applications," Society of Chemical Industry, London, 1955, p. 170.

(30) G. V. Samsonov, Yu. B. Boltaks, N. P. Kuznetsova, A. P. Bashkovich, and R. B. Pomonareva, *Kolloid Zh.*, **21**, 471 (1959).



Table III

Sym- bol	Definition	Units	Sym- bol	Definition	Units
$C$	Initial solution concentration	mequiv./cm. <sup>3</sup>	$r$	Radial space coordinate (distance from particle center)	cm.
$\bar{C}$	Concentration of fixed ionogenic groups <sup>a</sup> (dissociated and undissociated) in ion exchanger	mequiv./cm. <sup>3</sup>	$r_i$	Radius of unconverted particle core	cm.
$C_i$	Concentration of species $i$	mmoles/cm. <sup>3</sup>	$r_0$	Radius of particle	cm.
$C_i'$	Concentration of species $i$ at film-solution boundary	mmoles/cm. <sup>3</sup>	$R$	Gas constant	ergs mole <sup>-1</sup> deg. <sup>-1</sup>
$\bar{C}_{R^-}$	Concentration of dissociated fixed ionogenic groups in weak-acid ion exchanger <sup>a</sup>	mequiv./cm. <sup>3</sup>	$S$	Surface area of particles	cm. <sup>2</sup>
$\bar{C}_{RH}$	Concentration of undissociated fixed ionogenic <sup>a</sup> groups in weak-acid ion exchanger	mequiv./cm. <sup>3</sup>	$t$	Time	sec.
$\bar{C}_i^0$	Concentration of species $i$ in ion exchanger at particle surface <sup>a</sup> (see eq. 22)	mmoles/cm. <sup>3</sup>	$t_c$	Time for complete attainment of equilibrium	sec.
$D$	Effective diffusion coefficient	cm. <sup>2</sup> /sec.	$T$	Absolute temperature	deg.
$D_i$	Diffusion coefficient of species $i$ (assumed constant)	cm. <sup>2</sup> /sec.	$V$	Solution volume	cm. <sup>3</sup>
$F$	Fractional attainment of equilibrium ( $F = 0$ at $t = 0$ , and $F = 1$ at equilibrium)	dimensionless	$\bar{V}$	Volume of ion exchanger <sup>a</sup>	cm. <sup>3</sup>
$\mathcal{F}$	Faraday constant	coulombs/mole	$x$	Space coordinate for finite slab (distance from interface slab-solution)	cm.
$G(t)$	Tabulated conversion function (see eq. 2)	dimensionless	$x_i$	Thickness of converted shell in finite slab	cm.
$J_i$	Flux of species $i$	mmoles cm. <sup>-2</sup> sec. <sup>-1</sup>	$x_0$	Thickness of finite slab	cm.
$K_{H_2O}$	Ion product of water	mmoles <sup>2</sup> /cm. <sup>6</sup>	$y$	$\equiv \rho - 1/2$	dimensionless
$K_{RH}$	Dissociation constant of fixed weak-acid groups (see eq. 17)	mmoles/cm. <sup>3</sup>	$z_i$	Valence of species $i$ (negative for anions)	dimensionless
			$\alpha$	Degree of dissociation of H in weak-acid ion exchanger (see eq. 39)	dimensionless
			$\delta$	Film thickness	cm.
			$\rho$	$\equiv r_i/r_0$	dimensionless
			$\varphi$	Electric potential	ergs/coulomb
			$\tau$	Dimensionless time variable (see eq. 56)	dimensionless

<sup>a</sup> Symbols with over-bars are used for the interior of the ion exchanger.

$$t = 0, \bar{C}_B(0) = 0 \quad (31)$$

gives

$$|z_B| \bar{C}_B(t) = \frac{3DCt}{r_0\delta} \quad (32)$$

$F(t)$  equals fractional conversion of the ion exchanger

$$F(t) = \frac{|z_B| \bar{C}_B(t)}{\bar{C}} \leq 1 \quad (33)$$

Substitution of  $|z_B| \bar{C}_B$  in eq. 33 by eq. 32 gives the rate law eq. 11.

For the more general case with diminishing boundary concentration  $C_B'(t)$ , this concentration is first calculated from the material balance

$$V \frac{dC_B'}{dt} = J_B(t)S = J_B(t) \frac{3\bar{V}}{r_0} \quad (34)$$

After substitution with eq. 28 and integration over  $t$  with the initial condition

$$t = 0, |z_B| C_B'(0) = C \quad (35)$$

one obtains

$$|z_B| C_B'(t) = C \exp\left(-\frac{3D\bar{V}t}{Vr_0\delta}\right) \quad (36)$$

After substitutions with eq. 28 and 36, eq. 30 is now integrated over  $t$  with the initial condition (31)

$$|z_B| \bar{C}_B(t) = \frac{CV}{\bar{V}} \left[ 1 - \exp\left(-\frac{3D\bar{V}t}{Vr_0\delta}\right) \right] \quad (37)$$

If  $CV > \bar{C}\bar{V}$ , then eq. 33 holds, and one obtains with eq. 33 and 37 the rate law eq. 12. On the other hand, if  $CV < \bar{C}\bar{V}$ , then equilibrium is attained when  $|z_B| \bar{C}_B = CV/\bar{V}$ , so that

$$F(t) = \frac{|z_B| \bar{C}_B(t) \bar{V}}{CV} \quad (38)$$

and one obtains the rate law eq. 13 from eq. 37 and 38.

*Derivation of Eq. 18 and 19.* It is most convenient to write the flux equations for  $\text{Na}^+$  and for *total* (i.e., free plus associated) H and to take association of  $\text{H}^+$  with  $-\text{COO}^-$  into account by use of the degree of dissociation

$$\alpha \equiv \bar{C}_{\text{H}^+}/\bar{C}_{\text{H}} \quad (39)$$

where  $\bar{C}_{\text{H}}$  is used for *total* H. The flux equations then are

$$\bar{J}_{\text{Na}} = -D_{\text{Na}} \left( \text{grad } \bar{C}_{\text{Na}} + \bar{C}_{\text{Na}} \frac{\mathfrak{F}}{RT} \text{grad } \varphi \right) \quad (40)$$

$$\bar{J}_{\text{H}} = -D_{\text{H}} \left( \text{grad } (\alpha \bar{C}_{\text{H}}) + \alpha \bar{C}_{\text{H}} \frac{\mathfrak{F}}{RT} \text{grad } \varphi \right) \quad (41)$$

Electroneutrality and absence of electric current require that

$$\alpha \bar{C}_{\text{H}} + \bar{C}_{\text{Na}} = \bar{C}_{\text{R}^-} \quad (42)$$

$$\bar{J}_{\text{H}} + \bar{J}_{\text{Na}} = 0 \quad (43)$$

Combination of eq. 40 to 43 to eliminate  $\alpha \bar{C}_{\text{H}}$  and  $\text{grad } \varphi$  gives

$$\bar{J}_{\text{Na}} = - \frac{\bar{D}_{\text{H}} \bar{D}_{\text{Na}}}{\bar{D}_{\text{H}}(\bar{C}_{\text{R}^-} - \bar{C}_{\text{Na}}) + \bar{D}_{\text{Na}} \bar{C}_{\text{Na}}} \times (\bar{C}_{\text{R}^-} \text{grad } \bar{C}_{\text{Na}} - \bar{C}_{\text{Na}} \text{grad } \bar{C}_{\text{R}^-}) \quad (44)$$

To express  $\bar{C}_{\text{R}^-}$  in terms of  $\bar{C}_{\text{Na}}$  one uses the mass action law

$$\frac{\bar{C}_{\text{R}^-} \bar{C}_{\text{H}^+}}{\bar{C}_{\text{RH}}} = K_{\text{RH}} = \text{constant} \quad (17)$$

where  $\bar{C}_{\text{RH}}$  can be substituted by  $\bar{C} - \bar{C}_{\text{R}^-}$ . Further substitution with eq. 39 and 42 leads to a quadratic equation for  $\bar{C}_{\text{R}^-}$  with the solution

$$\bar{C}_{\text{R}^-} = 1/2(\bar{C}_{\text{Na}} - K_{\text{RH}} + A) \quad (45)$$

where  $A$  is defined as in eq. 19. Also, it follows from eq. 45 by differentiation that

$$\text{grad } \bar{C}_{\text{R}^-} = 1/2 \left( 1 + \frac{\bar{C}_{\text{Na}} - K_{\text{RH}}}{A} \right) \text{grad } \bar{C}_{\text{Na}} \quad (46)$$

Substituting  $\bar{C}_{\text{R}^-}$  and  $\text{grad } \bar{C}_{\text{R}^-}$  in eq. 44 by eq. 45 and 46 one obtains, after rearrangement, the flux equation (19).

*Derivation of Eq. 21, 23, and 25.* The fluxes of  $\text{Na}^+$  and  $\text{OH}^-$  across the shell are

$$\bar{J}_{\text{Na}} = -\bar{D}_{\text{Na}} \left( \text{grad } \bar{C}_{\text{Na}} + \bar{C}_{\text{Na}} \frac{\mathfrak{F}}{RT} \text{grad } \varphi \right) \quad (40)$$

$$\bar{J}_{\text{OH}} = -\bar{D}_{\text{OH}} \left( \text{grad } \bar{C}_{\text{OH}} - \bar{C}_{\text{OH}} \frac{\mathfrak{F}}{RT} \text{grad } \varphi \right) \quad (47)$$

If the concentration of  $\text{H}^+$  in the shell is negligible, then the conditions of electroneutrality and absence of electric current are

$$\bar{C}_{\text{Na}} = \bar{C}_{\text{OH}} + \bar{C} \quad (48)$$

$$\bar{J}_{\text{Na}} = \bar{J}_{\text{OH}} \quad (49)$$

If, as assumed,  $\bar{C}_{\text{OH}} \ll \bar{C}_{\text{Na}}$ , one obtains from eq. 40 and 47 to 49

$$\bar{J}_{\text{Na}} = -\bar{D}_{\text{OH}} \text{grad } \bar{C}_{\text{Na}} \quad (21)$$

The boundary condition at the particle surface is constant, as given in eq. 22. It is readily shown that the flux across the shell is quasi-stationary. At a time  $t(r_i)$ , at which the core radius is  $r_i$ , the condition for quasi-stationary behavior is

$$t = t(r_i), r_i \leq r \leq r_0, \frac{\partial \bar{C}_{\text{OH}}}{\partial t} = -\text{div } \bar{J}_{\text{OH}} = 0 \quad (50)$$

It follows from eq. 21 and 50 that

$$t = t(r_i), r_i \leq r \leq r_0, \frac{\partial \bar{C}_{\text{OH}}}{\partial r} = \frac{a}{r^2} \quad (51)$$

where  $a$  is independent of  $r$ . The value of  $a$ , at the time  $t(r_i)$ , is obtained by integration of eq. 51 over  $r$  with the boundary conditions

$$r = r_0, \bar{C}_{\text{OH}}(r_0) = \bar{C}_{\text{OH}}^0 \quad (52)$$

$$r = r_i, \bar{C}_{\text{OH}}(r_i) = 0$$

One finds

$$t = t(r_i), a = \bar{C}_{\text{OH}}^0 \frac{r_i r_0}{r_0 - r_i} \quad (53)$$

The amount of  $\text{OH}^-$  flowing into the particle at the time  $t(r_i)$  is now readily obtained from eq. 51 and 53 as the flux times the particle surface area

$$t = t(r_i), -(\bar{J}_{\text{OH}})_{r=r_0} S = \frac{3V \bar{D}_{\text{OH}}}{r_0} \left( \frac{\partial \bar{C}_{\text{OH}}}{\partial r} \right)_{r=r_0} = \frac{3V \bar{D}_{\text{OH}} \bar{C}_{\text{OH}}^0 r_i}{r_0^2 (r_0 - r_i)} \quad (54)$$

Complete conversion requires flow of an amount of  $\text{OH}^-$  equivalent to  $\bar{C}V$  into the particle; therefore

$$\frac{dF}{dt} = -(\bar{J}_{\text{OH}})_{r=r_0} \frac{S}{CV} = \frac{3\bar{D}_{\text{OH}} \bar{C}_{\text{OH}}^0 r_i}{\bar{C} r_0^2 (r_0 - r_i)} \quad (55)$$

Dimensionless variables are now introduced for convenience

$$\tau \equiv \frac{3\bar{D}_{\text{OH}} \bar{C}_{\text{OH}}^0 t}{\bar{C} r_0^2}; \rho \equiv \frac{r_i}{r_0} \quad (56)$$

so that eq. 55 becomes

$$\frac{dF}{d\tau} \equiv \frac{\rho}{1 - \rho} \quad (57)$$

Also, since the boundary at  $r_i$  is sharp and the core constitutes the unconverted exchanger, the ratio of shell volume to total particle volume equals  $F$ ; accordingly

$$F(\tau) = 1 - \rho^3 \quad (58)$$

The initial condition, corresponding to  $r_i = r_0$ , is

$$\tau = 0, \rho = 1, F(\tau) = 0 \quad (59)$$

To solve eq. 57 to 59, one differentiates eq. 58

$$\frac{dF}{d\rho} = \frac{dF}{d\tau} \frac{d\tau}{d\rho} = -3\rho^2 \quad (60)$$

which gives, with eq. 57

$$\frac{d\tau}{d\rho} = 3\rho^2 - 3\rho \quad (61)$$

(These operations are permissible since, as readily shown,  $\tau$  is a univalued and differentiable function of  $\rho$ .) Integration of eq. 61 with the initial condition (59) gives<sup>31</sup>

$$\tau = \rho^3 - \frac{3}{2}\rho^2 + \frac{1}{2} \quad (62)$$

With a change in variables

$$y \equiv \rho - \frac{1}{2} \quad (63)$$

Equation 62 becomes

$$y^3 - \frac{3}{4}y + \frac{1}{4}(1 - 4\tau) = 0 \quad (64)$$

The solution must obey the restriction  $0 \leq r_i \leq r_0$ , which, with eq. 56, 62, and 63, requires that

$$-1/2 \leq y \leq 1/2; 0 \leq \tau \leq 1/2 \quad (65)$$

Of the trigonometric solution of eq. 64,<sup>32</sup> the only root satisfying the restrictions (65) is

$$y = \sin \psi/3, \sin \psi = 1 - 4\tau \\ (-180^\circ \leq \psi \leq 180^\circ) \quad (66)$$

or, in explicit form

$$y = \sin[1/3 \sin^{-1}(1 - 4\tau)] \quad (|\sin^{-1}| \leq \pi/2) \quad (67)$$

Now,  $\rho$  is obtained from eq. 63 by substituting  $y$  with eq. 67, and  $F(\tau)$  is then obtained by substituting  $\rho$  in eq. 58. The result is the rate law eq. 23.

For a finite slab of thickness  $x_0$  and in contact with the solution at  $x = 0$ , the calculation is analogous. From eq. 50, one obtains immediately

$$0 \leq x_i \leq x_0, -\frac{\partial \bar{C}_{OH}}{\partial x} = \frac{\bar{C}_{OH}^0}{x_i} \quad (68)$$

so that, instead of eq. 54

$$t = t(x_i), \bar{J}_{OH} = \frac{\bar{D}_{OH} \bar{C}_{OH}^0}{x_i} \quad (69)$$

and thus

$$\frac{dF}{dt} = \frac{\bar{D}_{OH} \bar{C}_{OH}^0}{\bar{C}_{x_i x_0}}; F(t) = x_i/x_0 \quad (70)$$

The solution with the initial condition  $t = 0, F(t) = 0$  is the rate law eq. 25.

(31) NOTE ADDED IN PROOF. As was pointed out to this writer, a relation equivalent to eq. 62 has been derived previously by P. B. Weisz and R. D. Goodwin for burn-off of deposits in catalyst beads (*J. Catalysis*, 2, 397 (1963)). These authors, however, did not proceed to give the explicit solution, eq. 23.

(32) R. G. Hudson, "The Engineers' Manual," 2nd Ed., John Wiley and Sons, Inc., New York, N. Y., 1953, p. 4; the solution has been transformed for greater convenience by substitution of sin for cos and corresponding change in the argument.

## An Infrared Study of High-Area Metal Films Evaporated in Carbon Monoxide

by C. W. Garland, R. C. Lord, and P. F. Troiano

*Department of Chemistry and Spectroscopy Laboratory, Massachusetts Institute of Technology, Cambridge, Massachusetts (Received October 1, 1964)*

A new technique has been developed for the preparation of porous, high-area, unsupported metal films which are suitable for an infrared absorption study of chemisorbed CO. In essence, the method involves the flash evaporation of a metal in the presence of CO gas. Spectra of CO chemisorbed on platinum, palladium, and rhodium have been obtained in this way. The results are compared with those reported previously for reduced, supported samples and for vacuum-evaporated films; in general, the bands observed in the 1800-2100-cm.<sup>-1</sup> region are in good agreement with those seen on supported samples. In the case of platinum, two bands were also observed in the 300-500-cm.<sup>-1</sup> region.

### Introduction

Infrared spectroscopy has been widely applied to the study of the chemisorption of CO on transition metals. In all such studies, the main experimental problem has been that of preparing samples with high adsorptive capacity and acceptable infrared transmission. There have been two general approaches to this problem—the use of supported metal samples<sup>1-4</sup> and of evaporated metal films.<sup>5-8</sup> Although both approaches have led to much valuable information about the nature of chemisorbed species, the techniques which are currently used in each of these approaches involve some undesirable features.

With supported samples, the very presence of a supporting medium leads to difficulties in spectral interpretation. The effect of different supporting materials on the spectra of CO chemisorbed on nickel has been investigated by O'Neill and Yates.<sup>3</sup> This study showed large pressure-dependent variations in the ratio of linear to bridged CO species and significant changes in the strength of binding of both species, depending on whether silica, alumina, or titania supports were used. So far, however, no way has been devised for quantitatively assessing the effect of the presence of any of these supports on the spectrum of chemisorbed CO. A second complicating feature of the usual supported-sample preparation is the use of hydrogen for reducing the metal. This hydrogen may dissolve in the metal and thus constitute an impurity that may alter the electronic properties of the metal. Such electronic changes might then be expected to produce

observable spectral changes. This point has been well demonstrated in the case of CO adsorbed on nickel, for which Eischens<sup>4</sup> has found pronounced changes in the ratio of linear to bridged CO species depending upon how thoroughly the hydrogen has been removed from the metal after reduction. Another limitation of most supported samples is infrared absorption by the supporting material, especially at low frequencies.

There have been even greater difficulties in the use of evaporated metal samples. In two of the techniques which have been developed to date the sample is exposed to air before CO is chemisorbed.<sup>1,5</sup> It is clear that such samples are contaminated to some unknown extent. Blyholder<sup>6</sup> has evaporated metals onto infrared cell windows which were coated with vacuum-pump oil to produce a highly dispersed evaporated deposit. This technique, however, produces films which may be contaminated and are, in a sense, supported. The work of Pickering and Eckstrom<sup>7</sup> on the

(1) R. P. Eischens and W. A. Pliskin, *Advan. Catalysis*, **10**, 1 (1958).

(2) A. C. Yang and C. W. Garland, *J. Phys. Chem.*, **61**, 1504 (1957).

(3) C. E. O'Neill and D. J. C. Yates, *ibid.*, **65**, 901 (1961).

(4) R. P. Eischens in "The Surface Chemistry of Metals and Semiconductors," H. C. Gatos, Ed., John Wiley and Sons, Inc., New York, N. Y., 1960, p. 521.

(5) J. B. Sardisco, *Perkin-Elmer Instrument News*, **15**, No. 1, 13 (1963).

(6) G. Blyholder, *J. Chem. Phys.*, **36**, 2036 (1962).

(7) H. L. Pickering and H. C. Eckstrom, *J. Phys. Chem.*, **63**, 512 (1959).

(8) R. A. Gardner and R. H. Petrucci, *J. Am. Chem. Soc.*, **82**, 5051 (1960).

reflectance spectrum of CO adsorbed on vacuum-evaporated nickel and rhodium mirrors represents the best attempt to study "clean" metal surfaces. The spectra recorded for CO on their rather thick films were, however, quite different from those obtained on supported samples<sup>1,2</sup> and are presumably characteristic of adsorption on the bulk metals rather than on high-area, small-particle deposits which are of greater catalytic interest.

In view of the various difficulties mentioned above and the somewhat discordant results which have been obtained with different techniques, it seemed desirable to develop a new evaporation technique which would make it possible to record *transmission* spectra of CO chemisorbed on high-area, unsupported metal samples which were free from contamination by either hydrogen or air. Obviously, mirror-like films would suffer from high reflection losses and would have adsorptive capacities which were too low to be of much use. Fortunately, the preparation of porous metal films analogous to those described by Beeck and his co-workers<sup>9</sup> and by Harris and Beasley<sup>10</sup> offers a way of obtaining films which have good infrared transmission properties and high specific surface areas.

A technique for preparing porous metal films suitable for infrared studies of chemisorbed CO has been developed. This technique involves evaporating a metal in the presence of CO gas and is, to our knowledge, completely new. Hayward and Trapnell<sup>11</sup> have briefly mentioned another, perhaps similar, method which is being investigated by Eberhagen, Hayward, and Tompkins. No details of their method have been published, and a comparison of our techniques and results with theirs is not yet possible. Spectra of CO adsorbed on platinum, palladium, and rhodium are presented in this paper, and a more detailed infrared study of CO chemisorbed on nickel is reported in the following paper.<sup>12</sup> These transition metals were selected for their catalytic interest and also because infrared spectra had previously been obtained on these systems with one or more of the older methods cited previously.

### Experimental Method

**Cell.** The design of the infrared cell used in this work is illustrated in Figure 1. The body consists of a 34/45 standard-taper joint to which a short length of 22-mm. tubing has been attached. The wall of the 22-mm. tubing was blown out in such a way as to produce two 15 × 20 mm. openings. The rims of these openings were ground optically flat and parallel so that CaF<sub>2</sub> or CsI windows (A) could be sealed on with either clear glyptal or picein cement. The

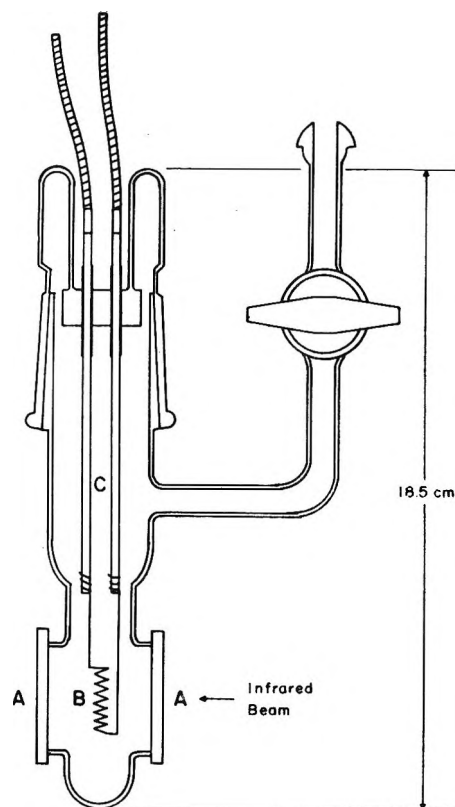


Figure 1. Cell for infrared studies of chemisorbed CO.

outer part of the standard-taper joint contains a well through which heavy tungsten leads (C) are introduced into the cell.

**Evaporation Techniques.** Tungsten filaments (B) were prepared from wire in the form of a coil about 2 cm. in length and 5 mm. in diameter. The spacing between turns was approximately 2 mm. The wires at the ends of the coil were brought up parallel to the coil axis. Two centimeters above the coil these wires were wound in a tight spiral to permit a press-fit over the heavy tungsten leads in the cell. These filaments were charged with the appropriate metal for evaporation either by placing small loops of the metal on each of the turns of the tungsten coil or by "weaving" short lengths of metal wire along the coil. With nickel and palladium a few small loops of the wire on the filament were sufficient for several evaporations. Platinum and rhodium, on the other hand, required

(9) O. Beeck, A. E. Smith, and A. Wheeler, *Proc. Roy. Soc. (London)*, **A177**, 62 (1940).

(10) L. Harris and J. K. Beasley, *J. Opt. Soc. Am.*, **42**, 134 (1952).

(11) D. O. Hayward and B. M. W. Trapnell, "Chemisorption," 2nd Ed., Butterworth, Inc., Washington, D. C., 1964.

(12) C. W. Garland, R. C. Lord, and P. F. Troiano, *J. Phys. Chem.*, **69**, 1195 (1965).

the weaving technique so as to produce a greater metal area during evaporation.

During a typical run, the cell was assembled and evacuated at room temperature to a pressure of  $10^{-6}$  mm. The filament was then slowly heated to drive off adsorbed or entrapped gases. (The temperature was raised in a series of small steps to prevent warping of the filament coil.) Pumping and heating were continued until a pressure no greater than  $5 \times 10^{-5}$  mm. was obtained at a temperature just below the point at which the metal would begin to melt and evaporate. During these final stages in the degassing procedure it was often necessary to turn the filament off for short periods of time to prevent cracking of the cell windows or rupturing of the window seals. After degassing, the filament was cooled to room temperature and the cell was pumped to a final pressure of  $10^{-6}$  mm.

Metal films were evaporated under vacuum or in the presence of small amounts of argon or CO. The evaporation was accomplished by presetting a power supply to give approximately 18 amp. through the filament for a potential drop of 20 v. The power was then switched on for short periods, and the metal was flash-evaporated onto the cell walls and windows. With nickel and palladium a single evaporation of about 2-4 sec. duration was sufficient to deposit a suitable film. Platinum and rhodium, on the other hand, required many 1-2-sec. evaporations to build up a deposit.

*Materials.* The CO gas used in this study was Matheson chemically pure (min. 99.5% CO) and was used without further purification. Platinum, rhodium, and palladium wires, stated to be 99.9% pure, were obtained from Engelhard Industries Inc., Newark, N. J. Wire diameters ranged from 0.0127 to 0.0254 cm. Tungsten wire of 0.0508-cm. diameter was obtained from the General Electric Co.

*Recording of Spectra.* The spectra of adsorbed gases were recorded on a Perkin-Elmer Model 421 double-beam grating spectrometer in the region from 4000 to 550  $\text{cm}^{-1}$ . Later in this work the range was extended to 300  $\text{cm}^{-1}$  using a Model 521 spectrometer. The spectrometers were flushed with dry nitrogen to remove atmospheric water vapor. No modifications in the instruments were required, and the spectra were generally recorded under normal operating conditions. In a number of cases, spectra were recorded with the use of an accessory which permitted the % transmission scale to be expanded as much as 20-fold. Scale expansions of fivefold proved extremely valuable in studying contours of relatively weak bands.

*Electron Micrographs.* A number of Pt films were

inspected using a Siemens Elmiskop I electron microscope. The beam voltage was typically less than 80 kv., and photographs of the metal deposits were most commonly made at a magnification of  $30,000\times$ . Metal films were evaporated onto Parlodion films cast over nickel electron-microscope grids. Several of these grids were laid on a window of the infrared cell, the cell was mounted in a horizontal position, and the metal evaporation was carried out in the usual manner. After evaporation, the grids were removed from the cell and rapidly placed in the microscope for study.

### Results and Interpretation

Metal films evaporated under high vacuum or in the presence of small amounts of argon were found to be unsuitable for infrared studies of adsorbed molecules. Thin films prepared at  $10^{-6}$  mm. were mirror-like and almost opaque to infrared radiation. Subsequent additions of CO gas did not produce detectable bands ascribable to chemisorbed CO. Films evaporated in argon at pressures between  $10^{-3}$  and 50 mm. were soot-like in appearance and transmitted much more infrared radiation than the vacuum-deposited films. Removal of the argon and admission of CO produced detectable bands in the region of 2000  $\text{cm}^{-1}$ . Unfortunately, these bands were extremely weak and, thus, unsuitable for further study and interpretation. Another complication was the presence of interference fringes in the spectra of these samples.

Films evaporated in the presence of CO gas were found to have desirable properties for infrared absorption studies. In this case reactive collisions in the gas phase are evidently quite efficient in producing a fine particle size and, hence, a high surface-to-volume ratio.

*Platinum Films. Results.* Platinum films have been evaporated in CO at pressures ranging from  $10^{-3}$  to 12 mm, and the resulting spectra have been recorded from 4000 to 300  $\text{cm}^{-1}$ . The range from 2 to 12 mm. was found to be the most useful in preparing films which exhibit good infrared transmission and CO adsorptive properties. Films prepared at these pressures were found to be relatively stable and showed no important spectral changes on prolonged standing (*i.e.*, several days).

Spectra of CO chemisorbed on a Pt film evaporated in 2 mm. of CO are shown in Figure 2. Spectrum 2-1 shows the original spectrum of CO, which appears to consist of only two bands. The more intense of these occurs at  $2053 \pm 2 \text{ cm}^{-1}$ , and the other, which is quite weak, appears at  $1840 \pm 10 \text{ cm}^{-1}$ . The assignment of a large uncertainty to the frequency of the latter

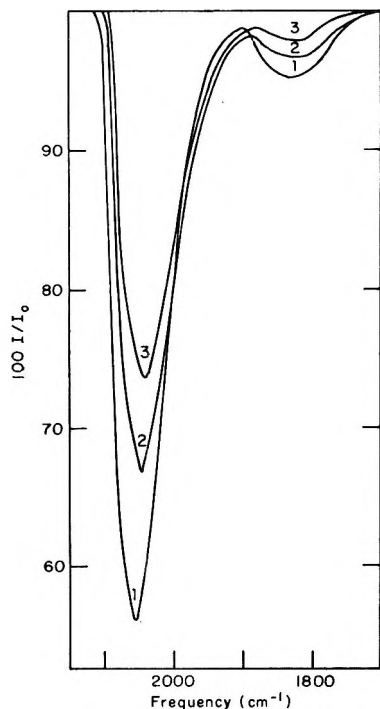


Figure 2. Spectra of CO chemisorbed on a Pt film: (1) original spectrum recorded after evaporation of film in 2 mm. of CO gas; (2) sample pumped 15 min.; (3) sample pumped 25 min.

band has been made because the band is sensitive to sample preparation, and, accordingly, its position varies from film to film. In addition, the band is so weak and broad that even with scale expansion it is difficult to locate the band center accurately. Although it is not apparent from the spectra presented here, there is also some evidence of a band at approximately  $2080 \pm 5 \text{ cm.}^{-1}$ . The band at  $2053 \text{ cm.}^{-1}$ , which is symmetrical at high coverages, develops a definite asymmetry when large amounts of CO are desorbed by pumping, and a very weak shoulder can be observed at  $2080 \text{ cm.}^{-1}$  in a number of spectra. The appearance of this shoulder cannot, however, be considered typical of the spectra recorded in this study.

Spectra 2-2 and 2-3 show the results of pumping for 15 and 25 min., respectively. Desorption causes a shift in the band maxima toward lower frequencies. For the sample used in Figure 2 the shift amounted to  $15 \text{ cm.}^{-1}$ , and the background transmission at  $2000 \text{ cm.}^{-1}$  decreased from 42 to 25% after a total pumping time of 25 min.

All Pt films prepared in this study, regardless of whether evaporated in 2 or 12 mm. of CO, produced spectra similar to those of Figure 2; *i.e.*, no new bands were observed when the CO pressure was varied. Occasional differences in band contours and frequencies

owing to a strong Christiansen filter effect<sup>13</sup> have been noted. This effect is characterized by a rapid increase in the transmission when the main absorption band is first reached and by a shift in the bands to lower frequencies by as much as  $20 \text{ cm.}^{-1}$ . No correlation between the CO pressure and the magnitude of this effect has been found.

Platinum films have also been examined in the region from  $600$  to  $300 \text{ cm.}^{-1}$  in an attempt to observe a frequency ascribable to the Pt-C stretching vibration. In most cases the transmission of the films was between 40 and 60% at  $500 \text{ cm.}^{-1}$ , and, in spite of several experimental difficulties, bands ascribed to adsorbed CO have been observed. Bands in this region were found to be extremely weak and in all cases were recorded with expansion of the transmission scale. The results obtained on a film evaporated in 2 mm. of CO are presented in Figure 3. Here the spectrum consists of a weak broad band at  $570 \pm 5 \text{ cm.}^{-1}$  and a weak but sharper band at  $477 \pm 2 \text{ cm.}^{-1}$ . All Pt films studied clearly showed the band at  $477 \text{ cm.}^{-1}$ , but in many cases the band at  $570 \text{ cm.}^{-1}$  was partially obscured by the sloping background. Spectral data are very difficult to obtain in this region during desorption, but it does appear that these bands are removed by pumping at about the same rate as those shown in Figure 2.

In order to characterize the metal samples, electron micrographs have been obtained for several Pt films evaporated in 2 mm. of CO. In all these films, the platinum appears to consist of small aggregates of particles with diameters of approximately  $45 \text{ \AA}$ . Scanning such films with the microscope showed that the deposits were quite uniform and free from holes. This uniformity unfortunately made it extremely dif-

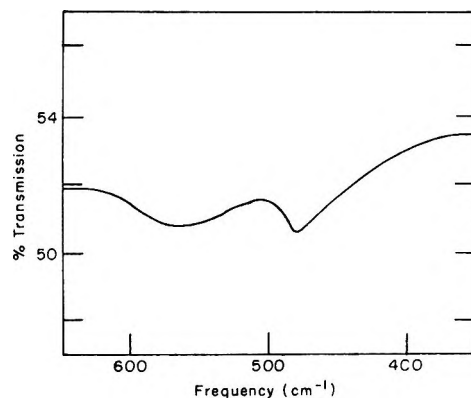


Figure 3. Low-frequency spectrum of CO chemisorbed on a Pt film evaporated in 2 mm. of CO gas.

(13) W. C. Price and A. N. Tetlow, *J. Chem. Phys.*, **16**, 1157 (1948).

difficult to find and measure single isolated particles even on the thinnest films. Because of this and limited resolution, it is not unreasonable to assign an uncertainty of  $\pm 10 \text{ \AA.}$  to the particle diameter.

*Interpretation.* Eischens and his co-workers<sup>1</sup> have reported the spectra of CO chemisorbed on a number of different types of Pt samples. Silica-supported samples show a relatively intense band at  $2070 \text{ cm.}^{-1}$  and rather weak absorption near  $1850 \text{ cm.}^{-1}$ . Alumina-supported samples, on the other hand, produce a broader band at  $2050 \text{ cm.}^{-1}$  and a more intense band near  $1820 \text{ cm.}^{-1}$ . Spectra of CO adsorbed on Pt in KBr pellets and on evaporated films are also described in Eischens' review. The pelleted samples show bands at  $2000$  and  $1850 \text{ cm.}^{-1}$ , in addition to a number of bands resulting from  $\text{CO}_2$  and water contamination. Evaporated films (made in an apparatus designed for preparing electron microscope samples and thus presumably vacuum deposited) show a single strong band at  $2050 \text{ cm.}^{-1}$  and only a very slight indication of absorption in the region around  $1800 \text{ cm.}^{-1}$ . Bands at  $2000 \text{ cm.}^{-1}$  and above were assigned by Eischens, *et al.*,<sup>1</sup> to a linear CO species bonded *via* the carbon atom to a single metal atom. Bands in the  $1800$ – $1850\text{-cm.}^{-1}$  region were assigned to a bridged carbonyl species between two adjacent metal atoms. The present results agree well with previous spectra of both supported and evaporated films although the relative band intensities agree more closely with those obtained on supported samples. The principal difference between our platinum deposits and supported samples is the ease with which our films "sinter" on desorption of CO (see also the more detailed data on nickel films<sup>12</sup>).

As mentioned earlier, two low-frequency bands were found at  $570$  and  $477 \text{ cm.}^{-1}$ . Unfortunately, no data on supported samples or vacuum-evaporated films are available in this region for comparison. (The fact that silica and alumina have poor transmission in this region makes studies on supported samples virtually impossible.) Pelleted Pt samples<sup>1</sup> have been examined and show a band at  $476 \text{ cm.}^{-1}$ . Force constant calculations<sup>14</sup> based on the isotopic frequency ratio for  $^{12}\text{CO}$  and  $^{13}\text{CO}$  on Pt suggest that the Pt–C stretching frequency should lie in this region. Hence the band observed at  $477 \text{ cm.}^{-1}$  is ascribed to the Pt–C stretching frequency. The band appearing at  $570 \text{ cm.}^{-1}$  has not been previously reported and may represent a bending mode of chemisorbed CO.

Since both the C–O and Pt–C stretching frequencies are known, it is possible to calculate approximate force constants for bond stretching and obtain some idea of bond orders. If valence forces and a negligible interaction between the Pt–C and the C–O bonds are as-

sumed, the calculation of the force constants can be made by analogy with Herzberg's treatment for the linear XYZ molecule.<sup>15</sup> If the mass of the Pt atom is further assumed to be infinite, values of  $15.6$  and  $4.1 \text{ mdyne/\AA.}$  are obtained for the C–O and Pt–C bonds, respectively. The isotopic-shift measurements of Eischens<sup>14</sup> indicated force constants of  $16$  and  $4.5 \text{ mdyne/\AA.}$  These values would indicate considerable double-bond character to the Pt–C bond, in agreement with the high degree of double-bond character found by Blyholder<sup>6</sup> for CO chemisorbed on iron.

*Palladium Films. Results.* The spectrum of CO chemisorbed on palladium has been studied with films evaporated in CO at pressures from  $5$  to  $20 \text{ mm.}$  Films prepared at lower pressures were found to be unsuitable because they produced interference fringes in the region of interest. The most useful spectra were recorded on films which were somewhat thicker than the Pt films and typically transmitted between  $20$  and  $40\%$  at  $2000 \text{ cm.}^{-1}$ . The transmission of Pd films was found to increase with wave length faster than that of the other films.

The spectrum of CO chemisorbed on a Pd film evaporated in  $9 \text{ mm.}$  of CO is shown in Figure 4. Here the spectrum consists of four bands located at  $2085 \pm 5$ ,  $1970 \pm 5$ ,  $1910 \pm 5$ , and  $1840 \pm 5 \text{ cm.}^{-1}$ . Regardless of the CO pressure used during evaporation, all

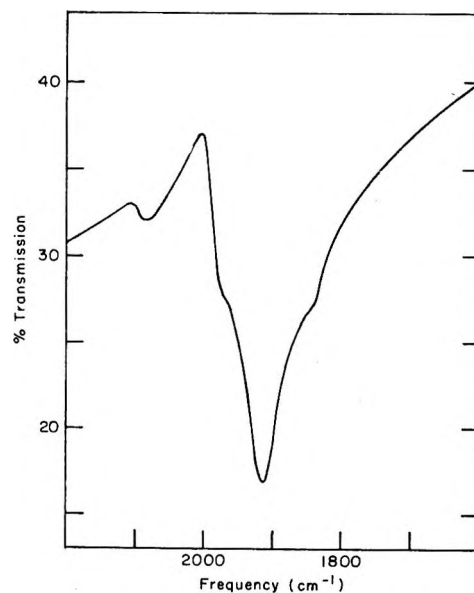


Figure 4. Spectrum of CO chemisorbed on a Pd film evaporated in  $9 \text{ mm.}$  of CO gas.

(14) R. P. Eischens, S. A. Francis, and W. A. Pliskin, *J. Phys. Chem.*, **60**, 194 (1956).

(15) G. Herzberg, "Infrared and Raman Spectra," D. Van Nostrand Co., Inc., Princeton, N. J., 1955.



of the spectra obtained in this study are similar to that given in Figure 4 in that no new features appear as the pressure is varied. The band intensities are somewhat variable, and the band at  $1840\text{ cm}^{-1}$  has been observed to be as intense as the  $1910\text{ cm}^{-1}$  band.

Desorption studies have been attempted on a number of Pd films; however, transmission losses occurring during the desorption of CO have made it impossible to obtain meaningful data. Studies in the region from  $600$  to  $300\text{ cm}^{-1}$  were also undertaken without success.

*Interpretation.* The spectrum shown in Figure 4 is in general agreement with those obtained by Eischens, *et al.*,<sup>14</sup> on silica-supported Pd samples. In their study, the spectrum at full coverage showed bands appearing at  $2074$ ,  $1930$ ,  $1895$ , and  $1845\text{ cm}^{-1}$ . The band above  $2000\text{ cm}^{-1}$  was assigned to a linear CO species, and the three bands with frequencies below  $2000\text{ cm}^{-1}$  were attributed to bridged CO species. There was no discussion of possible differences among these bridged species or among the Pd sites on which they were adsorbed. It does appear, however, from the adsorption-desorption data presented by Eischens, *et al.*, that the bridged species giving rise to their bands at  $1895$  and  $1845\text{ cm}^{-1}$  are most tightly bound and are probably due to adsorption on crystalline sites. This would be compatible with the results of a recent study of vacuum-deposited Pd films.<sup>5</sup> For such films, bands due to chemisorbed CO were observed at  $2062$ ,  $1905$ , and  $1869\text{ cm}^{-1}$ .

Thus, in terms of frequency and relative intensity, our bands at  $2085$ ,  $1910$ , and  $1840\text{ cm}^{-1}$  are in reasonable agreement with previous work. The appearance of a second band assigned to a bridged CO species and with a frequency around  $1900\text{ cm}^{-1}$  has also been observed in the case of rhodium (see next section) and nickel.<sup>12</sup> This rather high frequency for a bridged CO group could be rationalized by the familiar assumption that the M-C-M bond angle is much smaller than usual. Such a reduction in angle is more likely due to a lengthening of the M-C bond (caused by a change in hybridization of the metal orbital) rather than a shortening of the metal-metal distance in the surface.

The greatest interpretive difficulty involves the weak band we have found at  $1970\text{ cm}^{-1}$ . It would seem reasonable to relate this band to the  $1930\text{-cm}^{-1}$  band observed on silica-supported samples, except for the considerable frequency shift and the great difference in intensities. Also, there is no third "bridge" band observed in the  $1930$ - $1970\text{-cm}^{-1}$  region for vacuum-evaporated films. It is difficult to explain a bridged CO frequency as high as  $1970\text{ cm}^{-1}$ , and our results indicate that such an assignment may also be

incorrect for the  $1930\text{-cm}^{-1}$  band on supported samples. One might speculate on the presence of Pd surface sites which adsorb CO to form species approaching the bonding indicated by  $\text{Pd}=\text{C}=\text{O}$ . Such sites and the associated band frequencies might well be very sensitive to the method of sample preparation.

*Rhodium Films. Results.* Rhodium has been evaporated in CO at pressures ranging from  $3$  to  $12\text{ mm.}$ , and the spectra of the resulting films have been recorded from  $4000$  to  $300\text{ cm}^{-1}$ . The transmission of these films was in the range from  $40$  to  $60\%$  at  $2000\text{ cm}^{-1}$ , and the background was essentially flat throughout the region investigated.

Spectra of CO chemisorbed on Rh films evaporated in  $3\text{ mm.}$  of CO are shown in Figure 5. These spectra were recorded with an adjustable shutter in the reference beam to compensate partially for absorption owing to the cell and the film. Somewhat different spectra have been observed on Rh films which were evaporated at the same CO pressure. The most typical spectrum is labeled 1 in Figure 5 and will be discussed first.

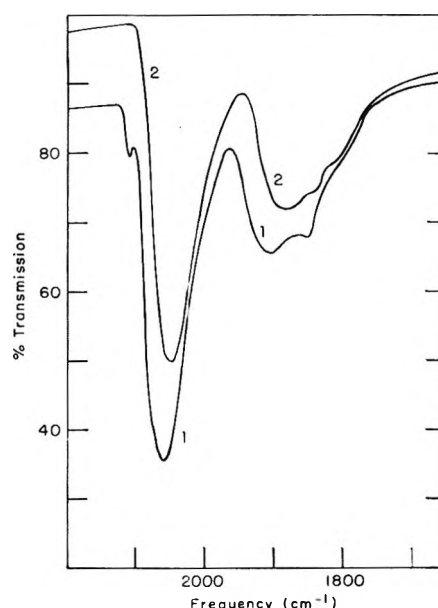


Figure 5. Spectrum of CO chemisorbed on a Rh film evaporated in  $3\text{ mm.}$  of CO gas: (1) most typical spectrum observed; (2) another spectrum observed on several samples.

On the high-frequency side of spectrum 5-1 there is a small sharp band at  $2111 \pm 1\text{ cm}^{-1}$  which is most easily observed and well resolved when the film is examined within a few hours of the time of preparation. In many cases, on longer standing this band

appears as only a weak shoulder. The main absorption band occurs initially at  $2058 \pm 5 \text{ cm.}^{-1}$  and after a time shifts to  $2055 \pm 5 \text{ cm.}^{-1}$ . There appear to be three bands in the region from 1900 to  $1800 \text{ cm.}^{-1}$ . The first of these occurs at  $1905 \pm 5 \text{ cm.}^{-1}$  and is often the most intense band in this region. The next band appears at  $1852 \pm 2 \text{ cm.}^{-1}$  and has been found to vary somewhat in intensity from film to film. Finally, there is a band appearing here as a shoulder at  $1817 \pm 5 \text{ cm.}^{-1}$ . Although this latter band is most often observed as a weak shoulder, it has been clearly resolved in at least one spectrum. There are also some indications of another weak band at  $2075 \pm 5 \text{ cm.}^{-1}$ , which is usually masked by the main absorption band but which has been seen as a shoulder in several spectra.

Spectrum 5-2 is an example of another spectrum which has been obtained on a number of Rh films. In this case the band at  $2111 \text{ cm.}^{-1}$  is missing, and the main absorption band is at  $2050 \pm 5 \text{ cm.}^{-1}$ . In the 1900- to  $1800\text{-cm.}^{-1}$  region the most intense band now appears at  $1885 \pm 5 \text{ cm.}^{-1}$  rather than  $1905 \pm 5 \text{ cm.}^{-1}$ . Although most of our spectra agree with either spectrum 5-1 or 5-2, other contours have been observed in the 1900- to  $1800\text{-cm.}^{-1}$  region. This is due to a wide variation in the relative intensity of the various bands, which indicates that the nature of the adsorption sites is quite sensitive to sample preparation.

These Rh films have also been studied extensively in the region from 600 to  $300 \text{ cm.}^{-1}$ . Although there are indications of weak absorption from approximately 575 to  $400 \text{ cm.}^{-1}$ , the quality of the spectra obtained was quite poor, and no bands definitely ascribable to chemisorbed CO have been observed.

*Interpretation.* The results presented above are quite similar to those obtained by Yang and Garland<sup>2</sup> on alumina-supported Rh. They studied both sintered and unsintered samples ranging from 2 to 16% Rh by weight. The sintered samples were heated to  $400^\circ$  and were free from residual water adsorbed on the support, while the unsintered samples were never heated above  $200^\circ$  and contained some residual water. In their study a species consisting of two linear CO molecules bonded to a single Rh atom was proposed to explain the presence of a doublet band appearing at 2040 and  $2108 \text{ cm.}^{-1}$  on sintered (dry) samples. A band observed on sintered samples with a frequency between 2045 and  $2062 \text{ cm.}^{-1}$  depending on the CO coverage was ascribed to a normal linear species with one CO per Rh atom. Finally, a band at  $1925 \text{ cm.}^{-1}$  for sintered samples was interpreted in terms of a bridged species consisting of a CO bonded to two Rh atoms each of which was also bonded to a linear CO.

A comparison of their results with those obtained here on Rh films evaporated in CO shows that the spectra obtained by Yang and Garland at intermediate coverages on 8% samples most closely resemble our spectrum 5-1. The only serious discrepancy appears to be associated with the absorption below  $2000 \text{ cm.}^{-1}$ . In this regard it should be pointed out that Yang and Garland also noted that the absorption in this region was quite sensitive to sample treatment and that this was the least reproducible region of the spectrum. It does, however, appear that the band assignments proposed for alumina-supported Rh are generally applicable to the present results.

It is, therefore, proposed that the band appearing at  $2111 \text{ cm.}^{-1}$  in spectrum 5-1 is one component of a weak doublet band ascribed to a species consisting of two linear CO molecules bonded to a single Rh atom.

An important difference in the spectra obtained on supported and evaporated films is the much greater intensity of the  $2108\text{-cm.}^{-1}$  band on supported samples. Since this band is associated with highly dispersed Rh sites, it is apparent that the evaporated deposits are relatively more crystalline. The band we have observed in the  $2050\text{-}2058\text{-cm.}^{-1}$  region can be easily assigned to the normal linear CO species. As one would expect from the weakness of the  $2111\text{-cm.}^{-1}$  component, there is no appreciable absorption near  $2040 \text{ cm.}^{-1}$ . Thus, our linear CO band has a symmetric contour in contrast to the results on supported samples. Unfortunately, we have no grounds for specific assignments of the several bands below  $2000 \text{ cm.}^{-1}$ . A variety of bridged CO species seems to exist for Rh as well as for Pd and Ni. Presumably, this variety depends on the existence of distinct surface sites which are sensitive to the method of sample preparation.

Small changes have been noted in spectra similar to spectrum 5-1 when the sample was left standing for some time. These changes, particularly the loss of the band at  $2111 \text{ cm.}^{-1}$ , are consistent with a slow sintering process occurring in the Rh films even at room temperature.

### Summary

Results obtained on metal films evaporated in the presence of CO indicate that, for the most part, these films produce spectra of chemisorbed CO which are remarkably similar to those obtained on supported metal samples. Spectral differences noted among the various types of samples can be largely interpreted in terms of support effects, variations in metal structure, and sintering. In general, there is much less correlation between our results and those obtained in previous

studies using vacuum-evaporation techniques. In contrast to our results, no bands were observed below  $1980\text{ cm}^{-1}$  for vacuum-prepared Rh films. In the case of Pd and Pt, the results are in somewhat better agreement, but, again, there are differences noted in bands observed below  $2000\text{ cm}^{-1}$ .

The problem of film sintering represents the major difficulty in obtaining the adsorption-desorption data that are necessary for a detailed characterization of

surface species. A possible solution to this problem would involve cooling the substrate to a point where sintering could largely be eliminated. In spite of this difficulty, the technique does offer the distinct advantage of permitting one to obtain spectra of chemisorbed CO on clean, unsupported metal samples. A detailed study of CO on nickel films, presented in the following paper,<sup>12</sup> will indicate the kind of results possible in a favorable case.

## Infrared Spectrum of Carbon Monoxide Chemisorbed on Evaporated Nickel Films

by C. W. Garland, R. C. Lord, and P. F. Troiano

*Department of Chemistry and the Spectroscopy Laboratory, Massachusetts Institute of Technology, Cambridge, Massachusetts (Received October 1, 1964)*

The infrared spectrum has been investigated for CO chemisorbed on nickel films which were evaporated in the presence of CO gas. For these unsupported samples, two limiting types of spectra were observed, depending on the CO gas pressure. When nickel is evaporated in 2 mm. of CO, the film is a dispersed, patchy deposit of  $65\text{-}\text{\AA}$ . particles. Films evaporated in 12 mm. of CO consist of  $200\text{-}\text{\AA}$ . particles connected in an open, chain-like network. The corresponding spectra are discussed in terms of these structural differences.

### Introduction and Method

Infrared spectra of CO chemisorbed on nickel have been reported previously for both supported and evaporated films. The earliest study was that of Eischens, Pliskin, and Francis<sup>1</sup> using a nonporous silica support. The sample contained about 8% Ni by weight and at full coverage showed infrared absorption bands at 2074, 2041, 1926, and approximately  $1870\text{ cm}^{-1}$ . A more detailed study is that by Yates and Garland<sup>2</sup> on alumina-supported Ni. In their work both adsorption-desorption studies and variations in the metal content of the samples were used in the characterization of the surface species. At full coverage on samples containing 10% Ni by weight, bands were observed at 2082, 2057, 2035, 1963, and  $1915\text{ cm}^{-1}$ . Samples con-

taining 25% Ni by weight showed a decrease in the relative intensity of the bands above  $2000\text{ cm}^{-1}$  when compared with the 10% samples. The band at  $2082\text{ cm}^{-1}$  showed the most pronounced loss in intensity.

Studies of CO chemisorbed on evaporated Ni films have been much less detailed than the studies on supported films. Reflectance spectra of CO on vacuum-evaporated Ni films have been recorded by Pickering and Eckstrom.<sup>3</sup> In their work a doublet at 2050 and  $2060\text{ cm}^{-1}$  is reported, as well as a weak band at

(1) R. P. Eischens, S. A. Francis, and W. A. Pliskin, *J. Phys. Chem.*, **60**, 194 (1956).

(2) J. T. Yates and C. W. Garland, *ibid.*, **65**, 617 (1961).

(3) H. L. Pickering and H. C. Eckstrom, *ibid.*, **63**, 512 (1959).

2030  $\text{cm}^{-1}$ . A similar reflectance study by Gardner and Petrucci<sup>4</sup> revealed only a single band at 2060  $\text{cm}^{-1}$ . Sardisco<sup>5</sup> has recorded the transmission spectra of CO adsorbed on Ni films prepared in a vacuum metallizer used to make specimens for electron microscopes. In this work a doublet at 2020 and 1980  $\text{cm}^{-1}$  was reported.

In view of the differences observed for silica- and alumina-supported samples and the conflicting data presented for evaporated films, an extensive investigation has been carried out of the spectra of CO chemisorbed on high-area, unsupported nickel films. The experimental method is new and is described in detail in the preceding paper.<sup>6</sup> The technique of film evaporation used for nickel is the same as that described for platinum, palladium, and rhodium. Nickel films were prepared by evaporating the metal (Baker Chemical, 99.9% pure) in the presence of CO at pressures ranging from  $10^{-3}$  to 44 mm. Spectra were then recorded from 4000 to 300  $\text{cm}^{-1}$ . It was found, however, that films prepared at pressures below 1 mm. have poor infrared transmission properties and show only weak absorption spectra superimposed on interference fringes. These films are thus quite similar to those obtained by evaporation in argon.<sup>6</sup> Films prepared at higher pressures transmit between 40 and 60% at 2000  $\text{cm}^{-1}$ , depending upon their mass, and show reasonably intense spectra of chemisorbed CO in the region from 2100 to 1600  $\text{cm}^{-1}$ .

It should be noted that, for purposes of comparison, the values of the % transmission of the metal films have arbitrarily been referred to 2000  $\text{cm}^{-1}$ . These values were obtained by drawing in a linear background from 1500 to 2300  $\text{cm}^{-1}$ . These background lines were used to obtain the values of  $I_0$  required to prepare the point-by-point plots of  $100I/I_0$  (shown in Figures 2 and 3). All the original spectra were recorded using fivefold expansion of the intensity scale on a Perkin-Elmer Model 521 spectrometer.

## Experimental Results

*Preliminary Observations.* With regard to the stability of the evaporated nickel films and the reproducibility of the spectra, it should be pointed out that the frequencies of the absorption band maxima have been observed to shift as a function of time in the spectra of many of the films prepared in this study. These shifts are most pronounced during the early stages of film development, *i.e.*, immediately after evaporation.

Spectra obtained from films evaporated in 2 mm. of CO with initial transmissions above 60% at 2000  $\text{cm}^{-1}$  are subject to the largest variations on standing. These changes involve not only a shift of the band

maxima to lower frequencies but also marked changes in the relative intensities of the bands. Frequency shifts in the spectra are less pronounced in films with lower initial transmissions, and the relative band intensities are unchanged on standing several hours. The band positions appear to reach nearly constant values after an "aging" period of about 30 min. The total shift in the band maxima amounts to something of the order of 5  $\text{cm}^{-1}$ . In view of this, detailed study has been limited to the more stable films having initial transmissions between 40 and 60% at 2000  $\text{cm}^{-1}$ . Spectra presented below are typical of these "stabilized" films.

Ni films evaporated in 12 mm. of CO appear to be relatively more stable than those evaporated in 2 mm. of CO, and they show no appreciable spectral changes on standing. They also differ from the films prepared at lower CO pressures in that the transmission throughout the infrared region increases more rapidly with increasing wave length.

Nickel films prepared in 2 mm. and in 12 mm. of CO exhibit reproducibly different spectra, and both have been examined in detail. These samples will be termed 2-mm. films and 12-mm. films, respectively. Intermediate CO pressures give rise to spectra which show a gradual transition from spectra characteristic of the 2-mm. films to those of the 12-mm. films. Higher pressures merely serve to shift the typical 12-mm. spectra to lower frequencies by amounts of the order of 10  $\text{cm}^{-1}$ .

*Electron Microscope Studies.* Electron micrographs of 2- and 12-mm. Ni films have been obtained in an effort to characterize the structure of these spectroscopically distinguishable metal deposits. Unfortunately, the method used to obtain the micrographs required that the films be exposed to air during the transfer to the microscope and that the films be evacuated to  $10^{-4}$  mm. prior to viewing.<sup>6</sup> Since both exposure to air and pumping were found to cause pronounced transmission losses, marked changes in the structure of the deposit before and even during the viewing of the film were anticipated. In an effort to establish the effects of this "pretreatment," films were exposed to air for periods ranging up to 4 days and were pumped on for periods up to 1 hr. prior to viewing. The results of these studies indicate that there are no major changes in the over-all film structure owing to this

(4) R. A. Gardner and R. H. Petrucci, *J. Am. Chem. Soc.*, **82**, 5051 (1960).

(5) J. B. Sardisco, *Perkin-Elmer Instrument News*, **15**, No. 1, 13 (1963).

(6) C. W. Garland, R. C. Lord, and P. F. Troiano, *J. Phys. Chem.*, **69**, 1188 (1965).

additional pretreatment. Such observations do not, however, preclude the possibility of minor structural changes which may have quite pronounced effects on the transmission. The difficulty in observing small changes resulted from the necessity of using low electron-beam energies. These were required since it was found that the films were easily sintered by the beam when voltages above 80 kv. were used. The use of lower energies or beam-spreading techniques resulted in a loss of resolution which made the observation of small structural changes virtually impossible.

In spite of the difficulties mentioned above, it is believed that the electron micrographs presented in Figure 1 reflect all of the major features of the deposits prior to exposure and pumping. The stability of these micrograph samples is perhaps due to the fact that they were typically much thinner than those used for infrared studies.

Figure 1(a) is an electron micrograph of a 2-mm. Ni film. The film appears to consist of randomly spaced patches of metal. These patches consist of smaller particles having diameters of approximately 65 Å. The sizes of the patches vary from single 65-Å particles to structured agglomerates containing hundreds of these individual particles. Thicker 2-mm. films, such as those used for infrared studies, would have a nonuniform porous structure which might best be described as spongy.

A typical 12-mm. Ni film is shown in Figure 1(b). The difference between the two types of film is immediately apparent. The first thing to be noted is the anticipated increase in the size of the individual particles in the agglomerates. In this case the average particle size is approximately 200 Å. The structure of the film is also vastly different in that, instead of random patches, the 12-mm. film exhibits a remarkable chain-like structure. The chains observed in these studies ranged from small chains containing 3 or 4 particles to large branched chains filling the whole field of view. It is also evident in this case that the individual particles are fused together rather than merely being in point contact.

*CO Chemisorbed on 2-mm. Ni Films.* Figure 2 summarizes the results of a typical study carried out on a Ni film which was evaporated in 2 mm. of gaseous CO.

Spectrum 2-1 shows the bands of chemisorbed CO obtained for full coverage at a CO pressure of 2 mm. In the region characteristic of carbonyl stretching frequencies associated with linearly adsorbed CO,<sup>7</sup> a prominent band is observed at  $2083 \pm 2$  cm.<sup>-1</sup> and a weaker band appears as a shoulder at  $2058 \pm 2$  cm.<sup>-1</sup>. In the region ascribed to bridged CO,<sup>3,7</sup>

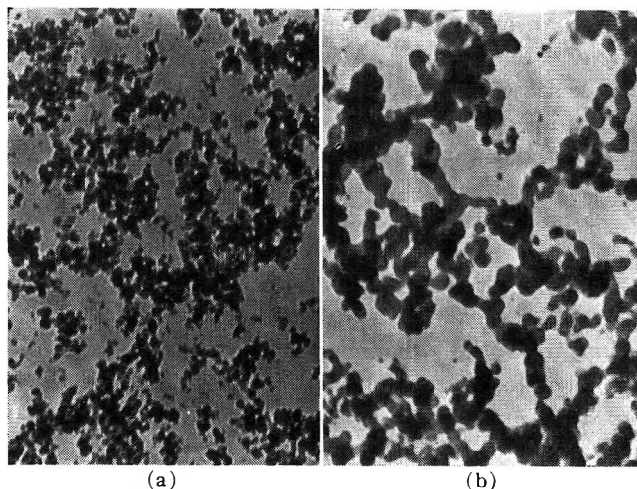


Figure 1. Electron micrographs of nickel films evaporated in (a) 2 mm. of CO gas and (b) 12 mm. of CO gas. The magnification scale and beam energy (80 kv.) were the same for both of these samples.

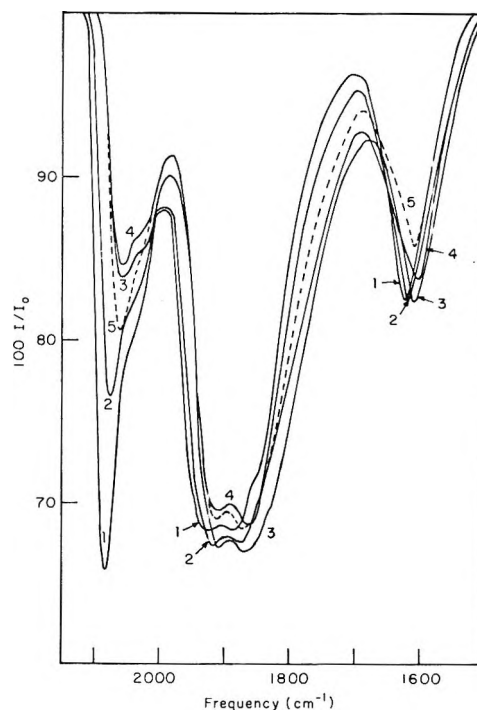


Figure 2. Spectra of CO chemisorbed on a 2-mm. Ni film: (1) original spectrum recorded in the presence of 2 mm. of gas; (2) sample pumped 1 min.; (3) sample pumped 15 min.; (4) sample pumped 50 min.; (5) 3 mm. of CO gas added to cell.

bands are observed at  $1925 \pm 5$  and  $1880 \pm 5$  cm.<sup>-1</sup>. Careful examination of many similar spectra indicates the possible existence of two additional bands in this

(7) R. P. Eischens and W. A. Pliskin, *Advan. Catalysis*, 10, 1 (1958).

region appearing as weak shoulders at approximately 1950 and 1840  $\text{cm}^{-1}$ . Although several spectra seem to indicate clearly the existence of these weak bands, it is quite difficult to demonstrate adequately their presence and exact position in the majority of the spectra recorded in this study. A further feature of the spectrum to be noted is the presence of a prominent band at 1620  $\text{cm}^{-1}$ . Even on "stabilized" films the position of this band has been found to vary and is thus somewhat more sensitive to sample preparation than the other bands. On various samples this band has been found in the range between 1630 and 1610  $\text{cm}^{-1}$ , but most often it appears at 1620  $\pm 5$   $\text{cm}^{-1}$ .

When the sample is left in contact with CO gas for periods in excess of 3 or 4 hr. several changes are noted in the spectrum. The intensity of the 2083- $\text{cm}^{-1}$  band decreases, and the shoulder at 2058  $\text{cm}^{-1}$  develops into a sharp, spike-like band. The development of this latter band is consistent with the formation of small amounts of gaseous  $\text{Ni}(\text{CO})_4$  in the cell.<sup>8,9</sup> This band is easily removed by pumping for 15 sec.

The possibility of studying relative binding strengths of various adsorbed species and the effect of surface coverage on band positions were investigated. A complete desorption-adsorption series of spectra could not be obtained since the transmission of the films was found to decrease markedly when CO was removed from the surface by pumping. Transmission losses were found to be most severe for the thicker films, *i.e.*, for films having initial transmissions below 40%. Losses for thinner films, in the range of 40 to 60% transmission at 2000  $\text{cm}^{-1}$ , were less pronounced. In general, pumping these thinner films for 1 hr. reduced the background transmission to one-half of its initial value. Pumping for longer periods reduced the transmission even further and made the recording of spectra quite difficult. Consequently, information concerning CO at low surface coverage, which could only be obtained after prolonged pumping, was not realized.

Spectra 2-2, 2-3, and 2-4 show the results obtained after pumping for 1, 15, and 50 min., respectively, at  $10^{-5}$  to  $10^{-6}$  mm. There are a number of changes to be noted in this series of spectra. The most obvious is the pronounced loss in intensity of the band at 2083  $\text{cm}^{-1}$  and what appears to be a somewhat less dramatic loss associated with the band at 2058  $\text{cm}^{-1}$ . There is also the development of a band appearing as a shoulder at 2025  $\pm 5$   $\text{cm}^{-1}$  which can be seen clearly in spectra 2-3 and 2-4. The apparent intensity loss and development associated with these bands may merely reflect the fact that they are more clearly resolved now that the masking effect of the band at 2083  $\text{cm}^{-1}$  has been

removed. A slight decrease in the intensity of the 1925- $\text{cm}^{-1}$  band relative to that of the 1880- $\text{cm}^{-1}$  band is also apparent; accompanying this change is a shift of these band maxima to lower frequencies.

The peak intensities of the bands below 2000  $\text{cm}^{-1}$  appear to remain constant or increase slightly during this relatively short desorption period. In this connection, however, it should be pointed out that the uncertainty in these values may in some cases be of the order of 1% or more. To a large extent this uncertainty arises from the difficulty in accurately determining  $I_0$  owing to small variations in the film transmission during the actual recording of the spectrum. After pumping this particular sample for 50 min., the background transmission at 2000  $\text{cm}^{-1}$  had dropped from an initial value of 47.5 to 29.5%.

Spectrum 2-5 shows the results of adding 3 mm. of CO gas to the sample in order to check the reversibility of the desorption. The CO remained over the sample for an equilibration period of 1 hr. before the spectrum was recorded. The results indicate that some CO can be reabsorbed, as evidenced by the growth of the 2058- $\text{cm}^{-1}$  band, but that the desorption is irreversible as far as the band at 2083  $\text{cm}^{-1}$  is concerned. It can also be seen that on reabsorption of CO the low-frequency bands shift toward slightly higher frequencies but do not quite achieve their initial values. Note also the loss of intensity in the 1620- $\text{cm}^{-1}$  band when CO is reabsorbed. Prolonged standing for periods in excess of 3 or 4 hr. produced a further intensification of the 2058- $\text{cm}^{-1}$  band which is again ascribed to the formation of  $\text{Ni}(\text{CO})_4$ . The early growth of the 2058- $\text{cm}^{-1}$  band is ascribed to the reabsorption of CO and not to the formation of  $\text{Ni}(\text{CO})_4$  because (a) the CO pressure is too low<sup>8</sup> to produce significant amounts of  $\text{Ni}(\text{CO})_4$  in the short time between dosing and recording the spectrum, (b) the band remains broad during early growth, which is typical of adsorbed CO, and (c) the band does not pump off as rapidly as would be expected if it were due to gaseous or physically adsorbed  $\text{Ni}(\text{CO})_4$ .

*CO Chemisorbed on 12-mm. Ni Films.* Presented in Figure 3 are the results of a typical study carried out on a Ni film which was evaporated in 12 mm. of gaseous CO.

Spectrum 3-1 shows the CO bands obtained for full coverage on a 12-mm. Ni film. The spectrum consists of three prominent bands at 2058  $\pm 2$ , 1880  $\pm 5$ , and 1620  $\pm 5$   $\text{cm}^{-1}$ . The 1620- $\text{cm}^{-1}$  band is again subject

(8) J. T. Yates, Ph.D. Thesis, Massachusetts Institute of Technology, June 1960.

(9) B. L. Crawford and P. C. Cross, *J. Chem. Phys.*, **6**, 525 (1938).

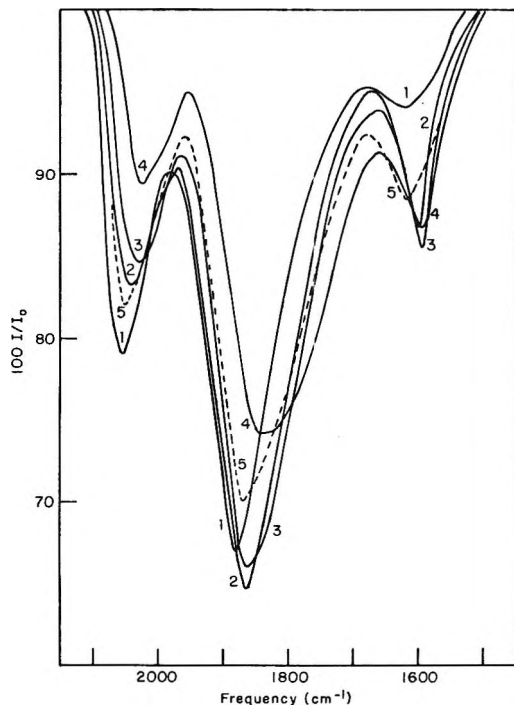


Figure 3. Spectra of CO chemisorbed on a 12-mm. Ni film: (1) original spectrum recorded in the presence of 12 mm. of CO gas; (2) sample pumped 5 min.; (3) sample pumped 15 min.; (4) sample pumped 45 min.; (5) 3 mm. of CO gas added to cell.

to the variations mentioned in connection with the 2-mm. films. There are also indications of a weak band appearing at approximately  $1950\text{ cm}^{-1}$  but none in the  $1840\text{-cm}^{-1}$  region. The principal differences between 2- and 12-mm. spectra are the loss of bands at  $2083$  and  $1925\text{ cm}^{-1}$  and the marked decrease in the intensity of the band at  $1620\text{ cm}^{-1}$ .

The results of pumping on a 12-mm. Ni film for varying periods of time are also shown in Figure 3. This series of spectra shows a number of important spectral changes during a relatively brief desorption period totaling only 45 min.<sup>10</sup> The first to be noted is the general shift in the bands below  $2000\text{ cm}^{-1}$  toward lower frequencies, which in this case amounts to approximately  $30\text{ cm}^{-1}$ . The most remarkable changes, however, are in the band intensities. The band at  $2058\text{ cm}^{-1}$  suffers a considerable loss in intensity, and spectrum 3-4 shows that a band at  $2025 \pm 5\text{ cm}^{-1}$  is the most prominent band above  $2000\text{ cm}^{-1}$  for lower coverages. Bands below  $2000\text{ cm}^{-1}$  actually appear to be intensified during the initial stages of desorption. This intensification is particularly apparent in the case of the band at  $1620\text{ cm}^{-1}$ , where the increase is much larger than any reasonable estimate of experimental uncertainty. It is also worth noting that, with both

the 2- and 12-mm. films, the intensities of bands in the  $1950\text{-}1850\text{-cm}^{-1}$  region appear to increase slightly and then decrease as pumping continues. This effect is probably real, but it could be an artifact caused by the experimental uncertainty in the intensities, which is of the order of 1%. Finally, it is apparent that the loss in intensity of the band at  $1880\text{ cm}^{-1}$  is relatively more pronounced in this case than with the 2-mm. films.

Spectrum 3-5 shows the changes produced by adding 3 mm. of CO gas to the cell after the desorption period. The effect is to reverse the desorption results by increasing the intensity of the bands at  $2058$  and  $1880\text{ cm}^{-1}$  and decreasing that of the  $1620\text{-cm}^{-1}$  band. In addition, the bands below  $2000\text{ cm}^{-1}$  shift toward higher frequencies by approximately  $25\text{ cm}^{-1}$ , nearly restoring the initial values. Prolonged standing in this case does not result in the formation of the spike-like band at  $2058\text{ cm}^{-1}$ , and thus little, if any,  $\text{Ni}(\text{CO})_4$  forms in the cell.

**300-600-Cm.<sup>-1</sup> Region.** Previous studies<sup>9,11</sup> on the infrared spectra of  $\text{Ni}(\text{CO})_4$  have shown that the Ni-C stretching frequency occurs near  $400\text{ cm}^{-1}$ . It was therefore anticipated that CO chemisorbed on Ni films would produce a band in the region from  $500$  to  $300\text{ cm}^{-1}$ . Spectra recorded from  $600$  to  $300\text{ cm}^{-1}$ , however, have not confirmed the existence of the Ni-C stretching frequency in this region. Unfortunately, the 100% transmission line and the background spectrum of the empty cell appear to have weak "bands" of their own in this region. These "bands" are probably connected, in some way, with the sample scattering and with the use of large slit widths. Such irregularities in the background would not be a serious handicap if they were reproducible. Experience has shown, however, that each film appears to have a somewhat different "spectrum" throughout this region.

In spite of these experimental difficulties, many 2- and 12-mm. Ni films have been examined in this region. At five- and tenfold scale expansion there appears to be a very weak band in the neighborhood of  $400\text{ cm}^{-1}$ , but the quality of the spectra is so poor and the reproducibility so bad as to preclude any definite assignment. The possibility that broad, weak bands do occur and have been missed in this work cannot be discounted. Since the integrated absorption coefficient is directly proportional to the frequency,<sup>12</sup> bands might well occur in this low-frequency region

(10) During desorption, the background transmission of this film at  $2000\text{ cm}^{-1}$  dropped from an initial value of 55.5 to 23.5%.

(11) L. H. Jones, *J. Chem. Phys.*, **23**, 2448 (1955).

(12) R. S. Mulliken, *ibid.*, **7**, 14 (1939).

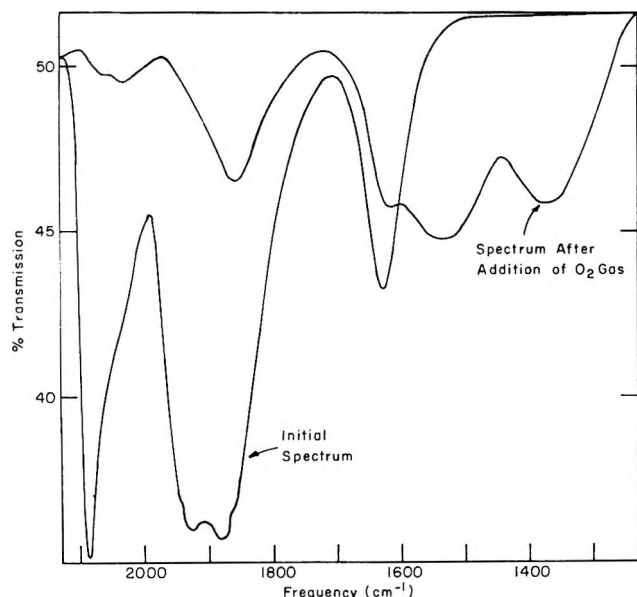


Figure 4. The effect of oxygen on the spectrum of CO chemisorbed on a 2-mm. Ni film.

which are too weak to be resolved in the presence of an irregular unreproducible background.

*Effect of Oxygen and Hydrogen on Chemisorbed CO.* The oxidation of chemisorbed CO has been studied at room temperature by adding small amounts of  $O_2$  gas to the films. The  $O_2$  pressure in the cell was typically of the order of a few millimeters. Since the oxidation was found to proceed quite rapidly, the spectra were recorded immediately after dosing. Results of the addition of 10 mm. of  $O_2$  gas to CO adsorbed on a 2-mm. Ni film are presented in Figure 4. The spectra were recorded using a fivefold scale expansion and have not been replotted as  $I/I_0$  since the difference in the transmission of the films before and after oxidation was in this case only about 1%.

The spectra indicate an extensive removal of CO from the Ni surface. There appears to be a complete disappearance of the bands at 2083 and 1925  $cm^{-1}$  and a drastic reduction in the intensity of the remaining bands. With respect to the band appearing at 1850  $cm^{-1}$  after oxidation, it is difficult to say whether this is, in fact, the original 1880- $cm^{-1}$  band which has been shifted or whether this is the band often seen as a weak shoulder at 1840  $cm^{-1}$ . Finally, there are two new bands appearing at 1530 and 1365  $cm^{-1}$  which are characteristic of the carboxylate ion formed by adsorbed  $CO_2$ .<sup>13,14</sup> Spectra obtained after the oxidation of 12-mm. Ni films are essentially identical with those of the 2-mm. films. In both cases gaseous  $CO_2$  is formed in the cell as indicated by the development of the doublet band at 2349  $cm^{-1}$ .

Hydrogen gas has also been added to a number of 2- and 12-mm. films to determine whether it has any effect upon the spectrum of chemisorbed CO. After the films were prepared and the initial spectrum of CO was recorded, the cell was filled with  $H_2$  at pressures ranging up to 0.5 atm. The sample was allowed to remain in contact with the  $H_2$  for some time at room temperature before the final spectrum was recorded. Studies were not carried out at elevated temperatures because of the difficulty in heating the cell. The results showed that the addition of  $H_2$  to these films at room temperature had no appreciable effect on the spectrum of the preadsorbed CO.

### Interpretation and Discussion

The results of previous investigations<sup>1-5</sup> of the infrared spectrum of CO chemisorbed on either supported or evaporated nickel films were reviewed briefly in the Introduction. It is clear that, in terms of the number and position of the bands, the results of the present study are most similar to those obtained on supported films. In particular the spectra of 2-mm. Ni films closely resemble the spectra obtained on 8 and 10% samples supported on silica and alumina, respectively. A summary of our results for the spectra of CO chemisorbed on 2- and 12-mm. Ni films is presented in Table I, along with a comparison with the data obtained for

Table I: Frequencies and Assignments of Infrared Bands Due to CO Chemisorbed on Evaporated Ni Films, Together with Previous Data for Supported Ni Samples

Band frequencies, $cm^{-1}$					
SiO <sub>2</sub> - sup- ported sample <sup>a</sup>	Al <sub>2</sub> O <sub>3</sub> - sup- ported sample <sup>b</sup>	2-mm. film	12-mm. film	Type of CO species (see text)	Type of Ni site
2074	2082	2083 ± 2	...	Linear	Amorphous
2041	{ 2057 2035	2058 ± 2	2058 ± 2	Linear	Semocrystalline
		2025 ± 5	2025 ± 5	Linear	Crystalline
1926	1963	1925 ± 5	...	Bridge, type I or II	Semocrystalline
~1870	1915	1880 ± 5	1880 ± 5	Bridge, type I	Crystalline
...	...	1620 ± 5	1620 ± 5	Bridge, type III	Crystalline

<sup>a</sup> See ref. 1. <sup>b</sup> See ref. 2.

supported films. The appearance of a band at 1620  $cm^{-1}$  on our evaporated films, however, represents a

(13) C. E. O'Neill and D. J. C. Yates, *Spectrochim. Acta*, **17**, 593 (1961).

(14) R. P. Eischens, *Z. Elektrochem.*, **60**, 782 (1956).

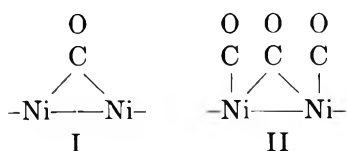


major departure from results obtained on supported films and will therefore be considered separately.

The differences among the frequencies of the CO bands observed on the three types of samples appear to be due to the support and are most pronounced in the region below 2000  $\text{cm}^{-1}$ . If the band positions for 2-mm. films are taken to be representative of unsupported Ni films in this region, one is led to the conclusion that the silica-supporting medium does not lead to important spectral changes but that alumina, on the other hand, increases the frequency of the bridged bands by some 40  $\text{cm}^{-1}$ .

The assignment of surface species and surface sites to the infrared absorption bands observed on 2-mm. Ni films closely parallels that of Yates and Garland.<sup>2</sup> The band located at 2083  $\text{cm}^{-1}$  is ascribed to a weakly held linear species bonded to the metal on "amorphous" Ni sites. The term "amorphous" is meant to signify a metal deposit with a very highly disordered structure in which the number and position of nearest neighbor atoms are much different from those in a crystalline deposit; comparable sites on supported samples were called "dispersed."<sup>2</sup> The assignment is made in light of the ease with which this species is removed from the surface by pumping and from the fact that the band is not observed on more compact films, *i.e.*, on 12-mm. films. Bands occurring at 2058 and 2025  $\text{cm}^{-1}$  are attributed to linearly adsorbed CO on semicrystalline and crystalline sites, respectively. The details of these assignments are extensively covered by Yates and Garland, and it is sufficient to note that the present results are consistent with their conclusions.

The assignment of bands below 2000  $\text{cm}^{-1}$  will be made by analogy with those made on the alumina-supported samples although certain difficulties arise from such an approach. It is assumed that the bands appearing at 1925 and 1880  $\text{cm}^{-1}$  on 2-mm. films correspond to the bands appearing at 1963 and 1915  $\text{cm}^{-1}$ , respectively, in the alumina-supported samples, the difference representing, in some way, the interaction of the metal with the alumina. Thus, the band at 1880  $\text{cm}^{-1}$  would be assigned to a normal bridged species, *i.e.*, structure I, adsorbed on a crystalline nickel site. This assignment is consistent with the high relative intensity of this band and the apparent strength of adsorption of the species associated with it. By



analogy with the assignments made by Yates and Gar-

land, one would ascribe the band at 1925  $\text{cm}^{-1}$  to a bridged species of structure II occupying a crystalline site. Another possibility is that this higher frequency band is related to a normal bridged species, like I, which is adsorbed on a semicrystalline site. In this connection, semicrystalline is meant to signify a metal deposit with a more irregular structure (with considerable lattice imperfections and edge atoms) than that of a crystalline film which approaches the structure of a bulk sample.

The results obtained on 12-mm. Ni films with the electron microscope indicate that these deposits are more compact than the 2-mm. films. One might, therefore, expect that the only major difference between the spectra of CO chemisorbed on 2- and on 12-mm. Ni films would be the loss of the band at 2083  $\text{cm}^{-1}$  which is characteristic of the amorphous sites. The results, as indicated in Figures 2 and 3, clearly show, however, that the loss of this band is only a part of the story since the band at 1925  $\text{cm}^{-1}$  has also disappeared. This is difficult to explain if the 1925- $\text{cm}^{-1}$  band is assigned to structure II on a crystalline site. Since the 12-mm. film is more crystalline and the CO pressure is higher, one would expect an enhanced 1925- $\text{cm}^{-1}$  band. If the 1925- $\text{cm}^{-1}$  band is assigned to a species on a semicrystalline site, its disappearance can be understood in terms of a drastic reduction of such sites on 12-mm. films. The relative intensities of bands ascribed to linear species (as best seen in spectra 2-4 and 3-4) seems to confirm the loss of semicrystalline character in 12-mm. films. Therefore, we favor an assignment of the band at 1925  $\text{cm}^{-1}$  to a bridged CO species adsorbed on a semicrystalline site. It does not seem possible to distinguish between structures I and II for this species.

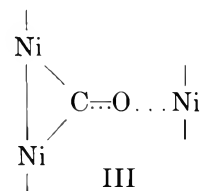
In general, our assignment of bands to various bridged species is consistent with the observed strengths of adsorption and hence with the types of sites involved in the adsorption. It should be admitted, however, that, owing to experimental difficulties, our adsorption-desorption data on unsupported films are far from complete. Such data would be useful in support of the correspondence between the observed bands and the proposed structures of the sites and the CO species.

The possibility that the band appearing at 1620  $\text{cm}^{-1}$  arises from film contamination has been considered since both adsorbed water and CO chemisorbed on NiO produce bands in this region. In view of the stringent outgassing procedure used in preparing the films, however, it is difficult to see how such contamination could occur. If water were present there would be every reason to expect a similar band in the spectra obtained with other transition metal

films prepared by the same method and not just on the Ni films. Since this is not the case,<sup>6</sup> the possibility of contamination by water is quite remote. O'Neill and Yates<sup>13</sup> have shown that CO chemisorbed on alumina-supported NiO samples produces bands of almost equal intensity near 1650 and 1450  $\text{cm}^{-1}$  which were attributed to  $\text{CO}_3$  and  $\text{CO}_3^-$  species. They also found that silica-supported samples show no absorption in this region. Bands observed by these authors were found to desorb in a normal fashion, in contrast to our anomalous adsorption-desorption results. Further, if the 1620- $\text{cm}^{-1}$  band observed in our work were due to CO adsorption on NiO sites, the addition of oxygen might be expected to increase the band intensity as more NiO is formed. That this is not the case can be clearly seen in Figure 4, which shows a decrease in the 1620- $\text{cm}^{-1}$  band intensity and the development of new bands at 1530 and 1365  $\text{cm}^{-1}$  which are consistent with the bands observed on silica-supported nickel in the presence of oxygen and carbon dioxide.<sup>13,14</sup> Finally, in contrast to our results, bands ascribed to linearly adsorbed CO were observed above 2100  $\text{cm}^{-1}$  on supported NiO samples. It therefore appears that an explanation of the 1620- $\text{cm}^{-1}$  band in terms of oxygen contamination giving rise to NiO sites is quite unlikely.

This band thus appears to represent a unique surface species which, to our knowledge, has not been previously observed in the study of CO chemisorbed on metals. The frequency is quite low for a normal carbonyl stretching vibration,<sup>15</sup> and thus consideration must be given to ways in which the frequency of a bridged CO species could be substantially lowered. One way in which this can occur is by an increase in the Ni-Ni spacing since the carbonyl stretching frequency is a function of the angle between the carbon-metal bonds. Halford<sup>16</sup> has treated the variation in frequency with bond angle for an  $\text{X}_2\text{C}=\text{O}$  type molecule, and his calculations indicate that, for X atoms heavier than hydrogen, a change in the bond angle from 90 to 180° would result in a shift of only about 100  $\text{cm}^{-1}$ . It thus seems improbable that a decrease in the normal carbonyl frequency of almost 300  $\text{cm}^{-1}$  can be attributed to a simple bridged species on a crystalline site characterized by a larger Ni-Ni spacing.

A more reasonable explanation would be that a carbonyl exhibiting a band at this low frequency must possess considerable single-bond character. This might arise through the weakening of the carbonyl bond *via* association of the oxygen atom with another Ni atom. A structure like III, where all of the Ni atoms are to be considered part of the same particle, might thus account for the appearance of the band at 1620  $\text{cm}^{-1}$ .



This would be in reasonable agreement with the frequencies observed for diketones which have formed chelates with metal atoms.<sup>15</sup> In particular, nickel acetylacetonate has a carbonyl band at 1598  $\text{cm}^{-1}$ .<sup>17</sup>

The remaining problem is then to show that such an assignment is also consistent with the limited desorption-adsorption data. In the case of 2-mm. Ni films, Figure 2 indicates that the species producing the band at 1620  $\text{cm}^{-1}$  is tightly bound and is pumped off slowly. Figure 3, on the other hand, clearly shows that on 12-mm. films the intensity of the 1620- $\text{cm}^{-1}$  band actually increases markedly during initial stages of pumping. At first it may seem remarkable that the concentration of an adsorbed species should increase as CO is removed from the surface. This is, however, just what one might expect if a species like III were present. At high initial coverage on a 12-mm. film it would appear that there are relatively few surface sites which are able to accommodate this species simply because the additional Ni site required for its formation is already occupied by a linear or perhaps a more "normal" bridged species. As CO is desorbed and the more weakly held surface species are removed, however, these additional sites could become available for participation in the formation of III. Hence, the concentration of III could gradually increase on pumping at the expense of other surface species. This would continue until finally this species itself was desorbed by prolonged pumping. Such variations in the concentration of III would thus be consistent with the observed changes in the band intensities shown in Figure 3.

The relatively larger proportion of species III noted on 2-mm. films seems to be consistent with the assumption that this species is favored by lower pressures. The fact that on 2-mm. films the 1620- $\text{cm}^{-1}$  band does not intensify on pumping suggests that the films are saturated with respect to this species. Desorption, therefore, would not lead to an increase in the concentration of III. It should also be noted that the

(15) L. J. Bellamy, "The Infrared Spectra of Complex Molecules," Methuen and Co. Ltd., London, 1958.

(16) J. O. Halford, *J. Chem. Phys.*, **24**, 830 (1956).

(17) K. Nakamoto, Y. Morimoto, and A. Martell, *J. Am. Chem. Soc.*, **83**, 4533 (1961).

readsorption of CO on both the 2- and 12-nm. films resulted in a decrease in the intensity of the 1620-cm.<sup>-1</sup> band. (See Figures 2 and 3.) This is again consistent with the idea that at higher pressures CO adsorbs on the third Ni site and reduces the amount of III.

A comparison of the relative intensities of the various bands obtained from CO chemisorbed on evaporated Ni samples with those obtained on supported samples (alumina or silica) again shows marked similarities. In general, relative band intensities appear to be consistent among the three types of samples above 1900 cm.<sup>-1</sup>. Below 1900 cm.<sup>-1</sup>, however, the absorption bands observed on the evaporated films are relatively more intense. Specifically, the band at 1880 cm.<sup>-1</sup> is quite weak in the spectra of supported films, and the band appearing at 1620 cm.<sup>-1</sup> is not observed. This then indicates that the distribution of surface sites is different for evaporated films. This difference could arise from a fundamental difference in the nature of

the evaporated deposit or from a reduction in the number of similar sites on supported samples through an interaction of the Ni particles with the support. The data obtained in the present work do not permit such a distinction to be made.

All nickel films prepared in this study showed pronounced losses in transmission and adsorptive capacity on pumping or heating. This suggests that the films are easily "annealed"; that is, the effective particle size in the deposit is increased, and therefore the transmission is decreased. The fact that no CO can be readsorbed on amorphous sites, *i.e.*, on those giving rise to the band at 2083 cm.<sup>-1</sup>, shows that these sites are most easily destroyed by the annealing process. These annealing effects represent the most serious disadvantage to the use of "flash-evaporated" films since the lack of detailed desorption-adsorption data has limited our ability to confirm certain band assignments fully.

# Thermoelectric Properties of the Molten Silver Nitrate–Sodium Nitrate System<sup>1</sup>

by Benson Ross Sundheim and Jordan D. Kellner

*Department of Chemistry, New York University, Washington Square, New York, New York 10003*  
(Received October 5, 1964)

Measurements of the final thermoelectric potential (in the Soret steady state) are reported for the system  $\text{AgNO}_3\text{--NaNO}_3$  over the range of composition between mole fraction of silver nitrate = 0.90 and 0.05. By combination of these results with the previously reported initial thermoelectric powers for this system, the various quantities of transports are calculated. The single ion entropy of the silver ion in pure silver nitrate is estimated at 19.0 e.u., leading to a value for the entropy of transport of the silver ion which is quite small. The reduced heat transported across a number fixed reference plane in an isothermal diffusion experiment (Dufour effect) is found to be everywhere positive, ranging from 1.1 to 3.6 kcal./mole and displaying a pronounced minimum near  $x = 0.7$ . No adequate basis for the theoretical interpretation of results of this kind seems to be extant.

Thermoelectric measurements in electrolytic solutions are of considerable interest because of the light they may be expected to shed on transport mechanisms.<sup>2</sup> Studies in fused salts are of particular interest because the absence of the usual dipolar solvent simplifies the system so as to present the ion motion in an especially direct way. Measurements of the initial thermoelectric potentials (uniform composition) have been previously reported<sup>3</sup> for the molten  $\text{AgNO}_3\text{--NaNO}_3$  system with silver electrodes. We report here on the determination of the final (Soret steady state) thermoelectric potentials for this system. By combining the two sets of data, the various quantities of transport of the system are obtained.

## Experimental Procedure

The design of the thermocell establishes a temperature gradient across a fine porosity sintered Pyrex disk whose upper surface is in contact with a large thermostated reservoir of the fused salt solution containing one electrode. The lower surface of the sintered disk is closed by a layer of silver which serves as the second electrode and which is thermostated independently. Considerable care is required to make a lower electrode which is adherent and leak-free and to which a good electrical connection can be made. First a coating of silver was laid down on the disk by vacuum evaporation. This was then reinforced by electroplating more silver on it. Finally, the sealing of

pinholes was accomplished by painting with a suspension of silver in amyl acetate, evaporating, and baking. A silver lead and a thermocouple junction were then mounted firmly against the surface and held in place by porcelain cement.

The temperature of the lower electrode was established by an air thermostat and that of the upper one maintained at a constant preselected difference from it by a differential thermocouple controller driving a saturable reactor which in turn operated the heater which was immersed in the reservoir. A thermocouple, corkscrew stirrer, and silver electrode completed the assembly in the upper compartment.

The temperature of the lower electrode was only approximately controlled since the steady-state thermopotentials are independent of the mean temperature over a range of at least 20°. The differential temperature controller maintained the temperature difference across the diaphragm to within several hundredths of a degree.

The dried salts were weighed, mixed mechanically, and introduced into the cell. The assembly was in-

(1) Abstracted in part from a dissertation submitted by J. D. Kellner to the Graduate School of Arts and Science of New York University in partial fulfillment of the requirements for the degree of Doctor of Philosophy.

(2) B. R. Sundheim, "Fused Salts," McGraw-Hill Book Co., Inc., New York, N. Y., 1964, Chapter 3.

(3) R. Schneebaum and B. R. Sundheim, *Discussions Faraday Soc.*, **32**, 197 (1961).

**Table I:** Quantities of Transport for  $\text{AgNO}_3\text{-NaNO}_3$  at  $310^\circ$ 

$x_1$	$\epsilon_{in}$		$\epsilon_{out}$		$Q_1^*$ kcal.	$Q_1^* - Q_2^*$ kcal.	$-\pi^*$ kcal.	$S_{\text{Ag}^+}$ e.u.	$\bar{S}_{\text{Ag}^+}$ e.u.	$-S^*_{\text{Ag}^+}$ e.u.	$\sigma$ mole/deg.
	$\mu\text{v./deg.}$	cal./deg.	$\mu\text{v./deg.}$	cal./deg.							
1.0	319	7.36	...	...	...	...	...	...	19.0	3.1	...
0.90	312	7.19	156	3.60	2.09	18.8	2.10	17.9	19.2	1.3	0.0310
0.75	322	7.42	205	4.74	1.56	4.69	2.76	19.0	19.6	0.5	0.00926
0.60	327	7.53	239	5.50	1.18	1.78	3.21	19.8	20.0	0.1	0.0043
0.50	331	7.64	248	5.72	1.12	1.12	3.34	20.0	20.4	0.3	0.00332
0.35	338	7.80	242	5.58	1.21	0.65	3.23	19.9	21.1	1.2	0.00276
0.20	345	7.96	215	4.96	1.75	0.44	2.89	19.3	22.2	2.9	0.00324
0.05	419	9.63	149	3.43	3.61	0.14	2.0	17.7	25.0	7.2	0.00555

roduced into the furnace and held at  $310^\circ$  to age the electrodes, since, at this point, there was always a large e.m.f., even at zero temperature gradient. After about 18 hr., this base e.m.f. was largely gone and the remaining asymmetry potential did not change much with time. After inserting the stirrer, thermocouple, and heater in the cell, the controller was energized and set for zero temperature difference. The cell was allowed to equilibrate for 1 hr. The silver-copper junctions from the electrodes were placed in an ice bath and the cell e.m.f. recorded to the nearest microvolt. Successive temperature differences were applied to the cell and, after each, the cell was returned to zero temperature difference to check the base e.m.f.

The cell e.m.f. *vs.* the temperature difference was plotted and the best straight line drawn through the points by the method of least squares. (No systematic curvature was found.) The temperature difference ranged from 1 to  $7^\circ$ . Seven different compositions were employed between 0.90 and 0.05 mole fraction of  $\text{AgNO}_3$ . The measurements were repeated several times to establish an index of precision.

The initial and final thermoelectric powers are given in Table I.

The experimental method is capable, in principle, of following the approach to the steady state as a function of time. The curves of e.m.f. *vs.* time were not used for the determination of quantities of transport because the initial temperature jump was not made sufficiently rapidly. However, their data were used as a rough check on the method by use of the characteristic time for the attainment of the Soret equilibrium. This quantity is the time required for the e.m.f. change to reach the fraction  $1/e$  of the steady-state value. It is possible to calculate the characteristic time from a knowledge of the ordinary diffusion coefficient and this value may be compared to the experimental one as a check on the internal consistency of the data. The approach to the steady state is exponential and is given by<sup>4</sup>

$$(D'/D)(1 - \exp[-t/\theta]) = s(t) \quad (1)$$

where  $D$  is the ordinary diffusion coefficient,  $\theta$  the characteristic time, and the measurement of the Soret coefficient,  $s$ , is made at the time  $t$ . The characteristic time is<sup>4</sup>

$$\theta = h^2/\pi^2 D \quad (2)$$

where  $h$  is the cell height, in this case the length of the path of the diffusing species in the cell. The time at which  $1/e$  of the temperature change is reached may be compared to the calculated  $\theta$ . The actual path length presumably is somewhat longer than the thickness of the disk due to the tortuosity of the path. It was concluded that these internal checks were satisfactory within the estimated experimental uncertainty, since the calculated value was 160 sec. and the experimental one was 180 sec.

## Discussion

The phenomenological equations describing this system may be presented in many ways.<sup>4</sup> Since there is only one independent composition variable, only one matter flux is required (and is associated with one independent heat of transport). We select the flux

$$\bar{J} = \bar{J}_1 - (x_1/x_2)\bar{J}_2 = cx_1(\bar{v}_1 - \bar{v}_2) \quad (3)$$

because it represents the relative motion of silver nitrate and sodium nitrate, because it is independent of the reference point chosen for the velocities, and because the heat of transport associated with it is a particularly useful quantity. [Here  $\bar{J}_1$  ( $\bar{J}_2$ ) is the flux of the neutral component  $\text{AgNO}_3$  ( $\text{NaNO}_3$ ).] The force conjugate to  $\bar{J}$  is  $-\bar{\nabla}_T\mu_1$ . The other fluxes used here are  $\bar{I}$ , the electrical current density, which is conjugate to  $-\nabla\phi$  (external electrical potential gradient) and  $\bar{q}'$ , the reduced heat flux (ref. 4, p. 26), which is

(4) H. J. V. Tyrrell, "Diffusion and Heat Flow in Liquids," Butterworth and Co., Ltd., London, 1961. A systematic survey of thermal diffusion with many references may be found here.

conjugate to  $-\bar{\nabla} \ln T$ . In terms of these variables, the equations are

$$\bar{J} = -L_{11}(\bar{\nabla}_T \mu_1 + Q^* \bar{\nabla} \ln T) - L_{12}(\bar{\nabla} \phi + \pi^* \bar{\nabla} \ln T) \quad (4)$$

$$\bar{I} = L_{21}(\bar{\nabla}_T \mu_1 + Q^* \bar{\nabla} \ln T) - L_{22}(\bar{\nabla} \phi + \pi^* \bar{\nabla} \ln T) \quad (5)$$

$$\bar{q}' = \bar{J}Q^* + \bar{I}\pi^* + [(L_{11} + L_{21})Q^* + L_{12} + L_{22}\pi^* - L_{33}]\bar{\nabla} \ln T \quad (6)$$

The phenomenological differential coefficients are

$$-T\varepsilon_i = -(\bar{\nabla} \phi / \bar{\nabla} \ln T)_{\bar{\nabla}_T \mu_1, \bar{I}} = tQ^* + \pi^* \quad (7)$$

$$-T\varepsilon_f = -(\bar{\nabla} \phi / \bar{\nabla} \ln T)_{\bar{J}, \bar{I}} = \pi^* \quad (8)$$

where  $t = (\bar{J}/\bar{I})_{\bar{\nabla}_T \mu_1, \bar{\nabla} \ln T} =$  Washburn transference number;  $Q^* = (\bar{q}/\bar{J})_{\bar{I}, \bar{\nabla} \ln T} =$  heat of transport  $= x_1 Q_1^* + x_2 Q_2^*$ ;  $\pi^* = (\bar{q}/\bar{I})_{\bar{J}, \bar{\nabla} \ln T} =$  Peltier heat;  $\varepsilon_i =$  initial thermoelectric power;  $\varepsilon_f =$  final (Soret steady state) thermoelectric power. See the Glossary for fuller definitions and for important relations.

In the  $\text{AgNO}_3\text{-NaNO}_3$  system it has been found<sup>5a</sup> that the potential of a concentration cell between silver electrodes

$$\Delta \phi = -(1/\mathfrak{F}) \int_1^{\text{II}} t \bar{\nabla}_T \mu_1 \cdot d\bar{r} \quad (9)$$

is represented adequately over the entire concentration range by

$$\Delta \phi = (1/\mathfrak{F})(\mu_1^{\text{II}} - \mu_1^{\text{I}}) \quad (10)$$

so that in this particular case  $t = -1$  and is independent of composition. Consequently, here

$$\varepsilon_i = -\pi^*/T \quad (11)$$

$$(\varepsilon_f - \varepsilon_c) = Q^*/T$$

The experimental values of these quantities are shown as functions of composition in Figure 1.

The Peltier heat can be related to the transported entropy<sup>2</sup> of the silver ion by constructing an entropy balance at the electrode. The entropy absorbed in the reaction at the electrode is  $S_{\text{Ag}} - \bar{S}_{\text{Ag}^+} - \bar{S}_{e(\text{Ag})}$  where  $S_{\text{Ag}}$  is the entropy of silver metal, which is 14.35 cal. mole<sup>-1</sup> deg.<sup>-1</sup> at this temperature.<sup>6</sup>  $\bar{S}_{e(\text{Ag})}$  is the partial molal entropy of the electron in silver metal and  $\bar{S}_{\text{Ag}^+}$  is the same quantity for the silver ion in the fused salt.

The entropy transported away from the electrode is  $-S^*_{\text{Ag}^+} - S^*_{e(\text{Ag})}$  where  $S^*_{\text{Ag}^+}$  is the entropy of transport of the silver ion and  $S^*_{e(\text{Ag})}$  is the entropy of transport of the electron in silver metal. Summing these terms and equating to the Peltier heat

$$\begin{aligned} \pi^*/T &= S_{\text{Ag}} - \bar{S}_{\text{Ag}^+} - \bar{S}_{e(\text{Ag})} - S^*_{\text{Ag}^+} - S^*_{e(\text{Ag})} \quad (12) \\ &= S_{\text{Ag}} - \bar{S}_{\text{Ag}^+} - \bar{S}_{e(\text{Ag})} \end{aligned}$$

where  $\bar{S}_{\text{Ag}^+}$  is the transported entropy of the silver ion, equal to the sum of  $\bar{S}_{\text{Ag}^+}$  and  $S^*_{\text{Ag}^+}$  and where  $\bar{S}_{e}$  is the "transported entropy" of the electron, equal to the sum of  $\bar{S}_e$  and  $S^*_e$ .

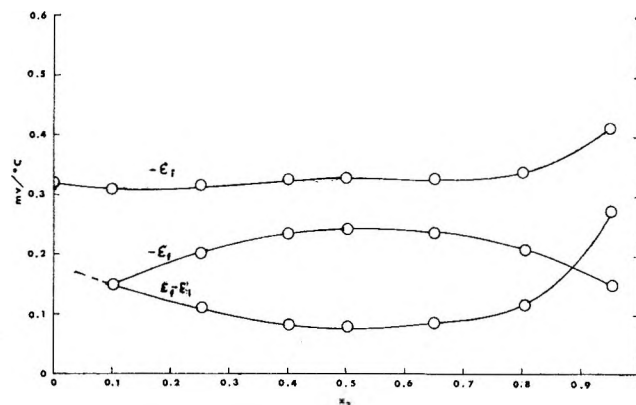


Figure 1. The initial and final thermoelectric powers as a function of composition.

The transported entropy of the electron in silver metal has been estimated<sup>7</sup> to be virtually zero, *i.e.*, smaller than the uncertainty in the thermocell e.m.f. Thus we have

$$-\varepsilon_f = S_{\text{Ag}} - \bar{S}_{\text{Ag}^+} - S^*_{\text{Ag}^+} \quad (13)$$

By estimating the value of the partial ionic entropy of silver ion and combining it with the experimentally obtained steady-state thermocell e.m.f., a value for the entropy of transfer of the silver ion can be obtained.

The entropy of a single ion is not experimentally accessible but if the ions are similar except for the sign of the charge, one could estimate it by taking one-half of the entropy of  $\text{AgNO}_3$  obtained from heat capacity measurements and third-law calculations.<sup>2,8</sup> In the case of a polyatomic ion such as  $\text{NO}_3^-$ , a correction term first must be subtracted to allow for the entropy of rotation and vibration. This correction is reduced somewhat due to restriction of rotation of the anion in the fused salt.<sup>9</sup> These considerations lead to a value

(5) (a) F. R. Duke, R. W. Laity, and D. Owens, *J. Electrochem. Soc.*, **104**, 299 (1957); (b) R. W. Laity, *J. Am. Chem. Soc.*, **79**, 1849 (1957).

(6) K. K. Kelly, U. S. Bureau of Mines Bulletin 584, U. S. Government Printing Office, Washington, D. C., 1960.

(7) M. I. Temkin and A. Z. Khoroshin, *Zh. Fiz. Khim.*, **26**, 500 (1952).

(8) C. Wagner, *Ann. Physik.*, **3**, 639 (1929).

(9) K. S. Pitzer, *J. Phys. Chem.*, **65**, 147 (1961).

of 19.7 e.u. for the internal entropy of the nitrate ion. The difference in mass between the two ions (appearing in the translational entropy) may be taken into account by adding  $3/2 \ln [M_{\text{Ag}^+}/M_{\text{NO}_3^-}]$  to the entropy of silver nitrate. A value of 19.0 e.u. for the entropy of  $\text{Ag}^+$  in pure  $\text{AgNO}_3$  finally is obtained. The entropy of  $\text{Ag}^+$  in solution is estimated at the various concentrations employed by assuming ideal entropy of mixing, *i.e.*, by subtracting  $R \ln x_1$ . Table I shows the values calculated in this way for the entropy of transfer of the silver ion at each experimental composition.

It may be noted that the uncertainties in some of these corrections will affect the absolute magnitude of the calculated entropy of transfer, perhaps to the extent of  $\pm 1$  e.u., but may be expected to have a minor effect on the relative values. The values are small over the greater part of the concentration range although they rise at the extremes. Pitzer<sup>9</sup> has suggested that  $S_i^*$  may be generally near zero in fused salts.

We now turn to the quantity  $Q^*$ . If we consider the isothermal, zero current interdiffusion of  $\text{AgNO}_3$  and  $\text{NaNO}_3$  in a number fixed reference frame ( $\bar{J}_1 = -\bar{J}_2$ ), we find

$$\begin{aligned} \bar{q}' &= \bar{J}Q^* = \bar{J}_1Q_1^* + \bar{J}_2Q_2^* = \bar{J}_1Q_1^*/x_2 \quad (14) \\ &= \bar{J}_1(Q_1^* - Q_2^*) \end{aligned}$$

since  $x_1Q_1 + x_2Q_2 = 0$ . In this special case since  $\bar{J} = \bar{J}_1/x_2$  we see that

$$Q^* = Q_1^* = (Q_1^* - Q_2^*)/x_2 \quad (15)$$

The quantities  $Q^*$  and  $Q_1^* - Q_2^*$  are shown as functions of composition in Figure 2. The latter quantity is the net (reduced) heat transported across the number fixed reference plane in an isothermal diffusion experiment (Dufour effect).  $Q^*$  is everywhere positive, its magnitude ranging from about 1.1 to 3.6 kcal. for the concentrations studied. It is very nearly symmetrical about  $x_1 = 0.5$ . [The curve of  $Q^*$  vs.  $x_1$  is fit quite well by  $Q = \ln x_1 + \ln(1 - x_1)$ .]  $Q^*/x_2 = Q_1^* - Q_2^*$  has a more pronounced minimum and is skewed toward  $x_1 \rightarrow 1$ . This quantity has been determined for a number of aqueous electrolytic solutions and the dependence on concentration generally observed resembles that found here. There does not appear to be any really satisfactory basis for interpreting the shape of this curve.

The Soret effect reflects a difference in mobilities in a thermal field, the more rapidly moving species accumulating in the hotter zone.<sup>10</sup> It is interesting that the mobilities of the cations in this system are approximately equal to each other in an electric field.<sup>5</sup>

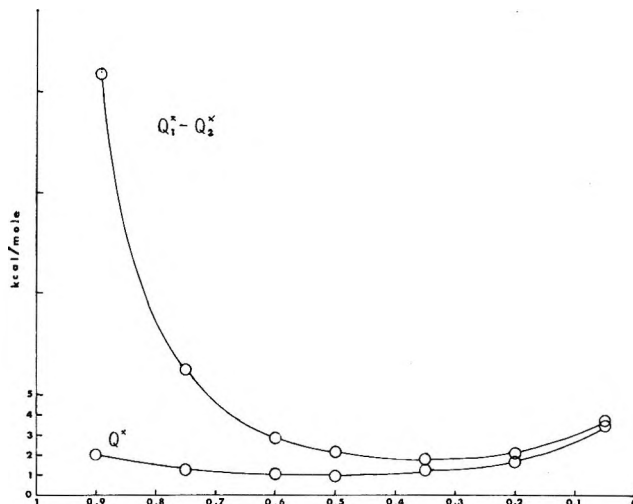


Figure 2. The quantities  $Q^*$  and  $Q_1^* - Q_2^*$  (reduced heat transported across a number fixed reference plane in an isothermal diffusion experiment).

Fundamental theories of transport properties in liquids, for example those expressed in terms of perturbations to the equilibrium distribution functions, have not reached the point of being applicable to specific systems. A less sophisticated but more pictorial model views transport as taking place by a series of activated transitions. Since the loci of the activation are distributed across the temperature field, differences in the net entropy flux arise. In its original form,<sup>11a,b</sup> it utilized implicitly a quasi-lattice model of the liquid state, which perhaps is better suited to fused salt systems than to other liquids. In a simplified formulation,<sup>11c,d</sup> it is found that

$$Q_1^* - Q_2^* = q_{H_1} - q_{H_2} \quad (16)$$

where  $q_{H_i}$  is the energy required for the breaking free of the given species from its surroundings. By assuming regular solutions with no volume effects it may be shown that

$$Q_1^* - Q_2^* = (\gamma n f / 2) (\epsilon_{11}^{1/2} - \epsilon_{22}^{1/2}) (x_1 \epsilon_{11}^{1/2} + x_2 \epsilon_{22}^{1/2}) \quad (17)$$

where  $\epsilon_{11}$  is the energy of activation of a molecule and  $\epsilon_{12}^2 = \epsilon_{11}\epsilon_{22}$ . In all simplified theories of this sort, the quantity  $Q^*/x_2$  is found to be only weakly dependent on the concentration.

(10) H. S. Green, "Molecular Theory of Fluids," Elsevier Publishing Co., Amsterdam, 1952.

(11) (a) K. Wirtz, *Naturwiss.*, **27**, 369 (1950); (b) K. Wirtz, *Physik. Z.*, **44**, 221 (1943); (c) I. Prigogine, L. de Broickere, and R. Amand, *Physica*, **16**, 577, 851 (1950); (d) K. Denbigh, *Trans. Faraday Soc.*, **48**, 1 (1952); (e) K. F. Alexander, *Z. physik. Chem.*, **203**, 204 (1954).

In passing to electrolytic solutions, considerations of ionic interactions in dilute nonionic solvents suggest<sup>12</sup> that the heat of transport should vary with  $m^{1/2}$ . The applicability of this approach to fused salts seems rather remote.

The positive value of the Soret coefficient in the  $\text{AgNO}_3\text{-NaNO}_3$  system means<sup>13</sup> that a silver ion is more difficult to remove from its environment than is a sodium ion. The greater ionic interactions in a silver nitrate melt as compared with those in a sodium nitrate melt are generally attributed<sup>14</sup> to the higher polarizability of the silver ion. The enthalpy of mixing in this system is given by the expression<sup>15</sup>

$$\Delta H_m = x_1 x_2 (677 - 156x_1) \text{ cal./mole}$$

This is a curve falling to zero at the extremes with a maximum near  $x = 0.5$ , quite different in shape and magnitude from that of  $Q^*$  vs.  $x_1$ . Thus arguments directed along the lines of interaction energies alone are not helpful.

It is remarkable that we know so little about the mechanisms of such elementary electrochemical transport processes. Further speculation must wait upon the accumulation of data on other systems.

*Acknowledgment.* It is a pleasure to acknowledge assistance to this work from the Office of Naval Research (Contract Nonr-285-37).

### Glossary

$\varepsilon_f$	Final thermoelectric power = $[d\phi/dT]_{J,I}$
$\varepsilon_{in}$	Initial thermoelectric power = $[d\phi/dT]_{T,I}$
$T$	Absolute temperature
$R$	Gas constant, 1.987 cal./deg. mole
$\pi$	Peltier heat $(q/I)_{J,\nabla \ln T}$
$Q^*$	Heat of transport = $(q/J)_{T,I}$
$x_1, x_2$	Mole fraction of $\text{AgNO}_3, \text{NaNO}_3$
$\bar{S}_{\text{Ag}^+}$	Transported entropy of $\text{Ag}^+$
$S^*_{\text{Ag}^+}$	Entropy of transport of $\text{Ag}^+$
$\bar{S}_{\text{Ag}^+}$	Partial molar entropy of $\text{Ag}^+$
$\bar{S}_{\text{Ag}^+} = \bar{S}^{\circ}_{\text{Ag}^+} - R \ln x_1$	
$\sigma$	Soret coefficient in moles/deg. = $\frac{1}{x_2} \left[ \frac{d \ln x_1}{dT} \right]_f$
$\bar{S}^{\circ}_{\text{Ag}^+}$	Partial molar entropy of $\text{Ag}^+$ when $x_1 = 1$ (pure salt)
$S^*_{\text{AgNO}_3} = S^*_{\text{Ag}^+} + S^*_{\text{NO}_3^-}$	
$S^*_{\text{NaNO}_3} = S^*_{\text{Na}^+} + S^*_{\text{NO}_3^-}$	
$\pi/T = -\varepsilon_f = S_{\text{Ag}} - \bar{S}_{\text{Ag}^+} - \bar{S}_{e(\text{Ag})} = S_{\text{Ag}} - S_{\text{Ag}} - S^*_{\text{Ag}^+}$	
$Q^* = T(\varepsilon_{in} - \varepsilon_f)$	
$Q_2^* = (-x_1/x_1)Q_1^*$	
$J_1$	Flux of $\text{AgNO}_3$ (moles/cm. <sup>2</sup> sec.)
$J_2$	Flux of $\text{NaNO}_3$ (moles/cm. <sup>2</sup> sec.)
$I$	Electrical current flux (faradays cm. <sup>2</sup> /sec.)
$q$	Reduced heat flux = second law heat flux = convected enthalpy
$J = J_1 - (x_1/x_2)J_2 = x_1 C(V_1 - V_2)$	
$t$	Washburn transport number = $(J/I)_{T,\mu}$
$M_i$	Mass of $i$ in atomic weight scale in a number fixed reference: $J = J_1/x_2; Q^* = Q_1^* = (Q_1^* - Q_2^*)x_2$

(12) E. Helfand, *J. Chem. Phys.*, **32**, 857 (1960).

(13) See ref. 4, pp. 272-290.

(14) J. G. Janz, *J. Chem. Educ.*, **39**, 59 (1962).

(15) O. J. Kleppa, R. B. Clark, and L. S. Hersch, *J. Chem. Phys.*, **35**, 175 (1961).



## Heat Capacities and Thermodynamic Properties of Globular Molecules.

XIII. Transition and Fusion of Pentaerythrityl Chloride and Bromide, Transition of Pentaerythrityl Iodide<sup>1a</sup>by H. Lawrence Clever, Wen-Kuei Wong, and Edgar F. Westrum, Jr.<sup>1b</sup>*Department of Chemistry, University of Michigan, Ann Arbor, Michigan (Received October 5, 1964)*

The heat capacities of crystalline pentaerythrityl iodide and of crystalline and liquid pentaerythrityl chloride and bromide above 290°K. have been determined by adiabatic calorimetry. The high entropies of fusion, 14.45 and 15.42 cal./ (mole °K.) found for pentaerythrityl chloride and bromide, respectively, indicate that these halides have no plastic crystal phase at atmospheric pressure. However, at temperatures corresponding to the same fraction of their respective melting points all three compounds show broad  $\lambda$ -anomalies in their heat capacity curves. These involve excess entropies of less than 1 cal./ (mole °K.).

Both pentaerythritol,<sup>2,3</sup> C(CH<sub>2</sub>OH)<sub>4</sub>, and pentaerythrityl fluoride,<sup>4</sup> C(CH<sub>2</sub>F)<sub>4</sub>, are globular molecules with apparent first-order solid-solid transitions and with the low entropies of fusion characteristic of plastic crystals.<sup>5</sup> The entropy increments of the transitions can be quantitatively accounted for by the changes in molecular symmetry.<sup>4a</sup> Although heat capacities of pentaerythrityl chloride, bromide, and iodide reveal no first-order transitions between 5 and 300°K., regions over which the heat capacity behaved anomalously and somewhat irreproducibly occurred near 235° for the chloride and near 290° for the bromide.<sup>6</sup> To determine whether or not these compounds are plastic crystals and to provide thermal data for the correlation of the thermodynamics of pentaerythritol<sup>3</sup> and of pentaerythrityl fluoride,<sup>4</sup> heat capacity measurements have been extended through fusion except for the iodide. Its tendency to decompose precluded accurate measurements above 423°K.

**Experimental**

The previously described Mark IV intermediate range thermostat,<sup>7</sup> a silver calorimeter (laboratory designation W-22), and a capsule-type, platinum resistance thermometer (laboratory designation A-7) were used. The quasi-adiabatic technique<sup>8</sup> and the computer program<sup>9</sup> for the conversion of data to thermodynamic functions have also been described previously. The

pentaerythrityl chloride, bromide, and iodide were those previously characterized for the earlier low-temperature work.<sup>6</sup> Given below for each sample are: its (a) mass *in vacuo*, (b) gram formula mass (g.f.m.), and (c) per cent of the total heat capacity (*i.e.*, that of calorimeter, sample, thermometer, and heater assembly) contributed by the compound.

	a. g.	b. g.	c. %
Pentaerythrityl chloride	71.6714	209.93	67-72
Pentaerythrityl bromide	66.4573	387.76	50-59
Pentaerythrityl iodide	86.7454	575.74	48-52

(1) (a) This research was supported in part by the U. S. Atomic Energy Commission. (b) To whom correspondence concerning this work should be directed.

(2) (a) I. Nitta and T. Watanabé, *Bull. Chem. Soc. Japan*, **13**, 28 (1938); (b) I. Nitta, S. Seki, and M. Momotani, *Proc. Japan Acad.*, **26** [9], 25 (1950); (c) I. Nitta, S. Seki, M. Momotani, K. Suzuki, and S. Nakagawa, *ibid.*, **26** [10], 11 (1950); (d) I. Nitta, T. Watanabé, S. Seki, and M. Momotani, *ibid.*, **26** [10], 19 (1950).

(3) E. F. Westrum, Jr., and D. H. Payne, to be published.

(4) (a) E. F. Westrum, Jr., and D. H. Payne, *J. Phys. Chem.*, to be submitted; (b) J. C. Trowbridge and E. F. Westrum, Jr., *ibid.*, **68**, 255 (1964).

(5) J. Timmermans, *Phys. Chem. Solids*, **18**, 1 (1961).

(6) D. H. Payne and E. F. Westrum, Jr., *J. Phys. Chem.*, **66**, 748 (1962).

(7) E. F. Westrum, Jr., and J. C. Trowbridge, to be published.

(8) E. F. Westrum, Jr., J. B. Hatcher, and D. W. Osborne, *J. Chem. Phys.*, **21**, 419 (1953).

(9) B. H. Justice, Appendix to Ph.D. Dissertation, University of Michigan; *cf.* U. S. Atomic Energy Commission Report TID-12722, 1961.

Table I: Heat Capacity Determinations on Pentaerythrityl Halides<sup>a</sup>

<i>T</i>	<i>C<sub>s</sub></i>	<i>T</i>	<i>C<sub>s</sub></i>	<i>T</i>	<i>C<sub>s</sub></i>	<i>T</i>	<i>C<sub>s</sub></i>	<i>T</i>	<i>C<sub>s</sub></i>	<i>T</i>	<i>C<sub>s</sub></i>		
Pentaerythrityl chloride						Pentaerythrityl bromide							
—Series I—						—Series I—						—Series VII—	
294.45	47.46	367.51	2789	359.55	83.97	304.54	54.33	433.03	7730	310.70	55.96		
301.58	49.47	367.75	2033	362.82	152.1	315.71	55.93	433.18	4460	319.74	58.17		
—Series II—						—Series II—						—Series IV—	
299.63	48.05	368.39	718	365.07	364	324.55	55.33	435.75	162.1	328.73	56.14		
309.63	49.06	373.53	65.72	366.44	953	333.52	55.21	Fusion run A		337.81	55.77		
319.46	50.45	382.67	66.42	367.02	1930	342.58	55.96	440.32	74.33	347.03	56.20		
329.08	52.53	—Series IV—			367.33	3280	351.52	56.36	444.88	74.45	356.34	56.90	
338.70	55.41	Fusion run A			367.53	4880	—Series II—		449.88	74.81	365.56	57.62	
348.26	58.28	—Series V—			367.66	6740	358.07	56.82	454.87	75.19	266.92	46.52	
357.28	69.72	Fusion run B			369.05	263	367.24	58.13	459.84	75.73	274.95	47.91	
363.52	190.5	—Series VI—			372.75	65.68	376.28	58.83	—Series V—		282.78	49.54	
—Series III—						—Series III—						—Series VIII—	
355.74	65.12	307.71	48.53	382.73	66.50	385.36	59.76	Fusion run B		268.38	46.13		
362.71	154	316.74	49.76	387.70	66.85	394.49	60.99	—Series VI—		276.71	48.72		
365.82	494	325.58	50.86	392.64	67.27	403.59	62.46	Fusion run B		285.13	51.09		
366.87	1085	334.41	53.81	397.60	67.54	412.59	63.42	—Series VI—		293.47	52.36		
367.27	1950	343.01	58.80	—Series VIII—		421.68	64.88	Fusion run B		301.89	53.91		
Pentaerythrityl iodide						Fusion run C						—Series IX—	
—Series I—						—Series IV—						—Series IX—	
258.58	48.79	388.29	62.15	332.59	53.79	426.67	71.80	428.28	87.52	310.56	55.69		
295.18	49.98	398.03	61.84	Enthalpy run A		431.78	628	431.84	828	319.31	58.08		
304.26	51.10	407.79	62.64	410.12	62.53	432.67	3850	432.58	5,190	328.04	56.08		
312.85	52.10	417.47	63.30	419.52	63.48	432.85	6160	432.82	3,850	338.82	55.68		
321.51	53.12	—Series III—			—Series V—		432.95	9310	433.05	5,530	345.65	55.57	
330.24	54.32	338.99	54.97	—Series V—		—Series III—		433.18	16,400	354.38	56.24		
—Series II—						—Series III—						—Series IX—	
335.43	54.47	347.63	56.29	354.09	57.29	433.23	30,700	435.46	189.2	310.56	55.69		
344.08	56.65	356.34	58.50	358.40	58.12	433.85	6160	—Series VI—		319.31	58.08		
351.64	57.54	365.01	60.73	362.65	58.74	432.95	9310	Fusion run B		328.04	56.08		
360.45	59.52	371.17	60.95	366.85	60.20	—Series III—		Fusion run B		336.82	55.68		
369.37	61.08	375.09	61.41	371.03	60.67	—Series III—		Fusion run B		345.65	55.57		
378.64	61.88	379.16	61.75	380.07	62.27	—Series III—		Fusion run B		354.38	56.24		
—Series II—						—Series III—						—Series IX—	
335.43	54.47	383.20	61.74	391.78	61.49	—Series III—		Fusion run B		310.56	55.69		
344.08	56.65	387.42	62.18	—Series V—		—Series III—		Fusion run B		319.31	58.08		
351.64	57.54	—Series III—			—Series V—		—Series III—		Fusion run B		328.04	56.08	
360.45	59.52	338.99	54.97	354.09	57.29	—Series III—		Fusion run B		336.82	55.68		
369.37	61.08	347.63	56.29	358.40	58.12	—Series III—		Fusion run B		345.65	55.57		
378.64	61.88	356.34	58.50	362.65	58.74	—Series III—		Fusion run B		354.38	56.24		
—Series II—						—Series III—						—Series IX—	
335.43	54.47	365.01	60.73	366.85	60.20	—Series III—		Fusion run B		310.56	55.69		
344.08	56.65	371.17	60.95	371.03	60.67	—Series III—		Fusion run B		319.31	58.08		
351.64	57.54	375.09	61.41	380.07	62.27	—Series III—		Fusion run B		328.04	56.08		
360.45	59.52	379.16	61.75	391.78	61.49	—Series III—		Fusion run B		336.82	55.68		
369.37	61.08	383.20	61.74	—Series V—		—Series III—		Fusion run B		345.65	55.57		
378.64	61.88	387.42	62.18	—Series V—		—Series III—		Fusion run B		354.38	56.24		

<sup>a</sup> Units: cal., g.f.m., °K.

All calculations are based upon the thermochemical calorie defined as 4.1840 j. and an ice point of 273.15°K.

## Results and Discussion

**Heat Capacities.** The heat capacities at saturation pressure, corrected for curvature, are listed in chronological order in Table I and depicted in Figure 1 along with earlier data on pentaerythrityl fluoride<sup>4</sup> over the common range of measurement. These data accord with the low-temperature results to within  $\pm 0.1\%$  except in the inherently irreproducible  $\lambda$ -regions. Nitta and Seki<sup>10</sup> have measured the vapor pressure of both solid and liquid pentaerythrityl bromide. No vapor pressure data on solid pentaerythrityl chloride or iodide

were found, but Mooradian and Cloke<sup>11</sup> report that the chloride boils at 100°C. at 12 torr pressure. Assuming Trouton's rule for pentaerythrityl chloride and using the pentaerythrityl bromide vapor pressures, the vaporization adjustments were found to be less than 0.02% for these substances and, therefore, were not made. The heat capacity measurements were extended about 30° into the liquid region for both pentaerythrityl chloride and bromide. Four or five series of runs were made through the solid-liquid transitions.

(10) I. Nitta and S. Seki, *J. Chem. Soc. Japan*, 62, 581 (1941).(11) A. Mooradian and J. B. Cloke, *J. Am. Chem. Soc.*, 67, 942 (1945).

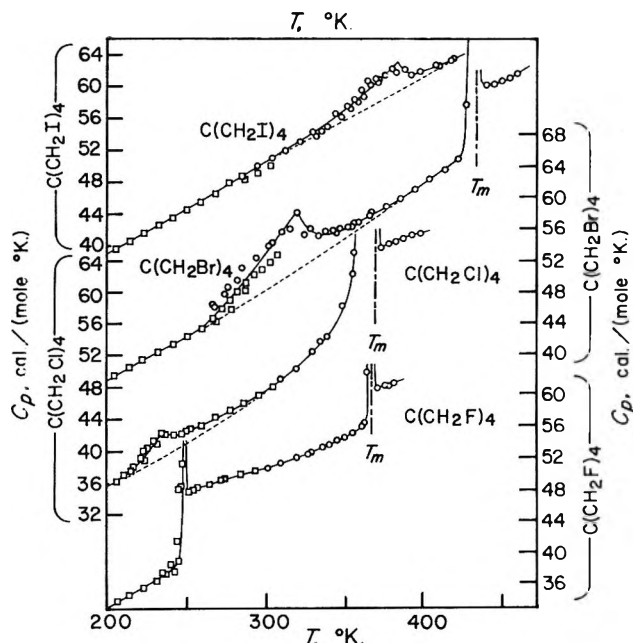


Figure 1. Intermediate-temperature heat capacities of the pentaerythrityl halides. The cryogenic calorimetric data<sup>4,6</sup> are represented by squares, those obtained in the intermediate temperature thermostat by circles.

**Thermodynamic Functions.** The derived<sup>9</sup> thermodynamic properties have been presented in Tables II–IV at selected temperatures. These values are predicated mainly on the 273.15°K. values of Payne and Wes-

Table II: Thermodynamic Properties of Pentaerythrityl Chloride<sup>a</sup>

$T$	$C_p$	$S^\circ$	$H^\circ - H^\circ_0$	$-(G^\circ - H^\circ_0)/T$
Crystal I				
273.15	44.68	57.51	7,293	30.81
298.15	47.44	61.54	8,444	33.22
300	47.67	61.84	8,532	33.40
310	49.00	63.42	9,015	34.34
320	50.56	65.00	9,512	35.28
330	52.56	66.59	10,027	36.20
340	55.37	68.20	10,567	37.12
350	59.56	69.86	11,140	38.03
360	65.83	71.62	11,766	38.94
368.23	...	72.39 <sup>b</sup>	12,037 <sup>b</sup>	39.70 <sup>b</sup>
Liquid				
368.23	...	86.84 <sup>b</sup>	17,357 <sup>b</sup>	39.70 <sup>b</sup>
370	65.38	87.15	17,473	39.93
380	66.29	88.90	18,131	41.19
390	67.02	90.64	18,800	42.44
400	67.59	92.34	19,471	43.66

<sup>a</sup> Units: cal., g.f.m., °K. <sup>b</sup> Assuming fusion to be isothermal.

trum<sup>6</sup> but in some instances are adjusted slightly as required by the present data. The probable error of the heat capacity data is considered to be about 0.15% and that of the functions 0.1%. An additional digit beyond those which are significant has occasionally been given for internal consistency and to permit interpolation.

Table III: Thermodynamic Properties of Pentaerythrityl Bromide<sup>a</sup>

$T$	$C_p$	$S^\circ$	$H^\circ - H^\circ_0$	$-(G^\circ - H^\circ_0)/T$
Crystal I				
250	42.32	61.42	6,745	34.44
260	43.60	63.10	7,174	35.51
270	45.25	64.78	7,618	36.56
273.15	45.85	65.31	7,762	36.89
280	47.33	66.46	8,081	37.60
290	49.86	68.16	8,566	38.63
298.15	52.24	69.58	8,982	39.45
300	52.82	69.90	9,079	39.64
310	56.12	71.69	9,624	40.64
320	59.63	73.53	10,202	41.64
340	55.52	77.00	11,328	43.68
350	56.07	79.25	11,886	45.29
360	56.98	80.75	12,451	46.16
370	58.10	82.25	13,026	47.04
380	59.19	83.75	13,613	47.93
390	60.34	85.25	14,210	48.81
400	61.65	86.75	14,820	49.70
410	63.08	88.00	15,444	50.33
420	64.91	89.75	16,083	51.46
425	66.65	90.25	16,411	51.64
433.45	...	91.53	17,016	52.27
Liquid				
433.45	...	106.95	23,700	52.27
435	74.17	107.22	23,757	52.60
440	74.29	108.07	24,128	53.23
450	74.83	109.74	24,874	54.46
460	75.78	111.39	25,626	55.68

<sup>a</sup> Units: cal., g.f.m., °K.

**Melting.** Experiments in evacuated glass tubes protected from direct light showed that pentaerythrityl iodide decomposes below its reported melting point of 506°K. Visible evidence of some decomposition was apparent at temperatures as low as 488–491°K. Consequently, to prevent possible damage to the silver calorimeter no heat capacity measurements were made above 423°K. Series III and VI for both chloride and bromide involved seven to nine short runs to characterize melting temperature and purity. The amount

**Table IV:** Thermodynamic Properties of Pentaerythrityl Iodide<sup>a</sup>

<i>T</i>	<i>C<sub>s</sub></i>	<i>S</i> <sup>o</sup>	<i>H</i> <sup>o</sup> - <i>H</i> <sup>o</sup> <sub>0</sub>	-( <i>G</i> <sup>o</sup> - <i>H</i> <sup>o</sup> <sub>0</sub> )/ <i>T</i>
260	45.47	69.20	7,648	39.79
270	46.68	70.91	8,109	40.87
273.15	47.06	71.48	8,256	41.26
280	47.88	72.63	8,581	41.98
290	49.11	74.34	9,067	43.08
298.15	50.12	75.75	9,471	43.98
300	50.35	76.03	9,564	44.15
310	51.62	77.73	10,073	45.24
320	52.94	79.38	10,596	46.26
330	54.38	81.00	11,133	47.26
340	55.97	82.66	11,685	48.29
350	57.71	84.27	12,253	49.26
360	59.49	85.92	12,839	50.26
370	61.18	87.58	13,442	51.25
380	62.67	89.25	14,062	52.25
385	63.38	90.06	14,377	52.72
390	61.51	90.86	14,688	53.20
395	61.59	91.65	14,995	53.68
400	61.98	92.43	15,304	54.16
410	62.77	93.97	15,928	55.12
420	63.54	95.49	16,559	56.06

<sup>a</sup> Units: cal., g.f.m., °K.**Table V:** Enthalpy of Melting of Pentaerythrityl Chloride and Bromide<sup>a</sup>

Designation	Number of runs	<i>H</i> <sub>370</sub> - <i>H</i> <sub>360</sub>	$\Delta H_m$
Pentaerythrityl chloride <sup>b</sup>			
Series III	7	5701	5313
Run A	1	5701	5312
Run B	1	5716	5327
Series VI	9	5645	5257 <sup>c</sup>
Run C	1	5715	5327
			Mean = 5320 ± 7
			$\Delta S_m = 14.45$
Pentaerythrityl bromide <sup>d</sup>			
<i>H</i> <sub>425</sub> - <i>H</i> <sub>415</sub>			
Series III	8	7345	6680
Run A	1	7346	6682
Run B	1	7346	6681
Series VI	8	7358	6693
			Mean = 6684 ± 4.5
			$\Delta S_m = 15.42$

<sup>a</sup> Units: cal., g.f.m., °K. <sup>b</sup>  $\Delta H_m$  for pentaerythrityl chloride includes an excess (premelting) enthalpy of 177 cal. between 330 and 360°K. <sup>c</sup> Rejected from average by Chauvenet criterion. <sup>d</sup>  $\Delta H_m$  for pentaerythrityl bromide includes an excess enthalpy (premelting) of 8 cal. between 410 and 425°K.

of liquid-soluble, solid-insoluble impurity can be estimated from a plot of the apparent melting temperature, *T*, against the fraction melted, 1/*F*. The temperature corresponding to 1/*F* = 1 is the triple point *T*<sub>1</sub> of the calorimetric sample, and the temperature corresponding to 1/*F* = 0 is the triple point *T*<sub>m</sub> of the pure sample. The mole fraction impurity, *N*<sub>2</sub>, is given by

$$N_2 = \frac{\Delta H_m(T_m - T_1)}{RT_m^2}$$

The respective values of *T*<sub>1</sub>, *T*<sub>m</sub>, and *N*<sub>2</sub> are 367.76, 368.23, and 0.0093 for pentaerythrityl chloride and 433.25, 433.45, and 0.033 for pentaerythrityl bromide.

*Enthalpy and Entropy of Melting.* The values of the enthalpy of fusion for pentaerythrityl chloride and bromide are summarized in Table V. Since the respective entropies of melting for the chloride and bromide are 14.46 and 15.42 cal./mole °K., neither crystal can be considered plastic. Nitta and Seki<sup>10</sup> obtain a value of 12.7 cal./mole °K. for the entropy of melting from their vapor pressure data on pentaerythrityl bromide. The accord is probably within the bounds of their uncertainties since very accurate vapor pressure data on both phases are needed to give precise values of the derived quantity.

Over ranges where the heat capacities of these three pentaerythrityl halides exhibited anomalous and somewhat nonreproducible behavior, thermal equilibration typically required several hours. Table VI presents the temperature range, peak temperature, and excess enthalpy and entropy for each. Each of the transformations appears at nearly the same fraction of the respective fusion temperature.

**Table VI:** Enthalpy and Entropy of Transformation<sup>a</sup>

Pentaerythrityl halide	<i>T</i> <sub>1</sub>	<i>T</i> <sub>2</sub>	<i>T</i> <sub>t</sub>	<i>T</i> <sub>t</sub> / <i>T</i> <sub>m</sub>	$\Delta H_t$	$\Delta S_t$
Chloride	200	280	235	0.64	61.5	0.259
Bromide	254	400	320	0.74	328	1.04
Iodide	300	420	385	0.76	151	0.412

<sup>a</sup> Units: cal., g.f.m., °K.

For example, the melting points of pentaerythrityl chloride and fluoride differ by only 1° and their transition temperatures differ by only 15°. However, the fluoride exhibits an apparent first-order transition char-

acterized by an entropy increment of 12.66 cal./mole °K.), while the chloride transformation is represented by a broad  $\lambda$ -type curve with excess entropy of only 0.26 cal./mole °K.). The sums of the transformation and melting entropy increments for the pentaerythrityl fluoride and chloride are 16.01 and 14.72 cal./mole °K.), respectively. The heat capacity measurements were made on small crystals of the pentaerythrityl chloride and iodide, and on the fused bromide. Although the effect of sample subdivision on the enthalpy of transformation is not known, the better defined thermodynamic state of the bromide may account for its relatively high  $\Delta H_t$  and  $\Delta S_t$  values.

The dipole moment data given in Table VII provide supplementary evidence that the pentaerythrityl fluoride differs significantly from the other halides. Since the rotational freedom of the  $-\text{CH}_2\text{X}$  group is increasingly hindered as the nonbonding radius of the halogen atom increases, and since a nonzero dipole moment can be expected only for an unsymmetrical conformation in

which the C-X bond moments reinforce one another, a dipole moment should exist for only those molecules in which the halogen atom is small and thus for which rotation of the  $-\text{CH}_2\text{X}$  group is possible. The maximum dipole moment will occur when the bond moments of the  $-\text{CH}_2\text{X}$  groups can assume parallel positions. According to Le Fèvre, Le Fèvre, and Smith<sup>16</sup> models of pentaerythrityl chloride and bromide show the  $-\text{C}-\text{H}_2\text{X}$  groups to be so interlocked that they cannot rotate. Furthermore, Thompson and Sweeney<sup>17</sup> indicate that it is sterically impossible for C-X bonds to be parallel in any of the pentaerythrityl halides except the fluoride. However, postulating a normal threefold rotation barrier, they predict a dipole moment of 3.62 D. for the fluoride and 3.71 D. for the chloride. The fact that the value for the fluoride is significantly less than the predicted value indicates that although the statistical contribution of the parallel rotational positions to the over-all structure of the molecule is not trivial, it does not assume prominence. Since rotation of the  $-\text{CH}_2\text{X}$  group cannot occur in the other halides, their nonzero dipole moments and heat capacity anomalies appear likely to be due to torsional oscillations of the  $-\text{CH}_2\text{X}$  groups. Temperature-dependent dielectric and n.m.r. studies of the solid would be helpful in further elucidating the mechanism of the transformation.

*Acknowledgment.* The financial support of the U. S. Atomic Energy Commission and the collaboration of Dr. Claus Wulff in some of the initiatory measurements on the pentaerythrityl chloride are appreciated.

**Table VII:** Dipole Moments of the Pentaerythrityl Halides in Benzene Solution at 25°<sup>a</sup>

Pentaerythrityl halide	Dipole moment <sup>b</sup>					
	0.77 <sup>c</sup>	...	...	...	1.6 <sup>g</sup>	1.4 <sup>h</sup>
Fluoride	0.77 <sup>c</sup>	...	...	...	1.6 <sup>g</sup>	1.4 <sup>h</sup>
Chloride	0.63 <sup>c</sup>	0.65 <sup>d</sup>	0.43 <sup>e</sup>	0 <sup>f</sup>	..	0.71 <sup>h</sup>
Bromide	...	0.68 <sup>d</sup>	0.50 <sup>e</sup>	0 <sup>f</sup>	..	...
Iodide	...	...	...	0 <sup>f</sup>	..	...

<sup>a</sup> The dipole moment of pentaerythrityl has not been determined in nonpolar solvents because of low solubility. Values determined by other methods are 2.0 D. by molecular beam,<sup>12</sup> 1.8 D. by dielectric study on the plastic solid,<sup>13</sup> and 0.9 D. from extrapolation of dielectric data on aqueous solutions.<sup>14</sup> <sup>b</sup> Units: Debye. <sup>c</sup> Ref. 15. <sup>d</sup> In carbon tetrachloride at 25° (ref. 16). <sup>e</sup> Ref. 17. <sup>f</sup> See A. D. Franklin, *J. Am. Chem. Soc.*, **73**, 3512 (1951), and L. Ebert, R. Eisenschitz, and H. U. Hartel, *Z. physik. Chem.*, **B1**, 94 (1928). <sup>g</sup> Ref. 4a (re-evaluated using densities of ref. 15). <sup>h</sup> Determined by a resonance method at four concentrations over the range 0.006 to 0.02 mole fraction halide.

(12) J. Estermann, *Z. physik. Chem.*, **B2**, 287 (1929).

(13) R. Kiriya, S. Yabumoto, and I. Nitta, *Bull. Chem. Soc. Japan*, **27**, 115 (1954).

(14) F. Oehme and M. Feinauer, *Chemiker-Ztg.*, **86**, 71 (1962).

(15) (a) H. Lumbroso and D. Lauransan, *Bull. soc. chim. France*, 513 (1959); (b) H. Lumbroso, *Compt. rend.*, **254**, 2750 (1962).

(16) C. G. Le Fèvre, R. J. W. Le Fèvre, and M. R. Smith, *J. Chem. Soc.*, 16 (1958).

(17) H. B. Thompson and C. C. Sweeney, *J. Phys. Chem.*, **64**, 221 (1960).

## Heat Capacities and Thermodynamic Properties of Globular Molecules.

### XIV. Tetraphosphorus Trisulfide, Tetraphosphorus Triselenide, and Tetraphosphorus Decasulfide between 5 and 350°K.<sup>1a</sup>

by H. Lawrence Clever, Edgar F. Westrum, Jr.,<sup>1b</sup>

*Department of Chemistry, University of Michigan, Ann Arbor, Michigan 48104*

and A. W. Cordes

*Department of Chemistry, University of Arkansas, Fayetteville, Arkansas 72701 (Received October 5, 1964)*

Thermal properties of three phosphorus chalcogenides were determined by adiabatic calorimetry and yielded entropies at 298.15°K. for P<sub>4</sub>S<sub>3</sub>, P<sub>4</sub>Se<sub>3</sub>, and P<sub>4</sub>S<sub>10</sub> of 48.60, 57.26, and 91.24 cal./(mole °K.), respectively. The P<sub>4</sub>S<sub>3</sub> transforms to a plastically crystalline state at 313.90°K. with  $\Delta S_t = 7.85$  cal./(mole °K.) and P<sub>4</sub>Se<sub>3</sub> shows an anomalous increase in heat capacity suggesting such an effect slightly above 350°K. Diffraction data on P<sub>4</sub>S<sub>3</sub> provided coefficients of thermal expansion on both phases and confirmation of the plastically crystalline nature of the Crystal I phase.

Many crystalline phases of high molecular symmetry show an apparent first-order solid–solid transition to a plastically crystalline phase<sup>2</sup> with a cubic or hexagonal structure. Compared to other molecular crystal phases this state of the compound is relatively easily deformed by pressure, has a relatively high vapor pressure, and has an entropy of fusion  $\leq 5$  cal./(mole °K.).

Several of the phosphorus chalcogenides are highly symmetrical molecules and solid–solid transitions have been reported for some of these. To elucidate further the range of existence and nature of the plastic crystalline phase, heat capacity measurements were made on tetraphosphorus trisulfide (P<sub>4</sub>S<sub>3</sub>), tetraphosphorus triselenide (P<sub>4</sub>Se<sub>3</sub>), and tetraphosphorus decasulfide (P<sub>4</sub>S<sub>10</sub>). The existence of solid–solid transitions has been reported for tetraphosphorus trisulfide<sup>3–5</sup> and there is some evidence that tetraphosphorus triselenide exists in two modifications<sup>6</sup>; transitions have not been reported in tetraphosphorus decasulfide. In addition, differential thermal analysis on tetraphosphorus trisulfide indicated an enthalpy of transition of 3.4 kcal./mole at  $312 \pm 1^\circ\text{K.}$ <sup>4</sup> Recent crystallographic studies have been made on the trisulfide,<sup>4</sup> triselenide,<sup>7</sup> and decasulfide.<sup>8</sup>

#### Experimental

*Cryostat and Calorimeter.* A gold-plated copper calorimeter (laboratory designation W-37) had a threaded, vacuum-tight seal with a 1.4-cm. diameter aperture and an annealed, gold gasket between the screw cap and the circular knife edge of the Monel metal top. This eliminated a soldered closure for these flammable compounds. The calorimeter, including cap and gasket, weighed 34.575 g. and had a volume of 32.45 cc. The thermometer–heater assembly was inserted in a well. Six metal vanes radiated from the central well through

(1) (a) Supported in part by the Selenium–Tellurium Development Association, Inc. (b) To whom correspondence concerning this paper should be directed.

(2) J. Timmermans, *Phys. Chem. Solids*, **18**, 1 (1961).

(3) A. Stock, *Ber.*, **43**, 150 (1910).

(4) Y. C. Leung, J. Waser, S. van Houten, A. Vos, G. A. Wieggers, and E. H. Wiebenga, *Acta Cryst.*, **10**, 574 (1957).

(5) (a) Y. C. Leung, J. Waser, and L. R. Roberts, *Chem. Ind. (London)*, 948 (1955); (b) S. van Houten, A. Vos, and G. A. Wieggers, *Rec. trav. chim.*, **74**, 1167 (1955).

(6) J. Mai, *Ber.*, **59**, 1888 (1926); **61**, 1807 (1928).

(7) E. Keulen and A. Vos, *Acta Cryst.*, **12**, 323 (1959).

(8) A. Vos and E. H. Wiebenga, *ibid.*, **8**, 217 (1955).

Table I

Compd.	Sample wt. (g. <i>in vacuo</i> )	Molecular mass	<i>d</i> , g./cc.	He, torr <sup>a</sup>
P <sub>4</sub> S <sub>3</sub>	27.496	220.09	2.08 <sup>b</sup>	13.3
P <sub>4</sub> Se <sub>3</sub>	19.429	360.78	3.17 <sup>c</sup>	15.5
P <sub>4</sub> S <sub>10</sub>	19.254	444.54	2.09 <sup>d</sup>	5.35

<sup>a</sup> Helium gas was added to aid thermal contact between calorimeter and samples. <sup>b</sup> Ref. 4. <sup>c</sup> Ref. 7. <sup>d</sup> Ref. 8.

the sample space to ensure rapid thermal equilibration of the entire assembly and sample.

The calorimeter was suspended within the Mark III cryostat<sup>9</sup> for the measurement of heat capacity by the quasiadiabatic technique.<sup>10</sup> A calibrated capsule-type platinum resistance thermometer (laboratory designation A-3) was used. Its temperature scale is considered to accord with the thermodynamic temperature scale

Table II: Heat Capacities of Phosphorus Chalcogenides<sup>a</sup>

<i>T</i>	<i>C<sub>s</sub></i>	<i>T</i>	<i>C<sub>s</sub></i>	<i>T</i>	<i>C<sub>s</sub></i>	<i>T</i>	<i>C<sub>s</sub></i>	<i>T</i>	<i>C<sub>s</sub></i>	<i>T</i>	<i>C<sub>s</sub></i>
Tetraphosphorus Trisulfide (P <sub>4</sub> S <sub>3</sub> )						Tetraphosphorus Triselenide (P <sub>4</sub> Se <sub>3</sub> )					
Series I		114.42	19.97	313.45	1590	Series I		237.95	36.33	10.07	1.86
5.52	0.142	123.41	21.35	313.79	3272	103.89	22.28	248.70	36.95	11.37	2.389
5.92	0.123	132.52	22.68	315.53	191.4			259.46	37.49	12.80	2.961
6.42	0.179	141.90	24.02	Series V		Series II		270.08	38.32	14.30	3.612
6.94	0.258	151.50	25.33	260.67	35.58	86.35	19.56	279.51	38.68	15.94	4.322
7.80	0.403	161.20	26.51	267.12	36.14	93.32	20.68	289.91	39.23	17.85	5.082
8.71	0.512	170.89	27.64	276.36	36.86	102.19	22.04	300.19	39.84	20.06	5.901
9.60	0.819	180.60	28.70	Enthalpy run E		111.66	23.46	310.36	40.50	22.59	6.750
10.70	1.104	190.34	29.76	Δ <i>Ht</i> run F		119.98	24.82	320.43	41.19	25.58	7.645
11.99	1.460	199.59	30.74	Enthalpy run G		130.01	26.26	330.38	42.03	28.76	8.464
13.46	1.941	208.51	31.51	Series VI		139.59	27.53	339.24	42.82	31.93	9.236
14.87	2.426	217.49	32.47	300.72	39.07	148.89	28.68	346.91	43.74	35.46	10.032
16.33	2.966	226.62	33.13	305.35	41.49	158.78	29.81	Series III		39.85	10.933
17.98	3.546	235.91	33.90	309.26	50.10	169.21	30.92	5.25	0.41	44.50	11.832
20.10	4.278	245.17	34.57	312.03	128.1	179.36	31.88	5.46	0.46	48.97	12.675
22.67	5.122	254.50	35.26	Δ <i>Ht</i> run H		189.63	32.81	6.02	0.48	53.74	13.573
25.17	5.862	263.82	35.89	313.71	2944	197.91	33.49	6.84	0.68	59.13	14.575
27.69	6.532	273.18	36.63	314.23	256.9	207.76	34.23	7.85	0.99	65.34	15.75
30.45	7.196	287.96	37.64	315.24	43.57	217.59	34.96	8.94	1.40	72.20	16.89
33.56	7.846	301.56	39.12	316.82	43.50	227.55	35.66			79.65	18.25
37.07	8.530	Δ <i>Ht</i> run A		321.84	43.30					88.34	19.82
41.10	9.185	326.87	43.36	323.84	43.36	Tetraphosphorus decasulfide (P <sub>4</sub> S <sub>10</sub> )					
45.78	9.893	336.17	43.46	338.62	43.55	Series I		196.86	58.59	33.34	11.160
51.24	10.669	345.53	43.85	346.63	43.57	120.63	42.77	206.90	60.09	37.38	12.926
57.41	11.523	Series III		Series VII		128.22	44.86	217.00	61.55	41.80	14.884
64.44	12.529	266.15	36.12	273.75	36.67	136.83	46.95	226.91	62.90	46.90	17.15
71.90	13.540	275.46	36.80	282.48	37.51	145.81	48.96	236.63	64.18	52.79	19.75
79.37	14.652	Enthalpy run B		286.49	37.82	154.70	50.88	246.20	65.31	58.88	22.39
87.28	15.92	Δ <i>Ht</i> run C		290.47	38.02	163.63	52.71	255.61	66.45	65.20	25.04
Series II		Enthalpy run D		292.16	37.96	172.57	54.40	265.23	67.62	71.54	27.36
81.06	14.926	Series IV		290.47	38.02	181.54	55.94	275.05	68.56	78.15	29.85
88.86	16.16	305.52	46.04	338.62	43.55			285.08	69.58		
96.73	17.29	311.69	208.2	Series II		120.63	42.77	206.90	60.09	37.38	12.926
105.32	18.58			273.75	36.67	128.22	44.86	217.00	61.55	41.80	14.884
				282.48	37.51	136.83	46.95	226.91	62.90	46.90	17.15
				286.49	37.82	145.81	48.96	236.63	64.18	52.79	19.75
				290.47	38.02	154.70	50.88	246.20	65.31	58.88	22.39
				292.16	37.96	163.63	52.71	255.61	66.45	65.20	25.04
						172.57	54.40	265.23	67.62	71.54	27.36
						181.54	55.94	275.05	68.56	78.15	29.85
								285.08	69.58		
						Series II		295.01	70.49	Series IV	
						81.81	31.29	304.88	71.35	5.72	0.42
						88.65	33.72	314.76	72.07	6.70	0.68
						95.03	35.63	324.73	72.92	8.22	0.98
						101.85	37.61	334.84	73.71	9.29	1.37
						109.15	39.69	345.10	74.45	10.35	1.76
						117.14	41.91			11.37	2.14
						125.69	44.15	Series III		12.38	2.49
						134.27	46.26	18.79	5.172	13.49	2.93
						Enthalpy run A		21.93	6.452	14.80	3.52
						187.23	56.98	24.52	7.499	16.15	4.08
								27.05	8.531	17.72	4.76
								29.91	9.698		

<sup>a</sup> Units: cal., mole, °K.

Table III: Thermodynamic Properties of Phosphorus Chalcogenides<sup>a</sup>

$T$	$C_p$	$S^\circ$	$H^\circ - H^\circ_0$	$-(G^\circ - H^\circ_0)/T$	$T$	$C_p$	$S^\circ$	$H^\circ - H^\circ_0$	$-(G^\circ - H^\circ_0)/T$
Tetraphosphorus Trisulfide ( $P_4S_3$ )					Tetraphosphorus Triselenide ( $P_4Se_3$ )				
Crystal II									
5	0.080	0.027	0.10	0.007	5	0.305	0.101	0.38	0.025
10	0.902	0.269	2.08	0.061	10	1.785	0.690	5.05	0.185
15	2.486	0.920	10.38	0.228	15	3.921	1.814	19.28	0.529
20	4.234	1.876	27.20	0.516	20	5.883	3.219	43.94	1.022
25	5.813	2.995	52.42	0.898	25	7.471	4.709	77.47	1.610
30	7.109	4.174	84.85	1.346	30	8.778	6.190	118.18	2.251
35	8.144	5.350	123.08	1.834	35	9.927	7.631	165.0	2.917
40	9.003	6.495	166.0	2.346	40	10.966	9.025	217.3	3.594
45	9.769	7.600	212.9	2.868	45	11.923	10.373	274.5	4.273
50	10.498	8.668	263.6	3.395	50	12.870	11.678	336.5	4.948
60	11.907	10.707	375.7	4.446	60	14.742	14.190	474.6	6.281
70	13.276	12.645	501.6	5.480	70	16.56	16.601	631.2	7.584
80	14.756	14.512	641.6	6.492	80	18.34	18.931	805.9	8.858
90	16.32	16.342	797.1	7.486	90	20.05	21.194	998.2	10.103
100	17.79	18.138	967.6	8.462	100	21.71	23.397	1,207.4	11.323
110	19.29	19.903	1,153.0	9.421	110	23.30	25.544	1,432.8	12.518
120	20.81	21.647	1,353.5	10.368	120	24.83	27.639	1,674	13.692
130	22.33	23.372	1,569	11.302	130	26.24	29.682	1,929	14.843
140	23.78	25.081	1,800	12.225	140	27.57	31.68	2,198	15.97
150	25.12	26.768	2,044	13.139	150	28.80	33.62	2,480	17.09
160	26.35	28.429	2,302	14.042	160	29.94	35.52	2,774	18.18
170	27.51	30.062	2,571	14.937	170	30.99	37.36	3,079	19.25
180	28.65	31.67	2,852	15.82	180	31.96	39.16	3,393	20.31
190	29.75	33.25	3,144	16.70	190	32.85	40.91	3,717	21.35
200	30.79	34.80	3,447	17.56	200	33.67	42.62	4,050	22.37
210	31.76	36.32	3,760	18.42	210	34.43	44.28	4,391	23.37
220	32.65	37.82	4,082	19.27	220	35.14	45.90	4,738	24.36
230	33.46	39.29	4,412	20.11	230	35.80	47.48	5,093	25.33
240	34.22	40.73	4,751	20.94	240	36.43	49.01	5,454	26.29
250	34.93	42.14	5,096	21.76	250	37.03	50.51	5,822	27.23
260	35.63	43.53	5,449	22.57	260	37.60	51.98	6,195	28.15
270	36.37	44.89	5,809	23.37	270	38.16	53.40	6,574	29.06
280	37.17	46.22	6,177	24.16	280	38.71	54.80	6,958	29.95
290	37.93	47.54	6,552	24.95	290	39.26	56.17	7,348	30.83
300	39.28	48.84	6,937	25.72	300	39.83	57.51	7,743	31.70
313.90	...	50.61 <sup>b</sup>	7,475 <sup>b</sup>	26.80 <sup>b</sup>	350	44.10	63.93	9,827	35.85
273.15	36.62	45.31	5,924	23.62	273.15	38.33	53.85	6,694	29.34
298.15	38.87	48.60	6,865	25.58	298.15	39.72	57.26	7,669	31.54
Crystal I									
313.90	...	58.46 <sup>b</sup>	9,939 <sup>b</sup>	26.80 <sup>b</sup>					
325	43.31	59.96	10,420	27.90					
350	43.77	63.18	11,508	30.31					

within 0.03°K. from 10–90°K. and within 0.04°K. from 90–350°K.

The heat capacity of the calorimeter–heater–thermometer assembly was determined in a separate series of measurements. Small adjustments were made for the slight differences in the quantities of helium and ther-

mal conductivity grease used in the various runs. Manual shield control was used below 70°K. Above this

(9) E. F. Westrum, Jr., *J. Chem. Educ.*, **39**, 443 (1962).

(10) E. F. Westrum, Jr., J. B. Hatcher, and D. W. Osborne, *J. Chem. Phys.*, **21**, 419 (1953).



Table III (Continued)

$T$	$C_p$	$S^\circ$	$H^\circ - H^\circ_0$	$-(G^\circ - H^\circ_0)/T$
Tetraphosphorus Decasulfide ( $P_4S_{10}$ )				
5	0.284	0.094	0.35	0.024
10	1.571	0.615	4.47	0.167
15	3.591	1.624	17.26	0.473
20	5.678	2.944	40.46	0.921
25	7.695	4.429	73.91	1.472
30	9.740	6.011	117.46	2.096
35	11.878	7.672	171.5	2.773
40	14.084	9.402	236.4	3.493
45	16.31	11.189	312.3	4.248
50	18.53	13.022	399.4	5.034
60	22.83	16.783	606.4	6.677
70	26.82	20.609	855.0	8.394
80	30.59	24.442	1,142.6	10.160
90	34.00	28.245	1,465.7	11.959
100	37.10	31.991	1,822	13.775
110	39.98	35.67	2,207	15.60
120	42.71	39.26	2,621	17.42
130	45.24	42.78	3,061	19.24
140	47.63	46.22	3,525	21.04
150	49.88	49.59	4,013	22.83
160	51.98	52.88	4,522	24.61
170	53.95	56.09	5,052	26.37
180	55.77	59.22	5,601	28.11
190	57.46	62.28	6,167	29.82
200	59.04	65.27	6,750	31.52
210	60.53	68.19	7,348	33.20
220	61.94	71.04	7,960	34.85
230	63.29	73.82	8,586	36.49
240	64.59	76.54	9,226	38.10
250	65.82	79.20	9,878	39.69
260	66.99	81.81	10,542	41.26
270	68.08	84.36	11,217	42.81
280	69.09	86.85	11,903	44.34
290	70.03	89.29	12,599	45.85
300	70.90	91.68	13,304	47.34
350	74.82	102.91	16,949	54.49
273.15	68.40	85.15	11,432	43.29
298.15	70.74	91.24	13,173	47.06

<sup>a</sup> Units: cal., mole, °K. <sup>b</sup> Assuming  $\Delta Ht$  to be isothermal at 313.90°K.

temperature three separate channels of recording electronic circuitry provided with proportional, rate, and reset control actions regulated the adiabatic shield to within approximately a millidegree of the calorimeter temperature. Thus the energy exchange between calorimeter and surroundings is reduced so that it is neg-

ligible in comparison with other sources of error. All measurements of temperature, time, potential, resistance, and mass are referred to calibrations or standards of the National Bureau of Standards.

**Samples.** The three samples were supplied by Dr. A. W. Cordes. The tri- and decasulfide samples were Eastman technical grade materials purified as follows. The trisulfide was subjected to boiling water in order to remove the higher sulfides which are readily hydrolyzed. The dried product was then subjected to repeated extraction with carbon disulfide with the first and last quarter of each extraction being discarded. The decasulfide was similarly purified by successive fractional extraction with carbon disulfide. This procedure is quite efficient because of the appreciable differences of the solubilities of the various phosphorus sulfides and sulfur in this solvent.<sup>11</sup>

The triselenide was prepared by the direct reaction of white phosphorus and selenium in tetrahydronaphthalene. The reaction was carried out in a sealed glass tube at 230°C. and 10 atm. pressure for 2 hr. A typical reaction involved 5 g. of phosphorus, 10 g. of selenium, and 150 ml. of solvent. The bright orange, highly crystalline product is obtained in greater than 90% yield. The sample was recrystallized once from tetrahydronaphthalene and several times from benzene.

All samples were dried under high vacuum, stored in sealed, evacuated glass vials, and transferred directly from the vials to the calorimeter in a nitrogen-filled dry-box (see Table I).

The approximate percentages of the total (*i.e.*, sample-calorimeter-heater-thermometer assembly) heat capacity due to each sample were 86% at 10°K., 40% at 180°K., and 50% at 350°K.

## Results

**Heat Capacity.** The experimentally determined heat capacities as a function of temperature are shown in Figure 1 and values for the individual determinations are presented in Table II in chronological order so that temperature increments across individual runs in a series may be estimated from adjacent mean temperatures. The data are stated in terms of the defined thermochemical calorie exactly equal to 4.1840 j. and an ice point of 273.15°K. An analytically determined curvature correction has been applied to the measured values of  $\Delta H/\Delta T$ . These data are considered to be characterized by a probable error of about 5% near 10°K., decreasing to 0.8% at 20°K. and to less than 0.2% above 30°K.

(11) A. Pitochelli, *Dissertation Abstr.*, 18, No. 58-1728, 1608 (1958).

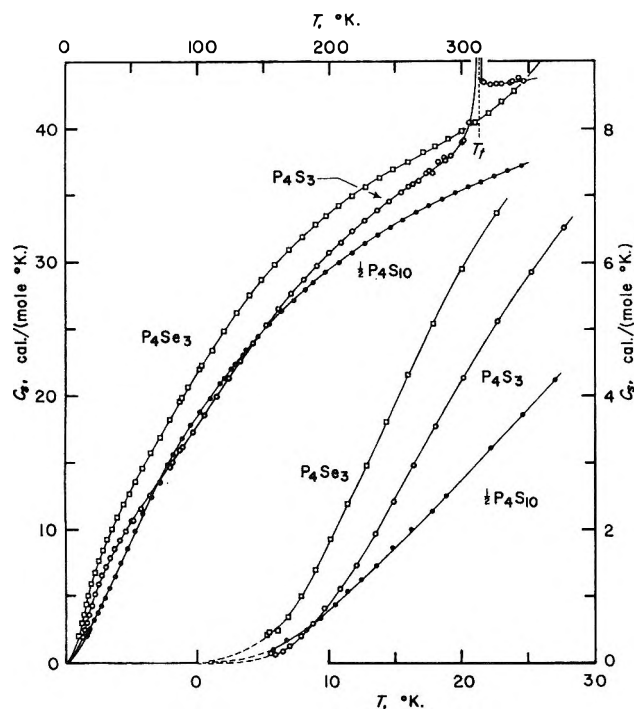


Figure 1. Heat capacities of three phosphorus chalcogenides.

**Thermodynamic Functions.** The molal values of heat capacity, entropy, enthalpy increment, and free energy function are listed in Table III for selected temperatures. These values have been obtained by smoothing or by integration of a least-squares polynomial fit by a digital computer through the data points. Both the fitting and the quadrature use computer programs previously described.<sup>12</sup> Below 5°K. the heat capacity data were extrapolated using the Debye limiting law. Since nuclear spin and isotopic mixing contributions have not been included in the entropy and free energy functions, these functions are therefore practical values for use in chemical thermodynamic calculations.

**Tetraphosphorus Trisulfide.** Examination of Figure 1 reveals a prominent hump in the heat capacity near 30°K. Attempts to represent the normal vibronic heat capacity of the lattice with combinations of Debye and Einstein functions suggest the excess heat capacity to approximate the form of a Schottky anomaly with a maximum of 4 to 6 cal./(mole °K.). No explanation for the origin of these low-lying energy levels is yet substantiated.

The apparently first-order solid-solid transition in  $P_4S_3$  occurs at 313.90°K. with heat capacities in excess of 3000 cal./(mole °K.), a  $\Delta Ht$  of  $2464 \pm 10$  cal./mole, and a  $\Delta St$  of  $7.85 \pm 0.03$  cal./(mole °K.). The transition was traversed by five series of runs (Table IV) to obtain the temperature and enthalpy of transition.

Table IV: Enthalpy of Transition of Tetraphosphorus Trisulfide<sup>a</sup>

Designation	No. of runs	$H_{320} - H_{300}^b$	$\Delta Ht^c$
Run A	1	3256	2454
Runs B, C, D	3	3237	2435 <sup>d</sup>
Series IV	5	3285 <sup>e</sup>	2483
Runs E, F, G	3	3268	2466
Series VI	10	3255 <sup>e</sup>	2453

$$\begin{aligned} \Delta Ht & 2464 \pm 10 \\ \Delta St & 7.85 \pm 0.03 \\ T_t & 313.90^\circ\text{K.} \end{aligned}$$

<sup>a</sup> Units: cal., mole, °K. <sup>b</sup> Contribution of the lattice to  $H_{320} - H_{300}$  is 805 cal. <sup>c</sup> Includes excess heat of 3 cal. from 290 to 300°K. <sup>d</sup> Rejected from average. <sup>e</sup> Corrected for quasi-adiabatic drift.

Several attempts to obtain the transition temperature by cooling curves failed. The transition tended to undercool about 30° and the enthalpy of transition was not sufficient to restore the system to the transition temperature. This tendency to undercool was confirmed during X-ray measurements described later in which the Crystal I phase persisted at 295°K. (19° below the transition temperature) for more than a week. The low value of  $\Delta Ht$  from Runs B, C, and D (*cf.* Table IV) probably resulted from incomplete conversion to Crystal II on cooling.

**Tetraphosphorus Triselenide and Tetraphosphorus Decasulfide.** The temperature dependence of the heat capacity shows no anomalies characteristic of the plastically crystalline phase for either  $P_4Se_3$  or  $P_4S_{10}$  up to a temperature of 350°K. An upturn in the  $P_4Se_3$  curve suggests a transition slightly above 350°K. Heat capacity measurements on both  $P_4Se_3$  and  $P_4S_{10}$  as well as  $P_4S_3$  will be extended through melting upon completion of a new intermediate range thermostat and silver calorimeter.

**Determination of the Coefficient of Thermal Expansion of Phosphorus Trisulfide.** X-Ray diffraction of a powdered trisulfide sample at 295 and 308°K. on Crystal II and at 319 and 337°K. on Crystal I yielded apparent linear coefficients of expansion of  $(2.5 \pm 0.6) \times 10^{-6} \text{ }^\circ\text{K.}^{-1}$  for Crystal II and  $(3.2 \pm 1.7) \times 10^{-6} \text{ }^\circ\text{K.}^{-1}$  for Crystal I. These values were obtained by assuming isotropic expansion. Relatively few diffraction lines were observable for the Crystal I phase. The relatively few X-ray diffraction lines observed for the Crystal I phase are consistent with the expectation

(12) B. H. Justice, Appendix to Ph.D. Dissertation, University of Michigan, U. S. Atomic Energy Commission Report TID-12722, 1961.

that it is plastically crystalline but did not permit the determination of symmetry or of unit cell dimensions.

### Discussion

In principle a detailed knowledge of the alignment of the molecular symmetry elements with those of the plastic crystal lattice should be consistent with the observed entropy of transition.<sup>13</sup> The Crystal II (low-temperature form) structure of  $P_4S_3$  is orthorhombic ( $D_{2h}$ <sup>16</sup>- $Pnmb$ ) with eight molecules in the unit cell.<sup>4</sup> The Crystal I (high-temperature, presumably plastic, form) structure is not known. Further confirmation of the plastic nature of this phase can be provided by the determination of the entropy of fusion.

The observed entropy of transition, 7.85 cal./( $\text{mole } ^\circ\text{K.}$ ) may be accounted for by the following mechanism.<sup>14</sup> Plastic crystal phases have close-packed structures; however, the low-temperature structures of both  $P_4S_3$  and  $P_4Se_3$  are roughly hexagonal closest packed. On assuming a cubic structure and matching symmetry elements of the  $C_{3v}$  molecule and the lattice<sup>13</sup> yields  $R \ln 48 = 7.69$  cal./( $\text{mole } ^\circ\text{K.}$ ) for the transitional entropy of disordering. This assumes the trigonal molecular axis may be randomly aligned in either direction along any of the four crystal cube diagonals and rotated sixfold about these positions so as

to bring either the three equivalent phosphorus atoms or the three selenium atoms into coincidence with other cube diagonals (hence,  $4 \times 2 \times 6$  orientations). The proximity in the van der Waals radii of sulfur and phosphorus (1.85 and 1.9, respectively<sup>15</sup>) facilitates this reorientation. The corresponding value for selenium (2.0) presages a similar effect in the triselenide. The remaining 0.16 cal./( $\text{mole } ^\circ\text{K.}$ ) will be assigned as entropy associated with the volume increment on transforming Crystal II to Crystal I. Confirmation of these tentative assignments must await a detailed knowledge of the structure of Crystal I and the transitional volume increment.

*Acknowledgment.* The authors appreciate the financial support of the Selenium-Tellurium Development Association, Inc., and the cooperation of J. T. S. Andrews and Dr. Yoichi Takahashi in some of the calorimetric measurements and of Bi-Cheng Wang in the X-ray determinations. Mrs. Carolyn Barber provided assistance in the evaluation of the data.

(13) G. B. Guthrie and J. P. McCullough, *Phys. Chem. Solids*, **18**, 53 (1961).

(14) This interpretation was suggested by Aaron Ribner.

(15) L. Pauling, "The Nature of the Chemical Bond," Cornell University Press, Ithaca, N. Y., 1960, p. 260.

## Calorimetric Determination of the Mean $\beta$ -Energy and Half-Life of Promethium-147<sup>1</sup>

by E. J. Wheelwright, D. M. Fleming, and F. P. Roberts

Hanford Laboratories, General Electric Company, Richland, Washington (Received October 10, 1964)

The mean  $\beta$ -energy of the  $\text{Pm}^{147}$  decay has been calorimetrically measured at periodic intervals extending over a 1-year period. Two independently prepared 1000-c. sources of highly purified  $\text{Pm}_2\text{O}_3$  were examined. The results obtained are self-consistent and are in excellent agreement with measurements made on the same sources by an independent scientist using a second calorimeter. Values of  $0.3330 \pm 0.0005$  w./g. of  $\text{Pm}^{147}$  and  $2.620 \pm 0.005$  years for the  $\beta$ -decay energy and the half-life, respectively, are believed to be the most reliable values yet published.

The only known published value of the mean  $\beta$ -energy of  $\text{Pm}^{147}$  is that of Hovi and Niemelä.<sup>2</sup> They report the mean  $\beta$ -energy of the  $\text{Pm}^{147}$  (1) calculated from the  $\beta$  energy spectrum, (2) calculated from Fermi's theory, and (3) calculated from their own calorimetric measurements to be  $64.1 \pm 1$ ,  $63.0 \pm 1$ , and  $70.4 \pm 4$  kev., respectively. Using the value of 2.619 years for the  $\text{Pm}^{147}$  half-life, which is slightly shorter than the 2.64 years used by Hovi and Niemelä, the three mean  $\beta$ -energy values are calculated to be 0.35, 0.35, and 0.39 w./g. of  $\text{Pm}^{147}$ , respectively. These three values are subject to several sources of error. The numerical integration of the  $\beta$ -energy spectrum and the maximum  $\beta$ -energy are each subject to errors of 1–2%. The small amount of  $\text{Pm}^{147}$  available to Hovi and Niemelä (0.792 c. or  $8.53 \times 10^{-4}$  g.) places serious limits on the accuracy of their calorimetric measurements and places a high dependence upon their absolute  $\beta$ -counting methods.

Values for the  $\text{Pm}^{147}$  half-life from 2.5 to 2.7 years have been reported in the literature.<sup>3–6</sup> These values were obtained by measuring the decay rate over extended periods of time or by absolute  $\beta$ -counting. They are subject both to the errors associated with the detection of the very soft  $\text{Pm}^{147}$   $\beta$ -energy and to the standardization of the detection equipment over an extended period of time.

When a relatively large quantity of highly purified  $\text{Pm}^{147}$  became available, it was deemed desirable to make an accurate measurement of the liberated energy

at periodic intervals extending over a significant portion of the isotope half-life. In addition to yielding a highly reliable value for the mean  $\beta$ -energy, such measurements yield an "absolute" value for the half-life, independent of radiochemical counting techniques.

### Experimental

**Materials.** The  $\text{Pm}^{147}$  used for these measurements was recovered as a crude rare earth fission product mixture from Hanford waste by precipitation processes. The crude mixture, containing 20,700 c. of  $\text{Pm}^{147}$  (cerium had been removed by a precipitation step), was then processed through a shielded ion-exchange unit to separate the  $\text{Pm}^{147}$  from its adjacent rare earth neighbors and all other contaminants. The ion-exchange process used was a "displacement-chromatographic" technique in which  $\text{Y}^{+3}$  was the barrier ion; 0.015 M ethylenediaminetetraacetic acid solution, adjusted to pH 8.7 with ammonium hydroxide, served as the eluent.<sup>7,8</sup> As the  $\text{Pm}^{147}$  "chromatographic

(1) Work performed under Contract AT-(45-1)-1350 between the General Electric Co. and the U. S. Atomic Energy Commission.

(2) V. Hovi and L. Niemelä, *Ann. Acad. Sci. Fennicae: Ser. A VI*, 103 (1962).

(3) (a) R. P. Schuman, M. E. Jones, and A. C. Mewherter, *J. Inorg. Nucl. Chem.*, 3, 160 (1956); (b) M. F. Merritt, P. J. Campion, and R. C. Hawkins, *Can. J. Phys.*, 35, 16 (1957).

(4) J. P. Cali and L. F. Lowe, *Nucleonics*, 17, 86 (1959).

(5) E. I. Wyatt, *et al.*, *Nucl. Sci. Eng.*, 11, 74 (1961).

(6) F. P. Roberts, E. J. Wheelwright, and W. Y. Matsumoto, U. S. Atomic Energy Commission Unclassified Report HW-77296 (1963).

band" was eluted from the final column, the solution was collected in 14 consecutive fractions, and the  $\text{Pm}^{147}$  was recovered from each by an oxalate precipitation followed by ignition to the oxide. The oxide composition shown in Table I was obtained from absorption spectrum measurements using a Cary Model 14 recording spectrophotometer and 1-cm. quartz cells. Analytical samples were prepared by dissolving a small amount of oxide from each sample in 2 ml. of 1.0 M  $\text{HClO}_4$ . The detection limit of samarium or neodymium in promethium by this method is a little less than 1%.

Table I: Promethium Purification Results

Fraction no.	g. of oxide	% composition		
		Nd	Pm	Sm
1	3.04	N.D.	10	90
2	2.12	N.D.	34	66
3	3.13	N.D.	64	36
4	3.43	N.D.	86	14
5	3.73	N.D.	97	2.8
6	3.21	N.D.	99	N.D.
7	2.05	N.D.	>99	N.D.
8	2.37	N.D.	>99	N.D.
9	2.55	N.D.	>99	N.D.
10	2.53	N.D.	99	N.D.
11	0.60	2	98	N.D.
12	0.45	6	94	N.D.
13	3.06	35	65	N.D.
14	2.20	50	50	N.D.

The oxide used for calorimeter source no. 1 was taken from fraction no. 8. This fraction was checked by emission spectroscopy. Only trace amounts of metallic impurities were found. Mass spectrographic measurements showed no masses except 147. Radiochemical analysis showed no detectable radiochemical impurities other than  $\text{Pm}^{146}$  and  $\text{Pm}^{148}$ . Both of these activities were less than  $10^{-4}\%$  of that of  $\text{Pm}^{147}$ . The formula of promethium oxide was verified. A small sample (0.1591 g.) was accurately weighed, dissolved in 1.0 M  $\text{HClO}_4$ , and diluted to a known volume with 1.0 M  $\text{HClO}_4$ . Aliquots of this solution were buffered to pH 4.8 and titrated with a standard ethylenediaminetetraacetic acid solution using a mercury electrode to detect the end point. The value obtained for the molar concentration agreed with the gravimetric value within 0.2% if the formula  $\text{Pm}_2\text{O}_3$  and the atomic weight of 147 for promethium are assumed. The purity of the promethium oxide used in source no. 1 is therefore  $99.9 \pm 0.1\%$ .

The oxide for calorimeter source no. 2 was taken from

a homogenized composite of fractions 5 through 10. The inclusion of the known samarium impurity in fraction 5 with possible undetected impurities in fractions 6 and 10 decreased the purity of this oxide to  $99.0 \pm 0.2\%$ .

Each of the two  $\text{Pm}^{147}$  calorimeter sources was prepared in the same manner. Promethium oxide was loaded into the smaller of two concentric aluminum cans by use of remote manipulators. The threaded lid of the inner can was screwed into place, and the can was removed from the "hot cell." Following surface decontamination, the loaded primary container was placed inside the secondary container, and the lid was screwed tight. The containers of known weight and the content were then accurately weighed on an analytical balance to determine the weight of  $\text{Pm}_2\text{O}_3$  in the source. The outer container was welded closed by a conventional "heliarc" technique.

*Calorimeter.* The calorimeter has been described previously.<sup>9</sup> For these measurements the calorimeter was operated isothermally rather than adiabatically, and some structural changes were made. A 0.635-cm. thick brass thermal shield was added in the access tube. The shield is in the form of a cylinder with a plugged end and is wound from top to bottom on the outside with a coil of copper tubing, through which thermostated water constantly circulates. The shield is completely covered with a 10.16-cm. thick cap of Styrofoam. The bottom of the Styrofoam cap and the thermal shield extend 15.24 cm. below the surface of the water bath to prevent heat losses.

The bath temperature was monitored by a thermistor submerged in the bath and connected electrically to a Wheatstone bridge circuit. Bath temperature deviations were corrected by bridge-controlled heat lamps located in the bath. Bath control during the measurements was always within  $\pm 1 \times 10^{-4}^\circ$ .

The calorimeter was calibrated by comparison with electrical energy introduced into the calorimeter by means of a 3099.216-ohm resistor in an aluminum sample container placed directly in the calorimeter sample holder. Temperature readout was by a thermistor imbedded in the absorber block. The electrical calibrating energy was measured to  $\pm 0.01\%$  by measuring the current and voltage at the calibrating coil with a Leeds and Northrup Type K-2 potentiometer.

(7) F. H. Spedding and J. E. Powell, *Chem. Eng. Progr. Symp. Ser.*, **50**, 7 (1954).

(8) E. J. Wheelwright and F. P. Roberts, U. S. Atomic Energy Commission Unclassified Report HW-78651 Rev. (1963).

(9) I. T. Myers, W. H. LeBlanc, and D. M. Fleming, *Rev. Sci. Instr.*, **32**, 1013 (1961).

*Procedure.* The  $\text{Pm}^{147}$  source was inserted into the calorimeter and allowed to attain thermal equilibrium. The resistance of the thermistor imbedded in the absorber block was then measured at approximately 1-hr. intervals and plotted as a function of time. The  $\text{Pm}^{147}$  source was removed from the calorimeter and replaced by the calibration resistor. Electrical power supplied to the coil was then adjusted in a stepwise manner until the resistance of the imbedded thermistor coincided with a point on the thermistor resistance *vs.* time curve. The time coordinate of this point was, therefore, the decay time at which the energy released to the calorimeter by the  $\text{Pm}^{147}$  source was identical with a known calibration energy. This procedure was repeated for each of the points given in Table II.

**Table II:** Calorimeter Results

Source no.	Decay time, days	Source power, $P_x$ , w.
1	37.0	0.45770
1	372.6	0.35863
1	372.7 <sup>a</sup>	0.35863
2	81.0	0.37830
2	255.5	0.33307
2	311.3	0.32004
2	311.7 <sup>a</sup>	0.32004
2	426.8	0.29457
2	427.4 <sup>a</sup>	0.29457

<sup>a</sup> Measurements made using an alternate thermistor.

## Results

By a method of least squares, the log of the  $P_x$  values in Table II was plotted as a function of decay time to yield two straight lines with identical slopes. Since time zero is the time of purification, the anti-log of the intercepts at time zero yields the power levels of the sources at purification. The  $\text{Pm}^{147}$  half-life was determined from the slope of the lines. The data are presented in Table III. Errors reported in Table III are standard deviations.

**Table III:** Data and Results

	Source no. 1	Source no. 2
Data purified	0030 hr. Jan. 14, 1963	0030 hr. Jan. 14, 1963
Grams of $\text{Pm}^{147}$ in source	1.4089 $\pm$ 0.0014	1.2063 $\pm$ 0.0024
Curies of $\text{Pm}^{147}$ in source	1310 $\pm$ 1	1120 $\pm$ 3
$\text{Pm}^{147}$ mean $\beta$ -energy, w./g.	0.3335 $\pm$ 0.0006	0.3325 $\pm$ 0.0007
$\text{Pm}^{147}$ half-life, years	2.620 $\pm$ 0.005	2.620 $\pm$ 0.005

The  $\text{Pm}^{147}$  mean  $\beta$ -energy and half-life results from the two sources are self-consistent and are believed to be significantly more accurate than previously reported values. The calorimetrically determined half-life value is singularly significant since the results are limited only by the accuracy of the calorimeter. Sample size or inert impurities do not affect the results. The only possible error is contamination of the source by other heat-producing radionuclides. Careful radiochemical analysis proved the  $\text{Pm}^{147}$  sources to be free of this error.

The two  $\text{Pm}^{147}$  sources were sent to the Mound Laboratory, Monsanto Research Corp., for calorimetric verification by K. C. Jordan.<sup>10,11</sup> The half-life values reported by Jordan were 2.6218  $\pm$  0.0017 years for source no. 1 and 2.6247  $\pm$  0.0006 years for source no. 2, with a weighted average of 2.6244  $\pm$  0.0006 years. Errors in each case were reported as probable errors. Since the measurements made by Jordan spanned only about 5% of 1 half-life, he reported that the error does not unequivocally cover all effects owing to the slow drifts in the measuring equipment or spurious heating effects such as the presence of unknown radionuclides. Jordan therefore enlarged the error to a value which previous experience had indicated would include the error for data taken over several half-lives and reported the  $\text{Pm}^{147}$  half-life to be 2.6244  $\pm$  0.0060 years with a 95% confidence.

Jordan reported the source power output, back-calculated to the date of purification, to be 0.46953 w. for source no. 1 and 0.40099 w. for source no. 2 with a probable error of  $\pm$  0.1%. Combining this error with the uncertainty in the amounts of  $\text{Pm}^{147}$  in each sample gives values of 0.3333  $\pm$  0.0006 and 0.3324  $\pm$  0.0008 w./g. for sources no. 1 and no. 2, respectively. The errors are standard deviations. These results are virtually identical with the Hanford values and lend confidence to their accuracy.

*Acknowledgment.* The authors express their thanks to a number of people who contributed to the success of these measurements. E. F. Lowery machined the small aluminum capsules and the auxiliary equipment needed to load the capsules without gross spread of contamination. J. L. Green, G. O. Hammer, T. R. Myers, C. A. Fulcher, and G. N. Buck performed many tasks associated with the purification of the pro-

(10) Mound Laboratory Progress Report, U. S. Atomic Energy Commission Unclassified Report MLM-1204, July 1964.

(11) Mound Laboratory Progress Report, U. S. Atomic Energy Commission Unclassified Report MLM-1221, Sept. 1964.

methium. K. C. Jordan and his associates at Mound Laboratory performed a valuable service by performing the corroborative calorimetric measurements. Finally,

the authors wish to thank Drs. R. L. Moore and W. C. Roesch under whose direction and encouragement this work was performed.

## The Decomposition Pressure and Melting Point of Thorium Mononitride<sup>1</sup>

by W. M. Olson and R. N. R. Mulford

*University of California, Los Alamos Scientific Laboratory, Los Alamos, New Mexico (Received October 10, 1964)*

Measurements of the decomposition pressure for the reaction  $\text{ThN(s)} = \text{Th(l)} + \frac{1}{2}\text{N}_2\text{(g)}$  in the temperature range 2416 to 2790° are described. ThN melts congruently at  $2790 \pm 30^\circ$  under a nitrogen pressure somewhat less than 1 atm. The presence of  $\text{ThO}_2$  as an impurity in the ThN was found to have a large effect on the melting point and decomposition pressure. The decomposition pressure-temperature relation for pure ThN is described by the equation  $\log p \text{ (atm.)} = 8.086 - 33,224/T + 0.958 \times 10^{-17}T^5$  ( $T$  in °K.). Insofar as could be determined from X-ray lattice parameter data, ThN exists over little or no stoichiometry range.

### Introduction

As part of a continuing effort to determine the melting points and decomposition pressures of the actinide mononitrides, these properties of ThN were measured. Some experiments were also done in an attempt to ascertain if ThN exists over a range of stoichiometry, and the effect of oxygen on the melting point and decomposition pressure was examined.

The decomposition pressure-temperature relation was determined by observing the apparent melting point as a function of nitrogen pressure. If ThN is heated in nitrogen, the nitride decomposes to liquid thorium and nitrogen gas when the temperature is such that the decomposition pressure exceeds the ambient nitrogen pressure. Since this reaction proceeds very rapidly, decomposition is easily detected by observing the apparent melting of the solid sample. Thus, measurement of the apparent melting point as a function of nitrogen pressure gives the equilibrium pressure-temperature relation for the decomposition of ThN. If the ambient nitrogen pressure is sufficiently high, ThN melts congruently.

Relatively little work on thorium mononitride has been reported in the literature. Chiotti<sup>2</sup> reports a melting point of  $2630 \pm 50^\circ$  in a helium atmosphere, but thorium metal was found in the sample after solidification, which indicates that decomposition of the nitride occurred. Therefore his observed melting point would be expected to be lower than the congruent melting temperature. Chiotti also reports a lattice parameter of  $a = 5.195 \text{ \AA.}$  for the face-centered cubic ThN before melting, and  $a = 5.144 \text{ \AA.}$  after melting. Street and Waters<sup>3</sup> report a lattice parameter of  $5.159 \text{ \AA.}$ , which is in agreement with the present work.

### Experimental

*Apparatus.* The apparatus and general technique used have been described previously.<sup>4</sup> Briefly, the

(1) Work done under the auspices of the U. S. Atomic Energy Commission.

(2) P. Chiotti, *J. Am. Ceram. Soc.*, **35**, 123 (1952).

(3) R. S. Street and T. N. Waters, Document AERE M-1115; Atomic Energy Research Establishment, Harwell, England, 1962.

ThN sample, in granular form, was heated in a 30° vee formed in the middle of a resistively heated tungsten strip within a vacuum-pressure vessel. The sample was observed and temperatures were measured with a calibrated Pyro microoptical pyrometer sighted through a prism and quartz window located at the top of the vessel. Pyrometer readings were corrected for window and prism absorptions and also for the emissivity of the tungsten vee.<sup>4</sup> The absolute accuracy of the temperatures reported is estimated to be  $\pm 30^\circ$ . The reproducibility is at least  $\pm 10^\circ$ .

*Preparation of ThN.* Thorium nitrides can be made directly from the elements or by reaction of the hydride with nitrogen or ammonia. The product of any of these reactions below 1500° is Th<sub>2</sub>N<sub>3</sub>. When Th<sub>2</sub>N<sub>3</sub> is heated under vacuum above about 1500°, ThN is formed as a golden yellow powder, which reacts readily in air to form ThO<sub>2</sub>.

The ThN used in the present studies was prepared in several ways. For most of the experiments it was made by induction melting crystal bar thorium in a tungsten crucible under about 2 atm. of spectroscopically pure nitrogen. At first the temperature was increased rapidly to 2000°. Then, after holding for about 15 min. at 2000°, the temperature was increased until melting occurred. The ThN ingot thus formed was removed readily from the crucible by breaking the tungsten away from the ingot. The ingot was a golden yellow color when first removed from the furnace, but within seconds a black surface film formed. Made in this way, the ThN contained 400 p.p.m. by weight of oxygen, whereas the crystal bar thorium starting material contained 130 p.p.m.

Ingot of ThN made by the induction melting process were stored under vacuum until needed, and then portions of the ingots were powdered in an argon atmosphere glovebox. A supply of the powder was transferred under argon to the vacuum can of the melting point furnace for storage during the runs. Argon was used to break the vacuum after each experimental run and was allowed to flow through the melting point furnace during loading. Samples were removed from the storage cup without removing the cup from the furnace. This procedure reduced contact between air and the reactive nitride powder.

In an effort to be certain that the nitride contained no oxygen, some of the samples were made in the melting point apparatus in the following manner and their melting points determined *in situ* without exposing the samples to air. A few thorium granules were placed in the tungsten vee and heated rapidly under nitrogen to the expected melting point of the nitride. Reaction between the metal and the nitrogen was so

rapid that the metal did not melt or vaporize appreciably. Melting point results obtained with this *in situ* material were essentially identical with those obtained from the induction-melted nitride. Larger amounts of thorium nitride were also made in the tungsten vee, but the time of heating was usually extended to about 1 hr., and the temperature employed was between 1500 and 1800°. In this procedure the nitrogen was pumped out after reaction, and the product was held at the reaction temperature under vacuum to decompose any Th<sub>2</sub>N<sub>3</sub> present. The use of spectroscopically pure nitrogen yielded ThN with no ThO<sub>2</sub> detectable by X-ray methods, whereas samples made with commercial "prepurified" nitrogen contained 5-10 vol. % ThO<sub>2</sub>.

In a number of experiments, hot pressed ThN samples were used. These were made by hot-pressing, in a graphite die, ThN made from hydride and nitrogen, and then firing the resulting compacts at 1800° under 3 atm. of nitrogen, after their surfaces had been machined to remove carbon contamination. The final product was found to contain 0.55 to 0.72 wt. % oxygen by fusion analysis. Micrographic examination revealed small amounts of a dark phase presumed to be ThO<sub>2</sub>, and X-ray diffraction patterns confirmed the presence of ThO<sub>2</sub>.

Thorium nitride was also prepared by arc melting thorium metal under approximately 0.8 atm. nitrogen pressure. This procedure, however, resulted in incomplete conversion; the product consisted of ThN dendrites in a thorium matrix.

*Procedure.* The decomposition experiments were done in the following manner. Approximately 5 mg. of powdered ThN was loaded into the tungsten vee, the apparatus was evacuated, and the sample was outgassed under vacuum at about 800° for a few minutes. Then, the desired pressure of spectroscopically pure nitrogen was admitted to the apparatus. The temperature was increased rapidly until the expected decomposition temperature was nearly reached and then was increased more slowly until the sample melted. Pyrometer readings were taken before and after melting, and the actual melting temperature was assumed to be the average of the two values. Usually the before and after readings differed by less than 10°. Pressure measurements were also made before and after melting, and the true decomposition pressure was assumed to be the average of these two values.

## Results

### 1. Decomposition Pressure and Congruent Melting

(4) W. M. Olson and R. N. R. Mulford, *J. Phys. Chem.*, **67**, 952 (1963).



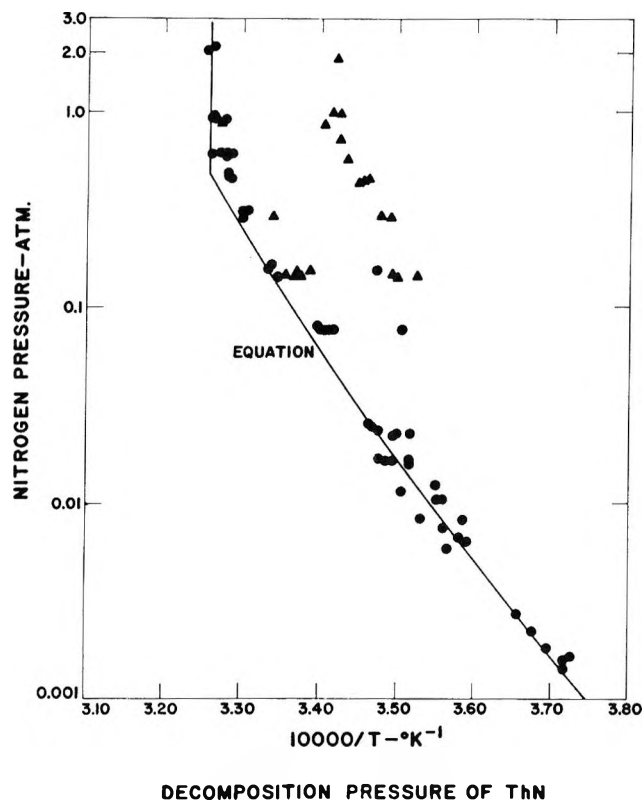


Figure 1. Log decomposition pressure of ThN vs. reciprocal of temperature: circles, pure ThN; triangles, ThN contaminated with oxygen.

*Point.* In Figure 1 the decomposition pressures obtained for ThN are plotted as  $\log p$  (atm.) vs.  $10,000/T$  ( $T$  in  $^{\circ}\text{K}$ ). The solid circles represent data obtained with oxygen-free nitride made either by the induction heating method or the *in situ* process. Although the data obtained from the oxygen-free nitride are considerably scattered, it is apparent that the points fall along a gentle curve which intersects the vertical line representing congruent melting. Because of this scatter and the curvature near the intersection, it is difficult to determine accurately the minimum pressure under which congruent melting occurs, but it appears to be less than 1 atm. The congruent melting temperature of oxygen-free ThN was found to be  $2790 \pm 30^{\circ}$ .

2. *Effect of Oxygen.* The data plotted as triangles in Figure 1 were obtained with the hot pressed ThN stock. Most of these points fall along a line about  $130^{\circ}$  lower than that passing through the data obtained with oxygen-free nitride. Since the hot pressed nitride contained 0.6 wt. % oxygen, compared to 0.04 found in the "oxygen-free" material, it seems obvious that oxygen lowers both the congruent melting point and the decomposition temperature. In an attempt to

confirm this conclusion, samples containing approximately 0.2, 0.6, 0.8, 1.2, and 2.4 wt. % oxygen, prepared by mixing powdered ThN with  $\text{ThO}_2$ , were run. Most of the data points thus obtained fell along the lower temperature line of Figure 1. Evidently; 0.2 wt. % or less of oxygen is sufficient to lower markedly the decomposition temperature of ThN, and greater amounts of oxide have little additional effect.

According to Lambertson, Mueller, and Gunzel,<sup>5</sup> the melting point of  $\text{ThO}_2$  is  $3220 \pm 50^{\circ}$ . Therefore a solid solution apparently is not formed between ThN and  $\text{ThO}_2$ , as one would expect the solid solution melting point to increase with increasing proportion of  $\text{ThO}_2$  instead of decreasing as observed.

Table I gives lattice parameters and other pertinent data for the ThN preparations. By comparing samples 2 and 4 it is seen that there is no large change of lattice parameter with oxygen content, and hence there is probably very small solubility of oxygen in ThN. Micrographic examination of the ThN- $\text{ThO}_2$  mixtures after melting suggested that a eutectic formed between the two compounds and that less than 0.2 wt. % oxygen was sufficient to produce the eutectic. Eutectic formation thus appears to be the most likely explanation for the observed lowering of the decomposition temperature.

3. *Stoichiometry of ThN.* As oxygen has little or no effect on the lattice parameter of ThN, it should be possible to determine whether ThN has a significant stoichiometry range by studying its lattice parameter as a function of nitrogen content. Samples 1 and 8 in Table I contained a thorium phase and were heat treated at 1800 and  $1000^{\circ}$ , respectively. The ThN in these samples thus had a composition on the thorium-rich boundary of the ThN single-phase region. Samples 3, 5, and 7 were heat-treated under nitrogen and are presumed to have had compositions on the nitrogen-rich phase boundary. There appears to be a difference of about 0.001 Å. in the lattice parameters of the two sets, which we interpret as evidence that ThN exists over only a very small range of composition, if any.

## Discussion

It is not possible to determine the standard heat of formation of ThN from the decomposition pressure data because the liquid thorium present in equilibrium with the nitride is saturated with nitrogen and has an unknown activity less than unity. The solubility undoubtedly varies with temperature. At higher tem-

(5) W. A. Lambertson, M. H. Mueller, and F. H. Gunzel, Jr., *J. Am. Ceram. Soc.*, **36**, 397 (1953).

**Table I:** Lattice Parameters for ThN

Sample no.	Method of preparation	Condition	ThN lattice parameter, Å.	Oxygen content, wt. %
1	Induction melted	1800° under vacuum, Th phase present	5.1608 ± 5	0.04
2	Induction melted	As prepared	5.1597 ± 7	0.04
3	Hot pressed	Melted in 2 atm. of N <sub>2</sub>	5.1585 ± 5	0.6
4	Hot pressed	As prepared	5.1582 ± 3	0.6
5	<i>In situ</i> , spectro N <sub>2</sub>	Melted in 1.5 atm. of N <sub>2</sub>	5.1585 ± 3	No ThO <sub>2</sub> by X-ray
6	<i>In situ</i> , spectro N <sub>2</sub>	Melted in 0.7 atm. of N <sub>2</sub> , held at 2000° under vacuum	5.1583 ± 3	No ThO <sub>2</sub> by X-ray
7	Induction melted	1000°, 4 days in 0.92 atm. of N <sub>2</sub>	5.159 ± 1	0.04
8	Arc melted in 0.7 atm. of N <sub>2</sub>	1000°, 4 days under vacuum, Th phase present	5.159 ± 1	No ThO <sub>2</sub> by X-ray
9	<i>In situ</i> , "prepurified" N <sub>2</sub>	As prepared	5.1590 ± 5	0.6-1.2 by X-ray

peratures more nitrogen will be dissolved in the liquid thorium, lowering its activity, and therefore the  $\log p$  vs.  $1/T$  plot would be expected to show some curvature, as indeed it does. The curvature might also be attributed to a temperature variation of composition of the ThN phase. Although results described in the preceding section suggest that the ThN phase does not vary in composition, it should be noted that a large stoichiometry range at high temperatures has been reported for UN.<sup>6</sup> Similar experiments to those reported here have been done on UN,<sup>4</sup> and similarly, by the lattice parameter criterion, it was concluded that UN was stoichiometric.

If it is assumed that the measured data are for a reaction in which the activity of the liquid thorium and perhaps also the ThN activity are less than unity, and that these activities approach unity as the temperature decreases, then the lowest experimental point can be used to calculate a limit for the standard free energy of formation of ThN. This can be done by combining an estimated standard entropy of formation with this experimental value. The lowest experimental point is  $P_{N_2} = 1.5 \times 10^{-3}$  atm. at 2703°K.  $\Delta S_f^{\circ 298}$  is taken as  $-20$  cal. deg.<sup>-1</sup> mole<sup>-1</sup> and  $\Delta C_{p,f}^{\circ}$  is assumed to be  $1.5$  cal. deg.<sup>-1</sup> mole<sup>-1</sup>. The conclusion from these calculations is that the standard heat of formation of ThN at 298°K. is more negative than  $-73$  kcal. mole<sup>-1</sup>.

Calorimetric measurements of the heat of formation of thorium nitride have been made by Neumann and co-workers.<sup>7,8</sup> A direct combination of thorium and nitrogen at 970° gave products that ranged in composition from ThN<sub>0.7</sub> to ThN<sub>0.9</sub> and a heat of 77.1 kcal./g.-atom of N. Which thorium nitride was actually obtained is questionable, but when a sample that analyzed ThN<sub>1.32</sub> was burned in oxygen, almost the same value was obtained (77.8 kcal./g.-atom of N); therefore it appears that the heat of formation of Th<sub>2</sub>N<sub>3</sub> was measured in the direct combination experi-

ment. If this is correct, then the standard heat of formation of thorium mononitride is at least equal to and probably more negative than  $-77,400$  cal./mole, the average of the two determinations of Neumann, *et al.* There appears to be no reliable way to estimate the difference in heats between ThN and Th<sub>2</sub>N<sub>3</sub>.

In previous work with UN<sup>3</sup> and PuN,<sup>9</sup> it was found that an empirical equation of the form  $\log p = A + B/T + CT^5$  fitted the experimental points well. The coefficients  $A$  and  $B$  were proportional to the standard entropy and enthalpy changes at temperature, respectively, and the  $CT^5$  term allowed for deviation of the liquid metal phase and possibly also the nitride from unit activity. The same form of equation was fitted to the present data.  $A$  was computed from the estimated entropy and heat capacity. In the present case we do not have a heat of formation value from which to compute the coefficient  $B$ , and therefore both the  $B$  and  $C$  coefficients were obtained by fitting to the experimental data instead of fitting just the  $C$  coefficient, as was done in the previous work. The resulting expression

$$\log p \text{ (atm)} = 8.086 - 33,224/T + 0.958 \times 10^{-17}T^5$$

can probably be used with reasonable accuracy to extrapolate the data at least down to the melting point of thorium.

*Acknowledgment.* We wish to thank F. H. Ellinger for the X-ray data reported herein and Maynard E. Smith for the fusion analyses for oxygen.

(6) R. Benz and M. G. Bowman, paper presented at 148th National Meeting of the American Chemical Society, Chicago, Ill., Sept. 1964.

(7) B. Neumann, C. Kröger, and H. Haebler, *Z. anorg. allgem. Chem.*, **207**, 145 (1932).

(8) B. Neumann, C. Kröger, and H. Kunz, *ibid.*, **218**, 379 (1934).

(9) W. M. Olson and R. N. R. Mulford, *J. Phys. Chem.*, **68**, 1048 (1964).

# The Estimation of Diffusion Coefficients for Ternary Systems of Strong and Weak Electrolytes

by Richard P. Wendt

Coates Chemical Laboratory, Louisiana State University, Baton Rouge, Louisiana (Received October 14, 1964)

Equations are derived for estimating phenomenological coefficients and diffusion coefficients for two classes of ternary systems: class I, containing only strong electrolytes as solutes, and class II, containing both weak and strong electrolytes as solutes. The approximate equations derived relate each of the four phenomenological coefficients for a ternary system to the concentrations and limiting equivalent conductivities of the ions in the system. From estimates of the phenomenological coefficients and from either known or estimated values for the chemical potential derivatives, the four diffusion coefficients for the system can be calculated. Estimated values for the coefficients are compared with observed values in the literature for four systems:  $\text{H}_2\text{O}-\text{NaCl}-\text{KCl}$ ,  $\text{H}_2\text{O}-\text{LiCl}-\text{KCl}$ ,  $\text{H}_2\text{O}-\text{LiCl}-\text{NaCl}$ , and  $\text{H}_2\text{O}-\text{Na}_2\text{SO}_4-\text{H}_2\text{SO}_4$ . Agreement between estimated and observed values is good for the first three systems but poor for the last system. From these comparisons the concentration range of validity of approximations made during the derivatives is inferred.

## Introduction

Diffusion coefficients are difficult to measure for multicomponent systems. Since 1955, when Dunlop and Gosting<sup>1</sup> at the University of Wisconsin first measured diffusion coefficients for a three-component system, the diffusion process has been studied for only several nonelectrolyte and electrolyte ternary systems.<sup>2</sup> Especially because of the many multicomponent electrolyte systems of industrial and biological interest, we feel it is important to present a general method for estimating phenomenological coefficients,  $(L_{ij})_0$ , and diffusion coefficients,  $(D_{ij})_0$ , for such systems from readily obtainable conductivity data.

The coefficients to be estimated appear in the following two sets of equations, either of which, according to nonequilibrium thermodynamics,<sup>3,4</sup> may be used to describe the isothermal diffusion process in a system containing  $n$  neutral components

$$(J_i)_0 = -\sum_{j=1}^{n-1} (L_{ij})_0 \text{grad } \mu_j \quad (i = 1, \dots, n-1) \quad (1)$$

$$(J_i)_0 = -\sum_{j=1}^{n-1} (D_{ij})_0 \text{grad } c_j \quad (i = 1, \dots, n-1) \quad (2)$$

Throughout this paper the notation corresponds to that used by Hooyman<sup>5</sup> and Gosting and co-workers.<sup>2,6</sup>

The subscript 0 refers to the solvent; the solvent-fixed flows of matter,  $(J_i)_0$ , are defined relative to the local velocity of the solvent and have here the dimensions moles/(cm.<sup>2</sup> sec.); the gradients of chemical potentials,  $\text{grad } \mu_j$  (ergs/mole of  $j$ ), are taken with time held constant;  $c_j$  is the concentration of  $j$ , in moles/cc.; and the solvent-fixed diffusion coefficients,  $(D_{ij})_0$ , are related to the solvent-fixed phenomenological coefficients,  $(L_{ij})_0$ , by

$$(D_{ij})_0 = \sum_{k=1}^{n-1} (L_{ik})_0 \mu_{kj} \quad (i, j = 1, \dots, n-1) \quad (3)$$

Here the  $\mu_{kj}$  are chemical potential derivatives

$$\mu_{kj} = \partial \mu_k / \partial c_j \quad (k, j = 1, \dots, n-1) \quad (4)$$

(1) P. J. Dunlop and L. J. Gosting, *J. Am. Chem. Soc.*, **77**, 5238 (1955).

(2) Brief summaries of work in this field are given as part of recent papers by L. A. Woolf, *J. Phys. Chem.*, **67**, 273 (1963); J. G. Albright, *ibid.*, **67**, 2628 (1963); and P. J. Dunlop, *ibid.*, **68**, 26 (1964).

(3) S. R. de Groot and P. Mazur, "Non-Equilibrium Thermodynamics," Interscience Publishers, Inc., New York, N. Y., 1962.

(4) D. D. Fitts, "Nonequilibrium Thermodynamics," McGraw-Hill Book Co., Inc., New York, N. Y., 1962.

(5) G. J. Hooyman, *Physica*, **22**, 751 (1956).

(6) P. J. Dunlop and L. J. Gosting, *J. Phys. Chem.*, **63**, 86 (1959).

The coefficients actually measured in diffusion experiments are cell-fixed,  $(D_{ij})_C$ , which are very nearly equal<sup>7</sup> to volume-fixed diffusion coefficients,  $(D_{ij})_V$ ; the  $(D_{ij})_0$  are related to the latter coefficients by<sup>5,6</sup>

$$(D_{ij})_0 = (D_{ij})_V + \frac{c_i}{c_0 \bar{V}_0} \sum_{k=1}^{n-1} \bar{V}_k (D_{kj})_V \quad (i, j = 1, \dots, n = 1) \quad (5)$$

where  $\bar{V}_k$  is the partial molar volume, in cc./mole, of component  $k$ . It can be seen from (5) that near infinite dilution  $(D_{ij})_0 = (D_{ij})_V$ , but even in relatively concentrated solutions (*ca.* 1.0 total molarity),  $(D_{ij})_0$  and  $(D_{ij})_V$  may differ by only 1–5%.<sup>6</sup> Therefore in the absence of values for the  $\bar{V}_k$  the equations derived for estimating the  $(D_{ij})_0$  also provide estimates of the  $(D_{ij})_V$ .

The same general procedure is followed here in two separate derivations. The first derivation is for ternary systems containing two strong electrolyte solutes having a common ion, and the second is for a class of ternary systems containing two electrolyte solutes which may only partially dissociate (see eq. 36). For both classes of systems the derivations rigorously follow the principles of nonequilibrium thermodynamics to obtain sets of exact equations. Approximations are then made for certain quantities in the exact equations so that the four coefficients  $(L_{ij})_0$  can be estimated from values for the limiting equivalent conductivities,  $\lambda_i^0$ , and the concentrations,  $c_i$ , of all ions in the given system. The four diffusion coefficients  $(D_{ij})_0$  can then be calculated from eq. 3 if values for the chemical potential derivatives  $\mu_{kj}$  are available. Methods are also discussed for estimating the  $\mu_{kj}$ , so that the  $(D_{ij})_0$ , and to a good approximation the  $(D_{ij})_V$ , can be estimated only from values for the  $\lambda_i^0$  and  $c_i$  of all ions.

An earlier approximate theory, derived by Gosting<sup>8</sup> for ternary systems containing strong electrolytes as solutes, suggested the general form of the theory presented here, but it differs from ours in an important way: all approximations are made early in the former derivation, with the result that explicit expressions are obtained for estimating only the  $(D_{ij})_0$  from values for  $\lambda_i^0$  and  $c_i$  of the ions. The coefficients  $(L_{ij})_0$  cannot be directly estimated, nor can available values for the  $\mu_{kj}$  be used to improve the estimates of  $(D_{ij})_0$  by using eq. 3. The equations derived here should therefore provide more accurate estimates of the  $(D_{ij})_0$  for the systems for which the  $\mu_{kj}$  are available, and the several approximations used for those systems can be more carefully examined by comparing estimated and observed values for the  $(L_{ij})_0$  and  $(D_{ij})_0$ . For the

systems of class I for which no observed values of the  $\mu_{kj}$  are available, our theory and Gosting's theory make equivalent predictions of values for the  $(D_{ij})_0$ . A more recent theory derived by Stockmayer<sup>9</sup> is applicable only to binary weak-electrolyte systems such as  $\text{H}_2\text{O}-\text{H}_2\text{SO}_4$ , but its rigorous derivation suggested several methods of achieving generality in the present multi-component theory.

The equations derived here are tested by using available thermodynamic and diffusion data for the ternary systems  $\text{H}_2\text{O}-\text{NaCl}-\text{KCl}$ ,  $\text{H}_2\text{O}-\text{LiCl}-\text{KCl}$ ,  $\text{H}_2\text{O}-\text{LiCl}-\text{NaCl}$ , and  $\text{H}_2\text{O}-\text{Na}_2\text{SO}_4-\text{H}_2\text{SO}_4$ . These data were only available at relatively high solute concentrations (*ca.* 0.5–3.0 total molarity) where the approximations made for quantities in the final equations were not expected to hold. Nevertheless, for the three strong electrolyte systems the predicted and observed values for the  $(D_{ij})_0$  are found to agree remarkably well. For the weak-electrolyte system  $\text{H}_2\text{O}-\text{Na}_2\text{SO}_4-\text{H}_2\text{SO}_4$  the agreement is relatively poor, but the order of magnitude, algebraic sign, and approximate concentration dependence of the  $(L_{ij})_0$  and  $(D_{ij})_0$  are correctly predicted.

## Theoretical

*Outline.* The two classes of systems will be separately treated but both derivations will follow the same general procedure. The first part of each derivation presents simple thermodynamic and stoichiometric relations between the chemical potentials, the stoichiometric coefficients, the concentrations, and the mass flows of all ions and neutral solutes comprising the system. Then the entropy-production expression is used to specify the independent flows and forces in the system. The condition of zero net electrical current flow is used in the third part to obtain exact relationships between the ionic and the neutral-solute phenomenological coefficients  $(L_{ij})_0$  which appear in the flow equations for ions and for neutral solutes, respectively. Approximations for the ionic  $(L_{ij})_0$  are made in the next part of the derivation which enable the neutral solute  $(L_{ij})_0$  to be estimated from values for the concentrations and limiting equivalent conductivities of all ions in the system. Finally; simple methods for estimating the neutral-solute chemical potential derivatives  $\mu_{kj}$  are discussed. The diffusion coefficients  $(D_{ij})_0$  can then be calculated from

(7)  $(D_{ij})_V = (D_{ij})_C$  if the  $\bar{V}_k$  are independent of concentration throughout the diffusion experiment; see G. J. Hooyman, *et al.*, *Physica*, **19**, 1095 (1953).

(8) L. J. Gosting in "Advances in Protein Chemistry," Vol. XI, Academic Press, Inc., New York, N. Y., 1956, pp. 536–539.

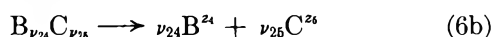
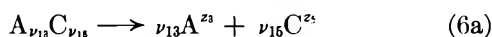
(9) W. H. Stockmayer, *J. Chem. Phys.*, **33**, 1291 (1960).

either known or estimated values for the neutral-solute  $(L_{ij})_0$  and  $\mu_{kj}$  by using eq. 3.

For any system of electrolytes not in the classes discussed here, the derivation would follow the general procedure outlined above, regardless of the kind or number of components in the system.

### Theory for Systems of Class I

*Thermodynamic Relations.* Consider two neutral strong electrolyte solutes  $A_{\nu_{13}}C_{\nu_{14}}$  and  $B_{\nu_{24}}C_{\nu_{25}}$  which completely dissociate according to the reactions



The first subscript on each stoichiometric coefficient  $\nu_{ij}$  refers to the neutral solute  $i$ ; here  $i = 1$  and  $i = 2$ . designate the solutes  $A_{\nu_{13}}C_{\nu_{14}}$  and  $B_{\nu_{24}}C_{\nu_{25}}$ , respectively. The second subscript on  $\nu_{ij}$  refers to the ion;  $j = 3$ ,  $j = 4$ , and  $j = 5$  designate the three ions  $A^{z_3}$ ,  $C^{z_4}$ , and  $B^{z_4}$ , respectively. Valences of the ions (including the algebraic sign) are represented by  $z_i$ .

Chemical potentials for the neutral solutes are defined by

$$\mu_i = \sum_{j=3}^5 \nu_{ij}\mu_j \quad (i = 1, 2) \quad (7)$$

Here and throughout the derivation we define  $\nu_{14} = \nu_{23} = 0$ . By taking the gradient of both sides of (7) and letting  $X_i = -\text{grad } \mu_i$  we obtain

$$X_i = \sum_{j=3}^5 \nu_{ij}X_j \quad (i = 1, 2) \quad (8)$$

Equation 8 is solved for  $X_3$ ,  $X_4$ , and  $X_5$ , finding

$$X_i = \sum_{j=1}^3 a_{ij}X_j \quad (i = 3, 4, 5) \quad (9)$$

where the coefficients  $a_{ij}$  have the values

$$\begin{aligned} a_{31} &= 0 & a_{32} &= 0 & a_{33} &= 1 \\ a_{41} &= -\frac{\nu_{25}}{\nu_{15}\nu_{24}} & a_{42} &= \frac{1}{\nu_{24}} & a_{43} &= \frac{\nu_{13}\nu_{25}}{\nu_{15}\nu_{24}} \\ a_{51} &= \frac{1}{\nu_{16}} & a_{52} &= 0 & a_{53} &= -\frac{\nu_{13}}{\nu_{16}} \end{aligned} \quad (10)$$

The solutes 1 and 2 are neutral; thus

$$\sum_{j=3}^5 \nu_{ij}z_j = 0 \quad (i = 1, 2) \quad (11)$$

The  $z_i$  are related by

$$z_i = a_{i3}z_3 \quad (i = 3, 4, 5) \quad (12)$$

where the  $a_{i3}$  are given by eq. 10.

The principle of conservation of mass is applied to the concentrations  $c_i$  and the flows  $(J_i)_0$  of the ionic species 3, 4, 5 to obtain

$$\sum_{i=1}^2 \nu_{ij}c_i = c_j \quad (j = 3, 4, 5) \quad (13)$$

$$\sum_{i=1}^2 \nu_{ij}(J_i)_0 = (J_j)_0 \quad (j = 3, 4, 5) \quad (14)$$

Because of (13), equations similar to (14) are valid for any reference frame.<sup>10</sup>

*Entropy Production.* For three-ion systems the entropy produced by isothermal diffusion is given by

$$T\sigma = \sum_{i=3}^5 (J_i)_0(X_i + z_i f E) \quad (15)$$

Here  $\sigma$  is the local rate of production of entropy per unit volume,  $T$  is the temperature of the isothermal system,  $f$  is the absolute value of the charge per mole of electrons,<sup>11</sup> and  $E$  is the local electric field. We replace each  $(J_i)_0$ ,  $i = 3, 4, 5$  in (15) by its equivalent from (14); after rearranging, (15) is rewritten

$$T\sigma = \sum_{i=1}^2 \sum_{j=3}^5 (J_i)_0 \nu_{ij} X_j + f E \sum_{i=1}^2 \sum_{j=3}^5 (J_i)_0 \nu_{ij} z_j \quad (16)$$

where as before  $\nu_{14} = \nu_{23} = 0$ . The coefficient of  $fE$  vanishes because of (11), and because of (8) the first term reduces to

$$T\sigma = \sum_{i=1}^2 (J_i)_0 X_i \quad (17)$$

Thus the entropy production can be expressed by either (15) or (17) and the linear laws can be written

(10) Macroscopic velocities  $v_i$  of neutral components can be defined by

$$\sum_{i=1}^2 \nu_{ij}c_i v_i = c_j v_j \quad (j = 3, 4, 5) \quad (a)$$

where  $v_j$  is the macroscopic velocity of ion  $j$ . Flows in general are measured with respect to an arbitrary reference frame R of velocity  $v_R$

$$(J_i)_R = c_i(v_i - v_R) \quad (b)$$

and cell-fixed flows are obtained by letting  $v_R = 0$

$$(J_i)_C = c_i v_i \quad (i = 1, \dots, 5) \quad (c)$$

Thus (a) also reads  $\sum_{i=1}^2 \nu_{ij}(J_i)_C = (J_j)_C$ . Both sides of (b) are multiplied by  $\nu_{ij}$  and summed over  $i = 1, 2$ ; (a) and (13) are introduced, and the general result which can be specialized to (14) is obtained

$$\begin{aligned} \sum_{i=1}^2 \nu_{ij}(J_i)_R &= c_j v_j - c_j v_R \\ &= (J_j)_R \end{aligned} \quad (d)$$

(11)  $f$  is given by eq. h of the Appendix

for flows of two neutral solutes (eq. 1 with  $n = 3$ ) or for flows of three ions

$$(J_i)_0 = \sum_{j=3}^5 (L_{ij})_0 (X_j + z_j fE) \quad (i = 3, 4, 5) \quad (18)$$

according to the linear-law postulate of nonequilibrium thermodynamics.<sup>3,4</sup>

*Relations between Phenomenological Coefficients.* For the irreversible process considered here, namely diffusion with no net electrical conduction, the flows of ions are related by the condition of zero net electrical current flow

$$\sum_{i=3}^5 z_i (J_i)_0 = 0 \quad (19)$$

We apply this condition to eq. 18 and find an expression for  $fE$

$$fE = - \frac{\sum_{k=3}^5 \sum_{l=3}^5 z_k (L_{kl})_0 X_l}{\sum_{m=3}^5 \sum_{n=3}^5 z_m (L_{mn})_0 z_n} \quad (20)$$

Here new subscripts  $k$ ,  $l$ ,  $m$ , and  $n$  have been introduced for convenience. Equation 20 could be used to calculate liquid junction potentials or diffusion potentials if the coefficients  $(L_{kl})_0$  and the gradients of ionic chemical potentials  $X_l$  were all known.

We use (20) to eliminate  $fE$  from eq. 18, which after rearrangement becomes

$$(J_i)_0 = \sum_{l=3}^5 X_l \left[ (L_{il})_0 - \frac{\sum_j \sum_k (L_{ij})_0 z_j z_k (L_{kl})_0}{\sum_m \sum_n z_m (L_{mn})_0 z_n} \right] \quad (i = 3, 4, 5) \quad (21)$$

The valences  $z_i$  in (21) are replaced by their equivalents according to (12), obtaining

$$(J_i)_0 = \sum_{l=3}^5 \Omega_{il} X_l \quad (i = 3, 4, 5) \quad (22)$$

where we define

$$\Omega_{il} = (L_{il})_0 - \frac{\sum_{j=3}^5 \sum_{k=3}^5 (L_{ij})_0 a_{j3} a_{k3} (L_{kl})_0}{\sum_{m=3}^5 \sum_{n=3}^5 a_{m3} (L_{mn})_0 a_{n3}} \quad (i, l = 3, 4, 5) \quad (23)$$

After using eq. 9 for  $X_l$  (22) becomes

$$(J_i)_0 = \sum_{j=1}^2 \sum_{l=3}^5 X_j a_{lj} \Omega_{il} \quad (i = 3, 4, 5) \quad (24)$$

The term in  $X_3$  has been eliminated by using the important identity<sup>12</sup>

$$\sum_{l=3}^5 a_{il} \Omega_{il} = 0 \quad (i = 3, 4, 5) \quad (25)$$

Thus for diffusion with no net electrical current flow the flows of ions 3, 4, 5 can be written as linear functions of only two variables,  $X_1$  and  $X_2$ , the chemical potential gradients of the neutral solutes. By using eq. 14 with<sup>13</sup>  $j = 3, 4$ , we obtain a new set of linear relations between the flows of neutral solutes and their conjugate forces

$$(J_1)_0 = \nu_{13}^{-1} \sum_{j=1}^2 \sum_{l=3}^5 X_j a_{lj} \Omega_{3l} \quad (26a)$$

$$(J_2)_0 = \nu_{24}^{-1} \sum_{j=1}^2 \sum_{l=3}^5 X_j a_{lj} \Omega_{4l} \quad (26b)$$

The coefficients of  $X_1$  and  $X_2$  in the above equations are then equated to the coefficients  $(L_{ij})_0$  in eq. 1 (with  $i = 1, 2$ ) to obtain a set of exact relations between the phenomenological coefficients for neutral solutes and those for ions

$$(L_{1j})_0 = \nu_{13}^{-1} \sum_{l=3}^5 a_{lj} \Omega_{3l} \quad (j = 1, 2) \quad (27a)$$

$$(L_{2j})_0 = \nu_{24}^{-1} \sum_{l=3}^5 a_{lj} \Omega_{4l} \quad (j = 1, 2) \quad (27b)$$

*Approximations for  $(L_{ij})_0$ .* This derivation has so far been rigorously performed according to the principles of nonequilibrium thermodynamics. If the nine ionic coefficients  $(L_{ij})_0$  in (18) were known at any particular composition, then the four neutral-solute coefficients  $(L_{ij})_0$  in eq. 1 (with  $n = 3$ ) could be calculated and compared with their measured values at that composition. Unfortunately, such data are not available; therefore, to make this derivation practically useful for estimating the neutral-solute  $(L_{ij})_0$ , we make approximations which enable us to relate some of the ionic  $(L_{ij})_0$  to the limiting equivalent conductivities of the ions in the system.

(12) The equivalent of  $\Omega_{ij}$ , as defined by (23) or (50), is introduced into the left-hand side of (25) or (51) and the sum of sums is written with a common denominator

$$\sum_l a_{il} \Omega_{il} = \frac{\sum_l \sum_m \sum_n a_{il} (L_{li})_0 a_{m3} (L_{mn})_0 a_{n3} - \sum_j \sum_k \sum_l a_{il} (L_{ij})_0 a_{j3} a_{k3} (L_{kl})_0}{\sum_m \sum_n a_{m3} (L_{mn})_0 a_{n3}}$$

In the triple sum at the right-hand side of the numerator the subscripts  $j$ ,  $k$ , and  $l$  are replaced by  $l$ ,  $m$ , and  $n$ , respectively; because all summations run over the same range both triple sums are equivalent, the numerator vanishes, and the identities (25) and (51) are proven.

(13) The two eq. 14 with  $j = 3, 4$  are chosen for convenience; any two of the three  $j = 3, 4, 5$  could be used.

First we assume that the cross-term phenomenological coefficients in the ionic flow eq. 18 are identically zero at all concentrations

$$(L_{ij})_0 = 0 \quad (i \neq j) \quad (i, j = 3, 4, 5) \quad (28)$$

Then the expressions for the  $\Omega_{il}$  become

$$\Omega_{il} = (L_{ii})_0 \delta_{il} - S^{-1} (L_{ii})_0 a_{i3} a_{i3} (L_{ii})_0 \quad (i, l = 3, 4, 5) \quad (29)$$

where

$$S = \sum_{k=3}^5 a_{k3}^2 (L_{kk})_0$$

and  $\delta_{il}$  is the Kronecker  $\delta$ , *i.e.*,  $\delta_{il} = 1$  for  $i = l$  and  $\delta_{il} = 0$  for  $i \neq l$ .

The main-term coefficients  $(L_{ii})_0$  or  $(L_{il})_0$  in (29) can be approximately related to their respective ionic limiting equivalent conductivities,  $\lambda_i^0$  or  $\lambda_l^0$ , by<sup>14</sup>

$$(L_{ii})_0 = \lambda_i^0 c_i / (|z_i| F^2 \times 10^7) \quad (i = 3, \dots, s+2) \quad (30)$$

Here  $\lambda_i^0$  has the units  $\text{cm}^2 \text{ ohm}^{-1} \text{ equiv.}^{-1}$ ,  $s$  is the number of ions in the system, and  $F$  is the Faraday constant with the units coulombs/equivalent.

Approximations (28) and (30) amount to the assumption that the mobilities of the ion are the same at appreciable concentrations as they are at infinite dilution; the approximations are exact near infinite dilution. Values of  $(L_{ij})_0$  for the neutral solutes can, however, be estimated at any values for all  $c_i$  by using eq. 30, 29, and 27, and values in the literature for  $\lambda_i^0$ .

*Estimation of  $\mu_{ik}$ .* Values for the chemical potential derivatives  $\mu_{ik}$  are available,<sup>6,15</sup> for example, for the system  $\text{H}_2\text{O}-\text{NaCl}-\text{KCl}$  of class I; these data, and the estimates of  $(L_{ij})_0$  obtained from (27) above, could be used to calculate approximate values for the four diffusion coefficients  $(D_{ij})_0$  for that system according to (3).

Miller<sup>16</sup> has discussed methods for estimating the  $\mu_{ik}$  in lieu of appropriate experimental data. The simple method which we use here is to write expressions for each chemical potential derivative and then assume that the mean ionic activity coefficients are independent of concentration. For systems of class I the chemical potentials  $\mu_i$  for neutral solutes, defined by eq. 7, may be written

$$\mu_i = \mu_i^0 + RT \ln \prod_{j=3}^5 (y_j c_j)^{\nu_{ij}} \quad (i = 1, 2) \quad (31)$$

where  $y_j$  is the activity coefficient of ion  $j$  and  $\mu_i^0$  is the chemical potential at the standard state for neutral solute  $i$ . We define mean ionic activity coefficients for the neutral solutes

$$(y_{\pm})_i = \left[ \prod_{j=3}^5 y_j^{\nu_{ij}} \right]^{1/\left(\sum_{j=3}^5 \nu_{ij}\right)} \quad (i = 1, 2) \quad (32)$$

The product of concentrations can be written

$$\prod_{j=3}^5 c_j^{\nu_{ij}} = (\nu_{13}c)^{\nu_{i3}} (\nu_{24}c_2)^{\nu_{i4}} (\nu_{15}c_1 + \nu_{25}c_2)^{\nu_{i5}} \quad (33)$$

by using (13). Thus (31) becomes

$$\mu_i = \mu_i^0 + RT \left[ \left( \sum_{j=3}^5 \nu_{ij} \right) \ln (y_{\pm})_i + \ln \nu_{13}^{\nu_{i3}} \nu_{24}^{\nu_{i4}} + \nu_{i5} \ln c_1 + \nu_{i4} \ln c_2 + \nu_{i6} \ln (\nu_{16}c_1 + \nu_{25}c_2) \right] \quad (31a)$$

To obtain estimates of the  $\mu_{ik}$  we assume<sup>17</sup>

$$\partial \ln (y_{\pm})_i / \partial c_j = 0 \quad (i, j = 1, 2) \quad (34)$$

Then the derivatives  $\mu_{ik}$  of  $\mu_i$  in (31a) can be estimated from

$$\mu_{ik} = RT \left[ \delta_{ik} \sum_{j=3}^4 (\nu_{ij}/c_i) + \frac{\nu_{i6} \nu_{k6}}{\nu_{16}c_1 + \nu_{25}c_2} \right] \quad (i, k = 1, 2) \quad (35)$$

where  $\delta_{ik}$  is the Kronecker  $\delta$ .

## Theory for Systems of Class II

This class of systems differs from class I because of the presence of four ions (instead of three for class I) and one equilibrium reaction among three of the ions (instead of none for class I).

*Thermodynamic Relations.* A system in this class contains one neutral undissociated solvent (designated by the subscript 0) and two neutral solutes (designated by the subscripts 1 and 2) which dissociate according to the reactions



(14) See eq. k of the Appendix.

(15) P. J. Dunlop, *J. Phys. Chem.*, **63**, 612, 2089 (1959).

(16) D. G. Miller, *ibid.*, **63**, 570 (1959).

(17) For activity coefficients  $\gamma_i$  defined as functions of molality,  $m_j$ , it can be shown that the assumptions

$$\frac{\partial \ln \gamma_i}{\partial m_j} = 0 \quad (i, j = 1, \dots, n-1) \quad (a)$$

imply ideality for the solvent as well as the solutes, but eq. a does not imply eq. 34; instead, eq. a implies small nonzero fixed values, given by  $\bar{V}_j/(1000c_0\bar{V}_0) \cong 0.02$ , for the derivatives  $\partial \ln (y_{\pm})_i / \partial c_j$  at the solute concentrations considered here (*ca.*  $10^{-3}$  mole/cc.). Therefore at very large solute concentrations, or for nonaqueous systems, care should be taken in making assumptions concerning activity coefficients. See ref. 16 and J. G. Kirkwood and I. Oppenheim, "Chemical Thermodynamics," McGraw-Hill Book Co., Inc., New York, N. Y., 1961, p. 171, for relevant thermodynamic derivations.

It must be assumed that the equilibrium reaction (36c) is very fast so that local equilibrium exists throughout the diffusion process.<sup>9</sup>

The chemical potentials of the neutral solutes 1 and 2 and the incompletely dissociated ion 3 are defined by

$$\mu_i = \sum_{j=4}^6 \nu_{ij} \mu_j \quad (i = 1, 2, 3) \quad (37)$$

Here we have set  $\nu_{15} = \nu_{24} = \nu_{34} = 0$ . It follows from (37) that the chemical potential gradients,  $-X_i$ , of ions and solutes are related by

$$X_i = \sum_{j=4}^6 \nu_{ij} X_j \quad (i = 1, 2, 3) \quad (38)$$

These linear equations may be solved for  $X_3, \dots, X_6$ , obtaining

$$X_j = \nu^{-1} \sum_{i=1}^3 a_{ji} X_i \quad (j = 3, \dots, 6) \quad (39)$$

Here  $\nu$  (without subscripts) is the determinant of the matrix of coefficients  $\nu_{ij}$  on the right-hand side of eq. 36

$$\nu = \begin{vmatrix} \nu_{14} & 0 & \nu_{16} \\ 0 & \nu_{25} & \nu_{26} \\ 0 & \nu_{35} & \nu_{36} \end{vmatrix} \quad (40)$$

and the  $a_{ji}$  are given by

$$\begin{aligned} a_{ji} &= (-1)^{i+j+1} \nu^{ij} \quad (i = 1, 2, 3) \\ &\quad (j = 4, 5, 6) \\ a_{31} &= a_{32} = 0 \\ a_{33} &= \nu \end{aligned} \quad (41)$$

The  $\nu^{ij}$  are the complementary minors of  $\nu$ .

Conservation of charge for the dissociation reactions (36) implies

$$\sum_{j=4}^6 \nu_{ij} z_j = 0 \quad (i = 1, 2) \quad (42a)$$

$$\sum_{j=5}^6 \nu_{3j} z_j = z_3 \quad (42b)$$

Solving for  $z_3, \dots, z_6$ , we obtain

$$z_j = \nu^{-1} a_{j3} z_3 \quad (j = 3, \dots, 6) \quad (43)$$

where the  $a_{j3}$  are given by (41).

Conservation of mass requires

$$\sum_{i=1}^2 \nu_{ij} c_i = c_j + \nu_{3j} c_3 \quad (j = 4, 5, 6) \quad (44)$$

and

$$\sum_{i=1}^2 \nu_{ij} (J_i)_0 = (J_j)_0 + \nu_{3j} (J_3)_0 \quad (j = 4, 5, 6) \quad (45)$$

Equation 45 is valid not only for the solvent-fixed but for any reference frame.<sup>10</sup>

*Entropy Production.* For the systems of class II the expression for the entropy production is

$$T\sigma = \sum_{i=3}^6 (J_i)_0 (X_i + z_i fE) \quad (46)$$

Three of the ion flows  $(J_i)_0$ ,  $i = 4, 5, 6$  are eliminated by using eq. 45; after rearrangement, (46) becomes

$$\begin{aligned} T\sigma &= \sum_{j=1}^2 (J_j)_0 \sum_{i=4}^6 \nu_{ji} X_i + (J_3)_0 (X_3 - \sum_{i=4}^6 \nu_{3i} X_i) + \\ &fE \left[ \sum_{j=1}^2 \sum_{i=4}^6 (J_j)_0 \nu_{ji} z_i + (J_3)_0 \left( z_3 - \sum_{i=4}^6 \nu_{3i} z_i \right) \right] \end{aligned} \quad (46a)$$

The coefficients of  $(J_3)_0$  and  $fE$  vanish because of (38) and (42), respectively; the term which remains is further simplified by using (38), obtaining

$$T\sigma = \sum_{i=1}^2 (J_i)_0 X_i \quad (47)$$

Therefore, two independent flows  $(J_i)_0$  and forces  $X_i$  of neutral solutes exist for this class of systems, and either the neutral-solute flow eq. 1, with  $i = 1, 2$ , or the ionic flow equations

$$(J_i)_0 = \sum_{j=3}^6 (L_{ij})_0 (X_j + z_j fE) \quad (i = 3, \dots, 6) \quad (48)$$

may be used to describe the isothermal diffusion process for this class of systems.

*Relations between Phenomenological Coefficients.* The condition of zero net electrical current flow,  $\sum_{i=3}^6 z_i (J_i)_0 = 0$ , is used to eliminate  $fE$  from eq. 48, which then reads

$$(J_i)_0 = \nu^{-1} \sum_{j=1}^2 \sum_{l=3}^6 X_j a_{lj} \Omega_{li} \quad (i = 3, \dots, 6) \quad (49)$$

where

$$\Omega_{li} = (L_{li}) - \frac{\sum_{j=3}^6 \sum_{k=3}^6 (L_{lj})_0 a_{j3} a_{k3} (L_{ki})_0}{\sum_{m=3}^6 \sum_{n=3}^6 a_{m3} (L_{mn})_0 a_{n3}} \quad (i, l = 3, \dots, 6) \quad (50)$$

The identity<sup>12</sup>

$$\sum_{l=3}^6 a_{l3} \Omega_{li} = 0 \quad (i = 3, \dots, 6) \quad (51)$$

has been used to obtain (49), which relates the flows of ions to chemical potential gradients of the two neutral solutes.

The first two equations in the set (45), which relate



flows of ions to flows of neutral solutes, are rearranged to read

$$(J_1)_0 = \nu_{14}^{-1}(J_4)_0 \quad (52a)$$

$$(J_2)_0 = \nu_{25}^{-1}\nu_{35}(J_3)_0 + \nu_{25}^{-1}(J_5)_0 \quad (52b)$$

Expressions (49) for  $(J_3)_0$ ,  $(J_4)_0$ , and  $(J_5)_0$  enable the flows  $(J_1)_0$  and  $(J_2)_0$  to be written as linear functions of  $X_1$  and  $X_2$

$$(J_1)_0 = \nu^{-1}\nu_{14}^{-1} \sum_{j=1}^2 \sum_{l=3}^6 X_j a_{lj} \Omega_{4l} \quad (53a)$$

$$(J_2)_0 = \nu^{-1}\nu_{25}^{-1} \sum_{j=1}^2 X_j \left[ \sum_{l=3}^6 a_{lj} (\nu_{35} \Omega_{3l} + \Omega_{5l}) \right] \quad (53b)$$

The coefficients  $(L_{ij})_0$  of  $X_1$  and  $X_2$  in (1) with  $i = 1, 2$  are equated to the corresponding coefficients in the flow eq. 53, obtaining the desired relations between neutral-solute and ionic phenomenological coefficients

$$(L_{1j})_0 = \nu^{-1}\nu_{14}^{-1} \sum_{l=3}^6 a_{lj} \Omega_{4l} \quad (j = 1, 2) \quad (54a)$$

$$(L_{2j})_0 = \nu^{-1}\nu_{25}^{-1} \sum_{l=3}^6 a_{lj} (\nu_{35} \Omega_{3l} + \Omega_{5l}) \quad (j = 1, 2) \quad (54b)$$

*Approximations for  $(L_{ij})_0$ .* As before, to obtain practical and useful expressions for predicting the four coefficients  $(L_{ij})_0$  from the exact eq. 54, we make the approximation that all cross-term ionic phenomenological coefficients are zero

$$(L_{ij})_0 = 0 \quad (i \neq l) \quad (i, j = 3, \dots, 6) \quad (55)$$

Then the coefficients  $\Omega_{il}$ , defined by eq. 50, become

$$\Omega_{il} = \delta_{il}(L_{ii})_0 - S^{-1}(L_{ii})_0 a_{i3} a_{i3} (L_{ii})_0 \quad (i, l = 3, \dots, 6) \quad (56)$$

where

$$S = \sum_{k=3}^6 a^2_{k3} (L_{kk})_0$$

The main-term coefficients  $(L_{ii})_0$  and  $(L_{il})_0$  in (56) are estimated from values for the limiting equivalent conductances according to eq. 30, which applies to all ions in any system.

*Estimation of  $\mu_{ik}$ .* For systems of this class, which contain a partially dissociated species, D (denoted by the subscript 3), the chemical potentials may be defined by ignoring the existence of D

$$\mu_i = \mu_i^0 + RT \ln \prod_{j=4}^6 (y_j c_j)^{\nu_{ij}} \quad (i = 1, 2) \quad (57)$$

As before, we define

$$(y_{\pm})_i = \left[ \prod_{j=4}^6 y_j^{\nu_{ij}} \right]^{1/\left(\sum_{j=4}^6 \nu_{ij}\right)} \quad (i = 1, 2) \quad (58)$$

where  $(y_{\pm})_i$  is now called the practical mean-ionic activity coefficient. By using eq. 44 (with  $c_3 = 0$ ) to introduce  $c_1$  and  $c_2$  into (57), and again making the assumption (34), equations are obtained for estimating the chemical potential derivatives  $\mu_{ik}$  in systems of class II

$$\mu_{ik} = \mu_i^0 + RT \left[ \delta_{ik} \sum_{j=4}^5 (\nu_{ij}/c_i) + \frac{\nu_{i6}\nu_{k6}}{\nu_{15}c_1 + \nu_{26}c_2} \right] \quad (i, k = 1, 2) \quad (59)$$

Estimates of  $\mu_{ik}$  may also be obtained by defining the  $\mu_i$  as functions of all ion concentrations  $c_i$

$$\mu_i = \mu_i^0 + RT \ln \prod_{j=3}^6 (y_j c_j)^{\nu_{ij}} \quad (i = 1, 2) \quad (60)$$

The activity coefficients for the ions,  $y_j$ , are not measurable quantities but nevertheless we can make the approximations

$$\partial \ln y_i / \partial c_k = 0 \quad (i = 3, \dots, 6) \quad (k = 1, 2) \quad (61)$$

Then the expressions for estimating the  $\mu_{ik}$  are

$$\mu_{ik} = RT \sum_{j=3}^6 \frac{\nu_{ij}}{c_j} \frac{\partial c_j}{\partial c_k} \quad (i, k = 1, 2) \quad (62)$$

If the ionic concentrations  $c_j$  can be written as functions of the neutral solute concentrations  $c_1, c_2$  then the derivatives  $\partial c_j / \partial c_k$  in (62) can be evaluated; the desired functions for  $c_1$  and  $c_2$  may be derived by using eq. 44, the equilibrium-quotient expression for reaction 36c

$$Q = c_6^{\nu_{36}} c_6^{\nu_{36}} / c_3 \quad (63)$$

and the condition of electrical neutrality

$$\sum_{i=3}^6 z_i c_i = 0 \quad (64)$$

Thus values of  $Q$  for the ternary system must be available to estimate the ion concentrations  $c_i$  for use with eq. 30 and to calculate the derivatives  $\partial c_j / \partial c_k$ .

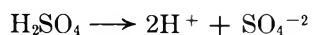
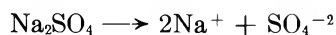
The accuracy of values estimated for the  $(D_{ij})_0$  from eq. 54 and 3 depend on the possibly crude approximations 30, 55 and 59, 62 for the ionic  $(L_{ij})_0$  and the neutral-solute  $\mu_{ik}$ , respectively, which must be used in lieu of experimental data. In general, the estimates for  $\mu_{ik}$  obtained using (59) and (62) will differ from each other for a given system in class II because one procedure neglects ion 3 and the other includes that ion. For a given system of class I, approximations similar to (59) and (62) would lead to equivalent estimates of the  $\mu_{ik}$  because no ions are neglected by either procedure. Of course for any

system the exact or measured values of the  $\mu_{ik}$  are independent of the explicit expressions used for the  $\mu_i$ .

### Tests of the Equations

**Calculations.** Phenomenological coefficients, chemical potential derivatives, and diffusion coefficients are estimated for three systems in class I:  $\text{H}_2\text{O}(0)\text{-NaCl}(1)\text{-KCl}(2)$ ,  $\text{H}_2\text{O}(0)\text{-LiCl}(1)\text{-KCl}(2)$ , and  $\text{H}_2\text{O}(0)\text{-LiCl}(1)\text{-NaCl}(2)$ , where the numbers in parentheses designate the respective neutral components in all subscript notations. Corresponding to the dissociation reactions (6) for solutes 1 and 2, the stoichiometric coefficients  $\nu_{ij}$  and  $z_i$  for all three systems have the values  $\nu_{13} = \nu_{15} = \nu_{24} = \nu_{25} = 1$ ,  $\nu_{14} = \nu_{23} = 0$ ,  $z_3 = z_4 = +1$ , and  $z_5 = -1$ . To estimate the main-term ionic phenomenological coefficients  $(L_{ij})_0$  from eq. 30, the limiting equivalent conductivities were taken to be<sup>18</sup>  $\lambda_{\text{Na}^+}^0 = 50.10$ ,  $\lambda_{\text{K}^+}^0 = 73.50$ ,  $\lambda_{\text{Li}^+}^0 = 38.68$ , and  $\lambda_{\text{Cl}^-}^0 = 76.35$  cm.<sup>2</sup> ohm<sup>-1</sup> equiv.<sup>-1</sup>. Values used for the quantities  $F$ ,  $R$ , and  $T$  were 96,493 coulombs equiv.<sup>-1</sup>,  $8.3144 \times 10^7$  ergs mole<sup>-1</sup> deg.<sup>-1</sup>, and 298.15°K., respectively. Concentrations of ions were calculated at each composition point  $c_1$ ,  $c_2$  according to (13), and the four coefficients  $(L_{ij})_0$  for flows of solutes 1 and 2 were estimated by using eq. 29 and 27. For the system  $\text{H}_2\text{O-NaCl-KCl}$  two methods were used to estimate the four diffusion coefficients  $(D_{ij})_0$  according to (3). In method A, values used for the chemical potential derivatives  $\mu_{ij}$  were estimated from eq. 35; in method B, observed values<sup>6,15</sup> for  $\mu_{ij}$  were used. Because no appropriate thermodynamic data are available, only method A was used to estimate diffusion coefficients for the systems  $\text{H}_2\text{O-LiCl-KCl}$  and  $\text{H}_2\text{O-LiCl-NaCl}$ .

Only for the system  $\text{H}_2\text{O-Na}_2\text{SO}_4\text{-H}_2\text{SO}_4$  of class II are there sufficient thermodynamic and diffusion data to compare estimated and observed values for diffusion coefficients and phenomenological coefficients. We designate the solutes and ions in this system as follows:  $\text{Na}_2\text{SO}_4 = 1$ ,  $\text{H}_2\text{SO}_4 = 2$ ,  $\text{HSO}_4^- = 3$ ,  $\text{Na}^+ = 4$ ,  $\text{H}^+ = 5$ , and  $\text{SO}_4^{2-} = 6$ . The reactions corresponding to (36) are



Thus the stoichiometric coefficients  $\nu_{ij}$  and  $z_i$  have the values  $\nu_{14} = \nu_{25} = 2$ ,  $\nu_{15} = \nu_{26} = \nu_{35} = \nu_{36} = 1$ ,  $\nu_{16} = \nu_{24} = \nu_{34} = 0$ ,  $z_3 = -1$ ,  $z_4 = z_5 = +1$ , and  $z_6 = -2$ . Values used for the  $\lambda_i^0$  were  $\lambda_3^0 = 51.2$ ,  $\lambda_4^0 = 50.10$ ,  $\lambda_5^0 = 349.8$ , and  $\lambda_6^0 = 80.02$  cm.<sup>2</sup> ohm<sup>-1</sup> equiv.<sup>-1</sup>.

Kerker's value for  $\lambda_3^0$  was used,<sup>19</sup> and values for the other  $\lambda_i^0$  were taken from ref. 18.

Concentrations of the ions,  $c_3, \dots, c_6$ , are given in Table I; they were calculated at  $c_1 = c_2 = 0.5 \times 10^{-3}$  and  $c_1 = c_2 = 1.0 \times 10^{-3}$  mole/cc. by using eq. 44, 63, 64, and a derived equation for  $c_5$

$$c_5 = \frac{1}{2}(c_2 - c_1 - Q) + \frac{1}{2}[(c_2 - c_1 - Q)^2 + 8Qc_2]^{1/2} \quad (65)$$

Values for  $Q$  were obtained from Baes' estimates<sup>20</sup> of the concentration dependence of  $Q$  for this ternary system. The four phenomenological coefficients were estimated by using eq. 30, 56, and 57 with values for the  $a_{ij}$  calculated from (41). The  $\mu_{ik}$  for the system  $\text{H}_2\text{O-Na}_2\text{SO}_4\text{-H}_2\text{SO}_4$  were estimated in two ways, according to eq. 59 (est. 1) and eq. 62 (est. 2). Equation 65 for  $c_5$  and appropriate equations from (44) for  $c_3$ ,  $c_4$ , and  $c_6$  were differentiated with respect to  $c_1$  and  $c_2$  while holding  $Q$  constant to obtain expressions for the derivatives  $\partial c_i / \partial c_k$  in (62). The apparently more accurate values obtained by est. 2 were used in method A2, and the observed values<sup>21</sup> for the  $\mu_{ik}$  were used in method B, to calculate the  $(D_{ij})_0$  from eq. 3.

**Table I<sup>a,b</sup>:** Ion Concentrations in the System  $\text{H}_2\text{O-Na}_2\text{SO}_4\text{-H}_2\text{SO}_4$

$c_1 \times 10^3$ ( $\text{Na}_2\text{SO}_4$ )	$c_2 \times 10^3$ ( $\text{H}_2\text{SO}_4$ )	$Q \times 10^2$	$c_3 \times 10^3$ ( $\text{HSO}_4^-$ )	$c_4 \times 10^3$ ( $\text{Na}^+$ )	$c_5 \times 10^3$ ( $\text{H}^+$ )	$c_6 \times 10^3$ ( $\text{SO}_4^{2-}$ )
0.5	0.5	0.363	0.552	1.000	0.448	0.448
1.0	1.0	0.745	1.096	2.000	0.904	0.904

<sup>a</sup> Concentrations  $c_i$  in moles/cc. <sup>b</sup> Values for  $Q$  obtained by using estimates in ref. 20.

### Results

Estimated and observed values for the neutral-solute phenomenological coefficients for the systems  $\text{H}_2\text{O-NaCl-KCl}$  and  $\text{H}_2\text{O-Na}_2\text{SO}_4\text{-H}_2\text{SO}_4$  are given in Table II.

The only assumptions used to estimate the four  $(L_{ij})_0$  for each system concern the ionic phenomenological coefficients and are given by eq. 28 and 30. At total concentrations  $c_1 + c_2$  of less than  $10^{-3}$  for the solutes  $\text{NaCl}$  and  $\text{KCl}$ , these assumptions seem to be valid; at

(18) R. A. Robinson and R. H. Stokes, "Electrolyte Solutions," Academic Press, Inc., New York, N. Y., 1959, p. 463.

(19) M. Kerker, *J. Am. Chem. Soc.*, **79**, 3664 (1957).

(20) C. F. Baes, Jr., *ibid.*, **79**, 5611 (1957).

(21) R. P. Wendt, *J. Phys. Chem.*, **66**, 1279 (1962).

**Table II<sup>a</sup>:** Estimated and Observed Values for Phenomenological Coefficients and Diffusion Coefficients

System <sup>b</sup>	$c_1$ $\times 10^3$	$c_2$ $\times 10^3$	Method	$(L_{11})_0$ $\times 10^{19}$	$(L_{12})_0$ $\times 10^{19}$	$(L_{21})_0$ $\times 10^{19}$	$(L_{22})_0$ $\times 10^{19}$	Method	$(D_{11})_0$ $\times 10^6$	$(D_{12})_0$ $\times 10^6$	$(D_{21})_0$ $\times 10^6$	$(D_{22})_0$ $\times 10^6$
H <sub>2</sub> O(0)-NaCl(1)-KCl(2)	0.25	0.25	Est. <sup>c</sup>	1.101	-0.358	-0.358	1.448	A <sup>g</sup>	1.461	0.014	0.186	1.977
			Obsd. <sup>d</sup>	1.057	-0.320	-0.294	1.409	B <sup>h</sup>	1.428	-0.046	0.075	1.865
			Obsd. <sup>i</sup>						1.380	-0.011	0.150	1.836
H <sub>2</sub> O(0)-NaCl(1)-KCl(2)	0.50	0.50	Est. <sup>c</sup>	2.203	-0.716	-0.716	2.897	A <sup>g</sup>	1.461	0.014	0.186	1.977
			Obsd. <sup>d</sup>	2.071	-0.611	-0.585	1.340	B <sup>h</sup>	1.478	-0.019	0.095	1.889
			Obsd. <sup>i</sup>						1.403	0.026	0.173	1.859
H <sub>2</sub> O(0)-NaCl(1)-KCl(2)	1.50	1.50	Est. <sup>c</sup>	6.608	-2.147	-2.147	8.691	A <sup>g</sup>	1.461	0.014	0.186	1.977
			Obsd. <sup>d</sup>	5.318	-1.510	-1.630	7.677	B <sup>h</sup>	1.788	0.174	0.345	2.118
			Obsd. <sup>i</sup>						1.464	0.199	0.387	1.901
H <sub>2</sub> O(0)-LiCl(1)-KCl(2)	0.25	0.20	Est. <sup>c</sup>	0.868	-0.260	-0.260	1.184	A <sup>g</sup>	1.195	0.013	0.251	1.841
			Obsd. <sup>j</sup>						1.141	0.012	0.221	1.822
H <sub>2</sub> O(0)-LiCl(1)-NaCl(2)	0.25	0.20	Est. <sup>c</sup>	0.877	-0.193	-0.193	0.853	A <sup>g</sup>	1.246	0.138	0.173	1.421
			Obsd. <sup>j</sup>						1.105	0.107	0.203	1.356
H <sub>2</sub> O(0)-Na <sub>2</sub> SO <sub>4</sub> (1)-H <sub>2</sub> SO <sub>4</sub> (2)	0.50	0.50	Est. <sup>c</sup>	1.167	-0.456	-0.456	3.795	A2 <sup>k</sup>	1.591	-0.498	-0.757	3.795
			Obsd. <sup>l</sup>	0.950	-0.262	-0.212	2.164	B <sup>l</sup>	1.371	-0.781	-1.175	4.900
			Obsd. <sup>m</sup>						1.096	-0.496	-0.617	2.785
H <sub>2</sub> O(0)-Na <sub>2</sub> SO <sub>4</sub> (1)-H <sub>2</sub> SO <sub>4</sub> (2)	1.00	1.00	Est. <sup>c</sup>	2.337	-0.918	-0.918	7.612	A2 <sup>k</sup>	1.588	-0.497	-0.748	3.802
			Obsd. <sup>l</sup>	1.564	-0.419	-0.529	3.174	B <sup>l</sup>	1.385	-0.849	-0.706	6.520
			Obsd. <sup>m</sup>						0.923	-0.401	-0.380	2.723

<sup>a</sup> Units:  $c_i$ , moles/cc.;  $(L_{ij})_0$ , moles<sup>2</sup>/(erg cm. sec.);  $(D_{ij})_0$ , cm.<sup>2</sup>/sec., corresponding to flows having units of moles/(cm.<sup>2</sup> sec.).  
<sup>b</sup> Numbers in parentheses designate components in subscript notation. <sup>c</sup> Estimated by using eq. 30, 29, and 27. <sup>d</sup> Calculated according to eq. 1d-1g, ref. 6, by using values for  $(D_{ij})_0$  and  $\mu_{ik}$  in ref. 23 and ref. 6, 15, respectively. <sup>e</sup> Estimated by using eq. 30, 56, and 54. <sup>f</sup> Observed values given in ref. 21. <sup>g</sup> Calculated from eq. 3 by using estimates of  $\mu_{ik}$  in Table III and estimates of  $(L_{ij})_0$  in this table. <sup>h</sup> Calculated from eq. 3 by using obsd. values for  $\mu_{ik}$  in Table III and estimates of  $(L_{ij})_0$  in this table. <sup>i</sup> Observed values given in ref. 23. <sup>j</sup> Calculated from eq. 5 by using observed values for  $(D_{ij})_0$  and  $\bar{V}_k$  in ref. 16. <sup>k</sup> Calculated from eq. 3 by using est. 2 values for  $\mu_{ik}$  in Table III and estimates of  $(L_{ij})_0$  in this table. <sup>l</sup> Calculated from eq. 3 by using observed values for  $\mu_{ik}$  in Table III and estimates of  $(L_{ij})_0$  in this table. <sup>m</sup> Calculated from eq. 5 by using observed values for  $(D_{ij})_0$  and  $\bar{V}_k$  in ref. 21.

**Table III<sup>a</sup>:** Estimated and Observed Values for Chemical Potential Derivatives

System <sup>b</sup>	$c_1 \times 10^3$	$c_2 \times 10^3$	Method	$\mu_{11} \times 10^{-14}$	$\mu_{12} \times 10^{-14}$	$\mu_{21} \times 10^{-14}$	$\mu_{22} \times 10^{-14}$
H <sub>2</sub> O(0)-NaCl(1)-KCl(2)	0.25	0.25	Est. <sup>c</sup>	1.4874	0.4958	0.4958	1.4874
			Obsd. <sup>d</sup>	1.4283	0.4096	0.4047	1.3884
H <sub>2</sub> O(0)-NaCl(1)-KCl(2)	0.50	0.50	Est. <sup>c</sup>	0.7437	0.2479	0.2479	0.7437
			Obsd. <sup>d</sup>	0.7411	0.2211	0.2157	0.7068
H <sub>2</sub> O(0)-NaCl(1)-KCl(2)	1.50	1.50	Est. <sup>c</sup>	0.2479	0.0826	0.0826	0.2479
			Obsd. <sup>e</sup>	0.3082	0.1146	0.1159	0.2720
H <sub>2</sub> O(0)-Na <sub>2</sub> SO <sub>4</sub> (1)-H <sub>2</sub> SO <sub>4</sub> (2)	0.50	0.50	Est. 1 <sup>f</sup>	1.2395	0.2479	0.2479	1.240
			Est. 2 <sup>g</sup>	1.3483	-0.0373	-0.0373	0.9955
			Obsd. <sup>h</sup>	1.1056	-0.1729	-0.1767	1.2701
H <sub>2</sub> O(0)-Na <sub>2</sub> SO <sub>4</sub> (1)-H <sub>2</sub> SO <sub>4</sub> (2)	1.00	1.00	Est. 1 <sup>f</sup>	0.6197	0.1239	0.1239	0.6197
			Est. 2 <sup>g</sup>	0.6730	-0.0171	-0.0171	0.4974
			Obsd. <sup>h</sup>	0.5838	-0.0279	-0.0223	0.8531
H <sub>2</sub> O(0)-LiCl(1)-KCl(2)	0.25	0.20	Est. <sup>c</sup>	1.5425	0.5509	0.5509	1.7904
H <sub>2</sub> O(0)-LiCl(1)-NaCl(2)	0.25	0.20	Est. <sup>c</sup>	1.5425	0.5509	0.5509	1.7904

<sup>a</sup> Units:  $c_i$ , moles/cc.;  $\mu_{ik}$ , cc. ergs/mole<sup>2</sup>. <sup>b</sup> Numbers in parentheses designate components in subscript notation. <sup>c</sup> Estimated by using eq. 35. <sup>d</sup> Observed values in ref. 6. <sup>e</sup> Observed values in ref. 15. <sup>f</sup> Estimated by using eq. 59. <sup>g</sup> Estimated by using eq. 62 and values for  $Q$  and  $c_i$  given in Table I. <sup>h</sup> Observed values in ref. 21.

least the good agreement between all estimated and observed<sup>22,23</sup>  $(L_{ij})_0$  at the relatively low concentrations implies no inconsistency of the assumptions for this system. A simple proportionality exists between estimates of corresponding  $(L_{ij})_0$  at each composition because all ions are univalent and because  $c_1 = c_2$ . This proportionality also exists inversely for the derivatives  $\mu_{ik}$  in Table III at the three compositions. In eq. 3 for calculating the  $(D_{ij})_0$  the proportionality constants will cancel and the estimates of all  $(D_{ij})_0$  will be independent of  $c_1$  or  $c_2$  for systems where  $c_1 = c_2$ , if the  $\mu_{ik}$  are estimated according to (35).

Diffusion data at low concentrations of the systems  $\text{H}_2\text{O}-\text{Na}_2\text{SO}_4-\text{H}_2\text{SO}_4$  are not available and the limits of validity of assumptions (55) and (30) for this system cannot be inferred from values in Table II. Furthermore, the estimates of  $Q$  for this system are of unknown accuracy at these high concentrations. Estimates of  $(L_{ij})_0$  for this system are, however, of correct algebraic sign and, except for  $(L_{22})_0$ , agree with observed<sup>21</sup>  $(L_{ij})_0$  to within  $0.20 \times 10^{-19}$  at the lower composition. Because  $(L_{22})_0$  depends strongly on  $(L_{55})_0$  (the main-term coefficient for the flow of  $\text{H}^+$ ) we suggest that the approximation (30) relating  $(L_{55})_0$  to  $\lambda_6^0$  is very inaccurate at total concentrations  $c_1 + c_2$  greater than approximately  $1.0 \times 10^{-3}$ .

For all systems none of the assumptions (28), (55), or (30) violates the Onsager relations<sup>24</sup>  $(L_{ij})_0 = (L_{ji})_0$ ,  $i \neq j$ , for the ionic phenomenological coefficients. Therefore, as expected, the estimates for the neutral-solute phenomenological coefficients are seen to satisfy the Onsager relation for neutral solutes,  $(L_{12})_0 = (L_{21})_0$ . Previous analyses<sup>6,15,21</sup> of experimental errors have explained the small differences between observed values for  $(L_{12})_0$  and  $(L_{21})_0$ .

Estimates of the  $\mu_{ik}$  in Table III are in good agreement with observed values at all compositions considered here for the system  $\text{H}_2\text{O}-\text{NaCl}-\text{KCl}$ . For the weak-electrolyte systems, eq. 62 (designated est. 2 in Table III) gives considerably better estimates of  $\mu_{12}$  and  $\mu_{21}$  than eq. 59 (designated est. 1), but est. 1 does a somewhat better job for the derivatives  $\mu_{11}$  and  $\mu_{22}$ . We chose est. 2 values to calculate the  $(D_{ij})_0$  for the system  $\text{H}_2\text{O}-\text{Na}_2\text{SO}_4-\text{H}_2\text{SO}_4$  because all diffusion coefficients were found to be somewhat more accurately estimated with those values than with values from est. 1.

In Table II, values for  $(D_{ij})_0$  estimated in two ways for the systems  $\text{H}_2\text{O}-\text{NaCl}-\text{KCl}$  and  $\text{H}_2\text{O}-\text{Na}_2\text{SO}_4-\text{H}_2\text{SO}_4$  are compared with observed values,<sup>23,25</sup> so that the effects of assumptions used in the estimates can be separately considered.

For the system  $\text{H}_2\text{O}-\text{NaCl}-\text{KCl}$ , the differences between  $(D_{ij})_0$  calculated by method A, which uses

estimates of  $\mu_{ik}$ , and values calculated by method B, which uses observed values of  $\mu_{ik}$ , are not appreciable except at the highest concentration,  $c_1 = c_2 = 1.50 \times 10^{-3}$  mole/cc. At that concentration the agreement between observed values for  $(D_{12})_0$  and  $(D_{21})_0$  and values estimated by method B is deceptively good; the estimated  $(L_{ij})_0$  in Table II are not in good agreement at the highest concentration of this system, and calculations of  $(D_{ij})_0$  using the poor estimates can only give fortuitously good results. The good agreement between estimated and observed<sup>26</sup> values for  $(D_{ij})_0$  for the systems  $\text{H}_2\text{O}-\text{LiCl}-\text{KCl}$  and  $\text{H}_2\text{O}-\text{LiCl}-\text{NaCl}$  may or may not be fortuitous. No thermodynamic activity data are available for those systems, and only if we assume the estimates of  $\mu_{ik}$  for these relatively dilute systems are as accurate as estimates of  $\mu_{ik}$  for the system  $\text{H}_2\text{O}-\text{NaCl}-\text{KCl}$  can we then infer the approximate validity of assumptions (28) and (30) for the ionic phenomenological coefficients.

Both methods used to estimate  $(D_{ij})_0$  for the weak-electrolyte system,  $\text{H}_2\text{O}-\text{Na}_2\text{SO}_4-\text{H}_2\text{SO}_4$ , give results which are generally in rather poor agreement with experiment. However, for the systems of this class no other theory is available<sup>27</sup> to estimate both the  $(L_{ij})_0$  and  $(D_{ij})_0$ . The present theory enables us to regard as fortuitous the few apparently accurate estimates of  $(D_{ij})_0$  made by method A2 (which uses est. 2 values of the  $\mu_{ik}$  from Table III) because the estimated and observed values for  $(L_{ij})_0$  are not in good agreement.

At the concentrations of the strong-electrolyte systems of class I considered here we conclude that this theory provides good estimates of the  $(L_{ij})_0$  and  $(D_{ij})_0$  and small second-order corrections to the  $(D_{ij})_0$  as estimated by the first-order approximate theory of Gosting and O'Donnell. For the one system of class

(22) Values for  $(D_{ij})_0$  for the system  $\text{H}_2\text{O}-\text{NaCl}-\text{KCl}$  that were recalculated by Fujita and Gosting (ref. 23) were used with observed values of  $\mu_{ik}$  (ref. 6 and 15) to calculate observed values for the  $(L_{ij})_0$  according to eq. 1d-1g of ref. 6.

(23) H. Fujita and L. J. Gosting, *J. Phys. Chem.*, **64**, 1256 (1960).

(24) L. Onsager, *Phys. Rev.*, **37**, 405 (1931); **38**, 2265 (1931).

(25) Observed values for the  $(D_{ij})_0$  for  $\text{H}_2\text{O}-\text{Na}_2\text{SO}_4-\text{H}_2\text{SO}_4$  were calculated according to eq. 5 by using values of  $(D_{ij})_v$  and  $\bar{V}_s$  given in ref. 21.

(26) For the systems  $\text{H}_2\text{O}-\text{LiCl}-\text{KCl}$  and  $\text{H}_2\text{O}-\text{LiCl}-\text{NaCl}$ , observed values for  $(D_{ij})_0$  were calculated by using eq. 5 and Miller's values (ref. 16) for  $(D_{ij})_v$  and  $\bar{V}_s$  (originally measured by Dunlop and Gosting, ref. 1). P. J. Dunlop, in *J. Phys. Chem.*, **68**, 3062 (1964), also presents recalculated values of  $(D_{ij})_v$  for these systems. His values do not differ significantly from Miller's.

(27) A first-order approximate theory for the system  $\text{H}_2\text{O}-\text{Na}_2\text{SO}_4-\text{H}_2\text{SO}_4$ , similar in form to that derived by Gosting<sup>3</sup> for systems of class I, was presented in the author's Ph.D. thesis (R. P. Wendt, University of Wisconsin, 1961, Library of Congress Card No. Mic 61-680). Values of  $(D_{ij})_0$  calculated from the present theory according to method A2, Table II, are found to equal those calculated according to the previous theory.

II examined, the theory provides poor estimates of  $(L_{ij})_0$  and  $(D_{ij})_0$  at the relatively high concentrations where data are available which can be compared with the estimates. At lower concentrations of all systems the assumptions concerning the ionic  $(L_{ij})_0$  become more accurate, the derivatives  $\mu_{ik}$  should have larger values, and the second-order corrections of the present theory should become more significant.

*Acknowledgment.* This research was supported in part by a grant-in-aid from the University Council on Research of Louisiana State University.

### Appendix

*Expressions Relating  $(L_{ii})_0$  to  $\lambda_i^0$ .* Limiting equivalent conductivities,  $\lambda_i^0$ , may be defined without using the formal theory of nonequilibrium thermodynamics

$$(I_i^0)_C = z_i c_i \lambda_i^0 E \quad (\text{a})$$

Here  $(I_i^0)_C$  is the electrical current density in coulombs/cm.<sup>2</sup> sec. corresponding to the flow  $(J_i^0)_C$  of ion  $i$  near infinite dilution, and  $E$  is the electric field, in volts/cm., causing the flow. The cell-fixed reference frame, indicated by the subscript C, is used because electrical current densities are measured relative to the cell in a conductance experiment. The total electrical current density at any concentration is given by

$$I_C = \sum_{i=1}^n (I_i)_C \quad (\text{b})$$

where the sum is taken over all ions in the system. The specific conductivities,  $k$ , actually measured in a conductance experiment appear in a form of Ohm's law

$$k = I_C/E \quad (\text{c})$$

To relate the ionic  $(L_{ij})_0$  of nonequilibrium thermodynamics (eq. 18 or 48) to the  $\lambda_i^0$  in eq. a, we assume

$$(L_{ij})_0 = 0 \quad (i \neq j) \quad (\text{d})$$

$$(J_i)_0 = (J_i^0)_C \quad (\text{e})$$

and

$$\text{grad } \mu_i = 0 \quad (\text{f})$$

The first two assumptions are valid near infinite dilution, and the last assumption is valid during a conductance experiment performed with an alternating electric field of sufficiently high frequency to prevent appreciable concentration changes anywhere in the conductance cell. By using (d) to (f), the flow equations (18) or (48) for ions become

$$(J_i^0)_C = (L_{ii})_0 z_i f E \quad (\text{g})$$

In (g) the quantity  $f$  must be related to the Faraday constant  $F$  (taken here to be 96,493 coulombs/equiv. of charge) by

$$f = 10^7 F \quad (\text{h})$$

if  $E$ ,  $(J_i)_C$ , and  $z_i$  are to have the dimensions volts/cm., moles/cm.<sup>2</sup> sec., and equivalents of charge/mole, respectively. At any concentration the definition of  $(I_i)_C$  requires

$$(I_i)_C = z_i F (J_i)_C \quad (\text{i})$$

If we use (g) and (h), then

$$(I_i^0)_C = z_i^2 (L_{ii})_0 F^2 \times 10^7 E \quad (\text{j})$$

By equating the right-hand sides of (a) and (j), we obtain eq. 30 for estimating  $(L_{ii})_0$  from values for  $\lambda_i^0$

$$(L_{ii})_0 = c_i \lambda_i^0 / (|z_i| F^2 \times 10^7) \quad (\text{k})$$

where the absolute value of  $z_i$  is used because main-term phenomenological coefficients are always positive.<sup>28</sup>

(28) See ref. 3, p. 31.

## The Occurrence of Metastable Tetragonal Zirconia as a Crystallite Size Effect

by Ronald C. Garvie

*U. S. Department of the Interior, Bureau of Mines, College Park Metallurgy Research Center, College Park, Maryland (Received October 15, 1964)*

Metastable tetragonal  $ZrO_2$  was prepared in two ways: (I) precipitation from alkaline aqueous solution and (II) low temperature calcination of zirconyl nitrate. Both methods are standard techniques for preparing active powders with large surface area. This suggested that the excess surface energy (relative to a large single crystal) present in I and II stabilized the tetragonal form. The maximum specific surfaces in I and II were 194 and 15.6  $m^2/g.$ , respectively, corresponding to crystallite sizes of 54 and 155  $\text{\AA}$ . The excess energy of the active powders ranged as high as 6.7 kcal./mole. There appeared to be a critical crystallite size, about 300  $\text{\AA}$ , above which the metastable tetragonal phase could not exist at room temperature. Thermodynamic calculations showed that, if the surface free energy of  $ZrO_2$  increased from 770 to 1130 ergs/cm.<sup>2</sup> upon passing from the tetragonal to the monoclinic structure at 300°K., then the occurrence of the metastable tetragonal form could be accounted for as a crystallite size effect.

### Introduction

This research was undertaken to determine the reason for the occurrence of metastable tetragonal  $ZrO_2$ . Normally, zirconia has a monoclinic structure at room temperature which transforms to a tetragonal structure at about 1100°. The enthalpy difference of the two structures at 1205° is 1420 cal./mole.<sup>1</sup> The high temperature form cannot be quenched, yet, surprisingly, it can exist at room temperature if the zirconia is prepared either by precipitation from alkaline aqueous solution or by calcining a salt such as the chloride or nitrate at low temperatures.<sup>2</sup>

Recently a "cubic" form of  $ZrO_2$ , obtained by precipitation, has been reported.<sup>3</sup> However, when this "cubic" phase is heated, certain broadened X-ray diffraction lines smoothly and gradually emerge as the characteristic tetragonal doublets. Thus, the "cubic" phase appears to be the tetragonal form with the doublets masked by line broadening.

Although Ruff and Ebert first prepared the metastable tetragonal phase in 1929 by igniting zirconium salts, there has been only one attempt to account for this puzzling behavior of  $ZrO_2$ .<sup>4</sup> Cypres, Wollast, and Raucq prepared the metastable phase by heating " $Zr(OH)_4$ ."<sup>5</sup> These authors studied the problem with the aid of differential thermal analysis, thermogravimetry, electrical conductivity, infrared absorption,

and X-ray diffraction. They concluded that small amounts (0.75 wt. %) of bound OH groups in solid solution stabilized the tetragonal form at room temperature. When the solid was heated in the region 600 to 900°, the OH groups were driven off as water, and simultaneously the formation of the monoclinic phase was noted.

The present author holds that this view is untenable owing to the experimental results obtained by Clearfield.<sup>3</sup> He prepared an amorphous precipitate of hydrous  $ZrO_2$  which was heated in distilled water under reflux. The following sequence of phases was observed in the precipitate: amorphous  $\rightarrow$  tetragonal + monoclinic  $\rightarrow$  monoclinic. Under these conditions, bound OH groups could not be driven off, and therefore it does not appear that OH groups have anything to do with the formation of the metastable tetragonal phase.

Moreover, the results of the infrared studies made by Cypres and co-workers (which constitute their strongest

(1) J. P. Coughlin and E. G. King, *J. Am. Chem. Soc.*, **72**, 2262 (1950).

(2) C. T. Lynch, F. W. Vahldiek, and L. B. Robinson, *J. Am. Ceram. Soc.*, **44**, 147 (1961).

(3) A. Clearfield, *Inorg. Chem.*, **3**, 146 (1964).

(4) O. Ruff and F. Ebert, *Z. anorg. allgem. Chem.*, **180**, 19 (1929).

(5) R. Cypres, R. Wollast, and J. Raucq, *Ber. Deut. Keram. Ges.*, **40**, 527 (1963).

evidence for bound OH groups) are open to question. They prepared samples for infrared analysis by grinding them in isobutyl alcohol. Powders formed by precipitation have very large specific surfaces and therefore would tend to adsorb polar molecules such as isobutyl alcohol. There is a possibility that the absorption peaks presented in their work arose from adsorbed alcohol.

A preliminary examination of Debye-Scherrer X-ray diffraction patterns of the metastable material prepared by this writer revealed the characteristic line broadening of a finely divided powder. Such powders are called active because they possess excess energy (relative to a large single crystal) and display unusual properties. For example, an increase in the heat of solution of samples of active MgO as high as 2 kcal./mole over coarse-grained material has been reported.<sup>6</sup> Again, one can obtain aluminum from alumina by heating the active oxide under vacuum at 500°.<sup>7</sup> It is suggested that the reaction, monoclinic  $ZrO_2 \rightleftharpoons$  tetragonal  $ZrO_2$ , has been so affected by the extremely fine state of subdivision of the material that the tetragonal phase occurs at room temperature. Buerger earlier suggested a crystallite size effect to account for the appearance of high cristobalite in samples of opal at room temperature.<sup>8</sup>

In this work, the formation of the metastable tetragonal phase was correlated with those physical properties which are most important in describing active powders, namely, mean crystallite size, surface area, and excess energy.

### Experimental Procedure

Zirconium dioxide was prepared in two ways: precipitation and calcination. In the former, a hot solution of zirconyl nitrate was added to a hot, stirred, 50 wt. % solution of sodium hydroxide, and the zirconium dioxide was precipitated as the hydrous oxide. Details of the procedure were taken from a paper by Hathaway and Clearfield.<sup>9</sup> In the latter, the anhydrous nitrate was calcined at 400° for 48 hr. The first preparation will be described hereafter as the precipitated oxide, and the second, as the calcined oxide. Samples of both types were heated in air at various temperatures up to 1000° for a constant time of 24 hr. Standard X-ray diffractometer techniques, using unfiltered iron radiation, were employed to determine the phases present and the mean crystallite size of the air-quenched product. The specific surface of the samples was measured by the B.E.T. method using the continuous-flow technique of Nelsen and Eggertsen.<sup>10</sup> Sample purity was checked by optical emission spectrography.

The crystallite-size measurements will be described in greater detail because of the uncertainties and difficulties associated with this technique. According to the Scherrer formula, the crystallite size,  $D$ , is inversely proportional to the true line broadening,  $\beta$ , of the diffraction peak, occurring at some angle,  $\theta$ . In this work the (111) line of both oxides was used for the size measurements.

Instrumental broadening is measured by scanning diffraction peaks of a standard substance whose crystallite size is known to be greater than 10,000 Å. The material used in this work was a thin cleavage flake of mica which has been used effectively to align a diffractometer.<sup>11</sup> A mica flake is a single crystal oriented to produce a series of strong sharp reflections of the (001) type when mounted on a diffractometer sample holder.

Values of  $\beta$  were obtained from the observed line broadening (defined as the line width at half-peak intensity) and the instrumental broadening by means of calibration curves published by Klug and Alexander.<sup>12</sup> These curves, assumed to be valid for all diffractometers of the same design, were reproduced on an enlarged scale and used directly to obtain  $\beta$ . This method is claimed to give a precision of  $\pm 10\%$  in the region 100–1000 Å. for a related series of samples and an absolute accuracy of  $\pm 25\%$ .<sup>13</sup>

### Results and Discussion

Spectrographic analyses of the precipitated and calcined oxides are given in Table I. The principal metallic impurity, other than hafnium, was sodium with a concentration of the order of 1%.

This writer assumes that the level of impurities listed in Table I does not affect the experimental results. This assumption is supported by evidence obtained by Mazdiasni, Lynch, and Smith, who observed the tetragonal phase at room temperature in ultra high purity zirconia prepared by thermal decomposition

(6) D. K. Thomas and T. W. Baker, *Proc. Phys. Soc. (London)*, **92**, 673 (1959).

(7) H. J. DeBoer, Ed., "Reactivity of Solids," Elsevier Publishing Co., New York, N. Y., 1961, p. 525.

(8) M. J. Buerger, "Phase Transformations in Solids," John Wiley and Sons, Inc., New York, N. Y., 1951, Chapter 6.

(9) A. J. Hathaway and A. Clearfield, "Preparation of Zirconia Solid Solutions by Coprecipitation," Basic Science Division Meeting of the American Ceramic Society, Columbus, Ohio, Oct. 1962.

(10) F. M. Nelsen and F. T. Eggertsen, *Anal. Chem.*, **30**, 1387 (1958).

(11) D. K. Smith, *Norelco Repr.*, **10**, 19 (1963).

(12) A. P. Klug and L. E. Alexander, "X-Ray Diffraction Procedures," John Wiley and Sons, Inc., New York, N. Y., 1954, Chapter 9.

(13) L. E. Alexander, Mellon Institute, Pittsburgh, Pa., private communication.

**Table I:** Optical Spectrographic Analyses of Zirconium Dioxide

Element <sup>a,b</sup>	Precipitated ZrO <sub>2</sub>	Calcined ZrO <sub>2</sub>
Al	0.003-0.03	n.d. <sup>c</sup>
B	0.001-0.01	n.d.
Cu	0.00003-0.0003	n.d.
Fe	0.3-0.03	0.0003-0.003
Hf	0.3-3	0.3-3
K	0.003-0.03	0.01-0.1
Mg	0.003-0.03	0.00001-0.0001
Mn	0.0001-0.001	n.d.
Na	0.3-3	0.3-3
Si	0.03-0.3	n.d.
Ti	0.01-0.1	0.003-0.03
V	0.0003-0.003	0.0003-0.003

<sup>a</sup> Elements sought but not detected: Ag, As, Ba, Be, Bi, Ca, Cd, Ce, Co, Cr, Cs, Ge, Hg, Li, Mo, Nb, Ni, P, Pb, Rb, Sb, Sn, Sr, Ta, Th, Ti, U, W, Zn. <sup>b</sup> Weight per cent. <sup>c</sup> Not detected.

of zirconium alkoxides.<sup>14</sup> They observed that the metastable phase persisted indefinitely at room temperature and conversion to the monoclinic phase only occurred upon heating the oxide above 400°.

Figure 1 shows the phases detected in this work, at room temperature, in samples of ZrO<sub>2</sub> heated to various temperatures. Initially, at low temperatures, only the tetragonal phase is present. At intermediate temperatures, partial transformation occurs, and a two-phase region is observed. Finally, above approximately 800°, complete transformation occurs, and only monoclinic ZrO<sub>2</sub> is observed. This sequence of phases can be correlated with changes in the tetragonal mean crystallite size, the specific surface, and the excess energy of the active samples as shown in Figures 2, 3, and 4, respectively.

In Figure 2, the tetragonal mean crystallite size, determined on quenched samples, is given as a function of the firing temperature. The initial values of  $D$  were 54 and 155 Å. for the precipitated and calcined oxides, respectively. When the samples were heated, the tetragonal crystallites grew to a maximum size of about 300 Å. before complete conversion took place. Figure 3 shows the variation in specific surface as a function of crystallite size. The curve labeled  $S_E$  is experimental. Initial values were 194 and 15.6 m.<sup>2</sup>/g. for the precipitated and calcined oxides, respectively. The  $S_T$  curve is theoretical and was obtained from the following equation, valid both for cubes of edge  $D$  or spheres of diameter  $D$ .

$$S_T = \frac{6}{\rho D} \quad (1)$$

where  $\rho$  = the density of the tetragonal phase. The small correction to account for the presence of the monoclinic phase in samples heated at higher temperatures was neglected. The discrepancy between the curves is probably due to the development of an internal surface in the powder (unavailable for nitrogen adsorption) owing to partial sintering when the samples were heated. Allred and co-workers observed

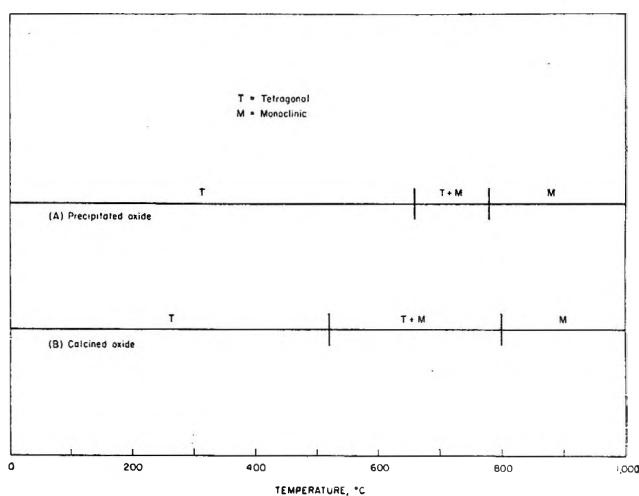


Figure 1. The phases present at room temperature in active powders of ZrO<sub>2</sub> heated to various temperatures.

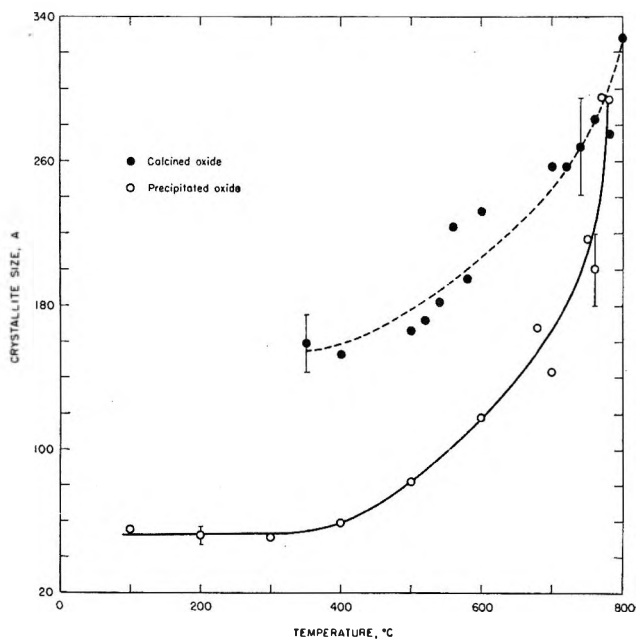


Figure 2. Experimental values of the mean crystallite size of metastable tetragonal ZrO<sub>2</sub> as a function of temperature.

(14) K. S. Mazdiyasi, C. T. Lynch, and J. S. Smith, "Preparation of Ultra-High Purity Submicron Refractory Oxides," 66th Annual Meeting, American Ceramic Society, Chicago, Ill., April 1964.



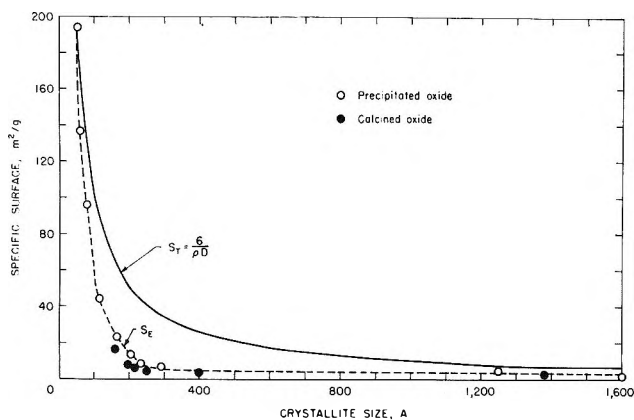


Figure 3. Comparison of theoretical and experimental values of the specific surface,  $S$ , as a function of crystallite size,  $D$ .

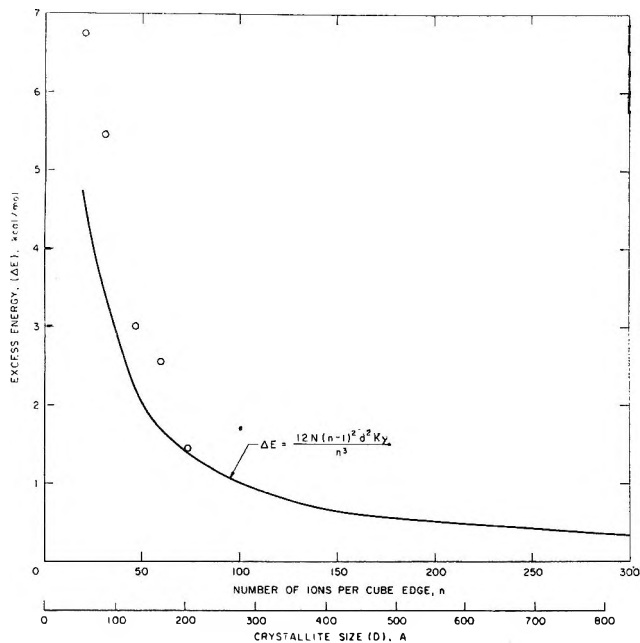


Figure 4. Comparison of theoretical and experimental values of the excess energy of active powders of  $ZrO_2$  as a function of crystallite size.

a similar discrepancy in a study of thorium dioxide powders.<sup>15</sup>

In Figure 4, the excess energy  $\Delta E$  (relative to a large single crystal) of active samples of the precipitated oxide is plotted as a function of the crystallite size,  $D$ . The experimental values of  $\Delta E$  (denoted by open circles) were obtained by heat of solution measurements.<sup>16</sup> These data show that excess energy ranging as high as 6.7 kcal./mole is present in active samples of precipitated  $ZrO_2$ . The data were fitted to the theoretical expression

$$\Delta E = \frac{12N(n-1)^2d^2K\gamma}{n^3} \quad (2)$$

where  $\Delta E$  = excess energy (kcal./mole);  $N$  = Avogadro's number;  $d$  = the diameter of the oxygen ion;  $K$  = a factor to convert ergs to kilocalories;  $\gamma$  = the surface energy (ergs/cm.<sup>2</sup>). Equation 2 was derived by using the same approach that Weissenbach employed for MgO.<sup>17</sup> The present author assumed that  $ZrO_2$  had the ideal fluorite lattice and that the powder was composed of cubes with  $n$  oxygen ions/edge. The value selected for the surface energy was 770 ergs/cm. and was obtained from data given by Livey and Murray.<sup>18</sup>

In summary, tetragonal  $ZrO_2$  at room temperature appears in active powders of  $ZrO_2$  characterized by small mean crystallite size, large specific surface, and appreciable excess energy. When the powders are heated, the crystallites grow so that the specific surface and excess energy diminish. Simultaneously, a phase transformation to the monoclinic structure occurs.

These phenomena lead one to make the following postulate. The two phases are in equilibrium at 300° when the crystallite size is about 300 Å. The fact that a two-phase region is observed may be attributed to a crystallite size distribution which can be considerable, as shown by Quinn and Cherin.<sup>19</sup> If the two structures are in equilibrium at the critical size of 300 Å., then their free energies must be equal. This is expressed in the equation

$$G_m + \gamma_m A_m = G_t + \gamma_t A_t \quad (3)$$

where  $G$  = the molar free energy of  $ZrO_2$  in the form of a large single crystal (cal./mole);  $\gamma$  = the surface energy (cal./cm.<sup>2</sup>);  $A$  = the molar surface (cm.<sup>2</sup>/mole). The subscripts,  $m$  and  $t$ , refer to the monoclinic and tetragonal phases, respectively.

Equation 3 states that there is a difference in the surface free energies of monoclinic and tetragonal  $ZrO_2$ ; the surface energy of the former structure is greater than the latter. This difference in surface energy, when associated with a large value of the molar surface, causes the molar free energies of the two structures to be equal when  $D$  is about 300 Å: and, hence, the formation of the tetragonal phase at room tempera-

(15) V. C. Allred, S. R. Buxton, and J. P. McBride, *J. Phys. Chem.*, **61**, 117 (1957).

(16) Heat of solution measurements were made by R. Barnay and K. Kelley, U. S. Bureau of Mines Thermodynamics Laboratory, Berkeley, Calif.

(17) B. Weissenbach, *Radex Rundschau*, **6**, 257 (1951).

(18) D. T. Livey and P. Murray, *J. Am. Ceram. Soc.*, **39**, 363 (1956).

(19) H. F. Quinn and P. Cherin, *Advan. X-Ray Anal.*, **5**, 94 (1962).

ture. The situation is displayed graphically in Figure 5.

The results obtained by Clearfield also point to the possibility of some critical crystallite size which governs the formation of the metastable phase.<sup>3</sup> He observed that the first crystalline product, obtained by heating amorphous, hydrous  $ZrO_2$  in distilled water under reflux, was a mixture of tetragonal and monoclinic crystallites, whose size was about 20 to 25 Å. After many hours of refluxing, the tetragonal phase disappeared, and only monoclinic crystallites, about 120 Å. in diameter, were observed. These data indicate a critical size, less than 120 Å., which is considerably smaller than that observed in the present work. The reason for this discrepancy is unknown, although it may be related to the fact that in Clearfield's experiments the crystallites grew in an aqueous medium.

It is of interest to calculate  $\gamma_m$  from eq. 3. The molar surfaces may be calculated from eq. 1. The surface energy of the tetragonal phase,  $\gamma_t$ , is known from the literature.<sup>18</sup> There remains only to calculate the molar free energy difference at 300°K., ( $G_t - G_m$ ). An estimate of this quantity may be obtained from a knowledge of the heat of transition (1420 cal./mole) and the transition temperature (1478°K.). If the heat and entropy of transition are assumed to be temperature independent then ( $G_t - G_m$ ) amounts to 1130 cal./mole at 300°K. When all the numerical quantities are substituted in eq. 3, the value of  $\gamma_m$  is 1810 ergs/cm.<sup>2</sup>.

Listed below are some values of the free surface energy in ergs/cm.<sup>2</sup> (at 0°K.) for some refractory oxides. The relatively small change in these values produced by increasing the temperature to 300°K. would not affect the semiquantitative argument:  $MgO$ ,<sup>20</sup> 1040;  $ThO_2$ ,<sup>21</sup> 1150;  $UO_2$ ,<sup>21</sup> 1030. But the value of  $\gamma_m$ , obtained above, is far higher than that usually found in refractory oxides and therefore is not probable.

The way out of this difficulty may lie in the nature of the high temperature monoclinic  $\rightleftharpoons$  tetragonal transformation itself which has been studied in detail at this research center.<sup>22</sup> The inversion which occurred in single crystals or well-sintered powders is of the type described by Ubbelohde as continuous.<sup>23</sup> The outstanding feature of a continuous transformation is the coexistence of both structures in a hybrid single crystal during the inversion. During the heating cycle, domains of the tetragonal structure grow in a matrix of the monoclinic form. Strain at the domain boundaries brings the reaction to a halt after a short time, and a constant ratio of phases is observed at some temperature,  $T$ , in the transition region. To change the phase ratio, the temperature must be changed.

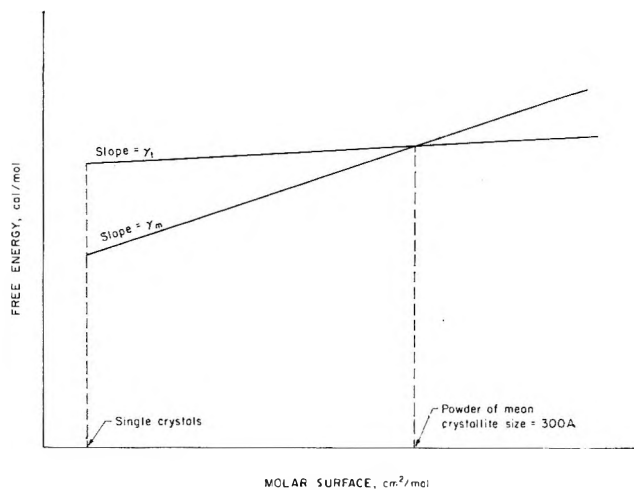


Figure 5. Schematic free-energy diagram of monoclinic and tetragonal  $ZrO_2$ .

This behavior is termed athermal kinetics. Consider a powdered monoclinic sample whose mean crystallite size is less than a domain. Coexistence of the two structures is impossible, and coexistence phenomena, such as athermal kinetics, should not be observed. Indeed, classical kinetics in which the amount of reactant (monoclinic phase) steadily diminished with time were noted for the inversion occurring in very fine-grained monoclinic powders.

One can predict, on the basis of the above discussion, that the heat of transition of a well-sintered powder is not the same as the heat of transition of very fine-grained powders whose mean crystallite size is less than a domain. The heat of transition of well-sintered powders would contain a contribution owing to the chemical difference of the two structures, as well as a contribution from the strain energy associated with the inversion. On the other hand, the heat of transition of a fine-grained powder would contain only the contribution arising from the chemical difference of the two forms. These ideas are expressed in the following equations. For well-sintered powders

$$\Delta H_{trans} = \Delta H_{chem} + \Delta H_{str} \quad (4)$$

For very fine-grained powders

$$\Delta H_{trans} = \Delta H_{chem} \quad (5)$$

The difference in  $\Delta H_{trans}$  shown by eq. 4 and 5

(20) G. Jara and C. Garland, *J. Am. Chem. Soc.*, **74**, 6033 (1952).

(21) G. C. Benson, P. I. Freeman, and E. Dempsey, *J. Am. Ceram. Soc.*, **46**, 43 (1963).

(22) C. Grain and R. Garvie, U. S. Bureau of Mines Report of Investigations, in press.

(23) A. R. Ubbelohde, *Quart. Rev. (London)*, **11**, 246 (1957).

should be detectable in a differential thermal analysis (d.t.a.) of the transition using coarse-grained and fine-grained powders. Accordingly, two samples of monoclinic  $ZrO_2$  were prepared; one was heated for 24 hr. at  $1500^\circ$  (coarse-grained), and one at  $900^\circ$  (fine-grained). The mean crystallite size of the former material was  $820 \text{ \AA}$ , and the latter,  $232 \text{ \AA}$ . D.t.a. experiments were carried out on both powders at a heating rate of  $10^\circ/\text{min}$ . The results are shown in Figure 6 (a and b). The area under the peak of the coarse-grained sample is much larger than that for the fine-grained sample, in good agreement with the prediction. The area under the d.t.a. peaks is proportional to the heat of transition. Therefore,  $\Delta H_{\text{trans}}$  for the fine-grained powder is obtained from the ratio of the small peak to the large peak when the latter is set equal to  $1420 \text{ cal./mole}$ . The results are given in Table II.

Table II

Sample	Area under peak, in. <sup>2</sup>	Sample weight, g.	Peak temp., °C.	Molar heat of transition, cal.
Coarse-grained	0.130	2.2823	1179	1420
Fine-grained	0.057	2.2870	1155	620

When the fine-grained sample was recycled through the inversion temperature, the same peak area was obtained (Figure 6c) as that observed for the coarse-grained sample. This observation agrees with the kinetic studies which established that classical kinetics are only observed during the first cycle.

The reason that eq. 3 yielded an unreasonable value for  $\gamma_m$  is now clear. The free energy of transition used in the calculation included a strain contribution. However, the metastable transformation is concerned with very fine-grained samples, and so the free energy of transition must be based on eq 5.  $(G_t - G_m)$  for fine-grained samples is then reduced to  $491 \text{ cal./mole}$  at  $300^\circ\text{K}$ ., and, when this value is substituted into eq. 3,  $\gamma_m$  amounts to  $1130 \text{ ergs/cm}^2$ .

This value of  $\gamma_m$  is about the same as that for thorium dioxide and uranium dioxide and is therefore acceptable. A good check on the hypothesis presented in this work would be to measure the surface tension of  $ZrO_2$  in the region  $1000$  to  $1200^\circ$  and observe if the predicted change in value of this parameter ( $1130$  to  $770 \text{ ergs/cm}^2$ ) really occurs.

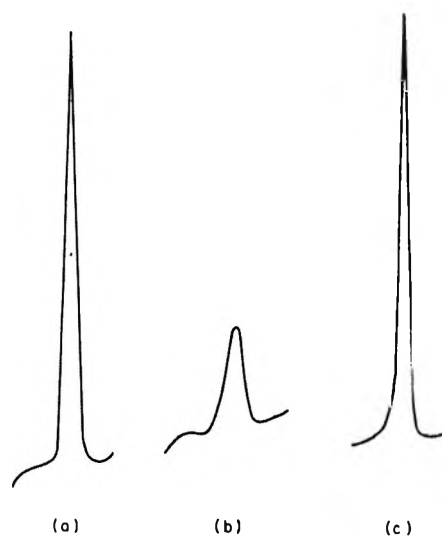


Figure 6. Comparison of the d.t.a. peaks of the monoclinic  $\rightarrow$  tetragonal transformation in coarse-grained and fine-grained  $ZrO_2$ .

It is interesting to note that metastable tetragonal  $HfO_2$  cannot be prepared.<sup>24</sup> If the hydrous precipitate or the nitrate is heated, the sequence of phases observed is amorphous  $\rightarrow$  monoclinic. The fact implies that the free-energy curves of the two structures intersect at such a small value of  $D$  that there is no long-range order in the solid, and only an amorphous phase can be observed.

### Conclusions

Current explanations for the occurrence of metastable tetragonal  $ZrO_2$  are based on contamination of the oxide by impurities, such as chemically bound OH groups. This interpretation is not convincing in the light of recent research on this phenomenon. A new explanation is offered in this work in which the stabilization of the high temperature phase is correlated with the intrinsic properties of active powders, namely, small mean crystallite size, large specific surface, and appreciable excess energy.

*Acknowledgments.* It is a pleasure to thank L. R. Furlong, supervisory research physicist, W. J. Campbell, supervisory research chemist, and E. E. Maust, Jr., chemical engineer, for their very helpful discussions and constructive criticisms.

(24) C. Grain, Bureau of Mines Metallurgy Research Center, College Park, Md., private communication.

# The Effect of Solvent and of Solutes on the Absorption Spectrum of Solvated Electrons<sup>1a</sup>

by M. Anbar<sup>1b</sup> and Edwin J. Hart

Chemistry Division, Argonne National Laboratory, Argonne, Illinois (Received October 17, 1964)

The properties of electron-pulse-generated solvated electrons in ethylenediamine and in some concentrated aqueous electrolytes are reported. In ethylenediamine, a single intense optical absorption band with a peak at 9200 Å. is found and is assigned to the solvated electron. The maximum of the hydrated electron ( $e_{aq}^-$ ) absorption band shifts from 7200 Å. for pure water to shorter wave lengths in concentrated solutions of  $MgCl_2$ , KF, NaOH, KOH,  $NaClO_4$ , and LiCl. These results are discussed and compared with the absorption spectrum of solvated electrons in other solvents and with the charge-transfer-to-solvent spectrum of the iodide ion in the same media. In a 12.4 M solution of KF, the rate constants of  $e_{aq}^-$  reaction with benzoate ion, acetone, nitrous oxide, and nitrate ion are lower than the corresponding rate constants in water.

The detailed studies on the absorption spectrum of dilute solutions of alkali metals in ammonia, which revealed the absorption spectrum of the solvated electron in ammonia,<sup>2</sup> were followed by the discovery and characterization of the absorption spectrum of the hydrated electron in aqueous solutions.<sup>3-5</sup> Recently the absorption spectra of solvated electrons in ethanol<sup>6</sup> and in methanol<sup>7</sup> were also determined. A recent study on alkali metal solutions in ethylenediamine<sup>8</sup> has assigned a certain absorption peak to the solvated electron in this medium. We have checked on this assignment by studying the absorption spectrum of solvated electrons formed by pulse radiolysis in ethylenediamine.

It has been found that the absorption spectrum of the hydrated electron is modified in concentrated solutions of ammonia.<sup>3,4</sup> It was of interest to investigate the effect of other solutes on the absorption spectrum of  $e_{aq}^-$ . In contrast to the case of ammonia where a shift to longer wave lengths was observed, various electrolytes tested affected the absorption spectrum of  $e_{aq}^-$  by a shift to shorter wave lengths. It is the purpose of this paper to describe these findings and to discuss them in relation to solvent effect on charge-transfer-to-solvent (c.t.t.s.) spectra.

## Experimental

Anhydrous ethylenediamine (Fluka, Puriss.) was further purified by refluxing over potassium metal and

redistilling under partial vacuum under a helium atmosphere. The pure air-free solutions were handled in syringes and transferred into the optical cell, as described elsewhere.<sup>9</sup> The half-life of the solvated electron in this solvent was about 2  $\mu$ sec. Other chemicals used were KF (Baker and Adamson),  $NaClO_4$  prepared from NaOH (Baker Analyzed) and 70%  $HClO_4$  (G. F. Smith), KOH (Mallinckrodt), LiCl (Baker Analyzed), and  $MgCl_2$  (Mallinckrodt).

The absorption spectrum of the solvated electron in ethylenediamine and in concentrated aqueous solutions was measured by determining the absorption of the transient formed on pulsed radiolysis at different wave lengths. Full details of the experimental setup have been previously described.<sup>10,11</sup>

(1) (a) Based on work performed under the auspices of the U. S. Atomic Energy Commission; (b) on sabbatical leave from the Weizmann Institute of Science, Rehovoth, Israel.

(2) W. L. Jolly, *Progr. Inorg. Chem.*, **1**, 235 (1959).

(3) J. W. Boag and E. J. Hart, *Nature*, **197**, 45 (1963).

(4) E. J. Hart and J. W. Boag, *J. Am. Chem. Soc.*, **84**, 4090 (1962).

(5) J. P. Keene, *Nature*, **197**, 47 (1963); *Radiation Res.*, **27**, 1 (1964).

(6) I. A. Taub, D. A. Harter, M. C. Sauer, and L. M. Dorfman, *J. Chem. Phys.*, **41**, 979 (1964).

(7) G. E. Adams, J. H. Baxendale, and J. W. Boag, *Proc. Roy. Soc. (London)*, **A277**, 549 (1964).

(8) R. R. Dewald and J. L. Dye, *J. Phys. Chem.*, **68**, 121 (1964).

(9) S. Gordon, E. J. Hart, M. S. Matheson, J. Rabani, and J. K. Thomas, *Discussions Faraday Soc.*, **36**, 193 (1963).

The rate of reactions of  $e_{aq}^-$  with different organic and inorganic reagents was determined by following the rate of decay of the absorption spectrum at the 7200 Å maximum. Details of the experimental procedure and calculation of the specific rate constants have been described.<sup>9,12,13</sup>

The absorption spectrum of NaI (Baker and Adamson) in ethylenediamine was measured using a Cary recording ultraviolet spectrophotometer. As the solvent did absorb strongly below 2500 Å, the spectra of  $2 \times 10^{-4}$ ,  $5 \times 10^{-4}$ ,  $10^{-3}$ , and  $5 \times 10^{-3}$  M NaI solutions in ethylenediamine were measured down to 2500 Å, using the pure solvent as reference. From these results the onset ( $\epsilon = 5$ ) of the absorption band was determined. Further, the spectra of aqueous NaI solutions were measured at the same concentrations and the parallel shift in the absorption curve was determined at half the height of the peak value. From these measurements it is concluded that the iodide band in ethylenediamine is shifted 170 Å toward longer wave lengths, compared with the iodide band in aqueous solution. In this treatment we assume that the extinction coefficient and the shape of the absorption curve of the iodide ion in ethylenediamine and water are not significantly different. This assumption seems justified in view of results with iodide ion in other media.<sup>14,15</sup>

## Results

The absorption spectrum of the electron-pulse-generated solvated electron in pure ethylenediamine ( $e_{eda}^-$ ) shows a single symmetrical band with a maximum at 9200 Å, falling to half its height at 7000 and 11,200 Å. (see Figure 1). Since these experiments were carried out at  $e_{eda}^-$  concentrations of the order of  $10^{-5}$  M, we attribute this band to the isolated solvated electron. No other absorption bands could be detected in the range 5000–12,000 Å. This implies that the band at about 12,000 Å reported by Dewald and Dye<sup>8</sup> in rather concentrated solutions of alkali metals in ethylenediamine is due, not to  $e_{eda}^-$ , but probably to units such as ion pairs and more complex ions as suggested by them. Attempts to detect any of the other bands observed by Dewald and Dye, by adding potassium ions up to  $2 \times 10^{-3}$  M to the pulse-radiolyzed solution, failed to produce additional bands.

As the  $G$  value of the solvated electron in ethylenediamine is unknown, its extinction coefficient cannot be calculated. However, by assuming the same yield for  $e_{eda}^-$  as the  $e_{aq}^-$  the extinction coefficient of  $e_{eda}^-$  has an approximate value of  $8000 M^{-1} \text{ cm}^{-1}$  at  $\lambda_{max}$ .

The absorption of  $e_{aq}^-$  was measured in concentrated electrolyte solutions. The results are summarized in Table I. It is evident that  $\lambda_{max}$  is shifted

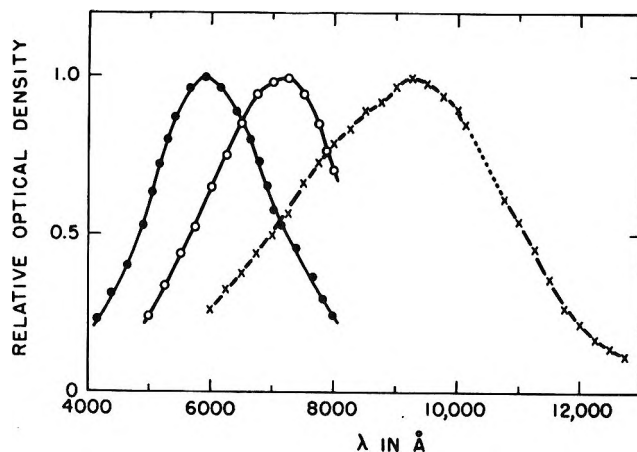


Figure 1. Spectra of electron pulse generated  $e_{aq}^-$  in 15 M aqueous solution and  $e_{eda}^-$  in ethylenediamine: ●, 15 M LiCl; ○, H<sub>2</sub>O (ref. 5); and ×, ethylenediamine.

from 7200 Å for pure water to shorter wave lengths in the electrolyte solutions. However, the shape of the absorption bands remains similar, and their extinction coefficients are only slightly lower than that of  $e_{aq}^-$  in pure water. The spectra of  $e_{aq}^-$  in 15 M LiCl and of  $e_{eda}^-$  in ethylenediamine are shown relative to water in Figure 1.

Table I: The Effect of Electrolytes on the Absorption Spectrum of  $e_{aq}^-$

Solute	Concn., M	$\lambda_{max}$ , Å	Relative $\epsilon$	$\lambda(0.5\epsilon_{max})$ , Å
None		7100	1.00	5700, 8300
MgCl <sub>2</sub>	4.6	6500	0.88	5000, 7950
KF	7.0	6500	0.72	5100, 7850
NaOH	15	6500	0.93	5050, 8150
KOH	15	6600	0.90	5200, 8160
NaClO <sub>4</sub>	10	6050	0.90	4850, 7450
KF	12.2	6050	0.83	5100, 7200
LiCl	15	5900	0.70	4800, 7200

The rates of reaction of several solutes with  $e_{aq}^-$  have been measured in 12 M KF and the specific rates are compared with those obtained in dilute solution (Table II). In all cases, the rates of reaction are lower than in dilute solution, although a primary salt effect is ex-

(10) S. Gordon, E. J. Hart, and J. K. Thomas, *J. Phys. Chem.*, **68**, 1262 (1964).

(11) J. K. Thomas, S. Gordon, and E. J. Hart, *ibid.*, **68**, 1524 (1964).

(12) E. J. Hart, S. Gordon, and J. K. Thomas, *ibid.*, **68**, 1271 (1964).

(13) M. Anbar and E. J. Hart, *J. Am. Chem. Soc.*, **86**, 5633 (1964).

(14) G. Stein and A. Treinin, *Trans. Faraday Soc.*, **56**, 1393 (1960).

(15) I. Burak and A. Treinin, *ibid.*, **59**, 1490 (1963).

pected to *increase* the rates of reaction of benzoate and nitrate ions with  $e_{aq}^-$ . Whereas the rate of the reaction of  $e_{aq}^-$  with  $NO_3^-$  is decreased in the concentrated solution by a factor of 5 and those with acetone and  $N_2O$  by a factor of 3-4, the rate of the  $e_{aq}^-$  reaction with benzoate ion is diminished by only a factor of 2.

**Table II:** The Reactivity of  $e_{aq}^-$  in Concentrated Electrolyte Solutions

Reactant (R)	$k(e_{aq}^- + R), M^{-1} \text{ sec.}^{-1}$	
	12.4 M KF	H <sub>2</sub> O
C <sub>6</sub> H <sub>5</sub> COO <sup>-</sup>	$(1.7 \pm 0.15) \times 10^9$	$(3.5 \pm 0.3) \times 10^{9a}$
CH <sub>3</sub> COCH <sub>3</sub>	$(1.6 \pm 0.2) \times 10^9$	$(5.9 \pm 0.2) \times 10^{9b,c}$
N <sub>2</sub> O	$(2.4 \pm 0.3) \times 10^9$	$(8.7 \pm 0.6) \times 10^{9c}$
NO <sub>3</sub> <sup>-</sup>	$(1.9 \pm 0.3) \times 10^9$	$(1.1 \pm 0.1) \times 10^{10c,d}$

<sup>a</sup> Ref. 13. <sup>b</sup> Ref. 12. <sup>c</sup> Ref. 9. <sup>d</sup> Ref. 11.

## Discussion

The analogy between the charge-transfer spectrum of halide ions and that of a trapped electron in the same medium had already been pointed out by Platzman and Franck in 1954.<sup>16</sup> No experimental evidence was available at the time to corroborate this suggestion. The absorption spectrum of iodide ions has been investigated in the presence of other ions<sup>14,17</sup> and in a number of solvents.<sup>15,17</sup> Having several absorption spectra of solvated electrons available, it was possible for us to examine quantitatively the Platzman and Franck hypothesis. The spectra of solvated electrons and of iodide ions are compared in Table III. The re-

**Table III:** A Comparison between the Spectra of Solvated Electrons and Ions in Different Media

Solvent	Solvated electrons		
	$\lambda_{max}, \text{\AA}$	$E_{\lambda_{max}}, \text{kcal./mole}$	Iodide ions $E_{\lambda_{max}}, \text{kcal./mole}$
H <sub>2</sub> O	7,200	39.7	126.5 <sup>a</sup>
MgCl <sub>2</sub> , 4.6 M	6,500	44.0	129.5 <sup>b</sup>
KF, 12 M	6,050	47.2	132.4 <sup>a</sup> (10 M)
LiCl, 15 M	5,900	48.4	135.0 <sup>b</sup> (12 M)
MeOH	6,300 <sup>c</sup>	45.4	130.1 <sup>d</sup>
EtOH	7,000 <sup>c</sup>	40.8	130.1 <sup>a</sup>
(CH <sub>2</sub> NH <sub>2</sub> ) <sub>2</sub> (en)	9,200	31.0	117.6
NH <sub>3</sub>	14,500 <sup>e</sup>	19.7	105.9 <sup>f</sup>
25% NH <sub>3</sub> in H <sub>2</sub> O	~7,800 <sup>g</sup>	37.1	123.6 <sup>a</sup>

<sup>a</sup> Ref. 15. <sup>b</sup> Extrapolated from value in ref. 15. <sup>c</sup> Ref. 6. <sup>d</sup> Ref. 17. <sup>e</sup> Ref. 2. <sup>f</sup> T. R. Griffiths and M. C. R. Symons, *Trans. Faraday Soc.*, **56**, 1125 (1960). <sup>g</sup> The first inflection in Figure 14, ref. 4.

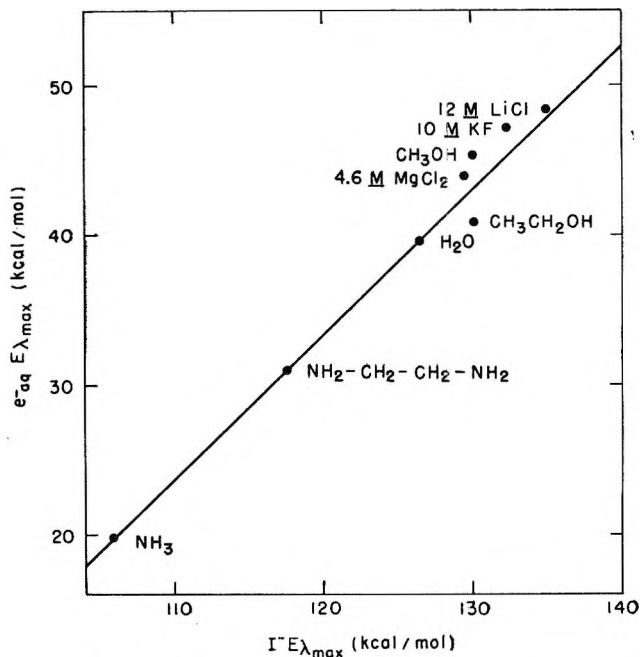


Figure 2. Comparison of  $E_{\lambda_{max}}$  of solvated electrons and iodide ions.

sults, presented in Figure 2, show a linear correlation between the effects of the medium on the spectra of solvated electrons and of iodide ions.<sup>18</sup>

The charge-transfer-to-solvent spectrum (c.t.t.s) of an anion,  $X^-$ , has been shown to follow the expression<sup>15,16,19</sup>  $E_{\lambda_{max}} = E_X + E_g - L_X - B$ , where  $E_X$  = electron affinity of the  $X$  radical;  $L_X$  = the heat of hydration of the  $X$  radical;  $E_g$  = the energy involved in removing the ion from its cavity in the solvent, without disturbing the persistent polarization of the medium; and  $B$  = the binding energy of the electron to the polarized medium in its excited state. In the case of hydrated electrons it has been shown<sup>20</sup> that  $E_{\lambda_{max}}$  of  $e_{aq}^-$  is equal to its energy of hydration. In this case  $E_X = L_X$  and  $B = 0$ ; thus  $E_{\lambda_{max}} = E_g$ . It has been suggested that the changes in  $E_{\lambda_{max}}$  of iodide are mainly due to changes in the  $E_g$  term.<sup>15</sup> Our results confirm this conclusion quantitatively and prove that

(16) R. L. Platzman and J. Franck, *Z. Physik*, **138**, 411 (1954).

(17) M. Smith and M. C. R. Symons, *Trans. Faraday Soc.*, **54**, 338, 346 (1958).

(18) It should be noted that the  $\lambda_{max}$  of the iodide ion was measured at 10 M KF and 12 M LiCl,<sup>14</sup> whereas  $\lambda_{max}$  of  $e_{aq}^-$  was measured at 12 M KF and 15 M LiCl. Correction for this difference in concentration would cause a shift of these points to the left in Figure 2 and, if the absorption spectra were measured at the same concentrations of added electrolyte, an even better correlation between  $e_{aq}^-$  and  $I^-$  spectra should result.

(19) G. Stein and A. Treinin, *Trans. Faraday Soc.*, **55**, 1086 (1959).

(20) J. H. Baxendale, *Radiation Res. Suppl.*, **4**, 139 (1964).

the effects of the medium on the spectrum of solvated electrons are the same as on that of iodide ions.

In the case of concentrated electrolyte solutions it was shown that changes in  $E_g$  are due to changes in the radius,  $r$ , of the cavity available to the ion in solution.<sup>14</sup> The contraction of the cavity results in a shift to shorter wave lengths. The effect of LiCl, KF, and MgCl<sub>2</sub> on this parameter has been discussed by Stein and Treinin,<sup>14</sup> and they predicted that anions which strongly bind the protons of H<sub>2</sub>O molecules will tend to decrease  $r$ . This prediction would imply a most extensive shift to the ultraviolet by OH<sup>-</sup> ions, contrary to our observations on the spectra of e<sub>aq</sub><sup>-</sup> in concentrated NaOH and KOH solutions (Table I). As the dielectric properties of these solutions are comparable to those of KF, the observed difference in behavior of OH<sup>-</sup> and F<sup>-</sup> must be due to a difference in the magnitude of  $r$ . The discrepancy may be explained, however, by the formation of well-defined OH(H<sub>2</sub>O)<sub>3</sub><sup>-</sup> complexes,<sup>21</sup> which leave larger cavities for e<sub>aq</sub><sup>-</sup>, than those produced by the mutual repulsion of protons.<sup>14</sup>

The effects of different solvents on  $E_{\lambda_{max}}$  are mainly due to changes in their dielectric properties which determine the value of  $E_g$ .<sup>15</sup> They affect the spectrum of the solvated electron in a manner similar to their effect on the charge-transfer spectra. In other words, the value of  $E_{\lambda_{max}}$  for solvated electrons may be predicted using Treinin's c. t. t. s. scale.<sup>15</sup>

The rate of reaction of hydrated electrons with oxidizing agents must be affected by the energy required to abstract the electron from its sphere of hydration. This is confirmed by our findings that the rates of e<sub>aq</sub><sup>-</sup> reactions are slowed down in concentrated KF solutions (Table II) in which an increase of 7.5 kcal./mole in  $E_{\lambda_{max}}$  was observed. It should be noted, however, that this decrease in rate is not equal for the different substrates examined and it appears that the more hydrated reactants, e.g., NO<sub>3</sub><sup>-</sup>, are affected to a greater extent. It is hard to believe that the primary salt effect on the BzO<sup>-</sup>-e<sub>aq</sub><sup>-</sup> reaction is greater than that on the NO<sub>3</sub><sup>-</sup>-e<sub>aq</sub><sup>-</sup> interaction. This would suggest that the major effect of the environment on the rate is by changing the hydration sphere of the activated complex, and that the changes in the size of the cavity of e<sub>aq</sub><sup>-</sup>, or the energetics of its hydration, are of relatively minor importance. This conclusion is supported by the finding that the rate of e<sub>aq</sub><sup>-</sup> reactions in water and alcohols is equal.<sup>6,13</sup>

In conclusion, it may be stated that our results have not only corroborated the quantitative theories of charge-transfer spectra but made it possible to predict the spectrum of solvated electrons in different solvents.

*Acknowledgment.* We gratefully acknowledge the value of our several discussions with Dr. R. L. Platzman.

(21) G. Yagil and M. Anbar, *J. Am. Chem. Soc.*, **85**, 2376 (1963).

## Influence of Electrolytes on the Solution Properties of Neutralized

### Poly-N-vinylimidazole

by Kang-Jen Liu<sup>1</sup> and Harry P. Gregor

Department of Chemistry of the Polytechnic Institute of Brooklyn, Brooklyn, New York  
(Received October 17, 1964)

The influence of counterions upon the solution properties of poly-N-vinylimidazole at different degrees of protonation was studied by viscometric and light scattering techniques. In the presence of sodium chloride (0.2–1.0 M) the viscosity of the polymer increased with the degree of protonation, but in the presence of sodium bromide or sodium nitrate the viscosity first decreased to a minimum and then increased with the degree of protonation. Intramolecular association with the formation of hydrogen bonds or triple ions was proposed as the basis for this behavior. Results of light scattering experiments showed a sharp drop in the second virial coefficient of the polymer at a point corresponding to the minimum viscosity. The apparent molecular weight decreased with protonation to a "true" value at the 100% neutralized point.

#### Introduction<sup>1</sup>

The size and shape of a given polyelectrolyte molecule in solution depends upon its net charge, the ionic strength of the solution, and the nature of the counterions present. The charged polyelectrolyte expands as a consequence of electrical repulsion between like charges; the addition of neutral salt reduces this expansion because counterions within the coil screen the electrical repulsion.<sup>2,3</sup> The work of Strauss, Woodside, and Wineman<sup>4</sup> on polyphosphate and studies on sodium carboxymethyl cellulose by Pals and Hermans<sup>5</sup> and by Schneider and Doty<sup>6</sup> have shown that the intrinsic viscosity decreased regularly with added neutral salt; Cox<sup>7</sup> has also described the influence of ionic strength upon the viscosity of ribonucleic acid solutions. Tanford<sup>8</sup> has discussed studies on the viscosity of polyvinylbutylpyridinium bromide by Fuoss and Strauss<sup>9,10</sup> and suggested the formation of  $-N^+Br^-N^+$  bonds within the polymer coil. These studies<sup>9,10</sup> had been carried out on polyvinylpyridine quaternized to only one degree (32%) in neutral salt solutions. Studies<sup>11–15</sup> on polyvinylpyridine quaternized with long hydrocarbon chain substituents (polysoaps) showed that these polymers were capable of pronounced micelle formation. Flory and Orofino<sup>16</sup> have studied the effects of changes in the degree of ionization

of polyacrylic acid in aqueous sodium chloride solutions upon its second virial coefficient and molecular dimensions. The behavior of a polybase at different degrees of ionization was reported by Gold and Gregor,<sup>17</sup>

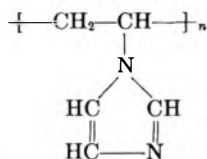
- (1) Taken in part from the dissertation of K. J. Liu, submitted in partial fulfillment of the requirements for the degree of Doctor of Philosophy in Chemistry at the Polytechnic Institute of Brooklyn, Brooklyn, N. Y., 1963.
- (2) D. T. F. Pals and J. J. Hermans, *J. Polymer Sci.*, **3**, 897 (1948).
- (3) R. M. Fuoss and U. P. Strauss, *ibid.*, **3**, 602 (1948).
- (4) U. P. Strauss, D. Woodside, and P. Wineman, *J. Phys. Chem.*, **61**, 1353 (1959).
- (5) D. T. F. Pals and J. J. Hermans, *Rec. trav. chim.*, **71**, 447 (1955).
- (6) N. S. Schneider and P. Doty, *J. Phys. Chem.*, **58**, 765 (1954).
- (7) R. A. Cox, *J. Polymer Sci.*, **47**, 441 (1960).
- (8) C. Tanford, "Physical Chemistry of Macromolecules," John Wiley and Sons, Inc., New York, N. Y., 1962.
- (9) R. M. Fuoss and U. P. Strauss, *J. Polymer Sci.*, **3**, 246 (1948).
- (10) R. M. Fuoss, *Discussions Faraday Soc.*, **11**, 125 (1951).
- (11) U. P. Strauss and N. L. Gershfeld, *J. Phys. Chem.*, **58**, 747 (1954).
- (12) U. P. Strauss, N. L. Gershfeld, and E. H. Crook, *ibid.*, **60**, 577 (1956).
- (13) D. Woermann and F. T. Wall, *ibid.*, **64**, 531 (1960).
- (14) U. P. Strauss, *J. Polymer Sci.*, **6**, 649 (1951).
- (15) U. P. Strauss and A. G. Boyes, *ibid.*, **22**, 63 (1956).
- (16) T. A. Orofino and P. J. Flory, *J. Phys. Chem.*, **63**, 283 (1959).
- (17) D. H. Gold and H. P. Gregor, *Z. physik. Chem. (Frankfurt)*, **15**, 93 (1958).



the present study is concerned with the influence of neutral salt on the properties of the same polymer.

### Experimental

The poly-N-vinylimidazole (PVI) used in this study was furnished by Badische Aniline and Soda Fabrik,



and was synthesized from the 1-vinylimidazole monomer. Its molecular weight was estimated to be  $1.38 \times 10^5$  by light scattering measurements, as will be discussed later. This product was obtained from the manufacturer in 1959 and was of much higher molecular weight than previous samples. The general properties and the purity of this polymer were described previously.<sup>17,18</sup> Stock solutions were prepared by weight and their titer determined potentiometrically with standard acid.

A three-bulb Ubbelohde dilution viscometer was used for all measurements. This viscometer permits dilution to be effected directly in the bulb without affecting the pressure gradient. The water-flow time was such that kinetic energy corrections were negligible. All viscosity measurements were taken at  $25 \pm 0.02^\circ$ . Routinely, viscosity measurements were made by first flushing with  $\text{CO}_2$ -free nitrogen, adding the desired solution, and bringing the system to the desired thermostat temperature. Efflux time measurements were repeated four times with each solution. The viscosity of PVI at different concentrations of sodium chloride, sodium bromide, and sodium nitrate was measured as a function of its degree of neutralization ( $\alpha$ ) with hydrochloric, hydrobromic, and nitric acid, respectively.

Light scattering measurements were performed at room temperature in a Brice-Phoenix photometer,<sup>19</sup> using incident unpolarized monochromatic blue light ( $\lambda = 436 \text{ m}\mu$ ). A cylindrical light scattering cell with flat faces at  $0$  and  $180^\circ$  was used. All solutions and solvents were filtered directly into the cell through an ultrafine frit (porosity  $0.45 \mu$ ) using four rinses. The same filtrates were used in the determination of refractive index increments, measured with a dipping refractometer at  $25 \pm 0.1^\circ$  in blue light.

### Results and Discussion

The viscosity results of  $0.1$  and  $0.01 \text{ M}$  PVI at different  $\alpha$ -values in different concentrations of various salts are shown in Table I. In sodium chloride solutions, this polyelectrolyte behaves normally, similar to

polyacids in salt solutions. In the absence of neutral salt,  $\eta_{sp}/C_p$  rises with  $\alpha$  as electrostatic repulsion acts to increase the hydrodynamic volume of the polymer coil, and then levels off and decreases. In the presence of appreciable concentrations of sodium chloride, the reduced viscosity increases by a much lesser extent as the result of counterion screening effects.

**Table I:** Reduced Viscosity ( $\eta_{sp}/C_p$ ) of PVI Solutions at  $25^\circ$

Salt	Concn., M	$\alpha$					
		0.0	0.2	0.4	0.6	0.8	1.0
In $0.01 \text{ M}$ PVI							
NaCl	1.0	0.88	0.89	0.91	0.91	1.02	1.03
NaCl	0.5	0.81	0.85	0.95	0.97	1.18	1.25
NaCl	0.2	0.78	1.02	1.34	1.64	1.73	1.87
NaCl	0	0.95	8.1	13.0	14.2	12.6	10.3
NaBr	0.5	0.91	0.28	0.29	0.93	1.08	1.12
NaBr	0.2	0.85	0.71	1.12	1.55	1.63	1.60
NaNO <sub>3</sub>	0.5	0.70	0.54	0.38	0.47	0.52	0.61
NaNO <sub>3</sub>	0.2	0.72	0.56	0.82	1.08	1.17	1.34
In $0.1 \text{ M}$ PVI							
NaCl	1.0	1.08	1.09	1.19	1.23	1.25	1.29
NaCl	0.5	1.03	1.10	1.36	1.48	1.52	1.60
NaCl	0.2	1.00	1.33	1.75	1.98	2.12	2.19
NaCl	0	1.02	5.31	6.21	6.63	7.26	5.88
NaBr	0.5	1.16	0.95	0.98	1.14	1.28	1.45
NaBr	0.2	1.03	0.93	1.29	1.65	1.85	1.97

In the presence of sodium bromide and sodium nitrate, the viscosity results were quite different from those with sodium chloride. As the polybase was protonated in the presence of bromide or nitrate, the reduced viscosity *decreased* to a minimum and then increased with increasing  $\alpha$ . Here, if only ion-pair formation between fixed and counterions took place when the polybase was protonated, the reduced viscosity would either increase (less than would be the case with lower ion binding) or would remain constant; the *decrease* in the reduced specific viscosity is the result of significant intramolecular association which causes polymer coil contraction. It may be reasonably postulated that this association is predominantly the result of triple-ion formation, as was also postulated by Tanford.<sup>8</sup> It could also be the result of hydrogen bonding of two nitrogens by a proton; the role of the anion here would be to stabilize the complex. Therefore, the protonation of a polybase may cause it to expand

(18) H. P. Gregor and D. H. Gold, *J. Phys. Chem.*, **61**, 1374 (1957).

(19) B. A. Brice, M. Halwer, and R. Speiser, *J. Opt. Soc. Am.*, **40**, 708 (1950).

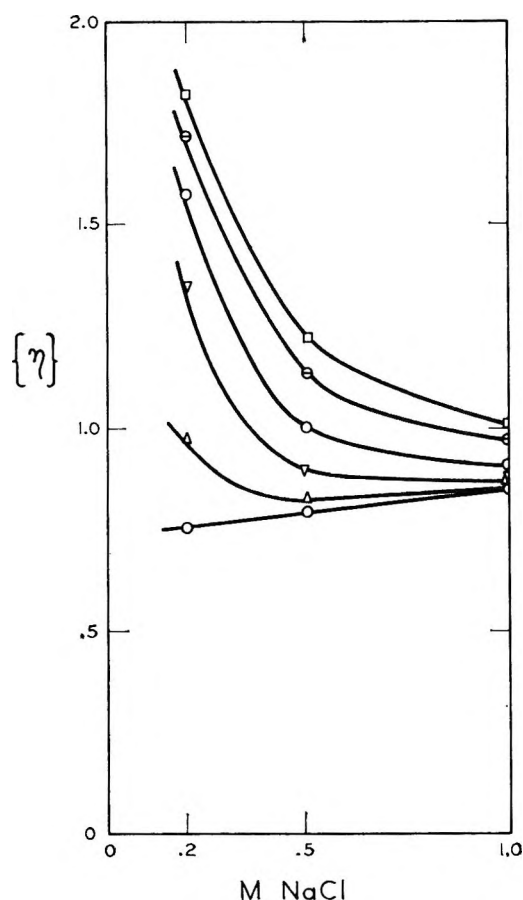


Figure 1. Intrinsic viscosity of PVI neutralized to different  $\alpha$ -values: 0 (O), 0.2 ( $\Delta$ ), 0.4 ( $\nabla$ ), 0.6 ( $\square$ ), 0.8 ( $\odot$ ), 1.0 ( $\square$ ), as a function of sodium chloride concentration.

or contract depending upon the compensating effects of electrostatic repulsion and intramolecular association.

The dependence of the intrinsic viscosity  $\{\eta\}$  (extrapolation of  $\eta_{sp}/C_p$  to zero polymer concentration) upon the concentration of sodium chloride is shown in Figure 1. The effect of increasing chloride concentration on the uncharged polymer is small. As the charge on the polymer increases, the contraction of the coil is observed with increases in the ionic strength of the solution.

The results of light scattering measurements confirm the interpretation of the viscosity data. It has been shown<sup>16,20</sup> that a polyelectrolyte in concentrated aqueous salt solutions can be treated as a two-component system. The Zimm plot has been generally applied.<sup>16,21</sup> The utilization of the experimental refractive index ( $dn/dc$ ) values in computations based on light scattering theories requires some discussion. For three-component systems, the light scattering constant  $H$  should be expressed<sup>22</sup> as

$$H = (32\pi^3 n^2) / (3\lambda^4 N) [(\partial n / \partial c) - (\partial \psi / \partial c)(\partial n / \partial \psi_0)]^2$$

where  $n$  is refractive index of the medium,  $\lambda$  is the wave length,  $N$  is Avogadro's constant,  $\psi_0$  is the volume fraction of solvent in the absence of polymer, and  $\psi$  is its value in the medium surrounding the polymer domain. Flory<sup>16</sup> has estimated these two latter terms and found that they can be neglected without introducing serious error. Figure 2 is a Zimm plot of PVI at  $\alpha = 1.0$  in

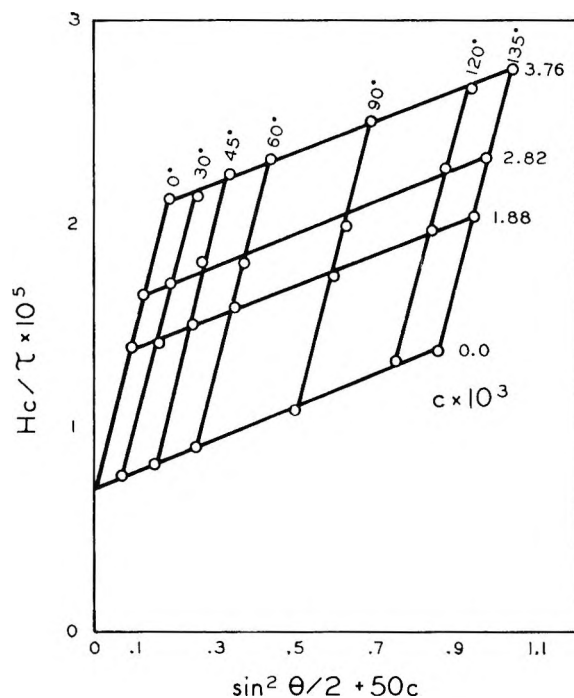


Figure 2. Zimm plot of fully neutralized ( $\alpha = 1$ ) PVI in 0.5 M sodium chloride. Concentration  $c$  in g. ml.<sup>-1</sup>.

0.5 M sodium chloride; similar plots were obtained at different  $\alpha$ -values and in other salts. The limiting slopes of the Zimm plot at zero polymer concentration are difficult to obtain accurately. The second virial coefficient ( $A_2$ ) and weight-average molecular weight are obtained from the light scattering equation

$$\frac{Hc}{\tau_0} = 1/M + 2A_2c + \dots$$

where  $c$  is the polymer concentration in g. ml.<sup>-1</sup>,  $\tau_0$  is the turbidity extrapolated from the Zimm plot to the zero scattering angle, and  $M$  is weight average molecu-

(20) H. Eisenberg and E. F. Casassa, *J. Polymer Sci.*, **47**, 29 (1960).

(21) U. P. Strauss and A. G. Boyes, *J. Phys. Chem.*, **65**, 1390 (1961).

(22) R. H. Ewart, C. P. Roe, P. Debye, and J. R. McCartney, *J. Chem. Phys.*, **14**, 687 (1946).

**Table II:** Weight-Average Molecular Weights and the Second Virial Coefficient of PVI at Various  $\alpha$ -Values in 0.5 M Salt

$\alpha$	$A_2 \times 10^4$	$\bar{M}_w \times 10^{-5}$
Sodium chloride		
0	7.50	4.35
0.20	6.25	2.85
0.41	9.12	1.54
0.70	15.75	1.28
1.00	19.00	1.40
Sodium bromide		
0	11.0	2.63
0.45	3.82	1.71
1.00	11.5	1.39
Sodium nitrate		
0	7.25	2.73
0.32	-0.37	..
1.00	7.50	1.35

lar weight. The calculated values are shown in Table II. The second virial coefficient values are indicative

of polymer-solvent relationships and correlate well with the observed *minimum* points of viscosity. The second virial coefficient of PVI shows a sharp drop in 0.5 M sodium nitrate at  $\alpha = 0.32$  and in 0.5 M sodium bromide at  $\alpha = 0.45$ , indicating a strong contraction of the polycation in that range. The apparent molecular weight decreases during protonation; this indicates that the polymer chains may have been somewhat associated at  $\alpha = 0$ , repelling each other as protonation proceeded. Therefore, molecular weights obtained at  $\alpha = 1.0$  are the most representative of true molecular weight. All of the second virial coefficients increased at high  $\alpha$ -values, indicating the effect of electrostatic repulsion in expanding the polycation coil. Therefore, the results of light scattering experiments are found to agree well with those from viscometric studies.

*Acknowledgment.* This investigation was supported in part by the Public Health Service Research Grant GM 02934 from the Division of General Medical Sciences, Public Health Service.

## Metal-Polyelectrolyte Complexes. X. Poly-N-vinylimidazole Complexes with Zinc(II) and with Copper(II) and Nitrilotriacetic Acid

by Kang-Jen Liu<sup>1</sup> and Harry P. Gregor

*Department of Chemistry of the Polytechnic Institute of Brooklyn, Brooklyn 1, New York  
(Received October 17, 1964)*

The binding of zinc by poly-N-vinylimidazole (PVI) in 1 *M* sodium nitrate at 0.1 and 0.01 *M* polymer concentrations was studied potentiometrically and by dialysis equilibrium. Formation constants computed from the data of each technique were in excellent agreement with a maximum coordination number of 4 being found. The enhancement of the successive intrinsic stepwise association constants due to the polymeric effect was observed; the four intrinsic formation constants  $\log \kappa_i$  could be read directly from the *Q*-plotting method of Scatchard, and were 1.72, 2.65, 3.35, and 3.76 as contrasted with 1.98, 2.19, 2.41, and 2.62 for the binding of imidazole by Zn(II). Analysis of the precipitated PVI-Zn(II) complex showed that the ratio of nonprotonated PVI to Zn(II) in the complex approached 1 with an excess of metal present and 4 with an excess of polymer. A turbidimetric study showed cross linking of polymer chains by Zn(II) at high polymer-metal ratios, with an approximately 400-fold increase in molecular weight. Nitrilotriacetic acid formed a 1:1:1 molar complex with Cu(II) and PVI; the tridentate ligand complex with the metal appeared to be attached to the chain by a single bond, with a formation constant of  $10^{4.0}$  as contrasted with the first and last stepwise constants of  $10^{3.50}$  and  $10^{3.76}$  for the binding of the polymer directly to Cu(II).

### Introduction

The role of the imidazole group in proteins and other natural products has been of broad interest; extensive work on its complexes with metallic ions has been reported.<sup>2-5</sup> The binding of Cu(II) and Ag(I) ions by poly-N-vinylimidazole (PVI) has been described previously.<sup>6</sup> In the present paper, the formation of complexes of PVI with Zn(II) was studied by both potentiometric titration and dialysis equilibrium experiments. The PVI-Cu(II) system was also studied by dialysis equilibrium techniques, and the results are compared with previous ones on potentiometric titrations.<sup>6</sup> PVI-Zn(II) complexes were precipitated from solution and analyzed to determine their stoichiometric relationship. The nature of the Zn(II)-PVI complex was studied turbidimetrically. A study of a mixed ligand system composed of a low molecular weight ligand with PVI and Cu(II) was also carried out.

### Experimental

**Materials.** Poly-N-vinylimidazole was obtained

from Badische Aniline und Soda Fabrik. It was essentially of high purity with a molecular weight (weight average) of  $1.38 \times 10^6$  estimated by light scattering measurements. Its general properties and purity were described previously.<sup>7,8</sup>

A stock solution of zinc nitrate (analytical grade reagent) which was approximately 0.2 *M* in the salt

(1) Taken in part from the dissertation of K. J. Liu, submitted in partial fulfillment of the requirements for the degree of Doctor of Philosophy in Chemistry at the Polytechnic Institute of Brooklyn, Brooklyn, N. Y., 1963.

(2) F. R. N. Gurd, J. T. Edsall, G. Felsenfeld, and D. S. Goodman, *Federation Proc.*, **11**, 224 (1952).

(3) C. Tanford and M. L. Wager, *J. Am. Chem. Soc.*, **75**, 434 (1953).

(4) J. T. Edsall, G. Felsenfeld, D. S. Goodman, and F. R. N. Gurd, *ibid.*, **76**, 3054 (1954).

(5) N. C. Li, J. M. White, and E. Doody, *ibid.*, **76**, 6219 (1954).

(6) D. H. Gold and H. P. Gregor, *J. Phys. Chem.*, **64**, 1461, 1464 (1960).

(7) H. P. Gregor and D. H. Gold, *ibid.*, **61**, 1347 (1957).

(8) H. P. Gregor and D. H. Gold, *Z. physik. Chem. (Frankfurt)*, **15**, 93 (1958).

and 0.005 *M* in nitric acid was diluted with water as needed. The acid prevented hydrolysis and its titer was considered in calculations. Zinc was determined by EDTA titration.<sup>9</sup> A copper nitrate solution was made according to the same procedure and determined also by EDTA titration.<sup>9</sup>

Solutions of CO<sub>2</sub>-free sodium hydroxide were prepared according to the procedure described by Kolthoff and Sandell.<sup>10</sup> The diluted solutions were standardized against freshly dried analytical grade potassium hydrogen phthalate and kept in a heavy-wall polyethylene bottle.

Common strong acids were prepared by dilution from analytical grade stock and kept also in heavy wall polyethylene bottles. Each acid prepared was routinely standardized with freshly standardized sodium hydroxide.

Zincon (2-carboxy-2'-hydroxy-5'-sulfoformazylbenzene) was selected as the analytical reagent for very dilute zinc(II) and copper(II) determinations.<sup>11</sup> Usually, finely powdered Zincon (0.130 g.) was dissolved in 2 ml. of 1 *M* sodium hydroxide and diluted to 100 ml., giving an approximately 0.002 *M* stock solution.

A stock solution of pure nitrilotriacetic acid (NTA) was prepared from freshly dried reagent grade stock. The concentrations were determined spectrophotometrically with a standardized copper(II) solution. All solutions reported here were made using distilled, CO<sub>2</sub>-free water.

**Potentiometric Titrations.** All titrations were made in the stepwise manner previously described<sup>6-8</sup> and at 24.0°. Hydrogen ion activities were determined with a Beckman Model G pH meter using a sleeve-type saturated calomel electrode. The point of incipient precipitation of zinc hydroxide was in the pH range of 5.7 to 6.3 at this salt concentration; no data above this pH level were used in the calculation.

Figure 1 shows the titration curve of 0.01 *M* PVI in the presence of various zinc(II) concentrations; similar curves were obtained for 0.1 *M* PVI.

**Dialysis Equilibrium Measurements.** In the presence of a relatively high concentration of neutral salt, the Donnan potential is swamped and the concentration of diffusible species is nearly the same on both sides of a membrane. Dialysis measurements, therefore, allow one to measure directly the binding of a metal ion to a polyelectrolyte. Cellophane tubing (Visking) was used in all dialysis experiments; it was washed thoroughly for at least 72 hr. with repeated changes of deionized water prior to use. The polymer was dialyzed using the same membrane for 24 days against daily changes of CO<sub>2</sub>-free deionized water before use in dialysis experiments. The test

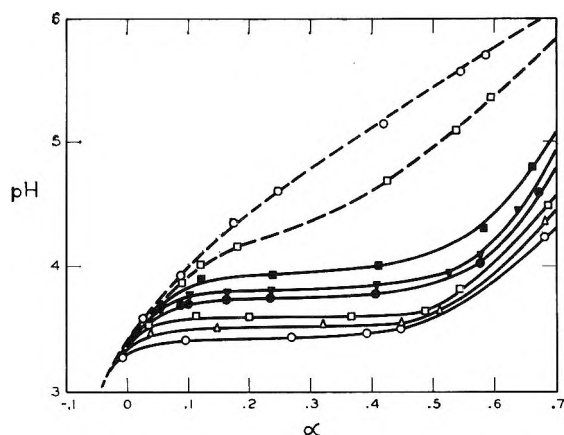


Figure 1. Titration of 0.01 *M* PVI in 1 *M* sodium nitrate with a zinc(II) nitrate concentration ( $M \times 10^{-4}$ ) of: 0 (---○---); 4.46 (---□---); 22.3 (■); 44.6 (▼); 66.9 (●); 223 (□); 446 (Δ); and 669 (○).

for the removal of diffusible polymer molecules was to measure the resistivity of the deionized water outside the membrane bag until no appreciable change was observed. The dialyzed solution was then filtered under nitrogen atmosphere and was ready for use.

The polymer solution (20 ml.) was placed in the membrane bag, which was placed into a tightly sealed bottle containing 50 ml. of copper(II) or zinc(II) nitrate solution; both inside and outside solutions were 1 *M* in sodium nitrate. The bottles were put on a shaker and rate experiments showed that 24 hr. was sufficient for equilibrium to be reached. Dialysis experiments were routinely run for 3 or 4 days. Experiments performed without PVI showed complete equilibrium. In all experiments, the volume inside the bag was unchanged within experimental error.

The pH levels inside and outside the membrane bag were measured with a Beckman Model G pH meter. No appreciable difference was observed ( $\pm 0.02$  pH unit). Metal ions were determined spectrophotometrically with a Zincon solution,<sup>11</sup> with the optical density measured with a Cary-14 spectrophotometer at  $\lambda = 620 \text{ m}\mu$  for Zn(II) and  $\lambda = 600 \text{ m}\mu$  for Cu(II) against a reagent blank; the calibration curves were quite linear, and were repeated for each series of experiments. The analytical error was less than  $\pm 0.4\%$ .

These experimental results are listed in Table I for the Zn(II)-PVI and Cu(II)-PVI systems.

**Analysis of PVI-Zn(II) Complex.** Approximately 500 ml. of PVI-ZnCl<sub>2</sub> solutions at different ratios were

(9) K. Ueno, "The Method of Complexometric Titrations," Kohnando Co., Tokyo, 1961.

(10) I. M. Kolthoff and E. B. Sandell, "Textbook of Quantitative Inorganic Analysis," The Macmillan Co., New York, N. Y., 1946.

(11) R. M. Rush and J. H. Yoe, *Anal. Chem.*, **26**, 1345 (1954).

**Table I:** Membrane Dialysis Equilibrium in 1 M Sodium Nitrate Solution<sup>a</sup>

—[Cu(II)] outside—			—[Zn(II)] outside—		
Initial, $M \times 10^4$	Final, $M \times 10^4$	pH, final	Initial, $M \times 10^4$	Final, $M \times 10^5$	pH, final
1.011	0.55	3.51	2.218	0.945	4.28
1.011	1.00	3.43	2.218	0.585	4.29
1.011	1.80	3.26	2.218	0.415	4.36
2.022	1.20	3.40	2.218	0.210	4.47
10.11	53.5	2.90	22.18	13.6	3.88
10.11	48.8	2.99	22.18	12.7	3.93
10.11	45.5	3.01	22.18	12.0	4.21

<sup>a</sup> Fifty ml. of metal nitrate solution dialyzed vs. 20 ml. of 0.01 M PVI in bag.

combined in a blender. The PVI concentration was 0.1 M, the pH was adjusted to 4.50 with hydrochloric acid, and no neutral salt was added. The initial PVI:Zn(II) ratios were 5:1, 4:1, 1:1, 1:4, and 1:10. The system was then kept in a sealed bottle for 1 month to ensure equilibrium. In all cases a precipitate was formed. At the latter three ratios, the well-defined precipitates could be filtered and washed quickly with  $10^{-4}$  M hydrochloric acid to remove adherent solution. The solution ratios rich in PVI gave gelatinous precipitates which could be collected only by centrifugation without washing. All precipitates were then dried in a vacuum oven at room temperature, ground to a fine powder, and redried. The composition of each (C, N, H, Cl, Zn) was determined.

**Turbidimetric Study.** A turbidimetric study of the Zn(II)-PVI complex at two Zn(II) concentrations,  $1.0 \times 10^{-5}$  and  $2.0 \times 10^{-6}$  M, with various polymer concentrations in a 0.06 M bicarbonate aqueous medium was performed at room temperature in a Brice-Phoenix light scattering photometer<sup>12</sup> using incident unpolarized monochromatic blue light. The light scattering of the polymer solution at corresponding concentrations in the absence of Zn(II) was also measured in all cases. The scattering light intensities were measured at 0 and 90° with a galvanometer recorder.

**Mixed Ligands.** A qualitative study to establish the formation of a mixed ligand complex with a polyelectrolyte-metal system in solution was first carried out. Polymer solutions were made up in two different concentrations in 0.06 M sodium bicarbonate buffer at pH 8.3, to which were added different amounts of Cu(II) and NTA. The degree of turbidity was observed visually. When the concentration of PVI was  $5 \times 10^{-4}$  M and that of Cu(II) was 0.5, 2, 3, and  $5.5 \times 10^{-4}$  M, the solutions were turbid; when  $5.0 \times 10^{-4}$  M NTA was added to the latter, a clear solution

resulted. Similarly, when the PVI concentration was  $1.0 \times 10^{-3}$  M and the solution was made 0.1 or  $1.1 \times 10^{-3}$  M in Cu(II), the solution became turbid; the addition of  $1.0 \times 10^{-3}$  M NTA to the latter solution also gave one which was nearly clear. A previous study<sup>6</sup> had shown that a Cu(II)(PVI)<sub>4</sub> complex is formed when a large excess of PVI over metal is present. Here, the molar concentration ratio of PVI to Cu(II) was 10:1 to 1.1:1 and the solutions were turbid as a result of cross linking of polymer chains by the metal. If one assumes that Cu(II) and NTA formed an equimolar tridentate and neutral complex, one which combined with PVI to form the PVI·Cu(II)·NTA complex, then no uncombined PVI would remain to be cross linked by the excess Cu(II) and form a turbid solution. Later experiments confirmed this hypothesis.

The mixed PVI·Cu(II)·NTA complex was studied quantitatively by dialysis equilibrium. The general procedure has been described previously. Both NTA or Cu(II) were determined spectrophotometrically by the addition of an excess of the other and observation of the absorbance of the Cu(II)·NTA complex at 734 mμ. When a standard Cu(II) solution was added to one of NTA, the optical density was linear with the reagent concentration up to the equimolar point; when NTA was added to Cu(II), the curve was also linear when corrected for absorbance of Cu(II) at that wave length.

## Calculations

**Potentiometric Titrations.** The use of potentiometric titrations to calculate formation constants for reactions between a metal ion and a ligand has been described in detail by Bjerrum.<sup>13</sup> Bjerrum's method was modified for metal ion-polyelectrolyte complexes by Gregor, Luttinger, and Loebel.<sup>14</sup> The average number of ligands bound per metal ion present in all forms ( $\bar{n}$ ) is expressed as a function of the free ligand concentration ( $A$ ) to give the formation curve of the system. For the PVI-Zn(II) system,  $\bar{n}$  is defined as

$$\bar{n} = \frac{[\text{PVI}]_t - [\text{PVI}] - [\text{PVIH}^+]}{[\text{Zn(II)}]_t} \quad (1)$$

where  $[\text{PVI}]_t$  is the total molar concentration of PVI,  $[\text{PVI}]$  for free PVI,  $[\text{PVIH}^+]$  for the ion, and  $[\text{Zn(II)}]_t$  for the total Zn(II) concentration.

(12) B. A. Brice, M. Halwer, and R. Speiser, *J. Opt. Soc. Am.*, **40**, 768 (1950).

(13) J. Bjerrum, "Metal Amine Formation in Aqueous Solutions." P. Hasse and Son, Copenhagen, 1941.

(14) H. P. Gregor, L. B. Luttinger, and E. M. Loebel, *J. Phys. Chem.*, **59**, 34 (1955).

It is readily shown from the material balance

$$[\text{PVI}]_t = [\text{PVI}] + [\text{PVIH}^+] + \sum_{i=1}^N i[\text{Zn}(\text{PVI})_i] \quad (2)$$

and electroneutrality requirement that

$$[\text{PVIH}^+] = [\text{PVI}]_t(1 - \alpha) - [\text{H}^+] + [\text{OH}^-] \quad (3)$$

where  $\alpha$  is the degree of neutralization. The hydrogen ion concentration was calculated from its activity, using the mean activity coefficient of the supporting electrolyte. The concentration of the hydroxide ion was generally negligible in our experiments.

It has been shown empirically<sup>8,14</sup> that over a wide range of  $\alpha$ , the titration of PVI could be expressed as

$$K_Q = \frac{[\text{H}^+][\text{PVI}]}{[\text{PVIH}^+]} (1/Z)^{n-1} \quad (4)$$

$Z$  is the ratio of charged to uncharged groups on the polymer chain;  $n$  is the Henderson-Hasselbach slope in the absence of added coordinating metal ion;  $K_Q$  is the average dissociate constant. In the presence of Zn(II), if a coordination number of 4 is assumed, the above expression can be transformed to

$$K_Q = \frac{[\text{H}^+][\text{PVI}]}{[\text{PVIH}^+]} \left\{ \frac{[\text{PVI}]}{[\text{PVIH}^+] + \frac{1}{2}(\alpha[\text{PVI}]_t + [\text{H}^+] - [\text{OH}^-] - [\text{PVI}])} \right\} \quad (5)$$

The equation is then solved for only unknown  $[\text{PVI}]$  through an iterative procedure. Plots of  $\bar{n}$  vs.  $p$ - $[\text{PVI}]$  are shown in Figure 2. The formation curve for the imidazole-Zn(II) system as determined by Edsall, *et al.*,<sup>4</sup> is also shown. The points corresponding to different Zn(II) ion concentrations at a constant polymer concentration fall on the same line, indicating the validity of this procedure.

The relationship between  $\bar{n}$  and the individual formation constants  $K_i$  which refer to the process



is given by the expression

$$\bar{n} = \frac{K_1[\text{A}] + 2K_1K_2[\text{A}]^2 + 3K_1K_2K_3[\text{A}]^3 + 4K_1K_2K_3K_4[\text{A}]^4}{1 + K_1[\text{A}] + K_1K_2[\text{A}]^2 + K_1K_2K_3[\text{A}]^3 + K_1K_2K_3K_4[\text{A}]^4} \quad (6)$$

where  $[\text{A}]$  refers to the free ligand concentration. One can also describe this relationship in terms of intrinsic formation constants which eliminate the statistical factor

$$\kappa_1 = K_1/4; \kappa_2 = 2K_2/3; \kappa_3 = 3K_3/2; \kappa_4 = 4K_4$$

The formation function then takes the form

$$\bar{n} = \frac{4(\kappa_1[\text{A}] + 3\kappa_1\kappa_2[\text{A}]^2 + 3\kappa_1\kappa_2\kappa_3[\text{A}]^3 + \kappa_1\kappa_2\kappa_3\kappa_4[\text{A}]^4)}{1 + 4\kappa_1[\text{A}] + 6\kappa_1\kappa_2[\text{A}]^2 + 4\kappa_1\kappa_2\kappa_3[\text{A}]^3 + \kappa_1\kappa_2\kappa_3\kappa_4[\text{A}]^4} \quad (7)$$

Bjerrum has shown that individual  $K_i$  and  $\kappa_i$ -values can be calculated from the formation curves. A more

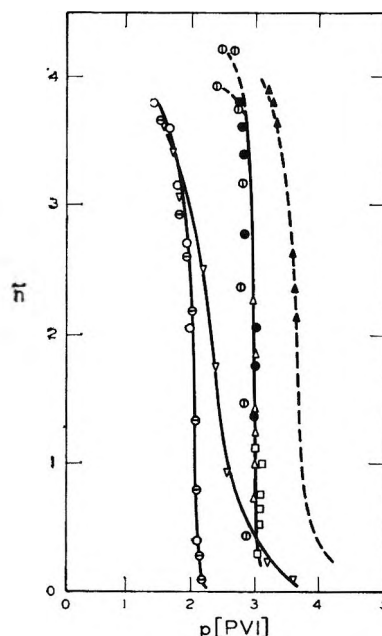


Figure 2. Bjerrum plot for the binding of Zn(II) by 0.1 M PVI in the presence of 0.0045 M (O) and 0.0089 M (⊖) Zn(II), and by 0.01 M PVI in the presence of 0.00045 M (⊙), 0.0023 M (Δ), and 0.0045 M (□) Zn(II), all in the presence of 1 M sodium nitrate. Results of dialysis experiments with PVI (0.01 M)-Zn(II) shown (●), and with PVI (0.01 M)-Cu(II) shown (▲), along with dotted curve for potentiometric titrations on the same system taken from ref. 6. Imidazole-Zn(II) from ref. 4 (▽).

elegant procedure was proposed by Scatchard and used by Edsall.<sup>4</sup> In this treatment the parameter  $Q$  is introduced

$$Q = \bar{n}/([N - \bar{n}][\text{A}]) \quad (8)$$

where  $N$  is the maximum coordination number. By plotting  $\log Q$  vs.  $\bar{n}$ , one obtains approximate values of the formation constants

$$\lim_{A \rightarrow 0} Q = \kappa_1 \quad (9)$$

$$\lim_{A \rightarrow \infty} Q = \kappa_4 \quad (10)$$

$$\lim_{\bar{n} \rightarrow 0} \frac{d \ln Q}{d \bar{n}} = \frac{3(\kappa_2 - \kappa_1)}{4\kappa_1} \quad (11)$$

$$\lim_{\bar{n} \rightarrow 4} \frac{d \ln Q}{d\bar{n}} = \frac{3(\kappa_4 - \kappa_3)}{4\kappa_3} \quad (12)$$

The Scatchard plots for the Zn(II) complexes are shown in Figure 3. To determine the limiting slopes defined by eq. 11 and 12, data of high precision at  $\bar{n} \rightarrow 0$  and  $\bar{n} \rightarrow 4$  are required; experimentally, it is in just these regions that accurate values are difficult to obtain. Edsall, *et al.*,<sup>4</sup> disregarded the scattering points at the extreme ends of their curves. A linear extrapolation was used for the PVI-Zn(II) system (method A). The values of  $\kappa$  thus obtained were then subjected to adjustment by iteration in eq. 7 to obtain the "best" values (method B). The results are listed in Table II; the values obtained by both methods are quite close. For comparison, values for the Zn(II)-imidazole complex by Edsall, *et al.*,<sup>4</sup> are also listed, as are values for the Cu(II) complexes, calculated from Scatchard plots shown in Figure 4.

**Table II:** Intrinsic Formation Constants for Zn(II) and Cu(II) with PVI and Imidazole at 1.0 Ionic Strength

Ligand and metal	Method	Log $\kappa_1$	Log $\kappa_2$	Log $\kappa_3$	Log $\kappa_4$
PVI (0.01 M), Zn(II)	A	1.88	2.28	3.40	3.80
	B	1.72	2.65	3.35	3.76
PVI (0.1 M), Zn(II)	A	1.22	1.56	2.39	2.72
	B	1.24	1.66	2.43	2.87
Imidazole, Zn(II) <sup>a</sup>		1.98	2.19	2.41	2.62
PVI (0.01 M), Cu(II) <sup>b</sup>	B	2.90	3.24	4.06	4.36
PVI (0.1 M), Cu(II)	B	2.02	2.33	3.07	3.38
Imidazole, Cu(II) <sup>a</sup>		3.76	3.39	3.03	2.66

<sup>a</sup> From Edsall, *et al.*; ionic strength = 0.16; method A, values obtained from linear extrapolation; method B, values obtained by iteration within eq. 7. <sup>b</sup> From Gold and Gregor.<sup>6</sup>

**Dialysis Equilibrium.** The metal ion concentrations outside the membrane as shown in Table I (in the absence of NTA) were equal to the corresponding concentrations in the bag under these experimental conditions. Therefore, the difference between the total (t) and the free metal ion concentration was that of bound (b) ions. Then, because a large excess of PVI was always present and assuming  $N = 4$ ,  $\bar{n} = 4[M]_b/[M]_t$ . Also,  $p[\text{PVI}]$  could be calculated directly from the known pH and metal ion concentrations employing eq. 1 and 3. Figure 2 shows also plots of  $\bar{n}$  vs.  $p[\text{PVI}]$  from dialysis experiments on both the Zn(II) and Cu(II) complexes. The dotted line of Figure 2 is that from potentiometric data on the Cu(II)-PVI complex.<sup>6</sup>

**Stoichiometry of PVI-Zn(II) Complexes.** By stoichiometry, each Zn(II) requires two  $\text{Cl}^-$ , the mole

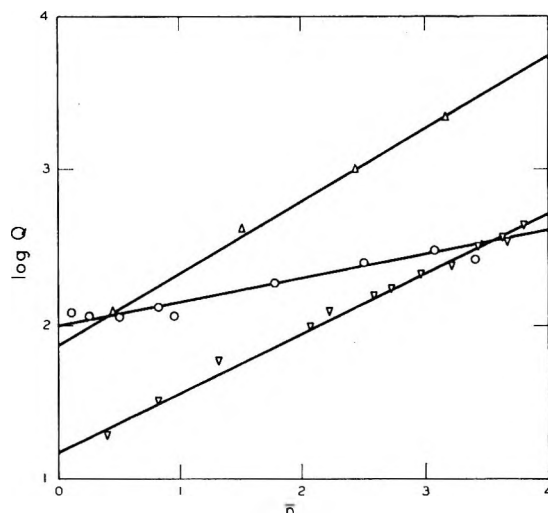


Figure 3. Scatchard  $Q$  plot for Zn(II)-imidazole and PVI complexes. PVI concentrations: 0.01 M ( $\Delta$ ); 0.1 M ( $\nabla$ ). Imidazole-Zn(II) from ref. 24 ( $\circ$ ).

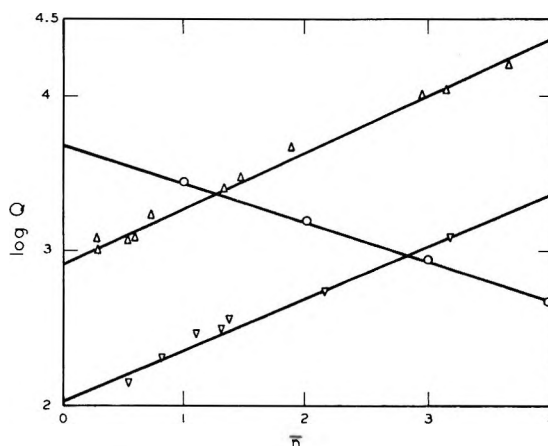


Figure 4. Scatchard  $Q$  plot for Cu(II)-imidazole and PVI complexes.<sup>6</sup> PVI concentrations: 0.01 M ( $\Delta$ ), 0.1 M ( $\nabla$ ). Imidazole-Cu(II) from ref. 4 ( $\circ$ ).

ratio of N:C:H is 2:5:6 (or 7 for  $\text{PVIH}^+$ ), and the excess of Cl over that required by  $\text{ZnCl}_2$  is due to  $\text{PVIH}^+ \cdot \text{Cl}^-$ . Taking Zn as the base, computations of composition were made and are shown in Table III.

**Turbidimetric Results.** The turbidity,  $\tau$ , was calculated from light scattering measurements at 90 and 0°, employing the relationship

$$\tau = Kn_0^2[(G/F)_{90}/(G/F)_0 - (G'/F)_{90}/(G'/F)_0]$$

where  $K$  is an instrument and cell constant,  $n_0$  the refractive index of the solvent,  $G$  the galvanometer reading, and  $F$  the filter correction at 90 and at 0° for the solution, with  $G'$  the corresponding galvanometer reading for the solvent alone. A plot of  $(\tau_{p+m} - \tau_p)/C_p$  vs.  $\log C_p$  at constant  $[\text{Zn(II)}]$  is shown in Fig-



**Table III:** Analytical Results of Isolated PVI-Zn(II) Complexes (Based upon Zn = 1)

Initial PVI:Zn	Zn, %	Cl, %	N, %	PVI·HCl <sup>a</sup>	PVI <sup>b</sup>	C		H	
						Exptl.	Calcd.	Exptl.	Calcd.
5:1	9.32	16.57	20.16	1.26	3.79	25.6	25.3	33.5	31.5
4:1	9.06	16.86	20.09	1.43	3.75	26.4	25.9	36.7	32.5
1:1	13.00	20.99	17.71	0.97	2.21	15.9	15.9	19.6	20.1
1:4	18.70	24.53	15.18	0.42	1.48	9.45	9.50	12.4	11.8
1:10	21.10	26.99	13.28	0.35	1.12	7.55	7.35	12.4	9.2

<sup>a</sup> From chlorine analysis: Cl (found) - 2Zn = PVI·HCl. <sup>b</sup> From nitrogen analysis: N (found) - PVI·HCl = PVI.

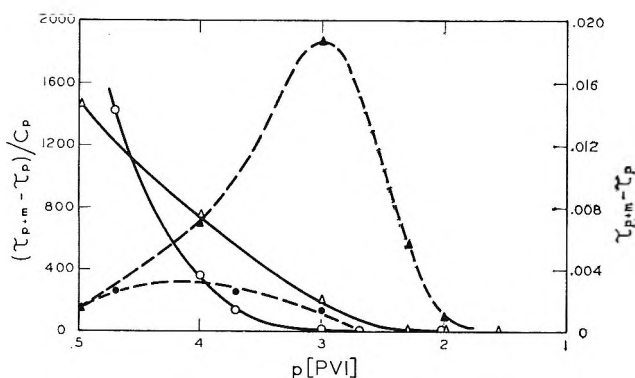


Figure 5. Plot of turbidity of PVI-Zn(II) complex ( $p + m$ ) less the turbidity of PVI alone, divided by the polymer concentration  $C_p$  ( $\text{g. ml.}^{-1}$ ) as a function of  $p$  [PVI] for solutions  $10^{-6} M$  ( $\Delta$ ) and  $2 \times 10^{-6} M$  ( $O$ ) in Zn(II) and  $0.06 M$  in sodium bicarbonate shown as solid lines. Curve for corrected turbidity shown as dashed lines. [PVI] is concentration in moles liter<sup>-1</sup>.

Figure 5, where  $\tau_{p+m}$  is the turbidity of the complex and  $\tau_p$  is that due to the same concentration of polymer alone, and where  $C_p$  is the polymer concentration in  $\text{g. ml.}^{-1}$ . The addition of PVI to Zn(II) caused a sharp increase in turbidity when  $[PVI]/[Zn]$  was about 100; the further addition of PVI resulted in a decrease in turbidity. The value  $(\tau_{p+m} - \tau_p)/C_p$  is the additional contribution to the turbidity of each polymer in the presence of Zn(II). The contribution of the polymer itself to the total turbidity of mixtures was always quite small. For example, at  $[PVI] = 10^{-3} M$ , the turbidity  $\tau \times 10^3$  was 0.2 for the polymer alone, but it was 1.8 and 2.4 in the presence of  $2 \times 10^{-6}$  and  $10^{-5} M$  zinc, respectively. Since the refractive index increment is about the same for the complex as for PVI alone because of the small fraction ( $<1\%$ ) of metal present, one can estimate the maximum average molecular weight of the cross-linked complex as  $6 \times 10^7$ .

**Mixed Ligand Complexes.** The results of dialysis experiments with NTA and PVI in the absence of Cu(II) showed no binding of the ligand to the polymer under the experimental conditions shown in Table IV.

The equilibrium concentration of NTA was that given by the volume increase, within experimental error. In Table IV for the NTA-PVI-Cu(II) system at two different total PVI concentrations  $[PVI]^0$ , there was always a sufficient excess of NTA over Cu(II) so that the concentration of free metal ion was negligible by comparison with that bound. Also, under these conditions the complex, at least in the external solution phase, had the composition Cu(II)·NTA as shown by Schwarzenbach.<sup>15</sup>

**Table IV:** Membrane Equilibrium<sup>a</sup>

pH	Cu(II)·NTA, $M \times 10^4$	NTA, $M \times 10^4$	NTA <sub>b</sub> , $\mu$ moles	Cu <sub>b</sub> , $\mu$ moles	Cu <sub>p</sub> , $\mu$ moles
[PVI] = 0.01 M					
4.36	4.73	3.5	67.1	67.9	0.8
4.46	4.94	3.6	63.3	66.4	3.1
7.00 <sup>b</sup>	5.40	7.5	32.6	63.2	30.6
7.14 <sup>b</sup>	5.42	7.8	30.5	63.0	32.5
8.42 <sup>b</sup>	6.61	6.5	31.1	64.7	23.6
8.77 <sup>b</sup>	6.71	6.9	26.7	54.0	27.3
[PVI] = 0.0025 M					
4.40	11.1	3.1	25.0	25.0	0.0
4.48	11.1	3.4	22.3	23.0	0.7
7.23	11.2	3.4	23.0	23.7	0.7
7.49	10.7	3.9	23.0	27.4	4.4
8.44	10.7	3.9	22.5	27.0	4.5
8.66	11.1	3.5	23.0	23.3	0.3

<sup>a</sup> Twenty ml. of PVI solution dialyzed vs. 50 ml. of solution  $0.0025 M$  in NTA and  $0.002 M$  in Cu(II), both solutions  $0.5 M$  in sodium nitrate. <sup>b</sup> Precipitate formed in bag; other systems clear. NTA and Cu(II)·NTA refer to solution concentrations, NTA<sub>b</sub> and Cu<sub>b</sub> to total amount bound to polymer, and Cu<sub>p</sub> is Cu(II) bound directly to polymer, as micromoles present.

The second and third columns of Table IV were values obtained by direct analysis of the external solution; the fourth column (NTA<sub>b</sub>) is the micromoles

(15) G. Schwarzenbach, G. Anderegg, W. Schneider, and H. Senn; *Helv. Chim. Acta*, **38**, 1147 (1955).

of NTA bound to the polymer, computed by differences. The column  $Cu_b$  is the total amount of metal bound to the polymer. If we assume a 1:1:1 complex or  $PVI \cdot Cu(II) \cdot NTA$ , then the amount of the  $Cu(II) \cdot n$ -PVI complex present can be computed by difference as  $Cu_p$ . An examination of Table IV reveals good evidence that the 1:1:1 complex was indeed present; the evidence is particularly strong at the lower PVI concentration. Other corroborative evidence was described earlier, where it was shown that free  $Cu(II)$  could cross link the polymer and that the  $PVI \cdot Cu(II) \cdot NTA$  complex remained linear.

### Discussion

The evidence from the potentiometric studies given here shows that the maximum coordination number of  $Zn(II)$  with the imidazole group on the PVI chain is 4, a finding quite in accord with its behavior with imidazole. The successive intrinsic association constants  $\kappa$  (Table II) show considerably greater successive increments with the  $Zn(II)$ -PVI system than with  $Zn(II)$  and imidazole. This phenomenon appears to be general with polymeric complexing systems; once the coordinating metal ion is attached to one group on the polymer chain, the other ligands coordinate more readily. With the  $PVI-Cu(II)$  complex and the imidazole- $Cu(II)$  complex, the slopes of the  $\log Q$  vs.  $\bar{n}$  are negative with the monomeric ligand and positive with the polymeric ligand (Figure 4). With imidazole and  $Cu(II)$ , the binding of the first ligand by the metal decreases its affinity for successive ligands; with the polymer, binding of the first ligand enhances successive binding, a clear demonstration of the polymeric effect on complex formation. It is also of interest to note that  $\kappa_1$  is always smaller in polybase complexing systems than in monomeric systems. This is due in large part to the increase in electrical free energy when a positively charged metal ion is added to a polymer chain already possessing a positive charge, as discussed previously by Gold and Gregor.<sup>6</sup> The enhancement of successive formation constants by the polymeric effect is substantially larger with PVI and  $Zn(II)$  than with  $Cu(II)$ ; Table II shows that  $\log \kappa_4 - \log \kappa_1$  is 2.04 for 0.01  $M$  PVI and  $Zn(II)$  but only 1.46 with  $Cu(II)$ . These differences are probably due to different steric strains in the two complexes.

The results of dialysis equilibrium experiments agreed well with those obtained from potentiometric titrations, showing the validity of the  $\bar{n}$  values calculated by the two methods.

Our stoichiometric studies of  $PVI-Zn(II)$  complexes showed that the ratio of PVI bound to  $Zn(II)$  decreased to a limiting value of unity when a large excess of metal

was present in solution; the same ratio approached a limiting value of  $N = 4$  when an excess of polymer was present in solution.

The turbidity studies on  $PVI-Zn(II)$  complexes showed intermolecular coordination by the metal (see Figure 5). Intermolecular binding does not require that four successive pendant imidazole groups be attached to the same zinc ion; steric considerations preclude this. Rather, binding is probably achieved by pairs of successive imidazole groups, each pair being well displaced along the chain.

From Table IV it may be seen that when the initial concentration of PVI was four times that of NTA, an increase in the pH favored the  $Cu(II) \cdot (PVI)_4$  complex rather than  $Cu(II) \cdot NTA$  complex and reduced the concentration of the mixed complex; polymer cross linking by  $Cu(II)$  increased, as shown by precipitate formation. When  $[PVI]^0$  was the same as  $[NTA]^0$ , the composition of the system hardly changed with pH, interpolymer cross linking was minimized, and no appreciable turbidity was observed.

The formation constant for the reaction between the  $Cu(II) \cdot NTA$  complex and PVI can be computed from the data of Table IV and that given earlier. When the concentration of PVI was  $2.5 \times 10^{-3} M$ ,  $p[PVI] \cong 4.0$ ; accordingly,  $\log K_f \cong 4.0$ ; at the 0.01  $M$  PVI concentration level,  $p[PVI] \cong 3.2$  and  $\log K_f$  again is 4.0. This formation constant may be compared with the stepwise formation constants for 0.01  $M$  PVI and  $Cu(II)$  given in Table II, where at the 0.01  $M$  PVI level  $\log K_1$  is 3.50 and  $\log K_4 = 3.76$ . Therefore, binding of the neutral  $Cu(II) \cdot NTA$  complex to PVI is stronger than for any of the stepwise reactions of  $Cu(II)$  and NTA. The electrical free energy term here is zero; this can readily account for the observed differences.

Our results may be compared with those of Jensen, Basolo, and Neumann,<sup>16</sup> who observed a substantial decrease in the rates of dissociation and racemization of  $Fe(phen)_3^{2+}$  in the presence of sodium polystyrene-sulfonate and attributed these effects to association of the metal complex with the polymer. In subsequent communications,<sup>17</sup> these authors employed the equilibrium dialysis technique and found that  $Co(phen)_3^{3+}$  and  $Fe(phen)_3^{3+}$  were somewhat more firmly bound than  $Ru(phen)_3^{2+}$ , and the binding constant was estimated to vary from  $10^4$  to  $10^5$  if a  $Co(phen)_3^{3+} \cdot PSS^-$  complex is assumed to exist. The binding of a number

(16) A. Jensen, F. Basolo, and H. M. Neumann, *J. Am. Chem. Soc.*, **80**, 2354 (1958).

(17) A. Jensen, F. Basolo, and H. M. Neumann, *ibid.*, **81**, 509, 512 (1959).

of nitroammine complexes of Co(III) to polystyrene-sulfonate were also studied, and the extent of binding was found to be much lower than with the phen complexes and to decrease with decreasing charge of the complex; the  $\text{Co(en)}_2\text{pyNO}_2^{2+}$  and particularly the  $\text{Co(bipy)}_2(\text{NO}_2)_2^+$  complex were much more strongly bound, suggesting that the existence of van der Waals forces or hydrophobic bonding<sup>18</sup> was more important than purely coulombic effects. Binding of phen complexes to the polymethacrylate anion was found to be considerably weaker than to the polystyrenesulfo-

nate anion, as expected. Our results indicate that hydrophobic bonding is not an important factor in  $\text{PVI}\cdot\text{Cu(II)}\cdot\text{NTA}$  complexes.

*Acknowledgment.* This investigation was supported in part by Public Health Service Research Grant GM 02934 from the division of General Medical Sciences, Public Health Service.

(18) See, *e.g.*, G. Némethy and H. A. Scheraga, *J. Chem. Phys.*, **36**, 3401 (1962).

## Kinetic Theory of Inhibition and Passivation in Electrochemical Reactions

by D. Gilroy and B. E. Conway

*Department of Chemistry, University of Ottawa, Ottawa, Canada (Received October 19, 1964)*

A kinetic theory of inhibition and passivation in anodic organic and metal dissolution reactions is given. Two types of cases arise. The first is one in which the inhibition results from effects of an inhibiting species, produced in a competing reaction, on the free available surface of the electrode and on the activation energy of the primary anodic reaction; the second case is one of self-inhibition which can arise in certain decompositions of adsorbed radicals, *e.g.*, in the oxidation of the formate ion. A reversal of the direction of the log [current]-potential relation is predicted, and the negative Tafel slope observed in the inhibition of an anodic reaction depends on its mechanism, on the isotherm for the inhibiting species, and on the number of electrons required for its production. Generally, the width, in units of electrode potential, of the region of normal and reverse Tafel behavior is determined by the magnitude of the interaction parameter  $f(\theta)$  in a Temkin type of isotherm for the adsorbed species. The sharpest current-potential relation is observed under Langmuir conditions. Application to several kinds of experimental results including passivation behavior at stainless steel indicates a sufficiently satisfactory agreement between theory and experiment that the general basis of the calculations is supported.

### Introduction

Most anodic reactions including metal dissolution,<sup>1</sup> organic oxidations, and even the oxidation of hydrogen<sup>2</sup> exhibit inhibition or passivation effects. These effects are usually manifested in galvanostatic current-voltage curves as transition regions<sup>3</sup> where there is a relatively abrupt change of the current-potential relation from one Tafel region to another; in potenti-

static determinations they are manifested as limiting currents with reversal of the direction of the current-potential relation. These effects, *e.g.*, in hydrogen

(1) N. Hackerman in "Surface Chemistry of Metals and Semiconductors," ed. by H. G. Gatos, J. W. Faust, and W. A. Lafleur, John Wiley and Sons, Inc., New York, N. Y., 1959, p. 313; see also P. V. Popat and N. Hackerman, *J. Phys. Chem.*, **65**, 1201 (1961).

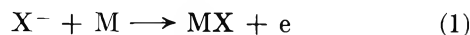
(2) Ya. M. Kolotykin, *Z. Elektrochem.*, **62**, 664 (1958); see also M. Breiter, K. Franke, and C. A. Knorr, *ibid.*, **63**, 226 (1959).

ionization,<sup>2</sup> can be distinguished from those associated with diffusion limitation of the rate, by this inversion; thus, diffusion limitation will tend to lead, under most conditions,<sup>4</sup> only to a constant limiting current with increasing potential whereas a true passivation under potential control is associated with a region of decreasing current with increasing potential following the attainment of a limiting critical current. The elements of a theory of these inhibition effects have been given in a brief form elsewhere,<sup>5-7</sup> and it is the purpose of the present paper to examine the kinetic origin of inhibition or passivation effects in more quantitative detail with applications to several anodic reactions. The basis of this treatment will be as follows; an anodic reaction will be considered which is inhibited by the appearance of another species, competing for sites upon the metal electrode surface, the coverage of which by this species can vary with potential. Kolotyrkin<sup>2</sup> has regarded the initiation of passivation as being associated with the appearance of a monolayer or less of an inhibiting species; Hackerman, *et al.*,<sup>1</sup> have studied the capacitative behavior of passive steel electrodes. In most cases, the inhibiting species will be a "surface" or "adsorbed" oxide, *e.g.*, the entity MOH or MO<sup>8,9</sup> generated from aqueous solution, but in other cases to be examined, the inhibition may arise in the primary reaction itself; *i.e.*, a self-passivation effect can occur.

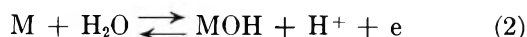
Much of the recent work on electrocatalytic oxidations has been carried out by means of the repetitive potentiostatic voltage-scanning method<sup>10</sup> in which the time- and potential-dependent Faradaic and pseudo-Faradaic currents are recorded by means of an oscilloscope. These current-potential relations exhibit peaks which can arise in two ways: (a) from charging processes associated with the production or removal of adsorbed intermediates,<sup>5b,11</sup> *e.g.*, H, OH, O, or organic radicals HCOO·,<sup>3</sup> CH<sub>3</sub>COO·, or CH<sub>3</sub>· in the Kolbe reaction<sup>3</sup> and (b) from kinetic processes exhibiting inhibition effects as the potential is changed. In another paper,<sup>11</sup> we have dealt with the significance of the adsorption peaks and associated adsorption pseudo-capacitance,<sup>12</sup> observed in the voltage-sweep method and in the related differential galvanostatic technique.<sup>13</sup> Here we shall examine the significance of Faradaic peaks in current-voltage curves and show how they can arise *kinetically* from inhibition effects in relation to the isotherm for adsorption of the intermediates involved.

### Kinetic Relations

*Case i. A Discharge Step Inhibited by a Competing Oxide or Similar Species.* We consider the general reaction



where X is an adsorbed radical produced from the anodic discharge of the ion X<sup>-</sup> (*e.g.*, in the formate oxidation reaction),<sup>3,11</sup> and competition for surface sites occurs between X and the OH species formed (*e.g.*, see ref. 8 and 14) in a reaction such as



Alternatively, the MO species may be involved as considered in case iii. Following previous formulations<sup>12,15,16</sup> of the rate equation for reaction 1 under general Temkin conditions<sup>12,16</sup> where both the rate and activation energy of reaction 1 depend on coverage through effects associated with the surface availability and interaction effects,<sup>17</sup> we can write

$$i_1 = F \frac{kT}{h} KC_X (1 - \theta_{OH}) \exp - [\Delta G_1^* - \beta VF + (1 - \beta)f(\theta)]/RT \quad (3)$$

where  $f(\theta)$  is the Temkin parameter<sup>12,15</sup> defining the rate of change of apparent standard free energy of adsorption<sup>18</sup> of species on the surface with the total

(3) B. E. Conway and M. Dzieciuch, *Can. J. Chem.*, **41**, 21, 28, 55 (1963); *Electrochim. Acta*, **8**, 143 (1963).

(4) An apparent exception might arise if, with increasing potential, conditions of diffusion control were initially reached but with further increase of potential, kinetic control were re-established owing to inhibition by competing adsorbed species. Other cases of anomalous Tafel behavior arise in reductions of anions, *e.g.*, S<sub>2</sub>O<sub>8</sub><sup>2-</sup>, but originate from well-known ionic double-layer effects and are quite different from the effects examined in this paper.

(5) (a) B. E. Conway, "Theory and Principles of Electrode Processes," Ronald Press, New York, N. Y., 1964; (b) E. Gileadi and B. E. Conway, "Modern Aspects of Electrochemistry," ed. by J. O'M. Bockris and B. E. Conway, Butterworth and Co., Ltd., London, 1964, Chapter V.

(6) During publication of the work referred to here,<sup>3</sup> similar principles have been proposed semiquantitatively by Bagotsky and Vasilev<sup>7</sup> for certain organic oxidations and have been developed further in the present paper.

(7) V. S. Bagotsky and Y. B. Vasilev, *Electrochim. Acta*, **9**, 869 (1964).

(8) J. O'M. Bockris, *J. Chem. Phys.*, **24**, 817 (1956); see also ref. 21.

(9) B. E. Conway and P. L. Bourgault, *Can. J. Chem.*, **37**, 292 (1959); **38**, 1557 (1960); **40**, 1690 (1962).

(10) F. Will and C. A. Knorr, *Z. Elektrochem.*, **64**, 258, 270 (1960).

(11) B. E. Conway, H. A. Kozłowska, and E. Gileadi, *J. Electrochem. Soc.*, in press; H. A. Kozłowska and B. E. Conway, in press.

(12) B. E. Conway and E. Gileadi, *Trans. Faraday Soc.*, **58**, 2493 (1962); *J. Chem. Phys.*, **39**, 3420 (1963); see also ref. 18.

(13) H. A. Kozłowska and B. E. Conway, *J. Electroanal. Chem.*, **7**, 109 (1964).

(14) K. Vetter and D. Berndt, *Z. Elektrochem.*, **62**, 378 (1958).

(15) R. Parsons, *Trans. Faraday Soc.*, **54**, 1053 (1958).

(16) A. N. Frumkin, P. Dolin, and B. V. Ershler, *Acta Physicochim.*, **13**, 779 (1940).

(17) M. Boudart, *J. Am. Chem. Soc.*, **74**, 1531, 3556 (1952).

(18) B. E. Conway and E. Gileadi, *Can. J. Chem.*, **42**, 90 (1964).

coverage  $\theta$  ( $= \theta_X + \theta_{OH}$ ) according to the model of Boudart<sup>17,19</sup> which we have applied to electrochemical kinetic problems<sup>12</sup> previously. Also in eq. 3,  $V$  is the metal-solution potential difference and ionic double-layer effects have been included in  $K$  for brevity (cf. ref. 12). Below the oxygen reversible potential, reaction 2 cannot proceed continuously and a quasi-equilibrium will be set up in which the coverage by OH will be dependent on potential according to the electrochemical isotherm

$$\frac{\theta_{OH}}{1 - \theta_{OH}} = K_2 \exp \left[ \frac{VF}{RT} \right] \exp[-f(\theta)/RT] \quad (4)$$

where  $K_2$  is a constant including the activity of the reactant in (2).  $\theta_X$  will tend to be small if step 1 is rate-determining with respect to a following desorption step such as



or



*Langmuir Case.* Here eq. 3 is written

$$i_1 = k_1(1 - \theta) \exp[\beta VF/RT] \quad (7)$$

where  $k_1$  is a combined constant at constant  $X^-$  and electrolyte concentration and

$$\frac{\theta_{OH}}{1 - \theta_{OH}} \doteq \frac{\theta}{1 - \theta} = K_2 \exp[VF/RT] \quad (8)$$

Then

$$i_1/i_{1,max} = \frac{1 - \theta}{1 - \theta_{max}} \exp[\beta(V - V_{max})F/RT] \quad (9)$$

where  $i_{max}$  is the maximum current in the inhibited process occurring at potential  $V_{max}$  and coverage  $\theta_{max}$ . Let  $\Delta V = V - V_{max}$ ; then from eq. 8

$$\left( \frac{\theta}{1 - \theta} \right)^\beta \left( \frac{\theta_{max}}{1 - \theta_{max}} \right)^\beta = \exp[\beta \Delta VF/RT] \quad (10)$$

and substituting from eq. 9

$$i_1/i_{1,max} = \left( \frac{\theta}{\theta_{max}} \right)^\beta \left( \frac{1 - \theta}{1 - \theta_{max}} \right)^{1-\beta} \quad (11)$$

By differentiation,  $\theta_{max} = \beta$ , so that  $\theta_{max} = 0.5$  when  $\beta = 0.5$ , which leads to the symmetrical relation

$$i_1/i_{1,max} = 2\theta^{1/2}(1 - \theta)^{1/2} \quad (12)$$

so that the  $i_1$ - $V$  curve is symmetrical with an inversion, i.e., with increasing potential two Tafel regions limitingly arise with slopes of  $2RT/F$  (normal discharge

reaction) and  $-2RT/F$  (inhibited reaction). As a function of  $\Delta V$ , using eq. 10

$$i_1/i_{1,max} = 2 \exp[\beta \Delta VF/RT] / (1 + \exp[\Delta VF/RT]) \quad (13)$$

*Temkin Case.* Here eq. 7 [cf. eq. 3] is written (cf. ref. 12, 15, 16)

$$i_1 = k_1(1 - \theta) \exp[\beta VF/RT] \exp[-(1 - \beta)f(\theta)/RT] \quad (14)$$

and eq. 4 is used for  $\theta$ . Proceeding as in the Langmuir case, elementary transformations lead to

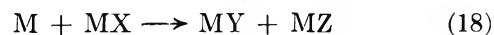
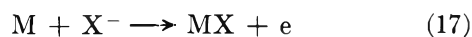
$$i_1/i_{1,max} = \frac{1 - \theta}{1 - \theta_{max}} \left( \frac{\theta/(1 - \theta)}{\theta_{max}/(1 - \theta_{max})} \right)^{1-\beta} \times \exp[(2\beta - 1)\Delta VF/RT] \quad (15)$$

or

$$i_1/i_{1,max} = \frac{1 - \theta}{1 - \theta_{max}} \left( \frac{\theta/(1 - \theta)}{\theta_{max}/(1 - \theta_{max})} \right)^\beta \times \exp[-(1 - 2\beta)f(\theta)/RT] \quad (16)$$

which in the usual case of  $\beta = 0.5$  gives again relations 11 and 12. Here, however, the shape of the  $i_1$ - $V$  curve will not be identical with that obtained from eq. 12 and 13 for the Langmuir case since the variation of  $\theta$  from small values toward unity will now occur over a wider potential range<sup>20</sup> determined by the magnitude of the general Temkin parameter  $f(\theta)$  in eq. 4 (see ref. 12). Numerical evaluation of the functions in eq. 13 and 16 leads to the results shown in Figure 1 expressed on a relative current density scale.

*Case ii. Inhibition in a Heterogeneous Decomposition Step,  $MX \rightarrow MY + MZ$ .* Here the reaction scheme considered is



where Y and Z may subsequently be desorbed to give final products. An example of step 18 may arise in the oxidation of formate<sup>3</sup> or in the Kolbe reaction<sup>3</sup>

(19) In this representation of the origin of coverage-dependent energies of adsorption, the principal effects are attributed to "induced heterogeneity"<sup>17</sup> which can account to a large extent for observed changes of heats of adsorption with coverage. Elsewhere,<sup>12</sup> we have compared the results of such a treatment with those arising when the kinetics are treated in terms of *intrinsic* heterogeneity. In the latter case, however, the  $f(\theta)$  factors can be specific for each of the adsorbed radicals present, and the kinetic analysis is then more complex.<sup>9,12</sup> This complication has not, we believe, been examined in the previous work<sup>7,15,16</sup> in which the Temkin isotherm (based on intrinsic heterogeneity) has been used.

(20) This potential range will also be related to the range of potentials over which the adsorption pseudocapacity for OH is appreciable, as treated in our previous papers.<sup>12</sup>

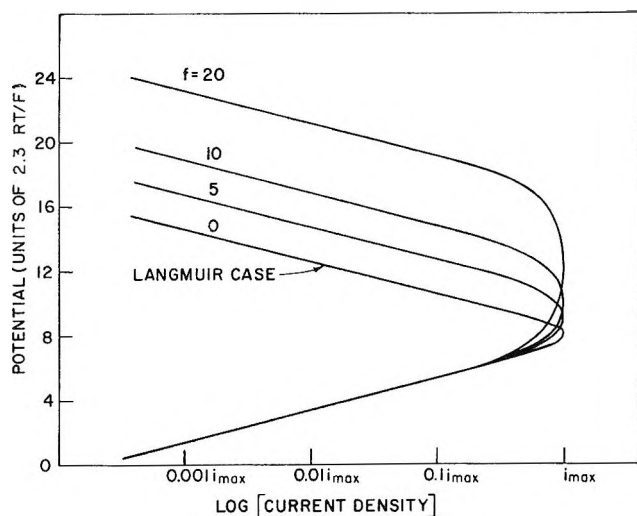
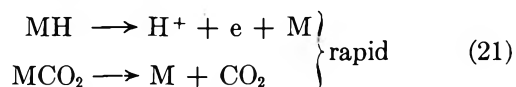
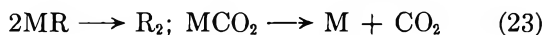


Figure 1. Theoretical current-potential relations for a discharge step inhibited by an adsorbed species produced in a single electron equilibrium (calculated for  $f = 0, 5, 10$ , and  $20RT$ ).

if  $\text{CO}_2$  is not immediately desorbed in the first-order decomposition step, *e.g.*



or in the Kolbe reaction after carboxylate ion discharge<sup>3</sup>



(a) *Inhibition by a Competing Species, e.g., OH.* The rate equation for reaction 18 is

$$i_s = k_5 \theta_X (1 - \theta) \quad (24)$$

where  $\theta$  is the total coverage by Y, Z, and OH and eq. 24 has been written for the Langmuir case. The  $1 - \theta$  term enters eq. 24 since two adsorption sites are considered to be required for Y and Z for every one occupied by X in step 18, regarded as rate-determining.

If  $\theta_{\text{OH}} \gg \theta_X$ , *i.e.*, when  $K_2$  (the electrochemical equilibrium constant for step 2) is greater than  $K_1$ ,  $1 - \theta \rightarrow 1 - \theta_{\text{OH}}$  and

$$1 - \theta = (1 + K_2 \exp[Vf/RT])^{-1} \quad (25)$$

and for quasi-equilibrium in step 1

$$\theta_X = \frac{K_1 \exp[Vf/RT]}{1 + K_2 \exp[Vf/RT]} = \frac{K_1}{K_2} \theta_{\text{OH}} \quad (26)$$

Hence

$$i_s = k_5 \frac{K_1}{K_2} \frac{K_2 \exp[Vf/RT]}{(1 + K_2 \exp[Vf/RT])^2} \quad (27)$$

At low coverage by X and OH when  $K_2 \exp[Vf/RT] \ll 1$ , it is seen from eq. 27 that the Tafel slope is  $RT/F$ ; when  $K_2 \exp[Vf/RT] \gg 1$  and  $\theta_X$  is still  $\ll 1$ , the Tafel slope becomes  $-RT/F$ , *i.e.*, an inversion due to inhibition arises. This is shown in Figure 2 where results of numerical calculations are given.

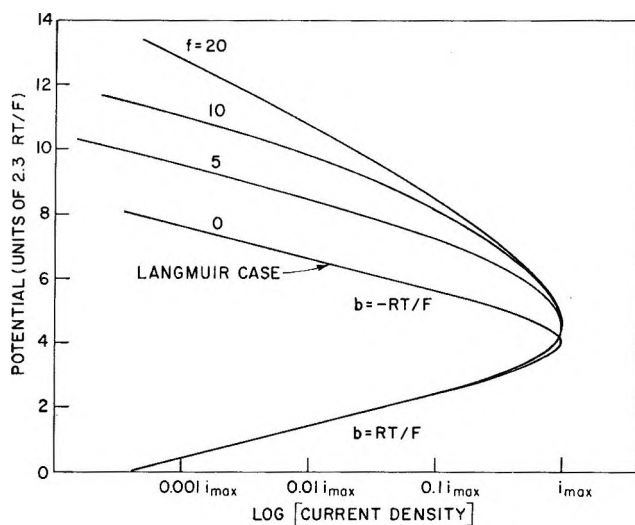


Figure 2. Theoretical current-potential relations for inhibition in a heterogeneous decomposition step of the type  $\text{M} + \text{MX} \rightarrow \text{MY} + \text{MZ}$  (calculated for  $f = 0, 5, 10$ , and  $20RT$ ).

The Temkin case corresponding to the above reaction sequence may be considered with reference to the rate equation for step 18 but now written in the form (*cf.* ref. 12, 18)

$$i_s = k_5 \theta_X (1 - \theta) \exp[\alpha f(\theta)/RT] \times \exp[-2(1 - \alpha)f(\theta)/RT] \quad (28)$$

which gives, when the symmetry factor  $\alpha$  for effects of changing adsorption energy of X, Y, Z, and OH in the induced heterogeneity model<sup>17</sup> is taken as 0.5

$$i_s = k_5 \theta_X (1 - \theta) \exp[-f(\theta)/2RT] \quad (29)$$

Following the same principles as before, the current-potential curve can be evaluated for this case as shown in Figure 2 for various values of  $f(\theta)$ . Inhibition effects are again predicted. The width of the potential range associated with the inhibition effect will be closely related to the potential range over which the coverage by OH and its associated pseudocapacity<sup>12</sup> are appreciable; this width will be determined by  $f(\theta)$  and may be estimated by methods reported previously.<sup>3</sup>

(b) *Case of Self-Inhibition.* The reaction scheme 1, 18 is of special interest in that inhibition effects can also arise *without* any involvement of a competing species produced in a parallel reaction, *e.g.* (2). Since experimental behavior which could correspond to this case has been observed<sup>11</sup> in the oxidation of formate in a completely anhydrous medium (pure HCOOH), this example is of some particular interest. The rate equation is again (*cf.* eq. 24)

$$i_s = k_s \theta_X (1 - \theta) \quad (30)$$

where  $\theta$  refers to the total coverage. Since reaction 18 is rate-determining,  $\theta_Y$  and  $\theta_Z$  are small and hence  $\theta \doteq \theta_X$ . Then

$$\theta_X = \frac{K_1 \exp[VF/RT]}{1 + K_1 \exp[VF/RT]} \quad (31)$$

and

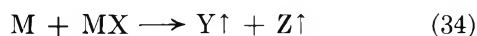
$$1 - \theta = (1 + K_1 \exp[VF/RT])^{-1} \quad (32)$$

instead of the result given by eq. 25. Hence

$$i_s = \frac{k_s K_1 \exp[VF/RT]}{(1 + K_1 \exp[VF/RT])^2} \quad (33)$$

This result is analogous to eq. 27 and gives limiting Tafel slopes again of  $RT/F$  when  $K_1 \exp[VF/RT] \ll 1$  and  $-RT/F$  when  $K_1 \exp[VF/RT] \gg 1$ , *i.e.*, a *self-inhibition* can arise without competition from a species produced in another reaction. The result under Temkin conditions is analogous and the current-potential behavior is the same as that for case iia under corresponding conditions.

(c) *Immediate Desorption of the Reaction Products.* Here reaction 18 is to be represented as

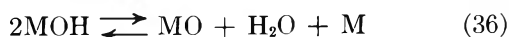
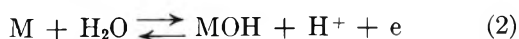


Two metal sites are considered necessary for decomposition of X as before. This changes the sign of the Temkin term in eq. 29 to give

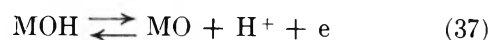
$$i_s = k_s \theta_X (1 - \theta) \exp[f(\theta)/2RT] \quad (35)$$

The resulting current-potential curves, shown in Figure 3, are the mirror images, taken about lines of constant potential through the respective  $i_{\max}$ , of those in Figure 2.

*Case iii. Competition from a Species Arising in a 2-Electron Quasi-equilibrium.* Competitive effects associated with surface oxides may arise<sup>8</sup> from equilibria of the type



or



In either case, the surface concentration of "MO" species in reaction 36 or 37 will depend on potential according to  $\exp[2VF/RT]$ , instead of  $\exp[VF/RT]$  for reaction 2. Such a "higher oxide" species may arise at higher anodic potentials, *e.g.*, as at platinum.<sup>14,21</sup> If the electrochemical quasi-equilibrium is in favor of "MO," inhibition will be mainly associated with such species and the Tafel line for an anodic process such as reaction 1 will then have a *negative* value of  $2RT/3F$  instead of  $2RT/F$  as in case i, *i.e.*, an *asymmetric* current-potential relation with slope reversal will arise (Figure 4). When hysteresis in oxide formation

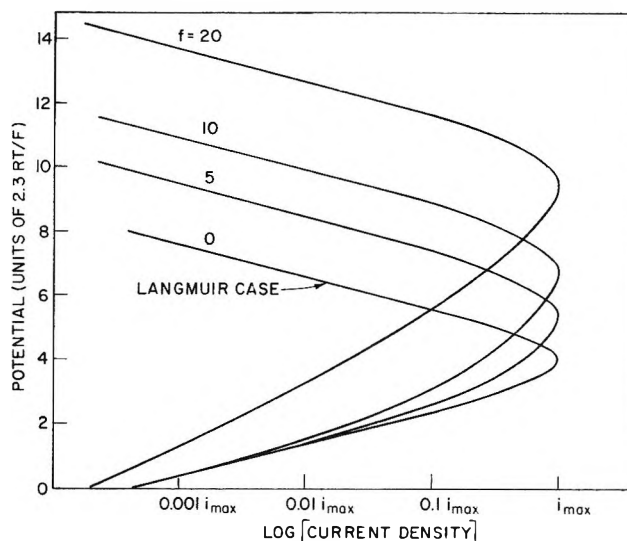


Figure 3. Theoretical current-potential relations for inhibition in a heterogeneous decomposition step of the type  $M + MX \rightarrow Y + Z$  with desorption of products (calculated for  $f = 0, 5, 10$ , and  $20RT$ ).

occurs as at Pt, the shape of the  $\ln [i]-V$  curve for a process such as reaction 1 may be different for the ascending (more anodic) direction of potential increase in a potentiostatic experiment and the descending direction, if there is a difference of surface oxide stoichiometry (or oxygen to metal atom ratio in the ad-layer) at high and at low potentials. This is the kind of behavior exhibited in a number of oxidations of organic substances, *e.g.*, of formate ion at Pt in aqueous solutions.<sup>11,22</sup> If "higher" oxide formation (*e.g.*, according to a reaction such as (36) or (37)) occurs at higher poten-

(21) S. Langer and J. Mayell, *J. Electrochem. Soc.*, **111**, 438 (1964); see also S. Gilman, *Electrochim. Acta*, **9**, 1025 (1964).

(22) A. Kutschker and W. Vielstich, *ibid.*, **8**, 985 (1963).

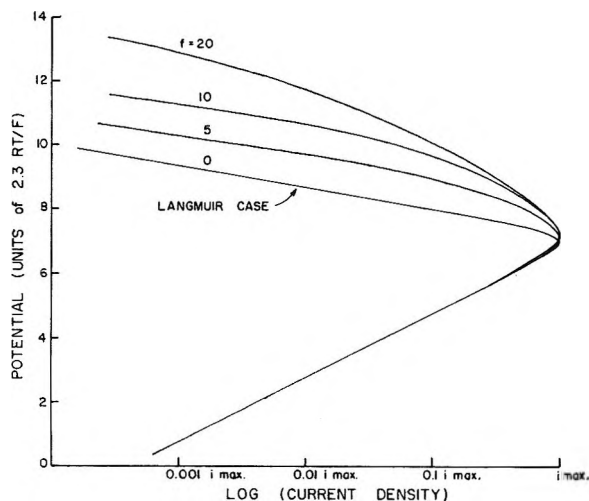
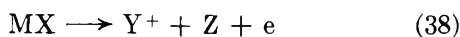
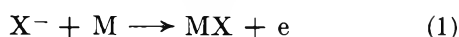


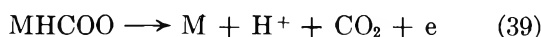
Figure 4. Theoretical current-potential relations for inhibition in a discharge step inhibited by an adsorbed species produced in a two-electron equilibrium.

tials and there is hysteresis with regard to the range of potentials over which such an oxide is formed and reduced, the descending current-potential curve for an oxidation such as (1) should have a lower negative slope in its region of reversal of slope than that observed in the ascending direction. The critical maximum current will also tend to be larger as observed. The exact kinetic behavior for a step such as (1) will obviously depend on the details of the electrochemical isotherm for adsorption of oxide species in the directions of ascending and descending potentials.

*Case iv. Discharge of an Intermediate Radical by an Electrochemical Mechanism.* Here the scheme



is considered. Such a reaction can occur in the electrochemical desorption of formate radicals in formate oxidation<sup>3</sup>



Self-inhibition obviously will not arise in this case. In the case of inhibition by MOH from (2), ( $\theta_{OH} \gg \theta_X$ )

$$\theta_X = \frac{K_1 \exp[V F / RT]}{1 + K_2 \exp[V F / RT]} \quad (40)$$

and the rate equation for reaction 38 is

$$i_{10} = k_{10} \theta_X \exp[\beta V F / RT] = \frac{k_{10} K_1 \exp[(1 + \beta) V F / RT]}{1 + K_2 \exp[V F / RT]} \quad (41)$$

from which it is clear that no passivation effects can

arise.<sup>23</sup> Similarly, under Temkin conditions, the same conclusion holds. When  $\theta_X \gg \theta_{OH}$ , the result is the same as that when no competing reaction is involved, and no inhibition effects arise. It will be noted, however, that although definite passivation effects are not predicted for this case, the effect of potential-dependent coverage by another species is to increase the Tafel slope from the value it would normally have (*viz.*  $RT/(1 + \beta)F$  in the above case), *i.e.*, the process is made more irreversible.

*Relation to Experimental Behavior.* Elsewhere,<sup>3,11</sup> we have examined the kinetics of oxidation of formate ion in aqueous and anhydrous formic acid solutions and discussed the evidence for the mechanisms (19), (20), (21), and the electrochemical desorption of MHCOO. In aqueous solutions at Pt, a symmetrical ascending current-potential curve exhibiting inhibition arises<sup>11</sup> over a range of potential of about 0.8 v. This can be fitted with remarkable exactness by a single value of the parameter  $f(\theta) = 15RT$  (see Figure 5) over a range of 0.8 v.<sup>24</sup> Similarly, the data of Bagotsky and Vasilev<sup>7</sup> for formic acid oxidation in phosphate buffer pH 4.26 can be fitted with  $f(\theta) = 6RT$  over 0.7 v. (Figure 6). The remarkably good agreement between the form of the experimental and theoretical relations lends strong support to the basis of the present theory of inhibition effects and the significance of the heterogeneity effects taken into account in the theory through the parameter  $f(\theta)$ . The fit of the theoretical relation to the experimental points round a curve is a more exacting test of the kinetic equations than comparison of predicted and experimental Tafel slopes. In the aqueous formate oxidation, the descending current-potential line has a smaller negative slope than the ascending one, suggesting a more sensitive dependence of the coverage by oxide species on potential than is the case in the ascending direction. This effect may be associated with the role of a higher oxide (*cf.* reactions 36 and 37) in the inhibition process, as discussed above.

In most inhibition processes involving organic oxidations, a further current-potential relation exists

(23) If a two-electron equilibrium is involved in the production of the passivating competitor, *e.g.*, by steps 36 or 37, then step 38 can be inhibited giving a forward Tafel slope of  $RT/(1 + \beta)$  ( $\theta_0 \ll 1$ ) and a reverse slope of  $-RT/(1 - \beta)$ , *i.e.*, approximately 0.040 and  $-0.120$  v., respectively.

(24) It has been argued that in the case of methanol oxidation,<sup>7</sup> OH radicals may preferentially participate in a cooxidation step analogous to  $MOH + HCOO^- \rightarrow H_2O + CO_2 + M$ , while O species are preferentially inhibiting. This does not appear to be the case here, since a symmetrical current-potential behavior arises which can only be accounted for if the inhibiting species arises in a one-electron quasi-equilibrium. In the formic acid case, inhibition may also arise from the chemical dissociative adsorption,  $M + HCOOH \rightarrow H_2O + M/CO$ , at the electrode surface.



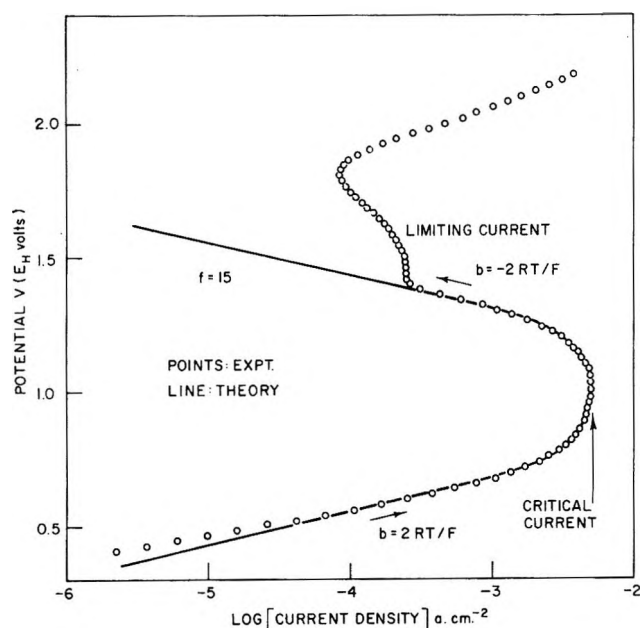


Figure 5. Current-potential behavior for oxidation of aqueous formate ion at 5° at smooth platinum:  $\circ$ , experimental points; line: theoretical calculation for inhibition by MOH species with  $f = 15RT$ .

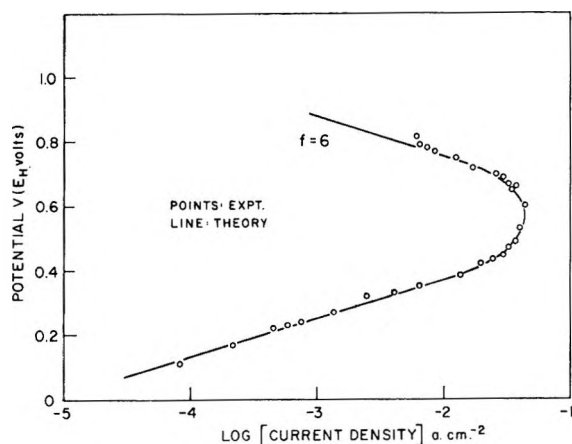
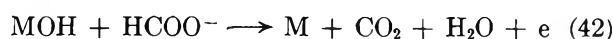


Figure 6. Current-potential behavior for oxidation of formic acid (phosphate buffer, pH 4.3) after Bagotsky and Vasilev<sup>7</sup>:  $\circ$ , experimental points; line: theoretical calculation for inhibition by MOH species with  $f = 6RT$ .

beyond the passivation region where the Tafel slope again acquires a normal sign, *e.g.*, in the Kolbe oxidation and in formate ion discharge. This can only arise on the basis of the above analysis if (a) discharge can occur onto the layer of inhibiting species after the latter is formed, in the steady state, to an appreciable extent of coverage, or (b) a new mechanism arises as the potential is made more anodic.

The formate oxidation in aqueous medium provides an interesting example since here a constant "limiting

current" over some 0.2 v. arises *after* the critical passivation current has been reached and reversal of the direction of the current-potential relation has occurred (Figure 5). The passivation effect is quantitatively accounted for on the basis of inhibition of formate ion discharge by the presence of a passivating "oxide" produced in a quasi-equilibrium process involving a one-electron change (*e.g.*, reaction 2). Any reaction following step 19 cannot become rate determining and at the same time bring about the increase in current, relative to  $i_1$ , which occurs in the "limiting current" region, so that an *additional* alternative reaction is required.<sup>25</sup> Discharge of the formate ion onto the oxide surface as



and



can account qualitatively, but rather satisfactorily, for the observed form of the current potential relation in formate oxidation.

The terms  $\theta_{\text{OH}}$  and  $\theta_0$  can be derived by assuming that the surface oxidizes according to reactions 2 and 37, which are in equilibrium. Then

$$\theta_{\text{OH}} = \frac{K_2 e^{VF/RT}}{1 + K_2 e^{VF/RT} + K_2 K_9 e^{2VF/RT}} \quad (44)$$

where  $K_2$  and  $K_9$  are the respective electrochemical equilibrium constants, and

$$\begin{aligned} i_{11} &= k_{11} \theta_{\text{OH}} e^{\beta VF/RT} C_{\text{HCOO}^-} \\ &= \frac{k_{11} K_2 e^{(1+\beta)VF/RT} C_{\text{HCOO}^-}}{1 + K_2 e^{VF/RT} + K_2 K_9 e^{2VF/RT}} \quad (44a) \end{aligned}$$

This gives a Tafel slope of  $2RT/F$  when the surface coverage is predominantly that produced by reaction 2, *i.e.*, when  $K_2 e^{VF/RT} > 1$  and  $K_2 e^{VF/RT} > K_2 K_9 e^{2VF/RT}$ . As the surface is further oxidized with increasing potential,  $K_2 K_9 e^{2VF/RT} > K_2 e^{VF/RT} > 1$  and a Tafel slope of  $-2RT/F$  is obtained. Thus step 42 has a critical passivation region which can have the appearance of a "limiting current" when the current-potential peak is broadened under Temkin conditions. Addition of  $i_1$  and  $i_{11}$  can therefore explain the experimental results depicted in Figure 5.

At higher potentials,  $\theta_0 \rightarrow 1$  and the current for reaction 43 is

(25) This conclusion differs from that proposed by Bagotsky and Vasilev,<sup>7</sup> who regard the *same* reaction as proceeding throughout the potential range on a surface the properties of which vary with its oxidation. On such a theory, it is difficult to see how increases of current can arise beyond a region in which current was previously decreasing with more anodic potentials.

$$i_{12} = k_{12}\theta_0 e^{\beta VF/RT} C_{\text{HCOO}^-}$$

$$= k_{12} e^{\beta VF/RT} C_{\text{HCOO}^-} \quad (45)$$

with a Tafel slope of  $2RT/F$ , as observed.<sup>11</sup> The overall scheme of reactions is then as shown in Figure 7.

*Case v. Passivation in Metal Dissolution.* The present treatment can be extended to metal passivation. As mentioned above, Kolotyркин<sup>2</sup> has argued that the initiation of passivation is associated with a monolayer or less of some species which inhibits the

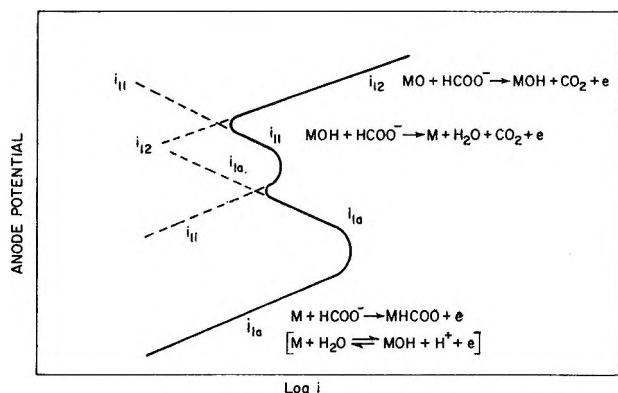
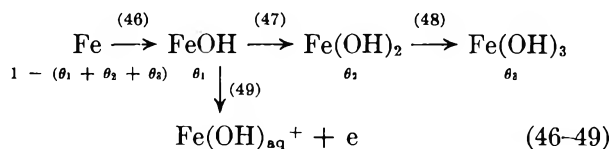


Figure 7. Over-all scheme of consecutive and alternative reactions in formate oxidation (theoretical).

process of dissolution of metal atoms (or adions<sup>26</sup>) from the lattice.<sup>27</sup>

The following scheme for the initiation of passivation of iron is considered



where FeOH, Fe(OH)<sub>2</sub>, Fe(OH)<sub>3</sub> are the initially inhibiting oxide species at coverages  $\theta_1$ ,  $\theta_2$ , and  $\theta_3$  arising in the anodic attack of iron. Denoting  $VF/RT$  by  $E$  for brevity, the steady-state condition for the corrosion oxidation gives

$$d\theta/dt = k_{15}\theta_2 \exp[\beta E] - k_{-15}\theta_3 \exp[-(1 - \beta)E] = 0 \quad (50)$$

or

$$\theta_3 = K_{15}\theta_2 \exp[E] \quad (51)$$

where the rate constants  $k_{15}$  and  $k_{-15}$ , and the equilibrium constant  $K_{15}$  refer to step 48.

Similarly

$$\theta_2 = K_{14}\theta_1 \exp[E]; \theta_3 = K_{14}K_{15}\theta_1 \exp[2E] \quad (52)$$

whence

$$\theta_1 = \frac{K_{13} \exp[E]}{1 + \left(1 + \frac{k_{16}}{k_{13}}\right) K_{13} \exp[E] + K_{13}K_{14} \exp[2E] + K_{13}K_{14}K_{15} \exp[3E]} \quad (53)$$

where  $K_{13}$  and  $K_{14}$  are equilibrium constants for steps 46 and 47, respectively. If coverage only by oxides up to the formal divalent state is involved, then eq. 53 has only the first three terms in its denominator.

If step 49 is the process that leads to net dissolution of iron,<sup>28</sup> the rate of corrosion is

$$i_{16} = k_{16}\theta_1 \exp[\beta E]$$

$$= k_{16}K_{13} [\exp(1 + \beta)E][A + B \exp(E) + C \exp(2E) + D \exp(3E)]^{-1} \quad (54)$$

where  $i_{16}$  and  $k_{16}$  refer to step 49, and  $A, B, C, D$ , are combined constants defined by comparison of eq. 54 with eq. 53. From eq. 54, it is clear that a passivation is accounted for, since, limitingly at high  $V$ , the minimum negative Tafel slope is  $-40$  mv., i.e.,  $[-RT/(2 - \beta)F]$ , and at low  $V$ ,  $+40$  mv., when  $\beta = 0.5$ , i.e., a reversal of slope and a critical current arises. Higher negative slopes may arise depending on the relative values of the terms in the denominator of eq. 54.

*Relation to Experimental Results.* Passivation of 304 stainless steel has recently been examined potentiostatically by Greene and Leonard<sup>29</sup> at various sweep

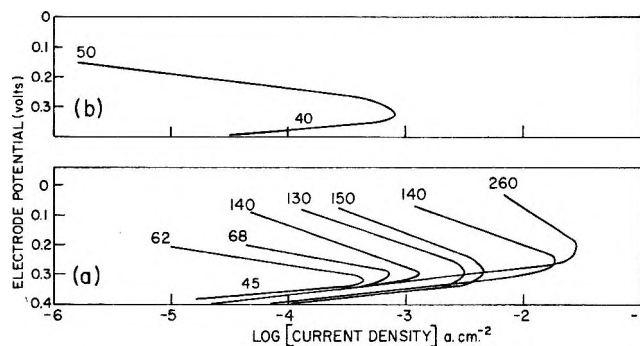


Figure 8. Current-potential relations for passivation of a stainless steel (from Greene and Leonard<sup>29</sup>). Slopes in mv. as indicated.

(26) B. E. Conway and J. O'M. Bockris, *Electrochim. Acta*, **3**, 340 (1961).

(27) Energetically, this may arise because (a) the metal atoms in the surface are stabilized by the presence of the ad-species, and (b) the local field influencing the removal of lattice atoms is changed on account of the dipole potential difference associated with the adsorption of passivating species, e.g., O, or OH (cf. ref. 3, 17).

(28) J. O'M. Bockris, D. Drazic, and A. R. Despic, *Electrochim. Acta*, **4**, 325 (1961).

rates in 1 *N* H<sub>2</sub>SO<sub>4</sub> at 25°. The lower Tafel slope has a value of 40–45 mv. and the slope in the current reversal region varies from –50 to –260 mv. depending on sweep rate. The highest sweep rate is 720 v. hr.<sup>-1</sup> and this gives the highest negative slope (–260 mv.) and the highest critical current (Figure 8). The lowest sweep rate gives reversed slopes of –50 to –62 mv. and lower critical passivation currents. This is as expected; the lower sweep rates allow more time for the inhibiting oxide layer to grow or for the higher valent species to be formed which could lead to lower negative slopes (*cf.* eq. 54). The *initiation* of passivation considered here will be expected to be associated with different effects from those arising with the normally thicker, steady-state passive film on iron, under aqueous aerated conditions.

*Case vi. Inhibition in a "Chemical" Step.* It has been suggested<sup>30</sup> that the oxidation of certain hydrocarbons occurs through a "chemical" reaction between the organic substance R and an electrochemi-

cally formed oxide species, *cf.* reactions 42 and 43. Various special cases can arise for this mechanism depending on coverage by R and the oxide species but when reactions 2, 36, or 37 are involved, an inhibition effect and reversal of Tafel lines will occur in a symmetrical manner (*cf.*, cases i and iia) with slopes of  $\pm RT/F$  and  $\pm RT/2F$ ; such low slopes are, however, not observed in hydrocarbon oxidation at platinum.<sup>30</sup>

*Acknowledgment.* Grateful acknowledgment is made to the Defence Research Board for support of this and related work on organic oxidation reactions on Grant No. 5412-01. We are also indebted to the U. S. Army Research and Development Laboratories for Contract MP 70 A1-63-4 on hydrocarbon oxidation studies. D. G. acknowledges the award of a postdoctoral fellowship.

(29) N. D. Greene and R. B. Leonard, *Electrochim. Acta*, **9**, 45 (1964).

(30) H. Wroblowa, B. J. Piersma, and J. O'M. Bockris, *J. Electroanal. Chem.*, **6**, 401 (1963).

# The Heat of Hydration of Cobalt Sulfate Hexahydrate to Heptahydrate.

## Their Solubilities and Heats of Solution<sup>1</sup>

by G. E. Brodale and W. F. Giauque

*Low Temperature Laboratory, Departments of Chemistry and Chemical Engineering, University of California, Berkeley, California (Received October 20, 1964)*

---

The heat of dilution of a saturated solution of  $\text{CoSO}_4 \cdot 7\text{H}_2\text{O}$  together with heats of solution of  $\text{CoSO}_4 \cdot 7\text{H}_2\text{O}$  and  $\text{CoSO}_4 \cdot 6\text{H}_2\text{O}$  have been measured to give  $\text{CoSO}_4 \cdot 6\text{H}_2\text{O}(\text{s}) + \text{H}_2\text{O}(\text{l}) = \text{CoSO}_4 \cdot 7\text{H}_2\text{O}(\text{s})$ ,  $\Delta H_{298.15^\circ\text{K.}} = -2455 \pm 10$  cal./mole. The solubilities of the two hydrates have been measured from 25 to 65°. The heat of the transition reaction,  $\text{CoSO}_4 \cdot 7\text{H}_2\text{O}(\text{s}) = 0.9122\text{CoSO}_4 \cdot 6\text{H}_2\text{O}(\text{s}) + 0.0878\text{CoSO}_4 \cdot 17.389\text{H}_2\text{O}(\text{l})$ , which occurs at 317.78°K., has been determined as  $2848 \pm 15$  cal./mole.

---

When investigating the heat capacities and heats of solution of solid hydrates, a common procedure is to work with samples which are predominantly one hydrate, but contain small amounts of a higher or lower hydrate, also under investigation. An analysis of the water content is used to evaluate the properties of the pure hydrates. However, cases have arisen where more than two water-containing phases are present and this invalidates the method. As a typical example, in the heat capacity work of Rao and Giauque<sup>2</sup> a sample of  $\text{CoSO}_4 \cdot 7\text{H}_2\text{O}$  was prepared and partially dehydrated to  $\text{CoSO}_4 \cdot 6\text{H}_2\text{O}$ . During the low temperature heat capacity measurements on this material a small amount of heat absorption occurred at the  $\text{CoSO}_4 \cdot 7\text{H}_2\text{O}$ -ice eutectic melting point showing that the sample contained small inclusions of saturated solution along with the hepta- and hexahydrates. Various delays in sampling and in the heat of solution measurements caused total water variation and possible "brine hole" migration. In any case a serious third-law "discrepancy" developed in the hexa- to heptahydrate reaction which could not be accepted without some explanation. The fact that the isomorphous hexahydrated sulfates of  $\text{Zn}^{2+}$  and  $\text{Mg}^{2+}$  have incompletely explained low temperature heat capacity irregularities helped obscure heat of solution errors as the principal source of the unpublished discrepancy in the work of Rao and Giauque.<sup>2</sup> The present work is designed to eliminate the source of error mentioned above and it has made it possible to use the heat capacity data to conclude that none of the phases involve residual entropy due to frozen-in disorder.

The general procedure was to prepare samples under conditions such that it would be very unlikely that more than two phases would be present. Crystals of  $\text{CoSO}_4 \cdot 7\text{H}_2\text{O}$  were left slightly wet so that the two phases were heptahydrate and saturated solution whether adhering or within "brine holes." Similar dilution measurements were made on a solution with the composition  $\text{CoSO}_4 \cdot A\text{H}_2\text{O}$ , where  $A = 23.309$ . For a saturated solution at 25°,  $A = 23.26$ .

In the case of lower hydrates, such as the hexahydrate in the present case, which must be crystallized at a higher temperature, excess solution, whether as inclusion or not, has always combined with adjacent lower hydrate when cooled into the range where the higher hydrate becomes stable. No eutectic calorimetric heat effect has ever been observed in such cases in various experiments in this laboratory. Thus, in the present case, we interpret the total water in the "hexahydrate" sample as distributed exclusively between the hexa- and heptahydrates, again enabling simple correction.

*Preparation of the Samples.* Two preparations of  $\text{CoSO}_4$  were made: (a) by crystallization from solution after treating  $\text{CoCO}_3$  with reagent grade  $\text{H}_2\text{SO}_4$ , and (b)

---

(1) This work was supported in part by the National Science Foundation.

(2) R. V. G. Rao and W. F. Giauque, *J. Phys. Chem.*, **69**, 1272 (1965).

(3) R. E. Barieau and W. F. Giauque, *J. Am. Chem. Soc.*, **72**, 5676 (1950).

(4) W. P. Cox, E. W. Hornung, and W. F. Giauque, *ibid.*, **77**, 3935 (1955).

by dissolving 99.999% cobalt metal<sup>5</sup> in reagent grade  $\text{H}_2\text{SO}_4$  (0.0004% residue on heating) and evaporation of excess  $\text{H}_2\text{SO}_4$ .

$\text{CoSO}_4 \cdot 7\text{H}_2\text{O}$  was prepared at ordinary temperatures and centrifuged to remove most of the adhering solution.

$\text{CoSO}_4 \cdot 6\text{H}_2\text{O}$  was prepared at about 55° and centrifuged at that temperature. We have found it convenient to thermostat a centrifuge roughly for this type of preparation. In several preliminary experiments the water content was left intermediate between the hexa- and heptahydrates to check against the possibility of an intermediate hydrate; however, the heat of solution data, while inferior to those given below, are linear with water content and thus do not support this possibility.

*Apparatus.* The heats of solution and dilution were measured in a calorimeter described by Kunzler and Giaque.<sup>6</sup> The samples were enclosed in small glass cylinders with thin glass cover plates attached to the ends by means of paraffin. The cover plates could be broken by a glass plunger to start the solution process. The total volume of the calorimeter was about 1 l.

*Analysis for Water Content.* The analysis for water content was by dehydration to 500° after careful preliminary heating to avoid spattering. In the case of the solubility measurements, and of the heptahydrate, soft-glass weighing bottles were used. For the hexahydrate, Pyrex containers were used and the residue was checked for decomposition to  $\text{Co}_3\text{O}_4$  by filtering and weighing the insoluble residue. The weight losses were in the range 0.01 to 0.03% of the anhydrous  $\text{CoSO}_4$ , which was about the limit of error of the determinations.

*Solubility of Cobalt Sulfate Hydrates.* The above type of correction requires a value of the solubility of  $\text{CoSO}_4 \cdot 7\text{H}_2\text{O}$  at the temperature of measurement, which was 25°. This solubility was determined as part of a more extensive investigation of the solubility of both the hepta- and hexahydrates over the range 25 to 65°. This was done in an attempt to see if any hydrates other than those expected above and below the hepta-hexa transition at 44.63°<sup>2</sup> were involved in the crystal preparation. No forms other than the ordinary hepta- and hexahydrates were found. The solubility data are given in Table I. The molecular weights of  $\text{CoSO}_4$  and water were taken as 154.9948 and 18.0153, respectively. In making corrections for buoyancy, the density of  $\text{CoSO}_4$  was taken as 3.70, that of  $\text{CoSO}_4 \cdot 7\text{H}_2\text{O}$  as 1.942, and that of  $\text{CoSO}_4 \cdot 6\text{H}_2\text{O}$ <sup>7</sup> as 2.006 g./cm.<sup>3</sup>. Also, the density of  $\text{CoSO}_4 \cdot 23.309\text{H}_2\text{O}$  was determined as  $d^{25}$  1.334 g./cm.<sup>3</sup>. The data in Table I are given in the order of the experiments.

*Heats of Dilution of Concentrated Aqueous Cobaltous*

Table I: Solubilities of  $\text{CoSO}_4 \cdot 7\text{H}_2\text{O}$  and  $\text{CoSO}_4 \cdot 6\text{H}_2\text{O}$

Temp., °C.	g. of $\text{CoSO}_4$ /100 g. of soln.	$A^a$	Solid phase	
Series 1				
62.23	36.462	14.992	$\text{CoSO}_4 \cdot 6\text{H}_2\text{O}$	
60.27	36.064	15.253		
55.69	35.164	15.863		
51.04	34.252	16.515		
48.23	33.729	16.897		
45.89	33.332	17.208		
43.52 <sup>b</sup>	32.907	17.541		
39.98	31.597	18.625		$\text{CoSO}_4 \cdot 7\text{H}_2\text{O}$
37.74	30.855	19.280		
31.04	28.830	21.239		
25.22	27.069	23.180		
Series 2				
34.06	29.771	20.295	$\text{CoSO}_4 \cdot 7\text{H}_2\text{O}$	
39.18	31.346	18.843		
41.19	31.983	18.297		
41.70	32.149	18.158		
42.37	32.367	17.978		
42.98	32.556	17.823		
43.56	32.764	17.655		
44.53	33.066	17.416		
44.92	33.184	17.323		$\text{CoSO}_4 \cdot 6\text{H}_2\text{O}$
45.66	33.327	17.212		
47.14	33.589	17.011	$\text{CoSO}_4 \cdot 7\text{H}_2\text{O}$	
50.76	34.244	16.517		
55.00	35.032	15.955		
25.00		(23.26)		Transition
44.63		(17.389)		

<sup>a</sup>  $A$  = moles of  $\text{H}_2\text{O}$ /mole of  $\text{CoSO}_4$ . <sup>b</sup> Supersaturated solution.

*Sulfate near Saturation.* The heats of dilution of concentrated cobalt sulfate solutions are given in Table II. In the experiments near 25° the concentrated sample was contained in two sample tubes which were broken separately as experiments 1 and 2. Thus the final conditions of experiment 1 were the initial conditions of experiment 2. The same type of sequence was used for experiments 3 and 4.

In making the corrections for temperature in Table II we made use of the equation given by Giaque, Barieau, and Kunzler<sup>8</sup> for the apparent molal heat capacity of aqueous  $\text{ZnSO}_4$  as a function of temperature and compo-

(5) Johnson, Matthey and Co., London, England.

(6) J. E. Kunzler and W. F. Giaque, *J. Am. Chem. Soc.*, **74**, 3272 (1952).

(7) A. Zalkin, H. Ruben, and D. H. Templeton, *Acta Cryst.*, **15**, 1219 (1962).

(8) W. F. Giaque, R. E. Barieau, and J. E. Kunzler, *J. Am. Chem. Soc.*, **72**, 5685 (1950).

**Table II:** Heats of Dilution of Concentrated Aqueous CoSO<sub>4</sub>

Prepn.	CoSO <sub>4</sub> (g)	Temp. of soln., °C.	A, sample <sup>a</sup>	A, initial calorimeter <sup>a</sup>	A, final calorimeter <sup>a</sup>	ΔH <sup>b</sup> obsd.	ΔH <sup>b</sup> cor. to 25.00°	ΔH <sup>b</sup> <sub>25</sub>	Remarks	
A	7.8182	25.05	23.309	∞	1018.4	-650	+2	-648	Expt. 1	
A	3.6979	25.09 <sup>c</sup>	23.309	1018.4	699.0	-404			Expt. 2	
A	11.5161	25.05	23.309	∞	699.0	-571	+2	-569	Calcd. 1 + 2	
B	7.3704	25.02	23.309	∞	925.4	-632	+1	-631	Expt. 3	
B	7.1810	25.07 <sup>d</sup>	23.309	925.4	980.2	-439			Expt. 4	
B	14.5514	25.02	23.309	∞	480.2	-537	+1	-536	Calcd. 3 + 4	
							ΔH <sup>b</sup> cor. to 44.63°	ΔH cor. to A, final = 700	ΔH <sub>44.63</sub> final = 700	
B	10.8947	45.24	17.383	∞	692.7	-1678	+23	+1	-2	-1656
B	10.0998	45.26	17.596	∞	715.0	-1693	+24	-18	+3	-1684
			(17.389) <sup>e</sup>							(-1670) <sup>f</sup>

<sup>a</sup> A = moles of H<sub>2</sub>O/mole of CoSO<sub>4</sub>. <sup>b</sup> Cal./mole. <sup>c</sup> Final temperature of expt. 1. <sup>d</sup> Final temperature of expt. 3. <sup>e</sup> Calculated. <sup>f</sup> Average.

**Table III:** Heat of Solution of CoSO<sub>4</sub>·7H<sub>2</sub>O

Prepn.	CoSO <sub>4</sub> (g)	Temp. of soln., °C.	A, sample <sup>a</sup>	A, final <sup>a</sup> soln.	Moles CoSO <sub>4</sub> in satd. soln. per mole CoSO <sub>4</sub> ·7H <sub>2</sub> O	ΔH <sub>t</sub> obsd., cal./mole CoSO <sub>4</sub> ·7H <sub>2</sub> O	ΔH <sup>b</sup> cor. for satd. soln.	ΔH <sup>b</sup> cor. to A, final = 700	ΔH <sup>b</sup> cor. to 25.00°	ΔH <sub>25</sub> <sup>b</sup> cal./mole, A, final = 700
A	11.4090	24.99	7.122	686.7	0.0076	3611	+4	-3	0	3612
A	11.5896	24.99	7.122	686.4	0.0076	3608	+4	-3	0	3609
B	10.4260	24.99	7.362	694.4	0.0228	3597	+13	-1	0	3609
										Av. ΔH <sub>25</sub> = 3610
							ΔH <sup>b</sup> cor. to 44.63°	ΔH <sub>44.63</sub> <sup>b</sup> A, final = 700		
B	9.4990	44.11	7.362	753.2	0.0357	3383	+58	+12	-4	3449

<sup>a</sup> A = moles of H<sub>2</sub>O/mole of CoSO<sub>4</sub>. <sup>b</sup> In cal./mole.

sition, since these solutions should have very similar properties and in any case the correction is small.

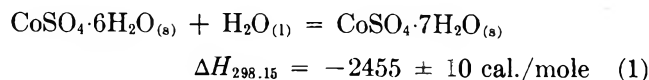
$$C_p, (\text{apparent}) = -218.7 + 0.6T + 191/A^{1/2}$$

For correcting the heat of solution for concentration, the present data show that in the range  $A = 500-700$ , aqueous CoSO<sub>4</sub> solutions have about the same heat of dilution as ZnSO<sub>4</sub> solutions. In the range  $A = 17-23$ , the relative partial heat content of the CoSO<sub>4</sub> solutions is less than that of aqueous ZnSO<sub>4</sub> by the order of 100 cal./mole, so that the curves are nearly identical.

*Heat of Solution of CoSO<sub>4</sub>·7H<sub>2</sub>O.* The heat of solution data for cobalt sulfate heptahydrate are given in Table III where they are also corrected for the saturated solution present in the samples.

*Heat of Solution of CoSO<sub>4</sub>·6H<sub>2</sub>O.* The heats of solution of samples with a water content CoSO<sub>4</sub>·6.078H<sub>2</sub>O are given in Table IV where they are also corrected for the amount of CoSO<sub>4</sub>·7H<sub>2</sub>O present.

*The Heat of Hydration of CoSO<sub>4</sub>·6H<sub>2</sub>O to CoSO<sub>4</sub>·7H<sub>2</sub>O.* From the data in the several tables the ΔH of the following reaction may be given as



*The Heat of Transition of CoSO<sub>4</sub>·7H<sub>2</sub>O to CoSO<sub>4</sub>·6H<sub>2</sub>O + Saturated Solution.* One of the principal purposes of the heat of solution measurements was the determination of the heat of transition in reaction 2, so that it

**Table IV:** Heat of Solution of  $\text{CoSO}_4 \cdot 6\text{H}_2\text{O}$ 

Prepn.	$\text{CoSO}_4(\text{g})$	Temp. of soln., °C.	A, sample <sup>a</sup>	A, final <sup>a</sup>	Moles		$\Delta H_t$ obsd., cal./mole $\text{CoSO}_4 \cdot 6\text{H}_2\text{O}$	$\Delta H^b$ cor. for $\text{CoSO}_4 \cdot 7\text{H}_2\text{O}$	$\Delta H^b$ cor. to A, final = 700	$\Delta H^b$ cor. to 25.00	$\Delta H_{25}^b, A_i$ final = 700
					$\text{CoSO}_4 \cdot 7\text{H}_2\text{O}$ per mole $\text{CoSO}_4 \cdot 6\text{H}_2\text{O}$	$\text{CoSO}_4 \cdot 6\text{H}_2\text{O}$					
B	13.4833	24.99	6.078	583.8	0.0846	1479	-305	-28	0	1146	
B	12.4599	25.00	6.078	585.1	0.0846	1498	-305	-28	0	1165	
B	13.4627	25.00	6.078	584.2	0.0846	1489	-305	-28	0	1156	
										Av.	1155
					Moles $\text{CoSO}_4$ in satd. soln. per mole $\text{CoSO}_4 \cdot 6\text{H}_2\text{O}$	$\Delta H^b$ cor. for satd. soln.	$\Delta H^b$ cor. to 44.63°	$\Delta H_{44.63}^b, A_i$ final = 700			
B	10.1517	46.59	6.350	712.4	0.0325	733	+58	+3	+33	827	

<sup>a</sup> A = moles of  $\text{H}_2\text{O}$ /mole of  $\text{CoSO}_4$ . <sup>b</sup> In cal./mole.

$$\text{CoSO}_4 \cdot 7\text{H}_2\text{O}_{(\text{s})} = \frac{(A-7)}{(A-6)} \text{CoSO}_4 \cdot 6\text{H}_2\text{O}_{(\text{s})} + \frac{1}{(A-6)} \text{CoSO}_4 \cdot A\text{H}_2\text{O}_{(\text{l})} \quad (2)$$

could be used to determine the over-all composition in the mixed hydrates used in the heat capacity work of Rao and Giauque.<sup>2</sup> Introducing the numerical value of  $\Delta = 17.389$ , the moles of  $\text{H}_2\text{O}$ /mole of  $\text{CoSO}_4$  in the saturated solution at the transition temperature, 44.63°, the transition reaction becomes

$$\text{CoSO}_4 \cdot 7\text{H}_2\text{O}_{(\text{s})} = 0.9122\text{CoSO}_4 \cdot 6\text{H}_2\text{O}_{(\text{s})} + 0.0878\text{CoSO}_4 \cdot 17.389\text{H}_2\text{O}_{(\text{l})} \quad (3)$$

There are three independent methods of combining the calorimetric observations to give the heat of reaction. 3. Two of the methods make use of the  $\Delta H$  of reaction 1, calculated to the transition temperature by means of the heat capacity data on the hydrates<sup>2</sup> together with the well-known heat capacity of liquid water to calculate  $\Delta H$  at 44.63°.

$$\Delta H_{44.63} = \Delta H_{25} + \int_{25}^{44.63} \Delta C_p dT = 2455 + 176 = 2631 \text{ cal./mole}$$

#### Combination 1

$$\text{CoSO}_4 \cdot 7\text{H}_2\text{O}_{(\text{s})} = \text{CoSO}_4 \cdot 6\text{H}_2\text{O}_{(\text{s})} + \text{H}_2\text{O}_{(\text{l})}, \quad \Delta H_{44.63} = 2631$$

$$0.0878[\text{CoSO}_4 \cdot 6\text{H}_2\text{O}_{(\text{s})} + 694\text{H}_2\text{O}_{(\text{l})}] = \text{CoSO}_4 \cdot 700\text{H}_2\text{O}, \quad \Delta H_{44.63} = 0.0878 \times 827 = 74$$

$$0.0878[\text{CoSO}_4 \cdot 700\text{H}_2\text{O} = \text{CoSO}_4 \cdot 17.389\text{H}_2\text{O} + 682.611\text{H}_2\text{O}], \quad \Delta H_{44.63} = 0.0878 \times 1670 = 147$$

By addition

$$\text{CoSO}_4 \cdot 7\text{H}_2\text{O}_{(\text{s})} = 0.9122\text{CoSO}_4 \cdot 6\text{H}_2\text{O}_{(\text{s})} + 0.0878\text{CoSO}_4 \cdot 17.389\text{H}_2\text{O}, \quad \Delta H_{44.63} = 2852 \text{ cal./mole} \quad (3)$$

#### Combination 2

$$0.9122[\text{CoSO}_4 \cdot 7\text{H}_2\text{O}_{(\text{s})} = \text{CoSO}_4 \cdot 6\text{H}_2\text{O}_{(\text{s})} + \text{H}_2\text{O}_{(\text{l})}], \quad \Delta H_{44.63} = 0.9122 \times 2631 = 2400$$

$$0.0878[\text{CoSO}_4 \cdot 7\text{H}_2\text{O}_{(\text{s})} + 693\text{H}_2\text{O} = \text{CoSO}_4 \cdot 700\text{H}_2\text{O}], \quad \Delta H_{44.63} = 0.0878 \times 3449 = 303$$

$$0.0878[\text{CoSO}_4 \cdot 700\text{H}_2\text{O} = \text{CoSO}_4 \cdot 17.389\text{H}_2\text{O}_{(\text{l})} + 682.611\text{H}_2\text{O}], \quad \Delta H_{44.63} = 0.0878 \times 1670 = 147$$

By addition

$$\text{CoSO}_4 \cdot 7\text{H}_2\text{O}_{(\text{s})} = 0.9122\text{CoSO}_4 \cdot 6\text{H}_2\text{O}_{(\text{s})} + 0.0878\text{CoSO}_4 \cdot 17.389\text{H}_2\text{O}_{(\text{l})}, \quad \Delta H_{44.63} = 2850 \text{ cal./mole} \quad (3)$$

#### Combination 3

$$\text{CoSO}_4 \cdot 7\text{H}_2\text{O}_{(\text{s})} + 693\text{H}_2\text{O} = \text{CoSO}_4 \cdot 700\text{H}_2\text{O}, \quad \Delta H_{44.63} = 3449$$

$$0.9122[\text{CoSO}_4 \cdot 700\text{H}_2\text{O} = \text{CoSO}_4 \cdot 6\text{H}_2\text{O}_{(\text{s})} + 694\text{H}_2\text{O}], \quad \Delta H_{44.63} = 0.9122 \times (-827) = -754$$

$$0.0878[\text{CoSO}_4 \cdot 700\text{H}_2\text{O}_{(\text{s})} = \text{CoSO}_4 \cdot 17.389\text{H}_2\text{O}_{(\text{l})} + 682.611\text{H}_2\text{O}], \quad \Delta H_{44.63} = 0.0878 \times 1670 = 147$$

By addition

$$\text{CoSO}_4 \cdot 7\text{H}_2\text{O}_{(\text{s})} = 0.9122\text{CoSO}_4 \cdot 6\text{H}_2\text{O}_{(\text{s})} + 0.0878\text{CoSO}_4 \cdot 17.389\text{H}_2\text{O}_{(\text{l})}, \quad \Delta H_{44.63} = 2842 \text{ cal./mole} \quad (3)$$

Combinations 1 and 2 agree well at 2852 and 2850 and the close agreement is obviously due to the fact that the measured  $\Delta H$  for reaction 1 dominates the contribution made by the experimental data obtained at 44.63°.

In combination 3 all of the data were obtained near 44.63° and the result, 2842 cal./mole, is in very satisfactory agreement.

We accept an average of  $2848 \pm 15$  cal./mole for the heat of transition at 44.63°.

## The Heat Capacities and Entropies of Cobalt Sulfate Heptahydrate and Hexahydrate from 15 to 330°K.<sup>1</sup>

by R. V. G. Rao and W. F. Giauque

*Low Temperature Laboratory, Departments of Chemistry and Chemical Engineering, University of California, Berkeley, California (Received October 20, 1964)*

The heat capacity of  $\text{CoSO}_4 \cdot 6\text{H}_2\text{O}$  has been determined from 15 to 330°K. and that of  $\text{CoSO}_4 \cdot 7\text{H}_2\text{O}$  from 15°K. to the hepta-hexa + solution transition, which was found to occur at 317.78°K. Values of  $S^\circ$ ,  $(F^\circ - H^\circ_0)/T$ , and  $(H^\circ - H^\circ_0)/T$  have been tabulated. The entropy change in the reaction  $\text{CoSO}_4 \cdot 7\text{H}_2\text{O} = \text{CoSO}_4 \cdot 6\text{H}_2\text{O} + \text{H}_2\text{O}(\text{g})$  has been determined from the free energy and heat of reaction at 298.15, 305.65, 309.80, and 313.35°K. to be 35.97, 35.92, 35.89, and 35.88 gibbs/mole, respectively. The corresponding values from the third law of thermodynamics are 35.92, 35.90, 35.88, and 35.87 gibbs/mole. The agreement indicates that there is no residual entropy due to structural disorder in either hydrate.  $\Delta H^\circ_0 = 13,771$  cal./mole for the above reaction.

The work reported here is part of a series of calorimetric and magnetic investigations on the hydrated sulfates of the elements of the first transition group. The present work measures the heat capacities of cobalt sulfate hepta- and hexahydrates. Such investigations are a desirable preliminary to detailed low temperature magnetic investigations for several reasons, including evidence that the crystalline forms stable at ordinary temperatures do not undergo transitions before reaching the temperatures of the magnetic investigation. It is especially important to show that no transition will occur in a single crystal which has been prepared and placed for axial measurements of its magnetothermodynamic properties. Also, evidence from the application of the third law of thermodynamics can show that there is no frozen-in disorder, such as that

possibly due to disordered hydrogen bonds, to complicate the interpretation of the magnetic systems. At one time some inaccurate preliminary unpublished heats of solution used in computing the entropy of hydration indicated disorder in the hexahydrate, and following this, Zalkin, Ruben, and Templeton<sup>2</sup> investigated the crystal structure of  $\text{CoSO}_4 \cdot 6\text{H}_2\text{O}$  at ordinary temperatures and found no evidence to support any type of hydrogen bond disorder. Their similar investigation<sup>3</sup> of the isomorphous  $\text{MgSO}_4 \cdot 6\text{H}_2\text{O}$  led to the same conclusion at ordinary temperatures. It has

(1) This work was supported in part by the National Science Foundation.

(2) A. Zalkin, H. Ruben, and D. H. Templeton, *Acta Cryst.*, **15**, 1219 (1962).

(3) A. Zalkin, H. Ruben, and D. H. Templeton, *ibid.*, **17**, 235 (1964).



been shown by Cox, Hornung, and Giauque<sup>4</sup> that  $\text{MgSO}_4 \cdot 6\text{H}_2\text{O}$  undergoes an irreversible transformation, with heat evolution over a range 100 to 140°K. and absorption over the range 235 to 265°K. This was believed due to decomposition of the hexahydrate to microcrystals of the mono- and heptahydrates during cooling.

Barieau and Giauque<sup>5</sup> had reported a similar irreversible transition in the isomorphous  $\text{ZnSO}_4 \cdot 6\text{H}_2\text{O}$ , which has heat evolution between 70 and 120°K. and absorption between 230 and 270°K., and in that case it is known that the hexahydrate is thermodynamically unstable with respect to the hepta- and monohydrate. No low temperature X-ray structural investigations of the hexahydrates of cobalt, zinc, or magnesium sulfates are available.

For these reasons we were concerned over the possibility that isomorphous  $\text{CoSO}_4 \cdot 6\text{H}_2\text{O}$  would be structurally altered on cooling. As will be discussed below, a small maximum rather similar to those in  $\text{ZnSO}_4 \cdot 6\text{H}_2\text{O}$  and  $\text{MgSO}_4 \cdot 6\text{H}_2\text{O}$  occurs in the heat capacity curve near 215°K. and it has so far not been possible to decide if this represents some form of transition. In any case, a rough estimate of the amount of entropy under the hump in the heat capacity curve was small enough (0.14 gibbs/mole) to encourage the belief that, despite our lack of knowledge concerning the hump, a third-law test for residual entropy was practicable, especially since no evidence supporting irreversibility could be found.

This led Brodale and Giauque<sup>6</sup> to reinvestigate the heats of solution of  $\text{CoSO}_4 \cdot 6\text{H}_2\text{O}$  and  $\text{CoSO}_4 \cdot 7\text{H}_2\text{O}$ , and with the assistance of these new data, agreement with the third law has been found. However, this result cannot be taken to prove that no structural changes would occur in a single crystal of  $\text{CoSO}_4 \cdot 6\text{H}_2\text{O}$  during cooling to liquid helium temperatures for a magnetic investigation of its properties.

*Preparation of  $\text{CoSO}_4 \cdot 7\text{H}_2\text{O}$  and  $\text{CoSO}_4 \cdot 6\text{H}_2\text{O}$  Used for the Heat Capacity Measurements.* The starting material used in the preparation of cobalt sulfate was Mallinckrodt reagent grade cobaltous chloride hexahydrate. It was stated to contain 0.15% nickel, 0.25% alkali salts, and remaining impurities, totalling only 0.088%. The nickel was removed by converting the cobalt to cobaltic hexaammine trichloride by oxidation with ammoniacal silver chloride. The method is a standard procedure<sup>7</sup> for the preparation of large amounts of *luteo*-cobalt chloride.

This material was heated on a hot plate and then over a gas burner. The hard cake produced was extracted with water and heated until it was a light blue powder without further evolution of ammonium chloride fumes.

C.P. concentrated sulfuric acid was added and the sulfate was heated with slow evaporation to dryness. This procedure was repeated to ensure elimination of chloride which was confirmed by test. The total heating time with sulfuric acid was about 80 hr. The cobalt sulfate was dissolved in warm distilled water and filtered and the resulting solution was used for crystallization of the hydrates. No trace of nickel was found by the sensitive dimethylglyoxime test,<sup>8</sup> which can detect one part of nickel in 5000 parts of cobalt.

The heptahydrate was crystallized by bubbling pure dry oxygen (which happened to be available in surplus from laboratory production) through the aqueous solution at room temperature. The wet crystals were further dried in a stream of oxygen, while they were mixed in a bottle which was slowly rotated about its horizontal symmetry axis by a motor, in an attempt to obtain uniform drying. The procedure continued until the analysis showed a water content slightly below that corresponding to heptahydrate.

The crystals were small and it had been hoped to avoid any entrapped solution; however, this was not entirely successful and, as will be shown later, the heat capacity measurements showed a small heat effect at the  $\text{CoSO}_4 \cdot 7\text{H}_2\text{O}$ -ice eutectic.

The  $\text{CoSO}_4 \cdot 6\text{H}_2\text{O}$  was prepared in a similar manner except that the crystallization was carried out at 55°. The drying procedure to remove  $\text{CoSO}_4 \cdot 7\text{H}_2\text{O}$  which was formed on cooling the adhering solution to ordinary temperatures was the same as for the heptahydrate and was continued until dehydration analyses indicated only a small remaining amount of  $\text{CoSO}_4 \cdot 7\text{H}_2\text{O}$  in the  $\text{CoSO}_4 \cdot 6\text{H}_2\text{O}$ .

*Apparatus and Samples.* The low temperature calorimeter used was similar to that described by Giauque and Egan<sup>9</sup> and the actual cylindrical copper calorimeter used has been described by Papadopoulos and Giauque.<sup>10</sup> It was 11 cm. long and 4.8 cm. in i.d. A double silk-covered gold resistance thermometer-heater was wound on the outside. After the sample

(4) W. P. Cox, E. W. Hornung, and W. F. Giauque, *J. Am. Chem. Soc.*, **77**, 3935 (1955).

(5) R. E. Barieau and W. F. Giauque, *ibid.*, **72**, 5676 (1950).

(6) G. E. Brodale and W. F. Giauque, *J. Phys. Chem.*, **69**, 1268 (1965).

(7) H. Biltz and W. Biltz, "Laboratory Methods of Inorganic Chemistry," adapted from the German by W. T. Hall and A. A. Blanchard, 2nd Ed., 1928, John Wiley and Sons, Inc., New York, N. Y.

(8) W. W. Scott, "Standard Methods of Chemical Analysis," Vol. 1, 5th Ed., D. Van Nostrand Co., Inc., New York, N. Y., 1939, p. 619.

(9) W. F. Giauque and C. J. Egan, *J. Chem. Phys.*, **5**, 45 (1937).

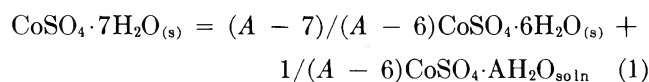
(10) M. N. Papadopoulos and W. F. Giauque, *J. Am. Chem. Soc.*, **77**, 2740 (1955).

had been added, the calorimeter was cooled to reduce the partial pressure of water vapor, evacuated, and 1 atm. of helium was added to assist thermal conduction. There were also eight radial copper vanes to assist heat distribution.

Laboratory standard copper-constantan thermocouple No. 105 was attached to the calorimeter throughout the measurements. During the experiment it was compared with several fixed points and showed exact agreement at the boiling points of normal hydrogen (20.36°K.) and nitrogen (77.34°K.). It read 0.03° low at the triple point of nitrogen (63.15°K.).

The weight of  $\text{CoSO}_4 \cdot 6.968\text{H}_2\text{O}$  in the calorimeter was 181.2521 g. and the weight of  $\text{CoSO}_4 \cdot 6.0033\text{H}_2\text{O}$  was 159.942 g., each *in vacuo*. One defined calorie was taken as 4.1840 absolute joules.

When third-law comparisons were originally made, discrepancies developed which cast doubt on the sampling as representative of the material used in the calorimeter. Unfortunately, the analytical samples of the stock material had not been taken at the time the calorimeter was filled and changes of water content could have occurred. In order to solve this problem Brodale and Giauque<sup>6</sup> made accurate measurements of the heat effect in the hepta-hexa transition reaction (eq. 1) which was found to occur at 317.78°K. The



symbol  $A$  represents the moles of water per mole of  $\text{CoSO}_4$  in the saturated solution at the transition temperature.

Three determinations of the transition temperature were made: 317.78, 317.79, and 317.78°K. Carpenter and Jette<sup>11</sup> reported 318.32°K. and Rohmer<sup>12</sup> reported 316.45°K. However, both of these values were determined by the intersection of solubility or vapor pressure curves, methods which are difficult to use accurately.

The value of  $A = 17.389$  at 317.78°K. was determined from the solubility measurements of Brodale and Giauque.<sup>6</sup>

The quantitative heat effect due to the transition of the small amount of heptahydrate in the hexahydrate sample was observed accurately during the heat capacity observations and this permitted the evaluation of the total water content of the material in the calorimeter.

In the case of the heptahydrate the evaluation was slightly more complicated since the heat capacity measurements showed the presence of 0.0248 mole of excess water in "brine holes" (entrapped solution) per mole of cobalt sulfate heptahydrate. Otherwise the

evaluation was straightforward. In the hexahydrate sample no entrapped solution was present since no heat effect was observed at the  $\text{CoSO}_4 \cdot 7\text{H}_2\text{O}$ -ice eutectic.

The "heptahydrate" sample consisted of 0.943 mole of  $\text{CoSO}_4 \cdot 7\text{H}_2\text{O}$ , 0.057 mole of  $\text{CoSO}_4 \cdot 6\text{H}_2\text{O}$ , and 0.025 mole of additional water per mole of cobalt sulfate. In estimating the excess water in the "brine holes" we made use of Rohmer's<sup>12</sup> solubility data to calculate  $A = 37.16$  for the  $\text{CoSO}_4 \cdot 7\text{H}_2\text{O}$ -ice eutectic at  $-2.7^\circ$ . This was combined with the heat of fusion of ice and an estimate of the heat of saturation to obtain a value for the heat of fusion of the eutectic,  $\Delta H = 46,800$  cal./mole of  $\text{CoSO}_4 \cdot 7\text{H}_2\text{O}$  which dissolved. The determination of the composition of the "heptahydrate" sample is less accurate than that of the hexahydrate because of the major dependence on accuracy of the transition heat.<sup>6</sup> However, since the specific heats of the hepta- and hexahydrates are not greatly different, the accuracy of the correction is not critically dependent on the composition of the heptahydrate, which may have an entropy error of about 0.03 gibbs/mole due to composition uncertainty. Below the  $\text{CoSO}_4 \cdot 7\text{H}_2\text{O}$ -ice eutectic temperature the "additional" water was present as ice and above the eutectic temperature it was present as saturated solution. Fortunately the amount of entrapped solution was so small that the variation of the heat effect due to the change of solubility and the related heat effect with temperature could be ignored in comparison with the major heat absorption at the eutectic.

In the case of the heat capacity measurements on  $\text{CoSO}_4 \cdot 6.0033\text{H}_2\text{O}$ , six separate series of runs were made in an attempt to understand the origin of the hump in the  $C_p$  curve near 215°K.

*Series 1.* The sample was cooled to 230°K. and measurements were made over the range 230-280°K. These measurements were primarily designed to check on the presence of any entrapped solution which would be present as liquid above the  $\text{CoSO}_4 \cdot 7\text{H}_2\text{O}$ -ice eutectic temperature. No eutectic heat was observed. It may be mentioned that no eutectic heat has ever been observed in numerous other experiments in this laboratory when the primary hydrate present was lower than the hydrate in equilibrium at the eutectic temperature.

*Series 2.* The calorimeter was cooled from room temperature to 169°K. in 2 hr., held at this temperature for 12 hr., raised to 220°K. in 40 min., and then cooled rapidly to 15°K. in 3.5 hr., followed by heat capacity measurements to 310°K.

(11) C. D. Carpenter and E. R. Jette, *J. Am. Chem. Soc.*, **45**, 578 (1923).

(12) R. Rohmer, *Ann. Chem.*, **11**, 611 (1939).

*Series 3.* The calorimeter was cooled slowly, over a period of 48 hr., from room temperature to  $80^\circ\text{K}$ ., followed by measurements over the range  $190\text{--}235^\circ\text{K}$ . The hump near  $215^\circ\text{K}$ . was observed.

*Series 4.* Measurements were made over the same range as in series 3, except that cooling was stopped at  $188^\circ\text{K}$ . and measurements were begun immediately. The same hump was observed.

*Series 5.* Measurements similar to those in series 3 and 4 were made except that the sample was held at  $188 \pm 1^\circ\text{K}$ . for 18 hr. before the series was started. The hump was present.

*Series 6.* A short series of measurements was made through the region of the hepta-hexa + solution transition to observe the transition heat due to the small amount of  $\text{CoSO}_4 \cdot 7\text{H}_2\text{O}$  present.

Careful observation near  $100^\circ\text{K}$ . failed to detect any spontaneous evolution of heat such as was observed in the case of  $\text{ZnSO}_4 \cdot 6\text{H}_2\text{O}$ <sup>5</sup> and  $\text{MgSO}_4 \cdot 6\text{H}_2\text{O}$ .<sup>4</sup> There were also many opportunities to observe any

such spontaneous heat evolution, had it occurred, during the several series of heat capacity measurements. Thus there is no evidence from the present work of any irreversible process. The data are given in Table I.

The transition heat absorbed due to the presence of a small amount of  $\text{CoSO}_4 \cdot 7\text{H}_2\text{O}$  present in the calorimeter, in combination with the weight of the sample, was used in determining the over-all composition of the sample within the calorimeter. However, as mentioned above, this was made possible only by means of the subsequent work of Brodale and Giauque<sup>6</sup> on reaction 1, where  $A = 17.389^6$  represents the moles of water per mole of  $\text{CoSO}_4$  in the saturated solution at the transition temperature.

The heat capacity of the sample which was primarily  $\text{CoSO}_4 \cdot 7\text{H}_2\text{O}$ , was investigated in two series of measurements.

*Series 1.* This consisted of a few measurements below, and a few above, the  $\text{CoSO}_4 \cdot 7\text{H}_2\text{O}$ -ice eutectic point to evaluate the amount of entrapped solution by means of the heat of eutectic melting.

*Series 2.* This series covered the range 15 to  $310^\circ\text{K}$ . and was followed by a measurement of the heat of transition of the amount of  $\text{CoSO}_4 \cdot 7\text{H}_2\text{O}$  present.

These data suffice to establish the composition and phases present in the calorimeter during the low tem-

**Table I:** Heat Capacity of  $\text{CoSO}_4 \cdot 6.0033\text{H}_2\text{O}^a$

Temp., $^\circ\text{K}$ .	$C_p^b$	Temp., $^\circ\text{K}$ .	$C_p^b$	Temp., $^\circ\text{K}$ .	$C_p$
—Series 1—		104.09	34.92	—Series 3—	
236.16	69.74	111.21	37.09	195.51	59.92
243.93	71.72	118.57	39.27	202.90	62.43
250.38	72.69	125.90	41.38	210.44	63.04
257.91	74.93	133.12	43.43	218.45	68.48
265.51	76.58	140.56	45.54	226.30	67.68
272.85	78.38	147.85	47.70	234.18	69.79
279.97	80.04	154.68	49.47		
		161.31	51.22	—Series 4—	
—Series 2—		168.07	52.94	195.14	59.78
16.88	2.10	174.94	54.64	203.41	62.18
18.84	2.81	181.48	56.35	211.61	64.67
20.42	3.30	188.50	58.11	219.65	68.34
22.09	3.84	195.97	60.09	227.44	67.93
24.88	4.88	203.87	62.27	234.95	69.44
28.34	6.22	212.00	65.52		
31.30	7.46	220.04	68.28	—Series 5—	
34.78	9.01	227.93	68.15	194.43	59.63
39.68	11.17	235.77	69.83	202.63	62.11
44.83	13.46	243.62	71.60	211.06	64.65
49.91	15.61	251.70	73.58	219.55	68.24
55.64	17.99	259.68	75.31		
62.02	20.56	266.92	77.00	—Series 6—	
68.33	23.01	273.82	78.90	303.80	85.82
74.73	25.41	280.73	80.16	310.36	87.30
81.82	27.82	287.80	81.89	318.32	90.13 <sup>c</sup>
89.29	30.58	294.99	83.71	324.17	90.04
96.85	32.67	302.02	85.57	330.67	91.49

<sup>a</sup>  $0^\circ\text{C}$ . =  $273.15^\circ\text{K}$ .; 1 gibbs = 1 defined cal./defined degree; mol. wt. of  $\text{CoSO}_4 \cdot 7\text{H}_2\text{O}$  = 281.102; mol. wt. of  $\text{CoSO}_4 \cdot 6\text{H}_2\text{O}$  = 263.087; 159.9424 g. in the calorimeter. <sup>b</sup> Gibbs/mole of  $\text{CoSO}_4$ . <sup>c</sup> Transition,  $\Delta T = 7.206$ .

**Table II:** Heat Capacity of  $\text{CoSO}_4 \cdot 6.968\text{H}_2\text{O}^a$

Temp., $^\circ\text{K}$ .	$C_p^b$	Temp., $^\circ\text{K}$ .	$C_p^b$	Temp., $^\circ\text{K}$ .	$C_p$
—Series 1—		66.81	24.58	204.83	70.09
248.49	81.36	73.55	27.42	212.51	72.35
254.37	82.79	80.20	30.17	220.11	74.24
260.11	84.72	87.17	32.84	227.51	76.10
266.22	87.71	94.48	35.41	234.87	77.98
272.87	88.10	101.87	38.10	242.36	79.84
279.90	88.76	109.06	40.52	249.87	81.59
286.37	90.16	116.09	42.95	257.45	83.69
—Series 2—		123.09	45.27	264.69	86.67
16.89	1.95	129.71	47.50	271.26	90.97
18.85	2.68	136.04	49.81	277.87	88.26
20.26	3.19	142.79	51.76	284.42	90.08
24.08	4.39	149.47	53.88	290.98	91.38
28.42	6.27	156.34	55.95	297.51	92.92
32.56	8.07	163.09	58.05	305.68	95.27
37.59	10.62	169.98	60.14	318.95	250.70 <sup>c</sup>
43.58	13.60	176.78	62.12	329.40	115.55
49.47	16.49	183.36	64.08	—Series 3—	
54.95	19.14	190.28	66.07	327.03	114.16
60.39	21.62	197.35	68.07	338.46	117.85

<sup>a</sup> See text for distribution of water;  $0^\circ\text{C}$ . =  $273.15^\circ\text{K}$ .; 1 gibbs = 1 defined cal./defined degree; mol. wt. of  $\text{CoCO}_4 \cdot 6\text{H}_2\text{O}$  = 263.087; mol. wt. of  $\text{CoSO}_4 \cdot 7\text{H}_2\text{O}$  = 281.102; 181.2521 g. in the calorimeter. <sup>b</sup> In gibbs/mole of  $\text{CoSO}_4$ . <sup>c</sup> Transition,  $\Delta T = 18.459^\circ$ .

perature measurements. The data are given in Table II.

Correction for the excess ice in the "heptahydrate" sample was made with the assistance of the heat capacity data of Giauque and Stout.<sup>13</sup> By simultaneous solution of the data in Tables I and II the heat capacities of  $\text{CoSO}_4 \cdot 6\text{H}_2\text{O}$  and  $\text{CoSO}_4 \cdot 7\text{H}_2\text{O}$  were obtained. They are given in Tables III and IV together with the derived thermodynamic properties.

It has been shown<sup>14</sup> by calorimetric measurements, that the application of magnetic fields of the order of 100 kgauss, near 1°K., extracts an entropy of  $R \ln 2$

Table III: Thermodynamic Properties of  $\text{CoSO}_4 \cdot 6\text{H}_2\text{O}^a$

Temp., °K.	$C_p$	$S$	$-(F^\circ - H^\circ_0)/T$	$(H^\circ - H^\circ_0)/T$
15	1.489	1.881	1.504	0.377
20	3.163	2.540	1.675	0.865
25	4.898	3.427	1.933	1.494
30	6.913	4.495	2.268	2.227
35	9.109	5.724	2.673	3.051
40	11.326	7.084	3.138	3.946
45	13.544	8.547	3.657	4.890
50	15.661	10.084	4.222	5.862
55	17.729	11.675	4.827	6.848
60	19.744	12.962	5.465	7.497
70	23.659	16.644	6.823	9.821
80	27.225	20.040	8.262	11.778
90	30.545	23.441	9.761	13.680
100	33.674	26.822	11.298	15.524
110	36.726	30.174	12.861	17.313
120	39.685	33.497	14.443	19.054
130	42.580	36.789	16.036	20.753
140	45.425	40.049	17.635	22.414
150	48.204	43.279	19.236	24.043
160	50.896	46.476	20.840	25.636
170	53.454	49.639	22.440	27.199
180	55.956	52.764	24.037	28.727
190	58.404	55.859	25.633	30.226
200	61.028	58.923	27.222	31.701
210	64.700	61.982	28.804	33.178
220	68.245	65.085	30.383	34.702
230	68.538	68.121	31.959	36.162
240	70.729	71.081	33.527	37.554
250	73.088	73.977	35.048	38.929
260	75.401	76.929	36.642	40.287
270	77.798	79.820	38.188	41.632
273.15	78.556	80.727	38.673	42.054
280	80.198	82.693	39.726	42.967
290	82.580	85.549	41.257	44.292
298.15	84.458	87.863	42.499	45.364
300	84.876	88.387	42.780	45.607
310	87.102	91.207	44.297	46.910
317.78	88.774	93.386	45.473	47.913
320	89.241	94.006	45.807	48.199
330	91.322	96.785	47.310	49.475

<sup>a</sup> Units are gibbs/mole.

= 1.377 gibbs/mole due to the electron system of  $\text{CoSO}_4 \cdot 7\text{H}_2\text{O}$ . This amount of entropy has been added to the values obtained by the ordinary extrapolation of the heat capacity measurements. Although a similar magnetic investigation has not been made on

Table IV: Thermodynamic Properties of  $\text{CoSO}_4 \cdot 7\text{H}_2\text{O}^a$

Temp., °K.	$C_p$	$S$	$-(F^\circ - H^\circ_0)/T$	$(H^\circ - H^\circ_0)/T$
15	1.388	1.849	1.496	0.353
20	3.072	2.467	1.656	0.811
25	4.822	3.339	1.902	1.437
30	5.850	4.393	2.227	2.166
35	9.258	5.627	2.623	3.004
40	11.845	7.034	3.084	3.950
45	14.292	8.572	3.608	4.964
50	16.767	10.207	4.186	6.021
55	19.197	11.920	4.809	7.111
60	21.516	13.671	5.475	8.196
70	26.053	17.352	6.909	10.443
80	30.165	21.103	8.449	12.654
90	33.965	24.879	10.063	14.816
100	37.564	28.644	11.734	16.910
110	41.052	32.389	13.442	18.947
120	44.456	36.108	15.176	20.932
130	47.793	39.799	16.928	22.871
140	51.061	43.460	18.693	24.767
150	54.199	47.091	20.464	26.627
160	57.374	50.692	22.242	28.450
170	60.409	54.272	24.030	30.242
180	63.381	57.799	25.798	32.001
190	66.290	61.304	27.575	33.729
200	69.109	64.777	29.350	35.427
210	71.880	68.215	31.118	37.097
220	74.596	71.622	32.882	38.740
230	77.071	74.991	34.639	40.352
240	79.651	78.326	36.391	41.935
250	82.083	81.630	38.136	43.494
260	84.494	84.895	39.870	45.025
270	86.779	88.127	41.598	46.529
273.15	87.492	89.138	42.141	46.997
280	89.058	91.324	43.316	48.008
290	91.378	94.489	45.026	49.463
298.15	93.332	97.048	46.413	50.635
300	93.783	97.627	46.727	50.900
310	96.292	100.743	48.420	52.323
317.78	98.321	103.155	49.730	53.425

<sup>a</sup> Units are gibbs/mole.

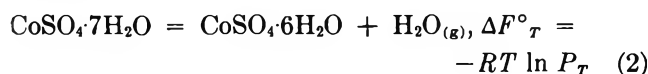
$\text{CoSO}_4 \cdot 6\text{H}_2\text{O}$ , an identical amount has also been added for the contribution of the electron system to the extrapolation of the entropy of this substance. The

(13) W. F. Giauque and J. W. Stout, *J. Am. Chem. Soc.*, **58**, 1144 (1936).

(14) W. F. Giauque, D. N. Lyon, E. W. Hornung, and T. E. Hopkins, *J. Chem. Phys.*, **37**, 1446 (1962).

heat capacity data of Fritz and Giauque<sup>15</sup> on  $\text{CoSO}_4 \cdot 7\text{H}_2\text{O}$  in the liquid helium region, were used in extending the calculations below 15°K. These data also show that the contribution of the electron system to  $(H^\circ - H^\circ_0)$  is trivial.

*Comparison of the Data with the Third Law of Thermodynamics.* Carpenter and Jette<sup>11</sup> have measured the vapor pressure of water over the phases  $\text{CoSO}_4 \cdot 7\text{H}_2\text{O}$ – $\text{CoSO}_4 \cdot 6\text{H}_2\text{O}$  at several temperatures in the range from 25° to the transition temperature. These data may be used to give the free energy change in reaction 2.



The heat of solution data of Brodale and Giauque<sup>6</sup> combined with the present heat capacity data and the well-known heat capacity of water vapor, derived from spectrographic data, give the heat of reaction 2 at various temperatures, from which  $\Delta S = (\Delta H - \Delta F)/T$  for reaction 2.

$$\Delta S \text{ (third law)} = \int_0^T C_{p(\text{hexa})} d \ln T + S_{\text{H}_2\text{O}_{(g)}} - \int_0^T C_{p(\text{hepta})} d \ln T$$

The entropy, heat capacity, and heat of vaporization of water are taken from the U. S. Bureau of Standards Tables<sup>16</sup>: for  $\text{H}_2\text{O}$  at 298.15°K.,  $S_{(g)} = 45.106$  gibbs/mole,  $C_p = 8.025$  gibbs/mole, and  $\Delta H_{\text{vap}} = 10,520$  cal./mole. The comparison is summarized in Table V.

The agreement in the last two columns of Table V is better than the accuracy of the several experiments involved and is consistent with the attainment of perfectly ordered crystalline states for  $\text{CoSO}_4 \cdot 6\text{H}_2\text{O}$  and  $\text{CoSO}_4 \cdot 7\text{H}_2\text{O}$  at limiting low temperatures.

**Table V:** Comparison of Entropy Values for the Reaction  $\text{CoSO}_4 \cdot 7\text{H}_2\text{O} = \text{CoSO}_4 \cdot 6\text{H}_2\text{O} + \text{H}_2\text{O}_{(g)}$ <sup>a</sup>

Temp., °K.	$\Delta H_T$	$\Delta F_T$	$(\Delta H - \Delta F)/T$	$\Delta S_{\text{third law}}$
298.15	12,975	2252	35.97	35.92
305.65	12,968	1990	35.92	35.90
309.80	12,963	1844	35.89	35.88
313.35	12,959	1717	35.88	35.87

<sup>a</sup> Units are defined cal./mole or gibbs/mole.

From the data in Tables III, IV, and V, and the value  $(H^\circ - H^\circ_0)/T = 7.941$  gibbs/mole for  $\text{H}_2\text{O}_{(g)}$ ,<sup>17</sup> the value of  $\Delta H^\circ_0$  for reaction 2 is found to be 13,771 cal./mole.

*Acknowledgment.* We thank G. E. Brodale for assistance with the calculations.

(15) J. J. Fritz and W. F. Giauque, *J. Am. Chem. Soc.*, **71**, 2168 (1949).

(16) National Bureau of Standards Circular 500, U. S. Government Printing Office, Washington, D. C., 1952.

(17) "Selected Values of Chemical Thermodynamic Properties," Series III, National Bureau of Standards, U. S. Government Printing Office, Washington, D. C., June 30, 1948.

## Kinetics of the Thermal Rearrangement between

### 3-Methyl-1,5-hexadiene and 1,5-Heptadiene

by Akira Amano and Masao Uchiyama

*The Department of Applied Chemistry, Tohoku University, Sakura-koji, Sendai, Japan  
(Received October 21, 1964)*

Gas phase thermal reaction of 3-methyl-1,5-hexadiene and 1,5-heptadiene has been studied in a static apparatus at a pressure of about 2 mm. and temperatures ranging from 178 to 250°. From the product distribution observed, it is concluded that the predominant mode of reaction is the unimolecular rearrangement between the two isomeric 1,5-diolefins. Other reactions such as cross-recombination and radical-induced decomposition are not detected under the given conditions. The equilibrium constant of the reversible system is effectively independent of temperature and is approximately 5.6 in favor of 1,5-heptadiene. The two rate constants can be expressed by the following equations:  $\log k_t (\text{sec.}^{-1}) = 9.84 - 32,500/4.575T$ , and  $\log k_b (\text{sec.}^{-1}) = 9.09 - 32,500/4.575T$ . The values of kinetic parameters are compatible with the assumption of a six-membered cyclic activated complex. The structure of the activated complex as well as the energetics of allylic radicals are also discussed.

Thermally induced migration of the allyl group has frequently been reported for molecules with functional groups such as  $\text{COOC}_2\text{H}_5$ , CN, etc., and is known as the Cope rearrangement.<sup>1</sup> Studies were further extended to molecules with methyl or phenyl group in place of the electronegative groups mentioned above. Produced from 3-phenyl-1,5-hexadiene,<sup>2</sup> 3-phenyl-1,5-heptadiene,<sup>2</sup> 3-methyl-4-phenyl-1,5-hexadiene,<sup>2</sup> 3-methyl-1,5-hexadiene,<sup>2,3</sup> 1,5-heptadiene,<sup>2,3</sup> and 3,4-dimethyl-1,5-hexadiene<sup>4</sup> were, thus, 1-phenyl-1,5-hexadiene, 4-methyl-1-phenyl-1,5-hexadiene, 1-phenyl-1,5-heptadiene, 1,5-heptadiene, 3-methyl-1,5-hexadiene, and 2,6-octadiene, respectively. The purely thermal rearrangement was considered to take place through a six-membered cyclic activated complex and is therefore similar to the Claisen rearrangement. Unfortunately, data given in the original papers are insufficient to estimate pressures under which these reactions were studied. It appears, however, that the experiments were carried out even in the condensed phase where a second-order process should predominate. Thus, according to Cope, *et al.*,<sup>2</sup> for example, in the products from 49 g. of 1,5-heptadiene only a total of 27.4 g. was recovered as 3-methyl-1,5-hexadiene and 1,5-heptadiene.

The present communication deals with the gaseous system: 3-methyl-1,5-hexadiene  $\rightleftharpoons$  1,5-heptadiene. By carrying out the reaction under an extremely low pressure, it is possible to avoid complicating factors such as polymerization and decomposition and hence to measure both equilibrium and kinetics of the reversible system. The present work was originally undertaken to obtain information as to the bond dissociation energy of the central C-C linkage of diallyl by observing the extent of cross-recombination between allylic radicals involved, but we have so far failed to detect such dissociation in the range of temperature selected.

#### Experimental

*Preparation of Crude Materials.* A mixture of 3-methyl-1,5-hexadiene and 1,5-heptadiene was prepared by the reaction of allylmagnesium bromide with a mix-

(1) A. C. Cope and E. M. Hardy, *J. Am. Chem. Soc.*, **62**, 441 (1940); A. C. Cope, K. E. Hoyle, and D. Heyl, *ibid.*, **63**, 1843 (1941); A. C. Cope, C. M. Hofmann, and E. M. Hardy, *ibid.*, **63**, 1852 (1941); D. E. Whyte and A. C. Cope, *ibid.*, **65**, 1999 (1943); A. C. Cope and L. Field, *ibid.*, **71**, 1589 (1949).

(2) H. Levy and A. C. Cope, *ibid.*, **66**, 1684 (1944).

(3) W. D. Huntsman, *ibid.*, **82**, 6389 (1960).

(4) W. von E. Doering and W. R. Roth, *Tetrahedron*, **18**, 67 (1962).

ture of 3-chloro-1-butene and 1-chloro-2-butene in absolute ether using a conventional technique of Grignard synthesis. Allylmagnesium bromide and chlorobutenes used in the above reaction were prepared by the methods described by Kharasch, Kritchevsky, and Mayo<sup>5</sup> and by Levy and Cope,<sup>2</sup> respectively. After a standard procedure, a fraction ranging from 79 to 94° was separated from the products of the Grignard reaction and was stored for use with subsequent purification.

**Isolation of Diolefins.** Prior to each experimental run, about 0.1 ml. of the crude fraction was introduced into a gas-liquid chromatographic column (300 cm., Apiezon Grease L on firebrick, at 70°, helium carrier gas rate 60 ml./min.) for complete separation of diolefins. Under these conditions, three well-defined peaks were obtained at retention times of 4.6, 7.4, and 11.0 min. with estimated column efficiency corresponding to about 900 theoretical plates. From the relation of boiling point *vs.* retention time of these and other structurally similar hydrocarbons, the three peaks in the order of retention time were assigned to 1,5-hexadiene, 3-methyl-1,5-hexadiene, and 1,5-heptadiene, respectively. This assignment, as will be described, was further confirmed by infrared absorption spectra. The eluates were separately collected in traps placed at the exit of the g.l.c. line using liquid nitrogen and were used for the kinetic experiments. Subsequent analysis by the same g.l.c. revealed that the sample of 3-methyl-1,5-hexadiene prepared by the above method contained not more than 1% of 1,5-heptadiene, while that of 1,5-heptadiene contained about 3.5% of 3-methyl-1,5-hexadiene. The contamination of these materials was taken into consideration in evaluating kinetic data.

**Infrared Spectra.** Infrared spectra of the three components from the g.l.c. were measured on a Perkin-Elmer Model 21 infrared spectrophotometer using NaCl optics. Reproduced in Figure 1 are the spectra which have not been reported previously. By comparison with an authentic sample and also with published spectral curves,<sup>6</sup> the first eluate from the g.l.c. was identified as 1,5-hexadiene. Since the second and the third eluates gave a sufficient number of absorptions characteristic to both 1,5-diolefin and CH<sub>3</sub>-group, they were identified as 3-methyl-1,5-hexadiene and 1,5-heptadiene, respectively (Figures 1a and 1b). A strong absorption observed at 960 cm.<sup>-1</sup> (Figure 1b), characteristic of out-of-plane deformation of CH in the *trans* form, indicates that at least a majority of the synthesized 1,5-heptadiene was in *trans* conformation. It should be noted, in this connection, that gas chromatograms of 1,5-heptadiene in the thermally rear-

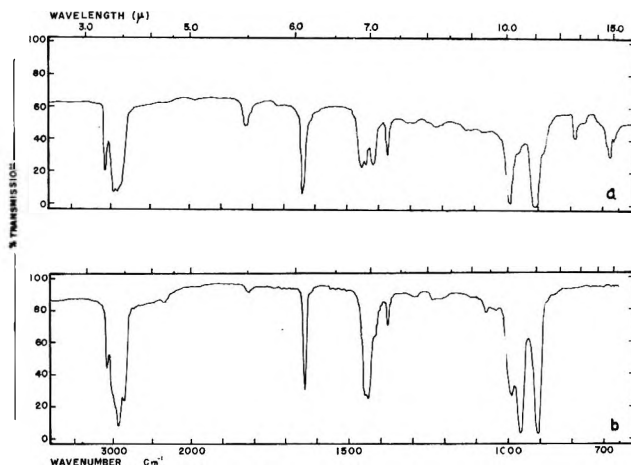


Figure 1. Infrared spectra using NaCl optics and 15- $\mu$  cell: a, 3-methyl-1,5-hexadiene; b, 1,5-heptadiene.

ranged product of 3-methyl-1,5-hexadiene frequently exhibited a shoulder on the descending part of the peaks. Although this matter was not pursued further, it may well be caused by a small amount of *cis*-1,5-heptadiene, the higher boiling isomer, which was present only in the reaction products.

**Apparatus and Procedure.** Rate and equilibrium of the rearrangement were measured in the gas phase by a static method using a standard vacuum line. A trap, containing either 3-methyl-1,5-hexadiene or 1,5-heptadiene from the preparative g.l.c., was connected to a high vacuum manifold through a glass tapered joint. After a thorough degassing, the reactant vapor was expanded into a calibrated volume and an all-glass Bourdon spoon gauge. The latter gauge was immersed in a thermostat and was used as a null-point indicator. Balancing pressure, supplied from ethylbenzene in a bulb connected to the reference side of the gauge, was controlled to maintain the pointer of the gauge at a calibrated null point by adjusting the temperature of the thermostat. The pressure of reactant vapor could thus be read to within  $\pm 0.2$  mm., corresponding to about 2% of the measured pressure, based on a standard table of the pressure *vs.* temperature relation of ethylbenzene. The reactant vapor in the calibrated volume was then transferred into a reaction vessel which was sealed by fusing a small connecting tube. Except for one run, the pressure of the reactant in the vessel was approximately 2 mm. The vessel, made of silica and about 120 ml. in volume, was equipped with

(5) M. S. Kharasch, J. Kritchevsky, and F. R. Mayo, *J. Org. Chem.*, **2**, 489 (1938).

(6) The Sadtler Research Laboratories, "The Sadtler Standard Spectra," No. 15330, Philadelphia, Pa.; American Petroleum Institute, Research Project 44, Infrared Data No. 1654, Pittsburgh, Pa.

a break-seal and a tapered joint through which it was connected to the vacuum manifold. The vessel was then removed from the manifold and was placed in an electric furnace. The temperature of the furnace dropped by a few degrees during the latter procedure, but reached a steady value in several minutes. The effect of the temperature variation was properly corrected in calculating kinetic results. The temperature of the furnace, ranging from 178 to 250°, was controlled electronically to within  $\pm 0.3^\circ$  and was measured by a Pt—Pt—Rh thermocouple to within  $\pm 0.1^\circ$ . After a lapse of the predetermined reaction time, ranging from 0.5 to 163 hr., the entire system was quenched by dropping the vessel into chilled water. The vessel was again connected to the manifold and the line was opened by breaking the seal with a magnetically operated iron plunger. All the condensable products were then collected in a small ampoule and were subjected to analyses.

*Analysis.* The ampoule was removed from the manifold and was loaded in a specially constructed "ampoule breaker" mounted at the inlet of the g.l.c. line. It was necessary to maintain the temperature of the breaker at about 100° to prevent the materials from condensing on the wall. The operating conditions of the g.l.c. were the same as those described for the isolation of diolefins. The analysis revealed that 3-methyl-1,5-hexadiene and 1,5-heptadiene were the sole components of the condensable products. Thus, only 1,5-heptadiene was formed from 3-methyl-1,5-hexadiene, and conversely 3-methyl-1,5-hexadiene from 1,5-heptadiene. The composition of the products was calculated from peak areas on the gas chromatogram using an experimentally determined correction factor of 1.16 for the ratio of peak area per mole of 1,5-heptadiene to that of 3-methyl-1,5-hexadiene. For a limited number of runs, analysis was also made for noncondensable products. Methane, ethylene, propylene, butenes, and butadiene were detected. Since these were formed in only negligible amounts, their presence was ignored in our kinetic treatment.

## Results and Discussion

*Scope of Reaction.* The possibility of the formation of intermediary allylic radicals by the rupture of the weakest central C—C linkage in the 1,5-diolefin skeleton must be excluded. If allylic radicals were formed as a primary act, cross-recombination of the radicals would result in the formation of both C<sub>6</sub>- and C<sub>8</sub>-diolefins and hydrogen abstraction by the radicals would produce considerable amounts of propylene and butenes. None of these compounds was produced to any noticeable extent, if at all. The only reaction

taking place at relatively mild conditions (below 250°) is, therefore, the reversible intramolecular rearrangement between 3-methyl-1,5-hexadiene and 1,5-heptadiene.

At temperatures considerably higher than those used in the present study, cleavage at the central C—C linkage would produce allylic radicals which in turn induce decomposition of the reactant molecules. Thus at 460°, according to Huntsman,<sup>3</sup> lower molecular weight gases as well as C<sub>6</sub>- and C<sub>8</sub>-diolefins were in fact major products from C<sub>7</sub>-diolefins. In this connection, it is interesting to refer to results reported on the pyrolysis of 1,5-hexadiene. According to Lebedev,<sup>7</sup> 1,5-hexadiene remained unchanged by a heat treatment for 8 days at 140–200°, but considerable polymerization took place after 10 days at 250°. Studies on the pyrolysis of the same compound at higher temperatures, reported by Hurd and Bollman<sup>8</sup> and by Bryce and Ruzicka,<sup>9</sup> indicate that the threshold temperature of decomposition may be as high as 350°. The absence of chemical reaction at lower temperature in the case of 1,5-hexadiene is compatible with present knowledge, since the rearrangement does not alter the skeletal structure. Transition from the low temperature rearrangement to the high temperature decomposition has an important bearing on the stability of the activated complex assumed for the rearrangement relative to the resonance energy in allylic radicals. This point will be discussed later.

*Equilibrium:* 3-Methyl-1,5-hexadiene  $\rightleftharpoons$  1,5-Heptadiene. Listed in Table I are the equilibrium data obtained at four different temperatures ranging from 210 to 260°. The equilibrium constant, *K* in the third column of Table I, is defined by the ratio (moles of heptadiene)/(moles of methylhexadiene). The equilibrium was reached from both sides of the equation, and the time allowed for its attainment was more than 15 times the estimated half-life. Since the values of *K* are practically independent of temperature, their arithmetic mean of 5.63 will be used to cover the whole temperature range studied.

In the paper on the thermal reaction of 1,5-diolefins, Huntsman<sup>3</sup> reported that, among various other hydrocarbons, 10% of 3-methyl-1,5-hexadiene and 56% of 1,5-heptadiene were found in the products from 3-methyl-1,5-hexadiene after 60 sec. at 460° while at the same temperature 10% of 3-methyl-1,5-hexadiene and

(7) S. V. Lebedev, *Chem. Abstr.*, **9**, 799 (1915).

(8) C. D. Hurd and H. T. Bollman, *J. Am. Chem. Soc.*, **55**, 699 (1933).

(9) W. A. Bryce and D. J. Ruzicka, *Can. J. Chem.*, **38**, 827, 835 (1960).



**Table I:** Equilibrium Data for 3-Methyl-1,5-hexadiene  $\rightleftharpoons$  1,5-Heptadiene

Temp., °C.	Reaction time, hr.	<i>K</i>
259.2	77	5.72 <sup>a</sup>
249.5	91	5.76 <sup>a</sup>
228.7	76	5.49 <sup>b</sup>
209.2	163	5.54 <sup>b</sup>

<sup>a</sup> Equilibrium was reached from 1,5-heptadiene. <sup>b</sup> Equilibrium was reached from 3-methyl-1,5-hexadiene.

49% of 1,5-heptadiene were found from 1,5-heptadiene after 58 sec. Since the reaction time was much longer than the half-life of the reaction (at 460° about 0.4 sec. and 3 sec. for the forward and the reverse reactions, respectively) and the rate of the rearrangement may be assumed to be faster than those of concurrent reactions, the two isomers obtained by Huntsman should roughly be in equilibrium with respect to one another. In excellent agreement with the present results, this leads to a value of 5.3 for the apparent equilibrium constant at 460°. The equilibrium constant can also be estimated using an empirical rule of group additivity proposed by Benson and Buss.<sup>10</sup> This rule predicts the value at 200° to be approximately 3.0 which tends to decrease, but very slightly, with increasing temperature. The agreement between the observed and the predicted values may be taken as a support for extending the rule to this class of compounds.

**Kinetics.** Summarized in Table II are the kinetic data for both the forward and the reverse reactions carried out at temperatures ranging from 178 to 246°. The values of  $k_f$  and  $k_b$ , the two rate constants, are also listed in the table. The rate constants were calculated using the opposing first-order rate equation:  $t(k_f + k_b) = \ln(KA_0 - B_0)/(KA - B)$ , in which  $t$  is the reaction time;  $A$  and  $B$ , the concentrations of reactant and product at time  $t$ ; and  $A_0$  and  $B_0$ , the initial concentrations of the corresponding species. Illustrated in Figure 2 are the plots for both  $k_f$  and  $k_b$  which indicate an over-all fit to the Arrhenius form. Temperature dependence of the rate constants can thus be expressed by the following equations:  $\log k_f$  (sec.<sup>-1</sup>) = 9.84 - 32,500/4.575*T* and  $\log k_b$  (sec.<sup>-1</sup>) = 9.09 - 32,500/4.575*T*. As indicated in Table II, two runs were carried out in the presence of a substantial amount of air which was accidentally introduced into the system. The fit of the rate constants from these runs to the same Arrhenius expression provides an evidence for the molecular nature of the reaction.

For the sake of comparison, the values of kinetic

**Table II:** Rate of Rearrangement

Temp., °C.	Time, hr.	Pressure, mm.	$k_f \times 10^6$ , sec. <sup>-1</sup>	$k_b \times 10^6$ , sec. <sup>-1</sup>
Forward reaction				
242.7	0.5	2.41	121	21.5
232.6	0.5	2.22	61.1	10.9
223.4	24.0	16.6	39.7	7.05
212.9	3.0	2.19	17.0	3.01
202.9	3.0	1.97	7.10	1.26
202.6	20.0	2.38	8.22	1.48
201.8°	14.0		9.60	1.71
192.3	21.2	2.18	3.80	0.675
191.9°	48.0		3.77	0.670
178.0	48.0		1.41	0.250
Reverse reaction				
246.6	0.5		145	25.8
246.4	0.5	2.37	128	22.7
245.2	0.5	2.51	129	23.0
222.5	3.0	1.70	41.4	7.35
197.3	12.0	1.71	4.96	0.880

<sup>a</sup> These runs were carried out in the presence of a substantial amount of air.

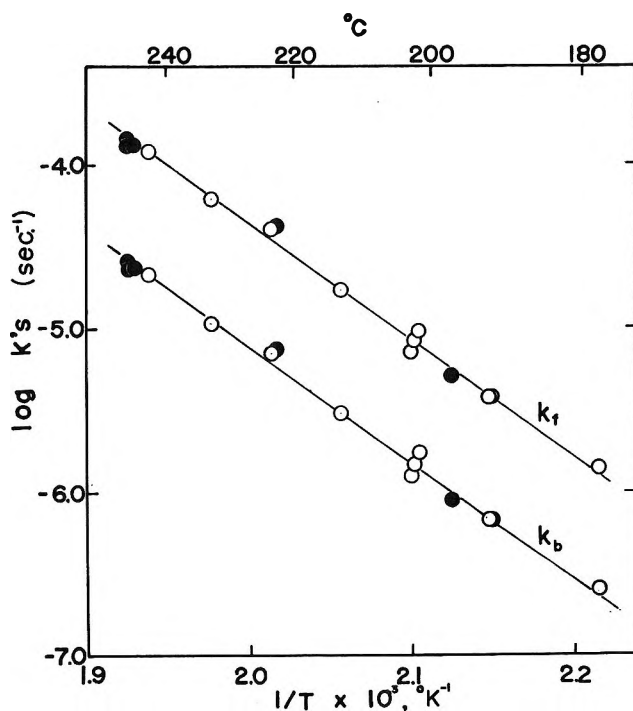


Figure 2. Arrhenius plots for the rate of rearrangement: O, rearrangement of 3-methyl-1,5-hexadiene; ●, rearrangement of 1,5-heptadiene. The upper and lower lines correspond to forward and reverse reactions, respectively.

(10) S. W. Benson and J. H. Buss, *J. Chem. Phys.*, 29, 546 (1958).

parameters which have hitherto been reported for the Cope rearrangement are listed in Table III. The

**Table III:** Reported Values of Kinetic Parameters for the Cope Rearrangement

Compd.	$A \times 10^{-10}$ , sec. <sup>-1</sup>	$E$ , kcal./ mole	$\Delta S^\ddagger$ , cal./ mole- °K.
(1-Ethylpropenyl)allylmalononitrile <sup>a</sup>	8.66	25.78	-11.1
1-Cyclohexenylallylmalononitrile <sup>a</sup>	6.31	26.16	-11.7
Ethyl (1,3-dimethyl-1-butenyl)allyl- cyanoacetate <sup>a</sup>	2.28	28.62	-14.0
3-Methyl-1,5-hexadiene <sup>b</sup>	0.69	32.5	-14.1
1,5-Heptadiene <sup>b</sup>	0.123	32.5	-16.0

<sup>a</sup> G. Foster, A. C. Cope, and F. Daniels, *J. Am. Chem. Soc.*, **69**, 1893 (1947). <sup>b</sup> Present study.

ease with which the rearrangement takes place, as reflected by the observed values of activation energy,  $E$ , is greatly enhanced by the attachment of electronegative groups to the carbon atom adjacent to a double bond. Thus at 200°, in accord with the order of electronegativity, malononitrile rearranges approximately  $10^6$  times faster than cyanoacetic ester which in turn rearranges approximately  $10^{3.5}$  times faster than simple 1,5-diolefins.

**Activated Complex.** As listed in Table III, the values of the  $A$ -factor obtained above correspond to -14.1 and -16.0 cal./mole-°K. in entropy of activation at 200° for the forward and the reverse reactions, respectively. The evaluation is based on the following relation:  $A = (\kappa kT/h)e^{\Delta S^\ddagger/R}$ , where the transmission coefficient,  $\kappa$ , is assumed to be unity. The large entropy decrease in each case is compatible with the formation of a cyclic activated complex which has been postulated for a number of similar reactions. The loss in entropy for the case of 3-methyl-1,5-hexadiene can be estimated to be approximately 23.8 cal./mole-°K., if the free internal rotations in the reactant molecule are assumed to be completely frozen in the complex. However, transformation of mechanical properties of the reaction system would not be as straightforward as assumed. Internal rotations in the reactant molecule may be restricted to a certain extent, and a part of the rotational motion may be retained in the complex as vibrational motion. Although rigorous treatment is impossible with our present knowledge, the estimated value of the entropy loss will be reduced considerably if these are taken into account.

A sketch of an imaginary 3-methyl-1,5-hexadiene molecule at an instant before commencing the reaction

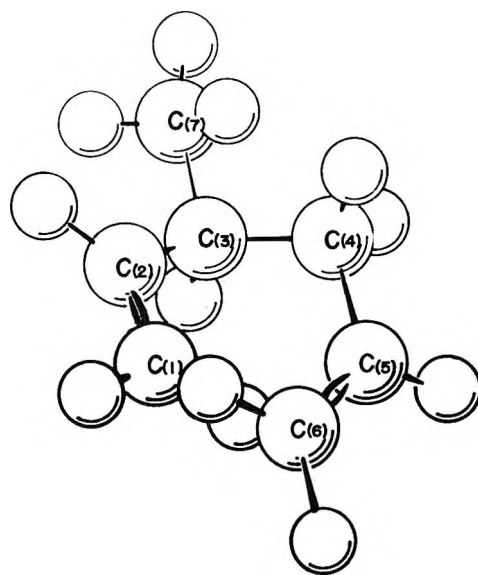


Figure 3. Schematic representation of 3-methyl-1,5-hexadiene.

is shown in Figure 3. In drawing the molecule, the C-2-C-3-C-4-C-5 skeleton is fixed at one of its *gauche* conformations, and two double bonds are allowed to rotate around the fixed axes in such a way that the distance between two terminal carbon atoms is minimized. The closest approach between C-1 and C-6 would then become 1.67 Å., based on the following molecular parameters: C-C distance = 1.54 Å., C=C distance = 1.35 Å., C< angle = 109° 28', and C≤ angle = 120°. The approach between C-1 and C-6 will be reduced to 1.54 Å. if the molecule is further allowed to twist around the C-3-C-4 axis by only about 3°. The calculation is admittedly crude, since the central C-3-C-4 bond length should be considered longer than 1.54 Å. It is however, sufficient to visualize the way by which 3-methyl-1,5-hexadiene can form a six-membered cyclic activated complex with a small torsional motion, and also the way by which the complex can decompose into *cis*-1,5-heptadiene. It is interesting to note that the thermally produced 1,5-heptadiene contained *cis* isomer whereas the latter was not present in the chemically synthesized 1,5-heptadiene. The figure also serves to make understandable the slower rate of the rearrangement observed for 1,5-heptadiene in which case the bulky methyl group would obstruct the bond formation between C-1 and C-6. That the retarding effect of the methyl group is purely steric can be seen in the values of kinetic parameters.

**Stabilization Energy in Allyl Radicals.** Following the conclusion drawn above, it becomes apparent that the more bulky groups attached to the terminal double-bonded carbon atoms, the slower would become the

rate of the rearrangement. Thus, according to Doering and Roth,<sup>4</sup> 2,6-octadiene was quite stable under conditions where other 1,5-diolefins would rearrange readily. If their statement is interpreted to mean that less than 1% of 2,6-octadiene had reacted after 24 hr. at 230°, the first-order rate constant would be less than  $10^{-7}$  sec.<sup>-1</sup> at 230°. Since there was no evidence of other reactions at the given conditions, the rate constant for the dissociation at the central C-C bond of 2,6-octadiene would also be deemed less than  $10^{-7}$  sec.<sup>-1</sup>. This puts the lowest limit for the bond dissociation energy of the central C-C bond as approximately 48-50 kcal./

mole, assuming  $10^{14}\sim 10^{15}$  sec.<sup>-1</sup> for the *A*-factor of the unimolecular decomposition. The maximum stabilization energy assignable for the allyl radical is therefore 18 kcal./mole. Studies along this line are currently being undertaken in our laboratory.

*Acknowledgment.* The authors are grateful to Professor Hiroshi Tokuhisa for his interest and to Professor Susumu Kinumaki and his group for the spectral data. Thanks are also due Mr. Toshihiko Amatatsu, Mr. Tadashi Kunii, and Mr. Hisahiko Takahashi for their assistance in the experimental work.

## Toward a Generalized Theory of Gas Chromatography at High Solute Concentrations

by D. L. Peterson and F. Helfferich

*Shell Development Company, Emeryville, California (Received October 22, 1964)*

The working formula of gas chromatography is based on the assumption that the mobile-phase velocity remains constant throughout the region of a solute pulse. Removal of this assumption leads to a more meaningful deduction of the usual result and eliminates contradictions otherwise encountered. In particular, the correct formula for the migration of solute concentration pulses in a column already equilibrated with a feed gas containing the solute at a high concentration results only when due allowance is made for the variation of mobile-phase velocity in the region of the pulse. The influence of this factor on the self-sharpening and nonsharpening character of concentration boundaries requires a new criterion, according to which it is possible for a nonlinear isotherm to produce a symmetrical chromatographic peak. Concentration-pulse migration-rate measurements at high solute concentrations make possible the measurement of nonlinear sorption isotherms. The method appears well suited to binary sorption equilibrium measurements, but less so for multicomponent equilibria.

### Introduction

Variations in solute concentration along the length of a chromatographic column are necessarily accompanied by changes in the velocity of the mobile phase. This occurs because sorbed solute advances only through the mobile phase, so that the total flux

of solute and carrier molecules must be greater where the amount sorbed is higher. While the working formulas of frontal analysis contain these different velocities preceding and following concentration fronts,<sup>1,2</sup> velocity differences in elution chromatography have ordinarily been presumed negligible and have

been omitted from derivations of pulse velocities. Indeed, only if the maximum concentrations attained during the entirety of passage of a pulse through a column are sufficiently small as to make this presumption plausible does the familiar relation<sup>3</sup> between retention volume  $V_R$ , stationary-phase volume  $V_s$ , void volume  $V_g$ , and concentrations of solute 1 in mobile and stationary phases,  $C_1$  and  $\bar{C}_1$ , respectively, apply

$$V_R = V_g + \bar{C}_1 V_s / C_1 \quad (1)$$

Otherwise, the higher velocity in the region of the pulse leads to a lower retention volume than given by eq. 1. Schay<sup>1</sup> has called attention to this phenomenon, and Golay<sup>4</sup> has presented a criterion by which one may decide the maximum allowable sample size consistent with the precision with which  $V_R$  is to be measured, such that the velocity effect may be neglected.

It is the purpose of this communication to show that velocity variations, except in two very special cases, are never absent from chromatographic experiments, and to discuss situations where they cannot be presumed so. Two cases are to be distinguished: (1) the use of large samples in a nonsorbed carrier gas, and (2) the use of small concentration pulses or steps in a feed gas containing solute at high concentration. The first case, of which use has been made in measurements of nonlinear isotherms from peak asymmetry,<sup>5</sup> is included in Golay's<sup>4</sup> discussion and will only be introduced here for purposes of comparison. Interest in the second owes to the possibility of measuring sorption equilibria at other than infinite dilution by simple retention volume measurements, as opposed to deductions from peak asymmetry. A description of the more elegant tracer-pulse technique for determining nonlinear isotherms directly from retention volumes, as well as a short critique of various other chromatographic methods for such purposes, was presented elsewhere.<sup>6,7</sup>

In the following, results anticipated from concentration-pulse measurements are compared, within the scope of linear, ideal chromatography, with those of other chromatographic procedures for the simplest example of only one sorbable solute in a nonsorbed carrier gas. Next, concentration-pulse migration in the general binary and in multicomponent systems is considered. A study of the influence of mobile-phase velocity on the criterion for self-sharpening boundaries follows. Finally, questions concerning the reduction to practice of these idealized results are taken up.

### Influence of Equilibrium

We begin with the recognition that mobile-phase velocities will be different in zones of different solute concentration and consider first only the influence of equilibrium on migration rates of boundaries and pulses. We thus assume that concentrations and mobile-phase velocity change discontinuously at a boundary between values which are everywhere constant within their respective zones (one-dimensional column and linear, ideal chromatography). In all but one of the following cases this condition is equivalent to the two assumptions: (1) local equilibrium and absence of all diffusional effects (no boundary or band broadening due to kinetic factors); and (2) the isotherm of the solute is linear in the range of concentrations contained in the boundary or band (no broadening due to equilibrium factors).

Use will also be made of the following assumptions: (3) the range of solute concentrations covered in the band or boundary is negligible compared to the concentration of carrier; (4) the mobile phase is an ideal gas; (5) there is no influence of heat of sorption; and (6) decreases in the void volume due to stationary-phase volume increases are negligible ( $V_g$  is constant).

It will be possible to relax certain of these assumptions in some cases<sup>8</sup> as summarized in Table I. The effects of removal of either assumption 1 or 2 form the subjects of later sections. We shall invariably assume that: (7) the pressure drop is negligible; and (8) solute concentrations in a supported stationary phase (g.l.c.) are not affected by the support.

The derivations are concerned with gas-solid or gas-liquid chromatography, in which the effects of mobile-phase velocity variations are far more significant than in liquid-phase chromatography, for which DeVault's treatment<sup>3</sup> will ordinarily be entirely adequate.

(1) G. Schay, "Theoretische Grundlagen der Gaschromatographie," Veb Deutsche Verlag der Wissenschaften, Berlin, 1961, Chapters 1 and 4.

(2) C. H. Bosanquet in "Gas Chromatography 1958," D. H. Desty, Ed., Butterworth and Co., Ltd., London, 1958, p. 107.

(3) D. DeVault, *J. Am. Chem. Soc.*, **65**, 532 (1943).

(4) M. J. E. Golay, *Nature*, **202**, 489 (1964).

(5) See, for example, J. F. K. Huber and A. I. M. Keulemans in "Gas Chromatography 1962," M. van Swaay, Ed., Butterworth, Inc., Washington, D. C., 1962, p. 26.

(6) F. Helfferich and D. L. Peterson, *Science*, **142**, 661 (1963).

(7) Tracer-pulse chromatography and possibly the influence of the velocity effect in chromatographic measurements at high solute concentrations appear to be contained in a treatment of F. I. Stalcup and H. A. Deans, *A.I.Ch.E. J.*, **9**, 107 (1963).

(8) Assumption 4 can, of course, in any event be removed through the introduction of an equation of state for real gases, but it is retained here for simplicity and clarity.

Table I: Underlying Assumptions of Derivations

Assumption	Case				
	Small sample	Large sample	Frontal analysis	Tracer pulse	Concentration pulse
1. Local equilibrium and no diffusional spreading	x	x	x	x	x
2. Linear isotherm in range of boundary	x	x	Removable	Condition met	x
3. Concentration change is small	x			Condition met	x
4. Gas-phase ideality		x	x	Not required	x
5. No heat of sorption	x	x	x	Condition met	x
6. $V_g$ is constant	x	x		Condition met	x
7. No pressure drop	x	x	x	x	x
8. Inert support in g.l.c.	x	x	x	x	x
9. Constant mobile-phase velocity	Superseded				
10. Equal equilibrium isotopic distribution				x	

Binary Mobile Phase with One Sorbable Component.

In this section we consider a binary feed gas consisting of one sorbable component (the solute) and one non-sorbable component (the carrier).

A. *Small-Sample Pulse in a Pure Carrier.* It will be instructive to consider first an ordinary chromatographic measurement at vanishing solute concentration, which technique is distinguished below by the term "small-sample case." It is pictured in Figure 1a, in which the shaded region shows the mobile- and stationary-phase concentration profiles  $C_1$  and  $\bar{C}_1$  of an idealized pulse of sorbable solute in moles per unit volume of the respective phase.<sup>9</sup> The broken outline shows the pulse after it has advanced a distance  $dz$  along the column. In this one instance, the usual additional assumption is tentatively made that: (9) the mobile-phase velocity  $v_i$  within the boundaries of the pulse is equal to the velocity  $v_0$  ahead of and behind the pulse. The rate of migration of the pulse, or what is equivalent in the present approximation, of the leading boundary, is obtained by writing the material balance around the element of column volume whose length is  $dz$ . If the length and void volume of the column are, respectively,  $L$  and  $V_g$ , then the amount of solute entering this element in the time  $dt$  during which the boundary traverses  $dz$  is  $C_1 V_g v_0 dt/L$ , and the increase within it is  $(C_1 V_g + \bar{C}_1 V_s) dz/L$ . Since none leaves, these two quantities must be equal and we have for the velocity of the boundary

$$v_b \equiv \frac{dz}{dt} = \frac{C_1 V_g v_0}{C_1 V_g + \bar{C}_1 V_s} \tag{2}$$

The retention volume is

$$V_R = V_g v_0 / v_b \tag{3}$$

Together, these equations lead to eq. 1 or in terms of the adjusted retention volume  $V_{R'} \equiv V_R - V_g$ , to

$$V_{R'} = \bar{C}_1 V_s / C_1 \tag{4}$$

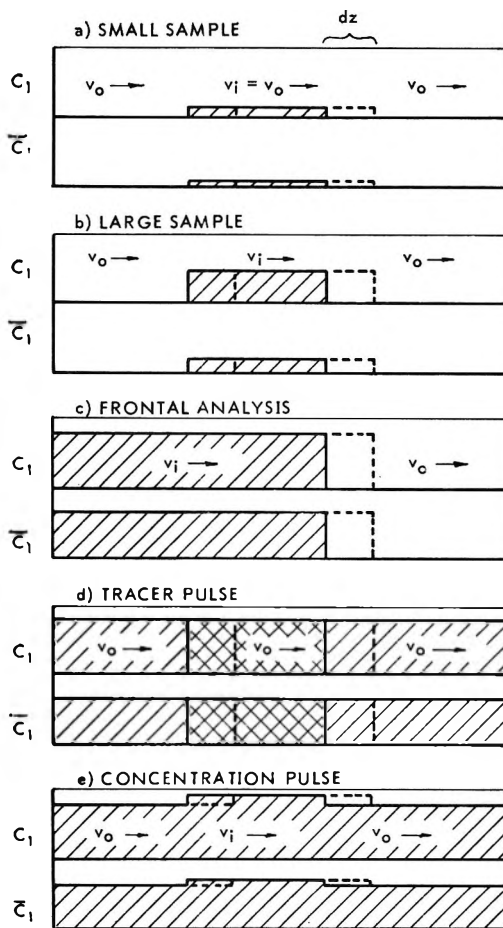


Figure 1. Illustration of solute concentration profiles in the mobile (upper half) and stationary (lower half) phases and of their progress through an element of column length  $dz$ .

B. *Large-Sample Pulse in a Pure Carrier.* This case, which differs from the small-sample case only through its divestiture of the assumption of constant velocity,

(9) The use of these concentration units is arbitrary, and any other choice may be made so long as the units are consistent.

is illustrated by Figure 1b. The amounts of solute of concern are

$$\begin{aligned} \text{entering: } & C_1 V_g v_i dt/L \\ \text{leaving: } & \text{none} \\ \text{increasing: } & (C_1 V_g + \bar{C}_1 V_s) dz/L \end{aligned}$$

The corresponding amounts of carrier are

$$\begin{aligned} \text{entering: } & (C - C_1) V_g v_i dt/L \\ \text{leaving: } & C V_g v_0 dt/L \\ \text{increasing: } & -C_1 V_g dz/L \end{aligned}$$

where  $C$  is the total molar concentration in the mobile phase. Equating the net flux to the increase, we obtain for the solute

$$v_b = \frac{C_1 V_g v_i}{C_1 V_g + \bar{C}_1 V_s} \quad (5)$$

and for the carrier

$$v_b = \frac{C v_0 - (C - C_1) v_i}{C_1} \quad (6)$$

Elimination of  $v_i$  leads to

$$v_b = \frac{C_1 V_g v_0}{C_1 V_g + \bar{C}_1 (C - C_1) V_s / C} \quad (7)$$

and with eq. 3 to

$$V_{R'} \equiv V_R - V_g = \frac{\bar{C}_1 (C - C_1) V_s}{C_1 C} = \frac{\bar{C}_1 V_s}{C_1} \left( 1 - \frac{C_1}{C} \right) \quad (8)$$

An expression equivalent to eq. 7 was derived by Golay.<sup>4</sup> Equation 8 reduces immediately to the small-sample result when  $C_1$  is negligible compared with  $C$ . If this is not true, the actual retention volume is lowered from that obtained with a small sample by the mobile-phase mole fraction of solute  $C_1/C$ . Because of the variation of  $C_1$  across a real band and with the length of column traversed, a criterion of negligible influence of  $v_i > v_0$  on a retention volume measurement must involve the initial, maximum value of  $C_1$  at the column entrance.

As a derivation of eq. 1 for a small sample, that represented by eq. 5 through 8 with  $C_1 \ll C$  is in closer alignment with physical reality and is more self-consistent than that represented by eq. 2 through 4 under reliance on the premise that  $v_i = v_0$ . That this premise leads to contradictions is quickly verified when one attempts to write the material balance for the carrier according to the small-sample approach; with  $v_i = v_0$  one obtains

$$v_b = v_0 \quad (9)$$

Combined with eq. 2 this leads to the requirement  $\bar{C}_1 = 0$ , whereas the solute is supposed to be sorbable. On the other hand, there arises no contradiction at any point in the derivation of eq. 8 if  $C_1$  is assumed to be small. These considerations verify the necessity that  $v_i > v_0$  no matter how small the size of a sorbable solute sample. That is, the sorbed molecules provide a continual source and sink within the band; coherence of the band exists, and *advance of sorbed molecules occurs only if the mobile-phase velocity is higher within the band than outside it.*

*C. Frontal Analysis in an Initially Solute-Free Column.* In frontal analysis, the different velocities on each side of the boundary persist at the respective ends of the column (Figure 1c). In terms of the effluent volume  $V_{R_0}'$ , which moves through the column with velocity  $v_0$ , its value from eq. 9 is

$$V_{R_0}' = C_c \bar{C}_1 V_s / C_1 C \quad (10)$$

in which  $C_c$  is the mobile-phase concentration of non-sorbed carrier. On the other hand, if the retention volume is measured by the volume of influent gas  $V_{R_1}'$ , then the result takes the form of eq. 1

$$V_{R_1}' = \bar{C}_1 V_s / C_1 \quad (11)$$

It may be noted that

$$V_{R_0}' = C_c V_{R_1}' / C \quad (12)$$

*i.e.*, that the (adjusted) amount of carrier entering equals, as it must, that leaving. A value of frontal analysis is in the measurement of nonlinear isotherms, where asymmetrical spreading of the front, in the rare cases where it is produced by nonlinearity, does not disturb the measurement of  $V_{R_1}'$ , which is, in practice, determined by the center of gravity of the front. Also, constancy of  $V_g$  with  $\bar{C}_1$  need not be assumed because the value appropriate to eq. 10 is a readily obtainable experimental quantity. The influence of the variation of mobile-phase velocity with solute concentration on the criterion for asymmetrical spreading is taken up in a later section.

*D. Tracer Pulse.* Figure 1d brings out the singular features of tracer-pulse chromatography. The cross-hatched areas depict a pulse containing tagged (*e.g.*, radioactive) solute molecules. The ordinarily closely approached approximation is made that: (10) the equilibrium distribution is the same for the tagged as for the untagged molecules.

With this assumption, although  $(C_1, \bar{C}_1)$  may represent a point on a nonlinear isotherm, the distribution of tagged molecules,  $\bar{C}_1^*/C_1^*$ , is, for all values of  $\bar{C}_1^*$  and

$C_1^*$ , constant and equal to  $\bar{C}_1/C_1$ . This means that apart from the influence of diffusional effects, band spreading cannot occur. Assumptions of mobile-phase ideality, zero heat of sorption, and constancy of void volume are superceded by that of equality of equilibrium distribution of both isotopes, which also ensures that  $v_1 = v_0$ .

For the tagged pulse we can write, in the same manner as above, for the amounts of *tagged solute* entering, leaving, and increasing within the volume element whose length is  $dz$  which is traversed by the leading boundary of the tracer pulse in time  $dt$

entering:  $C_1^*V_g v_0 dt/L = C_1 V_g v_0 dt/L$

leaving: none

increasing:  $(C_1^*V_g + \bar{C}_1^*V_s)dz/L = (C_1 V_g + \bar{C}_1 V_s)dz/L$

and obtain for the result of a tracer-pulse retention volume measurement

$$V_{R'} = \bar{C}_1 V_s / C_1 \tag{13}$$

*E. Concentration Pulse in a Partially Presaturated Column.* The conditions of a concentration-pulse measurement are shown in Figure 1e; the column is initially equilibrated throughout with a feed gas containing solute at a finite concentration (partial presaturation), and a pulse concentration change superimposed. A *step* concentration change (frontal analysis in a partially presaturated column) would, in this idealized binary case, travel at the same rate; the assumption of a linear isotherm in the range of  $C_1$  and  $\bar{C}_1$  covered by such a step could then be relaxed for the same reason as in the frontal analysis case in an initially solute-free column above. It is retained in the case of a concentration *pulse* because otherwise an asymmetrical peak will be obtained in practice for which  $V_{R'}$  will not be unambiguously defined.

Following the usual procedure, and introducing  $C_1 + \delta C_1$  and  $\bar{C}_1 + \delta \bar{C}_1$  for the concentrations of solute within the boundaries of the pulse, we have with respect to the volume element of length  $dz$  traversed by the boundary in time  $dt$

solute entering:  $(C_1 + \delta C_1)V_g v_i dt/L$

solute leaving:  $C_1 V_g v_0 dt/L$

solute increasing:  $(\delta C_1 V_g + \delta \bar{C}_1 V_s)dz/L$

carrier entering:  $(C - C_1 - \delta C_1)V_g v_i dt/L$

carrier leaving:  $(C - C_1)V_g v_0 dt/L$

carrier increasing:  $-\delta C_1 V_g dz/L$

Equating net fluxes to net increases, and eliminating  $v_i$ , we obtain

$$V_{R'}(C_1) = (C - C_1 - \delta C_1)\delta \bar{C}_1 V_s / C \delta C_1 \tag{14}$$

If  $\delta C_1 \ll (C - C_1)$ , then because we have presumed linearity of the isotherm in the range  $\delta C_1$ ,  $\delta \bar{C}_1$ , eq. 14 may be rewritten

$$V_{R'}(C_1) = C_c V_s \frac{d\bar{C}_1}{dC_1} / C \tag{15}$$

in which  $d\bar{C}_1/dC_1$  is the slope of the isotherm at  $C_1$ .

It will be noted that eq. 15 assumes the correct form (eq. 1) as  $C_1$  approaches zero

$$\lim_{C_1 \rightarrow 0} V_{R'}(C_1) = \bar{C}_1 V_s / C_1 \tag{16}$$

inasmuch as in the small-sample case it is assumed that  $C_1 \ll C$  and that  $\bar{C}_1/C_1 = \text{constant}$ . It is of particular importance to recognize that the limiting form of eq. 15 as the concentration change  $\delta C_1$  approaches zero, in contradistinction to the small-sample case, retains the factor  $C_c/C$  if  $C_1 \neq 0$  (concentration pulse) whereas it does not if  $C_1 = 0$  (small sample). Rather, the two cases are exactly parallel in the neglect of  $\delta C_1$  in the concentration-pulse case and of  $C_1$  in the small-sample case. The inadmissible assumption that  $v_i = v_0$  has a graver consequence in an attempted derivation of the concentration-pulse formula in that the result does not contain the factor  $C_c/C$ , while the contradiction  $\delta \bar{C} = 0$  also appears.<sup>10</sup>

That the factor  $C_c/C$  must appear may be somewhat surprising; its presence owes to the fact that the portion of sorbed molecules comprising the pulse (band width times  $V_s \delta \bar{C}_1/L$ ) is transported at an accelerated rate relative to the small-sample case. Equation 14 may be rewritten

$$v_b = \frac{\delta C_1 V_g v_0}{\delta C_1 V_g + \frac{(C_c - \delta C_1)}{C} \delta \bar{C}_1 V_s} = \frac{\delta C_1 V_g v_i}{\delta C_1 V_g + C_c \delta \bar{C}_1 V_s / C} \tag{17}$$

Thus the velocity of the boundary is inversely proportional to  $C_c \delta \bar{C}_1 / C = \delta \bar{C}_1 - C_1 \delta \bar{C}_1 / C$  rather than to  $\delta \bar{C}_1$  as in the small-sample case. This term expresses

(10) It might also be noted that in contrast to the frontal analysis case, a reduction to the form of eq. 1 is not produced by expressing the retention volume by the volume of carrier only,  $V_{R_c}(C_1)$  (compare eq. 10, 11, and 12). This latter quantity is  $C_c V_{R_c}(C_1)/C$ , so that

$$V_{R_c}(C_1) = C_c^2 V_s \frac{d\bar{C}_1}{dC_1} / C^2 \tag{15a}$$

the fact that the time required to transport the amount  $V_s \delta \bar{C}_1 / L$  through a given volume element is, in a concentration-pulse experiment, reduced according to the fraction of solute in the mobile phase.

Experimentally, it will always be more convenient to measure  $v_0$  than  $v_1$  (eq. 17) and to ensure that  $\delta C_1 \ll (C - C_1)$ . Evidently, a concentration pulse measurement will be subject to the same type of error as expressed by a comparison of the large-sample with the small-sample cases.

*Mobile Phase with More than One Sorbable Component.*

*A. Binary Case.* The previous section, in which one of the two components of a binary feed gas was presumed nonsorbable, represents a limiting case of the general binary problem. Also, it was shown therein that the concentration-pulse case contains those of the large and of the small sample, as well as of frontal analysis, as special cases. We therefore examine under the above heading only the concentration-pulse formula for pulse migration when the feed gas is a binary mixture in which both components are sorbed.

The procedure is extended to take into account the sorption of the second solute. The amounts of each solute entering and leaving, and the net gain within the volume element of length  $dz$  through which the boundary passes in the time  $dt$ , are

$$\text{solute 1 entering: } (C_1 + \delta C_1) V_g v_1 dt / L$$

$$\text{solute 1 leaving: } C_1 V_g v_0 dt / L$$

$$\text{solute 1 increasing: } (\delta C_1 V_g + \delta \bar{C}_1 V_s) dz / L$$

$$\text{solute 2 entering: } (C_2 + \delta C_2) V_g v_1 dt / L$$

$$\text{solute 2 leaving: } C_2 V_g v_0 dt / L$$

$$\text{solute 2 increasing: } (\delta C_2 V_g + \delta \bar{C}_2 V_s) dz / L$$

With the aid of eq. 3, the general form of the binary equation is found to be

$$V_{R'} = V_s \left[ \frac{\delta \bar{C}_1}{\delta C_1} - \frac{C_1}{C} \left( \frac{\delta \bar{C}_1}{\delta C_1} + \frac{\delta \bar{C}_2}{\delta C_1} \right) \right] \quad (18)$$

or since  $\delta C_1 + \delta C_2 = 0$ , and with assumption 2

$$V_{R'} = \frac{V_s}{C} \left( C_2 \frac{d\bar{C}_1}{dC_1} + C_1 \frac{d\bar{C}_2}{dC_2} \right) \quad (19)$$

It should be noted in eq. 19 that the contribution of each solute to the retention volume is weighted by the content in the gas phase of the *other* solute. If solute 2, say, is present in excess, then even if it has the greater isotherm slope, still that of the minor component, solute 1, is alone determining. Equation 18 is observed to simplify, with the appropriate substitutions, to eq. 15, 10, 8, or 1. In the special case of con-

stant total amount sorbed, as, for example, if solutes 1 and 2 were isotopes, and therefore had identical isotherms (except for negligible differences in equilibrium isotopic distribution), since then  $\delta \bar{C}_1 + \delta \bar{C}_2 = 0$  (aside from the negligible effect of changes in stationary-phase volume in g.l.c.)<sup>11</sup>

$$V_{R'} = V_s \frac{d\bar{C}_1}{dC_1} = V_s \frac{d\bar{C}_2}{dC_2} \quad (20)$$

Constancy of total amount sorbed ensures that the mobile-phase velocity does not vary with concentration, so that as in the formulas for small-sample and tracer-pulse migration, the concentration term ( $C_1/C$  or  $C_2/C$ ) is absent.

*B. Multicomponent Case.* Whereas the constraint  $\delta C_1 + \delta C_2 = 0$  in the binary cases limits the number of simultaneous boundaries to one, in ternary and higher systems an arbitrary concentration disturbance at the column inlet gives rise to generally more than one boundary. This fact is well known in frontal analysis of mixtures in an initially solute-free column, where a description of the migration rates of the various boundaries (of which there may be as many as  $n - 1$  in an  $n$ -component system) is straightforward.<sup>1</sup>

A particularly instructive example of multiple boundaries in a multicomponent system is found in the limiting case of  $n$  sorbable components, all at very low concentrations in a large excess of carrier gas. For a binary system with only one such trace component it is readily seen from eq. 15 that a pulse of pure carrier gas, which interrupts the continuous flow of the trace component, travels with a rate governed by the limiting slope of the isotherm exactly as is that of a solute pulse in ordinary small-sample chromatography. Thus the rates of migration of a solute "hole" in a column wherein the solute elsewhere exists at a constant, trace level, and of a trace-level solute pulse in an otherwise solute-free column, are equal. In the multicomponent system, if all the sorbable species are at trace levels, the sorbent will not be significantly loaded and the individual isotherms will not be influenced by one another. If the continuous flow of all trace components is interrupted by the injection of a pulse of pure carrier gas, a hole for each component will therefore arise and travel independently of the others, and at its characteristic rate, giving what might be called a mirror image of an ordinary small-sample multicomponent chromatogram.<sup>12</sup> The injected single pulse of pure carrier thus breaks up into  $n$  different pulses emerging at different

(11) It is partially because in liquid-phase chromatography the condition of constant total amount sorbed is much more closely approached that the velocity effect is likely to have little consequence there.



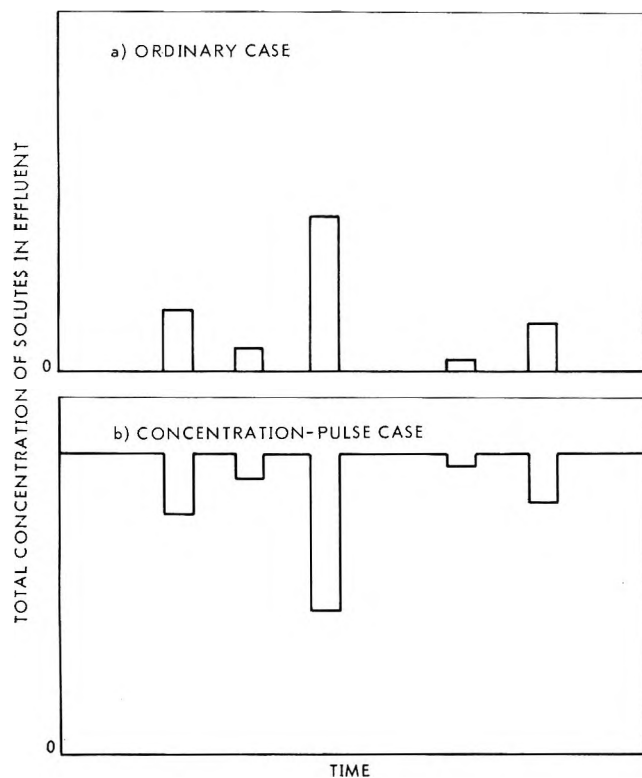


Figure 2. Comparison of idealized chromatograms of a hypothetical mixture obtained in the ordinary case with a small-sample pulse in a nonsorbed carrier and in the concentration-pulse case with a carrier pulse in a feed gas consisting of a nonsorbed carrier and of the solutes at trace levels.

times, each with one sorbable component missing and the others present at their inlet concentrations; a hypothetical chromatogram of this sort is compared in Figure 2 with one which would be obtained with the same mixture in an ordinary chromatographic analysis. This particular limiting case greatly aids a general understanding of chromatographic behavior in multicomponent systems. First, it helps to overcome the intuitive objection to the production of a multiplicity of boundaries by one disturbance. Second, it demonstrates that in multicomponent systems also, the migration rate of any disturbance, whether pulse, hole, or step, is chiefly governed by the trace component rather than by that one present in excess (compare eq. 19 for the binary case).

The prediction of rates of migration of concentration steps where this simple behavior does not occur, and more particularly, of pulses, appears to be an involved problem in multicomponent systems. It is a simple matter, however, to write the formula for the retention volume  $V_{R_m}'$  of an assumed stable boundary, m. For this purpose, the sum over the two components of the binary eq. 18 is replaced by one over all com-

ponents. It is then required for each component  $j$  of the mixture that

$$V_{R_m}' = V_s \left[ \frac{\delta \bar{C}_j}{\delta C_j} - \frac{C_j}{C} \sum_k \frac{\delta \bar{C}_k}{\delta C_k} \right] \quad (21)$$

Unlike eq. 19, which for the binary case is a unique relation between a single boundary and the relevant binary sorption isotherms, eq. 21 is by itself an inadequate description of the general case as it does not indicate with which particular values of  $\delta C_j$  and  $\delta \bar{C}_k$  the boundary is stable.

The complexity even of the binary concentration-pulse method, and more so, of those involving higher multiplicity, and further the differential nature of such measurements, are to be contrasted with the tracer-pulse technique. Equation 13, obtained above for the case of a tracer pulse of a single solute in a nonsorbed carrier, generalizes immediately to cases of any degree of complexity, and allows a direct, integral measurement of  $\bar{C}_j$  for any component of the mixture.

*Criterion for a Self-Sharpening Boundary.* The discussion so far has been limited to the influence of equilibrium on migration rates of steps and pulses. It is clear that these rates are determined by the isotherm slope. Strictly, this property is also shared by the tracer-pulse case and by frontal analysis wherein although a large concentration change or a nonlinear isotherm may be involved, the conditions of the respective experiments are such that the average slope in this range, and therefore the integral difference between the extremes, is in fact measured. Also, in the small-sample case an integral measurement results only because of the occurrence of isotherm linearity. In the present section, we relax this assumption in order to examine the combined influence of velocity variation and isotherm shape on band or boundary shape, still under the assumption of local equilibrium and absence of diffusional spreading.

The effect of isotherm curvature on the shapes of chromatographic bands<sup>3</sup> and sorption and exchange fronts<sup>13,14</sup> when velocities are assumed constant is well known. Suppose an elution chromatographic pulse encompasses concentrations on an isotherm characterized by decreasing isotherm slope with increasing mobile-phase concentration:  $(d^2 \bar{C}_1 / dC_1^2) < 0$ . Portions of the band which contain the highest values

(12) This general type of behavior, although not with trace components, has been observed by A. A. Zhukhovitskii and N. M. Turkel'taub, *Dokl. Akad. Nauk SSSR*, **143**, 646 (1962).

(13) F. Helfferich, "Ion Exchange," McGraw-Hill Book Co., Inc., New York, N. Y., 1962, Chapter 9.

(14) T. Vermeulen in "Advances in Chemical Engineering," Vol. II, Academic Press, New York, N. Y., 1958, p. 147 ff.

of  $C_1$  and  $\bar{C}_1$  then move with higher velocity than those containing lower values. This follows for the small-sample case when the migration rate is obtained from eq. 17 by setting  $C_e = C$  and  $v_i = v_0$

$$v_b = v_0 \left/ \left( 1 + \frac{\delta \bar{C}_1 V_s}{\delta C_1 V_g} \right) \right. \quad (22)$$

As discussed by DeVault,<sup>3</sup> this self-sharpening effect gives rise, with the other present assumptions retained, to a peak with a vertical front boundary and a diffuse rear boundary. The criterion for a self-sharpening front boundary is simply that  $(d^2\bar{C}_1/dC_1^2) < 0$ . From eq. 22 it is seen that the occurrence of higher velocities with increased concentrations reinforces this sharpening effect.

Now in the reverse example, that is, of a peak whose concentrations span an isotherm with positive curvature  $(d^2\bar{C}_1/dC_1^2) > 0$ , it is the front boundary which becomes diffuse and the rear boundary which is self-sharpening. The criterion for a self-sharpening rear boundary, if  $v_i = v_0$ , is  $(d^2\bar{C}_1/dC_1^2) > 0$ . From eq. 22 it is seen that, with isotherms of such curvature, the occurrence of higher velocities at higher concentrations counteracts the effect of equilibrium on the boundary shapes.

In the special example of a linear isotherm, with  $(d^2\bar{C}_1/dC_1^2) = 0$ , all regions of a band would migrate with equal rate if the mobile-phase velocity were constant. Spreading and sharpening through equilibrium effects would then be absent; the front as well as the rear boundary would retain their original shapes. It is apparent, then, that allowance for the velocity variation in the mobile phase will alter the self-sharpening criterion, and that an absence of sharpening and spreading through equilibrium effects will be found with a particular *nonlinear* isotherm shape; *i.e.*, it is possible for a *nonlinear isotherm to produce symmetrical peaks*.

The criterion for self-sharpening boundaries is presented below for the simplest case of a solute pulse in a nonsorbed carrier flowing through an initially solute-free column, and its significance considered; more general cases are thereafter briefly outlined. The criterion for self-sharpening front or rear boundaries for a single solute pulse in a nonsorbed carrier follows immediately from the formula for the retention volume derived without the limitation that  $v_i = v_0$ . It is required, then, that eq. 8 for a large sample applies with the same value of  $V_R'$  to all concentrations if the boundary is neither to sharpen nor to spread.<sup>15</sup> This means simply that it is in terms of  $\bar{C}_1(C - C_1)/C_1C$ , and not of  $\bar{C}_1/C_1$ , that the criterion is to be drawn. The same is true in the frontal analysis case (in an

initially solute-free column, eq. 10). A leading boundary (increasing  $C_1$  with time at a certain  $z$ ) is thus self-sharpening if the isotherm has a curvature which is lower than that of the function

$$\bar{C}_1 = kC_1/(C - C_1) \quad (23)$$

in which  $k$  is a constant. Then front boundaries are self-sharpening if

$$\frac{d^2\bar{C}_1}{dC_1^2} < \frac{2\bar{C}_1C}{C_1(C - C_1)^2} \quad (24)$$

and rear boundaries, if

$$\frac{d^2\bar{C}_1}{dC_1^2} > \frac{2\bar{C}_1C}{C_1(C - C_1)^2} \quad (25)$$

where  $\bar{C}_1$  is the isotherm under test.<sup>16</sup> The difference between the exact criteria 24 and 25 and those derived with  $v_i = v_0$  is greatest when the distribution coefficient  $\bar{C}_1/C_1$  is high and the total mobile-phase concentration  $C$  is low, and when the mole fraction of solute in the mobile phase  $C_1/C$  is large. The former conditions prevail particularly at lower column pressures, and the latter one in frontal analysis. It seems probable that under the conditions of gas-phase elution chromatography, the term on the right-hand sides of relations 24 and 25 could attain high values. The practical meaning of this circumstance is that the sort of band asymmetry characterized by a steeper leading than trailing boundary, and generally associated with isotherms having negative curvature, can also be produced by isotherms having appreciable positive curvature. In either event, reductions in  $C_1$  will not completely eliminate the asymmetry even if such a reduction is carried to the point where the isotherm is practically linear. If an experimental lower limit on  $C_1$  exists in the range of a nonlinear isotherm, then relations 24 and 25 imply that the resulting asymmetry in the chromatogram may be reduced by increasing the column pressure.<sup>17</sup>

The self-sharpening criterion for concentration steps and pulses of a single solute in a nonsorbed carrier (in partially presaturated columns) follows from eq. 14, which implies that the balance point occurs when

(15) Strictly, this assertion requires a demonstration that the migration velocity  $v_b(C_1)$  of each *portion* of the boundary, *e.g.*, that with extreme concentrations  $C_1$ ,  $\bar{C}_1$ , and  $C_1 + \delta C_1$ ,  $\bar{C}_1 + \delta \bar{C}_1$ , is solely a function of  $C_1$ . This is ensured by eq. 17.

(16) It is, of course, possible that conditions 24 or 25 apply only over a part of the range of concentrations occurring within the respective boundary. The rather complicated sharpening behavior of boundaries in such cases has been discussed by Tudge (A. P. Tudge, *Can. J. Phys.*, 39, 1600, 1611 (1961)) with the assumption that  $v_i = v_0$ . One can readily extend Tudge's results to the case where  $v_i \neq v_0$  with the aid of conditions 24 and 25.

$$\frac{\delta \bar{C}_1}{\delta C_1} = \frac{k}{(C_1 - C_1^0 - \delta C_1)} = \frac{k}{C - C_1} \quad (26)$$

where  $\delta C_1 = C_1 - C_1^0$  and  $\delta \bar{C}_1 = \bar{C}_1 - \bar{C}_1^0$ ,  $C_1^0$  and  $\bar{C}_1^0$  denoting here the concentrations ahead of the step. The criterion for a self-sharpening leading boundary is then

$$\frac{d^2 \bar{C}_1}{dC_1^2} < \frac{2(\bar{C}_1 - \bar{C}_1^0)(C - C_1^0)}{(C_1 - C_1^0)(C - C_1)^2} \quad (27)$$

which reduces to the form of relation 24 when  $\bar{C}_1^0 = C_1^0 = 0$ .

In similar fashion, the self-sharpening criteria for mixtures containing more than one sorbable component are determined by the requirement of independence of solute concentration of  $V_R'$  and of  $V_{R_m}'$  in eq. 19 and 21 for binary and general cases, respectively. Under conditions which guarantee that the total amount sorbed is constant (eq. 20 for the binary case) the criteria again reduce to those applicable when  $v_i = v_0$ .

### Influence of Nonequilibrium Effects

Up to this point, the assumption of local equilibrium and absence of diffusional spreading (assumption 1) has been retained throughout. Since this condition is essentially never met in actual operation, the question arises as to how far the deductions reached above are useful in practice.

In calculations of peak or boundary shapes in large-sample chromatography and in frontal analysis, the variation of mobile-phase velocity with solute concentration introduces a new complication in theories which are already quite complex even before kinetic limitations are introduced, and their effect does not concern us here. Rather, it is exactly those chromatographic methods which are well suited for rapid and convenient determinations of equilibrium properties for which a relaxation of assumption 1 does not interfere with the use of the equations derived for them. The experimental procedures of these techniques, tracer-pulse and concentration-pulse (or small-step) chromatography, have in common with ordinary small-sample chromatography the capacity of meeting the requirements of eq. 1, namely, the isotherm curvature within the covered range can be made negligible, and  $v_i$  can be brought very nearly equal to  $v_0$ . With these two conditions, and with a column long enough for end effects to be negligible, spreading of bands and boundaries by finite rates of sorption and desorption and by longitudinal diffusion is known from chromatographic theories and practical experience to follow the same simple laws as diffusion. Accordingly,

spreading introduced by these factors is symmetrical about the center of a band, or about the midpoint of a boundary. The derived equations relating the retention volume to the sorption isotherm thus still hold if assumption 1 is relaxed, provided one identifies the retention volume with these points about which symmetrical spreading occurs.

In the particular case of the tracer pulse, an even more general argument can be advanced which is independent of the condition of symmetrical spreading. Provided that each sorbable molecule in its passage through the column undergoes many sorption-desorption steps, a premise which is at the very heart of any chromatographic theory and experiment, eq. 13 is an exact expression for the *average* retention volume of the individual molecules of a species in an equilibrated column operated without any change in the input rate and composition, and under conditions which ensure a negligible pressure drop. This follows from a material balance around the whole column and is true regardless of spreading effects in the column, whatever their cause. If the sorbent does not distinguish between the isotopes, the average retention volume is the same for both isotopic species. Therefore, eq. 13 must also apply to the average retention volume of the tracer, that is, to that of the center of gravity of the tracer pulse.

### Application to Vapor-Liquid Equilibria

The relations presented for retention volume measurements at nonvanishing sorbent loadings (all cases except that of the small sample) are subject to a qualification in their reduction to practice. Specifically, the constantly sorbed solute under these conditions is a significant component of the stationary phase so that where stationary-phase concentrations are expressed in terms of the total volume including all solutes (gas-liquid as opposed ordinarily to gas-solid and liquid-solid chromatography), the true value of  $V_s$  is not immediately known. Incorporation of this complication is illustrated below for concentration and tracer pulses, and a special case of the latter described, in which  $V_s$  need not be known explicitly at all.

Equilibria involving liquids are conventionally expressed with the aid of the activity coefficient in the liquid phase

(17) The inverse proportionality of the isotherm curvature on the total mobile-phase concentration  $C$  in relations 24 and 25 is a mathematical expression of the ability of more condensed mobile phases to support the advance of sorbed solute at a given stationary-phase concentration with a smaller resultant increase in velocity than can more rarefied mobile phases. This is an independent reason why velocity variations, and their consequences, are quite minor in *liquid-phase chromatography*, where the mobile phase, too, is a condensed one.

$$\gamma_1(y_1) = y_1 P / x_1 p_1^0 \quad (28)$$

where  $x_1$  and  $y_1$  are the mole fractions of solute 1 in the liquid and gas phases, respectively,  $P$  is the column pressure, and  $p_1^0$  is the vapor pressure of liquid solute at the temperature of measurement. Under the assumption of gas-phase ideality and with  $M_s$  equal to the number of moles of stationary phase in the column (including solutes), the activity coefficient is related to concentrations through

$$\gamma_1(C_1) = \frac{M_s RT C_1}{V_s p_1^0 \bar{C}_1} \quad (29)$$

Substitution by eq. 1 leads to the relation between the limiting value of  $\gamma_1(C_1)$  as  $C_1$  approaches zero and the retention volume measured with a small sample

$$\gamma_1 = \frac{M_s RT}{p_1^0 V_{R_1}'} \quad (30)$$

Now in the concentration- and tracer-pulse methods,  $M_s$  includes a contribution  $x_1 M_s$  during the measurement of  $V_{R_1}'$ . If  $M_s'$  moles of nonvolatile, stationary solvent were originally present before the introduction of a single solute into the feed gas, then during the experiment  $M_s'$  is increased to  $M_s'/(1 - x_1)$ .<sup>18</sup> From eq. 13 we then have for tracer-pulse measurements with one sorbable component only

$$\gamma_1(C_1) = \frac{M_s' RT}{p_1^0 V_{R_1}'(C_1)(1 - x_1)} \quad (31)$$

from which  $x_1$  may be eliminated to give

$$\gamma_1(y_1) = \frac{1}{p_1^0} \left[ \frac{M_s' RT}{V_{R_1}'(y_1)} + y_1 P \right] \quad (32)$$

For concentration-pulse measurements involving only one sorbable component, one has from eq. 15, 28, and 29, and with  $M_s(1 - x_1) = M_s'$

$$\frac{dx_1}{dy_1} = \frac{P V_{R_1}'(y_1)(1 - x_1)^2}{M_s' RT(1 - y_1)} \quad (33)$$

where  $dx_1/dy_1$  is evaluated at  $y_1$ . Whereas gas-solid chromatographic results lead directly to sorption isotherms through a graphical integration of eq. 15, such is true of vapor-liquid results only if the term  $(1 - x_1)^2$  may be neglected in eq. 33. Otherwise, the most direct approach is to obtain the isotherm, as in the gas-solid case, on a *solute-free* basis, by graphical integration of

$$\frac{dx_1'}{dy_1} = \frac{P V_{R_1}'(y_1)}{M_s' RT(1 - y_1)} \quad (34)$$

where  $x_1'$  is the solute:solvent mole ratio

$$x_1' = \frac{x_1}{1 - x_1} \quad (35)$$

and from which  $x_1(y_1)$  may be evaluated immediately, and, through eq. 28,  $\gamma_1(y_1)$ . The derivation of multi-component  $\gamma$ 's is considered below only for the tracer-pulse case, for which a significant simplification occurs.

When the feed fluid in a tracer pulse contains more than one sorbable component, the only effect on eq. 13 is the contribution of these added solutes to the amount of stationary phase. Thus for the determination of the activity coefficient of the  $j$ th component, eq. 31 generalizes immediately to

$$\gamma_j(C_j) = \frac{M_s' RT}{p_j^0 V_{R_j}'(C_j)(1 - \sum_k x_k)} \quad (36)$$

If  $V_{R_j}'(C_j)$  is measured for each solute, eq. 36 may be rewritten in terms of the known  $y_k$

$$\gamma_j(y_j) = \frac{[M_s' RT + P \sum_k y_k V_{R_k}'(y_k)]}{p_j^0 V_{R_j}'(y_j)} \quad (37)$$

The method may be extended to the determination of vapor-liquid equilibria in the absence of a stationary solvent of negligible volatility. If the distinction of the stationary component is removed, and all species considered as volatile and present in the gas phase, then the total number of moles of solute is

$$M_s = \frac{P}{RT} \sum_k y_k V_{R_k}'(y_k) \quad (38)$$

An accurate knowledge of the value of  $M_s$  (or of  $V_s$ ) is then unnecessary and one has directly from eq. 13, 29, and 38

$$\gamma_i(y_i) = \frac{P}{p_i^0 V_{R_i}'(y_i)} \sum_k y_k V_{R_k}'(y_k) \quad (39)$$

## Conclusion

In the past, the formula for the rates of migration of chromatographic boundaries and pulses, and the influence of equilibrium on their shapes, have been taken directly over from liquid-phase chromatography to gas-phase chromatography, and, until recently, the efficacy of this procedure has gone unchallenged. Not only has it tended to conceal the fundamental essence of boundary and pulse migration, by carrying the implication that sorbed molecules can advance through a chromatographic column without contributing to the mobile-

(18) This solvent swelling will also decrease  $V_g$  from its original value, so that for most accurate work,  $V_g$  would be measured (by the retention volume of a pulse of nonsorbed molecules otherwise not present in the feed gas) for each solute concentration employed.

phase flux; it has also obscured what can, in practice, be a very important source of error in correlations of measured gas-liquid and gas-solid chromatographic retention volumes with equilibrium properties. On the other hand, removal of the unrealistic assumption that the mobile-phase velocity remains constant across a boundary or band is straightforward, and the derived result simplifies to the usual formula in the ordinary case under the more rigorous condition that the solute concentration is small. More important, when the solute concentration attains high values during a pulse measurement, or when it is maintained at a high level and pulses or steps are superimposed, correct deductions of migration rates and of boundary shapes are reached only when this variation in mobile-phase velocity is properly taken into account. Again, the resulting formulas simplify to the usual one only in the cases of constant total amount sorbed, or in tracer-pulse chromatography.

#### List of Symbols

$C$	Total molar concentration in the mobile phase, or molar concentration of subscripted component in the mobile phase
$\bar{C}$	Molar concentration of subscripted component in the stationary phase
$\gamma$	Activity coefficient of subscripted component in the stationary phase (eq. 28)

$k$	Concentration-independent constant in eq. 23 and 26
$L$	Column length
$M_s$	Moles of stationary phase in the column
$p^0$	Vapor pressure of subscripted component
$P$	Total column pressure
$R$	Molar gas constant
$t$	Time since the introduction of a pulse or step at the column inlet
$T$	Absolute temperature
$v$	Linear velocity of mobile phase or of a boundary
$V_g$	Void volume of the column
$V_R$	Retention volume measured at pressure $P$
$V_s$	Volume of stationary phase
$x$	Mole fraction of subscripted component in a liquid stationary phase
$y$	Mole fraction of subscripted component in the mobile phase
$z$	Distance from the column inlet

#### Superscripts

'	Adjustment of $V_R$ for $V_g$ (e.g., eq. 8), or solute-free basis
0	Initial values
*	Tagged component of a tracer pulse

#### Subscripts

1,2	Sorbable components
b	Boundary
c	Nonsorbable component
i	Inside region of pulse, or at column inlet
j	One member of a multicomponent feed
m	Multicomponent boundary (eq. 21)
o	Outside region of pulse, or at column exit

## Microwave Absorption and Molecular Structure in Liquids. LXII.

### The Three Dielectric Dispersion Regions of the Normal Primary Alcohols<sup>1</sup>

by S. K. Garg and C. P. Smyth

*Frick Chemical Laboratory, Princeton University, Princeton, New Jersey (Received October 22, 1964)*

The dielectric constants and losses of the ten normal alcohols from propyl through dodecyl have been measured at 20, 40, and 60° at 16 wave lengths from 30,000 to 0.22 cm. The data have been analyzed to obtain three different relaxation times for each alcohol, one in the region from 1 to  $22 \times 10^{-10}$  sec., one in the region from 1.7 to  $5 \times 10^{-11}$  sec., and one in the region from 1.7 to  $4 \times 10^{-12}$  sec. The long relaxation time is attributed, as in previous interpretations, to breaking of the hydrogen bonds in molecular aggregates followed by ROH rotation. The intermediate relaxation time is that characteristic of rotation of the free, monomeric molecule, and the short relaxation time is that for the relaxation of the hydroxyl group by rotation around its C-O bond.

Because of the possibility of strong hydrogen bonding between adjacent molecules, alcohols present a complex and interesting problem in liquid structure, which has been extensively studied by a variety of methods. The first considerable dielectric investigation of alcohols was carried out by Mizushima<sup>2</sup> and discussed by Debye.<sup>3</sup> Subsequent high-frequency measurements indicated two or more absorption regions.<sup>4-8</sup> By using low temperatures, Cole and his co-workers<sup>9-12</sup> were able to bring the dispersion of a few alcohols into the region of audio- and radiofrequencies, with the result that more numerous and more accurate points could be obtained than are possible in the microwave range. With the almost continuous coverage of the spectrum they were able to distinguish three separate dispersion regions, all of the Debye type. In this laboratory, approximate early measurements were made<sup>13</sup> on two octyl alcohols at 9.72 cm. wave length and more extensive measurements<sup>14</sup> were carried out later on several alcohols at 1, 3, and 10 cm. However, these measurements were not sufficiently complete to warrant an exhaustive interpretation. A number of solutions have been measured recently both in the centimeter region and in the infrared,<sup>15</sup> but the results remain to be interpreted. A few measurements in the millimeter wave region<sup>16,17</sup> have indicated the importance of such measurements in interpreting the dielectric behavior of the liquid alcohols in terms of

structure. The availability of apparatus for the measurement of dielectric constant and loss at 2.2 mm. wave length and at meter wave lengths, in addition

- (1) This research was supported by the U. S. Army Research Office (Durham) and by the National Science Foundation. Reproduction, translation, use, or disposal in whole or in part by or for the United States Government is permitted.
- (2) S. Mizushima, *Bull. Chem. Soc. Japan*, **1**, 47, 83, 115, 143, 163 (1926); *Physik. Z.*, **28**, 418 (1927).
- (3) P. Debye, "Polar Molecules," Chemical Catalog Co., New York; N. Y., 1929, p. 95.
- (4) P. Girard and P. Abadie, *Trans. Faraday Soc.*, **42A**, 40 (1946).
- (5) P. Abadie, *ibid.*, **42A**, 143 (1946).
- (6) R. Dalbert, M. Magat, and A. Surdut, *Bull. soc. chim. France*; D345 (1959).
- (7) C. Brot, M. Magat, and L. Reinisch, *Kolloid-Z.*, **134**, 101 (1953).
- (8) C. Brot, Thesis, University of Paris, 1956; *Ann. Phys. (Paris)*; [13] **2**, 714 (1957).
- (9) D. W. Davidson and R. H. Cole, *J. Chem. Phys.*, **19**, 1484 (1951).
- (10) R. H. Cole and D. W. Davidson, *ibid.*, **20**, 1389 (1952).
- (11) F. X. Hassion and R. H. Cole, *ibid.*, **23**, 1756 (1955).
- (12) D. J. Denney and R. H. Cole, *ibid.*, **23**, 1767 (1955).
- (13) W. P. Conner and C. P. Smyth, *J. Am. Chem. Soc.*, **65**, 382 (1943).
- (14) G. B. Rathmann, A. J. Curtis, P. L. McGeer, and C. P. Smyth, *ibid.*, **78**, 2035 (1956).
- (15) A. A. Antony, Thesis, Princeton University, 1963.
- (16) R. W. Rampolla, R. C. Miller, and C. P. Smyth, *J. Chem. Phys.*, **30**, 566 (1959).
- (17) J. A. Saxton, R. A. Bond, G. T. Coats, and R. M. Dickinson; *ibid.*, **37**, 2132 (1962).

to the long-used equipment for the centimeter and radio regions, has made possible a comprehensive investigation of the straight-chain alcohols from *n*-propyl through *n*-dodecyl alcohol. Sufficient data are available on methyl and ethyl alcohols to permit their consideration along with the higher alcohols. The alcohols above dodecyl have melting points so high as to be inconvenient for measurement in our millimeter wave apparatus.

### Experimental

**Method of Measurement.** The complex dielectric constant of the various normal primary alcohols ( $C_3$  to  $C_{12}$ ) was measured at wave lengths of 10.1, 3.22, 1.25, and 0.22 cm. by methods which have been previously described.<sup>18-21</sup> A Boonton Radio Corp. RX meter (Type 250A) was used for measurements in the frequency range 0.5 to 250 Mc./sec. A 50-ohm coaxial adaptor was used to connect the dielectric cell to the bridge terminals, the physical length of this connector being made small in order to keep corrections to a minimum. Standard transmission line equations were used to correct the measured data. The coaxial adaptor was constructed of stainless steel with very thin outer wall and hollow inner conductor so as to provide a poor thermal path between the dielectric cell and the bridge. The sample cell was simply an open circuit coaxial termination, whose capacitance is determined by the length of the cell and the relative radii of the central and outer conductor's opposing surfaces. The cell was calibrated by using standard dielectric liquids of known dielectric constants. The temperature control was provided by a water jacket surrounding the cell, which was further enclosed in a polystyrene foam block for insulation.

**Purification of Materials.** All substances were ob-

tained from Eastman Kodak Company. The method of purification and refractive indices are listed in Table I.

### Experimental Results

The dielectric constant  $\epsilon'$  and loss  $\epsilon''$  of each of the compounds investigated, together with the wave length and temperature at which the measurement was made, are listed in Table II.

As illustrated in Figure 1 for *n*-octyl alcohol, the data show that all of the alcohols measured have three dispersion regions. The dielectric constant and loss were initially plotted in a complex plane<sup>22</sup> as shown in Figure 2 for undecyl alcohol. For all substances studied, it was found that the first dispersion encountered was quantitatively described by a semi-circle with intercepts on the real axis at values  $\epsilon' = \epsilon_{01}$  and  $\epsilon' = \epsilon_{\infty 1}$ , representing the limiting low and high frequency dielectric constants for this dispersion. The lower frequency data were processed with the aid of an IBM 7094 computer,<sup>23</sup> and the values of  $\epsilon_{\infty 1}$  and relaxation time  $\tau_1$  for maximum absorption were determined.

Assuming that the observed results are the sum of overlapping dispersions, the contribution to  $\epsilon'$  and  $\epsilon''$  from this first or lower dispersion region was calculated and then subtracted from the high-frequency results and the remainder was used to estimate the shorter relaxation times  $\tau_2$  and  $\tau_3$ , and  $\epsilon_{\infty 3}$ .

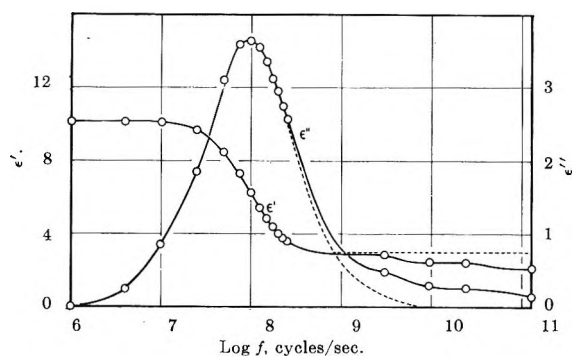


Figure 1. Dielectric constant and loss of *n*-octyl alcohol at 20° against log frequency (in cycles/sec.). Solid lines represent the observed data and dashed lines the calculated behavior for the first dispersion region.

Table I: Method of Purification and Refractive Indices

Compound	$n_{20}^D$	
Propyl alcohol <sup>a</sup>		
Butyl alcohol <sup>a</sup>	1.3994	
Amyl alcohol <sup>a</sup>	1.4099	1.414 (13°) <sup>c</sup>
Hexyl alcohol <sup>b</sup>	1.4180	
Heptyl alcohol <sup>b</sup>	1.4250	1.425 <sup>c</sup>
Octyl alcohol <sup>b</sup>	1.4292	1.430 <sup>c</sup>
Nonyl alcohol <sup>b</sup>	1.4338	
Decyl alcohol <sup>a</sup>	1.4372	
Undecyl alcohol <sup>b</sup>	1.4404	1.4404 <sup>c</sup>
Dodecyl alcohol <sup>a</sup>		

<sup>a</sup> Used as received from the manufacturer. <sup>b</sup> Fractionally distilled twice under reduced pressure. <sup>c</sup> Values from "International Critical Tables."

(18) H. L. Laquer and C. P. Smyth, *J. Am. Chem. Soc.*, **70**, 4097 (1948).

(19) W. M. Heston, A. D. Franklin, E. J. Hennelly, and C. P. Smyth; *ibid.*, **72**, 3443 (1950).

(20) F. H. Branin and C. P. Smyth, *J. Chem. Phys.*, **20**, 1121 (1952).

(21) W. E. Vaughan, W. S. Lovell, and C. P. Smyth, *ibid.*, **36**, 535 (1962).

(22) K. S. Cole and R. H. Cole, *ibid.*, **9**, 341 (1941).

(23) This work made use of computer facilities supported in part by National Science Foundation Grant NSF-GP 579.

Table II: Dielectric Constants and Losses

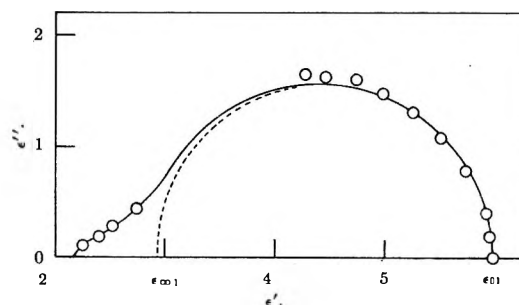
Wave length, cm.	20°		40°		60°		Wave length, cm.	20°		40°		60°	
	$\epsilon'$	$\epsilon''$	$\epsilon'$	$\epsilon''$	$\epsilon'$	$\epsilon''$		$\epsilon'$	$\epsilon''$	$\epsilon'$	$\epsilon''$	$\epsilon'$	$\epsilon''$
<i>n</i> -Propyl alcohol							<i>n</i> -Hexyl alcohol						
30,000	21.10		18.52		16.16		30,000	13.20		11.30		9.49	
3,000	21.00	0.56	18.56	0.56			7,500	13.19	0.22	11.20	0.04		
1,200	21.00	1.14	18.50	0.97	16.14	0.41	3,000	13.12	0.77	11.19	0.23	9.49	0.08
600	20.79	2.21	18.42	1.40	16.14	0.50	1,200	12.83	1.86	11.18	0.61	9.46	0.23
400	20.50	3.20	18.29	1.86	16.15	0.66	600	11.95	3.40	11.03	1.21	9.41	0.44
300	20.00	4.20	18.12	2.33	16.11	0.86	400	10.83	4.41	10.83	1.76	9.39	0.64
240	19.50	5.07	17.95	2.76	16.14	1.10	300	9.58	4.98	10.53	2.29	9.37	0.86
200	18.80	5.83			16.11	1.32	240	8.43	5.26	10.20	2.75	9.28	1.09
171	18.10	6.53	17.71	3.18	16.02	1.52	200	7.44	5.28	9.79	3.17	9.21	1.27
150	17.40	7.27	17.49	3.64	15.91	1.77	171	6.59	5.18	9.39	3.50	9.11	1.49
133	16.50	7.86	17.29	4.06	15.93	1.99	150	5.92	5.02	8.93	3.82	9.01	1.67
120	15.70	8.42	17.01	4.58	15.89	2.23	133	5.34	4.85	8.46	4.06	8.88	1.89
10.1	4.35	2.70	5.36	3.50	6.77	5.50	120	4.89	4.64	8.03	4.31	8.76	2.12
3.22	3.53	1.16	3.66	1.64	3.92	2.42	10.1	3.08	0.74	3.33	1.22	3.78	1.66
1.25	3.20	0.72	3.28	0.95	3.35	1.34	3.22	2.75	0.46	2.83	0.60	3.03	0.86
0.22	2.48	0.57	2.53	0.57	2.29	0.55	1.25	2.55	0.29	2.62	0.42	2.70	0.54
							0.22	2.31	0.17	2.27	0.22	2.26	0.27
<i>n</i> -Butyl alcohol							<i>n</i> -Heptyl alcohol						
30,000	17.68		15.20		13.07		30,000	11.55		9.82		8.22	
7,500	17.68	0.22	15.28	0.17	13.07		7,500	11.62	0.21	9.78	0.08		
3,000	17.66	0.62	15.30	0.27	13.05	0.18	3,000	11.54	0.81	9.78	0.29	8.22	0.06
1,200	17.49	1.41	15.28	0.58	13.09	0.26	1,200	11.21	1.91	9.75	0.62	8.22	0.21
600	17.15	2.78	15.22	1.12	13.08	0.45	600	10.15	3.34	9.59	1.18	8.19	0.35
400	16.54	3.98	15.11	1.64	13.04	0.66	400	8.88	4.12	9.34	1.69	8.05	0.60
300	15.74	5.02	14.98	2.19	13.05	0.88	300	7.69	4.39	9.02	2.18	8.10	0.78
240	14.79	5.98	14.76	2.79	13.05	1.12	240	6.64	4.43	8.66	2.57	8.02	0.94
200	13.88	6.64	14.57	3.27	13.01	1.34	200	5.83	4.29	8.27	2.88	7.92	1.15
171	12.91	7.17	14.31	3.70	12.96	1.59	171	5.23	4.06	7.81	3.15	7.82	1.33
150	11.95	7.57	14.01	4.21	12.98	1.79	150	4.74	3.87	7.39	3.36	7.71	1.51
133	10.97	7.91	13.60	4.70	12.94	2.10	133	4.38	3.64	6.99	3.52	7.56	1.63
120	10.02	8.20	13.25	5.30	12.98	2.33	120	4.05	3.47	6.58	3.64	7.47	1.83
10.1	3.69	1.54	4.18	2.56	5.39	3.79	10.1	2.93	0.60	3.15	0.88	3.49	1.30
3.22	3.16	0.74	3.24	1.04	3.48	1.70	3.22	2.62	0.36	2.76	0.51	2.89	0.71
1.25	2.88	0.53	2.95	0.66	3.02	0.93	1.25	2.48	0.24	2.55	0.34	2.64	0.46
0.22	2.37	0.33	2.39	0.39	2.36	0.49	0.22	2.24	0.16	2.24	0.19	2.23	0.25
<i>n</i> -Amyl alcohol							<i>n</i> -Octyl alcohol						
30,000	15.15		13.03		11.16		30,000	10.16		8.55		7.09	
7,500	15.15	0.22	13.03	0.14			7,500	10.15	0.25	8.55	0.09		
3,000	15.13	0.68	13.03	0.25	11.07	0.17	3,000	10.12	0.85	8.55	0.21	7.09	0.06
1,200	14.95	1.65	13.01	0.60	10.98	0.30	1,200	9.68	1.84	8.49	0.56	7.09	0.20
600	14.19	3.18	12.82	1.19	11.00	0.40	600	8.54	3.11	8.33	1.08	7.09	0.33
400	13.45	4.31	12.66	1.78	11.04	0.64	400	7.30	3.61	8.08	1.53	7.03	0.50
300	12.41	5.17	12.51	2.24	10.95	0.91	300	6.24	3.67	7.75	1.93	7.01	0.66
240	11.29	5.85	12.23	2.78	10.93	1.09	240	5.43	3.57	7.38	2.29	6.94	0.82
200	10.25	6.23	11.68	3.10	10.83	1.27	200	4.83	3.35	7.00	2.53	6.85	0.98
171	9.24	6.39	11.41	3.66	10.75	1.55	171	4.40	3.13	6.63	2.70	6.77	1.11
150	8.37	6.46	10.94	3.95	10.70	1.75	150	4.02	2.97	6.22	2.83	6.64	1.25
133	7.51	6.41	10.64	4.41	10.65	1.96	133	3.76	2.75	5.86	2.94	6.60	1.37
120	6.72	6.35	10.19	4.79	10.60	2.20	120	3.60	2.56	5.52	3.00	6.47	1.54
10.1	3.33	1.07	3.69	1.61	4.39	2.43	10.1	2.83	0.48	2.98	0.73	3.35	1.05
3.22	2.91	0.58	3.00	0.77	3.21	1.13	3.22	2.56	0.29	2.66	0.42	2.82	0.61
1.25	2.67	0.39	2.75	0.52	2.83	0.66	1.25	2.43	0.20	2.49	0.28	2.57	0.38
0.22	2.32	0.26	2.34	0.33	2.34	0.35	0.22	2.22	0.13	2.20	0.18	2.23	0.26



Table II (Continued)

Wave length, cm.	20°		40°		60°		Wave length, cm.	40°		60°	
	$\epsilon'$	$\epsilon''$	$\epsilon'$	$\epsilon''$	$\epsilon'$	$\epsilon''$		$\epsilon'$	$\epsilon''$	$\epsilon'$	$\epsilon''$
<i>n</i> -Nonyl alcohol							<i>n</i> -Undecyl alcohol				
30,000	9.17		7.61		6.33		30,000	5.98		5.07	
7,500	9.14	0.25	7.61	0.08			7,500	5.97			
3,000	9.02	0.81	7.62	0.20	6.33	0.06	3,000	5.95	0.19		
1,200	8.55	1.87	7.53	0.54	6.33	0.15	1,200	5.92	0.40	5.07	0.10
600	7.27	2.88	7.36	1.02	6.30	0.30	600	5.73	0.78	5.06	0.22
400	6.02	3.14	7.10	1.45	6.25	0.45	400	5.51	1.09	5.03	0.33
300	5.18	3.07	6.75	1.80	6.21	0.60	300	5.25	1.31	4.97	0.44
240	4.60	2.88	6.37	2.07	6.14	0.75	240	4.98	1.48	4.92	0.52
200	4.15	2.64	6.03	2.28	6.05	0.90	200	4.74	1.61	4.87	0.64
171	3.85	2.43	5.67	2.37	6.00	1.01	171	4.46	1.63	4.79	0.73
150	3.61	2.25	5.29	2.47	5.87	1.14	150	4.28	1.65	4.72	0.80
133	3.46	2.10	4.98	2.49	5.77	1.27	133	4.05	1.67	4.63	0.89
120	3.32	1.98	4.71	2.53	5.72	1.37	120	3.87	1.64	4.58	0.98
10.1	2.71	0.40	2.88	0.59	3.17	0.87	10.1	2.74	0.44	2.97	0.58
3.22	2.54	0.22	2.60	0.36	2.73	0.51	3.22	2.52	0.28	2.64	0.38
1.25	2.40	0.16	2.45	0.24	2.51	0.34	1.25	2.40	0.18	2.46	0.26
0.22	2.18	0.10	2.22	0.14	2.21	0.20	0.22	2.15	0.10	2.18	0.14
<i>n</i> -Decyl alcohol							<i>n</i> -Dodecyl alcohol				
30,000	7.86		6.55		5.61		30,000	5.46		4.65	
7,500	7.84	0.14					7,500	5.44	0.16		
3,000	7.76	0.64	6.54	0.17			3,000	5.42	0.37	4.65	0.09
1,200	7.38	1.41	6.52	0.40	5.61	0.14	1,200	5.27	0.66	4.61	0.22
600	6.39	2.21	6.37	0.81	5.54	0.27	600	5.06	0.93	4.60	0.28
400	5.46	2.43	6.17	1.11	5.50	0.35	400	4.85	1.13	4.57	0.36
300	4.80	2.39	5.93	1.37	5.49	0.47	300	4.58	1.27	4.53	0.45
240	4.36	2.30	5.62	1.58	5.42	0.59	240	4.35	1.35	4.49	0.53
200	4.00	2.12	5.38	1.76	5.36	0.72	200	4.15	1.39	4.41	0.61
171	3.75	1.97	5.08	1.82	5.28	0.79	171	3.95	1.41		
150	3.56	1.84	4.87	1.88	5.21	0.90	150	3.80	1.42		
133	3.42	1.73	4.65	1.94	5.15	0.98	133	3.66	1.41		
120	3.30	1.63	4.41	1.94	5.07	1.07	120	2.70	0.40	2.90	0.54
10.1	2.69	0.37	2.86	0.53	3.12	0.75	10.1	2.51	0.27	2.62	0.36
3.22	2.51	0.23	2.58	0.33	2.74	0.47	3.22	2.38	0.17	2.45	0.24
1.25	2.40	0.15	2.44	0.22	2.51	0.32	1.25	2.15	0.10	2.15	0.12
0.22	2.17	0.09	2.19	0.12	2.19	0.16	0.22				

The high-frequency data found after subtracting the contributions of the low-frequency Debye semicircular dispersion were first plotted in a complex plane as shown in Figure 3 for *n*-undecyl alcohol. The existence of two semicircular dispersion regions is clearly evident. Due to the great uncertainty in the value of  $\epsilon_{02}$  or  $\epsilon_{\infty 1}$ , particularly in the lower members of the series and at high temperatures, it was decided to make the final analysis of the data by Cole's method of linear plotting.<sup>24</sup> For a system with two mechanisms of dielectric relaxation a plot of  $\epsilon'$  against  $\epsilon''/\lambda$  or  $\epsilon''\lambda$ , where  $\lambda$  is the wave length, yields a curve with two different slopes corresponding to the relaxation times of the two mechanisms. This method, of course, assumes that all the processes involved have Debye behavior. The values of the relaxation times  $\tau_1$ ,  $\tau_2$ , and  $\tau_3$  for the

Figure 2. Arc plot for *n*-undecyl alcohol at 40°.

first, second, and third dispersion regions together with the value of the limiting optical dielectric constant

(24) R. H. Cole, *J. Chem. Phys.*, 23, 493 (1955).

$\epsilon_{\infty 3}$  for the third dispersion region obtained according to the above analysis are listed in Table III.

The temperature dependence of the relaxation time was used to calculate the free energies  $\Delta F^*$ ,  $\Delta H^*$ , and entropies  $\Delta S^*$  of activation (Table IV) for dielectric relaxation from values of  $\tau_1$ ,  $\tau_2$ , and  $\tau_3$  in the usual manner.<sup>25</sup>

**Table III:** Relaxation Times for First, Second, and Third Dispersion Regions

$t$ , °C.	$\tau_1 \times 10^{12}$ , sec.	$\tau_2 \times 10^{12}$ , sec.	$\tau_3 \times 10^{12}$ , sec.	$\epsilon_{\infty 3}$
<i>n</i> -Propyl alcohol				
20	430	21.9	2.12	2.24
40	286	17.7	1.80	2.21
60	132			
<i>n</i> -Butyl alcohol				
20	668	27.0	2.35	2.22
40	382	21.6	2.03	2.20
60	172	17.1	1.73	2.17
<i>n</i> -Amyl alcohol				
20	927	27.6	2.65	2.20
40	419	22.4	2.26	2.18
60	212	17.4	1.91	2.16
<i>n</i> -Hexyl alcohol				
20	1210	31.0	2.90	2.19
40	520	23.6	2.44	2.17
60	244	17.7	2.04	2.15
<i>n</i> -Heptyl alcohol				
20	1465	34.4	3.18	2.17
40	594	25.7	2.64	2.19
60	279	19.1	2.29	2.15
<i>n</i> -Octyl alcohol				
20	1780	38.7	3.23	2.17
40	668	29.2	2.70	2.12
60	298	20.3	2.24	2.14
<i>n</i> -Nonyl alcohol				
20	2150	45.0	3.44	2.16
40	768	32.6	2.86	2.14
60	334	22.9	2.37	2.12
<i>n</i> -Decyl alcohol				
20	2019	47.5	3.87	2.17
40	763	33.0	3.21	2.15
60	329	22.9	2.65	2.14
<i>n</i> -Undecyl alcohol				
40	890	38.7	3.30	2.12
60	350	25.8	2.81	2.11
<i>n</i> -Dodecyl alcohol				
40	954	43.8	3.87	2.11
60	372	29.7	3.08	2.09

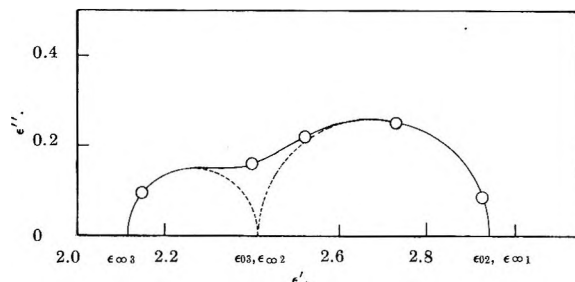


**Figure 3.** Arc plot of the second and third dispersion regions of *n*-undecyl alcohol at 40°.

**Table IV:** Activation Energies (kcal./mole) and Entropies (e.u./mole) of Normal Primary Alcohols ( $C_nH_{2n+1}OH$ )

$n$	$t$ , °C.	$\Delta F_1$	$\Delta H_1$	$\Delta S_1$	$\Delta F_2$	$\Delta H_2$	$\Delta S_2$	$\Delta F_3$	$\Delta H_3$	$\Delta S_3$
<i>n</i> = 3										
	20	4.61	5.0	1.2	2.87	1.5	-4.7	1.50	1.0	-1.7
	40	4.71			2.97			1.54		
	60	4.54								
<i>n</i> = 4										
	20	4.87	5.6	2.4	2.99	1.7	-4.4	1.57	0.9	-2.3
	40	4.89			3.10			1.62		
	60	4.72			3.18			1.65		
<i>n</i> = 5										
	20	5.06	6.8	5.9	3.00	1.8	-4.1	1.63	0.95	-2.3
	40	4.95			3.12			1.68		
	60	4.86			3.19			1.72		
<i>n</i> = 6										
	20	5.22	7.2	6.8	3.07	2.1	-3.3	1.68	1.05	-2.16
	40	5.09			3.15			1.73		
	60	4.95			3.20			1.77		
<i>n</i> = 7										
	20	5.33	7.4	7.1	3.13	2.3	-2.9	1.74	1.25	-1.7
	40	5.17			3.20			1.78		
	60	5.04			3.25			1.84		
<i>n</i> = 8										
	20	5.45	8.0	8.8	3.20	2.4	-2.7	1.75	1.2	-1.9
	40	5.22			3.29			1.80		
	60	5.08			3.29			1.82		
<i>n</i> = 9										
	20	5.56	8.6	10.4	3.29	2.6	-2.4	1.78	1.2	-2.0
	40	5.33			3.35			1.83		
	60	5.16			3.38			1.86		
<i>n</i> = 10										
	20	5.52	8.4	9.8	3.32	2.8	-1.8	1.85	1.2	-2.2
	40	5.33			3.36			1.91		
	60	5.15			3.38			1.94		
<i>n</i> = 11										
	40	5.43	7.8	7.6	3.46	3.0	-1.5	1.94	1.2	-2.35
	60	5.19			3.46			1.98		
<i>n</i> = 12										
	40	5.47	8.0	8.1	3.54	3.05	-1.5	2.02	1.0	-3.2
	60	5.23			3.55			2.06		

## Discussion

The data show that all of the alcohols measured have three dispersion regions. The relaxation times for the first dispersion region are much too large to correspond to the times ordinarily associated with molecular rotation. Figure 4 shows that the relaxation times  $\tau_1$  for the first dispersion region increase regularly with increase in molecular chain length except for a slight drop in the relaxation time of decyl alcohol at 20°. One would suspect the presence of an abnormal experimental error, but the values of the dielectric constant and loss are in good agreement with those obtained

(25) E. J. Hennelly, W. M. Heston, Jr., and C. P. Smyth, *J. Am. Chem. Soc.*, **70**, 4102 (1948).

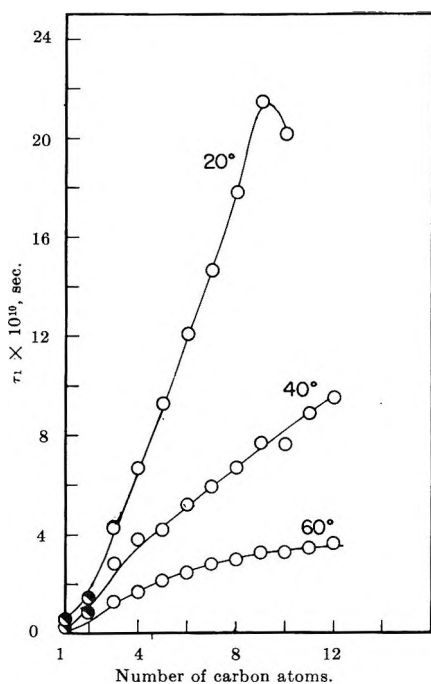


Figure 4. Dependence of low-frequency relaxation time ( $10^{-10}$  sec.) upon number of carbon atoms in primary alcohols: open circles, results of present investigation; half-filled circles, literature values from F. Buckley and A. A. Maryott, National Bureau of Standards Circular 589, U. S. Government Printing Office, Washington, D. C., 1958.

many years ago in this laboratory on a different sample,<sup>14</sup> and a similar drop is evident in the results of Brot, Magat, and Reinisch.<sup>7</sup> The previously reported<sup>6</sup> zigzag in the curve suggesting an odd-even effect of the chain as in melting points is not evidenced in Figure 4. The long relaxation times have been interpreted<sup>26-30</sup> in terms of the lifetime of a microcrystalline complex as determined by the time required for a monomeric molecule to break off from the complex. Hassion and Cole<sup>11</sup> explained the observed low-frequency dispersion region as due to an orientation of the OH moment in which one hydrogen bond is broken and another is formed. The heats and entropies of activation (Table IV) for the first relaxation process increase with increasing length of the alkyl group, which might suggest that the relaxation process for the low-frequency dispersion is due to molecular rotation. However, the values of the relaxation time are much too large for the orientation of a single molecule.

It appears that the alcohol molecules are in fact associated by hydrogen bridges in temporary microcrystalline structures. These structures are not stable, and at a given instant each of these has a finite length. At each instant some hydrogen bonds are ruptured and others are formed. The first dispersion region is connected with the molecules in these microcrystalline

structures. The dielectric relaxation process involves the breaking and reforming of the hydrogen bonds with the orientation of dipole moment, and the rate of breaking off is the determining factor for the relaxation time.

Since the relaxation times  $\tau_3$  reported here for the third dispersion region are much smaller than one would expect for the orientation of monomeric molecules, and depend very little on the length of the hydrocarbon chain, the mechanism leading to the dispersion should not involve considerable intermolecular interactions or large displacement of neighboring molecules. This is substantiated by the relatively low barrier  $\Delta H_3$  of approximately 1 kcal./mole associated with the process (Table IV), which is identical with the barrier height hindering OH rotation found from microwave spectroscopy.<sup>31</sup> A magnitude of  $\tau_3 = 3 \times 10^{-12}$  is not unreasonable for the relaxation of this process, a value of about  $6 \times 10^{-12}$  sec. having been obtained by Davies and Meakins<sup>32</sup> for the rotation of the OH group of 2,4,6-tri-*t*-butylphenol in decalin solution, while an even shorter time was apparent for cyclohexyl carbinol in the same solvent. Fong and Smyth<sup>33</sup> obtained for OH group relaxation at 20°:  $4 \times 10^{-12}$  sec. in *p*-phenylphenol,  $3.4 \times 10^{-12}$  sec. in 1-naphthol, and  $3.4 \times 10^{-12}$  sec. in 2,6-dimethylphenol, all in benzene solution. Since  $\tau_3$  is the relaxation time for the rotational orientation of the OH group, it should increase with molecular chain length only insofar as it is affected by increasing viscosity of the liquid or by change in steric hindrance within the molecule. Since small, nearly spherical molecules<sup>34</sup> and methoxy groups<sup>35</sup> have been found to show but slight increase in relaxation time with increase in viscosity of the medium, the relatively small increase in  $\tau_3$  with increasing molecular size is consistent with the picture which has been proposed.

Before deriving any conclusion on the basis of the magnitudes of the second relaxation times  $\tau_2$ , it should be emphasized that large errors are accumulated in these values. The lower frequency dispersion region

(26) E. Bauer, *Cahiers phys.*, **20**, 1 (1944); **21**, 21 (1944).

(27) E. Bauer and D. Massignon, *Trans. Faraday Soc.*, **42A**, 12 (1946).

(28) M. Magat, "Hydrogen Bonding," D. Hadzi, Ed., Pergamon Press, London, 1957, p. 309.

(29) M. Moriamez, Ph.D. Thesis, L'Université de Lille, 1959.

(30) L. Reinisch, *J. chim. phys.*, **51**, 113 (1 54).

(31) S. Mizushima, "Structure of Molecules and Internal Rotation," Academic Press, Inc., New York, N. Y., 1954.

(32) M. Davies and R. J. Meakins, *J. Chem. Phys.*, **26**, 1584 (1957).

(33) F. K. Fong and C. P. Smyth, *J. Am. Chem. Soc.*, **85**, 1565 (1963).

(34) C. P. Smyth, *Proc. Natl. Acad. Sci. U. S.*, **42**, 234 (1956).

(35) E. L. Grubb and C. P. Smyth, *J. Am. Chem. Soc.*, **83**, 4873 (1961).

is accurately characterized by the low-frequency data on the one hand and the millimeter dispersion region by the values of the 2-mm. measurements on the other, whereas the second dispersion is derived from the values obtained after subtracting the contribution of the first and third dispersion regions from the total dispersion. It is likely, therefore, that the relaxation times of the second dispersion region, particularly for the lower members of the series, may be in error by as much as 25 to 30%. The error should be much less for the higher members of the series and probably is not greater than 10% for octyl to dodecyl alcohols. The exact values of the relaxation times, therefore, should not be taken seriously, but the trend of these values is of significance.

Magat<sup>28</sup> suggested that the rotation of molecular segments near the end of a polymer chain might account for this second dispersion region. Denney and Cole,<sup>12</sup> on the basis of two rather than three dispersion regions, argued against Magat's theory because they found that the importance of the high-frequency dispersion region relative to that of the low-frequency region is not very temperature dependent. Hassion and Cole<sup>11</sup> attribute the high-frequency dispersion to the orientation of the oxygen-alkyl group moment during the shift of the hydrogen bond from one electron orbital of the bridged oxygen atom to the other. However, it seems that this process should also depend on the lifetime of the complex and should be involved in the low-frequency process.

The present data indicate that the importance of the second and third dispersion regions relative to that of the low-frequency dispersion region increases both with the temperature and with the length of the hydrocarbon chain (Figures 5 and 6). This is different from the findings of Cole and his co-workers who, at low temperatures,<sup>11,12</sup> found an inverse temperature dependence for the second dispersion region for ethanol and 2-propanol, but is in qualitative agreement with the later finding of Klages and Roth,<sup>36</sup> who measured higher even-number alcohol molecules ( $C_8-C_{16}$ ) between 20 and 60°. Since the accurate measurements of Cole and his co-workers were carried out at low temperatures and in supercooled liquids, it is not surprising that the behavior of these liquids under these conditions is different from that at higher temperatures.

From Table III it is clear that the relaxation times  $\tau_2$  are of the same order of magnitude as those for the unassociated alkyl bromide molecules<sup>25</sup> although larger because of the greater viscosities of the alcohols. They increase with the chain length much as do those of the alkyl bromides. The values of the activation energies are small and of the same order of magnitude

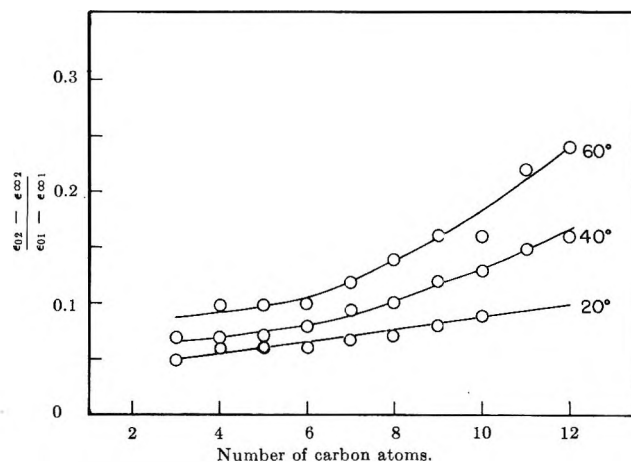


Figure 5. Dependence on chain length of ratio of fractional contributions of second and first dispersion regions.

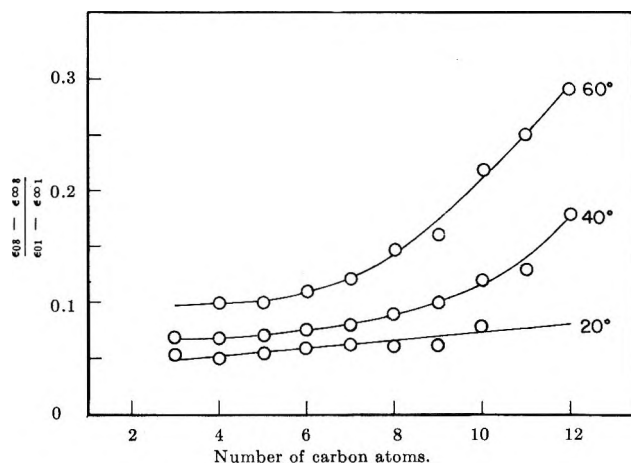


Figure 6. Dependence on chain length of ratio of fractional contributions of third and first dispersion regions.

as those for the single dispersion region of the alkyl bromides. It appears that the relaxation process for the second dispersion may reasonably be supposed to be that of the monomeric molecules. This does not exclude the possibility of a contribution from the dipoles of the molecules which are at the extremities of the polymer chains and are only bonded by their oxygen atoms to the neighboring molecules.

### Conclusions

The measurements which have been discussed confirm the existence of three dielectric dispersion regions in the pure liquid, straight-chain alcohols. The long relaxation times  $\tau_1$  associated with the low-frequency dispersion are what might be expected for the polymeric clusters resulting from the strong hydrogen

(36) G. Klages and D. Roth, *Z. Naturforsch.*, **14a**, 628 (1959).

bonding between the hydroxyl groups. These relaxation times increase with increasing alkyl chain length, which should increase the bulk of the cluster and, hence, its relaxation time. However, one would expect a distribution of cluster sizes and, hence, a distribution of relaxation times. The failure to observe such a distribution has been regarded as ruling out the orientation of the whole cluster as the mechanism of this relaxation process. The closeness of the activation energies for this process to the dissociation energy of the hydrogen bond has led to the belief that breaking of the hydrogen bond is an initial step in the relaxation process, but some molecular motion dependent upon chain length seems to be required to give the observed increase in  $\tau_1$  with increasing chain length. The aggregate of ROH molecules may be pictured as containing a chain of hydroxyl groups held together by hydrogen bonds. The slow relaxation mechanism may be described<sup>28</sup> as the breaking of one of these bonds followed by rotation of a now partially liberated ROH. The relaxation time is long because of the time required to break the hydrogen bond, dependent upon the length of the chain of the rotating ROH, but uninfluenced by all but the nearest portions of the molecular aggregate and, therefore, independent of the rest of the aggregate and essentially single-valued. A certain amount of dipole orientation by twisting of segments within the chain might be expected. If the segments consisted of different numbers of ROH's, a distribution of relaxation should be observed. The absence of such distribution indicates that, if such segmental orientation occurs, the segment consists of a single ROH. Relaxation in this way would be hindered by strong steric repulsions of the neighboring ROH's in the chain and by the viscosity of the liquid with the result that the relaxation time might be of the order of those observed for  $\tau_1$ . The values of  $\tau_1$  are much shorter than those observed for the solid long-chain alcohols,<sup>37,38</sup> where proton migration was indicated, in addition to bond breaking and molecular rotation, and where resistance to molecular rotation should be much greater than that in the liquid.

The very short relaxation time  $\tau_3$  is so close in size to that recently found for OH rotation in a number of compounds and so little dependent on temperature and on molecular size that it seems highly probable that this very high-frequency dispersion region results from hydroxyl group rotation. The very approximate values of the intermediate relaxation time  $\tau_2$  are of about the size and temperature dependence to be expected of free ROH molecules. The ROH molecule at each end of a chain may be able to rotate around its hydrogen bond to the rest of the chain to give dielectric relaxation with a relaxation time so near to that of the free molecule as to be indistinguishable from it in the measurements and analysis here reported. Since the OH dipole moment of 1.51 D. is but slightly smaller than the ROH molecular moment 1.66–1.70 and since only the hydroxyl groups on the monomeric ROH molecules are free to rotate, the orienting dipoles contributing to the third dispersion region should be similar both in moment and in number to those contributing to the second region, unless the number of orientable, terminal ROH's on the polymer chains is considerable. The contribution to the total dielectric relaxation made by the very high-frequency dispersion region associated with OH rotation may, therefore, be about the same as that from the intermediate dispersion region associated with ROH rotation. Figures 5 and 6 show that, within the considerable uncertainty of the values, this is the case, thus lending further credence to the mechanisms assigned to the second and third relaxation processes.

Differences between the values of  $\epsilon_{\infty 3}$  in Table III and the squares of the optical refractive index show the presence of further absorption in the infrared region. These will be discussed in a subsequent paper dealing with the atomic polarizations of a large number of compounds.

(37) J. D. Hoffman and C. P. Smyth, *J. Am. Chem. Soc.*, **71**, 431 (1949).

(38) R. J. Meakins, "Progress in Dielectrics," Vol. 3, J. B. Birks and J. Hart, Ed., John Wiley and Sons, Inc., New York, N. Y., 1963, pp. 182–189.

## Microwave Absorption and Molecular Structure in Liquids. LXIV.

### The Dielectric Behavior of Mixtures of Polar Nonassociative Liquids<sup>1,2</sup>

by Edward Forest and Charles P. Smyth

*Frick Chemical Laboratory, Princeton University, Princeton, New Jersey (Received November 30, 1964)*

Dielectric constants and losses have been measured at wave lengths of 575 m., 10.0, 3.22, and 1.25 cm. at 25° for four binary mixtures of chlorobenzene, bromobenzene, 1-chloronaphthalene, and 1-bromonaphthalene, and for solutions of 1-bromonaphthalene and 1-chloronaphthalene in benzene. The densities and viscosities have also been determined. The dielectric data of the binary mixtures have been interpreted in terms of two partly superimposed Debye regions whose relative contributions are in the same ratio as the molar concentrations of the components. The results for these binary systems are consistent with the assumption that the relaxation processes are those of molecules rather than larger liquid regions as proposed by some earlier workers for systems which they investigated.

#### Introduction

From his study of the dielectric constant and loss of binary polar mixtures as a function of temperature at constant frequency, Schallamach<sup>3</sup> suggested that dielectric relaxation involved relatively large regions in the liquid. Accordingly, if the polar components of a binary mixture are both associative or both nonassociative, so that mixing occurs on the molecular level, the dispersion region should appear to correspond to a single relaxation process. On the other hand, binary mixtures in which one is associative and the other nonassociative yield two dispersion regions. Denney<sup>4</sup> measured the dielectric constants and losses of such mixtures as a function of frequency at constant temperature and found his results to be in accord with those of Schallamach. The dispersion regions investigated by Schallamach and Denney in binary mixtures of nonassociative polar liquids occurred at temperatures of the order of -100°. Bos,<sup>5</sup> investigating binary polar mixtures, observed all of the familiar types of complex plane plots encountered in dielectric investigations. Binary mixtures of nitrobenzene and chlorobenzene, which should be representative of the nonassociative type, were found to give semicircular plots indicative of a single relaxation time. In view of the fact that chlorobenzene and nitrobenzene are molecules of similar size and shape, they might be expected, if dissolved in identical

environments, to yield no more than a slight widening of the dispersion region, which might not be experimentally detectable because of the preponderance of the nitrobenzene contribution arising from the fact that its moment is 2.5 times larger than that of chlorobenzene.<sup>6</sup>

In view of the relatively small amount of information available on polar mixtures of the nonassociative type at room temperature, an investigation has been undertaken. Another reason for studying this problem is the fact that many substances have recently been studied in which dielectric relaxation takes place by two simultaneously occurring processes. The results have been analyzed into plausible values for the relaxation times of the two processes, but the successful analysis of

(1) This research was supported by the U. S. Army Research Office (Durham). Reproduction, translation, publication, use, or disposal in whole or in part by or for the United States Government is permitted.

(2) This paper represents part of the work submitted by E. Forest to the Graduate School of Princeton University in partial fulfillment of the requirements for the degree of Doctor of Philosophy.

(3) A. Schallamach, *Trans. Faraday Soc.*, **42A**, 180 (1946).

(4) D. J. Denney, *J. Chem. Phys.*, **30**, 1019 (1959).

(5) F. Bos, Doctoral Dissertation, University of Leiden, Leiden, Holland, 1958.

(6) A. A. Maryott and F. Buckley, "Table of Dielectric Constants and Electric Dipole Moments of Substances in the Gaseous State." National Bureau of Standards Circular 537, U. S. Government Printing Office, Washington 25, D. C., 1953.

simple binary systems will give some evidence as to the soundness of the analyses of the single substances in which two relaxation processes occur. In this initial investigation, the molecules of the compounds chosen are rigid and have electric moments which are of the same order of magnitude.

### Experimental

1-Chloronaphthalene, purchased from Matheson Coleman and Bell, was vacuum distilled. The fraction collected within the temperature range 129.0–129.5° gave a refractive index  $n^{20}_D$  of 1.6330; literature value, 1.6332. Bromobenzene, purchased from Eastman Kodak Co., was distilled under atmospheric pressure and the fraction coming over between 156.0 and 156.5° was collected. The index of refraction,  $n^{20}_D$  1.5606, compared with a literature value of  $n^{20}_D$  1.5598. Chlorobenzene, from Eastman Kodak Co., was purified by fractional distillation under atmospheric pressure. The distillate coming over between 133.4 and 133.7° had an index of refraction  $n^{20}_D$  1.5246 compared with the literature value  $n^{20}_D$  1.5248. 1-Bromonaphthalene, from Eastman Kodak Co., was vacuum distilled at 4 mm. The fraction collected at 118° gave an index of refraction  $n^{20}_D$  1.6582 compared with a literature value of  $n^{20}_D$  1.6588.

The dielectric constants and losses of the mixtures were measured at wave lengths of 575 m. (giving  $\epsilon_0$ ), 10.0, 3.22, and 1.25 cm. at a temperature of 25° by methods which have been previously described.<sup>7-9</sup> The density balance and the viscosities were determined with an Ostwald type viscometer.

### Results

The maximum possible errors in the dielectric constant,  $\epsilon'$ , and the dielectric loss,  $\epsilon''$ , at loss tangents of about 0.2 are estimated as  $\pm 2$  and 5%, respectively. At the lower losses, the experimental error in the actual loss value is within  $\pm 0.05$ . The dielectric constants and losses were first plotted in the complex plane.<sup>10</sup> Figure 1, illustrating the Debye behavior of a mixture of 1-chloronaphthalene and benzene in a molar ratio of 1:4, is also typical of the behavior observed for 1-bromonaphthalene and benzene mixed in the same ratio. Figure 2 for the system 1-bromonaphthalene and chlorobenzene in the molar ratio 1:4 is typical of the complex plane plots observed for the dipolar mixtures. The dielectric constant and loss measurements were repeated in each case and the deviations observed from a symmetrical distribution could not be attributed to experimental error. The data were, therefore, analyzed to obtain two relaxation times,  $\tau_1$  and  $\tau_2$ , corresponding to the two polar components. Initial estimates of  $\tau_1$  and

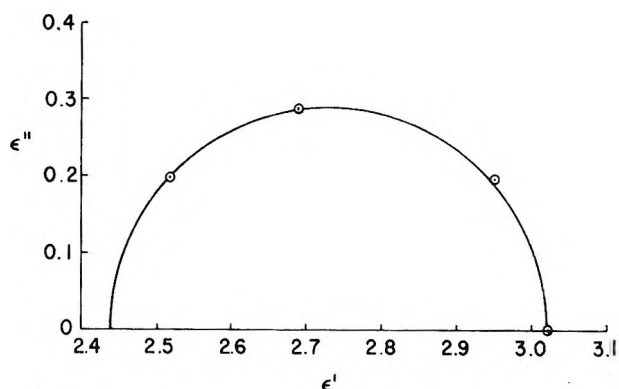


Figure 1. Complex plane plot for solution containing 0.20 mole fraction of 1-chloronaphthalene in benzene at 25°.

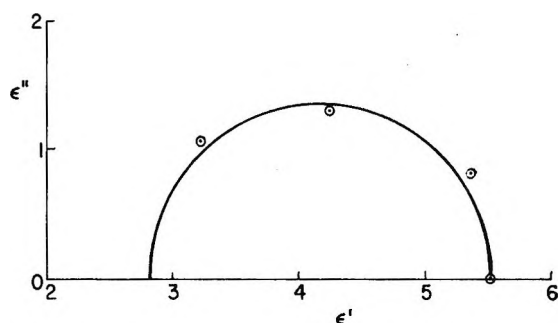


Figure 2. Complex plane plot for solution containing 0.20 mole fraction of 1-bromonaphthalene in chlorobenzene at 25°.

$\tau_2$ , the relaxation times of the two components,  $\epsilon_\infty$ , the optical dielectric constant, and  $C_1$ , the relative amount of the contribution of component 1, were varied to obtain the best fit of eq. 1 and 2 to the experimental data.<sup>11</sup>

$$\frac{\epsilon' - \epsilon_\infty}{\epsilon_0 - \epsilon_\infty} = C_1 \frac{1}{1 + (\omega\tau_1)^2} + C_2 \frac{1}{1 + (\omega\tau_2)^2} \quad (1)$$

$$\frac{\epsilon''}{\epsilon_0 - \epsilon_\infty} = C_1 \frac{\omega\tau_1}{1 + (\omega\tau_1)^2} + C_2 \frac{\omega\tau_2}{1 + (\omega\tau_2)^2} \quad (2)$$

In these equations,  $C_1 = 1 - C_2$ ,  $\omega$  is the angular frequency, and  $\epsilon_0$  is the static or low frequency dielectric constant.  $\epsilon_\infty$  was estimated by assuming additive contributions from the respective components, while  $C_1$  and  $C_2$  were estimated from the relative molar concentrations. Once estimates of  $C_1$ ,  $C_2$ , and  $\epsilon_\infty$  are obtained, initial estimates of  $\tau_1$  and  $\tau_2$  become apparent. The experimental and calculated values of  $\epsilon'$  and  $\epsilon''$  are

(7) H. L. Laquer and C. P. Smyth, *J. Am. Chem. Soc.*, **70**, 4097 (1948).

(8) W. M. Heston, A. D. Franklin, E. J. Hennelly, and C. P. Smyth, *ibid.*, **72**, 3443 (1950).

(9) F. H. Branin and C. P. Smyth, *J. Chem. Phys.*, **20**, 1121 (1952).

(10) K. S. Cole and R. H. Cole, *ibid.*, **9**, 341 (1941).

(11) K. Bergmann and C. P. Smyth, *J. Phys. Chem.*, **64**, 665 (1960).

given in Table I. The molar volumes, viscosities, and dispersion parameters are given in Table II. Since, in the case of each mixture, the number of equations relating the experimentally determined quantities  $\epsilon'$  and  $\epsilon''$  exceeds the number of adjustable parameters by two, the derived parameters form a unique set. Some latitude in the values of the parameters is possible through mutual compensation but the adjustable interval is relatively small. Figure 3 is a plot of  $\epsilon''$  vs. log fre-

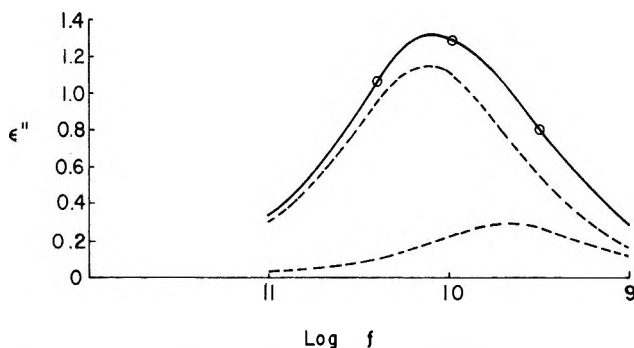


Figure 3. Plot of dielectric loss against log frequency for solution containing 0.20 mole fraction of 1-bromonaphthalene in chlorobenzene. The solid line represents the sum of the resolved dashed curves and the points are the experimentally determined loss values.

quency for the system 1-bromonaphthalene and chlorobenzene in the molar proportion 1:4. The dashed curves are the resolved dispersion regions, the solid line represents their sum, and the points are the experimentally determined loss values. Table III consists of the relaxation times, macroscopic viscosities, and molar volumes of the pure liquids used in this investigation at the temperature of measurement. The relaxation times, viscosities, and molar volumes were determined by other workers in this laboratory.<sup>12</sup>

### Discussion of Results

Chlorobenzene, bromobenzene, 1-chloronaphthalene, and 1-bromonaphthalene have nearly the same electric moment. Therefore, the internal field in the pure liquid state would not be expected to be very different from the internal field in the mixed state. This is evidenced by the fact that the static dielectric constant as well as the molar volume of a given mixture can be expressed by a simple mixing formula of the type

$$\epsilon_0 = X_A \epsilon_{0A} + X_B \epsilon_{0B} \quad (3)$$

where  $X_A$  and  $X_B$  are the mole fractions of the components,  $\epsilon_0$  is the static dielectric constant of the mixture, and  $\epsilon_{0A}$  and  $\epsilon_{0B}$  are the static dielectric constants of the pure components at the temperature of meas-

Table I: Observed and Calculated Dielectric Constants and Losses at 25°

Mixture concn., mole fraction	Wave length, cm.	$\epsilon'$		$\epsilon''$	
		Obsd.	Calcd.	Obsd.	Calcd.
0.493 bromobenzene in chlorobenzene	10.0	5.40	5.34	0.77	0.75
	3.22	4.27	4.33	1.47	1.45
	1.25	3.15	3.10	1.21	1.24
0.500 1-chloronaphthalene in chlorobenzene	10.0	4.97	4.85	1.00	0.94
	3.22	3.74	3.74	1.17	1.20
	1.25	3.05	2.94	0.82	0.80
0.196 1-chloronaphthalene in chlorobenzene	10.0	5.34	5.24	0.79	0.74
	3.22	4.26	4.33	1.36	1.34
	1.25	3.24	3.17	1.19	1.18
0.198 1-bromonaphthalene in chlorobenzene	10.0	5.28	5.17	0.81	0.76
	3.22	4.25	4.23	1.30	1.31
	1.25	3.23	3.14	1.06	1.08
0.199 1-bromonaphthalene in benzene	10.0	2.93		0.20	
	3.22	2.66		0.28	
	1.25	2.52		0.17	
0.199 1-chloronaphthalene in benzene	10.0	2.95		0.20	
	3.22	2.69		0.29	
	1.25	2.52		0.20	

urement. As one might expect, the dielectric constants of the mixtures of 0.20 mole fraction of 1-chloronaphthalene and 0.20 mole fraction of 1-bromonaphthalene, respectively, in benzene are considerably larger than predicted by eq. 3. It is apparent that the nonpolar benzene molecules separate the polar halonaphthalene molecules from each other, decreasing the probability of those molecular orientations which exist in the pure liquid and tend to decrease the effective moment and hence the dielectric constant.

The amplitudes,  $C_1$  and  $C_2$ , of the resolved regions are seen to be in the same ratio as the molar concentrations of the polar components in the mixtures. Since the polar components all have about the same moment, one would expect this to be the case. It is thus reasonable to attribute the resolved dispersion regions to the individual components. From this point of view, then, the longer resolved relaxation time has been associated with the component that has the longer relaxation time in the pure liquid state, although the relaxation time of each component is different from that in the pure liquid because of the difference in molecular environment. The additivity of the dielectric constant and the molar volume are consistent with the molecular or microscopic mixing thus indicated. This result is not necessarily in conflict with the conclusions of Schallamach<sup>3</sup> and Denney<sup>4</sup> for similar mixtures at extremely low temperatures ( $-100^\circ$ ), where only a single disper-

(12) E. J. Hennesly, W. M. Heston, Jr., and C. P. Smyth, *J. Am. Chem. Soc.*, **70**, 4102 (1948).



**Table II:** Molar Volumes, Viscosities, Squares of the Refractive Indices, and Dispersion Parameters at 25°

Mixture concn., mole fraction	$\epsilon_0$	Molar volume, cc.	Viscosity, cp.	$n^{20}_D$	$\epsilon_\infty$	$\tau_1 \times 10^{12}$ , sec.	$\tau_2 \times 10^{12}$ , sec.	$C_1$	$\tau_0 \times 10^{12}$ , sec.
0.493 bromobenzene in chlorobenzene	5.547	103.38	0.896	2.371	2.41	18	9.5	0.50	
0.500 1-chloronaphthalene in chlorobenzene	5.341	119.57	1.442	2.509	2.61	35	13	0.50	
0.196 1-chloronaphthalene in chlorobenzene	5.497	109.04	0.964	2.397	2.50	32	11	0.20	
0.198 1-bromonaphthalene in chlorobenzene	5.458	109.83	1.033	2.419	2.58	35	12	0.20	
0.199 1-bromonaphthalene in benzene	3.026	98.93	0.925	2.380	2.47				23.1
0.199 1-chloronaphthalene in benzene	3.020	98.68	0.85	2.356	2.44				18.2

**Table III:** Molar Volumes, Viscosities, and Relaxation Times of Pure Liquids<sup>12</sup>

Substance	Molar volume, cc.	Viscosity, cp.	$\tau \times 10^{-12}$ , sec.
Chlorobenzene	102.24	0.756	10.3
Bromobenzene	105.50	1.08	16.4
1-Chloronaphthalene	138.88	2.94	49.1
1-Bromonaphthalene	140.02	4.52	86.0

sion region was found. Schallamach attributed the relaxation process to relatively large regions in the liquid. With increasing temperature, however, the average lifetime of these regions as well as their size would be expected to decrease until, at room temperatures, their influence upon the relaxation process might well become negligible.

The relaxation time of 1-chloronaphthalene is seen to fall from  $49.1 \times 10^{-12}$  sec. in the pure liquid state (Table III) to  $35 \times 10^{-12}$  sec. in the equimolar mixture with chlorobenzene, and to  $32 \times 10^{-12}$  sec. in the 1:4 mixture with chlorobenzene (Table II). It is thus seen that the relaxation time of 1-chloronaphthalene is relatively insensitive to further dilution with chlorobenzene over a considerable range of concentration. The viscosities of the mixtures when compared to the viscosity of pure 1-chloronaphthalene show an analogous behavior, although not as pronounced. The relaxation time of 1-bromonaphthalene falls from  $86 \times 10^{-12}$  sec. in the pure liquid state to  $35 \times 10^{-12}$  sec. in the 1:4 mixture with chlorobenzene, almost equal to that of 1-chloronaphthalene in a similar ratio with chlorobenzene, the viscosities of the two mixtures differing by only 0.07 cp., while the viscosity of pure 1-bromonaphthalene is 1.58 cp. greater than that of 1-chloronaphthalene. It is likely that the introduction of the molecules of chlorobenzene results in considerably greater rotational and translational freedom of motion for the relatively flat halonaph-

thalene molecules, the greatest effect taking place at concentrations of chlorobenzene of less than 0.50 mole fraction.

Only a small gradual increase in the relaxation time of chlorobenzene is observed with increasing concentration of the halonaphthalenes. The relaxation time of chlorobenzene is greater in the presence of 1-bromonaphthalene than in the presence of 1-chloronaphthalene. This is probably due to the greater internal friction coefficient arising from the higher polarizability of the bromine. The relaxation time of 1-chloronaphthalene falls to  $18.2 \times 10^{-12}$  sec. and that of 1-bromonaphthalene to  $23.1 \times 10^{-12}$  sec. if benzene is substituted for chlorobenzene in the 1:4 mixture. This further decrease in the relaxation time which is accompanied by a similar decrease in the viscosity may be attributed to the decrease in the internal field and the internal friction coefficient. The equimolar mixture of chlorobenzene and bromobenzene appears to be slightly anomalous. The relaxation time of bromobenzene increases to  $18.5 \times 10^{-12}$  sec. while that of chlorobenzene decreases to  $9.5 \times 10^{-12}$  sec. These values are, however, so close to the pure component relaxation times that the slight anomalies may be the result of experimental error.

It is evident that the dielectric behavior of these binary mixtures of rather similar polar molecules can be represented in terms of the behaviors of the individual molecules. The two relaxation times change with concentration in a manner at least qualitatively predictable from the change in molecular environment, there being no evidence that larger liquid regions are involved in the relaxation processes. The satisfactory manner in which the dielectric behavior of these simple binary systems can be represented in terms of two relaxation times gives increased confidence in the methods of analysis which have been applied to single substances in which two relaxation processes can occur simultaneously.

## Wettability of Metals under Continuous Condensing Conditions

by Robert A. Erb

Chemistry Division, The Franklin Institute Laboratories, Philadelphia, Pennsylvania 19103  
(Received October 22, 1964)

The wettability of a number of metals has been measured under continuous condensing conditions in pure steam for extended periods of time. Water exhibits high contact angles on the noble metal samples studied; the average advancing angles are Au, 55–85°; Ag, 68–89°; Rh, 65–82°; Pd, 74°; and Pt, 50°. Water condensed in a filmwise manner on Ni, Cd, Ti, Cr, Type 316 stainless steel, copper-nickel 10%, and quartz samples, indicating zero or low contact angles on these surfaces. Experimental evidence relating the wettability of clean metal surfaces to surface oxide present is considered and the conclusion is established that a clean "high-energy surface" of metal substantially free of oxygen is not wettable by water.

### Introduction

The statement has often been made in surface chemistry that a clean "high-energy surface" is by nature wettable. That this is not a true general statement has been seen recently in the experimental work of White,<sup>1</sup> in which he showed that water has a fairly high contact angle on clean gold and that water will spread on gold only if a gross oxide film is present. Fowkes<sup>2</sup> has provided a theoretical basis for the non-wettability of oxide-free metal surfaces, relating to the dispersion-force nature of the interaction between water and the oxide-free metal surface. This approach predicts accurately the high interfacial tension between water and mercury (approximately 426 ergs/cm.<sup>2</sup>) and confirms the experimentally observed nonspreading of water on mercury.

The principal experimental problem in studying the wettability of solid metals (for example, in the forms of electroplated or mechanically polished specimens) is the requirement that organic surface contamination must be removed without subjecting the surface to powerful oxidizing treatments which could result in oxide formation. This problem has been overcome in our program by the use of a system in which the samples to be studied serve as vertical condensing surfaces in a pure steam atmosphere in a closed refluxing system where they may be washed continuously by the freshly condensed water for many weeks at a time. Under these conditions, physically adsorbed organic surface contamination is generally removed within a few hours and

chemisorbed contamination within a few days; this statement is based not only on our experience, but also on the extensive literature on the behavior of organic promoters of dropwise condensation on metal condensing surfaces.<sup>3</sup>

### Experimental

Two different apparatus were used in this study, each with outer vessels constructed of Type 316 stainless steel, with boiling water in the bottom part of the vessel and a condenser in the upper part. In the first apparatus a hollow, water-cooled copper core served as support for 2.5 × 7.6 cm. metal flats attached to its surface. In the second, eight vertical tubes, 1.3 cm. diameter × 13 cm. in length and closed at the bottom end, were internally water-cooled. Electrically heated Pyrex windows were provided in each apparatus for examination of the condensing surfaces.

Great care was taken to avoid organic contamination. The following steps were taken in this direction. (1) Grease-free fittings were used throughout, with Teflon or Viton seals for windows and top plate. (2) The stainless steel and Pyrex vessels were cleaned rigorously

(1) M. L. White, *J. Phys. Chem.*, **68**, 3083 (1964).

(2) F. M. Fowkes, *ibid.*, **67**, 2538 (1963); also in "Contact Angle, Wettability, and Adhesion," *Advances in Chemistry Series*, No. 43, American Chemical Society, Washington, D. C., 1964, pp. 99–111.

(3) R. A. Erb, "Dropwise Condensation: A Bibliography of the Literature on Dropwise Condensation from 1930 to 1964," to be published as an Office of Saline Water Research and Development Progress Report.

before being put into service, including refluxing with trichloroethylene, then with isopropyl alcohol, then with water, followed by a final wash with sodium dichromate-sulfuric acid cleaning solution and a rinse with pure water. (3) The water to be refluxed (about 5 l. in a charge) was redistilled in an all-Pyrex apparatus from alkaline permanganate solution in order to destroy any organic contamination. (4) During the condensation runs, pressure in the vessels was maintained above atmospheric to prevent laboratory air from entering the vessel. (5) The refluxing water was completely drained and replaced with organic-free water several times in each condensation run; this is an additional aid in eliminating residual organic contamination. (6) Steam was bled off many times during each run; this assisted in removal of noncondensable gases, as did the procedure used at the outset involving displacement of air with argon followed by evacuation by water aspirator.

For the first apparatus, the sample flats whose wettability is discussed later were prepared in the following ways. The solid silver sample had a rolled finish and was heated in a tube furnace to 600° in a nitrogen atmosphere. The other silver sample was electroplated from a cyanide bath on a Type 316 stainless steel base. The gold sample had a commercial rolled finish. The rhodium samples were electroplated to a thickness of 35  $\mu$  by Sel-Rex Corp. The palladium, platinum, and titanium samples were polished mechanically using aluminum oxide abrasives. The nickel and cadmium samples were electroplated with a matte finish on a copper-nickel 10% base. The fused quartz sample was given a final cleaning in sodium dichromate-sulfuric acid cleaning solution, with a distilled water rinse. The metal samples were rubbed lightly with Bon-Ami and water, with copious rinsing before mounting.

The tube samples for the second apparatus were prepared without mechanical polishing of the final surfaces. The Type 316 stainless steel tube and copper-nickel 10% tube were used as received, having a bright finish. The gold-, silver-, and rhodium-surfaced tubes were bright-electroplated by Sel-Rex Corp. The gold coating is 99.5% gold and 0.5% silver. The chromium-surfaced tube was bright-electroplated by Philadelphia Rustproof Co. The only treatment given these tubes before insertion in the apparatus was a quick wipe with ethanol on a cellulose wiping tissue.

Contact angles were measured on drop profile images using a Gaertner telemicroscope with protractor eyepiece and right-angle cross hairs. The flat plate apparatus has a slow condensation rate per unit area (because of a high ratio of condensing area to power input),

and measurements could be made on drops by direct observation through the telemicroscope. The tube apparatus had for this experimental run a condensation rate of water of about  $4 \times 10^{-3}$  g./cm.<sup>2</sup>-sec., which is one order of magnitude higher than that with the flat plate system. For convenience in measuring the contact angles of the rapidly growing, merging, and sweeping drops, the images and cross hairs were projected onto a ground-glass screen.

For each sample, both advancing and receding contact angles were measured. The advancing angles were measured at the leading edge of drops about to slide under gravitational influence. The receding angles were measured similarly at the trailing edge of drops at the start of sliding. Five advancing and five receding contact angles were measured for each substrate.

## Results and Discussion

Table I lists the average advancing and receding contact angles and their standard root-mean-square deviations for sample flats in the first apparatus after 3650 hr. of continuous condensation. The contact angle of water appears to be zero on the quartz sample, which is one indication of freedom of the system from organic contamination. The contact angles of water on the nonnoble metals, cadmium, nickel, and titanium, appear to be near zero, with any break in the condensed film of water occurring near the bottom of the sample, where the accumulated washing by condensed water is the greatest and where the oxide film might be partly removed by the washing action.

**Table I:** Wettability of Metal Surfaces after 3650 Hr. of Continuous Condensation with Pure Water

Sample	Average contact angle, deg.	
	Advancing	Receding
Silver (99.9%), heated in H <sub>2</sub> to 600°	85 ± 5	74 ± 2
Silver, plated on Type 316 stainless steel	89 ± 3	55 ± 11
Gold (99.9%)	85 ± 3	46 ± 2
Rhodium, plated on silver	65 ± 3	51 ± 7
Rhodium, plated on copper-nickel 10%	82 ± 2	73 ± 1
Palladium	74 ± 3	51 ± 7
Platinum	50 ± 6	30 ± 2
Titanium	90% filmwise condensation; 5% mixed	
Nickel	70% filmwise condensation; 20% mixed	
Cadmium	100% filmwise condensation	
Quartz	100% filmwise condensation	

Water has a fairly high advancing and receding contact angle on each of the noble metal surfaces studied here. Platinum is the most wettable of these, with a 50° advancing angle and a 30° receding angle.

Table II lists the advancing and receding contact angles of water on the tube condenser surfaces in an atmosphere of water vapor at 115°. Neither the condensation conditions nor the sample preparations were the same in the two apparatus, and the contact angles on the bright electroplated noble metal surfaces were somewhat lower than for the sample flats listed in Table I. The gold advancing angles averaged about 61° as compared to 85°, the silver was about 69° compared with 87°, and the rhodium about 65° compared with 73°. The essentially hydrophobic nature of the noble metals under continuous condensing conditions with high purity steam is confirmed, however.

It is of interest to note that water condenses in a filmwise fashion on the chromium, stainless steel, and copper-nickel 10% surfaces. This wettability, we believe, is due to the oxide films on the surfaces. Our

**Table II:** Wettability of Metal Tube Surfaces after 1500 Hr. of Continuous Condensation with Pure Water

Sample description	Average contact angle, deg.—	
	Advancing	Receding
7.6 $\mu$ Au over 5.1 $\mu$ Ni over copper-nickel 10% base	66 $\pm$ 3	55 $\pm$ 3
1.3 $\mu$ Au over 7.6 $\mu$ Ni over copper-nickel 10% base	55 $\pm$ 3	47 $\pm$ 2
13 $\mu$ Ag over 13 $\mu$ Ni over copper-nickel 10% base	68 $\pm$ 2	60 $\pm$ 1
13 $\mu$ Ag over Type 316 stainless steel base	70 $\pm$ 2	50 $\pm$ 2
0.25 $\mu$ Rh over 2.5 $\mu$ Au over copper-nickel 10% base	65 $\pm$ 2	55 $\pm$ 1
13 $\mu$ Cr over 25 $\mu$ Ni over copper-nickel 10% base	(Filmwise condensation over 95% of the area)	
Copper-nickel 10%	(Filmwise condensation over 95% of the area)	
Type 316 stainless steel	(Filmwise condensation over 100% of the area)	

experimental evidence for this could be seen when, after about 1900 hr. total condensation time, the dark oxide film on a small area near the bottom of the copper alloy tube had washed off, leaving a bright copper-colored area; on this area the water condensed in a dropwise fashion, with a contact angle in the order of 60–70°. Because the steam at this time was substantially oxygen-free, the bright area continued to exist without darkening.

Further evidence of the role of oxide in the wetta-

bility of the metals was provided in an experiment at 2000 hr. in which oxygen was introduced into the chamber in an amount equal to 0.3% of the chamber volume. Several effects could be seen. (1) The copper-nickel and the chromium samples, which had showed dropwise or mixed condensation in the areas most subject to washing, reverted to 100% filmwise condensation; this was accompanied by a darkening of the copper-nickel sample. (2) The contact angle on the silver surfaces was lowered temporarily (by perhaps 20°). (3) The gold and rhodium samples appeared to be unchanged as to wettability. The final wettability in contact with oxygen at this small partial pressure and the changes caused by the addition of the oxygen are closely related to the "nobility" of the metals under consideration.

Two factors appear to affect the degree of coverage of the metal surfaces by oxide under the continuous condensing conditions. One factor is the fraction of surface covered by oxygen (if less than a monolayer) or the thickness of oxide layer formed as a function of time and partial pressure of oxygen. For the noble metals, Rao, Damjanovic, and Bockris<sup>4</sup> have provided values for fractional surface coverage with adsorbed oxygen at a temperature of 20°: Au <0.03; Pd, 0.22; Pt, 0.22–0.27; Rh, 0.90. At room temperature, with partial pressures of oxygen between 10<sup>-4</sup> and 10<sup>-2</sup> mm., the oxide film thicknesses forming on silver and copper level off after a few hours at about 15 and 150 Å., respectively.<sup>5</sup>

The second factor, which is of particular importance for the case of metals which have more than a fractional monolayer of oxygen on the surface, is the solubility of the oxide film in water. For example, the solubility of Ag<sub>2</sub>O in water is 0.0053 g./100 ml. at 80°.<sup>6</sup> A calculation using the observed tube condensation rate of 4  $\times$  10<sup>-3</sup> g./cm.<sup>2</sup>-sec. and a density of Ag<sub>2</sub>O of 7.14 g./cm.<sup>3</sup> indicates that the quantity of water condensed in 0.5 sec. on a unit area would be sufficient to dissolve a 15-Å. film of Ag<sub>2</sub>O on the area. Thus it might be suggested that a silver surface under active condensation conditions in air-free steam would be substantially free of gross oxide surface films. The surface oxide layer on chromium and on stainless steel, on the other hand, appears to be tenaciously held; it is also conceivable that the oxide film on those materials above hydrogen in the electromotive force series might be replenished by limited reaction of the metal surfaces with the steam.

(4) M. L. B. Rao, A. Damjanovic, and J. O'M. Bockris, *J. Phys. Chem.*, **67**, 2508 (1963).

(5) N. Cabrera and N. F. Mott, *Rept. Progr. Phys.*, **12**, 163 (1948).

(6) "Handbook of Chemistry and Physics," 44th Ed., The Chemical Rubber Publishing Co., Cleveland, Ohio, 1961, p. 649.

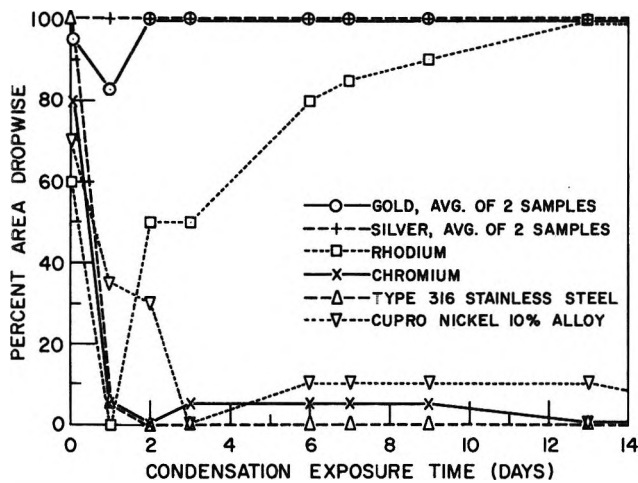


Figure 1.

Figure 1 shows graphically how these two factors operate and also shows the removal of organic surface contamination under the described conditions in the tube condensing apparatus. The first points describe the system after 0.5 hr. of condensation washing. Note that on all six materials, water condenses in a dropwise manner initially on from 60 to 100% of their area; this corresponds to the hydrophobic nature imparted to "high-energy surface" materials through exposure to laboratory air with its organic components. The stainless steel and chromium surfaces, however, quickly (in 1 day) become hydrophilic and with their tenacious oxide films remain that way. The copper-nickel 10% takes 3 days to become wettable; due to some oxide removal by the washing action the dropwise area varies from about 0 to 10%.

Among the noble metals, gold soon becomes 100% dropwise and remains so, as would be expected from its oxide-free surface. The hydrophobic nature of the silver (100% dropwise from 0.5 hr. on) could well relate to the somewhat high solubility of the thin initial oxide coating on its surface, which when dissolved off leaves the hydrophobic oxide-free metal surface. Any tendency for a net re-forming of the oxide is apparently negated in the steam atmosphere with its extremely low partial pressure of oxygen.

The behavior with rhodium is of great interest, in view of the possible 0.90 fractional surface coverage with oxygen at the start. The dropwise area drops

from 60% to 0 in the first day, suggesting that a wettable oxide surface is indeed present after the usual organic contamination is removed. A slow increase in hydrophobic behavior then occurs over a period of more than 1 week until the area becomes 100% dropwise; this confirms that the oxide layer is only very slightly soluble in water (much less so than silver oxide). The wettability characteristics of all the surfaces as shown at 14 days (336 hr.) have remained substantially unchanged through 2800 hr. exposure time in the present program.

In conclusion, it has been demonstrated experimentally that water has a high contact angle on a number of metal surfaces substantially free of oxide films, including gold, silver, rhodium, palladium, and platinum, under conditions of continuous condensation.

It should be emphasized here that the nonwettability of a clean, "high-energy" surface is not contrary to the basic principles of surface thermodynamics. In the past it has been stated that a liquid having a free surface energy of less than 75 ergs/cm.<sup>2</sup> would be expected to spread spontaneously on any clean "high-energy surface" because there would thereby be expected to result a decrease in the free surface energy of the system.<sup>7</sup> No decrease in the over-all surface energy of the system would, however, occur with spreading if  $|\gamma_{LV}\Delta A_{LV} + \gamma_{SL}\Delta A_{SL}| > |\gamma_{SV}\Delta A_{SV}|$  for the change from the drop configuration to the spreading configuration. ( $\gamma_{LV}$  is the liquid-vapor interfacial tension,  $A_{LV}$  is the liquid-vapor interfacial area, etc.) This is apparently the case for substantially oxide-free metal surfaces with respect to wetting by water.

This work is presently being extended with further studies of the wettability of these and other metals and inorganic materials under controlled condensation conditions over extended periods of time.

*Acknowledgment.* This work was supported by the Office of Saline Water, U. S. Department of the Interior, under Contract No. 14-01-0001-293. The thoughtful interest of Messrs. E. A. Cadwallader of the Office of Saline Water and Edmund Thelen of The Franklin Institute Laboratories is acknowledged with appreciation.

(7) H. W. Fox, E. F. Hare, and W. A. Zisman, *J. Phys. Chem.*, **59**, 1097 (1955).

## Thermodynamic Parameters of Hydrophobic Bond Formation

### in a Model System<sup>1,2</sup>

by Henry Schneider, Gordon C. Kresheck,<sup>3</sup> and Harold A. Scheraga

*Department of Chemistry, Cornell University, Ithaca, New York (Received October 24, 1964)*

In order to compare the theoretical and experimental values for the thermodynamic parameters for the formation of hydrophobic bonds, the standard free energy, enthalpy, and entropy changes were evaluated for the transfer of the hydrocarbon chains of acids and alcohols from water to the water-polystyrene interface. These parameters were computed from those of the acids and alcohols, which were determined from adsorption isotherms and calorimetric measurements, on the basis of the assumption that the contributions of the polar and nonpolar portions are additive. In the case of the acids, rough quantitative agreement with theory was found but not with the alcohols, the enthalpy change in this latter case becoming more negative with chain length instead of more positive. This trend is similar to that found for the transfer of alcohols from water to hydrocarbon solvents and is contrary to that found for the same type of transfer processes with hydrocarbons. The presence of a head group effect on the thermodynamics of adsorption, indicated by the different behavior of acids and alcohols, was confirmed by the findings that the butyrate ion and isoelectric amino acids with hydrocarbon chains comparable in length to those of the acids and alcohols were adsorbed to only a very small extent, if at all. It was concluded that the rough quantitative agreement between theory and experiment in the acid series provided support for the theory and that there may be a pronounced head group effect with some compounds on the thermodynamics of hydrophobic bond formation.

### Introduction

Thermodynamic parameters for the formation of hydrophobic bonds between nonpolar side chains of proteins have been evaluated recently<sup>4</sup> on the basis of a statistical mechanical theory of the structure of liquid water and of aqueous solutions of hydrocarbons.<sup>5,6</sup> In order to compare these theoretical values with experiment, it seemed necessary to resort to model systems because the interactions of interest in proteins are not readily accessible to study in a straightforward manner. In one of the model systems studied thus far, the adsorption of carboxylic acids at the polystyrene-water interface,<sup>7</sup> the extent of adsorption was found to increase with chain length, in agreement with theoretical considerations. The polystyrene-acid system was chosen as a model because of the expectation that the nonpolar portion of the adsorbed molecule would be in a state analogous to that in a hydrophobic bond in

that it would be near a nonpolar surface in the presence of water.

The favorable qualitative agreement between theory and experiment in the polystyrene-acid system<sup>7</sup> sug-

(1) This work was supported by a research grant (AI-01473) from the National Institute of Allergy and Infectious Diseases of the National Institutes of Health, U. S. Public Health Service, and by a research grant (GB-2238) from the National Science Foundation.

(2) Presented in part before the Division of Biological Chemistry at the 146th National Meeting of the American Chemical Society, Denver, Colo., Jan. 1964, and at the meeting of the American Society of Biological Chemists, Chicago, Ill., April 1964.

(3) National Institutes of Health Postdoctoral Fellow of the National Cancer Institute, 1963-1965.

(4) G. Némethy and H. A. Scheraga, *J. Phys. Chem.*, **66**, 1773 (1962).

(5) G. Némethy and H. A. Scheraga, *J. Chem. Phys.*, **36**, 3382 (1962).

(6) G. Némethy and H. A. Scheraga, *ibid.*, **36**, 3401 (1962).

(7) I. Z. Steinberg and H. A. Scheraga, *J. Am. Chem. Soc.*, **84**, 2890 (1962).

gested that it might be suitable for comparing theory and experiment quantitatively. This possibility was explored in the present study by determining the thermodynamic parameters for the adsorption of the hydrocarbon chains of straight chain carboxylic acids. These quantities were computed from the thermodynamic parameters for adsorption of these acids on the basis of the assumption that the contribution of the carboxyl group was the same for each acid and could be represented by the parameters for the adsorption of formic and acetic acids. The thermodynamic parameters for the adsorption of the acids themselves were determined during the course of this study from adsorption isotherm and calorimetric measurements. The possibility that the polar head group might alter the energetics of binding was investigated by comparing some aspects of the thermodynamics for adsorption of the acids with those of the sodium salt of butyric acid, alcohols, and amino acids in their isoelectric form. It was found that there was rough quantitative agreement between theory and experiment in the acid system and that the head group exerted a marked effect on the energetics of adsorption which was manifest in all cases but that of the acids.

Experiments designed to characterize the thermodynamic behavior of the transfer of compounds which do not have a polar head group (ethane, propane, and *n*-butane) from water to the water-polystyrene interface were also carried out. It was found not to be possible to evaluate the relevant thermodynamic parameters in these systems because the adsorption data could not be interpreted unequivocally, there being the possibility that the hydrocarbons were adsorbed in multilayers and, also, that they diffused into the matrix of the polystyrene particles. However, the experiments did provide a straightforward demonstration of the unusual variation with temperature of the enthalpy change for the transfer of hydrocarbons from water to hydrocarbon solvents,<sup>8</sup> or of the enthalpy of formation of a hydrophobic bond,<sup>4</sup> namely that  $\Delta H$  is positive at low temperatures and becomes more negative with increasing temperature, eventually passing through zero.

Several experiments were also carried out to see how proteins and synthetic polypeptides behaved at the polystyrene-water interface. It was found that these materials were strongly adsorbed.

## Experimental

**Materials and Methods. Polystyrene.** The polystyrene employed was a porous resin with a large surface area which was kindly supplied by the Dow Chemical Co., Midland, Mich. The styrene-divinyl-

benzene ratio used in its preparation was 1:1; hence the final product is extensively cross linked. The polymer was obtained in a water-swollen form which was prepared by the manufacturer by swelling the dry polymer in toluene, leaching out the toluene with acetone, and then replacing the acetone with water. All adsorption experiments were carried out with this water-swollen material after purifying it. The purification was considered necessary since some batches had a slight odor and materials soluble in toluene but insoluble in water could be extracted from the air-dried polymer. The odor was thought to be due to the presence of small amounts of the solvent in which polymerization was carried out and the soluble materials were thought to be low molecular weight and slightly cross-linked polymers. The purification procedure consisted of drying the polymer in air and then extracting it exhaustively in a Soxhlet apparatus first with toluene, then with acetone, and finally replacing the acetone with water. Drying the polymer in air caused it to shrink but it was readily re-swollen when it was extracted with toluene. Fine particles were removed after the purification had been carried out by elutriation in water.

The water-swollen polystyrene lost water rapidly when exposed to air and consequently it was always stored under water. For adsorption experiments, the polystyrene was weighed out as a slurry in water and the amount of polymer actually used was determined by dry weight at the end of the experiment.

The surface area of the dry polymer was 505 m<sup>2</sup>/g. as determined by nitrogen adsorption at low temperature (B.E.T.) and the pore size ranged from 0.005 to 0.1  $\mu$  as determined with an Aminco porosimeter.<sup>9</sup> When water-swollen, the volume of the polystyrene particles was about twice that when dry; hence, the surface area and pore size would be expected to be considerably greater in this wet state.

**Reagents.** The acids and alcohols used were the purest grades available commercially. The amino acids were chromatographically pure and were obtained from Mann Research Laboratories, Inc., New York, N. Y., as was DL-leucylglycylglycine. Glycylglycylglycine was purchased from the Nutritional Biochemical Corp., Cleveland, Ohio, and ribonuclease, 5 $\times$  crystallized Type 1A, was provided by the Sigma Chemical Co., St. Louis, Mo. Poly-L-proline II (DP = 150) and poly-DL-alanine (DP = 30) were gifts from

(8) W. Kauzmann, *Advan. Protein Chem.*, **14**, 1 (1959).

(9) We are indebted to Dr. D. R. Asher of the Dow Chemical Co., Midland, Mich., for supplying us with these data and also for supplying the polystyrene.

Dr. I. Z. Steinberg of the Weizmann Institute, Rehovoth, Israel. The hydrocarbon gases and sodium butyrate were provided by the Matheson Co., East Rutherford, N. J. The purity of the hydrocarbons was at least 99.7 mole % by the manufacturer's analysis. Laboratory distilled water was deionized before use.

*Determination of Adsorption Isotherms.* The extent of adsorption of all compounds other than the hydrocarbons and ribonuclease was determined by adding a known amount of a standardized solution of the adsorbate to a weighed amount of a polystyrene-water slurry in a screw-capped test tube and shaking gently for 2.5 hr. The amount of the various components employed varied with the amount of adsorption expected but in most instances about 0.3 g. of polystyrene (dry weight) was used with about 10 ml. of adsorbate solution. In experiments at  $4.0 \pm 0.1^\circ$  the suspensions were shaken in a temperature-controlled cold room; the suspensions were shaken in a thermostated water bath at the other temperatures employed, *viz.*, 15.0, 25.0, and  $40.0 \pm 0.1^\circ$ . Shaking for 2.5 hr. was more than sufficient to attain equilibrium since, from observations of the rate at which heat was absorbed or evolved during the calorimetric experiments, the reaction could be seen to be over in 5 min. In the case of ribonuclease, experiments were carried out as with the low molecular weight adsorbates except that the slurries were shaken for 24 hr. After the shaking period, the polystyrene was allowed to settle for 0.5 hr.; the equilibrium concentration of acid in the supernatant was then determined potentiometrically by titration with standard base, and the concentrations of sodium butyrate and the alcohols were determined by oxidation with dichromate.<sup>10</sup> The concentrations of the amino acids were determined colorimetrically with ninhydrin.<sup>11</sup> The concentration of polyalanine and polyproline was determined from optical density measurements at  $230 \text{ m}\mu$  on the basis of calibration curves while that of ribonuclease was determined at  $278 \text{ m}\mu$  taking the molar extinction coefficient as 9800.<sup>12</sup> When the concentration of adsorbates was determined by a spectrophotometric method, the supernatants were filtered through a cellulose acetate membrane (Type HAWP 013 000, Millipore Filter Corp., Bedford, Mass.) in order to remove minute amounts of particles of polystyrene which settled extremely slowly and which would interfere with the analysis. The dry weight of polystyrene in each tube was determined at the end of the run by transferring the slurry quantitatively to a sintered glass crucible, washing with water and acetone, and then drying in air at  $55\text{--}60^\circ$ .

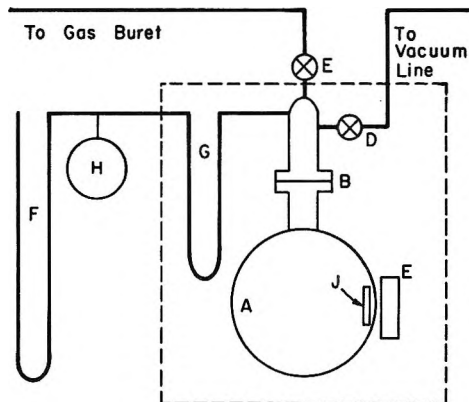


Figure 1. Apparatus for measuring gas adsorption at the polystyrene-water interface. See text for definitions of symbols.

A schematic diagram of the apparatus used to follow the interaction of dissolved hydrocarbon gases with water-swollen polystyrene is shown in Figure 1. The polystyrene-water slurry was placed in the vessel labeled A and could be stirred by the stirring bar and magnet arrangement labeled J and E, respectively. The volume of A up to the O-ring joint B was about 100 ml. and the total volume of the system was about 120 ml. The dry weight of polystyrene employed varied from 1 to 3 g. and the volume of water used was about 70 ml. The gas was introduced *via* stopcock E and the pressure in the reaction vessel was measured using the combination of the differential and absolute mercury manometers G and F. The amount of gas introduced was determined with the aid of a gas buret connected to stopcock E.

The bulb labeled H which contained air and could be connected to either a pressure or a vacuum line (by stopcocks not shown) was used to equalize the pressure on the two sides of the differential manometer in order to keep the volume of the system constant. The stopcocks E and D were of the greaseless variety (Lab-Crest needle valve, The Fischer and Porter Co., Warminster, Pa.) as was the O-ring joint, B, so that errors arising from the absorption of hydrocarbon by stopcock grease were absent. The portion of the apparatus thermostated ( $\pm 0.1^\circ$ ) is indicated by the dotted line.

Replicate determinations of the water solubility of propane and butane with this apparatus (substituting a vessel with a volume of 500 ml., containing water but no polystyrene, for the one used for the adsorption

(10) R. Sargent and W. Rieman, III, *Anal. Chim. Acta*, **14**, 381 (1956).

(11) S. Moore and W. H. Stein, *J. Biol. Chem.*, **176**, 367 (1948).

(12) J. Hermans, Jr., and H. A. Scheraga, *J. Am. Chem. Soc.*, **83**, 3283 (1961).



experiments) deviated from the mean value by less than 0.5% in most instances and were in good agreement with the values of other workers as quoted in ref. 13. In hydrocarbon adsorption experiments, results were reproducible to within  $\pm 2\%$ . The amount of hydrocarbon which had combined with the polystyrene was taken to be equal to the difference between the amount introduced into the system and the amount remaining in the vapor phase and that dissolved in solution at equilibrium. The amount in the vapor phase at equilibrium was determined from the partial pressure of the hydrocarbon and the volume of the vapor space in the reaction vessel, this latter quantity being computed from the volume of liquid and polystyrene used in the experiment and the volume of the reaction vessel when empty. The amount dissolved in solution was computed from solubility data for the hydrocarbons as a function of pressure and temperature and the volume of water used. The solubility values employed for propane and butane were those obtained with the present apparatus while the values of Morrison and Billet<sup>14</sup> were used for ethane. In computing the amount of gas introduced into the apparatus and that remaining in the vapor phase at equilibrium, small deviations from ideality, which were always less than 4%, were taken into account using the compressibility factor data of Silberberg, *et al.*<sup>15</sup> Application of the correction consisted of computing the number of moles in the volume of interest using the ideal gas law and then dividing this quantity by the compressibility factor for the appropriate temperature and pressure.

The procedure usually followed in determining an adsorption isotherm was first to outgas the water-polystyrene slurry by boiling gently at 25° at low pressure, introduce a known amount of gas, stir until equilibrium was attained, record the final pressure, and then add an increment of gas and repeat the process until the practical pressure limit of 2 atm. was reached or until the polystyrene began to cake at the top surface of the water. Caking occurred only with butane when the partial pressure was about 600 mm. at 25° and 350 mm. at 4° and was presumed to be caused by a large decrease in the density of the adsorbant as the result of the uptake of butane. Experiments were discontinued when the adsorbant began to cake because it was then no longer in intimate contact with the aqueous phase since it was a coherent mass floating on the surface of the water which could not be dispersed by the magnetic stirring arrangement.

All experiments with the exception of those involving ribonuclease were carried out in aqueous solution without the addition of buffer salts. Consequently,

the pH in experiments with the acids was 2 to 4, depending on the acid and its concentration, and that for CO<sub>2</sub> saturated water, *i.e.*, about 5.5, with the other compounds. The ribonuclease experiments were carried out in a pH 6.5 buffer (0.01 *M* glycine plus 0.15 *M* KCl).

*Evaluation of Thermodynamic Parameters.* In linear regions of the isotherms, the equilibrium constant for adsorption, *K*, and the number of binding sites per gram of adsorbent, *b<sub>T</sub>*, were determined graphically (least squares) with the aid of the equation

$$\frac{1}{b} = \frac{1}{(a)} \left( \frac{1}{b_T K} + \frac{1}{b_T} \right) \quad (1)$$

from the slope and intercept of a plot of the reciprocal of the number of moles of adsorbate bound per gram of adsorbant, 1/*b*, *vs.* the reciprocal of the activity (see below) of the adsorbate in the supernatant, 1/(*a*). Equation 1 can easily be shown to be a form of the Langmuir adsorption isotherm. The equilibrium constant, *K*, in this equation may be defined as<sup>16</sup>

$$K = \frac{\theta}{(1 - \theta)(a)} \quad (2)$$

where  $\theta$  represents the fraction of surface sites occupied, *i.e.*, *b/b<sub>T</sub>*. From the derivation of this isotherm given by Everett,<sup>17</sup> it is readily evident that the free energy change calculated from eq. 3, taking the standard

$$\begin{aligned} \Delta F^\circ &= -RT \ln K \\ &= -RT \ln \frac{\theta}{(1 - \theta)(a)} \end{aligned} \quad (3)$$

state to be mole fraction unity for the adsorbate in solution and on the surface, is the standard excess or unitary<sup>8</sup> free energy of adsorption,  $\Delta F_u^\circ$ . This quantity was of interest in rationalizing certain aspects of the isotherms of the acids; to obtain  $\Delta F_u^\circ$ , the units of *K* had to be changed from liters/mole to (mole fraction)<sup>-1</sup> since *K* was originally obtained from plots in which the units of (*a*) were moles/liter. The conversion was accomplished by multiplying *K* by 55.5, the number of moles of water in 1 l. This procedure is only an approximation since the solutions employed in determining the isotherms, especially those used in the case of the lower acids and alcohols, were too con-

(13) G. C. Kresheck, H. Schneider, and H. A. Scheraga, to be submitted.

(14) T. J. Morrison and F. Billet, *J. Chem. Soc.*, 3819 (1952).

(15) I. H. Silberberg, P. K. Kuo, and J. J. McKetta, Jr., *Petrol. Engr.*, 24, C9 (1952).

(16) D. C. Grahame, *J. Phys. Chem.*, 57, 665 (1953).

(17) D. H. Everett, *Trans. Faraday Soc.*, 46, 942 (1950).

centrated to allow the conversion to be carried out accurately in this way. However, the maximum error in  $K$  estimated to be introduced by this procedure was only 4% and could be ignored for the present purposes. It is necessary to point out that the values computed for the unitary parameters for adsorption of the side chains of the adsorbates were not altered by changing the units of  $K$  as described above since the conversion factor was eliminated when the contribution of the head group was subtracted out.

The enthalpy of adsorption was obtained by direct calorimetric determination. It was not evaluated from measurements of  $K$  as a function of temperature because sufficient precision to observe the trends of interest could not be obtained in this way. The unitary change in the entropy of adsorption was obtained from the relation

$$\Delta F_u^\circ = \Delta H^\circ - T\Delta S_u^\circ \quad (4)$$

In experiments with hydrocarbons the adsorption isotherms were found to be curved. In these cases an average equilibrium constant was evaluated at the point where one-half of the total number of binding sites was occupied using the procedure employed by Nisonoff and Pressman<sup>18</sup> for the binding of haptens to antibodies in heterogeneous systems.

The activity coefficients employed in experiments with *n*-butyl alcohol at 4° were those of Harkins and Wampler<sup>19</sup> for 0°. For experiments with ethanol and *n*-propyl alcohol at 4°, values calculated for 0° from the activity data of Knight<sup>20</sup> for water in alcohol solutions were used. The standard state for these activities was a hypothetical ideal 1 *M* solution. For the acids, the activity of the undissociated form was taken to be equal to the molar concentration of the monomeric species, the standard state being taken to be a hypothetical ideal 1 *M* solution. This concentration of the monomeric species was estimated from the measured value of the total concentration of acid in the supernatant, as determined by titration with base, its acid dissociation constant, and its dimerization constant,  $K_D$ , where  $K_D$  is defined as  $(HA)_2/(HA)^2$  and where HA represents the undissociated form of the acid. The dimerization constants employed were estimated on the basis of the results of Schrier, Pottle, and Scheraga,<sup>21</sup> who showed that at 25° the enthalpy for the dimerization of formic acid was zero and that the free energy of dimerization of acetic, propionic, and butyric acids could be represented by the sum of two terms, one for the contribution of the carboxyl group, which was taken to be equal to that for the dimerization of formic acid, and one for the contribution of the hydrocarbon tails the values of which agreed

with those predicted from the theory of Némethy and Scheraga<sup>4</sup> for the formation of hydrophobic bonds. The dimerization constants at other temperatures, evaluated on the basis of these findings, were 0.11, 0.19, and 0.30 for acetic, propionic, and butyric acids, respectively, at 4°. The values evaluated for acetic and propionic acids at 40° are 0.13 and 0.26, and for propionic acid at 15 and 25°, 0.20 and 0.22, respectively. The value of the dimerization constant for formic acid used in these calculations was 0.04 at 25°.<sup>21</sup>

For the purposes of the present study the accuracy of the dimerization constants employed was not of prime importance since it was found that if they were allowed to vary by as much as 20%, the computed concentration of monomer varied by only 1% or less, and errors of this magnitude would not affect the final results in a perceptible manner. The net effect of plotting the data in terms of the concentration of the undissociated monomeric species (taken equal to its activity) instead of the total acid concentration was to increase the equilibrium constant for adsorption by 5% or less and to increase the sharpness of the break observed in the isotherms for some of the acids. The effect on the thermodynamic parameters for the adsorption of the side chains was not perceptible within the experimental error. The reason for this is that these quantities were obtained by subtracting those for acetic or formic acids (ethanol in the case of the alcohols) from those of the higher homologs. Hence, any change in  $K$ , which is more or less the same for each member of the series, caused by using activities instead of concentrations is cancelled out in the subtraction process.

*Calorimetric Measurements.* Enthalpies of adsorption were obtained using an adiabatic solution calorimeter modeled after the one described by Benjamin.<sup>22</sup> Measurements were carried out at temperatures close to either 4 or 40° and were not corrected for small deviations (normally  $\pm 0.1^\circ$ ) from these temperatures. In all cases a weighed 40-ml. portion of an aqueous polystyrene slurry was placed outside the glass sample cell which contained a known volume and weight of a standardized solution of the adsorbate. The dry weight of polystyrene was determined after adsorption

(18) A. Nisonoff and D. Pressman, *J. Immunol.* **80**, 417 (1958).

(19) W. D. Harkins and R. W. Wampler, *J. Am. Chem. Soc.*, **53**, 850 (1931).

(20) W. Knight, Ph.D. Thesis, Princeton University, 1962.

(21) E. E. Schrier, M. Pottle, and H. A. Scheraga, *J. Am. Chem. Soc.*, **86**, 3444 (1964).

(22) L. Benjamin, *Can. J. Chem.*, **41**, 2210 (1963); we are indebted to Dr. Benjamin for providing us with information about the design of this instrument prior to publication.

following collection on a fritted glass filter. Minute pieces of glass, which resulted from breaking the sample cell, were present on the filter and a correction for their contribution to the weight of dry polystyrene, estimated as 0.03 g., was made. This correction was uncertain by  $\pm 0.015$  g. and affected the final heat of adsorption by an amount which depended on the weight of polystyrene but which was always less than 2%. Correction was also made for the heat associated with opening the sample cell. Since the heat capacity of the adsorbate solution in the sample cell amounted to less than 5% of the total heat capacity, it was estimated from the data of Bury and Davies.<sup>23</sup> The heat capacity of the water and the cell was determined and was used to obtain the heat capacity of the water-swollen polystyrene, which was found to contribute less than 5% to the total heat capacity. Weights were corrected to vacuum and the results were expressed in terms of the defined calorie which is equal to 4.184 absolute joules.

For purposes of calculation, the adsorption process was considered to take place in two steps. The first was a dilution process which was followed by the actual adsorption process. The heat of dilution of adsorbate was measured directly in separate experiments, and it was usually about  $\frac{2}{3}$  of the heat change observed in the presence of polystyrene. The amount of adsorbate bound at equilibrium in the calorimeter cell was computed from the known composition of the system and the adsorption isotherm assuming that only monomers of the undissociated form of the acid were adsorbed. The average deviation from the mean value of enthalpies of adsorption obtained in duplicate experiments was less than 0.1 kcal./mole in most cases.

## Results

**Carboxylic Acid Salts.** The amount of the butyrate ion adsorbed from aqueous solutions of the sodium salt as concentrated as 0.2 M was equal to zero within the experimental error ( $\pm 2\%$ ) of the determination of the concentration of free butyrate ion. On the basis of the results of the present and other studies<sup>24,25</sup> on the effect of chain length on the free energy of adsorption at other types of interfaces, the butyrate ion would be expected to be adsorbed more extensively than anions of the lower acids. Hence, it was concluded that in the homologous series of acids ranging from formic to butyric, only the undissociated form is adsorbed from aqueous solutions.

**Carboxylic Acids.** The shape of the adsorption isotherms varied with the carboxylic acid. Those for acetic, propionic, and *n*-butyric acids were linear at the higher concentrations (Figure 2) but exhibited a

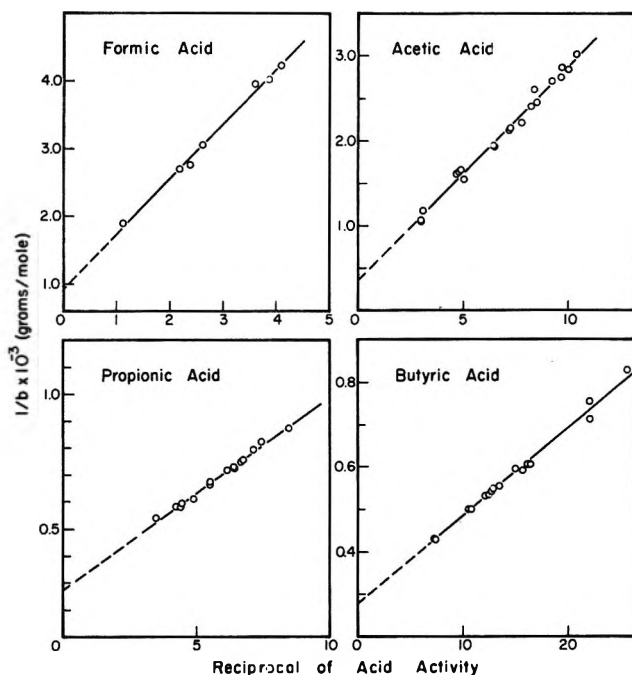


Figure 2. Adsorption isotherms (in the high-concentration region) of several acids at the polystyrene-water interface at 4°.

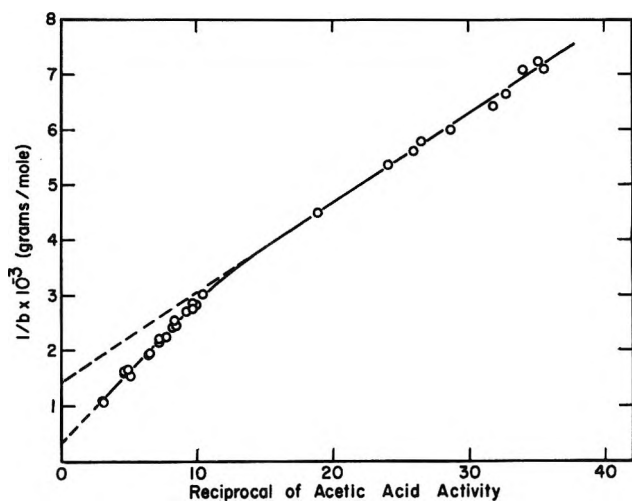


Figure 3. Adsorption isotherm of acetic acid at the polystyrene-water interface at 4°.

break at lower concentrations (Figures 3 and 4). On the lower concentration side of the break (*i.e.*, larger values of  $1/(a)$ ) the isotherm for acetic acid was linear while that for propionic acid seemed to be linear

(23) C. R. Bury and D. C. Davies, *J. Chem. Soc.*, 2413 (1932).

(24) D. Grahame and R. S. Hansen, *J. Phys. Chem.*, 60, 1153 (1956).

(25) A. F. H. Ward and L. Tordai, *Trans. Faraday Soc.*, 42, 408, 413 (1946).

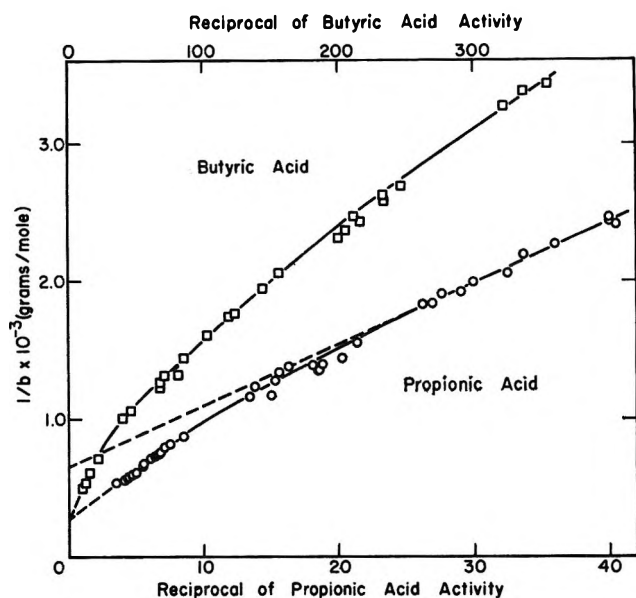


Figure 4. Adsorption isotherms of propionic and butyric acids at the polystyrene-water interface at 4°.

at the lowest concentrations studied. The isotherm for butyric acid curved continuously beyond the break. Because only small amounts of formic acid were adsorbed, a well-defined isotherm for this material could be obtained only at higher concentrations (Figure 2) and it was linear in this region.

The values of  $K$  and  $b_T$  for the linear portions of the isotherms shown in Figures 2, 3, and 4, all of which were determined at 4°, are summarized in Table I. This table also includes other relevant data. An estimate for  $b_T$  and  $K$  for the low concentration region of the isotherm for butyric acid was obtained on the assumption that the points for the 12 lowest concentrations lay on a straight line. Values for the minimum surface area available to the adsorbates are shown in Table I in the next to the last column. These quantities represent only minimal values since they were computed on the basis of the surface area of the dry polystyrene while that of the water-swollen material used is undoubtedly somewhat larger.

If only a monolayer of acid molecules was adsorbed the surface area available per molecule would be equal (or larger if a complete monolayer was not formed) to the actual area occupied by the particular orientation and conformation of the adsorbed molecule. Neither the orientation nor the conformation of the adsorbed acids is known, so that the surface area actually occupied can only be estimated roughly; for this purpose the values along the major axis of the acids evaluated by Blackburn and Kipling<sup>26</sup> were employed as a frame of reference and are shown in the last column of Table

I. If account is taken of the fact that the values for the area occupied by the adsorbates shown in Table I are minimal values, then it is evident that the adsorption isotherms may be considered as reflecting the formation of only a monolayer.

For the high-concentration region of the isotherms of propionic and butyric acid and for the linear portion of those for the alcohols (Table VI), the total number of binding sites was the same within the standard error. This fact is taken to indicate that, in the regions of the isotherm under consideration, these adsorbates may be bound to the same localized sites. The possible nature of these sites is discussed below.

In all likelihood, the orientation of the bound adsorbates varies to some extent with chain length. This view is reasonable since the final orientation would be the result of two opposing tendencies (i) that of the polar head group to interact with water and to minimize its extent of contact with the hydrocarbon surface of the resin, (ii) the opposite tendency of the nonpolar portion of the adsorbate. The consequences of these opposing tendencies would be (i) that a hydrophobic bond of full strength would not be formed, the extent of this effect decreasing with chain length; (ii) the energetics of adsorption of the head group would vary with chain length, the free energy becoming more positive with the longer chains. Effects of this sort may be responsible for the smaller number of binding sites found for formic and acetic acids when compared to those of the higher acids. In the case of these compounds the head group may control the orientation of the bound adsorbate and this orientation may be such that these molecules cannot be bound at some of the possible sites because of unfavorable interactions of the carboxyl group with the polystyrene surface.

The equilibrium constants for adsorption in the low-concentration region of the isotherms were significantly greater than the values for the high-concentration region (Table I). This fact suggested that there might be two classes of independent binding sites on the surface. However, the isotherms over the whole concentration range could not be fitted to equations derived on this assumption; hence, the breaks probably represent a transition in which the adsorbed molecules change their orientation as the concentration is increased. A transition of this sort has been proposed to occur during the adsorption of aliphatic alcohols and acids on a carbon surface.<sup>24</sup> In the present case it does not seem likely that the transition is caused by adsorbate-adsorbate interactions on the resin surface since it begins to occur when the fractional surface

(26) A. Blackburn and J. J. Kipling, *J. Chem. Soc.*, 1493 (1955).

**Table I:** Parameters of Adsorption Isotherms of the Carboxylic Acids

Region of isotherm	Temp., °C.	Acid	K, l./mole	$b_T \times 10^4$ , moles/g.	Minimum area occupied per molecule, Å. <sup>2</sup>	Area of molecule, Å. <sup>2</sup>	
High concentration	4.0	Formic	$1.14 \pm 0.15^a$	$1.08 \pm 0.08^a$	65	13.4	
		Acetic	$1.41 \pm 0.19$	$2.81 \pm 0.36$	30.0	19.6	
		Propionic	$3.91 \pm 0.24$	$3.60 \pm 0.15$	23.4	25.0	
		Butyric	$13.63 \pm 0.82$	$3.59 \pm 0.09$	23.5	31.4	
	15.0	Propionic	$4.07 \pm 0.41$	$3.36 \pm 0.12$	25.1	25.0	
	25.0	Propionic	$3.95 \pm 0.40$	$3.30 \pm 0.21$	25.4	25.0	
	40.0	Acetic	$1.00 \pm 0.25$	$2.75 \pm 0.29$	30.5	19.6	
		Propionic	$3.46 \pm 0.29$	$3.30 \pm 0.21$	25.4	25.0	
	Low concentration	4.0	Acetic	$8.69 \pm 1.43$	$0.70 \pm 0.09$	119.8	19.6
			Propionic	$14.64 \pm 1.47$	$1.53 \pm 0.12$	45.8	25.6
Butyric			~146	~0.98	85.6	31.4	

<sup>a</sup> The errors shown in this and all subsequent tables are the standard errors.

coverage is small and the minimum area available per molecule is large, the values for the fractional surface coverage being 0.1, 0.1, 0.3, and for the surface area 300, 234, and 70.5 Å.<sup>2</sup> for acetic, propionic, and butyric acids, respectively. It is suggested that the transition is caused by a combination of energetic and packing factors, that is, it is considered that at the lower surface coverages the adsorbate is free to interact with those regions of the surface which cause the largest free energy decrease. However, these high energy sites are visualized as extending over two or more possible low energy sites so that, when the concentration of acid in the aqueous phase increases, a point is reached eventually where it becomes more favorable energetically to pack the adsorbate on the low energy sites because now more molecules can be packed on with a concomitant greater over-all free energy decrease. Evidence in favor of this mechanism is provided by the data shown in Table II for the standard unitary free energy of adsorption in the two regions of the isotherms and the proportional changes in the free energy and number of binding sites on going through the transition.

It is readily apparent from Table II that on going through the transition from the low-concentration to

the high-concentration region, the standard free energy decreases by a factor of about 0.75 while the number of binding sites increases by a factor of at least 2.4.

The thermodynamic parameters for the adsorption of the acids are summarized in Table III. Since the binding of the acids in the high-concentration region of the isotherms could be characterized by a single equilibrium constant it would be expected that the enthalpy of adsorption would be independent of surface coverage in this region.<sup>17</sup> Such independence was actually found within the precision of the calorimetric measurements and is indicated in Table III by the fact that in some instances the same enthalpy value is shown for different values of  $1/b$ . In the low-concentration region of the isotherms, in the case of acetic and propionic acids, the enthalpy of adsorption was evaluated at one point in the linear region of the isotherm and was assumed to be independent of surface coverage. In the case of butyric acid, the enthalpy of adsorption was determined at two different surface coverages and different values were obtained,  $0.7 \pm 0.17$  at  $1/b = 1.34$  and  $1.9 \pm 0.07$  at  $1/b = 2.37$ . This result is not surprising since the isotherm in the low concentration region is always curved; hence, the free energy of binding varies with surface coverage and it would therefore be expected that  $\Delta H$  would do so also. The enthalpy change determined at  $1/b = 2.37$  is on that portion of the isotherm where an equilibrium constant for binding was estimated, assuming that the isotherm was linear, and this value of  $\Delta H$  was taken to approximate the actual values in this region.

Thermodynamic parameters for the adsorption of the hydrocarbon portions of the carboxylic acids at 4 and 40° are shown in Table IV. One set of these

**Table II:** Mechanism of Transition

Acid	$-\Delta F_u^\circ$ , high-concn. region, kcal./mole	$-\Delta F_u^\circ$ , low-concn. region, kcal./mole	Ratio of $\Delta F_u^\circ$ in the two regions	Ratio of $b_T$ in the two regions
Acetic	$2.40 \pm 0.08$	$3.40 \pm 0.10$	0.71	4.0
Propionic	$2.96 \pm 0.03$	$3.69 \pm 0.05$	0.80	2.4
Butyric	$3.65 \pm 0.03$	~4.96	0.74	3.7

**Table III:** Thermodynamic Parameters for the Adsorption of Carboxylic Acids

Region of isotherm	Acid	Temp., °C.	$-\Delta F_u^\circ$ , kcal./mole	$-\Delta H^\circ$ , kcal./mole	$\Delta S_u^\circ$ , e.u.	$(1/b)^a \times 10^2$ , g./mole
High concentration	Formic	4.0	$2.29 \pm 0.06$	$2.53 \pm 0.06$	$-0.87 \pm 0.30$	2.25
	Acetic	4.0	$2.40 \pm 0.08$	$2.18 \pm 0.07$	$0.79 \pm 0.38$	1.48, 3.4
	Propionic	4.0	$2.96 \pm 0.03$	$1.93 \pm 0.06$	$3.72 \pm 0.24$	0.59, 0.73, 0.91
	Butyric	4.0	$3.65 \pm 0.03$	$1.43 \pm 0.07$	$8.00 \pm 0.37$	0.50
	Acetic	40.0	$2.50 \pm 0.18$	$2.74 \pm 0.17$	$-0.77 \pm 0.90$	1.92
	Propionic	40.0	$2.98 \pm 0.05$	$2.65 \pm 0.10$	$1.05 \pm 0.40$	0.34, 0.69
Low concentration	Acetic	4.0	$3.40 \pm 0.10$	$2.15 \pm 0.07$	$4.51 \pm 0.44$	5.68
	Propionic	4.0	$3.69 \pm 0.05$	$2.12 \pm 0.07$	$5.67 \pm 0.31$	2.20
	Butyric	4.0	$\sim 4.96$	$\sim 1.90$	$\sim 11.04$	2.37

<sup>a</sup> The value of  $1/b$  indicates the degree of surface coverage at which the calorimetric measurements were made.

**Table IV:** Experimental and Theoretical Thermodynamic Parameters for Hydrophobic Bond Formation in the High Concentration Region of the Isotherms of the Acids

Temp., °C.	Side chain	Head group	Experimental values			Theoretical values				
			$-\Delta F_u^\circ$ , kcal./mole	$\Delta H^\circ$ , kcal./mole	$\Delta S_u^\circ$ , e.u.	$-\Delta F_u^\circ$ , kcal./mole	$\Delta H^\circ$ , kcal./mole	$\Delta S_u^\circ$ , e.u.	$\Delta Y^S$	$Z_R$
4.0	CH <sub>3</sub> -	Formic acid	$0.11 \pm 0.10$	$0.35 \pm 0.09$	$1.7 \pm 0.48$	0.2	0.5	2.5	2	1
	CH <sub>3</sub> CH <sub>2</sub> -		$0.67 \pm 0.07$	$0.60 \pm 0.08$	$4.6 \pm 0.36$	0.7	0.7	4.9	4	3
	CH <sub>3</sub> CH <sub>2</sub> CH <sub>2</sub> -		$1.36 \pm 0.07$	$1.10 \pm 0.09$	$8.87 \pm 0.37$	1.1	1.1	7.9	6	5
4.0	CH <sub>3</sub> -	Acetic acid	$0.56 \pm 0.08$	$0.25 \pm 0.09$	$2.93 \pm 0.43$	0.5	0.2	2.4	2	2
	CH <sub>3</sub> CH <sub>2</sub> -		$1.25 \pm 0.08$	$0.75 \pm 0.10$	$7.21 \pm 0.45$	0.9	0.6	5.5	4	4
40.0	CH <sub>3</sub> -	Acetic acid	$0.48 \pm 0.15$	$0.09 \pm 0.20$	$1.82 \pm 0.80$	0.6	-0.1	1.4	2	2

parameters was computed on the basis of the assumption that the thermodynamic parameters for the adsorption of formic acid represent the contribution of the carboxyl group to the corresponding parameters of the higher acids while the other was computed using acetic acid as the head group. It is readily evident that the experimental parameters agree with theoretical predictions<sup>4</sup> in that the free energy change becomes more negative as the length of the chain increases while the corresponding enthalpy and entropy changes become more positive. Theory predicts that, with increasing temperature,  $\Delta F$ ,  $\Delta H$ , and  $\Delta S$  should all become more negative and this seems to be the case with the experimental data for  $\Delta H$  and  $\Delta S$  for the CH<sub>3</sub> group using acetic acid as the head group. However, because of experimental errors it is difficult to be certain about this trend.

The experimental parameters for adsorption of the hydrocarbon tails also agree fairly well with the theoretical values shown in the right hand side of Table IV. The agreement here holds both at 4 and 40°. The theoretical parameters were computed for orienta-

tions of adsorbed acid molecules which were found to be possible using Courtaulds space-filling models. The number of water molecules which lose contact with hydrocarbon residues,  $\Delta Y^S$ , and the number of hydrocarbon-hydrocarbon contacts made,  $Z_R$ , assumed in the calculation, are shown on the right-hand side of the table. Better agreement could not be obtained with some other possible orientations. In the orientations to which the parameters in Table IV refer, the hydrocarbon portions of the acids were lying flat on a phenyl group while the carboxyl group faced the aqueous phase. In the case of butyric acid the  $\alpha$  and  $\beta$  carbons were considered to be in contact with the phenyl group while the terminal CH<sub>3</sub> residue interacted with the aliphatic backbone of the polystyrene adsorbent. Accordingly, the parameters computed using formic acid as the head group represent, for the CH<sub>3</sub> group, those for a hydrophobic bond of this residue with an aromatic ring (minimal contact being assumed), for the CH<sub>3</sub>CH<sub>2</sub> group, a hydrophobic bond with an aromatic ring, and for the CH<sub>3</sub>CH<sub>2</sub>CH<sub>2</sub> group, a bond involving both aromatic and aliphatic residues.

The parameters computed using acetic acid as the head group represent those for the contact of the  $\text{CH}_3$  group with an aromatic ring and of the  $\text{CH}_3\text{CH}_2$  group contact with an aromatic ring and aliphatic carbons. The values for a given side chain computed using acetic and formic acids as head groups are different because the groups under consideration are involved in different sorts of interactions. Thus, for example, in the case of the  $\text{CH}_3$  group, the value obtained using formic acid as the head group pertains to the interaction of the terminal  $\text{CH}_3$  residue of acetic acid to form a hydrophobic bond of minimum strength with an aromatic ring while the value obtained when acetic acid is used as the head group pertains to the terminal  $\text{CH}_3$  group of propionic acid forming a hydrophobic bond with an aromatic residue which is stronger than a bond of minimum strength.

In computing the theoretical parameters a small correction for the loss of rotational freedom of the hydrocarbon chains on forming the hydrophobic bond, which for  $\Delta F$  is equal to only a few tenths of a kilocalorie per mole, was not included although this term is included in the theory. The correction was omitted since better agreement was then obtained with experiment, as was found also in other model systems.<sup>21,27</sup> It is of interest to note that the agreement between the experimental and theoretical values in Table IV suggests that the assumed orientations on the binding sites are reasonable.

The thermodynamic parameters for adsorption of hydrocarbon tails of the acids in the low-concentration region of the isotherm, computed using formic acid to represent the head group, are shown in Table V.

**Table V:** Thermodynamic Parameters for Hydrophobic Bond Formation at 4° in the Low-Concentration Region of the Isotherms of the Acids

Side chain	$-\Delta F_u^\circ$ , kcal./mole	$\Delta H^\circ$ , kcal./mole	$\Delta S_u^\circ$ , e.u.
$\text{CH}_3-$	$1.11 \pm 0.14$	$0.38 \pm 0.09$	$5.38 \pm 0.60$
$\text{CH}_3\text{CH}_2-$	$1.40 \pm 0.11$	$0.41 \pm 0.09$	$6.56 \pm 0.51$
$\text{CH}_3\text{CH}_2\text{CH}_2-$	$\sim 2.67$	$\sim 1.80$	$\sim 16.09$

These numbers agree qualitatively with theory but theoretical parameters corresponding to them could not be obtained. It was possible to fit two out of three of the thermodynamic parameters, but in this case the third was off by a factor of  $\sim 2$ . Similar results were obtained when acetic acid was used as the head group. A possible reason for this behavior is that the assumption that acetic or formic acid can be used as the

head group is not valid in the low-concentration region of the isotherm. This would seem to be reasonable since, as can be seen by comparing the thermodynamic parameters for adsorption of the hydrocarbon tails in the two regions of the isotherms (Tables IV and V), the free energy of adsorption for a given residue is appreciably greater in the low-concentration region. Thus, in this region the hydrocarbon chain would be expected to exert a more prominent influence in orienting the adsorbate with the result that the energetics for adsorption of the head group will be different from that of formic acid and also will vary from acid to acid.

*Alcohols.* The adsorption isotherms for the alcohols are shown in Figures 5 and 6. At the highest concen-

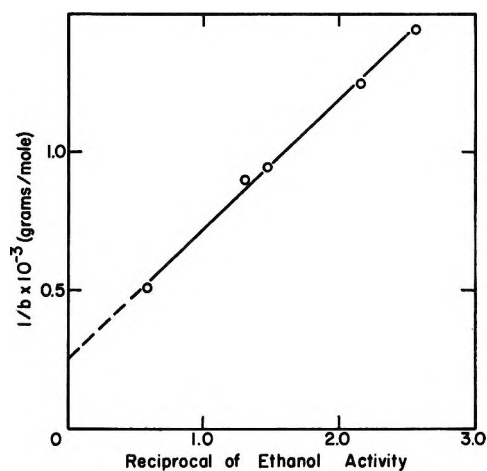


Figure 5. Adsorption isotherm of ethanol at the polystyrene-water interface at 4°.

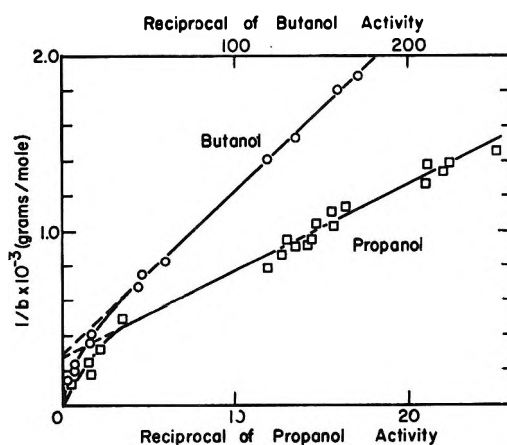


Figure 6. Adsorption isotherms of propanol and butanol at the polystyrene-water interface at 4°.

(27) E. E. Schrier, R. T. Ingwall, and H. A. Scheraga, *J. Phys. Chem.*, 69, 298 (1965).

Table VI: Binding and Thermodynamic Data for Adsorption of the Alcohols at 4°

Alcohol	$K$ , l./mole	$b_T \times 10^3$ , moles/g.	$-\Delta F_u^\circ$ , kcal./mole	$\Delta H^\circ$ , kcal./mole	$\Delta S_u^\circ$ , e.u.	$(1/b)^a \times 10^3$ , g./mole
Ethanol	$0.55 \pm 0.09$	$3.91 \pm 0.49$	$1.89 \pm 0.10$	$1.19 \pm 0.10$	$13.45 \pm 0.51$	0.98
<i>n</i> -Propyl alcohol	$5.46 \pm 1.48$	$3.60 \pm 0.51$	$3.15 \pm 0.25$	$0.70 \pm 0.10$	$13.89 \pm 0.97$	0.58
<i>n</i> -Butyl alcohol	$31.12 \pm 2.72$	$3.44 \pm 0.73$	$4.10 \pm 0.05$	$-0.12 \pm 0.10$	$14.36 \pm 0.40$	1.90

<sup>a</sup> The value of  $1/b$  indicates the degree of surface coverage at which the calorimetric measurements were made.

trations employed those for *n*-propyl and *n*-butyl alcohol depart from linearity and extrapolate to the origin. This behavior probably reflects the formation of multilayers at the higher concentration and was not observed in the case of the acids, presumably because sufficiently high concentrations were not employed. In the case of the higher alcohols and also of acids higher than *n*-butyric (not shown), the adsorption isotherms were curved over the whole concentration range employed for the other members of the series and appeared to extrapolate to the origin. Because of these complications their thermodynamics of adsorption was not studied.

Relevant binding and thermodynamic data for the adsorption of the alcohols are shown in Table VI. As pointed out previously, the number of binding sites for the alcohols are the same within the standard error as those for propionic and butyric acids and it was suggested, therefore, that all of these molecules are adsorbed on the same localized region of the surface.

The thermodynamic parameters for the adsorption of the hydrocarbon chains (using ethanol as head group) are shown in Table VII.

Table VII: Thermodynamic Parameters for Adsorption of the Nonpolar Portion of the Alcohols

Residue	$-\Delta F_u^\circ$ , kcal./mole	$\Delta H^\circ$ , kcal./mole	$\Delta S_u^\circ$ , e.u.
CH <sub>3</sub> -	$1.26 \pm 0.27$	$-0.49 \pm 0.14$	$0.44 \pm 1.10$
CH <sub>3</sub> CH <sub>2</sub> -	$2.22 \pm 0.11$	$-1.31 \pm 0.14$	$0.91 \pm 0.65$

As in the case of the acids, the free energy of adsorption became more negative with chain length; however, in distinct contrast, the enthalpy change became more negative. This variation of the enthalpy change with chain length disagrees with theoretical predictions<sup>4</sup> and suggests that the polar head group is affecting the energetics of adsorption.

*Amino Acids.* In order to see if a head group effect was present with another series of compounds, the binding to polystyrene of amino acids in their isoelectric

form was investigated. These compounds consist of a hydrocarbon portion and an electrically neutral but dipolar portion. Evidence for a head group effect in this series was found since there was little or no binding of amino acids which possessed an aliphatic hydrocarbon chain of three or four carbon atoms (*DL*-leucine, *-norleucine*, and *-norvaline*) within the precision with which the concentration of these materials in solution was determined ( $\pm 2\%$ ). Under the conditions employed (10 ml. of a 0.05 *M* solution and 0.2 g. of polystyrene), the concentration of the amino acids in the supernatant should have decreased by about 50% if they were bound as strongly as butyric acid. Some binding of  $\alpha$ -aminocaprylic acid and of the aromatic amino acids, tyrosine and phenylalanine, was observed (Table VIII), but not of glycine, *DL*-alanine, *L*-proline, *DL*-serine, *L*-glutamic acid, and *L*-aspartic acid.

Although polystyrene was a poor adsorbent for isoelectric amino acids and also for peptides such as gly-gly-gly-gly, it did combine with leucyl-gly-gly and high molecular weight polypeptides and proteins. Some of the results obtained with leucyl-gly-gly, polyproline (DP = 150), poly-*DL*-alanine (DP = 30), and ribonuclease<sup>28</sup> (pH 6.5) are shown in Table VIII.

The polystyrene surface adsorbed the ribonuclease very strongly since about 95% of the amount originally present in solution was bound. Whether or not ribonuclease unfolds on adsorption is not known. If it did unfold, then the adsorbed material should be digested by chymotrypsin in contrast to the folded material in solution, as indicated by the results of Rupley and Scheraga.<sup>29</sup> The adsorbed material was found not to be digested by chymotrypsin; hence, either (i) the molecule does not unfold on adsorption, or (ii) only regions not susceptible to chymotrypsin unfold, or (iii) the regions containing the susceptible portions unfold but are not digested by chymotrypsin.

(28) The failure to observe retardation (hence adsorption) of ribonuclease and some polypeptides on polystyrene chromatographic columns in the study of ref. 7 was probably due to the small surface area of the resin employed.

(29) J. A. Rupley and H. A. Scheraga, *Biochemistry*, 2, 421 (1963).



**Table VIII:** Adsorption of Amino Acids, Peptides, and Proteins

Compound	Concn. in supernatant at equilibrium, moles/l.	Moles bound/g. of adsorbent	% of original amount adsorbed
DL- $\alpha$ -Aminocaprylic acid	$1.7 \times 10^{-6}$	$1.5 \times 10^{-6}$	50
L-Tyrosine	$1.38 \times 10^{-3}$	$1.23 \times 10^{-4}$	12
DL-Phenylalanine	$3.05 \times 10^{-6}$	$8.9 \times 10^{-6}$	80
DL-Leucylglycylglycine	$1.08 \times 10^{-4}$	$9.19 \times 10^{-6}$	10
Poly-L-proline II	$6.25 \times 10^{-8}$	$3.96 \times 10^{-6}$	80
Poly-DL-alanine	$4.68 \times 10^{-6}$	$1.34 \times 10^{-6}$	91
Ribonuclease	$6.30 \times 10^{-6}$	$2.62 \times 10^{-6}$	95

It is of interest to note in this connection that it has been shown that the lowering of the thermal transition temperature of ribonuclease in aqueous alcohol solutions relative to that in water could be rationalized quantitatively on the assumption that the alcohols were bonded hydrophobically to hydrocarbon side chains which became available when the protein unfolded, thereby stabilizing this form.<sup>27</sup>

**Hydrocarbons.** The adsorption behavior of the hydrocarbons was more complicated than that of either the acids or the alcohols. In the case of butane at 4° (Figure 7), the isotherm turned downward at a concentration of about 0.001 (corresponding to a butane partial pressure of 220 mm.) while at 25° the isotherm extrapolated to the origin. The abrupt downturn may be the result of capillary condensation<sup>30</sup> while the extrapolation to the origin may represent the formation of multilayers. The isotherm for propane at 4° (Figure 8) was similar in shape to that for butane at 4°.

The average unitary free energy of adsorption for the point where one-half of the total number of binding sites are occupied, computed assuming the isotherms may justifiably be extrapolated as shown in Figures 8 and 9, was estimated to be -3.1 kcal./mole for ethane and -4.4 kcal./mole for propane. These values are close to those for the transfer of the hydrocarbons from water to nonpolar solvents at 4°<sup>31</sup> and are much larger than those expected for the adsorption of hydrocarbons at a polystyrene-water interface. The distinction being made here is that between the situations where the hydrocarbon chain is involved in only pairwise interactions with another chain in the presence of water (hydrophobic bonding) and that where the hydrocarbon chain is involved solely in multiple contacts with other hydrocarbon molecules or residues (solution in nonaqueous solvents). The high average values may be due, at least in part, to the occurrence

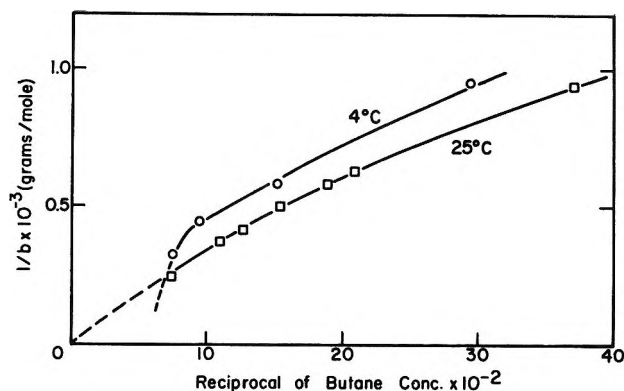


Figure 7. Adsorption isotherm of butane on polystyrene at 4 and 25°.

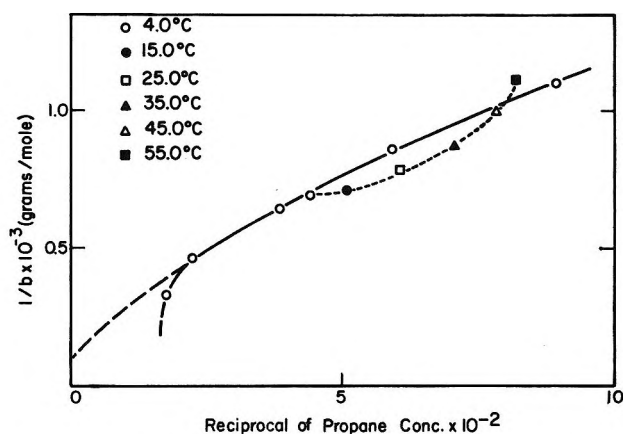


Figure 8. Adsorption isotherm of propane on polystyrene.

of multiple contacts analogous to that for solution in nonaqueous solvents since the attainment of equilibrium in the hydrocarbon systems took a relatively long time, suggesting that the adsorbates were diffusing into the matrix of the polystyrene particles. Thus, while adsorption of the acids and alcohols required 5 min. and solution of the gas in polystyrene-free water required ~1 hr., the attainment of equilibrium in the case of ethane required 4-5 hr. Even longer times were required for the other hydrocarbons, 80% of the gas being picked up in 4 hr., the remainder requiring 8-12 hr. for propane and 24-48 hr. for butane. The time for attainment of equilibrium was longer the higher the concentration of hydrocarbon. Another factor which could contribute to the high average free energy change was the use of the assumption that only a monolayer of hydrocarbon was adsorbed when, in fact, multi-

(30) S. J. Gregg, "The Surface Chemistry of Solids," 2nd Ed., Reinhold Publishing Corp., New York, N. Y., 1961, p. 68.

(31) G. Némethy, Ph.D. Thesis, Cornell University, June 1962.

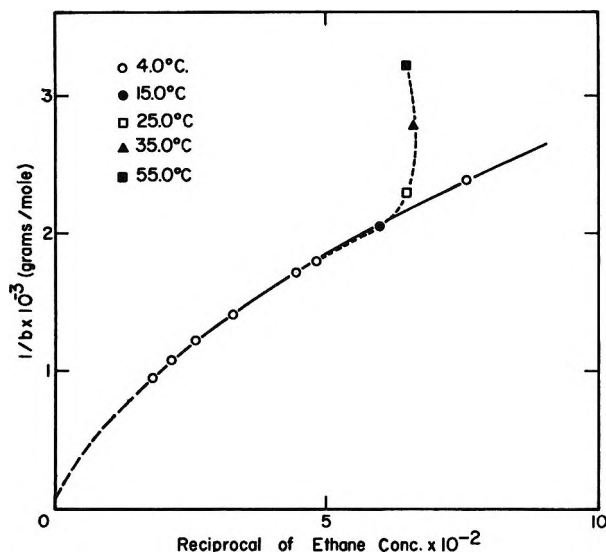


Figure 9. Adsorption isotherm of ethane on polystyrene.

layers were actually being formed. In order to see if only a monolayer is adsorbed it would be necessary to determine the surface area occupied by each adsorbed molecule. This would require determination of the total number of binding sites by extrapolation of the isotherm to  $1/c = 0$ . In the present case, sufficiently precise data to obtain a more accurate extrapolation than that shown in Figures 8 and 9 could not be obtained; hence, it was not possible to check for the formation of multilayers. It is obvious that the complex nature of the isotherms of the hydrocarbons and the difficulties associated with their interpretation preclude their use for obtaining the parameters of interest beyond the statements made above.

One of the unusual features of the enthalpy of formation of hydrophobic bonds or the transfer of hydrocarbons from water to a hydrocarbon solvent is that this parameter is positive at low temperatures and becomes more negative, actually passing through zero as the temperature increases. It is of interest to note that this phenomenon could be observed directly in experiments with the polystyrene-hydrocarbon system by following the changes in pressure of the system as a function of temperature. The results of typical experiments of this sort for ethane and propane (dashed lines at higher values of  $1/c$ ) are shown in Figures 8 and 9 from which it can be seen that the enthalpy change would be zero in the ethane system between 4 and 15° and between 25 and 35° in the propane system.

## Discussion

The tests applied here to the theory of Némethy and Scheraga for the thermodynamics of hydrophobic

bond formation were quite stringent in that attempts were made to predict for a model system the value of two thermodynamic parameters ( $\Delta F$  and  $\Delta H$ ,  $\Delta S$  being essentially a composite of these two) and also the effects of temperature and chain length. The favorable rough quantitative agreement in the acid series for the high-concentration region of the isotherm therefore supports the theory and also suggests that head group effects are not important in the carboxylic acid series.

The factors which prevented a *definitive* test of the theory from being carried out with the model system employed were due to the facts that in some instances the changes predicted by theory were small and within the experimental error (*e.g.*, the effects of temperature), the absence of information concerning the exact nature of the binding site and the orientation of the adsorbed acid, and two assumptions made in applying the theory. These were (i) that the structure of water within the pores of the polystyrene particles was the same as that of bulk water, and (ii) the partition function for water in the first layer adjacent to a hydrocarbon residue is the same when this residue is on a hydrocarbon surface as when it is in solution. With regard to the first of these assumptions, any alterations in water structure would be expected to be found only with pores with a radius less than 1000 Å. since the thermal expansion of water in pores of smaller radii is different from that of bulk water.<sup>32</sup> Whether or not this effect was important in the present study could not be determined since the pore size distribution for the water-swollen polystyrene was not known. With regard to the structure of water at hydrocarbon-water interfaces, the fact that the entropy change for their formation is more negative<sup>8</sup> than expected suggests that ordered clusters of water are present and this fact was taken into account in choosing the system investigated as a model. However, little is known about the detailed structure of this water; hence, effects involving it could not be computed exactly.

Perhaps the most striking result of the present study is the finding that the thermodynamics of adsorption of hydrocarbon chains at a polystyrene-water interface may vary in a pronounced manner with the nature of the polar, but electrically neutral head group to which they are attached. Because of this finding, salient questions at this point are: (i) are the effects observed peculiar to the water-polystyrene interface, and (ii) are the effects peculiar to hydrocarbon interfaces in general; *i.e.*, are the head group effects manifested also

(32) V. V. Karasev, B. V. Deryagin, and E. N. Eframa, *Colloid J. USSR*, **24**, 404 (1962).

in the interaction of hydrocarbon chains in aqueous solution or in the interaction of the nonpolar side chains of proteins? The answers to these questions are not clear at this time and it is difficult to come to any conclusion on the basis of the data for model systems available in the literature. Thus, with regard to the possibility that the effects are peculiar to the polystyrene-water interface, there is evidence that this is not the case since the same trends in the variation of the enthalpy change with chain length are found for the adsorption of  $C_4$  and  $C_6$  alcohols and acids at the air-water interface.<sup>33</sup> On the other hand, evidence conflicting with this view is provided by the fact that both the butyrate ion and butyric acid are adsorbed at a paraffin-water interface,<sup>34</sup> in contrast to the behavior observed at a polystyrene-water interface. However, the amount of the butyrate ion adsorbed at the paraffin-water interface is relatively small so that there is the possibility that the different sort of behavior observed in the paraffin and polystyrene systems is due primarily to a difference in the  $\zeta$  potential at the interface of these materials with sodium butyrate solutions.

With regard to the possibility that the head group effects are manifested only at interfaces, there are three pieces of evidence to consider. The first concerns thermodynamic data for the transfer of aliphatic hydrocarbons, acids, alcohols, and amino acids from water to hydrocarbon solvents or to 6-7 *M* urea. In the transfer of hydrocarbons and alcohols from water to hydrocarbon solvents, the trends in  $\Delta H$  with chain length are opposite in direction ( $\Delta H$  for hydrocarbons becoming more positive) of that for hydrocarbons, agreeing with theory.<sup>35</sup> This discrepancy is similar to that for the adsorption of the side chains of the acids and alcohols at polystyrene-water surfaces, with, in this instance, the trends for the acids agreeing with theory. On the basis of these data alone it could be concluded that the discrepancies are due to some influence of the hydroxyl group of the alcohols on the structure of water about the hydrocarbon portion. On the other hand, the trends in  $\Delta H$  are generally in the same direction for the transfer of hydrocarbons,<sup>36</sup> carboxylic acids,<sup>37</sup> amino acids,<sup>37</sup> and alcohols<sup>38</sup> from water to 6-7 *M* urea.

The second piece of evidence concerns the results of Schrier, Ingwall, and Scheraga<sup>27</sup> on the effects of alcohols on the thermal transition temperature of ribonuclease. These authors showed that if it was assumed that the alcohols were bound hydrophobically to nonpolar residues which became available when the protein was unfolded with a free energy change computed on the basis of the theory of Némethy and Scheraga,<sup>4</sup> excellent agreement was obtained between experimental

and theoretically predicted lowering of the thermal transition temperatures. Thus, these findings suggest that there is no head group effect in the case of the alcohols. The third piece of evidence concerns the nuclear magnetic resonance shift of water protons in aqueous solutions of sodium alkyl sulfates.<sup>39</sup> This study showed that hydrocarbon chains in water cause an upfield shift of the water proton resonance. The first four methylene groups adjacent to the head group have little effect, with the extent of the shift being directly proportional to the number of  $-CH_2-$  groups beyond the first four. These findings suggest that the sulfate group can perturb the structure of water along the four adjacent methylene groups and hence provide direct physical evidence for head group effects. It is readily evident that much more experimental work will have to be done in order to sort out the precise nature of the head group effects involved in the systems discussed and to evaluate their effects on hydrophobic bonds.

Recently, Feitelson<sup>40</sup> showed that the enthalpy and entropy for adsorption of the hydrocarbon chain of the cationic form of amino acids to sulfonated polystyrene resins were negative. These parameters were computed on the assumption that the contributions to the free energy of binding of the  $-NH_3^+$  group with the  $-SO_3^-$  group of the resin (taken equal to that for the  $NH_4^+$  ion) and that for the hydrocarbon tail were additive. The trends observed disagreed with theory, and therefore it was concluded that hydrophobic bonding was not involved. Since the present study indicates that the nature of the head group may affect the energetics of adsorption of the hydrocarbon portion of adsorbates, the conclusion of Feitelson must be accepted with reservation, especially in view of the fact that there are three head groups involved, namely, the un-ionized carboxyl and  $-NH_3^+$  group of the amino

(33) J. T. Davies and E. K. Rideal, "Interfacial Phenomena," Academic Press, New York, N. Y., 1961, p. 162.

(34) F. M. Fowkes and W. D. Harkins, *J. Am. Chem. Soc.*, **62**, 3377 (1940).

(35) G. Némethy, I. Z. Steinberg, and H. A. Scheraga, *Biopolymers*, **1**, 43 (1963).

(36) D. B. Wetlaufer, S. K. Malik, L. Staller, and R. L. Coffin, *J. Am. Chem. Soc.*, **86**, 508 (1964).

(37) G. C. Kresheck and L. Benjamin, *J. Phys. Chem.*, **68**, 2476 (1964).

(38) The enthalpy for the transfer of the alcohols from water to 5.7 *M* urea was determined during the course of the present study and was 0.475 and 0.962 kcal./mole for methanol and 1-butanol, respectively, at 25°.

(39) J. Clifford and B. A. Pethica, *Trans. Faraday Soc.*, **60**, 1483 (1964).

(40) J. Feitelson, *J. Phys. Chem.*, **67**, 2544 (1963).

acid and the  $-\text{SO}_3^-$  group on the resin surface. Feitelson also made the point that the use of hydrocarbon surfaces of ion-exchange resins in model systems for studying hydrophobic bonding may not be valid because of differences in the structure of water between

the resin and the bulk phases. This point has already been discussed above.

*Acknowledgment.* Thanks are due to Mrs. E. R. Stimson for technical assistance in determining the adsorption isotherms.

## Pulse Radiolysis of Aqueous Hydrogen Solutions. I. Rate Constants for

## Reaction of $e_{\text{aq}}^-$ with Itself and Other Transients. II.

### The Interconvertibility of $e_{\text{aq}}^-$ and $\text{H}^1$

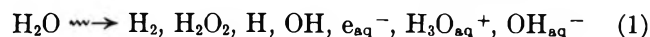
by Max S. Matheson and Joseph Rabani

*Chemistry Division, Argonne National Laboratory, Argonne, Illinois (Received October 26, 1964)*

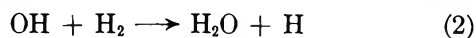
The technique of pulse radiolysis has been applied to aqueous solutions with (up to 100 atm.) and without dissolved  $\text{H}_2$  in the pH range 7–14. This work demonstrated the reaction  $\text{H} + \text{OH}_{\text{aq}}^- \rightarrow e_{\text{aq}}^-$ , by direct observation of the absorption of the  $e_{\text{aq}}^-$  formed as a product. The rate constants for this and several other reactions in this system have been determined. The values obtained are:  $k(\text{H} + \text{OH}_{\text{aq}}^-) = (1.8 \pm 0.6) \times 10^7$ ;  $2k(e_{\text{aq}}^- + e_{\text{aq}}^-) = (1.1 \pm 0.15) \times 10^{10}$  at pH 13.3;  $k(e_{\text{aq}}^- + \text{O}_{\text{aq}}^-) = (2.2 \pm 0.6) \times 10^{10}$  at pH 13;  $k(\text{O}_{\text{aq}}^- + \text{H}_2) = (8 \pm 4) \times 10^7$ ;  $k(e_{\text{aq}}^- + \text{H}) = (2.5 \pm 0.6) \times 10^{10}$ ;  $k(e_{\text{aq}}^- + \text{OH}) = (3.0 \pm 0.7) \times 10^{10} \text{ M}^{-1} \text{ sec}^{-1}$ .

#### Introduction

This work was originally undertaken to measure the rate constants for reaction of the hydrated electron,  $e_{\text{aq}}^-$ , with the other transient radiolysis products of process 1. A number of OH scavengers such as meth-



anol, ethanol, and ferrocyanide<sup>2</sup> had been used in our previous work to simplify the system. However,  $\text{H}_2$  seemed preferable as a scavenger for OH since the product of reaction 2 does not introduce a new species



to the system but an H atom, a species already present.

Another reaction which appeared likely to be useful

in simplifying the system further was reaction 3,



which had been suggested by Baxendale and Hughes<sup>3</sup> and by Friedman and Zeltmann.<sup>4</sup> This suggestion is supported by work in which externally produced H atoms were introduced into alkaline aqueous chloroacetate solutions<sup>5</sup> (since chloroacetate ion can be used

(1) Based on work performed under the auspices of the U. S. Atomic Energy Commission.

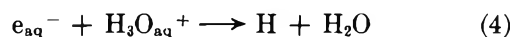
(2) S. Gordon, E. J. Hart, M. S. Matheson, J. Rabani, and J. K. Thomas, *Discussions Faraday Soc.*, **36**, 193 (1963).

(3) J. H. Baxendale and G. Hughes, *Z. physik. Chem.* (Frankfurt), **14**, 323 (1958).

(4) H. L. Friedman and A. H. Zeltmann, *J. Chem. Phys.*, **28**, 878 (1958).

to detect hydrated electrons<sup>6</sup>) or in which H atoms were produced by radiation in aqueous solutions of varying alkalinity.<sup>7</sup>

That some H atoms are produced in the irradiation of water was proposed by Allan and Scholes.<sup>8</sup> Supporting evidence for this proposal was obtained by showing that for added solutes reactive toward H atoms the relative rate constants of H atom reaction are the same in neutral solution containing an electron scavenger<sup>9</sup> as they are in acid solution where reaction 4 converts all hydrated electrons to H atoms.<sup>6,8</sup> By now it is



generally accepted that H atoms are produced with a yield of  $G_H \sim 0.6$  atom/100 e.v. absorbed in irradiated neutral water. However, it has been proposed that excited water molecules are the precursors of these H atoms.<sup>10</sup> To us the present evidence for excited water molecules is not conclusive and, in any case, such a precursor would not affect the results in this paper if the excited water molecules are converted to H atoms in less than 1  $\mu$ sec. Possible effects of longer lived  $H_2O^*$  on the rate constants are discussed later.

The development of pulse radiolysis techniques<sup>11</sup> and the direct observation of the spectrum of the hydrated electron with this method<sup>11d,12</sup> have enabled us to confirm reaction 3 directly. Also, we have used the technique of pulse radiolysis on aqueous solutions of various pH values saturated with up to 100 atm. of  $H_2$  to measure the rate constants of reaction of  $e_{aq}^-$  with itself and with other transient species. This work is described and discussed in this paper. A few preliminary results have been referred to previously.<sup>13</sup>

## Experimental

The experimental arrangement, including the linear accelerator and optical arrangement, has been described in earlier papers,<sup>11a,e</sup> and the setup used in the present work differs only in the substitution of the pressure cell (Figure 1) for the cell and mirror  $M_1$  of Figure 2 in ref. 11e. A 0.4- $\mu$ sec. pulse of 15-Mev. electrons with pulse currents in the range from 10 to 180 ma. was generally used. In a few experiments, 5- $\mu$ sec. pulses at 120 ma. were used to study the effect of high transient concentrations.

The pressure cell of Figure 1 is of welded stainless steel construction. The electron beam was focused to pass maximum current through the 1-cm. aperture, O, of the brass collimator. The focused beam entered the stainless steel cell through the 1.2-mm. thick, 1-cm. diameter aluminum window,  $W_1$ . Microscope slides placed in front of or behind cell C and darkened by irradiation indicated that cell C was uniformly

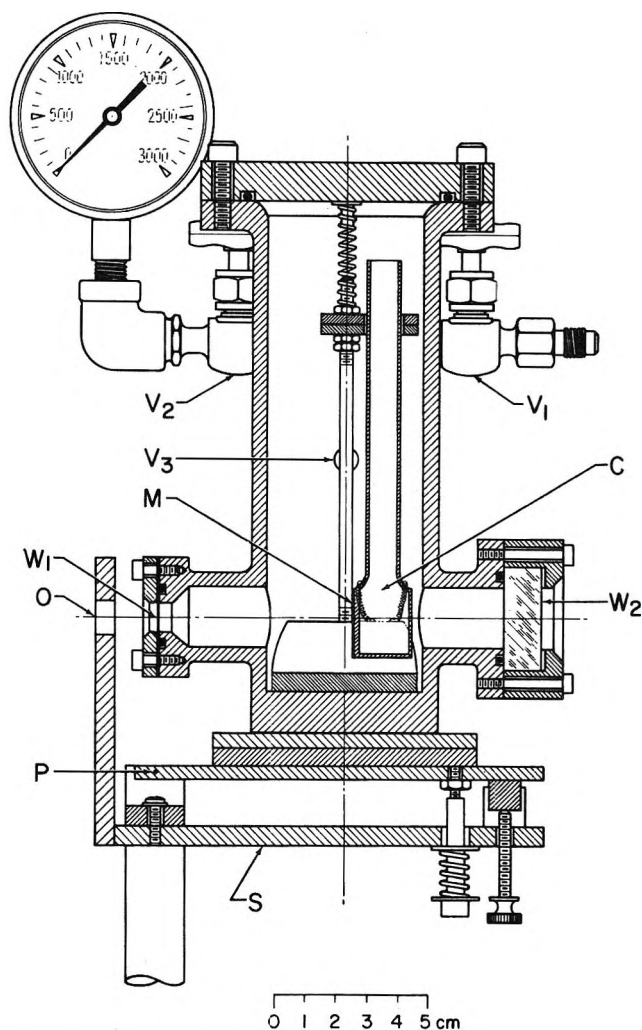


Figure 1. Pressure cell for pulse radiolysis.

- (5) (a) J. Jortner and J. Rabani, *J. Phys. Chem.*, **66**, 2081 (1962); (b) J. Jortner and J. Rabani, *J. Am. Chem. Soc.*, **83**, 4868 (1961).
- (6) (a) E. Hayon and J. Weiss, *Proc. 2nd Intern. Conf. Peaceful Uses At. Energy Geneva*, **29**, 80 (1958); (b) E. Hayon and A. O. Allen, *J. Phys. Chem.*, **65**, 2181 (1961).
- (7) (a) J. T. Allan, M. G. Robinson, and G. Scholes, *Proc. Chem. Soc.*, 381 (1962); (b) S. Nehari and J. Rabani, *J. Phys. Chem.*, **67**, 1609 (1963); (c) J. T. Allan and C. M. Beck, *J. Am. Chem. Soc.*, **86**, 1483 (1964).
- (8) J. T. Allan and G. Scholes, *Nature*, **187**, 218 (1960).
- (9) (a) J. Rabani, *J. Am. Chem. Soc.*, **84**, 868 (1962); (b) J. Rabani and G. Stein, *J. Chem. Phys.*, **37**, 1865 (1962); (c) G. Scholes and M. Simic, *J. Phys. Chem.*, **68**, 1731, 1738 (1964).
- (10) (a) E. Hayon, *Trans. Faraday Soc.*, **60**, 1059 (1964); (b) M. Anbar and D. Meyerstein, *J. Phys. Chem.*, **68**, 1713 (1964).
- (11) (a) M. S. Matheson and L. M. Dorfman, *J. Chem. Phys.*, **32**, 1870 (1960); (b) J. P. Keene, *Nature*, **188**, 843 (1960); (c) R. L. McCarthy and A. MacLachlan, *Trans. Faraday Soc.*, **56**, 1187 (1960); (d) E. J. Hart and J. W. Boag, *J. Am. Chem. Soc.*, **84**, 4090 (1962); (e) L. M. Dorfman, I. A. Taub, and R. E. Bühler, *J. Chem. Phys.*, **36**, 3051 (1962).
- (12) (a) J. P. Keene, *Nature*, **197**, 47 (1963); (b) J. P. Keene, *Discussions Faraday Soc.*, **36**, 304 (1963).
- (13) (a) M. S. Matheson and J. Rabani, *Radiation Res.*, **19**, 180 (1963); (b) M. S. Matheson, *Radiation Res. Suppl.*, **4**, 1 (1964).

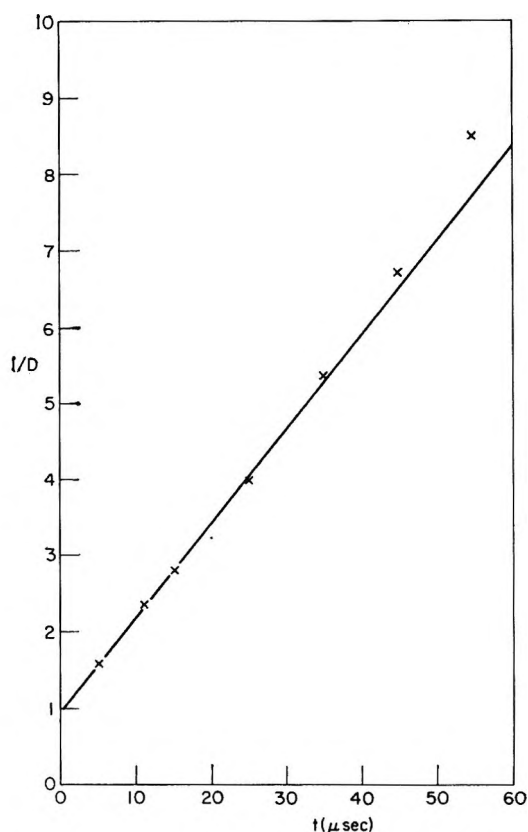


Figure 2. Second-order decay of absorption of  $e_{aq}^-$  at 5780 Å. in 0.2 M NaOH equilibrated with 100 atm. of  $H_2$ . Light path = 8 cm.;  $t = 0$  corresponds to middle of pulse. Plot is linear to 85% reaction.

irradiated. The cylindrical cell C was 2 cm. in diameter and 1 or 2 cm. in length. An aluminum mirror, M, protected by a copper coating, was evaporated on the window of the cell through which the electron beam entered. Light entered the pressure cell through the 16-mm. thick high purity silica window,  $W_2$ . The analyzing light beam from an HBO 107/1 Osram mercury lamp traversed the length of cell C two or four times. The transient changes in absorption were recorded photoelectrically and photographed on an oscilloscope screen.<sup>11e</sup> Three stainless steel cells were constructed and so machined that they could be interchanged on the support, S, shown in Figure 1. Minor adjustments were required since the mirror M was not independent but was deposited on the silica cell.

The silica cells were filled under an atmosphere of argon in a glove box. The triply distilled water had previously been degassed in syringes<sup>14</sup> which were then introduced into the glove box. The NaOH solutions (unless otherwise stated) were prepared by weighing freshly cut sodium in the glove box and adding the sodium in small pieces to a beaker containing a fraction

of a milliliter of triply distilled water. After the sodium had all reacted, the appropriate volumes of triply distilled water were added and the resulting alkaline solutions were put in syringes. The glove box technique and the preparation of NaOH from Na were adopted to avoid carbonate in the solutions, since it has been shown that OH (or  $O^-$ ) reacts with carbonate to give a long-lived transient absorbing also at 5780 Å.<sup>15,16</sup> By acidification and subsequent gas chromatographic analysis, the  $CO_2$  in 1 M NaOH prepared in the glove box was found to be 5.3  $\mu M$ . The carbonate introduced by NaOH would be proportionately lower in less alkaline solutions. Since three pressure cells were available, three silica cells could be filled for each set of experiments. With the silica cells in place, the pressure cells were closed in the glove box and then removed from it.

Next each pressure cell was connected to a cylinder of Matheson Co. Ultrapure hydrogen (impurities 1 p.p.m. of  $H_2O$ , 5 to 9 p.p.m. of argon) and flushed out briefly with a current of  $H_2$ . Then the cell was filled to a pressure of about 30 atm. of  $H_2$  and shaken as vigorously as possible without spilling solution from the silica cell. (The cell neck was made long (Figure 1) to minimize possible spillage.) Subsequently, the exhaust valve  $V_3$  was opened and the cell pressure decreased to just above atmospheric pressure. The pressurizing, shaking, and exhausting were repeated three times to assure removal of traces of air. Finally, the cell was filled to the desired pressure, usually 100 atm. (1500 p.s.i.g.). One of the cells was always filled with  $\sim 0.2$  M NaOH and 100 atm. of  $H_2$  to serve as a control and relative dosimeter. The initial optical density under presumably similar conditions varied as much as 20% in the three different cells when all were filled with the same solution. Perhaps the slight adjustments necessary for optical alignment changed the alignment with the beam, although the vertical axis of adjustment passed 1 cm. from O and the horizontal axis 5 cm. below aperture O, both axes intersecting at pivot point P.

When the hydrogen pressurized cells were pulse-irradiated it was found the rate of  $e_{aq}^-$  decay decreased from one pulse to the next, attaining a constant rate of decay after about 20 pulses. If a cell with 100 atm. of  $H_2$  was given 500 consecutive pulses (total dose about  $10^6$  rads) but the shutter of the oscilloscope camera opened only for the 20th and 500th pulse, the two

(14) C. Senvar and E. J. Hart, *Proc. 2nd Intern. Conf. Peaceful Uses At. Energy Geneva*, 29, 19 (1958).

(15) S. Gordon, E. J. Hart, M. S. Matheson, J. Rabani, and J. K. Thomas, *J. Am. Chem. Soc.*, 85, 1375 (1963).

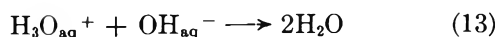
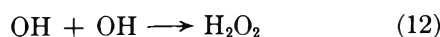
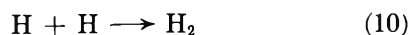
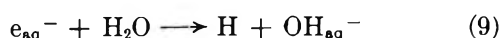
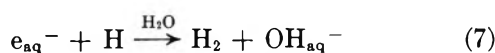
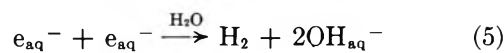
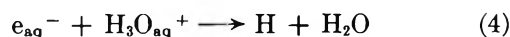
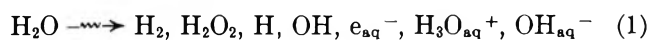
(16) G. E. Adams and J. W. Boag, *Proc. Chem. Soc.*, 112 (1964).

decay curves photographed as a single curve. For two reasons it was concluded that this effect was probably due to traces of impurities introduced from the gas phase. First, the effect of the initial pulses in slowing the rate occurred at all pH values from 7 to 14 and, therefore, these impurities could not have been added with the NaOH. Second, if water plus 100 atm. of  $H_2$  was pulse-irradiated until the limiting slow rate was attained and then the  $H_2$  was removed and replaced by repeated shaking with 1 atm. of argon, then the rate for the first pulse with argon was the same as that measured for pure deaerated water (of the same pH) with the usual syringe and unpressurized silica cell technique.<sup>2</sup> Experiments without  $H_2$  were generally made using deaerated triply distilled water (pH 7 to 14) in the usual syringe technique<sup>2</sup> and, of course, using only the decay curve for the first pulse. The attainment of the slower constant rate in the presence of 100 atm. of  $H_2$  after repeated pulsing indicated that the molecular  $H_2O_2$  produced by each pulse probably disappeared in a chain reaction with the  $H_2$ .

All experiments were carried out at room temperature, 23°. For  $H_2$ -saturated solutions the cell was given about 20 pulses to obtain a constant rate and then generally for each decay curve the absorption decays for three consecutive pulses were photographed superposed to give a single curve. For computer fitting of plots of 1/(optical density) vs. time, an IBM 1620 was used.

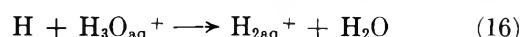
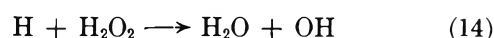
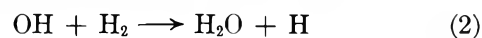
## Results and Discussion

In water, the following reactions should result from the irradiation pulse



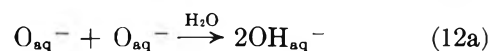
Except for (9), reactions 4 through 13 are generally fast, having rate constants  $10^{10} M^{-1} \text{ sec.}^{-1}$  or greater, e.g.,  $k_4^{15,17} = 2.2 \times 10^{10}$ ;  $k_8^{15,17b} = 1.2 \times 10^{10}$ ;  $2k_{10}^{18,19}$

$= 1.2$  or  $2.0$  or  $3.0 \times 10^{10}$ ;  $k_{11}^{18} = 1.2 \times 10^{10}$ ;  $2k_{12}^{18,20} = 0.8$  or  $1.2 \times 10^{10}$ ;  $k_{13}^{21} = 1.4 \times 10^{11} M^{-1} \text{ sec.}^{-1}$ . Although  $k_9(H_2O)^{22}$  is only about  $1.4 \times 10^3 \text{ sec.}^{-1}$ , a first-order reaction of about  $10^4 \text{ sec.}^{-1}$  was found in our work. This first-order reaction is probably due to impurities and in most experiments was a very small fraction of the initial decay rate. It is the initial decay rate which is most significant in the determination of rate constants. Other reactions such as 2, 3, 14, 15, and 16 are slower and need be considered only if the



stable reactant is present in sufficient concentration.  $k_2^{20a} = 4.5 \times 10^7$ ,  $k_{14}^{18} = 9 \times 10^7$ ,  $k_{15}^{20a} = 4.5 \times 10^7$ , and  $k_{16}$  is much smaller than these.<sup>13b</sup>

$H_2$  (100 Atm. at pH ~13): Determination of  $k(e_{aq}^- + e_{aq}^-)$ . In the pulse radiolysis of a solution at high pH (~13) and under 100 atm. of  $H_2$  (~0.08 M  $H_2$ ), reactions 4, 6a, 7, 10, 11, and 12a should be eliminated since reactions 2a, 3,<sup>23</sup> and 13 will be very fast. The



pK of OH is 11.9,<sup>20b</sup> so reactions 2a, 6a, and 12a replace reactions 2, 6, and 12. Reactions 8 or 8a and



9 should also not be important, since (3) following (9) and (2a), and (3) following (8) or (8a) will regenerate  $e_{aq}^-$ . Thus, under these conditions  $e_{aq}^-$  should disappear only by reaction 5, and a plot of  $1/D$  vs.  $t$  should be linear, since for the second-order disappearance of an absorbing species

(17) (a) L. M. Dorfman and I. A. Taub, *J. Am. Chem. Soc.*, **85**, 2370 (1963); (b) J. P. Keene, *Radiation Res.*, **22**, 1 (1964).

(18) (a) J. K. Thomas, *J. Phys. Chem.*, **67**, 2593 (1963); (b) J. P. Sweet and J. K. Thomas, *ibid.*, **68**, 1363 (1964).

(19) H. A. Schwarz, *ibid.*, **67**, 2827 (1963).

(20) (a) H. A. Schwarz, *ibid.*, **66**, 255 (1962); (b) J. Rabani and M. S. Matheson, *J. Am. Chem. Soc.*, **86**, 3175 (1964).

(21) M. Eigen and L. DeMaeyer, *Z. Elektrochem.*, **59**, 986 (1955).

(22) This work indicates previously published values are too high and S. Gordon and E. J. Hart have recently found  $k_9 \leq 25 M^{-1} \text{ sec.}^{-1}$ .

(23)  $k_3 \approx 2 \times 10^7 M^{-1} \text{ sec.}^{-1}$  can be estimated from ref. 7a,b assuming  $k(H + O_2) = 2 \times 10^{10} M^{-1} \text{ sec.}^{-1}$ .

$$1/D_t = 1/D_0 + (k/\epsilon_s^\lambda l)t \quad (17)$$

where  $D_0$  and  $D_t$  are the optical densities at times 0 and  $t$ ,  $\epsilon_s^\lambda$  is extinction coefficient of absorbing species  $s$  at the wave length  $\lambda$ , and  $l$  is the optical path length for the analyzing light. Figure 2 indicates the linearity obtained.

In Table I are summarized the results of experiments at 100 atm. of  $H_2$  and pH 13.3 with varying electron pulse intensities. The intensity of the pulse can be obtained from the initial optical density at 5780 Å.,  $D_0$  in Table I. In most of these experiments a 0.4- $\mu$ sec. pulse was used, and, since  $e_{aq}^-$  decays very little during 0.4  $\mu$ sec., extrapolation to the middle of the pulse yields a value of  $D_0$  very close to that appropriate for a pulse of equivalent total energy and negligible duration. However, with the 5- $\mu$ sec. pulses considerable  $e_{aq}^-$  decayed during the pulse, and  $D_0$  was taken arbitrarily at the end of the pulse.

Table I: " $k$ " for 100 Atm. of  $H_2$  and 0.2  $M$  NaOH Using Variable Pulse Intensities

$D_0^{5780}$	" $k$ " <sup>a</sup>	% linearity of plot	No. of expts.
2.32 <sup>b,c</sup>	1.2	75	3
1.80 <sup>c</sup>	1.0	90	3
1.43	1.05	90	3
1.25 <sup>c</sup>	1.2	85	3
1.20	1.2	90	2
1.07	1.05	85	3
0.600	1.35	80	5
0.460	1.05	90	3
0.370	1.3	85	6
0.300	1.3	80	9
0.240	1.3	80	1
0.200	1.25	80	1
0.150	1.4	75	6

<sup>a</sup> " $k$ " measured from initial linear portion of plot as  $[d(1/D)/dt] \times \epsilon l$ . <sup>b</sup> With a 1-cm. cell, two passes with 0.1  $M$  NaOH.  $D_0$  multiplied by 4 for comparison with other results where  $l = 8$  cm. <sup>c</sup> Using a 5- $\mu$ sec. pulse.  $D_0 = D$  at the end of pulse; others, 0.4- $\mu$ sec. pulse and  $D_0$  extrapolated to middle of pulse.

In estimating the per cent linearity in the table there was a small error but we believe the error is not more than 5%. In plots such as Figure 2 the initial slope was drawn though the greatest number of experimental  $1/D$  values possible while still excluding points which would deviate from the straight line by more than the experimental error. The deviation from linearity would be consistent with the presence of a small amount of a reaction of  $e_{aq}^-$  with an impurity present at a constant concentration, since the deviation,

which from computer calculations seems to require a first-order reaction, cannot be due to  $e_{aq}^- + H_2O$  at this pH because this reaction would be immediately reversed by  $H + OH_{aq}^-$ . The reaction is not with  $H_2O_2$  either, since in the presence of the high concentration of  $H_2$  used,  $H_2O_2$  regenerates  $e_{aq}^-$  as previously discussed. The same  $e_{aq}^-$  decay at a given intensity was obtained whether the solution was purified by a series of pulses of higher, or of lower, or of equal intensity. A factor of 8 in pulse intensity was tried. The fact that the deviation could not be eliminated by repeated pulse irradiation in the presence of  $H_2$  could be explained by a relatively high concentration of impurity with low reactivity toward  $e_{aq}^-$ , or by a metal ion impurity which regenerates after each pulse, perhaps by reaction with water.<sup>24</sup> The impurity may have been introduced with the  $H_2$  in filling the cell, perhaps from connecting tubing. If metallic impurities were introduced with the sodium, the amount should be proportionately less for lower pH values.

The principal decay of  $e_{aq}^-$  is definitely second order over a 15-fold range of pulse intensity (Table I), and yields (using only the results at  $D_0 = 0.460$  and higher and correcting for the small first-order reaction)  $2k_5 = (1.08 \pm 0.05) \times 10^{10} M^{-1} sec^{-1}$ .  $\epsilon_e^{5780} = 10,600 (\pm 10\%) M^{-1} cm^{-1}$  was used throughout this paper.<sup>25</sup> When the error in  $\epsilon_e^{5780}$  is included  $2k_5 = (1.1 \pm 0.15) \times 10^{10} M^{-1} sec^{-1}$ , in satisfactory agreement with previous values:  $(0.85 \pm 0.15) \times 10^{10}$  at pH 10.9<sup>2</sup> and  $<(1.3 \pm 0.2) \times 10^{10}$  at pH 13<sup>17a</sup> all at 23°. The latter value of Dorfman and Taub, which becomes  $<(1.4 \pm 0.2) \times 10^{10}$  using the above  $\epsilon_e^{5780}$  or  $\leq(1.2 \pm 0.2) \times 10^{10}$  if corrected for the first-order rate found in their solutions, was measured in 0.5  $M$  aqueous ethanol and the agreement with our values shows two things. First, it shows that the reaction of  $e_{aq}^-$  with  $\alpha$ -ethanol radicals was not important, and second, that reaction 8a did not affect significantly the measurement of  $2k_5$  in the aqueous ethanol system. The effect of ionic strength could account for a value of  $2k_5$  higher at pH 13 than at pH 10.9. As already noted, at pH 13.3 H atoms are converted in less than 1  $\mu$ sec. to  $e_{aq}^-$ ; therefore, reaction 5 must yield  $H_2$  and not H atoms, otherwise  $e_{aq}^-$  would be stable for milliseconds in irradiated basic solutions containing sufficient  $H_2$  in the absence of H atom scavengers. Conclusive evidence that  $e_{aq}^- + e_{aq}^-$  yields  $H_2$  came from the pulse radiolysis of  $C_2H_5OD$  in  $D_2O$ , where  $G(D_2)$  was found equal to  $G_{D_2} + \frac{1}{2}G_e$ .<sup>17a</sup>

(24) (a) G. E. Adams, J. H. Baxendale, and J. W. Boag, *Proc. Chem. Soc.*, 241 (1963); (b) M. Anbar and D. Meyerstein, *ibid.*, 23 (1964).

(25) J. Rabani, W. A. Mulac, and M. S. Matheson, *J. Phys. Chem.*, 69, 53 (1965).



The alternative suggestion that reaction 5 yields  $H + H$  or  $e_{aq}^- + H$  in a cage, the pair in the cage then combining 100% to form  $H_2$ , can be shown to be not reasonable. The theory of the effect of scavengers on cages has been treated mathematically many times.<sup>26</sup> In particular, Jortner, Ottolenghi, and Stein<sup>27</sup> have studied the cages of  $e_{aq}^-$  or  $H$  atoms plus halogen atoms. They found that  $10^{-4} M H_3O_{aq}^+$  scavenged over half the  $e_{aq}^-$  in the cage,  $[e_{aq}^- + I]$ , while  $1 M CH_3OH$  scavenged all the  $H$  atoms in the cage  $[H + I]$ . Since, as will be seen later,  $k_3 \simeq 10^{-3} k_4 \simeq 10k_{H+CH_3OH}$ , and, if the parameters of the assumed  $[H + H]$  or  $[e_{aq}^- + H]$  cages are similar to those of the  $[H + I]$  and  $[e_{aq}^- + I]$  cages, then it would be reasonable to expect  $0.2 M OH_{aq}^-$  to scavenge a large fraction of the cages. Moreover, increasing the  $OH_{aq}^-$  concentration from  $0.2$  to  $1 M$  did not slow the  $e_{aq}^-$  decay rate, contradicting the effect expected if  $H$  atoms were present in cages. Finally, on the basis of the Samuel-Magee theory and assuming a cage of  $3\text{-}\text{Å}$ . initial separation,  $2\text{-}\text{Å}$ . reaction radius, and  $1\text{-}\text{Å}$ . mean free path, one calculates 75% of the  $H$  atoms escape recombination.

As noted in the Experimental section, care was used to avoid carbonate in the NaOH solutions since carbonate gives a transient absorbing at 5780.<sup>15,16</sup> In experiments with  $0.072 M Ba(OH)_2$ , 50 atm. of  $H_2$ , 8-cm. light path, and  $0.4\text{-}\mu\text{sec}$ . pulse, the following results were obtained: Initial optical density,  $D_0 = 0.950$ , " $k$ " =  $1.1 \times 10^{10} M^{-1} \text{sec}^{-1}$ ;  $D_0 = 0.400$ , " $k$ " =  $1.2 \times 10^{10}$ ;  $D_0 = 0.200$ , " $k$ " =  $1.2 \times 10^{10}$ . This is further evidence that the carbonate radical ion was not significantly present in our work.

*Variable  $H_2$  Concentration at pH 13.3. Determination of  $k(O_{aq}^- + H_2)$  and  $k(e_{aq}^- + O_{aq}^-)$ .* When an aqueous solution at pH 13.3 (NaOH) was purified by pulse irradiation under 50 atm. of  $H_2$  and then irradiated by a pulse of electrons,  $D_0^{5780} = 0.790$  was obtained for the initial optical density. After removal of the  $H_2$  by repeated purging and shaking with argon, this same solution under 2 atm. of argon was pulse-irradiated only once with a pulse intensity equal to that used previously with 50 atm. of  $H_2$  and now gave  $D_0^{5780} = 0.410$  in the absence of  $H_2$ . The optical path length was 8 cm. in both cases. This  $D_0$  ratio corresponds to  $G_{OH}/(G_e + G_H) = 0.9$ , a reasonable result. The 0.9 was used in later calculations, although it is not considered more precise than literature values. The fact that the  $D_0$  increase obtained by adding 50 atm. of  $H_2$  (to convert  $OH$  to  $H$ ) corresponds to  $G_{OH}$  gives further support to reaction 3.

For the experiment above, carried out in a pressure cell but in the absence of  $H_2$ , the plot of  $1/D$  vs.  $t$  was linear up to 65% reaction of  $e_{aq}^-$ , the slope giving

" $k$ " =  $\epsilon_e^{5780} [d(1/D)/dt] = 4.7 \times 10^{10} M^{-1} \text{sec}^{-1}$ . However, a similar experiment at pH 13 (NaOH also prepared in a glove box from Na), using the simple unpressurized silica cell and syringe technique<sup>2</sup> with pulse irradiation, gave an initial  $[e_{aq}^-] = 1.2 \times 10^{-5} M$  and " $k$ " =  $3.3 \times 10^{10} M^{-1} \text{sec}^{-1}$  with 55% linearity. This latter value of " $k$ " is preferred, since the pulse intensity is 2.5-fold higher which would minimize reactions of  $e_{aq}^-$  with impurities. Secondly, " $k$ " was measured in the absence of  $H_2$  at three other pH values both in the pressure cells and with the syringe technique, with the result that agreement was found at pH 11.5 and 12.5, while " $k$ " was about 30% higher in the pressure cell at pH 10.5. From this result it was concluded that sometimes impurities were reintroduced with the argon, and therefore, for rate constants to be measured in the absence of  $H_2$ , the syringe technique was preferred throughout the work reported in this paper.

In solutions of pH  $\geq 13$  which contain only NaOH,  $H$  and  $H_3O_{aq}^+$  will not be important after the pulse, because reactions 3 and 13 will be very fast. Reaction 3 also reverses 9. Reaction 8 is replaced by reaction 8a because the  $pK$  of  $H_2O_2$  is 11.8.<sup>28</sup> Comparison of  $2k_5$  measurements above showed (8a) to be negligible, and there is other evidence that may support this conclusion.<sup>5a</sup> Since the  $pK$  of  $OH$  is 11.9,<sup>20b</sup> only reactions 5 and 6a are left for consideration. Thus  $k_{6a}$  can be obtained from eq. 18, where the initial slope in the experiment above (initial  $[e_{aq}^-] = 1.2 \times 10^{-5} M$ )

$$"k" = 2k_5 + \sum_i k(e + \chi_i) \frac{[\chi_i]_0}{[e_{aq}^-]_0} \quad (\chi_i \neq e_{aq}^-) \quad (18)$$

gave " $k$ " =  $3.3 \times 10^{10} M^{-1} \text{sec}^{-1}$ , and where  $[\chi_i]_0$  and  $[e_{aq}^-]_0$  are initial concentrations of reactants  $\chi_i$  and  $e_{aq}^-$ . Using  $[O_{aq}^-]_0/[e_{aq}^-]_0 = G_{O^-}/(G_H + G_e) = 0.9$  as measured above,  $k_{6a} = 2.4 \times 10^{10} M^{-1} \text{sec}^{-1}$ . Comparing our value for " $k$ " =  $1.3 \times 10^{10}$  in the presence of  $0.5 M$  ethanol at pH 11 to 12.6 with " $k$ " =  $3.3 \times 10^{10}$  at pH 13 with only NaOH present, the difference should be due only to reaction 6a. The fact that (9) proceeds in the presence of ethanol gives

(26) (a) R. A. Wijsman, *Bull. Math. Biophys.*, **14**, 121 (1952); (b) A. H. Samuel and J. L. Magee, *J. Chem. Phys.*, **21**, 1080 (1953); (c) R. M. Noyes, *J. Am. Chem. Soc.*, **77**, 2042 (1955); **78**, 5486 (1956); *J. Phys. Chem.*, **65**, 763 (1961); (d) J. C. Roy, R. R. Williams, and W. H. Hamill, *J. Am. Chem. Soc.*, **76**, 3274 (1954); (e) A. Kuppermann, "Actions Chimiques et Biologiques des Radiations, Cinquième Série," M. Haissinsky, Ed., Academic Press, New York, N. Y., 1961, p. 85.

(27) J. Jortner, M. Ottolenghi, and G. Stein, *J. Phys. Chem.*, **66**, 2029, 2037, 2042 (1962).

(28) M. G. Evans and N. Uri, *Trans. Faraday Soc.*, **45**, 224 (1949); J. Jortner and G. Stein, *Bull. Res. Council Israel*, **A6**, 239 (1957).

a negligible correction. This comparison yields  $k_{6a} = 2.2 \times 10^{10} M^{-1} \text{sec.}^{-1}$ .

The above calculation is equivalent to assuming  $2k_{12a} = 2k_5$  so that  $[e_{aq}^-]/[O_{aq}^-]$  remains about constant as the reaction proceeds. However, a computer calculation with  $2k_{12a} = 0$ ,  $2k_5 = 1.0 \times 10^{10}$ , and  $k_{6a} = 2.2 \times 10^{10} M^{-1} \text{sec.}^{-1}$  and neglecting other reactions gave a  $1/D$  vs.  $t$  plot which agreed with the experimental points to at least 80% reaction. Since we have found<sup>20b</sup>  $2k_{12a} \sim 2 \times 10^9$  and since in this experiment  $k_{6a}$  is not sensitive to a small amount of reaction of  $e_{aq}^-$  with impurity, we set  $k_{6a} = (2.2 \pm 0.6) \times 10^{10} M^{-1} \text{sec.}^{-1}$ , where the error limits include the error in  $\epsilon_e$ <sup>5780</sup>.

The effect of  $H_2$  concentration on  $D_0$  and "k" in 0.2 M NaOH is shown for different pulse intensities in Table II. In these experiments the pressure cell was

**Table II:** The Effect of  $H_2$  Concentration on  $D_0$ <sup>5780</sup> and "k" in 0.2 M NaOH

Atm. of $H_2$ <sup>a</sup>	$D_0$ <sup>b</sup>	"k"	% linearity	Relative pulse intensity	No. of expts.
100	1.20	1.2	90	6	2
40	1.00	1.2	85	6	2
20	0.87	0.95	70	6	2
6	0.87	1.25	75	6	2
>1	0.60	1.3	70	6	2
100	0.63	1.3	80	3	2
40	0.77	1.3	80	3	2
20	0.59	1.1	50	3	2
>1	0.33	1.5	75	3	2
100	0.20	1.25	80	1	1
>1	0.14	...	0 <sup>c</sup>	1	4

<sup>a</sup> The  $H_2$  concentration in the experiments at >1 atm. corresponded to saturation at a pressure slightly greater than 1 atm. <sup>b</sup> 0.4- $\mu$ sec. pulse, 8-cm. light path. <sup>c</sup>  $D_{max} = 0.155$  obtained  $\sim 3 \mu$ sec. after pulse.  $D_0$  here was not extrapolated but measured as close to the pulse as possible.

filled to 100 atm. of  $H_2$ , the solution purified by irradiation, and then the decay observed at different  $H_2$  pressures as the pressure was reduced in steps as indicated going down column one in the table. For the four experiments in the last line of the table the solution was previously pulse-irradiated at 100 atm. of  $H_2$  for each separate experiment at 1 atm. of  $H_2$ , although repeated pulsing at 1 atm. of  $H_2$  did not change the decay curve perceptibly. As was discussed above, at pH 13.3 in the absence of  $H_2$  only reactions 5 and 6a need be considered. At pH 13.3 in the presence of a small amount of  $H_2$ ,  $e_{aq}^-$  will be formed over a period of several microseconds by the sequence of (2a) and

(3), with (2a) as the rate-controlling step. Reaction 2a is pseudo-first-order; therefore at high intensities,  $e_{aq}^-$  will decay after the pulse due to the rapidity of the second-order reactions 5 and 6a, while at low intensities, (2a) may initially predominate over (5) and (6a) so that  $e_{aq}^-$  increases for a while after the pulse.

To test this prediction, the usual syringe technique was used to prepare a solution under slightly less than 1 atm. of  $H_2$  at pH 13. When this solution was irradiated with a low-intensity pulse which gave  $[e_{aq}^-]_0 = 1.27 \times 10^{-6} M$ ,  $d(1/D)/dt$  was observed to be zero at  $t = 0$ . For this same solution with a 40% higher pulse intensity, the optical density was found to decay initially with time, while with a 40% lower pulse intensity the optical density increased initially with time. Water at pH 13 irradiated with the same pulse intensity yielded "k" =  $4.2 \times 10^{10} M^{-1} \text{sec.}^{-1}$ . For the experiment with initial zero slope, "k"  $[e_{aq}^-]_0^2 = k_{2a}[O_{aq}^-]_0[H_2]$ . With the above values of "k" and  $[e_{aq}^-]_0$ , setting  $[O_{aq}^-]_0/[e_{aq}^-]_0 = 0.9$  and  $[H_2] = 6.6 \times 10^{-4} M$ , we obtain  $k_{2a} = (8 \pm 4) \times 10^7 M^{-1} \text{sec.}^{-1}$ .

Schwarz<sup>20a</sup> has reported  $k_2 = 4.5 \times 10^7 M^{-1} \text{sec.}^{-1}$ . Thus it appears that  $k_{2a}$  is similar to or slightly greater than  $k_2$  although previous results<sup>29,30</sup> have been interpreted by assuming  $O_{aq}^- + H_2$  is slow. Gordon and Hart<sup>29</sup> found that the yield of HD in  $\gamma$ -irradiated aqueous  $D_2$  solutions decreased above pH 9. They proposed that OH dissociated to  $O^-$  which was unreactive toward  $D_2$ . Friedman and Zeltmann<sup>4</sup> confirmed these results but suggested that reaction 3 could also explain the effect, although they could not demonstrate which was the correct explanation. The present work suggests the conversion of H atoms to  $e_{aq}^-$  is responsible in part at least for the alkaline effect in aqueous  $D_2$ . Reaction 3 does not seem to explain all the details quantitatively, and probably impurity effects ( $OH + CO_3^{-2}$  or  $HCO_3^-$ ) should be considered. Hochanadel<sup>30</sup> found that in the competition of  $H_2O_2$  and  $H_2$  for OH, the apparent reactivity of  $H_2$  decreased relative to the reactivity of  $H_2O_2$  as the pH was increased above  $\sim 10$ . However, our results show  $k_{2a} \simeq k_2$ . A possible explanation of Figure 6 in Hochanadel's paper would be that  $HO_2^-$  is more reactive than  $H_2O_2$  toward OH or  $O^-$  radicals. Other explanations are possible, since in the pH range above 10, H atoms are converted to  $e_{aq}^-$ , OH to  $O_{aq}^-$ , and  $H_2O_2$  to  $HO_2^-$ , also  $O_{aq}^-$  can react with  $O_2$  to give  $O_3^-$ ,<sup>31</sup> and OH or  $O^-$  can react with any carbonate<sup>15,16</sup> present in the alkali.

(29) S. Gordon and E. J. Hart, *J. Am. Chem. Soc.*, **77**, 3981 (1955).

(30) C. J. Hochanadel, *Radiation Res.*, **17**, 286 (1962).

(31) G. Czapski and L. M. Dorfman, *J. Phys. Chem.*, **68**, 1169 (1964).

$H_2$  (100 Atm.) at pH 10.5. The Determination of  $k(e_{aq}^- + H)$  and  $k(e_{aq}^- + H_2O)$ . At 100 atm. of  $H_2$  all OH are quickly converted to H atoms. At pH 10.5 the half-life for conversion of H to  $e_{aq}^-$  is about 100  $\mu\text{sec.}$ , while the measured decay of  $e_{aq}^-$  in our experiments was about 4  $\mu\text{sec.}$  Also, at pH 10.5 all the radiation-produced  $H_3O_{aq}^+$  are suppressed. Thus, after

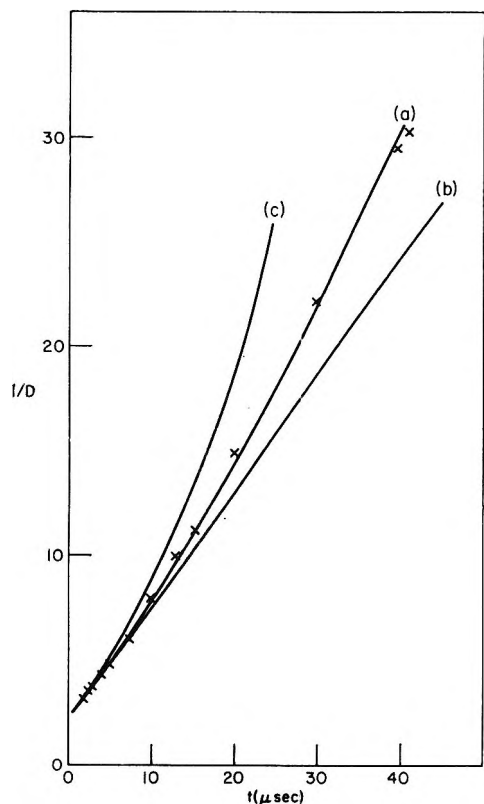


Figure 3. Decay of  $e_{aq}^-$  absorption at 5780 Å, pH 10.50, 100 atm. of  $H_2$ , light path 8 cm.,  $t = 0$  corresponds to the beginning of electron pulse. Points are experimental; solid lines are computer calculated decays. For the computer calculations, the pulse of 0.4  $\mu\text{sec.}$  half-width and 0.5  $\mu\text{sec.}$  base width was assumed equivalent to two rectangular pulses of 0.2 and 0.3  $\mu\text{sec.}$  width whose intensities were adjusted by trial and error to  $4.42 \times 10^{26}$  and  $3.43 \times 10^{26}$  e.v.  $l^{-1} \text{sec.}^{-1}$  in curve a and  $4.8 \times 10^{26}$  and  $3.7 \times 10^{26}$  e.v.  $l^{-1} \text{sec.}^{-1}$  in curve b or c. Curve a:  $G_e = G_{OH} = 2.6$ ;  $G_H = 0.5$ ;  $G_{H_2O_2} = 0.7$ ;  $G_{H_2} = 0.45$ ;  $G_{H^+} = 3.6$ ;  $G_{OH^-} = 1.0$ ;  $k_2 = 4.5 \times 10^7$ ;  $k_3 = 2 \times 10^7$ ;  $k_5 = 5 \times 10^9$ ;  $k_6 = 3 \times 10^{10}$ ;  $k_7 = 2.5 \times 10^{10}$ ;  $k_8 = 1.2 \times 10^{10}$ ;  $k_9 = 1.8 \times 10^{12}$ ;  $k_{10} = 1.0 \times 10^{10}$ ;  $k_{13} = 1.43 \times 10^{11} M^{-1} \text{sec.}^{-1}$ . All other  $k = 0$ . Curve b: Same as (a) except that  $G_e = G_{OH} = 2.7$ ;  $G_{H^+} = 3.7$ ;  $k_6 = 3.4 \times 10^{10}$ ;  $k_7 = 2.9 \times 10^{10}$ ; and  $k_9 = 0 M^{-1} \text{sec.}^{-1}$ . Curve c: Same as (b) except that  $k_7 = 2.6 \times 10^{10}$  and  $k_9 = 3.6 \times 10^{12} M^{-1} \text{sec.}^{-1}$ . These curves illustrate the necessity of a first-order reaction to account for the curvature;  $k_9$  and  $k_{10}$  have opposing effects on curvature. However,  $k_7$  accounts for most of the initial decay and therefore is not appreciably affected by uncertainties in  $k_9$  and  $k_{10}$ .

the pulse  $e_{aq}^-$ , H,  $H_2O_2$ , and  $H_2O$  are present, so that reactions 5, 7, 8, and 9 are important in  $e_{aq}^-$  decay. In fact, (7) was introduced because reactions 8 and 9 could not explain the increased initial rate observed at pH 10.5 in comparison with pH 13.3, where only (5) was important. To calculate  $k_7$ , we assumed  $G_{OH} = G_e$ ,  $G_H = 0.2G_e$ , and  $G_{H_2O_2} = 0.25G_e$ . With these assumptions and using our experimental "k"s in eq. 18, Table III was obtained. It can be seen in the Table that inclusion of a pseudo-first-order rate constant,  $k_9(H_2O)$ , of 1 to  $2 \times 10^4 \text{sec.}^{-1}$  gives the most consistent  $k_7$  values when the pulse intensity is varied. In Figure 3 one of these experiments is fitted with a computer calculated curve with the result that  $k_9(H_2O) = 1 \times 10^4 \text{sec.}^{-1}$  gives a much better fit than 0 or  $2 \times 10^4 \text{sec.}^{-1}$ . Computer calculations fitting other experiments also show that the decay curves cannot be fitted unless a first-order reaction with  $k \approx 1 \times 10^4 \text{sec.}^{-1}$  is included. This determines an upper limit for  $k_9$  since, as was previously discussed, contributions of impurity reactions cannot be excluded.

Table III: Calculation of  $k(e_{aq}^- + H)$

$D_0^a$	$k_7^b$				pH
	$k_9(H_2O) = 0^c$	$k_9(H_2O) = 1^c$	$k_9(H_2O) = 2^c$	$k_9(H_2O) = 4^c$	
0.46	2.9	2.7	2.6	2.3	10.5 <sup>d</sup>
0.21	4.0	3.6	3.2	2.6	10.5 <sup>d</sup>
0.15	2.8	2.4	1.9	1.0	10.5 <sup>d</sup>
0.40	3.0	2.8	2.6	2.1	10.6 <sup>e</sup>
0.12	3.6	2.9	2.3	0.9	10.6 <sup>e</sup>

<sup>a</sup> Light path was 8 cm. <sup>b</sup> In units of  $10^{10} M^{-1} \text{sec.}^{-1}$ . <sup>c</sup> In units of  $10^4 \text{sec.}^{-1}$ . <sup>d</sup> NaOH with 100 atm. of  $H_2$ . <sup>e</sup>  $Ba(OH)_2$  with 10.5 atm. of  $H_2$ .

With respect to  $k_7$ , the best results should be obtained at high pulse intensities where first-order reactions are minimized. Therefore, we deduce from Table III that  $k_7 = 2.7 \times 10^{10} M^{-1} \text{sec.}^{-1}$ , while the computed curve giving the best fit in Figure 3 was calculated using  $k_7 = 2.5 \times 10^{10} M^{-1} \text{sec.}^{-1}$ . We have found that for curves with slight upward curvature we tend to draw initial slopes slightly higher than the initial slopes of computer-fitted curves; therefore, we choose as the best value  $k_7 = (2.5 \pm 0.6) \times 10^{10} M^{-1} \text{sec.}^{-1}$ . Although other reactions are occurring, reaction 7 accounts for two-thirds of the initial rate of decay of  $e_{aq}^-$  in Figure 3, which means that small errors in the other rate constants do not seriously affect the precision of  $k_7$ .

*No  $H_2$  at pH 10.5. Determination of  $k(e_{aq}^- + OH)$ .* In water containing only NaOH at pH 10.5  $H_3O_{aq}^+$

will be eliminated by reaction 13. The half-life of (3) is about 100  $\mu\text{sec.}$ , but reactions 5 to 12 inclusive must be considered. A typical plot of  $1/D$  vs.  $t$  is shown in Figure 4. The addition of 0.5  $M$  ethanol will scavenge H and OH, suppressing reactions 6, 7, 10, 11, and 12. If water at pH 10.5 with and without 0.5  $M$  ethanol is irradiated with equal pulse intensities, the initial "k" without ethanol is greater than the initial "k" with ethanol and the difference is due to reactions 6 and 7. From the measured difference in experiments using the syringe technique and assuming the same  $G$  values as used for the  $k_7$  calculation,  $k_6 = 3.1 \times 10^{10} M^{-1} \text{sec.}^{-1}$  is obtained. About 60% of the total initial rate of decay of  $e_{\text{aq}}^-$  in water at pH 10.5 is due to reaction 6. The fit of a computer-calculated curve to the experimental points obtained with water at pH 10.5 is shown in Figure 4. From these and other experiments, we set  $k_6 = (3.0 \pm 0.7)$

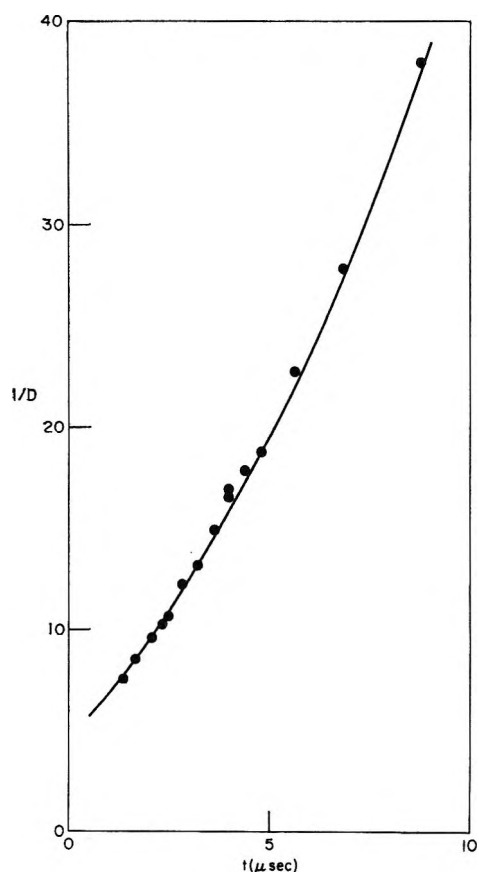


Figure 4. Decay of  $e_{\text{aq}}^-$  absorption at 5780  $\text{\AA}$ ., pH 10.50, no  $\text{H}_2$ ,  $l = 2$  cm. Pulse assumed to be two rectangular pulses  $8.06 \times 10^{26}$  and  $6.08 \times 10^{26}$  e.v.  $l^{-1} \text{sec.}^{-1}$  and 0.2 and 0.3  $\mu\text{sec.}$ , respectively.  $G$  and  $k$  values as for Figure 3a except that  $k_2 = 0$ ;  $k_7 = 2.6 \times 10^{10}$ ;  $k_9 = 2.5 \times 10^{12}$ ;  $k_{11} = 1.2 \times 10^{10}$ ; and  $2k_{12} = 1 \times 10^{10} M^{-1} \text{sec.}^{-1}$ ;  $k_9$  necessary for curvature;  $k_6$  accounts for most of initial decay.

$\times 10^{10} M^{-1} \text{sec.}^{-1}$ . Thus we see that  $e_{\text{aq}}^-$  reacts almost equally fast with either OH or  $\text{O}_{\text{aq}}^-$ .

$\text{H}_2$  (100 Atm.) at pH 11.6. Determination of  $k(\text{H} + \text{OH}^-)$ . Evidence has already been presented in support of reaction 3, and further evidence will be presented later. Reaction 3 is first order in  $[\text{OH}_{\text{aq}}^-]$  so that the half-life can be fixed by a suitable choice of pH. At pH 11.6 the half-life for this reaction was found to be about 10  $\mu\text{sec.}$ , so that only a small fraction of H atoms is converted to  $e_{\text{aq}}^-$  during the pulse. This means that at the end of the pulse  $[e_{\text{aq}}^-]_0$ ,  $[\text{H}]_0$ , and  $[\text{H}_2\text{O}_2]_0$  can be deduced from the initial optical density and relative  $G$  values for the species. (All OH is assumed to convert to H.) In order to calculate  $k_3$ , one may use eq. 19.

$$\left[ \epsilon_e^{5780} \times l \times \frac{d}{dt} \left( \frac{1}{D} \right) \right] [e_{\text{aq}}^-]^2 = 2k_6[e_{\text{aq}}^-]^2 + k_9[e_{\text{aq}}^-][\text{H}_2\text{O}] + k_7[e_{\text{aq}}^-][\text{H}] + k_8[e_{\text{aq}}^-][\text{H}_2\text{O}_2] - k_3[\text{H}][\text{OH}_{\text{aq}}^-] \quad (19)$$

where the first term in brackets on the left-hand side is an effective bimolecular rate constant which will vary with pulse intensity and with time after the pulse. If the initial slope of a  $1/D$  vs.  $t$  plot and the initial optical density are measured in an experiment, then all the quantities in eq. 19 are known for time zero except  $k_3$ , which can then be calculated. This method will be most precise if the left-hand side, *i.e.*, the initial slope, is close to zero.

In Figure 5 are shown the oscilloscope traces obtained with 100 atm. of  $\text{H}_2$  at pH 11.6. At pH 11.6

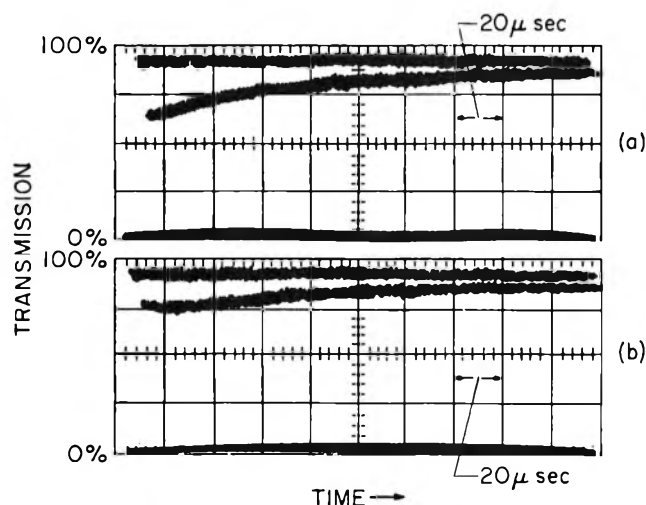


Figure 5. Oscilloscope traces showing  $e_{\text{aq}}^-$  absorption at 5780  $\text{\AA}$ . in 0.004  $M$  NaOH and 100 atm. of  $\text{H}_2$ . In (a) the pulse intensity is higher so that  $e_{\text{aq}}^-$  decay always exceeds formation by (3). In (b),  $[e_{\text{aq}}^-]$  continues to increase after the pulse due to reaction 3.

at high pulse intensity the  $e_{aq}^-$  absorption decays continuously (Figure 5a), whereas at low pulse intensities the  $e_{aq}^-$  concentration increases for several microseconds after the pulse (Figure 5b). At pH 13.3 reaction 3 takes place during the pulse and a rapid decay is observed at all intensities. Using data from Figure 5 in eq. 19 gave  $k_3 = (2.0 \pm 0.2) \times 10^7 M^{-1} \text{sec.}^{-1}$ . For this calculation the following values were used:  $2k_5 = 1 \times 10^{10} M^{-1} \text{sec.}^{-1}$ ,  $k_9[\text{H}_2\text{O}] = 2 \times 10^4 \text{sec.}^{-1}$ ,  $k_7 = 2.6 \times 10^{10}$ , and  $k_8 = 1 \times 10^{10} M^{-1} \text{sec.}^{-1}$ . If  $k_9[\text{H}_2\text{O}]$  is taken as zero,  $k_3 = 1.6 \times 10^7 M^{-1} \text{sec.}^{-1}$ . As we have seen  $k_9$  is small but the effective first-order component of  $e_{aq}^-$  decay in some of our solutions is about  $10^4 \text{sec.}^{-1}$ , so we choose a best value for  $k_3$  as  $(1.8 \pm 0.6) \times 10^7 M^{-1} \text{sec.}^{-1}$ , including the uncertainty arising from errors in  $\epsilon_e^{5780}$  and in the other  $k$  values. A value of  $k_3/k_{\text{H}+\text{O}_2} = (0.6 \text{ to } 1.2) \times 10^{-3}$  can be calculated.<sup>7a,b,32</sup> From the pulse radiolytic<sup>33</sup> formation of  $\text{HO}_2$ ,  $k_{\text{H}+\text{O}_2} = 2.1 \times 10^{10} M^{-1} \text{sec.}^{-1}$ , yielding  $k_3 = (1.2\text{--}2.5) \times 10^7 M^{-1} \text{sec.}^{-1}$ . This agreement is satisfactory, since  $k_3/k_{\text{H}+\text{O}_2}$  was not measured directly but was estimated by combining several rate constant ratios.

**Further Evidence for Reaction 3.** The variation with pH of initial optical density at 5780 Å. using 100 atm. of  $\text{H}_2$  and constant pulse intensity provides further evidence for the conversion of H to  $e_{aq}^-$  in alkaline solutions. See Figure 6.  $D_0$  varied as much as 20% between identical solutions in the three different pressure cells. Therefore, the  $D_0$  values in Figure 6 were measured by rotating the solutions at each pH among the three cells and taking  $D_0$  measurements three to eight times at each pH. One of the cells in each set always contained 0.2 M NaOH as a control.

Between neutral and pH 11.5,  $D_0$  is about constant and is due to  $G_e$ . Neutral becomes slightly acid due to  $\text{H}_3\text{O}_{aq}^+$  formed by the pulse. Above pH ~11.5 there is a sharp, approximately twofold increase.  $D_0$  is probably constant between pH 13 and 14 although the unusually large scatter of points at pH 14.07 makes this conclusion uncertain. At the higher pH values if H and  $\text{OH}(\text{O}^-)$  are converted to  $e_{aq}^-$ , the ratio of  $D_0(\text{pH } 13\text{--}14)/D_0(\text{pH } 7\text{--}11.5)$  should equal  $(G_e + G_{\text{OH}} + G_{\text{H}})/G_e \approx 2.2$ , which agrees closely enough with the ratio in Figure 6 of ~2.5.

Measurements of the decay of absorption at 4358 Å. are in agreement with the absorption decay at 5780 Å. This suggests that the same species is involved and we find  $\epsilon_e^{5780}/\epsilon_e^{4358} = 3.2$ , whereas Keene<sup>11b</sup> gives 3.5 for this ratio. Since in our case more than half of the  $e_{aq}^-$  would be due to reaction 3, this result again supports the reaction of  $\text{H} + \text{OH}_{aq}^-$ . Table IV shows the experimental comparison.

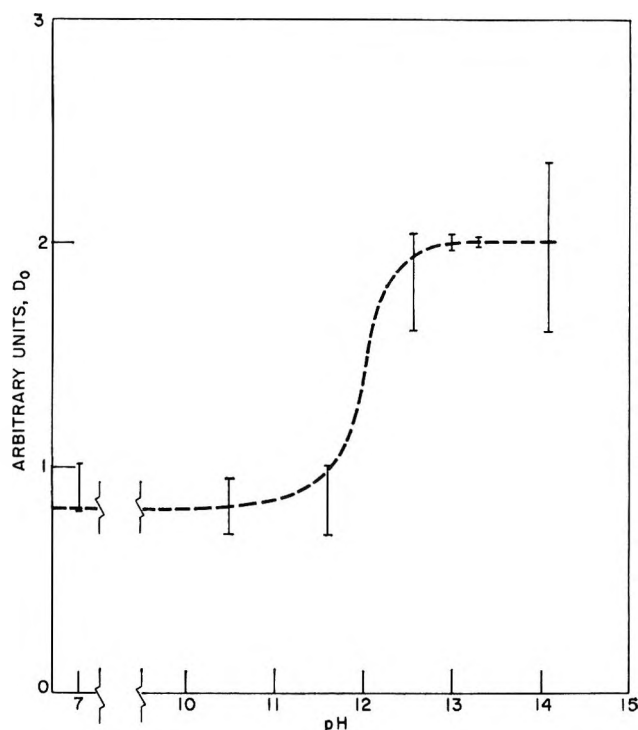


Figure 6. Effect of pH on initial optical density at 5780 Å. Same pulse intensity as for Figure 3. Initial optical density from extrapolation of  $1/D$  vs.  $t$  plots to middle of pulse.

Table IV: Decay of  $e_{aq}^-$  Absorption<sup>a</sup>

Pulse length, $\mu\text{sec.}$	$k^c$		% linearity		$D_0$	
	4358 Å.	5780 Å.	4358 Å.	5780 Å.	4358 Å.	5780 Å.
0.4	1.4	1.3	80	85	0.115	0.360
5 <sup>b</sup>	1.05	1.2	$\geq 80$	85	0.385	1.25

<sup>a</sup>  $\text{H}_2$  (100 atm.), pH 13.3, 8-cm. light path. <sup>b</sup>  $D_0$  taken at end of pulse. <sup>c</sup> In units of  $10^{10} M^{-1} \text{sec.}^{-1}$ .

Using equal pulse intensities, the initial optical density at 5780 Å. in 0.134 M NaOH under 100 atm. of  $\text{H}_2$  was compared to the final optical density measured *in situ* after 10 sec. in the modified Fricke dosimeter.<sup>17a</sup> The resulting ratio  $D_0^{5780}/D_{\infty}^{3020} = 2.1$  (four experiments) corresponds satisfactorily to  $G(e_{aq}^-) = G_e + G_{\text{H}} + G_{\text{OH}}$  as would be expected if reaction 3 occurs.

**The Effective Bimolecular Decay Constant for  $e_{aq}^-$  as a Function of pH.** In Figure 7 the variation of the effective initial bimolecular decay constant for  $e_{aq}^-$ , " $k$ " in eq. 18, is plotted as a function of pH. The

(32) A. O. Allen, *Radiation Res. Suppl.*, **4**, 54 (1964).

(33) S. Gordon, E. J. Hart, and J. K. Thomas, *J. Phys. Chem.*, **68**, 1262 (1964).

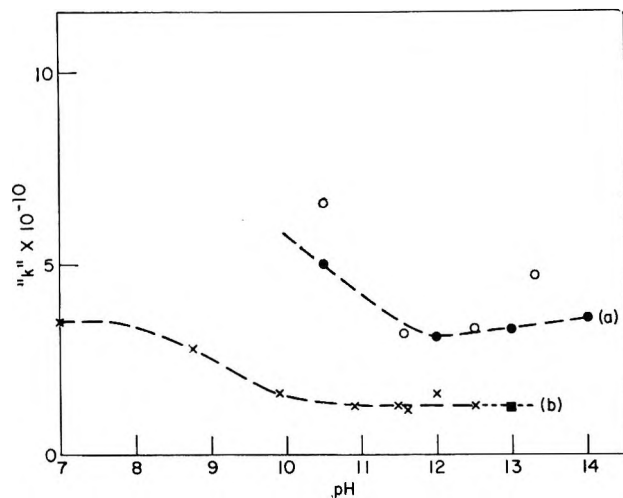


Figure 7. Initial slope of  $1/D$  vs.  $t$  plots as a function of pH. (a): No ethanol; ●,  $l = 2$  cm., pulse intensity as in Figure 4; ○,  $l = 8$ , pressure cells, intensity as in Figure 3. (b): 0.5 M ethanol; ×,  $l = 2$ , intensity as in Figure 4; ■, from Dorfman and Taub.<sup>17a</sup> These "k" values from initial slopes are slightly higher than computer values, especially where rapid decay occurred. In water at pH 7 (see Figure 8) no "k" is given because the decay is very rapid and the resultant error is large.

values of "k" were measured (a) in "pure" water, and (b) with 0.5 M ethanol added.

These plots can be accounted for quantitatively using the mechanism and the rate constants already reported in this paper. The 0.5 M ethanol scavenges all H and OH eliminating reactions 3, 6 or 6a, and 7, which explains the lower values of "k" on curve b as compared to a. As the pH is increased from pH 7, "k" decreases both in the presence and absence of ethanol due to the suppression of reaction 4. Since  $k_6$  is not much greater than  $k_{6a}$ , "k" (curve a) changes little at pH 11.9, the pK of OH. The open circles were obtained with the pressure cells after purification by irradiation under  $H_2$  followed by replacement of the  $H_2$  with 1 atm. of argon. The differences from curve a may be due to impurities or other experimental errors. If the small increase (curve a) above pH 12 is real it may be due to a salt effect or to impurities.

A further test of the mechanism and rate constants is shown in Figure 8, where the decay of  $e_{aq}^-$  in pure neutral pulse-irradiated water is shown plotted vs.  $t$ . Both the initial slope and the strong curvature are accounted for quantitatively.

*Errors Due to the Possible Existence of Excited Water Molecules.* It is obvious that excitation is produced in irradiated water. Although the evidence for  $H_2O^*$  does not seem to be conclusive, we shall discuss the possible effects of  $G_{H_2O^*} \approx 0.6^{10}$  on our rate constants. If  $H_2O^*$  decomposes to H and OH in less than 1  $\mu$ sec.,

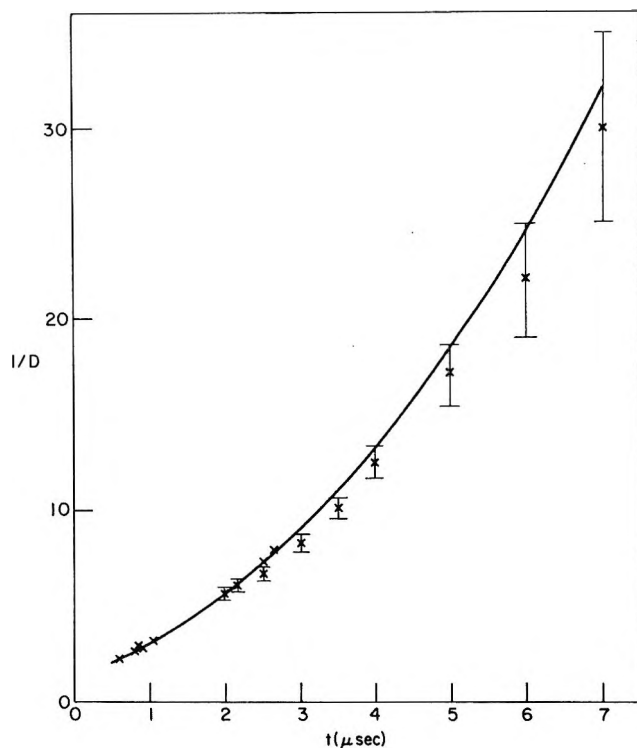


Figure 8. Decay of  $e_{aq}^-$  absorption at 5780 Å. in neutral water, no  $H_2$ ,  $l = 4$  cm. Pulse assumed to be two rectangular pulses  $1.2 \times 10^{26}$  and  $9.5 \times 10^{26}$  e.v.  $l^{-1}$   $sec^{-1}$  of 0.2 and 0.3  $\mu$ sec., respectively.  $G$  values as in Figure 3a.  $k_4 = 2 \times 10^{10}$ ,  $2k_5 = 1 \times 10^{10}$ ,  $k_6 = 3.0 \times 10^{10}$ ,  $k_7 = 2.5 \times 10^{10}$ ,  $k_8 = 1.1 \times 10^{10}$ ,  $k_9 = 2 \times 10^{10}$ ,  $2k_{10} = 3.0 \times 10^{10}$ ,  $k_{11} = 1.5 \times 10^{10}$ ,  $2k_{12} = 1.2 \times 10^{10}$ ,  $k_{13} = 1.43 \times 10^{11}$   $M^{-1}$   $sec^{-1}$ . In this plot the  $k$ 's could be varied a reasonable amount and a fit still be obtained because  $e_{aq}^-$  decays by so many reactions. Reactions 10, 11, and 12 have an opposite effect on curvature as compared to reaction 9.

then our rate constant measurements are not affected by  $H_2O^*$ , or, if  $H_2O^*$  reacts in alkaline solution with  $OH_{aq}^-$  to give  $e_{aq}^-$  and OH in less than 1  $\mu$ sec. then the rate constants measured in alkaline solution are not affected. If  $H_2O^*$  reacts with a half-life longer than  $\sim 10$   $\mu$ sec., the rate constants from computer curve fitting will be in error to the extent that the  $G_H$  and  $G_{OH}$  used are in error. An error of +10% in  $2k(e_{aq}^- + e_{aq}^-)$  will be introduced if  $k(e_{aq}^- + H_2O^*) = 10^{10}$   $M^{-1}$   $sec^{-1}$ . If  $H_2O^*$  yields  $e_{aq}^-$  during measurement, an error up to -10% may be introduced. The rate constant for  $O_{aq}^- + H_2$  was obtained by comparing the rate of formation of  $e_{aq}^-$  in the presence of 1 atm. of  $H_2$  with the measured decay in the absence of  $H_2$ , so that  $k(O_{aq}^- + H_2)$  would seem to be correct even if  $H_2O^*$  reacts in the microsecond region. For the rate constants  $k(H^+ + OH_{aq}^-)$ ,  $k(e_{aq}^- + O_{aq}^-)$ ,  $k(e_{aq}^- + OH)$ , and  $k(e_{aq}^- + H)$  the estimated error

depends upon the precise assumptions, but it does not seem likely that  $\text{H}_2\text{O}^*$  reaction in the microsecond range would introduce an error greater than  $\sim 30\%$ . The kinetics observed in our work gave no indication of  $\text{H}_2\text{O}^*$  playing a role, but this cannot be taken as conclusive evidence against  $\text{H}_2\text{O}^*$ .

### Conclusion

From experiments in the pulse radiolysis of water at pH 10–13, with and without 100 atm. of  $\text{H}_2$ , a mechanism has been shown to account for the radiolysis of water at high intensities. In particular, very good evidence for the reaction  $\text{H} + \text{OH}_{\text{aq}}^- \rightarrow \text{e}_{\text{aq}}^- + \text{H}_2\text{O}$

has been found. Many rate constants have been measured, so that the proposed mechanism is a quantitative one.

*Acknowledgment.* We wish to thank W. A. Mulac for invaluable assistance in all phases of these experiments and Gene Clift for careful Linac operation. We wish also to thank Dr. Klaus Schmidt for programming the computer calculations. Discussions with our colleagues, Drs. L. M. Dorfman (now of Ohio State University), S. Gordon, E. J. Hart, I. A. Taub (now of Mellon Institute), and J. K. Thomas, have been very helpful.

## Solvents Having High Dielectric Constants. XV. Thermodynamic

### Properties of Solutions of Hydrochloric Acid in N-Methylacetamide

#### by Electromotive Force Measurements<sup>1</sup>

by Lyle R. Dawson, William H. Zuber, Jr., and Hartley C. Eckstrom

*Department of Chemistry, University of Kentucky, Lexington, Kentucky (Received October 31, 1964)*

The e.m.f. of the cell  $\text{Pt}, \text{H}_2; \text{HCl}(m); \text{AgCl}-\text{Ag}$  in N-methylacetamide has been measured for 15 to 20 concentrations at  $5^\circ$  temperature intervals over the range  $35$  to  $70^\circ$ . Vapor pressures, relative partial molal enthalpies, and relative partial molal heat capacities of the solute have been calculated. Standard thermodynamic values  $\Delta G^\circ$ ,  $\Delta H^\circ$ , and  $\Delta S^\circ$  for the cell reaction have been determined. The standard potential of the Ag–AgCl electrode ranges from 0.21187 at  $35^\circ$  to 0.17194 at  $70^\circ$ .

Platinum–hydrogen and silver–silver chloride electrodes have been shown to be stable and reproducible in N-methylacetamide (NMA) by Dawson and co-workers<sup>3</sup> in this laboratory. In this solvent having a very high dielectric constant (165.5 at  $40^\circ$ ) the standard potential of the silver–silver chloride electrode is 0.20573 v. at  $40^\circ$ .

Mean molal activity coefficients of HCl in NMA at  $40^\circ$  were found to be larger than those for similar solutions in water at corresponding concentrations. Also,

the activity coefficients decrease with increasing molality much less than in aqueous solutions.

The purpose of the present investigation was to determine the standard reduction potentials of the silver–silver chloride electrode over the temperature range

(1) (a) Taken from a Ph.D. dissertation submitted by W. H. Zuber, Jr.; (b) this work was supported in part by a research grant from the U. S. Atomic Energy Commission.

(2) L. R. Dawson, R. C. Sheridan, and H. C. Eckstrom, *J. Phys. Chem.*, **65**, 1829 (1961).

35–70°. From these data various thermodynamic values for the reaction  $\frac{1}{2}\text{H}_2 + \text{AgCl} \rightleftharpoons \text{Ag} + \text{HCl}$  and thermodynamic properties of solutions of the electrolyte in NMA were calculated.

### Experimental

The preparation of the electrodes has been described adequately earlier.<sup>2–4</sup> An all-glass type of electromotive force cell of the design recommended by Harned and Morrison<sup>5</sup> was used. Shielding was provided to avoid leaks of potential. The measurements were made in a mechanically stirred mineral oil bath thermostated to  $\pm 0.03^\circ$ .

For measurements above  $45^\circ$ , the electromotive force cell was provided with a stopcock fitted between the two electrode compartments as in the cell described by Bates and co-workers.<sup>6</sup> The stopcock was needed at the higher temperatures to prevent the migration of silver ions into the hydrogen electrode compartment.

For preparing the various solutions, the procedure was essentially the same as that described previously.<sup>2</sup> All experimental results used represent averages of two or more series of determinations over the same concentration range with new stock solutions and freshly prepared electrodes for each series.

After preparing the cell and placing it in position, a hydrogen flow of about 1 bubble/sec. was continued for 2 hr. before e.m.f. readings were taken. Readings were made every hour until equilibrium was attained, as evidenced by constancy of the e.m.f. values. All measurements were reduced to 760 mm. pressure of hydrogen.

The vapor pressure of pure NMA was measured over the temperature range 30 to  $80^\circ$  with a closed-end manometer. Below  $100^\circ$  it is less than 10 mm.; therefore, the correction to the e.m.f. for the vapor pressure of NMA is very small in the temperature range of this study.

Since heat data calculated from e.m.f. measurements are quite sensitive to experimental error, it may be considered that the results reported here have an accuracy no better than  $\pm 150$  joules or an uncertainty of approximately 0.8%.

### Results and Discussion

A summary of e.m.f. data for HCl in NMA at  $45^\circ$  is shown in Table I. Similar experimental values were obtained for 15 to 20 concentrations at each of the 5° temperature intervals throughout the range; however, space limitations do not permit presentation of all of these results. Values of  $E'$  were calculated from the equation<sup>2</sup>

$$E + \frac{2(2.303)RT}{F} \log m - \frac{2(2.303)RT}{F} \alpha \sqrt{m} = E' = E^\circ - \frac{2(2.303)RT}{F} \beta m$$

A plot of  $E'$  vs.  $m$  at each temperature should yield a straight line with slope =  $2(2.303)RT\beta/F$  and intercept  $E^\circ$ . In each case, a least-squares fit of the calculated values of  $E'$  was obtained, and from this the intercept,  $E^\circ$ , was determined.

Table I: Summary of E.m.f. Data for HCl in NMA at  $45^\circ$ <sup>a</sup>

$m_{\text{HCl}}$	E.m.f., v.	$E'$ , v. <sup>b</sup>
0.004834	0.49462	0.20086
0.005383	0.48919	0.20125
0.008038	0.46820	0.20192
0.011195	0.44875	0.20030
0.015941	0.42881	0.19932
0.016871	0.42792	0.20147
0.018039	0.42216	0.19929
0.019662	0.41975	0.19927
0.025930	0.40320	0.19968
0.029910	0.39516	0.19923
0.029922	0.39603	0.20012
0.037775	0.38330	0.19973
0.044065	0.37385	0.19841
0.051970	0.36502	0.19826
0.056855	0.36132	0.19927
0.065805	0.35222	0.19782
0.068832	0.35037	0.19832
0.085124	0.33866	0.19766
0.108844	0.32596	0.19766
0.129468	0.31554	0.19614
0.139437	0.31217	0.19656
0.155698	0.30569	0.19570

<sup>a</sup> Corrected to 1 atm. <sup>b</sup> Average deviation in  $E' = 0.00057$  v.

Values of  $E^\circ_{\text{AgCl-Ag}}$  in NMA together with similar data in water are shown in Table II.

Utilizing these data, the mean molal activity coefficients,  $\gamma_{\pm}$ , were calculated as described earlier.<sup>2</sup>

In order to calculate the partial molal quantities it was necessary to express  $E^\circ$  as a function of the form  $A + BT + CT^2$ . Appropriate constants were determined for the concentration range 0.005 to 1.0  $m$  from which

(3) L. R. Dawson, E. D. Wilhoit, and P. G. Sears, *J. Am. Chem. Soc.*, **78**, 1569 (1956).

(4) R. G. Bates, "Electrometric pH Determinations," John Wiley and Sons, Inc., New York, N. Y., 1954, pp. 179–183.

(5) H. S. Harned and J. O. Morrison, *Am. J. Sci.*, **33**, 161 (1937).

(6) R. B. Bates and G. D. Pinching, *J. Res. Natl. Bur. Std.*, **42**, 419 (1949).



**Table II:** Comparison of  $E^\circ$  for the Cell Reaction  $\frac{1}{2}\text{H}_2 + \text{AgCl} = \text{Ag} + \text{HCl}$  in Water and in NMA

Temp., °C.	$\alpha(\text{NMA})$	$\beta(\text{NMA})$	$E^\circ$ in NMA	$E^\circ$ in $\text{H}_2\text{O}$
35	0.018247	0.074553	0.21187	0.21566
40	0.019217	0.033267	0.20573	0.21207
45	0.020322	0.035053	0.20091	0.20834
50	0.021534	0.024607	0.19456	0.20449
55	0.022843	0.030989	0.18972	0.20051
60	0.024309	0.041589	0.18357	0.19641
70	0.027899	0.045096	0.17194	0.18785

**Table III:** Summary of Activity Coefficients for HCl in NMA

$m_{\text{HCl}}$	$\gamma_{\pm}$							
	35°	40°	45°	50°	55°	60°	65°	70°
0.00200	0.985	0.986	0.985	0.984	0.983	0.983	0.982	0.981
0.00500	0.976	0.978	0.975	0.975	0.975	0.974	0.973	0.971
0.01000	0.966	0.971	0.970	0.966	0.966	0.965	0.964	0.961
0.02000	0.952	0.963	0.961	0.955	0.955	0.956	0.953	0.950
0.03000	0.942	0.958	0.956	0.948	0.948	0.950	0.947	0.943
0.04000	0.933	0.954	0.953	0.942	0.943	0.946	0.943	0.938
0.05000	0.925	0.952	0.950	0.937	0.939	0.943	0.940	0.935
0.06000	0.919	0.951	0.949	0.934	0.936	0.942	0.938	0.933
0.07000	0.912	0.950	0.948	0.931	0.934	0.940	0.937	0.931
0.08000	0.907	0.950	0.948	0.929	0.933	0.940	0.937	0.930
0.09000	0.901	0.927	0.948	0.927	0.931	0.940	0.937	0.930
0.10000	0.896	0.950	0.948	0.925	0.930	0.940	0.937	0.930

partial molal quantities for hydrogen chloride in NMA are presented in Tables IV and V.

**Table V:** The Relative Partial Molal Heat Capacity of Hydrochloric Acid in NMA (joules/mole deg.; multiply tabulated value by  $-1$ )

$m_{\text{HCl}}$	35°	40° <sup>a</sup>	45°	50°	55°	60°	65°	70°
0.005	67.5	68.5	69.5	70.5	71.8	72.9	74.0	75.1
0.01	71.9	73.1	74.3	75.4	76.6	77.8	78.9	80.1
0.02	86.4	87.4	89.2	90.6	92.0	93.4	94.8	96.2
0.03	102.5	104.2	105.8	107.5	109.2	110.8	112.5	114.2
0.04	112.1	114.0	115.8	117.6	119.4	121.2	123.1	124.9
0.05	161.1	163.7	166.4	169.0	171.6	174.2	176.8	179.4
0.06	144.1	146.5	148.8	151.3	153.5	155.8	158.2	160.5
0.07	160.0	162.6	165.2	168.7	170.4	173.0	175.6	178.2
0.08	176.7	179.6	182.4	185.3	188.2	191.0	193.9	196.2
0.09	192.8	196.0	199.1	202.2	205.4	208.5	211.6	214.7
0.10	210.1	213.5	216.9	220.3	223.8	227.2	230.6	234.0

<sup>a</sup> See ref. 2.

From the experimental data, thermodynamic quantities  $\Delta G^\circ$ ,  $\Delta H^\circ$ , and  $\Delta S^\circ$  for the cell reaction at eight temperatures were calculated in the usual manner. A summary of these values may be found in Table VI.

Approximate measurements of the vapor pressure of NMA yielded results ranging from 0.28 mm. at 35° to 1.87 mm. at 70° and 11.77 mm. at 100°. Using these

**Table IV:** The Relative Partial Molal Heat Content of Hydrochloric Acid in NMA (joules/mole)

$m_{\text{HCl}}$	35°	40° <sup>a</sup>	45°	50°	55°	60°	65°	70° <sup>a</sup>
0.005	$2.171 \times 10^3$	$1.831 \times 10^3$	$1.486 \times 10^3$	$1.135 \times 10^3$	$0.779 \times 10^3$	$0.417 \times 10^3$	$0.050 \times 10^3$	$-0.322 \times 10^3$
0.01	2.238	1.875	1.507	1.133	0.753	0.367	-0.025	-0.422
0.02	2.692	2.257	1.814	1.365	0.909	0.445	-0.025	-0.502
0.03	3.116	2.599	2.074	1.541	0.999	0.449	-0.109	-0.676
0.04	3.375	2.809	2.234	1.652	1.059	0.457	-0.153	-0.773
0.05	4.409	3.597	2.772	1.934	1.082	0.218	-0.660	-1.550
0.06	4.094	3.358	2.620	1.870	1.108	0.335	-0.450	-1.247
0.07	4.423	3.616	2.797	1.964	1.119	0.260	-0.611	-1.495
0.08	4.762	3.872	2.967	2.047	1.113	0.165	-0.797	-1.774
0.09	5.092	3.796	3.132	2.129	1.110	0.076	-0.975	-2.040
0.10	5.429	4.370	3.294	2.201	1.091	-0.036	-1.181	-2.342

<sup>a</sup> See ref. 2.

the equation  $E^\circ = 0.445372 - 4.22430 \times 10^{-4}T - 1.09049 \times 10^{-6}T^2$  was obtained.

Harned and Owen<sup>7</sup> have shown that  $\bar{L}_2 = F(A - BT^2)$  and  $\bar{J}_2 = 2FBT$  where  $\bar{L}_2$  is the relative partial molal enthalpy of the solute and  $\bar{J}_2$  is the relative partial molal heat capacity of the solute. From the dependence of  $E^\circ$  and  $E$  on temperature, values for the constants  $A$  and  $B$  were calculated. Summaries of these

data, a value of  $(55.6 \pm 8.4) \times 10^3$  joules/mole was calculated for the heat of vaporization of N-methylacetamide in the temperature range 30 to 100°.

At each temperature the standard reduction potential for the silver chloride-silver electrode is less in

(7) H. S. Harned and B. B. Owen, "The Physical Chemistry of Electrolytic Solutions," Reinhold Publishing Corp., New York, N. Y., 1958, pp. 433-436.

**Table VI:** Standard Thermodynamic Changes for the Cell Reaction

Temp., °C.	$E^\circ$ , v.	$G^\circ \times 10^{-4}$ , joules	$H^\circ \times 10^{-4}$ , joules	$S^\circ$ , joules/deg.
35	0.21187	20.44	43.59	75.13
40	0.20573 <sup>a</sup>	19.85	43.53	75.62
45	0.20091	19.39	43.61	76.13
50	0.19456	18.77	43.55	76.68
55	0.18972	18.31	43.64	77.19
60	0.18357	17.71	43.61	77.74
65	0.17786	17.16	43.62	78.25
70	0.17194	16.59	43.63	78.80

<sup>a</sup> See ref. 2.

NMA than it is in water.<sup>7</sup> For example, at 35°  $E^\circ_{\text{AgCl}-\text{Ag}(\text{NMA})} = 0.21187$  and  $E^\circ_{\text{AgCl}-\text{Ag}(\text{H}_2\text{O})} = 0.21566$ . Since  $\Delta G^\circ = -nFE^\circ$ ,  $\Delta G^\circ$  for the cell reaction is more negative in water than in NMA; also, the equilibrium constant for the reaction is larger in water.

At each concentration, the activity coefficients are larger in NMA than in water.<sup>7</sup> The experimental activity coefficients in NMA approach more rapidly the values predicted by the Debye-Hückel theory as the concentration of solute decreases as would be expected because of the higher dielectric constant of NMA. The higher activity coefficients in NMA indicate that solutions of HCl in this solvent are more nearly ideal than are solutions of HCl in water.

## The Dispersion of the Conductance of a Salt in Low Dielectric Solvents

by T. R. Nanney<sup>1</sup> and W. R. Gilkerson

Department of Chemistry, University of South Carolina, Columbia, South Carolina (Received November 2, 1964)

The conductances of solutions of tetra-*n*-butylammonium picrate in 50 mole % *o*-dichlorobenzene-benzene solvent and in chlorobenzene have been measured at 25° as a function of frequency from 1 to 100 kc. The conductances increase with increasing frequency. The magnitude of the effect, at low salt concentrations, approaches that which one would predict from relaxation of the ion atmosphere (Debye-Falkenhagen effect), while at higher salt concentrations the magnitude of the effect approaches that which one would predict from relaxation of the ion-pair equilibrium. Ion-pair recombination rates calculated from the frequency dependence of the effect are in agreement with theory (Onsager).

This work was undertaken in an effort to detect the predicted<sup>2</sup> dispersion of the low-field conductance of a weak electrolyte due to relaxation of the ion-pair equilibrium. The detection of such an effect would be important not only for its theoretical implications, but also because present theories predict that the method can be used to determine rate constants for ionic recombination. An earlier report<sup>3</sup> from this laboratory of an observation of this effect in aqueous boric acid solutions in the 10-kc. frequency range was subsequently found<sup>2b,4</sup> to be incorrect. Our next effort was in the megacycle frequency range using

aqueous acetic acid and a modified Twin-T bridge. These results at best showed no difference in conductance between acetic acid and nitric acid. The corrections necessary at these frequencies due to inductance in leads and cells were larger than the expected effect to be measured. We next turned to electrolytes

(1) Tennessee Eastman Fellow.

(2) (a) R. G. Pearson, *Discussions Faraday Soc.*, **17**, 187 (1954);  
(b) W. R. Gilkerson, *J. Phys. Chem.*, **66**, 669 (1962).

(3) W. R. Gilkerson, *J. Chem. Phys.*, **27**, 914 (1957).

(4) R. P. Bell and R. R. Robinson, *Trans. Faraday Soc.*, **58**, 2358 (1962).

in low dielectric solvents where observations could possibly be made in the kilocycle frequency region using more conventional conductance bridges. We report here the results of the latter investigation. The salt, tetra-*n*-butylammonium picrate ( $\text{Bu}_4\text{NPi}$ ) and solvent systems, chlorobenzene (CB) and 50 mole % *o*-dichlorobenzene in benzene (ODCB-B), were chosen to satisfy two requirements: the conductance in the low-frequency range has been well studied<sup>5a,b,c,6</sup> and the fraction of ion pairs dissociated is small in the concentration range where one would predict a maximum effect.

### Experimental

**Materials.** Chlorobenzene (Dow Chemical Co.) was passed through a  $33 \times 2$ -cm. column packed with alumina (Merck, chromatographic grade) and distilled, b.p.  $28^\circ$  (13 mm.). The specific conductance was  $4.8 \times 10^{-11}$  mho/cm. Benzene (Merck, reagent grade) was passed through the alumina-packed column, recrystallized, refluxed over sodium for 2 hr., and distilled, retaining a middle cut. No conductivity was observable. *o*-Dichlorobenzene (Eastman, White Label) was passed through alumina and distilled, b.p.  $56^\circ$  (10 mm.), specific conductance  $4.5 \times 10^{-11}$  mho/cm.  $\text{Bu}_4\text{NPi}$  was prepared as previously,<sup>7</sup> m.p.  $89.8^\circ$  (reported<sup>7</sup>  $89.8^\circ$ ).

**Measurements.** All solutions were made up by weight in a nitrogen-filled drybox. The cell principally used in this work is similar to a design by Sadek and Fuoss<sup>8</sup> and has been described previously.<sup>7</sup> In the present work, the guard electrode was connected directly to the ground electrode for all measurements. Used in this fashion, the cell has an air capacity,  $C_0$ , of 24.72 pf. and a lead capacitance,  $C_L$ , of 34.6 pf. as determined from the capacity of the cell filled with pure CB, ODCB-B, and air. The cell constant is thus calculated to be  $0.0885/C_0$  (in pf.) =  $0.00358 \text{ cm.}^{-1}$ . One other cell was used: this was a dipping type with cylindrical nickel electrodes, obtained from Balsbaugh Laboratories, Duxbury, Mass., Type 2TN25. This cell had  $C_0 = 23.30$  pf.,  $C_L = 5.4$  pf., and cell constant  $0.00380 \text{ cm.}^{-1}$ .

The bridge was similar to one already described.<sup>7,9</sup> In one set of measurements, using the 2TN25 cell, the detector circuit was replaced by a General Radio Type 1232-A tuned amplifier and null detector. The ratio arms in the bridge, the Leeds and Northrup Campbell-Shackelton ratio box, were replaced by the ratio arms of a General Radio 716-C capacitance bridge, with  $f_0$  set at 100 kc. at all oscillator frequencies. Using the regular detector, the precision of a single conductance measurement at 1, 10, and 100 kc. amounted to

$\pm 0.2, 0.4,$  and  $1.0 \times 10^{-9}$  mho, respectively. The cells were placed in an oil-filled bath thermostated at  $25.00^\circ$ . During a typical set of measurements on one solution, the temperature variation was  $\pm 0.008^\circ$ .

The 20,000-ohm secondary standard resistor was a Leeds and Northrup Co. Type 4642. The dielectric constant for the ODCB-B solvent mixture is<sup>6</sup> 6.041 while that of CB is<sup>10</sup> 5.621, all at  $25^\circ$ .  $\Lambda_0$  for the salt was taken as 30 in 50% ODCB-B,<sup>8</sup> with the ion pair dissociation constant,  $K$ , being  $2.74 \times 10^{-7}$ . The corresponding values in CB were<sup>5c</sup> 41.5 and  $4.1 \times 10^{-8}$ .

The conductances of solutions, solvents, empty cell, and resistor were determined at 1, 2, 5, 10, 20, 50, and 100 kc. The bridge was initially rebalanced at each frequency. The conductance increase,  $\Delta G$ , at frequency  $f$  was taken as the conductance at  $f$  minus that at 1 kc. Measurements were performed in the sequence: 1 kc.,  $f$  kc., 1 kc. The mean of the two 1-kc. values immediately preceding and succeeding the determination at  $f$  was taken to be the best value at 1 kc. to be used in calculating  $\Delta G$ . This was done to minimize the effect of thermal drift.<sup>11</sup> The increase in the loss factor,  $\Delta\epsilon''$ , was calculated using the relation  $\Delta\epsilon'' = \Delta G/2\pi f C_0$ .

### Results

The increase in loss factor of solution minus the increase in loss factor of solvent at each frequency for solutions of  $\text{Bu}_4\text{NPi}$  in ODCB-B are shown in Figure 1 while the results for CB as solvent are shown in Figure 2, plotted *vs.*  $\log f$ . In each figure is also plotted  $\Delta\epsilon''$  for the pure solvent. The height of the bar at each point represents the uncertainty due to variation in the two 1-kc. conductance values used to calculate  $\Delta G$ . The large uncertainties at 2 and 5 kc. are principally due to the fact that the conductance increases are small at these frequencies, typically of the order of  $1 \times 10^{-9}$  mho while the uncertainty in the 1-kc. values for the more concentrated solutions were of the same order of magnitude. The uncertainty decreased generally as the concentration of salt decreased.

(5) (a) R. L. McIntosh, D. J. Mead, and R. M. Fuoss, *J. Am. Chem. Soc.*, **62**, 506 (1940); (b) P. H. Flaherty and K. H. Stern, *ibid.*, **80**, 1034 (1958); (c) J. B. Ezell and W. R. Gilkerson, *J. Phys. Chem.*, **68**, 1581 (1964).

(6) W. R. Gilkerson and R. E. Stamm, *J. Am. Chem. Soc.*, **82**, 5295 (1960).

(7) H. L. Curry and W. R. Gilkerson, *ibid.*, **79**, 4021 (1957).

(8) H. Sadek and R. M. Fuoss, *ibid.*, **76**, 5905 (1954).

(9) H. Eisenberg and R. M. Fuoss, *ibid.*, **75**, 2914 (1953).

(10) A. Maryott, National Bureau of Standards Circular No. 514, U. S. Government Printing Office, Washington, D. C.

(11) H. P. Schwann, G. Schwarz, J. Maczuk, and H. Pauly, *J. Phys. Chem.*, **66**, 2626 (1962).

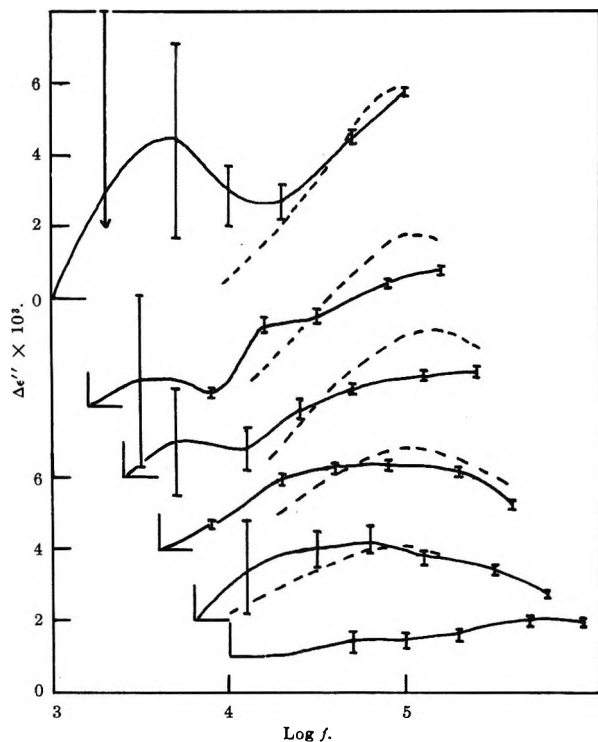


Figure 1. Observed loss factors, solid lines, for  $\text{Bu}_4\text{NPI}$  in 50% ODCB-B at  $25^\circ$ , referred to 1 kc.: in order, top to bottom (concentration in  $\mu\text{M}$ ); 101.9, 43.52, 24.35, 6.62, 2.19, and 0.00. Except in the case of the pure solvent, the loss due to solvent has been subtracted from the total observed loss. The origin for each solution is indicated by the appropriate right angle to the left. Dashed lines were calculated from eq. 1, multiplied by an arbitrary factor of 0.42. Height of error bars indicates experimental uncertainty.

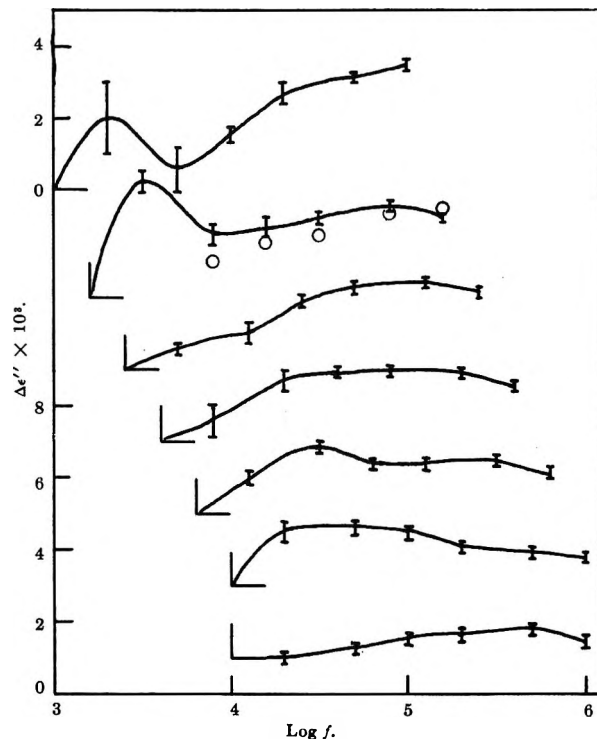


Figure 2. Observed loss factors for  $\text{Bu}_4\text{NPI}$  in CB at  $25^\circ$ , referred to 1 kc.: in order, top to bottom (concentration in  $\mu\text{M}$ ); 103.4, 49.34, 22.40, 10.01, 3.80, 1.41, and 0.00; open circles, repeat experiment in Balsbaugh cell,  $42.7 \mu\text{M}$ . The origin for each solution is indicated by the appropriate right angle to the left.

Typically,  $G_0$ , the low frequency (1 kc.) conductance of the solutions in the cell varied from  $4.64 \times 10^{-5}$  mho for the most concentrated solution in ODCB-B to  $0.225 \times 10^{-5}$  mho for the most dilute solution in CB. The magnitudes of the various increases in conductance with increasing oscillator frequency may be seen in Figure 3, where the increase in conductance divided by the frequency,  $\Delta G/f$ , is plotted vs.  $\log f$  for the most and the least concentrated solutions in ODCB-B, the pure ODCB-B solvent, and the 20,000-ohm resistor. The latter showed an increase of  $2.3 \times 10^{-9}$  mho at 100 kc.

Reproducibility of the effect for a solution in CB may be seen in Figure 2, where the open circles are results obtained at a later date with a different batch of salt and solvent and using a different cell, the 2TN-25, and bridge ratio arms. Early in the investigation the effect was also observed in ODCB-B using a different Balsbaugh cell with an air capacity of 104.7 pf. In this case the observed dispersion was approximately

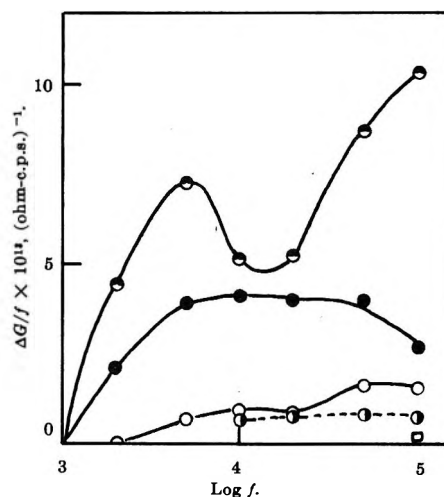


Figure 3. Increase in conductance over the 1-kc. value,  $\Delta G$ , divided by the frequency  $f$  vs.  $\log f$  for: upper half-filled circles, highest salt concentration in 50% ODCB-B; filled circles, lowest concentration in 50% ODCB-B; open circles, pure 50% ODCB-B; right half-filled circles, air; all in the Sadek and Fuoss cell. The square represents the result for the 20-kilohm resistor.

four times as large as that observed using the Sadek and Fuoss cell of air capacity 24.72 pf. Thermal drift was too great for precise measurements with the larger cell, however. These observations together with those made on air, the pure solvents, and the 20,000-ohm resistor clearly point to a solution dispersion effect.

### Discussion

The losses,  $\Delta\epsilon''$ , over and above that due to ionic conduction, are presumed to be due to some process in the solutions and not to some spurious effects characteristic of either bridge or cell. In Figure 3, the loss due to the cell with and without solvent present can be seen to be significantly less than that occurring with solutions present. The loss cannot be due to bridge inequalities since the observed change in the conductance of the 20,000-ohm resistor was so small over the same frequency range. The maxima, Figures 1 and 2, in  $\Delta\epsilon''$  occurring in the kilocycle region in the more concentrated solutions is probably due to electrode polarization.

The increasing loss in the most concentrated solutions in both solvents at higher frequencies is indicative that a maximum is probably occurring in the 0.1 to 1-Mc. region. As the concentrations are decreased, the maxima shift toward lower frequencies. The maxima are occurring at such low frequencies that it is improbable that they are due to Debye absorption (relaxation of dipole rotation). This latter effect has been studied by Kraus and co-workers,<sup>12,13</sup> Strobel and Eckstrom,<sup>14</sup> and Davies and Williams,<sup>15</sup> who find maxima in the 100–1000-Mc. region for salts which exist principally as pairs in solution.

The results will be discussed in terms of the three relevant theories: (1) the Debye–Falkenhagen effect,<sup>16</sup>  $\Delta\epsilon''_1$ , eq. 1, due to relaxation of the ion atmosphere; (2) the ion-pair relaxation effect,  $\Delta\epsilon''_2$ , eq. 2, as calculated by Pearson<sup>2a</sup>; and (3) the ion-pair relaxation effect,  $\Delta\epsilon''_3$ , eq. 3, as calculated by Gilkerson.<sup>2b</sup>

$$\Delta\epsilon''_1 = [z^2e^2\kappa/10.23kT][(1-h)/\omega\tau] \quad (1)$$

$$\Delta\epsilon''_2 = [64N_0z^2e^2q^2c\alpha/9000\pi kT] \times [\omega\tau'/(1+4\omega^2\tau'^2)] \quad (2)$$

$$\Delta\epsilon''_3 = [2\pi N_0z^2e^2qsc\alpha/3000kT] \times [\omega\tau'/(1+\omega^2\tau'^2)] \quad (3)$$

where  $q = z^2e^2/2\epsilon kT$ ,  $\epsilon$  is the dielectric constant for the solvent,  $s$  is a mean distance between two dissociating ions,<sup>2b</sup>  $\omega$  is  $2\pi f$ ,  $\tau = C/G_0$ , and all other quantities have their usual significance. The second factor in brackets on the right in each equation contains the frequency-dependent portion of the equation.  $\tau'$  is the Langenvin relaxation time whose reciprocal is given by eq. 4

$$1/\tau' = k_d + (2-\alpha)k_r c\alpha/(1-\alpha) \quad (4)$$

where  $k_d$  is the rate of ion pair dissociation and  $k_r$  is the rate of ion recombination. The latter is given, according to Onsager,<sup>17</sup> by eq. 5. Here,  $\Lambda_0$  is the limit-

$$k_r = 1.200\pi N_0 z e \Lambda_0 / F \epsilon \quad (5)$$

ing equivalent conductance of the pair of ions, and  $F$  is the Faraday constant. It is to be noted that if the quantity  $s$  in eq. 3 is taken to be  $q$ , the Bjerrum distance, the  $\Delta\epsilon''_3$  essentially reduces to Pearson's result, eq. 2, except for the frequency factor.  $\omega\tau'$  is multiplied by a factor of 2 in the latter.

There are two aspects of each of the three equations, eq. 1, 2, and 3, which bear comparison; the first is the frequency dependence and the second is the magnitude of the effect. If a plot of the frequency dependent portions of eq. 1, 2, and 3 are made, it is found that  $\Delta\epsilon''_1$  and  $\Delta\epsilon''_3$  should exhibit a maximum at about the same frequency,  $f_0 (= 1/2\tau\tau')$ , while Pearson's result, eq. 2, should exhibit a maximum at  $f_0/2$ .

The maximum values of  $\Delta\epsilon''$ ,  $\Delta\epsilon''_m$ , and the frequencies,  $f_m$ , at which they occurred were read from Figures 1 and 2 for each solution where a maximum occurred in the accessible frequency range. The uncertainty in  $\log f_m$  was taken to be  $\pm 0.10$  unit (leading to an uncertainty of  $\pm 25\%$  in  $f_m$ ) except for  $1.001 \times 10^{-5} M$  salt in CB, where, due to a lengthy flat in  $\Delta\epsilon''$ , an uncertainty of  $\pm 0.20$  in  $\log f_m$  was assigned. The values of  $f_m$  so obtained are plotted in Figure 4 vs. the coefficient of  $k_r$  in eq. 4,  $(2-\alpha)c\alpha/(1-\alpha)$ , for both solvents. The solid line in each case was calculated using Onsager's value for  $k_r$ , eq. 5, and the frequency function corresponding to eq. 3. The dashed lines were calculated assuming eq. 5 and Pearson's frequency function, eq. 2 to be correct. The experimental results tend to agree with the solid line. The values of  $k_r$  calculated from eq. 5 were  $5.62 \times 10^{10} M^{-1} \text{sec.}^{-1}$  in 50% ODCB-B and  $8.35 \times 10^{10} M^{-1} \text{sec.}^{-1}$  in CB at 25°.

The ratios,  $\Delta\epsilon''_m/\Delta\epsilon''_1$  and  $\Delta\epsilon''_m/\Delta\epsilon''_3$  were calculated at their maxima. In the case of  $\Delta\epsilon''_3$ , the distance  $s$  was taken to be equal to  $q$ . The ratios are plotted vs. the ion concentrations,  $c\alpha$ , in Figure 5. Note that as the ion concentration approaches zero, the ratio  $\Delta\epsilon''_m/\Delta\epsilon''_3$  increases; whether the ratio

(12) A. H. Sharbaugh, C. Schmelzer, H. C. Eckstrom, and C. A. Kraus, *J. Chem. Phys.*, **15**, 47 (1947).

(13) A. H. Sharbaugh, H. C. Eckstrom, and C. A. Kraus, *ibid.*, **15**, 54 (1947).

(14) H. A. Strobel and H. C. Eckstrom, *ibid.*, **16**, 817 (1948).

(15) M. Davies and G. Williams, *Trans. Faraday Soc.*, **56**, 1619 (1960).

(16) P. Debye and H. Falkenhagen, *Physik. Z.*, **29**, 121, 401 (1928).

(17) L. Onsager, *J. Chem. Phys.*, **2**, 595 (1934).

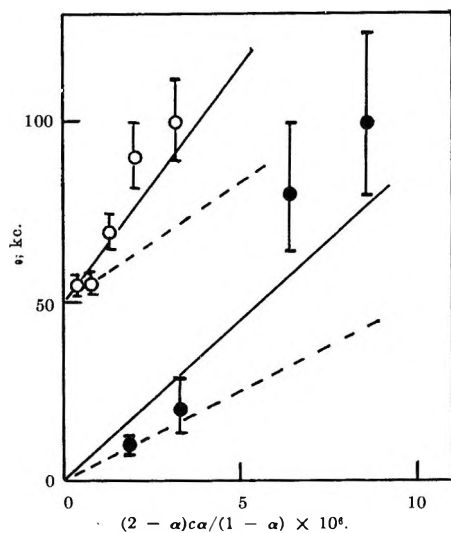


Figure 4. Plot of the frequency,  $f_0$ , at which maximum loss occurs, for  $\text{Bu}_4\text{NPi}$  at  $25^\circ$ , vs.  $(2 - \alpha)c\alpha/(1 - \alpha)$ : open circles, CB solvent, origin displaced up by 50 kc.; closed circles, 50% ODCB-B solvent. Solid line calculated from eq. 1; dashed line calculated from eq. 2.

actually approaches unity at infinite dilution is difficult to say from the present data, but this could well be the case. At the other extreme, as the ion concentration increases, the ratio  $\Delta\epsilon''_m/\Delta\epsilon''_s$  does appear to approach unity as a limit. A plot of either of the foregoing ratios vs. the degree of dissociation,  $\alpha$ , the stoichiometric salt concentration,  $c$ , or the ion-pair concentration,  $c(1 - \alpha)$ , yields two distinct curves, one for each solvent. It thus appears that the deviation of the observed losses from either of those calculated using eq. 1 or 3 (taking  $s = q$ ) is a function of the ion concentration. It is not clear at this point what other parameters, such as the solvent, might be important in this regard. In order to explain the intermediate values completely, it will probably be necessary to await the solution of the conductance equation following Onsager and Fuoss' latest approach,<sup>18</sup> but with alternating fields. This last should be a sticky task.

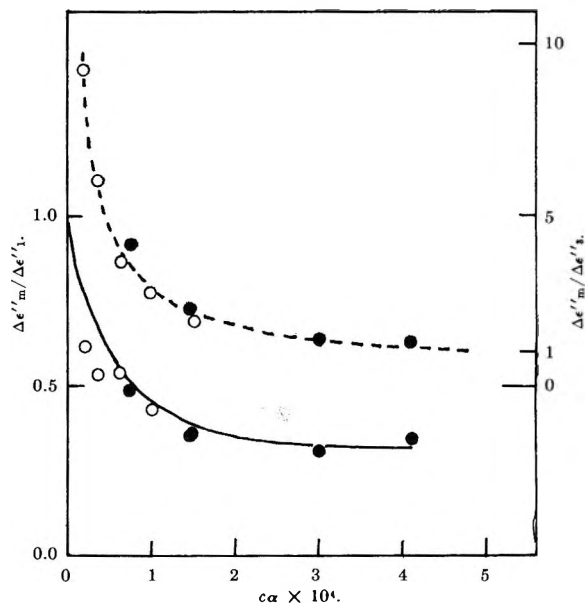


Figure 5. Ratios of the maximum observed loss factors,  $\Delta\epsilon''_m$ , to those calculated from eq. 1 and 3 ( $\Delta\epsilon''_1$  and  $\Delta\epsilon''_3$ , respectively) vs. the ion concentration,  $c\alpha$ : open circles, CB solvent; closed circles, 50% ODCB-B solvent; upper set, right-hand ordinate; lower set, left-hand ordinate.

In conclusion, while we are unable to account completely for the variation with concentration of the magnitude of the dispersion of the conductance of tetra-*n*-butylammonium picrate in the two low dielectric solvents used, the frequency dependence does allow the calculation, from the slope of a plot such as Figure 4, of rates of ionic recombination in satisfactory agreement with theory.

*Acknowledgment.* We wish to thank the Research Corporation for a grant in support of this work and also to acknowledge support in part by the Office of Ordnance Research (now Army Research Office), Durham.

(18) R. M. Fuoss and L. Onsager, *J. Phys. Chem.*, **66**, 1722 (1962); **67**, 621 (1963).

## The Fluorescence of Benzene and Benzene- $d_6$

by John A. Poole<sup>1</sup>

Department of Chemistry, University of Rochester, Rochester, New York (Received November 4, 1964)

A study has been made of the quantum yields of fluorescence of benzene and benzene- $d_6$  in the pressure range 5–15 mm. and at the temperatures 30, 60, and 90°. The exciting lines were monochromatically chosen to correspond to the transition  ${}^1B_{2u} \leftarrow {}^1A_{1g}$ . The yields for benzene- $d_6$  exceeded those for benzene in all cases. The Stern–Volmer plots showed a small but finite slope, and the addition of 80 mm. of cyclohexane resulted in a decrease in fluorescence yield except in the case of benzene at 30° where no such decrease was observed. The high values for the emission yields of biacetyl, sensitized by the benzenes, at 30° substantiates the hypothesis that the primary process involving  ${}^1B_{2u}$  removal is intersystem crossing to the  ${}^3B_{1u}$  state. The energy required for this process is about twice the difference in zero point energies for benzene and benzene- $d_6$ . Thus, intersystem crossing seems to depend upon vibrational energy content. The fluorescence yields decreased with increasing temperature and decreasing wave length of the exciting line. The nonradiative process involving intersystem crossing appears to be faster for the light benzene.

The  ${}^1B_{2u} \leftarrow {}^1A_{1g}$  transition in benzene vapor occurs in the region 2200–2800 Å. Ishikawa and Noyes have reported<sup>2</sup> the quantum yield of fluorescence ( $Q_f$ ) of benzene as a function of pressure at 29° as follows:  $1/Q_f = 0.0335P + 3.89$ .  $P$  is the benzene pressure in millimeters and the incident mercury lines were 2537 and 2654 Å. Therefore,  $Q_f$  (20 mm.) = 0.22. A value of 0.12 was observed for the benzene-sensitized emission yield of biacetyl, at biacetyl and benzene pressures of 0.10 and 20 mm., respectively. If no internal conversion occurs (*i.e.*,  ${}^1A_{1g} \leftarrow {}^1B_{2u}$  as a nonradiative process), then 78% of the absorbed energy must be accounted for by singlet–triplet intersystem crossing<sup>3</sup> (*i.e.*,  ${}^3B_{1u} \leftarrow {}^1B_{2u}$ ). In a benzene–biacetyl mixture the maximum sensitized emission yield is expected to be 0.12 if it is assumed that only 15% of triplet state biacetyl molecules emit radiation.<sup>4</sup> However, Almy, *et al.*,<sup>4a</sup> give the accuracy of this figure as  $0.145 \pm 0.03$ , so that with introduction of no further errors in the work of Ishikawa and Noyes, the uncertainty in the yield of triplet state benzene molecules is fairly large. In any event, these results show that the single most important process in this system must be intersystem crossing to the triplet state.

A comparative study has been made of benzene and of benzene- $d_6$  to ascertain the importance of inter-

system crossing to the triplet state. Zero point energies of these compounds differ sufficiently to affect markedly triplet state yields provided an activation energy is required for intersystem crossing.

### Experimental

Benzene was Mallinckrodt, A.R. grade. Benzene- $d_6$  (stated purity, 99.5%) was obtained from Merck Sharp and Dohme of Canada. Both were chromatographically purified and only the middle portion was retained. Biacetyl was Eastman White Label and cyclohexane was Eastman Spectrograde. Both were degassed and distilled under vacuum. A conventional stopcock-free and grease-free high vacuum system was used and all materials were introduced and stored after trap-to-trap distillation procedures.

The fluorescence cell was of fused quartz, 12.3 cm.

(1) Department of Chemistry, Temple University, Philadelphia, Pa. 19122.

(2) H. Ishikawa and W. A. Noyes, Jr., *J. Chem. Phys.*, **37**, 583 (1962).

(3) The term intersystem crossing is used to describe radiationless transitions between electronic states of different multiplicity. Internal conversion is used when states of the same multiplicity are involved.

(4) (a) G. M. Almy and P. R. Gillette, *J. Chem. Phys.*, **11**, 188 (1943); (b) H. L. J. Backstrom and K. Sandros, *Acta Chem. Scand.*, **14**, 48 (1960); (c) G. B. Porter, *J. Chem. Phys.*, **32**, 1587 (1960).

in length with windows 3.8 cm. in diameter and a center side arm 2.2 cm. in diameter through which emission was observed. The cell (total volume, 276.6 cc.) was painted black and encased in an electrically heated aluminum block furnace.

The light source was a Hanovia Quartz Alpine Sun Burner, Type S-100, focused by a condensing lens onto the entrance slit of a Bausch and Lomb monochromator of the following specifications: grating blaze 2000 Å., focal length 500 mm., grating area 100 × 100 mm., 1200 grooves/mm., reciprocal linear dispersion 16 Å./mm., and entrance and exit slits 4.0 mm. No exit slit condensing lens was used. The radiation passed through two 15-cm. circular apertures and fell directly on the quartz cell. The emergent beam was focused by a quartz lens, stopped by a 17.5-cm. circular aperture and directed to a calibrated RCA 935 phototube. The potential drop across a 25-kilohm resistor was recorded on a Varian G-10 graphic recorder. The perpendicular emission was directed to a calibrated RCA 1P28 photomultiplier tube after passing through either a Corning 9863 or a Corning 3389 glass filter. The former was used in conjunction with benzene fluorescence and the latter for the measurement of biacetyl emission. The current from this photomultiplier was read on an RCA ultrasensitive d.c. microammeter. The associated electronics have been described elsewhere.<sup>5</sup> The 2537-Å. line was reversed in the light source so that there was no danger of mercury sensitization of the substances in the cell. This system produced an absorption of approximately 10<sup>12</sup> quanta/sec. in the cell. The exact amount depends upon pressure, temperature, incident intensity, and wave length.

The methods used for determining  $Q_f$  (the quantum yield of fluorescence of benzene) and  $Q_e$  (the quantum yield of biacetyl emission, sensitized by benzene) were similar to those used by Ishikawa and Noyes.<sup>2</sup> A value of 0.145 was assumed for the absolute emission yield in the green of biacetyl excited at 4358 Å.<sup>4a</sup> The phototube sensitivities (*i.e.*, spectral responses of the phototube to a given wave length based on a value of 100 for maximum sensitivity) were: (i) RCA 935, 58 and 87 for 4358 and 2638 Å., respectively, and (ii) RCA 1P28, 52 and 65 for 5250 ± 20 and 2900 ± 50 Å., respectively. The per cent transmission of Corning glass filters 3389 and 9863 to 5250 and 2900 Å. were 88 and 85%, respectively. A low dispersion Hilger spectrograph was used for photographing the spectra.

## Results

Self-absorption of the emitted fluorescence at the pressures used should be negligible and is neglected.

Thus, the absolute quantum yield of fluorescence,  $Q_f$ , is defined as the ratio of photons emitted to photons absorbed in some volume element of the cell. Diffusion out of this volume before emission is negligible in view of the short lifetime of benzene in the <sup>1</sup>B<sub>2u</sub> state.<sup>6</sup> The following notation will be used, where *f* and *e* correspond to benzene fluorescence and biacetyl emission, respectively:  $I_t^0$  = intensity transmitted by evacuated cell, in mv.;  $I_t$  = intensity transmitted by cell when filled, in mv.;  $I_0$  = intensity with cell removed, in mv. (the phototube remaining stationary);  $I_f^0$  or  $I_e^0$  = intensity of scattered light plus fluorescence, if any from evacuated cell, *i.e.*, background reading, in μa.; and  $I_f$  or  $I_e$  = intensity of emission from cell when filled, in μa. An arbitrary yield,  $Q_f'$ , defined in eq. 1

$$Q_f' = \frac{I_f - I_f^0}{I_0 - I_t} \quad (1)$$

may be converted to an absolute value by comparison with a standard of known yield, *e.g.*, biacetyl at 4358 Å. Corrections must be made for light loss by filter absorption as well as for phototube spectral sensitivity variations as shown by eq. 2, where  $S_\lambda(i)$  = spectral

$$Q_f = Q_f' C_1 \frac{S_{5250}(1P28) \times S_{2638}(935) \times \% T_{5250}(3389)}{S_{2900}(1P28) \times S_{4358}(935) \times \% T_{2900}(9863)} \quad (2)$$

response of phototube *i* to wave length  $\lambda$ ,  $\% T_\lambda(i)$  =  $\%$  transmission of Corning glass filter *i* to wave length  $\lambda$ , and  $C_1$  is a constant which depends on the experimental arrangement. It is determined by observing emission of biacetyl excited at 4358 Å.  $C_1$  was determined to have the value 1.15 ± 0.05; therefore,  $Q_f$  was calculated as 1.44  $Q_f'$ . Similarly, if  $Q_e^*$  is the arbitrary emission yield of biacetyl (using an equation similar to 1) sensitized by benzene, then the absolute yield is given as 1.72  $Q_e^*$ . The corrections applied to the arbitrary yields differ slightly from those used by Ishikawa and Noyes.<sup>2</sup> If their values are used, then  $Q_f$  and  $Q_e$  in this paper should be multiplied by 0.86 and 0.97, respectively, *e.g.*, (0.86)( $Q_f$  - Poole) = ( $Q_f$  - Ishikawa, Noyes), etc.

The procedure outlined for the determination of absolute yields will be valid when the fraction of light absorbed in the cell is small, *i.e.*, less than 0.20. This is because the emission is observed from a volume element located near the center of the cell, and the number of photons absorbed in this volume should be used.

(5) J. H. Heicklen and W. A. Noyes, Jr., *J. Am. Chem. Soc.*, **81**, 3858 (1959).

(6) J. W. Donovan and A. B. F. Duncan, *J. Chem. Phys.*, **35**, 1389 (1961).



Thus, the method is valid if the decrease in this volume is proportional to that absorbed in the entire cell, and if reflection corrections are negligible. In the general case, the procedure requires the calculation of the arbitrary yield,  $Q_f''$ , as shown by eq. 3<sup>7-9</sup>

$$Q_f'' = \frac{1}{kP} \frac{I_t - I_t^0}{\sqrt{I_t^0 I_t}} - f \frac{I_t^0}{\sqrt{I_t^0 I_0}} \left[ 1 + \frac{I_t^0/I_0}{(1-f)^2} \right] \frac{I_t}{I_0} \quad (3)$$

where  $k$  is the absorption coefficient at pressure  $P$  and  $f = 0.04$ . The filter and phototube corrections are now applied to  $Q_f''$ .

These two methods were applied to some experimental data for benzene at 30° with 2638-Å. exciting light. At pressures of 11 and 17 mm. no difference resulted in the calculated values of  $Q_f$ . At 31 mm. the difference was about 4%. Since agreement within experimental error was observed, the results of this investigation were treated by the simpler method based on eq. 1 to calculate arbitrary yields. Smooth curves were drawn through the experimental values of  $(I_t^0 - I_t)/I_t^0$  and  $(I_t - I_t^0)/I_t^0$ . From these, the  $1/Q_f$  vs.  $P$  curves were determined by a least-squares procedure. These equations are given in Table I. Extrapolation to pressures outside the indicated ranges should be regarded with caution since the behavior of  $Q_f$  at very small pressures has not been experimentally observed. At 15 mm. the ratios  $Q_f(\text{benzene-}d_6)/Q_f(\text{benzene})$  are about 1.4 and there is no gross change in this ratio with temperature although both benzenes show a decrease in fluorescence yield with increasing temperature.

**Table I:** Relationship between  $1/Q_f$  for Benzene and Benzene-*d*<sub>6</sub><sup>a</sup>

Temp., °C.	Equation	Pressure range, mm.
Benzene		
30	$1/Q_f = 3.2 + 0.027P$	10-32
60	$1/Q_f = 3.7 + 0.018P$	10-32
90	$1/Q_f = 4.1 + 0.024P$	6-22
Benzene- <i>d</i> <sub>6</sub>		
30	$1/Q_f = 1.9 + 0.047P$	4-15
60	$1/Q_f = 2.1 + 0.043P$	5-15
90	$1/Q_f = 2.2 + 0.080P$	3-15

<sup>a</sup> Incident radiation 2638 Å.

The effect of pressure was investigated by addition of 80 mm. of cyclohexane, which does not absorb the incident radiation. In all cases the benzenes were admitted to a pressure of 15 mm. The results are listed in Table II. It should be noted that the values

of  $Q_f$  recorded in Table II differ slightly from those expected on the basis of the equations listed in Table I. This is because the yields quoted in Table II were obtained from only a few experiments whereas those listed in Table I represent mean values of a larger number of experiments. The important point is that the change upon addition of cyclohexane is representative. Thus, after either  $Q_f$  or  $Q_e$  was determined in the absence of cyclohexane, the added gas was immediately introduced into the cell and the comparative values of the yields in the presence of cyclohexane were determined. Table II gives an indication of the effect on light yields of the addition of an inert foreign gas with many degrees of freedom, at high pressure. In most cases a decrease in yield is observed. This change was greater in the case of benzene-*d*<sub>6</sub>. No change is observed for benzene at low temperatures. For a given benzene (at a given temperature) the change upon addition of cyclohexane was about the same for  $Q_f$  and for  $Q_e$ .

**Table II:** The Effect of Cyclohexane Addition on the Fluorescence Yields of Benzene and Benzene-*d*<sub>6</sub>, and on the Emission Yield of Biacetyl, Sensitized by the Benzenes<sup>a</sup>

Temp., °C.	—No added gas—		Cyclohexane added		% reduction in $Q_f$	% reduction in $Q_e$
	$Q_f$	$Q_e$	$Q_f$	$Q_e$		
Benzene						
30	0.29	0.135	0.29	0.132	0	2
90	0.21	0.043	0.16	0.030	24	30
Benzene- <i>d</i> <sub>6</sub>						
30	0.43	0.124	0.35	0.106	19	14
90	0.28	0.045	0.17	0.029	39	36

<sup>a</sup> Cyclohexane pressure 80 mm.; benzene pressure, 15 mm.

Measurements of  $Q_f$  and  $Q_e$  were made at several wave lengths. These data are recorded in Table III. In these cases the cell temperature was 30°. For these measurements the following parameters were used to obtain absolute yields:  $S_{2537}(935) = 60$  and  $S_{2520}(935) = 56$ . The results listed in Table III do not have the precision of those at 2638 Å. since not as many determinations were made at each given pressure. Probably within the over-all error (ca. 20%) they are representative. In these experiments a different pressure range was used to maintain a fractional absorption

(7) R. E. Hunt and T. L. Hill, *J. Chem. Phys.*, **15**, 111 (1947).

(8) F. C. Henriques and W. A. Noyes, *J. Am. Chem. Soc.*, **62**, 1038, (1940).

(9) H. J. Groh, Jr., Ph.D. Thesis, University of Rochester, 1952.

less than 0.20. In all cases the emission yields appear to decrease with decreasing wave length, the yields from benzene again being less than those for benzene- $d_6$ . At 2400 and 2345 Å., no emission could be observed for either benzene.

**Table III:** Fluorescence Yields for Benzene and Benzene- $d_6$  and Emission Yields of Biacetyl, Sensitized by the Benzenes<sup>a</sup>

Wave length, Å.	Pressure, mm.	$Q_f$		$Q_e$
		Benzene	Benzene- $d_6$	
2345	10	0	0	
2400	10	0	0	
2520	0.5	0.23		
	0.9	0.19		
	1.2	0.19		
	2.0	0.20		0.076
	2.1	0.20		
	2.6	0.18		
	1.0			0.26
2537	2.0		0.25	0.077
	4.2		0.23	
	1.0	0.22		
2537	2.0	0.21		
	10	0.17		
	1.2		0.33	
	3.0		0.28	
	5.2		0.26	

<sup>a</sup> At 30°.

## Discussion

The 2200-2800-Å. transition in benzene vapor has been well established<sup>10-12</sup> and the upper state has been assigned  $^1B_{2u}$ .<sup>13,14</sup> The zero-zero bands for benzene and for benzene- $d_6$  have been placed at 38,090 and 38,290  $\text{cm}^{-1}$ , respectively.<sup>11</sup> The electronic energy of the  $^1B_{2u}$  state is 4.88 e.v., and the corresponding  $^3B_{1u}$  energy has been placed at 3.6 e.v.<sup>14</sup>

The longest wave length used in this investigation was 2638 Å. In benzene this exciting line lies between the absorption bands  $H^0_0$  ( $400 \rightarrow 240$ ) and  $H^1_0$  ( $2 \times 400 \rightarrow 2 \times 240$ ), where 400 and 240 represent frequencies of the  $\nu_{20}$  vibration (a C-C-C  $\perp$  bending mode<sup>15</sup>) in the lower and upper electronic state, respectively. A similar situation exists for benzene- $d_6$  except that all frequencies are shifted somewhat to lower values. The main aspects of the absorption and fluorescence spectra of benzene and of benzene- $d_6$  can be understood in terms of only three vibrational carbon frequencies of the excited and ground states.<sup>15,16</sup> These are  $\nu_{20}$ ,  $\nu_2$  (a C-C stretching mode), and  $\nu_{18}$  (a C-C-C  $\parallel$  bending mode). In going from 2638 to 2537 and 2520-Å. exciting light, the initial population of higher vibra-

tional quantum states increases. Radiation at 2638 Å. lies near the long wave length cutoff for this transition. The purpose of this choice was to excite benzene molecules to low vibrational levels of the first excited singlet state. From a study of the fluorescence spectrum of benzene it has been established<sup>17</sup> that at pressures equivalent to those used in this investigation, the spectrum is of the high pressure type, with very little contribution of resonance fluorescence even at the lowest pressures used. Therefore, emission originates from lower levels than are directly excited, especially in the cases of 2537 Å. and shorter wave lengths. Thus, vibrational deactivation is less important in the case of 2638-Å. exciting light, although due to the absence of the zero-zero band, there must be some vibrational deactivation at the longest wave lengths used.

Since the absolute yield of fluorescence is less than unity, and no photochemical reactions of benzene have been observed in connection with this transition, the loss of excitation energy must be accounted for by other processes than emission from the first excited singlet state. These may be internal conversion to the  $^1A_{1g}$  ground electronic state and intersystem crossing to the  $^3B_{1u}$  state followed by intersystem crossing from the triplet to the ground electronic state.

Ishikawa and Noyes have given evidence<sup>2</sup> which favors singlet-triplet intersystem crossing as the important process for removal of excited singlet molecules by nonradiative processes. Similarly, Cundall, Fletcher, and Milne<sup>18</sup> as well as the data presented in this paper support the conclusion that internal conversion to the ground electronic state must be a relatively unimportant process compared to intersystem crossing. The data in Table II show that at 30° internal conversion is a negligible process. At 90° the  $Q_e$ -values for the pure substances are much lower and this is a reflection of the instability of triplet biacetyl at this temperature. Here it must be noted that the  $Q$ -values may be in error by as much as 20%.

(10) G. B. Kistiakowsky and A. K. Solomon, *J. Chem. Phys.*, **5**, 609 (1937).

(11) H. Spöner, G. Nordheim, A. L. Sklar, and E. Teller, *ibid.*, **7**, 207 (1939).

(12) W. F. Radle and C. A. Beck, *ibid.*, **8**, 507 (1940).

(13) M. Goepfert-Mayer and A. L. Sklar, *ibid.*, **6**, 645 (1938).

(14) R. Pariser, *ibid.*, **24**, 250 (1956).

(15) G. Herzberg, "Infrared and Raman Spectra," D. Van Nostrand Co., Inc., Princeton, N. J., 1945, p. 118.

(16) P. Pringsheim, "Fluorescence and Phosphorescence," Interscience Publishers, Inc., New York, N. Y., 1949, p. 261.

(17) C. K. Ingold and C. L. Wilson, *J. Chem. Soc.*, 935, 941 (1936).

(18) R. B. Cundall; F. J. Fletcher, and D. G. Milne, *Trans. Faraday Soc.*, **60**, 1146 (1964).

In addition to these experimental results, there is also some other evidence that internal conversions do not readily occur in such systems.<sup>19,20</sup>

The cross section for collisional quenching of excited singlet benzenes at 30° and 2638 Å. was estimated from the data in Table I. In this calculation the rate constant for the fluorescence step was taken as  $1/(6.2 \times 10^{-7} \text{ sec.})$ .<sup>2</sup> The cross sections are 0.11 and 0.20 Å.<sup>2</sup> for benzene and for benzene- $d_6$ , respectively. These figures are only about 1/300 as large as the gas kinetic collision diameters. Thus, the benzenes exhibit very little self-quenching. In fact, when cyclohexane at a pressure of 80 mm. is added at 30° there is no apparent change in light yield with benzene, and the change in the case of benzene- $d_6$  is very small. Thus, the nonradiative destruction of  $^1B_{2u}$  benzene molecules appears to be a first-order process, primarily an intersystem crossing. The fact that a small but finite slope was always observed for the  $1/Q_f$  vs.  $P$  plots indicates that collisional processes, although relatively unimportant, do occur to a small extent in the over-all quenching mechanism. The extrapolated values for the fluorescence yields are less than unity in the limit of small pressures but these data should really be experimentally checked in this small pressure region. In this connection, Parmenter has some evidence<sup>21</sup> that, even at pressures in the region 0.005 mm., the fluorescence yield of benzene is much less than unity.

Concerning the first-order removal of excited singlet benzenes, an Arrhenius-type analysis of the data in Table I at 30, 60, and 90° produced a straight line. From the slope of this line an apparent activation energy for the processes gave  $1400 \pm 300$  for benzene and  $1200 \pm 300$  cal./mole for benzene- $d_6$ . In both cases, this amounts to about  $460 \text{ cm.}^{-1}$ . This energy corresponds roughly to a quantum of vibrational energy for the lower modes in the excited state. For example,  $\nu_{18}$  in  $^1B_{2u}$  benzene is  $520 \text{ cm.}^{-1}$ , and in benzene- $d_6$  this corresponds to  $497 \text{ cm.}^{-1}$ ; similarly, the  $\nu_4$  mode in benzene is  $513 \text{ cm.}^{-1}$ , etc. Thus, this process seems to require some vibrational energy in excess of the zero point energy difference. It would seem that energy in some fairly rigid mode is required for nonradiative removal of  $^1B_{2u}$  benzene molecules. Here, more detailed work must be done. That is, a more complete temperature dependence study must be made as well as an attempt to increase the accuracy of the experimental method.

Since the fluorescence yield of benzene- $d_6$  always exceeds that of benzene, radiationless processes must assume somewhat more importance in the case of

light benzene. This is probably related to the observation that deuteration of a compound seems to increase the lifetime of the phosphorescing state at low temperatures. That is, here again the radiationless process (*i.e.*, triplet-singlet intersystem crossing to the ground electronic state) is faster for the case where H atoms are involved compared to the D atom.

In Table II the per cent reductions in  $Q_f$  and in  $Q_e$  upon addition of cyclohexane seem to be approximately the same at a given temperature. Thus, it appears that the decrease in  $Q_e$  is a reflection of the fact that collisions with cyclohexane result in removal of  $^1B_{2u}$  molecules before either fluorescence or intersystem crossing can occur, *i.e.*, by internal conversion processes. There is also the possibility of a singlet-triplet and then triplet-singlet process all enhanced by the presence of cyclohexane, although this is less likely since in this case the relative rates would have to be the same.

The data in Table III indicate that there is some wave length at which the fluorescence of the benzenes becomes very small and shorter wave lengths fail to produce fluorescence at all. The behavior of benzene in this wave length region, *i.e.*, the question of energy dissipation under these conditions, is an open question. Even if singlet-triplet intersystem crossing is invoked as an explanation, the resulting triplet state molecules must transfer their energy to a biacetyl molecule which decomposes before it can emit the usual phosphorescence in view of the low value observed for  $Q_e$  under these conditions. In any event, even at these short wave lengths the fluorescence yield of benzene- $d_6$  exceeds that for the light benzene. The solution to most of these problems must await a determination of light yields in these systems with techniques such that the over-all experimental error does not exceed a few per cent.

*Acknowledgment.* The author is greatly indebted to Professor W. A. Noyes, Jr., for his help and encouragement throughout the course of this investigation. He also wishes to thank Drs. P. Sigal and A. Zahra for many helpful discussions. This work was supported by Contract AFOSR-206-63 with the Office of Aerospace Research, Office of Scientific Research, U. S. Air Force.

(19) H. S. Spomer, *Radiation Res. Suppl.*, 1, 558 (1959).

(20) G. W. Robinson and R. P. Frosch, Contribution No. 2799, Gates and Crellin Laboratory, California Institute of Technology.

(21) C. S. Parmenter, Indiana University, Department of Chemistry, private communication.

## Carbon-13 Magnetic Resonance Spectra of 1-Substituted 1-Hexynes

by Daniel D. Traficante

*The Frank J. Seiler Research Laboratory, O.A.R., United States Air Force Academy, Colorado*

and Gary E. Maciel

*Department of Chemistry, University of California, Davis, California (Received November 5, 1964)*

The  $C^{13}$  chemical shifts of the acetylenic carbon atoms in 1-hexyne ( $C_4H_9-C\equiv C_\alpha-X$ ,  $X = H$ ) and seven derivatives ( $X = CH_3, Br, Cl, I, COCH_3, C\equiv CC_4H_9$ , and  $C_6H_5$ ) were obtained. The peaks assigned to the  $C-\alpha$  resonances covered a range of 90.3 p.p.m. while those assigned to the resonance of  $C-\beta$  covered a range of 28.6 p.p.m. No correlation was found between the chemical shifts and the inductive and/or resonance characteristics of the substituents  $X$ . On the basis of the opposite trends of the  $C-\alpha$  and  $C-\beta$  shifts with changes in halogen substituents  $X$ , it was concluded that the neighbor anisotropy model is incapable of accounting for the general features of these results.

As the number of publications dealing with  $C^{13}$  magnetic resonance spectroscopy has grown in the past few years, systematic studies of substituted ethanes,<sup>1</sup> methanes,<sup>1</sup> benzenes,<sup>2-4</sup> carbonyl compounds,<sup>5</sup> and aromatic hydrocarbons<sup>6-8</sup> have been reported.<sup>9</sup> The trends reported in these papers have given rise to interesting correlations and have indicated promising avenues for additional research.

Conspicuously absent from the growing volume of  $C^{13}$  data is a systematic study of acetylenic compounds. Fragmentary data on  $C^{13}$  shifts have been reported for substituted acetylenes,<sup>9,10</sup> but the choice of compounds employed has covered a rather narrow range of substituent types, or has involved disubstituted acetylenes, and has not permitted a systematic evaluation of the effect of substituents on the  $C^{13}$  shifts of sp-hybridized carbon atoms. In order to fill this gap, we have obtained the  $C^{13}$  n.m.r. spectra of a series of 1-substituted 1-hexynes,  $C_4H_9-C\equiv C-X$ , with a representative selection of eight substituents  $X$ .

### Experimental

*$C^{13}$  Magnetic Resonance Measurements.* The  $C^{13}$  n.m.r. spectra were obtained at a frequency of 15.085 Mc./sec. by measuring  $C^{13}$  resonances in natural abundance, using dispersion mode and rapid passage techniques as described previously by Lauterbur.<sup>6</sup> The sample container was similar to that described by Spiesecke and Schneider<sup>1</sup> except that no provision was

made for spinning the sample. It consisted of two concentric, thin-walled spherical bulbs about 0.1 and 1.6 cc. in volume, a geometry which obviates the need for bulk susceptibility corrections in these results. The small inner bulb contained a reference consisting of an approximately 1:1:1 (weight ratio) mixture of  $NaO_2-C^{13}CH_3$ ,  $Na_2C^{13}O_3$ , and water ( $C^{13}$  enrichment about 56%), with a trace of ferric acetylacetonate (to sharpen the signal of the reference lines by decreasing the spin-lattice relaxation times). In a calibration spectrum of benzene in this cell, the acetate resonance was found to be  $-54.1$  p.p.m. with respect to the benzene doublet center, and the separation of the acetate and carbonate resonances was determined to be 15.5

(1) H. Spiesecke and W. G. Schneider, *J. Chem. Phys.*, **35**, 722 (1961).

(2) H. Spiesecke and W. G. Schneider, *ibid.*, **35**, 731 (1961).

(3) P. C. Lauterbur, *J. Am. Chem. Soc.*, **83**, 1846 (1961).

(4) G. B. Savitsky, *J. Phys. Chem.*, **67**, 2723 (1963).

(5) J. B. Stothers and P. C. Lauterbur, *Can. J. Chem.*, **42**, 1563 (1964).

(6) P. C. Lauterbur, *J. Am. Chem. Soc.*, **83**, 1838 (1961).

(7) H. Spiesecke and W. G. Schneider, *Tetrahedron Letters*, **14**, 468 (1961).

(8) P. C. Lauterbur, *ibid.*, **8**, 274 (1961).

(9) P. C. Lauterbur, "Determination of Organic Structures by Physical Methods," F. C. Nachod and W. D. Phillips, Ed., Academic Press, Inc., New York, N. Y., 1962, Chapter 7.

(10) R. A. Friedel and H. L. Retcofsky, *J. Am. Chem. Soc.*, **85**, 1300 (1963).

p.p.m. The latter separation was used to calibrate the charts, and the former shift was used to convert the raw data to shifts with respect to benzene. Each shift is the result of at least five field scans in both increasing and decreasing senses, and the data of Table I may be considered reliable to about  $\pm 0.4$  p.p.m.

**Materials.** Spectra were obtained directly from 1-hexyne supplied by Beacon Chemical Industries and 2-heptyne and 1-butyne-3-one supplied by K and K Laboratories without further purification.

**Table I:** Carbon-13 Chemical Shifts of the Acetylenic Carbons in 1-Substituted 1-Hexynes

$n\text{-C}_6\text{H}_9\text{-C}\equiv\text{C}_\alpha\text{-X}$		
X	$\delta_{\text{C}^{13}\alpha}$ <sup>a</sup>	$\delta_{\text{C}^{13}\beta}$ <sup>a</sup>
H	58.7	43.0
CH <sub>3</sub>	(50.4) <sup>b</sup>	(47.0) <sup>b</sup>
Cl	72.0	59.9
Br	90.3	48.9
I	132.0	31.9
COCH <sub>3</sub>	41.7	31.3
C <sub>6</sub> H <sub>5</sub>	45.6	36.7
$n\text{-C}_4\text{H}_9\text{C}\equiv\text{C}$	60.7	50.0

<sup>a</sup> In p.p.m. with respect to benzene. <sup>b</sup> The assignment of these shifts may be reversed from the correct situation and should be considered tentative.

1-Chloro-1-hexyne was prepared by the method of Straus, Kollek, and Heyn<sup>11</sup> for the preparation of 1-bromo-1-heptyne. From a mixture of 6.67 g. (0.119 mole) of KOH, 145 ml. of a 5.25% solution of NaOCl in water, and 8.54 g. (0.104 mole) of 1-hexyne, after refluxing with vigorous stirring for 11 days, was obtained, after fractional distillation, 1.62 g. (7.5%) of product which had b.p. 70° (130 mm.),  $n_{\text{D}}^{25}$  1.4350 [lit.<sup>12</sup> b.p. 38° (15 mm.),  $n_{\text{D}}^{25}$  1.4335].

1-Bromo-1-hexyne was prepared by the method of Straus, Kollek, and Heyn<sup>11</sup> for the preparation of 1-bromo-1-heptyne. To a mixture of 18.35 g. (0.328 mole) of KOH, 145 ml. of water, and 16.7 g. (0.104 mole) of bromine, was added, with vigorous stirring, 8.54 g. (0.104 mole) of 1-hexyne. After stirring overnight, the mixture was extracted once with 30 ml. of pentane. The organic layer, after fractional distillation, afforded 7.52 g. (45%) of product which had b.p. 74–78° (74 mm.),  $n_{\text{D}}^{25}$  1.4630 [lit.<sup>12</sup> b.p. 38° (15 mm.),  $n_{\text{D}}^{25}$  1.4630].

1-Iodo-1-hexyne was prepared by the method of McCusker and Vogt<sup>13</sup> for the preparation of 1-bromo-1-heptyne, except that iodine and hexyne were used as the starting materials. From 8.4 g. (0.102 mole) of 1-

hexyne and 26.0 g. (0.102 mole) of iodine was obtained, after fractional distillation, 7.93 g. (35%) of product which had b.p. 79–82° (26 mm.),  $n_{\text{D}}^{25}$  1.5156 [lit.<sup>12</sup> b.p. 75° (20 mm.),  $n_{\text{D}}^{25}$  1.5151].

3-Octyne-2-one was prepared by the method of Kroeger and Nieuwland.<sup>14</sup>

1-Phenyl-1-hexyne was prepared by the method of Johnson, Schwartz, and Jacobs.<sup>15</sup>

Dodeca-5,7-diyne was prepared by the method of Black, Horn, and Weedon,<sup>16</sup> using cuprous chloride as the catalyst.

## Results

Carbon-13 magnetic resonance spectra were obtained on eight compounds of the type  $n\text{-C}_2\text{H}_9\text{-C}\equiv\text{C-X}$  corresponding to X = H, CH<sub>3</sub>, Cl, Br, I, C<sub>6</sub>H<sub>5</sub>, COCH<sub>3</sub>, and C≡C- $n\text{-C}_4\text{H}_9$ . In each case the spectrum consisted of two peaks in the carbonyl region corresponding to the signals of NaO<sub>2</sub>C<sup>13</sup>CH<sub>3</sub> and Na<sub>2</sub>C<sup>13</sup>O<sub>3</sub> in the reference bulb, two signals in the region expected for acetylenic resonances on the basis of previously reported data,<sup>9,10</sup> a relatively complicated pattern due to the carbon resonances of the  $n$ -butyl group, and signals due to the presence of carbon in X (in COCH<sub>3</sub>, CH<sub>3</sub>, or C<sub>6</sub>H<sub>5</sub>). In the case of the prototype, 1-hexyne, the resonance peaks of the acetylenic carbons were split into doublets by the ≡CH proton as has been previously reported for systems of the type C<sup>13</sup>≡CH and C≡C<sup>13</sup>-H,<sup>9,10</sup> These splittings render the assignment of shifts in 1-hexyne unequivocal.

In the substituted 1-hexynes the two acetylenic resonance lines seem to fall into a recognizable pattern: the peak corresponding to the less shielded carbon is, in each case, somewhat broader and shorter than that of the more shielded carbon. A typical spectrum is that of dodeca-5,7-diyne (X =  $n\text{-C}_4\text{H}_9\text{C}\equiv\text{C}$ ) which is reproduced in Figure 1. Among the 1-substituted 1-hexynes, the only possible exception to this pattern is in the spectrum of 2-heptyne (X = CH<sub>3</sub>) where the difference in shielding between the acetylenic carbons is only 3.4 p.p.m. and the corresponding two peaks partially overlap and have a similar appearance. In this case specific assignments were not possible. In the general case we interpret the broadness of the less shielded resonance to be due to the presence of an ad-

- (11) F. Straus, L. Kollek, and W. Heyn, *Ber.*, **63B**, 1868 (1930).
- (12) D. J. Pflaum and H. H. Wenzke, *J. Am. Chem. Soc.*, **56**, 1106 (1934).
- (13) P. A. McCusker and R. R. Vogt, *ibid.*, **59**, 1307 (1937).
- (14) J. W. Kroeger and J. A. Nieuwland, *ibid.*, **58**, 1861 (1936).
- (15) J. R. Johnson, A. M. Schwartz, and T. L. Jacobs, *ibid.*, **60**, 1882 (1938).
- (16) H. K. Black, D. H. S. Horn, and B. C. L. Weedon, *J. Chem. Soc.*, 1707 (1954).

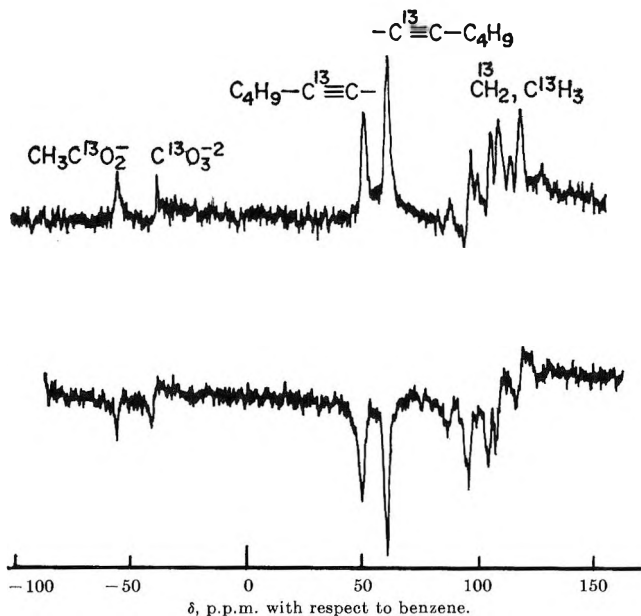


Figure 1.  $C^{13}$  n.m.r. spectrum of dodeca-5,7-diyne, image of decreasing field sweep (upper), increasing field sweep (lower).

jacent alkyl group, probably a result of appreciable splitting by the methylene hydrogens. The sharper appearance of the resonance line for the more shielded carbon can then be rationalized in terms of a larger number of bonds separating the alkyl group from the corresponding carbon atom, and a smaller  $C^{13}$ -H spin-spin coupling constant. This interpretation is in agreement with the proton- $C^{13}$  splitting data reported for methyl acetylene:  $J_{C^{13}-CH_3} = 10.6$  c.p.s.,  $J_{C^{13}=C-CH_3} = 4.8$ .<sup>17</sup> This is equivalent to assigning the broader, lower field resonances to C- $\beta$  nuclei and the sharper, higher field peaks to the C- $\alpha$  nuclei, and results in the assigned shifts collected in Table I.

While the indicated assignments are unequivocal only in the case of 1-hexyne, strong arguments can be presented in two other instances from additivity considerations, and in the remaining cases the assignments based on the inferred trends seem reasonable. Thus, the 10.4 p.p.m. greater shielding of C- $\alpha$  than C- $\beta$  in 3-octyne-2-one (X =  $CH_3CO$ ) indicated in Table I is in accord with the shifts of the acetylenic carbons of 1-hexyne and 1-butyne-3-one ( $\delta_{C^{13}-H} = 48.1$  and  $\delta_{C^{13}-COCH_3} = 45.6$  p.p.m. with respect to benzene). Assuming additivity of the effects of the substituents  $n-C_4H_9$  and  $CH_3CO$  on the  $C^{13}$  shifts of acetylenic groups to which they are attached, one would predict a shift difference of 13.2 p.p.m. in the same direction as the observed difference of 10.4 p.p.m. Similarly, the 8.9 p.p.m. greater shielding assigned in Table I to C- $\alpha$  compared to C- $\beta$  for X =  $C_6H_5$  is in good agreement with the value 9.4 p.p.m. which one would predict by considering the  $C^{13}$

shifts in 1-hexyne and phenylacetylene ( $\delta_{C^{13}-H} = 50.3$ ,  $\delta_{C^{13}-C_6H_5} = 44.0$  p.p.m. with respect to benzene)<sup>10</sup> on the assumption of additivity of substituent effects.

## Discussion

The  $C^{13}$  chemical shifts of the  $\alpha$ -acetylenic carbon atoms listed in Table I vary over a range of 90.3 p.p.m., considerably larger than the range of  $\alpha$ -carbon shifts in ethyl compounds or of the shifts of the substituted carbon atom in phenyl compounds reported by Spiesecke and Schneider,<sup>1,2</sup> and larger than the range anticipated for acetylenic carbons on the basis of previously available data.<sup>9</sup> The shifts of the  $\beta$ -carbons cover the narrower span of 28.6 p.p.m., larger than the range of  $\beta$ -carbon shifts in ethyl compounds and of *ortho* carbon shifts in phenyl compounds.<sup>1,2</sup> Thus, the effect of substituents on  $C^{13}$  shifts of acetylenic carbons appears to be greater on the carbon atoms to which they are attached than on the carbon atoms separated from them by two bonds. In attempting to interpret the shifts and to relate them to the influences on electronic configuration which are at their origin, we have tried to correlate the shifts directly with the substituent constants  $\sigma_I$  and  $\sigma_R$  due to Taft<sup>18,19</sup> and to the  $C^{13}$  shifts of substituted ethanes and benzenes.<sup>1,2</sup> Although in most cases a correlation could be demonstrated for the three halogen substituents, all the relationships failed for other substituents and are clearly not general.

It is tempting to interpret this complete lack of correlation between acetylenic shifts and the molecular constants to which other  $C^{13}$  shifts have been related in terms of an overwhelming influence of anisotropy effects in these pseudo-linear systems. The linearity of the system  $C-C_\beta \equiv C_\alpha-Y$  (where Y is the atom in the group X which is attached to C- $\alpha$ ) provides a geometry in which anisotropy in the magnetic susceptibility of the molecules would be expected to be large, and might be expected to dominate other effects closely related to electron densities, bond orders, etc. An interpretation based on the "neighbor anisotropy" concept<sup>1,2</sup> seems consistent with the facts that: (a) the  $C^{13}$  shifts of C- $\alpha$  for the halogen substituents decrease in the order  $I > Br > Cl$ , the same order as the neighbor anisotropy effects reported for the methylene resonances in haloethanes by Spiesecke and Schneider<sup>1</sup>; and (b) the  $C^{13}$  shifts of C- $\beta$  for these substituents increase in the order  $I < Br < Cl$ , the same trend reported by Spiesecke and

(17) G. J. Karabatsos, J. D. Graham, and F. M. Vane, *J. Am. Chem. Soc.*, **84**, 37 (1962).

(18) R. W. Taft, Jr., E. Price, I. R. Fox, I. C. Lewis, K. K. Andersen, and G. T. Davis, *ibid.*, **85**, 709 (1963).

(19) R. W. Taft, Jr., E. Price, I. R. Fox, I. C. Lewis, K. K. Andersen, and G. T. Davis, *ibid.*, **85**, 3146 (1963).

Schneider<sup>1</sup> for the neighbor anisotropy effects of the halogens on the C<sup>13</sup> chemical shifts of the methyl groups in haloethanes. However, the magnetic anisotropy model cannot predict opposite signs for the contribution to long-range shielding at two points which both lie on the axis of symmetry of the susceptibility tensor. In fact, the trends of opposite sign in the  $\alpha$  and  $\beta$  acetylenic resonances can be considered evidence against a rationalization of these shifts based on a simple model of magnetic anisotropy. Caution has previously been expressed in reference to employing the rather flexible concept of magnetic anisotropy in explanations of C<sup>13</sup> chemical shifts,<sup>20,21</sup> and Schaefer, Reynolds, and Yonemoto<sup>21</sup> have suggested contributions to C<sup>13</sup> shifts in

aliphatic and aromatic halogen compounds due to intramolecular effects of the van der Waals type. The present results seem to emphasize the need for a critical consideration of the importance of anisotropy effects and the need for alternative explanations. It appears that more work, both experimental and theoretical, may be necessary before a satisfactory explanation for the present data will be possible, or before a completely acceptable discussion of earlier data can be given.<sup>22</sup>

(20) P. C. Lauterbur, *J. Chem. Phys.*, **38**, 1406 (1963).

(21) T. Schaefer, W. F. Reynolds, and T. Yonemoto, *Can. J. Chem.*, **41**, 2969 (1963).

(22) The authors are grateful to the referee whose comments on this section were most helpful.

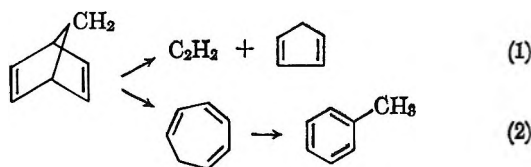
## The Thermal Unimolecular Decomposition of Norbornylene<sup>1a</sup>

by B. C. Roquitte<sup>1b</sup>

Division of Pure Chemistry, National Research Council, Ottawa 2, Canada (Received November 9, 1964)

The thermal decomposition of norbornylene in the gas phase has been examined between temperatures from 266 to 304° and pressures from 5 to 43 mm. Up to 50% decomposition, ethylene and cyclopentadiene, formed in equal quantities, were the only products. At higher conversion, a third product was detected, which, however, was never more than 2% of the total product. The decomposition is first order, uninhibited by the usual free radical scavengers, namely, NO, O<sub>2</sub>, propylene, and toluene. The first-order rate constant for the over-all decomposition may be expressed as  $k = 7.08 \times 10^{13} e^{-43,470/RT}$  sec.<sup>-1</sup>.

The thermal decomposition of norbornadiene (bicyclo[2.2.1]heptadiene, BCHD)<sup>2-4</sup> was found to follow first-order kinetics. Two modes of decomposition of BCHD have been detected (eq. 1 and 2).



Norbornylene (bicyclo[2.2.1]heptene, BCH) has a similar structure but only one double bond, and it was

of interest to examine its thermal decomposition to see whether it follows the same modes of decomposition as BCHD. A brief report on the pyrolysis of BCH in a flow system was published<sup>5</sup> while this in-

(1) (a) Issued as N.R.C. No. 8369; (b) National Research Council Postdoctoral Fellow, 1962-1964; Radiation Research Laboratories, Mellon Institute, Pittsburgh 13, Pa.

(2) W. G. Woods, *J. Org. Chem.*, **23**, 110 (1958).

(3) J. H. Birely and J. P. Chesick, *J. Phys. Chem.*, **66**, 568 (1962).

(4) B. C. Roquitte, *Can. J. Chem.*, **42**, 2134 (1964).

(5) W. C. Herndon, W. B. Cooper, Jr., and M. J. Chambers, *J. Phys. Chem.*, **68**, 2016 (1964).

vestigation was in progress. Our kinetic data, however, were obtained in a static system under a wider range of pressures and additives using different techniques.

### Experimental

**Reagents.** Norbornylene, acquired from Aldrich Chemical Co., was outgassed and distilled under vacuum several times. The middle fraction was further purified by gas chromatography. On analysis by gas chromatography, the purified sample was found to contain one component only. This sample was stored under vacuum at  $-78^{\circ}$  and used for all the experiments reported here. The sample of cyclopentadiene, used for gas chromatographic calibration, was prepared from dicyclopentadiene<sup>6</sup> (Eastman Kodak Co.) and further purified gas chromatographically. Phillips research grade ethylene was subjected to bulb-to-bulb distillation, and the middle cut was retained for gas chromatographic calibration. Research grade toluene, obtained from Phillips Petroleum Co., was outgassed and used as such. Nitric oxide (Matheson, 98.7%) was purified by repeated distillation from  $-160$  to  $-196^{\circ}$ . Matheson oxygen (99.5%) was used without further purification.

**Apparatus.** The experiments were carried out in a static system. Two cylindrical Pyrex reaction vessels mounted in an electrically heated vertical furnace were used. One of these was filled with thin-walled Pyrex tubing to increase the surface to volume ratio 25-fold. Each reaction vessel was provided with a thermocouple well extending to the center and the reaction temperatures were measured with a standardized platinum-platinum-10% rhodium thermocouple. During an experiment, the temperature of the furnace could be maintained constant to within  $0.1^{\circ}$ . The rate of the reaction was followed manometrically with a wide-bore mercury manometer read with a cathometer.

**Analysis.** At the completion of an experiment, the reaction mixture was removed from the reaction zone by condensation into an ampoule at  $-196^{\circ}$ , and sealed under vacuum. It was introduced into the inlet system of an F and M temperature-programmed gas chromatograph Model 720 by means of an ampoule crusher. The products were initially identified by comparison of their retention times with those of known compounds. For quantitative analysis of the products, an 8.6-m. silicone grease column (25% by wt. on Celite) was used. The reaction products, ethylene and cyclopentadiene, were individually confirmed by mass spectrometric analysis. The ultraviolet absorption spectrum of the product cyclopentadiene was in good agreement with that given in the literature.<sup>7</sup> At con-

versions higher than 50%, an unknown peak was observed in the gas chromatograph; it was estimated to be not more than 2% of the total reaction products. In the kinetic experiments with added gases such as NO, O<sub>2</sub>, propylene, and toluene the reactant was introduced into the reaction vessels after the added gas.

### Results

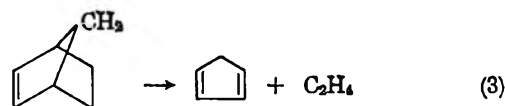
From the analytical results shown in Table I, it

**Table I:** Analysis of the Reaction Mixture from the Decomposition of Norbornylene<sup>a</sup>

$P_0$	$P_I$	$P_E$	$P_C$	Temp., °C.	% de-compn.	Additive
22.43	11.22	11.11	11.22	266.0	50.3	Pkd
8.60	3.93	3.90	3.91	275.0	45.7	
32.40	9.48	9.45	9.50	284.5	29.2	Tol
14.35	4.67	4.66	4.67	284.5	32.5	
10.90	5.36		5.29	304.0	49.2	NO
13.90	6.90	6.92	6.89	304.0	49.9	

<sup>a</sup> All pressure values are given in mm.;  $P_0$  = initial pressure,  $P_I$  = pressure increase during an experiment,  $P_E$  = pressure of ethylene,  $P_C$  = pressure of cyclopentadiene, Tol = toluene, and Pkd = reaction vessel filled with Pyrex tubings.

appears certain that BCH decomposes simply into ethylene and cyclopentadiene.



In several experiments, the ratio of the final pressure  $P_{\alpha}$ , to the initial pressure  $P_0$ , was determined, and the values obtained are summarized in Table II. It appears

**Table II:** Comparison of Final and Initial Pressures in the Decomposition of Norbornylene<sup>a</sup>

$P_0$ , mm.	$P_{\alpha}/P_0$	Temp., °C.	Additive
5.25	2.02	294.5	
8.50	1.99	288.0	NO
11.10	1.98	275.0	Tol
12.50	2.01	305.0	Pkd
17.20	2.01	304.0	
43.80	1.98	294.5	

<sup>a</sup>  $P_0$  = initial pressure,  $P_{\alpha}$  = final pressure, Pkd = reaction vessel filled with Pyrex tubings, and Tol = toluene.

(6) R. B. Moffett, *Org. Syn.*, **32**, 41 (1952).

(7) L. W. Pickett, E. Paddock, and E. Sackter, *J. Am. Chem. Soc.*, **63**, 1073 (1941).



that the ratio is very close to 2, even in the presence of radical scavengers, within experimental uncertainty, indicating that one molecule of BCH decomposes to two molecules of products.

The quantitative analysis of the products indicated that ethylene and cyclopentadiene were present in equimolecular amounts, and the increase in pressure  $P_I$  was equal to the pressure of ethylene  $P_E$  and the pressure of cyclopentadiene  $P_C$ , within experimental error. This was also true when the decomposition was carried out in a packed reaction vessel or in the presence of radical scavengers, at least up to 50% decomposition. To test for possible back reactions, an equimolar mixture of ethylene and cyclopentadiene was introduced into the reaction vessel at 304°. After 5 hr., no BCH could be detected in the reaction mixture by gas chromatography. This proves beyond reasonable doubt that there was essentially no back reaction under our experimental conditions.

The kinetic data on the thermal decomposition of BCH are shown in Table III. It may be noted that

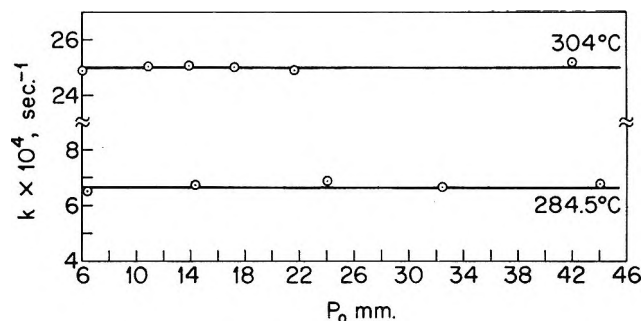


Figure 1. Effect of initial pressure upon the rate constant for the decomposition of BCH.

These facts indicate that the decomposition of BCH was a first-order, homogeneous reaction, unaffected by free radical chain processes. The ratio  $t_{1/4}/t_{1/8}$  is equal to 2.16 in good agreement with the value of 2.15 calculated from the first-order equation, and the plot of  $\log P_0/(2P_0 - P_t)$  against time is linear; these facts strongly confirm the first-order nature of the reaction.

The variation with temperature of the rate constant for the decomposition of BCH is shown in Figure 2, where  $\log k$  is plotted against  $1/T$ . From the slope of the best straight line, the activation energy of the reaction was found to be 43.47 kcal./mole, and the  $A$

Table III: Rate Constants for the Decomposition of Norbornylene under Various Experimental Conditions

$P_0$ , mm.	$k \times 10^4$ , sec. <sup>-1</sup>	Temp., °C.	Additive <sup>a</sup>
9.25	1.71	266.0	
11.10	1.93	266.0	
8.60	3.17	275.0	
11.10	3.50	275.3	
14.35	6.74	284.5	
32.40	6.65	284.5	
5.25	13.21	294.5	
7.80	13.05	295.0	
13.75	13.78	294.5	Pkd
15.80	12.90	295.0	NO
31.50	12.85	294.5	
43.80	12.78	294.5	
15.00	12.85	294.7	Tol
24.00	13.03	294.2	C <sub>3</sub> H <sub>6</sub>
14.60	12.68	294.2	O <sub>2</sub>
10.90	25.03	304.0	
13.90	25.03	304.0	
17.20	25.00	304.0	
21.60	24.90	304.0	

<sup>a</sup> Pkd = reaction vessel filled with Pyrex tubings and Tol = toluene.

the rate constant for the decomposition was not affected by the addition of radical scavengers and/or by the increase of surface/volume ratio.

In Figure 1 the rate constants at temperatures 284.5 and 304° are plotted against pressure. In the pressure range 5–43 mm., the rate constants did not change within the experimental uncertainty.

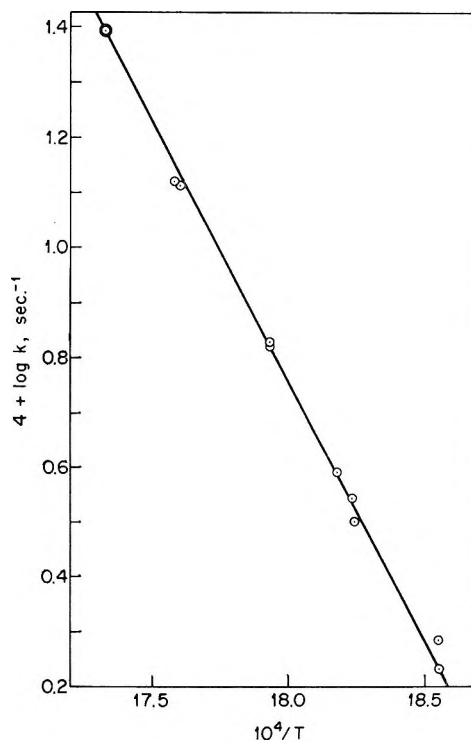


Figure 2. Variation of rate constant for the decomposition of BCH with temperature.

factor  $7.08 \times 10^{13} \text{ sec.}^{-1}$ ; these values are to be compared with the activation energy, 42.75 kcal., and  $A$  factor,  $7.80 \times 10^{13}$  reported in the flow system.<sup>5</sup>

### Discussion

From the analysis of the results mentioned in the foregoing section, it appears that the decomposition of BCH is a first-order reaction taking place homogeneously in the gas phase. Failure to inhibit the decomposition by free radical scavengers seems to suggest that the reaction is free from radical chain processes. Since the increase of surface-volume ratio by a factor of 25 did not affect the rate, it is safe to conclude that, under our experimental conditions, heterogeneous reactions do not appear to be important.

It is of interest to compare the thermal decomposition of BCH with that of BCHD. The latter, in the temperature range 300–360°, exhibits two modes of decomposition<sup>4</sup> (eq. 1 and 2), whereas BCH decomposes only according to eq. 3. The isomerization of BCHD to cycloheptatriene and/or toluene is a minor reaction, which presumably takes place by the rupture of the bridgehead C–C bond; it appears that such an isomerization reaction is not taking place in BCH. This probably implies that the bridgehead C–C bond in BCH is stronger than that in BCHD because of lesser strain in the ring. Since no induction period was observed, it appears that the decomposition of BCH does not proceed through an intermediate such as I

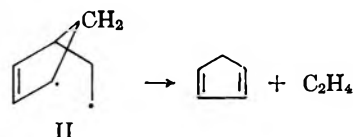


I

unless it is very short-lived. This was also true for BCHD.

The frequency factor observed for the decomposition of BCH is comparable to that found for other unimolecular decompositions. The frequency factor obtained for BCHD, however, is an order of magnitude greater than that of BCH; on the other hand, it may be noted that the frequency factor  $7.08 \times 10^{13} \text{ sec.}^{-1}$  found in this study for the reverse Diels–Alder reaction is of the same order of magnitude as the  $A$  factor,  $1.0 \times 10^{13} \text{ sec.}^{-1}$ , observed for the decomposition of dicyclopentadiene.<sup>8</sup> The activation energy for the decomposition of BCH is about 6.4 kcal. lower than that of BCHD.

The formation of ethylene and cyclopentadiene from BCH may occur through the intermediate formation of a biradical such as II. Since we have no



direct evidence for the existence of such a biradical it may be concluded that if one is involved, it must be very short-lived.

*Acknowledgment.* The author is thankful to Drs. K. O. Kutschke and R. A. Back for their interest in this work.

(8) G. A. Benford and A. Wassermann, *J. Chem. Soc.*, 362 (1939).

## Galvanostatic Studies of Carbon Monoxide Adsorption on Platinum Electrodes

by S. B. Brummer and J. I. Ford

*Tyco Laboratories, Inc., Waltham, Massachusetts (Received November 10, 1964)*

The adsorption of CO on smooth platinum from solutions of 1 *N* HClO<sub>4</sub> saturated with 1 atm. of CO at 40° has been studied using anodic and cathodic galvanostatic transients. It is found that when a large anodic current,  $i_a$ , is applied to the electrode, the potential increases rapidly to  $\sim 1.2$  v. (*vs.* H<sub>2</sub>/H<sup>+</sup> in the same solution), falls to  $\sim 1.0$  v., slowly starts to increase again, and finally becomes almost steady, probably owing to O<sub>2</sub> evolution. The charge passed in the various regions of this transient is insensitive to the current density in the range 2.3 to 147 ma./cm.<sup>2</sup> and, also, to the starting potential, in the range 0.1 to 0.8 v. During the application of such a current, three processes contribute to the charge passed,  $Q_a$ . These are (I) oxidation of adsorbate, (II) oxidation of a species in solution, and (III) surface oxidation of the electrode. By applying a cathodic current,  $i_c$ , at various times during the anodic transient, it is possible to measure (III) directly. From the charge passed in deposition of H atoms prior to H<sub>2</sub> solution,  $Q_H$ , one can follow changes in the concentration of adsorbed CO. The effect of (II) can be assessed by varying  $i_a$ . It is found that  $\theta_H (Q_H/Q_H^{\max})$  increases almost linearly with  $Q_a$  and this relation is independent of  $i_a$ . Oxidation of the electrode is impeded, even when the adsorbed CO has been removed, but does occur during the progress of (I). In addition, it is a function of  $i_a$ . Thus, the coincidence of the  $\theta_H$ - $Q_a$  curves, for the different current densities, does not mean that we are solely observing (I); there must also be a contribution from (II). The sum of (II) and (III) is virtually independent of  $i_a$ , and (II) is not limited by diffusion.  $Q_a$  is corrected for (II) and (III); then, it is found that 390  $\mu\text{coulombs/real cm.}^2$  (based on  $Q_H^{\max} = 210 \mu\text{coulombs/cm.}^2$ ) is required to oxidize all of the adsorbed CO. Of this, 60  $\mu\text{coulombs/cm.}^2$  is weakly adsorbed and requires three electrons per Pt surface atom for removal. The remainder, from  $\theta_H = 0.1$  to  $\theta_H = 1.0$ , requires 1.77 electrons per site. This would correspond to  $\sim 23\%$  of the adsorbed CO in a doubly bonded or "bridged" structure. From cathodic charging curves; it is found that the electrode is less than 2% bare at 0.3 v. The rate of adsorption of CO at low potentials is limited by diffusion in solution.

### I. Introduction

In a previous paper,<sup>1</sup> it was shown that the oxidation of HCOOH on platinum is "poisoned" by the slow adsorption of a material from solution, particularly at low potentials. In a more recent paper,<sup>2</sup> quantitative measurements were made of the maximum (poisoning) adsorption from HCOOH solutions. It was shown<sup>1,2</sup> that the adsorbed species is not likely to be HCOOH itself. It has been suggested<sup>3,4</sup> that the poisoning species is formed from the decomposition of HCOOH on the electrode, and the slow kinetics of the process<sup>1</sup> support such an explanation. The inadequacy of the

identification of the species adsorbed from HCOOH solutions as CO has been indicated previously.<sup>2</sup> Despite considerable work on the adsorption of CO on Pt, using voltammetric and galvanostatic

- (1) S. B. Brummer and A. C. Makrides, *J. Phys. Chem.*, **68**, 1448 (1964).
- (2) S. B. Brummer, *ibid.*, **69**, 562 (1965).
- (3) R. Slott, Thesis, Massachusetts Institute of Technology, 1963.
- (4) D. R. Rhodes and E. F. Steigelmann, Abstract No. 213, Toronto Meeting of the Electrochemical Society, Theoretical Division, May 1964. *J. Electrochem. Soc.*, **112**, 16 (1965).
- (5) S. Gilman, *J. Phys. Chem.*, **66**, 2657 (1962).
- (6) S. Gilman, *ibid.*, **67**, 78 (1963).

techniques, no data suitable for comparison with the data previously obtained with HCOOH solutions<sup>2</sup> are presently available. It is the purpose of the present investigation to present such quantitative information.

The main experimental method used was to apply large anodic galvanostatic transients to "strip" previously adsorbed CO. Two examples of such transients are shown in Figure 1. These traces were obtained at 50 ma./cm.<sup>2</sup>. At lower current densities more complex traces are found. This method has been used by Warner and Schuldiner.<sup>9</sup> Their measurements, which were made at 25°, indicate that the region AB in Figure 1a (they have used a slightly different description of the transient) represents the oxidation of adsorbed CO. When the time of measurement exceeds ~1 msec., they found, also, a small contribution from CO oxidizing from solution. After correction for double-layer charging, they estimated the charge corresponding to oxidation of adsorbed CO,  $Q_{CO}$ , as 453, 435, and 428  $\mu$ coulombs/cm.<sup>2</sup>, for 1, 0.1, and 0.0 atm. of CO, respectively. They claim, also, that the wave BC corresponds, at very high current densities, to the deposition of a monolayer of oxygen, just as in the absence of CO. Thus, they appear to have found that the oxidation of the adsorbed CO and of the electrode occur completely separately. Also, a chemisorbed monolayer (428  $\mu$ coulombs/cm.<sup>2</sup> is approximately equivalent to one CO molecule per platinum surface atom assuming a two-electron oxidation of the CO to CO<sub>2</sub>) is observed at low CO pressures. They assert that  $Q_{CO}$  increases at higher pressures due to physical adsorption on this layer.

Gilman<sup>5-8</sup> has adopted a completely different approach. He has adsorbed the CO at a constant potential and then "stripped" it with a linear potential sweep. Thus, he obtains a transient current-potential (time) curve, which he integrates to obtain a charge which includes  $Q_{CO}$ . The electrode oxidation during this transient is considered to proceed to the same extent as in the absence of CO. Thus, a "solvent correction" is subtracted from the charge under the current-potential trace to obtain a charge which is independent of the sweep speed over a wide range, and is equated to  $Q_{CO}$ . Gilman finds that, for 1 atm. of CO<sup>6</sup> and for 0.01 atm. of CO,<sup>7</sup>  $Q_{CO}$  is ~270  $\mu$ coulombs/cm.<sup>2</sup> (per "real" cm.<sup>2</sup>—see later. All results will be expressed in these terms. Warner and Schuldiner's results are already essentially in these units). Gilman<sup>5,6</sup> has shown that about 20% of the platinum atoms are still available for deposition of hydrogen, even with the maximum adsorption of CO.

Gilman's results for the maximum adsorption of CO

on platinum were taken with 1 *N* HClO<sub>4</sub> at 30°. Warner and Schuldiner's measurements refer to 1 *M* H<sub>2</sub>SO<sub>4</sub> at 25°. It would be surprising, indeed, if the serious discrepancy between their values for  $Q_{CO}$  arises from this small difference in their experimental procedure, although the results of Fasman, Padyukova, and Sokol'skii<sup>10</sup> suggest some complex effects of temperature. It is more likely that the discrepancy arises from a serious error in the allowance made for the oxidation of the electrode, in the determination of  $Q_{CO}$ .

In order to test this and to provide data for comparison with adsorbed HCOOH, the following technique was adopted. The electrode was cleaned with an anodic current (20–150 ma./cm.<sup>2</sup> for ~1 sec.) and allowed to adsorb CO (at 1 atm.) for 2 min., from a quiescent solution, while under potentiostatic control. Then an anodic current,  $i_a$ , and, at various times during this anodic transient, a cathodic current,  $i_c$ , were applied. The latter was used to measure  $Q_O$ , the charge density to reduce the electrode previously oxidized during  $i_a$ , and  $Q_H$ , the charge density to deposit H atoms on the surface.  $Q_H$ , or rather  $\theta_H$  ( $= Q_H/Q_H^{\max}$ , where  $Q_H^{\max}$  is the maximum value of  $Q_H$ , measured in absence of CO) is a measure of the extent of removal of adsorbed CO; thus, not only can we correct the anodic charge,  $Q_a$ , for electrode oxidation by subtracting  $Q_O$  but, also, we can follow the effectiveness of the anodic transient in cleaning the electrode. In this way, we should obtain an unambiguous value of  $Q_{CO}$ . This technique is illustrated in Figure 2.

## II. Experimental

The main experimental technique is illustrated in Figure 2 and has been described above. Most of the details of the circuit and the cell have been described previously.<sup>1,2</sup> Experiments were performed with 1 *N* HClO<sub>4</sub> at 40° with a smooth platinum wire electrode (thermocouple grade) of ~0.6 cm.<sup>2</sup> geometric area. Potentials were measured against Pt, H<sub>2</sub>/H<sup>+</sup> in the same solution, and are reported thus. The CO was C.P. grade (Matheson). The solutions were pre-electrolyzed prior to use, although there was no evidence that this made any difference to the results.

Unless otherwise stated, results are given on the

(7) S. Gilman, *J. Phys. Chem.*, **67**, 1898 (1963).

(8) S. Gilman, *ibid.*, **68**, 70 (1964).

(9) T. B. Warner and S. Schuldiner, NRL Report 6058, U. S. Naval Research Laboratory, Washington, D. C., April 1964; *cf.* Abstract No. 209, Toronto Meeting of the Electrochemical Society, Theoretical Division, May 1964; *J. Electrochem. Soc.*, **111**, 992 (1964).

(10) A. B. Fasman, G. L. Padyukova, and D. V. Sokol'skii, *Dokl. Akad. Nauk SSSR*, **150**, 856 (1963).

basis of "real  $\text{cm}^2$ ." There is no unambiguous way to estimate the real area of a platinum electrode, a problem which has been discussed previously in some detail.<sup>2</sup> The area was computed on the basis that a monolayer of H atoms is present on platinum<sup>11-13</sup> prior to  $\text{H}_2$  evolution. This would correspond to 210  $\mu\text{coulombs}/\text{cm}^2$ . To ensure that the surface was clean for the measurement of  $Q_{\text{H}}^{\text{max}}$ , the electrode was cycled without stirring between 0.25 and 1.25 v. at 0.1 c.p.s., a galvanostatic pulse being applied from 0.6 v. on the anodic sweep. The value of  $Q_{\text{H}}^{\text{max}}$  determined in this way is very reproducible and is independent of the current density in the range used, 1-300  $\text{ma.}/\text{cm}^2$ .

As has been indicated above,  $Q_{\text{H}}$  was also measured in the presence of CO. The assumption will be made that  $\theta_{\text{H}}$  ( $Q_{\text{H}}/Q_{\text{H}}^{\text{max}}$ ) is a measurement of the cleanliness of the surface at the time of the measurement. Much of the general background of this procedure has been presented previously.<sup>2</sup> The  $\theta_{\text{H}}$ -values, in the presence of CO, could be incorrect for one or more of the following reasons. (A) Some of the more loosely adsorbed CO could be desorbed during the measurement of  $\theta_{\text{H}}$ , particularly since hydrogen has a high affinity for platinum. Note, however, that the equilibrium condition under CO atmosphere, in the potential region where  $\theta_{\text{H}}$  is measured, is coverage with CO itself, not with hydrogen. (B) Some CO which is oxidized from the electrode during the anodic transient could be replaced by readsorption during the measurement of  $\theta_{\text{H}}$ . (C) CO, or its oxidation product  $\text{CO}_2$ , could be reduced during the measurement. Regarding (A), if the CO were desorbed during the cathodic pulse, one might expect to find discontinuities in the range of  $\theta_{\text{H}}$  observed, independent of the initial condition of the electrode. Specifically,  $\theta_{\text{H}}$  might tend to unity. In fact, a continuous range of  $\theta_{\text{H}}$  was observed from 0 to 1. Concerning (B), CO is adsorbed during the measurement of  $\theta_{\text{H}}$  at a rate which is largely governed by the rate of diffusion to the electrode from the solution. This is discussed in the next section, and merely involves the measurement of  $\theta_{\text{H}}$  with a large current density and, then, a small correction to the observed values. Regarding (C), there is no evidence for CO reduction, and reduction of the oxidation product,  $\text{CO}_2$ , is too slow<sup>14</sup> to be relevant here. To justify this point, we note that in CO solutions, the maximum value of  $\theta_{\text{H}}$  is just 1 after the small correction mentioned above, whereas if CO or  $\text{CO}_2$  were reduced we should find a higher value.

### III. Results and Discussion

*Adsorption of CO during Measurement of  $\theta_{\text{H}}$ .* In order to examine the adsorption of CO at low poten-

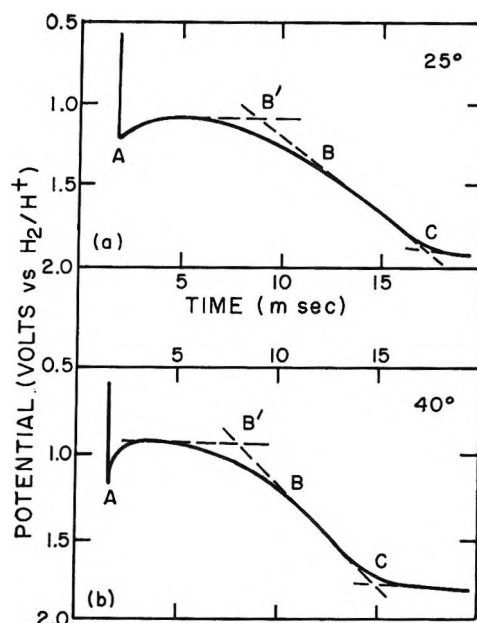


Figure 1. Anodic galvanostatic transients taken from 0.3 v., 2 min. after cleaning pulse, with 1 atm. of CO, at  $\sim 50 \text{ ma.}/\text{cm}^2$ . At 25°, point B is not very well defined, but at 40° quite a sharp break is observed. The overshoot also is more pronounced at 40°

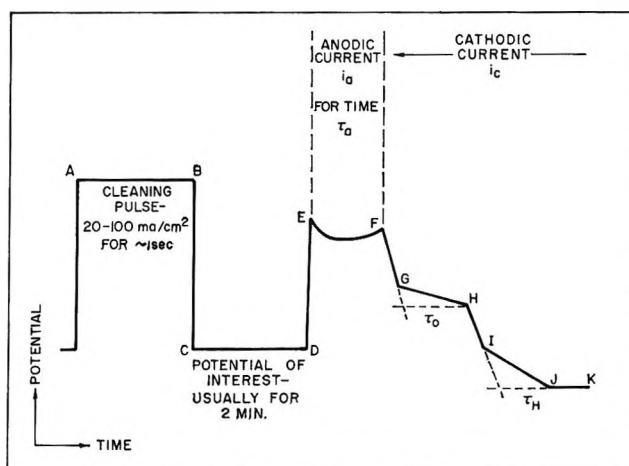


Figure 2. Potential-time sequence used to clean the electrode and to measure the surface oxidation and cleanliness during the progress of the anodic transient.

tials, *i.e.*, during the measurement of  $\theta_{\text{H}}$ , the following procedure was adopted. The electrode was cleaned anodically, as shown in Figure 2, allowed to adsorb

(11) M. W. Breiter, H. Kammermaier, and G. A. Knorr, *Z. Elektrochem.*, **60**, 37, 119 (1956).

(12) M. W. Breiter, "Transactions of the Symposium on Electrode Processes," John Wiley and Sons, Inc., New York, N. Y., 1961.

(13) A. N. Frumkin, "Advances in Electrochemistry and Electrochemical Engineering," Vol. 3, John Wiley and Sons, Inc., New York, N. Y., 1963.

(14) J. Giner, *Electrochim. Acta*, **8**, 857 (1963).

CO for 2 min., and then subjected to an anodic pulse of 73 ma./cm.<sup>2</sup> such that 560  $\mu$ coulombs/cm.<sup>2</sup> passed. This is a condition which (see later) should correspond to the complete oxidation of the adsorbed material. Then, various cathodic currents ( $\sim 2$ –150 ma./cm.<sup>2</sup>) were applied to measure  $\theta_H$  and  $Q_0$ . The results are shown in Figure 3.

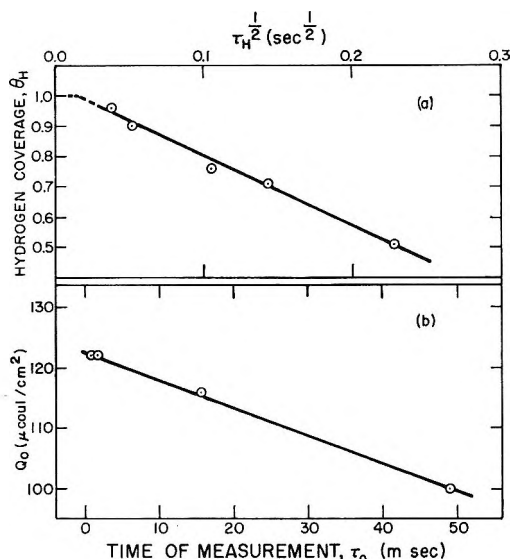


Figure 3. The variation of  $\theta_H$  and  $Q_0$  with the time of measurement. The electrode was prepared at 0.3 v. for 2 min. in the usual way (Figure 2). Then 560  $\mu$ coulombs/cm.<sup>2</sup> of anodic charge was passed at 73 ma./cm.<sup>2</sup> and  $\tau_H$  and  $\tau_0$  were varied by varying  $i_c$ . The experiment was carried out with 1 atm. of CO at 40°.

We see that  $\theta_H$  vs.  $\tau_H^{1/2}$  is an excellent straight line over the range investigated, 0.5–0.95 in  $\theta_H$  and 52–1.5 msec. in  $\tau_H$ . It is suggested that  $\theta_H$  decreases with increase in  $\tau_H$  due to readsorption of CO while taking the measurement. It should be noticed that CO is normally adsorbed in this low potential region and the only reason  $\theta_H$  can be measured in a CO-saturated solution is that the H atom adsorption is sufficiently fast ( $H^+ : CO \approx 1000$  in 1 N HClO<sub>4</sub>). The linearity of the  $\theta_H$  vs.  $\tau_H^{1/2}$  plot suggests that CO readsorption is limited by diffusion in the solution phase. The charge,  $Q^d$ , as a function of time,  $\tau$ , for the two-electron oxidation of CO, when limited by semi-infinite linear diffusion, is given by<sup>5</sup>

$$Q^d = 1.1\tau^{1/2} \text{ mcoulombs/geometric cm.}^2 \quad (1)$$

In this work, a real cm.<sup>2</sup> is approximately equivalent to 0.6 geometric cm.<sup>2</sup>, thus

$$Q^d = 660\tau^{1/2} \mu\text{coulombs/cm.}^2 \quad (2)$$

with  $\tau$  in seconds. This corresponds to

$$\frac{dQ^d}{d(\tau^{1/2})} = 33 \times 10^{-10} \text{ mole/cm.}^2 \quad (3)$$

This slope of the line in Figure 3a is  $50 \times 10^{-10}$  mole/cm.<sup>2</sup>. The agreement between these values is reasonable but could be made better by assuming that the CO, when first adsorbed, blocks two H sites (Pt atoms), making the predicted slope  $66 \times 10^{-10}$  mole/cm.<sup>2</sup>. It is rather surprising that the rate of readsorption can be so readily explained in terms of diffusion control even when the electrode is already 50% covered. This may arise from the high mobility of the incipiently adsorbed CO. The measurements which show<sup>5,9</sup> that CO is retained on Pt even when the pressure is reduced to zero argue against such mobility. However, a mobile film may exist at relatively low coverages with what may be a "bridged,"<sup>15</sup> i.e., two-site, adsorbate. At times less than about  $2.3 \times 10^{-4}$  sec., the rate of adsorption is apparently controlled by some process other than diffusion. A maximum value of  $2.3 \times 10^{-4}$  sec. can be suggested for the time of formation of a CO–Pt bond on a bare surface; (the dotted region in Figure 3a is obviously oversimplified).

In order to minimize the effect of this readsorption on the measured values of  $\theta_H$ , the cathodic current was adjusted to the highest convenient value, 147 ma./cm.<sup>2</sup>. In addition, all  $\theta_H$ -values were corrected, proportionately, according to the dotted line in Figure 3a. The maximum correction of the  $\theta_H$ -values, in this way, for  $\theta_H \rightarrow 1$  is  $\sim 5\%$ .

$Q_0$  also varies with the time of its measurement. This is probably due to reduction of oxide by CO. Assuming that one can write

$$(\theta_{\text{oxide}})_{\tau_0} = (\theta_{\text{oxide}})_{\tau_0 \rightarrow 0} - k\tau_0 \quad (4)$$

and that

$$\theta_{\text{oxide}} = \frac{Q_0}{2Q_H^{\text{max}}} \quad (5)$$

one can evaluate that  $k$  is  $\sim 0.4\%/msec.$  (Figure 3b). In the present measurements, the maximum observed, relevant value of  $\theta_{\text{oxide}}$  is  $\sim 0.85$  and the corresponding value of  $\tau_0$  is  $\sim 2.2$  msec. This would constitute a possible, albeit insignificant, error in  $Q_0$  of  $\sim 1\%$  or, for  $\theta_{\text{oxide}} \approx 0.85$ , about 3.5  $\mu$ coulombs/cm.<sup>2</sup>.

*General Features of the Anodic Transients.* Anodic galvanostatic transients at 25 and 40° are illustrated in Figure 1. There are some significant differences between the two traces. In particular, at 40° the over-

(15) R. P. Eischens and W. Pliskin, *Advan. Catalysis*, **10**, 18 (1958).

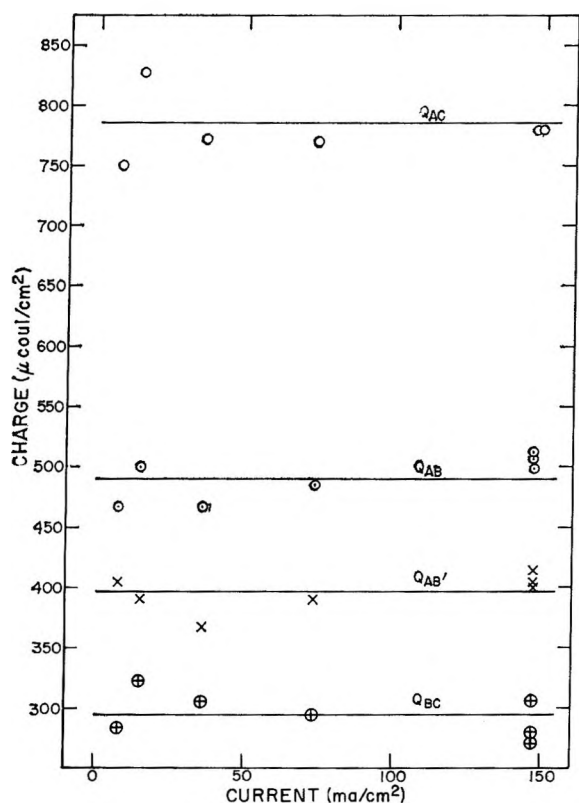


Figure 4. Variation of charge with current density for transients taken at 40°. Transients were taken from 0.3 v., 2 min. after cleaning pulse, with 1 atm. of CO.

shoot is more pronounced and the point B is more distinct. Some quantitative aspects of the transients are shown in Figure 4 and summarized in more detail in Table I. These results were taken in the range 7.35 to 147 ma./cm.<sup>2</sup> from 0.3 v. At low current densities (*viz.*, 1.5 ma./cm.<sup>2</sup>), the transient changed character—there was almost no overshoot and  $Q_{AC}$  was somewhat larger, indicating a considerable contribution from diffusion. Similar results were found, starting the transients in the region 0.1–0.8 v.

Table I: Various Properties of Anodic Transients Taken from 0.3 v., 2 Min. after Cleaning (charges in μcoulombs/cm.<sup>2</sup>)

Temp., °C.	$Q_{AC}$	$Q_{AB}$	$Q_{BC}$	$Q_{AB}^1$	$Q_{AC} - Q_{AB}^1$
25	766 ± 27			348 ± 13	418 ± 14
40	785 ± 28	491 ± 14	295 ± 15	397 ± 12	388 ± 22

As the charges are independent of the current density over a wide range (Figure 4), it might be supposed that  $Q_{AB}$  is a measure of  $Q_{CO}$ . This would be similar to the

results of Warner and Schuldiner.<sup>9</sup> We will show, however, that if any charge could be equated to  $Q_{CO}$  it is not  $Q_{AB}$  but  $Q_{AB}^1$ . Also, we will show that the electrode oxidation varies with the current density and thus the nondependence of  $Q_{AC}$ , and the other charges, on  $i_a$  is probably fortuitous.

*The Variation of  $\theta_H$  with  $Q_a$ .* In Figure 5, we show the variation of  $\theta_H$  with  $Q_a$  for a range of anodic current densities  $i_a$ .  $\theta_H$  increases essentially linearly with  $Q_a$ , independent of current density. At low values of  $Q_a$ , *i.e.*, during the early part of the transient,  $\theta_H$  increases less rapidly with  $Q_a$  than during most of the transient. Also,  $\theta_H$  is zero when  $Q_a$  is zero, *i.e.*, the electrode is completely covered with adsorbed CO.

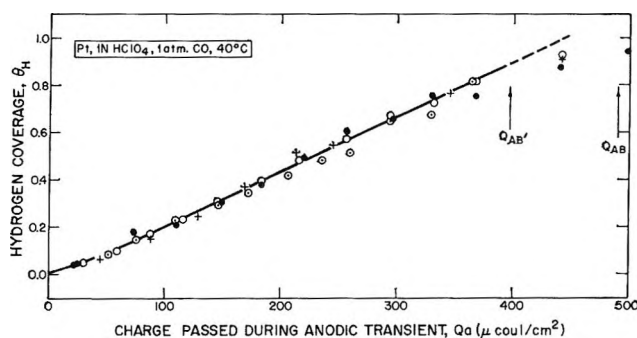


Figure 5. Variation of  $\theta_H$  with  $Q_a$  for various current densities. Transients were taken from 0.3 v., 2 min. after cleaning pulse, with 1 atm. of CO. Anodic current densities:  $\circ$ , 2.35 ma./cm.<sup>2</sup>;  $\bigcirc$ , 7.35 ma./cm.<sup>2</sup>;  $\bullet$ , 73.5 ma./cm.<sup>2</sup>;  $+$ , 147 ma./cm.<sup>2</sup>; cathodic current density, 147 ma./cm.<sup>2</sup>.  $\theta_H$  values are slightly corrected according to dotted line in Figure 3a.

Gilman<sup>5,6</sup> found that ~20% of the surface is bare but, in the present work, direct cathodic charging from 0.3 v. showed that H<sub>2</sub> evolution is strongly retarded by adsorbed CO (*viz.*, at 50 ma./cm.<sup>2</sup>, the overpotential is ~0.6 v.) and that less than 2% of the surface is available for H atom deposition before H<sub>2</sub> evolution commences. This suggests that H<sub>2</sub> is evolved, under these extremely cathodic conditions, on top of the adsorbed CO. The  $\theta_H$ - $Q_a$  line curves over a little before  $\theta_H = 1$ , but if we extrapolate the line to  $\theta_H = 1$  (which presumably corresponds to a clean surface), we obtain a  $Q_a$  value of 446 μcoulombs/cm.<sup>2</sup>. This value does not agree either with  $Q_{AB}$  or  $Q_{AB}^1$  (Table I). Since we observe a common relation between  $\theta_H$  and  $Q_a$  independent of current density, it is tempting to consider that contributions from solution oxidation are negligible and that the above value of  $(Q_a)_{\theta_H \rightarrow 1}$  corresponds only to the charge required to oxidize the adsorbed species. Certainly, since  $\theta_H$  is one (neglecting the tendency of the points at higher  $Q_a$  values to be

away from the line), this would be a better procedure than any arbitrary assumptions about the various parts of the transients shown in Figure 1.

If we examine the oxidation of the electrode during the passage of the anodic charge (Figure 6), the situation becomes more complex. The oxidation of the electrode during the anodic transient is significant in the region shown in Figure 5 and varies with the current density. Thus, the excellent overlap of the respective  $\theta_H$ - $Q_a$  lines for the different current densities can only take place if there is another process occurring. This process (consuming a charge  $Q_s$ ) must be more significant for smaller current densities and, also, must be such that  $Q_s + Q_o$  is independent of  $i_a$ . Thus, to evaluate  $Q_{CO}$ , we must determine the contribution of  $Q_s$  to  $Q_a$  and, also, we must make an appropriate correction for electrode oxidation.

*The Correction for Electrode Oxidation During the Anodic Transient.* The simplest approach is to assume that the charge used to oxidize the electrode,  $Q_o^{AN}$ , is the same as the charge passed in reducing the electrode,  $Q_o$ . Some workers have found, however, that  $Q_o^{AN}/Q_o$  is greater than one.<sup>16,17</sup> Feldberg, Enke, and Bricker<sup>17</sup> have suggested that platinum is oxidized and reduced in two equal stages, the second step in the reduction being very slow. They believed that, given sufficient time and reducing conditions between anodizations, the second reduction would occur and  $Q_o^{AN}/Q_o$  would tend toward two. In this instance, 0.3 v. for 2 min. between anodizations with a

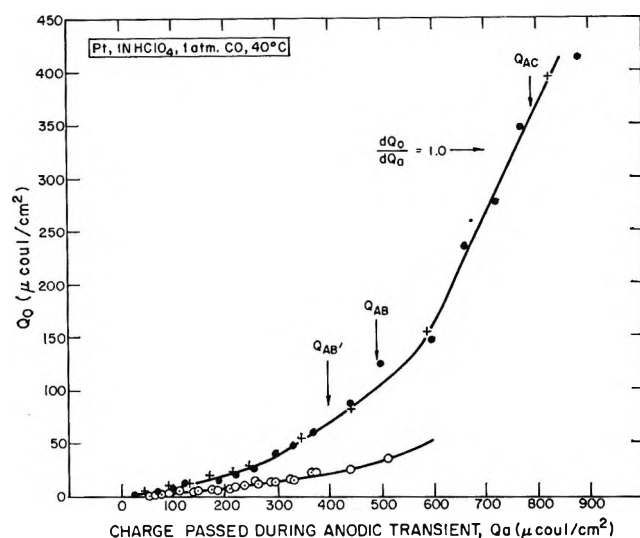


Figure 6. Variation of  $Q_o$  with  $Q_a$  for various current densities. The transients were taken after 2 min. at 0.3 v. with 1 atm. of CO. Anodic current densities:  $\circ$ , 2.35 ma./cm.<sup>2</sup>;  $\square$ , 7.35 ma./cm.<sup>2</sup>;  $\bullet$ , 73.5 ma./cm.<sup>2</sup>;  $+$ , 147 ma./cm.<sup>2</sup>; cathodic current density, 147 ma./cm.<sup>2</sup>.

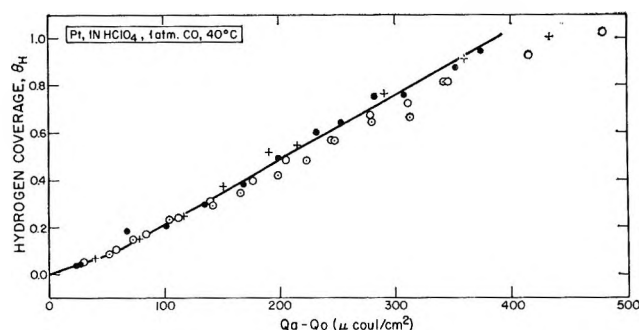


Figure 7. Variation of  $\theta_H$  with  $Q_a - Q_o$ . Transients taken after 2 min. at 0.3 v. with 1 atm. of CO. Anodic current densities  $\circ$ , 2.35 ma./cm.<sup>2</sup>;  $\square$ , 7.35 ma./cm.<sup>2</sup>;  $\bullet$ , 73.5 ma./cm.<sup>2</sup>;  $+$ , 147 ma./cm.<sup>2</sup>. Cathodic current density, 147 ma./cm.<sup>2</sup>.

reducing species in solution, one might expect  $Q_o^{AN}/Q_o$  to tend toward two.

The value of  $Q_o$  for the 73.5 ma./cm.<sup>2</sup> and 147 ma./cm.<sup>2</sup> transients is  $\sim 350$   $\mu$ coulombs/cm.<sup>2</sup> (Figure 6). If  $Q_o^{AN}/Q_o$  were two,  $Q_o^{AN}$  would be  $\sim 800$   $\mu$ coulombs/cm.<sup>2</sup>. This would give, at best, 85 (785 for  $Q_{AC} - 700$ )  $\mu$ coulombs/cm.<sup>2</sup> for  $Q_{CO}$ . This is much too low and suggests that complete electrode coverage with CO, which is found, corresponds to about 1 molecule of CO/5 Pt surface atoms, which is hardly likely. Also, this value of  $Q_o^{AN}$  is greater than that found in the absence of CO which, after a small correction for double-layer charging, was  $\sim 440$   $\mu$ coulombs/cm.<sup>2</sup>, i.e.,  $\sim 1$  monolayer of oxide. Thus, we could hardly expect  $Q_o^{AN}/Q_o$  to be greater than 1.25 (440/350). We observe (Figure 6) that, during the latter part of the transient (but before the point C of Figure 1),  $dQ_o/dQ_a$  is 1.0. This implies that all the anodic charge passed in this region is used in oxide formation and that this oxide is fully reduced, coulomb for coulomb, on current reversal. This suggests that  $Q_o^{AN}/Q_o$  is 1.0. Thus, it would seem reasonable to assume that  $Q_o^{AN}/Q_o$  is 1.0 and to correct the  $Q_a$  values for electrode oxidation by subtracting the observed  $Q_o$  quantities.

*The Evaluation of  $Q_{CO}$ .* In Figure 7, we see the variation of  $\theta_H$  with charge passed during the anodic transient corrected for electrode oxidation. (The line in the figure has been drawn through the highest current density points.) As before, we have essentially a linear relation. Now, however, the value of  $(Q_a)_{\theta_H \rightarrow 1}$  is 390  $\mu$ coulombs/cm.<sup>2</sup>. Also, it is apparent that the smaller current densities are less efficient in cleaning the electrode than the larger currents, particularly at

(16) K. J. Vetter and D. Berndt, *Z. Elektrochem.*, **62**, 378 (1958).

(17) S. W. Feldberg, C. A. Enke, and C. E. Bricker, *J. Electrochem Soc.*, **110**, 826 (1963).



longer times of electrolysis. As indicated previously, this implies that some other process occurs, involving transport of CO from solution.

We can determine from eq. 2 that the maximum amount of CO which could diffuse to the electrode during the 147 ma./cm.<sup>2</sup> transient, up to the time when  $\theta_H = 1$ , is equivalent to 36  $\mu\text{coulombs/cm.}^2$ . This makes no allowance for the fact that the electrode is partly covered with CO and with oxygen during this time, and we can be fairly confident that the CO does not readily oxidize on top of either. Thus, the average fraction of the surface available for CO oxidation from solution, during this part of the transient, is about one-third. Then to a first approximation, the worst error due to oxidation of diffusing CO is about 12  $\mu\text{coulombs/cm.}^2$ . If we were to consider the slope of the line in Figure 3a as the best guide to the diffusional rate of CO under the present conditions, we might modify this to 18  $\mu\text{coulombs/cm.}^2$ . It is to be noted that this is the *maximum* charge which would pass during the 147 ma./cm.<sup>2</sup> anodic transient, as a result of oxidation from solution.

If we examine the deviations of the lower current density points from the line of Figure 7 and try to correct them assuming that  $Q_s$  (charge consumed in process from solution) is given by eq. 2, we find that the correction is much too large. Even if we assume, as above, that the process cannot occur on top of adsorbed CO or oxygen, we would still be overcorrecting the lower current density points (even without Figure 3a). This implies that  $Q_s$  is determined not by diffusion to the electrode but by a discharge reaction of some kind as was noted by Warner and Schuldiner.<sup>9</sup> We may estimate the rate of this process by assuming that  $Q_s$  is given by

$$Q_s = \bar{\theta}_{\text{bare}} \tau_a k' \quad (6)$$

Here,  $k'$  is the desired rate constant in ma./cm.<sup>2</sup> of bare surface,  $\tau_a$  is the time of electrolysis, defined in Figure 2, and  $\bar{\theta}_{\text{bare}}$  is the mean fraction of the surface which is bare during the transient.  $\bar{\theta}_{\text{bare}}$  was assumed to be given by

$$\bar{\theta}_{\text{bare}} = 1/2(\theta_H^{\tau=0} + \theta_H^{\tau=\tau_a}) - 1/2(\theta_O^{\tau=0} + \theta_O^{\tau=\tau_a}) \quad (7)$$

*i.e.*

$$\bar{\theta}_{\text{bare}} = 1/2(\theta_H - \theta_O)^{\tau=\tau_a} \quad (8)$$

It was assumed that the results at 147 ma./cm.<sup>2</sup> needed no correction since even  $Q^d$  itself is insignificant. Thus, a value of  $k'$  of 1 ma./cm.<sup>2</sup> of bare surface was chosen to force the lowest current density points to overlap with the 147 ma./cm.<sup>2</sup> transient. The remaining current

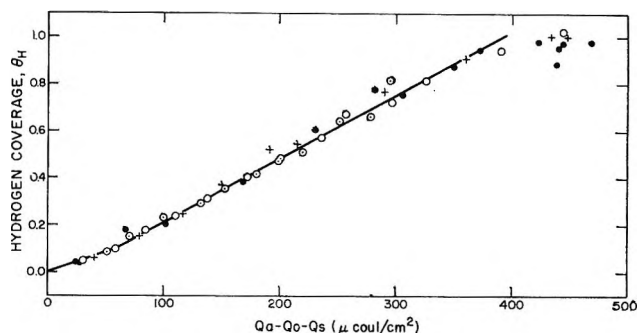


Figure 8. Variation of  $\theta_H$  with charge passed during the anodic transient,  $Q_a$ .  $Q_a$  is corrected for electrode oxidation and for oxidation from solution. Current densities as in Figure 5, values of  $Q_0$  from Figure 6 and  $Q_s$  obtained from eq. 6-8.

densities were similarly corrected using this value for  $k'$ . The result is shown in Figure 8.

Some allowance should be made for double-layer charging during the transient. It is found that, during the time that  $\theta_H$  goes from zero to one, the potential is essentially constant and, therefore, charging terms of the type  $C\Delta E$  ( $C$  is capacity,  $E$  is potential) are negligible. However, as pointed out by Warner and Schuldiner,<sup>9</sup> the double-layer capacity changes during the transient due to the removal of CO. Consequently, charge would flow into the double layer. We can attempt to evaluate this charge as follows.  $Q_{d.l.}$  (the charge on the electrode) is given by

$$Q_{d.l.} = \int_{\text{E.C.M.}}^E C(E) dE \quad (9)$$

where  $C(E)$  is the double-layer capacity,  $E$  is the potential at which the CO is oxidized (against a reference electrode), and E.C.M. is the point of zero charge. Then, if we assume that  $C(E)$  is independent of potential, and that the E.C.M. is the same in presence as in absence of CO, we can write

$$\Delta Q = (C^{\text{HClO}_4} - C^{\text{CO}})(E - \text{E.C.M.}) \quad (10)$$

Here,  $\Delta Q$  is the charge which passes (at constant potential) during the oxidation of CO, corresponding to double-layer effects,  $C^{\text{HClO}_4}$  is the (potential independent) capacity, in absence of CO, and  $C^{\text{CO}}$  is that in presence of a monolayer of CO. This equation differs from that given by Warner and Schuldiner.<sup>9</sup> If we take  $C^{\text{HClO}_4}$  as 40  $\mu\text{f./cm.}^2$ ,<sup>8</sup>  $C^{\text{CO}}$  as 8  $\mu\text{f./cm.}^2$ ,<sup>9</sup> E.C.M. as  $\sim 0.2$  v., and  $E$  as 0.95 v.,  $\Delta Q$  is  $\sim 25$   $\mu\text{coulombs/cm.}^2$ . Then,  $Q_{\text{CO}}$  would be  $\sim 365$   $\mu\text{coulombs/cm.}^2$  ( $390 - 25$ ).

In the oxygen region, the double-layer charge is  $C\Delta E$ , *i.e.*, about 33  $\mu\text{coulombs/cm.}^2$ . With this cor-

(18) S. Schuldiner and R. M. Roe, *J. Electrochem. Soc.*, **110**, 332 (1963).

rection, the points which cluster beyond the top end of the line in Figure 8 would be much closer to the end of the line.

The correction for double-layer charging is not, then, very large. It is significant, though, that although the measurements themselves may be reproducible to about 1%, the actual evaluation of  $Q_{CO}$ , by any technique, may have an uncertainty of  $\pm 10\%$ , due to the complicated corrections which must be made. The present study shows that both Gilman and Warner and Schuldiner were incorrect in their assignment of charge to the various processes which occur during anodic transients with CO. It is suggested that under 1 atm. of CO,  $Q_{CO}$  is 365  $\mu\text{coulombs/cm.}^2$ . This value is in excellent agreement with  $Q_{AB1}$  (Table I), which is 372 after the above correction for double-layer effects. This is rather surprising, and the fact that  $Q_{AB1}$  is independent of  $i_a$  is probably fortuitous.

Figure 8 shows the behavior of adsorbed CO. During the removal of about the first 60  $\mu\text{coulombs/cm.}^2$  of adsorbed CO,  $dQ_{CO}/dQ_H$ , *i.e.*, the number of electrons to oxidize the adsorbate per Pt surface atom, is three. This would involve, on the average, 1.5 CO molecules per site. This probably refers to a small amount of physical adsorption of CO on top of the chemisorbed CO. Warner and Schuldiner<sup>9</sup> also have postulated physically adsorbed CO, although on the basis of the present experiments, their evidence is not really valid. One would expect that physically adsorbed CO would be the easiest to be removed.

For the rest of the surface coverage (0.1–1.0 for  $\theta_H$ ),  $dQ_{CO}/dQ_H$  (without the double-layer correction) has a constant value of 1.77. We could assume, after Eischens and Pliskin<sup>15</sup> and Gilman,<sup>5–8</sup> that the CO is present in two forms, a "bridged" or two-site form ( $dQ_{CO}/dQ_H$  equals one), and a "linear" or one-site form ( $dQ_{CO}/dQ_H$  equals two). If, at any time during this region of the removal of CO, a fraction  $\alpha_B$  of the adsorbed CO were in the bridged form, then

$$1.77 = \alpha_B + 2(1 - \alpha_B) \quad (11)$$

and  $\alpha_B$  would be 0.23. If we took double-layer charging into account,  $\alpha_B$  would be 0.39. These must be regarded as the outside limits of  $\alpha_B$ . Gilman,<sup>6</sup> from measurements made during the adsorption of the CO at 30°, reported a value of 0.31 for  $\alpha_B$  at saturation under 1 atm. One can note also that, since the slope  $dQ_{CO}/dQ_H$  is constant, the ratio of the two forms is constant. This implies that their oxidation kinetics are similar or that they can easily revert from one form to the other to maintain a fixed ratio.

#### IV. Summary and Conclusions

Using a rapid, programmed sequence of currents and potentials, it is possible to examine the adsorption of CO on platinum electrodes from solution in what appears to be an unambiguous way. The particular virtue of the present method is that we can see clearly the quantitative limit on the assumptions involved in deriving  $Q_{CO}$ , whereas in the previous work<sup>5–9</sup> this was not possible. In view of the radically different assumptions used in evaluating  $Q_{CO}$ , it is hardly surprising that the values at 1 atm. are so different, *viz.*, 270  $\mu\text{coulombs/cm.}^2$  (Gilman), 453  $\mu\text{coulombs/cm.}^2$  (Warner and Schuldiner), and 365  $\mu\text{coulombs/cm.}^2$  in this work. It is believed that the method described here yields a reliable value for  $Q_{CO}$  and could be more generally used to elucidate adsorption from solution on platinum electrodes.

In the following paper, a comparison is made between the properties of adsorbed CO and adsorbed HCOOH.

*Acknowledgment.* It is a pleasure to acknowledge the support of the Office of Naval Research under Contract Nonr-3765(00). This work was presented in part at the 126th meeting of the Electrochemical Society in Washington, D.C.

## Comparison of Adsorbed Formic Acid and Carbon Monoxide on Platinum Electrodes

by S. B. Brummer

*Tyco Laboratories, Inc., Waltham, Massachusetts (Received November 10, 1964)*

The low potential anodic oxidation of HCOOH on platinum is poisoned by the slow adsorption of an interfering species on the electrode. It has been suggested that this species is CO formed by decomposition of the HCOOH. A comparison is made between the properties of the adsorbed films formed on platinum in HCOOH and CO-saturated solutions. Both the coulometric behavior and the oxidation kinetics of the adsorbed films suggest that they are not the same.

### Introduction

In a previous paper,<sup>1</sup> it was shown that the low potential oxidation of HCOOH on platinum in HClO<sub>4</sub> solutions is poisoned by the slow adsorption of a species from the solution. Evidence that the oxidation is poisoned may also be found in the experiments of Buck and Griffith,<sup>2</sup> Slott,<sup>3</sup> Rhodes and Steigelmann,<sup>4</sup> and Giner.<sup>5</sup>

Slott and Rhodes and Steigelmann suggest that this poisoning results from adsorbed CO which is formed from decomposition of the HCOOH on the electrode, and the slow kinetics of the process<sup>1</sup> agree with some such hypothesis. The evidence of Rhodes and Steigelmann on this point is: (a) that during an anodic linear potential sweep, a current peak is observed with HCOOH solution which is similar to that found in CO-saturated solutions, and (b) the charge passed during this peak is the same in HCOOH as in CO-saturated solution. As was pointed out previously,<sup>6</sup> this evidence is not conclusive. Thus, the electrode normally oxidizes in the vicinity of the current peaks and it is well known that material not previously desorbed from platinum is invariably desorbed in this potential region. Also, the area under the peaks, a little more than 100  $\mu$ coulombs/cm<sup>2</sup>, is much too low to correspond to maximum coverage with HCOOH<sup>6</sup> or CO.<sup>7</sup> Thus, the coincidence of the areas under the peaks is not conclusive, particularly as Rhodes and Steigelmann found it necessary to use an arbitrary upper potential limit to terminate the charge integration under the peak. In order to compare the properties of the adsorbed layers and to at-

tempt to decide whether the poison for HCOOH oxidation is CO, measurements were made on the adsorbed films with anodic and cathodic galvanostatic transients.<sup>6,7</sup> In this paper, the coulometric properties of the adsorbed films, presented previously, are compared and some new results on the oxidation kinetics of the films are presented.

*Comparison of Shape of Galvanostatic Transients.* As was pointed out previously,<sup>1</sup> the simple comparison of large galvanostatic transients does not suggest that CO<sub>ads</sub> and HCOOH<sub>ads</sub> are the same. Thus, while for CO the potential increases and then overshoots considerably<sup>7,8</sup> during the application of the current, this is rarely found for HCOOH, and, in fact, only for relatively low current densities.<sup>1,2</sup> More usually,<sup>1,6,9</sup> one finds a relatively flat plateau in the HCOOH system and, when there is an overshoot, it is relatively minor. These differences in shape, however, might arise from

(1) S. B. Brummer and A. C. Makrides, *J. Phys. Chem.*, **68**, 1448 (1964).

(2) R. P. Buck and L. R. Griffith, *J. Electrochem. Soc.*, **109**, 1005 (1962).

(3) R. Slott, D.Sc. Thesis, Massachusetts Institute of Technology, 1963.

(4) D. R. Rhodes and E. F. Steigelmann, Abstract No. 213, Theoretical Division of the Toronto Meeting of the Electrochemical Society, May 1964.

(5) J. Giner, *Electrochim. Acta*, **9**, 63 (1964).

(6) S. B. Brummer, *J. Phys. Chem.*, **69**, 562 (1965).

(7) S. B. Brummer and J. I. Ford, *ibid.*, **69**, 1355 (1965).

(8) T. B. Warner and S. Schuldiner, *J. Electrochem. Soc.*, **111**, 992 (1964).

(9) M. W. Breiter, *Electrochim. Acta*, **8**, 447, 457 (1963).

differences in the relative contributions of the processes of adsorbate oxidation(I), of electrode oxidation (II), and of oxidation from solution (III) in the two cases, albeit it has been shown that the last two are relatively unimportant until (I) is finished.<sup>6,7</sup>

*Comparison of Coulometry for Adsorbed Films.* In the case of HCOOH,<sup>6</sup> it was shown that the oxidation of the maximum adsorption requires 310  $\mu\text{coulombs/real cm.}^2$  (1 "real"  $\text{cm.}^2 = 210 \mu\text{coulombs of H-atom coverage}$ ).<sup>6,7</sup> This material is adsorbed in the range  $10^{-3}$  to 1 M HCOOH, below 0.35 v. vs.  $\text{H}_2/\text{H}^+$  in the same solution. The electrode is only about 73% covered with this species. The oxidation of this material involves two electrons per Pt site. During this oxidation, the oxidation of the electrode is very strongly impeded. For CO,<sup>7</sup> the oxidation of the adsorbate, at 1 atm. pressure, requires 390  $\mu\text{coulombs/cm.}^2$  (in neither case is this value corrected for double-layer effects; these would constitute about 25  $\mu\text{coulombs/cm.}^2$ ). This material is adsorbed from 0.1 to 0.8 v. vs.  $\text{H}_2/\text{H}^+$  (the whole measured range) and the electrode is apparently completely covered. The oxidation of this material initially ( $\sim 10\%$  of electrode coverage) involves three electrons per site, but over most of the range, 1.77 electrons per site are involved. The oxidation of the electrode is impeded during the removal of the adsorbed CO but to a lesser extent than for the HCOOH. This direct comparison of the properties of the adsorbed films does not suggest that they are the same. However, there are some factors which must be taken into account.

Regarding the charges 310 and 390  $\mu\text{coulombs/cm.}^2$ , respectively, for  $\text{HCOOH}_{\text{ads}}$  and  $\text{CO}_{\text{ads}}$ , one may note that the latter value probably contains a contribution from CO physically adsorbed on the main chemisorbed layer.<sup>7</sup> If this is subtracted, we obtain 370  $\mu\text{coulombs/cm.}^2$  for  $Q_{\text{CO}}$  (assuming 1.77 electrons per site for the last 10% of coverage, also). This value is still too high but it could be that since the CO pressure in the HCOOH solutions is zero, a lower value of  $Q_{\text{ads}}$  (charge to oxidize the adsorbate) results. The estimates of Warner and Schuldiner<sup>8</sup> and Gilman<sup>10</sup> indicate  $\sim 5$  and 20% difference, respectively, between 1 atm. and zero pressure of CO. Taking Gilman's figure, the value of  $Q_{\text{CO}}$  above (390  $\mu\text{coulombs/cm.}^2$ ) could be made very close to the value for  $Q_{\text{HCOOH}}$ . However, as has been pointed out,<sup>7</sup> there is reason to suppose that Gilman's values for  $Q_{\text{CO}}^{\text{max}}$  are not correct.

It is also curious that CO itself is not adsorbed on a one-molecule per Pt surface atom basis, although the CO produced from HCOOH would have to be to account for the two electrons per surface atom found for the oxidation of  $\text{HCOOH}_{\text{ads}}$ . It may be that this is due

to the mode of adsorption of HCOOH prior to CO formation which is, perhaps, more likely to give one-site rather than two-site adsorption of the CO produced. The latter must then be assumed to be immobile. One has to account for the fact that the  $\text{HCOOH}_{\text{ads}}$  only covers 73% of the surface whereas  $\text{CO}_{\text{ads}}$  covers the whole surface in a similar kind of way; *i.e.*, the HCOOH cannot fit onto the bare surface in any way which could lead to further  $\text{CO}_{\text{ads}}$  production.

We may note that the oxidation of the electrode during the removal of  $Q_{\text{ads}}$  is easier in CO-saturated solution than in HCOOH solution.<sup>6,7</sup> However, this may be determined by solution effects rather than by the properties of the unremoved adsorbate.

*Oxidation Kinetics of the Adsorbed Films.* In Figure 1, we have plotted the potential during a 14.7 ma./ $\text{cm.}^2$  anodic transient against the surface bareness. The surface bareness is defined by  $\theta_{\text{H}}$ , which is the fraction of the surface available for cathodic galvanostatic H-atom deposition.<sup>6,7</sup> These transients were made from 0.3 v. vs.  $\text{H}_2/\text{H}^+$  in the same solution. The

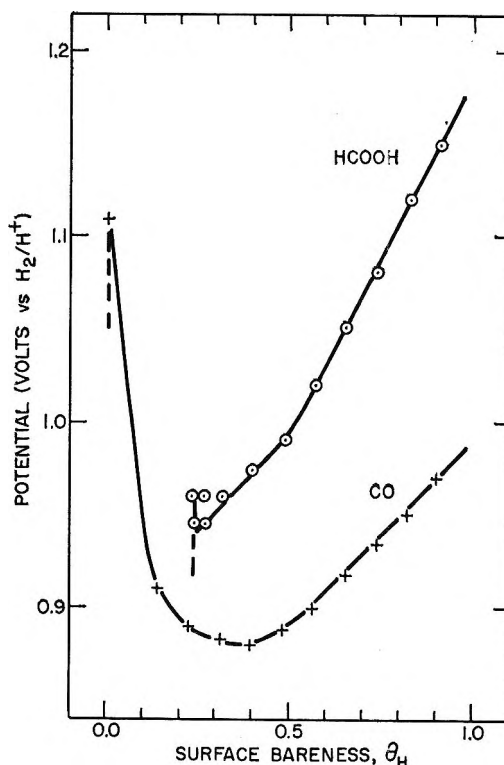


Figure 1. The variation of potential with surface bareness during a 14.7 ma./ $\text{cm.}^2$  anodic galvanostatic transient. HCOOH measurement was taken in a 0.2 M solution in 1 N  $\text{HClO}_4$ . The CO measurement was made with 1 N  $\text{HClO}_4$ , saturated with 1 atm. of CO.

(10) S. Gilman, *J. Phys. Chem.*, **66**, 2657 (1962).

solutions were made up in 1 *N* HClO<sub>4</sub> and, as previously, the measurements were made at 40°. The anodic current was chosen to minimize *iR* losses and electrode oxidation, on the one hand, and to avoid significant oxidation from solution, on the other. We find that, over the whole range of surface coverage, CO<sub>ads</sub> is easier to oxidize than the HCOOH<sub>ads</sub>. We note from Gilman's measurements<sup>11</sup> that CO at zero pressure oxidizes more readily than CO at 1 atm., which means that the CO curve, for comparison with HCOOH, should come at an even lower potential. One cannot argue that the two adsorbates are CO<sub>ads</sub> but are differently bonded (see above) and, therefore, their oxidation kinetics are different, since the evidence is that both the two-site ("bridged") and one-site ("linear") forms of CO<sub>ads</sub> are oxidized at the same rate. Thus, it was found<sup>7</sup> that the ratio of one-site to two-site adsorbate is constant during most of the removal of the CO<sub>ads</sub>. This could, of course, occur as a result of a rapidly attained equilibrium between the two species during the oxidation. That argument can be firmly rejected in this context, however, first, because it is likely that the CO<sub>ads</sub> layer is immobile—thus even at zero pressure it is strongly adsorbed—and secondly,

because if it were mobile, in this way, then a CO<sub>ads</sub> layer formed from HCOOH solutions would also be mobile and would attain the same equilibrium. However, we have seen that a striking difference between the two adsorbed films is the number of electrons per Pt atom required to oxidize them.

### Conclusions

While the differences between CO<sub>ads</sub> and HCOOH<sub>ads</sub> are not large, it does not appear likely, from the evidence presented here, that the poison for HCOOH oxidation is CO. It has been pointed out by Giner<sup>6</sup> that the poison resembles a species found on Pt in CO<sub>2</sub>-saturated solution which he has called "reduced CO<sub>2</sub>."<sup>12</sup> It would not seem, then, that this species is CO.

*Acknowledgment.* It is a pleasure to acknowledge support by the Office of Naval Research under Contract Nonr-3675(00). This work was presented in part at the 126th Meeting of the Electrochemical Society in Washington, D. C.

(11) See ref. 10, Figure 5.

(12) J. Giner, *Electrochim. Acta*, **8**, 857 (1963).

## The Radiolysis of Acetone in Air-Free Aqueous Solutions

by Peter Riesz

*Radiation Biology Section, Laboratory of Physiology, National Cancer Institute, National Institutes of Health, Bethesda, Maryland (Received November 12, 1964)*

The products from the radiolysis of aqueous air-free acetone solutions have been identified as 2,5-hexanedione, isopropyl alcohol, hydroxyacetone, hydrogen peroxide, and hydrogen and their yields have been determined over a wide range of concentration ( $10^{-3}$  to 1 *M*) and pH (1.0 to neutral). The marked dependence of the yields of isopropyl alcohol, 2,5-hexanedione, and hydrogen on both pH and acetone concentration can be understood in terms of the competition of acetone and hydrogen ions for the hydrated electron formed by the irradiation of water. Hydrated electrons react either with acetone to form an anion radical which is the precursor of isopropyl alcohol, or with hydrogen ions to give hydrogen atoms. About two-thirds of the hydrogen atoms produced react with acetone by abstraction to give acetyl radicals and hydrogen gas, and the remainder reacts by addition. This mechanism is supported by the effect of addition of *n*-propyl alcohol to acetone solutions before radiolysis. As a good scavenger for H and OH but a very poor one for hydrated electrons, *n*-propyl alcohol suppresses the formation of 2,5-hexanedione but not that of isopropyl alcohol.

The radiolysis of air-free aqueous acetone solutions was first investigated by Fricke, Hart, and Smith,<sup>1</sup> who found that at pH 3 the yield of hydrogen first increases and then decreases with increasing acetone concentration. In 1960, Allan and Scholes<sup>2</sup> presented evidence to show that acetone and hydrogen ions compete for the hydrated electron,  $e_{aq}^-$ ,<sup>3,4</sup> and thus provided an interpretation for the decreasing hydrogen yield observed by the earlier workers.<sup>1</sup> Subsequent studies based on competition kinetics<sup>5</sup> as well as the recent direct determination of rate constants by the technique of pulse radiolysis<sup>6</sup> have confirmed that acetone is an excellent scavenger for hydrated electrons. The same conclusion was reached in the present work, some aspects of which were reported earlier.<sup>7,8</sup> Since, apart from hydrogen, the radiolysis products from air-free aqueous acetone solutions have not been previously determined, it seemed of interest to study the chemical consequences of the reactions of hydrated electrons, hydrogen atoms, and hydroxyl radicals with acetone.

### Experimental

All irradiated solutions were made up in purified water obtained by redistilling ordinary distilled water first from alkaline permanganate, second from acid di-

chromate, and finally with no reagent added. Baker and Adamson reagent grade acetone was used as received in most experiments. Identical results were obtained after purification of acetone through the sodium iodide complex followed by two distillations through a 0.5-m. Nester spinning band column. 2,5-Hexanedione was fractionated under atmospheric pressure and the middle third was retained. Isopropyl alcohol (Fisher reagent), hydrogen peroxide (35%, inhibitor-free, Buffalo Electrochemical Corp.), and sulfuric acid (Baker and Adamson reagent) were used as received. Hydroxyacetone and *o*-aminobenzaldehyde were obtained from Bios Laboratories. Hydroxyacetone was purified by fractional distillation at 15 mm. and the fraction which boiled between 42 and 45° was collected.

- (1) H. Fricke, E. J. Hart, and H. P. Smith, *J. Chem. Phys.*, **6**, 229 (1938).
- (2) J. T. Allan and G. Scholes, *Nature*, **187**, 213 (1960).
- (3) G. Czapski and H. A. Schwarz, *J. Phys. Chem.*, **66**, 471 (1962).
- (4) E. J. Hart and J. W. Boag, *J. Am. Chem. Soc.*, **84**, 4090 (1962).
- (5) J. Rabani and G. Stein, *J. Chem. Phys.*, **37**, 1865 (1962).
- (6) E. J. Hart, S. Gordon, and J. K. Thomas, *J. Phys. Chem.*, **68**, 1271 (1964).
- (7) P. Riesz, *Radiation Res.*, **16**, 566 (1962).
- (8) P. Riesz, *Radiation Res. Suppl.*, **4**, 152 (1964).

This fraction contained 85.8% hydroxyacetone as determined by titration of an aqueous solution with periodic acid.<sup>9</sup> Water-insoluble polymer was removed from *o*-aminobenzaldehyde by the method of Forist and Speck.<sup>10</sup>

The pH of solutions was adjusted by addition of sulfuric acid. Dissolved gases were removed by the multiple-cell technique of Hart.<sup>11</sup> The acetone concentrations of solutions to be irradiated were determined after degassing by measuring the optical density at 270 m $\mu$ . All glassware brought into contact with these solutions was cleaned by annealing in an electric furnace. Irradiations were carried out with a Co<sup>60</sup>  $\gamma$ -source at dose rates of about  $2 \times 10^{20}$  e.v./l.-min. except for some experiments in which the effect of radiation intensity was studied. Dose rates were determined by the Fricke dosimeter with  $G(\text{Fe}^{11}) = 15.6$ .

The total yield of gaseous products (hydrogen plus methane plus ethane) was measured by extracting about 20 ml. of the irradiated solution in a Van Slyke gas analysis apparatus. Hydrogen was determined by gas chromatography using a 5A molecular sieve and a thermal conductivity detector with argon as carrier gas. For all other products a hydrogen flame ionization detector and helium carrier gas were used. Methane and ethane yields were measured using a silica gel column. For the nongaseous products 10–20- $\mu$ l. samples of irradiated solution were injected directly into the inlet system of the gas chromatograph with a Hamilton syringe. For quantitative work the unknown samples were bracketed by standards of approximately the same concentration and containing the same amount of acetone. Isopropyl alcohol was identified by comparison of the retention volume with that of a standard sample on five different columns at several temperatures, namely Carbowax 20 M, Carbowax 1000, Ucon (Polar), Flexol plasticizer, and Tween 80 columns; for quantitative assay a Ucon (Polar) column at 70° was used. Acid solutions were neutralized before injection to prevent the formation of 2,5-dimethylfuran from 2,5-hexanedione in the inlet system of the gas chromatograph. 2,5-Hexanedione was identified by comparison of the retention volume with that of a standard sample on Carbowax 1000, Tween 80, and on diethylene glycol adipate columns at several temperatures, and determined on the adipate column at 130°. Reduction of the irradiated solutions with sodium borohydride resulted in the complete removal of the 2,5-hexanedione peak and the appearance of the predicted amount of 2,5-hexanediol. Diacetone alcohol and pinacol were determined on a Tween 80 column at 100° and a diethylene glycol adipate column at 160°, respectively. Hydroxyacetone was identified by the excitation and

fluorescence spectra of the irradiated solution after treatment with *o*-aminobenzaldehyde. The observed spectra were identical with those of 3-hydroxyquinoline, which is the condensation product of hydroxyacetone and *o*-aminobenzaldehyde. Further evidence for the formation of hydroxyacetone was the isolation and determination of 1,2-propanediol from an irradiated solution which had been reduced with sodium borohydride. The yield of 1,2-propanediol was determined by gas chromatography on a diethylene glycol adipate column at 160°. Assays were made by the method of Huggins and Miller.<sup>12</sup> A Bowman-Aminco spectrophotofluorimeter was used with an excitation wave length of 370 m $\mu$  and the fluorescence was measured at the 445-m $\mu$  peak. Concentrations of a few micromoles/liter can be accurately determined by this method. Hydrogen peroxide was determined by the iodide method.<sup>13</sup>

## Results and Discussion

Air-free aqueous acetone solutions were irradiated with Co<sup>60</sup>  $\gamma$ -rays in neutral and acid solutions over the concentration range of  $10^{-3}$  to 1 *M*.

The major radiolysis products were identified as hydrogen, hydrogen peroxide, isopropyl alcohol, 2,5-hexanedione, and hydroxyacetone. Smaller amounts of pinacol, diacetone alcohol, methane, and ethane were also observed. The *G*-values of hydrogen and of 2,5-hexanedione were independent of dose over the range  $10$ – $150 \times 10^{20}$  e.v./l. while those of isopropyl alcohol, hydroxyacetone, and hydrogen peroxide decreased with increasing dose:

Figure 1 shows the formation of isopropyl alcohol in acid solutions as a function of dose and acetone concentration. The dependence of hydrogen peroxide formation in neutral and acid solutions on dose and acetone concentration is shown in Figure 2. In both neutral and acid solutions a steady-state concentration,  $(\text{H}_2\text{O}_2)_{ss}$ , is reached with increasing dose. With increasing acetone concentration,  $(\text{H}_2\text{O}_2)_{ss}$  decreases markedly in acid solutions but increases slightly in neutral solutions. Since the observed  $\text{H}_2\text{O}_2$  yields,  $G(\text{H}_2\text{O}_2)$ , were always lower than the molecular  $\text{H}_2\text{O}_2$  yield,  $G_{\text{H}_2\text{O}_2}$ , and since it was shown by control experiments that none of the observed radiolysis products react with  $\text{H}_2\text{O}_2$  under the conditions of these experi-

(9) I. M. Kolthoff and V. A. Stenger, "Volumetric Analysis," Vol. 3, Interscience Publishers, Inc., New York, N. Y., 1957, p. 486.

(10) A. A. Forist and J. C. Speck, Jr., *Anal. Chem.*, **22**, 903 (1950).

(11) E. J. Hart, *J. Am. Chem. Soc.*, **73**, 68 (1951).

(12) C. G. Huggins and O. N. Miller, *J. Biol. Chem.*, **221**, 711 (1956).

(13) C. J. Hochanadel, *J. Phys. Chem.*, **56**, 597 (1952).

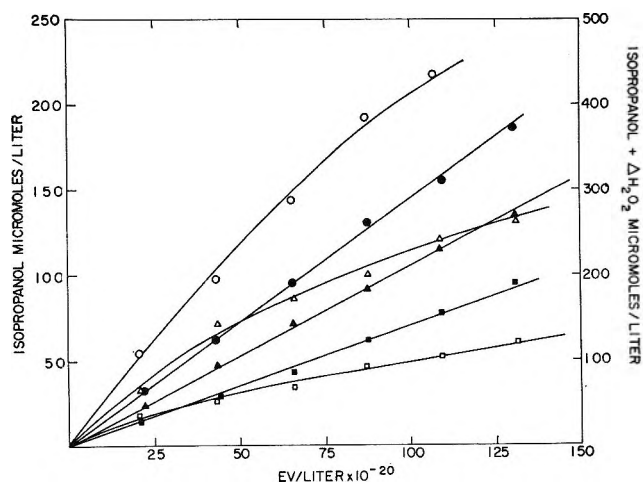


Figure 1. Isopropyl alcohol formation in air-free acetone solutions at pH 1.15 at different acetone concentrations; at 0.098 *M*: □, IH and ■, (IH +  $\Delta\text{H}_2\text{O}_2$ ); at 0.207 *M*:  $\Delta$ , IH and  $\blacktriangle$ , (IH +  $\Delta\text{H}_2\text{O}_2$ ); and at 0.386 *M*: ○, IH and ●, (IH +  $\Delta\text{H}_2\text{O}_2$ ).

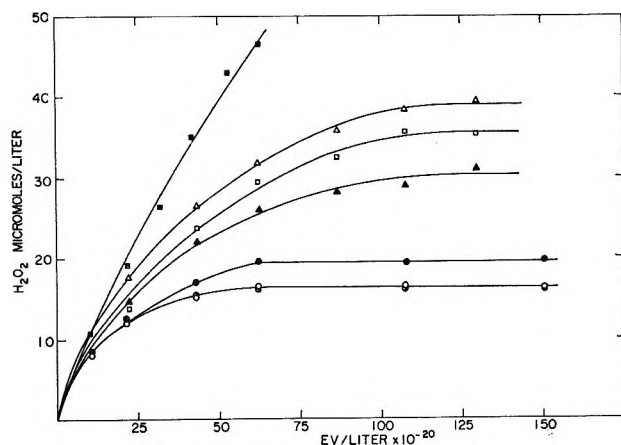


Figure 2. Hydrogen peroxide formation in air-free acetone solutions at neutral pH and pH 1.15 at different acetone concentrations; at pH neutral: ○, 0.01 *M*, ○, 0.10 *M*, and ●, 0.39 *M*; at pH 1.15: ■, 0.011 *M*,  $\Delta$ , 0.13 *M*, □, 0.21 *M*, and  $\blacktriangle$ , 0.49 *M*.

ments, it follows that  $\text{H}_2\text{O}_2$  is removed by reaction with one or more radical intermediates.

In order to identify these intermediates, the effect of adding  $\text{H}_2\text{O}_2$  to neutral acetone solutions before irradiation was studied. Figure 3 shows that a large decrease of the isopropyl alcohol yield and an approximately equal increase of the 2,5-hexanedione yield occurs in neutral solutions of 0.1 *M* acetone. As the  $\text{H}_2\text{O}_2$  concentration falls to the stationary-state concentration, the slopes of the isopropyl alcohol and 2,5-hexanedione yields approach those obtained in the absence of added  $\text{H}_2\text{O}_2$ . These results show that  $\text{H}_2\text{O}_2$  is removed by reaction with the radical precursor of isopropyl alcohol

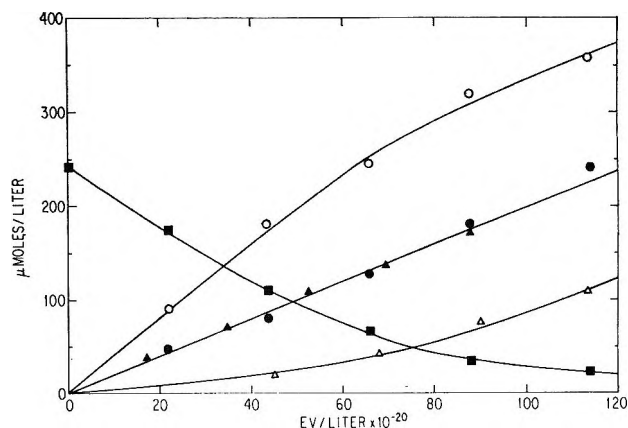


Figure 3. Formation of 2,5-hexanedione and of isopropyl alcohol in neutral 0.1 *M* acetone solutions with and without added hydrogen peroxide: ○, 2,5-hexanedione (243  $\mu\text{M}$   $\text{H}_2\text{O}_2$ ); ●, 2,5-hexanedione, no  $\text{H}_2\text{O}_2$  added;  $\Delta$ , isopropyl alcohol (247  $\mu\text{M}$   $\text{H}_2\text{O}_2$ );  $\blacktriangle$ , isopropyl alcohol, no  $\text{H}_2\text{O}_2$  added; and □,  $\text{H}_2\text{O}_2$ .

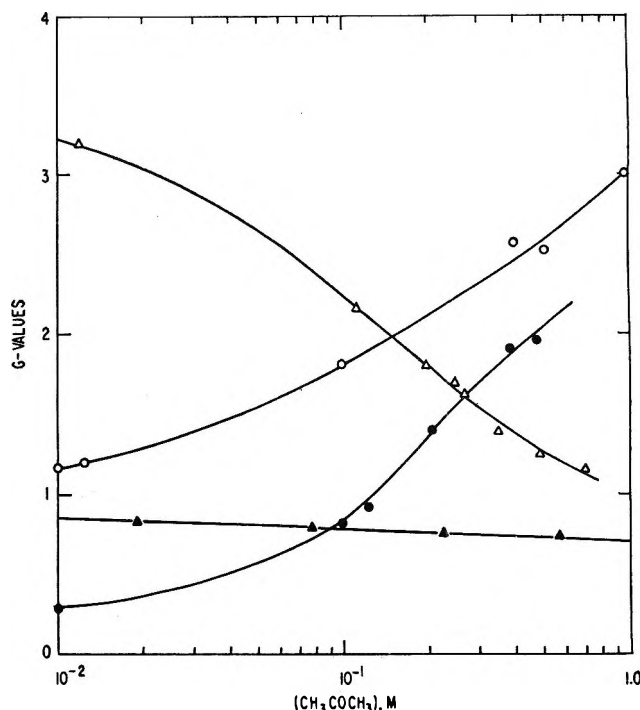


Figure 4. Hydrogen and isopropyl alcohol yields in acid and neutral acetone solutions:  $\Delta$ ,  $\text{H}_2$ , pH 1.15;  $\blacktriangle$ ,  $\text{H}_2$ , pH neutral; ●, IH +  $\Delta\text{H}_2\text{O}_2$ , pH 1.15; and ○, IH +  $\Delta\text{H}_2\text{O}_2$ , pH neutral.

but not with the acetylonyl radical which is the logical radical precursor of 2,5-hexanedione. In agreement with this inference, it is found that a plot of sum of the yields of isopropyl alcohol (IH) plus the difference between observed and molecular  $\text{H}_2\text{O}_2$  yields ( $\Delta\text{H}_2\text{O}_2$ ) is linear as a function of dose as shown in Figure 1.

The effects of acetone concentration and pH on the yields of hydrogen and on the sum of the yields of iso-



propyl alcohol plus  $\Delta\text{H}_2\text{O}_2$  are shown in Figure 4. In  $10^{-2} M$  acetone at pH 1.2, the  $G$ -value for hydrogen is 3.2 and no isopropyl alcohol can be observed. With increasing acetone concentration at this pH, the  $\text{H}_2$  yield falls and the isopropyl alcohol yield rises, approaching the values for neutral solutions. This behavior is consistent with the assumption that hydrated electrons react with acetone to form an anion radical which leads to isopropyl alcohol. In acid solutions the hydrogen ions compete with acetone for hydrated electrons, converting them to hydrogen atoms, which react principally to give  $\text{H}_2$  and acetyl radicals. However, not all of the hydrogen atoms formed in  $0.01 M$  acetone at pH 1.2 are accounted for by the abstraction process. This question will be discussed later.

The qualitative features of Figure 2 can be understood in terms of the same competition. If  $\text{H}_2\text{O}_2$  is removed by the radical precursor of isopropyl alcohol which is produced by the reaction of  $e_{\text{aq}}^-$  with acetone, the steady-state  $\text{H}_2\text{O}_2$  concentration at pH 1.2 should decrease with increasing acetone concentration. Figure 2 shows this to be the case.

It also follows from the proposed competition that at a fixed acetone concentration the hydrogen yield should fall and that of isopropyl alcohol plus  $\Delta\text{H}_2\text{O}_2$  rise with increasing pH. The data shown in Figure 5 confirm this prediction. The effect of pH on the hydroxyacetone yields is also shown.

The yields of 2,5-hexanedione and of hydroxyacetone in neutral solutions and at pH 1.2 are presented in Figure 6. In dilute acetone solutions the 2,5-hexanedione yields are larger at pH 1.2 than at neutral pH; this difference disappears at higher acetone concentrations. Such a result is to be expected if acetyl radicals are produced by the reaction of hydrogen atoms and hydroxyl radicals, but not of hydrated electrons, with acetone. At high acetone concentrations, the reaction of hydrated electrons with hydrogen ions to give hydrogen atoms is suppressed even in the acid solutions.

The  $G$ -value for pinacol from  $0.2 M$  acetone solutions at pH 1.2 irradiated with a dose of  $10^{22}$  e.v./l. is approximately 0.05. No pinacol was found from neutral solutions.  $G$  for diacetone alcohol from  $0.1 M$  neutral acetone solutions is about 0.06 at a dose of  $3.6 \times 10^{22}$  e.v./l. These small yields do not contribute significantly to the material balance, but they demonstrate the presence of the 2-hydroxy-2-propyl radical in these solutions.

The amounts of methane and ethane produced by radiation are directly proportional to dose and acetone concentration, and are independent of pH. The  $G$ -values for the "direct" products, methane and ethane, from  $1 M$  acetone solutions are 0.22 and 0.0039, re-

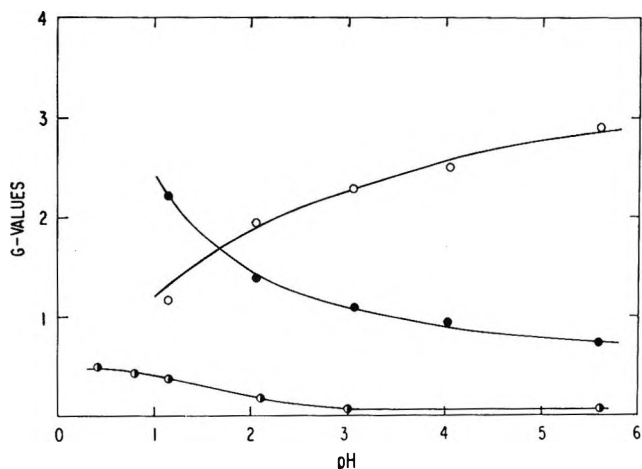


Figure 5. Yields of isopropyl alcohol, hydrogen, and hydroxyacetone in  $0.1 M$  acetone solutions: ○,  $2,5\text{-IH} + \Delta\text{H}_2\text{O}_2$ ; ●,  $\text{H}_2$ ; and ○,  $\text{CH}_3\text{COCH}_2\text{OH}$ .

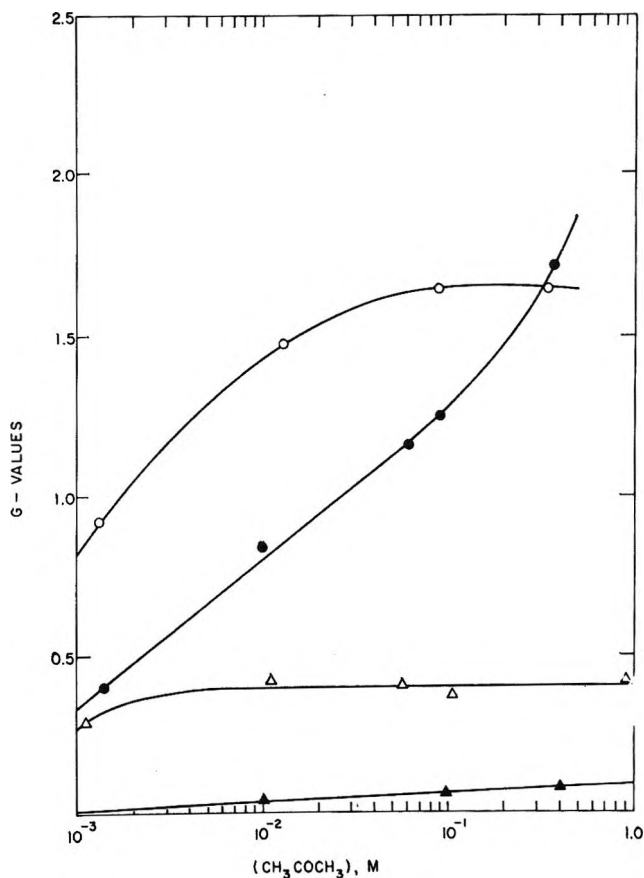
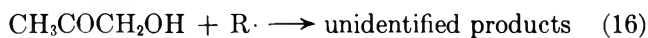
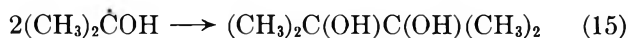
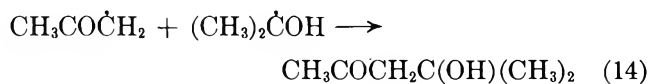
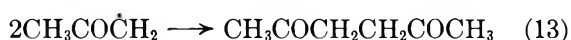
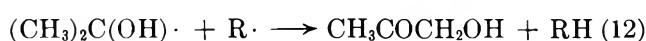
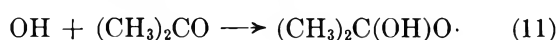
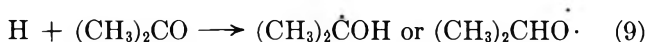
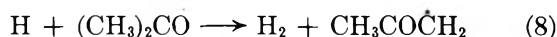
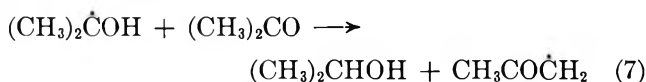
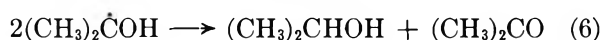
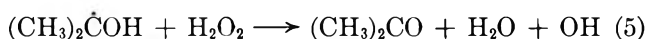
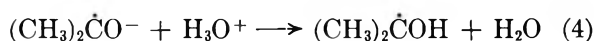
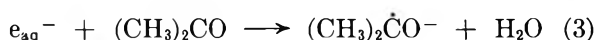
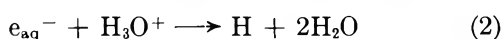
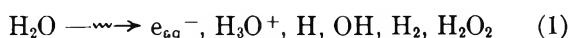


Figure 6. 2,5-Hexanedione and hydroxyacetone yields in neutral and acid acetone solutions: ○, 2,5-hexanedione, pH 1.15; ●, 2,5 hexanedione, pH neutral; △, hydroxyacetone, pH 1.15; and ▲, hydroxyacetone, pH neutral.

spectively. If one assumes that the absorbed energy is divided between water and acetone on the basis of

electron fractions, one finds from the results of Barker<sup>14</sup> on the radiolysis of liquid acetone that  $G(\text{CH}_4)$  is 0.12 and  $G(\text{C}_2\text{H}_6)$  is 0.017.

The material balance was investigated in neutral and acid  $10^{-2}$  M acetone solutions by repeated measurements of the acetone concentration by gas chromatography before and after irradiation at a dose of  $250 \times 10^{20}$  e.v./l. At pH 1.2, the observed  $G$ -value for acetone removal is 4.1, while the value calculated from the observed products is  $2G(\text{hexanedione}) + G(\text{isopropyl alcohol}) + G(\text{hydroxyacetone}) = 3.2 \pm 0.3$ . This indicates a product deficiency of  $0.9 \pm 0.3$  at  $10^{-2}$  M acetone in acid solutions. At this low acetone concentration, hydroxyacetone competes successfully with acetone for radicals and the products of this reaction have not been identified. Results on the formation of hydroxyacetone as a function of dose at pH 1.2 show that a steady-state concentration of 3  $\mu\text{moles/l.}$  is reached in  $10^{-3}$  M acetone and of 30  $\mu\text{moles/l.}$  in  $10^{-2}$  M acetone. At higher acetone concentrations where the reaction of hydroxyacetone with radicals is suppressed, the disappearance of acetone cannot be determined with acceptable precision. In neutral solutions, the observed value for acetone removal is  $2.9 \pm 0.4$  and the value calculated from the products is  $2.3 \pm 0.2$ . Extensive attempts to discover missing products by gas chromatography were unsuccessful. The dimerization product of the isopropoxyl radical, diisopropylperoxide, was synthesized and shown not to be a radiolysis product. Tests for the presence of organic hydroperoxides were negative.



The results shown in Figures 1-6 for solutions containing acetone concentrations of about 0.1 M or greater can be understood in terms of the mechanism in eq. 1-16. Reactions operating through the enol form of acetone have been neglected, since they appear unlikely because of the low enol content ( $2.5 \times 10^{-4}\%$ ) of acetone under our conditions; furthermore, no products requiring the assumption of such a pathway have been observed.

An essential feature of the mechanism, that hydrated electrons lead to a radical precursor of isopropyl alcohol (reaction 3) is clearly demonstrated by the effect of adding *n*-propyl alcohol to neutral acetone solutions before radiolysis. Alcohols are known to be efficient scavengers for H and OH radicals, but to be very unreactive toward hydrated electrons.<sup>15</sup> The results of Table I show that *n*-propyl alcohol almost completely suppresses the formation of 2,5-hexanedione but does not decrease the isopropyl alcohol yield.

Table I: Effect of Added Solutes on the Radiolysis of Neutral Acetone Solutions

Solutions Added solute	Concn., M	Acetone, M	$G(\text{hexanedione})$	$G(\text{isopropyl alcohol})$
None		0.10	1.6	1.1
$\text{H}_2\text{O}_2$	$250 \times 10^{-6}$	0.086	2.5	0.3
<i>n</i> -Propyl alcohol	0.16	0.078	<0.05	1.2

Isopropyl alcohol formation at low acetone concentration ( $10^{-2}$  M) occurs almost entirely by the disproportionation of 2-hydroxy-2-propyl radicals (reaction 6), while at high acetone concentration (0.5 M) isopropyl alcohol is made by the reaction of 2-hydroxy-2-propyl radicals with acetone (reaction 7). That reaction 6 contributes very predominantly in 0.1 M neutral acetone can be seen from the effect of adding  $\text{H}_2\text{O}_2$  before radiolysis. Reactions 7 and 5, followed by 10, both lead to approximately the same number of acetyl radicals in neutral solution, since only a very small fraction of the OH radicals is removed by (11). However, an increased contribution of reaction 5 at the ex-

(14) R. Barker, *Trans. Faraday Soc.*, 375 (1963).

(15) E. J. Hart, J. K. Thomas, and S. Gordon, *Radiation Res. Suppl.*, 4, 74 (1964).

pense of (6) leads to an increased production of acetyl radicals and therefore of 2,5-hexanedione by reaction 13. For every 2-hydroxy-2-propyl radical removed by reaction 5, an additional acetyl radical is produced. Hence the decrease of the isopropyl alcohol yield should be equal to the increase of the 2,5-hexanedione yield. The observed results in Figure 3 and Table I are in agreement with this conclusion.

A stationary-state treatment of the competition between reactions 5 and 6 shows that the steady-state hydrogen peroxide concentration,  $(\text{H}_2\text{O}_2)_{ss}$ , is proportional to the square root of the dose rate, while for competition between (5) and (7),  $(\text{H}_2\text{O}_2)_{ss}$  is independent of the dose rate. From the results of Table II it can be seen that in 0.01 *M* acetone reaction 6 is the principal path for isopropyl alcohol formation, while in 1.0 *M* acetone reaction 7 predominates. This result provides part of the explanation for the increase in the yields of isopropyl alcohol and of 2,5-hexanedione which occurs when the acetone concentration is increased above 0.1 *M* in neutral solutions. The change from reaction 6 to 7 increases both the isopropyl alcohol and the hexanedione yields by 0.5 ( $G_a - \Delta\text{H}_2\text{O}_2$ )  $\sim$  1. At high acetone concentrations, yields will also be increased by the suppression of the back reaction in the spurs to form water and the consequent increase in the radical yields.

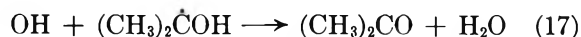
**Table II:** Effect of Dose Rate and Ionic Strength on the Steady-State  $\text{H}_2\text{O}_2$  Concentration in Neutral Acetone Solutions

Acetone, <i>M</i>	$\text{NaClO}_4$ , <i>M</i>	$(\text{H}_2\text{O}_2)_{ss}$ , $\mu\text{M}^a$	$(\text{H}_2\text{O}_2)_{ss}$ , $\mu\text{M}^b$
0.01	0	16.6	6.2 $\pm$ 0.6
0.10	0	16.5	7.8 $\pm$ 0.8
0.39	0	19.6	17.9
1.14	0	21.8	20.6
0.01	0.0045	16.9	
0.01	0.0227	17.2	
0.01	0.0906	18.6	
0.01	0.181	19.1	
0.01	0.327	20.6	

<sup>a</sup> Dose rate =  $2.03 \times 10^{20}$  e.v./l.-min. <sup>b</sup> Dose rate =  $0.128 \times 10^{20}$  e.v./l.-min.

The reactions which are responsible for the decrease of the isopropyl alcohol and of the 2,5-hexanedione yields at acetone concentrations below 0.1 *M* have not been identified. From reactions 3, 4, 5, and 6, it follows that in neutral solutions  $2G(\text{isopropyl alcohol}) + \Delta\text{H}_2\text{O}_2 = G_a = 2.8$ , while the observed value for 0.1 *M* acetone in neutral solution is 2.9 ( $\Delta\text{H}_2\text{O}_2 \simeq 0.7$ ). It follows that in  $10^{-2}$  *M* acetone solution 2-hydroxy-2-propyl radicals are removed by one or more other reactions. The yield

of 2,5-hexanedione to be expected in neutral solution from reactions 8, 10, and 13 would be  $0.5[G_{\text{OH}} + \Delta\text{H}_2\text{O}_2 + \{G(\text{H}_2) - G_{\text{H}_2}\} - G(\text{hydroxyacetone})] \simeq 1.6$ ; the value observed in 0.1 *M* acetone solutions is 1.3. However, the observed hexanedione yield in neutral  $10^{-2}$  *M* solutions is only 0.8 and therefore acetyl radicals are also removed by other processes such as reaction 16. Reaction 17 does not play any role since in order for it



to compete with reaction 10 at the dose rates used in these experiments, the ratio  $k_{17}/k_{10}$  would have to be of the order of  $10^6$ . Recent measurements by Thomas<sup>16</sup> have shown that  $k_{10} = 7.7 \times 10^7 \text{ M}^{-1} \text{ sec.}^{-1}$  and hence it follows that the ratio  $k_{17}/k_{10}$  cannot be of the order of  $10^6$ .

Experiments on the effect of ionic strength on  $(\text{H}_2\text{O}_2)_{ss}$  in neutral solution suggest the possibility that neutralization of the anion radical (reaction 4) does not always occur before reaction 6. In dilute acetone solutions,  $(\text{H}_2\text{O}_2)_{ss}$  is proportional to  $(2k_6/k_6)^{1/2}$  (dose rate)<sup>1/2</sup>. Although the data of Table II show considerable scatter when  $2 \log [(\text{H}_2\text{O}_2)_{ss,i}/(\text{H}_2\text{O}_2)_{ss,o}]$  is plotted against  $\mu^{1/2}/(1 + \mu^{1/2})$  (where  $\mu$  is the ionic strength and the subscripts *i*, *o* denote ionic strengths *i* and *o*, respectively), they indicate a slope of about  $0.4 \pm 0.1$  compared to the value of 1.02 to be expected from the Brønsted equation for a reaction between two univalent anions. Since the rate of reaction 6 will be different for radical anions and for uncharged radicals, it follows that the relative contributions of reactions 6 and 7 to isopropyl alcohol formation may not be the same in acid and neutral solutions.

A possible mechanism for the formation of hydroxyacetone is indicated by reactions 11 and 12. Since an increase of the acetone concentration from  $10^{-2}$  to 1 *M* has no effect on the hydroxyacetone yields in acid solutions, it follows that hydroxyacetone is not produced by the reaction of hydroxyl with acetyl radicals. A second mechanism to be considered is the reaction of acetyl radicals with hydrogen peroxide to give hydroxyacetone and hydroxyl radicals. The addition of 240  $\mu\text{M}$   $\text{H}_2\text{O}_2$  to 0.36 *M* acetone at pH 1.2 increases the initial hydroxyacetone yield from 0.4 to 0.7 and the ratio  $R = G(\text{hydroxyacetone})/G(\text{hexanedione})$  from 0.24 to 0.33. From reactions 11, 14, and 18 it follows



that  $R = k_{18}(\text{H}_2\text{O}_2)/k_{13}(\text{CH}_3\text{CO}\dot{\text{C}}\text{H}_2)$ . Addition of 240  $\mu\text{M}$   $\text{H}_2\text{O}_2$  increases the average  $\text{H}_2\text{O}_2$  concentration during the initial formation of the hydroxyacetone yield

(16) J. K. Thomas, private communication.

by a factor of about 20. The steady-state acetylonyl radical concentration is increased by less than a factor of 2, due to the conversion of  $e_{aq}^-$  to OH by reactions 3, 4, and 5. Hence, the ratio  $R$  would be expected to increase at least 10-fold. It may be inferred that the contribution of reaction 18 under those conditions is not important.

The actual mechanism for the observed production of hydroxyacetone is not known at present. The addition of hydroxyl radicals to the enol form of acetone can be neglected since the rate constant of this reaction would have to be of the order of  $10^6$  times greater than  $k_{10}$ . A highly speculative process is suggested in reactions 11 and 12. Reaction 11 consists of the addition of a hydroxyl radical to acetone to give the hydroxyisopropoxyl radical. From this species hydroxyacetone could be formed by a transfer of a hydrogen atom to another radical, accompanied by an intramolecular rearrangement (reaction 12). Figure 5 shows that the hydroxyacetone yield is very low and constant between pH 6 and 3, increases below pH 3, and levels off at pH 0.4. Clearly, further work on the formation of hydroxyacetone is needed.

The hydrogen yield in acid solutions (pH 1.15) of  $10^{-2}$  M acetone is 3.2, as shown in Figure 4. Under these conditions 94% of the hydrated electrons are converted to hydrogen atoms and hence, if all of the hydrogen atoms reacted by abstraction from acetone, the hydrogen yield would be 3.9 instead of 3.2. This suggests that about 25% of the hydrogen atoms react by addition to acetone (reaction 9). This conclusion is supported by the observation that  $H_2$  yields from neutral solution are less than 1.0, the value to be expected from a molecular yield of 0.45 and a "direct H atom yield" of 0.55.

From the competition of hydrogen ions and of acetone for hydrated electrons (reactions 2 and 3) and from the abstraction and addition of hydrogen atoms to acetone (reactions 8 and 9) it follows that eq. 19 applies

$$\frac{1}{G(H_2) - fG_{H_2} - G_H \left( \frac{k_8}{k_8 + k_9} \right)} = \frac{1}{G_a} \frac{k_8 + k_9}{k_8} + \frac{1}{G_e} \frac{k_8 + k_9}{k_8} \frac{(\text{acetone})}{(H^+)} \quad (19)$$

where  $f$  is a correction factor for the decrease of the molecular hydrogen yield in the presence of acetone which can be calculated from the data of Anderson and Hart.<sup>17</sup> Recent work by Hayon<sup>18</sup> has shown that the direct H atom yield is not decreased by electron scavengers. The hydrogen yields from aqueous acetone solutions at pH 1.2 plotted according to eq. 19 are

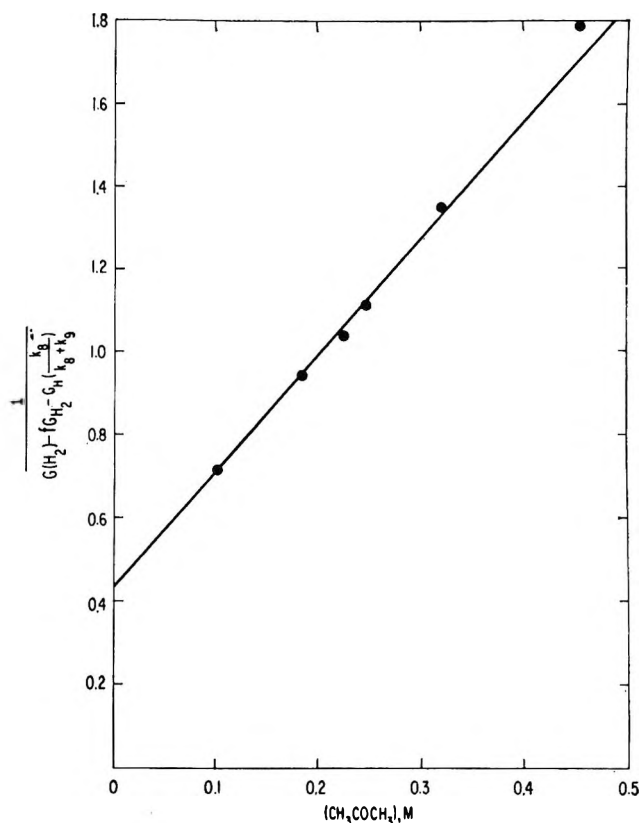


Figure 7. Results of the hydrogen determinations at pH 1.15 plotted as described in text: ●,  $H_2$ .

shown in Figure 7. From the observed slope and from the literature values<sup>19,20</sup> of  $G_e = 3.10$ ,  $G_H = 0.55$ , and  $G_{H_2} = 0.45$  one finds  $k_9/k_8 = 0.33 \pm 0.06$  and  $k_2/k_3 = 2.1 \pm 0.2$ . The value of  $k_9/k_8$  is in good agreement with the value of 0.3 previously found by Nehari and Rabani.<sup>21</sup> Absolute rate measurements by pulse radiolysis<sup>22</sup> give a value of  $4.0 \pm 0.4$  for  $k_2/k_3$  in neutral solutions, which corresponds to a value of  $2.2 \pm 0.2$  at an ionic strength of 0.11, in good agreement with the present results.

Recently, Gordon, Hart, and Thomas<sup>23</sup> have observed transients in the flash radiolysis of aqueous deaerated neutral acetone solutions. A very similar transient was observed<sup>23</sup> from air-free isopropyl alcohol solutions. The observed absorption appears to be due to the 2-hy-

(17) A. R. Anderson and E. J. Hart, *J. Phys. Chem.*, **65**, 804 (1961).

(18) E. Hayon, *ibid.*, **68**, 1242 (1964).

(19) A. O. Allen, "The Radiation Chemistry of Water and Aqueous Solutions," Van Nostrand Company, Inc., Princeton, N. J., 1961, p. 47.

(20) J. Rabani and G. Stein, *J. Chem. Phys.*, **37**, 1865 (1962).

(21) S. Nehari and J. Rabani, *J. Phys. Chem.*, **67**, 1609 (1963).

(22) S. Gordon, E. J. Hart, M. S. Matheson, J. Rabani, and J. K. Thomas, *Discussions Faraday Soc.*, **36**, 193 (1963).

(23) S. Gordon, E. J. Hart, and J. K. Thomas, *J. Phys. Chem.*, **68**, 1262 (1964).

droxy-2-propyl radical in agreement with the proposed mechanism. Adams, Baxendale, and Boag<sup>24</sup> have demonstrated by pulse radiolysis that the ketyl radical ion,  $(\text{C}_6\text{H}_5)_2\dot{\text{C}}-\text{O}^-$ , is the primary product from the addition of  $e_{\text{aq}}^-$  to benzophenone in alkaline solutions. In neutral solutions, the rapid neutralization of the ketyl ion produces the neutral radical,  $(\text{C}_6\text{H}_5)_2\dot{\text{C}}-\text{OH}$ .

*Acknowledgment.* The author wishes to thank Dr. E. J. Hart and Dr. C. R. Maxwell for valuable discussions and Mr. C. L. Spears and Mr. J. A. Oliver for technical assistance.

(24) G. E. Adams, J. H. Baxendale, and J. W. Boag, *Proc. Roy. Soc. (London)*, **A277**, 549 (1964).

## Mass Spectrometric Knudsen Cell Measurements of the Vapor Pressure of Palladium and the Partial Pressure of Palladium Oxide

by J. H. Norman, H. Gene Staley, and Wayne E. Bell

*General Atomic Division of General Dynamics Corporation, John Jay Hopkins Laboratory for Pure and Applied Science, San Diego, California (Received November 12, 1964)*

Thermodynamic values derived from measurements of the vapor pressure of palladium and the partial pressure of  $\text{PdO}(\text{g})$  in equilibrium with  $\text{Pd}(\text{s})$  in an oxygen atmosphere are  $\Delta H^\circ_{298} = 91.0$  kcal./mole for  $\text{Pd}(\text{s}) = \text{Pd}(\text{g})$ , and  $\Delta H^\circ_{298} = 83.4$  kcal./mole and  $\Delta S^\circ_{298} = 18.8$  e.u. for  $\text{Pd}(\text{s}) + \frac{1}{2}\text{O}_2 = \text{PdO}(\text{g})$ . The palladium vapor pressure data measured over the range 1485 to 1710°K. are represented by  $\log P_{\text{Pd}} (\text{atm.}) = (-19,370/T) + 6.120$ .

### Introduction

In a previous study, Alcock and Hooper,<sup>1</sup> using a transpiration method, found that the volatility of palladium is slightly increased in oxygen, which suggests the formation of a gaseous oxide of palladium. Norman, *et al.*,<sup>2</sup> using a mass spectrometric method, identified the gaseous oxide  $\text{PdO}$ . The present mass spectrometric investigation was undertaken to measure the partial pressure of the gaseous oxide in equilibrium with palladium metal in an oxygen atmosphere.

In the measurement of the partial pressure of  $\text{PdO}$ , it was desirable to use the vapor pressure of palladium as a reference. A survey of the literature showed that the vapor pressure of the metal has been measured by four previous investigators<sup>1,3-5</sup>; however, the results are not in accord. Vapor pressure data measured by Haefling and Daane<sup>3</sup> using a Knudsen cell loss-in-weight technique are higher by an order of magnitude

than those derived from the Langmuir-type measurements of Dreger and Margrave<sup>4</sup> and Hampson and Walker.<sup>5</sup> The Knudsen and Langmuir data could be reconciled if the evaporation coefficient for palladium were assumed to be 0.1; however, this coefficient is typically higher for metals. The vapor pressure data obtained by Alcock and Hooper<sup>1</sup> using a transpiration method are in accord with the Langmuir data. Second-law heats of vaporization derived from published data

(1) C. B. Alcock and G. W. Hooper, *Proc. Roy. Soc. (London)*, **A254**, 551 (1960).

(2) J. H. Norman, H. G. Staley, and W. E. Bell, *J. Phys. Chem.*, **68**, 662 (1964).

(3) J. F. Haefling and A. H. Daane, *Trans. Met. Soc. AIME*, **212**, 115 (1958).

(4) L. H. Dreger and J. L. Margrave, *J. Phys. Chem.*, **64**, 1323 (1960).

(5) R. F. Hampson and R. F. Walker, *J. Res. Natl. Bur. Std.*, **66A**, 177 (1962).

vary from 77 to 107 kcal./mole. In view of the discord in published data, measurement of the vapor pressure of palladium was undertaken as the first step in the present investigation.

### Experimental

A Consolidated Electrodynamics Corp. Model 21-703 mass spectrometer modified for Knudsen cell studies was employed. For the palladium vapor pressure measurements, a quartz cell contained in a molybdenum outer cell was used. The quartz cell was completely sealed except for a circular orifice, through which the cell was loaded. During the course of the vapor pressure measurements, the effective orifice area, as determined by mercury effusion measurements, increased from 0.0119 to 0.0147 cm.<sup>2</sup>.

In order to calibrate the mass spectrometer, three samples of palladium (about 5 mg. each) were totally evaporated from the quartz cell at temperatures around 1450°. The ionizing voltage used was 21.7 e.v. Three calibration factors were obtained; the factors obtained in the second and third evaporation experiments differed by 14 and 21%, respectively, from the factor obtained in the first experiment. The difference was undoubtedly caused by an increase in orifice size, and it is apparent from the magnitude of the over-all difference (21%) that practically all of the 24% increase in orifice size indicated by the mercury effusion experiments occurred during the calibration experiments. The third calibration factor was accepted for use in the vapor pressure evaluation.

At the end of the total-evaporation experiments, the quartz cell, in position within the outer cell, was loaded through the orifice, and regular Knudsen effusion experiments were performed.

For studies of the gaseous oxide, an alumina Knudsen cell contained inside a molybdenum outer cell was used. A knife-edge slit, 0.005 × 0.95 cm., served as the orifice. A 0.16-cm. o.d. alumina tube was inserted through the base of the cell to provide for admission of oxygen. At the total pressures used, the maximum mean free path was twice the slit width, which indicates that Knudsen conditions existed.

The cells were heated by electron bombardment from a series of filaments mounted around and on top of the cell. Heat shields were used on the bottom and around the cell, but no shielding was used on top. The furnace was similar in most respects to that described previously by Norman, *et al.*<sup>6</sup> Experimental temperatures were determined from optical pyrometric measurements by viewing the inner cell through small holes in the outer cell near the top and bottom of the inner cell. The difference between the measured top

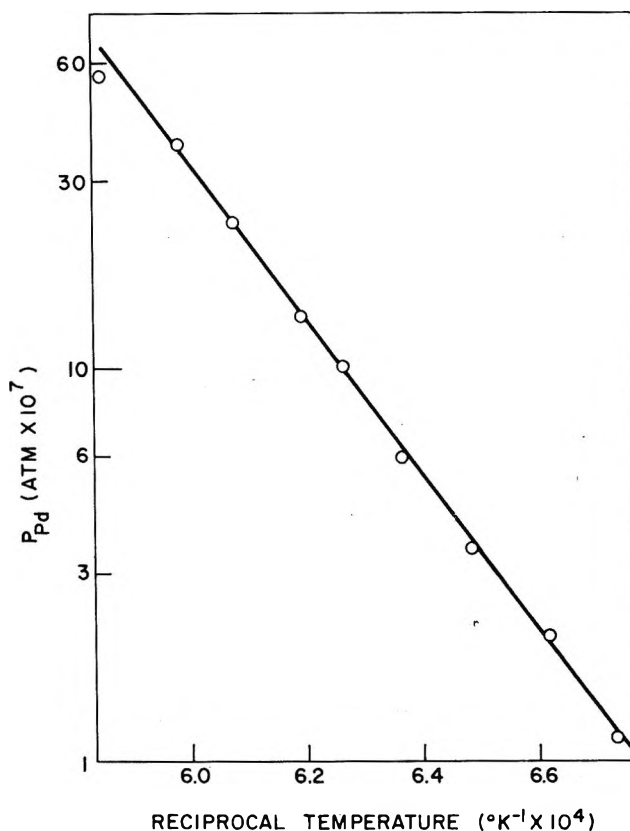


Figure 1. Palladium vapor pressures as a function of reciprocal temperature.

and bottom cell temperatures did not exceed 5° during an experiment.

Palladium metal in the form of foil obtained from the Baker Division, Engelhard Industries, was used. The impurities found in this foil were 0.07% Pt and traces of Ag, B, Fe, Mg, and Si. The foil was cut into strips for loading into the cells. Liquid Carbonic industrial grade oxygen, which has been found to contain 400 p.p.m. of N<sub>2</sub> as the major contaminant, was used. Ratios of cell orifice areas to evaporating areas were about 1/600 or less for the alumina cell.

*Vapor Pressure of Palladium.* Measurements of the vapor pressure of palladium were made over the temperature range 1485 to 1710°K. The data are plotted in Figure 1 as a function of reciprocal temperature. The line drawn through the data corresponds to  $\Delta H^\circ_{1600} = 90$  kcal./mole and  $\Delta S^\circ_{1600} = 29.2$  e.u. for the reaction



where 1600°K. is the mean temperature of the measurements.

(6) J. H. Norman, P. Winchell, and H. G. Staley, *J. Chem. Phys.*, **41**, 60 (1964).

In a third-law treatment of the data, using entropy values given by Stull and Sinke,<sup>7</sup> one derives  $\Delta H^\circ_{1600} = 88.65 \pm 0.08$ , where the uncertainty is the standard deviation of the mean for nine measurements. The third-law  $\Delta H^\circ_{1600}$  agrees with the second-law value given above within the uncertainty of the second-law determination. Using the third-law  $\Delta H^\circ_{1600}$ , one obtains

$$\log P_{\text{Pd}} (\text{atm.}) = \frac{-19,370}{T} + 6.120 \quad (2)$$

which is representative of the vapor pressure data. A third-law treatment of the data using free-energy functions given by Stull and Sinke yields  $\Delta H^\circ_{298} = 90.96 \pm 0.07$  kcal./mole for reaction 1. This value may be compared with the third-law  $\Delta H^\circ_{298}$  values  $91.0 \pm 0.8$  kcal./mole reported by Dreger and Margrave and  $89.2 \pm 0.2$  kcal./mole reported by Hampson and Walker.

In Figure 2 the vapor pressure curve representative of eq. 2 is compared with curves derived from equations given by previous investigators. The extent of each curve reflects the temperature range over which data were measured, with the exception that Dreger and Margrave performed one measurement at  $1220^\circ\text{K}$ . ( $1/T = 8.20 \times 10^{-4}$ ), which is considerably outside the range indicated by the curve representing their data. The measurement yielded the vapor pressure value  $2.54 \times 10^{-10}$  atm., which compares with  $1.87 \times 10^{-10}$  obtained from an extension of their curve. Figure 2 shows that the data of the present investigation are in good agreement with the results of Dreger and Margrave and of Alcock and Hooper. The data of Hampson and Walker are higher by a factor of about two. The reported vapor pressures of Haefling and

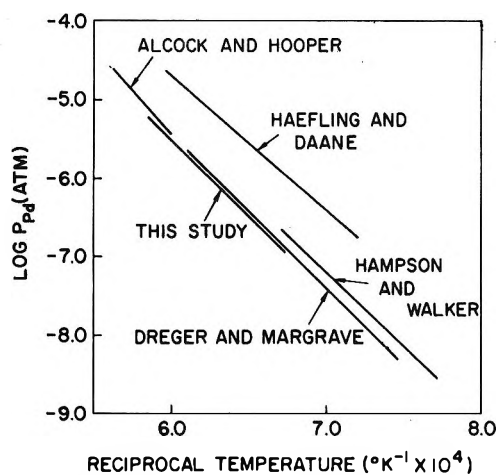


Figure 2. Comparison of palladium vapor pressure curves derived from data of various investigators.

Daane are in wide disagreement with the other data and would appear to be incorrect.<sup>7a</sup>

*Vaporization of Palladium in Oxygen.* To obtain enthalpy data for the vaporization reaction



as well as for reaction 1, intensities of  $\text{PdO}^+$  and  $\text{Pd}^+$  were measured as a function of temperature in the range  $1700$  to  $1950^\circ\text{K}$ . During the measurements, a constant flux of oxygen flowed through the Knudsen cell.

In this work, temperatures ranging around the melting point of palladium were necessary in order to get measurable  $\text{PdO}^+$  signals. The ion intensities measured above the melting point of palladium were corrected by the heat and entropy of fusion<sup>8</sup> in order

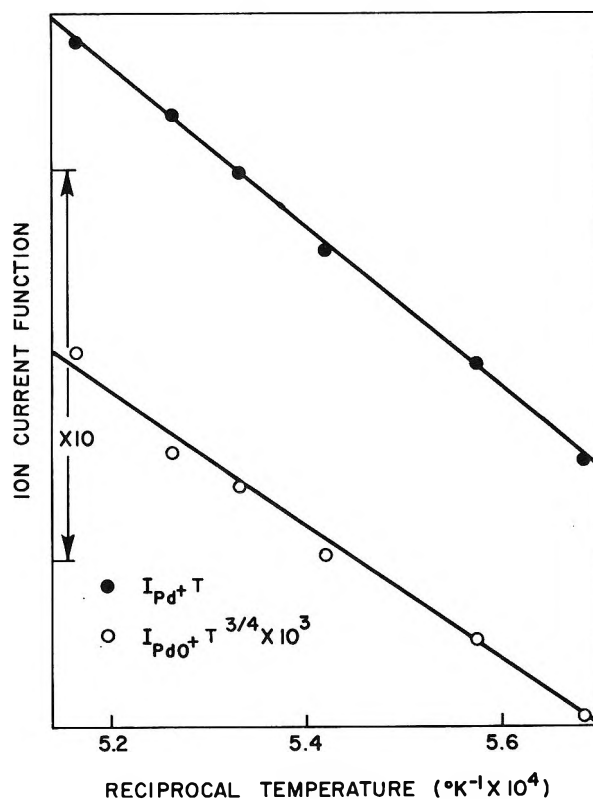


Figure 3. Ion current function data for  $\text{PdO}^+$  and  $\text{Pd}^+$  as a function of reciprocal temperature (data were corrected for fusion of palladium).

(7) D. R. Stull and G. C. Sinke, "Thermodynamic Properties of the Elements," American Chemical Society, Washington, D. C., 1956.

(7a) NOTE ADDED IN PROOF. Zavitsanos [P. D. Zavitsanos, *J. Phys. Chem.*, **68**, 2899 (1964)] recently reported the vapor pressure and heat of vaporization of palladium measured using a Knudsen cell target-gain-in weight technique. He obtained the third-law  $\Delta H^\circ_{298}$  value of  $89.8 \pm 0.9$  kcal./mole, in agreement with the values cited above. His contentions on the results of previous investigators are similar to ours.

to obtain the pressures which would have been observed if palladium had remained solid over the entire range of study. This makes possible fitting all the data to a single curve describing reaction 3.

A typical set of temperature-dependence data, measured using 21.7-e.v. ionizing electrons, is presented in Figure 3. The data are expressed in terms of ion-current functions,  $I_{\text{Pd}^+}T$  for reaction 1 and  $I_{\text{PdO}^+}T^{1/4}$  for reaction 3. In the latter term, the temperature factor,  $T^{1/4}$ , occurs because the pressure of oxygen in the cell was proportional to  $T^{1/4}$  under the conditions of constant influx of the gas.

The temperature-dependence studies yielded  $\Delta H^\circ_{1850} = 79.1 \pm 0.6$  kcal./mole for reaction 3 on the basis of four determinations and  $\Delta H^\circ_{1850} = 91.2 \pm 1.7$  kcal./mole for reaction 1 on the basis of three determinations, where 1850°K. was the mean temperature of the measurements. The uncertainties are standard deviations of the mean. The  $\Delta H^\circ_{1850}$  value for reaction 1 agrees reasonably well with values determined in the Pd vapor pressure work.

Intensities of the ions  $\text{PdO}^+$ ,  $\text{Pd}^+$ , and  $\text{O}_2^+$  were measured simultaneously at 1900°K. The ion signals were correlated by using values for the relative ionization cross sections of Pd and  $\text{O}_2$  given by Otvos and Stevenson.<sup>9</sup> Multiplier gains inversely proportional to molecular weight were used with these cross sections according to the treatment described by Inghram and Drowart.<sup>10</sup> Appearance potentials, 8.1 e.v. for  $\text{Pd}^+$  and 9.1 e.v. for  $\text{PdO}^+$ , as reported previously,<sup>2</sup> and an ionization potential of 12.5 e.v. for  $\text{O}_2$  were employed. Palladium vapor pressures given in Figure 1 were used as reference values. This procedure gave partial-pressure values of  $6.2 \times 10^{-8}$  atm. for  $\text{PdO}(\text{g})$  and  $3.9 \times$

$10^{-3}$  atm. for  $\text{O}_2$  at 1900°K. Combining the free-energy value derived from these partial-pressure values with the  $\Delta H^\circ_{1850}$  value cited above, one arrives at  $\Delta S^\circ_{1900} = 14.2$  e.u. for reaction 3.

On the basis of the average of heat capacity data for MO-type molecules given by Kelley,<sup>11</sup>  $C_p$  for  $\text{PdO}(\text{g})$  is estimated to be  $8.45 + 0.30 \times 10^{-3}T - 0.83 \times 10^5 T^{-2}$  cal./°K.-mole. Combining this with heat capacity data for Pd(s) and  $\text{O}_2$  given by Kelley, one arrives at  $\Delta C_p = -0.93 - 1.58 \times 10^{-3}T - 0.63 \times 10^5 T^{-2}$  cal./°K.-mole for reaction 3.

Using the values of  $\Delta H^\circ_{1850}$  and  $\Delta S^\circ_{1900}$  given above and the  $\Delta C_p$  value, one calculates  $\Delta H^\circ_{298} = 83.4 \pm 3.0$  kcal./mole and  $\Delta S^\circ_{298} = 18.8 \pm 2.5$  e.u. for reaction 3. The uncertainties were estimated. Within the uncertainty, the  $\Delta S^\circ_{298}$  value is in accord with the typical entropy of formation (20.6 e.u.) for MO-type gaseous molecules cited by Searcy.<sup>12</sup>

*Acknowledgments.* This research was supported in part by the U. S. Atomic Energy Commission under Contract AT(04-3)-164. The authors are indebted to Drs. U. Merten and A. Searcy for helpful discussions.

(8) R. Hultgren, R. L. Orr, P. D. Anderson, and K. K. Kelley, "Selected Values of Thermodynamic Properties of Metals and Alloys," John Wiley and Sons, Inc., New York, N. Y., 1963.

(9) J. W. Otvos and D. P. Stevenson, *J. Am. Chem. Soc.*, **78**, 546 (1956).

(10) M. C. Inghram and J. Drowart, "Proceedings of the International Symposium on High Temperature Technology," McGraw-Hill Book Co., Inc., New York, N. Y., 1960.

(11) K. K. Kelley, Bureau of Mines Bulletin 584, U. S. Government Printing Office, Washington, D. C., 1960.

(12) A. W. Searcy in "Survey of Progress in Chemistry," A. F. Scott, Ed., Academic Press, Inc., New York, N. Y., 1963.



## Properties of Organic-Water Mixtures. II. Solubilities and Activity

### Coefficients of Sodium Chloride and Potassium Chloride in *N,N*-Dialkylamides Containing Water<sup>1</sup>

by C. F. Coleman

*Chemical Technology Division, Oak Ridge National Laboratory, Oak Ridge, Tennessee  
(Received November 16, 1964)*

The selectivity of different amides for water over salt was evaluated by determining activity coefficients through measurement of salt distribution or solubility under conditions of (1) amide saturated with both water and salt, (2) amide saturated with water at limited salt concentrations, and (3) amide saturated with salt at limited water contents. Both solubilities and activity coefficients of sodium and potassium chloride proved to be controlled mainly by the water content of the amide. Solubility decreased with decreasing water content, while the selectivity for water, proportional to  $\gamma_{\pm(o)}/\gamma_{\pm(aq)}$ , increased to maxima often exceeding  $10^3$  at water contents around 0.5 to 1%.

As part of a continuing program directed toward a better understanding of selective hyperfiltration membrane behavior and of the basis for choosing membrane materials, the selectivity of a series of amides for water over salt was examined by measuring the solubilities and activity coefficients of sodium and potassium chlorides. The solubility of water and/or salt in different amides, and in hydrocarbon solutions of one of them, was measured under three separate conditions: amide saturated with both water and salt, saturated with water at limited salt contents, and saturated with salt at limited water contents. Liquid-liquid equilibrations were used for the first and second conditions, and a salt-packed column technique<sup>2</sup> for the third. The sodium and potassium chloride solubilities in the organic-rich phase were low and were measured by use of radioactive tracers.

#### Experimental

*Methods.* Solubility of water in the organic phases was measured in liquid-liquid equilibrations with salt absent, present at limited concentrations, or present at saturation (excess solid salt present). Solubility of salt was also measured in the latter liquid-liquid equilibrations. When the water content of organic phases was limited to less than saturation, salt solubility was

measured by saturation in slow flow through a salt-packed column.

Aqueous and organic phases were equilibrated, usually at equal volumes, in screw-cap vials (or in glass-stoppered graduated cylinders for direct measurement of phase-volume changes) rotated end-over-end in a thermostat at  $25 \pm 0.02^\circ$ . Phase separation was usually rapid and clean. The organic-rich (upper) phase was sampled first, then removed for sampling of the water-rich phase. Both water and salt contents were always less in the upper than in the lower phase.

Packed column saturation was carried out essentially as previously described.<sup>2</sup> The columns were  $\leq 2$  mm. i.d., with a wider top portion to serve as liquid reservoir. They were jacketed with water circulated from a thermostat at  $25 \pm 0.05^\circ$ . They contained 0.1 to 0.2 g. of tracer-tagged salt, supported on a plug of glass wool and diatomaceous filter aid. The flow resistance depended mainly on the thickness of the filter aid layer, which was chosen so as to give a flow of about 0.05 ml./min. under an applied pressure equal

(1) Research sponsored by The Office of Saline Water, U. S. Department of the Interior, under Union Carbide Corporation's contract with the U. S. Atomic Energy Commission.

(2) K. A. Kraus, R. J. Raridon, and W. H. Baldwin, *J. Am. Chem. Soc.*, **86**, 2571 (1964).

Table I: Identification and Molecular Weights of Amides

Amido group	N,N-Dialkylamide <sup>a</sup> (mol. wt.)			
$\begin{array}{c} \text{O} \\ \parallel \\ \text{=NC}(\text{CH}_2)_{10}\text{CH}_3 \end{array}$	$\text{Me}_2\text{Lr}^b$ (227.4)			
$\begin{array}{c} \text{O} \\ \parallel \\ \text{=NC}(\text{CH}_2)_8\text{CH}_3 \end{array}$		$\text{Et}_2\text{Dec}$ (227.4)		
$\begin{array}{c} \text{O} \\ \parallel \\ \text{=NC}(\text{CH}_2)_6\text{CH}_3 \end{array}$			$\text{Pr}_2\text{Oct}^c$ (227.4)	
$\begin{array}{c} \text{O} \\ \parallel \\ \text{=NCCH}_2\text{CH}_3 \end{array}$		$\text{Pr}_2\text{Pr}$ (157.3)	<i>i</i> - $\text{Pr}_2\text{Pr}^d$ (157.3)	$\text{Bu}_2\text{Pr}$ (185.3) <i>i</i> - $\text{Bu}_2\text{Pr}^d$ (185.3)
$\begin{array}{c} \text{O} \\ \parallel \\ \text{=NCCH}_3 \end{array}$		$\text{Pr}_2\text{Ac}$ (143.2)		$\text{Bu}_2\text{Ac}$ (171.3)
$\begin{array}{c} \text{O} \\ \parallel \\ \text{=NC} \\   \\ \text{C}_6\text{H}_4 \end{array}$		$\text{Et}_4\text{Phth}^e$ (276.4)		

<sup>a</sup> Source: Eastman Organic Chemicals, except as noted. <sup>b</sup> Hallcomid M-12, The C. P. Hall Co. <sup>c</sup> Prepared by W. H. Baldwin, ORNL. <sup>d</sup> *i* indicates isoalkyl. <sup>e</sup>  $\text{Et}_4\text{Phth}$ , m.p.  $\sim 39^\circ$ , is readily handled as a supercooled liquid at  $25^\circ$ . Its melting point is depressed below  $25^\circ$  by a relatively small water content.

to 10–30 in. of water. Twice, input amide inadvertently contained more than enough water for saturation when saturated with salt, and the effluent split into two phases. Each organic (lighter) phase so produced agreed well in both water and salt content with the corresponding organic phase obtained by the liquid–liquid distribution technique, providing a useful cross-check for both methods; however, such operation was generally avoided because of its excessively rapid consumption of the salt column.

**Analysis.** Sodium and potassium chloride were determined by counting  $^{24}\text{Na}$  and  $^{42}\text{K}$  in a well-type scintillation counter. Water was determined by Karl Fischer titration, precision around 1%. Chloride (for checks independent of the tracer metal analyses) was determined by Mohr titration, precision around 0.1%. Samples for chloride and water analyses and column-effluent samples for counting were weighed. Liquid–liquid distribution aqueous samples required dilution before counting and were measured on volume basis; the corresponding organic samples were counted directly, on either weight or volume basis. Phase densities required for subsequent calculations were measured with a 500- $\mu\text{l}$ . pipet as a pycnometer.

Amide solubilities in the water-rich phases were determined in separate equilibrations: a 25-ml. portion of an aqueous solution was agitated in the thermostat with consecutive increments of an amide until a visible amount remained undissolved. Much less than 0.01 ml. of excess amide was easily visible. (Direct Kjeldahl nitrogen determination gave inconsistent results in preliminary tests with some of the high-weight amides and was not pursued.)

**Materials.** The radioactive tracers were obtained from the Radioisotopes Division of ORNL:  $^{24}\text{Na}$  (15.0 hr. half-life), >99% purity,  $\sim 10$  curies/g. of Na, >1 mc./ml., and  $^{42}\text{K}$  (12.47 hr. half-life), >99% purity, >0.2 curie/g. of K, >1 mc./ml. Tracer-tagged solid NaCl or KCl was prepared by mixing normal salt and tracer in concentrated solution and then either evaporating the solution to dryness or precipitating the salt with ethanol and drying it. An aliquot of the mixed solution was withdrawn to check the final specific activity and also to obtain a decay curve for a check on the radiochemical purity.

NaCl, KCl, and  $\text{MgCl}_2 \cdot 6\text{H}_2\text{O}$  were reagent grade salts, stated to meet ACS specifications.

Most of the amides (Table I) were obtained from Eastman Organic Chemicals. They were used as received, after being tested for free acid or base. Dimethylauramide ( $\text{Me}_2\text{Lr}$ ) was prepared from Hallcomid M-12, which contains some homologs with longer and shorter acyl chains, by scrubbing to remove any component light enough to have significant solubility in water. Dipropyloctanamide ( $\text{Pr}_2\text{Oct}$ ) was prepared by W. H. Baldwin, ORNL Chemical Division, by reaction of dipropylamine with octanoic acid chloride.<sup>3</sup> After hydrolysis of any excess reactant and scrubbing to remove free acid or base, it was distilled at about 1 mm. pressure.

Diethylbenzene used to dilute the amide in some tests contained 5% *o*-, 61% *m*-, 28% *p*-diethylbenzene, 5% *sec*-butylbenzene, and 1% ethylisopropylbenzene.<sup>4</sup>

(3) L. M. Rice, *et al.*, *J. Am. Chem. Soc.*, **76**, 3730 (1954).

(4) C. A. Blake, *Anal. Chem.*, **35**, 1759 (1963).

## Results and Discussion

**Equilibrium Compositions.** The phase compositions (in terms of weight %) resulting from equilibrating amides with water and with saturated salt solutions are shown in Table II. The two amides of lowest equivalent weight, dipropylacetamide ( $\text{Pr}_2\text{Ac}$ ) (143) and tetraethylphthalamide ( $\text{Et}_4\text{Phth}$ ) ( $276/2 = 138$ ) were miscible in all proportions with water. All the amides showed miscibility gaps with saturated potassium chloride and sodium chloride solutions; several showed still wider miscibility gaps with saturated magnesium chloride solution, as expected from the lower water activity in the latter. However, dipropylacetamide became miscible in all proportions, and the miscibility gap between dibutylacetamide and water was narrowed instead of widened, when water was replaced by saturated magnesium chloride. This suggests that there is some interaction between this salt and these two amides. The distribution coefficient ( $D = M_{\text{MgCl}_2, \text{org}}/M_{\text{MgCl}_2, \text{aq}}$ ) of magnesium chloride from saturated aqueous solution to dibutylacetamide was about 0.3, in contrast with less than 0.001 to all of the heavier amides examined.

The miscibility gaps are markedly unsymmetrical when considered on a mole fraction basis. The most nearly symmetrical pair on a weight basis was diisopropylpropionamide-water ( $i\text{-Pr}_2\text{Pr}$ ), with about 6 wt. % of each in the other, but with mole fractions of 0.38 water in amide *vs.* only 0.007 amide in water. The solubility of water in the amides varied with both their molecular weight and their structure. The latter is striking in the set of 14-carbon isomers, where  $\text{Pr}_2\text{Oct}$  (with chain lengths 3,3,8) showed the lowest water content of all the water-amide systems tested, while  $\text{Me}_2\text{Lr}$  (1,1,12) showed the highest. The isomeric pairs  $\text{Pr}_2\text{Pr}$ - $i\text{-Pr}_2\text{Pr}$  and  $\text{Bu}_2\text{Pr}$ - $i\text{-Bu}_2\text{Pr}$  showed a smaller but interesting effect in that the shift from straight to branched alkyls decreased the water content in amide but increased the amide content in water.

The solubilities of water in amides are compared in Figure 1 by plotting the activity of water  $a_1$  *vs.* mole fraction. Pure water is taken as the reference state for both phases, so that  $a_1$  is the same in both phases at equilibrium. Values of  $a_1$  for the various (binary) salt solutions (Table III) were obtained from tabulations of Robinson and Stokes.<sup>5</sup> Since amide contents of the aqueous phases were very small, assumption of Raoult's law is reasonable and indicates very small decreases of  $a_1$  on saturation with the amide. The maximum effect, 0.007 mole fraction  $i\text{-Pr}_2\text{Pr}$  in water, indicating a decrease of  $a_1$  from 1 to 0.993, is barely

**Table II:** Equilibria of Amides with Water and with Saturated Salt Solutions

Amide	Salt <sup>a</sup>	Aqueous phase		Organic phase		$D(\text{salt})^b$
		Wt. % amide	Wt. % salt	Wt. % water	Wt. % salt	
$\text{Pr}_2\text{Ac}$	None	(Miscible)				
	KCl	1.1	26.1	16.8	0.86	$2.35 \times 10^{-2}$
	NaCl	0.4	26.3	11.2	0.42	$1.18 \times 10^{-2}$
	$\text{MgCl}_2$	(Miscible)				
$\text{Bu}_2\text{Ac}$	None	1.5		14.4		{ K $3.50 \times 10^{-2}$ Na $3.91 \times 10^{-3}$
	KCl	<0.05	26.4	6.88	0.027	$7.7 \times 10^{-4}$
	NaCl	<0.03	26.3	5.90	0.034	$9.7 \times 10^{-4}$
	$\text{MgCl}_2$	0.1	35.3	21.6	13.3	$2.9 \times 10^{-1}$
$\text{Pr}_2\text{Pr}$	None	5.2		9.5		{ K $2.46 \times 10^{-2}$ Na $2.12 \times 10^{-3}$
	KCl	0.2	26.3	5.12	0.012	$3.5 \times 10^{-4}$
	NaCl	0.15	26.4	4.04	0.007	$2.1 \times 10^{-4}$
	$\text{MgCl}_2$	0.2	35.3	1.46	0.04	$8 \times 10^{-4}$
$i\text{-Pr}_2\text{Pr}$	None	6		6.46		{ K $6.9 \times 10^{-4}$ Na $5.6 \times 10^{-4}$
	KCl	<0.5	26.3	3.92	0.008	$2.3 \times 10^{-4}$
	NaCl	<0.5	26.3	3.08	0.006	$1.7 \times 10^{-4}$
	$\text{MgCl}_2$	<0.5	35.3	1.12	0.04	$8 \times 10^{-4}$
$\text{Bu}_2\text{Pr}$	None	0.5		4.20		{ K $8.6 \times 10^{-5}$ Na $7.7 \times 10^{-5}$
	KCl	<0.1	26.4	2.82	0.002	$7.0 \times 10^{-5}$
	NaCl	<0.1	26.5	2.60	0.002	$6.1 \times 10^{-5}$
	$\text{MgCl}_2$	<0.1	35.3	0.88	<0.01	$<2 \times 10^{-4}$
$i\text{-Bu}_2\text{Pr}$	None	0.8		3.52		{ K $8.1 \times 10^{-5}$ Na $7.6 \times 10^{-5}$
	KCl	<0.1	26.4	2.58	0.002	$7.0 \times 10^{-5}$
	NaCl	<0.1	26.5	2.33	0.002	$5.1 \times 10^{-5}$
	$\text{MgCl}_2$	<0.1	35.3	0.78	<0.01	$<2 \times 10^{-4}$
$\text{Pr}_2\text{Oct}$	None	<0.1		2.35		{ K $7.1 \times 10^{-4}$ Na $6.4 \times 10^{-4}$
	KCl	<0.1	26.5	1.64	0.007	$1.97 \times 10^{-4}$
	NaCl	<0.1	26.5	1.51	0.007	$1.88 \times 10^{-4}$
$\text{Et}_2\text{Dec}$	None	<0.1		3.30		{ K $2.0 \times 10^{-3}$ Na $3.2 \times 10^{-2}$
	KCl	<0.1	26.5	2.20	0.007	$2.1 \times 10^{-4}$
	NaCl	<0.1	26.5	1.95	0.007	$1.9 \times 10^{-4}$
$\text{Me}_2\text{Lr}$	None	<0.5		17.4		{ K $2.5 \times 10^{-2}$ Na $3.0 \times 10^{-2}$
	KCl	<0.1	26.5	3.45	0.012	$3.5 \times 10^{-4}$
	NaCl	<0.1	26.5	2.50	0.011	$3.1 \times 10^{-4}$
$\text{Et}_4\text{Phth}$	None	(Miscible)				
	KCl	0.5				
	NaCl	0.3	26.3	8.0	0.05	$1.41 \times 10^{-1}$
	$\text{MgCl}_2$	0.8				

<sup>a</sup> Excess solid present in all saturated salt solutions. "None" indicates equilibration either with pure water or with water containing only radiotracer. <sup>b</sup> Distribution coefficient,  $D(\text{salt}) = [(\text{tracer count rate/ml.})_{\text{org}}/(\text{tracer count rate/ml.})_{\text{aq}}]$ .

visible at the scale of Figure 1. With the exception discussed above of increased miscibility and high salt content in  $\text{Bu}_2\text{Ac}$  with saturated  $\text{MgCl}_2$ , the salt contents of amide phases were so low that they are assumed to have no effect on the water activity-mole fraction relation. Hence, a single smooth curve is drawn through the set of points for each amide. These

(5) R. A. Robinson and R. H. Stokes, "Electrolyte Solutions," 2nd Ed., Academic Press, New York, N. Y., 1959, pp. 476, 510.

**Table III:** Solubilities of Salts in Amides Containing Limited Concentrations of Water

Amide	% water	G. of KCl/ kg. of soln.	% water	G. of NaCl/ kg. of soln.	
Pr <sub>2</sub> Ac	0.33	0.0067	0.48	0.0053	
	0.54	0.0072	0.75	0.0071	
	0.74	0.0091	1.08	0.0098	
	1.02	0.0128	1.40	0.0134	
	1.30	0.0168	1.52	0.0143	
	2.14	0.0394	2.13	0.0258	
	2.44	0.056	4.24	0.128	
	4.49	0.170	8.0	0.99	
	8.2	1.08	10.1	2.54	
	10.8	1.98			
Bu <sub>2</sub> Ac	0.12	0.0019	0.08	0.0014	
	0.54	0.0039	0.41	0.0018	
	0.66	0.0042	0.60	0.0023	
	0.68	0.0045	0.72	0.0024	
	1.17	0.0068	0.81	0.0025	
	1.21	0.0074	0.84	0.0027	
	1.65	0.0117	1.01	0.0030	
	1.93	0.0152	1.08	0.0039	
	4.26	0.079	1.64	0.0075	
	5.65	0.161	1.80	0.0081	
			2.78	0.0264	
			3.20	0.036	
			3.39	0.047	
Bu <sub>2</sub> Pr	0.37	0.0020	0.23	0.00055	
	0.64	0.0029	0.50	0.00078	
	0.92	0.0040	0.71	0.00109	
	1.00	0.0046	0.86	0.0014	
	1.83	0.0108	1.33	0.0039	
	2.22	0.0146	2.08	0.0108	
	<i>i</i> -Bu <sub>2</sub> Pr	0.31	0.0026	0.53	0.0014
		0.56	0.0037	0.63	0.0014
		0.73	0.0042	0.71	0.0015
		0.97	0.0056	0.75	0.0018
1.05		0.0061	0.98	0.0034	
1.29		0.0084	1.26	0.0043	
2.08		0.0173	2.03	0.0124	

constitute a strikingly consistent family of curves. Even more remarkable is the similarity of these curves, especially those for Bu<sub>2</sub>Pr, *i*-Bu<sub>2</sub>Pr, Et<sub>2</sub>Dec, and Pr<sub>2</sub>Oct, to the corresponding curves for the esters glycol diacetate and glycerol triacetate.<sup>2</sup>

**Salt Solubility.** The solubilities of sodium and potassium chloride in the various amides (Tables II and III) are compared in Figure 2. On the weight per cent basis, there is not much difference between the two salts. Over-all, in comparison with the total range covered, these solubilities fall along a rather narrow band, showing that as a first approximation the salt

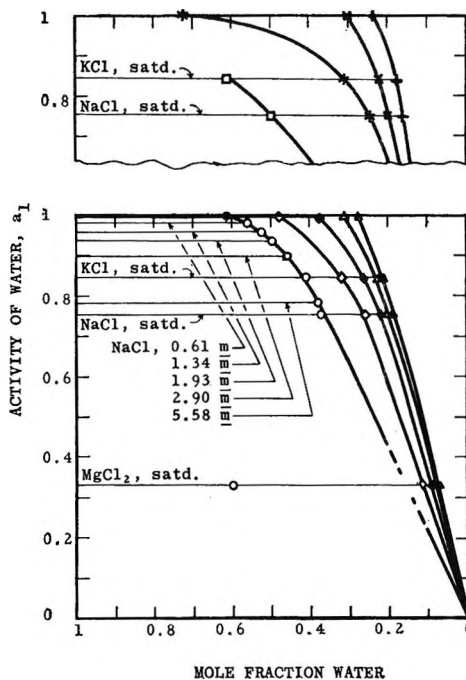


Figure 1. Activity of water in two-phase water-amide systems: □, dipropylacetamide (completely miscible with water and with saturated MgCl<sub>2</sub> soln.); O, dibutylacetamide; ◇, dipropylpropionamide; ◆, diisopropylpropionamide; Δ, dibutylpropionamide; ▲, diisobutylpropionamide; +, dipropyloctanamide; ×, diethyldecanamide; \*, dimethylauramide. For the Bu<sub>2</sub>Ac-MgCl<sub>2</sub> point, the mole fraction of water is calculated as  $m_{H_2O}/(m_{H_2O} + m_{Bu_2Ac} + 3m_{MgCl_2})$ . If MgCl<sub>2</sub> is assumed to exist as an ion cluster instead of dissociating, the mole fraction of water is higher, 0.70 instead of 0.60. For all other points the salt content is negligible.

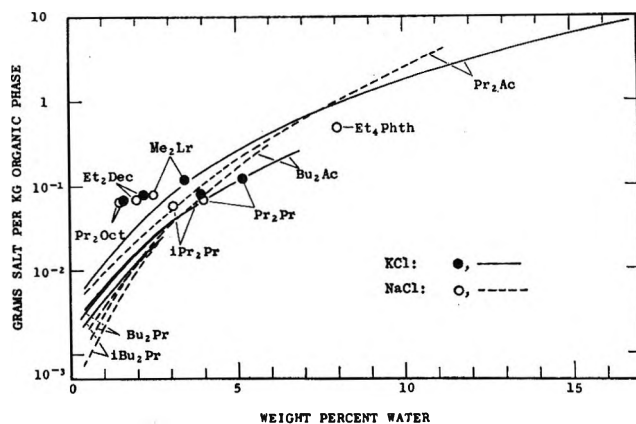


Figure 2. Solubilities of NaCl and KCl in amides containing water. Curves from data in Tables II and III.

solubility is essentially controlled by the amount of water present in the amide. Locally, they show some smaller but systematic trends. At a given water content, solubility is somewhat lower in the nearly symmetrical compounds than in the compounds with

longer acyl chains, and in the heavier compounds than in the lighter compounds of similar shape.

**Salt Activity Coefficients.** For evaluation of activity coefficients, concentrations in each phase will be expressed as  $m$  = moles of salt/kg. of water, even when water is only a minor component, and the activities in all phases will be referred to the same standard state as in pure aqueous salt solution. Thus, a salt's activity will be identical in all phases at equilibrium, and in particular its activity at saturation in any phase will be the same as its known activity at saturation in pure aqueous solution. Choice of this concentration scale and standard state, as previously used in ref. 2, provides a useful relation between activity coefficients and the selectivity for water over salt

$$\frac{\gamma_{\pm(o)}}{\gamma_{\pm}} = \frac{m}{m(o)} = \frac{D(\text{water})}{D(\text{salt})} \quad (1)$$

where  $D$  is the concentration distribution coefficient defined as

$$D(x) = \frac{\text{mass of } x/\text{volume of organic-rich phase}}{\text{mass of } x/\text{volume of aqueous-rich phase}}$$

$\gamma_{\pm}$  is the mean activity coefficient of the salt, and subscript (o) indicates the organic-rich phase. Equation 1 is an identity, since  $\gamma_{\pm(o)}m(o) = \gamma_{\pm}m = a_{\pm}$ , and

$$\frac{D(\text{water})}{D(\text{salt})} = \frac{\left\{ \frac{\text{kg. of water/l.}_{(o)}}{\text{kg. of water/l.}_{(aq)}} \right\} \left\{ \frac{\text{moles of salt}}{\text{kg. of water}} \right\}_{(aq)}}{\left\{ \frac{\text{moles of salt/l.}_{(o)}}{\text{moles of salt/l.}_{(aq)}} \right\} \left\{ \frac{\text{moles of salt}}{\text{kg. of water}} \right\}_{(o)}} = \frac{m}{m(o)}$$

The values of  $\gamma_{\pm}$  required for calculation of  $\gamma_{\pm(o)}$  were obtained, some by extrapolation, from Robinson and Stokes.<sup>5</sup> Activity coefficients of the salts were virtually the same in the water-rich phases as in pure aqueous solution; *i.e.*, they were not changed significantly by the presence of the small amounts of amide. The concentration of salts in solutions containing only tracers ranged from  $10^{-5}$  to  $5 \times 10^{-5}$   $m$  NaCl, corresponding to  $\gamma_{\pm} = 0.995 \pm 0.002$ , and  $10^{-4}$  to  $10^{-3}$   $m$  KCl, corresponding to  $\gamma_{\pm} = 0.98 \pm 0.01$ .

The activity coefficients obtained for sodium and potassium chlorides at saturation are shown in Figures 3 and 4, and for the salts present only as tracer, in Figure 5. The curves all reach maxima at around 0.5 to 1% water in the organic-rich phase. At lower water contents they decrease sharply, as required by the choice of  $m$  = moles of salt/kg. of water for the concentration scale. At higher water contents they

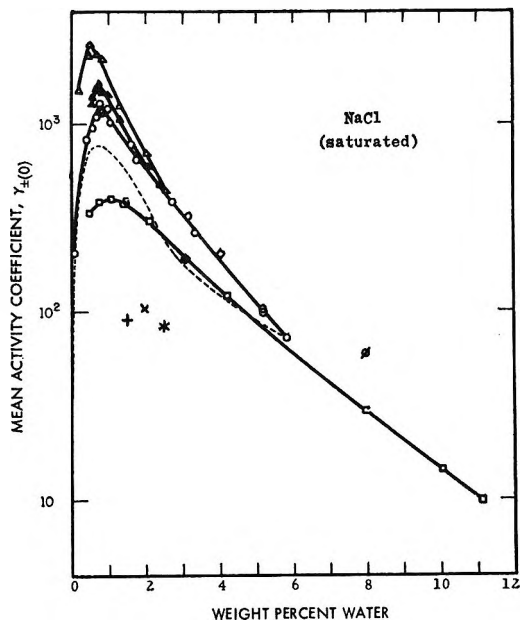


Figure 3. Variation of NaCl activity coefficients with water contents of amides; solutions saturated with NaCl; Bu<sub>2</sub>Ac-DEB curve from Figure 8, - - - -; □, dipropylacetamide; ○, dibutylacetamide; ◇, dipropylpropionamide; ◆, diisopropylpropionamide; Δ, dibutylpropionamide; ▲, diisobutylpropionamide; +, dipropyloctanamide; ×, diethyldecanamide; \*, dimethylauramide; ●, tetraethylphthalamide.

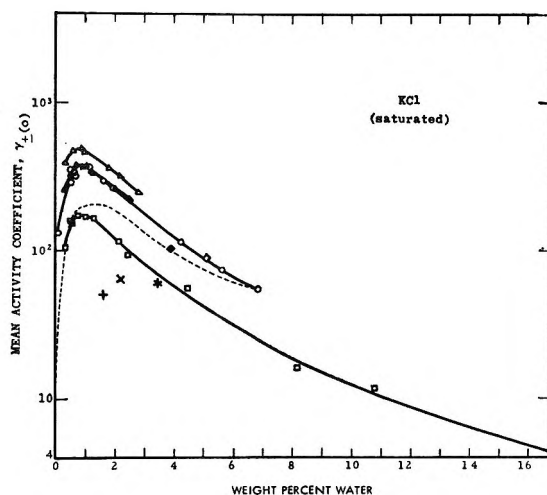


Figure 4. Variation of KCl activity coefficients with water contents of amides; solutions saturated with KCl; Bu<sub>2</sub>Ac-DEB curve from Figure 8, - - - -; □, dipropylacetamide; ○, dibutylacetamide; ◇, dipropylpropionamide; ◆, diisopropylpropionamide; Δ, dibutylpropionamide; ▲, diisobutylpropionamide; +, dipropyloctanamide; ×, diethyldecanamide; \*, dimethylauramide.

decrease more gradually, and with strikingly similar slopes as the per cent water increases. The close similarity of all the  $\gamma_{\pm(o)}$  vs. per cent water curves in shape,

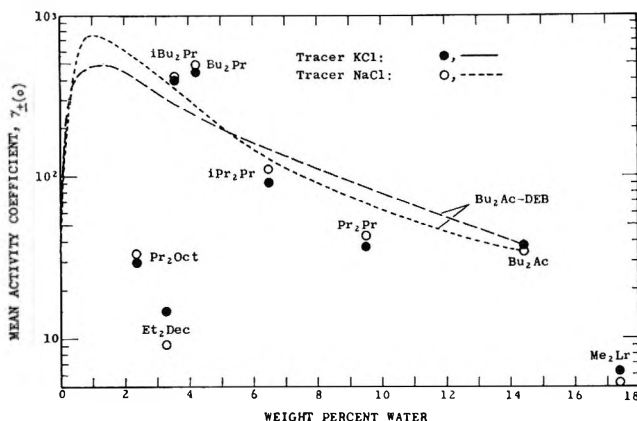


Figure 5. Variation of activity coefficients with water contents of amides equilibrated with water containing only tracer KCl or NaCl;  $Bu_2Ac-DEB$  curves from Figure 8.

and to a considerable extent in magnitude, suggests that the water content itself is the most important parameter controlling the activity coefficients of the salts. While there are smaller differences that appear to correlate consistently with choice of amide, salt, and aqueous concentration, there is a major, overriding dependence of  $\gamma_{\pm(o)}$  on the water content for both sodium and potassium chloride and for different amides. Moreover, these curves are strikingly similar to the curves reported by Kraus, Raridon, and Baldwin for glycol and glycerol acetates (Figures 3 and 4 in ref. 2). They noted the major importance of the water content in controlling the selectivity of distribution of salts to those esters. The present demonstration of the same kind of relation in the amide systems suggests that it may have considerable generality, and that the equilibrium organic-phase water content may prove to control salt solubility and water-salt selectivity in still more diverse systems.

Kraus, *et al.*, also showed useful correlation between  $\gamma_{\pm(o)}$  in the liquid esters and the salt-rejection performance of the related cellulose acetate hyperfiltration membranes. This suggests, by extension, that effective hyperfiltration membranes might be prepared from polyamides related to the liquid amides described here.

As noted above, within the over-all similarities there are smaller differences that appear to correlate consistently with sodium *vs.* potassium, with aqueous salt concentration, and with size and shape of the amides. Thus, the values of  $\gamma_{\pm(o)}$  are generally higher for sodium than for potassium chloride. However, if the ratio  $\gamma_{\pm(o)}/\gamma_{\pm}$  is plotted *vs.* water content, there is a crossover: The sodium values remain somewhat higher than the potassium values near the maxima at low water

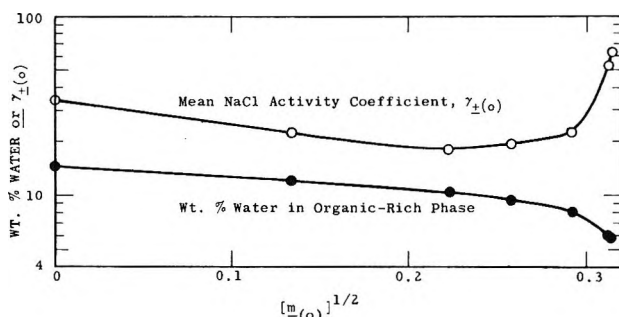


Figure 6. Effect of varying NaCl content on NaCl activity coefficient and water content in dibutylacetamide. The corresponding NaCl contents of the water-rich phases were: tracer only, 3.4, 7.4, 10.2, 14.5, 24.6, and 26.3 wt. %.

contents, but they drop below the potassium values at high water contents. The values of  $\gamma_{\pm(o)}$  at the maxima decrease in the order  $Bu_2Pr > i-Bu_2Pr > Bu_2Ac > Pr_2Ac$ . The points for the three amides with long acyl chains are noticeably lower than the points and curves for the more nearly symmetrical compounds. When the aqueous sodium chloride concentration was decreased from saturation (Figure 6),  $\gamma_{\pm(o)}$  decreased through a minimum that matches in position the minimum in  $\gamma_{\pm}$  *vs.* wt. % NaCl. The ratio  $\gamma_{\pm(o)}/\gamma_{\pm}$  plotted *vs.* water content would show a shallower minimum at the same position.

*Four-Component System.* The foregoing results show a rather closely similar variation of water-salt selectivity *vs.* water content at the widely differing saturation water contents obtained in the amides of differing molecular weights. Since increasing molecular weight can be looked upon as an increasing dilution of the amide groups with the hydrocarbon portions, it is of interest to compare the effect of actual dilution by a hydrocarbon with the effect of varying molecular weight (Table IV).

When dibutylacetamide was diluted with diethylbenzene, the solubility of water in the organic phase (Figure 7) dropped rapidly, and most rapidly with the first increments of the hydrocarbon diluent. The distribution of salts from aqueous to organic phase dropped even more rapidly, however, so that their activity coefficients in the organic phase,  $\gamma_{\pm(o)}$  as defined above, at first increased (Figure 8). They reached maxima in the organic mixtures that dissolved around 0.5 to 1% water, then dropped to the values found in the diethylbenzene alone. When these  $\gamma_{\pm(o)}$  curves are replotted against the water content, they are skewed sharply toward the zero-water side (dotted curves in Figures 3-5), closely similar both to the curves obtained at limited water contents and to the loci of points obtained at water saturation of the amides of

**Table IV:** Equilibria of Bu<sub>2</sub>Ac-Diethylbenzene Mixtures with Water and with Saturated Salt Solutions

Bu <sub>2</sub> Ac in Bu <sub>2</sub> Ac + DEB		Equilibrated with water <sup>a</sup>		Equilibrated with satd. KCl soln. <sup>b</sup>			Equilibrated with satd. NaCl soln. <sup>c</sup>		
Wt. %	Mole %	Wt. % water	D(salt) <sup>d</sup>	Wt. % water	Wt. % KCl	D(KCl)	Wt. % water	Wt. % NaCl	D(NaCl)
100	100	14.4	{ K 3.5 × 10 <sup>-3</sup> Na 3.9 × 10 <sup>-3</sup>	6.88	0.03	7.7 × 10 <sup>-4</sup>	5.90	0.034	9.7 × 10 <sup>-4</sup>
92.0	90.0	8.4		{ K 6.6 × 10 <sup>-4</sup> Na 8.4 × 10 <sup>-4</sup>	4.68	0.01	3.4 × 10 <sup>-4</sup>	3.80	0.01
84.9	81.5	5.2	{ K 2.8 × 10 <sup>-4</sup> Na 2.6 × 10 <sup>-4</sup>	3.34	0.006	1.68 × 10 <sup>-4</sup>	2.75	0.005	1.34 × 10 <sup>-4</sup>
75.1	69.5	3.34		{ K 1.00 × 10 <sup>-4</sup> Na 7.3 × 10 <sup>-5</sup>	2.21	0.003	7.2 × 10 <sup>-5</sup>	2.12	0.002
65.1	59.5	2.74	{ K 5.6 × 10 <sup>-5</sup> Na 4.3 × 10 <sup>-5</sup>	1.38	0.001	4.0 × 10 <sup>-5</sup>	1.33	<0.001	2.2 × 10 <sup>-5</sup>
51.9	45.8	1.05		{ K 1.9 × 10 <sup>-5</sup> Na 1.2 × 10 <sup>-5</sup>	0.72	<0.001	2.2 × 10 <sup>-5</sup>	0.65	<0.001
35.4	30.0	0.66	{ K 1.3 × 10 <sup>-5</sup> Na 8 × 10 <sup>-6</sup>	0.35	<0.001	2.1 × 10 <sup>-5</sup>	0.34	<0.001	6 × 10 <sup>-6</sup>
0	0	0.015		{ K 3 × 10 <sup>-6</sup> Na 4 × 10 <sup>-6</sup>	0.012	<0.001	1.0 × 10 <sup>-5</sup>	0.012	<0.001

<sup>a</sup> Aqueous phases: ≤1.5% wt. % Bu<sub>2</sub>Ac. Tracer potassium of sodium chloride present. <sup>b</sup> Aqueous phases: <0.05 wt. % Bu<sub>2</sub>Ac, ≥26 wt. % KCl. <sup>c</sup> Aqueous phases: <0.03 wt. % Bu<sub>2</sub>Ac, ≥26 wt. % NaCl. <sup>d</sup> Distribution coefficient,  $D(\text{salt}) = (\text{count rate/ml.})_{\text{org}} / (\text{count rate/ml.})_{\text{aq}}$ .

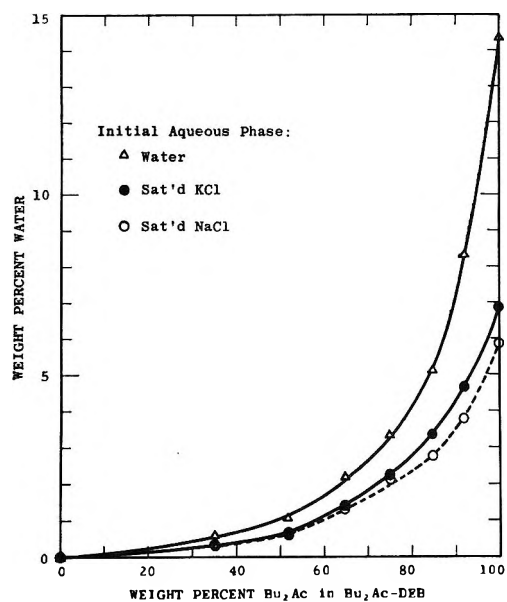


Figure 7. Variation of water content with dibutylacetamide content in dibutylacetamide-diethylbenzene mixtures. Solutions were equilibrated with saturated NaCl, saturated KCl, or water containing only tracer NaCl or KCl.

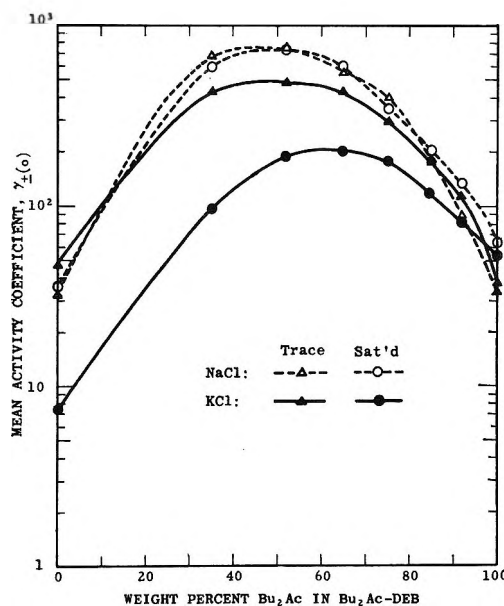


Figure 8. Variation of activity coefficients with dibutylacetamide content in dibutylacetamide-diethylbenzene mixtures. Solutions were equilibrated with saturated NaCl, saturated KCl, or water containing only tracer NaCl or KCl.

different molecular weights. Thus, the influence of the hydrocarbon diluent on  $\gamma_{\pm(o)}$ , like the influence of the variables examined in the three-component systems, also appears to occur primarily through its effect on the water content of the organic phase.

## Conclusions

Solubilities and activity coefficients of NaCl and KCl in a range of N,N-dialkylamides depend primarily on the water content of the organic phase, whether or not that water content is at saturation. Smaller dif-

ferences within the over-all similarities appear to correlate consistently with salt and with size and shape of amide.

Except where complete miscibility intervenes or where salt solubility is unusually great, the activity of water dissolved in amide varies with its mole fraction in a series of similar smooth curves.

In both of these aspects, these amides closely resemble the esters described by Kraus, Raridon, and Baldwin.<sup>2</sup> The remarkable similarity between the two different systems suggests that the water content may prove to be the major factor controlling salt

solubility and water-salt selectivity in still more diverse systems.

The similarity in water-salt selectivity of these amides to that of those esters<sup>2</sup> (which correlate well with cellulose acetate hyperfiltration membranes) suggests that effective hyperfiltration may also be obtainable with membranes based on related polyamides.

*Acknowledgment.* It is a pleasure to thank Dr. K. A. Kraus and Dr. G. Scatchard for helpful discussions, and Mr. F. A. Kappelmann and Mr. J. P. Eubanks for extensive technical assistance.

## Rate Constants of Some Reactions of H Atoms in Aqueous Solution

by Gil Navon and Gabriel Stein

*Department of Physical Chemistry, Hebrew University, Jerusalem, Israel (Received November 17, 1964)*

Using a variety of scavengers, the rate constants of the reactions of these with atomic hydrogen in aqueous solution are compared when H atoms are produced (a) in the gas phase by a high-frequency electrodeless discharge and introduced into the aqueous solution and (b) by irradiation of the aqueous solution with ionizing radiations. With the help of this comparison it is shown that the diffusion model proposed previously may be used for the calculation of the rate constants from experiments using the first method. The reaction of atomic hydrogen with nitrate and nitrite ions was investigated under various conditions and rate constants determined. Phosphate ions inhibit these reactions, probably through complex formation with atomic hydrogen. Hydroxyl ions catalyze them, probably through the formation of hydrated electrons.

### Introduction

Hydrogen atoms and solvated electrons have recently been recognized as two distinct reducing species interconverted in aqueous solutions by an acid-base equilibrium. They are of kinetic importance in many chemical reactions, of which those occurring in solutions irradiated with ionizing radiations or ultraviolet light have been specially investigated in the last few years. A large number of directly determined absolute rate constants have become known for the reactions of the solvated electron through the application of pulse

radiolysis techniques, which enable one to measure the transient absorption spectrum of the solvated electron itself.<sup>1,2</sup> This technique has not been applicable to investigations of the reactions of H atoms, which does not have a convenient optical absorption spectrum. In the absence of a specific detection technique in this case, the specific rates of reactions of H atoms have

(1) S. Gordon, E. J. Hart, M. S. Matheson, J. Rabani, and J. K. Thomas, *Discussions Faraday Soc.*, **36**, 193 (1963).

(2) J. H. Baxendale, *et al.*, *Nature*, **201**, 468 (1964).



been derived kinetically from measurements on the products of its reactions with various substrates.

A systematic correlation of such constants is of interest for our knowledge of elementary reaction mechanisms. However, both in radiation and in photochemistry, atomic hydrogen itself is not the major primary product, nor can it be obtained for such kinetic studies as the only reactive radical present. Therefore, it is of importance to have an independent method to measure rate constants of the reactions of H atoms. Such a method was developed using<sup>3,4</sup> an electrodeless high-frequency discharge in hydrogen gas, producing H atoms which are then introduced into the aqueous solution. This method has the advantage that other reactive species like the hydrated electron or hydroxyl radical are absent and H atoms are the primary products at all pH values. We have recently improved the accuracy of the experimental results obtainable by this method.<sup>5</sup> A method was developed to treat the results obtained applying diffusion kinetics, so that the rate constants could be derived.<sup>4</sup> In the present paper, we reconsider the theoretical treatment. By correlation with recently obtained rate constants of H-atom reactions with various substrates in solutions irradiated with ionizing radiations, it was found that the method of H-atom production used by us may be utilized to obtain rate constants of improved accuracy under varying experimental conditions. To widen the range of rate constants available, we investigated the action of H atoms on nitrate ions, which is a relatively slow one.<sup>6,7</sup>

## Experimental

The method of producing the hydrogen atoms and introducing them into the solution has been described in detail.<sup>3</sup> Briefly, hydrogen gas at 27 mm. pressure is pumped through an electrodeless discharge operated at 30 Mc.p.s., through the experimental solution (cooled to 4° to decrease evaporation), followed by a liquid air-cooled trap to retain volatile products. Control determinations are made in every case by carrying out runs without lighting the discharge. The dose rate of H atoms,  $A$ , was usually determined before and after every experimental run, using a  $10^{-3}$  M ferricyanide solution as the dosimeter,<sup>8</sup> and taking  $Y/A = 0.74$  for this system, where  $Y$  is the reduction yield per second of the product(s).

**Analysis.** Nitrite ion was determined according to the method of Shin,<sup>9</sup> by coupling the diazonium salt of sulfanilamide with *N*-(1-naphthyl) ethylenediamine dihydrochloride. We found this method accurate, obtaining a reproducibility of about  $\pm 1\%$ . Problems were encountered in the determination of nitrate ion.

We finally adopted a modification of the method given by Hagino.<sup>10</sup> This consists of the reduction of nitrate to nitrite by strong shaking of 10 ml. of test solution and 1 ml. of 5 M  $\text{NH}_3$  solution with about 0.2 g. of Zn dust for 4 min. After decantation, 1 to 2 ml. is taken, and the nitrite is determined as above. The yield of the reduction varies between 85 and 95% of the theoretical value in the different solutions. However, the accuracy of the determination did consistently reach  $\pm 3\%$  if a blank solution and the test solution

**Table I:** Reduction of Nitrate Ion in Neutral and Acid Solutions

Initial concn., $M$	pH	Dose rate $\times 10^4$ , mole l. <sup>-1</sup> min. <sup>-1</sup>	Time of reaction, min.	% re- duction	$Y/A$	$k \times 10^{-7}$ , l. mole <sup>-1</sup> sec. <sup>-1</sup>
$10^{-2}$	7	2.84	10	4.1	0.143	0.91
$10^{-2}$	7	2.43	15	3.9	0.108	0.60
$10^{-3}$	7	2.34	10	4.6	0.020	0.92
$10^{-3}$	7	3.28	7	5.2	0.023	1.31
Average $k = 0.93 \times 10$						
$10^{-3}$	4.7	2.67	6	2.5	0.018	0.91
$10^{-3}$	2.0	2.20	6	4	0.030	1.34
$10^{-3}$	1.1	2.74	6	4	0.028	1.20

**Table II:** The Reduction of  $10^{-3}$  M Nitrate in Basic Solutions

$[\text{OH}^-]$ , $M$	Dose rate $\times 10^4$ , mole l. <sup>-1</sup> min. <sup>-1</sup>	Time of reaction, min.	% re- duction	$Y/A$	$k_0[S]$ $\times 10^{-4}$	$k \times 10^{-6}$
0.004	1.22	6.75	7.3	0.089	2.8	4.7
0.01	2.84	5.0	15.3	0.108	6.6	5.8
0.01	3.06	5.5	18.0	0.107	6.8	6.0
0.02	0.82	7.5	16.3	0.264	8.7	3.9
0.05	0.95	5.0	11.0	0.232	8.3	1.5
0.12	2.39	5.0	43.1	0.361	28.0	2.3
0.12	0.76	5.0	27.0	0.713	48.4	4.0
0.20	2.76	5.0	63.5	0.460	45.5	2.25
Average $k = 3.8 \times 10^6$						

(3) G. Czapski and G. Stein, *J. Phys. Chem.*, **63**, 850 (1959).

(4) G. Czapski, J. Jortner and G. Stein, *ibid.*, **65**, 956 (1961).

(5) G. Navon and G. Stein, *Israel J. Chem.*, **2**, 151 (1964).

(6) S. Nehari and J. Rabani, *J. Phys. Chem.*, **67**, 1609 (1963).

(7) A. Appleby, G. Scholes, and M. Simic, *J. Am. Chem. Soc.*, **85**, 3891 (1963).

(8) G. Czapski and G. Stein, *J. Phys. Chem.*, **64**, 219 (1960).

(9) M. B. Shin, *Ind. Eng. Chem., Anal. Ed.*, **13**, 33 (1941).

(10) K. Hagino, *Nippon Kagaku Zasshi*, **82**, 841 (1961); *Chem. Abstr.*, **55**, 26861 (1961).

Table III: Comparison of Rate Constants

Reactant	$k_s(D^{1/2}\varphi/k_r)^{2/3}$	$k_{rad}^b$	$(D^{1/2}\varphi/k_r)^{2/3} \times 10^{11}$	$k_{diff. calcd. using mean value}$
Co(NH <sub>3</sub> ) <sub>6</sub> <sup>2+</sup>	$3.6 \times 10^{-10c}$	$1.4 \times 10^{10d}$	2.6	$1.8 \times 10^6$
ClCH <sub>2</sub> COO <sup>-</sup>	$9.6 \times 10^{-10e}$	$1.9 \times 10^{10f}$	5.1	$4.8 \times 10^6$
NO <sub>3</sub> <sup>-</sup>	$1.85 \times 10^{-10g}$	$1.5 \times 10^{10h}$	1.2	$0.9 \times 10^7$
Fe <sup>2+</sup>	$5.55 \times 10^{-10i}$	$1.7 \times 10^{10j}$	3.3	$2.8 \times 10^7$
OH <sup>-</sup>	$4.4 \times 10^{-10k}$	$2.4 \times 10^{10l}$	(1.9)	$2.2 \times 10^7$
H <sub>2</sub> O <sub>2</sub>	$1.5 \times 10^{-10m}$	$5.4 \times 10^{10n}$	2.8	$7.5 \times 10^7$
HCOO <sup>-</sup>	$(2.5) \times 10^{-10o}$	$2.0 \times 10^{10p}$	(1.3)	$1.2 \times 10^8$
NO <sub>2</sub> <sup>-</sup>	$1.5 \times 10^{-10q}$	$8.7 \times 10^{10r}$	1.7	$7.5 \times 10^8$
FeCl <sub>2</sub> <sup>+</sup>	$(9.6) \times 10^{-10s}$	$4.6 \times 10^{10t}$	(2.6)	$4.8 \times 10^8$
Fe(CN) <sub>6</sub> <sup>3-</sup>	$3 \times 10^{-10u}$	$4.0 \times 10^{10v}$	0.75	$1.5 \times 10^9$
Fe(Cytochrome-C)	$4.8 \times 10^{-10w}$	$1.0 \times 10^{10z}$	(0.37)	$2.4 \times 10^9$
Mean value: $2.1 \times 10^{-11}$				

<sup>a</sup> Calculated as  $(A/6W)^{2/3}/[Sr]$ , see eq. 10 in text. <sup>b</sup> The absolute values were calculated assuming a value of  $k(H + O_2) = 2.0 \times 10^{10}$  l. mole<sup>-1</sup> sec.<sup>-1</sup> which is based upon the value  $k(H + Fe^{2+}) = 1.7 \times 10^7$  l. mole<sup>-1</sup> sec.<sup>-1</sup> of Schwarz (ref. 16) and the constant ratio  $k(H + O_2)/k(H + Fe^{2+}) = 1200$  (W. G. Rothschild and A. O. Allen, *Radiation Res.*, **8**, 101 (1958)). The values of ref. 7 are taken assuming  $k(H + Fe(CN)_6^{3-}) = 4.0 \times 10^9$ . This choice gives the best fit with the data of other authors. <sup>c</sup> G. Navon and G. Stein, *J. Phys. Chem.*, **69**, 1390 (1965). <sup>d</sup> D. Meyerstein, personal communication. <sup>e</sup> J. Jortner and J. Rabani, *J. Phys. Chem.*, **66**, 2078 (1962). <sup>f</sup> See ref. 7. <sup>g</sup> The present work. <sup>h</sup> The value of  $1.0 \times 10^7$  l. mole<sup>-1</sup> sec.<sup>-1</sup> can be calculated from the ratio in ref. 6,  $k(H + NO_3^-)/(H + CH_3COO^-) = 25$ , together with  $k(H + NO_2^-)$  and the ratio  $k(H + NO_2^-)/k(H + CH_3COO^-) = 2200$ , J. Rabani and G. Stein, *J. Chem. Phys.*, **37**, 1865 (1962). The value of  $2.2 \times 10^{10}$  may be calculated from ref. 7, see footnote b above. <sup>i</sup> G. Czapski,

J. Jortner, and G. Stein, *J. Phys. Chem.*, **65**, 960 (1961). <sup>j</sup> See ref. 16. Following Allen<sup>16</sup> the value adopted is the value for the short lifetime of FeH<sup>2+</sup> approximation. <sup>k</sup> In ref. 17 the ratio  $k(H + OH^-)/k(H + ClCH_2COO^-) = 4.5$  was measured. Recalculated by our method, the result given in the table is obtained. <sup>l</sup> From  $k(H + HCOO^-)/k(H + OH^-) = 11$  and  $k(H + OH^-)/k(H + CH_3COO^-) = 60$ , ref. 5. Cf. J. Rabani and M. S. Matheson, *Radiation Res. Suppl.*, **4**, 1 (1964), who give  $1.5-2.3 \times 10^7$  l. mole<sup>-1</sup> sec.<sup>-1</sup>. <sup>m</sup> G. Czapski, J. Jortner, and G. Stein, *J. Phys. Chem.*, **65**, 964 (1961). <sup>n</sup> The geometrical mean of  $4.4 \times 10^7$  l. mole<sup>-1</sup> sec.<sup>-1</sup> (calculated from the ratio  $k(H + O_2)/k(H + H_2O_2) = 450$  given by C. J. Hochanadel, *Radiation Res.*, **17**, 286 (1962)) and  $6.7 \times 10^7$  l. mole<sup>-1</sup> sec.<sup>-1</sup> calculated from the value of 300 given for the above ratio by J. K. Thomas, ref. 17. In both cases, a rate constant of  $k(H + O_2) = 2.0 \times 10^{10}$  was assumed (see footnote b). <sup>o</sup> G. Czapski, J. Rabani, and G. Stein, *Trans. Faraday Soc.*, **58**, 2160 (1962). They found the ratio  $k(H + Fe(CN)_6^{3-})/k(H + HCOO^-) = 12$ . <sup>p</sup> The geometrical mean of  $2.6 \times 10^8$  (from the ratio  $k(H + HCOO^-)/k(H + O_2) = 0.013$  calculated by J. Rabani, *J. Phys. Chem.*, **66**, 361 (1962), from the results of E. J. Hart, *J. Am. Chem. Soc.*, **76**, 4312 (1954)), and  $1.5 \times 10^8$  ref. 7 (see footnote c). <sup>q</sup> J. Jortner, E. Hayon, G. Navon, and J. Rabani, unpublished results. <sup>r</sup> From  $k(H + Fe(CN)_6^{3-})/k(H + NO_2^-) = 4.6$  (J. Rabani and G. Stein, *J. Chem. Phys.*, **37**, 1865 (1962)). <sup>s</sup> G. Navon and G. Stein, to be published. <sup>t</sup> Derived from  $k(H + FeCl_2^+)/k(H + O_2) = 2.3$  (H. A. Schwarz, *J. Am. Chem. Soc.*, **79**, 534 (1957); H. A. Schwarz and J. M. Hritz, *ibid.*, **80**, 5636 (1958)). <sup>u</sup> See footnote s. <sup>v</sup> From the value of  $k(H + O_2)/k(H + Fe(CN)_6^{3-}) = 5$  given by J. Rabani, *J. Phys. Chem.*, **66**, 361 (1962). <sup>w</sup> G. Czapski, N. Frohwirth, and G. Stein, to be published. <sup>x</sup> From the value of  $k(H + Fe(CytC))/k(H + CHOO^-) = 50$  given by J. Rabani and G. Stein, *Radiation Res.*, **17**, 327 (1962).

were analyzed in parallel. Chloride and bromide were found not to interfere with this determination, even at high concentrations. Iodide interferes seriously. So does phosphate, but in this case, improved results could be obtained if the time of shaking was reduced to 2 min.

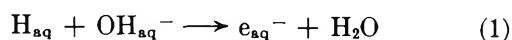
All materials used were analytical grade; the water used was triply distilled.

## Results

*Reaction of H Atoms with Nitrate and Nitrite Ions.* To extend the range of reactions investigated by the present method, the rate constants of the reaction of H atoms were determined with nitrate ions at neutral and acid pH values and with nitrite in neutral solutions. For nitrate ions the reaction results in the formation of NO<sub>2</sub> and subsequently from this by hydrolysis, of nitrite. The reaction was followed by the determination of nitrate in the solution. Allowance was made for the slight decrease in nitrate concentration observed in the control experiments without discharge, due to

nitrate being carried off by the gas stream. As the analysis for nitrate is not very accurate, triplicate determinations were carried out. The results are shown in Tables I and II and the final result is incorporated in Table III. Similarly, we reinvestigated the action of H atoms on nitrite ion, which was previously examined in this laboratory by Hayon, Jortner, Navon, and Rabani some years ago, but remained unpublished. Our result, with better reproducibility, agreed very well with the results obtained by Hayon, *et al.*, and is included in Table III.

We also examined the reaction of H atoms with nitrate and nitrite ions in alkaline solutions. For nitrate in alkaline solution, the extent of reduction is increased over that in acid or neutral solutions, and increases with OH<sup>-</sup> concentration. We assume that this is due to the formation of solvated electrons according to



Increased reaction yields are then expected since

solvated electrons react much faster with nitrate ions<sup>1,2</sup> than do H atoms ( $k_e + \text{NO}_3^- \sim 1 \times 10^{10}$ ). Similarly, in the case of nitrite ions, we reinvestigated the reaction in alkaline solution, which was previously examined by Hayon, *et al.*

In both cases, the rate constant of the reaction between  $\text{OH}^-$  ions and H atoms can be calculated as follows. The term  $k_s[\text{S}]$ , where  $k_s$  is the rate constant of the reaction of H atoms with the scavenger and  $[\text{S}]$  is the scavenger concentration, appears in calculations when systems containing one scavenger only are considered. In the case of more than one scavenger being present, we now take this expression to represent the sum of all parallel processes.  $Y$  represents the total reduction yield of nitrate or nitrite, respectively, due to all competing processes. Assuming that every hydrated electron produced reduces one nitrate or nitrite ion, the yield  $Y$  is the sum of reduction by H atoms and of the yield of solvated electrons

$$k_s[\text{S}] = k_{\text{H} + \text{NO}_3^-}[\text{NO}_3^-] + k_{\text{H} + \text{OH}^-}[\text{OH}^-] \quad (2)$$

Inserting the appropriate rate constants for the reaction of H atoms with nitrate and nitrite, we obtained for  $k_{\text{H} + \text{OH}^-}$  the value of  $3.8 \times 10^6$  l. mole<sup>-1</sup> sec.<sup>-1</sup> from experiments with nitrate, and the value of  $3.6 \times 10^6$  l. mole<sup>-1</sup> sec.<sup>-1</sup> from experiments with nitrite, this latter in good agreement with the value previously obtained by Hayon, *et al.* Both of these values are lower than the value of  $2.2 \times 10^7$  l. mole<sup>-1</sup> sec.<sup>-1</sup> derived previously using the chloroacetic acid system<sup>11</sup> in a similar manner. We retain the higher value in Table III, since for competition experiments of this kind, the higher concentration of scavenger that can be used with chloroacetic acid allows experimental conditions which ensure that the necessary approximations in deriving the equation will hold, such as that all hydrated electrons produced will react with the scavenger but will not recombine or react with H atoms. The higher value agrees also with the results obtained in radiation chemistry (see note 1 to Table III).

*The Effect of Added Phosphate.* In alkaline solutions containing either nitrate or nitrite, the effect of added phosphate present as  $\text{HPO}_4^{2-}$  and  $\text{PO}_4^{3-}$  ions, was investigated. The results are shown in Table IV, and indicate an inhibition of the reduction processes. Similar observations were made by us (to be published) in the case of oxidation of iodide and bromide ion by atomic hydrogen and by Shirom and Stein (to be published) in a photochemical system, where solvated electrons and H atoms were formed in aqueous solutions of ferrocyanide. The effect of these higher concentrations of phosphate may be due to the formation

of a complex between H atoms and phosphate ions. This effect will be discussed in detail in connection with these more detailed examinations. The expression in Table IV for  $k(\text{inhib.})$  is not intended to suggest a mechanism but serves merely to give a quantitative form to our experimental results.

*Calculation of Rate Constants.* Czapski, Jortner, and Stein<sup>4</sup> developed and compared the calculation of H-atom rate constants using this experimental method, assuming three models: homogeneous, diffusion, and forced convection. We now conclude that of these, the diffusion model is the most appropriate for the following reasons.

Consider the limiting case applicable for low solute concentration. Then the steady-state concentration of the hydrogen atoms is determined by their recombination. The solution of the diffusion equation (eq. 9 and 13 of ref. 4)

$$(\partial H / \partial t)_{\text{transport}} = D(\partial^2 H / \partial X^2) = k_r[\text{H}]^2 \quad (3)$$

is<sup>12</sup>

$$[\text{H}]^{-1/2} = [\text{H}]_0^{-1/2} + (k_r/6D)^{1/2} X \quad (4)$$

where (eq. 15 in ref. 4)

$$[\text{H}]_0 = (3A^2/2k_r D \varphi^2)^{1/3} \quad (5)$$

with the notation as in ref. 4.

Using the value of  $k_r = 3 \times 10^{13}$  mole<sup>-1</sup> cm.<sup>3</sup> sec.<sup>-1</sup> for the rate constant of the recombination of H atoms,  $D = 6 \times 10^{-5}$  cm.<sup>2</sup> sec.<sup>-1</sup> for the diffusion coefficient of atomic hydrogen, setting  $A = 10^{-7}$  mole sec.<sup>-1</sup> for the dose rate, and  $\varphi = 1$  cm.<sup>2</sup> for the average effective surface area for the diffusion of H atoms (this value will be derived later), one obtains  $H_0 = 3 \times 10^{-8}$  mole cm.<sup>-3</sup> and for the distance from the surface at which the concentration of atomic hydrogen reduces to  $H_0/2$

$$X_{1/2} = ([\text{H}]^{-1/2} - [\text{H}]_0^{-1/2})(6D/k_r)^{1/2} = 1.4 \times 10^{-5} \text{ cm.} \quad (6)$$

In the presence of a scavenger,  $X_{1/2}$  will be even lower. Thus the reaction is accomplished within a very thin layer with a thickness of the order of  $10^{-5}$  cm. Therefore, neither the homogeneous model nor the forced convection model is adequate for our method, the first because only a very small portion of the total volume is used for the reaction, the second because in such a thin layer, effects due to forced convection must be negligible. As we shall see, however, the diffusion

(11) J. Jortner and J. Rabani, *J. Phys. Chem.*, **66**, 2078, 2081 (1962).

(12) The corresponding equation in ref. 4 (eq. 14) is erroneous.

**Table IV:** Effect of Phosphate upon the Reduction of Nitrate and Nitrite (in all experiments  $[\text{OH}^-] = 0.02 \text{ M}$ )

Salts present	Dose rate $\times 10^4$ , mole l. <sup>-1</sup> min. <sup>-1</sup>	Time, min.	% reduction	Y/A	$k_s[\text{S}]$	$k(\text{inhib.})^a$
$10^{-3} \text{ M KNO}_3$	2.2	7	6.3	0.078	$3.83 \times 10^4$	$1.2 \times 10^6$
$0.8 \text{ M K}_2\text{HPO}_4$						
$0.4 \text{ M NaOH}$						
$10^{-3} \text{ M KNO}_2$	0.82	7.5	16.3	0.264	$8.7 \times 10^4$	
$0.02 \text{ M NaOH}$						
$1.24 \times 10^{-4} \text{ M KNO}_2$	2.33	1	39	0.202	$1.26 \times 10^6$	
$0.02 \text{ M NaOH}$						
$1.24 \times 10^{-4} \text{ M KNO}_2$	2.32	1	33	0.180	$1.05 \times 10^6$	
$0.16 \text{ M K}_2\text{HPO}_4$						
$0.08 \text{ M NaOH}$						
$1.24 \times 10^{-4} \text{ M KNO}_2$	2.44	1	15.5	0.0785	$0.41 \times 10^6$	$2.1 \times 10^6$
$0.8 \text{ M K}_2\text{HPO}_4$						
$0.4 \text{ M NaOH}$						

<sup>a</sup>  $k(\text{inhib.}) = \Delta(k_s[\text{S}])/C(\text{phosphate})$ .

model yields useful rate constants. Using eq. 21, 23, 24, and 25 of ref. 4

$$Y = k_s[\text{S}] \int [\text{H}] dv \quad (7)$$

$$Y/A = \Delta/W \quad (8)$$

$$W = 2\Delta^3 + 3\Delta^2 + \Delta \quad (9)$$

$$W = k_r A / \{6(k_s[\text{S}])^{1/2} D^{1/2} \varphi\} \quad (10)$$

After determining  $Y/A$ , the ratio of the reduction yield rate to the dose rate of H atoms, we can calculate the quantity  $W$  from which  $k_s$ , the rate constant of the reaction of H atoms with the substrate may be calculated through eq. 10. This calculation involves the use of the constants  $A$ , dose rate of H atoms,  $D$ , diffusion constant of H atoms,  $k_r$ , rate constant of recombination of H atoms, and  $\varphi$ , surface area effective for the diffusion of H atoms into the system from the gas phase. This last is a specific constant depending on the experimental conditions in our apparatus, which we were unable to determine accurately. Therefore, we were faced with the problem of deriving a reliable value for this parameter.

Recently, absolute rate constants have been obtained for the reactions of atomic hydrogen using high-intensity pulsed electron beam irradiation techniques, and conversion of solvated electrons to H atoms, *e.g.*, by reaction with  $\text{H}^+$ .<sup>13,14</sup> This method suffers from the disadvantage that the formation of H atoms is indirect, and that H atoms are not the only reactive intermediate. However, in those cases where the method is applicable, absolute rate constants can be calculated. It will be seen that a systematic comparison of these rate constants with those obtained in the present

method enable us to derive rate constants from our measurements.

In Table III, the rate constants of some reactions of H atoms, determined with techniques of radiation chemistry, are given. These rate constants were obtained at room temperature. Many of them are derived from comparison of the ratios of reaction velocities in competition experiments. With these limitations, they are accurate probably within a factor of two. As the basis for the calculation of the data in Table III, we accepted, following Allen,<sup>15</sup> as the most reliable rate constant the value given by Schwarz<sup>16</sup> of  $1.7 \times 10^7$  l. mole<sup>-1</sup> sec.<sup>-1</sup> for the reaction  $\text{H} + \text{Fe}^{2+}$ . The independent measurements<sup>17</sup> of the absolute rate constant for the reaction of H atoms with  $\text{O}_2$  and  $\text{H}_2\text{O}_2$  are in agreement then with the values calculated in this manner. It will be seen that the known rate constants cover a range extending over four orders of magnitude, from  $10^6$  to  $10^{10}$  l. mole<sup>-1</sup> sec.<sup>-1</sup>.

Incorporating the experimental results in the present and in the following paper, the same range is now covered using the technique of H-atom production employed by us, and the results are also shown in Table III. The values of  $k_s(D^{1/2}\varphi/k_r)^{2/3}$  recorded in the first column of Table III are experimental values calculated using eq. 8–10 and the measured values of  $Y$  and  $A$ . These values were found to be proportional

(13) H. A. Schwarz, *Radiation Res. Suppl.*, **4**, 89 (1964).

(14) H. Fricke and J. K. Thomas, *ibid.*, **4**, 34 (1964).

(15) A. O. Allen, *ibid.*, **4**, 54 (1964).

(16) H. A. Schwarz, *J. Phys. Chem.*, **67**, 2827 (1963).

(17) (a) J. K. Thomas, *ibid.*, **67**, 2593 (1963); (b) J. P. Sweet and J. K. Thomas, *ibid.*, **68**, 1363 (1964).

to the rate constants  $k_{\text{rad}}$  taken from radiation chemistry.

It will be seen that using an average value of the proportionality constant,  $(D^{1/2}\varphi/k_r)^{2/3} = 2.1 \times 10^{-11}$ , in order to calculate  $k_{\text{diff}}$  for the experimental results, the deviation between  $k_{\text{diff}}$  and  $k_{\text{rad}}$  is usually less than a factor of two over the entire range of four orders of magnitude.

Let us now examine if this empirical value of  $(D^{1/2}\varphi/k_r)^{2/3}$  is in accord with the diffusion model.

Following Schwarz,<sup>16</sup> we take  $D = 6 \times 10^{-5}$  cm.<sup>2</sup> sec.<sup>-1</sup>,  $k_r = 3 \times 10^{13}$  mole<sup>-1</sup> cm.<sup>3</sup> sec.<sup>-1</sup> and assume an average activation energy of 5 kcal. for all reactions in Table III. This last introduces a factor of approximately two when one passes from our experimental temperature of 4° to room temperature, of the radiation chemistry experiments. We thus obtain a value of  $\varphi = 1$  cm.<sup>2</sup> for the surface area. This is very reasonable indeed and corresponds approximately to the surface area of one bubble. In our experiments one bubble enters the solution at a time.

It should be noted that even if the diffusion model is valid, a deviation between  $k_{\text{rad}}$  and  $k_{\text{diff}}$  calculated by the present method is expected because (1) the activation energy might change from one reaction to the other probably in the direction of lower activation energy for faster reaction, and (2) depletion of the reactant [S] from the surface exposed to the action of the H atoms. This must be more important for faster reactions where lower concentrations are used. However, the good correlation indicates that these two factors do

not cause a large resulting effect in our system. Perhaps, as they have an opposite effect on the measured rate constant they tend to cancel one another. We remark that we carried out a series of experiments using the reduction of ferricyanide by H atoms, over a range of over 100-fold change of initial concentration, and found no appreciable change in the rate constant derived as discussed above. This indicates that depletion does not play a very pronounced role. Thus, the present method may be used for the determination of rate constants. The present result supports the adequacy of the diffusion model.

The error in rate constant derived in our instrument is greater than the error in the measurements of rate constant ratios in radiation chemistry. However, it approaches in accuracy the direct determination of absolute rate constants and the determination of absolute rate constants by means of several consecutive ratios by means of radiation experiments. Taking into account these limitations, the agreement between our technique and radiation chemistry is satisfactory and permits us now to take advantage of this method.

In particular, advantage may be taken of the wide pH range over which in the present technique H atoms are the only primary intermediate available for chemical reaction.

*Acknowledgment.* We wish to thank Dr. G. Czapski for valuable discussions. This research was supported in part by the U. S. Atomic Energy Commission Biology Division.

## Electron Transfer between Atomic Hydrogen and Cobalt(III)

### Complexes in Aqueous Solution

by Gil Navon and Gabriel Stein

*Department of Physical Chemistry, Hebrew University, Jerusalem, Israel (Received November 17, 1964)*

The reaction of atomic hydrogen, produced by an electrodeless high-frequency discharge, with some complex ions of the type  $\text{Co}^{\text{III}}(\text{NH}_3)_5\text{X}$  was studied in aqueous solutions. The rate constants for the reduction of the complex ions with  $\text{X} = \text{NH}_3, \text{H}_2\text{O}, \text{OH}^-, \text{F}^-, \text{Cl}^-, \text{Br}^-,$  and  $\text{I}^-$  were found to be  $k_s = 1.85 \times 10^6, 4.5 \times 10^5, 3.1 \times 10^7, 1.1 \times 10^6, 7.3 \times 10^7, 4.6 \times 10^8,$  and  $3.3 \times 10^9$  l. mole<sup>-1</sup> sec.<sup>-1</sup>, respectively. Through comparison between the rates of these reactions and the rates of other known analogous reactions, probable mechanisms are proposed. Assuming the validity of Marcus' electron-transfer reaction theory, the  $\text{H}-\text{H}_{\text{aq}}^+$  isotopic exchange rate was estimated.

#### Introduction

Atomic hydrogen is known to act both as a reducing agent giving  $\text{H}_{\text{aq}}^+$  and as an oxidizing agent, acting either by hydrogen abstraction from organic molecules or together with  $\text{H}_{\text{aq}}^+$  to give the  $\text{H}_2$  molecule.<sup>1</sup> Baxendale<sup>2</sup> calculated for atomic hydrogen an oxidation reduction potential of +2.1 v. for the couple  $\text{H} \rightarrow \text{H}_{\text{aq}}^+ + e_{\text{aq}}^-$  (thus acting as a reducing agent) and -2.1 v. for the couple  $\text{H}_2 \rightarrow \text{H} + \text{H}_{\text{aq}}^+ + e_{\text{aq}}^-$  in acid solution of  $a_{\text{H}^+} = 1 M$ .

These recent developments encourage one to apply to atomic hydrogen the theory of oxidation-reduction reactions.

The mechanisms of electron-transfer reactions were recently elucidated by a number of workers both experimentally and theoretically.<sup>3</sup> Some of the best investigated electron-transfer reactions are the reductions of cobalt(III) complexes by various reducing agents. These complexes are very convenient for such investigations having a well-defined structure, being relatively inert to substitution.

In this work we shall attempt to compare the reducing ability of hydrogen atoms with other reducing agents. This comparison is of interest because hydrogen atoms are unique among the reducing agents, having the simplest structure, small size, absence of charge, and consequently also no strongly bound hydration shell.

The measurement of rate constants of atomic hy-

drogen is conveniently accomplished by the quantitative technique developed in this department<sup>4</sup> using atomic hydrogen produced in the gas phase and introduced into aqueous solutions. This method has the advantage of the absence of other species like hydrated electrons and hydroxyl radicals, which occur in aqueous solutions irradiated with ionizing radiations.

The reliability and the method of estimating absolute rate constants by this method are discussed in the preceding paper.<sup>5</sup>

#### Experimental

The method of producing the atomic hydrogen in the gas phase and introducing it into the solution is described in ref. 4. The dose rate was determined for every single experiment by the reduction of  $10^{-3} M$   $\text{K}_3\text{Fe}(\text{CN})_6$  solution,<sup>6</sup> taking  $Y/A = 0.74$  for this concentration.<sup>7</sup>

(1) G. Stein, *Discussions Faraday Soc.*, **29**, 235 (1960); Proceedings of the 5th International Conference on Free Radicals, Stockholm, 1960.

(2) J. H. Baxendale, *Radiation Res. Suppl.*, **4**, 114 (1964).

(3) For reviews, see (a) H. Taube, *Advan. Inorg. Chem. Radiochem.*, **1**, 1 (1959); (b) J. Halpern, *Quart. Rev. (London)*, **15**, 207 (1961); (c) N. Sutin, *Ann. Rev. Nucl. Sci.*, **12**, 285 (1962).

(4) (a) G. Czapski and G. Stein, *J. Phys. Chem.*, **63**, 850 (1959); (b) G. Czapski, J. Jortner, and G. Stein, *ibid.*, **65**, 956 (1961).

(5) G. Navon and G. Stein, *ibid.*, **69**, 1384 (1965).

(6) G. Czapski and G. Stein, *ibid.*, **64**, 49 (1960).

(7) G. Navon and G. Stein, unpublished results.

Table I

Salt	Initial concn., <i>M</i>	Dose rate $\times 10^4$ , <i>M</i> min. <sup>-1</sup>	Time of reaction, min.	Yield of Co(II) $\times 10^4$ , <i>M</i>	<i>Y/A</i>	<i>k</i>
Co(NH <sub>3</sub> ) <sub>6</sub> Cl <sub>3</sub>	0.08	1.36	5	2.02	0.293	1.75 $\times 10^6$
	0.04	0.84	6	1.20	0.236	1.90 $\times 10^6$
						Av. 1.85 $\times 10^6$
[Co(NH <sub>3</sub> ) <sub>5</sub> F](ClO <sub>4</sub> ) <sub>2</sub>	1.5 $\times 10^{-2}$	0.19	3.25	0.204	0.330	0.92 $\times 10^6$
	1.5 $\times 10^{-2}$	0.70	2.8	0.114	0.058	0.85 $\times 10^6$
	6 $\times 10^{-3}$	0.13	4.5	0.150	0.257	1.36 $\times 10^6$
	6 $\times 10^{-3}$	0.76	6.0	0.156	0.0342	1.26 $\times 10^6$
	3 $\times 10^{-3}$	0.82	6.0	0.048	0.0097	(0.68 $\times 10^6$ )
						Av. 1.1 $\times 10^6$
[Co(NH <sub>3</sub> ) <sub>5</sub> Cl](ClO <sub>4</sub> ) <sub>2</sub>	2.44 $\times 10^{-3}$	0.63	4	1.01	0.40	5.5 $\times 10^7$
	2.2 $\times 10^{-3}$	0.91	4	1.56	0.42	8.3 $\times 10^7$
	1.8 $\times 10^{-3}$	0.36	4.5	0.834	0.509	7.7 $\times 10^7$
	7.2 $\times 10^{-4}$	0.47	5	0.618	0.261	8.1 $\times 10^7$
	7.2 $\times 10^{-4}$	0.47	4.5	0.456	0.217	6.5 $\times 10^7$
						Av. 7.3 $\times 10^7$
[Co(NH <sub>3</sub> ) <sub>5</sub> Br](ClO <sub>4</sub> ) <sub>2</sub>	1.41 $\times 10^{-3}$	1.19	5	4.15	0.70	4.4 $\times 10^8$
	7.05 $\times 10^{-4}$	1.13	5	3.05	0.541	4.8 $\times 10^8$
						Av. 4.6 $\times 10^8$
[Co(NH <sub>3</sub> ) <sub>5</sub> I](ClO <sub>4</sub> ) <sub>2</sub>	9.8 $\times 10^{-5}$	1.03	2	0.83	0.404	3.35 $\times 10^9$
	4.9 $\times 10^{-5}$	1.05	1	0.327	0.31	2.94 $\times 10^9$
	4.15 $\times 10^{-5}$	0.90	1	0.267	0.28	3.68 $\times 10^9$
						Av. 3.3 $\times 10^9$

The amount of reduction was estimated in all cases, except for the Co(NH<sub>3</sub>)<sub>5</sub>I<sup>2+</sup> reduction, by the determination of the Co(II) formed, using the method given by Katakis and Allen<sup>8</sup> by extracting Co(SCN)<sub>2</sub> into methyl isobutyl ketone and reading the absorbance at 620  $\mu$ . It was found convenient to extract the NH<sub>4</sub>-SCN solution with the organic solvent before use in order to reduce the blank absorbance due to traces of Fe<sup>3+</sup>.

We followed the rate of the reduction of the Co(NH<sub>3</sub>)<sub>5</sub>I<sup>2+</sup> ion by its absorbance at 383  $\mu$ . The optical density measurements were done immediately after the reaction to exclude any interference by the reaction:  $2\text{Co}(\text{NH}_3)_5\text{I}^{2+} + \text{I}^- \rightarrow 2\text{Co}^{2+} + 10\text{NH}_3 + \text{I}_3^-$ .

According to Yalman,<sup>9</sup> this reaction has a bimolecular rate constant of 0.2 l. mole<sup>-1</sup> sec.<sup>-1</sup> at 45°. Taking account of the concentrations used in the present work, the extent of the above reaction was negligible during the time of the measurements (about 5 min. after the reaction).

All of the solutions were prepared without added buffer. The pH was regulated by the addition of HClO<sub>4</sub> or NaOH solutions when necessary. When

not otherwise mentioned, the pH of the solutions was slightly acidic:  $4 < \text{pH} < 6$ .

The concentration of the solutions was estimated by optical absorbance measurements using the spectra given by Linhard and Weigel.<sup>10</sup> A Beckman B spectrophotometer was used for all the spectrophotometric measurements.

**Materials.** Co(NH<sub>3</sub>)<sub>5</sub>CO<sub>3</sub>NO<sub>3</sub> was prepared by the method described by Basolo and Murmann<sup>11</sup> and was used further for the preparation of the [Co(NH<sub>3</sub>)<sub>5</sub>F](NO<sub>3</sub>)<sub>2</sub> and [Co(NH<sub>3</sub>)<sub>5</sub>I](NO<sub>3</sub>)<sub>2</sub>.<sup>11</sup> [Co(NH<sub>3</sub>)<sub>5</sub>F](ClO<sub>4</sub>)<sub>2</sub> and [Co(NH<sub>3</sub>)<sub>5</sub>I](ClO<sub>4</sub>)<sub>2</sub> were prepared from the nitrate salts by grinding the salts in with concentrated solutions of NaClO<sub>4</sub> acidified with HClO<sub>4</sub>, filtering, and repeating this procedure several times.

[Co(NH<sub>3</sub>)<sub>5</sub>Br](ClO<sub>4</sub>)<sub>2</sub> was prepared similarly to its iodide analog. [Co(NH<sub>3</sub>)<sub>5</sub>Cl](ClO<sub>4</sub>)<sub>2</sub> was prepared

(8) D. Katakis and A. O. Allen, *J. Phys. Chem.*, **68**, 1359 (1964).

(9) R. J. Yalman, *J. Am. Chem. Soc.*, **75**, 1842 (1953).

(10) M. Linhard and M. Weigel, *Z. anorg. allgem. Chem.* (Leipzig), **266**, 49 (1951).

(11) F. Basolo and R. K. Murmann in "Inorganic Synthesis," Vol. IV, J. C. Bailar, Jr., Ed., McGraw-Hill Book Co., Inc., New York, N. Y., 1953.

Table II

[Co(NH <sub>3</sub> ) <sub>5</sub> H <sub>2</sub> O](ClO <sub>4</sub> ) <sub>3</sub> concn., M	pH	Dose rate × 10 <sup>4</sup> , M min. <sup>-1</sup>	Time, min.	Yield of Co(II) × 10 <sup>4</sup> , M	Y/A	k <sub>s</sub> [S] × 10 <sup>-4</sup>	k <sub>H<sub>2</sub>O</sub> × 10 <sup>-6</sup>
1.6 × 10 <sup>-2</sup>	1.80	1.19	4	0.126	0.0265	0.782	4.9
8 × 10 <sup>-3</sup>	1.80	0.59	3	0.036	0.0202	0.374	4.7
8 × 10 <sup>-3</sup>	1.85	2.50	4	0.126	0.0126	0.552	6.9
4.5 × 10 <sup>-2</sup>	1.92	0.68	4.75	0.132	0.0412	0.87	1.9
1.6 × 10 <sup>-2</sup>	3.18	1.49	4	0.164	0.0275	0.93	5.8
4.5 × 10 <sup>-2</sup>	3.88	0.53	4.75	0.162	0.0650	1.21	2.7
							Av. 4.5
k <sub>OH<sup>-</sup></sub> × 10 <sup>-7</sup> Assumed pK = 6.44, 6.74							
3.1 × 10 <sup>-3</sup>	6.66	0.53	4.5	0.60	0.254	6.03	3.10
1.6 × 10 <sup>-3</sup>	7.15	0.59	5	0.540	0.182	4.27	3.18
8.0 × 10 <sup>-3</sup>	7.39	0.50	5	0.696	0.278	6.58	0.91
2.45 × 10 <sup>-3</sup>	10.7	2.31	5	1.97	0.170	9.8	4.00
4.9 × 10 <sup>-3</sup>	11.0	2.61	4	2.96	0.284	20.4	4.16
							Av. 3.1
							3.4

by adding a concentrated acidified NaClO<sub>4</sub> solution to a solution of [Co(NH<sub>3</sub>)<sub>5</sub>Cl]Cl<sub>2</sub> which was prepared according to Hynes, Yanowski, and Shiller.<sup>12</sup>

[Co(NH<sub>3</sub>)<sub>5</sub>H<sub>2</sub>O](ClO<sub>4</sub>)<sub>3</sub> was prepared from [Co(NH<sub>3</sub>)<sub>5</sub>CO<sub>3</sub>]NO<sub>3</sub> according to Sebera and Taube.<sup>13</sup> Reagent grade Co(NH<sub>3</sub>)<sub>6</sub>Cl<sub>3</sub> of City Chemical Corp. was used without further purification. All other chemicals used on this work were of reagent grade. The water was triply distilled. During the experiments, the reacting solutions were cooled to 4° to decrease evaporation. Rate constants in Tables I and II are calculated for room temperature.<sup>5</sup>

## Results

The reduction yields and the calculation of the rate constants of the reaction between atomic hydrogen and the cobalt(III) complexes are reproduced in Tables I and II. The rate constants were calculated from the diffusion model<sup>4b,5</sup> assuming the values of the constants  $k_r$ , the recombination constant of atomic hydrogen,  $D$ , its diffusion coefficient, and  $\varphi$ , the effective surface are such that they fulfill the relation,<sup>5</sup>  $(D^{1/2}\varphi/kr)^{2/3} = 2.1 \times 10^{-11}$ . The mean deviation in the rate constant is  $\pm 15\%$  except in the reduction of Co(NH<sub>3</sub>)<sub>5</sub>H<sub>2</sub>O<sup>3+</sup> where it is  $\pm 30\%$ . The absolute value of the rate constants is thought to be correct within a factor of 2, as discussed before.<sup>5</sup> The value of  $1.4 \times 10^6$  l. mole<sup>-1</sup> sec.<sup>-1</sup> for the reaction of atomic hydrogen with Co(NH<sub>3</sub>)<sub>6</sub>Cl<sub>3</sub>, which was found in radiation chemistry,<sup>14</sup> is in reasonable agreement with our value of  $1.8 \times 10^6$  l. mole<sup>-1</sup> sec.<sup>-1</sup>.

The rate constant,  $k_2$ , for the reaction of atomic hydrogen with Co(NH<sub>3</sub>)<sub>5</sub>OH<sup>2+</sup> was calculated by using the relation

$$k_2[S] = k_1[\text{Co}(\text{NH}_3)_5\text{H}_2\text{O}^{3+}] + k_2[\text{Co}(\text{NH}_3)_5\text{OH}^{2+}] \quad (1)$$

Its value depends somewhat upon the equilibrium constant of the reaction  $\text{Co}(\text{NH}_3)_5\text{OH}_2^{3+} \rightleftharpoons \text{Co}(\text{NH}_3)_5\text{OH}^{2+} + \text{H}^+$ . A value of pK = 6.03 at 20° and  $\mu = 1$  M and  $\Delta H = 9.5$  kcal. was found in the literature.<sup>15</sup> This value corresponds to pK = 6.44 at 4° and the same ionic strength. Although the ionic strength in our experiments was 10<sup>-3</sup> to 10<sup>-2</sup> M we calculated the rate constant assuming pK = 6.44. A somewhat better agreement was obtained when pK = 6.74 was used, but the change in the average rate constant was within our experimental error.

## Discussion

The reactions of Co(III) complexes with atomic hydrogen are compared in Tables III and IV with some reactions of these complexes and similar ones with other reducing agents.

(12) W. A. Hynes, L. K. Yanowski, and M. Shiller, *J. Am. Chem. Soc.*, **60**, 3053 (1938).

(13) D. Sebera and H. Taube, *ibid.*, **83**, 1785 (1961).

(14) D. Meyerstein, personal communication.

(15) Unpublished result of D. J. Bearcroft, D. Sebera, A. Zwickel, and H. Taube, cited in: A. Zwickel and H. Taube, *J. Am. Chem. Soc.*, **81**, 1288 (1959).



**Table III:** Relative<sup>a</sup> Rate Constants of Some Electron-Transfer Reactions

X	Co(NH <sub>3</sub> ) <sub>6</sub> X <sup>2+</sup> + Ru(NH <sub>3</sub> ) <sub>6</sub> X <sup>2+</sup> <sup>b</sup>	Co(NH <sub>3</sub> ) <sub>6</sub> X <sup>2+</sup> + H <sup>c</sup>	Cr(NH <sub>3</sub> ) <sub>6</sub> X <sup>2+</sup> + Cr <sup>2+</sup> <sup>d</sup>	CrX <sup>2+</sup> + Cr <sup>2+</sup> <sup>e</sup>
F	...	1.5 × 10 <sup>-2</sup>	5.3 × 10 <sup>-3</sup>	2.9 × 10 <sup>-4</sup>
OH	1.5 × 10 <sup>-4</sup>	0.46	...	2 × 10 <sup>-2</sup> <sup>j</sup>
Cl	1 <sup>f</sup>	1 <sup>g</sup>	1 <sup>h</sup>	1 <sup>i</sup>
Br	6.15	6.3	6.3	6.7
I	25.8	45	108	...

<sup>a</sup> Relative to chloro-substituted complexes. <sup>b</sup> at 25°, ref. 17. <sup>c</sup> This work. <sup>d</sup> At 25°, ref. 16. <sup>e</sup> At 0°, D. L. Ball and E. L. King, *J. Am. Chem. Soc.*, **80**, 1091 (1958). <sup>f</sup>  $k = 2.6 \times 10^2 M^{-1} \text{sec}^{-1}$ . <sup>g</sup>  $k = 7.3 \times 10^7 M^{-1} \text{sec}^{-1}$ . <sup>h</sup>  $k = 5.1 \times 10^{-2} M^{-1} \text{sec}^{-1}$ . <sup>i</sup>  $k = 9 M^{-1} \text{sec}^{-1}$ . <sup>j</sup> Calculated from A. Anderson and N. A. Bonner, *J. Am. Chem. Soc.*, **76**, 3826 (1954), assuming  $E_a = 13 \text{ kcal}$ .

**Table IV:** Relative<sup>a</sup> Reduction Rates of Co(NH<sub>3</sub>)<sub>6</sub>X<sup>3+</sup> Complex Ions by Some Reducing Agents

X	Ru(NH <sub>3</sub> ) <sub>6</sub> X <sup>3+</sup> <sup>b</sup>	Cr(dipy) <sub>3</sub> X <sup>3+</sup> <sup>c</sup>	H <sup>d</sup>	Cr <sup>2+</sup> <sup>e</sup>
NH <sub>3</sub>	3 × 10 <sup>-3</sup>	1.1 × 10 <sup>-2</sup>	40	1.6 × 10 <sup>-4</sup>
H <sub>2</sub> O	1 <sup>f</sup>	1 <sup>g</sup>	1 <sup>h</sup>	1 <sup>i</sup>
OH <sup>-</sup>	0.01	0.6	74	3.0 × 10 <sup>6</sup>
Cl <sup>-</sup>	87	15	160	10 <sup>6</sup>

<sup>a</sup> Relative to the aqua-substituted complexes. <sup>b</sup> At 25°; ref. 17. <sup>c</sup> At 4°; A. Zwickel and H. Taube, *Discussions Faraday Soc.*, **29**, 73 (1960). <sup>d</sup> This work. <sup>e</sup> See ref. 17 for references. <sup>f</sup>  $k = 3.0 M^{-1} \text{sec}^{-1}$ . <sup>g</sup>  $k = 2.1 \times 10^3 M^{-1} \text{sec}^{-1}$ . <sup>h</sup>  $k = 4.5 \times 10^6 M^{-1} \text{sec}^{-1}$ . <sup>i</sup>  $k = 0.55 M^{-1} \text{sec}^{-1}$ .

From Table III one can see the parallelism in the relative rate constants along the series X = F, OH, Cl, Br, and I.

The same trend is common to all the reactions listed in Table III, although they are very different from each other in their mode of reaction. While the reduction by Cr<sup>2+</sup> is known to proceed *via* an inner-sphere activated complex<sup>3a,16</sup> (as one can judge from the fact that the product of the reaction is CrX<sup>2+</sup>), the reduction by Ru(NH<sub>3</sub>)<sub>6</sub><sup>2+</sup> was said to proceed *via* an outer-sphere activated complex because it is substitution inert.<sup>17</sup> The atomic hydrogen is different from the other agents as it has no hydration or any other coordination layer. Its electronic structure is also very different from the other reagents.

All this confirms the conclusion<sup>3a</sup> that this "conduction" of electron depends upon the properties of the ligand itself.

In the case of conjugate organic ligands a correlation with the mobile bond order (atom-atom polarizability<sup>18</sup>) was tried.<sup>19-21</sup>

Here, in the present case, where the halide and hydroxide anions serve as the electron mediators, a very good correlation exists between the relative rate constants and their polarizabilities. A similar correlation between the rate of Fe(CN)<sub>6</sub><sup>3-</sup>-Fe(CN)<sub>6</sub><sup>4-</sup> electron transfer and the polarizability of the cations catalyzing this reaction was found recently.<sup>22</sup>

It seems that the more polarizable ligand can facilitate the electron transfer by two mechanisms. First, as the polarizable electron cloud, in contrast to the nucleus, can follow the electron transfer, it does not contribute to the Franck-Condon<sup>23</sup> type of reorganization energy.

The other possible mechanism is by increasing the covalent interaction between the reactants. The increasing delocalization of the metal electrons and their orbital expansion can be seen also from the reduction of the electron repulsion terms along the nephelauxetic series.<sup>24</sup> However, for NH<sub>3</sub> and H<sub>2</sub>O this series is reversed, except for H atoms.

It is very difficult to discriminate between these two mechanisms as they usually run parallel.

Endicott and Taube<sup>17</sup> noted that the relative rate constants of aquo and hydroxy complexes may be diagnostic of the difference between inner- or outer-sphere mechanism. If this criterion is applicable, then the reaction of hydrogen atom, which proceeds much faster with the hydroxy than with the aquo complex, is defined unequivocally as an inner-sphere reaction.

A large amount of energy is needed for the reaction of hydrogen atom to give a bare proton by direct electron transfer. On the other hand, for the production of the stable product H<sub>3</sub>O<sup>+</sup> a large amount of reorganization energy is needed. These may be the reasons why in spite of its very high reduction potential the atomic hydrogen reacts in many cases relatively slowly as compared to the hydrated electron, for instance.

In other cases, the hydrogen atom may react through a bridged activated complex like Co(NH<sub>3</sub>)<sub>5</sub>XH<sup>2+</sup>

(16) A. E. Ogard and H. Taube, *J. Am. Chem. Soc.*, **80**, 1084 (1958).

(17) J. F. Endicott and H. Taube, *ibid.*, **86**, 1686 (1964).

(18) C. A. Coulson and H. C. Longuet-Higgins, *Proc. Roy. Soc. (London)*, **A191**, 39 (1947).

(19) J. Halpern and L. E. Orgel, *Discussions Faraday Soc.*, **29**, 32 (1960).

(20) R. T. M. Fraser, *J. Am. Chem. Soc.*, **83**, 4920 (1961).

(21) P. V. Manning, R. C. Jarnagin, and M. Silver, *J. Phys. Chem.*, **68**, 265 (1964).

(22) M. Sporer, A. Ron, A. Lowenstein, and G. Navon, in press.

(23) W. F. Libby, *J. Phys. Chem.*, **56**, 863 (1952).

(24) C. E. Schäffer and C. K. Jørgensen, *J. Inorg. Nucl. Chem.*, **8**, 143 (1958).

which gives either  $\text{Co}^{\text{II}}(\text{NH}_3)_5\text{X}^{2+} + \text{H}^+$  or  $\text{Co}^{\text{II}}(\text{NH}_3)_6^{2+} + \text{HX}$  which dissociates immediately to  $\text{H}^+$  and  $\text{X}^-$ . A similar mechanism seems to be established in the reduction of  $\text{Fe}(\text{CN})_6^{3-}$  by atomic hydrogen.<sup>25</sup>

For such a mechanism no excessive reorganization energy is needed and rates may be fast. On the other hand, a necessary thing for such an activated complex is the existence of an available pair of electrons.

The fact that  $\text{Co}(\text{NH}_3)_6^{3+}$  reacts faster than  $\text{Co}(\text{NH}_3)_5\text{OH}_2^{3+}$  seems somewhat curious and is not in accord with the above explanation. However, the chlorides were used as the perchlorate is not sufficiently soluble. Therefore catalysis by chloride may have occurred.

According to Marcus,<sup>26</sup> a relation exists between the rate constant  $k_{12}$  of an outer-sphere oxidation-reduction reaction with a net chemical change and the rate constants  $k_{11}$  and  $k_{22}$  of the exchange of the reactants separately. This relation is

$$k_{12} = (k_{11}k_{22}K_{12}f)^{1/2} \quad (2)$$

where

$$\log f = (\log K_{12})^2/4 \log (10^{-22}k_{11}k_{22})$$

and  $K_{12}$  is the equilibrium constant for the oxidation-reduction reaction.

If relation 2 is applicable to the reaction between atomic hydrogen and the  $\text{Co}(\text{NH}_3)_6^{3+}$  complex ion, one can calculate an order of magnitude for the H,

$\text{H}^+$  electron exchange rate constant. We take<sup>27</sup>  $E^\circ = -0.1$  v. for the couple  $\text{Co}(\text{NH}_3)_6^{2+} \rightarrow \text{Co}(\text{NH}_3)_6^{3+} + e$ ;  $E^\circ = 2.1$  v.<sup>2</sup> for  $\text{H} \rightarrow \text{H}^+ + e$ ;  $k_{11} \leq 3.3 \times 10^{-12}$  l. mole<sup>-1</sup> sec.<sup>-1</sup> for the  $\text{Co}(\text{NH}_3)_6^{2+,3+}$  electron exchange<sup>17,28</sup> at 25°, and  $k_{12} = 1.8 \times 10^6$  l. mole<sup>-1</sup> sec.<sup>-1</sup> measured in this work. The rate constant for the isotopic exchange between H and  $\text{H}^+$  is calculated to be  $k_{22} \geq 4 \times 10^{-4}$  l. mole<sup>-1</sup> sec.<sup>-1</sup>. Owing to the question of the applicability of Marcus' equations to this case, the value of  $k_{22}$  calculated should not be taken too seriously. However, it does not contradict the upper limits for the rate constant  $k(\text{D} + \text{H}^+) < 200$  and  $k(\text{D} + \text{H}^+) < 4.5$  l. mole<sup>-1</sup> sec.<sup>-1</sup> given by Friedman and Zeltman<sup>29</sup> and Kurien and Burton,<sup>30</sup> respectively.

*Acknowledgment.* This research was supported in part by the U. S. Atomic Energy Commission, Biology Division.

(25) G. Navon and G. Stein, unpublished results.

(26) R. A. Marcus, *J. Phys. Chem.*, **67**, 853 (1963), and the previous papers in the series.

(27) W. M. Latimer, "Oxidation Potentials," Prentice-Hall, Inc., New York, N. Y., 1952.

(28) D. R. Stranks, *Discussions Faraday Soc.*, **29**, 73 (1960); N. S. Biradar and D. R. Stranks, *Trans. Faraday Soc.*, **58**, 2421 (1963).

(29) H. L. Friedman and A. H. Zeltman, *J. Chem. Phys.*, **28**, 878 (1958).

(30) K. C. Kurien and M. Burton, Summary of Proceedings of the Fourth Informal Conference on the Radiation Chemistry of Water, 14, University of Notre Dame, Notre Dame, Ind., March 23-25, 1961, p. 14.

## Pore Area and Adsorption Hysteresis for Packed Spheres

by Raymond Venable and William H. Wade

Department of Chemistry, The University of Texas, Austin, Texas (Received November 19, 1964)

The desorption isotherms for water from packed spheres and a commercial gel were obtained and analyzed for their pore volume distributions. In addition, nitrogen film areas were obtained during the desorption process. From these latter measurements pore area distributions were obtained. The calculated distributions provide some insight into the geometry of the packed spheres.

Several recent papers<sup>1,2</sup> have delineated the importance of capillary condensation for certain powdered adsorbent samples which can be treated as an assemblage of spheres. In addition, Wade<sup>3</sup> has provided several techniques where the packing coordination number of the spheres could be estimated for a single sample of Al<sub>2</sub>O<sub>3</sub> whose coordination number was increased by compression of loosely packed powders.

For such systems Kiselev, *et al.*,<sup>1</sup> have predicted the shapes of N<sub>2</sub> isotherms for both the adsorption and desorption branches. The adsorption branch is assumed to obey the B.E.T. equation—which is not usually found to be true—up to a critical pressure where the porous medium completely saturates. (The authors point out the existence of special cases where this is not strictly true.) The existence of such a singular pressure requires uniform packing geometry of identical spheres. Such powder packs have never been obtained, and Wade<sup>3</sup> could find no such behavior for his samples. Although it may be possible to prepare samples of more and more uniform dimensions, it is hard to envision obtaining a simple geometric packing for an entire assemblage by a compressional process.

Kiselev, *et al.*, in treating the desorption process empty the pores once again at a pressure unique for given radii spheres packed in a single geometric pattern. They state that the pores open when the pendular rings around the spheres forming the necks appear as an unbroken circle. Although this is a pleasing, simple picture in that the liquid meniscus at the instant of pore emptying would be hemispherical with two identical radii of curvature, it must be incorrect. The inscribed circle condition is correctly applied to the pore-filling process. Prior to pore opening, the filled windows must additionally dilate and the description of

the resulting meniscus is quite complex and to the present time not analytically described. The spherical radii,  $r_{\text{sph}}$ , used by Kiselev, *et al.*, eq. 5 and 6, must be too small and a more correct representation will be offered later.

Furthermore, in describing pore structure is has been common practice to assume cylindrical symmetry and make use of the geometrical relationship

$$\frac{V_p}{\Sigma_p r_{\text{sph}}} = 1/2 \quad (1)$$

where  $V_p$  is the true pore volume,  $\Sigma_p$  is the pore area, and  $r_{\text{sph}}$  is the spherical pore radius using the Kelvin equation in the form

$$\ln p/p^0 = \frac{2\gamma \bar{V}}{R_G T r_{\text{sph}}} \quad (2)$$

$\gamma$  being the liquid surface tension,  $\bar{V}$  is the molar volume,  $R_G$  is the gas constant,  $T$  is the absolute temperature, and  $r_{\text{sph}}$  is the radius of the spherical meniscus. In general,  $V_p/r_{\text{sph}}$  is summed over the pore volume distribution and the resulting area is compared with the B.E.T. area obtained from a nitrogen isotherm

$$1/2 \Sigma \frac{V_p}{v_{\text{sph}} + t} \stackrel{?}{=} \Sigma_{\text{B.E.T.}} \quad (3)$$

where  $t$  is the thickness of film remaining subsequent to pore opening. Quite good agreement is commonly found between the measured and calculated areas and de Boer<sup>4</sup> has discussed the applicability to several sys-

(1) B. G. Aristov, A. P. Karanaukhov, and A. V. Kiselev, *Russ. J. Phys. Chem.*, **36**, 1159 (1962).

(2) W. H. Wade, *J. Phys. Chem.*, **68**, 1029 (1964).

(3) W. H. Wade, *ibid.*, **69**, 322 (1965).

tems. Everett<sup>5</sup> has tabulated quantities similar to the constant,  $1/2$ , in eq. 1 for other pore structures. For instance, a similar quantity,  $V_p/\Sigma_p R$ , has the value of 0.304 for pores formed by cubically packed spheres and 0.117 for hexagonally close-packed spheres where  $R$  is now the adsorbent sphere radius. This coupled with a discussion of the validity of eq. 3 for a variety of more complex pore structures by de Boer<sup>4</sup> should dictate against the indiscriminate application of eq. 3 without some knowledge of pore geometry.

Wade<sup>2</sup> has demonstrated the feasibility of measuring areas of frozen adsorbate films on adsorbent spheres. Such areas taken from the desorption branch of an isotherm should yield an analogous pore area distribution and a combination of the two distributions will yield an experimental measurement of Everett's parameter,  $\alpha_R = V_p/\Sigma_p R$ .

### Experimental

Two high surface area alumina specimens were investigated, both having been the subject of previous investigations.<sup>2,3,6</sup> One is a commercial alumina gel produced by Alcoa, Inc., and designated by them as XF-20. In this study it will be referred to as sample A. The other material is a high-purity  $\gamma$ - $\text{Al}_2\text{O}_3$  produced by Whittaker, Clark, Daniels, Inc., and is designated by them as Alucer MA. It was compressed in a hydraulic press to produce samples of greatly decreased porosity. Three such samples are discussed here and bear the designation B, C, and D as in the previous study.<sup>3</sup>

The water desorption isotherm for sample A was obtained on a commercial quartz beam vacuum microbalance manufactured by Worden Laboratories, Houston, Texas. Weighing was always done with the balance at null, the restoring torque on the beam being applied by a Helmholtz coil interacting with an Alnico V magnet rigidly mounted on the beam. The null position was detected by a 50 $\times$  microscope and the coil current read as a voltage drop across a standard 10-ohm resistor with a Rubicon Model B potentiometer. Pressures were read from an accompanying oil manometer. The desorption isotherms for samples B-D were obtained by standard volumetric techniques. These four isotherms are displayed in Figure 1 where the ordinates have been converted to liquid cubic centimeters per gram for subsequent calculations.

The surface areas of samples A and C were measured for samples pre-equilibrated with various amounts of water preadsorbed as previously detailed.<sup>2</sup> The film areas corresponding to the water adsorption branch have been published,<sup>3,6</sup> but since experimental film area hysteresis has not been noted previously they are

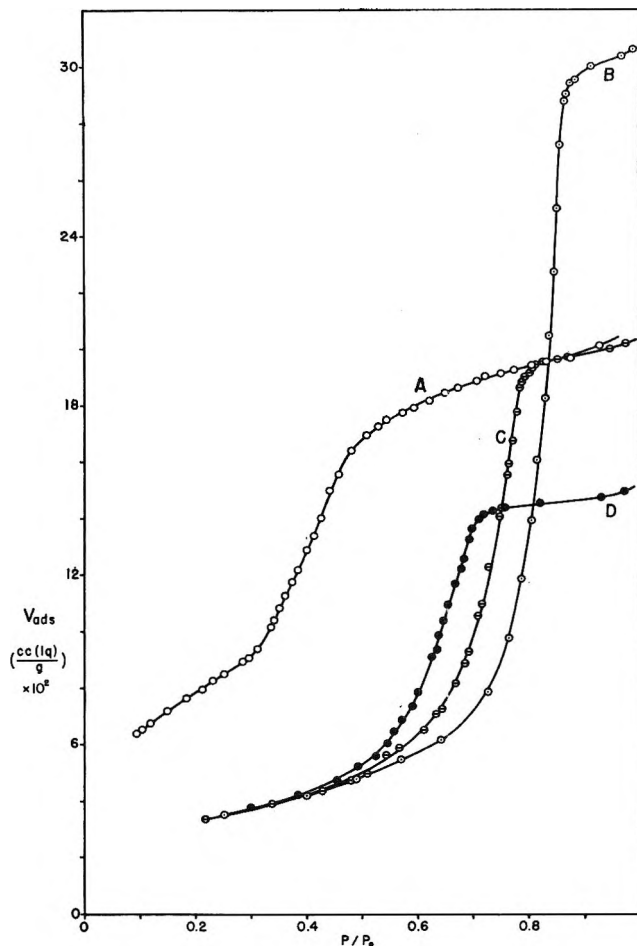


Figure 1. Desorption isotherms for samples A-D.

reported in Figure 2 along with the measured film areas taken from the water desorption branches. It will be noted that there is indeed hysteresis in the film areas and the loops occur in the same relative pressure region as observed in the adsorption-desorption isotherms themselves.

### Results and Discussion

The desorption isotherms for samples B-D in Figure 1 when combined with the adsorption branches<sup>3</sup> show that as the porosity decreases in proceeding from B to C to D, the width of the hysteresis loop increases. Pore emptying is likewise accomplished only at lower pressures when proceeding from sample B to D. Previous calculations<sup>3</sup> of the average coordination number,  $n$ , of B, C, and D yielded approximate values of 6, 8, and 10. The coordination number of packed

(4) J. H. de Boer, *Proc. Colston Res. Soc.*, **10**, 68 (1958).

(5) D. H. Everett, *ibid.*, **10**, 95 (1958).

(6) W. H. Wade and N. Hackerman, *J. Phys. Chem.*, **68**, 1592 (1964).

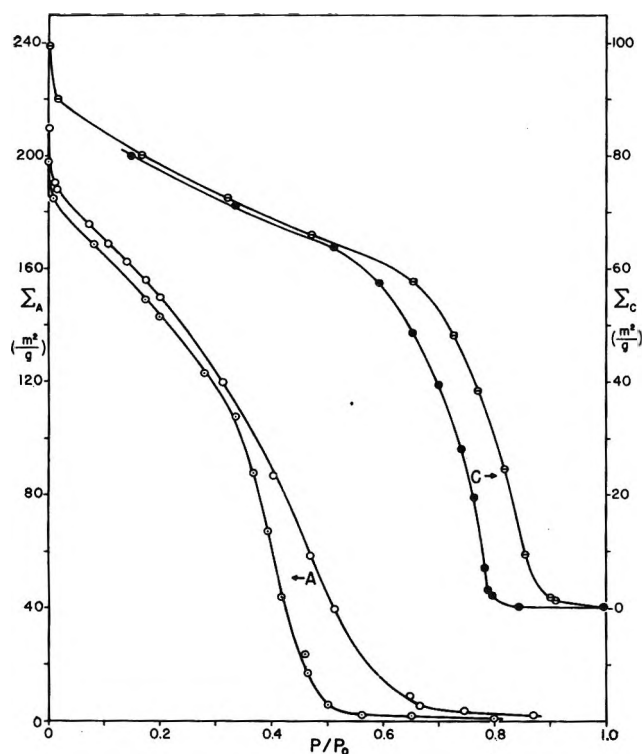


Figure 2. Adsorption and desorption film areas for samples A and C.

spheres is not singularly related to a single packing geometry but, commonly, two or more different pack porosities can have the same coordination number.<sup>7</sup> Thus considering only the packing models of Graton and Fraser,<sup>8</sup> the coordination numbers of 6, 8, and 10 correspond to packs with square, triangular and square, and triangular and rectangular pore windows. (The windows are, of course, made up of circular arcs but for abbreviation will be designated as above.) A given pore volume will always empty through the largest pore and thus Graton and Fraser's  $n = 6$  and 8 packs should empty at the same pressure and the  $n = 10$  sample at a somewhat lower pressure. Using the model of Kiselev, *et al.*,<sup>1</sup> packed spheres with coordination numbers of 6 or 8 empty through the square windows at a relative pressure when the pendular rings no longer overlap. The window opens at the point where it is just no longer circular in cross section. For a square array of packed spheres, the radius of the inscribed circle is equal to  $r_{sph}$  in eq. 3, and from geometric considerations is

$$r_{sph} = (\sqrt{2} - 1)R - t \quad (4)$$

where  $t$  is the thickness of the residual adsorbate uniform film and once again  $R$  is the radius of the adsorbent spheres. Previously, it was found<sup>6</sup> that the thick-

ness of the uniform film on samples B-D could be represented by the Frenkel-Halsey-Hill equation as

$$t = \left\{ -\frac{65.0}{\ln p/p^0} \right\}^{1/3} (\text{\AA.}) \quad (5)$$

over the relative pressure region  $0.3 < p/p^0 < 0.98$ . Calculations show  $R$  to have the value of 75.4  $\text{\AA}$ . By utilizing eq. 2, 4, and 5, one can predict that samples B and C, if they conform to the Graton and Fraser and Kiselev models, should empty at a pressure of 15.8 mm., whereas experimentally they are found to empty at different pressures, both of which are higher than those predicted. It should be immediately obvious that detailed agreement would not be expected, for the isotherms do not show a discontinuous drop as the simple model predicts. This is due to two causes: a distribution of sphere radii and a packing geometry which is not simple but retains much random character during formation.

Sample D also shows the same behavior but on the average the pore necks are smaller and thus the pores empty at lower pressures. Once again using Kiselev's model, pore emptying occurs when the pendular rings at the ends of the rectangular windows separate. The next step in the analysis is not clear to this author. Apparently a hemispherical meniscus is once again assumed at the ends of the rectangles and, for sample D, eq. 2, 5, and one similar to (4) would be applied. The menisci separate at  $(\sqrt{8/6} - 1)R - t$  and thus

$$r_{sph} = (\sqrt{8/6} - 1)R - t \quad (6)$$

Clearly, this approach is incorrect for the liquid meniscus in these rectangular pores cannot approach a hemispherical shape with two identical radii of curvature.

The condition of equilibrium over any point on a liquid meniscus is that  $(1/e_1 + 1/e_2)$  is constant where  $e_1$  and  $e_2$  are the principal radii of curvature. At the present time the conversion of this to an analytical description of complex meniscus shapes as discussed here is not available. Thus it is proposed to treat the complex radii of curvature as a single equivalent radius of curvature,  $r_{eq}$ , which is the radius of a circle whose area is equal to the actual pore area when it opens

$$r_{eq} = \left\{ \frac{A_w}{\pi} \right\}^{1/2}$$

where  $A_w$  is the window area. This still nonrigorous approach lacks simplicity because of some inconvenience

(7) S. Kruyer, *Trans. Faraday Soc.*, **54**, 1758 (1958).

(8) L. C. Graton and H. J. Fraser, *J. Geol.*, **43**, 785 (1935).

in evaluating  $A_w$ . If spheres forming the window are of uniform radius,  $R$ , then an angle  $\phi$  may be defined (Figure 3) as one-half the angle formed at the intersection of the two tangents drawn from the points of contact of any one sphere with the two adjacent spheres. The shaded area of the construction in Figure 3 is the segment of the window pertinent to this sphere. It is the segment of the pore area diminished by the uniform film and pendular rings. Geometrical considerations yield the expression

$$A_w' = R^2 \cot \phi + \pi C^2 \frac{\phi}{180} + 2B\sqrt{A^2 - R^2} - B\sqrt{r_m^2 - B^2} - r_m^2 \sin^{-1} \frac{R}{r_m} - \frac{RC^2}{A^2} \sqrt{A^2 - R^2} - C^2 \sin^{-1} \frac{R}{A} \quad (7)$$

where  $A = R + t + r_m$ ,  $B = [R(R + t)/A] - R$ ,  $C = R + t$ , and  $r_m$  is the lesser radius of curvature of the pendular rings. If the complete window is a regular polygon, then

$$A_w = \frac{360}{2\phi} A_w' \quad (8)$$

If not, then  $A_w'$  must be summed for each value of  $\phi$  and overlapping triangular areas eliminated.  $A_w$  and  $r_{eq}$  have been evaluated using the C.D.S. 1604 computer at The University of Texas for a variety of sphere radii packed in regular triangular, square, pentagonal, and hexagonal arrays.  $r_{eq}$  is plotted in Figure 4 for water adsorbed on Alucer MA as a function of pressure. The thickness of the uniform film,  $t$ , is given by eq. 5 and the size of the pendular rings related by

$$\log p/p^0 = -2.275 \left\{ \frac{1}{r_m} - \frac{2}{\sqrt{A^2 - R^2} - r_m + R + t} \right\} \quad (9)$$

as before.<sup>2</sup> The ring-hand side of each of the four window arrays terminates at the maximum relative pressure at which the pores can remain open, as given by the condition in (4), (4'), and their analogs. Each region is calculated as centered about  $R = 75.0 \text{ \AA}$ . and is arbitrarily extended to limits on  $R$  of 60 and 90  $\text{\AA}$ . for it was felt that this should include 90% of the adsorbent spheres. The rectangular inset framing represents the limits of occurrence of the hysteresis loop for sample C, the pressure limits from the isotherm, and the  $r_{eq}$  limits from the application of eq. 2 assuming  $r_{eq} = r_{sph}$ . The line set in the rectangle is a plot of eq. 2 in the region of interest. For a given sphere radius and packing geometry,  $r_{eq} = r_{sph}$  at the

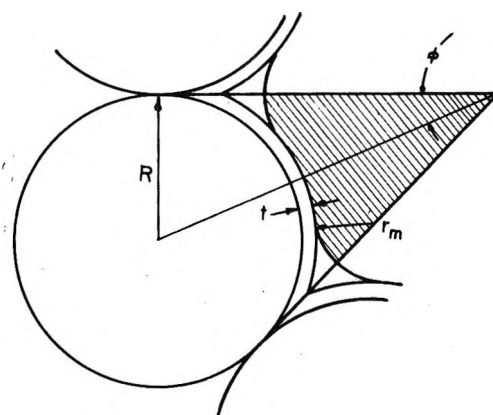


Figure 3.  $A_w$  (shaded area) for pore window diminished by a uniform film and the two segments of pendular rings.

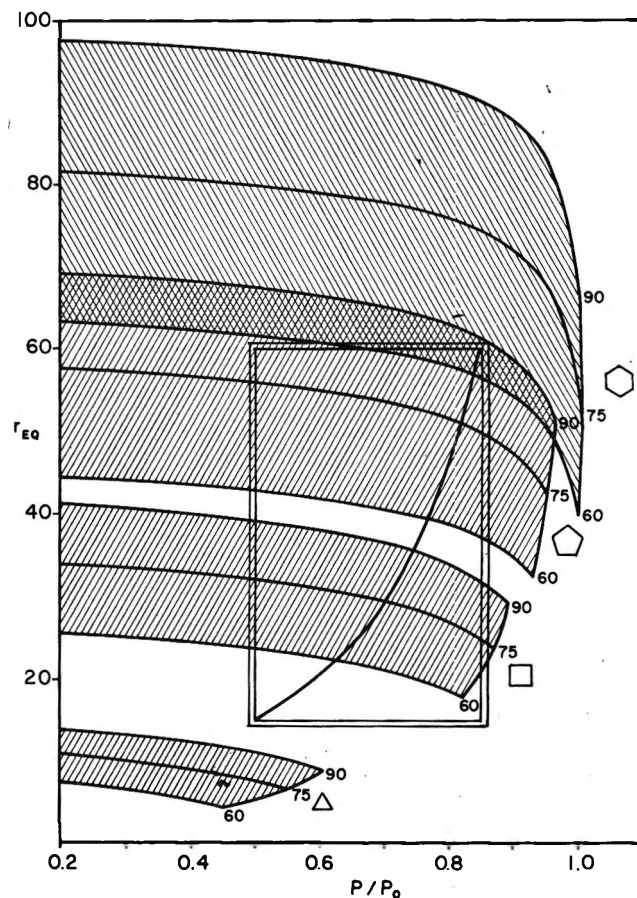


Figure 4. Equivalent radius of triangular, square, pentagonal, and hexagonal windows as a function of relative pressure for 60-, 75-, and 90- $\text{\AA}$ . radius spheres.

pressure corresponding to the pore emptying. For cubic packing with  $R = 75 \text{ \AA}$ , this pressure is 16.7 mm., which is within the region of the hysteresis loop which, when coupled with the measured coordination

number of  $n = 8$  would indicate a packing such as cases II and IV discussed by Graton and Fraser. However, at this pressure the desorption branch is far from vertical and the evident distribution of pore openings poses an insoluble problem. This distribution can arise from a distribution in sphere radii for a single given packing geometry, a distribution of packing geometries for a single sphere size, or a random distribution in both packing geometry and sphere size. Undoubtedly the latter is the more realistic. The most sensible view is that pore volumes communicate through a wide distribution of pore windows with a given pore volume emptying through its largest window. For sample B at  $p = 20$  mm. ( $p/p^0 = 0.84$ ) such windows should need to be regular pentagons made of the larger sphere sizes, regular hexagons of smaller sphere sizes, flattened hexagons of larger sphere size, or some appropriate combination of sphere sizes in pentagonal or hexagonal arrays. For sample C at  $p = 18$  mm. ( $p/p^0 = 0.76$ ) they could be both square and pentagonal arrays of a variety of sphere sizes. For sample D at  $p = 15.5$  mm. ( $p/p^0 = 0.65$ ) the largest windows are probably regular square arrays and even for this sample it is still improbable that triangular arrays of even the largest spheres are the largest windows. Furthermore, for sample D there are probably very few pentagonal or hexagonal windows unless they are so flattened that they differ little from square (or diamond) or triangular arrays.

The desorption isotherms in combination with eq. 2 were used to obtain uncorrected pore volume distributions. These derivations of  $V_{\text{meas}} = f(r_{\text{sph}})$  are shown in Figure 5 along with analogous pore area distributions obtained from the measured desorption pore areas. It is immediately apparent that the maxima for the two types of distributions for samples A and C occur at the same pressures and the shape of the distribution curves are quite similar. Barrett, Joyner, and Halenda<sup>9</sup> have discussed the detailed analysis of desorption data to yield true pore volume distribution. They note that corrections must be made to account for the thinning of residual adsorbate in previously opened pores and the uniform film retained in the pores opened in a given desorption increment. Unfortunately, the detailed treatment is limited to cylindrical capillaries and will not be employed here. With an eye toward the calculation of Everett's geometry constant, the quantity  $(V_p - V_{\text{ads}})/\Sigma_t R$  was calculated for Graton and Fraser's four geometries with  $n = 6, 8, 10,$  and  $12$ .  $V_{\text{ads}}$ , the volume adsorbed in empty pores at any coverage, and  $\Sigma_t$ , the adsorbate film area in the pore, were evaluated by eq. 1 and 2 in ref. 3 connecting these quantities through  $t$  and  $r_m$  to eq. 5 and 9 in this paper

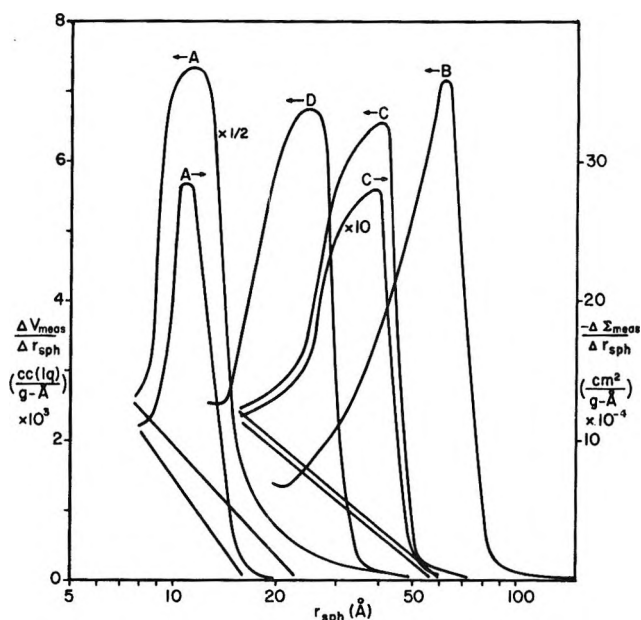


Figure 5. Uncorrected pore volumes and area distributions.

relating  $t$  and  $r_m$  to the pressure. The constant  $\alpha_R$  defined as

$$\alpha_R = \frac{V_p - V_{\text{ads}}}{\Sigma_t R} \quad (10)$$

is plotted in Figure 6 as a function of the relative pressure. The curves are terminated at  $p/p^0 = 5$  mm., for below this point eq. 5 is no longer applicable.  $\alpha_R$  is found to be insensitive to the adsorbed state at low relative pressures having the values calculated by Everett. At high pressures  $\alpha_R$  decreases rapidly; however, on the desorption branch the pores will be closed at these pressures. The pressures corresponding to the maxima in Figure 5 for samples B, C, and D are noted in Figure 6 on the  $n = 6, 8,$  and  $10$  lines since they correspond to the measured values of  $n$ . They are located on the knees of the curves where  $\alpha_R$  is not appreciably lower than for outgassed spheres. Thus for present purposes it should be sufficient to correct  $\Delta V_{\text{meas}}/\Delta r_{\text{sph}}$  and  $\Delta \Sigma_{\text{meas}}/\Delta r_{\text{sph}}$  only for the thinning of adsorbate film and pendular rings of the previously opened pores. This was done in the following way. Increments in  $r_{\text{sph}}$  ( $2 \text{ \AA.}$ ) were chosen and thus were established increments in  $\Delta V_{\text{meas}}$  and  $\Delta \Sigma_{\text{meas}}$ . Assuming  $n = 6, 8,$  and  $10$  and once again using eq. 1 and 2 in ref. 3,  $\Delta V_{\text{ads}}/\Delta r_{\text{sph}}$  and  $\Delta \Sigma_t/\Delta r_{\text{sph}}$  could be evaluated as a function of  $p/p^0$  and are given in Figure 7. These two quantities must then be weighted by the fraction of total

(9) E. P. Barrett, L. G. Joyner, and P. P. Halenda, *J. Am. Chem. Soc.*, **73**, 373 (1951).

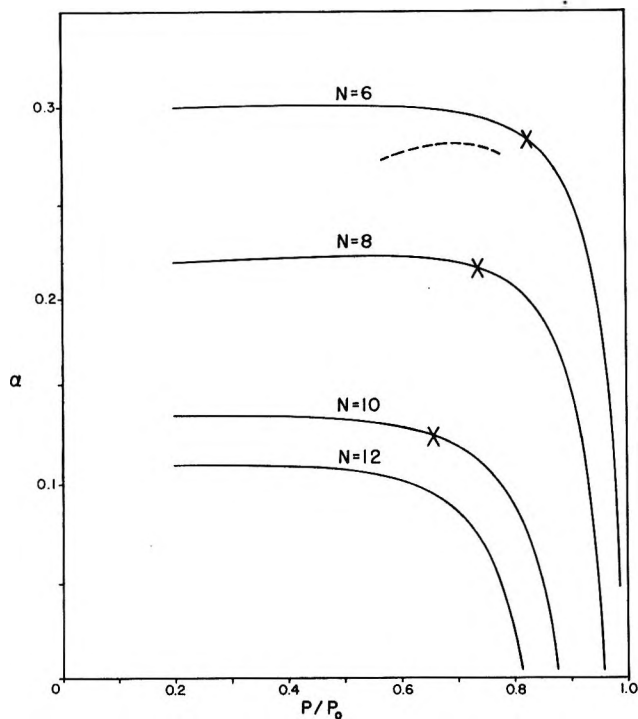


Figure 6. The variation of the geometry constant,  $\alpha_h$ , as a function of relative pressure for spheres of radius 75 Å. packed with coordination numbers of 6, 8, 10, and 12.

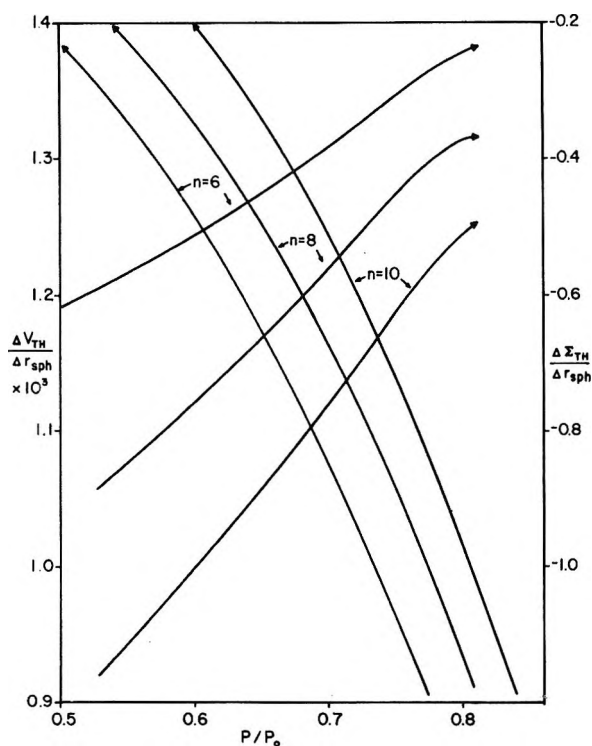


Figure 7. The slope of  $V_{\text{ads}} = f(r_m)$  and  $\Sigma_t = f(r_m)$  vs. relative pressures in the region of hysteresis.

pore space opened prior to the present increment. This was done by graphical integrations of initially corrected pore volume and area distributions (the primed quantities below) and the quantities

$$\frac{\Delta V_{\text{TH}_1}}{\Delta r_{\text{sph}}} = \frac{\Delta V_{\text{ads}}}{\Delta r_{\text{sph}}} \left\{ \frac{\sum_{r_{\text{sph}} \text{ av}}^{r_{\text{sph}} \text{ hi}} \left( \frac{\Delta V_{\text{meas}}}{\Delta r_{\text{sph}}} \right)' \Delta r_{\text{sph}}}{\sum_{r_{\text{sph}} \text{ lo}}^{r_{\text{sph}} \text{ hi}} \left( \frac{\Delta V_{\text{meas}}}{\Delta r_{\text{sph}}} \right)' \Delta r_{\text{sph}}} \right\} \quad (11)$$

$$\frac{\Delta \Sigma_{\text{TH}_1}}{\Delta r_{\text{sph}}} = \frac{\Delta \Sigma_t}{\Delta r_{\text{sph}}} \left\{ \frac{\sum_{r_{\text{sph}} \text{ av}}^{r_{\text{sph}} \text{ hi}} \left( \frac{\Delta \Sigma_{\text{meas}}}{\Delta r_{\text{sph}}} \right)' \Delta r_{\text{sph}}}{\sum_{r_{\text{sph}} \text{ lo}}^{r_{\text{sph}} \text{ hi}} \left( \frac{\Delta \Sigma_{\text{meas}}}{\Delta r_{\text{sph}}} \right)' \Delta r_{\text{sph}}} \right\} \quad (12)$$

become the corrections for thinning of the open pores. The initially corrected distributions are the uncorrected distributions terminated at their extremities by a sloping straight line such as those drawn in Figure 5 and thus are just first approximations of (11) and (12) corresponding to linear desorption isotherms. The resulting pore area and volume distributions are drawn in Figure 8 for sample C. The values of  $\alpha_R$  taken from

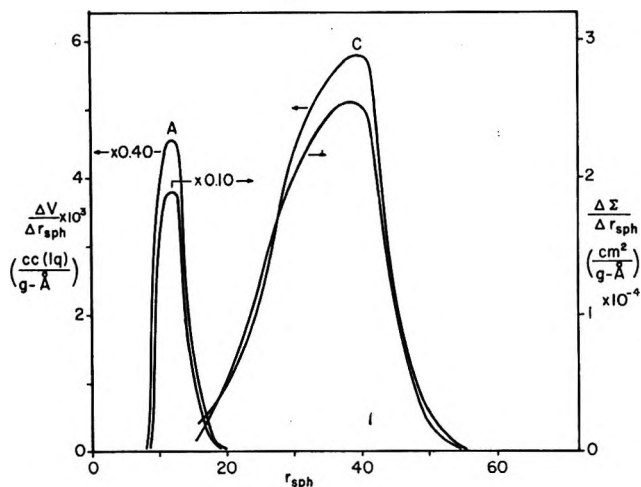


Figure 8. Corrected pore volume and area distributions for samples A and C.

the ratios of these two distributions for  $R = 75.4 \text{ \AA}$ . are traced in Figure 6. Little significance should be placed on the variation of  $\alpha_R$  with  $p/p^0$  since it is the resulting ratio of two graphical differentiations both of which needed to be smoothed. The average experimental value of  $\alpha_R$  is 0.27 lying between the values for  $n = 6$  and 8 for Graton and Fraser's models. If the true, fully corrected pore volume and area distributions are



desired, the adsorbate remaining in the empty pores could be calculated to a good approximation by

$$V_{\text{TH}_2} = V_{\text{ads}} \left\{ \frac{\left( \frac{\Delta V_{\text{meas}}}{\Delta r_{\text{sph}}} \right)' \Delta r_{\text{sph}}}{\sum_{r_{\text{sph lo}}^{r_{\text{sph hi}}} \left( \frac{\Delta V_{\text{meas}}}{\Delta r_{\text{sph}}} \right)' \Delta r_{\text{sph}}} \right\} \quad (13)$$

$$\Sigma_{\text{TH}_2} = \Sigma_f \left\{ \frac{\left( \frac{\Delta \Sigma_{\text{meas}}}{\Delta r_{\text{sph}}} \right)' \Delta r_{\text{sph}}}{\sum_{r_{\text{sph lo}}^{r_{\text{sph hi}}} \left( \frac{\Delta \Sigma_{\text{meas}}}{\Delta r_{\text{sph}}} \right)' \Delta r_{\text{sph}}} \right\} \quad (14)$$

for any given segment of the distribution. These quantities are the fraction of total volume adsorbed and film area in pores of a given  $r_{\text{sph}}$  and for a given increment in  $\Delta r_{\text{sph}}$  and must be added to the appropriate values in Figure 8. This second correction shifts the distributions to slightly larger values of  $r_{\text{sph}}$ , but  $\alpha_R$  remains 0.27 as would be expected from Figure 6.

Film area hysteresis was also noted for the commercial alumina gel, sample A. It is probably not valid to treat the pore volume as the interstices between packed spheres as can be done for many silica gels, but without more information it certainly cannot be treated as an assembly of capillaries. The uncorrected pore area and volume distributions for this same are shown in Figure 5. A rather arbitrary correction for the thinning of adsorbate in open pores can be made by assuming that the lower break in the desorption isotherm at  $p/p^0 = 0.30$  corresponds to complete depopulation of the pore structure and curves of analytic form similar to those for sample C applied as correction for open pore thinning. The resulting distributions are also given in Figure 6. These distributions can then be handled in two ways. Treating the pores as capillaries the quantity

$$\alpha_r = \frac{\left( \frac{\Delta V_{\text{meas}}}{\Delta r_{\text{sph}}} \right)'}{\left( \frac{\Delta \Sigma_{\text{meas}}}{\Delta r_{\text{sph}}} \right)' r_{\text{sph av}}} \quad (15)$$

was evaluated over the two distributions. The average value obtained is  $\alpha_r = 0.55$  compared to the value of 0.50 commonly used. It is difficult to assess the expected agreement but the 10% difference is probably within experimental error.

If rather than as capillaries, the pore spaces are considered as formed from packed spheres, the quantity

$$\alpha_R = \frac{\left( \frac{\Delta V_{\text{meas}}}{\Delta r_{\text{sph}}} \right)'}{\left( \frac{\Delta \Sigma_{\text{meas}}}{\Delta r_{\text{sph}}} \right)' R} \quad (16)$$

can be evaluated over the distributions. The average value of  $\alpha_R$  is found to be 0.26 using  $R = 28.3 \text{ \AA}$ , as calculated from eq. 5 in ref. 3 for  $n = 6$ . This value of  $\alpha_R$  is quite similar to that for sample C. Without more information it is not possible to delineate further this sample's pore structure.

In Table I are listed values of  $\alpha_r$  and  $\alpha_R$  for spheres packed in Graton and Fraser's four arrays.

Table I

Packing	$\alpha_R$	$\alpha_r$
Cubic	0.303	0.579
Orthorhombic	0.218	0.417
Tetragonal-spheroidal	0.144	0.300
Hexagonal close	0.117	0.518

$\alpha_R$  is the geometrical pore volume to pore area ratio divided by the sphere radius for completely uncovered spheres and consists of the values approached  $p/p^0 = 0$  in Figure 6. It would appear to be a very definitive parameter. Unfortunately, this is not so. If rather than the sphere radius,  $r_{\text{eq}}$  is divided into the volume to area ratio to yield  $\alpha_r$ , a much smaller spread is observed. In calculating  $r_{\text{eq}}$  for the middle two packings where two different window areas occur, the large window was chosen in each case for it will control the pore opening. The average value of  $\alpha_r$  in Table I is 0.45 which differs only by 10% from the value of 0.5 for capillary geometry. Perhaps this explains why the condition expressed in (3) is so often observed. If one has spheres packed randomly over the four distributions in Table I or even if they are packed uniformly in cubic or hexagonal close-packed arrays, they exhibit the same capillaries. To illustrate this, evaluating  $\alpha_r$  for sample C yields a value of 0.55 and shows that (3) would be a suitable if misleading test for this sample. In conclusion, the experimental pore area distributions give some insight into the common success of treating complex pore shapes as capillaries.

*Acknowledgment.* The authors gratefully acknowledge the Robert A. Welch Foundation and the American Petroleum Institute for their financial support and continued interest. Miss Josephine Barto wrote the necessary computer programs and did many of the auxiliary calculations and Mr. Arnold C. Falk performed many of the film area measurements.

## Electrical Properties of Ferromagnetic $\text{CrO}_x$ ( $1.89 < x < 2.02$ )

by D. S. Chapin, J. A. Kafalas, and J. M. Honig

*Lincoln Laboratory,<sup>1</sup> Massachusetts Institute of Technology, Lexington, Massachusetts  
(Received November 20, 1964)*

The resistivity ( $\rho$ ) and Seebeck coefficients ( $\alpha$ ) of hot-pressed  $\text{CrO}_x$  ( $1.89 < x < 2.02$ ) have been determined in the temperature ( $T$ ) range 0–450°K.  $\rho$  increased slightly with rising  $T$ ; no significant anomaly was encountered at the Curie point of the samples. Plots of  $\alpha$  vs.  $T$  exhibited four types of temperature dependence. Both  $\alpha$  and  $\rho$  change only slightly with  $x$ . The data are interpreted in terms of a band scheme recently proposed by Goodenough.

In this paper we report on measurements of the electrical properties of  $\text{CrO}_x$  ( $1.89 < x < 2.02$ ). This study was motivated in part by the striking physical properties of  $\text{CrO}_2$ . The oxide is ferromagnetic and quasi-metallic.<sup>2a</sup> Also, above 200°K. the thermal expansion coefficient along the  $c$  axis of the rutile structure is negative, while that along the  $a$  axis is positive, so that the volume expansion coefficient remains nearly independent of temperature.<sup>2b</sup> The only systematic electrical measurements to date seem to be those of Kubota and Hirota,<sup>3</sup> who observed an anomalous resistivity maximum near the Curie temperature of 119°. It seemed highly desirable to check their work and to extend the measurements over a wider range of conditions, in the hope that this might clarify the conduction mechanism which was not understood.<sup>4</sup> The data cited below are examined in terms of a model recently proposed by Goodenough<sup>5</sup> for a systematic interpretation of the electrical properties of metallic oxides.

A review of the physical properties and methods of preparations of  $\text{CrO}_2$  has been provided by Kubota and Hirota<sup>6</sup> (KH); further information is provided by the duPont group.<sup>7,8</sup> While single crystals have been grown by hydrothermal methods, the resulting specimens were too small for use in electrical measurements by conventional techniques. Our attempts to grow large single crystals of  $\text{CrO}_2$  were likewise unsuccessful. Therefore, all measurements presented here were carried out on hot-pressed polycrystalline material.  $\text{CrO}_2$  begins to decompose above 250°<sup>8</sup>; this sets an upper limit to the temperature range in which measurements could be carried out.

### Experimental

*Preparation of  $\text{CrO}_x$ .* Mallinckrodt  $\text{CrO}_3$  and Baker or Kern  $\text{Cr}_2\text{O}_3$  powders were mixed in appropriate quantities to produce  $\text{CrO}_x$  with  $x \approx 2$ , placed in a cylindrical 0.96 × 2.5 cm. boron nitride cell with a Pt foil liner, and subjected to a pressure of 20 kbars at approximately 400°. In a typical case, the resulting ferromagnetic pellet had a density of 4.81 g./cc., compared to a literature value of 4.80 g./cc., and to a density of 4.90 g./cc. calculated from lattice parameters. Analyses of the resulting specimens for impurity content were made on a CEC 21-10 spectrograph and are tabulated in Table I. Parallelepiped specimens approximately 8 × 6 × 3 mm. in dimensions were cut and measured to the nearest 0.01 mm.; two holes, 0.76 mm. in diameter, were ultrasonically drilled through the sample perpendicular both to the long axis and to the

(1) Operated with support from the U. S. Air Force.

(2) (a) J. B. Goodenough, "Magnetism and the Chemical Bond," F. A. Cotton, Ed., John Wiley and Sons, Inc., New York, N. Y., 1963; (b) K. Siratori and S. Iida, *J. Phys. Soc. Japan*, **15**, 2362 (1960); **17**, 208 (1962).

(3) B. Kubota and E. Hirota, *ibid.*, **16**, 345 (1960).

(4) J. B. Goodenough, ref. 2a, p. 243.

(5) J. B. Goodenough, paper submitted to International Colloquium of CNRS on Oxygen Compounds of Transition Elements in the Solid State, Bordeaux, Sept. 1964.

(6) B. Kubota and E. Hirota, *Natl. Tech. Rept. (Osaka)*, **No. 4**, 372 (1961) (translation available OTS, SLA).

(7) T. J. Swoboda, P. Arthur, Jr., H. L. Cox, J. N. Ingraham, A. L. Oppegard, and M. S. Sadler, *J. Appl. Phys.*, **32**, 3745 (1961).

(8) F. J. Darnell and W. H. Cloud, paper submitted to International Colloquium of CNRS on Oxygen Compounds of Transition Elements in the Solid State, Bordeaux, Sept. 1964.



**Stoichiometry.** Chromium content (and therefore  $x$ ), in  $\text{CrO}_x$  was determined by oxidation-reduction titration of the oxidized chromium in solution with standardized ferrous ammonium sulfate to a precision of 1 part in 1000 or better. In some runs, Cr was also determined from the weight loss on calcination of  $\text{CrO}_2$  to  $\text{Cr}_2\text{O}_3$  at  $800^\circ$ . The two sets of determinations differed by less than 1% in every case.

## Results

**Resistivity Measurements.** Because of the polycrystalline nature of the specimens, measurements of resistivity ( $\rho$ ) as a function of temperature ( $T$ ) were frequently erratic. In the worst cases, severe hysteresis effects were encountered, which could not be eliminated; however, in many runs, readings tended to stabilize after subjecting the sample to several cycles. The results of two relatively good runs for  $x = 1.904$  and  $x = 2.013$  are shown in Figure 1. In Figure 1a, the initial  $\rho$  measurements lay above the remainder and passed through a flat maximum near the Curie temperature of  $T_c = 119^\circ$ ; the remaining points fell on a nearly straight line, with no visible anomalies near  $T_c$ , and with no difference in readings taken for ascending or descending temperatures. Figure 1b shows the resistivities for  $\text{CrO}_{2.013}$  taken with rising temperature. Here, the slight dependence of  $\rho$  on  $T$  is again noteworthy. If these data can be taken at face value, there is an initial decrease of  $\rho$  as  $T$  rises from 4 to  $50^\circ\text{K}$ . and a rather shallow maximum in  $\rho$  some  $40^\circ$  below the Curie point; the slight discontinuity near  $100^\circ\text{K}$ . may be fortuitous.

These data are representative of measurements obtained on the  $\text{CrO}_x$  system for  $1.89 < x < 2.02$ . All resistivities fell in the range of 2–75 mohm-cm., which is relatively low for metallic oxides at these temperatures. Data taken with  $\text{CrO}_{1.943}$ ,  $\text{CrO}_{1.994}$ , and  $\text{CrO}_{2.013}$  down to liquid helium temperatures showed no evidence for a transition to semiconductor characteristics. For  $x < 2$ ,  $\rho$  increased slightly with  $T$ , the temperature variation becoming less and less pronounced as  $x$  approached 2. For  $x > 2$ , the change of  $\rho$  with  $T$  was nonsystematic and did not exceed  $\pm 12\%$  of the mean. Any maxima observed by us during initial heating of the sample were relatively flat, extended over a considerable temperature range, and did not necessarily peak at the Curie point.

Measurements of this type on polycrystalline samples are always subject to criticism; however, while no reliance can be placed on the numerical values, the qualitative features and trends should be of significance.

**Temperature Dependence of Seebeck Coefficient.** Since Seebeck coefficients ( $\alpha$ ) are determined, as nearly as

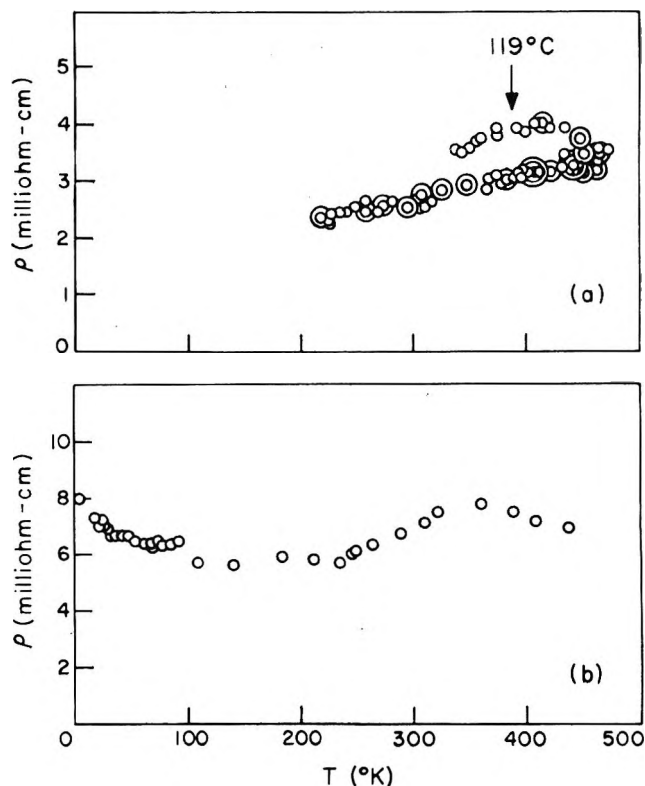


Figure 1. Representative plots of resistivity vs. temperature for two  $\text{CrO}_x$  samples: (a)  $x = 1.994$ ; the upper portion of the curve represents the initial results; the lower portion, the measurements obtained in later cycles with increasing or diminishing temperatures; (b)  $x = 2.013$ ; data taken on the first cycle with rising  $T$  only.

possible, under conditions of no electric current flow, these measurements should not be as drastically affected by the polycrystalline nature of the sample as the resistivity measurements. Indeed, the fluctuations in  $\alpha$  were generally much less than those in  $\rho$ .

For the Sommerfeld model of a metal, the expression for  $\alpha$  due to diffusion effects is given by<sup>11</sup>

$$\alpha = z \frac{\pi^2 k^2 T}{3 e \mu} \quad (1)$$

where  $k$  is Boltzmann's constant,  $e$  the electronic charge,  $z = \pm 1$  depending on whether one deals with a p- or n-type metal, and  $\mu$  is the Fermi level taken relative to the appropriate band edge. For the other extreme of an extrinsic semiconductor conforming to the simple Wilson model, the relation of interest reads<sup>11,12</sup>

(11) A. H. Wilson, "The Theory of Metals," Cambridge University Press, London, 1953, Chapter VIII.

(12) R. W. Ure, Jr., "Thermoelectricity: Science and Engineering," R. R. Heikes and R. W. Ure, Jr., Eds., Interscience Publishers, Inc., New York, N. Y., 1961, pp. 46, 53.

$$\alpha = \frac{z}{T_e} (2kT - \mu) \quad (2)$$

in which the second term generally dominates the first. Thus, plots of  $\alpha$  vs.  $T$  or of  $\alpha$  vs.  $1/T$  should show the dependence of  $\mu$  on  $T$ . Representative graphs of this type are shown for  $\text{CrO}_{1.906}$  in Figure 2. A similar graph of  $\alpha$  vs.  $T$  for the lower temperature range is shown in Figure 3 for  $\text{CrO}_{1.994}$ . It is seen that  $\alpha$ , which is negative and small relative to most oxidic materials, changes little with  $T < 240^\circ\text{K}$ ., and then increases numerically with rising  $T$ . From an examination of these data as well as those for other samples (not shown here) one can distinguish four temperature regions:  $T < 240^\circ\text{K}$ .;  $240 < T < 323^\circ\text{K}$ .;  $323 < T < 389^\circ\text{K}$ .; and  $T > 392^\circ\text{K}$ . The sharp break separating the  $\alpha$  vs.  $1/T$  plots into two linear regions near  $T \approx 50^\circ$  is particularly noteworthy.

*Galvano-Thermomagnetic Measurements.* Experiments were carried out at the Massachusetts Institute

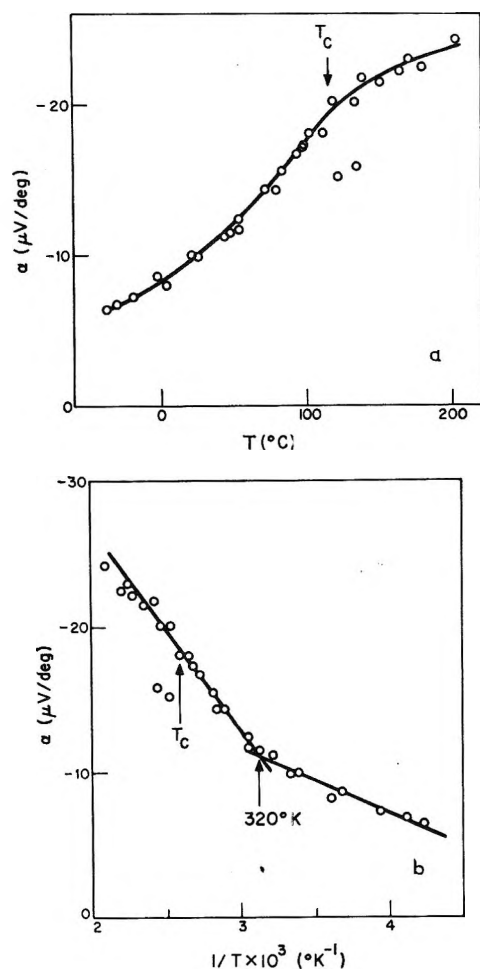


Figure 2. Representative plots of Seebeck coefficients (a) vs.  $T$  or (b) vs.  $1/T$  for  $\text{CrO}_{1.906}$ .

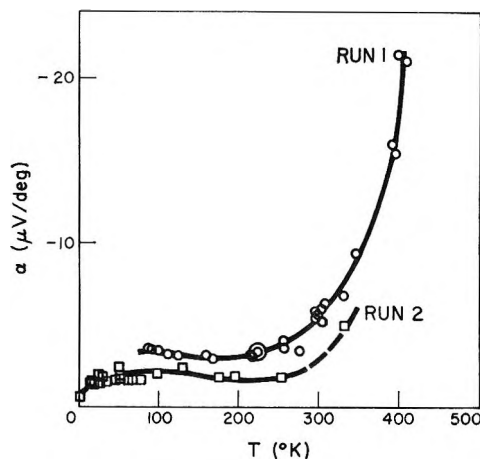


Figure 3. Representative plots of Seebeck coefficients vs.  $T$  for  $\text{CrO}_{1.994}$  in the temperature range below the Curie point.

of Technology National Magnet Laboratory to determine magneto-resistivity, Hall, magneto-Seebeck, Nernst, and Ettingshausen-Nernst effects in steady magnetic fields up to 100 kgauss. No effects could be detected in any of the attempted measurements.

## Discussion

*The Goodenough Model.* Any model adopted for  $\text{CrO}_2$  must provide an understanding as to why the material: (a) is ferromagnetic, (b) is a relatively good electrical conductor, and (c) does not display galvano-thermomagnetic effects. To date, only the model proposed by Goodenough<sup>5</sup> seems to provide a basis for understanding these facts; the pertinent features are outlined below. Beginning with the separated atoms, as indicated on the extreme left and right of Figure 4, one draws the atomic energy levels for the cation and anions. In the rutile structure for  $\text{CrO}_2$ , each Cr is surrounded approximately octahedrally by O, and each O, approximately trigonally by Cr. In the crystal fields referred to above,<sup>13</sup> the d levels of Cr are first split into two  $e_g$  and three  $t_{2g}$  sublevels; moreover, because of the distinction between the  $c$  and  $a$  axes in rutile structures, a further splitting of the  $t_{2g}$  states into a  $t_{2g}^{\parallel}$  and two  $t_{2g}^{\perp}$  levels takes place. The relative stability of these sets of levels depends on the  $c/a$  axial ratio of the crystal. The crystal field acting on the O splits each of the three p states into one  $p_{\pi}$  and two  $p_{\sigma}$  levels. The centers of gravity of the cationic and anionic atomic levels are separated by a distance  $E_M - E_I$  on the energy scale, where  $E_M$  and  $E_I$  refer, respectively, to the Madelung and the ionization energies for the "effective" charges on the ions.

(13) L. E. Orgel, "An Introduction to Transition-Metal Chemistry." Methuen and Co. Ltd., London, 1960.



single crystal  $\text{CrO}_2$ . It is evident that for these very low mobilities no galvano-thermomagnetic phenomena can be anticipated at currently available magnetic fields.

*Investigation of Band Characteristics Based on the Seebeck Effect.* In an extension of the above model, one can investigate certain features of the  $(\alpha)$   $\pi^*$  band using the dependence of the Seebeck coefficient on temperature. If eq. 1 were an adequate representation of the situation, a plot of  $\alpha/T$  vs.  $T$  should reveal the dependence of  $\mu$  on temperature. Graphs that explore primarily the high or low temperature range are shown in Figure 5; again these are representative of the results obtained with all samples. It is striking that only above the Curie point does  $\alpha/T$  become approximately independent of  $T$ ; in other words, eq. 1 as it stands is inadequate for the interpretation of the Seebeck coefficient data in the range  $0 < T < 392^\circ\text{K}$ .

We now discuss the four types of temperature dependence in some detail. For  $T < 240^\circ\text{K}$ ,  $\alpha$  is very small and almost independent of  $T$ . It is suggested that in this range the phonon-drag phenomena<sup>17,18</sup> play an important role. For single crystal material these manifest themselves by the presence of peaks occurring in the  $20\text{--}60^\circ\text{K}$ . range in plots of  $\alpha$  vs.  $T$ . For polycrystalline material this effect is very greatly diminished but not entirely suppressed; in this view, the almost flat regions in Figure 3 are the remnants of a peak which is greatly broadened over a wide temperature range.

The kinks in Figures 5 and 2a draw attention to an anomaly which occurs for all stoichiometries in the vicinity of  $50^\circ$ , roughly  $70^\circ$  below the Curie point of the material. It seemed logical to correlate this phenomenon with the relatively sudden change in temperature dependence of the lattice parameter  $a$  at about that temperature.<sup>2b</sup> For, with a constant number of charge carriers, the  $(\alpha)$   $\pi^*$  band remains approximately half-filled, so that the quantity  $\mu \approx 0.5\Delta\epsilon$  should vary with band width  $\Delta\epsilon = \epsilon_t - \epsilon_b$  (see Figure 4). Now  $\Delta\epsilon$  is determined by the degree of overlap of the appropriate  $t_{2g}^{\parallel}$  and  $p_{\pi}$  atomic wave function, and the overlap itself depends inversely on the interatomic Cr-O spacing, i.e., on the  $a$  value. In the deKronig and Penney idealization<sup>19,20</sup> of a solid (which is consistent with the simple Sommerfeld model of a metal considered here), the band width is proportional to the potential energy barrier separating the atoms, and the latter can be taken to vary approximately as  $1/a$  in the limiting case. On the basis of these very crude arguments one would anticipate that plots of  $\alpha/T$  vs.  $a$  should remove the  $50^\circ$  anomaly in  $\alpha$  vs.  $T$  or  $\alpha$  vs.  $1/T$  plots. Indeed, this is the case, as is shown in Figure 6

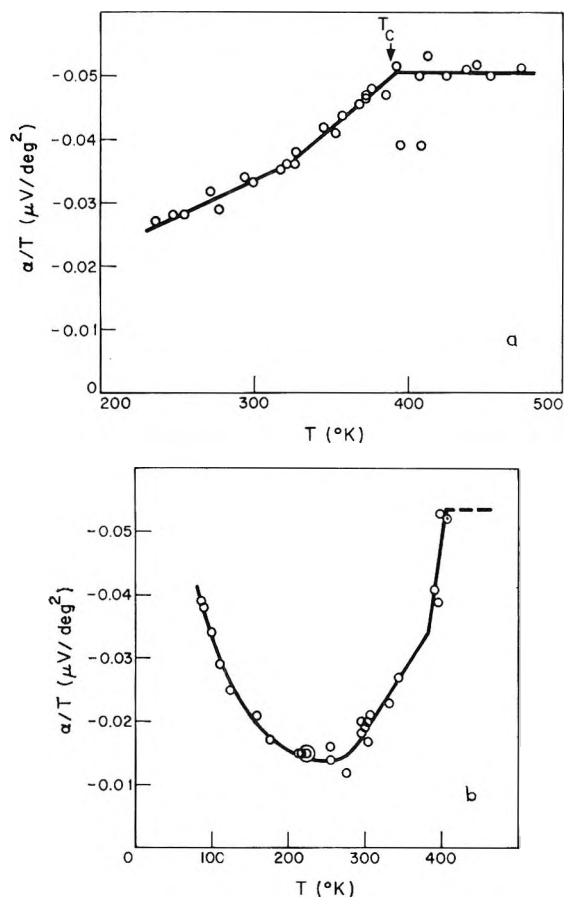


Figure 5. Plots of  $\alpha/T$  vs.  $T$  for  $\text{CrO}_x$ : (a)  $x = 1.906$ ; (b)  $x = 1.994$ .

for  $\text{CrO}_{1.906}$ , which is representative of all samples studied. In this view the change in the  $\alpha$  vs.  $T$  behavior is correlated with alterations in the  $(\alpha)$   $\pi^*$  band width engendered by the change in the  $a$  vs.  $T$  dependence near  $50^\circ$ .

Finally, we must deal with the observation that below the Curie point  $\alpha/T$  is a strong function of  $T$ , whereas above  $T_c$ , this ratio is independent of  $T$ . Manifestly, this changeover will have to be correlated with the ferromagnetic properties of the material. It seems reasonable to assume that the increasing spin disorder with rising temperature for  $T \leq T_c$  increases the degree of scattering of the charge carriers. This effect can be taken into account by a generalization of eq. 1

(17) D. K. C. McDonald, "Thermoelectricity," John Wiley and Sons, Inc., New York, N. Y., 1962.

(18) H. M. Rosenberg, "Low Temperature Solid State Physics," Clarendon Press, Oxford, 1963, p. 278 ff.

(19) R. L. deKronig and W. G. Penney, *Proc. Roy. Soc. (London)*, **A130**, 499 (1931).

(20) V. Rojansky, "Introductory Quantum Mechanics," Prentice-Hall, Inc., New York, N. Y., 1946, p. 49.

$$\alpha = \frac{\pi^2 k^2 T}{3 e} + \left( \frac{\partial \ln l}{\partial \epsilon} \right)_{\epsilon = \mu} \quad (4)$$

which takes into account the scattering of charge carriers through the mean free path,  $l$ . If in the temperature range  $0.2T_c < T < T_c$  the magnetic scattering dominates other scattering processes, then  $l$  diminishes sharply with increasing disorder of the spins, thereby allowing  $\alpha$  to rise. Beyond the Curie point,  $l$  remains

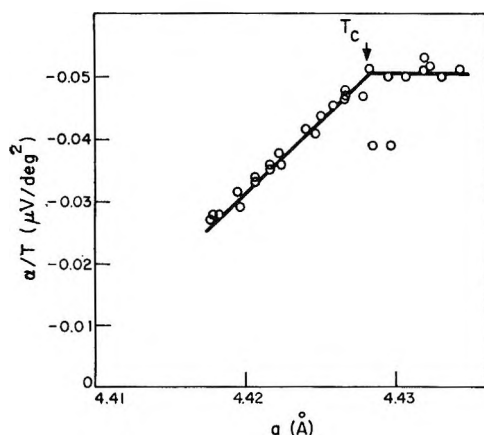


Figure 6. Plot of  $\alpha/T$  vs. crystal parameter  $a$  for  $\text{CrO}_{1.906}$ .

constant, and  $\alpha$  would then be expected to vary roughly as  $T$ , as is experimentally observed. In an alternate reformulation of eq. 4, one uses the fact that quite generally<sup>21</sup>  $\alpha = S^*/e$ , where  $S^*$  is the entropy carried per charge carrier. Separating out the magnetic contribution from the remainder, one may write

$$|\alpha| = \frac{S_n^*}{e} + \frac{S_{\text{mag}}^*}{e} \quad (5)$$

For  $\text{CrO}_2$ , with a body-centered array of spins which are completely ordered at  $0^\circ\text{K}$ . and essentially randomized at  $T = T_c$ , the entropy at the Curie point<sup>22</sup> due to the magnetic disorder is approximated by  $S_{\text{mag}}/k = 0.59$ . If  $S_{\text{mag}}$  were equated with  $S_{\text{mag}}^*$  this would correspond to a value of  $\alpha_{\text{mag}} = 52 \mu\text{v./deg}$ . An upper limit for the experimentally observed magnetic contribution to  $\alpha$  is about  $20 \mu\text{v./deg}$ , which is in reasonable relation to  $S_{\text{mag}}/e$ . Using eq. 5, the value of  $\mu$  estimated from  $\alpha$  at  $200^\circ\text{K}$ . is 0.80 e.v. On the Goodenough model this implies a band width of roughly 1.6 e.v., which is somewhat greater than, but of the same order of magnitude as, the  $\Delta\epsilon$  deduced for  $\text{V}_2\text{O}_3$  from heat capacity anomalies near the semiconductor-metal transition temperature range.<sup>23</sup> However, because of the many simplifying assumptions which enter

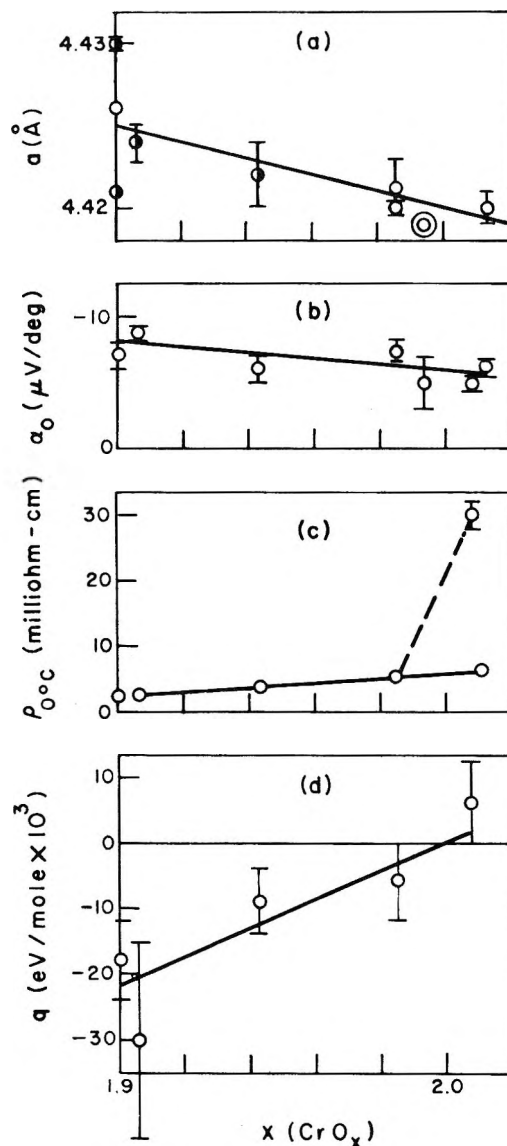


Figure 7. Dependence of various experimental parameters on sample stoichiometry. Half-shaded circles in (a) represent two-phase mixtures of  $\text{CrO}_2$  and  $\text{Cr}_2\text{O}_3$ .

the derivation of eq. 5, this numerical result should be accepted with caution.

*Changes of Properties with Stoichiometry.* The variation of the crystal parameter  $a$ ,  $\alpha$  at  $0^\circ$ ,  $\rho$  at  $0^\circ$ , and activation energy for conduction ( $q$ ) are shown in Figure 7 for various  $\text{CrO}_x$  stoichiometries in the range  $1.89 < x < 2.02$ . Generally, there is a systematic trend of the measurements with  $x$ . In the indicated range the variation of  $a$  is less than  $0.1\%$ , which is within the ex-

(21) C. A. Domenicali, *Rev. Mod. Phys.*, **26**, 237 (1954).

(22) C. Domb, *Advan. Phys.*, **9**, 149, 245 (1960).

(23) J. Feinleib, personal communication.



perimental error and indicates the incipient formation of a second phase,  $\text{Cr}_2\text{O}_3$ , in  $\text{CrO}_2$  as  $x$  decreases. The present data do not, however, preclude the possibility that  $\text{CrO}_2$  exhibits a single-phase defect structure down to  $x = 1.96$ .

According to the discussion of the preceding section, the very slight change of  $a$  with  $x$  should entail only slight changes of  $\alpha$  with  $x$  when  $T$  remains fixed. As Figure 7b shows for  $0^\circ$ , this is indeed the case.

The resistivity of the oxide increases slightly with  $x$  in the range  $1.90 \leq x \leq 2.02$ . The difficulty attendant to  $\rho$  measurements is illustrated by one run in which the calculated resistivity is larger by a factor of six than all other measurements. (See Figure 7c.) Because of the polycrystalline nature of the specimens, no undue importance should be attached to this finding. The same caution should be applied with regard to the activation energies (derived from the linear portions of  $\ln \rho$  vs.  $1/T$  plots) exhibited in Figure 7d. What these really indicate is that  $\rho$  is very insensitive to large temperature changes for all stoichiometries.

Consistent with the Goodenough model, neither  $\alpha$  nor  $\rho$  changes markedly with  $x$ , since any changes in stoichiometry in the indicated range will not appreciably alter the degree of filling of the ( $\alpha$ )  $\pi^*$ -band.

*Comparison with Prior Work.* Finally, concerning the comparison of our work with that by KH, there is

excellent agreement as to the sign and magnitude of the Seebeck coefficients measured in the two laboratories. However, our resistivities are lower by roughly two orders of magnitude than the comparable values cited by KH. Furthermore we observed only a very slight increase of  $\rho$  with rising temperature and, at best, a flat maximum in the  $\rho$ - $T$  curves in the vicinity of the Curie point. This is consistent with the metallic behavior of  $\text{CrO}_2$  as predicted by the Goodenough model, but is in marked contrast to the findings by KH. These workers observed an over-all decrease in  $\rho$  by a factor of two to three with rising temperature, with a distinct maximum in this curve near the Curie point. These differences can probably be ascribed to the different methods of sample preparation.

*Acknowledgments.* The authors gratefully acknowledge their indebtedness to Dr. J. B. Goodenough who drew their attention to the  $\text{CrO}_2$  problem, discussed the results, and communicated to them the energy band scheme for  $\text{CrO}_2$  prior to its publication. They are similarly indebted to Dr. J. Feinleib and to Dr. H. Zeiger for stimulating discussions. Thanks are due Dr. M. Gardels, Mr. E. Owens, and Mr. J. Cornwell for their analytical work. The assistance of Miss Mary Finn and Mr. J. Sanchez in the X-ray analyses and of Messrs. R. Germain and J. Eaton in the measurements is gratefully acknowledged.

# Thermodynamics of Vaporization of Liquid Thallous Iodide<sup>1</sup>

by Daniel Cubicciotti

Stanford Research Institute, Menlo Park, California 94026 (Received November 23, 1964)

The vapor pressure of liquid thallous iodide was measured by a quasi-static method from the melting point to the boiling point. The results can be represented by the equation,  $\log p = -7313/T + 22.215 - 4.18 \log T$ . The only important species in the vapor was found to be monomer (TII). This was established by combining transpiration measurements with the vapor pressure measurements. The heat and entropy of evaporation at 1000°K. were 25.2 kcal. and 23.3 e.u., respectively. The heat of sublimation at 298°K. was 33.3 kcal.

## Introduction

Vapors saturated with liquid thallous chloride and bromide have been found<sup>2,3</sup> to contain some dimer in addition to the predominant monomeric species. Between the melting and the normal boiling point, the dimer to monomer ratio was greater for the chloride than for the bromide. The present investigation was made to compare the behavior of the iodide with the other halides.

A qualitative examination of the vapors produced from liquid thallous iodide was made using a Bendix Time-of-Flight mass spectrometer. In this experiment the sample was contained in a copper cell having a narrow slit orifice. With the sample above its melting point, the shutter-dependent peaks observed were:  $Tl^+$  (relative intensity not examined because of interference by  $Hg^+$  peaks),  $TII^+$  (very strong),  $Tl_2I^+$  (weak), and  $Tl_2I_2^+$  (very weak). No higher-molecular-weight species were observed. A very rough evaluation of these data indicated that the dimer intensity was less than 1% of the monomer.

## Experimental

The vapor pressure was measured by the quasi-static method of Rodebush, *et al.* The details of our apparatus for this measurement have been described elsewhere.<sup>4</sup> For the present work the cell was made of fused quartz and required about 200 g. of TII. The inert gas used was high-purity dry nitrogen. The transpiration apparatus has also been described in ref. 4. In the present work, high-purity dry nitrogen was again used as a carrier gas.

Thallous iodide was made by dissolving pure thallium (99.95% from American Smelting and Refining Co.) in dilute  $HNO_3$  and adding sufficient dilute HI to precipitate TII. The precipitate was collected on a sintered glass filter and air-dried. This material was prepared for analysis by fuming in concentrated  $H_2SO_4$ , diluting, and reducing with  $SO_2$ . The resulting solution was analyzed for thallium by the chromate method,<sup>4,5</sup> as in the bromide case. Analysis of three samples indicated  $61.69 \pm 0.05\%$  thallium compared with 61.69 theoretical for TII. The freezing point of this material was found to be  $441.6 \pm 0.5^\circ$  and it showed a solid transition at  $178 \pm 1^\circ$ . A slight attack of the quartz container was observed after several days of operation. The analysis of the samples after use showed 61.78, 61.70, and 61.66% thallium.

Temperatures in both sets of measurements were determined with a platinum-10% rhodium thermocouple that had been checked against a similar N.B.S.-calibrated thermocouple.

## Results

Vapor pressures were obtained by the quasi-static method over the range from a few millimeters to 1 atm. Three separate samples were run. The results are

(1) This work was made possible by the support of the Research Division of the U. S. Atomic Energy Commission under Contract No. AT(04-3)-106.

(2) D. Cubicciotti, *J. Phys. Chem.*, **68**, 1528 (1964).

(3) D. Cubicciotti, *ibid.*, **68**, 3835 (1964).

(4) F. J. Keneshea and D. Cubicciotti, *J. Chem. Phys.*, **40**, 191 (1964).

(5) O. L. Forchheimer and R. P. Epple, *Anal. Chem.*, **23**, 1445 (1951).

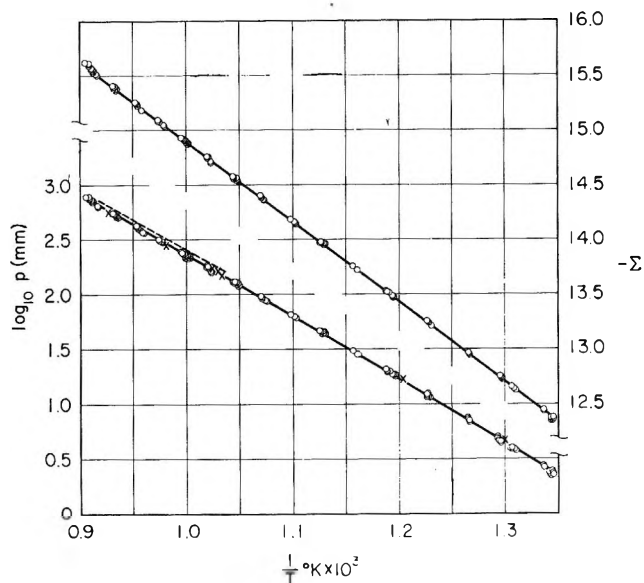


Figure 1. Vapor pressure of thallos iodide: lower curve, points by quasi-static method; crosses by transpiration; dotted line, data of von Wartenberg and Bosse; upper curve,  $\Sigma$ -plot of quasi-static data.

shown in Figure 1. The different samples gave results that were indistinguishable. The pressures can be represented by the equation

$$\log p(\text{mm.}) = \left[ -\frac{7313}{T} + 22.215 - 4.18 \log T(^{\circ}\text{K.}) \right] \pm 1\%$$

from 470 to 830°. The results are compared in Figure 1 with the boiling point data of von Wartenberg and Bosse.<sup>6</sup> Their data have the same slope as the present data but are displaced toward lower temperatures by a few degrees. The same difference was observed with the bromide<sup>3</sup> and chloride.<sup>2</sup>

The mass spectrometric investigation indicated that the dimer was a negligibly small percentage of the monomer. Thus, data were treated as monomer pressures by the usual  $\Sigma$ -plot treatment. The heat capacity of gaseous TII was calculated from molecular constant data to be 8.9 and that of the liquid measured for this work<sup>7</sup> and found to be 17.2 cal./mole deg. The expression used for  $\Sigma$  was

$$\Sigma = -\log p(\text{mm.}) - 4.18 \log T(^{\circ}\text{K.})$$

The  $\Sigma$ -plot is also shown in Figure 1. The data fell on a straight line and the heat of evaporation calculated from its slope was

$$\Delta H(T) (\text{cal./mole}) = 33,500 - 8.3T$$

At 1000°K. the heat of evaporation is 25.2 kcal. and the

entropy is 23.8 e.u. Combining this heat of evaporation with  $H_{1000} - H_{298} = 14.4$  kcal. for the condensed phase<sup>7</sup> and with  $H_{1000} - H_{298} = 6.3$  for the gas (calculated from molecular constants) gave for the heat of sublimation

$$\Delta H(\text{subl., } 298^{\circ}) = 33.3 \text{ kcal./mole}$$

Barrow, *et al.*,<sup>8</sup> have measured the vapor pressure over the solid. Combining their reported vapor pressures with our heat contents for the solid,<sup>7</sup> we calculate a value of 32.4 kcal. for the heat of sublimation at 298°K. (A recalculation of their heats of sublimation, reported as second-law values, with our heat contents gave 32.3).

Since our values for the heats of sublimation to monomer for the chloride and bromide agreed with those of Barrow, *et al.*, within 0.2 kcal., we wondered if there were some systematic error in our results that gave rise to the 0.9-kcal. difference. If there were some other species evaporating from the liquid, in addition to monomer, it could influence the slope of the vapor pressure curve. Accordingly, we made a few transpiration measurements, calculating the results on the basis of a molecular weight of 331. The transpiration results are shown as crosses on the vapor pressure curve. They fall well within experimental error on the vapor pressure curve. Therefore, the species evaporated was the monomer TII. In the highest temperature transpiration measurements a little iodine was found in the collectors along with the thallos iodide. The amount of iodine was always less than 0.5% of the sample in the collector (and less than 0.005% of the total TII in the transpiration cell); therefore, it was assumed that it did not affect the results.

Extrapolation of our data and those of Barrow, *et al.*, and Volmer<sup>9</sup> over the solid to the melting point gave vapor pressures at the melting point that agreed within 2%.

The absolute entropy of crystalline TII at 298°K. can be obtained from the vapor pressure data combined with the absolute entropy calculated for the gas and the heat capacities above room temperature. This calculation was made using the present data and those of Barrow, *et al.* The data used for these calculations and the resulting absolute entropies at 298°K. are shown in Table I. The data of Barrow, *et al.*, give an

(6) H. von Wartenberg and O. Bosse, *Z. Elektrochem.*, **28**, 384 (1922).

(7) D. Cubicciotti and H. Eding, "Heat Contents of Thallos Halides," to be published.

(8) R. F. Barrow, E. A. N. S. Jeffries, and J. M. Swinstead, *Trans. Faraday Soc.*, **51**, 1650 (1955).

(9) F. Volmer, *Physik. Z.*, **30**, 590 (1929).

**Table I:** Calculation of Absolute Entropy of Solid TlI at 298°K. from Vapor Pressure Data

$T$ , °K.	$\log p$ (mm.) <sup>a</sup>	$\Delta H(\text{vap.}, T)$ <sup>b</sup>	$\frac{\Delta S}{T}$ (vap., T)	$S^\circ(T)$ , gas <sup>c</sup>	$(S_T - S_{298})$ , solid <sup>d</sup>	$S^\circ_{298}$ , solid
(A) From present data						
1000	2.363	25.2	22.8	76.5	23.0	30.7
952.5	2.085	25.6	23.2	76.1	22.1	30.8
909.1	1.808	25.9	23.6	75.7	21.4	30.7
869.8	1.520	26.2	24.0	75.3	20.6	30.7
833.3	1.235	26.6	24.4	74.9	19.9	30.6
800.0	0.945	26.8	24.7	74.5	19.2	30.6
769.2	0.648	27.1	25.0	74.2	18.6	30.6
(B) From data of ref. 8, using S-1, S-2, and S-4						
507.3	-3.901	31.3 <sup>e</sup>	30.7	70.4 <sup>e</sup>	7.4 <sup>d</sup>	32.3
545.5	-2.949	31.2	30.4	71.0	8.4	32.2
513.8	-3.719	31.3	30.9	70.5	7.6	32.1
620.5	-1.458	30.8	29.7	72.2	10.1	32.4
615.7	-3.740	31.3	30.8	70.5	7.6	32.1
620.1	-1.460	30.8	29.8	72.2	10.1	32.3

<sup>a</sup> From Figure 1. <sup>b</sup>  $\Delta H(T) = 33,500 - 8.3T$ . <sup>c</sup> Calculated from molecular constants. <sup>d</sup> From ref. 7. <sup>e</sup>  $\Delta H(T) = 32.18 + 1.19T - 5.63 \times 10^{-3}T^2$ .

average value of 32.2 e.u. while the present data give 30.7 e.u.

To help us resolve this discrepancy, Westrum has measured the entropy of the solid at 298°K. calorimetrically. His value for  $S^\circ_{298}$  is  $30.56 \pm 0.05$  e.u.<sup>10</sup> Since this value is in good accord with the one we obtained from the absolute entropy of the gas and the vapor pressures we determined over the liquid, the heat of sublimation derived from the liquid data (33.3 kcal./mole) is to be preferred to that derived from the solid data.

The dissociation energy of the gaseous molecule TII was calculated from the heat of formation of the solid and our value of the heat of sublimation as shown in Table II. This thermochemical value is about 0.2 e.v. larger than the spectroscopic value<sup>11</sup> (2.6). The same difference was observed with TIBr.<sup>3</sup>

**Table II:** Thermochemical Calculation of TII Dissociation Energy

Reaction	$\Delta H$ , kcal.	Ref.
Tl(s) + $\frac{1}{2}$ I <sub>2</sub> (s) = TII(s), 298°K.	-29.6	<sup>a</sup>
TII(s) = TII(g), 298°K.	33.2	This work
Tl(s) = Tl(g), 298°K.	43.6	<sup>b</sup>
$\frac{1}{2}$ I <sub>2</sub> (s) = I(g), 298°K.	25.5	<sup>a</sup>
TII(g), 0° = TII(g), 298°K.	2.5	Calcd., molecular constants
Tl(g), 0° = Tl(g), 298°K.	1.5	<sup>a</sup>
I(g), 0° = I(g), 298°K.	1.5	<sup>a</sup>
TII(g) = Tl(g) + I(g), 298°K.	64.9	
	(2.81 e.v.)	

<sup>a</sup> G. N. Lewis and M. Randall, "Thermodynamics," revised by K. S. Pitzer and L. Brewer, McGraw-Hill Book Co., Inc., New York, N. Y., 1961, Appendix 7. <sup>b</sup> R. Hultgren, R. L. Orr, P. D. Anderson, and K. K. Kelley, "Thermodynamic Properties of Metals and Alloys," John Wiley and Sons, Inc., New York, N. Y., 1963, p. 290.

*Acknowledgment.* The author is indebted to Mr. W. E. Robbins who carried out much of the experimental work.

(10) Private communication from Prof. Edgar F. Westrum, Jr., University of Michigan.

(11) See T. L. Cottrell, "The Strengths of Chemical Bonds," 2nd Ed., Butterworth and Co., Ltd., London, 1958.

## Production, Identity, and Annealing of the Radiolytic Products Formed in Crystalline Cesium Bromate by Cobalt-60 γ-Rays<sup>1</sup>

by G. E. Boyd and Q. V. Larson

Oak Ridge National Laboratory, Oak Ridge, Tennessee 37831 (Received November 24, 1964)

Yields for bromate ion decomposition and for the production of oxygen gas, bromide ion, and oxidizing fragments in the radiolysis of crystalline CsBrO<sub>3</sub> by <sup>60</sup>Co γ-rays were determined as a function of dose, temperature, and dose rate. At 57° all of the yields except those for O<sub>2</sub>(g) increased nonlinearly with dose. For large doses the concentration of oxidizing fragments became constant, and further radiolysis produced bromide and oxygen. Radiolysis at 300° gave only bromide and oxygen; at lower temperatures increasing amounts of oxidizing fragments including hypobromite, bromite, and bromine species with higher oxidation numbers were formed, and the amounts of Br<sup>-</sup> and O<sub>2</sub>(g) decreased. The radiolytic decomposition of BrO<sub>3</sub><sup>-</sup> increased from -196 to 40° and then decreased with increasing temperature until a maximum stability was reached at ca. 100°; at 200° the decomposition was nearly the same as at 40°, and at 300° it was significantly greater. Post-irradiation heating of the crystals removed their color, alkaline reaction, and oxidizing properties, increased their bromide content, and decreased the initial bromate decomposition. The yields of all the radiolysis products were independent of the dose rate. The behavior of the thermally labile oxidizing fragments was explained in terms of their decomposition to bromide and oxygen and their back-reaction to re-form bromate ion. The reaction of BrO<sub>2</sub><sup>-</sup> ion with lattice oxygen produced thermally or by γ-rays is proposed to account for the annealing of the chemical radiation damage produced in CsBrO<sub>3</sub>.

The decomposition modes exhibited by molecular ions in crystals when they are exposed to energetic ionizing radiations have been the object of an increasing number of investigations. Researches on the radiolysis of the alkali metal halates, nitrates, sulfates, and phosphates, for example, have been directed toward identifying the nature of the products formed and toward establishing a mechanism for the decomposition. Quite generally, ionizing radiations act to degrade oxygenated anions by breaking their oxygen-central atom bonds to form oxygen gas and a reduced valence state of the central atom. Diverse, partially fragmented species including free radicals, positively charged molecular ions, etc., may be created and stabilized in the crystal lattice.

In the study to be reported in this paper, bromate ions in highly purified CsBrO<sub>3</sub> crystals were radiolyzed by <sup>60</sup>Co γ-rays. An attempt was made to identify the species formed and to measure the variation of their

yields with dose, temperature, and dose rate. Irradiations were carried out at low temperatures to enhance the stabilization of the highly labile radiolytic intermediates and at elevated temperatures to study the thermal annealing of the radiation damage. Aqueous solutions of the yellow-colored irradiated solid were slightly alkaline and possessed oxidizing properties. Readily detectable quantities of bromide ion were produced, and oxygen gas was released on dissolving the crystals. Part of the oxidizing power of the solution was attributed to hypobromite ion which was identified spectrophotometrically. A preliminary account of some of these observations has been given<sup>2,3</sup>; in this

(1) Presented before the Division of Physical Chemistry, 148th National Meeting of the American Chemical Society, Chicago, Ill., Sept. 1964. Research sponsored by the U. S. Atomic Energy Commission under contract with Union Carbide Corp.

(2) G. E. Boyd, E. W. Graham, and Q. V. Larson, *J. Phys. Chem.*, **66**, 300 (1962).

(3) G. E. Boyd and Q. V. Larson, *ibid.*, **68**, 2627 (1964).

research detailed measurements were made with CsBrO<sub>3</sub> because this salt was the most easily radiolyzed of all the alkali metal bromates.

### Experimental

Two *ca.* 175-g. preparations of pure, crystalline CsBrO<sub>3</sub> were formed by treating Cs<sub>2</sub>CO<sub>3</sub> with HBrO<sub>3</sub> prepared from reagent grade KBrO<sub>3</sub> by cation exchange. The Cs<sub>2</sub>CO<sub>3</sub> employed (DeReval International Rare Metals Co. and Penn Rare Metals, Inc., Revere, Pa.) was shown by flame spectrophotometric analysis to be pure and quite free from the other alkali metals. The twice-crystallized preparations (designated as CsBrO<sub>3</sub>-4 and CsBrO<sub>3</sub>-5) contained less than 5 p.p.m. of bromide ion and alkali metals as follows: CsBrO<sub>3</sub>-4: <1, 7, 4, and 392 p.p.m. of Li, Na, K, and Rb, respectively; CsBrO<sub>3</sub>-5: <0.5, 5, 4, and 350 p.p.m. of Li, Na, K, and Rb, respectively. The anhydrous solids were stored away from light.

Approximately 5-g. aliquots of the finely divided crystals were irradiated with <sup>60</sup>Co  $\gamma$ -rays in three different sources: (a) an air-cooled <sup>60</sup>Co storage facility where the temperature was 57° and the dose rate was  $1.3 \times 10^{18}$  e.v. g.<sup>-1</sup> min.<sup>-1</sup>; (b) a Ghormley-Hochanadel (G-H) type source where the temperature was 35° and the rate was  $1.58 \times 10^{18}$  e.v. g.<sup>-1</sup> min.<sup>-1</sup>; and (c) a low intensity G-H source where the rate was  $1.61 \times 10^{17}$  e.v. g.<sup>-1</sup> min.<sup>-1</sup>. The samples irradiated at -78° in source a were immersed in powdered Dry Ice in a large dewar placed at the center of the source. Irradiations at -196 and -86° were conducted in source b using a special dewar in which the samples were immersed in liquid N<sub>2</sub>, or in a Dry Ice-acetone mixture. The irradiations at 100, 200, and 297° were performed in (b) with the samples placed at the center of a small, cylindrical oven whose temperature was controlled to  $\pm 2^\circ$ . All samples irradiated at room temperature or below were stored at -78 or -196° until analysis or thermal annealing as described.

Dose rates were measured with Fricke dosimeter solutions taking  $G(\text{Fe}^{\text{III}}) = 15.6$  and a molar absorptivity index of 2200 at 3050 Å. or, for source a, with aqueous ceric sulfate-sulfuric acid solutions calibrated by irradiation in source b. The value of  $G[\text{Ce}(\text{III})]$  employed was computed from the Ce(IV) concentration<sup>2</sup> and then corrected to 57° with data taken in a recent study of the temperature dependence of the Ce(III) yield.<sup>4</sup> The dose rate in the CsBrO<sub>3</sub> was computed by multiplying the rate in the dosimeter solution by the ratio of the energy absorption mass attenuation coefficients at 1.25 Mev. for the solution and the compound.

Chemical analyses for radiolytic products were per-

formed on aqueous solutions of the crystals: bromide ion was determined by microtitration with standard AgNO<sub>3</sub> solution; BrO<sub>3</sub><sup>-</sup> ion decomposition was measured by microargentometric titration of the total Br<sup>-</sup> ion in the solution after a treatment with excess arsenite to reduce the oxidizing fragments; total oxidizing power (*i.e.*, the oxidizing capacity with respect to arsenite) was determined by the addition of excess AsO<sub>2</sub><sup>-</sup> to a 0.1 *N* NaOH solution of the irradiated CsBrO<sub>3</sub> and back-titration with standardized I<sub>2</sub> solution after adjusting the pH to 9.0-9.5; hypobromite and "bromite" were measured following the procedures of Chapin<sup>5</sup> and of Hashmi.<sup>6,7</sup> Complete reduction of the oxidizing fragments by AsO<sub>2</sub><sup>-</sup> was slow, and to obtain quantitative results it was necessary to heat the solutions at *ca.* 100° for 1 hr. Separate experiments showed that BrO<sup>-</sup> ion was reduced rapidly by AsO<sub>2</sub><sup>-</sup> so that presumably bromite ion was the slowly reacting species.<sup>8</sup> The conditions under which the CsBrO<sub>3</sub> was dissolved did not appear to have an effect on the analytical results: identical titers were obtained independently of whether crystals irradiated at 35° were dissolved in pure water and allowed to stand for periods up to 2 hr. before AsO<sub>2</sub><sup>-</sup> addition, or whether they were dissolved directly in water containing excess AsO<sub>2</sub><sup>-</sup>. The selective reduction of hypobromite by NH<sub>4</sub><sup>+</sup> ion in the Hashmi method was rapid. This procedure for the estimation of BrO<sup>-</sup> was checked by spectrophotometric analysis using the characteristic ultraviolet absorption band at 330 m $\mu$  shown by this ion in a 0.1 *N* NaOH solution. The molar absorptivity index at this wave length was measured as 290 in good agreement with Farkas and Klein.<sup>9</sup>

Oxygen yields were measured by gas chromatography. In these experiments the crystals were irradiated under vacuum and the gas evolved on dissolving them in water was collected in a closed system and passed through a 1.7-m. column of Linde 5A molecular sieve maintained at 50°. A thermal conductivity detector was employed. No gas was detected above the radiolyzed CsBrO<sub>3</sub> before it was dissolved. Several

(4) C. J. Hochanadel and J. A. Ghormley, *Radiation Res.*, **16**, 653 (1962).

(5) R. M. Chapin, *J. Am. Chem. Soc.*, **56**, 2211 (1934).

(6) M. H. Hashmi and A. A. Ayaz, *Anal. Chem.*, **35**, 908 (1963)

(7) Hypobromite was estimated from the difference between the initial oxidizing power toward AsO<sub>2</sub><sup>-</sup> and that determined after the addition of an excess of NH<sub>4</sub><sup>+</sup> ion or phenol. The oxidizing power remaining after the destruction of BrO<sup>-</sup> will be termed "bromite"; however, bromine species of oxidation number greater than that of BrO<sub>2</sub><sup>-</sup> also were present in small amounts.

(8) Chlorite ion in bicarbonate solution is not reduced by AsO<sub>2</sub><sup>-</sup>. See L. Farkas, M. Lewin, and L. R. Bloch, *J. Am. Chem. Soc.*, **71**, 1988 (1949).

(9) L. Farkas and F. S. Klein, *J. Chem. Phys.*, **16**, 886 (1948).

per cent of N<sub>2</sub>(g) usually were observed indicating either occlusion of air by the crystals or a slight in-leakage. Corrections were made for atmospheric oxygen from the observed N<sub>2</sub>(g) content. No H<sub>2</sub>(g) was observed except in one heavy irradiation ( $21.0 \times 10^{23}$  e.v. mole<sup>-1</sup>) when an amount corresponding to a 100-e.v. yield of 0.002 was measured. Possibly this low yield was a consequence of the scavenging of electrons by BrO<sub>3</sub><sup>-</sup>.<sup>10</sup>

The irradiated crystals were colored golden yellow and when they were dissolved in water a distinct alkaline reaction was produced: the pH of 0.15 M solutions formed by dissolving irradiated and unirradiated CsBrO<sub>3</sub> in freshly boiled triple-distilled water was 9.4 and 5.3, respectively. The alkaline reaction and the color of the irradiated crystals were removed completely by heating them in air at 300° for 1 hr.

Optical absorption measurements in the visible and ultraviolet were made on aqueous solutions of the irradiated salt with a Model 14 PM Cary recording spectrophotometer with 1-cm. path length matched quartz cells. The reference cell was filled with a solution of unirradiated CsBrO<sub>3</sub> at the same concentration as the irradiated salt in the other cell to reduce the interference by the intense ultraviolet absorption of bromate ion.<sup>11</sup> In the experiments which showed BrO<sub>2</sub><sup>-</sup> ion small quantities of BrO<sup>-</sup> were added to the reference cell to reduce the overlap of its strong band with that of bromite. As in our previous work,<sup>2</sup> we were unable to detect any Br<sub>2</sub> in the irradiated crystals. The hypobromite observed in alkaline aqueous solutions therefore was not formed by the hydrolysis of radiolytic bromine.

The thermal stability of the oxidizing fragments was determined by heating the irradiated crystals in air for varying periods. Five-gram quantities held in a porcelain boat were placed at the center of a tube furnace whose temperature was controlled to  $\pm 3^\circ$ . The temperature was measured with a thermocouple and recorded continuously.

## Results

The action of <sup>60</sup>Co γ-rays on crystalline CsBrO<sub>3</sub> decomposed bromate ion to give bromide ion, oxygen gas, and other products which in neutral or alkaline aqueous solutions showed an oxidizing capacity with respect to arsenite ion. The amount of bromide ion was increased significantly by the reaction with AsO<sub>2</sub><sup>-</sup> so that most, if not all, of the oxidizing fragments must have contained bromine. The dose and temperature dependence of the yields for BrO<sub>3</sub><sup>-</sup> decomposition and for Br<sup>-</sup> ion, O<sub>2</sub>(g), and oxidizing fragment production are shown in Figure 1 where it will be noted that the conversion of BrO<sub>3</sub><sup>-</sup> was carried to approximately 7%.

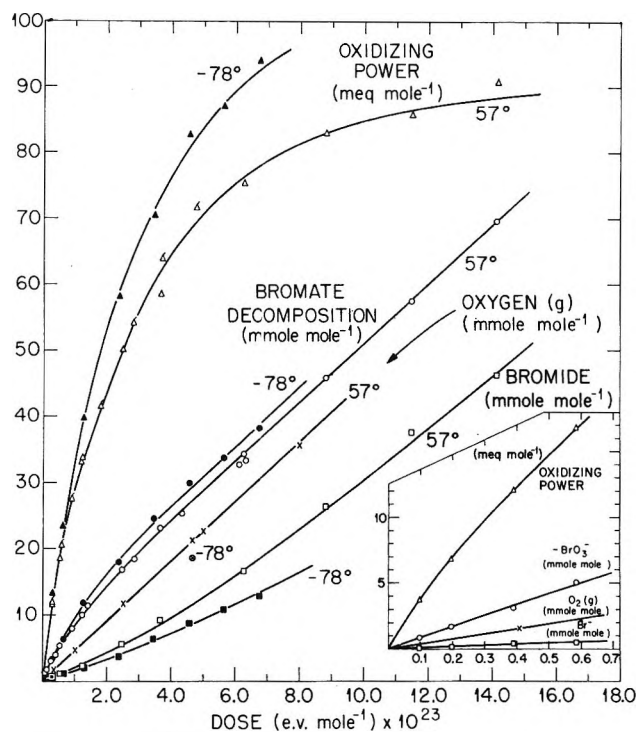


Figure 1. Radiolysis of crystalline CsBrO<sub>3</sub> with <sup>60</sup>Co γ-rays from source a. Insert shows data for radiolysis at low dose with source b.

The decomposition yield of bromate ion increased rapidly for small doses and then became linear with dose above  $ca. 5 \times 10^{23}$  e.v. mole<sup>-1</sup>. In contrast, the Br<sup>-</sup> ion yield was small initially but became proportionately greater with increasing dose and approached a linear dose dependence. The yield of oxidizing fragments initially was strongly dose dependent, but this steadily decreased until the yield at large doses was essentially independent of the dose. The yield of oxygen was linear with the dose over the entire range.

Detailed measurements at 35° for small doses (Figure 1A) showed that the oxidizing fragment yield was nonlinear to less than  $0.1 \times 10^{23}$  e.v. mole<sup>-1</sup>, while, in contrast, the yield of bromide ion was linear with dose below  $0.7 \times 10^{23}$  e.v. mole<sup>-1</sup> within the experimental error. The bromate decomposition yield also was nonlinear down to the smallest dose, although the departure from linearity was much smaller than with the oxidizing fragments. Initial 100 e.v. yields for decompositions smaller than 0.1 mole % at 35° were:  $G_0(-\text{BrO}_3^-) = 5.5$ ;  $G_0(\text{Br}^-) = 0.55$ ;  $G_0(\text{O}_2) = 2.4$ ; and  $G(\text{"Ox"}) = 5.0$ .<sup>11a</sup>

(10) A. Treinin and M. Yaacobi, *J. Phys. Chem.*, **68**, 2487 (1964).

(11) The molar absorbance index was unity for BrO<sub>3</sub><sup>-</sup> at 275 mμ and for Br<sup>-</sup> at 230 mμ.

(11a) NOTE ADDED IN PROOF.  $G(\text{"Ox"})$  is given in "molecule-equivalents" per 100 e.v.

A complex behavior was exhibited by the temperature dependence of the radiolysis (Figure 1). The decomposition of  $\text{BrO}_3^-$  ion and the yield of oxidizing fragments were greater at  $-78^\circ$  than at  $57^\circ$ , whereas the yields of  $\text{Br}^-$  ion and  $\text{O}_2(\text{g})$  were both greater at  $57^\circ$  than at  $-78^\circ$ . A further investigation of the yields as a function of temperature for a constant dose (Table I) showed that the concentration of oxidizing fragments decreased with increased temperature above  $-78^\circ$  until at  $300^\circ$  none was found in the radiolyzed crystal. At this latter temperature only bromide and  $\text{O}_2(\text{g})$  were formed, and the yield of  $\text{Br}^-$  ion was linear with dose. The bromate decomposition was found to increase in the range  $-196$  to  $40^\circ$ , to decrease when the temperature was raised to  $100^\circ$ , and then to increase again so that at  $200^\circ$  the decomposition was approximately the same as at  $40^\circ$ . The rapid increase in bromate radiolysis between  $200$  and  $300^\circ$  suggests that the thermal dissociation of excited  $\text{BrO}_3^{*-}$  has become the dominant process.

**Table I:** Temperature Dependence of the Yields in the Radiolysis of  $\text{CsBrO}_3$  by  $^{60}\text{Co}$   $\gamma$ -Rays<sup>a</sup>

Temp., $^\circ\text{C}$ .	Oxidizing fragments (mequiv. mole <sup>-1</sup> )	Bromate decompn. (mmoles mole <sup>-1</sup> )
-196	53.2	14.1
-86	57.8	15.6
40	45.9	15.8
100	30.0	10.2
200	11.0	15.5
297	0.0	40.0

<sup>a</sup> Dose of  $2.6 \times 10^{23}$  e.v. mole<sup>-1</sup> in source b.

Spectrophotometric measurements (Figure 2) on alkaline aqueous solutions of salt irradiated at  $35^\circ$  showed hypobromite and bromite ions. The ultraviolet absorption band of  $\text{BrO}^-$  at  $330 \text{ m}\mu$  was clearly evident, and a weaker band at  $285 \text{ m}\mu$  which may be assigned to  $\text{BrO}_2^-$  was observed. The band at  $330 \text{ m}\mu$  was rapidly and irreversibly bleached on adding excess  $\text{NH}_4^+$  ion to the solution.

The dose dependence of the yields of  $\text{BrO}^-$  ion and "bromite" is shown in Figure 3 which also reveals that the ratio of the yields of these two species remained constant, independent of the dose from the beginning of the irradiation, and that both products separately tended to "steady-state" yields for large doses. The foregoing observations have suggested that these oxidizing species, or their precursors, were formed independently in the radiolysis (*i.e.*,  $\text{BrO}^-$  was not generated by the thermal or radiolytic decomposition of "bromite").

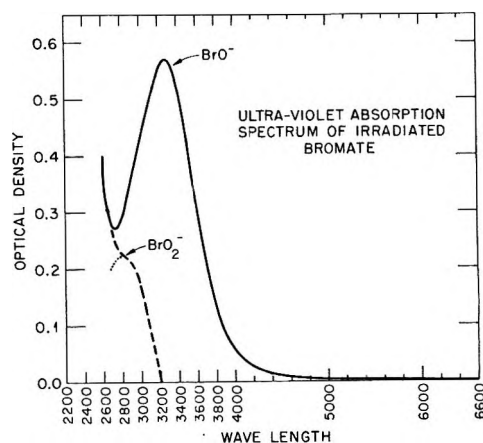


Figure 2. Ultraviolet absorption spectrum of an aqueous solution of  $\gamma$ -irradiated bromate.

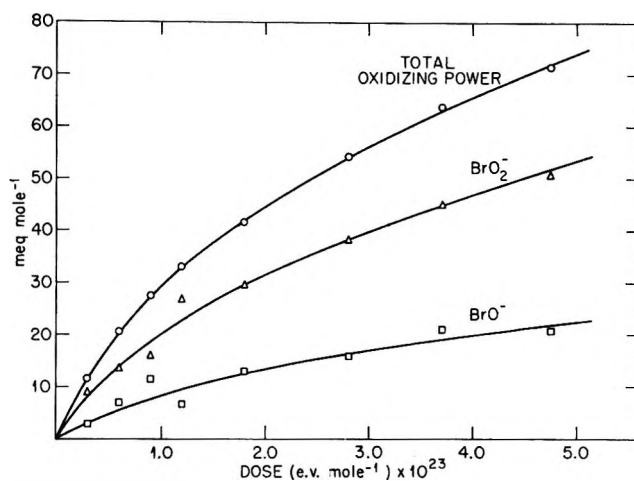


Figure 3. Radiolysis of crystalline  $\text{CsBrO}_3$  with  $^{60}\text{Co}$   $\gamma$ -rays from source a at  $57^\circ$ .

The larger yield of oxidizing power at  $-78^\circ$  than at  $57^\circ$  (Figure 1) and the data of Table I suggested that at least some of the oxidizing fragments were reactive thermally; therefore, heating the crystals after the irradiation might alter their concentration. The results from an isothermal annealing of  $\text{CsBrO}_3$  at several temperatures are shown in Figure 4. The oxidizing fragments were removed at all temperatures above that of the irradiations by a reaction which was quite rapid initially followed by a much slower process. Some of the fragments produced at  $-78^\circ$  evidently were more reactive than those formed at  $57^\circ$ .

To determine if either decomposition or recombination reactions, or both, were responsible for the removal of the oxidizing fragments, experiments were conducted in which the crystals were heated for 1 hr. at several temperatures, rapidly cooled, and analyzed for bromate decomposition, oxidizing power, and bro-



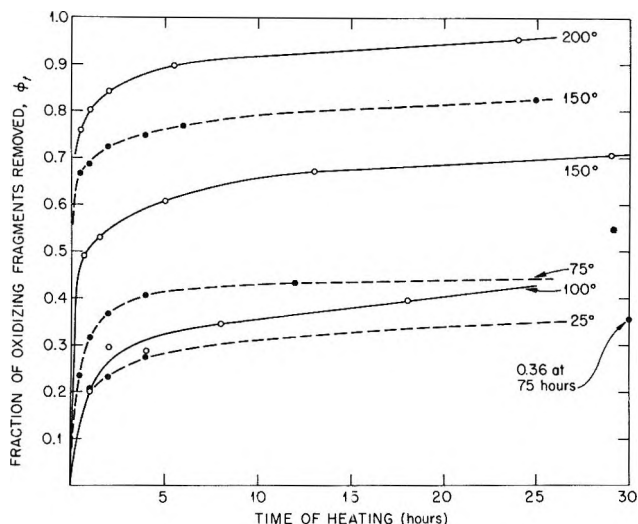


Figure 4. Isothermal annealing of oxidizing fragments produced in crystalline CsBrO<sub>3</sub> by <sup>60</sup>Co γ-rays (dashed curves: irradiation at -78° to 6.75 × 10<sup>23</sup> e.v. mole<sup>-1</sup>; solid curves: irradiation at 57° to 14.1 × 10<sup>23</sup> e.v. mole<sup>-1</sup>).

mid ion content. The results given in Table II show that as the oxidizing power was removed the amount of bromide ion increased, as might be expected if decomposition had occurred, but, more importantly, *the amount of BrO<sub>3</sub><sup>-</sup> ion decomposed also became less*. This latter result indicates that a thermal recombination reaction to form BrO<sub>3</sub><sup>-</sup> ion from the oxidizing fragments must have taken place. When the irradiated crystals were heated for 1 hr. at 200°, approximately three-

Table II: Isochronal Annealing of CsBrO<sub>3</sub> Irradiated at -78°<sup>a</sup>

Temp. of anneal., °C.	Oxidizing power (mequiv. mole <sup>-1</sup> )	Direct Br <sup>-</sup> (mmoles mole <sup>-1</sup> )	BrO <sub>3</sub> <sup>-</sup> decompn. (mmoles mole <sup>-1</sup> )
-78	93.9	12.7	38.2
25	85.6	13.1	30.2
100	54.3	15.25	25.5
150	29.6	17.2	22.8
200	14.3	19.1	20.8
250			(22.6)

<sup>a</sup> Dose of 6.75 × 10<sup>23</sup> e.v. mole<sup>-1</sup>.

fourths of the oxidizing fragments which disappeared recombined to BrO<sub>3</sub><sup>-</sup> ion and the remainder decomposed to yield Br<sup>-</sup>. Studies similar to the foregoing but not so detailed were conducted with CsBrO<sub>3</sub> irradiated to a dose of 3.11 × 10<sup>23</sup> e.v. mole<sup>-1</sup> at 35°. Heating for 1 hr. at 300° removed all the oxidizing frag-

ments and caused approximately 40% of them to recombine to bromate. The amounts of O<sub>2</sub>(g) and Br<sup>-</sup> ion found in the heated crystals were in a ratio of 1.5 to 1.

Isochronal annealing experiments also were performed to determine the effect of heating on the relative amounts of BrO<sup>-</sup> and "bromite." Hypobromite was found (Table III) to be destroyed more rapidly than "bromite"; consequently, as the crystals were annealed, the average oxidation number of bromine in the fragments increased.

Table III: Changes in the Amounts of "Bromite" and Hypobromite Formed in CsBrO<sub>3</sub> Irradiated at -78° by Heating for 1.0 Hr. at Various Temperatures<sup>a</sup>

Temp., °C.	Oxidizing power (mequiv. mole <sup>-1</sup> )	"Bromite" (mequiv. mole <sup>-1</sup> )	Hypobromite (mequiv. mole <sup>-1</sup> )
-78	62.6	45.5	17.1
25	53.5	42.1	11.4
50	50.9	(37.1)	(13.8)
100	42.3	32.4	9.9
158	31.6	25.4	6.2
200	17.5	13.4	4.1
250	5.4	5.1	0.3
300	0		

<sup>a</sup> Dose of 2.62 × 10<sup>23</sup> e.v. mole<sup>-1</sup>.

In our earlier study,<sup>2</sup> the bromate decomposition appeared to be nearly independent of the dose rate. Further careful studies of this variable were made in this work because of its importance in establishing the radiolytic mechanism. Yields for the production of bromide ion, oxidizing power, and bromate decomposition were measured with dose rates differing by a factor of 10. Within experimental errors no dose rate dependence was detected (Table IV).

Table IV: Dose Rate Dependence of Radiolytic Yields in the Irradiation of CsBrO<sub>3</sub> with <sup>60</sup>Co γ-Rays at 35°

Dose rate <sup>a</sup> (e.v. g. <sup>-1</sup> min. <sup>-1</sup> )	Dose to CsBrO <sub>3</sub> (e.v. mole <sup>-1</sup> )	BrO <sub>3</sub> <sup>-</sup> decompn. (mmoles mole <sup>-1</sup> )	Oxidizing power (mequiv. mole <sup>-1</sup> )	Direct Br <sup>-</sup> (mmoles mole <sup>-1</sup> )
1.613 × 10 <sup>17</sup>	3.51 × 10 <sup>23</sup>	18.90	51.04	4.55
1.579 × 10 <sup>18</sup>	3.44 × 10 <sup>23</sup>	18.73	50.42	4.63

<sup>a</sup> Fricke dosimeter solution: ε 2200 at 3050 Å.; G(Fe<sup>III</sup>) = 15.6.

## Discussion

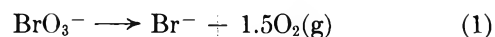
*General.* The yields shown in Figure 1 as a function of dose and irradiation temperature possess several features of interest which appear to have a bearing on the mechanism of the radiolytic decomposition. The oxidizing fragment concentration, for example, saturated at large doses, suggesting that a reaction which removed the fragments was present. This reaction may have been either a decomposition and/or a recombination of a thermal or of a radiolytic nature. The fact that the yields of  $O_2(g)$  and  $Br^-$  ion were greater at  $57^\circ$  than at  $-78^\circ$  showed that thermal decomposition occurs. However, the fact that the bromate decomposition was less at  $57^\circ$  than at  $-78^\circ$  strongly indicates that a thermal back-reaction converting oxidizing fragments to  $BrO_3^-$  ion also must have taken place. If only decomposition of the oxidizing fragments had occurred, a larger bromate decomposition yield at  $57^\circ$  than at  $-78^\circ$  would have been observed. The oxidizing fragments may be removed from the  $CsBrO_3$  crystals by heating them in the absence of radiation (Figure 4) at temperatures well below their melting point. The data in Table II show further that some of the fragments were decomposed because the yield of  $Br^-$  ion increased and that some must have back-reacted because the bromate ion decomposition also decreased. If the action of heating had been solely to decompose the oxidizing fragments, the total bromate decomposition would have remained constant independent of the temperature. Evidently, therefore, true thermal annealing to reconstitute  $BrO_3^-$  proceeds in the crystal both in the absence and in the presence of radiation (*cf.* Tables I and II). *The observation that chemical radiation damage can be annealed and, moreover, that this annealing reaction is an important determinant in the over-all decomposition of bromate ion was one of the most interesting findings in this research.* The initial, nonlinear dose dependence of the yield for bromate decomposition (Figure 1) may be explained by the annealing reaction.

Bromide ion is considered to be formed mainly by the thermal decomposition of precursor oxidizing fragments, although production to a small extent *via* primary radiolysis of bromate probably also occurred. The linear increase in  $Br^-$  ion yield with dose for small doses (Figure 1a) and the apparent temperature independence of this yield are consistent with a direct process. The dose rate independence of the bromide yield (Table IV) suggests that  $Br^-$  was not formed by the radiolysis of long-lived intermediates.

The yield of  $O_2(g)$  increased linearly with dose to total doses as large as  $21 \times 10^{23}$  e.v. mole $^{-1}$ . If oxygen was produced by the same processes as was bromide,

the rate of increase of its yield should have become progressively larger with dose (*i.e.*, initially,  $O_2(g)$  was generated simultaneously with the formation of the oxidizing fragments and by the total decomposition of  $BrO_3^-$  ion; at large doses oxygen was formed additionally by thermal decomposition of the fragments). Clearly, therefore, it is necessary to assume that a reaction consuming oxygen was present. This was the annealing reaction, and we assume that energetic oxygen atoms are produced in the crystal lattice which scavenge the oxidizing fragments.

The linear dose dependence of the yields for  $BrO_3^-$  decomposition and for  $O_2(g)$  and  $Br^-$  ion formation above *ca.*  $10 \times 10^{23}$  e.v. mole $^{-1}$ , and the parallelism of their yield curves (Figure 1) should be noted. At large doses where the oxidizing fragment concentration becomes constant, the net radiolytic decomposition reaction is simply to give bromide and oxygen gas (eq. 1). The decomposition of bromate by radiation at



$297^\circ$  (Table I) followed eq. 1, and the yields of  $Br^-$  and  $O_2(g)$  were linear with dose over the entire range, as expected.

*Nature of the Oxidizing Fragments in the Irradiated Crystal.* A discussion of the identity of the oxidizing fragments will be facilitated by comparing the data in Figure 1 with results taken in a study of the radiolysis of crystalline  $KClO_3$  by X-rays.<sup>12</sup> Many features exhibited in the decomposition of  $CsBrO_3$  also were observed with  $KClO_3$ : (a) the yield of  $O_2(g)$  was linear with dose; (b) chloride was produced at a rate which initially increased with the dose and above *ca.*  $10 \times 10^{23}$  e.v. mole $^{-1}$  the rate became approximately constant; and (c) the yield of oxidizing fragments increased with dose, but for doses exceeding  $10 \times 10^{23}$  e.v. mole $^{-1}$  it became constant, independent of dose indicating a "steady state." In addition, the oxidizing fragments in the  $KClO_3$  crystals were identified by spectrophotometry as  $ClO^-$ ,  $ClO_2^-$ ,  $ClO_2$ , and  $Cl_2O_6$ . Because of their great instability, the identity of the oxidizing fragments from the bromate radiolysis has not been identified so completely. Hypobromite and bromite ions appear in alkaline aqueous solutions of irradiated alkali metal bromates, and, by analogy with  $KClO_3$ , it might be assumed that  $BrO_2^-$ ,  $BrO_2$ , and  $BrO^-$  also exist in the crystalline salts. However, the oxidizing power of solutions of radiolyzed  $CsBrO_3$  is greater than expected if only the latter species were produced. Oxides such as  $BrO_2$ ,  $BrO_3$ ,  $Br_2O$ ,  $Br_2O_5$ , etc., are reported to be quite unstable,<sup>13</sup> and it seems

(12) H. G. Heal, *Can. J. Chem.*, **37**, 979 (1959).

unlikely that they will exist in the radiolyzed crystals at other than low temperatures. The possibility that highly oxidized states of bromine are produced by radiation and are stabilized in the crystal lattice has been suggested by considerations to which we now turn.

The average oxidation number,  $\bar{Z}$ , of bromine in the oxidizing fragments and the average number of oxygen atoms per bromine were derived from the data in Figure 1 in an attempt to establish the stoichiometry of an average oxidizing fragment. The number of mmoles/mole of bromine associated with the oxidizing fragments was found by subtracting the value taken from the curve for Br<sup>-</sup> ion yield for a given dose from that taken from the curve for BrO<sub>3</sub><sup>-</sup> ion decomposition. The ratio of the mequiv./mole of oxidizing power to the mmole/mole of bromine thus obtained yielded the average mequiv./mmole involved in the reduction of the oxidizing fragment to bromide ion, and hence to  $\bar{Z} + 1$ . The value of  $\bar{Z}$  for the irradiations at 35 and 57° was constant at  $3.3 \pm 0.1$  independent of the dose, while for the irradiations at -78°,  $\bar{Z} = 2.9 \pm 0.1$  for small doses and decreased slightly with increasing dose. The average amount of oxygen in an oxidizing fragment was estimated by subtracting the amount of O<sub>2</sub>(g) observed in the radiolyzed crystals from the amount estimated from the bromate decomposition assuming 1.5 moles of O<sub>2</sub>(g) released per mole of BrO<sub>3</sub><sup>-</sup>. This difference, divided by the amount of bromine in the oxidizing fragments, yielded the stoichiometric composition. The composition of an "average fragment" increased from BrO<sub>2.3</sub> for doses less than  $1 \times 10^{23}$  e.v. mole<sup>-1</sup> to BrO<sub>2.8</sub> for doses greater than  $10 \times 10^{23}$  e.v. mole<sup>-1</sup>. The foregoing estimates thus require that species in addition to BrO<sup>-</sup>, BrO<sub>2</sub><sup>-</sup>, and BrO<sub>2</sub> be present in small amounts in the radiolyzed crystal. Conceivably the free radical BrO<sub>3</sub> may exist, or BrO<sub>4</sub><sup>-</sup> ion may be formed.

This work has demonstrated that the oxidizing frag-

ments are thermally labile and decompose to form bromide and oxygen or recombine to give bromate ion. The alkali metal hypobromites are quite unstable and break down to give Br<sup>-</sup> and O<sub>2</sub>(g); therefore, it seems logical to identify the radiolysis fragments which decompose as BrO<sup>-</sup> and possibly BrO<sub>2</sub> and BrO<sub>3</sub>. Bromite ion may be implicated as one of the fragments which reacts to reconstitute bromate according to eq. 2.



Reactions of this type occur in the radiolysis of KNO<sub>2</sub>,<sup>14</sup> where nitrate ions were observed in the crystal, and in radiolyzed KClO<sub>3</sub>,<sup>12</sup> whose aqueous solutions show perchlorate ions.<sup>15</sup> The oxidation of bromite according to eq. 2 will take place with an estimated free energy decrease of 8.7 kcal. mole<sup>-1</sup>. Moreover, this reaction will be favored by the CsBrO<sub>3</sub> crystal lattice. The presence of a BrO<sub>2</sub><sup>-</sup> ion at a BrO<sub>3</sub><sup>-</sup> site creates a "strain energy" in the crystal which will be released when the ion is converted to BrO<sub>3</sub><sup>-</sup>. An alternative mechanism for the reconstitution of BrO<sub>3</sub><sup>-</sup> ions would be *via* electron capture by BrO<sub>3</sub> free radicals trapped in the crystalline lattice. Although this alternative seems unlikely, because of the great instability of BrO<sub>3</sub>, electron spin resonance measurements on radiolyzed KNO<sub>3</sub> and NaClO<sub>3</sub> at 77°K. have shown the presence of NO<sub>3</sub><sup>16</sup> and of ClO<sub>2</sub>,<sup>17</sup> respectively, in the crystals. Accordingly, the results from an e.s.r. study with crystalline KBrO<sub>3</sub> now in progress<sup>18</sup> are awaited with interest.

(13) M. Schmeisser and K. Brändle, *Advan. Inorg. Chem. Radiochem.*, **5**, 41 (1963).

(14) A. R. Jones and R. L. Durfee, *Radiation Res.*, **15**, 546 (1961).

(15) Perchlorate ion was assumed to be formed by the reaction of Cl<sub>2</sub>O<sub>8</sub> in the crystal with water on dissolving the solid. However, ClO<sub>4</sub><sup>-</sup> is produced in solid chlorates by thermal decomposition.

(16) R. Livingston and H. Zeldes, *J. Chem. Phys.*, **41**, 4011 (1964).

(17) P. W. Atkins, J. A. Brivati, N. Keen, M. C. R. Symons, and P. A. Trevalion, *J. Chem. Soc.*, 4785 (1962).

(18) H. Zeldes, private communication.

## Relation between Specific Heat and Total Emittance in Tantalum, Niobium, Tungsten, and Molybdenum<sup>1</sup>

by H. V. L. Narasimhamurty, A. S. Iyer, and M. Hoch

Materials Science Program, University of Cincinnati, Cincinnati, Ohio (Received September 8, 1964)

The ratio of specific heat to total emittance  $C_p/\epsilon$  is determined by measuring the cooling rate of metal rods and disks of various sizes and shapes under vacuum. The method does not require any instrumentation of the sample and permits easy preparation of the surface. The value of  $C_p/\epsilon$  was found to be constant for tantalum, niobium, tungsten, and molybdenum in the temperature range 1250–2350°K.

### Introduction

The method developed in our laboratory to measure thermal conductivities<sup>2</sup> requires the knowledge of the total emittance of the material investigated. The determination of total emittance is one of the most difficult problems. The value obtained depends very strongly on surface contamination and surface preparation. A method is required which permits the determination of the total emittance of a sample without having to instrument the sample; further, the shape of the surface should be simple in order to be able to prepare it easily for the measurements.

The present work describes such a method where the ratio of specific heat to total emittance is obtained. As the specific heat is not a surface property, it will not vary from sample to sample and can be determined relatively easily. The shape of the material used can be either long cylinders or disks. In the case of disks, the flat surface can be prepared in any fashion, and thus the variation of emittance with surface preparation investigated. No instrumentation of the sample is required, and, as the measurements are carried out under vacuum, contaminations can be held to a minimum.

The method is first demonstrated on tantalum samples of various shapes, and then measurements on molybdenum, tungsten, and niobium are presented.

### Theory

When a sample is heated to a high temperature under vacuum and if  $\dot{q}_1$  is the power input to the specimen,  $\dot{q}_g$  is the thermal energy gain of the specimen, and

$\dot{q}_r$  is the radiation loss, then the instantaneous power balance can be written as

$$\dot{q}_1 = \dot{q}_g + \dot{q}_r \quad (1)$$

According to the Stefan–Boltzmann law

$$\dot{q}_r = \text{radiation loss} = \sigma F(\epsilon\epsilon_0)A(T^4 - T_0^4) \quad (2)$$

where  $\sigma$  = Stefan–Boltzmann constant,  $1.354 \times 10^{-12}$  cal./cm.<sup>2</sup> °K.<sup>4</sup> sec.);  $A$  = surface area of the sample at temperature  $T$  in cm.<sup>2</sup>;  $T$  = blackbody temperature of the sample in °K.;  $T_0$  = temperature of the surroundings to which energy is radiated in °K.; and  $F(\epsilon\epsilon_0)$  = a function of the total emittances of the body and surroundings, respectively. The thermal energy gain is

$$\dot{q}_g = mC_p \frac{dT}{d\theta} \quad (3)$$

where  $m$  = mass of the sample in grams;  $C_p$  = specific heat at temperature  $T$  in cal./(g. °K.);  $dT/d\theta$  = slope of the time–temperature curve at temperature  $T$  in °K./sec.

From eq. 1–3

(1) This research has been supported in part by the Air Force Materials Laboratory, Research and Technology Division, Air Force Systems Command, United States Air Force, under Contract No. AF 33(616)-7123.

(2) M. Hoch, D. A. Nitti, C. F. Gottschlich, and P. E. Blackburn, "Progress in International Research on Thermodynamic and Transport Properties," American Society of Mechanical Engineers, Academic Press, New York, N. Y., 1962, p. 512.

$$\dot{q}_1 = mC_p \frac{dT}{d\theta} + \sigma F(\epsilon\epsilon_0)A(T^4 - T_0^4) \quad (4)$$

When  $\dot{q}_1 = 0$

$$mC_p \frac{dT}{d\theta} = -\sigma F(\epsilon\epsilon_0)A(T^4 - T_0^4) \quad (5)$$

When  $T \gg T_0$

$$mC_p \frac{dT}{d\theta} = -\sigma F(\epsilon\epsilon_0)AT^4 \quad (6)$$

The function  $F(\epsilon\epsilon_0)$  depends upon the total emittances  $\epsilon$  and  $\epsilon_0$  and on the relative configuration of specimen and environment. The geometry employed in this study is that of a cylindrical body of finite length radiating partially to an open helix a small distance away and partially to a closed concentric shell of radius large compared with that of the specimen. This configuration may be regarded as intermediate between the case of a completely enclosed body large compared to the dimensions of the enclosure and that of a body small compared to the dimensions of the enclosure. For the first case, Hottel<sup>3</sup> gives the expression

$$F(\epsilon\epsilon_0) = \frac{1}{1/\epsilon + 1/\epsilon_0 - 1} \quad (6')$$

For the second case

$$F(\epsilon\epsilon_0) = \epsilon \quad (6'')$$

It is seen that if  $\epsilon_0 = 1$ , i.e., if the surroundings are made perfectly black, (6') reduces to (6'') so that the emittance function is essentially unaffected by the proximity of the induction coil. Therefore, eq. 6 reduces to

$$mC_p \frac{dT}{d\theta} = -\sigma\epsilon AT^4 \quad (7)$$

Rearranging eq. 7

$$\frac{C_p}{\epsilon} \frac{d(1/T^3)}{d\theta} = \frac{3\sigma A}{m} \quad (8)$$

where  $C_p/\epsilon = g(T)$ , some function of temperature;  $d(1/T^3)/d\theta =$  slope of the curve  $1/T^3$  vs.  $\theta$

$$A \simeq A_0[1 + 2\alpha(T - 300) + 2\beta(T - 300)^2] \quad (9)$$

where  $\alpha$  and  $\beta$  are the first and second coefficients of linear thermal expansion and  $A_0 =$  surface area of the specimen at room temperature in  $\text{cm}^2$ . From eq. 8

$$\frac{C_p}{\epsilon(1 + 2\alpha T' + 2\beta T'^2)} \times \frac{d(1/T^3)}{d\theta} = \frac{3\sigma A_0}{m} \quad (10)$$

where

$$T' = T - 300 \quad (10')$$

In eq. 10,  $C_p$  and  $\epsilon$  are both monotonously increasing with temperature; the expression  $(1 + 2\alpha T' + 2\beta T'^2)$  changes only 2% between 300 and 2000°K.; the right-hand side is a constant. Thus,  $d(1/T^3)/d\theta$  will vary only little with temperature, and its evaluation is easy. The functional form used will be

$$a + b\theta = \frac{1}{T^3} + c \left[ \frac{1}{T^3} \right]^2 + d \left[ \frac{1}{T^3} \right]^3 + \dots \quad (11)$$

## Experimental

**Equipment.** The cylindrical heating chamber was 30 cm. high and had an internal diameter of 15.5 cm. The heating coil, concentric with the heating chamber, was made of 0.5-cm. diameter copper tubing, was 20 cm. in length, 3.75 cm. in internal diameter, and had 34 turns. The heating chamber had three sight windows, one at the top and two at the side.

The vacuum system consisted of a Veeco CT-200 5.08-cm. brass cold trap, an NRC H-4-P diffusion pump, and a Welch Duo-Seal mechanical pump. The pressure was measured by a Veeco DG-2 cold cathode discharge gauge.

The power was supplied by a Thermionic generator. A Thermodot TD-1 coupled with a Speedomax Type G Recorder Model 5-6000 Series was used as a radiation detector. The temperature was measured by a Leeds and Northrup disappearing filament optical pyrometer.

**Procedure. Materials.** Tantalum specimens of different sizes and shapes were used. Samples 1, 2, and 3 were cylindrical; samples 4 and 5 were flat disks machined in our laboratory from a 2.55-cm. diameter bar. Only one sample each of tungsten, niobium, and molybdenum was used. All materials were obtained from the Fansteel Metallurgical Corp.

A 0.16-cm. transverse hole was drilled 0.5 cm. from one end through samples 1, 2, W, Nb, and Mo; a 0.25-cm. transverse hole was drilled through sample 3, 0.4 cm. from one end. Tantalum wire of 0.065-cm. diameter was run through the hole in the samples and up to a suspension ring seated within the flange of the upper window of the heating chamber so that the sample was suspended concentric with the coil. The suspension was a four-point 2-V type suspension. Samples 4 and 5 were supported by resting on a tungsten tripod. The sample dimensions are given in Table I.

The samples were cleaned with acetone and loaded into the vacuum furnace. For the data "as received"

(3) A. J. Brown and S. M. Marco, "Introduction to Heat Transfer," McGraw-Hill Book Co., Inc., New York, N. Y., 1951, p. 61.

**Table I:** Dimensions of the Samples

Material	Length, cm.	Diameter, cm.	Total area $A_0$ , cm. <sup>2</sup>	Mass, g.	$K = 3\sigma A_0/m$ , cal./sec. g. °K. <sup>4</sup>
Tantalum					
Sample 1	10.250	1.270	43.43	215.013	$0.8205 \times 10^{-12}$
Sample 2	10.150	1.260	42.67	208.113	$0.8327 \times 10^{-12}$
Sample 3	4.430	0.635	9.47	22.903	$1.6795 \times 10^{-12}$
Sample 4	0.246	1.920	7.27	11.516	$2.5643 \times 10^{-12}$
Sample 5	0.246	2.580	12.45	21.411	$2.3620 \times 10^{-12}$
Niobium	10.16	1.270	43.17	110.886	$1.5814 \times 10^{-12}$
Molybdenum	10.16	1.265	42.89	129.259	$1.3478 \times 10^{-12}$
Tungsten	10.16	1.275	43.25	248.7	$0.7064 \times 10^{-12}$

no further treatment was given to the samples. For the other measurements, the samples were heated for 0.5 hr. at 2350°K. In this way, a uniform "equilibrium" surface was obtained.

*Temperature Calibration.* If the emitting surface is gray in the spectrally sensitive region, the Thermodot can be utilized for the evaluation of the blackbody temperature. Metals which emit selectively over broad spectral regions are not truly gray.

The response of the recorder was correlated with the reading of the optical pyrometer. The pyrometer was focused through the top viewing port onto the upper surface of the sample. The optical head of the Thermodot was focused onto the cylindrical surface of the sample through one of the lateral viewing ports of the chamber. The measured temperature which corresponds to the surface temperature of the sample was corrected for glass absorption and for nonblackbody conditions.

Since the optical pyrometer was used as the temperature-measuring instrument, the distance over which the recorder moves in covering a certain temperature interval was set to equal the distance over which the optical pyrometer drum rotates to cover the same temperature interval.

At various temperatures the sample temperature was determined by the optical pyrometer; thus, the output of the Thermodot was calibrated over the whole temperature range by the optical pyrometer before each measurement.

After the calibration, the sample was heated to the highest desired temperature and held for 10 min. The heater was then shut off, and the cooling curve traced. From the cooling curve,  $1/T^3$  was plotted *vs.*  $\theta$ , and the coefficients in eq. 11 were obtained.

## Results and Discussion

Table II contains typical time-temperature values as read from the cooling curve. These data were

plotted according to eq. 11, the coefficient determined by least-squares analysis, and values of  $C_p/\epsilon$  obtained.

**Table II:** Cooling Data on Sample 1

Temp. $T$ , °K.	Time $\theta$ , sec.
1712	0
1687	2.50
1664	5.25
1631	8.0
1605	11.50
1583	14.375
1550	19.125
1515	24.625
1475	32.40

Within experimental error, in all cases, constants  $c$  and  $d$  in eq. 11 were equal to zero. Tables III–V give the temperature intervals, the number of points used in the computation,  $C_p/\epsilon$ , and its standard error for the different kinds of samples.

**Table III:** Evaluation of  $C_p/\epsilon[1 + 2\alpha(T - 300) + 2\beta(T - 300)^2]$  for Tantalum, Samples As Received

Sample	Temp. range, °K.	No. of points	$C_p/\epsilon[1 + 2\alpha(T - 300) + 2\beta(T - 300)^2]$ , cal./g. °K.
1	1522–1325	8	$0.123 \pm 0.003$
1	1602–1326	10	$0.106 \pm 0.002$
2	1784–1461	9	$0.205 \pm 0.002$
2	1775–1518	10	$0.226 \pm 0.010$
3	1555–1294	12	$0.121 \pm 0.002$
3	1553–1382	8	$0.135 \pm 0.002$

Table III contains the data on the tantalum samples as received; the values of  $C_p/\epsilon$  do not agree with each other and are lower than in Table IV. This is expected because surface contamination will increase  $\epsilon$ ; the difference in surface preparation also affects  $\epsilon$ .

Table IV contains  $C_p/\epsilon$  data on the tantalum samples after the treatment described. The value of  $C_p/\epsilon$  is the same independent of sample shape; the treatment given was sufficient to give each sample the same surface. The lowest temperature was 1252°K.; the highest, 2340°K.; in this temperature range,  $C_p/\epsilon$  is constant. The best value from all the data is  $C_p/\epsilon = 0.21 \pm 0.01$  cal./g. °K., for this type of material.

Table V contains the data on Nb, W, and Mo.

Rudkin, Parker, and Jenkins<sup>4</sup> have measured the

(4) R. L. Rudkin, W. J. Parker, and R. J. Jenkins, "Temperature—Its Measurement and Control in Science and Industry," Vol. 3, Reinhold Publishing Corp., New York, N. Y., Part 2, 1962, p. 523.

**Table IV:** Evaluation of  $C_p/\epsilon[1 + 2\alpha(T - 300) + 2\beta(T - 300)^2]$  for Tantalum, Various Shapes

Sample	Temp. range, °K.	No. of points	$C_p/\epsilon[1 + 2\alpha(T - 300) + 2\beta(T - 300)^2]$ , cal./g. °K.
1	2090-1905	8	0.212 ± 0.007
1	2180-1740	8	0.196 ± 0.003
1	1712-1475	9	0.234 ± 0.004
1	1842-1529	11	0.223 ± 0.001
2	1832-1570	10	0.226 ± 0.001
3	1741-1487	7	0.220 ± 0.002
3	1676-1297	11	0.220 ± 0.009
4	1970-1555	7	0.207 ± 0.006
4	2340-2015	6	0.220 ± 0.008
4	1770-1442	8	0.207 ± 0.003
4	1527-1262	8	0.209 ± 0.003
5	2152-1715	6	0.203 ± 0.003
5	2145-1722	6	0.216 ± 0.007
5	2302-1965	5	0.191 ± 0.010
5	1662-1312	10	0.222 ± 0.005
5	2020-1682	8	0.187 ± 0.006
5	2245-1992	4	0.211 ± 0.023
5	1690-1277	10	0.203 ± 0.003
5	1695-1282	8	0.206 ± 0.005
5	2136-1275	8	0.199 ± 0.003
5	2242-1638	8	0.182 ± 0.003

**Table V:** Evaluation of  $C_p/\epsilon[1 + 2\alpha(T - 300) + 2\beta(T - 300)^2]$ 

Sample	Temp. range, °K.	No. of points	$C_p/\epsilon[1 + 2\alpha(T - 300) + 2\beta(T - 300)^2]$ , cal./g. °K.
Niobium	2094-1733	10	0.439 ± 0.013
	2154-1766	9	0.400 ± 0.004
Molybdenum	2112-1698	10	0.420 ± 0.017
	2165-1933	6	0.400 ± 0.021
Tungsten	1930-1589	9	0.168 ± 0.004
	2087-1757	9	0.163 ± 0.006

specific heat and total emittance of tungsten, molybdenum, and rhenium, using wire samples of 0.254-cm. diameter. They noted the constancy of  $C_p/\epsilon$  for tungsten between 1000 and 2800°K. as  $C_p/\epsilon = 0.124$  cal./g. °K. From their data for molybdenum between 1500 and 2800°K.,  $C_p/\epsilon = 0.303$  cal./g. °K. For rhenium between 1400 and 2700°K., their data give  $C_p/\epsilon = 0.123$  cal./g. °K. The agreement for tungsten and molybdenum between this and Rudkin's<sup>4</sup> work is fair; closer agreement cannot be expected as their wire samples had different surface structure than the material used here. Important, however, is the fact that the ratio  $C_p/\epsilon$  is constant.

The specific heat  $C_p$  can be determined with an accuracy of 4-5% in the 1000-3000°K.<sup>5</sup> temperature range and thus the emittance  $\epsilon$  is obtained. It must be noted that  $\epsilon$  can be determined by measurement of  $C_p/\epsilon$  and estimation of  $C_p$ .

### Error Considerations

The major errors in the determinations are due to the measurement of the temperature. The error in reading the pyrometer is 6°K. Taking an average temperature of 1500°K., this amounts to an uncertainty of 1.2% in  $1/T^3$ . The error in calibration of the pyrometer is 6° at 1500°K. The uncertainty in the corrections owing to window absorption and non-black body conditions (spectral emissivity) is taken as 10% of the measured correction, giving 2 and 13°, respectively, amounting to 0.4 and 2.5% in  $1/T^3$ . The total uncertainty in  $1/T^3$  is 3.2%. To determine  $C_p/\epsilon$  the slope of the curve of  $\theta$  vs.  $1/T^3$  is required (eq. 8). Though values of  $1/T^3$  are uncertain to 3.2%, the slope of the curve can have larger errors than that. This is borne out by inspecting the last column of Tables III-V where the error in the slope is between 5 and 8%. Thus, the over-all accuracy of  $C_p/\epsilon$  is 10%.

In the derivation of the equations, the assumption is made that the surface temperature of the sample is uniform. "Surface" means the thin layer of the material from which all the energy is radiated. If this surface temperature is not uniform, eq. 7 does not hold; instead, the radiated energy has to be obtained by averaging over  $T^4$ . The other assumption made is that the temperature of the bulk is the same as or close to that of the surface and that the temperature gradients within the sample are negligible. If large temperature gradients exist in the sample, the value of  $C_p$  used in eq. 7 has to be obtained again by averaging. However, the specific heat varies slowly with temperature. For tantalum,<sup>5</sup>  $C_p$  increases only 1% between 1500 and 1600°K.; thus, a temperature gradient within the sample of 30-40°K. will give an uncertainty in  $C_p$  of 0.5%. For the same reason, a possible temperature difference of 20-30°K. between the radiating surface layer and the bulk material will introduce only a negligible error.

The reproducibility and self-consistency of the data in Tables IV and V indicate that these two assumptions are satisfied in the present case. For materials which are translucent (and the "radiating surface layer" is thick) and which are poor heat conductors, eq. 7 will not be applicable.

(5) M. Hoch and H. L. Johnston, *J. Phys. Chem.*, **65**, 855, 1184 (1961).

## On the Calculation of the Vibrational De-excitation Probabilities

by H. Shin\*

Department of Chemistry, Cornell University, Ithaca, New York  
(Received August 26, 1964)

In the evaluation of the essential part of the vibrational de-excitation probability per unit time,  $P$ , it is a common practice<sup>1-6</sup> to use the Laplace method<sup>7</sup> assuming there is a most probable value  $E^*$  of the initial relative translational energy  $E$  for the transition. Use of this method has been concerned only with the second-order term in the expansion of the exponent of the relevant integral around  $E = E^*$ , however, and the contribution of the terms higher than the second order have not been subjected to a critical investigation. In this note we discuss the correction terms which result from these higher-order terms and how significant they are compared to the leading term. For this study we assume the repulsive interaction  $V(x) = A \exp(-x/a)$ .

The de-excitation probability per unit time is obtained from the transition probability per collision  $p(E)$  by  $P = \int_0^\infty p(E)Z(E) dE$ , where  $Z(E)dE$  is the number of collisions per unit time suffered by each molecule, in which the initial relative translational energy is between  $E$  and  $E + dE$ . Both  $p(E)$  and  $Z(E)$  are predominantly controlled by their exponential parts so that we can write  $P = \alpha \int_0^\infty \exp(f(E)/\hbar) dE$ , where  $\alpha$  is the composite of the pre-exponential part in  $p(E)$  and  $Z(E)$ .

For small  $\hbar$ ,  $P$  can be given in terms of an integral representation

$$P = \alpha \int_c \exp\left[\frac{1}{\hbar} f(E)\right] dE \quad (1)$$

where  $c$  is some contour in the  $E$  plane. To determine  $P$  for  $1/\hbar \gg 1$ , we adjust the contour so that  $Re f(E)$  is everywhere as small as possible. Then the largest value of  $Re f(E)$  throughout the contour will be at a saddle point for  $f(E)$ . Near this point  $f(E) = f(E^*) + \frac{1}{2}f''(E^*)(E - E^*)^2 + \frac{1}{6}f'''(E^*)(E - E^*)^3 + \dots$ , where  $E^*$  is the solution of  $df(E)/dE = 0$ . Changing the variable of the integral to  $E = E^* + w_1(E^*) +$

$w_2(E^*)t$ , where  $w_1(E^*) = -f''(E^*)/f'''(E^*)$  and  $w_2(E^*) = (6i\hbar/f'''(E^*))^{1/3}$ , we obtain

$$P \sim \exp\left\{\frac{1}{\hbar} f(E^*) + \frac{1}{3\hbar} \frac{[f''(E^*)]^3}{[f'''(E^*)]^2}\right\} \times \int_{c'} \exp\left\{\frac{1}{\hbar} [i\hbar t^3 - \varphi(t^*)t]\right\} dt \quad (2)$$

where

$$\varphi(t^*) = \frac{[f''(E^*)]^2}{2[f'''(E^*)]} \left[ \frac{6i\hbar}{f'''(E^*)} \right]^{1/3}$$

Here  $c'$  is a new contour in the  $t$  plane, and  $t^*$  is the saddle point. In this integral  $Re(i\hbar t^3 - \varphi(t^*)t)$  is monotonic along the path, except at the saddle point, and we may apply the Laplace method to evaluate it asymptotically at  $t^* = -(\varphi/3i\hbar)^{1/2}$ . Use of this procedure then simply gives

$$\int_{c'} \exp\left\{\frac{1}{\hbar} [i\hbar t^3 - \varphi(t^*)t]\right\} dt \sim \exp\left\{\frac{1}{3\hbar} \frac{[f''(E^*)]^3}{[f'''(E^*)]^2}\right\} \quad (3)$$

Therefore, the exponent of  $P$  is

$$\frac{1}{\hbar} f(E^*) + \frac{2}{3\hbar} (f''(E^*))^3 / (f'''(E^*))^2$$

We now evaluate  $P$  by substituting an explicit expression for  $p(E)$ , *i.e.*,  $f(E)$  and its derivatives in the above expressions, which is obtained in terms of the WKB wave functions.<sup>4,8</sup> For  $V(x) = A \exp(-x/a)$ , this approach gives<sup>9</sup>

\* Department of Chemistry, University of Nevada, Reno, Nev.

(1) L. Landau and E. Teller, *Physik. Z. Sowjetunion*, **10**, 34 (1936).  
(2) R. N. Schwartz, Z. I. Slawsky, and K. F. Herzfeld, *J. Chem. Phys.*, **20**, 1591 (1952); R. N. Schwartz and K. F. Herzfeld, *ibid.*, **22**, 767 (1954).

(3) E. E. Nikitin, *Opt. i Spektroskopiya*, **6**, 141 (1959).

(4) B. Widom, *Discussions Faraday Soc.*, **33**, 37 (1962).

(5) J. T. Vanderslice and S. Weissman, *J. Chem. Phys.*, **37**, 2247 (1962).

(6) D. Rapp and T. E. Sharp, *ibid.*, **38**, 2641 (1963).

(7) N. G. de Bruijn, "Asymptotic Methods in Analysis," 2nd Ed., North-Holland Publishing Co., Amsterdam, 1961, Chapters 4 and 5.

(8) L. Landau and E. M. Lifshitz, "Quantum Mechanics," Pergamon Press, Ltd., London, 1958, pp. 178-183.

(9) H. Shin, *Can. J. Chem.*, **42**, 2351 (1964); *J. Chem. Phys.*, **42**, 59 (1965).



$$f(E) = \sqrt{2\pi\mu a} \sum_{n=1}^{\infty} \left[ (-1)^n \frac{\Delta^n}{n!} \times \Gamma(n - 1/2) E^{1/2-n} \right] - \frac{\hbar E}{kT} \quad (4)$$

where  $\mu$  is the reduced mass of the colliding molecules and  $\Delta$  ( $>0$ ) is the magnitude of the change in the oscillator's energy owing to the transition. From eq. 4 we obtain  $E^* = (\mu/2)^{1/3} (a\pi\Delta kT/\hbar)^{2/3} - \Delta/2$  and

$$f''(E^*) = - \frac{\sqrt{2\pi\mu a \Delta \Gamma(5/2)}}{E^{*5/2}} \times \left[ 1 - \frac{5}{4} \left( \frac{\Delta}{E^*} \right) + \frac{35}{24} \left( \frac{\Delta}{E^*} \right)^2 - \dots \right]$$

$$f'''(E^*) = \frac{\sqrt{2\pi\mu a \Delta \Gamma(7/2)}}{E^{*7/2}} \times \left[ 1 - \frac{7}{4} \left( \frac{\Delta}{E^*} \right) + \frac{63}{24} \left( \frac{\Delta}{E^*} \right)^2 - \dots \right]$$

When these expressions are substituted into eq. 2 and 3, with the aid of eq. 4, we obtain the final expression for  $P$ , in the asymptotic limit  $\hbar \rightarrow 0$

$$P \sim \exp \left\{ - \left( 1 + \frac{4}{75} \right) 3 \left[ \sqrt{\frac{\mu}{2}} \frac{\pi a \Delta k T}{\hbar} \right]^{2/3} \frac{1}{kT} + \frac{\Delta}{2kT} \right\} \quad (5)$$

If this expression is compared to the previous result<sup>1-6</sup> obtained by neglecting the higher-order terms in  $f(E)$ , it can be readily seen that  $-(4/25)(\mu/2)^{1/3}(a\pi\Delta kT/\hbar)^{2/3}/kT$  is the correction term resulting from the inclusion of these neglected terms. Therefore, the leading term of the exponent in these previous works is about 5.3% overestimated.

Since for various molecules the leading term is 15-30 at ordinary temperatures,<sup>2, 6</sup> taking account of the higher-order terms in  $f(E)$  may reduce the de-excitation probability by a factor of 2 to 5. Therefore, although the inclusion of such terms does not seriously change  $P$ , it is still an important factor to be concerned in any critical comparison between theories and experiments.

## Carbon-13 Chemical Shift Viewed as a Constitutive Property. II. Substituted Hydrocarbons

by George B. Savitsky, Robert M. Pearson, and Keishi Namikawa

Department of Chemistry, University of California, Davis, California (Received September 16, 1964)

It has been shown<sup>1</sup> that C<sup>13</sup> chemical shifts in simple unsubstituted hydrocarbons can be calculated by constitutive additivity with 2 p.p.m. standard error. Although substitution of hydrocarbons by polar groups leads to significant deviations from the constitutive rule, it is possible that these deviations may become useful and theoretically important parameters, as deviations from other constitutive properties, e.g., exaltations of molar refraction. The purpose of this paper is to present some patterns and trends in these deviations which begin to emerge from the available experimental data.

### Experimental

The C<sup>13</sup> chemical shifts were measured according to the procedure previously described.<sup>2</sup> All chemical shifts are reported in p.p.m. with respect to benzene (64.9 p.p.m. are subtracted from literature values originally reported in p.p.m. from CS<sub>2</sub>). All commercial reagents were checked for purity.

**Determination of Polar Bond Contributions to C<sup>13</sup> Chemical Shifts.** Assuming that the contribution of C-H bonds to C<sup>13</sup> chemical shifts is not affected by polar substituents, the constitutive contribution of a polar bond -X to the C<sup>13</sup> shift can be determined by subtracting 3 times the value of the -H bond parameter<sup>1</sup> (i.e., 95.4 p.p.m.) from the C<sup>13</sup> chemical shift of the corresponding CH<sub>3</sub>X. Some values of -X bond parameters thus obtained are listed in Table I. The =O bond parameter of the carbonyl oxygen was obtained by subtracting the values of -CH<sub>3</sub> and -H bond parameters<sup>1</sup> from the chemical shift of acetaldehyde.

**Monosubstituted Alkanes.** It was previously shown<sup>2</sup> that in the monosubstituted alkane series CH<sub>3</sub>X, C<sub>2</sub>H<sub>5</sub>X, *i*-C<sub>3</sub>H<sub>7</sub>X, and *t*-C<sub>4</sub>H<sub>9</sub>X, the effect of replacement of the hydrogen atoms bonded to the  $\alpha$ -carbon by methyl groups on the shift of that carbon varied significantly with the nature of X. This, in fact, implies

(1) G. B. Savitsky and K. Namikawa, *J. Phys. Chem.*, **68**, 1956 (1964).

(2) G. B. Savitsky and K. Namikawa, *ibid.*, **67**, 2430 (1963).

(10) A. V. Kleinberg and A. N. Terenin, *Dokl. Akad. Nauk SSSR*, **101**, 1031 (1955).

**Table I:** Some Values of Polar Bond Parameters Obtained from Literature by Using Constitutive Rule

Bond -X	Bond parameter in p.p.m. with respect to benzene	Ref.
-F	-42.1	a
-Cl	8.4	a
-Br	23.9	a
-I	55.6	a
-OCH <sub>3</sub>	-26.1	a
-N(CH <sub>3</sub> ) <sub>2</sub>	-14.2	a
-COCH <sub>3</sub>	9	a
-NO <sub>2</sub>	-32	b
-OH	-14.7	c
-CHO	3.7	a
-COOH	13.8	c
-CN	29	c
-CH <sub>2</sub> Cl	15.4	c
-CH <sub>2</sub> Br	12.9	c
-CH <sub>2</sub> I	10.1	c
-CH <sub>2</sub> OH	16.5	c
=O	-128.2	d

<sup>a</sup> H. Spiesscke and W. G. Schneider, *J. Chem. Phys.*, **35**, 722 (1961). <sup>b</sup> P. C. Lauterbur, *Ann. N. Y. Acad. Sci.*, **70**, 841 (1958). <sup>c</sup> See ref. 2. <sup>d</sup> J. B. Stothers and P. C. Lauterbur, *Can. J. Chem.*, **42**, 1563 (1964).

deviations from the constitutive rule exist in this series. However, if we combine the approximate correlation which was found<sup>2</sup> between the effect of replacement of the hydrogen atom on the  $\alpha$ -carbon by a methyl group and the C-X bond distance,  $d_X$ , with the values of constitutive bond parameters, the deviation,  $D_X$  in p.p.m., for a given X, from the constitutive rule in this series will be given by

$$D_X = n(1.50 - d_X)22.6 \quad (1)$$

where  $n$  is the number of carbon bonds attached to the monosubstituted  $\alpha$ -carbon. This expression compactly, although approximately, summarizes the correlation obtained in ref. 2. Thus, from the knowledge of the bond distance,  $d_X$ , and constitutive bond parameters, the chemical shifts of the  $\alpha$ -carbon in  $C_2H_5X$ ,  $i-C_3H_7X$ , and  $t-C_4H_9X$  can be estimated to within about 3-p.p.m. accuracy for X = F, Cl, Br, I, OH, NO<sub>2</sub>, and COOH.

*Allyl and Benzyl Derivatives.* There are six bond parameters involving single carbon-to-carbon bonds which were assigned various constitutive values in simple hydrocarbons.<sup>1</sup> Actually the empirical expression for the constitutive correlation (1) has been derived only for a bond of one type, *i.e.*, -CH<sub>3</sub>. It remains to be seen if the same expression is applicable

to the remaining five types of single bonds in mono-substituted alkanes. There are no sufficient data available at present which would allow us to test the applicability of expression (1) to the bonds -CH<sub>2</sub>-, -CH<, and  $\begin{array}{c} / \\ -C- \\ \backslash \end{array}$ . Besides, considerable branching would make unambiguous spectral assignments in the alkane region very difficult. On the other hand, the test for the -CH= and  $\begin{array}{c} // \\ -C \\ \backslash \end{array}$  bonds can be readily made by unambiguously determining the chemical shifts on the  $\alpha$ -carbon of allyl derivatives (CH<sub>2</sub>=CH-CH<sub>2</sub>X) and methylene carbon shifts in benzyl derivatives (C<sub>6</sub>H<sub>5</sub>-CH<sub>2</sub>-X), both of these carbons leading to clearly defined triplets in the alkane region. We have accordingly measured the shifts on the above-mentioned carbons in both series for some of the representative X's. The results of these measurements are compared in Table II with the calculated values using constitutive

**Table II:** The  $\alpha$ -Carbon Shifts of Some Allyl Derivatives and Methylene Carbon Shifts of Some Benzyl Derivatives Calculated from Bond Parameters and Expression 1

Carbon	Exptl.	Calcd.	Difference
CH <sub>2</sub> =CH-CH <sub>2</sub> Cl	84.4	82.6	1.8
CH <sub>2</sub> =CH-CH <sub>2</sub> Br	96.2	94.5	1.7
CH <sub>2</sub> =CH-CH <sub>2</sub> I	121.9	122.1	-0.2
CH <sub>2</sub> =CH-CH <sub>2</sub> OH	65.8	67.4	-1.6
C <sub>6</sub> H <sub>5</sub> -CH <sub>2</sub> -Cl	81.4	81.5	-0.1
C <sub>6</sub> H <sub>5</sub> -CH <sub>2</sub> -Br	96.6	93.4	3.2
C <sub>6</sub> H <sub>5</sub> -CH <sub>2</sub> -I	122.9	121.0	1.9
C <sub>6</sub> H <sub>5</sub> -CH <sub>2</sub> -CN	106.0	108	-2
C <sub>6</sub> H <sub>5</sub> -CH <sub>2</sub> -OCH <sub>3</sub>	54.2	54.9	-0.7

bond parameters and the constitutive correction (1). The close agreement between the calculated and experimental results covering a wide range of shifts and C-X bond distances indicates that the approximate expression (1) is also applicable to the two types of single bonds mentioned above.

The fact that expression (1) implies a constitutive correction which is associated only with C-C bonds, and not with less polarizable C-H bonds, seems to be in general agreement with the idea previously proposed<sup>2</sup> that trends in carbon shifts of monosubstituted alkanes can be qualitatively understood in terms of the inductive polarizabilities of the C-X and C-C bonds. Furthermore, if such is indeed the case, no constitutive correction associated with the C-C bond in the sym-

metrically disubstituted ethanes  $\text{CH}_2\text{X}-\text{CH}_2\text{X}$  would have to be required to predict the carbon shifts because of the compensation of the inductive effects of the two identical polar groups by one another. This is also borne out by experiment. The carbon chemical shifts of  $\text{CH}_2\text{Cl}-\text{CH}_2\text{Cl}$ ,  $\text{CH}_2\text{Br}-\text{CH}_2\text{Br}$ , and  $\text{CH}_2\text{I}-\text{CH}_2\text{I}$  calculated by the constitutive rule without the use of the constitutive correction (1) are 87.4, 100.4, and 129.3 p.p.m., respectively. The values experimentally obtained by us are 84.9, 98.0, and 126.3 p.p.m., in the same order. These predictions are within 3 p.p.m. of the experimental values. If the correction (1) were applied, the error would be as high as 8 p.p.m. for  $\text{X} = \text{Br}$ , and 11 p.p.m. for  $\text{X} = \text{I}$ .

**Polar Substituents Attached to  $\pi$ -Systems.** If one calculates the carbon chemical shifts on the substituted carbon in the  $\text{C}_6\text{H}_5\text{X}$  series<sup>3</sup> from constitutive bond parameters, considerable deviations result for various groups, as can be seen from Table III.

**Table III:** Deviations of Chemical Shifts from Constitutive Rule on the Substituted Carbon in the  $\text{C}_6\text{H}_5\text{X}$  Series

X	Exptl. <sup>a</sup>	Calcd.	Dev.
I	32.3	22.6	9.7
Br	5.4	-9.1	14.5
$\text{COCH}_3$	-9.3	-24	15
Cl	-6.4	-24.6	18.2
OH	-27.6	-47.7	20.1
$\text{N}(\text{CH}_3)_2$	-22.4	-47.2	24.8
$\text{OCH}_3$	-30.2	-59.1	28.9
F	-35.1	-75.1	40.0
$\text{NO}_2$	-19.6	-65	45

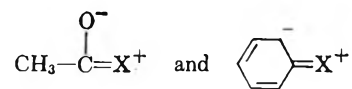
<sup>a</sup> H. Spiesecke and W. G. Schneider, *J. Chem. Phys.*, **35**, 731 (1961).

These deviations do not seem to be simply related to either inductive or resonance parameters. However, if one calculates the deviations on the carbonyl carbon in the  $\text{CH}_3-\text{CO}-\text{X}$  series (shown in Table IV), one finds that for the groups of the same mesomeric sign (I, Br, Cl, OH,  $\text{N}(\text{CH}_3)_2$ ,  $\text{OCH}_3$ ) these deviations parallel closely those of the  $\text{C}_6\text{H}_5\text{X}$  series.

In fact, the two sets of deviations,  $D_X$  (for  $\text{C}_6\text{H}_5\text{X}$  series) and  $D_X'$  (for  $\text{CH}_3-\text{COX}$  series) are fairly well related by the linear expression

$$D_X = 4.0 + 0.27D_X' \quad (2)$$

Thus, for all the common X with the same mesomeric sign listed in both tables the chemical shifts of  $\text{C}_6\text{H}_5\text{X}$  can be estimated from those of  $\text{CH}_3\text{COX}$  with an error not exceeding 2.5 p.p.m. by using (2). For these groups resonance structures of the types



place the carbons in the two systems under consideration in analogous electronic environments, and this may account for the observed parallelism between their

**Table IV:** Deviations of Chemical Shifts from Constitutive Rule on the Carbonyl Carbon in the  $\text{CH}_3-\text{CO}-\text{X}$  Series

X	Exptl.	Calcd.	Dev.	Ref.
I	-29.3	-47.8	18.5	a
$\text{COCH}_3$	-69.8	-94.5	24.7	b
Br	-40.9	-79.6	38.7	c
Cl	-41.1	-95.1	54.0	b
OH	-49.3	-118.2	68.9	b
$\text{N}(\text{CH}_3)_2$	-40.7	-117.5	76.8	c
$\text{OCH}_3$	-41.9	-129.6	87.7	b

<sup>a</sup> G. E. Maciel, private communication. <sup>b</sup> See ref. d, Table I. <sup>c</sup> Determined by us.

constitutive corrections. It is somewhat difficult, however, to rationalize the very large positive deviations in case of the carbonyl compounds. Stothers and Lauterbur<sup>4</sup> have already observed the shielding effect of the electronegative substituents on the carbonyl carbon. As a possible explanation for this they suggested that the electron-withdrawing substituents reduce the polarization of the  $\text{C}=\text{O}^-$  bond such that the electron density is increased at the carbonyl carbon thereby increasing the screening of the nucleus. The argument seems to be qualitatively correct, but the deviations in  $\text{CH}_3-\text{CO}-\text{X}$  compounds do not follow the order of induction except for halogens. For example, the  $\text{OCH}_3$  group results in significantly higher shielding than Cl. Making use of a recent theory which assumes the dominance of paramagnetic shielding in  $\text{C}^{13}$  chemical shifts, Pople<sup>5</sup> satisfactorily estimates the carbonyl carbon shifts in formaldehyde by assuming a polar MO for the  $\text{C}=\text{O}$   $\pi$ -bond

$$\Psi_{\pi z}(\text{C}-\text{O}) = 0.6\phi(\text{C};p_z) + 0.8\phi(\text{O};p_z)$$

To account quantitatively for the large upfield effect of the  $\text{OCH}_3$  group in terms of Pople's formulation, one

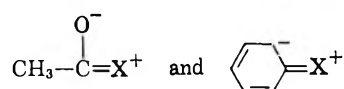
(3) The chemical shifts on substituted carbon in  $\text{C}_6\text{H}_5\text{X}$  series were calculated by using only one Kekulé-Lewis structure as in a previous article.<sup>1</sup> Accordingly the constitutive bond parameters corresponding to the  $-\text{CH}=\text{}$ ,  $=\text{CH}$ , and  $-\text{X}$  bonds were summed up. The carbonyl shifts in  $\text{CH}_3\text{COX}$  series were calculated by summing up the bond parameters corresponding to  $-\text{CH}_3$ ,  $=\text{O}$ , and X.

(4) See ref. d, Table I.

(5) J. A. Pople, *Mol. Phys.*, **7**, 301 (1963-1964).

would have to assume that the  $\text{OCH}_3$  group attached to the carbonyl carbon would reverse the polarity of the carbonyl bond by induction if other factors were not important, which seems to be rather unlikely. In this type of calculation, however, we have so far tacitly assumed that the average energy of excitation,  $\Delta E$ , which appears in the denominator of Pople's expression for paramagnetic shielding<sup>5</sup> is practically constant in a homologous series of molecules. This may not and need not be actually so, and as little as 10% uncertainty in  $\Delta E$  may lead to about 40-p.p.m. uncertainty in the carbonyl shifts. Furthermore, the constitutive corrections in these systems may reflect not only the interaction of substituents with the  $\pi$ -systems but also an additional effect of changing from  $\text{sp}^3$  to  $\text{sp}^2$  hybridization.

The effect of resonance on the carbon shifts in these systems is very difficult to assess even on a qualitative basis. It must be borne in mind that in the contributing resonance structures, such as



the carbons in question are merely resonance transmitting. They cannot be qualitatively compared with *ortho* and *para* carbons in substituted benzenes on which the development of charge can be discussed in terms of enhanced screening. On the other hand, resonance may contribute to a more asymmetric charge distribution around the carbons in question and hence to increased anisotropy of their electronic environment.

Another feature of resonance which cannot be ignored is the extent to which it may affect the average excitation energy,  $\Delta E$ , in these molecules.

Thus, according to Jaffé and Orchin,<sup>6</sup> substitution of a group with a lone pair as  $\text{NR}_2$ ,  $\text{OR}$ , or halogen, into the carbonyl group, as in amide, ester, or acid chloride results in a pronounced effect on the  $n \rightarrow \pi^*$  transition energy. The atoms with the lone-pair electrons influence such transitions both by resonance and inductive effect. Even in the absence of inductive effect the  $\pi^*$  level is raised by resonance, thus leading to higher excitation energies. The lone-pair atoms, O, N, and Cl, are more electronegative than carbon and hydrogen, and the lone-pair electrons on the carbonyl oxygen are held more firmly than they would be in ketones and aldehydes. The effects of resonance and induction are difficult to separate, but the  $n \rightarrow \pi^*$  excitation energies follow the order  $\text{O} > \text{N} > \text{Cl} > \text{H}$  in  $\text{CH}_3\text{COX}$  compounds, where O, N, Cl, and H are the atoms of the group X immediately attached to the carbonyl. It is noteworthy that the deviations in carbonyl shifts in

ester, amide, and acid chloride with respect to acetaldehyde follow exactly the same trend. If  $n \rightarrow \pi^*$  transition energies are to be assumed to follow the same order as the average excitation energies,  $\Delta E$ , then this would be in agreement with Pople's formulation,<sup>5</sup> according to which high excitation energies lead to high-field shifts. The very range of variation in  $n \rightarrow \pi^*$  transition energy (it is about 30% higher in esters than in acetaldehyde) accounts for the right order of magnitude of the deviations from constitutive additivity in these molecules.

It would thus be tempting to conclude that, at least in the case of carbonyl shifts, the energy of excitation,  $\Delta E$ , plays the dominant role.

However, in the case of the benzene series such an explanation is untenable, since substitution by X usually leads to the lowering in  $\Delta E$ . If other factors in the  $\text{C}_6\text{H}_5\text{X}$  series are more important, the empirical correlation (2) will have to be regarded, at best, as being merely fortuitous.

We have thus been unable to find a simple and unambiguous explanation for the trends in deviations from constitutive additivity in these two systems. We feel, however, that the statement of the problem and the factors involved, conflicting as they seem to be at present, may help in the future attempts to understand the delicate interplay of various effects which contribute to the over-all  $\text{C}^{13}$  chemical shifts in substituted hydrocarbons.

*Acknowledgment.* The authors wish to express their gratitude to the Research Corp. for the financial support of this work and to Professor G. E. Maciel for helpful discussions and suggestions.

(6) H. H. Jaffé and M. Orchin, "Theory and Applications of Ultraviolet Spectroscopy," John Wiley and Sons, Inc., New York, N. Y., 1962, pp. 178-181.

## Carbon-13 Isotope Effects in the Oxidation of Acetic Acid

by Mieczysław Zieliński<sup>1</sup>

Enrico Fermi Institute for Nuclear Studies, University of Chicago, Chicago, Illinois (Received October 5, 1964)

The oxidation of organic compounds by the Van Slyke-Folch<sup>2</sup> "wet" method is a convenient and widely applied procedure. Acetic acid, because of its critical importance in metabolism, is often a sample material

for such oxidation and, also frequently, isotopically labeled acetic acid or acetate is the isolate under study.

Earlier investigations<sup>3,4</sup> have demonstrated that there is an appreciable kinetic isotope effect associated with the wet oxidation of acetic acid (as acetate) labeled with C<sup>14</sup>; the results, however, are discrepant. Evans and Huston<sup>3</sup> do not indicate the degree or increment of decomposition involved in their experiments (in which specific activity measurements were made on "two consecutive fractions of roughly the same weight"), but Eyring and Cagle<sup>5</sup> estimated their results to be equivalent to a 5% isotope effect in the oxidation of the carboxyl-labeled acetate. In the later experiments,<sup>4</sup> an effect of  $1.7 \pm 0.5\%$  was observed in the oxidation of carboxyl-labeled acetate, but a  $4.0 \pm 0.6\%$  effect in that of the methyl-labeled compound was observed.

Because of the intrinsically more accurate measurements possible of C<sup>13</sup> isotope effects compared with those of C<sup>14</sup>, it was of interest to attempt to resolve the discrepancy described above by investigations of the oxidation of acetate containing C<sup>13</sup> at the natural abundance level.

### Experimental

Samples of acetate mixed with excess solid sodium hydroxide were pyrolyzed quantitatively in copper vessels to methane and carbonate—the former being oxidized to carbon dioxide over copper oxide, the latter being converted to carbon dioxide with phosphoric acid. Isotope ratio measurements on these samples permitted evaluation of the ratio ( $C^{13}H_3C^{12}OOH/C^{12}H_2C^{13}OOH$ ) =  $Q$ .  $Q_0$  was found to be 1.0074 for the acetate used, and the average of the methane-carbon and carboxyl-carbon isotope ratios was identical with that obtained for carbon dioxide resulting from complete combustion (over copper oxide) of the original acetate,  $R_0$ .

The partial oxidation experiments were carried out using the Van Slyke-Folch procedure. Values of  $Q_t$  and  $R_t$  (the ratio indicated above and the ratio  $C^{13}O_2/C^{12}O_2$  at time  $t$  or degree of reaction  $f$ ) were obtained in each of three runs.

Where  $k_1$  is the specific rate constant for the oxidation of  $C^{12}H_3C^{12}OOH$ ,  $k_2$  that for  $C^{12}H_3C^{13}OOH$ , and  $k_3$  that for  $C^{13}H_3C^{12}OOH$ , it can be shown that

$$\frac{k_1}{k_2} = \left[ \frac{1 + Q_t k_3/k_2}{1 + k_3/k_2} \right] \frac{\ln [1 - f]}{\ln \left[ 1 - \frac{(1 + Q_0) R_t}{1 + (k_3/k_2) R_0} \right]}$$

Use of this formula with the present data requires a value for  $k_3/k_2$ ; this we take from the C<sup>14</sup> results of Zlotowski and Zielinski to be  $0.9879 \pm 0.004$ , assuming that the C<sup>14</sup> kinetic isotope effect would be twice the C<sup>13</sup> effect.

From the three experiments we obtain  $k_1/k_2 = 1.0098 \pm 0.0030$ . Combination with the assumed value for  $(k_3/k_2)$  yields  $k_1/k_3 = 1.0221 \pm 0.005$ . Though the value of  $k_1/k_3$  is not independent of the earlier C<sup>14</sup> results, it is, nevertheless, of interest to compare these isotopic rate constant ratios for the C<sup>13</sup> effects with those calculated directly from the C<sup>14</sup> data. We have  $(k_1/k_2)_{\text{calcd}} = 1.0087$  (compare with 1.0098) and  $(k_1/k_3)_{\text{calcd}} = 1.021$  (compare with 1.0221). The present results are thus consistent with the earlier findings of Zlotowski and Zielinski for the wet oxidation of acetic acid.

*Acknowledgment.* The author expresses his thanks to Professor Robert N. Clayton for making possible his stay at the Enrico Fermi Institute and for assistance in the preparation of this note. Also, the author expresses appreciation to Professor Peter E. Yankwich, the referee of this note, for introducing substantial changes which made the whole note clearer and more systematic. The research was supported in part by a grant from the National Science Foundation (NSF-GP-2019).

(1) Department of Nuclear Chemistry, University of Warsaw, Poland.

(2) D. D. Van Slyke and J. Folch, *J. Biol. Chem.*, **136**, 509 (1940).

(3) E. A. Evans and J. L. Huston, *J. Chem. Phys.*, **19**, 1214 (1951).

(4) I. Zlotowski and M. Zielinski, *Nukleonika*, **4**, 5 (1959).

(5) H. Eyring and F. W. Cagle, *J. Phys. Chem.*, **56**, 889 (1952).

### Magnetic Resonance of the Triplet State of Oriented Pyrene Molecules<sup>1a</sup>

by O. Hayes Griffith<sup>1b</sup>

*Gates and Crellin Laboratories of Chemistry,<sup>1a</sup> California Institute of Technology, Pasadena, California (Received November 2, 1964)*

Bree and Vilkos<sup>2</sup> have recently completed an optical polarization study of the lower singlet states of pyrene in a fluorene matrix at 77°K. The crystal structure of fluorene is orthorhombic, the space group is Pnam, and there are four molecules per unit cell.<sup>3</sup> This crystal is a convenient matrix because the long axes of the fluorene molecules are all parallel to the crystalline  $c$  axis. We report here the observation of electron

(1) (a) Supported by the National Science Foundation under Grant No. GP-930; (b) National Science Foundation Predoctoral Fellow; (c) Contribution No. 3181.

(2) A. Bree and V. V. B. Vilkos, *J. Chem. Phys.*, **40**, 3125 (1964).

(3) D. M. Burns and J. Ibal, *Proc. Roy. Soc. (London)*, **A227**, 200 (1955).

spin resonance of the lowest triplet state of pyrene in a fluorene matrix.

The fluorene ( $C_{13}H_{10}$ ), kindly supplied by D. E. Wood, was prepared from commercial reagent grade fluorenone. The fluorenone was purified by column chromatography (column: alumina; wash: spectral quality cyclohexane) and was reduced with hydrazene hydrate.<sup>4</sup> The resulting fluorene was then chromatographed as mentioned previously and sublimed.<sup>5</sup> The pyrene ( $C_{16}H_{10}$ ) was prepared by zone refining (30–50 zones) commercial reagent grade pyrene. The crystals of pyrene-doped fluorene were grown from a melt initially containing 1.0 mole % of pyrene, but the actual concentrations of pyrene in the crystals were not determined.<sup>6</sup> These crystals were found to cleave in the (001) plane, and the positions of the *a*, *b*, and *c* axes were determined by X-ray crystallographic techniques. The actual crystal fragments used in the e.s.r. experiments were initially oriented with a polarizing microscope and were not subjected to X-irradiation until after the e.s.r. experiments were complete. The crystals were illuminated *in situ* with a General Electric BH-6 Hg arc lamp, and the temperature of the sample was maintained at 100°K. throughout the experiments with a conventional nitrogen gas flow system. A Varian X-band spectrometer was used to obtain the spectra. Magnetic fields corresponding to the extrema (or near extrema) splittings were measured with a rotating coil gaussmeter, and the remainder of the fields were measured with a Hall-effect probe.

The e.s.r. spectra were recorded with the magnetic field, **H**, in the *ac*, *bc*, and *ab* planes of the pyrene-doped fluorene crystals. Two e.s.r. lines displaced symmetrically about  $g \approx 2.0030$  were observed with **H** in the *ac* or *bc* planes, and the maximum splitting between these two lines occurred when **H** was perpendicular to the cleavage plane. In general, four lines were observed with **H** in the crystallographic *ab* plane. All of the e.s.r. lines decayed rapidly upon removal of the light source (lifetime < 1–2 sec.).

Using the method of Hutchison and Mangum,<sup>7,8</sup> the *g* values and zero field splitting parameters of the Hamiltonian  $\mathcal{H} = \beta \mathbf{H} \cdot \mathbf{g} \cdot \mathbf{S} + DS_z^2 + E(S_x^2 - S_y^2)$  were found to be  $g_{zz} = 2.0033$ ,  $g_{yy} = 2.0026$ ,  $g_{xx} = 2.0033$ ,  $D(xy)/hc = \pm 0.0806 \text{ cm.}^{-1}$ ,  $D(z)/hc = \pm 0.0810 \text{ cm.}^{-1}$ , and  $E/hc = \pm 0.0182 \text{ cm.}^{-1}$ . The estimated errors in the *g* values, *D*, and *E* are  $\pm 0.0005$ ,  $\pm 0.0012$ , and  $\pm 0.0009$ , respectively. The limits of error are uncomfortably large because the e.s.r. signals were very weak, frequently being only a factor of 1.5 to 8 above the noise level. Employing these values of the parameters in the above spin-Hamiltonian and allowing for the symmetry properties of the fluorene lattice, the posi-

tions of all observed lines can be predicted within experimental error. Therefore, it is clear that the e.s.r. signals result from one type of molecule, and this molecule occupies a substitutional site in the fluorene lattice. It remains to show that this molecule is pyrene.

Single crystals of fluorene exhibited a faint blue-green phosphorescence at boiling nitrogen temperatures, and corresponding weak lines were present in the phosphorescence emission spectra of these crystals. However, under the same experimental conditions that the e.s.r. spectra were obtained from the pyrene-doped fluorene crystals, no e.s.r. signals were observed from single crystals of fluorene, and therefore it is highly unlikely that the above e.s.r. spectra are due to either fluorene or an impurity in fluorene. The zone-refined pyrene undoubtedly contains impurities, the most troublesome of which is probably naphthacene<sup>9</sup> ( $C_{18}H_{12}$ ). A single crystal of naphthacene-doped fluorene was grown from a melt containing 0.01 mole % of naphthacene, and no e.s.r. signals were observed at 100°K. in these crystals. The pyrene-doped fluorene crystals exhibited a reddish phosphorescence at low temperatures similar to the phosphorescence of pyrene in a hydrocarbon glass. The maximum of the only line observed in the 77°K. phosphorescence spectra of the pyrene-doped fluorene crystals occurred at  $16,750 \pm 60 \text{ cm.}^{-1}$ , which is in good agreement with the phosphorescence maximum reported for pyrene in glasses at 77°K.<sup>10</sup> The emission lines observed in the fluorene

(4) J. H. Weissberger and P. H. Grantham, *J. Org. Chem.*, **21**, 1160 (1956).

(5) Fluorene prepared by this procedure exhibited far lower phosphorescence intensity at 77°K. than did zone-refined commercial reagent grade fluorene. According to D. E. Wood (private communication), some samples of fluorene prepared by this technique (with additional zone refining in some cases) produced a negligible phosphorescence.

(6) Cold traps were used during the crystal preparations to prevent possible contamination from stopcock grease, and the chemicals were melted only under reduced pressures of prepurified nitrogen gas to minimize oxidation and decomposition.

(7) C. A. Hutchison, Jr., and B. W. Mangum, *J. Chem. Phys.*, **34**, 908 (1961).

(8)  $D(xy)$  is the value of *D* obtained along with *E* from the (extrema) splittings corresponding to the molecular *x* and *y* directions, and  $D(z)$  is the value of *D* obtained using *E* and the (extremum) splitting corresponding to the molecular *z* direction. The agreement of these two values of *D* constitutes a partial verification of the proper choice of molecular axes. Using these values of *D* and *E*,  $(D^2 + 3E^2)^{1/2} = 0.0868 \pm 0.002$ . This value is in only fair agreement with the value  $0.0929 \text{ cm.}^{-1}$  obtained by Smaller [B. Smaller, *J. Chem. Phys.*, **37**, 393 (1963)] (and confirmed by us) from the  $\Delta m = \pm 2$  transition of randomly oriented pyrene molecules.

(9) However, the zone-refined, crystalline pyrene appeared white rather than the yellow color characteristic of small concentrations of naphthacene.

(10) McClure reports [D. S. McClure, *J. Chem. Phys.*, **17**, 910 (1949)] that for pyrene in a rigid glass at 77°K. the phosphorescence maximum occurs at  $16,800 \text{ cm.}^{-1}$ , the ratio of phosphorescence yield to fluorescence yield is 0.001, and the mean lifetime is about 0.2 sec.

crystal were apparently quenched in the pyrene-doped fluorene crystal. All of the above evidence supports the conclusion that the e.s.r. spectra observed in the pyrene-doped fluorene crystals arise from the (lowest) triplet state of pyrene.

Further splitting of the fine-structure e.s.r. lines into hyperfine lines was not observed in any of the spectra recorded,<sup>11</sup> and, therefore, it is not possible to determine uniquely the orientations of the pyrene molecules in the fluorene lattice. However, one of the principal magnetic axes of pyrene lies approximately along the crystalline *c* axis (the long axis of fluorene), and the other two magnetic axes correspond to the short axis and a normal to the molecular plane of fluorene. It appears, therefore, that the molecular plane and long axis of the pyrene molecule are oriented with respect to the fluorene lattice in the same manner as the displaced fluorene molecule. If we assume this to be the case, then the molecular *z*, *y*, and *x* axes of pyrene would be parallel to the long axis, the short axis, and the normal to the molecular plane of the pyrene molecule, respectively.<sup>12</sup>

*Acknowledgments.* We are indebted to Professor Harden M. McConnell for the generous use of his laboratory facilities. We are also indebted to Dr. Richard E. Marsh for help concerning the X-ray photography, to Professor Melvin W. Hanna for helpful discussions, and to Mrs. Lelia M. Coyne for obtaining the optical spectra.

(11) The lack of resolution is presumably due to the large number of protons interacting with the electron and to crystal disorder. Laue photographs disclosed that the first crystals obtained were badly disordered. The crystals used for the e.s.r. study were of much better quality but could have been sufficiently disordered to reduce resolution of the hyperfine structure.

(12) By convention,<sup>7</sup> *D* and *E* for pyrene were arbitrarily chosen to have opposite signs. If *D* and *E* were chosen to have the same sign then the *x* and *y* axes would be interchanged. This indeterminacy affects only the relative signs of *D* and *E* and not their magnitudes. We are indebted to Dr. J. H. van der Waals for a discussion on this point.

### Computation of Statistical Complexions. III. An Exact High Speed Method

by E. W. Schlag, R. A. Sandsmark, and  
W. G. Valance

Department of Chemistry, Northwestern University,  
Evanston, Illinois (Received November 6, 1964)

There has been a substantial increase in interest in obtaining information about kinetic rate processes on a

molecular level. For such experiments it is necessary that one is able to define initial states as closely as possible in order to be able to discriminate between various possible theoretical models on the basis of the experimental results. One such approach has been to study the reactions of monoenergetically excited species.<sup>1</sup> One then wishes to compute a set of theoretical transition probabilities for reaction or energy transfer and then use this set to generate the appropriately predicted laboratory observable.<sup>2</sup> If the set of transition probabilities involves any statistical factors, then one needs to know the number of states that all have a total energy between *E* and *E* + *dE*, known simply as the density of states  $\rho(E)$  at *E*. For example, in the RRKM version of unimolecular rate theory, the transition probability for reaction at *E* is just proportional to a simple ratio<sup>3</sup> of two such numbers, that for an activated complex (at a reduced *E*) to that for excited molecules at *E*. Similar considerations may arise for some theories of energy transfer.<sup>2</sup> Hence, ideally, one would like to generate a set  $\rho(E)$  for all *E* of interest, for all relevant species. The primary information for such a computation would just be the frequency spectrum of each of the species.

In detail, the generation of such a complete set of  $\rho(E)$  just amounts to a computation which takes the molecule to be a collection of noncommensurate and perhaps anharmonic oscillators. The approximation that considers all oscillators to be identical leads to serious inaccuracies.<sup>4</sup> One can, however, simplify the problem by neglecting anharmonicity effects, which may often be a justifiable approximation.<sup>5</sup> There has been some question as to the formula to be employed in the computation of this density at *E*. Rice and Marcus<sup>3</sup> presented a modification of the classical value for use at higher energies. (At lower energies they suggested a detailed count of possible complexions.) Rabinovitch and Diesen<sup>6</sup> pointed to inadequacies in this expression for typical high energies of kinetic

(1) For examples, see: (a) B. S. Rabinovitch and M. C. Flowers, *Quart. Rev. (London)*, **18**, 122 (1964); (b) G. B. Porter and B. T. Connelly, *J. Chem. Phys.*, **33**, 81 (1960); (c) A. N. Strachan, R. K. Boyd, and K. O. Kutschke, *Can. J. Chem.*, **42**, 1345 (1964).

(2) For a discussion of the various methods of calculating laboratory observables from transition probabilities and their difficulties, see R. V. Serauskas and E. W. Schlag, *J. Chem. Phys.*, in press, and references cited therein.

(3) R. A. Marcus and O. K. Rice, *J. Phys. Colloid Chem.*, **55**, 894 (1951).

(4) This can be seen from the expression developed by L. S. Kassel for nonidentical harmonic oscillators, *ibid.*, **32**, 1065 (1928).

(5) See E. W. Schlag, R. A. Sandsmark, and W. G. Valance, *J. Chem. Phys.*, **40**, 1461 (1964), for a typical evaluation of the anharmonic contributions to the density of states.

(6) B. S. Rabinovitch and R. W. Diesen, *ibid.*, **30**, 735 (1959). See also G. Z. Whitten and B. S. Rabinovitch, *ibid.*, **38**, 2466 (1963).

interest, and introduced an empirical correction factor. Schlag and Sandsmark<sup>7</sup> suggested a nonempirical finite series, which had a leading term identical with the single term expression given by Marcus and Rice.<sup>3</sup> Further terms become important at lower energies. Schlag and Sandsmark, however, had developed only the first three terms of their series. More recently, further terms in this series were developed by an inverse Laplace transform expansion technique.<sup>8,9</sup> In particular, Thiele has given a general coefficient<sup>10</sup> from which, as he has shown, the first four terms of the series of Schlag and Sandsmark can be generated by a multinomial formula. In view of the apparent usefulness of an exact and simple method for generating  $\rho(E)$ , it was decided to generate the complete series for several molecules from this multinomial formula and compare this method of counting with a detailed combinatorial calculation.<sup>7</sup> This was programmed on a computer since the collation of terms becomes an impossible bookkeeping task.

The general term in the series is generated by a proper collection of Thiele's specific terms. The number of terms in this series, when complete, is approximately half the number of vibrational degrees of freedom. The complete series was computed for methyl chloride, cyclopropane, cyclopropane-*d*<sub>6</sub>, CBr<sub>3</sub>Cl, CCl<sub>2</sub>O, CHBr<sub>3</sub>, C<sub>2</sub>H<sub>4</sub>, C<sub>4</sub>H<sub>2</sub>, and benzene.<sup>11</sup> The typical computation time was about 1 min. to calculate a complete set of densities,  $\rho(E)$ , for all  $E$  up to 250 kcal. When one compares the densities obtained from the complete series with exact combinatorial calculations,<sup>7</sup> one finds only small discrepancies for these molecules at 10 kcal. and above, at most 10%, the discrepancy being further reduced at higher energies (see Table I). Below this energy, the densities fluctuate more strongly about the average value given by the series. This causes no difficulty since it takes but a few seconds to compute the values up to 10 kcal. by the exact combinatorial method.<sup>7</sup> Hence, one can reduce the exact

calculation of densities to a very high speed computer subroutine. For an arbitrary group of frequencies, the subroutine will generate the value for all densities,  $\rho(E)$ , up to 250 kcal.<sup>12</sup>

*Acknowledgment.* The support of this work by a grant from the Petroleum Research Fund of the American Chemical Society is gratefully acknowledged.

(7) E. W. Schlag and R. A. Sandsmark, *J. Chem. Phys.*, **37**, 168 (1962).

(8) (a) P. C. Haarhoff, *Mol. Phys.*, **6**, 337 (1963); (b) P. C. Haarhoff, *ibid.*, **7**, 101 (1963).

(9) E. Thiele, *J. Chem. Phys.*, **39**, 3258 (1963).

(10) It should be pointed out that these are only the coefficients for the expansion about the pole  $\beta = 0$ . The effect of higher poles can be shown to just lead to oscillations on top of this smoothed function, without changing its average value as a function of energy. The effect of these higher poles will only be important for the first few kcal./mole. Computationally, this is adequately handled by a simple direct count up to 10 kcal./mole (see below). The Dirichlet integral technique of Schlag and Sandsmark effectively also rejects these oscillatory terms when it replaces a multiple sum by a multiple integral. Since only the first 10 kcal./mole are involved, a direct count procedure is to be preferred to explicitly including quantum corrections in the series techniques.

(11) Frequencies chosen were those listed in ref. 6.

(12) A copy of the program written in IBM Fortran IV (IBSYS system) with instructions is available upon request.

## Comparison of Water Sorption and Deuterium-Hydrogen Exchange Sites in Poly-L-valine<sup>1a</sup>

by W. W. Brandt and R. S. Budrys<sup>1b</sup>

*Department of Chemistry, Illinois Institute of Technology, Chicago, Illinois 60616 (Received November 30, 1964)*

Measurements of deuterium-hydrogen (D-H) exchange capacities and rates on dissolved polypeptides or proteins have become one of the standard methods to determine the chain conformations of these macromolecules.<sup>2</sup> H atoms which are readily exchanged are usually assumed to be easily accessible. In solid polymers, on the other hand, D-H exchange capacities may

(1) (a) This work was supported by PHS Grant AM-4324. Material supplementary to this article has been deposited as Document No. 8130 with the ADI Auxiliary Publications Project, Photoduplication Service, Library of Congress, Washington 25, D. C. A copy may be secured by citing the document number and by remitting \$2.50 for photoprints, or \$1.75 for 35 mm. microfilm. Advance payment is required. Make checks or money orders payable to: Chief, Photoduplication Service, Library of Congress. (b) Abstracted in part from the work of R. S. B. to be submitted in partial fulfillment of the research requirements for the Ph.D. degree in the Department of Chemistry, Illinois Institute of Technology.

(2) H. A. Scheraga, "Protein Structure," Academic Press, Inc., New York, N. Y., 1961.

Table I

Molecule	Discrepancy at (in %)		
	10 kcal.	15 kcal.	20 kcal.
Methyl chloride	8.16	-0.52	-1.73
Cyclopropane	-9.45	-3.47	-2.00
Cyclopropane- <i>d</i> <sub>6</sub>	3.70	-0.33	-0.80
CBr <sub>3</sub> Cl	-0.01	-0.02	-0.01
CCl <sub>2</sub> O	0.88	-0.19	0.04
CHBr <sub>3</sub>	1.37	-0.01	-0.22
C <sub>2</sub> H <sub>4</sub>	0.32	0.00	
C <sub>4</sub> H <sub>2</sub>	-3.80	1.50	-1.42
Benzene	3.86	-1.93	-1.70



likewise yield a measure of the accessibility of amide groups, provided diffusion to or from the neighborhood of the polymer exchange site is relatively fast and not rate controlling.

A second possible measure of the accessibility of polar groups is the "monolayer area," derived from sorption isotherm data using B.E.T. theory. Various polypeptide-sorbate systems have been treated in this fashion.<sup>3-5</sup>

There is considerable doubt whether the two measures of sorption site accessibility mentioned above should agree. Hnojewyj and Reyerson found that sorption and exchange sites in poly-L-glutamic acid are not identical, while earlier studies on proteins seemed to indicate their equivalence.<sup>6</sup> More recent work of Ehrlich and Bettelheim<sup>7</sup> showed that sorption and exchange sites in mucopolysaccharides are probably different.

In view of these findings, one may suspect that a number of sorption and exchange sites are in fact identical, but that some are not. To test this idea, D-H exchange experiments were carried out on two poly- $\alpha$ -amino acids for which sorption isotherm data are already available.<sup>3b,4</sup>

### Experimental

The poly-L-valine (PV) and poly-L-leucine (PL) used in the present work are the ones described earlier.<sup>3b,4</sup> One of the two PV samples used had previously been exposed to TFA (trifluoroacetic acid). The exchange experiments were carried out using a quartz balance of conventional design. The samples were degassed, exposed to D<sub>2</sub>O vapor, and after a definite time the D<sub>2</sub>O vapor was quickly removed and replaced by a new batch of undiluted vapor. The procedure was repeated until there was no further change in the sample weight. The results are plotted as the number of moles of D exchanged per polymer repeat unit against the cumulative time of exposure.

### Results and Discussion

From Figure 1 one notes that the PV used has a much higher exchange capacity than PL. Thus, there is a definite correlation to the sorption uptake for HCl and TFA on fresh samples of the two polymers. A numerical agreement of the number of exchange sites and of sorption sites cannot be tested because the isotherms do not permit an unambiguous estimate of the sorption "monolayer." The relatively high exchange and sorptive capacity of PV are in accord with the low quality of its  $\beta$  structure, as judged from X-ray diffraction patterns.

Interestingly, the number of D atoms introduced into PV is distinctly larger than what corresponds to complete exchange at the polymer chain end groups only. The converse is true for PL.

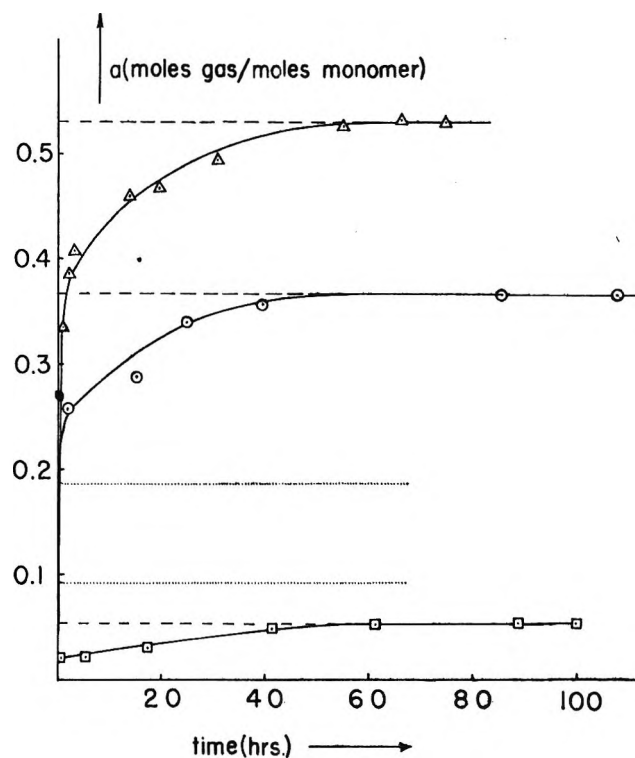


Figure 1. Deuterium-hydrogen exchange capacities at 75.2°:  $\square$ , poly-L-leucine;  $\circ$ , poly-L-valine in original form; and  $\Delta$ , poly-L-valine after prolonged exposure to trifluoroacetic acid. Dotted lines indicate approximate D-H exchange expected if only chain ends are involved; upper line, poly-L-valine; lower line, poly-L-leucine.

Aside from the gross correlation of sorptive and exchange capacities, there is an interesting discrepancy: the PV sample which was previously exposed to TFA takes up much less of this sorbate, compared to the original sample.<sup>3b</sup> This is in accord with the improvement in the polymer secondary structure, seen in the X-ray diffraction patterns.<sup>3b</sup> On the other hand, the D-exchange capacity is markedly increased. We conclude that the accessibility, measured as the D-H

(3) (a) L. Pauling, *J. Am. Chem. Soc.*, **67**, 555 (1945); (b) W. W. Brandt and R. S. Budrys, *J. Biol. Chem.*, **239**, 1442 (1964).

(4) W. W. Brandt and R. S. Budrys, *J. Phys. Chem.*, **69**, 600 (1965).

(5) L. H. Reyerson and W. S. Hnojewyj, *ibid.*, **67**, 1945 (1963), and references cited there.

(6) W. S. Hnojewyj and L. H. Reyerson, *ibid.*, **67**, 711 (1963).

(7) S. H. Ehrlich and F. A. Bettelheim, *ibid.*, **67**, 1954 (1963).

exchange capacity, depends on the polymer secondary structure in a way not yet understood, and that at least some of the exchange sites are not functioning as sorption sites.

As an additional comment, sorption data reported earlier<sup>8</sup> show D<sub>2</sub>O to be sorbed more extensively than

H<sub>2</sub>O, confirming the findings of Hnojewyj and Reyerson on similar systems.<sup>9</sup>

(8) W. W. Brandt and R. S. Budrys, ADI, Library of Congress, Document No. 8130.

(9) W. S. Hnojewyj and L. H. Reyerson, *J. Phys. Chem.*, **65**, 1694 (1961).

## COMMUNICATIONS TO THE EDITOR

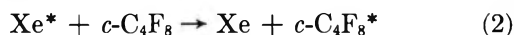
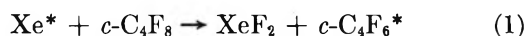
### The Importance of Xenon Fluorides in the Xenon-Photosensitized Reactions of the Perfluoroalkanes

*Sir:* No work has been reported on the xenon-photosensitized reactions of perfluoroalkanes since the work of Dacey and Hodgins in 1950.<sup>1</sup> They found that CF<sub>4</sub> was decomposed into a solid polymer and fluorine by Xe(<sup>3</sup>P<sub>1</sub>) with unit quantum efficiency although a product balance was not obtained. We are of the opinion that the xenon fluorides play a major role in this and other xenon-photosensitized reactions of the perfluoroalkanes. Following the development of a suitable all-quartz resonance lamp of improved design,<sup>2</sup> we investigated the reactions of C<sub>2</sub>F<sub>6</sub>, C<sub>3</sub>F<sub>8</sub>, and *c*-C<sub>4</sub>F<sub>8</sub>. Most of our work was done with the latter compound; hence, we will confine our discussion to it.

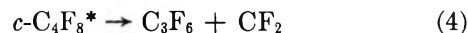
The products resulting from the xenon-photosensitized reaction of *c*-C<sub>4</sub>F<sub>8</sub> were CF<sub>4</sub>, C<sub>2</sub>F<sub>6</sub>, C<sub>3</sub>F<sub>8</sub>, and a larger amount of a higher molecular weight fluorocarbon probably comprised mostly of C<sub>8</sub> compounds. Small amounts of C<sub>2</sub>F<sub>4</sub> and traces of *c*-C<sub>3</sub>F<sub>6</sub> and C<sub>3</sub>F<sub>6</sub> were found by vapor phase chromatographic analysis. XeF<sub>2</sub> was identified among the products by the absorption bands 549 and 564 cm.<sup>-1</sup>.<sup>3</sup> The higher molecular weight fluorocarbons were not positively identified.

With a reaction cell volume of 142 cc. and a constant lamp intensity of 2 × 10<sup>15</sup> quanta/sec. (determined by photolysis of CO<sub>2</sub>), the reaction proceeds with a pressure drop that is linear with time (Figure 1).

To explain these results, the following mechanism is proposed. The Xe(<sup>3</sup>P<sub>1</sub>) may either abstract two fluorines from the fluorocarbon or pass its energy to the fluorocarbon without reaction. It is assumed that the

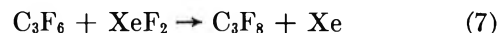
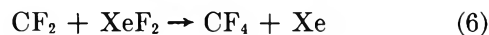
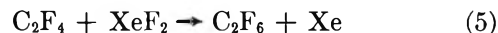


energy-rich *c*-C<sub>4</sub>F<sub>8</sub>\* from reaction 2 decomposes in one of the two ways known to occur with its thermal de-



composition.<sup>4-6</sup> The quantities of energy required for these reactions are 74 and 87 kcal., respectively.

The products of reactions 3 and 4 are fluorinated by the XeF<sub>2</sub> formed by reaction 1, thus accounting for all the low molecular weight fluorocarbons found except the trace of *c*-C<sub>3</sub>F<sub>6</sub>, which is assumed to be formed when reaction 4 occurs. It is known that XeF<sub>2</sub> is a fluorinat-



ing agent, although Chernick, *et al.*, have found that it is slow to react with perfluoroolefins at room temperature.<sup>7</sup> Near the thin quartz window separating the xenon discharge from the reaction space, the tempera-

(1) J. R. Dacey and J. W. Hodgins, *Can. J. Res.*, **28B**, 173 (1950).

(2) G. H. Miller, and J. R. Dacey, *Rev. Sci. Instr.*, in press.

(3) D. E. Milligan and D. R. Sears, *J. Am. Chem. Soc.*, **85**, 823 (1963).

(4) B. Atkinson, and A. B. Trenwith, *J. Chem. Soc.*, 2082 (1953).

(5) J. N. Butler, *J. Am. Chem. Soc.*, **84**, 1393 (1962).

(6) A. Lifshitz, H. Carroll, and S. Bauer, *J. Chem. Phys.*, **39**, 1661 (1963).

(7) T. C. Shieh, N. C. Yang, and C. L. Chernick, *J. Am. Chem. Soc.*, **86**, 5021 (1964).

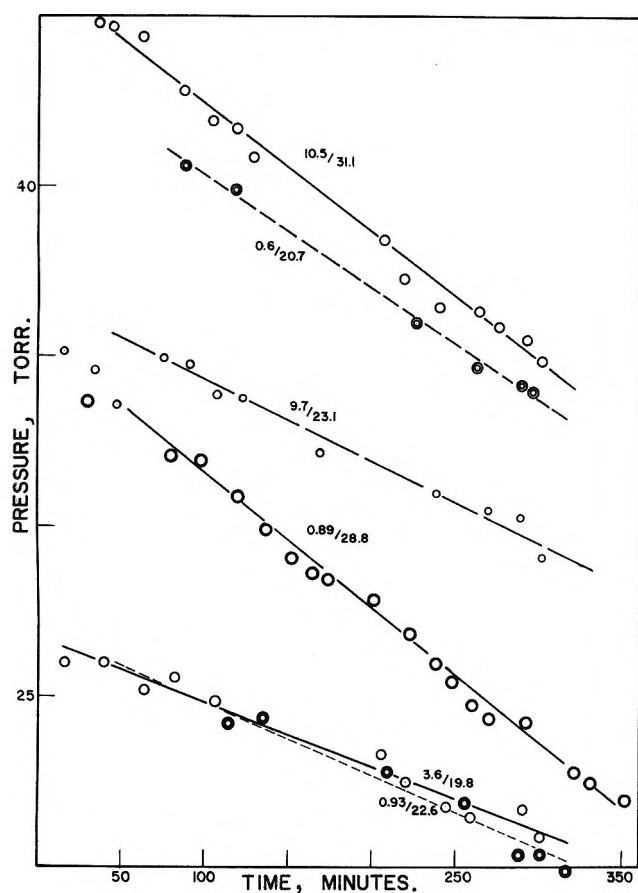
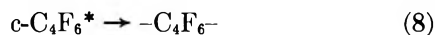


Figure 1. Pressure of reaction cell as a function of time. Indicated ratios are the initial pressures Xe/*c*-C<sub>4</sub>F<sub>6</sub>. The 0.6/20.7 curve is displaced upward by 20 torr units.

ture could be in excess of 200°, so that with our system fluorination with XeF<sub>2</sub> seems probable.

For reaction 1, the energy available is approximately 254 kcal. (194 kcal. from Xe at 1469 Å. and about 60 kcal. from two Xe-F bonds). Approximately 220 of this is required to break two C-F bonds; the remainder is insufficient to fragment the *c*-C<sub>4</sub>F<sub>6</sub> but could open the



ring. Various isomers of this diradical could form, depending on how the cyclic radical was formed and opened. The condensation of two of these radicals to form a C<sub>8</sub> fluorocarbon yields the main product found.



This product may be more or less fluorinated by the XeF<sub>2</sub>. Its formation would cause the pressure drop observed, the rate being constant for a constant rate of formation of Xe.\* We conclude that the main initial step is reaction 1.

It is interesting that Xe, when activated with 1469-Å.

light, not only acts as an energy carrier but also redistributes the fluorine between the reaction products.

*Acknowledgment.* This work was supported by Grant 9530/13 from the Defense Research Board of Canada.

UNIVERSITY OF CALIFORNIA  
SANTA BARBARA, CALIFORNIA  
ROYAL MILITARY COLLEGE OF CANADA  
KINGSTON, ONTARIO, CANADA

GLENN H. MILLER

J. R. DACEY

RECEIVED MARCH 4, 1965

### The Spectroscopy and Photosensitization of Various Photochromic Spiroprans

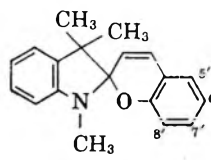
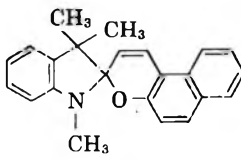
*Sir:* The purpose of this communication is to report on the emission spectra, assignment of excited states, photosensitization, certain aspects of the absorption spectra of several spiroprans, and mechanisms for the photochromic process. More complete details of results and interpretation will follow in the future. Table I presents a summary of the most pertinent information relative to the points described above.

The 6'-nitro derivative has an emission with sharp vibrational structure showing a 1450 vibrational progression in 2MeTHF. Such a spacing corresponds to an NO stretching frequency. The spectrum is also sharp in EPA and the emission origin is slightly blue shifted compared to 2MeTHF. The separation of the origin of emission from the longest wave length band maximum is approximately 8800 cm.<sup>-1</sup> (4200 cm.<sup>-1</sup> from the onset). All of these facts strongly indicate that the emission corresponds to a phosphorescence originating from an n,π\* triplet state. Furthermore, it has been possible to enhance the emission by sensitizing with benzophenone at 77°K. as well as to enhance photocoloration at -100°. This is consistent with the state assignment. Enhancement has very recently been shown for two different compounds.<sup>1</sup> Thus, the mechanism for the photochromic process would appear to be excitation (to lowest π,π\* or n,π\* singlet states), internal conversion to the lowest n,π\* singlet, intersystem crossing to the lowest, n,π\* triplet, followed by molecular rearrangement to the colored species. Obviously, the earlier steps would be bypassed by sensitization.

The emission for 6'-nitro,8'-methoxy (Table I) is assigned as a phosphorescence originating in an n,π\* triplet state. The mechanism for the photochromic

(1) T. Bercovici and E. Fischer, *J. Am. Chem. Soc.*, **86**, 5687 (1964).

**Table I:** Spectroscopic and Photosensitization Properties of Various Spiroprans

Compound	Solvent <sup>a</sup>	Absorption, colorless form		Emission origins		Color of colored form	Photosensitization		
		Onset in Å.	Longest $\lambda_{max}$ , Å.	Colorless form, Å.	Colored form, Å.		Photo-sensitizer	Emission <sup>b</sup>	Photocolor-ation <sup>c</sup>
 1,3,3-Trimethylindolino-benzospiropyran (TIB)	EPA	~3700	3200 (sh)	4140	5330 (sh)	Pink-red	Benzophenone	No	Yes w
	2MeTHF	~3600	3200 (sh)	4080	5900	Pink-red	Benzophenone	...	No
	HC	~3650	3200 (sh)	4080	6500	Pink	Benzophenone	No	Yes vs
6-Nitro TIB	EPA	~3950	3300	4670	6150 (max.)	Pink-red	Benzophenone	...	Yes w
	2MeTHF	~3950	3350	4740	6190 (max.)	Pink-red	Benzophenone	Yes	Yes w
6-Nitro, 8-methoxy TIB	EPA	...	...	5080	6270	Blue	...	...	...
	2MeTHF	~4000	3540	5180	6180 (max.)	Blue	...	...	...
 1,3,3-Trimethyl-indolino- $\beta$ -naphthospiropyran	2MeTHF		3595	3660 and 7100 (max.)	6050	Pink-red	Benzophenone	...	Yes vw
	EPA		3585	3700 and 7200 (max.)	6100	Pink-red	Quinoxaline	...	Yes vw

<sup>a</sup> EPA: 2 parts of ethyl ether, 5 parts of isopentane, 2 parts of ethyl alcohol; 2MeTHF: 2-methyltetrahydrofuran; HC: 2 parts of methylcyclohexane, 1 part of 3-methyl pentane. <sup>b</sup> Refers to photosensitization of emission of colorless form at 77°K. <sup>c</sup> Refers to comparative formation of colored form by sensitization relative to that without sensitizer, at -100°. vs = very strong (~50:1); w = weak (1.5-3:1); vw = very weak (<1.5:1).

process is expected to be comparable to that given for the nitro case.

The 1,3,3-trimethylindolino- $\beta$ -naphthospiropyran has two emissions. The one at higher energy is assigned as a fluorescence originating from a  $\pi, \pi^*$  singlet state and the one at lower energy is assigned as a phosphorescence originating from a  $\pi, \pi^*$  triplet state. The mechanism for sensitization is expected to be similar to that for the cases noted previously except for the nature of the states.

The parent benzospiropyran emission (Table I) is long-lived (~0.4 sec.). It is therefore assigned as originating in a triplet state. The exact assignment is

uncertain at the moment. The mechanism of photochromism is expected to be similar to that given for other cases. Data have been obtained for other compounds, but the state assignments have not yet been completely ascertained.

*Acknowledgment.* This study was performed under Contract AF 33(615)-1733 from the U. S. Air Force, Systems Engineering Group, Wright-Patterson AFB, Ohio.

DEPARTMENT OF CHEMISTRY  
UNIVERSITY OF HOUSTON  
HOUSTON, TEXAS 77004

RALPH S. BECKER  
J. K. ROY

RECEIVED FEBRUARY 3, 1965